JAERI-Conf
95-003

PROCEEDINGS OF THE 6TH JAPAN-CHINA BILATERAL SYMPOSIUM ON RADIATION CHEMISTRY

November 6~11, 1994, Waseda University, Tokyo, Japan

March 1995

(Eds.) Yoshimasa HAMA[*1], Yosuke KATSUMURA[*2]
Nobuyuki KOUCHI[*3] and Keizo MAKUUCHI

日本原子力研究所
Japan Atomic Energy Research Institute

本レポートは，日本原子力研究所が不定期に公刊している研究報告書です。
入手の問合わせは，日本原子力研究所技術情報部情報資料課（〒319-11 茨城県那珂郡東海村）あて，お申し越しください。なお，このほかに財団法人原子力弘済会資料センター（〒319-11 茨城県那珂郡東海村日本原子力研究所内）で複写による実費頒布をおこなっております。

This report is issued irregularly.
Inquiries about availability of the reports should be addressed to Information Division, Department of Technical Information, Japan Atomic Energy Research Institute, Tokai-mura, Naka-gun, Ibaraki-ken 319-11, Japan.

© Japan Atomic Energy Research Institute, 1995

編集兼発行　日本原子力研究所
印　　刷　いばらき印刷㈱

JCBSRC '94

The 6th Japan-China Bilateral Symposium on Radiation Chemistry

November 6-10, 1994

Waseda University
Tokyo, Japan

Sponsored and Organized
by
Waseda University
Japanese Society of Radiation Chemistry
Japan Atomic Energy Research Institute
China Radiation Research and Radiation Processing Society

Supported by
Radiation Application Development Association

Honorary Chairman

Y. Tabata (Tokai Univ.)

Organizing Committee in Japan

Y. Hama	(Waseda Univ.): Chairman
T. Dohke	(Waseda Univ.)
Y. Ohki	(Waseda Univ.)
J. Sohma	(Kanagawa Univ.)
K. Fueki	(Nagoya Univ.)
M. Imamura	(RIKEN)
S. Takamuku	(Osaka Univ.)
H. Yoshida	(Hokkaido Univ.)
K. Ishigure	(Univ. of Tokyo)
M. Nishikawa	(Kanagawa Institute of Tech.)
H. Yamaoka	(Kyoto Univ.)
T. Shida	(Kyoto Univ.)
Y. Hatano	(Tokyo Institute of Technology)
T. Sawai	(Tokyo Metropolitan Isotope Research Center)
S. Sato	(Japan Atomic Research Institute)
N. Tamura	(Radiation Application on Development Association)
M. Takehisa	(Radia Industry Co. Ltd.)
K. Oda	(The Furukawa Electric Industry Co.)
K. Ueno	(Sumitomo Electric Industry Co. Ltd.)
K. Mizusawa	(Nissin-High Voltage Co. Ltd.)

Organizing Committee in China

Wu Jilan	(Peking Univ.): Chairman
Chen Wenxiu	(Beijing Normal Univ.)
Lin Nianyun	(Shanghai Institute of Nuclear Research)
Ma Zueteh	(Shanghai Univ. of Science and Tech.)
Wang Bingling	(Beijing Radiation Application Center)
Liu Renzhong	(Shanghai Institute of Nuclear Research)
Zhang Zhiping	(East China Univ. of Chemical Tech.)
Sun Jiazhen	(Changchun Institute of Applied Chem.)
Xu Jun	(Changchun Institute of Applied Chem.)
Zhang Manwei	(Univ. of Science and Tech.)
Wang Jiaju	(China Institute of Atomic Energy)
Shen Huaiyu	(Shanghai Organic Chemistry Institute)
Chen Xingfang	(Jilin Univ.)
Cao Jin	(East China Univ. of Chemical Tech.)
Hu Fumin	(Chengdu Research Center for Sillicones)
Wei Genshuan	(Peking University)
Gu Dangsheng	(Ministry of Chemical Industry)
Pan Xiumiao	(Dept. of Research and High Technologies of R. P. C.)

Steering Committee in Japan

Y. Hama	(Waseda Univ.): Chairman
Y. Katsumura	(Univ. of Tokyo): Secretary General
S. Tagawa	(Osaka Univ.): Chairman of Program Committee
T. Ichikawa	(Hokkaido Univ.)
M. Ogasawara	(Hokkaido Univ. of Education)
T. Miyazaki	(Nagoya Univ.)
S. Nishimoto	(Kyoto Univ.)
H. Matsuyama	(Kyoto Univ.)
N. Kouchi	(Tokyo Institute of Technology)
K. Makuuchi	(Japan Atomic Research Institute)
M. Washio	(Sumitomo Heavy Industries, Ltd.)

Steering Committee in China

Wu Jilan	(Peking Univ.): Chairman
Wang Binling	(Beijing Radiation Application center):Secretary General
Chen Wenxiu	(Beijing Normal Univ.): Chairman of Program Committee
Liu Renzhong	(Shanghai Institute of Nuclear Research)
Wei Genshuan	(Peking Univ.)
Cao Jin	(East China Univ. of Chemical Tech.)

CONFERENCE LOCATION

International Conference Center, Waseda University Center for Scholarly Information, Nishiwaseda 1-20-14, Shinjuku-ku, Tokyo, Japan

The symposium organizers of The 6th Japan-China Bilateral Symposium on Radiation Chemistry gratefully acknowledge the financial support provided by the following organization in Japan.

Beam Operation Co., LTD.

Ebara Corporation

Eikosha, LTD

JEOL LTD.

Micro Device Co., LTD.

Nissin-High Voltage Co., LTD.

Radia Industry Co., LTD.

Radiation Application Development Association.

SUMITOMO ELECTRIC INDUSTRIES, LTD.

Sumitomo Heavy Industries, LTD.

Japan Atomic Energy Research Institute

Japanese Society of Radiation Chemistry.

Waseda University

JAERI-Conf 95-003

Proceedings of the 6th Japan-China Bilateral Symposium on Radiation Chemistry

November 6-11, 1994, Waseda University, Tokyo, Japan

(Eds.) Yoshimasa HAMA*1, Yosuke KATSUMURA*2, Nobuyuki KOUCHI*3 and Keizo MAKUUCHI

Department of Material Development
Takasaki Radiation Chemistry Research Establishment
Japan Atomic Energy Research Institute
Watanuki-cho, Takasaki-shi, Gunma-ken

(Received February 7, 1995)

This is the proceedings of The 6th Japan-China Bilateral Symposium on Radiation Chemistry held on November 6 - 11, 1994 at International Conference Center of Waseda University in Tokyo. 125 papers (90 papers in oral and 35 papers in poster) including 2 plenary lectures and 22 invited papers were presented. In the plenary lecture, Prof. Tabata presented on recent progress of accelerators for beam application in Japan, and Prof. Wu presented on some progress on radiation chemistry and radiation processing of substances of biological interests and biological applications of radiation technology in China. In two special sessions on irradiation facility and dosimetry, 7 papers and 10 ones, respectively, were presented. The other papers presented were classified into 5 sessions which consist of gas and liquid phase(24 papers) polymers(32 ones), biological system(14 ones), radiation processing(26 ones) and solid phase(10 ones). In each session, 2 to 5 invited papers were presented.

Keywords: Radiation Chemistry, Irradiation Facility, Polymer, Biological System, Radiation Processing, Pulse Radiolysis, Dosimetry

---

*1 Waseda University
*2 The University of Tokyo
*3 Tokyo Institute of Technology

JAERI-Conf 95-003

第6回日中放射線化学シンポジウム論文集

1994年11月6日－11日、早稲田大学、東京

日本原子力研究所高崎研究所材料開発部

（編）浜　義昌[*1]・勝村　庸介[*2]・河内　宣之[*3]

幕内　恵三

（1995年2月7日受理）

本論文集は平成6年11月6－11日に早稲田大学において開催された第6回日中放射線化学シンポジウムに関するものである。2件の基調講演と22の招待講演を含み、合計125件の発表があった。そのうち35件がポスター発表として行われた。基調講演において、田畑教授から日本におけるビーム利用加速器の最近の進歩について、呉教授からは中国における生物関連分野の放射線化学および放射線プロセスの進歩についての発表が行われた。照射施設と線量測定に関する2特別セッションが設けられ、それぞれ7件と10件の発表が行われた。そのほかの発表は5セッションに分類された。ガス・液相関係では24件、高分子関係では32件、生体システム関係では14件、放射線プロセス関係では26件、固相関係では10件の発表がそれぞれ行われた。各セッションでは2－5件の招待講演が行われた。

高崎研究所：〒370－12　群馬県高崎市綿貫町1 2 3 3

*1　早稲田大学

*2　東京大学

*3　東京工業大学

Contents

Preface

Yoshimasa Hama

Opening Remarks

Wu Jilan

Setsuo Takamuku

1. Plenary Lectures

1.1 Recent Progress of Accelerators for Beam Application in Japan ····· 1

Yoneho Tabata

1.2 Some Progress on Radiation Chemistry of Substances of Biological Interests and Biological Applications of Radiation Technology in China ····· 4

Wu Jilan and Fang Xingwang

2. Irradiation Facilities

2.1 * A Typical R&D Center on Radiation Processing in China ····· 11

Sun Jiazhen

2.2 * Synchrotron Radiation Facilities for Chemical Applications ····· 21

Yoshihiko Hatano

2.3 * Irradiation Facilities and Research Activities in JAERI-Takasaki ····· 29

Waichiro Kawakami

2.4 * Current Status of Radiation Chemical Research in India ····· 35

C. Gopinathan and J.P. Mittal

2.5 * Pulse Radiolysis Facilities and Activities in Japan ····· 36

M. Ogasawara

2.6 EB Processing at Tsukuba EB Center ····· 46

Yutaka Yamase, Yasuyuki Aikawa and Toyoaki Inamura

2.7 An Economic Benefit Analysis on the Cobalt-60 Irradiation Facility of Beijing Radiation Research Center ····· 51

Wang Binlin

3. Gas and Liquid Phase (1)

3.1 * Dynamics of Superexcited Molecules as Studied by Two Dimensional Spectroscopy ····· 54

Masatoshi Ukai

3.2 * The Study on the Primary Processes of Radiation Chemistry in Liquid Alkanes by Means of Picosecond Pulse Radiolysis ····· 59
Y. Yoshida and S. Tagawa

3.3 Isotope and Temperature Effects on Positronium Formation in Water ····· 64
Testuya Hirade

3.4 Electron Mobilities and Electron-ion Recombination Rate Constants in Nonpolar Solvents ····· 69
K. Shinsaka, T. Odaka, K. Isoda, H. Yamada, M. Ukai, N. Kouchi and Y. Hatano

3.5 The Reactions of Excited Radical Ions Produced by Pulse Radiolysis ····· 76
Tetsuro Majima, Akito Ishida and Setsuo Takamuku

3.6 Selecting Ethanol as an Ideal Organic Solvent Probe in Radiation Chemistry γ-radiolysis of Acetone-ethanol System and Acetophenone-ethanol System ····· 81
Jin Haofang, Wu Jilan, Fang Xingwang and Zhang Xujia

3.7 Hydroxylethylation of Baicalin by γ-ray Irradiation of Baicalin in Ethanol ····· 91
Cai Zhongli, He Yongke and Wu Jilan

3.8 A Comparative Study on the Protection Effect in the Radiation-induced Oxidation of Liquid Paraffins and Polypropylene ····· 96
Y.S. Soebianto, I. Kusuhata, Y. Katsumura, K. Ishigure, J. Kubo, S. Hamakawa, K. Azami, H. Kudoh and T. Seguchi

4. Polymers (1)

4.1 * Relationship between Energy Profile and Chemical Structural Change in Polymers Irradiated by Ion-beam ····· 101
Yoshimasa Hama, Kenichi Hamanaka, Hideya Matsumoto, Hisaaki Kudoh, Tsuneo Sasuga and Tadao Seguchi

4.2 WAXD and SAXS Study on Gamma-radiation Damage to Polyamide-1010 Crystal Structure ····· 105
L. Zhang, H. Zhang and D. Chen

4.3 Radiation Damage of Polymers Studied by Positron Annihilation (Positron and Gamma-ray Irradiation Effects) ····· 110
T. Suzuki, Y. Oki, M. Numajiri, T. Miura, K. Kondo and Y. Ito

4.4 * The Radiation Chemistry of Poly(Arylene Ether Phosphine Oxide)s ····· 115
D.J.T. Hill, J.L. Hopewell, J.H. O'Donnell and P.J. Pomery

4.5 Mechanism of Radiation-induced Degradation of Poly(Methyl Methacrylate) ····· 120
Tsuneki Ichikawa, Ken-ichi Oyama and Hiroshi Yoshida

4.6 Radiation Stability of Pyridine Resin for Reprocessing ····· 125
M. Nogami, Y. Fujii and T. Sugo
4.7 Inhibition of Radiation-oxidation by Pure Hydrocarbon Type Radical Scavengers ····· 129
Junichi Kubo and Kazushige Otsuhata
4.8 Degradation of Elastomers by Heat and/or Radiation ····· 136
M. Ito
4.9 Aging Effect on Radiation-induced Degradation of Polypropylene ····· 141
M. Imai, M. Sekiguchi, M. Tabei, Y. Yamada and H. Shimizu
4.10 Effect of Isotacticity on Radiation Stability of Polypropylene ····· 146
Qiao Jinliang, Zhang Fengru, Wei Genshuan, Zhang Juhong and Wu Jilan
4.11 Structural Changes in the Crystal-amorphous Interface of Isotactic Polypropylene Film Induced by Annealing and γ-irradiation ····· 152
Sei-ichi Nishimoto, Hideo Seike, Malinee Chaisupakitsin, Fumio Yoshii and Keizo Makuuchi
4.12 The Effect of Monomer Molecular Weight on Grafting Reaction ····· 157
Wu Minghong, Ding Zhongli and Ma Zueteh
5. Gas and Liquid Phase (2)
5.1 * Radiation and Photochemistry of Fullerenes ····· 166
Jai P. Mittal
5.2 The Research of Some Transient Species of Fullerenes with Pulse Radiolysis and Laser Photolysis ····· 167
S.D. Yao, Z.R. Lian, W.F. Wang, J.S. Zhang and N.Y. Lin
5.3 Radiolytic Reduction Reaction of Colloidal Silver Bromide Solution ····· 179
Yasuhisa Oya, Takehiro Zushi, Kunihiko Hasegawa and Tatsuo Matsuura
5.4 Simulation of Radiation-induced Ozone Decomposition in Water in the Presence of Organic Compounds ····· 184
H. Arai, H. Namba, T. Miyata, M. Arai, A. Sakumoto and H. Sunaga
5.5 The Model of Initial Intratrack Chemical Processes of Water Radiolysis ····· 189
M. Domae, Y. Katsumura, K. Ishigure and V.M. Byakov
5.6 Radiolysis of Concentrated Nitric Acid Solutions ····· 194
R. Nagaishi, P.Y. Jiang, Y. Katsumura, M. Domae and K. Ishigure
5.7 Radiolysis of Water at Elevated Temperatures with γ-rays and Fast Neutrons ····· 199
Y. Katsumura, G.R. Sunaryo, D. Hiroishi and K. Ishigure
6. Biological System (1)

6.1 * Excitation Transfer, Charge Transfer and Hydrogen Abstraction Reaction, Kinetics Studies of Modification of DNA Components ····· 204
N.Y. Lin

6.2 Kinetic Observation of Rapid Electron Transfer between Thymine and Thymidine Anion Radicals and Caffeic Acid: A Pulse Radiolysis Study ····· 211
Z.H. Zuo, S.D. Yao, H.C. Lee, W.Z. Lin, J.-S. Zhang and N.Y. Lin

6.3 Cellular Non-protein Thiol Depletion and Radiosensitization of Hypoxic Cells by Nitroazole Derivatives Possessing and NPSH-reactive Side Chain ····· 216
Ling Zhou and Sei-ichi Nishimoto

6.4 A Study on Radiosensity of Listeria Monocytogenes in the Food ····· 221
Hu Jinhui, Wang Zhixin, Du Qiang and Yan Di

6.5 * The Effects of γ-irradiation on the Garlic Oil Contents in Garlic Bulbs and the Radiolysis of Allyl Trisulfide ····· 225
Wei Genshuan, Wang Guanghui, Yang Ruipu and Wu Jilan

6.6 Radiation Crosslinking for Signal Responsive Chemical Delivery Systems ····· 231
Isao Kaetsu, Kumao Uchida, Shinji Ueta, Koichi Sudani and G.O. Phillips

7. Poster Presentation (1)

7.1 Variation in Yield Ratios of Fragment Ions and of Ion-pairs from CF_2Cl_2 Following Monochromatic Soft X-ray Absorption ····· 236
I.H. Suzuki, N. Saito and J.D. Bozek

7.2 The Specialty Committee of Radiation Processing of CIRA ····· 241
Hou Fuzhen

7.3 Photoionization Potentials of Fullerenes (C_{60}-C_{84}) in Non-polar Liquid ····· 243
Iwao Shimoyama, Kazumichi Nakagawa, Chiemi Fujikawa, Katsuyuki Morii, Tadaoki Mitani and Ryuji Kato

7.4 Radiation Damages on Superionic Conductors ····· 248
T. Awano, M. Ikezawa and T. Matsuyama

7.5 Electron Transfer and Recombination Reactions of Polymer Anions Produced by Ionizing Radiation ····· 252
Masaaki Ogasawara

7.6 Intramolecular Electron Transfer in Nitrite Reductase Studied by Pulse Radiolysis ····· 255
K. Kobayashi, S. Tagawa, T. Kouzuma, Deligeer, K. Yamaguchi, N. Nakamura, S. Suzuki and S. Shidara

7.7 Ion Beam Irradiation Effects on Aromatic Polymers ····· 260
Satoshi Shukushima and Keiji Ueno

7.8 Ion-irradiated Polymer Studied by a Slow Positron Beam ····· 265
Y. Kobayashi, I. Kojima, S. Hishita and T. Suzuki
7.9 One-touch Alanine Dosimetry System for Radiation Processing ····· 270
S. Kashiwazaki, S. Matsuyama, H. Yaguu, H. Hara and T. Kojima
7.10 Radiation Induced Solid-state Polymerization of Long-chain Acrylates Containing Fluorocarbon Chain ····· 275
Y. Shibasaki and Zhi-qin Zhu
7.11 Decolorization and Degradation of Melanoidins in Wastewater by Ionizing Radiation ····· 280
M. Sekiguchi, T. Tanabe and T. Sawai
7.12 Discrimination of Damages Depending on the Types of Lactic Dehydrogenase Isozymes in Electron Beam Irradiation ····· 285
A. Ohta, T. Matsubayashi, Liu Xiao-Lan and H. Takizawa
7.13 EPR Study of N^{+}-ion-induced Free Radical Formation in Antibiotic-producers ····· 293
Xie Liqing, Zhang Yinfen, Chen Ruyi, Gao Juncheng, Zhang Pelling and Ying Hengfeng
7.14 Adhesion of Yeast Cells on Surface of Polymers Produced by Radiation Polymerization ····· 298
Zhaoxin Lu, Masaaki Takehisa and Zongchuan Xie
8. Polymers (2)
8.1 Enhanced Interfacial Radiation-induced Reaction for Improving the Interfacial Adhesion of Incompatible Polymer Blend PP/BR ····· 303
Liu Chang-hai, Yang Hui-li and Xu Jun
8.2 * Morphology and Properties of Polyurethane/poly(ST) or Poly(MMA) Interpenetrating Polymer Networks by Co60 γ-ray ····· 308
Zhi-ping Zhang, Geng-chao Wang and Sheng-kang Ying
8.3 Radiation Crosslinking Film ····· 317
Wang De-ren and Fang Mei-zhen
8.4 Low Temperature Gamma-ray Irradiation Effects on Polymer Materials ····· 321
H. Kudoh, N. Kasai, T. Sasuga and T. Seguchi
8.5 Radiation Effects on Epoxy Composites at Cryogenic Temperatures ····· 326
H. Yamaoka, K. Miyata, S. Nishijima and T. Okada
9. Dosimetry
9.1 * Dosimetry Systems for Radiation Processing in Japan ····· 331
N. Tamura

9.2 Dosimetry of A 3-5 MeV Linear Electron Accelerator for Radiation Processing ····· 338
Xie Liqing, Song Hongbin, Wang Pengcheng, Zhang Yenfen, Gu Hongchun and Liu Xiaoguang
9.3 Dosimetry Study for Electron Beam Irradiation in Radiation Processing ····· 344
H. Sunaga, Y. Haruyama, H. Takizawa, T. Kojima and K. Yotsumoto
9.4 The Status of Radiation Processing Dosimetry in China ····· 349
Cheng Wenxiu, Li Chenghua, Pang Ruicao and Zhang Yanli
9.5 * Effects of Additives on PVG Dosifilm ····· 356
Chen Wenxiu and Liu Aiguo
9.6 Recent Progress in Application of JAERI Alanine/ESR Dosimetry System ····· 362
T. Kojima
9.7 Dosimetry Study on A p-n Junction Semiconductor Detector ····· 367
Zheng Zheng, Zhao Yongfu, Dai Honggui and Xie Zongchuan
10. Biological System (2)
10.1 Capturing of *Staphylococcus aureus* onto an Interface Containing Graft Chains ····· 372
William Lee, Kyoichi Saito, Shintaro Furusaki, Takanobu Sugo and Keizo Makuuchi
10.2 An Intelligent Biopolymer Gel with Pendant L-proline Methyl Ester ····· 377
Masaru Yoshida, Agneza Safranj, Hideki Omichi and Ryoichi Katakai
10.3 * IAEA Education and Training Programs in Radiation Technology ····· 383
Ma Zue-teh
10.4 Feasibility Study on Utilization of Vitrified Radioactive Waste as Radiation Sources ····· 392
K. Makuuchi, F. Yoshii and K. Hyakutake
10.5 Production of an Intense Slow Positron Beam using a Compact Cyclotron ····· 396
Masakazu Washio, Masafumi Hirose and Kazuyoshi Takahashi
10.6 The Recent Industrial EB Applications in Japan ····· 401
Koji Nakai, Masayuki Kashiwagi and Kenichi Mizusawa
11. Radiation Processing (1)
11.1 * Effect of Irradiation on PTC Performances of Carbon Black Filled Polymer Composites ····· 408
Cheng Xinfang, Jia Wentao, Tang Hao, Yang Huali and Li Shuhua
11.2 An Investigation on Radiation Crosslinked Foam of LDPE/EVA Blends ····· 414
Siqin Dalai and Chen Wenxiu

11.3 Radiation Modification of LDPE Sheets and its Application ····· 419
Li Chaoshun, Zhang Zihui, Rao Zhigong, Zheng Xinmiao, Xu Ziyan and Wang Binglin

11.4 Electron Beam Curing of Dimer Acid-based Urethane Acrylates for Pressure Sensitive Adhesives ····· 424
T. Sasaki, S. Takeda and K. Shiraishi

11.5 * The Application of FT-IR Spectrum Method in Photocuring Process for Polyester Acrylate ····· 428
Cao Jin, Lu Xian Liang and Zhang Zhen Li

11.6 Radiation Polymerization and Crosslinking of *N*-isopropylacrylamide in Aqueous Solution and in Solid State ····· 434
Agneza Safranj, Noriyasu Nagaoka, Masaru Yoshida, Hitoshi Kubota, Hideki Omichi and Ryoichi Katakai

12. Poster Presentation (2)

12.1 Collisional Deexcitation Processes of Ne($^3P_2$) by Rare Gas Atoms ····· 439
Deba Bahadur Khadka, Yuji Fukuchi, Masashi Kitajima, Masatoshi Ukai, Noriyuki Kouchi and Yoshihiko Hatano

12.2 Studies of Some Elementary Processes Involving Electrons in the Gas Phase by Pulse-radiolysis Microwave-cavity Technique ····· 444
Takeyoshi Sunagawa, Takeshi Makita, Hirofumi Musasa, Yoshitsugu Tatsumi and Hiroshi Shimamori

12.3 Photoredox Chemistry of Chloro Complexes of Main Group Metals ····· 449
Nobuyoshi Shinohara and Masaaki Oshima

12.4 Photoionization of C_{60} and C_{70} in Alkane Liquids ····· 453
Ryuzi Katoh, Klaus Lacmann and Werner F. Schmidt

12.5 Magnetic Field Effects in the Ion-pair Recombination Process ····· 458
Kunihiro Kokubu, Hiroshi Hasegawa and Yoshimasa Hama

12.6 Pulse Radiolysis of Cyclodextrin Inclusion Complexes ····· 462
Y. Yamamoto, Y. Naka, Y. Yoshida and S. Tagawa

12.7 Uniform Irradiation of High-energy Intense Ion Beams to Large Area by Two-dimensional Beam Scanning ····· 467
T. Agematsu, S. Okumura and K. Arakawa

12.8 High Energy Ion Irradiation Effects on Polymer Materials ····· 472
H. Kudoh, T. Sasuga and T. Seguchi

12.9 Space Charge Distribution in Gamma-irradiated Low Density Polyethylene ····· 476
M. Kojima, Y. Tanaka, T. Takada and Y. Ohki

12.10 A New Leuco Dye Dosifilm PVG ····· 481
Liu Aiguo, Chen Wenxiu and Jia Haishun
12.11 Radiation Induced Crosslinking of Polytetrafluoroethylene ····· 487
Akihiro Oshima, Yoneho Tabata, Shigetoshi Ikeda, Kazushige Otsuhata, Hisaaki Kudoh and Tadao Seguchi
12.12 Kinetic Behavior of Nitric Oxide in Biological System Studied by Pulse Radiolysis ····· 492
M. Miki, K. Kobayashi and S. Tagawa
12.13 Radicals of Some Aminoacids and Their Derivatives at 77K Produced by Synchrotron Radiation in Vacuum Ultraviolet Range
Ⅱ. N-acetyl-DL-alanine ····· 497
Atsuko Minegishi, Junkichi Sohma and Kiminori Ushida
12.14 Protecting Effect on Gamma-ray Damage of DNA by Tea Catechin ····· 502
H. Yoshioka, G. Akai, H. Yoshioka, K. Yoshinaga and K. Hasegawa
12.15 γ-radiation Induced Polymerization of Unsaturated Liposomes Containing Unsaturated Lipid, Cholesterol, and Saturated Aliphatic Acid ····· 507
F. Hosoi, H. Omichi, K. Akama, S. Tokuyama and Y. Nakano
12.16 Microemulsion Polymerization of Butyl Acrylate Irradiated by γ-ray ····· 512
Zhicheng Zhang, Xiangling Xu, Lei Shi and Manwei Zhang
12.17 The Measurement of Dose Distribution in the Product Boxes by Alanine/ESR Dosimeter ····· 517
Xie Liqing, Zhang Yinfen, Lan Liqiao and Zhou Ruiyng

13. Solid Phase

13.1 Quantum Mechanical Tunneling Reaction in Solid Hydrogen and Solid Alkane at Low Temperature, Tunneling of Hydrogen Atom and Hydrogen Molecule ····· 522
T. Miyazaki
13.2 Asymmetrical Distorted Structure, Dynamics, and Reactions of the Silacyclohexane and Related Radical Cations: ESR and *ab-initio* MO Study ····· 527
Kenji Komaguchi, Masaru Shiotani and Mitsuo Ishikawa
13.3 * The Factor that Determines Photo-induced Crystalline-state Reaction ····· 531
Y. Takenaka
13.4 Optical Absorption Analysis on Diamond Crystals Modified by H_2^+ Implantation and Subsequent Annealing ····· 536
Z.Q. Ma, H. Naramoto, Y. Aoki, S. Yamamoto, T. Takeshita and P.C. Goppelt-Langer

13.5 Generation and Bleaching of γ-ray-induced Loss of Er^{3+}-doped Silica-core Optical Fiber ····· 542
Takeshi Koyama, Nobuyuki Dohguchi, Yoshimichi Ohki, Hiroyuki Nishikawa, Yasuo Kusama and Tadao Seguchi

13.6 Self-trapped Holes in Alkali Silver Halide Crystals ····· 547
T. Awano, M. Ikezawa and T. Matsuyama

13.7 Ion Beam Induced Luminescene and Damage Study on Single-and Poly-crystalline Al_2O_3:Cr ····· 552
N.T. My, Y. Aoki, H. Takeshita, S. Yamamoto, P. Goppelt-Langer and H. Naramoto

13.8 * Effect of Carbon K-shell Excitation on H^+ Desorption and Color Center Formation in Anthracene Crystal ····· 557
Iwao Shimoyama, Kazumichi Nakagawa, Aiko Kimura, Ryuji Kato, Masahiro Kotani, Tetsuji Sekitani, Jun'ya Maruyama and Ken'ichiro Tanaka

14. Radiation Processing (2)

14.1 * A Research on Gas-phase Grafting of Acrylic Acid onto Polytetrafluoroethylene by Preirradiation ····· 562
Hu Fumin, Fen Wen, Wang Yufang and Huang Guanglin

14.2 Radiation Induced Graft of Acrylonitrile on Silk Protein in $ZnCl_2$ Solution ····· 569
Zhicheng Zhang and Jiegen Chu

14.3 Effects of Preirradiation Graft Polymerization of Acrylic Acid onto Polyethylene Film ····· 574
Feng Wen, Hu Fumin, Yuan Lihua, Zhu Po and Chen Zefang

14.4 Preparation of Carboxy-group-contained Polyvinyl Alcohol Amidoxime Chelate Fiber by Preirradiation Grafting and its Adsorbability for Au(Ⅲ) Ions ····· 579
Lei Rao, Jun Xu, Wenbing Xie and Jinyu Yao

14.5 Stability of Guest Molecules in Urea Canal Complexes by Canal Polymerization ····· 584
Fumio Yoshii and Keizo Makuuchi

14.6 Preparation of Polymer Microspheres by Radiation-induced Polymerization ····· 588
Yukihiko Naka, Yukio Yamamoto, Yoichi Yoshida and Seiichi Tagawa

14.7 * Synthesis of Nanometer Metallic Powders or its Oxides by γ-ray Reduction of Salts Aqueous Solution ····· 593
Zhang Manwei, Zhu Yingjie, Qian Yitai and Chen Zuyao

14.8 Preparation of a New Thermo-sensitive Material by Preirradiation Grafting … 598
Minghong Wu, Zhongli Ding, Hongding and Zueteh Ma
14.9 International Standard of Radiation Sterilization Current Trend of Dose Setting and the Issues …… 603
Masaaki Takehisa
14.10 Electron Beam Sterilization for Dishes …… 607
Wang De-ren and Fang Mei-zhen
14.11 Evaluation of Sterilization Dose for Disposable Hypodermic Needles Manufactured under Ultra-clean Condition …… 610
M. Tabei and M. Sekiguchi
14.12 Removal of Gaseous Xylene by Electron Beam Irradiation …… 615
K. Hirota, H. Mätzing and H.-R. Paur
14.13 On the Mechanism for Chemical Reactions in the Electron Beam Irradiated Fuel Gas …… 620
Shin-ichi Ohno, Hideki Namba and Okihiro Tokunaga
List of Participants …… 625
Author Index …… 629
Invited lectures are marked asterisk

目　　次

まえがき　浜　義昌

1. 基調講演

1.1 日本におけるビーム利用加速器の最近の進歩 …… 1
田畑　米穂

1.2 中国における生物関連分野の放射線化学および放射線プロセスの進歩 …… 4
呉　季蘭

2. 照射施設

2.1 * 中国における放射線プロセスのR＆Dセンター …… 11
孫　家珍

2.2 * 化学利用放射光施設 …… 21
簇野　嘉彦

2.3 * 原研高崎の照射施設と研究活動 …… 29
川上　和市郎

2.4 * インドにおける放射線化学研究の現状 …… 35
ジェイ・ピー・ミッタル

2.5 * 日本国内のパルスラジオリシス施設と研究活動 …… 36
小笠原　正明

2.6 つくば電子照射センターにおける電子線利用 …… 46
山瀬　豊

2.7 * 北京放射線研究センターにおけるコバルト60照射施設の経済分析 …… 51
王　炳林

3. ガス・液相 (1)

3.1 * 二次元分光法による超励起分子のダイナミクス …… 54
鵜飼　正敏

3.2 * ピコ秒パルスラジオリシス法による液中アルカン中の放射線初期過程の研究 …… 59
吉田　陽一

3.3 水中におけるポジトロニウム形成の同位体および濃度効果 …… 64
平出　哲也

3.4 非極性溶媒における電子の移動度と電子・正イオン再結合反応 …… 69
新坂　恭士

3.5 電子・レーザーパルス照射法によるラジカルイオンの光反応 …… 76
真嶋　哲朗

3.6 アセトン－エタノール及びアセトフェノン－エタノールのγ線照射研究の
理想的溶媒としてのエタノールの選択 …… 81
金　浩芳
3.7 γ線照射によるエタノール中のバイカリンのハイドロキシエチル化 …… 91
蔡　中麗
3.8 液体パラフィンとポリプロピレンにおける放射線誘起酸化反応の保護効果に
対する添加物の比較実験 …… 96
ソエビアント・ヤンティ・サバリナ
4. 高分子（1）
4.1 * 高分子のイオン照射におけるエネルギー付与プロファイルと化学構造変化の
相関 …… 101
浜　義昌
4.2 ＷＡＸＤとＳＡＸＳ法によるポリアミド1010結晶のγ線損傷の研究 …… 105
張　利華
4.3 消滅ポジトロン法によるポリマーの放射線損傷－ポジトロンとγ線照射 …… 110
鈴木　健訓
4.4 * ポリアクリレンエーテルフォスフィンオキシドの放射線化学 …… 115
ディビット・ジェイムス・ヒル
4.5 ポリメチルメタアクリレートの放射線分解機構 …… 120
市川　恒樹
4.6 再処理用ピリジン型樹脂の耐放射線性 …… 125
野上　雅伸
4.7 純炭化水素型ラジカル捕捉剤による放射線劣化防止 …… 129
久保　純一
4.8 熱と放射線によるエラストマーの劣化 …… 136
伊藤　政幸
4.9 ポリプロピレンの照射劣化における経時変化 …… 141
今井　正彦
4.10 ポリプロピレンの放射線耐性のイソタクティシティ効果 …… 146
喬　金梁
4.11 加熱およびγ線照射によって誘起されるイソタクチックポリプロピレンフィルムの
結晶・非結晶界面における構造変化 …… 152
西本　清一
4.12 モノマー分子量のグラフト反応への影響 …… 157
呉　明紅
5. ガス・液相（2）

5.1 * フラーレンの放射線化学と光化学 …… 166
ジェイ・ピー・ミッタル
5.2 パルスラジオリシス及びレーザーフォトリシス法によるフラーレンの短寿命活性種の研究 …… 167
姚　思徳
5.3 コロイド臭化銀溶液の放射線還元反応 …… 179
大矢　恭久
5.4 有機物共存下における水中オゾンの放射線反応のシミュレーション …… 184
新井　英彦
5.5 拡散モデルによる水溶液の放射線分解拡張スパーの初期過程の研究 …… 189
堂前　雅史
5.6 高濃度硝酸溶液の放射線分解 …… 194
氷石　隆二
5.7 γ線と高速中性子による高温水の放射線分解 …… 199
勝村　庸介
6. 生体システム（1）
6.1 * ＤＮＡ構成要素中の動力学研究－励起・電荷移動と水素引き抜き …… 204
林　念芸
6.2 パルスラジオリシス法によるチミン及びチミジンアニオンラジカルとカフェイン酸との速い電子移動の動力学研究 …… 211
姚　思徳
6.3 非タンパク質性チオール（ＮＰＳＨ）捕捉能を側鎖に持つニトロアゾール誘導体の低酸素細胞に対する放射線増感作用機構 …… 216
周　玲
6.4 食品中のリステリアモノシトゲンの放射線感受性の研究 …… 221
胡　金慧
6.5 * γ線照射香辛料のオイル成分の影響とアリルトリサルフィドの放射線分解 …… 225
魏　根栓
6.6 放射線による信号応答性薬物伝達システムの開発 …… 231
嘉悦　勲
7. ポスター発表（1）
7.1 単色軟Ｘ線吸収によるCF_2Cl_2からのフラグメントイオンとイオンペア収量比の変動 …… 236
鈴木　功
7.2 ＣＩＲＡ放射線プロセス特別委員会 …… 241
候　福珍

7.3 無極性溶媒中のフラーレン（C_{60}-C_{84}）のイオン化ポテンシャル …… 243
中川 和道
7.4 超イオン伝導体の放射線損傷の研究 …… 248
淡野 照義
7.5 放射線により生成したポリマーアニオンの電子移動反応と再結合反応 …… 252
小笠原 正明
7.6 パラスラジオリシス法を用いた銅型亜硝酸還元酵素のタンパク質内電子移動 …… 255
小林 一雄
7.7 芳香族ポリマーへのイオンビーム照射効果 …… 260
宿島 悟志
7.8 低速陽電子によるイオン照射高分子の研究 …… 265
小林 慶規
7.9 放射線加工分野に適したワンタッチアラニン線量計測システム …… 270
柏崎 茂
7.10 フッ化炭素鎖を含むアクリル酸長鎖エステルの放射線固相重合 …… 275
柴崎 芳夫
7.11 排水中のメラノイジンの放射線照射による脱色と分解 …… 280
関口 正之
7.12 電子線照射に対する乳酸脱水素酵素の活性障害のアイソザイム識別 …… 285
太田 顕成
7.13 ＥＳＲ法によるantibiotic-producer中のN⁺イオン照射による
生成ラジカルの研究 …… 293
謝 立青
7.14 放射線重合法によるポリマー表面へのイースト菌の吸着 …… 298
陸 兆新
8. 高分子（2）
8.1 放射線反応によるポリマーブレンド（ＰＰ／ＢＲ）の界面接着特性 …… 303
徐 俊
8.2 Co^{60}照射によるポリウレタン／ポリスチレンあるいはＰＭＭＡ中に形成される
相溶性高分子ネットワークの形態と特性 …… 308
張 志平
8.3 放射線架橋フィルム …… 317
王 徳仁
8.4 高分子材料の極低温γ線照射効果 …… 321
工藤 久明
8.5 極低温におけるエポキシ系複合材料の照射効果 …… 326
山岡 仁史

9. 線量測定

9.1 * 日本における放射線加工処理用の線量計測システム …… 331
田村 直幸

9.2 放射線プロセス用3－5MeV電子線形加速器の線量測定 …… 338
謝 立青

9.3 電子線による放射線プロセスにおける線量測定 …… 344
須永 博美

9.4 * 中国における放射線プロセス用線量計測の現状 …… 349
陳 文秀

9.5 線量測定用ＰＶＧフィルムの添加物効果 …… 356
陳 文秀

9.6 原研アラニン／ＥＳＲ線量測定システムの応用における最近の進歩 …… 362
小嶋 拓治

9.7 ｐ－ｎ接合半導体検出器による線量測定 …… 367
鄭 正

10. 生体システム（2）

10.1 グラフト鎖を有する界面への黄色ブドウ状球菌の捕捉 …… 372
ウィリアム・リー

10.2 放射線プロセスによる側鎖にＬ－プロリンアルチルエステルをもつインテリジェントバイオポリマーゲル …… 377
吉田 勝

10.3 * 放射線技術分野におけるＩＡＥＡの教育研修プログラム …… 383
馬 瑞徳

10.4 ガラス固化体の放射線源利用 …… 392
幕内 恵三

10.5 小型サイクロトロンを用いた低速陽電子の発生 …… 396
鷲尾 方一

10.6 最近の日本における電子線の工業利用状況 …… 401
水澤 健一

11. 放射線プロセス（1）

11.1 * 放射線照射したカーボンブラック充填高分子複合体のＰＴＣ特性 …… 408
陳 欣方

11.2 ＬＤＰＥ／ＥＶＡブレンドによる放射線架橋発泡体の製造 …… 414
斯欽 達来

11.3 放射線によるＬＤＰＥシートの改質と利用 …… 419
李 朝順

11.4 ダイマー酸からのウレタンアクリレートの電子線硬化による感圧接着剤 …… 424
佐々木 隆
11.5 ポリエステルアクリレートの熱硬化へのＦＴ－ＩＲ法の適用 …… 428
曹 瑾
11.6 固相および水溶液におけるＮ－イソプロピルアクリルアミドの放射線重合と
それの架橋 …… 434
サフランニ・アグネサ
12. ポスター発表（2）
12.1 希ガス原子による$Ne(^3P_2)$の衝突脱励超過程 …… 439
テバ・バハドゥル・カドカ
12.2 気体中の電子付着、電子の熱平衡化、ペニングイオン化過程の研究 …… 444
嶋森 洋
12.3 典型金属元素のクロロ錯体の光化学的酸化還元 …… 449
篠原 信好
12.4 アルカン溶液中でのC_{60}，C_{70}の光イオン化 …… 453
加藤 隆二
12.5 イオン対再結合過程におよぼす磁場の影響 …… 458
国分 晋裕
12.6 シクロデキストリン包接錯体のパルスラジオリシス法 …… 462
山本 幸男
12.7 高エネルギー、高強度イオンビームの二次元定着による大面積均一照射 …… 467
上松 敬
12.8 高分子材料の高エネルギーイオン照射効果 …… 472
工藤 久明
12.9 γ線照射低密度ポリエチレンの空間電荷分布 …… 476
小嶋 雅之
12.10 新しいルイコ染料入りＰＶＧ線量測定フィルム …… 481
陳 文秀
12.11 ポリテトラフルオロエチレンの放射線架橋 …… 487
大島 明博
12.12 パルスラジオリシス法を用いた生体系における一酸化窒素の動的解析 …… 492
小林 一雄
12.13 真空紫外域シンクロトロン光の77K照射でアミノ酸及びその誘導体に生成する
ラジカルⅡ．Ｎ－アセチル－ＤＬ－アラニン …… 497
峯岸 安津子
12.14 ＤＮＡのγ線損傷に対する茶カテキンの防御効果とその機構 …… 502
吉岡 闊江

12.15 不飽和ポリン脂質、コレステロール、脂肪酸からなる混合脂質リボソームの
γ線照射重合 …… 507
細井 文雄
12.16 γ線照射によるブチルアクリレートのミクロ乳化重合 …… 512
張 志成
12.17 アラニン／ＥＳＲ線量測定法による照射製品箱中の線量分布 …… 517
謝 立青
13. 固 相
13.1 低温、固体水素および固体アルカン中における量子力学的トンネル反応、水素原子
および水素分子のトンネル効果 …… 522
宮崎 哲郎
13.2 シラシクロヘキサンおよび関連カチオンラジカルの非対称歪構造、および反応:
ＥＳＲ法とab initio ＭＯ法による研究 …… 527
塩谷 優
13.3 * 光誘起結晶相反応を支配する因子 …… 531
竹中 康之
13.4 H_2^+注入と引き続く熱処理により改質したダイヤモンド結晶の光学吸収による
解析 …… 536
馬 忠権
13.5 Er^{3+}ドープ光ファイバにおけるγ線誘起損失 …… 542
小山 武志
13.6 アルカリ銀ハライド結晶中のセルフトラップドホールの研究 …… 547
淡野 照義
13.7 Al_2O_3:Crにおけるイオンビーム誘起発光と照射損傷過程の研究 …… 552
青木 康
13.8 * アントラセン単結晶のH^-放出と色中心生成における炭素Ｋ殻励起効果 …… 557
中川 和道
14. 放射線プロセス (2)
14.1 * 前照射法による気相アクリル酸のポリテトラフルオロエチレン表面への
グラフト …… 562
胡 福敏
14.2 $ZnCl_2$溶液中の絹タンパクへのアクリロニトリルの放射線グラフト …… 569
張 志成
14.3 前照射法によるアクリル酸のポリエチレンフィルムへのグラフト …… 574
馮 文

14.4 前照射グラフト法によるカルボキシグループを含むポリビニルアルコール
アミドキシムキレートファイバーの作成とAu（Ⅲ）イオンの吸着特性 …… 579
饒　蕾
14.5 包接重合における尿素包接化合物の中のゲスト分子の安定性 …… 584
吉井　文男
14.6 放射線重合による高分子ミクロフェアの合成 …… 588
仲　幸彦
14.7 金属塩水溶液のγ線照射還元法による金属と酸化物のナノメータサイズの
粉末の合成 …… 593
張　曼維
14.8 前照射グラフト法による新感熱材料の製作 …… 598
呉　明紅
14.9 放射線滅菌の国際規格：線量設定の最近の動向 …… 603
武久　正昭
14.10 微生物培養用皿の電子線滅菌 …… 607
王　徳仁
14.11 超清浄環境下で製造されたディスポーザブル注射針の滅菌線量の評価 …… 610
田部井　雅枝
14.12 電子線照射によるガス状キシレンの除去 …… 615
広田　耕一
14.13 電子線照射排煙における化学反応について …… 620
大野　新一
参加者リスト …… 625
著者索引 …… 629

アステリスク付の講演は招待講演を示す。

Preface

The 6th Japan–China Bilateral Symposium on Radiation Chemistry (JCBSRC'94) was held on November 6 – 11, 1994 at International Conference Center of Waseda University in Tokyo. This symposium was sponsored by Waseda University, Japanese Society of Radiation Chemistry, Japan Atomic Energy Research Institute and China Radiation Research and Radiation Processing Society.

Since the first symposium has been held in Shanghai in 1983, the symposium has been held five times mutually in China and Japan. The second symposium has been held in Osaka in 1985, the third in Changchun in 1987, the forth in Kyoto in 1989 and the latest one has been held in Beijing in 1991.

The symposium was attended by 155 participants from 5 countries which consisted of 121 from Japan including 24 foreigners studying in Japan, 31 from China, 1 each from Australia, India and U.S.A.. 125 papers including 2 plenary lectures and 22 invited papers were presented. These consisted of 79 papers from Japan, 42 from China, 2 from India, 1 each from Australia and U.S.A.. It is first attempt to invite scientists of other countries than Japan and China. I am sure that our attempt gives fresh stimulation to this symposium.

I believe that this symposium has contributed to the congress of radiation chemistry researches and to the friendly interchange between Japan and China. I hope that this symposium is fruitful for all participants and for the future of our association.

I would like to express my sincere thanks to all members of Japanese and Chinese Organizing Committee and Steering Committee. I thank, especially, Secretary General, Professor Y. Katsumura of The University of Tokyo, Program Committee Chairman, Professor S. Tagawa of Osaka University and Professor Wu Jilan of Chairman of Chinese Organizing Committee for their constant efforts to ensure a successful symposium. Finally, I would like to extend my thanks to the related organizations providing financial support to this symposium.



Yoshimasa Hama
Chairman of Organizing Committee
JCBSRC'94

Ladies and Gentlemen:

I am very glad to meet so many old Japanese friends, scholars, especially at this very exciting meeting: the 6th Japan-China Bilateral Symposium on Radiation Chemistry. Also I am glad to see my old friends Prof. Joseph Silverman from USA and Dr. Mittel from India and guest from Australia to be present at the meeting.

At first, please allow me to express our thanks on behalf of Chinese delegation to Prof. Yoneho Tabata, Honorary Chairman, Prof. Yoshimasa Hama, Chairman of the 6th Symposium and all members of the Organising Committee for preparing the symposium.

I also would like to express my honour to Japanese side for supporting Chinese younger to this symposium, which, I think, is a significant act to develop our friendship and bilateral exchange in Radiation Chemistry in the future.

With the efforts from both Japan and China, the symposium has been a significant occasion for scientists in both countries. Through the symposium, we have learned a lot of things from Japanese colleagues and introduced our progresses in Radiation Chemistry. At this moment, when we all are enjoying the happy reunion and cheering the opening of the 6th Symposium, I hope we will have a good discussion and be able to exchange information and ideas in the field during the symposium.

Once again, thanks to all the members who contributed to the preparation of the symposium.

I wish that the 6th Japan-China Bilateral Symposium on Radiation Chemistry have a complete success.

Thank you.

Wu Jilan

Greetings

On behalf of the Japanese Society of Radiation Chemistry, I would like to express a few words of greetings at the opening of the 6th Japan-China Bilateral Symposium on Radiation Chemistry.

My hearty welcome is extended to the scientists coming to Japan from China and also from other countries. Originally this bilateral symposium, started in Shanghai in 1983, was organized by Prof. Ma Zueteh of the Shanghai Univ. of Sience and Technology and Prof. K. Hayashi of Osaka University. During these ten years, radiation chemistry can be said to be expanding wider and also each field is becoming more specific.

Radiation research has become strongly connected with the increasing need for the utilization of radiation in the development of basic science and technology. The scientific fields of radiation research cover a wide range of fields such as physics, chemistry, biology, medicine, and material science.

I hope the fundamental research on radiation chemistry contributes to the development of mechanistic chemical kinetics and also to radiation technology.

The Japanese Society of Radiation Chemistry has, since its inception, endeavored to promote and develop radiation chemistry and has recognized that one of the important means to achieve this end is the exchange of scientific information between radiation scientists all over the world as well as through scientists in different research fields. I find it very significant to have this opportunity of presenting and discussing the latest achievements which have been carried out all over the world.

I sincerely hope the success of this symposium and the fruits of this symposium will significantly contribute to the development of basic science. Finally, I would like to gratefully acknowledge the cooperation of the many people who organized this symposium, especially the members of the organizing committee.

S. Takamuku

Setsuo Takamuku

1. Plenary Lectures

1.1 Recent Progress of Accelerators for Beam Application in Japan

Yoneho Tabata
Japan Atomic Energy Commission

Introduction

Radiation utilization has been promoted in Japan as the other mainstay of development and utilization of nuclear technology along with energy utilization.Research and development(R&D) for practical application of radiation has been implemented steadily in the fields of industry, agriculture, medicine and others.

Much attention has been focused on utilization of accelerators in recent years.R&D related to accelerators have been actively performed in a wide range of application fields.

Due to the recent progress of the accelerator technology, a variety of beams is now being utilized.

The present status of R&D using accelerators in Japan is introduced.

1.TIARA

Ion Accelerators at Takasaki Radiation Chemistry R.E.

Ion accelerators for advanced radiation application named TIARA have been operated since 1991 in Takasaki, Japan Atomic Energy Research Institute(JAERI).R&D for advanced radiation technology is being conducted, including the development of radiation-resistant materials, new functional materials and biotechnology.For example, materials for the space environment, radiation effects on semiconductors have been studied by simulating the space radiation environment, and radiation tolerant semiconductors are being developed.

While, production of new radioisotopes has been tried by using AVF Cyclotron with an equipment of ISOL.

They have recently succeeded to identify new elements of P^{125} and Pr^{127} and determined their lifetimes of 3.3sec and 7.7sec, respectively.

2.HIMAC

Heavy Ion Medical Accelerators in Chiba

The National Institute of Radiological Sciences(NIRS) has applied a heavy-ion beam to cancer treatment research.Conventional cancer-therapy using radiation has a reduced effect on locally developing cancer and tumor cells that have a less-than-normal oxygen concentration.In addition, a conventional irradiation dose must be limited because it adversely affects normal cells around the target.In contrast, a beam of heavy-ion particles efficiently destroys locally developing cancer and tumor cells with a less-than-normal oxygen concentration.Damage to normal cells is minimized due to the highly localized dose distribution of the heavy ion beam.From 1987 to 1993, the NIRS constructed a heavy-ion accelerators(HIMAC) equipped with a cancer treatment device.After completion of biological experiments, the first clinical trial with HIMAC has started on June 21, 1994.The treatment with heavy ions for the first group of three patients who suffer from head and neck cancer has finished by August 10, 1994. In these treatments, carbon-12 beam was used. Each patient receive eighteen fractionated irradiation over the period of six weeks. The three treated have already been released from

hospital and they are well and now back to their daily lives. The three patients will be medically examined for about six months, followed by a medical evaluation of the effect of the irradiation.

Following the head & neck cancer, the irradiation treatment will be extended to other parts of organs such as central nerve system(brain tumor) and lung cancer beginning at the end of October.

After becoming operational, the HIMAC facility will be opened for domestic and international research collaboration as well as the treatment of patients.

3.RIKEN

Institute for Physical and Chemical Research

RIKEN led Japan in successful acceleration of heavy ions and has made a major contribution to the development of 'Heavy-Ion Science'. At present, RIKEN is promoting following six research projects.

A search for superheavy elements. Theoretically speaking, there should be a total of about 6000 nuclear species. Stable nuclei in nature is about 270. Existence of unstable nuclei of about 2000 has been confirmed. As the remainder are likely to exhibit unexpected behavior patterns, their discovery could pave the way to a new conceptualization of nuclear properties.

The study of hot and high-density nuclei. Collisions between high-energy heavy ions and target nuclei produce temporary nuclear matter that is thought to have high temperature and density. Study of nuclei in such a condition will play an important role in understanding neutron stars and quark matter.

Nuclear physics using radioisotope(RI)beams. RIKEN's use of RI beams has led to the discovery of forms of nuclear matter such as neutron halos and neutron skins. Properties of these forms of matter are being studied.

The study of highly-charged atoms. The study of highly-charged atoms in multiply ionized and highly excited states is expected to elucidate fundamental problems in quantum physics of atomic process such as the relativistic quantum effect.

Solid-state physics with muons. RIKEN uses slow muons μ^+ for analyzing structure of materials by μSR. On the other hand, muon catalysed fusion μCF by μ^- is being investigated.

Biological applications. By exposing cells to heavy-ions, it is possible to study on cancer development and cell mutations.Furthermore, RIKEN is developing new radioactive-multitracer techniques that exploit the advantages provided by short-lived RI.

4.SPring -8

Super Photon ring-8 Gev

The JAERI and the RIKEN are jointly constructing one of the largest synchrotoron radiation facilities(SPring-8) in the world in Harima Science Garden City in Hyogo Prefecture.A part of beam line become available for use in 1997, and the facility will be completed in 1998.

The facility provides high quality photons with very low emittance and high intensity in a wide range of wave lengths.

SPring-8 will be the largest and highest performance facility of its kind in the world, with an energy-level of 8Gev.The facility consists of three accelerators:the Linear Accelerator(total length 140m) for injection of electrons with an energy level of 1Gev;the Synchrotron, a race-track-shaped system with a circuference of 396m which accelerates electrons up to 8Gev;and a round-shaped Storage Ring, with a circumference of 1,436m which keeps 8Gev electrons in orbit.In addition, synchrotoron radiation extraction devices called Beam Lines are placed around the Storage Ring.

This should lead to great progress in research and development in various scientific fields such as material sciences, information and electronic sciences, and life sciences.Analysis of dynamic phenomena, where molecular scale changes occur over an extended period, and investigation of micro-scale structures and the properties of materials under extreme physical or chemical conditions will be made at this facility.

One important objective of SPring-8 is for it to become the center of excellence in research on synchrotron radiation.For that purpose, it will be available for researchers from domestic industries, universities, and national institutions and also from foreign countries.

5.JAERI, Tokai

A super-conducting electron linear accelerator(20Mev) for free electron laser has been constructed at JAERI, Tokai.They can provide tunable laser beams ranging from 10 to 50μm.

The linear accelerator will be extended up to 200Mev, 4mA in near future.

A tandem Van de Graaff(20Mev) together with a superconducting linear accelerator is being operated.Several tenth several hundredth Mev heavy ions are available at the facility.

6.Universities and KEK

Femtosecond Pulse Radiolysis

Femtosecond pulse radiolysis system by using a superconducting CW linac has been proposed by us.This was presented at the previous ICRR in Toronto(1991) and at the previous Bilateral Symposium in Peijing(1991).

Components and devices for femtosecond pulse radiolysis have been extensively investigated at Nuclear Research Laboratory, University of Tokyo in Tokai.Subpicosecond pulse was obtained recently by magnetic pulse compression method.

On the other hand, KEK and Tokai University have been trying to improve quality of beam from cathode.This is a very important and essential step to achieve a very short, intense femtosecond pulse.

Recently, high quality beam with low emittance and high brightness was obtained by using La B6 single crystal as the cathode.

Combination of both approaches mentioned above will lead the femtosecond program to better result in near future.

1.2 Some Progress on Radiation Chemistry of Substances of Biological Interests and Biological Applications of Radiation Technology in China

JILAN WU and XINGWANG FANG
Department of Technical Physics, Beijing University, Beijing 100871, PR China

Abstract Studies in China on the detection method of irradiated food, mechanism of DNA damage induced by peroxidation, radiolysis of natural products and herbs are reviewed on the update open literature, and some progress on applications of radiation technology is summerized.

In China, more attention has been paid to the Radiation Chemistry research of substances of biological interest and natural products and applications of radiation technology in biomedicine. From the invited talks and contributed papers of Chinese at this symposium, one can get an overview of the recent achievements in radiation research and radiation processing. Here, we would only report some progress in China of our interests.

I. RADIATION CHEMISTRY OF SUBSTANCES OF BIOLOGICAL AND BIOMEDICAL INTEREST

The formation of peroxide from fatty part of pork under γ irradiation

Recent research results reveal that DNA damage induced by lipid-peroxidation may be involved in processes of ageing and tumorigenisis. Interaction of lipid peroxidation products with DNA was studied [1,2]. In the linoleic acid-DNA system, a Schiff base product with fluorescence was formed by the reaction of DNA with peroxidized linoleic acid and it increased with increasing of reaction time. DNA damage induced by liposome peroxidation was also reported. Among the four typical bases, the damage of guanine was much more serious than those of the other three.

The study of peroxide formation from fat and lipid under γ irradiation is important not only for the detection of irradiated food but also for the control of the food quality. It was discovered that the organic peroxide thus formed was proportional to the dose applied. (Fig. 1) [3]. Moreover, the peroxide content of irradiated pork during storage increased much more rapidly than that of unirradiated reference (Fig. 2). These results indicate that for the purpose of preservation (extension of the shelf-life), the irradiation technology applying to sausage seems doubtful.

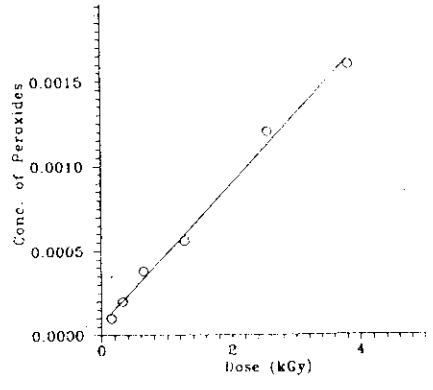


Fig. 1 The dependence of the formation of organic peroxides on absorbed dose of the irradiated pork.

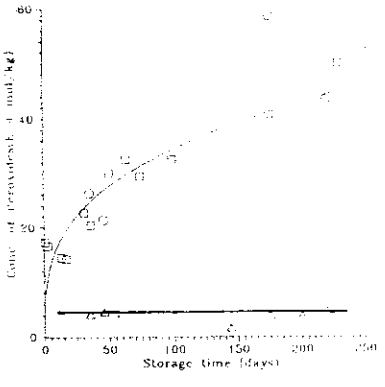


Fig. 2 The difference in the formation rate of peroxide between irradiated peroxidation and autooxidation at -18 °C. unirradiated (Δ) and irradiated (□, 2.18 kGy; ○, 3.12 kGy) pork

Study on the excitation of phosphoryl group (≡P=O) by photolysis, γ and pulse radiolysis of model compound TBP [5]

≡P=O is an important functional group of DNA. The extinction coefficient of its P=O bond is very low, thus it is very difficult to study the chemistry of the excitation state of this P=O. Yet, we have successfully detected TBP* molecule and measured its G value by different methods. Fig.3 and Fig.4 show the results obtained by pulse radiolysis, in which ketyl radical is formed *via* energy transfer from TBP*.

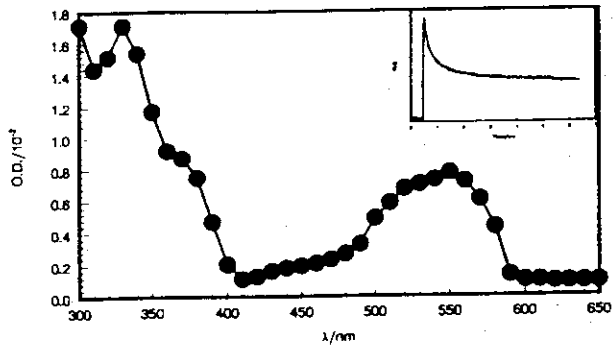


Fig. 3 Transient spectrum of N_2 degassed benzophenone (0.04 mol dm^{-3}) in TBP, 20μs after pulse. Insert, decay of absorbance at 550 nm, 5 Gy/pulse.

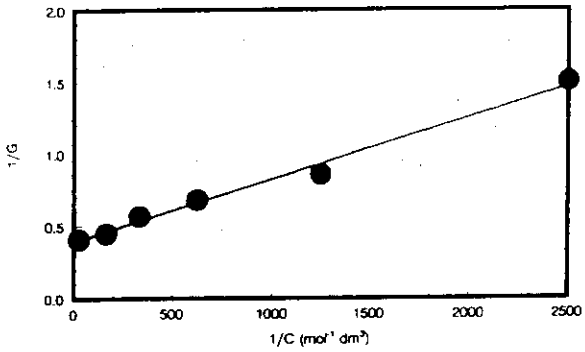


Fig. 4 Dependence of G(ketyl radical) on the concentration of Benzophenone in TBP. Degassed by N_2 , 5 Gy / pulse.

The competition kinetics was also examined employing the following reactions and Tab. 1 complied the ratios of the rate k_2 to k_1 obtained from different systems by different methods.

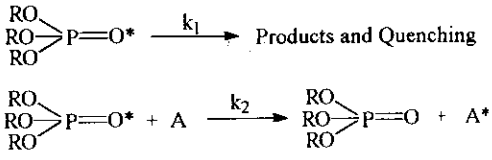


Table 1. Comparison of $*k_2/k_1$ and estimated τ of singlet of TBP obtained by different methods.

Method	k_2/k_1	$\tau_{singlet}$ / s
Photolysis of Φ_2SO-TBP	240	1.2×10^{-7}
γ radiolysis of Φ_2SO-TBP	250	1.2×10^{-7}
Pulse radiolysis of Φ_2CO-TBP	840	4.2×10^{-7}

* Assuming the second reaction is diffusion controlled with $k_2 = 2.0\times 10^9$ dm^3 mol^{-1} s^{-1}

The above mentioned results indicate that the radiation decomposition of TBP might be mainly due to the excitation of phosphoryl group, *i.e.* the following reactions may occur:

$$TBP^* \longrightarrow TBP^\bullet + R^\bullet \quad ; \qquad TBP^* \longrightarrow \text{Acid products}$$

This discovery might be very helpful to clarify the mechanism of the damage of DNA by UV and γ irradiation.

Radiation Chemistry of Metallothionein

Metallothionein (MT). a special protein containing 20 thiol groups, has high potential application as a medicine. The rate constants (Table 2)of MT reacting with various active species from radiolysis of water have been studied by pulse radiolysis and γ radiolysis.

The pulse radiolysis of metallothionein shows the formation of disulphide anion [6,7].

$$RS^\bullet + RS^- \rightleftharpoons RSSR^{\bullet-}$$

Fig. 5 shows that the $RSSR^{\bullet-}$ radical anion was formed by intermolecular reaction, however, final radiolytic products analysis indicated that the disulphide linkage was mainly formed intramolecularly [8].

Moreover, a very interesting phenomenon was discovered that the modified MT containing disulphide can be strongly adsorbed by PO_4^{3-} of DNA (Fig. 7).

Table 2. Compilation of the rate constants of some reactions involved in the radiolysis of metallothionein (RS^-) and cysteine (CyS^-)

Reaction	Rate constant / $dm^3\ mol^{-1}\ s^{-1}$	
	RS^-	Cys^-
$OH + RS^- \longrightarrow RS^\bullet$	6×10^{10}	3.4×10^{10}
$RS^\bullet + RS^- \longrightarrow RSSR^{\bullet-}$	1.8×10^9	1.9×10^9
$^*RSSR^{\bullet-} \longrightarrow RS^- + RS^\bullet$	7×10^4	3.2×10^5
$RS + RSSR^{\bullet-} \longrightarrow RSSR + RS^-$	9.2×10^8	4×10^9
$RSSR^{\bullet-} + O_2 \longrightarrow RSSR + O_2^{\bullet-}$	3×10^7	4.3×10^8

* The units of rate constant for this reaction are s^{-1}.

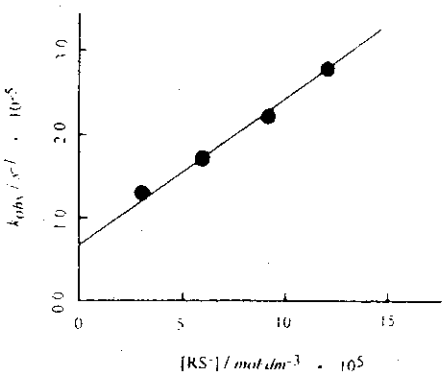


Fig. 5 The build-up kinetics of $RSSR^{\bullet-}$ showing its dependence on RS^- concentration. Bubbled with N_2O, 1 Gy/pulse, monitored at 450 nm.

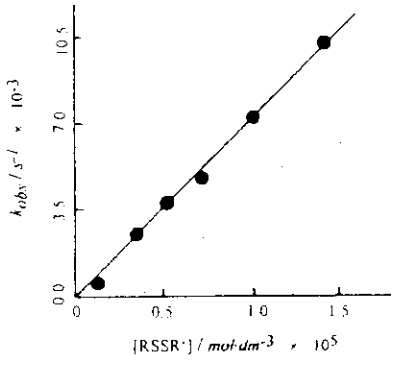


Fig. 6 The decay kinetics of $RSSR^{\bullet-}$ monitored at 450 nm, Solution bubbled with N_2O (O_2 free).

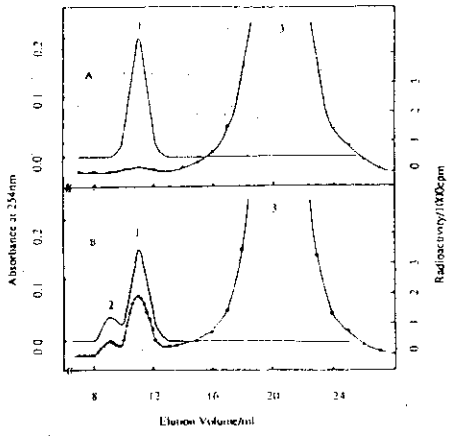


Fig .7 Gel-filtration Chromatography profiles of mixtures of sodium [^{32}P]phosphate with (A) native and (B) pre-irradiated MT after 24-h incubation at 25 °C, performed on a Sephadex G-50 column eluated by 0.01 mol dm^{-3} Tris HCl containing 0.1 mol dm^{-3} phosphate buffer (pH7.0). Peak 1 and 2, monomeric and dimeric forms of MT; peak 3, free [^{32}P]phosphate. (—) absorbance at 254 nm, (-o-) [^{32}P]phosphate radioactivity.

Radiation Chemistry of medicine

(1) Using ethanol as a solvent probe to detect the active site of baicalin [10]

The results show that the active sites of baicalin are at its π conjugated system containing carbonyl group (ring B and C) and the capability of scavenging electron by carbonyl groups is evidently lower than that of acetophenone. The conjugated system of ring B and C can capture OH, $RO^{\bullet}$, $H^{\bullet}$ and $RO_2^{\bullet}$ radicals effectively. It is helpful to explain the pharmacological effect of flavonoid.

(2) Studying the effect of water on the radiation decomposition of the chief components of herbs [11]

Table 3. The variation of bioactive components with H_2O contents in γ-irradiated herbs. Absorbed dose: rhubarb 150 kGy, other herbs 10 kGy.

Herb		content of components (%)			
Scutellaria	H_2O	0	15	30	45
Baicalensis	Baicalin	13.78	13.25	12.98	12.71
Glycyrrhiza	H_2O	0	19	30	40
Uralensis	Glycyrrhizic Acid	1.6	1.24	1.08	1.06
Radix Gentianae	H_2O	0	17.3	29.2	39.4
Marcrophyllae	Gentiopicrin	4.16	3.34	3.24	3.36
rhubarb	H_2O	0	15	23	35
	Anthraquinone	2.13	1.94	2.01	1.86

Table 3 reveals that water is able to promote the γ radiolysis of herbs, but it seems that water takes an effort on the surface of herbs, a detailed study has been undertaken on rhubarb-H_2O system.

The additives such as fructose and glucose can inhibit the γ radiation decomposition of herbs.

(3) Determination of one electron reduction potentials of some radiosensitive compounds by pulse radiolysis [12]

Anthraquinone-2-sulphate (AQS), duroquinone (DQ) and methyl viologen (MV^{2+}) were used as references. The results were shown in Table 4.

Table 4. Rate constants of electron transfer and equilibrium constants for reaction

$$D^{\bullet -} + A \underset{k_{-}}{\overset{k}{\rightleftharpoons}} D + A^{\bullet -}$$

and calculated values of their one-electron reduction potentials

D	A	k / $dm^3\ mol^{-1}\ s^{-1}$	k_{-} / $dm^3\ mol^{-1}\ s^{-1}$	K	ΔE /mV	$E(D/D^{\bullet -})$/mV
Miso	MV^{2+}	1.92×10^{8}	1.70×10^{9}	0.113	-56.0	-391, +3
911	AQS	1.15×10^{9}	1.28×10^{8}	8.98	56.4	-431, +2
CMNa	DQ	6.71×10^{8}	2.09×10^{7}	32.1	88.9	-464, +2
SMU-1	AQS	6.06×10^{9}	7.43×10^{7}	81.5	113	-488, +2
SMU-2	AQS	6.99×10^{9}	3.90×10^{7}	179.1	133	-508, +2
S3	AQS	6.96×10^{9}	7.02×10^{7}	99.1	118	-493, +2
SMD	AQS	2.58×10^{9}	6.69×10^{7}	38.6	93.6	-469, +2
SNN	AQS	3.54×10^{9}	3.05×10^{8}	11.6	62.7	-438, +2
BSO	AQS	4.69×10^{9}	1.01×10^{8}	46.4	98.3	-473, +2

II. RESEARCH ON BIOMEDICAL APPLICATIONS OF RADIATION TECHNOLOGY

Since 1980, especially late 80's, the radiation technology for biomedical application in China have been rapidly developed and its bright future is attracting a great of attentions.

Progress on γ-sterilization of biomedical products

(1) Evaluation of irradiated herbs [11]

Evaluation of pharmacological efficacy after γ radiation was performed on 124 types of herbs and fruitful results were obtained, which shows a hopeful prospect to sterilizing herbs by γ rays, yet important rules as following step should be obeyed:

a. Herb to be irradiated must exist in dry state.
b. It is encouraged to make bolus by mixing powered Chinese medicine with honey to inhibit the radiation deconstruction of herbs.
c. The producer must strictly control the manufacture procedure to minimize the microbiological contamination, which subsequently lowers the dose applied.

(2) Improvements on hygienic level of glucoamylase[13]

γ-sterilization of industrial glucoamylase under 2 kGy can greatly reduce the contamination of gemma bacillus and other putrefactive microbes and thus stabilize the pH value during preparation. Glucoamylase thus treated can be preserved at good quality even without antiseptics.

(3) New treatment for enhancing the radiation tolerance of polypropylene

Serial studies of radiation effects on PP have been carried out, such as the effect on the morphology of polypropylene in the presence of some additives [14]. To limit ETO method for sterilization, the new treatment of PP must be cheaper and safer than this conventional treatment. A lot of trails have been performed. Some treated PP present good radiation tolerance in the absence of additive Trinuvin 770, a well-known photo-oxidant stabilizer which might have blocking effect on autonomic nerve.

Progress on the Use of radiation processing for synthesis of biomaterials

Many studies focused on immobilization, synthesis of hydrogel, grafting hydrophilic monomer to biocompatiable polymer matrix and fundamental studies.

(1) Immobilization of Drugs, Enzymes and Cells

Slow release anti-cancer drugs(5-Fluorouracilum, Mitomycinum, Bleomycinum and Ara-C) were prepared by radiation co-polymerization of monomer such as HEMA. The release rate and amount of drugs can be controlled by regulating the content of hydrophilic or hydrophobic monomer(MMA<EMA<BMA) and crosslinking reagent in drug-copolymer composite and by changing the radiation dose and drug content. Pore structure of the composite may accelerate the release rate[15,16]. Radiation polymerization was used to immobilize testosterone propionate into crosslinked network of polyhydroxyethyl methacrylate to prepare slow release male sex hormone drug which is applied for testicular prosthesis[17].

The immobilization of enzymes (horseradish peroxidase (HRP), glucose oxidase), cells (baker's yeast, E. Coli), proteins (bovine serum albumin (BSA)) by radiation polymerization was also studied. The monomers used were 2-hydroxyethyl methacrylate, acrylic acid, acrylamide and N-2-propyl acrylamide [18-21].

Generally, two methods have been applied for immobilization. One method is radiation polymerization. Addition of crosslinking agent will significantly low the dose applied for gel formation

and modification other properties. The other was graft co-polymerization, for example, the acrylic acid was grafted *via* radiation onto segmented polyetherurethane (SPEU) film, a kind of biocompatible material, and the peroxidase was immobilized onto the grafted SPEU film by chemical binding [22].

Immobilization of cell membrane of E. Coli by radiation technology was successfully performed. Nylon 6 was grafted with HEMA, which had "live" free radicals. The matrix containing free radicals was used to immobilize cell membrance of E. Coli by radiation entrapment at low temperature [20].

It should be pointed out that a number of irradiated oxidoreductase (catalase and HRP) are facile to be of post deactivated, especially in the air [23].

(2) Hydrogels

Recently, a lot of attentions have been paid to radiation synthesis of thermo-sensitive polymers and the hydrogel dressing. An activated copolymer, poly(N-isopropylacrylamide-co-N-acryloxy succinimide) (NASI) has been prepared. The active ester group of NASI has high chemical stability and good physical properties and shows both high reactivity and selectivity toward amino nucleophiles, thus, the BSA and HRP have been immobilized onto the active copolymer. The BSA (or HRP) / copolymer conjugates still maintain the original thermo-sensitive properties of the linear poly NIPAAm [24]. Other reports revealed that NIPAAm was grafted onto surface of ethyl-vinyl acetate (EVA slice) by means of pre-irradiation grafting due to poly-NIPAAm's weak mechanical strength, and the grafted surface of EVA slice expresses higher mechanical strength than and similar thermosensitivity to poly-NIPAAm gel. The response to the change of temperature through the lower critical solution temperature (LCST) of the graft is more swift than that of the gel. The LCST of the grafted surface shifts to higher and the drop of swelling around the LCST decreases with increasing hydrophilicity of the graft when co-grafting NIPAAM with acrylic acid or acrylamide [25].

A radiation prepared hydrogel base wound dressing carrying special drug is developed for hospital applications. Main chemical materials used are polymers (*e.g.* PVA, PVP, PEG), difunctional monomers (*e.g.* itaconic diallyl ester) and chloramphenicolum. The dressing is possessed of high water absorbability. Standard tests for biomedical material were made and clinical results obtained proved its practice [26].

Besides the progress mentioned above, "radiation chemistry and environment" has attracted more attentions recently. In order to reduce chemical fumigation, a new ^{60}Co facility (500 kCi) has been set up in Beijing for irradiation of rice to kill insects. A plan to promote the use of γ sterilization to substitute ethylene oxide sterilization has been made, and a plan of establishing pilot plant to treat fuel gas by electron beam irradiation is undergoing.

REFERENCES

1. Liu X.Q. and Cao E. H. (1994)*Shengwu Huaxue yu Shengwu Wuli Jingzhan* (Chinese) **21**, 3.
2. Liu X. Q., Cao, E. H. and Zhu Y. R. (1993) *Acta Biophys. Sinica* **9**, 493.
3. Qi S. C., Wu J. L. and Zhu Y. (1993)*Radiat. Phys. Chem.* **42**, 371.
4. Qi S. C. and Wu J. L. Use of peroxide method for identifying irradiated food. *in press.*
5. Wu J. L. *et al.* Study of the excitation of phosphoryl group by photolysis, γ radiolysis and pulse radiolysis of model compound TBP, *poster in this volume.*
6. Fang X. W., Li F. M., Wu J. L. *et al.* (1993)*Wuli Huaxue Xuebao* (Chinese) **9**, 702.
7. Fang X. W., Wu J. L.,Wei G. S. *et al.* Generation and reactions of the disuphide radical anion derived from metallothionein: a pulse radiolysis study. *to be submitted.*
8. Fang X. W., Wu J. L. and Wei G. S. (1994)*Radiat. Res.* **138**, 165.
9. Fang X. W., Wu J. L. and Wei G. S. Associations of metallothionein with phosphate. *Radit. Phys. Chem. in press.*
10. Cai Z. L., Zhang, X. J. and Wu J. L. (1995)*Radiat. Phys. Chem.* **45**, 217.
11. Wu J. L., Zhang X. J., Yuan R. Y. *et al.* Radiolysis of herbs, *Radiat. Phys. Chem. in press.*
12. Zuo Z. H., Yao S. D., Li H. C. *et al.* (1994)*Fushe Yanjiu yu Fushe Gongyi Xuebao* (Chinese) **12**, 129.
13. Chen R. Y., Lan J. M., Yan Y. Q. *et al.* (1993)*Radit. Phys. Chem.* **42**, 935.

14. Chen W. X. and Yu S. (1993)*Radiat. Phys. Chem.* **42**, 207.
15. Li X. M., Yuan Z. J., Chen W. M. *et al.* (1989) *Fushe Yanjiu yu Fushe Gongyi Xuebao* (Chinese) **7**, 36.
16. Xie H. J. Song J. Z. and Peng T. (1993)*Radiat. Phys. Chem.* **42**, 931.
17. Liu R. Z., Lei S. Q., Li X. M. *et al.* (1992) *Fushe Yanjiu yu Fushe Gongyi Xuebao* (Chinese) **10**, 65.
18. Wang G. H., Ha H. F., Wang X. *et al.*(1988)*Radiat. Phys. Chem.* **31**, 705.
19. So Z. X., Cao J., Wang F. J. *et al.* (1986) *Fushe Yanjiu yu Fushe Gongyi Xuebao* (Chinese) **4**, 47.
20. Cao J., Chen P. and Yu Y.(1991) *Fushe Yanjiu yu Fushe Gongyi Xuebao* (Chinese) **9**, 219.
21. Ha H. F., Gao J. H. and Wu J. L. (1990) *Fushe Yanjiu yu Fushe Gongyi Xuebao* (Chinese) **8**, 75.
22. Ha H. F., Wang G. H. and Wu J.L. 1988)*Radiat. Phys. Chem.* **31**, 761.
23. Ha H. F. and Chen Y. Q. (1993) *Fushe Yanjiu yu Fushe Gongyi Xuebao* (Chinese) **11**, 70.
24. Zhai M. L., Ha H. F. and Wu J. L. (1993)*Radit. Phys. Chem.* **42**, 919.
25. Ding Z. L., Pa H. T., Ye H. *et al.* (1994) *Fushe Yanjiu yu Fushe Gongyi Xuebao* (Chinese) **12**, 11.
26. Chen J., Yang, Y. Q., Qian P. B. et al. (1993)Radiat. Phys. Chem. **4**, 915.

2. Irradiation Facilities

2.1 *A Typical R&D Center on Radiation Processing in China

Sun Jiazhen
Changchun Institute of Applied Chemistry
Chinese Academy of Sciences

INTRODUCTION

The industrial application of radiation processing has been growing rapidly in China since 1980's in such fields as manufacturing radiation crosslinked heat shrinkable materials, radiation crosslinked wire and cables, sterilization of medical products and so on. Changchun Institute of Applied Chemistry(CIAC), as one of the earliest organizations in which fundamental research work on radiation polymer chemistry was carried out, play a major role for R & D of radiation processing of polymers in China and nowadays has owned the largest enterprise of manufacturing radiation crosslinked heat shrinkable materials in China. The R & D activities at CIAC can be said to be very typical in China from which it can be seen how a chinese research institute transfer its results of fundamental research work into large scale production.

FUNDAMENTAL RESEARCH WORK

In the bigining of 60's , to meet the needs of our country and caught up with the rapid development of radiation chemistry in the world, some theoretical research work on radiation polymer chemistry was carried out in CIAC and then a 200,00 ci Co-60 source was the only radiation source by which most of research work was performed and thus this also constitutes one of characteristics of our current manufacturing, that is, most of radiation is performed through γ rays.

1. Radiation modification of fluoropolymers

Fluoropolymers, owing to their superior high temperature and chemical resistance, are widely used in some special fields. The marked weakness of them such as the sensitivity to high energy radiation and creeping of PTFE and the cracking of FEP, however, limit their application in some fields to a great extent. And thus we tried to solve the above problems by way of radiation crosslinking.

For FEP it was reported that it could be crosslinked by radiation performed above its glass transition temperature(1) . Owing to the

unavailablness of suitable solvent for FEP, the characterization of crosslinked polymer, however, was thought to be very difficult to conducted then . After carefully selection it was finally found in our laborotary that fluoro-chloro oil(oligmer of trifluoro chloro ethylene) could dissolve FEP at high temperature which made it possible to get the fraction of crosslinked part in irradiated FEP. On the basis of thus obtained sol data we calculated gelation dose and concerned parameters by using Charlesby - Pinner equation. Table 1 lists the obtained results.

As we all know that PTFE had been taken as typical radiation degradative polymer in all previous literatures and its radiation crosslinking was thought to be impossible. The observation of the fact that radiation stability of PTFE is increased upon raising irradiation temperature,however, encourage us to explore the possibility to crosslink the polymer by radiation. After many year's exploration, we finally found a very strict condition in 1980's only under which PTFE could be crosslinked by radiation. The finding of the condition resulted from an accidental phenomenon observed in an unsuccessful experiment in which we irradiated PTFE around 300 ℃ in vacuo. Then owing to the unevenness of temperature distribution in heater, irradiated PTFE sheets were found to appear semi- transparent in middle part caused by locally overheat and white color in two end of sheet as usual , the unusual hardness and strength of the semi-transparent part made us deeply convince that PTFE was crosslinked there. After further detailed work the crosslinking condition of PTFE was discovered, that is: 0.2 - 1 Mrad at 330 - 340 ℃ and in vacuo. Crosslinked PTFE was found to gain a great improvement in both mechanical properties and radiation stability as shown in figures 1- 4 which overcomes the creeping properties of PTFE.

2. Modification of Charlesby - Pinner equation

Charlesby - Pinner eqation is a basic one to describing relationship of sol fraction to irradiation dose from which we can get many important parameters concerning with crosslinking of polymers. During application, however, it was found that for certain polymers such as those having too rigid or soft polymer chains, the relation between $(s + s^{1/2})$ and $1/R$ will be nonlinear. On the basis of large number of experimental work and summarizing previous lectures, we finally presented a eqation which introduce a parameter β concerning with glass transition temperature Tg and internal rotating steric factor σ of polymer.

$$R(S + S^{1/2}) = 1/q_o U_r + \alpha_o R^{\beta}/q_o$$

$$\beta = 0.002Tg + 0.206$$

$$Tg = A(\alpha - a)$$

This equation is applicable to most of polymer systems.

3. Radiation grafting for preparing functional materials

(1) Radiation grafting palladium - acrylonitrile complex on inorganic compound to prepare polymer catalyst and thus obtained catalyst has higher active hydrogenation and better antitoxic than that obtain by chemical method.

(2) Radiation grafting of polymer metrix to prepare ionic polymer sensor - Ionic Selected Electrode(ISE)

i. Electrode for Cl^- & NO_3^- ions

Concerning property parameters:	
Slope (mv/log C)	*58*
Detection concentration(M)	$8\times10^{-1} \sim 5\times10^{-5}$
PH region	*4 ~ 9.5*
Stability (mv/8hr)	*±0.9*
Internal resistance(Ω)	*< 25*
Life time (month)	*> 4*
Respond time (second)	*< 10*

ii. Gadolinium ISE sensor - functional polymer active material

Slope of electrode	*52 ~ 59 mv/log C*
Detection limit	3.2×10^{-6} *M*

(3) Radiation grafting of acrylic acid on EVA to increase the hydrophilicity of grafted polymers.

4. Radiation crosslinking of polymer blends

The regularity of radiation crosslinking of polymer blends were investigated. These system include LDPE/EVA, LDPE/CPE, PMMA/PEO, PDMVS/LDPE and so on. Among them PMMA/PEO blend was found to be most interested which indicated that PMMA, a radiation degradative polymer, can be crosslinked in such a blend system in the dose range of 1 - 20 Mrad and composition of PMMA being 30 - 70%. The crosslinking degree of PMMA was found to be the largest for blend containing 70% PMMA.

5. The Effect of antioxidant on radiation crosslinking of polymer

Antioxidant was reported to affect radiation crosslinking of polymers owing to its absorption radiation energies and scavenging radiation induced radicals. The effect of structure and varieties of varying antioxidants on crosslinking process and changes in their stabilizing activities after exposure to radiation was examined which showed that for antioxidant examined in our work the activities of antioxidant was not affected by radiation ; the inhibitory effect of antioxidant on crosslinking of LDPE was not dependent on the concentration of antioxidant in the range of 0.5 - 2 phr and the post irradiation effect of LDPE was observed to be greatly inhibited by the presence of antioxidant.

APPLIED RESEARCH WORK

In the end of 70's to meet the needs of industrial division we set up a pilot factory in Jilin Radiation Chemistry Institue to manufacture EB crosslinked heat shrinkable tubings in a small scale. In the middle of 80's , required by the power department, we successfully developed 10- 35 KV radiation crosslinked power cable termination and set up a heat shrinkable material factory which belongs to CIAC. After that we developed varieties of heat shrinkable tubings, irregular shape heat shrinkable articles, heat shrinkable sheet and sleeves for bus bar prot ection, heat shrinkable sheet for communication cable joint and cap for the end protection of cable. Besides that we also developed varieties of chemical formulations of radiation crosslinked wire and cables including 6.6 KV cable for airport runway; 105 ℃ grade high voltage wire for color TV; 125 ℃ grade flame retardant wire; non-halogen low smoke flame retardant wire and cables; 10 KV aerial cables , oil resistant cables for locomotive and heat shrinkable sleeves for pipe joint protection.

THE DEVELOPMENT OF RADIATION PROCESSING AT CIAC

The Heat Shrinkable Materials Factory of CIAC was established at 1987 when eight persions from research laboratory began to manufacture power cable accessories and heat shrinkable tubings with a 600,00 Ci Co- 60 source. With the rapid development of Chinese economy the radiation processing at CIAC has been growing at high speed. Today CIAC has owned 7 joint-venture branch factories spreaded in Shenzheng, Beijing, Shanghai, Xinjiang ,Nanjing,Xian and Shijiazhuang and 16 sales company all over China. The heat shrinkable products manufactured in these factories have occupied more than half of the market in China and some of them have been exported to Southeast Asia. Now it can be said that CIAC has become the largest R & D center of radiation processing in China. In March of this year a 1.5 Mev electron accelerator

imported from Russia was put into operation and the problem of radiation ability being insufficient that CIAC met in past years is expected to solved, which lay a good foundation for the more rapid development of radiation processing at CIAC. The figures below give a quantitative description of the development of radiation processing at CIAC.

REFERENCE

(1) Bowers, G. H. and Lovejoy, E. R. Industrial & Engineering Chemistry Products Research & Development 1962, 1, 89

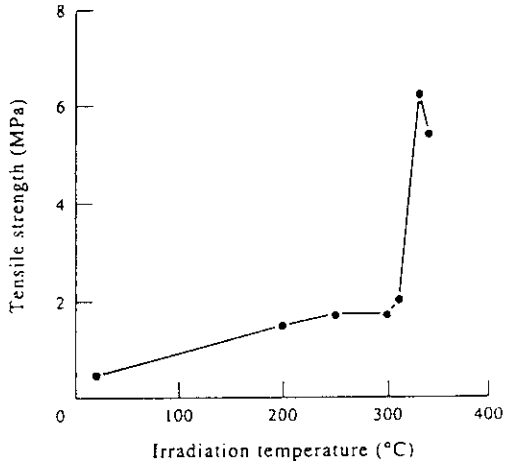


Fig. 1. Tensile strength at 200°C of PTFE absorbed 20 kGy.

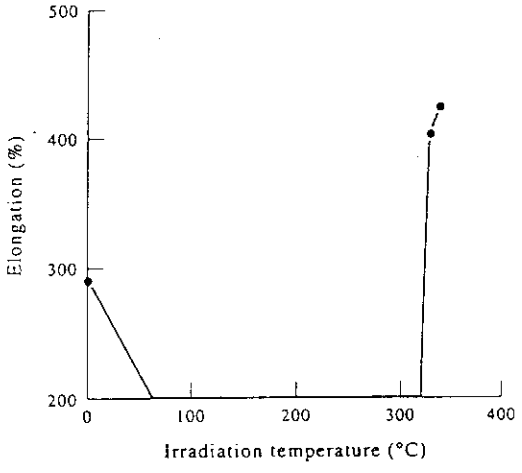


Fig. 2. Elongation at 200°C of PTFE absorbed 20 kGy.

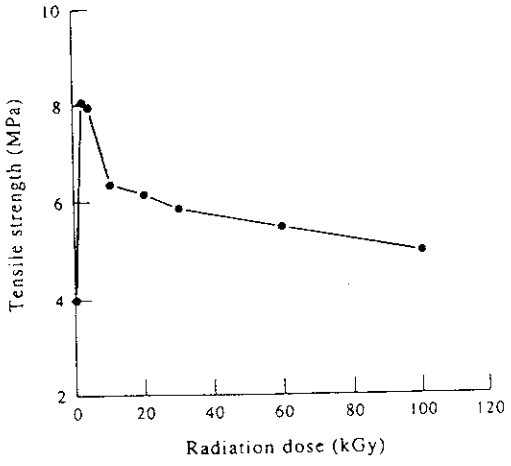


Fig. 3. Effect of dose on tensile strength at 200°C of PTFE irradiated at 330°C.

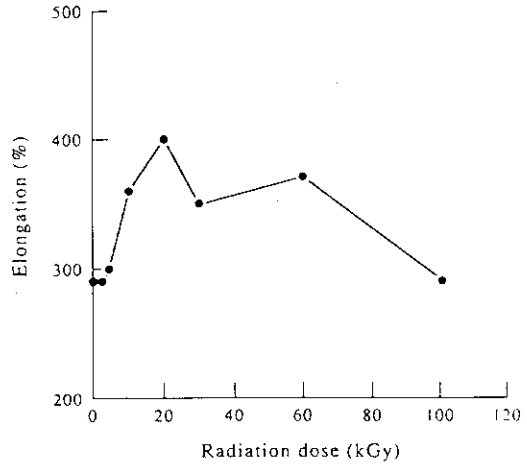


Fig. 4. Effect of dose on elongation at 200°C of PTFE irradiated at 330°C.

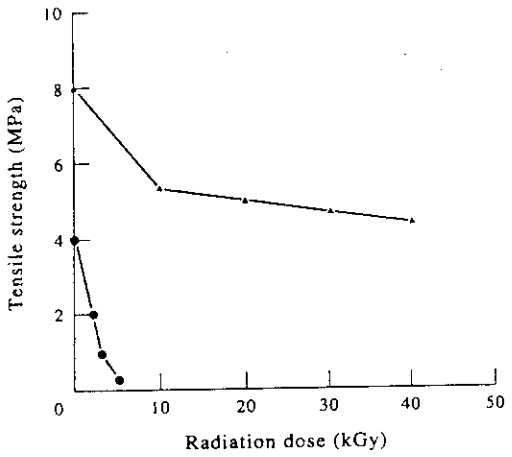


Fig. 5. Effect of aging dose on tensile strength at 200°C of PTFE. —●—, Control PTFE; —▲—, crosslinked PTFE.

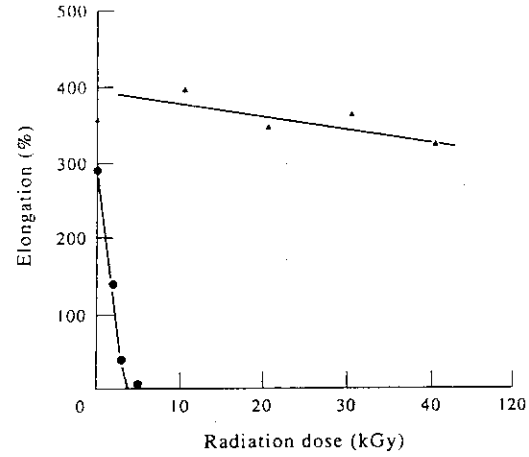


Fig. 6. Effect of aging dose on elongation at 200°C of PTFE. —●—, Control PTFE; —▲—, crosslinked PTFE.

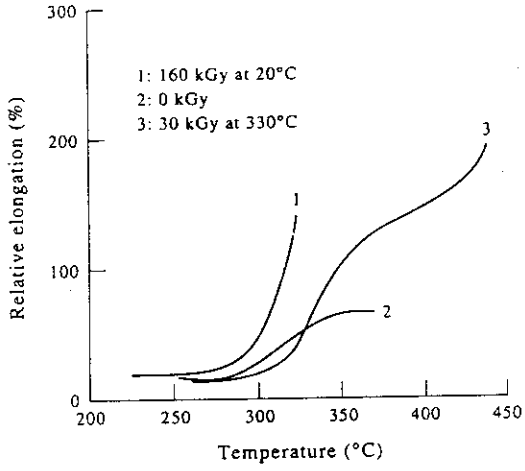


Fig. 7. Effect of radiation on TMA curves of PTFE.

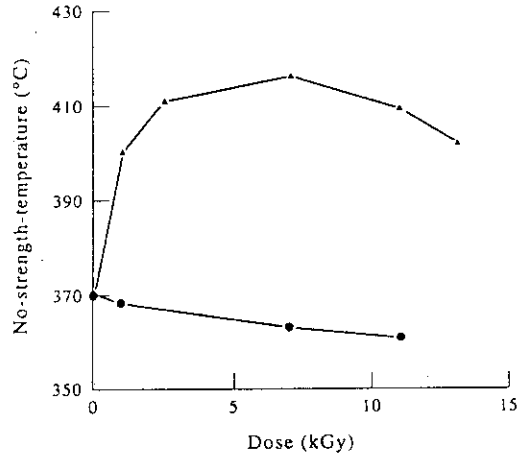


Fig. 8. Effect of radiation on NST of PTFE. —●—, Control PTFE; —▲—, crosslinked PTFE.

Table 1 Values of p_0/q_0 and gelation dose of FEP irradiated at different temperatures

Irradiation temperature (°C)	p_0/q_0	Gelation dose (Mrad)
150	1.35	12.3
210	0.85	10.0
220	0.80	8.0
240	0.42	2.5

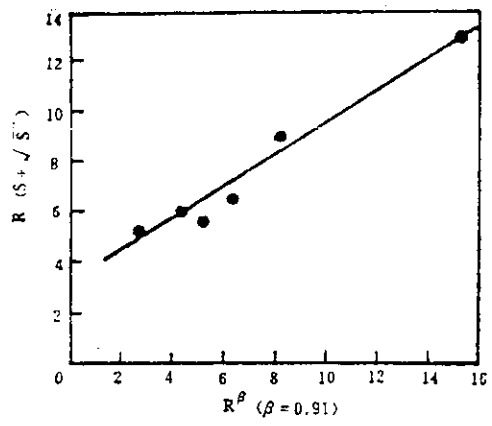


图 2-c 氟-46 的辐照交联(本实验室工作)
Fig. 2-c Radiation crosslinking of F-46 (our laboratory)

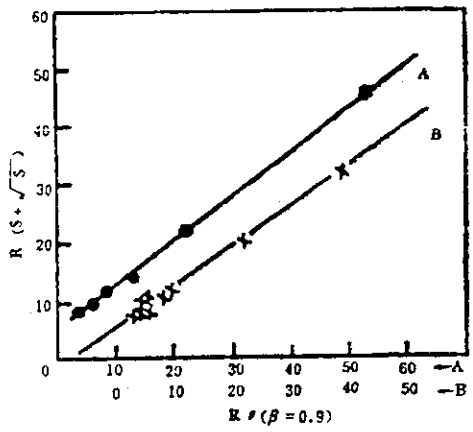


图 2-d PVAc 的辐射交联[11]
Fig. 2-d Radiation crosslinking of PVAc[11]

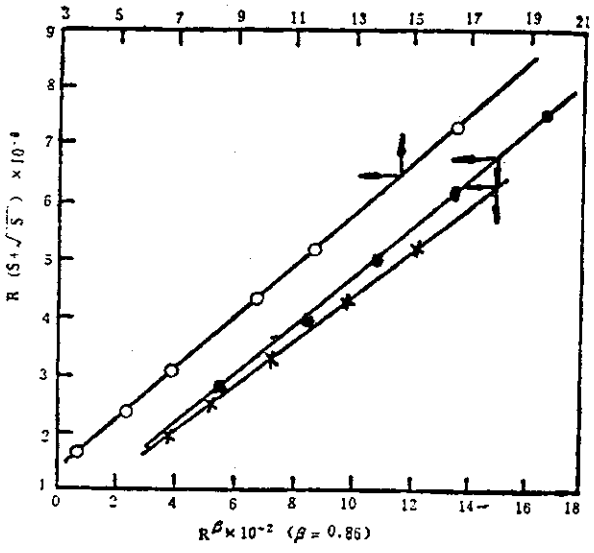


图 3-a PET 的辐射交联[20]
Fig. 3-a Radiation crosslinking of PET[20]
●——N_2 ×——真空 ○——空气

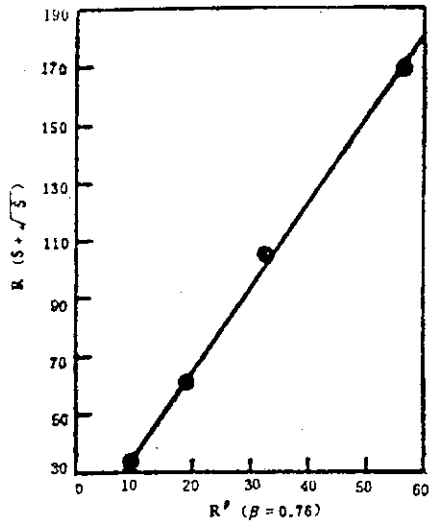


图 3-b 聚丙烯的辐射交联[21](本实验室工作)
Fig. 3-b Radiation crosslinking of polypropylene(our laboratory)

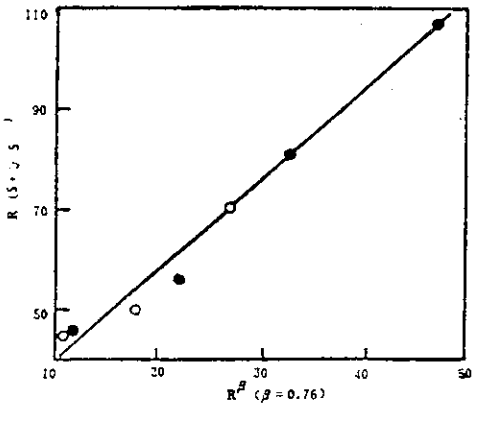


图 3-c 聚丙烯的辐射交联[21]
Fig. 3-c Radiation crosslinking of polypropylene[21]

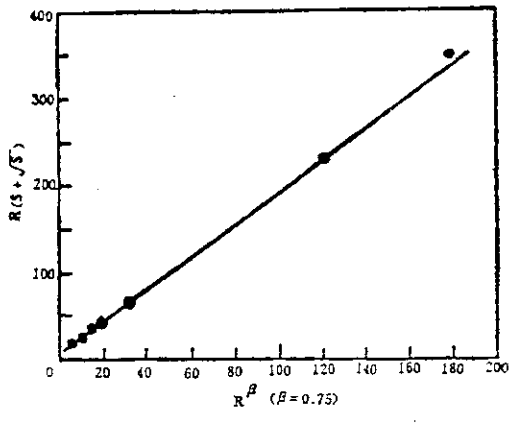


图 3-d 聚己烯的辐射交联[19]
Fig. 3-d Radiation crosslinking of polyhexene[19]

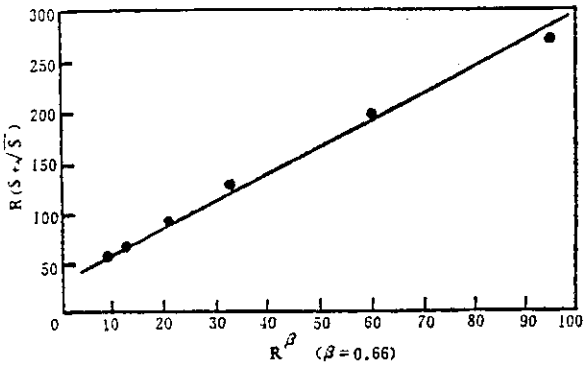


图 3-e 聚戊烯的辐射交联[19]
Fig. 3-e Radiation crosslinking of polypentene[19]

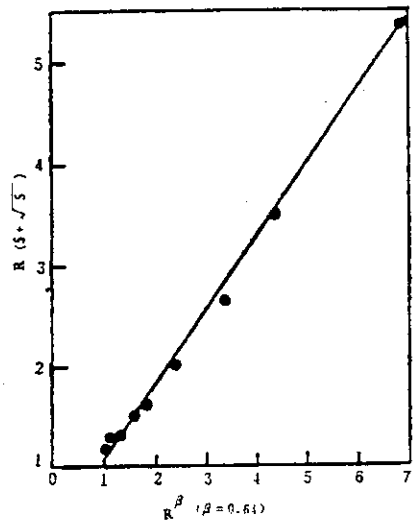


图 4-a 天然橡胶的辐射交联[17]
Fig. 4-a Radiation crosslinking of natural rubber[17]

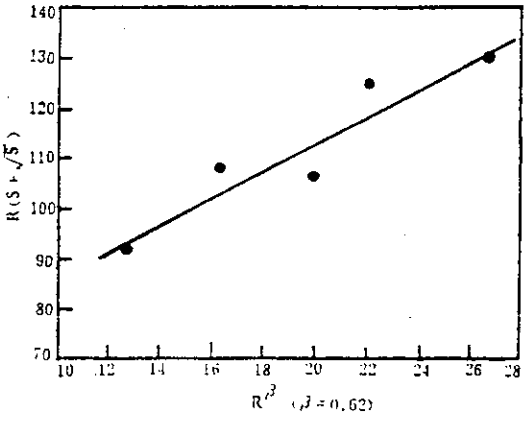


图 4-b 聚氧化乙烯的辐射交联[18]
Fig. 4-b Radiation corsslinking of polyethylene oxide[18]

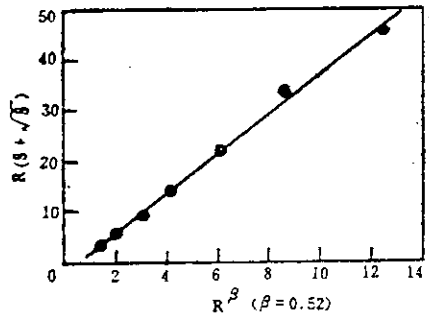


图 4-d 聚乙烯的辐射交联[14]
Fig. 4-d Radiation crosslinking of polyethylene[14]

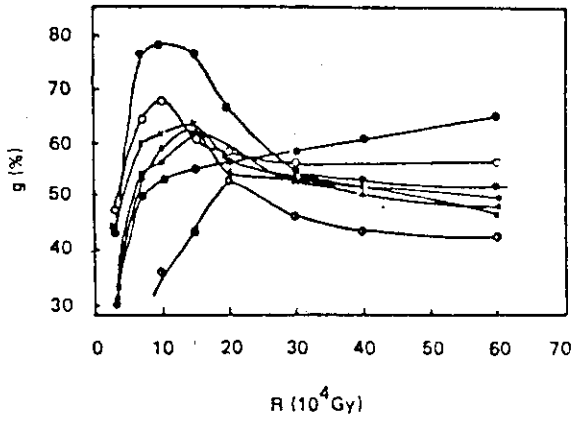
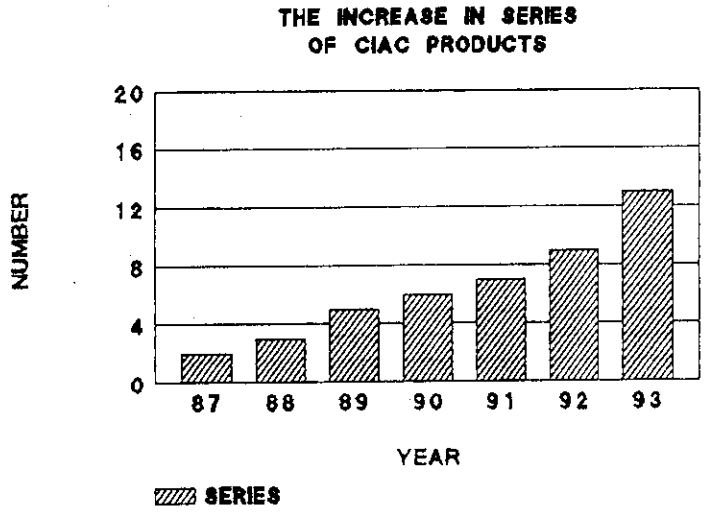
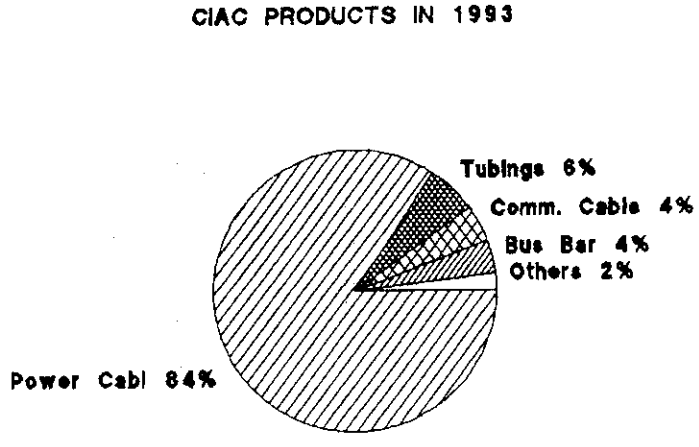


FIG. 1. Relationship between gel content (g) and irradiation dose (R). The content of PMMA: ⊗, 0%; ○, 30%; ●, 70%; ■, 60%; ▲, 50%; X, 40%; ◑, 75%.

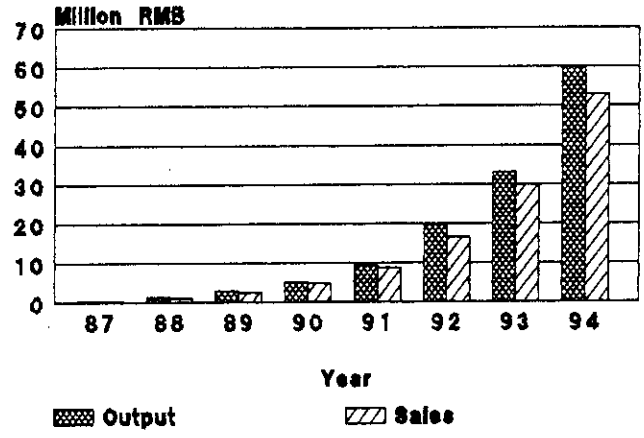
Tab 5. Gel fraction g in melt mixing PIB-EPR blend system obtained under different dose

R(10 kGy)	g(%)	PIB (%)				
		0	50	60	70	80
0	g_B	0	0	0	0	0
4	g_{EPR}	50.1	25	20	15.0	10
	g_{PIB}	0	23	25	19.7	10.1
8	g_{EPR}	71.5	35.8	28.6	21.4	14.3
	g_{PIB}	0	17.7	18.5	25.4	17.1
15	g_{EPR}	82.9	41.4	33.1	24.9	16.6
	g_{PIB}	0	19.4	21.3	30.6	21.1
30	g_{EPR}	87.5	43.7	35.0	26.3	17.5
	g_{PIB}	0	17.9	14.6	32.6	21.3

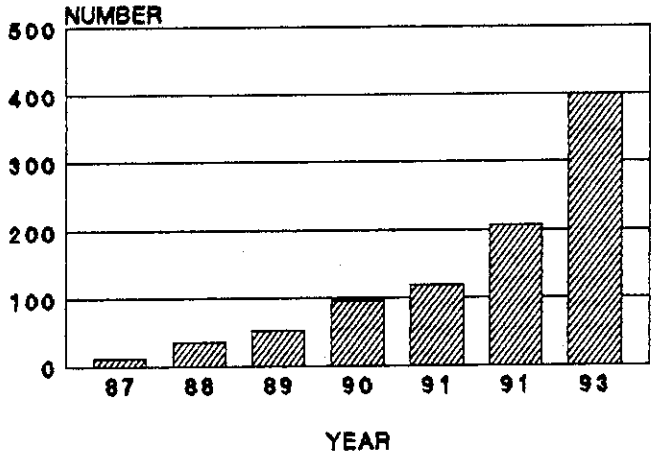




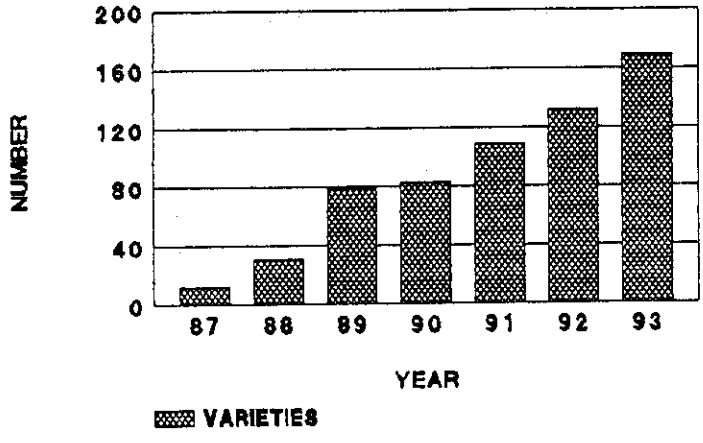
OUTPUT AND SALES OF CIAC PRODUCTS



THE ANNUAL INCREASE IN STAFF



THE INCREASE IN VARIETIES OF CIAC PRODUCTS



2.2 *Synchrotron Radiation Facilities for Chemical Applications

Yoshihiko HATANO
Department of Chemistry
Tokyo Institute of Technology
Meguro-ku, Tokyo 152

INTRODUCTION

Synchrotron radiation (SR) research is of great importance in understanding radiation chemistry, physics, and biology (Hatano, 1987; Hatano and Inokuti, 1994). It is also clearly recognized in the international chemical community that chemical applications of SR are greatly advanced (Weston et al., 1989; Hatano et al., 1995) and divided into

1) Molecular Spectroscopy and Dynamics Studies－Gases, Surfaces, and Condensed Matter－,
2) Radiation Chemistry and Photochemistry,
3) X-ray Structural and XAFS Studies－Crystals, Surfaces, and Liquids－,
4) Analytical Chemistry, and
5) Synthesis or R&D of New Materials.

In this paper, a survey is given of recent advances in the application of SR to the chemistry of excitation and ionization of molecules (Hatano, 1994), i.e., SR chemistry, in the wavelength region between near-ultraviolet and hard X-rays. The topics will be chosen from those obtained at some leading SR facilities (Ohta et al., 1994).

SR CHEMISTRY AS A BRIDGE BETWEEN RADIATION CHEMISTRY AND PHOTOCHEMISTRY

Figure 1 shows the wavelengths of electromagnetic radiation from the infrared to the γ-ray regions and corresponding photon energies (Hatano, 1987). Characteristic x-rays, ^{60}Co-γ rays, and VUV light from discharge lamps are indicated by the arrows. Figure 1 clearly demonstrates that SR bridges the wide gap in the photon energy between radiation chemistry and photochemistry, i.e., "electron-collision chemistry" and "photon-collision chemistry", respectively.

It is important to recognize that a major part of both photoabsorption and photoionization intensities lies in the wide gap between the two for almost all molecules (Hatano, 1987). The experimental data for cross section values in this wavelength region have been incomplete in general because of experimental difficulties related to suitable photon sources and window materials. As an alternative, electron energy-loss spectroscopy has been used. Even then, cross section data are limited, particularly for chemically important complex molecules such as hydrocarbons and other organic molecules (Hatano, 1987).

INTERACTION OF PHOTONS WITH MOLECULES AND ITS RELATION TO THE EFFECTS OF IONIZING RADIATION

The absorption of a single photon results in an electronic transition of

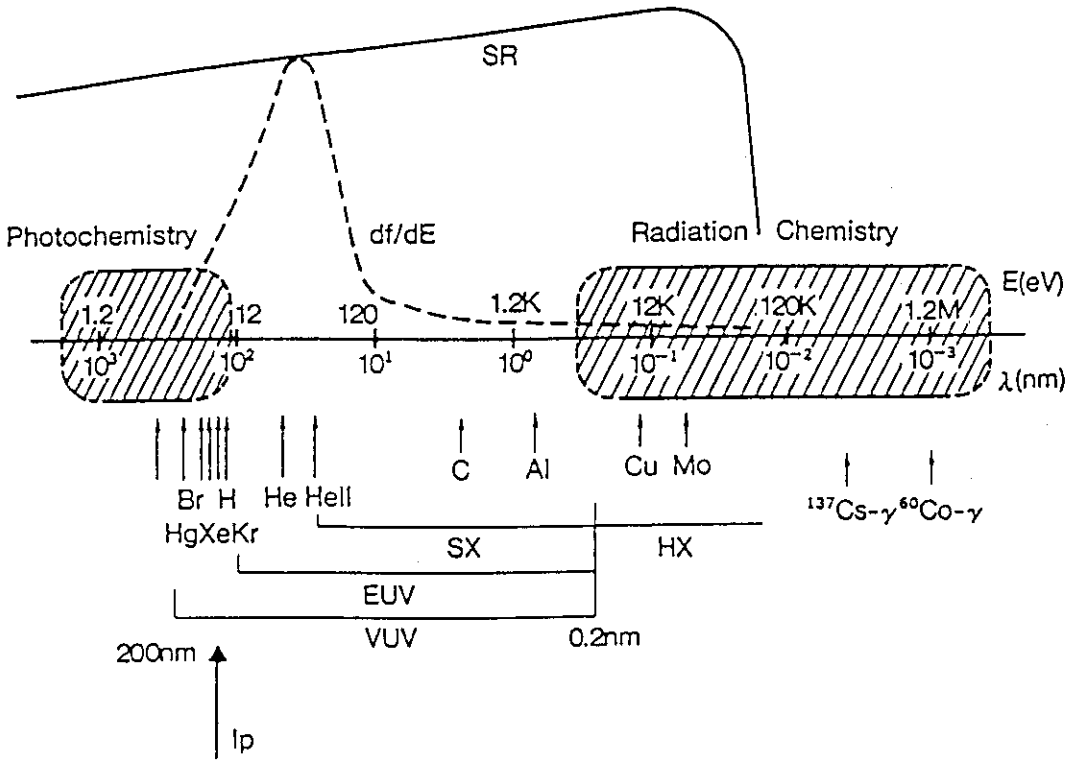


Fig.1. Synchrotron radiation (SR) chemistry as a bridge between radiation chemistry and photochemistry (Hatano, 1987).

a molecule from the ground state 0 to a final state j (Inokuti, 1986). The transition probability is expressed in terms of the optical oscillator strength f_j. It is in turn expressed in terms of E_j/R, the transition energy measured in the unit of the Rydberg energy R (=13.6 eV), and of M_j^2, the dipole matrix element squared as measured in atomic units, as

$$f_j(E_j) = (E_j/R)\, M_j^2. \qquad (1)$$

A set of E_j and f_j characterizes a discrete spectrum. To discuss a continuous spectrum, one expresses the oscillator strength in a small region of the excitation energy between E and E+dE as (df/dE)dE, and calls df/dE the oscillator-strength distribution, or, more precisely, the spectral density of the oscillator strength. The total sum of the oscillator strength including discrete and continuous spectra is equal to the total number Z of electrons in the molecule, viz.,

$$\sum_j f_j(E_j) + \int_I (df/dE)dE = Z, \qquad (2)$$

where I represents the (first) ionization potential. Equation (2) is called the Thomas-Kuhn-Reiche (TKR) sum rule.

The oscillator-strength distribution is proportional to the cross section

for the absorption of a photon of energy E.

A decisive step in the physical and physicochemical stages of the action of any ionizing radiation on matter is collisions of secondary electrons in a wide energy range with molecules. At energies T higher than about 10^2 eV, the total cross section $Q_j(T)$ to excite a molecule to the state j is at least approximately given by the Bethe cross section (Inokuti, 1971). Using the Bethe cross section and further assumptions, Platzman (Platzman, 1967; Hatano, 1968) showed that the number of product species j formed per 100 eV absorbed is approximately proportional to the dipole matrix element squared

$$M_j^2 = \int_J^\infty \phi_j(E) \frac{R}{E} \frac{df}{dE} dE, \tag{3}$$

where $\phi_j(E)$ is the quantum yield and J is the threshold energy, both for the formation of j. With the use of the W value, one may write

$$G_j = \frac{100}{W} \frac{M_j^2}{M_i^2} \tag{4}$$

where M_i^2 is the dipole matrix element squared for ionization, i.e.,

$$M_i^2 = \int_I^\infty \eta(E) \frac{R}{E} \frac{df}{dE} dE, \tag{5}$$

where $\eta(E)$ is the quantum yield for ionization. Since

$$\eta(E) = \sigma_i(E)/\sigma_t(E), \tag{6}$$

where $\sigma_i(E)$ and $\sigma_t(E)$ are, respectively, the photoionization cross section and the photoabsorption cross section, Eq. (4) means that the radiation chemical yield G_j is obtained from optical cross section data. Equation (4) is therefore called the optical approximation. Optical cross section data are, thus, of fundamental importance in understanding not only the interactions of photons with molecules, but also the actions of any ionizing radiation with matter.

It is important to obtain photoabsorption and related cross sections for polyatomic molecules such as hydrocarbons and other organic molecules and relate them with molecular structure. With this idea, photoabsorption and photoionization cross sections for molecules in several stereo-isomer series have been systematically measured and compared with each other (Koizumi et al., 1985, 1986, and 1989). The main purpose of these investigations is to reveal how df/dE changes with changing molecular structures; for this purpose isomers have been chosen as examples.

Figure 2 shows, as an example, the absorption cross sections of C_3H_6 isomer molecules, cyclopropane and propylene (Koizumi et al., 1985; Hatano, 1987 and 1994). Similar cross section data have been obtained also for the other isomer series, giving the common new features of absorption cross sections or oscillator strength distributions summarized as follows:

1) The values of σ_t show a maximum at 70-80 nm (16-18 eV) for each molecule.
2) In the high energy side of the maximum the values of σ_t are almost the same among the isomer molecules, e.g., cyclopropane and propylene, and equal to the sum of the cross sections for the constituent atoms.

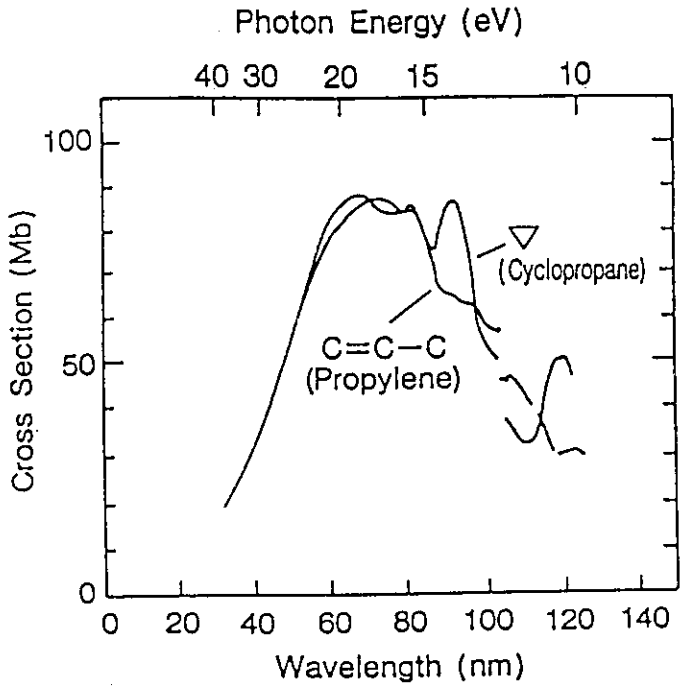


Fig.2. Photoabsorption cross sections for cyclopropane and propylene (Koizumi et al., 1985; Hatano, 1987 and 1994).

3) In the low energy side, the cross sections have different peaks and shoulders depending on an isomer, i.e., on its molecular structure. The sum of the cross sections in this energy region is, however, almost equal among the isomer molecules.

FORMATION AND DECAY PROCESSES OF SUPEREXCITED MOLECULES

A molecule that has received energy exceeding its ionization threshold (I_p) does not necessarily ionize because there are in general other decay channels such as dissociation into neutral fragments, and the ionization process competes with the neutral fragmentation. Various pathways are schematically represented in the following for a molecule AB (Platzman, 1962; Hatano, 1983 and 1994).

$$AB + \text{energy} (>I_p) \rightarrow AB^+ + e^- \quad ; \text{Direct ionization} \quad (7)$$

$$\rightarrow AB' \quad ; \text{Superexcitation} \quad (8)$$

$$\rightarrow AB^+ + e^- \quad ; \text{Autoionization} \quad (9)$$

$$\rightarrow A + B \quad ; \text{Dissociation} \quad (10)$$

$$\rightarrow \text{Others} \quad (11)$$

In this mechanism AB' is a superexcited molecule which decays through autoionization or dissociation. The cross section σ_i corresponds to the sum of the cross sections for both direct- and auto-ionization processes, while σ_t to the sum of the cross sections for direct ionization and superexcitation. The value of η in the energy region below I_p is zero, while above I_p it increases with increasing energy, and eventually approaches unity in the energy region well above I_p; however, in the energy region close to I_p the dissociation process plays a very important role in the decay of a superexcited molecule.

It has been pointed out both theoretically and experimentally that superexcited states, and hence neutral fragments formed from their dissociation play an important role in radiolysis. The neutral fragments are translationally, vibrationally, or sometimes electronically excited, because of a large internal energy of superexcited states. Such fragments are called hot atoms or free radicals, and have anomalous chemical reactivities (Hatano, 1989).

In order to understand the electronic structure and dissociation dynamics of superexcited states, electron impact spectroscopy and more recently spectroscopy combined with SR have been extensively applied (Hatano, 1983 and 1994). It has been concluded that a major part of the superexcited states of molecules are molecular high Rydberg states converging to various ionic states and are classified into the following three types: 1)vibrationally excited states, 2)doubly excited states, and 3)inner-core excited states (Hatano, 1994).

In summary, photoabsorption cross sections, photoionization cross sections and photoionization quantum yields are of great importance as key features of superexcited states, which characterize the primary processes, (7) -(11), of both photolysis and radiolysis of molecules.

REACTION DYNAMICS BY MEANS OF SR PULSE PROPERTIES

The outstanding pulse properties of SR with a subnanosecond pulse width and a pulse-to-pulse interval from nanoseconds to submicroseconds as combined with other SR properties, i.e., a wide wavelength-tunability, a high degree of polarization, and a long term stability in pulse shape, timing, and intensity have been applied to molecular spectroscopy and reaction dynamics which are closely related with radiation chemistry.

It has been clearly demonstrated that the SR pulse properties are a promising tool for studying bimolecular processes (Hatano et al., 1981). The rate constant for the energy transfer from a state-specified Xe excimer to some molecules has been measured using a delayed coincidence single photon counting technique. Using a similar technique the SR pulse properties have been applied also to one of the important subjects of research in radiation chemistry that is the measurement of fluorescence lifetimes and excitation spectra of liquid alkanes (Wickramaaratchi et al., 1985, Shinsaka et al., 1985). The obtained results are compared with those by techniques using different kinds of excitation sources, i.e., α, β, γ, and X-rays, accelerated electron beams, UV photons from discharge lamps, and laser photons.

Comments on SR studies of condensed matter from the viewpoint of radiation chemistry

I had the opportunity to summarize the future problems needing more work in the chemical application of SR (Hatano, 1987), in which I made comments on

SR studies of condensed matter from the viewpoint of radiation chemistry. They are summarized as follows.

1) To understand or to substantiate more the radiation chemistry of condensed matter, SR should be applied not only directly to molecules in the condensed phase but also to those in high density gases and clusters.
2) The SR joined properties should be more actively used. It is interesting not only to join the SR properties with each other but also to join them with lasers of electron beams.
3) It is worthwhile to make an attempt of measuring product yields by using a chemical scavenger method, in particular, the radical sampling technique using radioactive compounds.
4) For better substantiation of specific ionization phenomena in the condensed phase as opposed to those in the gas phase, SR has been applied to the measurement of the ionization threshold energy values of liquids and also to the experiment for an attempt to get evidence for Rydberg states near the threshold in liquid alkanes. A key experiment, however, for this purpose should be the measurement of the absolute ionization efficiency values in liquids.
5) A wide wavelength-tunability of SR is useful to study the track structure of ionizing radiation interacting with matter.

In the past several years since I made these comments, the related SR studies have been rapidly in progress. The followings are good examples of these studies as chosen from the Proceedings of the Annual Discussion Meeting of Radiation Chemistry in Japan published in the past five years, as well as from the scientific program of the present Symposium.

a) Effect of innershell excitation on the color-center formation in anthracene single crystals (See A10-9 Shimoyama et al. at the present Symposium and Kimura et al., 1994).

Interesting oscillating structures near the C K-edge energy at 285 eV have been observed in the absolute quantum yield of optical emission from the S_1 state formed by the photoexcitation of crystalline anthracene in the photon energy region of 100-600 eV. This observation has reminded me of similar structures in W (Suzuki and Saito, 1985) or $G_{f,i}$ values (Holroyd et al., 1992). Interesting structures have been also observed by the same group in the photoconductivity excitation spectra of supercritical Xe doped with anthrance. This group has extended recently these experiments further into the ion desorption from benzene monolayer (See also A10-9 Shimoyama et al. at the present Symposium), and has also applied SR as a helpful light source to studies of the photoioizaion potentials of C_{60}-C_{84} in nonpolar liquids (See P8-4 Shimoyama et al., and also P9-4 Katoh et al. at the present Symposium) and of the electron-ion recombination in dense C_2H_6.

b) VUV-light induced electron emission from low-vapor pressure organic liquids (Koizumi, 1994; Koizumi et al., 1993 and 1994).

As pointed out above in the list of comments, the measurement of absolute photoionization efficiency curve as a function of the photon energy is a key experiment to understand the essential features of ionization phenomena in condensed matter, i.e., to differentiate the ionization of condensed matter from that of gases.

A systematic investigation has been recently successful in this measurement by means of VUV-photons not from SR sources but from discharge lamps. Obtained results and discussion in a series of this investigation is helpful to substantiate the mechanism of the ionization of liquids. This investigation

has been recently further extended to that of the pressure dependence of photoconductivity in liquids.

c) Picosecond SR pulse radiolysis (Ogata and Tagawa, 1989).

The time structure of SR has been applied to one of the important objectives of radiation research, that is the investigation of LET or track-structure effects. The fluorescence lifetimes of the S_1 state in liquid n-dodecane and of the excimer state in polystyrene have been measured by means of a SR pulse of hundreds psec with the photon energy of 3-30 keV and compared with those measured by means of a 1-3 MeV H^+ or He^+ pulse and a 28 MeV e^- pulse.

d) Free radical formation in the SR-VUV photolysis of polycrystalline aminoacids and derivatives (See P9-15 Minegishi et al. at the present Symposium).

The product free radicals have been observed by means of ESR spectroscopy in the SR-VUV photolysis of acetyl-alanine and related compounds in polycrystalline states as a function of the wavelength in the region of 115-245 nm. The formation mechanism of detected free radicals has been ascribed to the neutral fragmentation of highly excited states including superexcited states of these molecules.

REFERENCES

Hatano Y. (1968) *Bull.Chem.Soc.Jpn.*, **41**, 1126.

Hatano Y. (1983) Comments on At.Mol.Phys., **13**, 259.

Hatano Y. (1987) "The Chemistry of Synchrotron Radiation", in "Radiation Research", eds. Fielden E.M., Fowler J.F., Hendry J.H. and Scott D., Taylor & Francis, London, Vol.2, pp.35-41.

Hatano Y. (1989) *Radiochim.Acta*, **43**, 119.

Hatano Y. (1994) "Dynamics of Superexcited Molecules" in "Dynamics of Excited Molecules", ed. Kuchitsu K., Elsevier, Amsterdam, pp.151-216.

Hatano Y., Ohno M., Kouchi N., Koizumi H., Yokoyama A., Isoyama G., Kitamura H. and Sasaki T. (1981) *Chem.Phys.Lett.*, **84**, 454.

Hatano Y. and Inokuti M. (1994) "Photoabsorption, Photoionization, and Photodissociation Cross Sections" in "Atomic and Molecular Data for Radiotherapy and Related Research", eds. Inokuti M., IAEA, Vienna, in press.

Hatano Y., Holroyd R.A. and Sham T.K. (org.) (1995) "Symposium on Chemical Applications of Synchrotron Radiation" in Pacifichem '95.

Holroyd R.A., Sham T.K., Yang B.-X. and Feng X.-H. (1992) *J.Phys.Chem.*, **96**, 7438.

Inokuti M. (1971) *Rev.Mod.Phys.*, **43**, 297.

Inokuti M. (1986) *Photochem.Photobiol.*, **44**, 279.

Kimura A., Nakagawa K., Tanaka K., Kotani M. and Kotoh R. (1994) *Nucl.Instr. Methods*, B91, 67.

Koizumi H. (1994) *Chem.Phys.Lett.*, **219**, 137.

Koizumi H., Yoshimi T., Shinsaka K., Ukai M., Morita M., Hatano Y., Yagishita A. and Ito K. (1985) *J.Chem.Phys.*, **82**, 4856.

Koizumi H., Hironaka K., Shinsaka K., Arai S., Nakazawa H., Kimura A., Hatano Y., Ito Y., Zhang, Y.W., Yagishita A., Ito K. and Tanaka K. (1986) *J.Chem. Phys.*, **85**, 4276.

Koizumi H., Shinsaka K. and Hatano Y. (1989) *Radiat.Phys.Chem.*, **34**, 87.

Koizumi H., Lacmann K. and Schmidt W.F. (1993) *Nucl.Instr.Methods*, A327, 75.

Koizumi H., Lacmann K. and Schmidt W.F. (1994) *J.Elect.Spectr. Related Phenom.*, **67**, 417.

Ogata A. and Tagawa S. (1989) *Rev.Sci.Instr.*, **60**, 2197.

Ohta T., Suga S. and Kikuta S. (eds.) (1994) "Synchrotron Radiation Facilities in Asia", Ionics Publishing, Tokyo.
Platzman R.L. (1962) *Vortex*, **23**, 372.
Platzman R.L. (1967) "Radiation Research", ed. Silini G, North-Holland, Amsterdam, p.20.
Shinsaka K., Koizumi H., Yoshimi T., Kouchi N., Nakamura Y., Toriumi M., Morita M., Hatano Y., Asaoka S. and Nishimura H. (1985) *J.Chem.Phys.*, **83**, 4405.
Suzuki I.H. and Saito N. (1985) *Bull.Chem.Soc.Jpn.*, **58**, 3210.
Weston R.E., Bancroft G.M. and Hatano Y. (org.) (1989) "Symposium on Chemical Applications of Synchrotron Radiation" in Pacifichem '89.
Wickramaaratchi M.A., Press J.M., Holroyd R.A. and Weston, Jr. R.E. (1985) *J. Chem.Phys.*, **82**, 4745.

2.3 *Irradiation Facilities and Research Activities in JAERI-Takasaki

Takasaki Radiation Chemistry Research Establishment
Japan Atomic Energy Research Institute
1233 Watanuki-machi, Takasaki, Gunma, Japan 370-12

Abstract

Takasaki Radiation Chemistry Research Establishment, Japan Atomic Energy Research Institute conducts R&D on radiation application using Co-60 irradiation facilities and electron accelerators. In addition, the advanced radiation technology project is in progress using newly built ion irradiation facilities.

The R&D on radiation application include those on modification of polymers, synthesis of new materials, environmental conservation and resources utilization. In synthesis of new materials, a production technology of silicon carbide fibers as heat resistant ceramic fibers is developed using radiation cross-linking. And development studies on selective absorbents of toxic gases, heavy metals and uranium in sea water are carried out using radiation graft polymerization. In environmental conservation, EB treatment process of flue gases from coal-fired power plant and municipal waste incinerators have developed.

In the advanced radiation technology project, studies on radiation effect on semiconductors and organic materials, synthesis of organic/inorganic functional materials creation, development in biotechnology and ion beam technology are carried out. On radiation effect on semiconductors, single event phenomena caused by heavy-ion impingement in electronic devices, radiation induced defects in SiC, radiation response of SiC MOS structure are studied. On organic functional materials, creation of functional surface and intelligent materials are studied using ion beams irradiation and radiation graft polymerization including the synthesis of porous membranes responding to environmental changes such as temperature, pH. On developing of analyzing technology using ion beams, advanced structure analyzing methods such as dual beam analysis systems for the on-site analysis of the surface region, in-situ microstructural observation system during ion irradiation, a time-resolved X-ray absorption spectrometer, positron annihilation spectroscopy are developed for synthesis of new materials.

Introduction

Takasaki Radiation Chemistry Research Establishment(TRCRE), Japan Atomic Energy Research Establishment(JAERI) was founded at 1963 as a center for research and development of radiation chemistry in Japan. Large irradiation facilities of Co-60 gamma-ray irradiation and EB accelerators were constructed, and developmental studies have been carried out in the radiation processing fields; radiation polymerization, modification of polymer materials, preparation of new materials/functional materials, environmental conservation and resource utilization technology. Various useful results have been produced through R&D works on radiation processing technologies using gamma rays and electron beams. Radiation processing technologies have extended in industries where many Co-60 gamma-rays and electron beams irradiation facilities have been introduced.

In 1988, JAERI proposed the advanced radiation technology (ART) project, a new research project in fields of material science, biotechnology and beam technology using ion beams. In 1993, construction of ion beams irradiation facilities(TIARA: Takasaki Ion Accelerators for Advanced Radiation Application) was completed. From January, 1994, all facilities including four ion beam accelerators are operated for research. These are AVF Cyclotron, 3 MV Tandem-type accelerator, 3 MV single-ended type accelerator and 400 kV ion implanter.

1. Irradiation Facilities

In Table 1, gamma-ray irradiation facilities and electron accelerators in TRCRE are shown. We have four Co-60 irradiation facilities, and there are 10 irradiation cells which have water pools for Co-60 source storage. We have 1.1 M Ci Co-60 source in total, about 140 kCi are imported every year to keep this ability.

We also have three electron accelerators, they are Cockcroft-Walton type (2 MeV, 60kW), Cascade type(3MeV, 75kW) and low energy, self-shield linear cathode type (300 keV, 30kW). The Cockcroft-Walton type is a dual beams type of horizontal and vertical beams.

Table 2 shows ions and their energy obtaind from TIARA[1]. This facility is composed of research building, cyclotron building where AVF Cyclotron is installed, and multiple beams building where 3 MV Tandem-type accelerator, 3 MV single-ended type accelerator and 400 kV ion implanter are installed. And more than 20 experimental apparatus including irradiation chambers for various uses are installed.

From the AVF cyclotron, scanning beams are available for wide uniform irradiation of organic materials and solar cells. Micro-ion beams are available from both Tandem and single-ended accelerators[2]. We also can get dual ion beams with Tandem accelerator and ion implanter and single ended accelerator and ion implanters, triple ion beams with Tandem, single ended accelerators and ion implanter.

Table 1 Gamma-rays irradiation facilities and electron accelerators

Name	Radiation Source(kCi)		Equipment
	Capacity	Activity	
Co-60 Irradiation Facility 1	1500	400	3 irradiation cells Stored in water-filled pool
Co-60 Irradiation Facility 2	500	420	3 irradiation cells Stored in water-filled pool
Food Irradiation Facility	400	315	2 irradiation cells Stored in water-filled pool
Irrad. Facility for Rad. Engineering	8 and 0.03	0.84 0.02	2 irradiation cells Stored in lead container

Name	Energy (MeV)	Current (mA)	Type
Electron Accelerator 1	2	30	Cockcroft-Walton type (Dual beams)
Electron Accelerator 2	3	25	Cascade type (Dynamitron)
Low Energy Electron Accelerator	0.3	100	Linear cathode type (self-shielded)

Table 2 Ions obtained from TIARA Facilities

Accelerator	Ions	Energy(MeV)
AVF Cyclotron	H	5 - 90
	D	5 - 53
	He	10 - 108
	C	30 - 330
	Ar	100 - 530
	Other (Kr, Ne, O,···)	
3 MV Tandem Accelerator	H, D, He	0.8 - 6
	C, N, O	0.8 - 15
	Al, Si, S, V, Cr	0.8 - 18
	Fe, Ni, Cu, Ag	0.8 - 18
	Au	0.8 - 21
3 MV Single-Ended Accelerator	H, D, He, e	0.4 - 3
400 kV Ion Implanter	H, P, Ar, Mn, As, Ag,···	20 - 400

2. Research Activities

2.1 Research of radiation resistance of materials

Radiation damage of devices and single event upsets(SEU) of integrated circuits(ICs) by cosmic rays that is heavy ions cause serious problems in control system of artificial satellite. So, total dose effects on devices including solar cells are evaluated using heavy ion irradiation system and proton irradiation system. And also mechanism of SEU are studied using a micro ion beam irradiation system.

Basic study of SEU, such as elementary process of charge collection in ICs after heavy ion irradiation using the micro ion beam irradiation system connected to Tandem accelerator are carried out. Fig. 1 shows an example of transients current in a p-n junction diode induced by a single ion exposure[3]. It is shown that SEU is a very rapid phenomena and induced electric charge depend on ion.

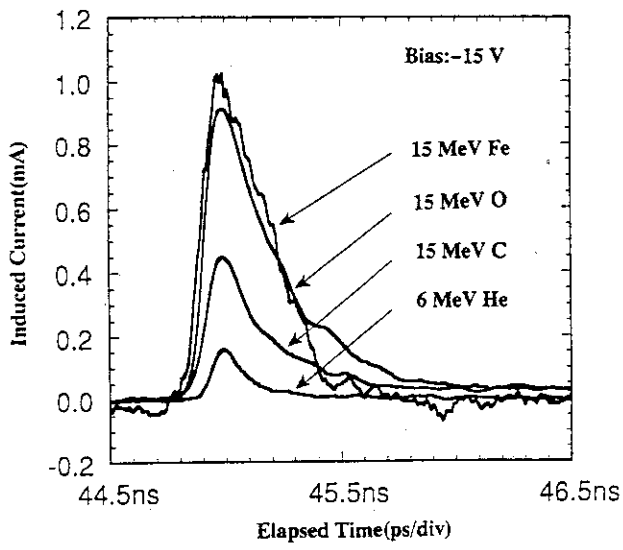


Fig.1 Transients current in a p-n junction diode induced by a single ion exposure

In study on radiation resistance of organic materials which are used in space as structural materials and in fusion reactor as insulating materials, radiation damage of organic composite materials and various organic polymer materials are studied using ion beams and other radiations in wide range of temperature including 4K. And aging of electric wire and cables which are used in nuclear power plants are also studied to establish a methodology of their life time estimation in a shorter testing time.

2.2 Synthesis of new materials and functional materials

Development of materials used in extreme environments, for example, preparation of radiation resistant SiC semiconducting materials by a CVD method, and preparation of super heat resistant SiC fiber using radiation crosslinking are carried out.

We have developed a new process for SiC fiber production using EB under a collaborated research with other organizations. This fiber has been manufactured from polycarbosilane(PCS) by a process as shown in Fig.2[4,5]. The SiC fiber is prepared through processes of melt spinning of PCS, infusible treatment using EB and pyrolysis. In the conventional process, infusible treatment is done by oxidation curing. But the fibers ("Nicalon") contain oxygen of about 10% during the curing process of thermal oxidation, the heat resistance in this case is around 1200°C. In EB process, polycarbosilane fibers are cured using electron beam crosslinking in He atmosphere. The cured PCS fibers were heat-treated in Ar gas up to about

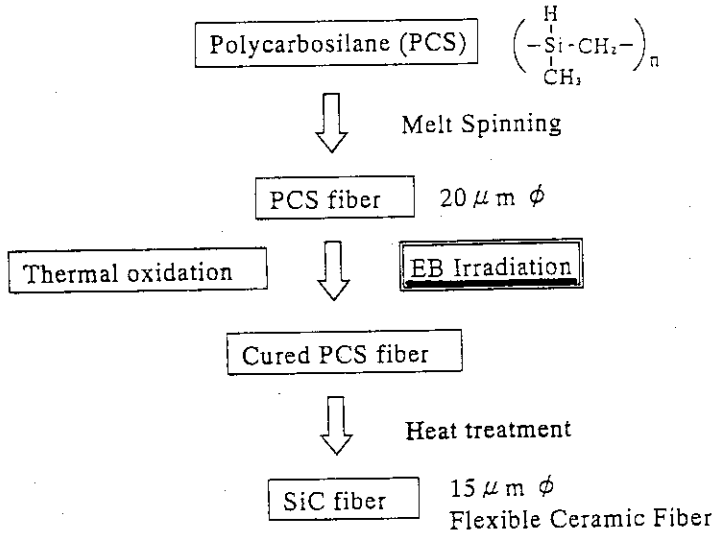


Fig.2 Process of SiC fibers preparation from PCS

1500K. The content of oxygen is very small, less than 0.4%. Heat resistance of SiC fibers are compared in Fig.3. Comparing with the conventional fiber, the new fiber(2,000K) is improved by 500K. This technology was transfered to an industry.

In research on synthesis of new materials and functional materials, we are also studying preparation of intelligent materials using ion track, and preparation of absorbent of pollutant gases, heavy metals in waste water and uranium in sea water using graft-polymerization.

Study on synthesis of porous membranes responding to environmental changes such as temperature, pH and electric field have been carried out using heavy ions[6]. Energetic ions induce severe damages in organic materials. The latent effects leave columnar passage. These latent tracks can be chemically etched out, and the diameter of the resultant pores can be controlled easily by etching conditions. An intelligent filter responding to temperature is developing by irradiation of CR-39 polymer using swift heavy ions and followed by chemical etching and gamma ray induced grafting of acryloyl-L-proline methyl ester on inner surface of micro-pores.

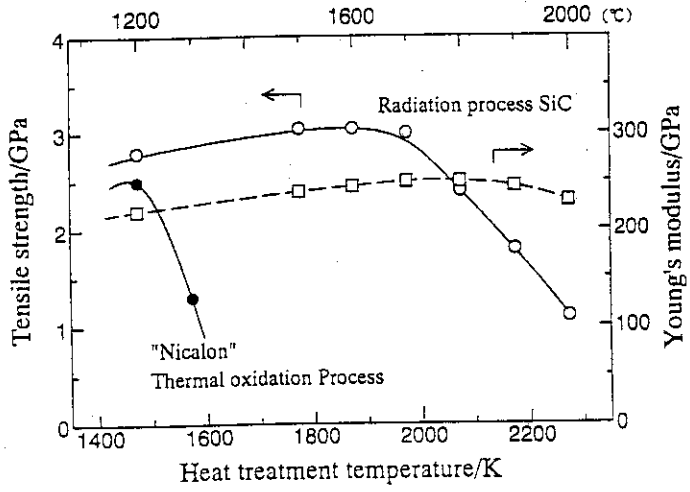


Fig.3 Comparison of heat resistance of SiC fibers

The other application of radiation is use of radiation graft polymerization, for synthesis of absorbent of various pollutants and metals[7,8]. In JAERI, many research works have been carried out using radiation graft polymerization as shown in Table 3. The first example which was transfered to an industry is production of battery separator, in this case, polyethylene film are irradiated by EB and acrylic acid are grafted on the surface. After alkali treatment, battery separator are obtained. The second is absorbent for toxic gases such as NH_3, H_2S. In this case, nonwoven polypropylene are irradiated by EB, and stylenes or GMA are grafted. After sulfonation, absorbent are obtained. Transfer of this technology to an industry is now proceeding. The other are heavy metal ions absorbent of functionalized hollow fiber membrane and nonwoven organic fibers using radiation graft polymerization.

Table 3 Preparation of various absorbents using radiation graft-polymerization

Substrates	Monomers	Treatment & Functional Groups	Utilizations
Polyethylene Films (25μ m)	Acrylic Acid $CH_2CHCOOH$	Alkali Treatment -COOK or -COONa	Battery Separators
Nonwoven Polypropylene(1-20μ m)	Glycidyl Methacylate(GMA)	Sulfonation $-SO_3H$	Absorbents for Gases(NH_3 etc)
Polyethylene Hollow Fiber(id:0.62mm)	GMA	Iminodiacetic Acid (IDA) $-N(CH_2COOH)_2$	Co Absorbent
Fibrous or Nonwoven Polypropylene (1-20μ m)	Acrylnitrile CH_2CHCN	Amidximation with Hydroxyamin $-C(NOH)(NH_2)$	Absorbents for U from Sea Water Heavy Metal Ions

2.3 Development of advanced analyzing technology

Dual/triple ion beam irradiation system, in-situ microstructural observation system during ion beam irradiation, and positron annihilation spectroscopy system are developing.

Dual beam analysis systems[9] have been installed to do the on-site analysis on the surface region modified by low energy ion beams and laser beams at low temperatures.

The ion beam analysis will be made using two kinds of ions; high energy heavy ions from the Tandem accelerator for ERDA and NRA, and light ions from the single-ended accelerator for RBS-channeling analysis.

In-situ microstructural observation during ion irradiation, an analytical electron microscope(JEOL 4000FSX) is connected to the 400 kV ion implantor, and it is possible to do the in-situ analysis of evolution of implants and induced defects during ion bombardments.

2.4 Others

In the field of environment conservation and utilization of resources, development of radiation technology of EB treatment of exhaust gases are carried out. Development of radiation treatment of biological resources and study on food irradiation and decontamination of microorganism are carried out.

Two pilot-scale tests for EB treatment of exhaust gases from coal-burning boiler and incinerator of municipal waste have been carried out under the joint researches of JAERI and other organizations, and are now under evaluation.

On biotechnology, the mechanisms of radiation resistance are studied focusing on repair of DNA double strand break of D. radiodurans. Further, a cell surgery technique is developing by local irradiation technique using focused beams and penetration-controlled beams. For these researches, a micro-ion beam generation system for local irradiation, apparatus for depth control irradiation are installed.

On ion beam technology, developments of technologies on micro ion beam generation, single ion hitting and new ion sources are carried out. In radiation engineering, dosimetry and traceability are studying.

3. Use of TIARA Facilities

TIARA is open for researchers from outside institutions, all research proposals including from JAERI will be assessed by the TIARA Program Committee and Program Advisory Committee composed of JAERI and non-JAERI members at the same level in advance, and the results obtained are reported as TIARA annual report.

Fig.4 shows change of number of research subjects adopted since 1991, there are more than 90 in 1994. The research field are materials for space and fusion reactor, bio-technology, new functional materials and so on.

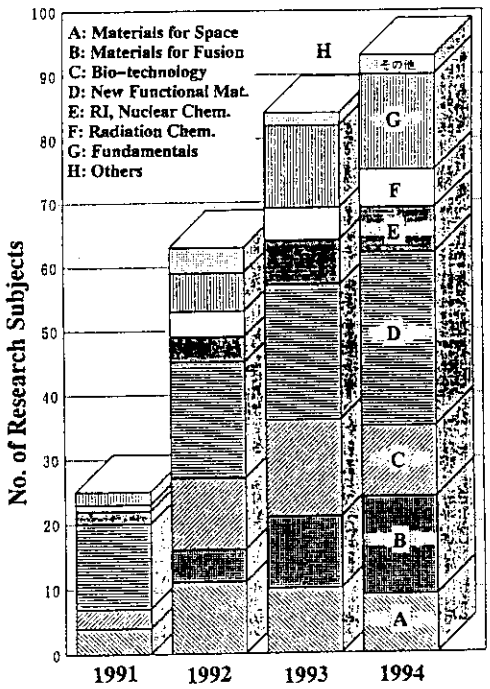


Fig.4 Number of research subjects using TIARA faclities

References

1. Watanabe,H., S.Tanaka, K.Nishimura, I.Takada,Y.Nakamura,K.Mizuhashi,N.Ohnuma,N.Akiyama and M.Maruyama;"Design and Construction of TIARA Facilities", TIARA Annual Report, Vol.2,211-220(1992).
2. Kamiya,T.,T.Suda,T.Hirao,I.Nashiyama and R.Tanaka;"Beam Positioning and Single Ion Hit for Heavy Ion Microbeam", TIARA Annual Report, Vol.3,193-195(1993).
3. Hirao,T, T.Nishijima,T.Kamiya, H.Yutoh,H.Itoh and I.Nashiyama;"Measurement of Transient Current by Microbeams", TIARA Annual Report, Vol.2,9-12(1992).
4. Seguchi,T.,M.Sugimoto and K.Okamura;"Heat Resistant SiC Synthesis and Reaction

Mechanisms from Radiation-Cured Polycarbosilane Fiber", 6th European Conf. on Composite Materials,20-24 Sept.,1993,Bordeaux.
5. Takeda,M.,Y.Imai,H.Ichikawa,T.Ishikawa, T.Seguchi and K.Okamura;"Properties of the Low Oxygen Content SiC Fiber on High Temperature Heat Treatment"; Ceram. Eng. Sci.Proc. 12(7-8) pp.1007-1018(1991).
6. Asano,M.,M.Yoshida,M.Tamada,H.Omichi,M.Fukuda,T.Agematsu,S.Okamura and K. Arakawa;"Uniformity of Beam Fluence Distribution Obtained by the Multiple Cou lomb Scattering Using Thin Metal Foils",TIARA Annual Report, Vol.2,83-86(1992).
7. Okamoto,J.,T.Sugo,K.Fujiwara and H.Sekiguchi;"The Synthesis of a New Adsorbent for Removal of Toxic Gas by Radiation-induced Graft Polymerization", Radiat. Phys. Chem. Vol.35,Nos 1-3,pp.113-116,1990.
8. N.Kabay, A.Katakai,T.Sugo and H.Egawa;"Preparation of Fibrous Adsorbents Conta ing Amidoxime Groups by Radiation-Induced Grafting and Application to Uranium Recovery form Sea Water", J. of Applied Polymer Science, Vol.49,599-607(1993).
9. P.Goppelt-Langer, S.Yamamoto, Y.Aoki,H.Takehisa and H.Naramoto;"Light Element Profiling Using Heavy Ion Beams",TIARA Annual Report, Vol.3,137-138(1993).

2.4 *Current Status of Radiation Chemical Research in India

C. Gopinathan and J.P. Mittal*
Chemistry Group
Bhabha Atomic Research Centre
Trombay, Bombay-400 085,India

Radiation Chemistry work in India first started at the Chemistry Division, Bhabha Atomic Research Centre as early as 1966, when radiation effects on solvents used in the processing of spent reactor fuel were studied. Radiation Chemistry work in the period 1950-66 was mostly of an applied nature. For example, comprehensive work was done on production of wood polymer composites by gamma radiation polymerisation of various monomer impregnated woods. A variety of high strength composites were also produced. Some of these went into commercial production. Other studies of interest to the Indian Atomic Energy Programme were also undertaken, such as studies of radiation damage to lubricants, paints and greases to be used under high radiation environment, and ways of improving their radiation resistance.

From 1966 onwards a comprehensive research programme on basic studies was initiated. For example, study of trapped transient species produced in low temperature systems was carried out using both absorption spectrophotometric and ESR techniques. Steady state gamma radiolysis studies also included room temperature aqueous and organic systems. In the late 1970s and early 80s theoretical work on the primary events and diffusion kinetics was carried out. The applied work during this period included production of radiation processed biomaterials such as a strip for the detection of Jaundice.

A fully computerised modern pulse radiolysis facility (7MeV electrons, 25 nanosecond, 50 nanesecond and 2 micro second pulses) was commissioned in 1986. About 25 scientists are now using this facility and over 100 Journal publications have appeared. Among the more important achievements include : (i)Evaluating the reaction mechanism of a number of reactions of free radicals with important biological compounds, (ii) An exhaustive study of the radiation chemistry of Buckminister fullerenes in solution, (iii) Assessment of the kinetics of nanoparticle formation during radiolytic reduction of metal salt solution, (iv) An improved understanding of aromatic substitution reactions including the identification of the site of attak and (v) Understanding of reactions occurring in microheteriogeneous system. Much of this work has attracted international attention.

Applied work has also been continued and commercial applications are expected soon.

2.5 *Pulse Radiolysis Facilities and Activities in Japan

M. Ogasawara

Hokkaido University of Education
Hachiman-cho 1-2, Hakodate 040, Japan

Abstract Pulse radiolysis studies in Japan have been reviewed in special reference to the facilities and the people who have engaged in the experiments. Main achievement is summarized with the list of selected publications.

INTRODUCTION

The first pulse radiolysis experiments in Japan was made by Katayama in 1964 in Hokkaido University. It was only two years behind the well known experiments in England by Boag and Hart on hydrated electron. Since then, about ten pulse radiolysis facilities have been constructed. In this paper I would like to overview the facilities as well as the activities concerning the pulse radiolysis in Japan. My intention is to give the readers a rough idea of what is Japanese contributions in this particular field of radiation chemistry. The description may inevitably be influenced by my own experience, but I do hope that the readers notice at least part of the important achievement accomplished in the last two decades in this country. For more precise understanding the readers may refer the papers in the list of the selected publications attached at the end of the article, which was completed in collaboration with many people enlisted in the acknowledgment. I must confess, however, that the list is far from a perfect one because of the limitation of my ability and the time given to prepare this article. Many other important publication should be added after this.

PULSE RADIOLYSIS FACILITIES IN JAPAN

Important facilities in Japan are summarized chronologically in Fig. 1 together with the "family tree" of the people engaged in the pulse radiolysis experiments.

The pulse radiolysis system constructed by Katayama was made up with 4 MeV Mitsubishi linear electron accelerator(LINAC) which was introduced in Hokkaido University in the beginning of 1960s. I myself joined his group in 1966 as a graduate student and had rather a tough experience of setting up the delicate optical system.

Only one or two years after Hokkaido University another pulse radiolysis system started to work in Radiation Center of Osaka Prefecture, now one of the institutes in the University of Osaka Prefecture. People in this institute made a great contribution with this machine to radiation chemistry. Kawabata, Okabe, and Horii observed the electron trapped in single crystal of D_2O which had absorption bands peaking at 630 nm and >1000 nm (see the list of UOP). A lot of important works have been done on this species and other reaction intermediates in this institute.

In Institute of Physical and Chemical Research (RIKEN), Arai, now a professor of Kyoto Institute of Technology, Kira and Imamura started more systematic studies on reaction intermediates from 1969 (see the list of RIKEN). They used 2 MeV van de Graaff for liquid and solid samples and 600 keV Febetron 706 for gas samples.

The facility consists of 600 keV Febetron in Tokyo Institute of Technology started to work in the early 70s by the effort of Hatano and his coworkers. The facility was equipped with (1)

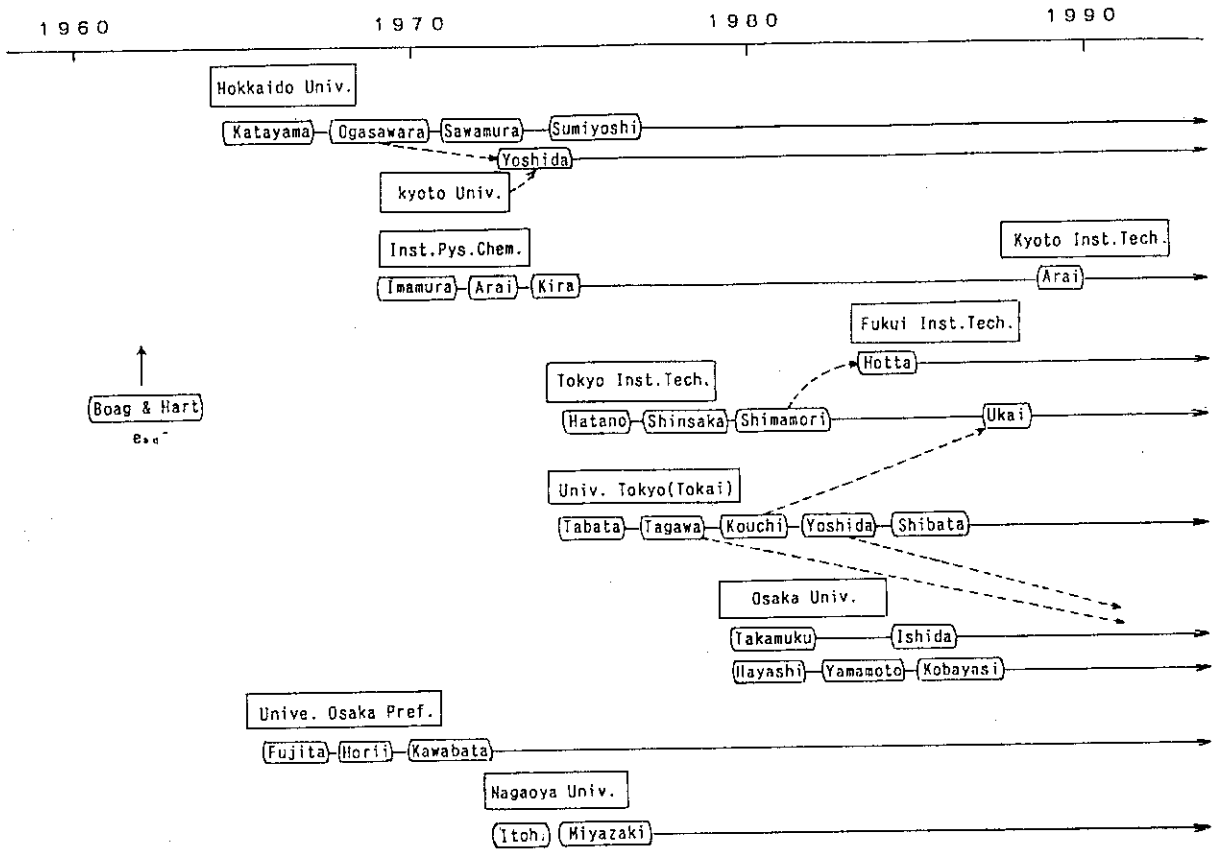


Fig. 1 Pulse radiolysis facilities in Japan and part of the people engaged in the experiments

time-resolved optical emission and absorption spectroscopy, (2)time-resolved DC-conductivity, and (3)time-resolved microwave conductivity. Shimamori, one of the strongest members of Hatano's group moved to Fukui Institute of Technology and completed an equivalent system with Hotta (see the list of FIT).

At the end of 70s modern and powerful machines were introduced in the University of Tokyo (Tokai) and Osaka University successively. They were 28 MeV and 38 MeV LINACs able to produce 10-20 ps pulse. Achievement obtained by these facilities should be highlighted in the history of pulse radiolysis studies in Japan. The readers will notice in Fig. 2 a sudden increase in the number of publications concerning pulse radiolysis in these years.

Facility in Nagoya University was started in the early 70s. Miyazaki completed a low temperature measurement system which was able to make experiments at liquid helium temperature. Interesting results concerning tunneling reaction in solid phase and radical ions of polymer were obtained by this facility (see the list of NU).

DEVELOPMENT OF PULSE RADIOLYSIS TECHNIQUE IN JAPAN

The basic pulse radiolysis system is composed of a radiation source, usually LINAC, and a detection system. Typically, a sample in optical absorption cell is irradiated by short pulses of ionizing radiation from LINAC. The transmission of the sample can be measured as function of time by means of a light beam .

In 1970 the group of Hunt in Toronto succeeded in obtaining picosecond time-resolution

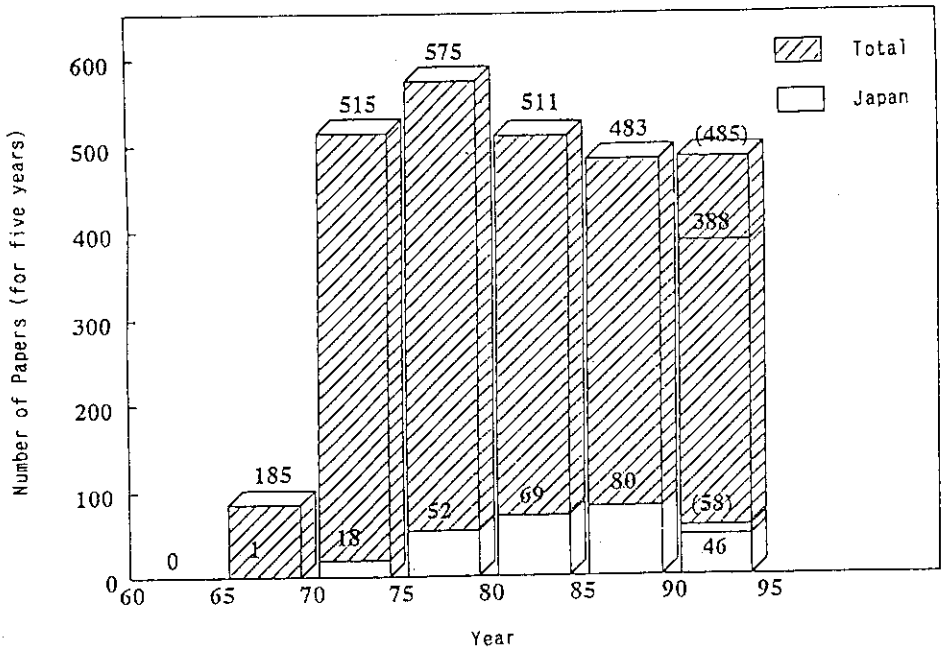


Fig. 2 Number of the published papers concerning pulse radiolysis
(From CA: presented by Prof. Takamuku)

by their stroboscopic pulse radiolysis system. In Japan, Katayama and Sumiyoshi in Hokkaido University constructed this type of system in the late 70 s (see the list of HU). In stroboscopic picosecond pulse radiolysis the train of bunches is used as it is obtained from the LINAC. Electrons in the accelerating tube respond to positive or negative electric field of the radiofrequency, and thus the electron pulse contains a train of bunches or fine structure. Their repetition rate is dependent on the frequency of the radiofrequency which is 350 ps for the S-band and 770 ps for the L-band. A set of Čerenkov light flashes is produced when the fine structure electron pulses travels through the air before hitting a sample; the flash is used to measure the concentration of the absorbing species produced in the sample at a fine point in time. The time sweep, which is limited within the interval between the structure pulses though, is accomplished by varying the length of the optical delay path.

This type of system has a shortcoming: it takes a long time, sometimes a day and a night, to get just a time-profile of the absorbance at a fixed wavelength. To get rid of this task, the LINAC which can produce a picosecond single beam was developed in Argone National laboratory in the United State in the early 70s. A similar one was completed in the University of Tokyo(Tokai). The principle is that the velocity of the electron beam emitted from an electron gun is modulated by the electric field at the gap of the prebuncher to form a single bunch within one radiofrequency period. The optical detection setup for single bunch picosecond measurement is not much different from that for nanosecond pulse radiolysis except for the streak camera which is used as a photo-detector.

This system has, however, an inherent limitation of time resolution, so that the group of Tabata of the University of Tokyo developed completely new systems called Twin Linac System and LL Twin System. Twin Linac System utilizes synchronized 10 ps electron pulses from two LINACs: one of the beams is used for producing Čerenkov light for analyzing the sample The time is swept by shifting the phase of the microwave in the two LINACs. In LL Twin Linac System analyzing light was taken from a synchronized laser apparatus. The laser light makes it possible to monitor the region from the visible to the near infrared region. Owing to these systems, it is possible to get time-resolved spectra in picosecond time-domain

in the wavelength range from 200 nm to 1600 nm.

In the same university, on the other hand, Shibata has engaged in developing an ion-beam pulse radiolysis system. The system contains two accelerators: one is a van de Graaff and another is a Tandetron accelerator. The pulsing system consists of a chopper and a retracer. The ion-beam is swept along the horizontal plane by 4 MHz sinusoidal wave from a chopper. The ions can pass through the aperture when the beam goes across the aperture from the right to the left and vice versa. Thus, the pulsed ion beam with the repetition rate of 8 MHz can be obtained.

ACHIEVEMENT IN THE PULSE RADIOLYSIS STUDIES IN JAPN

Initiation mechanism of radiation-induced-polymerization: The primary events induced by ionizing radiation in polymeric systems drew much attention in connection with initiation mechanism. Katayama observed transient absorption in pulse-irradiated α -methylstyrene in the uv region and assigned it to the radical anion of α -methylstyrene (see the list of HU). However, both the effects of additives on the polymerization rate and the composition of the copolymer strongly suggested a cationic mechanism. The problem was solved by elegant experiments by Egusa in 1977 in which he observed two types of dimer cations of styrene in solution. One of them, bonded dimer cation, is formed by the opening of the vinyl double-bond, which corresponds to the initiation step of the polymerization (see the list of RIKEN).

Pulse radiolysis of alkanes: The pulse radiolysis studies of liquid alkanes are important for understanding radiation effect on polyethylene or related polymers. Tagawa observed, on pulse radiolysis of n-dodecane, radical cation, excited states, alkyl radicals. The alkane radical cation had an absorption band in the visible with its maximum at 800 nm. The position of the absorption maximum changed from 600 nm to 900 nm depending on the carbon number of the alkane. This was one of the first observations of alkane radical catins (see the list of UT).

Radical-Ions in Solution: Chemistry of radical ions has been expanded and deepened considerably by use of pulse radiolysis. Undoubtedly, Japanese scientists play a dominant role in this subject. Arai and his coworkers found that solute cations were produced efficiently in irradiated dichloroethane, acetone, and benzonitrile solutions of aromatic haydrocarbons. They confirmed the existence of equilibrium between monomer cation and dimer cation of aromatic hydrocarbons (see the list of RIKEN). The observation of the dimer cation of styrene radical cation, explained above, is a direct consequence of these studies. They also found that anion radicals of olefin derivatives. My own studies on the radical ions of PMMA, poly(4-vinylbiphenyl), and substituted polyacetylene are extensions of this methodology to polymers (see the list of HU).

Pulse Radiolysis Study Related to Organic Synthesis: The chemistry of radical-ions in Japan was advanced tremendously when a powerful 38 MeV LINAC which could produce 20 ps single pulse with 50 nC was constructed in the Radiation Laboratory in the Institute of Scientific and Industrial Research, Osaka University. Takamuku and his coworkers started from reactions of aromatic radical anions with halides. The simplest case is the reaction of naphthalene radical anions with alkyl halides where the well known dissociative electron transfer reaction takes place. It was the case for the radical anion of 4-alkylbiphenyl when the number of carbon in the alkyl group was less than two. But, when the chain length of the alkyl group was extended more than that, intramolecular S_N2 reaction took place instead and the spyrocyclic radical was formed. They also demonstrated many interesting reactions involving radical ion of organic compounds (see the list of OU).

Pulse radiolysis of Gaseous Systems: Gas phase pulse radiolysis has been conducted by the groups led by Arai (see the list of RIKEN and KIT), Hatano (see the list of TIT) and Shimamori (see the list of FIT). They have done excellent works on (1)deexcitation of excited rare gas atoms, (2)electron-ion recombination in gases, (3)electron thermalization and attachment in gases. Since there is no space left, I can only touch the experiment(3) carried out by Hatano and Shimamori. They measured the rate of thermal electron attachment to oxygen molecules by using microwave conductivity technique combined with the pulse radiolysis method. They found that the attachment rate for O_2-C_2H_4 mixtures showed a significant deviation from those obtained by simple mechanism. By their extensive works in collaboration with the group of Notre Dame, the mechanism involving electron attachment to van der Waals molecule is widely accepted now.

Reactions Related to Biological Systems: Pulse radiolysis has been successfully applied to biological systems by Kobayashi in Osaka University. The readers may find a significant number of his papers in the list of OU.

ACKNOWLEDGMENT

I would like to express my sincere thanks to following scientists for their sending me their publication lists, figures, brochures, and comments. Without their help I could not complete this article: Prof. Takashi Sumiyoshi, Hokkaido University; Prof. Hiromi Shibata, the University of Tokyo; Prof. Noriyuki Kouchi, Tokyo Institute of Technology; Prof. Tetsuo Miyazaki, Nagoya University; Prof. Hiroshi Shimamori, Fukui Institute of Technology; Prof. Shigeyoshi Arai, Kyoto Institute of Technology; Prof. Setsuo Takamuku, Osaka University; Prof. Yukio Yamamoto, Osaka University; Prof. Hideo Horii, University of Osaka Prefecture

LIST OF PUBLICATIONS

HOKKAIDO UNIVERSITY (HU)

Katayama M., Hatada M., Hirota K., Yamazaki H. and Ozawa H. (1965) Pulse radiolysis applied to polymerization reactions: The intermediate in the radiation-induced polymerization of -methylstyrene. Bull. Chem. Soc. Jpn. 38, 1965.

Katayama M. (1965) The transient absorption of irradiated α-methylstyrene. Bull. Chem. Soc. Jpn. 38, 2208.

Sumiyoshi T., Sawamura S., Koshikawa Y. and Katayama M. (1982) Transient species in picosecond pulse radiolysis of liquid carbon tetrachloride. Bull. Chem. Soc. Jpn. 55, 2341.

Sumiyoshi T., Miura N., Aikawa M. and Katayama M. (1982) Pulse radiolysis studies on methyl methylthiomethyl sulfoxide in aqueous solution. Bull. Chem. Soc. Jpn. 55, 2347.

Aikawa M., Sumiyoshi T., Miura N. and Katayama M. (1982) Dynamic studies on electron transport across micellar phase. Intermicellar migration of hydrated electrons. Bull. Chem. Soc. Jpn. 55, 2352.

Ogasawara M., Kajimoto N., Izumida T. Kotani K. and Yoshida H. (1985) Pulse radiolysis study of the electron-transfer reactions from aromatic radical anions to styrene and substituted styrene. J. Phys. Chem. 89, 1403.

Sumiyoshi T., Tsugaru K., Yamada T. and Katayama M. (1985) Yields of solvated electrons at 30 picoseconds in water and alcohols. Bull. Chem. Soc. Jpn. 58, 3073.

Yoshida H. and Ogasawara M. (1986) Application of the pulse radiolysis technique to reactions of organic radical ions. J. Raioanal. Nucl. Chem. Articles 101, 339.

Honda E., Tokuda M., Yoshida H., Ogasawara M. (1987) Fast reactions of organic anion radicals with organic halides in hexamethylphosphoric Triamide studied by pulse radiolysis. Bull. Chem. Soc. Jpn. 60, 851.

Ogasawara M., Tanaka M. and Yoshida H. (1987) Reaction of solvated electron with poly(methyl methacrylate) and substituted poly(methyl methacrylate) in hexamethylphosphoramide studied by pulse radiolysis. J. Phys. Chem. 91, 937.

Hagiwara H., Sawamura S., Sumiyoshi T. and Katayama.M. (1987) Pulse radiolysis study of transient species in LiCl-KCl melt. Radiat. Phys. Chem. 30, 141.

Tanaka M., Yoshida H. and Ogasawara M. (1988) Formation and reaction of polymer ions in solutions studied by pulse radiolysis. Radiat. Phys. Chem. 32, 719.

Sumiyoshi T., Katayama M. and Schnabel W. (1988) On the reduction of N-alkoxypyridinium ions. Bull. Chem. Soc. Jpn. 61, 1893.

Sumiyoshi T., Sugita N., Watanabe K. and Katayama M. (1988) Pulse radiolysis studies of solvent radical cations in liquid 1,2-dichloroethane. Bull. Chem. Soc. Jpn. 61, 3055.

Tanaka M., Yoshida H. and Ogasawara M. (1989) Ionic processes in pulse-irradiated fluid solutions of poly(4-vinylbiphenyl). Radiat. Phys. Chem. 34, 591.

Sumiyoshi T., Suzuki T., Katayama M. and Schnabel W. (1989) Energy transfer from excimers of aromatic compounds to acylphosphine oxide. Radiat. Phys. Chem. 34, 561.

Tanaka M., Ogasawara M. and Yoshida H. (1990) Ionic reactions of polymers in solution-generation and

characterization of ion radicals of polymers. Radiat. Phys. Chem. 36, 243.
Suzuki T., Imamura M., Sumiyoshi T., Katayama M. and Fujimoto M. (1990) One-electron-transfer reactions of molybdenum(V) and manganese(III) porphyrins with solvated electrons and solvent radicals in 2-methyltetrahydrofuran. Inorg. Chem. 29, 1123.
Sumiyoshi T., Watanabe K., Shogen S., Kawasaki M. and Katayama M. (1990) Formation mechanism of the complexes between DMSO and halogen atoms. II. Laser flash photolysis studies. Bull. Chem. Soc. Jpn. 63, 1584.
Sumiyoshi T. and Katayama M. (1990) Formation mechanism of the complexes between DMSO and halogen atoms. I. Pulse radiolysis studies. Bull. Chem. Soc. Jpn. 63, 1293.
Miki H., Nakajima A., Tamura M. and Ogasawara M. (1990) Reaction of metal-substituted myoglobins with excess electrons studied by pulse radiolysis and low-temperature gamma-radiolysis. Radiat. Phys. Chem. 36, 689.
Tanaka M., Yoshida H. and Ogasawara M. (1991) Intramolecular electron transfer in polymers with aromatic side groups as a stepping stone. J. Phys. Chem. 95, 955.
Yoshida H., Ogasawara M. and Tanaka M. (1992) Pulse radiolysis study on electron migration along polymer chain-ion radicals on poly(4-vinylbiphenyl-co-vinylpyrene). Radiat. Phys. Chem. 39, 35.
Ogasawara M., Suganuma T., Junke N., Yamaoka H. and Yoshida H. (1992) Localization and migration of excess electron in aromatic substituted polyacetylenes in solution. Radiat. Phys. Chem. 40, 111.
Sumiyoshi T. and Katayama M. (1992) Reactivity of the transient UV-band produced in irradiated liquid carbon tetrachloride with various alcohols. Bull. Chem. Soc. Jpn. 65, 1038.
Sumiyoshi T. and Katayama M. (1992) Reactivity of alcohols towards the chlorine atom in carbon tetrachloride. Trends in Phys. Chem., 7.
Sumiyoshi T., Sakai H., Kawasaki M. and Katayama M. (1992) Pulse radiolysis-laser flash photolysis studies of diphenyl sulfide in liquid halocarbons. Chem. Lett., 617.
Sumiyoshi T., Kawasaki M. and Katayama M. (1993) Photochemistry of diphenyl sulfide/halogen and mesitylene/halogen complexes in liquid halocarbons. Bull. Chem. Soc. Jpn. 66, 2510.
Imamura T., Sumiyoshi T., Takahashi K. and Sasaki Y. (1993) Radiolytic studies of ruthenium oxo-acetato trinuclear complexes in acetonitrile. J. Phys. Chem. 97, 7786.
Ogasawara M. (1993) Application of pulse radiolysis to the study of polymers and polymerizations(Ed. by Okamura S .). p 233, Springer-Verlag, Berlin Heiderberg.

UNIVERSITY OF OSAKA PREFECTURE (UOP)

Kawabata K., Horii H. and Okabe S. (1972) Optical absorption spectrum of trapped electron in crystalline ice at -150℃. Pulse radiolysis study. Chem. Phys. Lett. 14, 225.
Kawabata K., Okabe S. and Horii H. (1973) Radiation produced traps in crystalline ice. Chem. Phys. Lett. 20, 586.
Fujita S., Horii H. and Taniguchi S. (1973) Pulse radiolysis of mercuric ion in aqueous solution. J. Phys. Chem. 77, 2868.
Fujita S., Horii H., Mori T. and Taniguchi S. (1975) Pulse radiolysis of HgO in neutral aqueous solution. J. Phys. Chem. 79, 960.
Fujita S., Horii H., Mori T. and Taniguchi S. (1975) Pulse radiolysis of $Hg(CN)_2$ in aqueous solution. Bull. Chem. Soc. Jpn. 48, 3067.
Fujita S., Horii H., Mori T. and Taniguchi S. (1976) Pulse radiolysis of $HgBr_2$ in aqueous solution. Bull. Chem. Soc. Jpn. 49, 1250.
Fujita S., Horii H., Mori T. and Taniguchi S. (1976) An initial intermediate on pulsed electron irradiation of aqueous solutions of mercuric iodide. Chem. Lett., 865.
Horii H., Fujita S., Mori T. and Taniguchi S. (1976) Int. J. Radiat. Phys. Chem. 8, 521.
Fujita S., Horii S., Mori T. and Taniguchi S. (1977) New radioluminescence effects of aqueous HgI_2 solutions after high energy electron irradiation. J. Chem. Phys. 8, 521.
Fujita S., Horii H., Mori T. and Taniguchi S. (1978) Studies of emission species observed on pulse radiolysis of mercuric halides in aqueous system. J. Phys. Chem. 82, 1693.
Horii H., Fujita S., Mori T. and Taniguchi S. (1979) Formation of benzyl radicals by pulse radiolysis of benzyltriphenylphosphonium chloride in aqueous solutions. Bull. Chem. Soc. Jpn. 52, 3099.
Irie S., Horii H. and Irie M. (1980) Macromolecules 13, 1355.
Fujita S. and Steenken S. (1981) Pattern of OH radical addition to uracil and methyl- and carboxyl-substituted uracils. Electron tranfser of OH adducts with N, N., N', N''-tetramethyl-p-phenylenediamine and tetranitromethane. J. Amer. Chem. Soc. 103, 2540.
Fujita S. (1982) Radiolysis of uracil in N2O saturated aqueous solutions. Dose-rate effects of the pK value for the yield of consumption. Int. J. Radiat. Biol. 42, 205.
Horii H., Fujita S., Mori T. and Taniguchi S. (1982) Pulse radiolysis of aqueous solution of substituted phosphonium ions. Radiat. Phys. Chem. 19, 231.
Horii H., Abe Y., Taniguchi S., Maeda S. and Watanabe T. (1983) Absorption spectrum of the 2,3-dihydroxy-2-propanol(triose reductone) radical. Chem. Lett., 1313.
Fujita S. (1984) Radiolysis of nuclosides in aqueous solutions: Base liberation by the base attack mechanism. Int. J. Radiat. Biol. 45, 371.
Horii H., Abe Y. and Taniguchi S. (1986) Absorption spectrum of the aquaric acid radical. Chem. Express 1 83, 1986.
Horii H., Abe Y. and Taniguchi S. (1986) Pulse radiolysis study of reaction of OH radicals with triose reductone. Bull. Chem. Soc. Jpn. 59, 721.
Horii H. and Taniguchi S. (1986) Oxidation intermediates of borohydride and tetraphenylborate ion in aqueous solutions by pulse radiolysis. J. Chem. Soc., Chem. Communn., 915.
Fujita S. and Negata Y. (1988) Pulse radiolytic studies of radicals produced from methylated uracils via oxidation by SO_4^-. Radiat. Res. 114, 207.
Fujita S., Nagata Y. and Dohmaru T. (1988) radicals produced by the reactions of SO_4^- with uridine and its derivatives. Studied by pulse radiolysis and γ -radiolysis. Int. J. Radiat. Biol. 54, 417.
Nakata K., Horii H. and Morita N. (1993) Detection of oxidation radicals of 2,3-dioxyoguluno-δ -lactone by pulse radiolysis. J. Chem. Soc., Chem. Commun., 1172.
Horii H., Nakata K., Yamamoto I., Akiba M. and Morita N. (1993) Oxidation intermediates of L-ascorbic acid 2-glucoside by pulse radiolysis. Bioelectrochemistry and Bioenergetics 32, 277.

INSTITUTE OF PHYSICAL AND CHEMICAL RESEARCH (RIKEN)

Arai S., Kira, A. and Imamura, M. (1970) Pulse radiolysis studies of deaerated alcoholic solutions of alkali halides and pottassium hydroxide. J. Phys. Chem. 74, 2102.
Kira A., Arai S. and Imamura M. (1971) Pyrene dimer cation as studied by pulse radiolysis. J. Chem. Phys. 54, 4890.
Arai S., Kira A. and Imamura M. (1971) Pulse radiolysis studies of acetone solutions of biphenyl and anthracene: Formation of ions and excited singlet state. J. Chem. Phys. 54, 5073.

Arai S., Kira A. and Imamura M. (1972) Thermodynamic constants and rate constants of the formation of the pyrene dimer cation. J. Chem. Phys. 56, 1972.

Kira A., Arai S. and Imamura M. (1972) Pulse radiolysis study of dimer cation formation of aromatic hydrocarbons in benzonitrile solution. J. Phys. Chem. 76, 1119.

Tagawa S., Arai, S. Kira A and Imamura M. (1972) Pulse radiolysis study of polymerization of vinylcarbazole in benzonitrile solutions. J. Polym. Sci. Polym. Lett. Ed. 10, 295.

Kira A., Arai S. and Imamura M. (1973) A pulse radiolysis study of the formation of trans-stilbene ions in organic solvents. Int. J. Radiat. Phys. Chem. 5, 127.

Seki H., Arai S., Shida T. and Imamura M. (1973) Transient absorption spectra of the chlorophyll a anion and cation. J. Amer. Chem. Soc. 95, 3404.

Arai S., Tagawa S. and Imamura M. (1974) Low-temperature pulse radiolysis. I. Negative ions of halogenated compounds. J. Phys. Chem. 78, 519.

Tagawa S., Arai S., Imamura M. and Tabata Y. (1974) Polymerization and dimerization of vinylcarbazole. II. Relation between reactive intermediates and final products in irradiated benzonitrile solutions. Macromolecules 7, 262.

Hoshino M., Arai S. and Imamura M. (1974) Low-temperature pulse radiolysis. II. Time-dependent spectra of anions of aromatic ketones. J. Phys. Chem. 78, 1473.

Hoshino M., Arai S., Imamura M. and Namiki A. (1974) Absorption spectra of anions aromatic ketones in ethanol glasses at 4.2 K. Chem. Phys. lett. 26, 582.

Tagawa S., Tabata Y., Arai S. and Imamura M. (1974) Solvent effects on both transient optical specra and products in radiation-induced polymerization and dimerization of vinylcarbazole. J. Polym. Sci. Polym. Lett. Ed. 12, 545.

Arai S., Hoshino M. and Imamura M. (1975) Low-temperature pulse radiolysis. III. Ionic species produced from aliphatic ketones. J. Phys. Chem. 79, 702.

Arai S. , Kira A. and Imamura M. (1976) Mechanism of the formation of cationic species in the radiolysis of butyl chlorides. 1. J. Phys.Chem. 80, 1968.

Hoshino M., Arai S. and Imamura M. (1976) J. Phys. Chem. 80, 2724.

Arai S., Kira A. and Imamura M. (1977) Low-temperature pulse radiolysis and α -irradiated matrix studies of dimer anions of olefin derivatives. J. Phys. Chem. 81, 110.

Egusa S., Arai S., Kira A., Imamura M. and Tabata Y. (1977) Cationic polymerization of styrene by means of pulse radiolysis. Radiat. Phys. Chem. 9, 419.

Arai S., Oka T., Kogoma M. and Imamura M. (1978) Near Infrared absorption of neon, argon, krypton, and xenon. J. Phys. Chem. 68, 4595.

Egusa S., Tabata Y., Arai S., Kira A. and Imamura M. (1978) Pulse radiolysis study on the initial processes of radiation-induced cationic polymerization of styrene and γ -methylstyrene. J. Polym. Sci. Polym. Chem. Ed. 16, 729.

Arai S. and Imamura M. (1979) Mechanism of the formation of cationic species in the radiolysis of butyl chlorides. 2. J. Phys. Chem. 83, 337.

Oka T., Kogoma M., Imamura M. and Arai S. (1979) Energy transfer of argon excited diatomic molecules. J. Chem. Phys. 70, 3384 (1979).

Ogasawara M., Arai S. and Imamura M. (1979) Radiation-induced polymeriazation of nitroethylene as studied by low-temperature pulse radiolysis. J. Polym. Sci. Polym. Lett. Ed. 17, 649.

Hoshino M., Arai S. and Imamura M. (1980) Electron transfer from 2-methyltetrahydrofuran radical to tetracyanoethylene at low temperature. Radiat. Phys. Chem. 15, 377.

Takao S., Kogoma M., Oka M., Imamura M. and Arai S. (1980) Optical absorption spectra and kinetic behavior of helium excited diatomic molecule (a $^3\Sigma_u^+$). J. Chem. Phys. 73, 148 (1980).

Hoshino M., Arai S., Imamura M., Ikehara K. and Hama Y. (1980) Mechanism of benzophenone ketyl radical formation in acid alcohols studied by pulse-radiolysis and rigid-matrix technique. J. Phys. Chem. 84, 2576.

Doba T. and Arai S. (1981) Reaction cross section of helium. J. Chem. Phys. 75, 488.

Kasama K., Oka T., Arai S., Kurusu H. and Hama Y. (1982) Near-infrared absorption bands and kinetic behavior of rare gas excited diatomic molecules. J. Phys. Chem. 86, 2035.

Ito Y. and Arai S. (1984) Kinetic study of excited diatomic molecules of krypton and xenon. Bull. Chem. Soc. Jpn. 57, 3062.

NAGOYA UNIVERSITY (NU)

Kato N., Miyazaki T., Kawai Y. and Fueki K. (1984) Temperature effect on decay of ions and radicals in supercooled liquids as studied by pulse radiolysis and γ -radiolysis: 1-propanol and ethanol. Bull. Chem. Soc. Jpn. 57, 3052.

Kato N., Miyazaki T., Fueki K., Miyata S. and Kawai Y. (1984) Temperature effect on decay of ions in viscous liquids as studied by pulse radiolysis and γ -radiolysis at 88-230 K. 2-methytetrahydrofuran and methylcyclohexane-2- methylbutane. J. Phys. Chem. 88, 1445.

Matsushima M., Kato N., Miyazaki T. and Fueki K. (1987) Formation and reactions of poly(4-vinylbiphenyl) anions in pulse radiolysis and γ -radiolysis: Comparison of their kinetic behavior with that of biphenyl anion. Radiat. Phys. Chem. 29, 231.

Kato N., Miyazaki T., Fueki K. and Saito A. (1988) Pulse radiolysis study of formation of poly(4-vinylbiphenyl) anions in 2-methyltetrahydrofuran solution at 100-120 K. Int. J. Chem. Kinetics 20, 877.

Kato N., Miyazaki T., Fueki K., Yokoi T. and Kitano T. (1989) Pulse radiolysis study on electron-transfer reactions in polymer solutions at low temperature. Macromolecules 22, 4124.

Miyazaki T., Shiba T., Fueki K. and Kamiya Y. (1991) Isotope and temperature effects on the reaction of proton transfer to benzene anions in ethanol at very low temperatures. A tunneling reaction. J. Phys. Chem. 95, 9115.

Miyazaki T., Kamiya Y., Fueki K. and Yasui M. (1992) New band of emission from high-energy-electron-irradiated ice at very low temperarure. J. Phys. Chem. 96, 9558.

Miyazaki T., Nagasaka S., Kamiya Y. and Tanimura K. (1993) Formation of excited OH radicals in high-energy-electron-irradiated ice at very low temperature. J. Phys. Chem. 97, 10715.

TOKYO INSTITUTE OF TECHNOLOGY (TIT)

Shimamori H. and Hatano Y. (1976) Thermal electron attachment to O_2 in H_2 and D_2. Chem. Phys. Lett. 38, 242.

Ueno T. and Hatano Y. (1976) Measurement of the rate constant of the penning ionization of nitrogen by helium metastable states as studied by pulse radiolysis. Chem. Phys. Lett. 40, 283.

Shmamori H. and Hatano Y. (1976) Mechanism of thermal electron attachment in O_2-N_2 mixtures. Chem. Phys. 12, 439.

Shimamori H. and Hatano Y. (1977) Thermal electron attachment to O_2 in the presence of various compounds as studied by microwave cavity technique combined with pulse radiolysis. Chem. Phys. 21, 187.

Ueno T., Kouchi N., Takao S., and Hatano Y. (1978) Pulse radiolysis studies of the lowest triplet state of benzene in

the gas phase. J. Phys. Chem. 82, 2373.
Kokaku Y., Toriumu M. and Hatano Y.(1980) Effect of van der Waals molecules on thermal electron attachment in some O_2-hydrocaron mixtures. J. Chem. Phys. 73, 6167.
Ueno T., Yokoyama A., Takao S. and Hatano Y. (1980) De-excitation rate constants of He(2^3S) by atoms and molecules as studied by the pulse radiolysis method. Chem. Phys. 45, 261.
Yokoyama A., Takao S., Ueno T. and Hatano Y. (1980) Measurements of de-excitaion rate constants of Ne($^3P_2$, $^3P_0$ nd $^3P_1$) by N_2 and SF_6 using pulse radiolysis method. Chem. Phys. 45, 439.
Yokoyama A. and Hatano Y. (1981) De-excitaion rate constants of Ne($^3P_2$, $^3P_1$ and $^3P_0$) by atoms and molecules as studied by the pulse radiolysis method. Chem. Phys. 63, 59.
Hatano Y. and Shimamori H. (1981) Electron attachment in dense fluid gases. Electron and Ion Swarms (Ed. by Cristophorou L. G.) p. 103. Pergamon Press, New York.
Hatano Y. and Kimizuka Y. (1982) Direct observation of penning electrons by pulse radiolysis-microwave cavity technique. Radiat. Phys. Chem.19, 255.
Toriumi M. and Hatano Y. (1983) Thermal electron attachment to van der Waals molecules(O_2, C_2H_6). J. Chem. Phys. 79, 3749.
Nakamura Y., Shinsaka K. and Yoshihiko H. (1983) Electron mobilities and electron-ion recombination rate constants in solid, liquid, and gaseous methane. J. Chem. Phys. 78, 5820.
Toriumi M. and Hatano Y. (1984) Thermal electron attachment to van der Waals molecules (O_2.C_2H_4). J. Chem. Phys. 81, 3748.
Toriumi M. and Hatano Y. (1985) Thermal electron attachment to van der Waala molecules (O_2N_2). J. Chem. Phys. 82, 254.
Ukai M., Tanaka Y., Koizumi H., Shinsaka K. and Hatano Y. (1986) Temperature dependence of the rate constants for deexcitation of He(2_1P) by SF_6 and Ar. J. Chem. Phys. 84, 5575.
Suzuki E. and Hatano Y. (1986) Electron thermalization processes in a He-Kr bicomponent systems and a Ne pure system. J. Chem. Phys. 85, 5341.
Ukai M., Koizumi H., Shinsaka K. and Hatano Y. (1986) Temperature dependence of the rate constants for deexcitation of Ar($^1P_1$) and Ar($^3P_1$) by SF_6 and N_2. J. Chem. Phys. 84, 3199.
Suziki E. and Hatano Y. (1986) Electron thermalization processes in rare gases with the Ramsuer minimum. J. Chem. Phys. 84, 4915.
Koizumi H., Ukai M., Tanaka Y., Shinsaka K. and Hatano Y. (1986) Temperarue dependence of the deexcitation of He (2^3S) by atoms and molecules as studied by pulse radiolysis method. J. Chem. Phys. 85, 1931.
Shinsaka K., Codama M., Srithanaratana, Yamamoto M. and Hatano Y. (1988) Electron-ion recombination rate constants in gasesous, liquid, and solid argon. J. Chem. Phys. 88, 7529.
Ukai M., Nakazawa H., Shinsaka K. and Hatano Y. (1988) Deexcitation cross section of He(2^1P) by atoms and molecules. J. Chem. Phys. 88, 3623.

UNIVERSITY OF TOKYO (UT)

Tabata Y. (1976) Study on cationic polymerization by means of pulse radiolyis. J. Polym. Sci. Symposium No. 56. 409.
Wahio M., Tagawa S. and Tabata Y. (1980) Direct observation of the kinetic behavior of a charge-transfer reaction on the cation-scavenging reaction for cation radical of N-vinylcarbazole and N-ethylcarbazole by using a pulse radiolysis technique. J. Phys. Chem. 84, 2876.
Tagawa S., Schnabel W., Washio M. and Tabata Y. (1981) Picosecond pulse radiolysis studies on polymer degradation of polystyrene and poly-α-methylstyrene. 18, 1087.
Washio M., Tagawa S. and Tabata Y. (1983) Pulse radiolysis of polystyrene and benzene in cyclohexane, chloroform and carbon tetrachloride. Radiat. Phys. Chem. 21, 239.
Itagaki H., Horie K., Mita I., Wahio M., Tagawa S. and Tabata Y. (1983) Intermolecular excimer formation of oligostyrene from dimer to tridecamer; The measurements of rate constants for excimer formation, singlet energy migration, and relaxation of internal rotation. J. Chem. Phys. 79, 1983.
Tagawa S., Washio M., Kobayashi H., Katsumura Y. and Tabata Y. (1983) Picosecond pulse radiolysis studies on geminate ion recombination in saturated hydrocarbon. Radiat. Phys. Chem. 21, 45.
Kobayashi H., Ueda T., Kobayashi T., Washio M., Tabata Y. and Tagawa S. (1983) Picosecond single electron pulse for pulse radiolysis studies. Radiat. Phys. Chem. 21, 13.
Tagawa S., Nakashima N., Yoshihara K. (1984) Absorption spectrum of the triplet state and the dynamics of intramolecular motion of polystyrene. Macromolecules 17, 1167.
Kawanishi S., Hagiwara M., Katsumura Y., Tabata Y. and Tagawa S. (1985) Effect of aromatic additives on the radiation resistance of ethylene-propylene-diene-terpolymer studied by optical emission spectroscopy of both steady-state and picosecond pulse radiolysis. Radiat. Phys. Chem. 26, 705.
Tagawa S., Washio M., Hayashi N. and Tabata Y. (1985) Pulse radiolysis studies on radiation resistance of epoxy resin. J. Nucl. Mat. 133 & 134, 785.
Tabata Y., Tagawa S., Washio M. and Hayashi N. (1985) Study on sensitized degradation and crosslinking of polymers by means of picosecond pulse radiolysis. Radiat. Phys. Chem. 25, 305.
Itagagi H., Horie K., Mita I., Washio M., Tagawa S., Tabata Y., Sato H. and Tanaka Y. (1985) Multicomponent fluorescence decay and molecular motion of diastereoisomeric styrene dimers on pico- and nano-second timescales. Chem. Phys. Lett. 120, 547.
Tagawa S. (1986) Pulse radiolysis and laser photolysis studies on radiation resistance and sensitivity of polystyrene and related polymers. Radiat. Phys. Chem.. 27, 455.
Itagaki H., Horie K., Mita I., Washio M., Tagawa S., Tabata Y., Sato H. and Tanaka Y. (1987) Local molecular motion of polystyrene model compounds measured by using picosecond pulse radiolysis. 1. Diastereoisomeric styrene dimers; Multicomponent Fluorescence decay curves, concentration dependence, and alkyl end-group effect on excimer formation. Macromolecules 20, 2774.
Aoki Y., Kouchi N., Shibata H., Tagawa S. and Tabata Y. (1988) Radiation effects of ion beams on polystyrene resist films. Nucl. Inst. Methods Phys. Res. B 33, 799.
Kouchi N., Tagawa S., Kobayashi H. and Tabata Y. (1989) New ion accelerator facility for the study of radiation effects and radiation chemistry at the University of Tokyo. Radiat. Phys. Chem. 34, 453.
Kouchi N., Aoki Y., Shibata H., Tagawa S., Kobayashi H. and Tabata Y. (1989) Pulsing of MeV ion beams and its application to ion beam pulse radiolysis studies of polystyrene thin films. Radiat. Phys. Chem. 34, 759.
Shibata H. and Tagawa S. (1991) Radiation effects of high energy ion beams on plystyrene-emission spectra. J. Photopolymer Sci. Tech. 4, 169.
Shibata H., Yoshida Y., Tagawa S., Aoki Y. and Namba H. (1993) Ion beam pulse radiolysis studies on liquid scintillators. Nucl. Inst. Methods Phys. Res. A327, 53.

Krushev V. V., Koizumi H., Ichikawa T., Yoshida H., Shibata H., Tagawa S. and Yoshida Y. (1994) Relation between track structure and LET effect on free radical formation for ion beam-irradiated alanine dosimeter. Radiat. Phys. Chem. 44, 521.

OSAKA UNIVERSITY (OU)

Mah S., Yamamoto Y. and Hayashi K. (1984) Primary processes of the radiation-induced cationic polymerization of α -methylstyrene enhanced by triphenylsulfonium haxafluorophosphate. Radiat. Phys. Chem. 23, 137.

Yamamoto Y., Nishida S., Yabe K., Hayashi K., Takeda S. and Tsumori K. (1984) Effects of quarternary ammonium salts on reactions of aromatic radical anions formed in tetrahydrofuran by pule radiolysis. J. Phys. Chem. 88, 2368.

Shimizu N., Kobayashi K. and Hayashi K. (1984) The reaction of superoxide radical with catalase. J. Biol. Chem. 259, 4414.

Ishida A, Toki S. and Takamuku S. (1986) Electron-transfer reactions induced by ionizing radiation and photoionization : Its application for organic synthesis. Mem. Inst. Sci. Ind. Res., Osaka Univ. 43, 47.

Nakabayashi K., Toki S. and Takamuku S. (1986) Triplet states of cyclic olefins and dienes. On the lifetime and chemical reactivities studied by pulse radiolysis. Chem. Lett. 1889.

Hayashi K. (1986) Application of radiation technology in biomedical materials; Fundamentals and Applied. Radiat. Phys. Chem. 27, 317.

Yamamoto Y. and Hayashi K. (1986) Promotion of radiation-induced cationic polymerization by onium salts. Mem. Inst. Sci. Ind. Res., Osaka Univ. 43, 69.

Yamamoto Y., Nishida S. Ma X-. H. and Hayashi K. (1986) Pulse radiolysis of trans-stilbene in tetrahydrofuran. Spectral shift snd decay kinetics of the radical anions in the presence of quarternary ammonium salts. J. Phys. Chem. 90, 1921.

Kobayashi K., Shimizu N. and Hayashi K. (1986) The reactions of superoxide radical with catalase. Superoxide and Superoxide Dismutase in Chemistry, Biology and Medicine., 228.

Kimura N. and Takamuku S. (1986) Solvent effects on the unimolecular dissociation of radical anions studied by pulse radiolysis. Bull. Chem. Soc. Jpn. 59, 3653.

Kimura N. and Takamuku S. (1987) One-electron reduction of aromatic halides and the solvent effects on the unimolecular dissociation of the radical anion. Radiat. Phys. Chem. 29, 179.

Yamamoto Y., Nishida S. and Hayashi K. (1987) Pulse radiolysis study of salt effects on reactions of aromatic radical cations with Cl⁻. Rate constants in the absence and presence of quarternary ammonium salts. J. Chem. Soc., Faraday Trans. I 83, 1795.

Yamamoto Y., Ma X-. H. and Hayashi K. (1987) Pulse radiolysis study of the formation of aromatic radical cations enhanced by diphenyliodonium salts. J. Phys. Chem. 91, 5343.

Ma X-. H., Yamamoto Y. and Hayashi K. (1987) Radiation-induced cationic polymerization of tetrahydrofuran by diphenyliodonium and triphenyl-sulfonium hexafluorophosphates. Macromolecules 20, 2703.

Kobayashi K., Amano M., Kanbara Y. and Hayashi K. (1987) One-electron reduction of the oxyform of 2,4-diacetyldeuteroheme P-450cam. J. Biol. Chem. 262, 5445.

Mizuno K. and Otsuji Y. (1988) Cis-trans isomerization of 1,2-bis(4-methoxyphenyl) cyclopropanes via a cationic chain mechanism. Chem. Lett., 433

Ishida A., Yamashita S. and Takamuku S. (1988) Hydroxyalkylation and lactone formation from dialkyl malonate by a Eu^{III}/Eu^{II} photoredox system. Bull. Chem. Soc. Jpn. 61, 2229.

Kobayashi K., Iyanagi T., Ohara H. and Hayashi K. (1988) One electron reduction of hepatic NADH-cytochrome b_5 reductase from pig liver microsome. J. Biol. Chem. 263, 7493.

Shimizu N., Kobayashi K. and Hayashi K. (1988) Studies on the equilibria and kinetics of the reactions of ferrous calalase with ligands. J. Biochem. 104, 136.

Chikai Y., Yamamoto Y. and Hayashi K. (1988) A pulse radiolysis study of the formation of dimer radical cations of aromatic olefins. Bull. Chem. Soc. Jpn. 61, 2281.

Yamamoto Y., Aoyama T. and Hayashi K. (1988) Pulse radiolysis study of salts effects on reactions of aromatic radical cations with Cl. Part 2. Spectral shifts and decay kinetics of diphenylpolyene radical cations in the presence of tetrabutylammonium hexafluorophosphate. J. Chem. Soc., Faraday Trans. I 84, 2209.

Shimizu N., kobayashi K. and Hayashi K. (1989) Kinetics of the reaction of superoxide anion with ferric horseradish peroxidase. Biochim. Biophy. Acta 995, 133.

Kobayashi K., Une H. and Hayashi K. (1989) Electron transfer process in cytochrome oxidase after pulse radiolysis. J. Biol. Chem. 264, 7976.

Ishida A. and Takamuku S. (1989) Progress of reaction systems by use of high energy electron beam. J. High-Temp. Soc. 15, 248.

Aoyama T., Yamamoto Y. and Hayashi K. (1989) A pulse radiolysis study of ion pairing of diphenylpolyene radical anions with tetrabutyl-ammonium and sodium cations in tetrahydrofuran. J. Chem. Soc., Faraday Trans. I 85, 3353.

Kobayashi K., Hayashi K. and Sono M. (1989) Effects of tryptophan and pH on the kinetics of superoxide radical binding to indoleamine 2,3-dioxygenase studied by pulse radiolysis. J. Biomol. Chem. 264, 15280.

Kobayashi K., Hayashi H. and Swallow J. (1990) Reaction of the NAD radical with higher oxidation states of horseradish peroxidase. Biochemistry 29, 2080.

Teramoto M., Yamamoto Y. and Hayashi K. (1990) Effect of triphenylmethane on the radiation-induced cationic polymerization by diphenyliodonium hexafluorophosphate in dichloromethane. J. Polm. Sci. Polym. Lett. Ed. 28, 253.

Gao D., Yamamoto Y. and Hayashi K. (1990) Effects of cyclodextrins on the radiation-induced polymerization of sodium p-styreneshulphonate in aqueous solution. J. Chem. Soc. Chem. Commun. 910.

Kobayashi K., Amano M. and Hayashi K. (1990) One electron reduction of the oxforma of cobalt substituted hemoprotein. Biochim. Biophys. Acta 1037, 297.

Kobayashi K. and Hayashi K. (1990) Reduction of the oxyform in hemoproteins to the ferry forms. J. Amer. Chem. Soc. 112, 6051.

Tojo S., Toki S. and Takamuku S. (1991)Acyclic 1,4-radical cations. Direct observation and stability. J. Org. Chem. 56, 6240.

Takamuku S. and Yamamoto Y. (1991) Pulse radiolysis study related to organic synthesis. Pulse radiolysis. 431.

Ishida A., Ito H. and Takamuku S. (1991) Reaction of syn-and anti-benzylideneaniline radical anions. Chem. Lett. 1537.

Naito I., Morihara H., Ishida A., Takamuku S., Isomura K. and Taniguchi H. (1991) Photochemistry of 2H-azirine-formation of nitrile ylide evidenced by laser flash photolysis and pulse radiolysis. Bull. Chem. Soc. Jpn. 64, 2757.

Yamamoto S., Yamamoto Y. and Hayashi K. (1991) Ion pairig

of radical ions studied by pulse radiolysis. Bull. Chem. Soc. Jpn. 64, 346.
Nakabayashi K., Fukumoto W., Yasuda M., Shima K. and Takamuku S. (1992) Cycloreversion of 1,4-diphenylbicyclo [3.2.0]hpt-2-ene via triplet state. Evidencefor adiabatic process on the triplet surface. Chem. Lett. 803.
Kimura N. and Takamuku S. (1992) Competitive intramolecular electron transfer and SN_2 reactions of radical anions. Effects of solvent polarity on the reaction mechanism. Bull. Chem. Soc. Jpn. 65, 1668.
Kobayashi K., Harada Y. and Hayashi K. (1992) Kinetic behavior of monodehydroascorbate radical studied by pulse radiolysis. Biochemistry 30, 8310.
Tojo S., Toki S. and Takamuku S. (1992) Formation and reactivity of dimer radical cations of 4-methoxystyrene. Radiat. Phys. Chem. 40, 95.
Ishida A., Sugita D. and Takamuku S. (1992) Photoinduced formation and reaction of benzalaniline radical anions-comparison with the radiation induced reactions. J. Photochem. Photobiol., A Photochem. 65, 197.
Ishida A., Naito I. and Takamuku S. (1992) Radical anion of nitrile ylide by dual beam irradiation of 3-(4-biphenylyl)-2H-azirine at low temperature. Chem. Lett., 1913.
Ishida A., Yamamoto K. and Takamuku S. (1992) Electron-laser dual beam irradiation of 2-methylbenzophenone. Bull. Chem. Soc. Jpn. 65, 3186.
Yamamoto Y., Shiraki S. and kawamura Y. (1992) Effects of cyclodextrin complexation on one0electron reduction and electron transfer of aromatic sulfonates. J. Chem. Soc., Perkin Trans. 2, 2241.
Yamamoto Y. (1992) Ion pairing of radical ions studied by pulse radiolysis. Trends in organic chemistry 3, 93.
Ishida A. and Takamuku S. (1993) Hydroxymethylation via radical intermediates. The Chemistry of Functolond Groups Supp. E., p. 657. John Wiley & Sons Ltd., London.
Tamai S., Mizuno K., Hashida T., Otsuji Y., Ishida A. and Takamuku S. (1994) Properties of radical cations generated by the pulse radiolysis of 1,ω -bis(diarylethenyl)alkanes. Trapping of distonic 1,4-radical cations by molecular dioxygen. Chem. Lett., 149.
Ito S., Hirano K., Furuta A., Komatsu M., Ohshiro Y., Ishida A., Takamuku S.. Kohzuma T., Nakamura N. and Suzuki S. (1993) Physicochemical properties of 2,2'methylthio-4-methlphenol. A model compound of the novel co-factor of galactose oxidase. Chem. Lett., 2099.
Nakabayashi K., Tahara Y., Yasuda M., Shima K. and Takamuku S. (1993) Cycloreversion of aryl-substituted cyclobutene by direct photolysis and pulse radiolysis. Bull. Chem. Soc. Jpn. 66, 698.
Kimura N. and Takamuku S. (1994) Mechanistic evaluation of dissociative electron transfer and nucleophilic substitution reactions. J. Amer. Chem. Soc. 116, 4087.
Yamamoto Y. (1993) Pulse radiolysis of onium salts and radiation-induced cationic polymarization. Radiation Curing in Polymer Science and Technology, Vol. II (Ed. by Fouassier J. P. and Rabek J. F.), p. 555. Elsevier, London.
Kobayashi K., Miki M. and Nishino T. (1993) Electron transfer process in milk xantine dehydrogenase as studied pulse radiolysis. J. Biol. Chem. 268, 24642.
Kobayashi K., Iwamoto T. and Honda K. (1994) Biochem. Biophys. Res. Communn. 201, 1348.
Kobayashi K. and Miki M. (1994) A direct demonstration of reaction of nitric oxide with superoxide anion by the use of pulse radiolysis. Frontiers of Reactive oxygen species in biology and medicine (Ed. by Asada K. and Yoshikawa T.), p. 223. Elsevier, Amsterdam.
Abe Y., Amuro N., Nishino T., Okazaki T. and Kobayashi K. (1994) The role of arginine-173 of rat manganese-superoxide dismutase studied by site-directed mutagenesis. Frontiers of Reactive oxygen species in biology and medicine (Ed. by Asada K. and Yoshikawa T.), p. 135. Elsevier, Amsterdam.
Yamakura F., Matsumoto T. and Kobayashi K. (1994) Analysis of the metal specific activity of Mn- and Fe-superoxide dismutase by using the Fe- and Mn-substituted enzymes. Frontiers of Reactive oxygen species in biology and medicine (Ed. by Asada K. and Yoshikawa T.), p. 115. Elsevier, Amsterdam.

FUKUI INSTITUTE OF TECHNOLOGY (FIT)

Shimamori H. and Hotta H. (1983) Mechanism of thermal electron attachment to O_2 as studied by observing isotope effects of attachment rates for $^{18}O_2$ systems. J. Chem. Phys. 78, 1318.
Shimamori H. and Hotta H. (1984) Mechanism of thermal electron attachment to O_2: Isotope effect studies of $^{18}O_2$ in rare gases and some hydrocarbons. J. Chem. Phys. 81, 1271.
Shimamori H. and Hotta H. (1986) Mechanism of thermal electron attachment to NO_2. J. Chem. Phys. 84, 3195.
Shimamori H. and Hotta H. (1986) Examination of the effects of van der Waals molecules on the thermal electron attachment to NO_2 at relatively high pressures. J. Chem. Phys. 85, 887.
Shimamori H. and Hotta H. (1986) Temperature dependence of electron attachment to NO_2. J. Chem. Phys. 85, 4480.
Shimamori H. and Hotta H. (1988) Thermal electron attachment to NO. I. The mechanism and the three-body rate constants. J. Chem. Phys. 89, 2938.
Shimamori H. and Nakatani Y. (1988) Rate constants for thermal electron attachment to CF_3I,CH_3I, C_2H_5I, 1-C_3H_7I, and 2-C_3H_7I determined between 250 and 350 K. Chem. Phys. Lett. 150, 109.
Shimamori H., Nakatani Y. and Hotta H. (1989) Thermal electron attachment to NO. II. Temperature dependence and implication of attachment to van der Waals molecules. J. Chem. Phys. 90, 232.
Shimamori H., Suzuki E., Hatano Y., Nonaka H., Ohshima Y., Kondow T. and Kchitsu K. (1989) Thermal electron attachment to carbon suboxide. J. Chem. Phys. 91, 4148.
Shimamori H. and Nakatani Y. (1992) Mechanism of thermal electron attachment to SO_2. J. Chem. Phys. 96, 1967.
Shimamori H., Tatsumi Y., Ogawa Y. and Sunagawa T. (1992) Electron-energy dependence of electron attachment to c-C_7F_{14}, CH_3I and CH_2Br_2 studied by the pulse-radiolysis microwave-cavity technique combined with microwave heating. Chem. Phys. Lett. 194, 223.
Shimamori H., Tatsumi Y., Ogawa Y. and Suganuma T. (1992) Low-energy electron attachment to molecules studied with microwave heating. J. Chem. Phys. 97, 6335.
Shimamori H., Tatsumi Y. and Sunagawa T. (1993) Thermal electron attachment to C_6F_5X and C_6H_5X(X=I, Cl, and F). *J. Chem. Phys.* 99, 7787.
Shimamori H., Sunagawa T., Ogawa Y. and Tatsumi Y. (1994) Low-energy electron attachment to C_6F_5X(X=f, Cl, Br, and I). Phys. Lett. 227, 609.

KYOTO INSTITUTE OF TECHNOLOGY (KIT)

Mori T., Kanou K., Ishikawa Y. and Arai S. (1992) Formation of highly excited oxygen atoms O($2p^3 3s$, ^5P) in electron irradiation of mixtures of rare gases nd O2. J. Chem. Phys. 96, 8258.
Mori T., Kanou K., Mizuta K., Kuramasu T., Ishikawa Y. and Arai S. J. Chem. Phys. 97, 9094.
Mizuta K., Kuramasu T., Ishikawa Y. and Arai S. (1994) Quenching rate constants of excited halogen atoms in quartet states. J. Chem. Phys. 100, 4876.

2.6 EB Processing at Tsukuba EB Center

Yutaka Yamase, Yasuyuki Aikawa, Toyoaki Inamura
Tsukuba Electron Beam Center, Sumitomo Heavy Industries, Ltd.

1. Introduction

Since opening of EB Center in June 1989 at Tsukuba we have accumulated rich experiences on electron beam process for various products.

Based on this 5 years experience we would like to introduce the latest development we have reached in electron beam processing.

Now we are confident ourselves that this technology is useful in various field of applications. Main fields we are processing are 1) plastics 2) wafers and 3) sterilization.

2. Outline of EB Center

Our center is located western part of Tsukuba City, 50km north east of Tokyo. Size of plant site and main facilities are as shown below. In Fig 1, 2 and 3 plant layout and pictures are shown.

Site Area	11,000 m^2
Plant Area	2,000 m^2
Accelerator	1-5 MeV x 40mA Dynamitron
Handling System:	Cart Conveyor (maximum 24 carts)
	Sheet Handling System

As for ozone treatment the Center is equipped with both catalysis and absorption system to reduce ozone condensation.

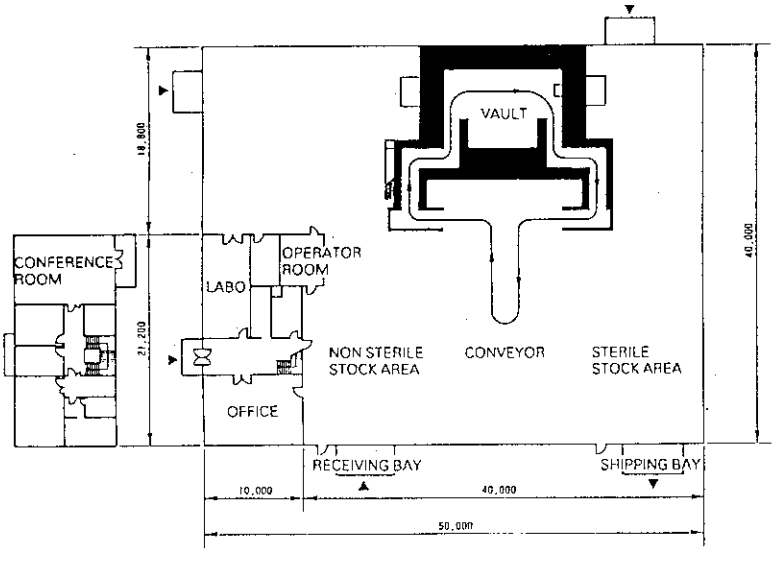


Fig 1. Plant Layout

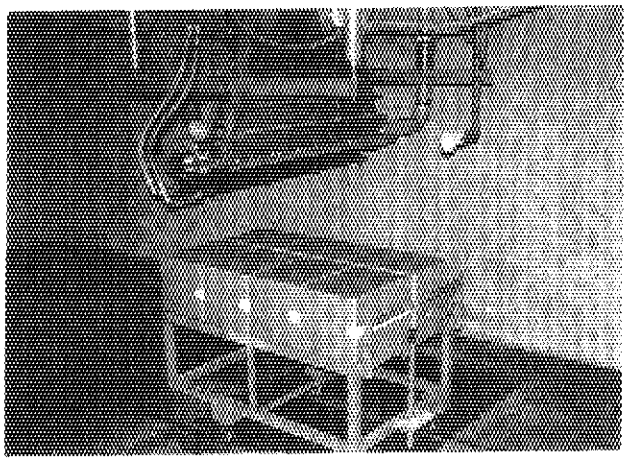


Fig 2. Cart passing under scan horn

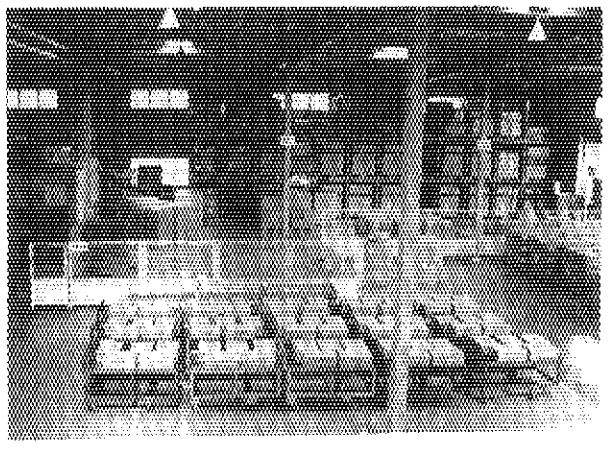


Fig 3. Stock area

3. Details of Processed Products

1) Industrial Materials

(1) Plastics

We are processing many field of plastic materials but followings are two major products:

-1) PE Sheets

Cross linked PE Sheets are used mainly to produce sealing tapes for petroleum pipe lines. Chart of dosage versus gelation ration is shown in Fig 4. Normal dosage to apply is around 100 KGy.

-2) PTFE Degradation

PTFE is the material widely used in various industrial fields for its excellent characteristics such as high heat resistibility, good non-adhesivity and corrosion resistibility.
When applying as a chemical additives it has to be grounded to fine powder.

By applying EB irradiation grinding characteristics of PTFE is improved remarkably and to produce fine powder of under 10 μm diameter can be produced easily. In Fig 5 relation between mean particle diameter versus dosage is shown.

(2) Silicon Wafers

Electron beam is also effective for improving switching characteristics of silicon wafers for power devices.

In addition to above, we process other industrial materials such as heat shrinkable tubings at Tsukuba Electron Beam Center.

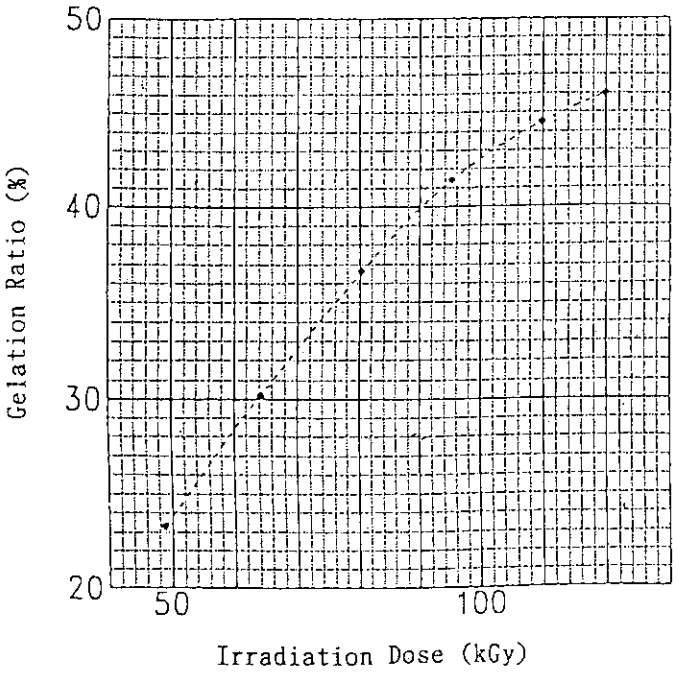


Fig 4.

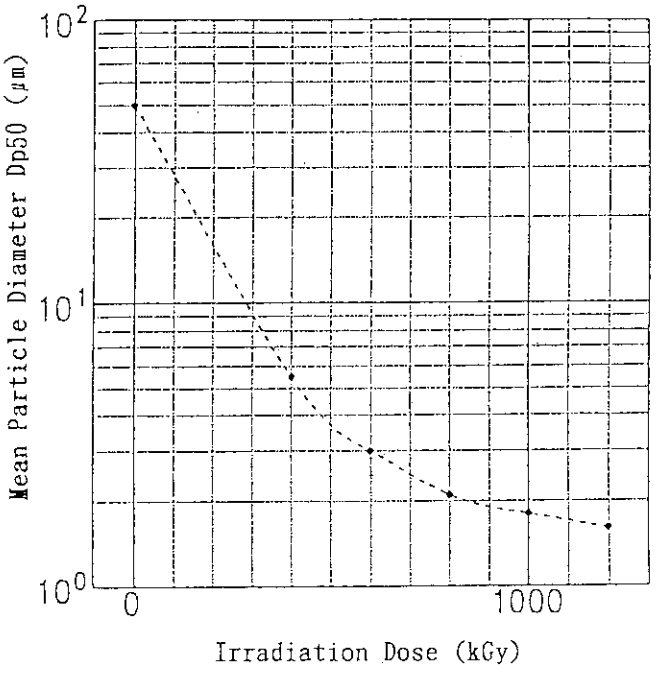


Fig 5.

2) Sterilization

(1) Features of EB Sterilization

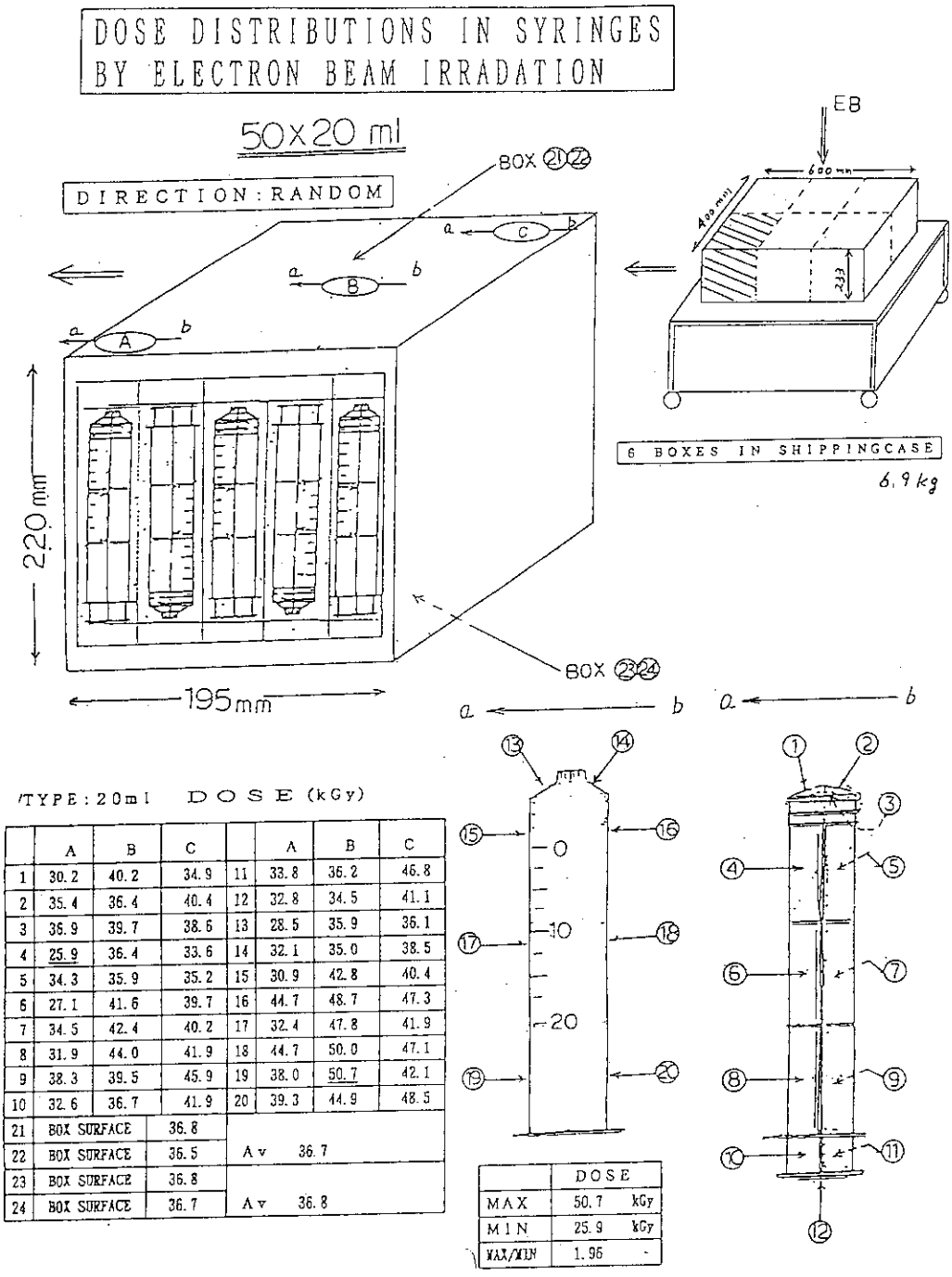
We received approval of Ministry of Health and Welfare as EB sterilization facility in 1991 which, of course, was first in Japan. Even before the approval we had started EB sterilization with those products which did not require governmental approval. Requests for the EB sterilization has remarkably increased recently since those advantages as shown below have well acknowledged to the public.

Advantages

1. Quick process time
2. No residuals
3. Little temperature rise
4. No pressure applied
5. No special package for gas sealing required
6. Easy validation by dosimetory
7. Less coloring and degradation

But because penetrations is less than that of γ ray dose distribution must be checked carefully prior to actual processing. Example of dose distribution test is shown in Fig 6.

In this example 60 dosimeters are used for three syringes. Maximum dosage gained is 50.7 KGy at syringe B No. 19 and minimum 25.9 KGy at syringe A No. 4.



	A	B	C		A	B	C
1	30.2	40.2	34.9	11	33.8	36.2	46.8
2	35.4	36.4	40.4	12	32.8	34.5	41.1
3	36.9	39.7	38.6	13	28.5	35.9	36.1
4	25.9	36.4	33.6	14	32.1	35.0	38.5
5	34.3	35.9	35.2	15	30.9	42.8	40.4
6	27.1	41.6	39.7	16	44.7	48.7	47.3
7	34.5	42.4	40.2	17	32.4	47.8	41.9
8	31.9	44.0	41.9	18	44.7	50.0	47.1
9	38.3	39.5	45.9	19	38.0	50.7	42.1
10	32.6	36.7	41.9	20	39.3	44.9	48.5
21	BOX SURFACE		36.8				
22	BOX SURFACE		36.5	Av 36.7			
23	BOX SURFACE		36.8				
24	BOX SURFACE		36.7	Av 36.8			

	DOSE	
MAX	50.7	kGy
MIN	25.9	kGy
MAX/MIN	1.96	-

Fig 6.

(2) Quality Assurance

Quality assurance is one of the most important factors in sterilization process. This procedure is strictly performed in accordance with GMP. Flow chart of the system is shown in Fig 7. This system is consisting of three parts. First part is machine calibration. Through this procedure we know that machine is operating exactly with the specification shown on instrument panel. This calibration is done periodically. Second is dosimetory calibration. Dosimeter can be traced back to the standard of National Physics Laboratories of Great Britain.

Combining above two final part is test irradiation to determine appropriate dose to apply. Example of this procedure is already shown.

With this system we are able to assure our process perfectly.

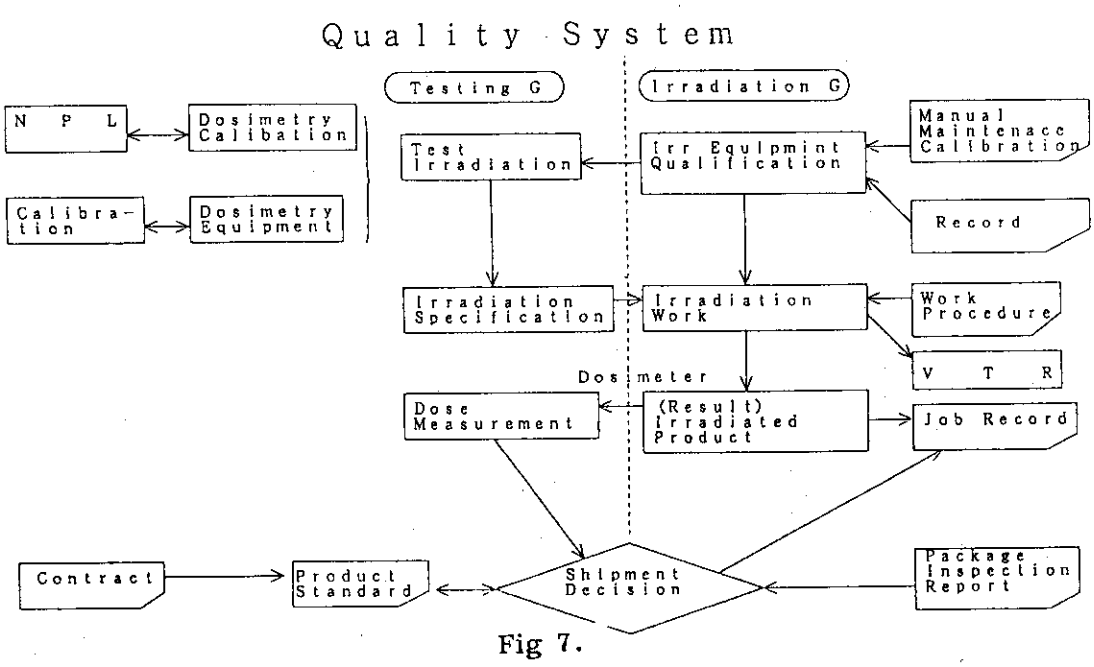


Fig 7.

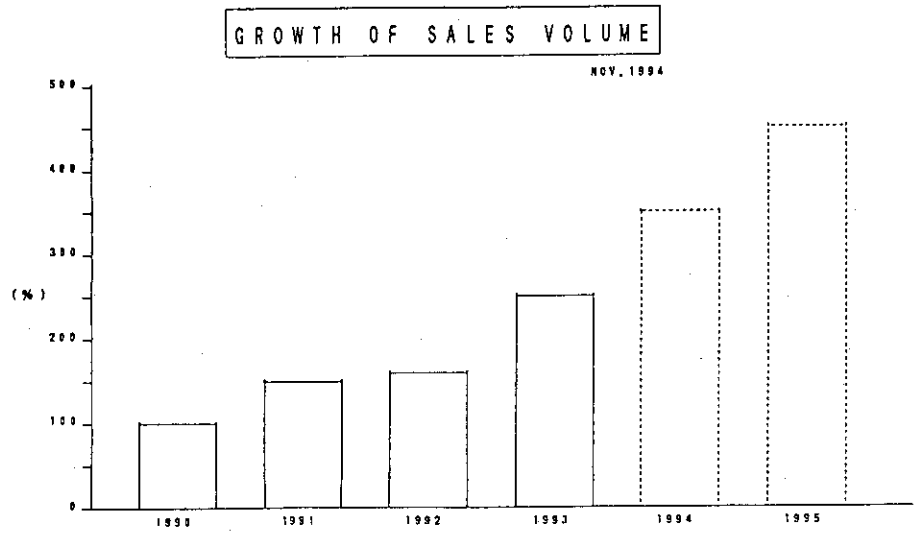
(3) EB Sterilized Products

Followings are list of typical products sterilized by EB.

Labo Wares	Petri dishes, Flasks, Pippets, Micro plates
Medical Devices	Sutures, Syringes, Canulas Dialyzers, Plasters
Misc. Products	Gauzes, Bandages, Drapes, Gowns, Gloves
Sanitary Wares	Tampons
Containers	Eye drops, Germ Free Medicines, Sterilized bags
Others	Caps for various pep drinks

4. Sales Growth

Sales amount growth since starting up of the facility is as follows. Sterilization has become backbone of this remarkable growth. This is due to that EB sterilization has been acknowledged widely as effective and economical method.



2.7 An Economic Benefit Analysis on the Cobalt-60 Irradiation Facility of Beijing Radiation Research Center

Wang Binlin

Beijing Radiation Application Research Centre
No. A6, Dayangfang, Andingmenwai, Chaoyang District,
Beijig , 100012, China

Abstract the peculiarity, the investment and annual operating cost of the 3.7×10^{16} Bq (MCi) cobalt-60 irradiation facility at Beijing Radiation Application Research Centre are described. Its economic benefits each year are analyzed according to severrai year operating practice . Some related questions on carrying out radiation processing are raised and discussed.

INTRODUCTION

With the development of the radiation processing industry, the establishments of cobalt-60 source irradiation facility have been unceasingly increasing, Now, in China, there are more than 70 cobalt-60 source irradiation facilities, with a capacity of ten thousand Curie($3.7\times 1\ 0^{14}$ Bq) each, in which more than 40 sets have a capacity of one hundre thousand Curie (3.7×10^{15} Bq) each. The designed cobalt-60 source loading capacity for the irradiation facility of Beijing Radiation Application Research Centre is one million Curie(3.7×10^{16} Bq) and the practical loading by now is eight hundred thousand Curie (2.96×10^{16} Bq) . Taking this as an example, I will make a preliminary analysis for its economic benefits according to the operating practice in several years , for your reference only.

This irradiation facility was based on a research work on the Radiation Sterilization of Medical Products in the periods of the Sixth Five-Year Plan, and it was listed as one of the State Key Importation Projects, "Radiation Sterilization Test Development Bases" in the Seventh Five-Year Plant, supported by the State Science and Technology Commission [1] . At the same time, this project was also supported by the IAEA , being brought into the Regional Co-operation Project(CPR/8/002). This project was consisted of a productive factory of 50 million syringes and one hundred million needles per year, and a radiation sterilization base. Therefore, in choosing the type of the cobalt-60 source irradiation facility, The sterilization of medical products was considered as main objective. A facility providing with a closed irradiation cell, a rotary door for the products passing in and out, and a mode of pneumatically transferring products by rail,was chosen. The main advantages of this facility are safety, saving building area, high automation level,good dosage uniformity, high radiation availability, etc. Its shortage is that it can not irradiate products which need low dose[2] . After setting up of this facility, because the fifty million syringes and one hundred million needles per year did not be produced and irradiated according to the plan, for a variety of reasons, the source of goods to be irradiated was not enough seriously. Through an active promotion of the scientific and technical personnel at our Centre, the situation has been improved uninterruptedly. Till 1992,the facility was running in full load of goods, with an annual operation hours of more than 8,000, acquiring better economic benefits.

CAPITAL INVESTMENT AND OPERATING COST

Investment:	(Million yuan, RMB)
Equipment for irradiation facility	3.550
Cobalt-60 source(330 KCi)	1.350
Necessary home-made equipment	0.800
Civil works	2.200
Others (traffic vehicles, boxes for goods, etc)	0.60

Annual operating cost	(Million yuan, RMB,according to practical consumption in 1992)
Depreciation of equipment	0.435(10 years)
Consumption of cobalt-60 source	0.438
Depreciation of civil works	0.088
Wages	0.125
Charges for water, electricity and steam	0.105
Others	0.060

ANALYSIS FOR ECONOMIC BENEFITS

Because there are a variety of products(several dozens) to be irradiated at this facility, the prices for them are different and the quantities for each kind of product are also different, an average value is taken as a basis for calculation in this paper .

The income in 1992 was 2.55 million yuan(RMB), i.e. the average income per year was 7,300 yuan for per thousand Curie of cobalt-60 source. It was similar to that of the provinces Jiangsu, Hunan, etc. in our country [3] [4] . Below calculations are based on the level of this income per year.

When the cobalt-60 source loading at our Centre is 150 ,000 Curie, with a presupposition that the source of goods to be irradiated is guaranteed, it is in equilibrium between the income and the cost, when the loading is 350,000 Curie, the ratio for the income and the cost is 2:1. If the cobalt-60 source is one million Curie, the ratio becomes 3:1.

The investment recovery time is listed in the following table.

Source loading (KCi)	Annual revenue (Million yuan)	Investment recovery period (Year)
350	2.55	7.6
500	3.65	4.8
800	5.84	3.5
1,000	7.30	3.0

The loan interest did not be taken into account in calculating.
If a facility is built with an investment by a loan, the investment recovery periods will be prolonged properly in foregoing table.

DISCUSSION

1.If the products to be irradiated are enough, then, the cobalt-60 source loading is higher, the econimic benefits are better, So, for a facility being built at present, it must be made to reach the designed cobalt-60 source loading capacity. For a cobalt-60 facility newly built, a fact that whether there are enough items to be irradiated or on must be carefully made sure.

2.Generally speak, better economic benefits will be acquired in irradiating the items which need a low dose. For example, the dose needed for garlics is about 3--4 order magnitude less than that for thermal shrinkable materials and butyl rubbers, but the charge collected for irradiation could not be increased proportionally with the increase of the dose. For this reason, for some small cobalt-60 irradiation sources, items which need low dose should be more developed.

3.The key point to raise economic benefits for radiation processing is to extend the market of irradiated products. In China, there are large amounts of products which can be or should be processed by irradiation technology. But now, only a few products are so treated.Why ? I think, principally because the proper authority in the government did not establish strict standards and did not adopt supervision measures on the requirements for the production quality and the sterilization techniques. For example, most women-used sanitary towels sold in market did not reach the hygienic standards, according to an investigation of the All-China Women's Federation, while this problem can be easily solved by the use of the irradiation technology, But the department responsible for this work failed to make laws and adoopt measures to force related factories to fulfil hygienic requirements. For another example, the ethylene oxide sterilization, which previously began to be used and has been keeeping its processing price lower. The occurence is accounted for the imperfect equipment at most sterilization plants, without the environment monitor and ethyline oxide residue testing means. These lead to a low processing cost. If the State strengthens the control and demands all ethylene oxide sterilization units to improve monitoring system and rigorously enforce the sterilization technology, this situation will be changed and the great part of medical products will be diverted to radiation sterilization.
4.Owing to the fact that the irradiation facility and its main spare parts are imported from abroad, and so is the cobalt-60 source, for them to pay US dollars is needed, while the charge for radiation processing are collected in RMB, which has an alterable exchange rate with US dollar, the analysis above-mentioned will be changed with the advance of time.

REFERENCE

(1) Wang Binlging et al.(1987).A study on the radiation sterilization of medical products. Journal of Beijing Normal University (natural science section), Feb. 1987.
(2) Wang Bingling et al. (1989).An industrial cobalt-60 radiation facility in China. In the 4th Japan -China, May 1989.
(3) The Department of Scientific and Technical Conditions of the Science and Technology Commission of Jiangsu Province (1989). A repore at the national second radiation processing work forum, Chengdu, Sichuan Province, China , Oct. 1989.
(4) The Ressearch and Development Centre for Irradiation Application Technology of Hu'nan province (1989) . A report at the national second radiation processing work forum, Chengdu, Sichuan Province, China,Oct.1989.

3. Gas and Liquid Phase (1)

3.1 *Dynamics of Superexcited Molecules as Studied by Two Dimensional Spectroscopy

Masatoshi Ukai
Department of Chemistry, Tokyo Institute of Technology
Ookayama, Meguro-ku, Tokyo 152, Japan

ABSTRACT Two dimensional (2D) yield spectra of vuv fluorescence radiation from excited fragment atoms produced in the neutral dissociation (ND) of N_2 and O_2 have been measured as a function of both excitation photon wavelength and fluorescence wavelength. The 2D spectrum presents *a location map of superexcited states* or *a pictorial correlation diagram for ND*, which shows both repulsive and well-defined vibrational superexcited states. Features in the 2D spectra are explained by the threshold structures due to the energy limits of dissociative excitation and the structures of superexcitation. The multi-step predissociation is shown to populate various kinds of fragments as a general rule. A highly state selective dissociation is also shown for Rydberg states converging onto $O_2^+ (c\,^4\Sigma_u^-)$, v'=1.

INTRODUCTION

Decay dynamics of superexcited molecules is one of the most important property of photophysics and photochemistry in the extreme-ultraviolet (euv) region, which provides the detailed information on the primary processes of the interaction of ionizing radiation with matter. Superexcited molecule in the gas phase present the most fundamental examples of the short-lived intermediates which show the complex decay behavior under the competition between autoionization and neutral dissociation (ND) (Hatano 1994), i.e.,

$$AB^{**}\ (\text{superexcited state}) \begin{cases} \rightarrow AB^+ + e^- \\ \rightarrow A + B \end{cases}$$

However, apart from the general idea on the competitive decay behavior, the decay property of superexcited molecules is not understood well. Especially their ND process is one of the unrevealed mysteries in the energy region well beyond the ionization potential (IP). This is due to the small amplitudes of cross sections and the experimental difficulties to observe neutral dissociation.

The recent progress of the tunable synchrotron radiation (SR) with high brilliance has given the opportunity to make detailed experimental studies of the molecular superexcited states as the dissociating states (Ukai *et al* 1991, 1992a, 1992c, 1994a) as well as autoionizing states (Ukai *et al* 1991, 1992a).

In this paper we show the recent results of the entitled study performed from the point of view of ND. To observe ND we disperse the fluorescence radiation from neutral atomic fragments produced by dissociative excitation (DE),

$$AB + h\nu\ (\lambda_{ex}) \rightarrow \begin{cases} A^* + B \\ \rightarrow A + h\nu'(\lambda_f) \end{cases}$$

which is the most representative ND well beyond IP. Dispersed spectra of fluorescene are presented as a two dimensional (2D) spectrum surface of fluorescence yields as a function of both the SR

wavelength and fluorescence wavelength (2D-FES: Fluorescence Excitation Spectrum). This is a kind of *a location map* or *a bird-eye's view* for featuring the ND of superexcited states. As typical examples we demonstrate the ND of O_2 and N_2 superexcited states under the competition with autoionization.

EXPERIMENT

The experiment was performed using the SR light source from a 2.5 GeV positron storage ring at Photon Factory. The SR from a 3m-normal incidence monochromator (Ito *et al* 1994) was typically 1×10^{11} photons/s at 50 nm with 0.1 nm band width. Vacuum-uv fluorescence emitted from excited fragments was dispersed using a 1200 lines/mm grating with a curvature radius of 20 cm at an angle of 64°. The dispersed images of fluorescence spectrum were obtained simultaneously using a position sensitive detector behind a microchannel plate coated with CsI (Ukai *et al* 1992b, 1994b).

RESULTS AND DISCUSSION

Figure 1 shows the 2D-FES emitted from dissociatively excited neutral N atoms as a function of excitation photon wavelength (λ_{ex}) for $39< \lambda_{ex} <62$ nm (photon energy: 20-31.7 eV) (Ukai *et al* 1994c). This is obtained at λ_{ex} shorter than the first IP (15.52 eV) at 85.0 nm. In the present region of λ_{ex}, the atomic fluorescence due to dissociative-ionization-excitation is not energetically accessible (λ_{ex} =35.8 nm (34.6 eV) for the lowest threshold $N^+(^3P)+N^*(3s\,^4P)$). This means that each of "vertical lines" in Fig. 1 presents the partial yield spectrum of NI fluorescence due to the ND of N_2^{**}. The fluorescence from molecular ions is absent. The diagonal line in the region of $55< \lambda_{ex} <62$ nm is due to the scattered incident photon from the gas cell, which appears at the secondary position. The smooth variation of the fluorescence yields shows that a considerable amount of contribution from the ND of repulsive N_2^{**} is involved. However, the potential curves for these repulsive N_2^{**} are not identified. It is possible that some repulsive potential curves of the Rydberg states having the ion cores of correlation-states locate in this region.

Some of the structures in the 2D-FES in Fig. 1 are explained by those due to DE thresholds (Ukai *et al* 1994c). With increasing the photon energy in passing through an energy limit of DE, a new DE channel becomes accessible. In DE, excitation photon energy $E_{ex}=hc/\lambda_{ex}$ (h, the Planck constant; c, light velocity) is divided into the bond-dissociation energy of a ground state molecule D, the internal energy of the excited fragment, E_{A^*}, that of the ND counterpart atom, E_B, and the kinetic energy reliese, KE. E_{A^*} is further divided into the fluorescence energy, E_f ($=hc/\lambda_f$) and the internal energy of the lower state of fluorescence transition, E_g. Thus at E_{ex} corresponding to a DE limit or for KE=0, the total amount excitation energy is partitioned as

$$E_{ex} = D + E_f + E_g + E_B .$$

This means that the trace of the appearance energy of fluorescence of E_f is related to E_{ex} linearly. This relation is rewritten by the relation between λ_{ex} and λ_f:

$$\lambda_{ex} = hc\,\lambda_f / [\,hc + (D + E_g + E_B)\,\lambda_f\,].$$

The threshold for the lowest DE for producing two vuv-fluorescent fragments $N^*(3s\,^4P)+N^*(3s\,^4P)$ lies at λ_{ex} =40.8 nm (30.4 eV). Below λ_{ex} =40.8 nm, ^4S (E_B =0 eV), ^2D (2.38 eV), or ^2P (3.58 eV) from the ground $(2s)^2(2p)^3$ configuration of N is accessible as the ND counterpart. Also

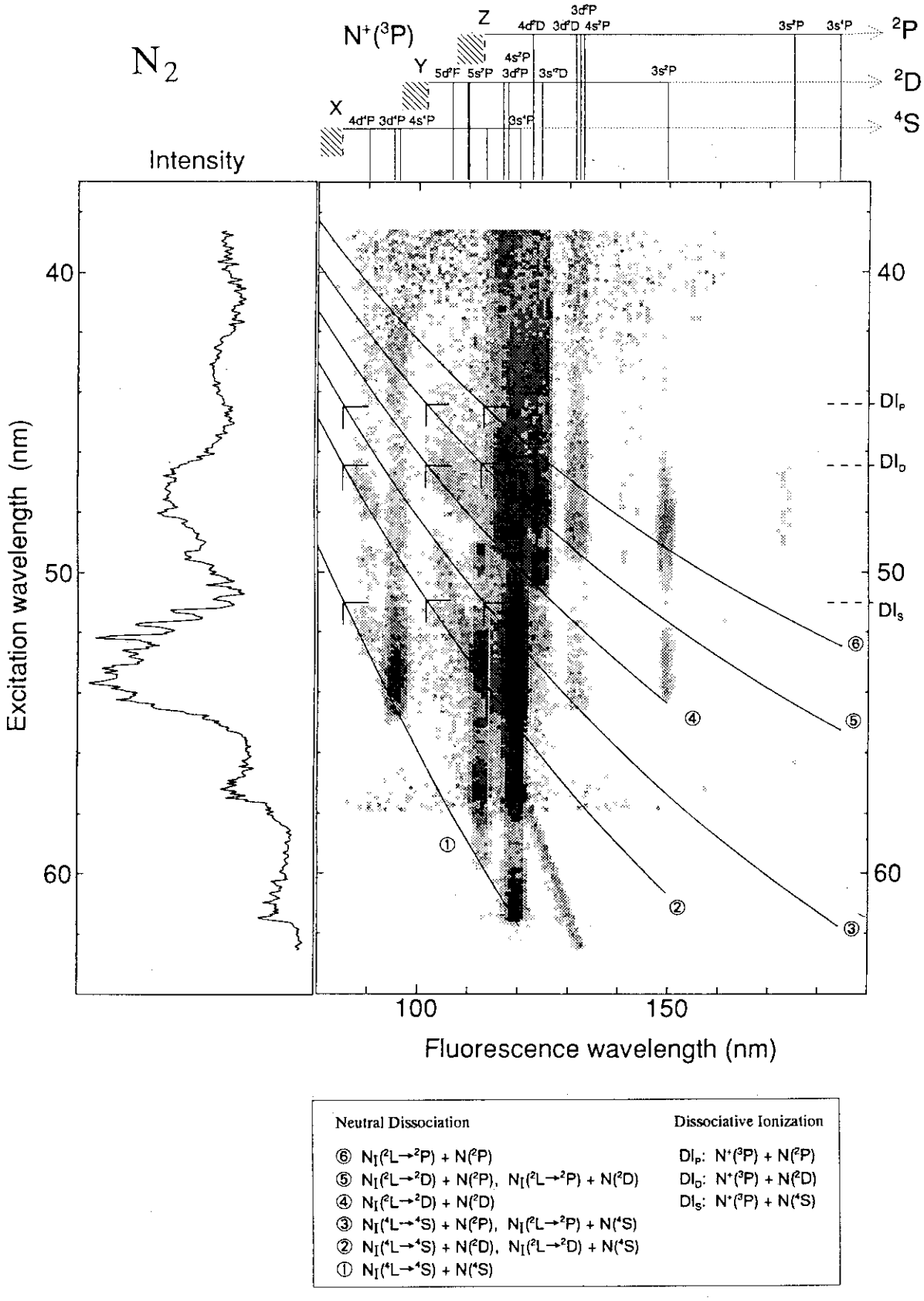


Fig. 1 A 2D FES for N_2 as a function of excitation photon wavelength (vertical) and fluorescence wavelength (horizontal) emitted from excited N atoms produced in the ND of superexcited N_2^{**}. The intensity of fluorescence yield is shown by a gray scale plot increasing from light to dark. A single dimensional excitation spectrum for undispersed vuv-fluorescence is shown for reference.

the possible lower state of fluorescence is ^4S, ^2D, or ^2P in the present region of λ_{ex}. Nine conbintaion cases of differnt E_B and E_g are possible, which are drawn as curves ① – ⑥ in Fig.1. Because the spin forbidden NI transition is unlikely, accessible spin state of N^* is assigned by the lower state. Although the ND producing N^* with the internal energy greater than the first IP (N^+ (^4P), 14.53 eV) is possible, yet most of such N^* atoms decay via autoionization rather than fluorescent decay. This is why fluorescence lines in Fig. 1 are explained by three series $nl\,^4L \rightarrow ^4S$, $nl\,^2L \rightarrow ^2D$, and $nl\,^2L \rightarrow ^2P$ toward the series limits at 85.3, 102.0, and 113.2 nm, respectively, for $\lambda_f = hc/(14.53 - E_g)$ requested by $E_{A^*} = E_f + E_g < 14.53$ eV.

Apart from the DE threshold structures, the vibrational structures due to well-definced superexcited Rydberg states converging onto N_2^+ ($D\,^2\Pi_g$ and $C\,^2\Sigma_u^+$) are also observed at λ_{ex} for $50 < \lambda_{ex} < 62$ nm in Fig. 1.

A similar ND behavior is observed in the 2D-FES for O_2. The smooth variation of the fluorescence yields and discrete structures in the 2D-FES for $50 < \lambda_{ex} < 60$ nm (photon energy: 24.8–20 eV) in Fig. 2 also shows the ND of both repulsive and well-defined vibrational O_2^{**} (Ukai *et al* 1994b). The discrete structures are due to the ns σ_g and nd π_g Rydberg series converging to O_2^+ ($c\,^4\Sigma_u^-$) of which ionic potential was shown to have only two vibrational bound states of v=0 and 1. However, the behavior of enhanced fluorescence yields is different at λ_{ex} to excite v'=0 or v'=1

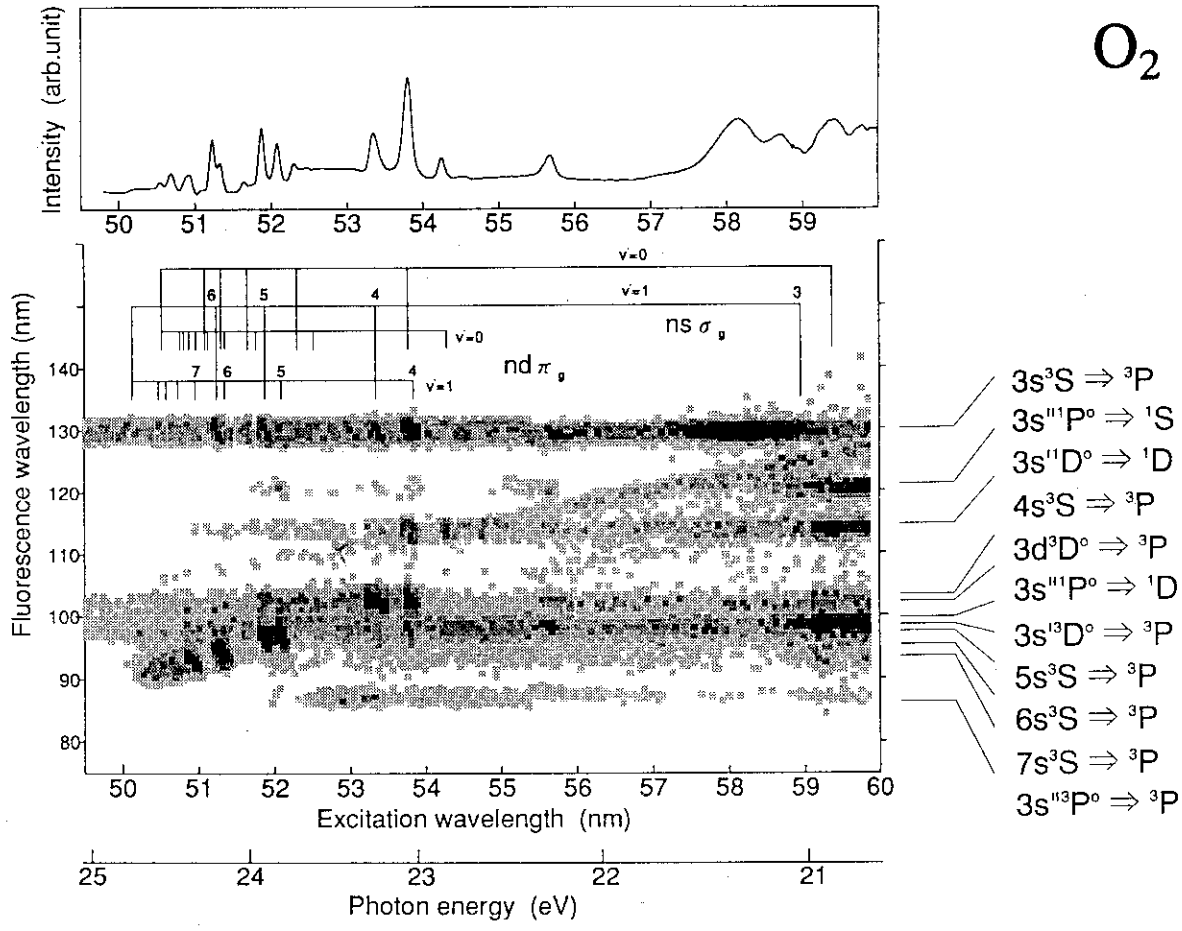


Fig. 2 A 2D FES for O_2 as a function of excitation photon wavelength (horizontal) and fluorescence wavelength (vertical) emitted from excited O atoms produced in the ND of superexcited O_2^{**}. A single dimensional excitation spectrum for undispersed vuv-fluorescence is shown for reference.

level. The yields of several OI lines at λ_{ex} for v'=0 are enhanced simultaneously, which is ascribed to the partitioning in a multi-channel predissociation. At λ_{ex} for v'=1 of each n (principal quantum number) states of O_2^{**} ($c\,^4\Sigma_u^-$ (ns σ_g or nd π_g)), the fluorescence yields from O(ns ^{3}S) (n $\geqq$ 3) atoms are emphasized selectively, where the n quantum number is conserved;

$$O_2^{**}\ (c\,^4\Sigma_u^-\ (ns\ \sigma_g\ \text{or nd}\ \pi_g)) \rightarrow O(ns\,^3S) + O.$$

This is an evidence of the state-to-state selective ND (Ukai *et al* 1994b), being against the general idea of multi-step predissociation in this region. By the addition of an ns σ_g Rydberg electron to c $^4\Sigma_u^-$ ion both around the Franck-Condon region and at the DE limit one can draw the potential curve for O_2^{**} ($c\,^4\Sigma_u^-$ (ns σ_g)) connected to the DE limit of O(ns ^{3}S)+O(^{1}D). Analogously to the dissociation of O_2^+ ($c\,^4\Sigma_u^-$) via tunneling, (calculated tunneling rates of 10^{11} s^{-1} for v'=1 and 10^8 s^{-1} for v'=0), at λ_{ex} for v'=1 O_2^{**} emerged on the repulsive wall, after the tunneling through the barrier, undergoes fast ND into O(ns ^{3}S)+O(^{1}D) limit. The absence of the selective enhancement at λ_{ex} for v'=0 suggests that the tunneling ND is no more important for v'=0 levels. The enhanced yield in the O(3s ^{3}S $\rightarrow$ ^{3}P) line at $c\,^4\Sigma_u^-$ (3s σ_g), v'=1 is followed by enhancement around 58 nm, which is the direct ND of free O_2^{**} on repulsive wall into the of O(3s ^{3}S)+O(^{1}D) limit (Ukai *et al* 1992b).

This work has been performed under the approval of the Photon Factroy Program Advisory Committee for proposal Nos. 92-156 and 94G196. The author thanks S. Machida, M. Kitajima, Dr K. Kameta, Prof. N. Kouchi, Prof. Y. Hatano, Prof. T. Hayaishi, and Prof. K. Ito for collaboration.

REFERENCES

Hatano Y., (1994) *Dynamics of Excited Molecules*, ed. K. Kuchitsu (Elsevier, Amsterdam), chapterIV.

Ito K., Morioka Y., Ukai M., Kouchi N., Hatano Y., and Hayaishi T., (1994) Nucl. Instrum. Method, *in press*.

Ukai M., Kameta K., Chiba R., Nagano K., Shinsaka K., Kouchi N., Hatano Y., Umemoto H., Ito Y., and Tanaka K., (1991) J. Chem. Phys., **95**, 4142.

Ukai M., Kameta K., Kouchi N., Nagano K., Hatano Y., and Tanaka K., (1992a) J. Chem. Phys., **97**, 4835.

Ukai M., Kouchi N., Kameta K., Terazawa N., Chikahiro Y., Hatano Y., and Tanaka K., (1992b) Chem.Phys.Lett., **195**,298.

Ukai M., Kameta K., Kouchi N., Hatano Y., and Tanaka K., (1992c) Phys. Rev. A **46**, 7019.

Ukai M., Kameta K., Machida S., Kouchi N., Hatano Y., and Tanaka K., (1994a) J. Chem. Phys., **101**, 5473.

Ukai M., Machida S., Kameta K., Kitajima M., Kouchi N., Hatano Y., and Ito K., (1994b) Phys. Rev. Lett., *submitted*.

Ukai M., Machida S., Kameta K., Kitajima M., Kouchi N., Hatano Y., Hayaishi T., and Ito K., (1994c) *to be published*.

3.2 *The Study on the Primary Processes of Radiation Chemistry in Liquid Alkanes by Means of Picosecond Pulse Radiolysis

Y. Yoshida and S. Tagawa

The Institute of Scientific and Industrial Research, Osaka University
8-1 Mihogaoka, Ibaraki, Osaka 567, Japan

The primary processes of radiation chemistry in liquid alkanes were studied by using picosecond pulse radiolysis. Especially, the geminate ion recombination, the formation process of excited states and ion-molecular reaction of radical cations were directly observed and the primary processes were discussed. Also, future picosecond and femtosecond pulse radiolysis to elucidate the unsolved problem in the primary processes was discussed.

Introduction

The most important process of radaiation chemistry in liquid alkanes is the geminate ion recombination[1] of alkane radiacal cations and electrons which are produced by the ioniziation. Figure 1 shows the behavior of the geminate process. After the thermalization of the electron emitted from the parent alkane by ionization, the parent radical cation and electron diffuse under the Coulomb interaction. Most pairs recombinaed very quickly on the picosecond time-scale, due to the long-range Coulomb interaction in non-polar liquid. Small fraction of the geminate pairs escapes the recombination and becomes the free ions.

The geminate ion recombination is an inhomogenious reaction and the kinetics is described the diffusion theory under the Coulomb potential, so called, the Smoluchowski equation, as follows[2].

$$\frac{\partial \omega}{\partial t} = D\nabla\left(\nabla\omega + \omega\frac{1}{kT}\nabla V\right) \quad (1)$$

where ω, D, k, and V are the survival probability of the geminate pairs, the sum of the diffusion coefficients of the pairs, the Boltzman constant, and the Coulomb potential, respectively. The equation shows the rapidity of the geminate ion recombination depends on the D.

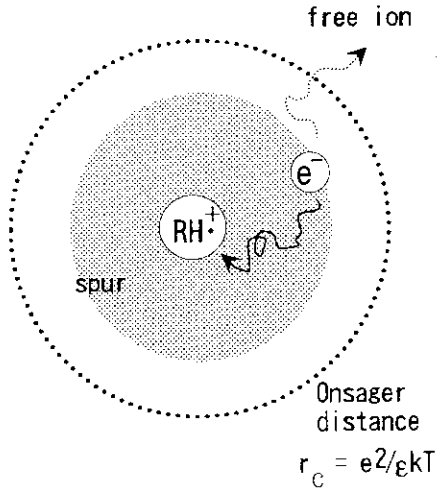


Fig. 1 Concept of the geminate ion recombination.

The geminate ion recombination has been studied theoretically and experimentally by many researchers. However, it had been difficult for a long time to observation of the geminate decays in neat alkanes by using pulse radiolysis, because the decays are so quick. Usually, the geminate decay of solute pairs instead of the alkane radical cations and electrons had been studied[3], because the solute geminate decays were slow due to the large diffusion coefficients. Recently, the transient absorption spectra of alkane has been

made clear and the new picosecond pulse radiolysis system has been enabled the direct observation of geminate ion recombination[4].

Picosecond Pulse Radiolysis

In the picosecond pulse radiolysis system for absorption spectroscopy, so called "Twin Linac System"[5], which was composed of two picosecond electron linear accelerators, one linac was used for radiation source and the other linac was used for the production of Cherenkov light as analyzing light. The system was successful to observe the time-dependent behavior of short-lived species at the wavelength from ultra violet to visible region. However, absorption peaks of most important species in primary processes, such as electrons and cation radicals of alkanes, are in infrared region, which can not observed by the Twin system, because the intensity of the Cherenkov light becomes lower in the infrared region.

A simpler system by using picosecond diode laser instead of the other linac has been developed to observe the absorption spectroscopy in infrared region. Figure 1 shows the block diagram of the new system which is called as LL-twin system. Both pulse widths of the 28 MeV electron pulse from linac and analyzing light from the diode laser are below 10 ps. The linac and diode laser are operated simultaneously by the trigger from the synchronized circuit system. The time profile is obtained by changing the trigger timing through the delay system. The timing jitter between the two triggers is 10 ps. Total time-resolution is about 20 ps which mainly depend on the pulse widths and the timing jitter.

The analyzing light through the sample cells is detected by Si or Ge Photo diode. The output charge from the detector is amplified by the charge amplifier and converted the digital number by a A/D converter. The digital data are stored in the multiparameter and the absorbance is calculated by a personal computer.

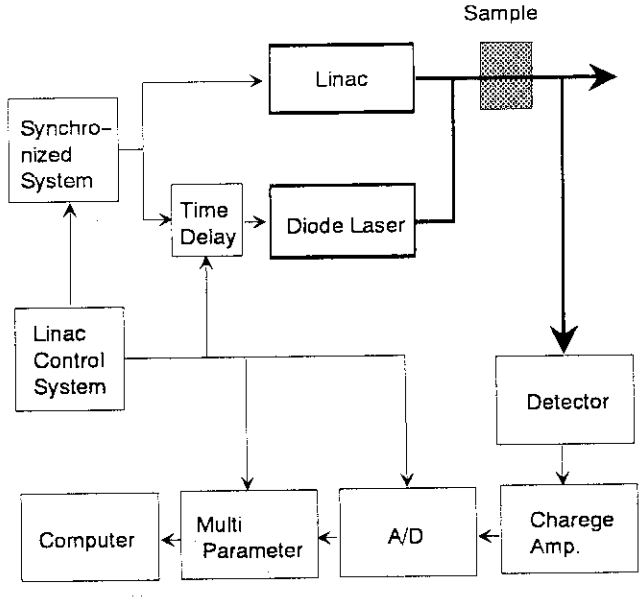


Fig.2 Block diagram of picosecond pulse radiolysis system for absorption spectroscopy by using picosecond diode laser (LL-twin System).

Transient Absorption Spectra of Alkanes

The absorption spectra obtained in alkanes had not been made clear, because the intermediate species were very short-lived and the spectra were broad. Recent pulse radiolysis study showed the assignments of the spectra.

Figure 3 shows the transient absorption spectra obtained in nanosecond pulse rdaiolysis of neat n-dodecane (a) and the n-dodecane solution containing 100 mM CCl_4. The major four absorption bands of 240, 650, 850, and >1000 nm are observed. The bands at 650 and >1000 nm were scavenged by CCl_4. From the scavenging result and the time-dependent behavior which will be discussed at next section, the bands at 650, 850 and >1000 nm are assigned to be excited states, radical cations and electrons, respectively. The bands around 240 nm is due to alkyl radicals.

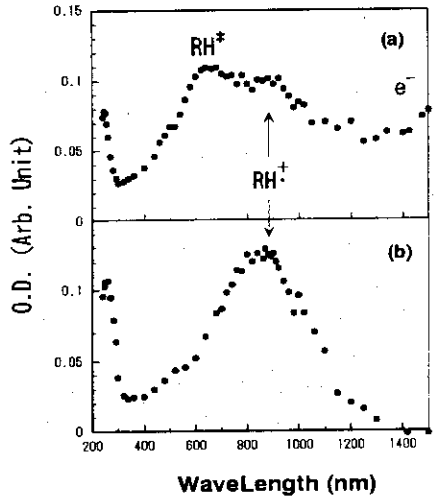


Fig. 3 Transient absorption spectra obtained in nanosecond pulse radiolysis of neat n-dodecane (a) and n-dodecane + 100 mM CCl_4 (b).

Primary Processes in Neat Alkanes

Figure 4 shows the time-dependent absorption obtained in the LL-twin pulse radiolysis in neat n-dodecane monitored at 660, 806, and 1300 nm, respectively. Both decays of the cation radicals at 806 nm and the electrons at 1300 nm agree with the theoretical decays based on the Smoluchowski equation[6] with the initial distribution of the exponential type and the initial separation of 6.6 nm (solid lines). The characteristic lifetime of the geminate pairs, which means the time when the 43 % of geminate pairs are survived, is 26 ps. The decay at 660 nm is complicated because of the overlap of the decay of cation radicals, the formation of excited states from the geminate ion recombination. The lifetime of the lowest excited states of n-dodecane is 4.3 ns..

It is known that the radical cations also decays by the ion-molecular reaction with alkane molecules. However, the ion-molecular reaction could not observed in the time-region from 50 ps to 1 ns. Therefore, main decay process

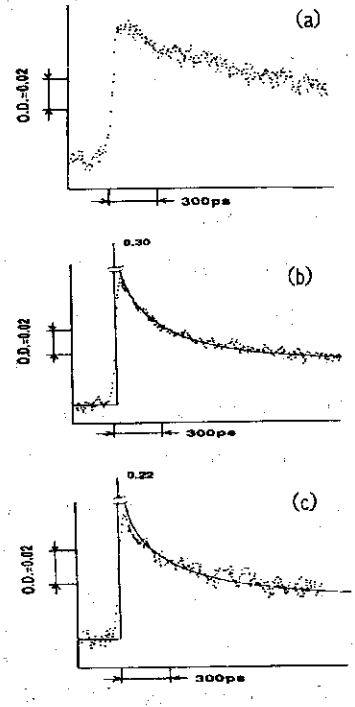


Fig. 4 Time-dependent absorption obtained in the LL-twin pulse radiolysis in n-dodecane monitored at 660 nm (a), 806 nm (b), and 1300 nm (c).

Table 1 Mobiliies of electrons, characteristic lifetimes, initial spatial distributions and initial separation.

liquids	mobilities (cm^2/Vs)	lifetime (ps)	distributions	initial separation (nm)
trans-decalin	0.013	35	exponential	6.1
n-dodecane	0.024	26	exponential	6.6
methylcyclohexane	0.044	16	exponential	6.2
n-hexane	0.071	9.4	exponential	6.0
cis-decalin	0.10	5.6	exponential	5.6
cyclohexane	0.23	3.2	exponential	6.1
isooctane	5.3	0.43	exponential	9.3
neopentane	50	0.63	gaussian	13.2
TMS	100	0.31	gaussian	13.2

exponential $R(r,r_0)=(1/r_0)\exp(-r/r_0)$

gaussian: $R(r,r_0)=(4r^2/\pi^{0.5}r_0^3)\exp(-r/r_0)$

in this time region is the geminate ion recombination.. Nanosecond pulse radiolysis studies shows that the ion-molecular reaction takes place in the long time region.

In other alkanes, such as cyclohexane and n-hexane,, the decays of the electrons agree with the Smoluchowski equation. The mobilities of the electrons, the characteristic lifetimes, initial spatial distributions, and initial separation are summarized in Table 1. The difference of the initial distribution depends on the slow down processes of electrons at ionization.

The decays of radical cations could not be observed clearly, because of both of the overlap of the cation radical bands and excited states band, and very short lifetimes of the cation radicals due to the rapid ion-Molecular reactions.

Pulse Radiolysis in Future

The unsolved problem in primary processes of alkanes is the elucidation of formation processes of alkyl radicals which are observed at 240 nm in figure 2. The possible main process is the formation from the highly excited radical cations and highly excited states.[7] In order to elucidate the problem, a new pulse radiolysis system which has higher time resolution in wider wavelength region is necessary.

The new plane for picosecond pulse rdaiolysis at Osaka university is the development of a new system by using the picosecond pulse from the L-band linac and Ti-Sapphire femtosecond laser. The linac and laser operated simultaneously with the time-jither within 10 ps by the synchronization technique of rf signals. The observable wavelength region will covered from ultraviolet (~250 nm) to infrared (~ 2 μm) by using SHG, THG, and OPO techniques.

The next plane for femtosecond pulse radiolysis also will depend on femtosecond laser technique. Femtosecond pulse linac will adopt laser-plasma acceleration technique. The very intense laser makes very high acceleration field in plasma and the pulse width will be femtosecond principality. The time-jitter between the electron pulse and the analyzing light is in the order of femtosecond, because the same

laser pulse is also used as the analyzing light. The workshop on the femtosecond linac has been started recently.

[References]

1 Y. Yoshida, S. Tagawa et al. "Pulse Radiolysis" ed.byY.Tabata, CRC Press, 343-355 (1991).

2 M. Tachiya, J. Chem. Phys., 56, 4377 (1972).

3 Y. Yoshida, S.Tagawa and Y. Tabata, Radiat. Phys. Chem., 28, 201 (1986).

4 Y. Yoshida, S. Tagawa and Y. Tabata, Radiat. Res., II, 69-74 (1992).

5 Y.Yoshida, T. Ueda, T. Kobayashi, H. Shibata and S. Tagawa, Nucl. Instrum. Meth., A327,41-43 (1993).

6 K. H. Hong and J. Noolandi, J. Chem. Phys. 68, 5163 (1978).

7 S. Tagawa N. Hayashi, Y. Yoshida, M. Washio and Y. Tabata, Radiation Phys. Chem., 34 503 (1989)

3.3 Isotope and Temperature Effects on Positronium Formation in Water

Tetsuya HIRADE
Department of Chemistry and Fuel Research,
JAPAN ATOMIC ENERGY RESEARCH INSTITUTE,
Tokai, Naka, Ibaraki, 319-11, JAPAN

Abstract -- I obtained the yields of the ortho-positronium formation in the mixture of heavy water and light water at room temperature, and that in pure water from room temperature to near the boiling temperature with the positron annihilation lifetime. The yield in pure light water at R.T. is 27.1%. The yield decreases linearly with increasing deuterium concentration and reaches 23.2% in pure heavy water. This is probably due to the spatial distribution of excess electrons in the positron spur, i.e. the terminal spur of positron truck. The spatial distribution, the size of the spur, might be larger in heavy water than in light water and the spatial distribution might change linearly with the change of the concentration. The temperature rise causes linear increase in the yield of ortho-Ps. It becomes 32.8% at 93C. It is probably due to the less localizing sites for electron and positron at higher temperature. Then, the yield increases with increasing the temperature. The site might be correlated with the cluster.

INTRODUCTION

Fundamental processes of radiation chemistry in water have been extensively studied. As the primary processes after irradiation are fast and inhomoginious reactions. It is necessary to have fast enough experimental techniques to know the primary processes.

Recently, some experimental techniques have been improved so much, and it is becoming possible to see the process of electron slowing down in the spur. The techniques, such as a pulse-radiolysis (PR), are based on the idea that cation-electron recombination time depends on the length between a cation and a thermalized electron in the spur[1].

There are many difficulties in understanding the positron annihilation in liquids, because the primary processes as positronium (Ps) formation are very fast reactions and inhomoginious processes. However, there is a basic idea on the processes of the Ps formation, which is the "spur reaction model" proposed and modified by Ole E. Mogensen[2,3,4]. According to this model, Ps is formed by the reaction of one of the excess electrons and a positron in the positron spur, i.e., the terminal spur of the positron track. The Ps formation is similar to the geminate recombination of an excess electron and a cation.

The yield of Ps formation depends on properties of solvents. Ps must be formed before solvation (or localization) of electron and/or positron, because solvated (or localized) electron and/or positron might not be able to form Ps and the solvated (or localized) positron will annihilate in about 400ps[3]. Which means that the rates of solvation (or localization) of electron and positron affect the yield of Ps formation. The reactivity of hole and electron affects the yield of Ps formation. As if the reactivity is smaller, positron have more posibility to react with electron to form Ps[5]. The thermalization distance of electron and positron in the positron spur affects the yield too, because longer distance of thermalization make the probability of electrons and positron escaping from the opposite charged particles larger, therefore the yield of Ps formation (and the geminate recombination) shall be lower[2].

In 1990, Charles D. Jonah et al. tried to find out the mechanism of electron thermalization in water with PR measurement at several D fractions[1]. They measured the decay of the hydrated electron at several fractions of D in water, and the changes in the rates of decay were quantified by the difference in the decay curves at 3.35 ns. The change in amount of decay at 3.35 ns depended linearly on the fraction of D_2O molecules, not D, in the solution. They interpreted this results as follows. The excitation of the solvent molecule should be similar for the isotopic molecules, so it could not be the cause of thermalization. As the strength of the OH stretch at approximately 3400cm^{-1} is the same in H_2O and HDO[6]. It can explain their experimental results that the OH stretch is efficient in thermalization.

The Ps yields of pure H_2O and D_2O have been measured and explained by several groups[7,8]. The yields were almost same as those I obtained in this work: about 27～28% ortho-Ps intensity for H_2O and 23～24% for D_2O. Ole E. Mogensen explained that the more excess electrons escape from the positron spur in D_2O than in H_2O, because the free ion yield in D_2O is larger[2]. Hence the Ps yield is lower in D_2O.

J. Facetti et al. explained with a different idea[8]. They interpreted that the difference of the Ps yields in H_2O and D_2O is caused by the difference of the hydrated electron yields from the initial ionizations in H_2O and D_2O in the spur. According to them, the G values of solvated electron yield from direct ionization, G_{direct}, and that from excited state, G_{ext}, are $G_{direct/H2O}$=3.3, $G_{direct/D2O}$=2.7, $G_{ext/H2O}$=0.4 and $G_{ext/D2O}$=0.5, respectively. Then, the ratio between H_2O and D_2O on the total of the hydrated electron yields from initial ionization, i.e. $(G_{direct/H2O}+G_{ext/H2O})/(G_{direct/D2O}+G_{ext/D2O})$, is 1.16. This value is exactly same as that on the ortho-Ps yields of H_2O and D_2O, 27.7/23.9=1.16. However, higher yield of hydrated electrons in H_2O means that the probability of Ps formation should be lower, because the hydrated electron and positron can not form a Ps. Besides, $G_{direct/H2O}$=3.3 and $G_{direct/D2O}$=2.7 are the maximum ionization yield according to the Ref.[9] from which J. Facetti et al. obtained the G values. So real G values, $G_{direct/H2O}$ and $G_{direct/D2O}$, might be lower than 3.3 and 2.7, respectively.

J. Ch. Abbe et al. measured the temperature dependences of Ps formation in some polar liquids, including light water. They have just measured at three temperatures in the case of light water[10]. They believe that there are two different paths to form Ps. One is the formation of free electron and free positron, the other is that of localized electron and localized positron. The first path is not affected by temperature change, but the second is. Probably, the most interesting point is that the Ps yield increases with increasing the temperature in water and methanol, but it decreases in ethanol and propanol. They mentioned that loosely bound electrons to the aliphatic groups would contribute to Ps formation in ethanol but not in methanol.

In this paper I describe the measurement of the lifetime of positron in H_2O, D_2O and HDO mixture. From these results, I discuss the electron thermalization distance in the spur with comparing the results of PR experiment done in the same solution by Charls D. Jonah et al.[1]. The temperature dependence of the yield of ortho-Ps in pure light water measured from room temperature to near boiling temperature is also shown and discussed.

EXPERIMENTAL

The positron lifetime spectra were measured by use of standard fast-fast coincidence apparatus. The detectors consisted of about 5cm^3 volume plastic scintillators (Pilot-U) coupled to Hamamatsu H3378-01 photomultiplier tubes. About 20μCi $^{22}NaCl$ between two 1.1mg/cm^2 Kapton foils was used as the positron source. RESOLUTION[11] analyses was performed to fit the time resolution spectrum by a sum of three Gaussians. The full width at half maximum (fwhm) of the resolution spectrum obtained with ^{22}Na source was about 200ps. The lifetime spectra were fitted by three exponentially decaying terms folded with the resolution curve by use of POSITRONFIT[12]. The contribution due to annihilation in the source materials was subtracted before the final analyses.

I used the method which can adjust the drift of time-zero of apparatus[13]. The spectra were measured for periods of one hour, and afterwards about 10 separately measured spectra were added taking into account the drift in time-zero. The applied correction procedure was similar to that normally used in hard-wear spectrum stabilizer. First, one of the separately measured spectra was chosen as the reference spectrum, and time windows were selected below and above time-zero for that spectrum. Second, the drift in time-zero for another lifetime spectrum relative to the time-zero of the reference spectrum was calculated by varying time-zero of that lifetime spectrum so that the ratio between the counting in the two selected time windows was equal to that of the reference spectrum. Linear interpolation within the about 25ps channel width was used in the calculation of the counting in the windows. Third, this procedure was done for all separately measured spectra.

The lifetime spectra of water are difficult to analyze with free three terms, because the longest

lifetime is not so long and there may exist the fourth lifetime component, i.e. probably short-lived ortho-Ps component[13]. Then the second component lifetime was needed to be fixed to 395ps.

H_2O sample was prepared in two different methods. One is prepared by the deionization, and another is distilled twice. There is no difference between these samples, then I decided to use the distilled H_2O. The isotopic purity of D_2O was 99.75% and used without any purification. All samples are degassed by freeze-thaw method to avoid the effect of oxygen.

RESULTS

The examples of results of analyses of the lifetime spectra at several deuterium, D, concentrations at room temperature are shown in Table 1. One example of the analyses without fixing the second component lifetime are shown at top of Table 1. The lifetime of second component, τ_2, tends to be too big, probably, because of the fourth lifetime component[13].

Figure 1 shows the dependence of the intensity of the third component, i.e. ortho-Ps, on the concentration of deuterium, D. It decreases linearly with increasing the concentration.

Figure 2 shows the temperature dependence of the ortho-Ps yield in light water. Ortho-Ps yield increases linearly with increasing the temperature.

Table 1 The results of analyses of the lifetime spectra at several deuterium concentration.

	fraction of D(%)	τ_1(ns)	I_1(%)	τ_2(ns)	I_2(%)	τ_3(ns)	I_3(%)	variance
(1)	0*	0.220	28.3	0.465	46.4	1.88	25.3	1.014
(2)	0**	0.151	12.4	0.395F	60.5	1.82	27.1	1.495
(3)	0**	0.148	11.7	0.395F	61.4	1.83	26.9	0.928
(4)	50	0.149	10.8	0.395F	64.0	1.88	25.3	1.094
(5)	100	0.149	8.8	0.395F	67.9	1.93	23.2	1.121

* (1) is the results of the same spectrum for (2) with a free 3-term-fit.

**(2) is the results of the sample which is distilled twice, and (3) is that of the deionized sample.

F means that the value was fixed on the computer analysis.[12]

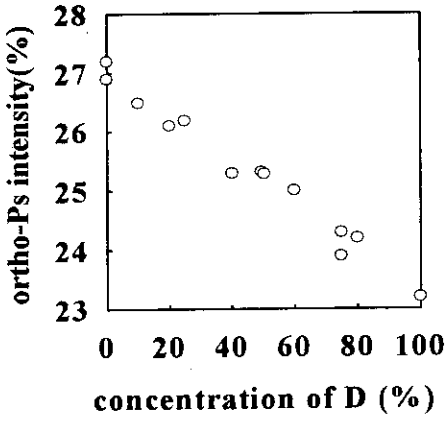


Fig.1 D concentration dependence on ortho-Ps intensity

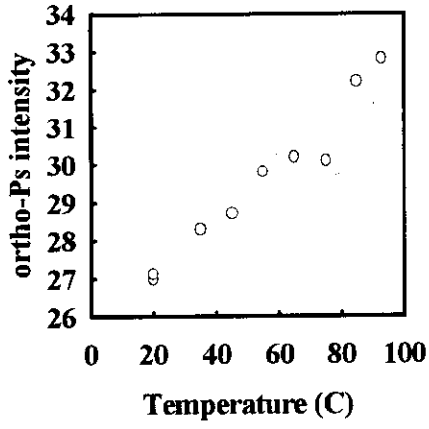


Fig.2 Temperature dependence on ortho-Ps intensity in H_2O

DISCUSSION

Thermalization distance of excess electrons

In the case of water, excess electron is solvated by water molecules in very short time as 0.3ps[14]. On alcohols, there are two paths of the solvation, the fast solvating time and the dielectric relaxation time caused by the orientation of the molecules are almost same[15]. Which means that one of the mechanism of the solvation might be the orientation of molecules around an electron. On the other hand, orientation of water molecules is not the mechanism of the hydration. The main mechanism of hydration

of electron might be movement of the electron itself to the site where the electron can be localized, and then it might be hydrated. The rates for localization(k_{loc}) and hydration(k_{sol}) were measured with the femtosecond laser technique[16].

Table 2 The rates of localization and solvation in H_2O and D_2O [16].

	H_2O	D_2O
k_{loc} (s^{-1})	$0.9x10^{13}$	$0.83x10^{13}$
k_{sol} (s^{-1})	$0.42x10^{13}$	$0.4x10^{13}$

Then, the concentration of D does not affect the rate of the hydration so much. Hence this process may not cause large change of the yield of Ps. Furthermore, the yield of Ps formation in H_2O is higher than in D_2O. This phenomena must not come from the difference of the rates of localization or solvation, because the rate in H_2O is a little faster than in D_2O. If it is the main mechanism which gives a difference on the yield of Ps formation, the yield of Ps formation should be lower in H_2O than in D_2O. The reactivity of the cation and the electron in the spur in D_2O might be smaller than that in H_2O[5], so it also can not be the cause of the difference on the yield of Ps formation.

There may be no reason of the change observed on the yield of Ps formation except for the spatial distribution of electrons in the positron spur, i.e., the thermalization distance of excess electrons in the positron spur depends linearly on the concentration of D, not D_2O. This conclusion is clearly different from that of PR experiment done by C. D. Jonah et al.

In the case of Ps formation, it is mainly observed that the reaction of an electron and a positron which can move fast, i.e., almost dry electron and positron. On the other hand, for the PR, you have to see the hydrated electrons. Then, what is the difference between the Ps formation and the geminate recombination of a cation and a hydrated electron? The most reliable answer might be the diffusion process. It is needed to take into account that there are effects of water molecules on the diffusion of the hydrated electrons. For Ps formation, there is no effect of the diffusion of hydrated electron, as almost all reactions are occurred before electron and/or positron become hydrated.

Ps formation in polar liquids

The temperature dependence on the Ps Yield in water and methanol shows completely opposite tendency of that in ethanol and propanol[17]. It is, probably, important to know the mechanism of Ps formation in alcohols to know what happens in water.

There are two kinds of electron scavengers that show the different types of the inhibition of the Ps formation in polar liquids[10]. $Te(OH)_6$, CH_3NO_2, Pb_2^+, BrO_4^-, SeO_4^{2-} and NO_3^- shows a full inhibition of Ps formation, and H^+, Ag^+, Cd_2^+ and Ti^+ show a partial inhibition. For PR experiment, there are two types of electron scavengers, too[15]. Acetone, chlorobenzene, carbontetrachloride and nitromethane inhibit the formation of whole solvated electrons, and fluorobenzene, H^+ and toluene inhibit just part of the solvated electrons, i.e. slowly formed solvated electrons.

M. A. Lewis et al. proposed a model to explain the PR experimental results as follows[15]. The fast formed solvated electrons are formed before thermalization. In this case, the energy of electrons are used to break hydrogen bond and orient molecules. At lower temperature, the fraction of the cluster of molecules is larger, and breaking the hydrogen bond and orienting the molecules to form the solvation might be more difficult. Which means that the probability of solvation with fast process would be lower. The mechanism of the slowly formed solvated electrons is that electrons are at first thermalized, and localized at the appropriate sites, then solvated. At lower temperature, the magnitude of the slowly formed solvated electrons increases, because of the increase of the sites for localization. The electrons before the fast formed solvation, i.e. hot electrons, can not be scavenged by fluorobenzene, H^+ and toluene. Hence, They inhibit the solvation partly.

Ps formation can be, perhaps, divided into two part. The first is not affected by temperature and not inhibited by H^+, Ag^+, Cd_2^+ and Ti^+, but by $Te(OH)_6$, CH_3NO_2, Pb_2^+, BrO_4^-, SeO_4^{2-} and NO_3^-. The second is affected by temperature and inhibited by all of the scavengers shown above[10]. It is quite

natural to think that the second part is correlated with the slowly formed solvation. The first might be due to the initial encounter pair of an electron and a positron. The second has not been known so well, especially the temperature dependence in methanol and ethanol[17]. The conclusion from PR indicates that there are more sites for electron (and positron?) localizing at lower temperature. Hence, Ps yield should be lower at lower temperature. It can explain the results of water and methanol. However, the PR experiment was done on ethanol and propanol. The mechanism of solvating positron, anti-particle of electron, must be different from that of electron in polar liquids. It might be difficult to localize positron in ethanol and propanol. Electron can be localized around H atom of OH group. If there exist a few hydrogen bonds, H atom at the end of the hydrogen bond is positively charged more. On the other hand, O atom is located between C atom and H atom, hence the negative charge might diffuse a little on the C atoms. That tendency might be larger in larger molecules. Water and methanol molecules are small, then positron can be localized as electron can. If positron can stay free after electron localized, the positron can pick off the localized electron to form Ps. It is probably the reason why temperature dependences of water and methanol are opposite of that of ethanol and propanol.

The appropriate site to localize electron or positron might correlated with hydrogen bond, i.e. cluster, as mentioned above.

CONCLUSIONS

The ortho-Ps intensity decreases linearly with increasing the concentration of D. This phenomena is caused by the difference of the thermalization distance of excess electrons in the spur. The size of the positron spur changes linearly with increasing the concentration of D.

The model of Ps formation in polar liquids such as water, methanol, ethanol and propanol is proposed. There are, very probably, two paths of Ps formation. One is the Ps formation from the initial encounter pair, which is not affected by temperature and not inhibited by H^+, Ag^+, Cd_2^+ and Ti^+. The other is the Ps formation from free electron and positron, or localized electron and free positron.

Acknowledgment - This study was started through the argument with Dr. Ole Erik Mogensen, but I could not argue with him about the results, unfortunately. I thank him for important suggestion on this work.

REFERENCES

1. C. D. Jonah and A. C. Chernovitz, CAN. J. Phys. 68, 935, (1990)
2. O. E. Mogensen, J. Chem. Phys. 60, 998, (1974)
3. O. E. Mogensen, POSITRON ANNIHILATION, North-Holland Publishing Company, 763, (1982)
4. O. E. Mogensen, "Positron Annihilation in Chemical Physics", (Springer, Heidelberg, to be published)
5. B. Lévay, S. J. G. Lund and O. E. Mogensen, Chem. Phys. 48, 97, (1980)
6. S. I. Ikawa and S. Maeda, Spectrochim. Acta. Part A 24, 655, (1967)
7. B. Lévay and A. Vértes, Radiochem. Radioanal. Letters 37, 27, (1979)
8. J. Facetti, J. Ch. Abbe, G. Duplatre, A. G. Maddock and A. Haessler, Radiat. Phys. Chem. 15, 541, (1980)
9. A. Singh, W. J. Chase and J. W. Hunt, Disc. Farad. Soc. 63, 28, (1977)
10. J. Ch. Abbe, G. Duplatre, A. Haessler and J. Talamoni, Radiat. Phys. Chem. 28, 19, (1986)
11. P. Kirkegaard, M. Eldrup, O. E. Mogensen and N. J. Pedersen, Computer Phys. Commun. 23, 307, (1981)
12. P. Kirkegaard, N. J. Pedersen and M. Eldrup, PATFIT-88, Risø-M-2740, (1989)
13. T. Hirade and O. E. Mogensen, Chem. Phys. 170, 249, (1993)
14. J. M. Wiesenfeld and E. P. Ippen, Chem. Phys. Lett. 73, 47, (1980)
15. M. A. Lewis and C. D. Jonah, J. Chem. Phys. 90, 5367, (1986)
16. A. Migus, Y. Gauduel, J. L. Martin and A. Antonetti, Phys. Rev. Lett. 58, 1559, (1987) S. Pommeret, A. Antonetti and Y. Gauduel, J. Am. Chem. Soc. 113, 9105, (1991)
17. J. Talamoni, J. Ch. Abbe, G. Duplatre and A. Haessler, Radiat. Phys. Chem. 21, 431, (1983)

3.4 Electron Mobilities and Electron-ion Recombination Rate Constants in Nonpolar Solvents

K.Shinsaka,[a] T.Odaka, K.Isoda, H.Yamada, M.Ukai, N.Kouchi and Y.Hatano
Department of Chemistry, Tokyo Institute of Technology, Meguro-ku, Tokyo 152, Japan; [a]Department of Electronics, Kanazawa Institute of Technology, Nonoichi-machi, Ishikawa-ken 921, Japan

Abstract Electron mobilities, μ_e, and electron-ion recombination rate constants, k_r, in liquids, dense gases, and solids of several nonpolar solvents such as hydrocarbons and rare gases have been measured by means of dc conductivity-pulse radiolysis, and for some solvents as functions of temperature, density and external dc-electric field strength. The k_r values in liquids vary in proportion to μ_e, up to ~ 100 cm^2/Vs in liquids; in accordance with the reduced Debye equation, $k_D=4\pi e\mu_e/\varepsilon$, where k_D is the recombination rate constant, e is the electron charge and ε is a dielectric constant of the solvent. In dense gases and liquids with higher μ_e values than ~ 100 cm^2/Vs, however, the k_r values deviate from the diffusion-controlled rate constant k_D to k_r values much slower values, where a k_r value seems to decrease lower with increasing the magnitude of relative mean-free-path, l/a, in which l is a mean-free-path of excess electrons and a is a reaction radius or with increasing inefficiency of electron-energy dissipation. The efficiency in electron-energy dissipation may be brought by lowering temperature or by increasing density. The effects of an external electric field on μ_e and k_r depend on a solvent and its phases, liquid or dense gaseous state. In liquid neohexane, for example, both μ_e and k_r show a gradual decrease with increasing an electric field, whereas in dense xenon gas these two values increase gradually with increasing electric field and decrease steeply after each peak value.

INTRODUCTION

The behavior of excess electrons is of great importance in the fundamental processes of radiation chemistry. It is greatly reflected in the mobility of excess electrons in the medium. Electron-ion

recombination has an important role in the loss processes of excess electrons and also in the initial precursor processes followed by many subsequent reactions leading to various final products. Electron-ion recombination in dilute gases has been intensively investigated experimentally (McGowan and Mitchell, 1984) and theoretically (Flannery) as one of the fundamental reactions in contrast to the liquids where the understanding of electron-ion recombination has been far behind. Since our work (Wada et al., 1977) on the liquid state was started, the knowledge of recombination in nonpolar liquids has made great advances. These are summarized recently in some review articles (Shinsaka and Hatano, 1990 and 1993; Hatano, 1994)

It has been known that in polar solvents, excess electrons are solvated in the initial early stage of radiolysis and therefore mobility of excess electrons becomes as low as ordinary ions,$\sim 10^{-3}cm^2/Vs$, and that the recombination proceeds between a solvated electron and a positive ion in a diffusion-controlled process. In nonpolar solvents, however, the solvation of excess electrons happens only to a very small extent if occurs. Therefore excess electrons can move much faster; mobilities of excess electrons are more than $\sim 10^{-1}cm^2/Vs$ and the recombination reaction proceeds very fast. A pulse radiolysis-dc conductivity method is useful for the measurement of electron mobilities and recombination rate constants of such fast reactions.

In the following, we describe the method of the measurement of electron mobilities and electron-ion recombination rate constants, and some features in the results.

EXPERIMENTAL

High purity samples were thoroughly purified further to get rid of a trace of electron-attaching impurities in various ways depending on the samples.

The values of μ_e and k_r were determined by analyzing a trasient electric current through a sample in a conductivity cell induced by irradiation of an X-ray pulse under a dc electric field.(Wada et al., 1977;Shinsaka and Hatano, 1990) At a low pulse dose, the contribution

of electron-ion recombination is negligible and the best fit value of μ_e is obtained for the theoretical decay of the transient current. At a high pulse dose, however, electron-ion recombination becomes effective, and the best fit value of k_r is determined for the approximate expression of the theoretical decay of the transient current by using the same value of μ_e already determined at a low pulse dose.

RESULTS AND DISCUSSION

Table 1 shows our experimental values of electron-ion recombination rate constants and electron mobilities in some nonpolar liquids with values by other researchers. Electron-ion recombination in nonpolar solvents is characterized by its very high reaction rate, which is 3～6 orders of magnitude larger than the neutralization rate constant for the well-known recombination of H_3O^+ and OH^- in aqueous solution(2.3×10^{-10} cm^3s^{-1} at 298K). Such very high recombination rate constants are mainly caused by much higher electron mobilities of electrons than those of ions. The observed electron-ion recombination rate constant, k_r, in the electron-mobility range up to ～100 $cm^2V^{-1}s^{-1}$ obeys the reduced Debye equation, as k_r values are nearly equal to the corresponding k_D values. However, k_r values in the solvents with a high electron mobility such as liquid methane, argon and krypton deviate from k_D with increasing μ_e as the ratio $k_r/k_D < 1$. About ten research groups have tried to explain the deviation theoretically in different ways from each other(Shinsaka and Hatano,1990). Although the complete explanation still remains unrealized, it has been made clear that two factors are very effective in determining recombination rate constants. One is a relative magnitude of a mean-free-path of excess electrons to a reaction radius a ; with increasing ratio 1/a, the recombination shows a larger deviation from a diffusion-controlled process, which is shown by a Monte Carlo simulation for electron-ion recombination(Tachiya, 1987a). The other is the efficiency of electron energy dissipation, of which importance was indicated semiempirically(Warman,1983); with increasing the efficiency of electron-energy dissipation, the recombination becomes more diffusion-controlled.

Table 1
Electron-ion recombination rate constants k_r and electron mobilities μ_e in nonpolar liquids

Liquid	T[K]	k_r[cm^3s^{-1}]	μ_e[$cm^2V^{-1}s^{-1}$]	k_r/k_D
n-Pentane	296	1.3×10^{-7}[a]	0.14[a]	1.0
n-Hexane	293	1.0×10^{-7}[b]	0.09[b]	1.2
Cyclohexane	293	3.2×10^{-7}[b]	0.35[b]	1.2
Neopentane	283	4.7×10^{-5}[c]	55[c]	0.9
Tetramethylsilane	296	8.0×10^{-5}[a]	100[a]	0.9
	298	8.5×10^{-5}[d]	104[d]	0.9
Neohexane	273	1.1×10^{-6}[e]	11[e]	1.0
Methane	123	3.0×10^{-4}[f]	420[f]	0.6
Argon	87	7.0×10^{-5}[g]	490[g]	0.11
Krypton	200	3.7×10^{-4}[h]	357[h]	0.61

[a]Allen and Holroyd,1974 [b]Baxendale et al.,1974 [c]Namba et al.,1979
[d]Nakamura et al.,1980 [e]Isoda et al.,1992 [f]Shinsaka et al.,1989
[g]Shinsaka et al.,1988 [h]Honda et al.,1992

The effects of an external electric field on μ_e and k_r depend on a solvent and its phases, liquid or dense gaseous states. In liquid neohexane, for example, both μ_e and k_r show a gradual decrease with increasing an electric field as the shown in Figs.3 and 4. In a dense xenon gas, however, both μ_e and k_r increase gradually with increasing an electric field and decrease steeply after each peak value as shown in Fig.1 and the ratio k_r/k_D also indicates a peak as shown in Fig.2.

The k_r/k_D ratio in dense gaseous xenon at a very low electric field is much less than unity(0.25) even at a low μ_e value (15 cm^2/Vs).

The k_r value in liquid methane or argon increases roughly in proportion to the external electric field in the range of a low electric field and decreases abruptly in a higher range of an electric field as a similar variation in dense xenon gas as shown in Figs.1 and 2. However, the μ_e values in liquid methane and argon are almost

constant in a low electric field region and decrease steeply with further increase in the electric field.

The k_r/k_D ratio in the liquid state is larger than that in a dense gaseous state, which increases with increasing a density in a low electric field region as shown in Fig.4. The k_r/k_D ratio in dense gaseous methane increases with increasing temperature at almost the same density (Shinsaka et al.,1989). These facts indicate that the k_r value seems to become lower with increasing the inefficiency of electron-energy dissipation. The efficiency in electron-energy dissipation may be brought by lowering a temperature or by increasing a density. The gradual increase in k_r with increasing an electric field in liquid methane (Nakamura, et al.,1983), argon (Shinsaka et al.,1988) and in dense gaseous methane (Shinsaka et al.,1989), argon (Shinsaka,et al.,1988), and krypton (Honda et al.,1992) may occur due to the increase in probability of encounter between electrons and a positive ions by disentangling the trajectory of excess electrons (Tachiya,1987b) or by the increase in the drift velocity. The steep decrease in k_r may occur due to the electron heating which means that the electron gains its kinetic energy from the external electric field more than that of thermal equilibrium.

It is surprising that the k_r/k_D values in solid methane(Nakamura, et al.,1983) and argon (Shinsaka et al.,1988) are close to unity even in a high electron-mobility region where the μ_e value in solid argon is 1690 cm^2/Vs at 80 K and this may be caused by a highly efficient mode of electron-energy dissipation in these solids such as crystal lattice vibrations.

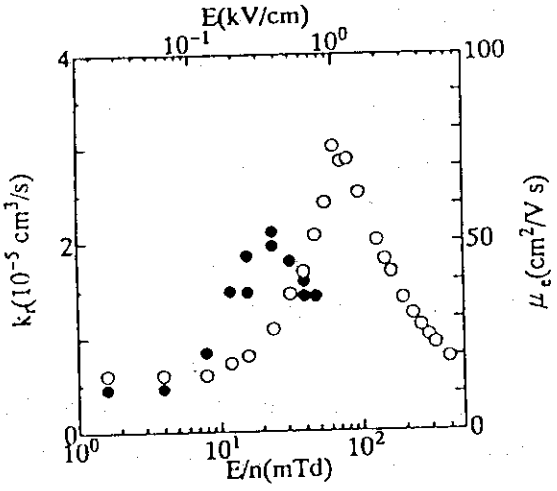


Fig.1 Electric field dependence of μ_e(○) and k_r(●) in dense Xe gas
(T=291K, n=1.6× $10^{21}cm^{-3}$)
(Odaka et al.,1994)

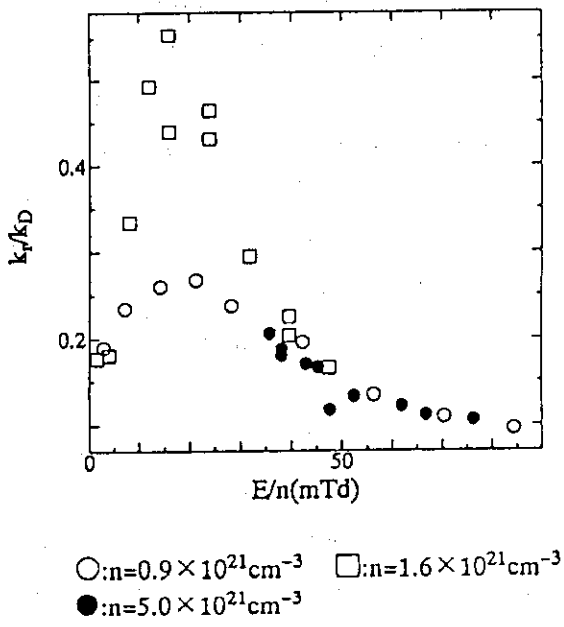


Fig.2 Electric field dependence of k_r/k_D in dense Xe gas
(T=291K)
(Odaka et al.,1994)

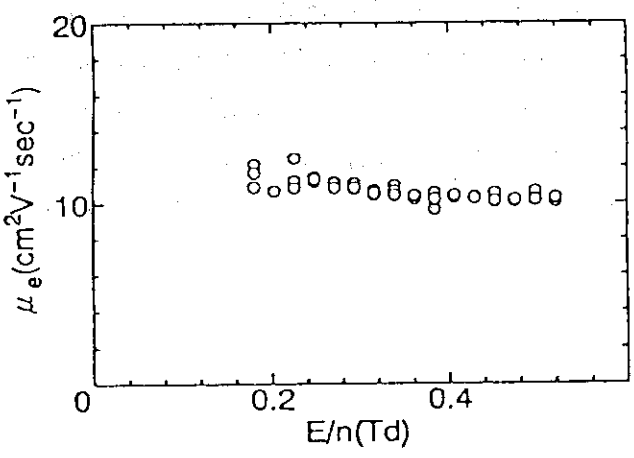


Fig.3 Electric field dependence of μ_e in liquid neohexane
(T=273K, n=4.57× $10^{21}cm^{-3}$)
(Isoda et al., 1992)

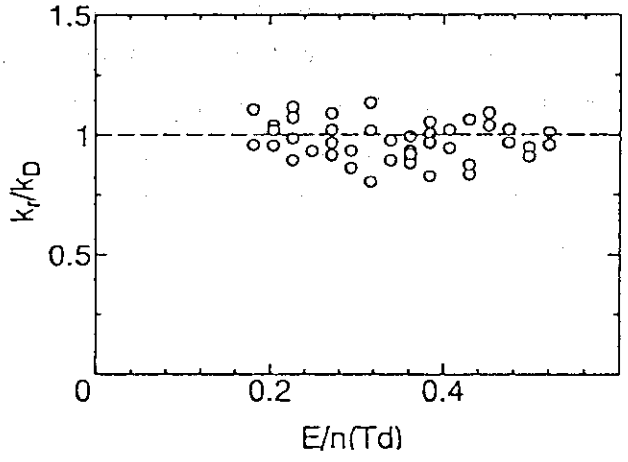


Fig.4 Electric field dependence of k_r/k_D in liquid neohexane
(T=273K, n=4.57× 1021cm-3
(Isoda et al.,1992)

REFERENCES

Allen A.O. and Holroyd R.A.(1974) J.Phys.Chem.78,796.

Baxendale J.H., Keene J.P. and Rasburn E.J.(1974) J.Chem.Soc.Faraday Trans.I,70,718.

Flannery M.R. Adv.Atom.Molec.Opt.Phys. 32, in press.

Hatano Y.(1994),"Electron-ion Recombination in Dense Molecular Media" in "Linking the Gaseous and Condensed Phases of Matter-The Behavior of Slow Electrons-",eds., Christophorou L.G. Illenberger E. and Schmidt W.F.NATO ASI Series B,Vol.326,pp.467-486.

Honda K., Endou K., Yamada H., Shinsaka K., Ukai M., Kouchi N. and Hatano Y.(1992) J.Chem.Phys. 97, 2386.

Isoda K., Yamada H., Shinsaka K., Ukai M., Kouchi N. and Hatano Y.(1992) Abstract,Jpn.Annu.Symp.Radiat.Chem, p.59.

McGowan J.Wm. and Mitchell J.B.A.(1984) "Electron-Molecular Positive Ion Recombination" in "Electron-Molecule Interactions and Their Applications" eds., Christophorou L.G, vol.2, Academic Press, Orlando, pp.65-88.

Nakamura Y., Shinsaka K. and Hatano Y.(1983) J.Chem.Phys. 78,5820.

Nakamura Y., Namba H., Shinsaka K. and Hatano Y.(1980) Chem.Phys.Lett. 76,311.

Namba H., Shinsaka K. and Hatano Y.(1979) J.Chem.Phys. 70,5331.

Odaka T., Isoda K. Shinsaka K. Ukai M. Kouchi N. and Hatano Y.(1994) Abstract,Jpn.Annu,Symp.Radiat.Chem, p.93.

Shinsaka K. and Hatano Y.(1990) "Electron-Ion Recombination in Dense Molecular Media" in "Nonequilibrium Effects in Ion and Electron Transport" eds., Gallagher J.W., Hudson D.F., Kunhardt E.E. and Van Brunt R.J., Plenum Press, New York, pp.275-289.

Shinsaka K., Codama M., Srithanratana T., Yamamoto M. and Hatano Y.(1988) J.Chem.Phys. 88,7529.

Shinsaka K., Codama M., Nakamura Y., Serizawa K. and Hatano Y.(1989) Radiat.Phys.Chem. 34,519.

Shinsaka K. and Hatano Y.(1993) Nucl, Instr. Methods, A327, 7.

Tachiya M.(1987a) J.Chem.Phys. 87,4108.

Tachiya M.(1987b) J,Chem.Phys. 87,4622.

Wada T., Shinsaka K., Namba H. and Hatano Y.(1977) Can.J.Chem. 55,2144.

Warman J.M.(1983) J.Phys.Chem. 87,4353.

3.5 The Reactions of Excited Radical Ions Produced by Pulse Radiolysis

Tetsuro Majima,* Akito Ishida, and Setsuo Takamuku

The Institute of Scientific and Industrial Research, Osaka University, Mihogaoka 8-1, Ibaraki, Osaka 567, Japan

Abstract The reactions of *cis*- and *trans*-stilbene radical cations in the photoexcited state (*c*-$St^{+\cdot}$*, *t*-$St^{+\cdot}$*) have been studied by pulse radiolysis-laser flash photolysis combined method. *c*-$St^{+\cdot}$* isomerizes to *t*-$St^{+\cdot}$ in the quantum yield of 0.3-0.4, while *t*-$St^{+\cdot}$* does not isomerize into *c*-$St^{+\cdot}$. *t*-$St^{+\cdot}$* is quenched by anisole via hole transfer quenching, while *c*-$St^{+\cdot}$* is not quenched. The lifetime of *t*-$St^{+\cdot}$* is estimated to be 100-200 ps, while that of *c*-$St^{+\cdot}$* is extremely shorter. The short lifetime of *c*-$St^{+\cdot}$* is attributed to the fast adiabatic isomerization process to *t*-$St^{+\cdot}$* and to the fast internal conversion from *c*-$St^{+\cdot}$* because of an allowed transition from the doublet excited state to the doublet ground state.

INTRODUCTION

Radical cations of aromatic compounds are predominantly generated with γ-radiolysis in rigid matrices at 77 K (Shida, 1988) or pulse radiolysis in solutions at room temperature (Arai et al., 1967). Such radical cations have relatively strong absorptions at longer wavelengths than those at which the precursor compounds absorb. Therefore, radical cations can be excited by irradiation of a laser flash at the wavelength where the radical cations absorb, within the lifetime of the radical cations. We have developed the pulse radiolysis-flash photolysis combined system (Ebbesen, 1988; Ebbesen et al., 1988; Sumiyoshi et al., 1992 and 1993; Ishida et al., 1992) composed with the first irradiation of a ns electron pulse and the second irradiation of a ns laser flash with an interval time of approximately 30 ns-1μs, in order to study radical ions in the photoexcited states. In the present work photochemical $c \rightarrow t$ one way isomerization of *cis*-stilbene radical cation (*c*-$St^{+\cdot}$) to *trans*-stilbene radical cation (*t*-$St^{+\cdot}$) is studied with transient absorption measurements using this technique.

EXPERIMENTAL

A solution containing a substrate in 1,2-dichloroethane (DCE) was irradiated firstly with an electron pulse (28 MeV, 8 ns duration, 0.7 kGy $pulse^{-1}$, diameter of 0.4 cm) and secondary with a laser flash (532 nm, 5 ns duration, 100 mJ $pulse^{-1}$, diameter of 0.5 cm) at a delay time of 50 ns after the electron pulse at room temperature. The probe beam from a 450 W Xe-lamp synchronized with the electron pulse was passed through the irradiation cell and monitored by a PMT after a monochromator.

RESULTS AND DISCUSSION

Pulse radiolyses of *c*-St or *t*-St in 1,2-dichloroethane at room temperature generate selectively *c*-$St^{+\cdot}$ and *t*-$St^{+\cdot}$ with the absorption maxima at 515 and 480 nm, respectively (Shida, 1988). Decay of $St^{+\cdot}$ is analyzed by neutralization with Cl^- formed from dissociative electron attachment to DCE and bimolecular reaction with a neutral St to give dimer radical cations ($St_2^{+\cdot}$) which decompose into the thermodynamically stabler *t*-$St^{+\cdot}$ and *t*-St at room temperature.

The excitation of $St^{+\cdot}$ at 532 nm generates $St^{+\cdot}$ in the photoexcited state ($St^{+\cdot}$*) with the excited energy of 53 kcal mol^{-1} (eq. 1). The asterisk denote the excitation from the doublet ground state to the doublet excited state. The excitation of *t*-$St^{+\cdot}$ at 532 nm did not cause any changes of the transient absorption spectrum and the time profiles of optical densities at 480 nm (OD_{480}) (Fig. 1). Therefore, *t*-$St^{+\cdot}$ does not isomerize into *c*-$St^{+\cdot}$ with the irradiation but decays rapidly to *t*-$St^{+\cdot}$ (eq. 2). On the other hand, the spectrum of *c*-$St^{+\cdot}$ with a maximum at 515 nm changed to that of *t*-$St^{+\cdot}$ with a maximum at 480 nm immediately after the laser flash (Fig. 2). OD_{515} decreased, while OD_{480} increased immediately after the laser flash. Therefore, photochemical $c \rightarrow t$ one way isomerization of *c*-$St^{+\cdot}$ to *t*-$St^{+\cdot}$ proceeds within a laser flash (eq. 3), similarly to results reported by Ebbesen (1988) and Kuriyama et al (1994).

$$St^{+\cdot} + h\nu\ (532\ nm) \rightarrow St^{+\cdot}* \quad (1)$$

$$t\text{-}St^{+\cdot}* \rightarrow t\text{-}St^{+\cdot} \quad (2)$$

$$c\text{-}St^{+\cdot}* \rightarrow t\text{-}St^{+\cdot} \quad (3)$$

$$c\text{-}St^{+\cdot}* \rightarrow c\text{-}St^{+\cdot} \quad (4)$$

$$t\text{-}St^{+\cdot}* + A \rightarrow t\text{-}St + A^{+\cdot} \qquad (k_A = k_{diff} = 7.8\times10^9\ M^{-1}\ s^{-1}) \quad (5)$$

$$c\text{-}St^{+\cdot}* \rightarrow t\text{-}St^{+\cdot}* \quad (6)$$

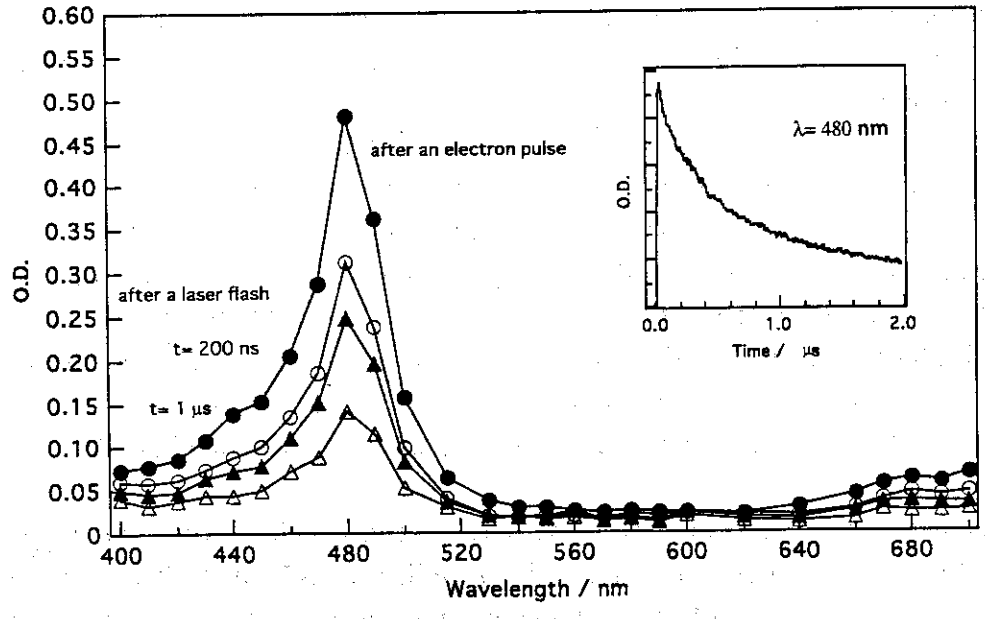


Fig. 1. Transient absorption spectra recorded immediately (●) after the electron pulse, and immediately (○), 200 ns (▲), and 1 μs (△) after the laser flash in the experiment of *t*-St (5 mM) in Ar-saturated DCE. Inset: kinetic traces illustrating the time profile of OD_{480}.

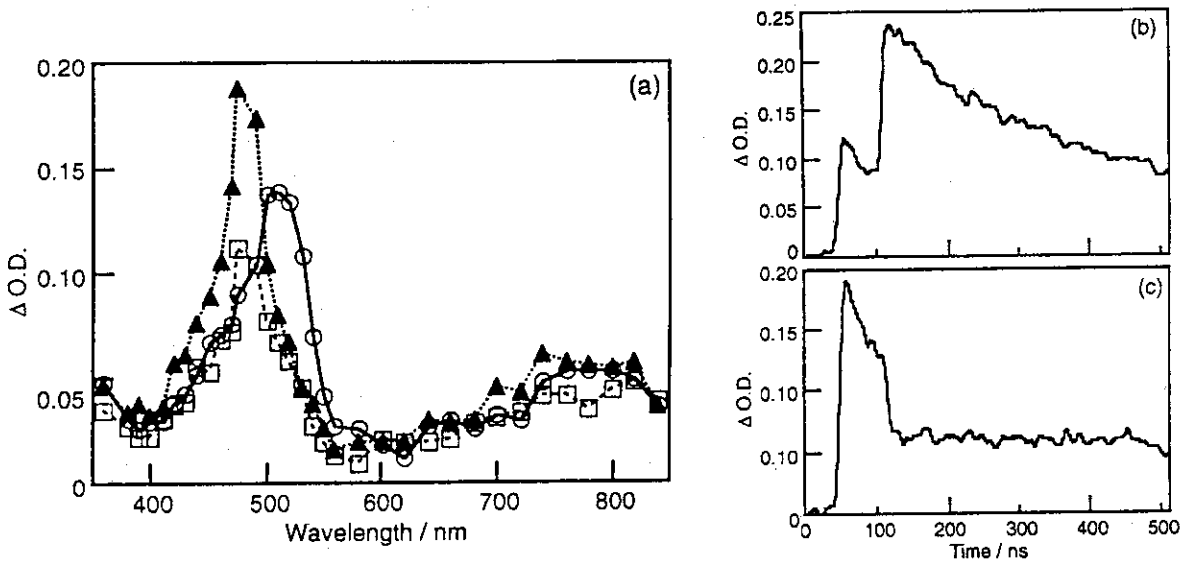


Fig. 2. Transient absorption spectra recorded 77 ns (○) after the electron pulse, and 40 ns (▲) and 260 ns (□) after the laser flash in the experiment of *c*-St (5 mM) in Ar-saturated DCE (a). Kinetic traces illustrating the time profiles of OD_{480} (b) and OD_{515} (c).

The concentrations of *c*-$St^{+\cdot}$ disappeared ($[c\text{-}St^{+\cdot}]_{disapp}$= 1.2×10^{-5} M) and *t*-$St^{+\cdot}$ formed ($[t\text{-}St^{+\cdot}]_{form}$= 1.0×10^{-5} M) immediately after the laser flash were calculated from the differences of OD at λ nm before and after the laser flash, the absorption molar coefficients of *c*-$St^{+\cdot}$ and *t*-$St^{+\cdot}$ at λ nm, and the optical path length of 0.4 cm. The values demonstrate that the photochemical conversion of *c*-$St^{+\cdot}$ per a flash is approximately 80 % on the basis of concentrations of *c*-$St^{+\cdot}$ before irradiation of the laser flash ($[c\text{-}St^{+\cdot}]_0$= 1.5×10^{-5} M), that the chemical yield of *t*-$St^{+\cdot}$ from *c*-$St^{+\cdot}$* is 83 % per a flash, and therefore that isomerization of *c*-$St^{+\cdot}$ proceeds almost stoichiometrically to *t*-$St^{+\cdot}$.

The number of laser photons absorbed by *c*-$St^{+\cdot}$ generated in the pulse radiolysis were calculated to be 3.0×10^{-5} einstein l^{-1} from OD_{532}= 0.13 for *c*-$St^{+\cdot}$ for the laser beam path (1.0 cm) using an actinometry of T-T absorption of zinc tetraphenylporfirin dichloride at 470 nm in cyclohexane ($\varepsilon_T\phi_T$= 50000 M^{-1} cm^{-1} at 470 nm) (Ebbesen, 1988). Therefore, the quantum yield of photochemical $c \rightarrow t$ isomerization of *c*-$St^{+\cdot}$ was calculated to be approximately 0.3-0.4 which is similar to 0.25-0.35 estimated from the value of $|\Delta OD_{480}|$ and the absorbed laser photons in excitation of *c*-$St^{+\cdot}$ at 500-590 nm (Ebbesen, 1988). Therefore, *c*-$St^{+\cdot}$* isomerizes into *t*-$St^{+\cdot}$ in 30-40 % and is deactivated to *c*-$St^{+\cdot}$ via internal conversion in 60-70 % yield (eq. 4).

Quenching of $St^{+\cdot}$* can be induced using hole transfer quechers which can not work as a hole acceptor for $St^{+\cdot}$ but for $St^{+\cdot}$*. Hole donor ability of $St^{+\cdot}$* is higher than that of $St^{+\cdot}$ because of the excited energy of $St^{+\cdot}$*. Although a number of aromatic compounds have been attempted as the hole transfer quencher of *c*-$St^{+\cdot}$*, most of them worked as a hole acceptor of *c*-$St^{+\cdot}$. Anisole did not work a hole acceptor of $St^{+\cdot}$, since $E_{1/2}^{ox}$= 1.76 V of A (Zwei et al,

1964) is higher than $E_{1/2}^{ox}$= 1.25 and 1.14 V of *c*-St and *t*-St vs. Ag/Ag^+ in acetonitrile. The reduction potentials of *c*-$St^{+\cdot}$* and *t*-$St^{+\cdot}$* are expected to be 1 or 2 V higher than those of *c*-$St^{+\cdot}$ and *t*-$St^{+\cdot}$ because of the excited energy of 53 kcal mol^{-1}. Therefore, the hole transfers from $St^{+\cdot}$* to A proceed essentially with highly exothermic energy ($\Delta E_{1/2}^{ox}$< -1 V), and at the diffusion-controlled rate in DCE, $k_A = k_{diff} = 7.8 \times 10^9\ M^{-1}\ s^{-1}$.

Pulse radiolysis of A itself in DCE provided radical cations of A ($A^{+\cdot}$) and anisole dimer ($A_2^{+\cdot}$) which absorb at around 350 and 450-700 nm and are stable in the time scale of 1 μs (Takamuku et al., 1989). Pulse radiolysis of *c*-St or *t*-St in the presence of excess A ([A]/[St]= 40-220) produced initially $A^{+\cdot}$ and $A_2^{+\cdot}$ as main radical cations and $St^{+\cdot}$ in a part. Then, the hole transfer from $Q^{+\cdot}$ ($A^{+\cdot}$ or $A_2^{+\cdot}$) to St proceeded to give $St^{+\cdot}$ at the rate constant of 7.8×10^9 $M^{-1}\ s^{-1}$ which is equivalent with k_{diff} because of the highly exothermic energy of the hole transfer process, $Q^{+\cdot} + St \rightarrow St^{+\cdot} + Q$. Finally $St^{+\cdot}$ was generated at the concentration of 1.4×10^{-5} M which was nearly equal to $[St^{+\cdot}]_0$ in the absence of A.

The irradiation of *t*-$St^{+\cdot}$ in the presence of A caused a decrease of OD_{480} immediately after the flash (Fig. 3a). $|\Delta OD_{480}|$ increased with increasing [A]: $|\Delta OD| = \varepsilon^t \cdot [t\text{-}St^{+\cdot}]_{disapp} + \varepsilon^Q \cdot [Q^{+\cdot}]_{disapp}$, where ε^Q and $[Q^{+\cdot}]_{disapp}$ denote the absorption molar coefficients of $Q^{+\cdot}$ and the molar concentrations of $Q^{+\cdot}$ disappeared immediately after the laser flash. Therefore, hole transfer quenching of *t*-$St^{+\cdot}$* by A occurs with the rate constant of $k_A = k_{diff} = 7.8 \times 10^9\ M^{-1}\ s^{-1}$ (eq. 5). From the Stern-Volmer relation of $[t\text{-}St^{+\cdot}]_{disapp}/[t\text{-}St^{+\cdot}]_0$ and [A], the lifetime of *t*-$St^{+\cdot}$* was estimated to be approximately 200 ps.

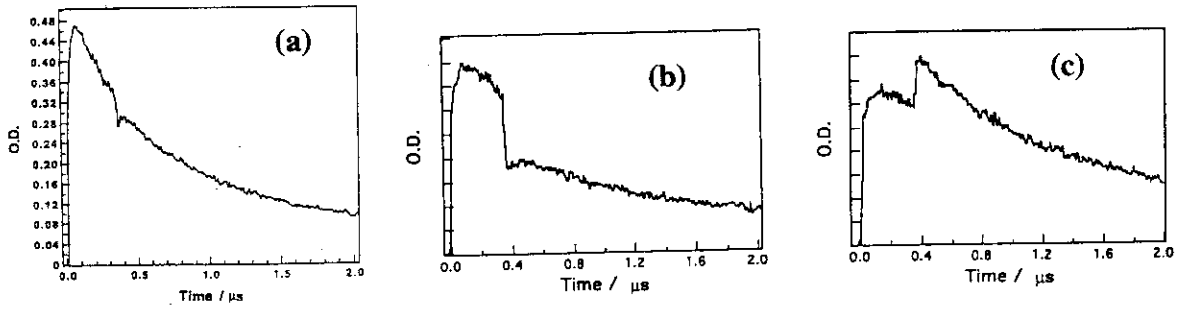


Fig. 3. Kinetic traces illustrating the time profile of (a) OD_{480} in the experiment of *t*-St (5 mM), (b) OD_{515} and (c) OD_{480} in the experiment of *c*-St (5 mM) in the presence of A (1 M).

The irradiation of *c*-$St^{+\cdot}$ in the presence of A caused different behaviors of changes of OD immediately after the flash (Fig. 3b, 3c), where $|\Delta OD| = \varepsilon^c \cdot [c\text{-}St^{+\cdot}]_{disapp}^{A} - \varepsilon^t \cdot [t\text{-}St^{+\cdot}]_{form}^{A} + \varepsilon^Q \cdot [Q^{+\cdot}]_{disapp}$. Concentrations of *c*-$St^{+\cdot}$ disappeared ($[c\text{-}St^{+\cdot}]_{disapp}^{A}$) and *t*-$St^{+\cdot}$ formed ($[t\text{-}St^{+\cdot}]_{form}^{A}$) in the presence of A were calculated from $|\Delta OD_{515}|$ and $|\Delta OD_{480}|$. $[t\text{-}St^{+\cdot}]_{form}^{A}$ decreased with increasing [A], while $[c\text{-}St^{+\cdot}]_{disapp}^{A}$ did not change within experimental errors. Consequently, the results show that *c*-$St^{+\cdot}$* was not quenched by a hole transfer quencher A at [A]= 0.2-1.3 M because of the shorter lifetime but the formation of *t*-$St^{+\cdot}$ were queched by A. Therefore, *c*-$St^{+\cdot}$* is not be quenched by A but is deactivated via internal conversion (eq. 4) or converts to *t*-$St^{+\cdot}$* via adiabatic isomerization from *c*-$St^{+\cdot}$* to *t*-$St^{+\cdot}$* on the energy surface of $St^{+\cdot}$* (eq.

6). Then t-$St^{+\cdot}$* formed is deactivated to t-$St^{+\cdot}$ (eq. 2) or quenched by A at the diffusion-controlled rate (eq. 5). Therefore, the lifetime of t-$St^{+\cdot}$* was estimated to be approximately 100 ps from the Stern-Volmer relation of $[t\text{-}St^{+\cdot}]_{disapp}/[t\text{-}St^{+\cdot}]_0$ and [A]. Since the estimation involves the large experimental errors more than 50 %, the lifetime of 100 ps is almost equivalent to 200 ps on the basis of the experiment of t-$St^{+\cdot}$.

The potential surface of $St^{+\cdot}$* is supposed to be a slope upon rotation from c to t with no minimum at the 90 degree twisted geometry (Ebbesen, 1988). On the other hand, the second doublet excited state of c-$St^{+\cdot}$* is assumed to cross avoidedly with the first doublet excited state which leads to t-$St^{+\cdot}$ in the ground state via an allowed crossing (Kuriyama et al, 1994). It is found in the present work that c-$St^{+\cdot}$* isomerizes rapidly into t-$St^{+\cdot}$* and decays into c-$St^{+\cdot}$ through internal conversion. On the other hand, t-$St^{+\cdot}$* decays into t-$St^{+\cdot}$ as the deactivated process with τ_f= 100-200 ps.

CONCLUSIONS

We have found that anisole acts as a selective donor molecule for t-$St^{+\cdot}$* via hole transfer process, but not for c-$St^{+\cdot}$*. The lifetime of t-$St^{+\cdot}$* is estimated to be approximately 100-200 ps, while that of c-$St^{+\cdot}$* is extremely shorter. Therefore, the fast adiabatic isomerization from c-$St^{+\cdot}$* to t-$St^{+\cdot}$* proceeds on the energy surface of $St^{+\cdot}$*.

Acknowledgment. We wish to thank Professor Katsumi Tokumaru, Tsukuba University, and Professor Seiichi Tagawa, Osaka University, for useful discussions. We are also grateful to Mr. Masayuki Fukui at Osaka University for help with the experiments. This work was partly supported by a Grant-in-Aid (No. 05453121) from the Ministry of Education, Science and Culture of Japan.

REFERENCES

Arai S., Grev D. A. and Dorfman L. M. (1967)*J. Chem. Phys.* **46**, 2572.

Ebbesen T. W. (1988) *J. Phys. Chem.* **92**, 4581.

Ebbesen T. W., Akaba R., Tokumaru K., Washio M., Tagawa S. and Tabata Y. (1988) *J. Am. Chem. Soc.* **110**, 2147.

Ishida A., Yamamoto K. and Takamuku S. (1992) *Bull. Chem. Soc. Jpn.* **65**, 3186.

Kuriyama Y., Hashimoto F., Tsuchiya M., Sakuragi H. and Tokumaru K. (1994)*Chem. Lett.* 1371.

Shida T. (1988) *Electronic Absorption Spectra of Radical Ions*, Elsevier, Amsterdam.

Sumiyoshi T., Sakai H., Kawasaki M. and Katayama M. (1992) *Chem. Lett.* 617.

Sumiyoshi T., Kawasaki M. and Katayama M. (1993) *Bull. Chem. Soc. Jpn.*. **66**, 2510.

Takamuku S., Komitsu S. and Toki S. (1989) *Radiat. Phys. Chem.* **34**, 553.

Zweig A., Hodgson W. G. and Jura W. H. (1964) *J. Am. Chem. Soc.* **86**, 4124.

3.6 Selecting Ethanol as an Ideal Organic Solvent Probe in Radiation Chemistry γ-radiolysis of Acetone-ethanol System and Acetophenone-ethanol System

Jin Haofang, Wu Jilan, Fang Xingwang and Zhang Xujia

Technical Physics Department, Peking University, Beijing 100871, P. R. China

ABSTRACT: Radiolysis of acetone-ethanol solution and acetophenone-ethanol solution has been studied in this work. The dependences of G values of the final γ radiolysis products such as H_2, 2,3-butanediol and acetaldehyde on additive concentration in liquid ethanol have been obtained. There are two kinds of new final products, isopropanol and 2-methyl-2,3-butanediol are detected in irradiated acetone-ethanol solution. As for acetophenone-ethanol system, more new final products are found.

In addition, experiments of pulse radiolysis upon acetophenone-ethanol solution have also been performed. The absorption spectrum with λmax at 315nm and 440nm is observed, which is assigned to ketyl radical ion $C_6H_5(CH_3)CO^-$ And the reaction mechanism of the two systems is proposed respectively with a moderate success.

Keywords: Radiolysis, Probe, Acetone, Acetophenone, Disproportionation

INTRODUCTION

Developing the theory of radiation chemistry requires accurate knowledge of the yields of intermediates and final products in irradiated systems. Radiation chemistry of water has been studied extensively and abundant experimental data have been obtained over a great variety of conditions[1,2,3]. The wealth of theoretical and experimental information makes water a useful model to predict the reaction mechanism of H, e^-_{aq} and OH with organic compounds. Now, many biological compounds are hydrophobic and they are not soluble in water. Therefore, the radiolysis of cyclohexane[4,5,6], which is a symmetrical nonpolar organic media , has been extensively investigated due in part to the fact that all C-C bond and all C-H bond are equivalent in cyclohexane, it means fewer numbers of products are obtained comparing with that of the straight-chain hydrocarbon. Meanwhile, the majority of biological compounds are still insolube in cyclohexane, therefore, the application of cyclohexane as a model in radiation chemistry is confined . Since the 1960's, radiation chemists have shown great interest in the radiolysis of ethanol and a lot of experiments have been carried out[7,8,9,10]. Being a classical polar organic solvent, ethanol shares some similarity with water in radiation chemistry. For example, both of their polar character has influence on the solvation and reactions of the electron and other charged species produced upon irradiation. The predominant advantage of liquid ethanol is that most of the organic compounds are easily soluble in ethanol. Nevertheless, many previous experiments performed often employed various additives as probe to study the behaviour of transient species such as e^-_{solv} H and α-hydroxyethyl, little has been done to survey the products resulting from the reaction of additive with intermediates. Therefore, it is often difficult to achieve a material balance between final products and intermediates, which may lead to an incorrect interpretation of the established mechanism. Recently, by using styrene, MPP and acrylic acid as additives [9,11,12] , Wu found that α-hydroxyethyl radical did not undergo disproportionation in liquid ethanol and the reaction mechanism was proposed. Later, using acetone as additive[13], Zhang has studied the dependences of the major final products on acetone concentration and started on surveying the products resulting from the reaction of acetone and intermediates of irradiated ethanol. A new final product, 2-methyl-2,3-butanediol is obtained. However, the material balance is still unresolved and the obtained ratio of rate constants $k(e^-_{solv}+CH_3CHO/e^-_{solv}+CH_3COCH_3)=5$ is inconsistent with that of obtained from pulse radiolysis experiments, and it seems abnormal for ketone to capture solvated electron in ethanol solution comparing that in aqueous solution. The purpose of this paper is in hope of clarifying the reaction mechanism by re-examining the study of acetone-ethanol system and identifying that ethanol can act as an ideal organic solvent in radiation chemistry. It can be further used as solvent probe in acetophenone-ethanol solution. Because of the structure similarity between acetophenone and flavonoids, our purpose of this work is to present the results and to gather all the information in order to use the radiolysis of the acetophenone-ethanol system as a tool for studying the flavonoid radical chemistry and the

pharmacological function of flavonoids.

EXPERIMENTAL

Absolute ethanol and acetone(Beijing Chemical Plant) were used after purification. The aldehyde content was reduced less about 10^{-6} mol dm^{-3}. The samples were deaerated with high purified nitrogen gas(>99.99%), irradiated at about 20°C with ^{60}Co γ-ray at dose rate 2.0Gy s^{-1}. The yield of hydrogen was determined by GC (instrument: Shimadzu GC-9A; column: 5A molecular sieve; detector: TCD; carrier gas: nitrogen). Those of 2,3-butanediol and acetaldehyde were also performed with GC(instrument: Shimadzu GC-9A; column: PEG, 2m glass column; detector: FID; a special column: chromosob106 for detecting C_2-C_5 alcohol was employed.)

Acetophenone(A.R.) was used as supplied after purification. The new radiolytic products were detected also with Shimadzu GC-9A(column: OV-1, 2m glass column). Shimadzu GC-14A MS (column: OV-1 25m capillary column, FID detector) was used to identify the P1, P2 P3 and P4.

The pulse radiolysis was carried out using a Van de Graff 2.8 Mev electron generator(High Voltage Eng. Co.) delivering 0.4μs electron pulse of 1-50Gy in the Max-Planck Institute of Germany. The pulse radiolysis set-up and detection techniques have been described in detailing[19]. Dosimetry was performed by the SCN^- method(0.01 mol dm^{-3} KSCN, N_2O-saturated) using $G((SCN)_2^{\cdot-})=6.0$ and $\varepsilon_{480}=7600$ mol^{-1} dm^3 cm^{-1}. Unless otherwise stated, dose per pulse used was around 1Gy.

RESULTS AND DISCUSSION

I. THE γ–RADIOLYSIS OF ACETONE-ETHANOL SYSTEM

The yields of the three major products, hydrogen, acetaldehyde and 2,3-butanediol are plotted as functions of the concentrations of acetone C in Fig.1. The most remarkable result is that acetone inhibits the formation of 2,3-butanediol and unaffects hydrogen, while the $G(CH_3CHO)$ values rise significantly with increasing acetone concentration. All of these are approximately consistent with the results obtained by Zhang. In addition, two new final products are found. One of the products has been detected by using gas chromatography and GC-MS[M/Z 59(100), 45(10), 71(10), 89(8)]. As for isopropanol, it is identified with the standard compound which appears in the same region . And depending on the known concentrations of the two standard compounds, the G values of the two products are calculated, both of them increases with the increasing concentration of acetone(as illustrated in Fig.1), which is parallel with that of released acetaldehyde and the consumption of acetone. (as shown in Fig.1)

It should be noted that all the concentrations of acetone scaled on the plot are initial concentration. (e.g. before irradiated)

The present results are consistent with many of the features of the mechanism proposed for the radiolysis of liquid ethanol by Wu[9]. The following is just a refinement of their established mechanism which is relying on the present results and consideration of the yields of the new final products. (The square brackets indicate that the entities are within in spur.)

When γ-radiolysis upon liquid ethanol, following reactions occur initially.

$$C_2H_5OH \longrightarrow [C_2H_5OH^+ + e^-] \quad G=2.0 \quad (1)$$

$$\longrightarrow [CH_3CHOH^+ + H^{\cdot} + e^-] \quad G=2.0 \quad (2)$$

$$[CH_3CHOH^+ + CH_3CH_2OH] \longrightarrow [CH_3CHO + CH_3CH_2OH_2^{\cdot}] \quad G=2.0 \quad (3)$$

$$[CH_3CH_2OH_2^+ + e^-] \longrightarrow [CH_3CH_2OH + H] \quad G=0.3 \quad (4)$$

$$[CH_3CH_2OH^+ + e^-] \longrightarrow CH_3CHO + H_2 \quad G=1.7 \tag{5}$$

$$\longrightarrow CH_3CH_2O\,(G=0.3) + H_2\ (G=0.15) \tag{6}$$

$$[e^- + CH_3CH_2OH] \longrightarrow e^-_{solv} \quad G=1.7 \tag{7}$$

$$CH_3CH_2O + CH_3CH_2OH \longrightarrow CH_3CHOH + CH_3CH_2OH \quad G=0.3 \tag{8}$$

$$e^-_{solv} \longrightarrow CH_3CH_2O^- + H \tag{9}$$

$$e^-_{solv} + CH_3CH_2OH_2^+ \longrightarrow CH_3CH_2OH + H \quad G=1.7 \tag{9'}$$

$$H + C_2H_5OH \longrightarrow H_2 + CH_3CHOH \quad G=4.15 \tag{10}$$

$$CH_3CHOH \longrightarrow (CH_3CHOH)_2 \quad G=2.1 \tag{18}$$

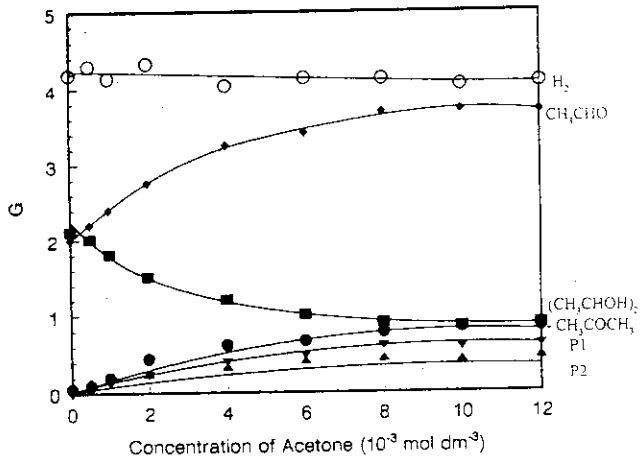


Fig. 1 The dependences of G values on acetone conc.;
system saturated with N_2; dose rate:2Gy/s; dose:6000Gy

While absence of additives and dose>160Gy, reactions(11) and(12) become important:

$$e^- + CH_3CHO \longrightarrow CH_3CHO^- \tag{11}$$

$$CH_3CHO^- + CH_3CH_2OH_2^+ \longrightarrow CH_3CHOH + CH_3CH_2OH \tag{12}$$

However, if acetone present as additive in this system, an alternative to reaction(10) as a fate for the solvated electrons e^-_{solv} might be:

$$e^-_{solv} + CH_3COCH_3 \longrightarrow CH_3CO\cdot CH_3 \quad G=1.7 \tag{13}$$

$$CH_3CO\cdot CH_3 + CH_3CH_2OH_2^+ \longrightarrow CH_3C\cdot OHCH_3 + CH_3CH_2OH \quad G=1.7 \tag{14}$$

Thus, acetaldehyde is released. Then, what about the fate of CH_3COHCH_3 radical. Considering the new products, following reactions might occur:

$$2CH_3C\cdot OHCH_3 \longrightarrow CH_3COCH_3 + CH_3CHOHCH_3 \quad G=0.35 \tag{15}$$

$$CH_3COHCH_3 + CH_3CHOH \longrightarrow CH_3HC(OH)C(OH)(CH_3)_2 \quad G=0.6 \tag{16}$$

$$CH_3CHOH + CH_3COHCH_3 \longrightarrow CH_3COCH_3 + CH_3CH_2OH \quad G=0.3 \tag{17}$$

Comparing the consumption of acetone and the redox potential of CH_3CHOH and CH_3COHCH_3 radical ($E_{CH_3COHCH_3/CH_3COCH_3}$=-1.3V, E_{CH_3CHOH/CH_3CH_2OH}=-1.1V), we could assume that reaction(17) may occur. According to the assumption mentioned above, it is reasonable to interpret the experimental result. In

the presence of acetone, hydrogen remains constant ($G(H_2) = 0.15 + 1.7 + 2.33 = 4.18$), because neither the reaction of H atom addition to acetone nor H abstraction from acetone occurs within the range of acetone concentration(up to 1.2×10^{-2} mol dm^{-3}). The $G(CH_3CHO)$ value rises significantly with increasing acetone concentration, which demonstrates definitely that acetone competes to capture the e^-_{solv} with acetaldehyde [reactions(11) and (13)]. When acetone captures all of the e^-_{solv} of the system, acetaldehyde is released to reach finally the limiting value 3.7($G(CH_3CHO) = 2.0 + 1.7 = 3.7$) accompanying by the formation of $CH_3CO{\cdot}CH_3$ anion radical(G=1.7). Neutralization reaction of $CH_3CO{\cdot}CH_3$ anion radical and $CH_3CH_2OH_2^+$ forms CH_3COHCH_3 radical (G=1.7))[reaction(14)] subsequently. From the G values of final products, considering the assumed way of disappearance of CH_3COHCH_3 radicals, the consuming yield of CH_3COHCH_3 radical($G = 0.3 + 0.6 + 0.35 \times 2 = 1.6$) is obtained, which is agreement with the forming yield of $CH_3CO{\cdot}CH_3$ anion radical. On the other hand, the yield of $(CH_3CHOH)_2$ measured is also coincident with the yield of CH_3CHOH radical. In other words, a material balance between intermediates and final products of this system is obtained. From the discussion above, it seems that there is some correlation between disproportionation and the number of β hydrogen atom possessed by alcohol radicals. The more β hydrogen atoms a radical owns, the easier the disproportionation occurs.

According to the suggested mechanism, kinetic analysis of the data is studied, and following equations are given by:

$$d[e^-_{solv}]/dt = k_i D - k_{11}[e^-_{solv}][CH_3CHO] - k_{13}[e^-_{solv}][CH_3COCH_3] \quad (1)$$

$$d[CH_3CHO]/dt = k_{ii} D - k_{11}[e^-_{solv}][CH_3CHO] \quad (2)$$

D is the dose rate, k_i and k_{ii} are the rate constant of producing e^-_{solv} and acetaldehyde respectively, reaction(9) and neutralization reaction(9)' are neglecting when acetone(10^{-3} mol dm^{-3}) presents.

When the steady-state has been established, $d[e^-_{solv}]/dt=0$, so:

$$[e^-_{solv}] = kD/(k_{11}[CH_3CHO] + k_{13}[CH_3COCH_3]) \quad (3)$$

Thus an intergrating equation is obtained[13]:

$$[CH_3CHO]/2 - 1.7k_{13}[CH_3COCH_3]/4k_{11} \times \ln(1 + 2k_{11}[CH_3CHO]/3.7k_{13}[CH_3COCH_3]) = kD \quad (4)$$

D is the dose, and k is an conversion coefficient($k=1.3\times10^{-23}$).

Substituting the data of curve $G(CH_3CHO)$ against concentrations of acetone in Fig. 1 into equation(4). one can obtain the ratio of rate constant against every experimental acetone concentration. It is apparent that the ratio varies at low concentration due to the assumption that $[CH_3COCH_3]$ remains constant during irradiation which is far deviating from the actual process. While at high concentration, the consumption of acetone can be neglected contrasting to its initial concentration, thus a constant approaching to 1 is obtained which is well fitted the steady state processing. When requiring a procedure depending on computer, $k(e^-_{solv}+CH_3CHO)/k(e^-_{solv}+CH_3COCH_3)=0.96$ is achieved by simulation which is coincident with the value obtained by pulse radiolysis experiment.(Tab.1)

Tab. 1 The ratio(k) of rate constants $k(e^-_{solv}+CH_3CHO)/k(e^-_{solv}+CH_3COCH_3)$ obtained from different methods

Conc.	Low($<4\times10^{-3}$ mol dm^{-3})	High($>4\times10^{-3}$ mol dm^{-3})
Steady Steate Application	Variations(5.0 - 1.5)	Approach to the Constant 1
Computer Simulation	0.96	0.96
Pulse Radiolysis	0.84	0.84

From the discussion above, we may be able to explain the discrepancy between the calculated value(k)

of Zhang's and that from pulse radiolysis. Being the simplest ketone, acetone is an easily volatile reagent. It is largely consumpted when degassed, therefore, the $[CH_3COCH_3]$ should be redetermined after degassed but Zhang neglects this effect. On the other hand, it will lead to a great error at low acetone concentration supposing that $[CH_3COCH_3]$ keeps constant.

The results obtained in acetone ethanol system demonstrate the effect of carbonyl group to scavenge solvated electrons in irradiated ethanol solution resembles that in aqueous solution. Thus, we could employ ethanol as solvent probe to study other ketone compounds, especially some hydrophobic aromatic carbonyl compounds.

II. THE γ-RADIOLYSIS AND PULSE RADIOLYSIS OF ACETOPHENONE-ETHANOL SYSTEM

Acetophenone, an important aromatic carbonyl compound , reveals great importance in biological reaction, especially in electron transfer and oxidative phosphorylation. A lot of experiments have been done[14,15,16], however , most of the studies carried out previously in the literatures investigated the reaction of solvated electron with acetophenone generally in aqueous solutions. Actually, acetophenone is less soluble in water which means the system studied has to be confined to a low acetophenone concentration. It is difficult to observe the effect of acetophenone on the intermediates as a function of concentration. On the other hand, the techniques often used are pulse radiolysis and flash photolysis, little has been done to study the products with γ-radiolysis in irradiated ethanol solution, in which acetophenone is easily soluble. Thus, there are still many disputations about the absorption spectra of the transient species. In course of this work, both γ-radiolysis method and pulse radiolysis are performed, the results are well agreement.

When γ-radiolysis acted upon acetophenone-ethanol solutions, the dependences of G values of the final products on acetophenone concentration were obtained.(as shown in Fig. 2)

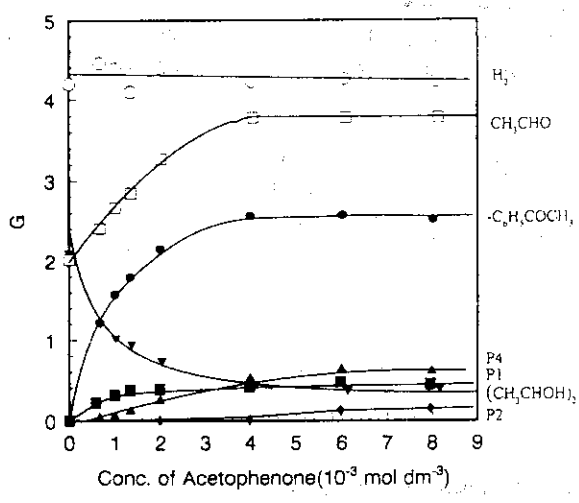


Fig. 2 The dependencesof G values on acetophenone conc.
system saturated with N_2; dose rate 2.0Gy/s; dose:3000Gy

It is found that when increasing acetophenone concentration, the $G(H_2)$ values remains unchangeable, in contrast the $G(CH_3CHO)$ values rise significantly and the $G((CH_3CHOH)_2)$ values decrease rapidly in this range of acetophenone concentration. It indicates that acetophenone being an effective e^-_{solv} scavenger like acetone, competes to capture the e-solve with acetaldehyde which is formed in γ-radiolysis of ethanol.[reactions (11),(19)]

$$C_6H_5COCH_3 + e^-_{solv} \longrightarrow C_6H_5(CH_3)CO^-_{solv} \qquad G=1.7 \qquad (19)$$

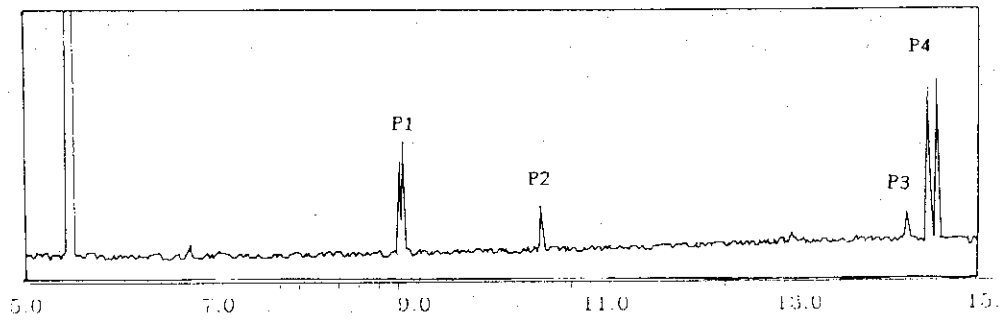


Fig. 3 GC-spectrum of the new final products in irradiated acetophenone ethanolsolution(FID); 25m OV-1 capillary column; [acetophenone]=6.12mM; dose rate:2.0Gy/s, Dose:3000Gy

P1,P2,P3 and P4 are the four new final products, and are detected by GC-MS(see Fig.3) and their structure are also determined.(see Fig.4). Estimating calibration factors from those of other compounds with similar structure are used to calculate the G values of the new final products and the trends of the G values with increasing acetophenone concentration are illustrated in Fig. 2.

Considering the behaviour of the intermediates in acetone-ethanol system and the formation of the new final products of this system, following reactions may occur :

$$C_6H_5(CH_3)CO^{\cdot} + CH_3CH_2OH_2^{+} \rightarrow C_6H_5(CH_3)COH + CH_3CH_2OH \quad G=1.7 \qquad (20)$$

$$2C_6H_5(CH_3)COH \longrightarrow P4 \quad G=0.6 \qquad (21)$$

$$C_6H_5(CH_3)COH + CH_3CHOH \rightarrow P1 \quad G=0.4 \qquad (22)$$

$$C_6H_5COCH_3 + CH_3CHOH \longrightarrow \longrightarrow P3 \quad G=0.15 \qquad (23)$$

$$C_6H_5COCH_3 + CH_3CHOH \longrightarrow \longrightarrow P4 \quad G=0.1 \qquad (24)$$

$$2CH_3CHOH \longrightarrow (CH_3CHOH)_2 \quad G=0.35 \qquad (25)$$

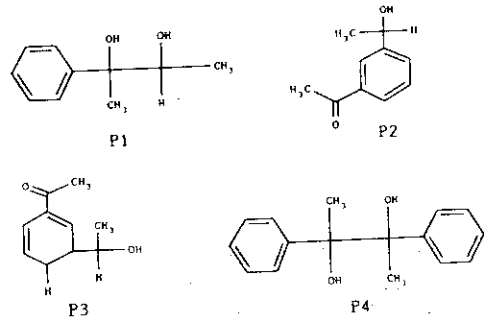


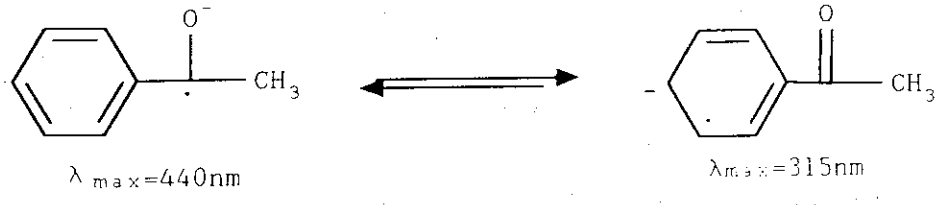
Fig. 4 The structures obtained four finl products P1,P2,P3 and P4 respectively on GC detecting sequence

It is obvious that acetophenone can scavenge all the e^{-}_{solv}(G=1.7) to form ketyl radical ion $C_6H_5CO^{-}CH_3$ and subsequently produce ketyl radical $C_6H_5COHCH_3$(G=1.7). On the other hand, the obtained values of G_{P1}=0.4 and G_{P4}=0.6 reveal that recombination reaction takes place both between $C_6H_5COHCH_3$ ketyl radicals and hydroxyethyl radical(G=0.4) and among $C_6H_5COHCH_3$ radicals(G=0.6x2=1.2). Meanwhile, the total consumption of $C_6H_5COHCH_3$(G=1.6) to form P1 and P4 is obtained, which is coincident with the loss of e^{-}_{solv}(G=1.7) captured by acetophenone. In other words, a good material balance between e^{-}_{solv} and radiolytic products P1 and P4 is obtained. However, there is still uncertain about the way of producing P2 and P3, maybe they are formed via the disproportionation reaction of $(CH_3CHOH)C_6H_5COCH_3$ radical.

From the discussion above, one can find that there are almost no disproportionation reaction occurs among ketyl radicals($C_6H_5COHCH_3$), only recombination reaction exists between CH_3CHOH radical and ketyl radicals. On the other hand, it should be noted that the material balance is still unresolved in this system as a whole and the fate of a part of the loss of the acetophenone (G=0.5) and CH_3CHOH radical (G=1.1) is

unknown. Relating to the fact that CH_3CHOH radical can be added to the solutes in irradiated garlic-ethanol[17] and baicalin system[18], we could suppose that the adduct of two CH_3CHOH radical added to benzene ring of acetophenone might be formed.

The result of pulse radiolysis experiment(see Fig.5 and 6) is another evidence to support the suggestion that acetophenone is an effective electron scavenger. The absorption spectra is characterized with absorption peaks at λmax=315nm and 440nm, both peaks decay unimolecularly with the same observed rate constant of $1.9 \times 10^5 s^{-1}$. When N_2O saturated acetophenone ethanol was pulsed, no obvious absorption can be observed in the wavelength range used(300-750nm). Therefore, the optical spectra presenting on pulse radiolysis of Ar degassed acetophenone ethanol solution might be assigned to one species, an electron adduct of acetophenone . The 440nm peaks is well-known and has been ascribed to ketyl radical ion $C_6H_5CO^-CH_3$ in previous literature. Thus, one might postulate that an electron charge transfer from the carbonyl group to the benzene ring might exist as following:



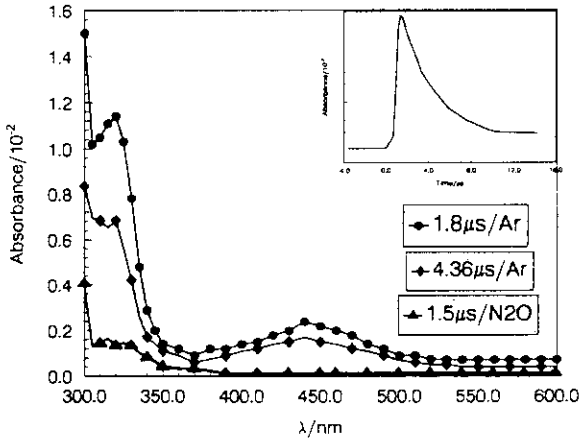


Fig.5 Transient spectra of Ar(N_2O) saturated acetophenone ethanol solution(1mM,neutral); insert: absorbance decay at 310nm; pulse dose:1Gy

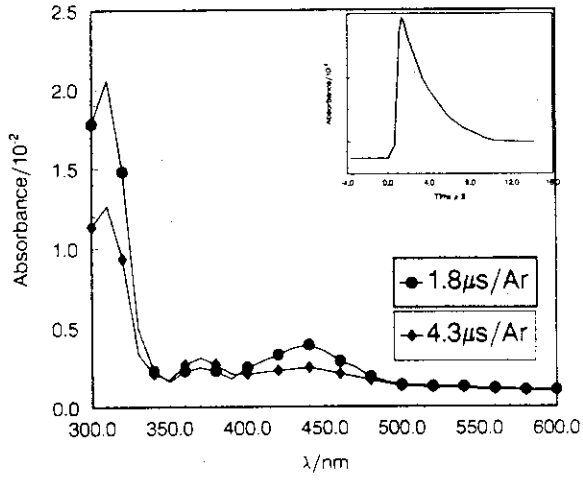


Fig. 6 Transient spectra of Ar saturated acetophenone aqueous solution(2mM, 0.2M t-BuOH, PH 6.5); insert:absorbance decay at 440nm, dose:1Gy

The species with λmax=315nm and λmax=440nm might decay by ethanolysising. Electron adducts of arene are known to hydrolysis to form cyclohexdienyl radicals, thus one might assume that the electron adducts of acetophenone could ethanolysis and a pseudo first order decay could be observed.

In addition, comparing Fig. 3 and Fig. 4, we may can infer that ethanol can act as a more convenient solvent than water when applied in pulse radiolysis owing to there is less disturbance of extra additives which is often introduced in water solution. One can get a more direct observation of transient species in ethanol solution.

Using the previously determined data in γ-radiolysis experiment, according to the differential equations(5,6) given, taking $k_{18}/k_8=4$, one can get the simulation curve of $G(CH_3CHO)$ varying with the concentration of acetophenone(see Fig.7)

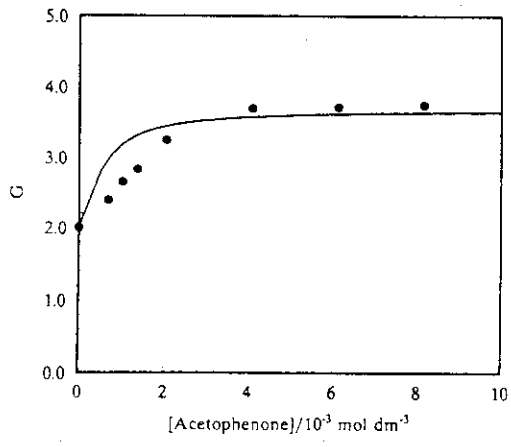


Fig. 7 The simulation curve for acetophenone competing the solvated electrons with acetaldehyde

$$d[e^-_{solv}]/dt = k_I D - k_{11}[e^-_{solv}][CH_3CHO] - k_{19}[e^-_{solv}][C_6H_5COCH_3] \quad (5)$$

$$d[CH_3CHO]/dt = k_{II} D - k_{11}[e^-_{solv}][CH_3CHO] \quad (6)$$

Comparing the structures of acetophenone and flavonoids such as baicalin, (see Fig.8) one can find that the A ring combing a carbonyl group of C ring in baicalin is similar to acetophenone. As a whole, baicalin combines a much greater conjugation system than that of acetophenone and demonstrates dominant difference of scavenging effect contrasting to acetophenone. Acetophenone can effectively scavenge e^-_{solv} produced in liquid ethanol while baicalin can't. (see Fig.9). We may can draw a conclusion that the larger conjugation structure in baicalin far weaken the character of the carbonyl group function and make baicalin difficult to capture the electron, which is vital in human body and not disturb the normal electron transferring in body when baicalin used as medicine. From the discussion above, we could find that the curing effect of flavonoids acting as medicine is really closely relating to their possessing big conjugation system.

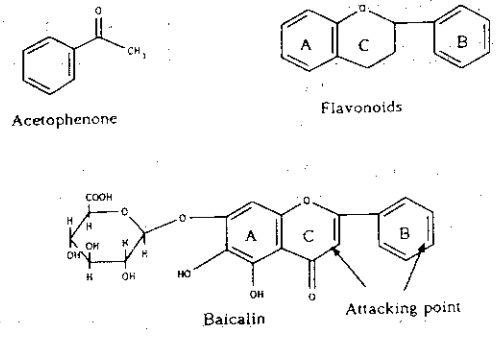


Fig. 8 Comparision of the structures of acetophenone, flavonoids and baicalin

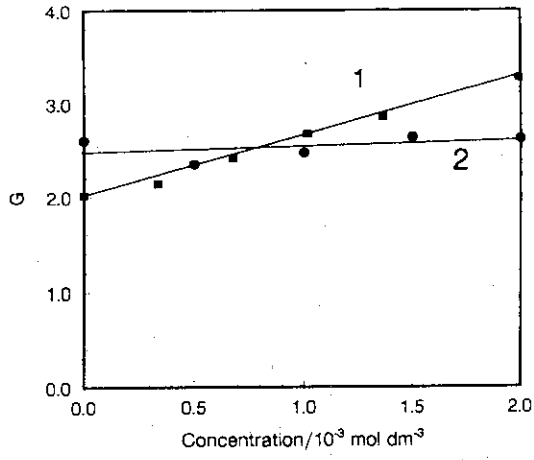


Fig. 9 The dependences of acetaldehyde G values on additives concentration.
1: acetophenone ethanol solution; dose rate: 2.0Gy/s; dose: 3000Gy
2: baicalin ethanol solution; dose rate: 0.5Gy/s; dose: 969Gy.

SUMMARY

In this paper:

(1) A good material balance between intermediates and final products in acetone ethanol solution was obtained, which demonstrate that some products in ethanol solution might be predicted. The achieved ratio of rate constant $k(e^-_{solv} + CH_3CHO)/k(e^-_{solv} + CH_3COCH_3)=0.96$ is well agreement with that of pulse radiolysis, which indicates that we can employ ethanol as a solvent probe to study the chemical behaviour of carbonyl group of ketone compounds.

(2) Both γ-radiolysis and pulse radiolysis of acetophenone ethanol solution confirm that acetophenone id an effective electron scavenger and there might be electron adducts isomers, both of them decays at the same rate constant via ethanolysising.

(3)Relating to the behaviour of CH_3CHOH radical in aqueous solution and liquid ethanol[13]as well as that of other kinds of alcohol radicals in ethanol solutions, one can find that different medium will affect the behaviour of alcohol radical. For example CH_3CHOH radical can undergo both recombination and disproportionation reaction at the almost same rate in aqueous ethanol, but very few disproportionation reaction of CH_3CHOH radical are observed in the radiolysis of liquid ethanol. At the same time, it seems that the number of β hydrogen atom belonging to the alcohol radical also takes an important role in disproportionation reaction.(see Tab.2), the more β hydrogen atoms a radical owns, the easier the disproportionation occurs.

Tab. 2 The influence of the number of β hydrogen atoms on reaction types

Radicals	CH_3CHOH	$(CH_3)_2COH$	$C_6H_5(CH_3)COH$
Number of β H Atoms	3	6	3
Reactions Type	R	D	R

R: Standing for Recombination Reaction
D: Standing for Disproportionation Reaction

References:

1. A. O. Allen, The Radiation Chemistry of Water and Aqueous Solutions. Van Norstrand, Princeton, NJ, 1961

2. R. S. Dixon, Radiat. Res. Rev., 2, 237(1970)
3. A. J. Swallow, A. B. Ross and W. P. Helman, Radiat. Phys. Chem., 17, 127(1981)
4. Zhang N., Wu J. L, Radiat. Phys. Chem., 38, 383(1991)
5. Asmus K. D., Warman J. M. and Schuler R. H. J. Phys. Chem., 74, 246(1970)
6. Spinks J. W. T. and Woods R. T. (1990) An Introduction to Radiation Chemistry
7. Bolton G. L. and Freeman G. R. , J. Am. Chem. Soc., 98, 6825(1976)
8. Mahan Y and Freeman G. R. , J. Phys. Chem., 89, 4347(1985)
9. Wu J. L. and Zhang X. J., Report on the 4th Japan-China Bilateral Symposium on Radiation Chemistry. 55 pp.
10. Mahan Y. and Freeman G. R. J. Phys. Chem., 91, 1561(1987)
11. Wei G. S and Wu J. L. et al, Chemical Journal of Chinese Universities, 13, 1109(1992)
12. Zhang X. J., Wu J. L., Ha H. F., Acta Physico Chimica Sinica, 6, 298(1990)
13. Zhang X. J., Wu J. L., Zhou Y. R., Radiat. Phys. Chem., 43, 335(1994)
14. A. G. Pribush and S.A. Brusnetseva, Radiat. Phys. Chem., 16, 277(1980)
15. Hayon, T. Ibata, N.N. Lictin and M. Simic, J. Phys. Chem., 76, 2072(1972)
16. D. W. Willans, Radiat. Phys. Chem., 10, 335(1977)
17. Wang. G.H., Ph. D. Thesis of Peking University(1994)
18. Cai Z. L., Ph. D. Thesis of Peking University(1993)
19. von Sonntag, C.,Schuchmann, H.-P. In *Oxygen Radicals in Biological System, Part C., Methods in Enzymology, vol.233;* Packer, L., Ed.; Academic Press: Orlando, FL, 1994, p3

3.7 Hydroxylethylation of Baicalin by γ-ray Irradiation of Baicalin in Ethanol

Cai Zhongli
Department of Technical Physics, Peking University
& Xiamen Torch High-Tech Industrial Development Co.

He Yongke and Wu Jilan
Department of Technical Physics, Peking University

Abstract Via γ -irradiation of baicalin in ethanol, hydroxylethyl groups were introduced into B & C ring of baicalin. Eight hydroxylethylation products were isolated by reverse HPLC and their molecular structures were postulated through their UV, IR, MS and fluorescence spectra. The primary binding constants of baicalin and its hydroxylethylation products in HSA were got by the fluorescence method.

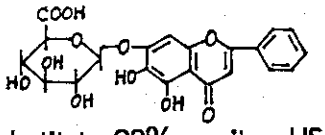
Key words hydroxyethylation, baicalin, radiation

INTRODUCTION

Hydroxyalkyl group is one of the most useful sustituents for organic synthesis and modification of natural medicinal components. Although the usefulness of radical intermediates in hydroxyalkylation has not been fully recognized, several successful regioselective hydroxymethylations via radical intermediates, including radiation chemical processes have been reported[1,2]. In this paper, we demonstrated that partly regioselective hydroxyethylation of baicalin could be carried out via γ -ray irradiation of baicalin in ethanol.

EXPERIMENT

MATERIALS

Baicalin()-supplied by Chinese Medicine & Biological Product Institute,98% purity; HSA -provided by Beijing Municipal Blood Station, 99% purity; Ethanol(G.R.) was from Beijing Chemical Plant.

IRRADIATION

The sample saturated with high purity nitrogen was irradiated in 1.5×10^{4} Ci Co^{60} source with the absorbed dose 3.0KGy, dose rate 0.50Gy/s.

ISOLATION AND PURIFICATION

The irradiated sample (2.5mM baicalin ethanol solution) was concentrated 25 times at 50℃ water bath by rotary evaporator, then diluted 3 times by triple distillated water so that 90% baicalin was precipitated. Finally the clear filtered solution was isolated by Varian Model 5060 HPLC (ODS column 8x300mm), with UV detection at 276nm, column temperature 28±1℃, injection volumn 500μ l. The eluent was 37%CH_3OH+63%(0.01%CF_3COOH–H_2O). The initial flow rate, kept 3.2ml/min for two minutes, then fell linearly to 0.8ml/min in 3 minutes, finally rose linearly to 3.2ml/min in 55 minutes.

Eight fractions (t_R 9.7, 19.2, 21.9, 24.6, 30.2, 46.5, 53.6, 60.4min) were collected, recrystallized for identification.

IDENTIFICATION

UV spectra of the above HPLC peaks were scanned by Philips PU 4895 HPLC/UV on–line instrument. IR spectra of KBr discs (1mg sample/100mg KBr) were recorded by PE 683 IR Spectrometer (Perkin–Elmer); CI–MS were measured by TSQ 45–B Model GC/MS/MS/DS(Finnigan MAT) with reaction gas CH_4, the temperature of ionization source 130℃, electron energy 70ev, injection temperature 250℃, solid sample injected directly. FAB–MS was measured by VG ZAB–HS Organic Massspectrometer with Ar beam energy 8Kev, bridge current 1mA, substrate thioglycerin. The fluorescence spectra of their ethanol solution were scanned by Shimadzu RF–540 Spectrofluorophotometer with excitation wave 280 nm.

MEASUREMENT OF THE BINDING CONSTANTS OF BAICALIN AND ITS HYDROXYLETHYLATION PRODUCTS IN HSA

Due to the low solubibity of baicalin in neutral water, the compounds were solved in ethanol($1x10^{-4}$M) first, then added into 2.0ml $2.0x10^{-6}$M HSA(0.05M PBS, PH7.3) by 20, 40, 60, 80, 100μ l, respectively, shaken even, kept in dark at room temperature for 10 hours. The fluorescence spectra of 2.00ml above mixtures were scanned from 300 to 500nm with excitation wave 280nm.

RESULTS AND DISCUSSION

IDENTIFICATION

1. UV Spectra

The on–line UV spectra of eight products all consisted of four peaks, with the maximum absorption at 210, 240, 290, 365nm, similar to that of dihydrobaicalin

[λ_{max}^{EtOH}(nm): 239, 288, 362][3]. Comparing them with the spectra of baicalin [λ_{max}^{EtOH}(nm): 215, 245, 278, 316)][3], we found that k absorption band for A–C ring conjugated system of baicalin(o–acetylalkoxy benzene) shifted from 278 to 290 nm and the band for B–C ring disappeared. This implied that the products all kept the A–C conjugated structure,while that of B–C ring had been destroyed.

2. Fluorescence Spectra

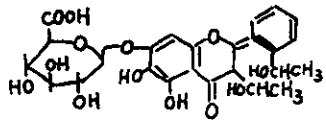
The fluorescence spectra of baicalin and its products under 280nm excitation light all had a main emission peak around 410nm, which implied that A–C conjuated structures were the same.

3. IR spectra

Two IR spectra for P_3 and P_6 were recorded. IR spectrum for P_3 wasυ_{max}^{KBr}(cm^{-1}): 3415, 2975, 2925, 1725, 1648, 1555, 1493, 1448;for P_6,υ_{max}^{KBr}(cm^{-1}):3427, 2923, 2854, 1723, 1623, 1493, 1447. Lower vibration absorption frequency (1648/1623) for keto group of aglycone than that of baicalin (1659) implied that the original $C_{2,3}$ double bond of P_3/P_6had been saturated[4].

4. MS Spectra

The main CI–MS data of 7 products were shown in Table 1, while FAB–MS of P_2 was m/z(%):537(87),447(100),411(80). Analysing the fragments,we postulated that P_{1-4} were dihydroxyethylation baicalin and P_{5-8}monohydroxyethylation baicalin; $C_{2,3}$ bond were all saturated and at least contained one · $CHOHCH_3$ group; Their A–C ring conjugated structure kept the same as that of baicalin; The structure of P_1 might be



,while its main fragment (m/z 327):

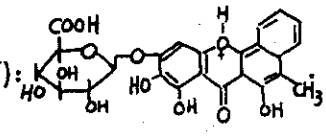


Table 1 The Main CI–MS Fragments and Their Abundances of The Products

	345	344	331	330	329	327	317	316	315	314	313	299	298	297	271	270	269	238	210	176	169	168	159	158	140	130
1						30																28		40		
3		5	16	12	21		29	100	18	9		5	4	2	15		6	5				6	6	7	20	6
4	4	19	2	2	2		100		70	2	1		37			14		2				1		2	1	1
5							2	1				5	2	2	10	2	5	9	100	3		13	12	39	6	10
6											8		6	3		100	17		28		2	17	6	14	6	1
7									100		73	13	2	1		73		2		9	3		13	8	13	11
8									3	3		6		6		87	42	100	66			8		89	23	19

THE BINDING CONSTANTS OF BAICALIN AND ITS HYDROXYETHYLATION PRODUCTS IN HSA

Baicalin and its hydroxyethylation products all strongly quenched the fluorescence of HSA. Moreover, HSA also quenched the fluorescence of baicalin and its hydroxyethylation products. This implied that nonfluorescent complexes between HSA and baicalin/its products were formed. According to the relation between the relative fluorescent intensity of HSA at 335nm and the concentration of its quenchers ($F_0/F=1+K[Q]$)[5], the primary binding constants K(10^5 M^{-1}) of baicalin and its products in HSA were got as below: 2.0(baicalin), 1.1(P_8), 0.4(P_7), 0.8(P_6), 0.6(P_5), 0.5(P_4),0.3(P_3), 1.4(P_2), 0.3(P_1).

CONCLUSION

Via γ –ray irradiation of baicalin in ethanol, we could introduce one or two hydroxyethyl groups exclusively at B or C ring of baicalin and saturate $C_{2,3}$ bond, with the G value 0.1(P_1), 0.1(P_2), 0.3(P_3), 0.2(P_4),0.2(P_5), 0.4(P_6), 0.5(P_7), 0.7(P_8), respectively[6]. The formation of hydroxyethylation products may be explained by the following mechanism[6]:

$$C_2H_5OH\sim\sim \xrightarrow{\gamma\text{ –ray}} H\cdot, e_s^-, CH_3CHO,\ H_2, CH_3CH_2OH_2^+ \quad (1)$$

$$e_s^- + C_2H_5OH \longrightarrow C_2H_5O^- + H\cdot \quad (2)$$

$$e_s^- + CH_3CHO \longrightarrow CH_3CHO^- \xrightarrow{+CH_3CH_2OH_2^+} R\cdot \quad (3)$$

$$H\cdot + C_2H_5OH \longrightarrow R\cdot + H_2 \quad (4)$$

$$2R\cdot \longrightarrow \text{2,3–butandiol} \quad (5)$$

$$H\cdot + B \longrightarrow BH\cdot \quad (6)$$

$$R\cdot + B \longrightarrow BR\cdot \quad (7)$$

$$BH\cdot + R\cdot \longrightarrow BHR \quad (8)$$

$$BR\cdot + R\cdot \longrightarrow BR_2 \quad (9)$$

(R=$CH_3\dot{C}HOH$, B=baicalin)

It was different from the mechanism of uracil hydroxymethylation [2] that no baicalin radical anion was involved in the hydroxyethylation. As a result, no dimer was detected.

Due to the higher polarity, $C_{2,3}$ single bond and hydroxyethyl group, the hydroxyethylation products not only were the useful intermediates for further structure modification, but also might have weaker mutagenity and stronger effect to prevent from and cure gastric ulcer than baicalin did[7,8] . Moreover, the hydroxyethylation of baicalin did not greatly influence its binding ability in HSA, which might play an important role in carrying medicines to reach pathogenic targets[13].

This project is subsidized by Science Fund for Doctor Stations of The State Education Commission, P.R. China.

REFERENCE

1. A. Akito and S. Takamuku(1993),
   The Chemistry of Hydroxy, Ether and Peroxide Groups, Vol.2,
   Edited by S. Patai,John Wiley & Sons Ltd.,657;
2. A. Ishida, S. Takamuku(1986), Radiat. Phys. Chem., 27,165;
3. Huang liang and Yu Dequan(1988),
   "The application of UV Spectra in Organic Chemistry", Part Two,Science Press;
4. B.L. Shaw and T.H. Simpson(1955), J. Chem. Soc. 655;
5. Chen Guozhang, Huang Xianzhi, Zheng Zhuzi, Xu Jingou and
   Wang Zhunben ed(1990), " Analytical Methods of Fluorescence", Science Press,118;
6. Cai Zhongli(1993), Peking University Doctoral Degree Dissertation;
7. B. Havesteen(1983), Biochem. Pharmac. 32(7), 1141;
8. Beijing Medical College, Beijing Chinese Medicine College(1983),
   "Chemistry on the Components of Chinese Herb", People's Health Press, 276;
9. H. Ogata(1990), Biochem. Pharmaco., 39(9),1495.

3.8 A Comparative Study on the Protection Effect in the Radiation-induced Oxidation of Liquid Paraffins and Polypropylene

Yanti S. Soebianto[1], Isami Kusuhata[1], Yosuke Katsumura[1], Kenkichi Ishigure[1], Junichi Kubo[2], Satoru Hamakawa[2], Kiyoshi Azami[2], Hisaaki Kudoh[3], and Tadao Seguchi[3]
Department of Quantum Engineering and Systems Science, Faculty Engineering, The University of Tokyo, 7-3-1 Hongo, Bunkyo-ku, Tokyo 113, Japan.
[2]Central technical Laboratory, Nippon Oil Company, 8 Chidori-cho, Naka-ku, Yokohama 231, Japan.
[3]Takasaki Radiation Chemistry Research Establishment, Japan Atomic Energy Research Institute, Watanuki-machi, Takasaki, Gunma, 370-12 Japan.

ABSTRACT. Comparison of protection effect of additives in liquid paraffins and polypropylene (PP) irradiation under pure oxygen atmosphere has been carried out. Gas product analysis and mechanical properties measurement of PP films indicate that the presence of additives reduces O_2 uptake, gas evolution and molecular degradation. These facts are attributed to energy and charge transfer, and radical scavenging action of the additive molecules regardless the physical state difference of the substrates. Oxidation pathway in liquid paraffin is shorter than that in solid PP, and the main part of the consumed O_2 are converted into carboxylic acids. The excess of H_2 evolution observed in PP oxidation is produced during the oxidation step, and transformation of the additives in their function as protector.

INTRODUCTION.

The presence of either antioxidant or energy and charge scavengers in the polypropylene (PP) matrix is known to have improved its mechanical strength after irradiation and to suppress the oxidation during storage of the irradiated PP[1]. The improvement of mechanical strength and reduction of the gas evolution have been attributed to energy and charge transfer as well as radical scavenging by the added molecules, as those observed in the model compounds[2].

Although the presence of additives either in PP matrix or the liquid paraffins give the same effect, the protection mechanism in both substrates are supposed to be different due to the difference in their physical states. In the PP matrix, additives are only distributed in the amorphous phase. On the other hand, in the liquid paraffins which are considered the model of amorphous polymers, the additives are well mixed.

The purpose of this paper to present the comparison of protection mechanism in both substrates. Product analysis has been carried out to evaluate the protection mechanism. Vacuum radiolysis is discussed as the basic protection mechanism.

EXPERIMENTAL.

Samples. Liquid n-hexadecane ($C_{16}H_{34}$, C), squalane ($C_{30}H_{62}$, S), and additives: tetralin (T), naphthalene (N), octahydrophenanthrene (OP), and phenanthrene (P) have been described in the previous publications[2]. The concentration of each additive in n-$C_{16}H_{34}$ ($C_{30}H_{62}$) was 200 mM (ca. 4*wt*%). Each sample of 5.0 ml was put in a glass ampoule having a breakable seal, evacuated, filled in with 600 torr of pure O_2, and sealed off. Polypropylene (PP) sheets with 97.9% tacticity were received from Nippon Oil Co.Ltd.(E130G Nippon Oil). The additives incorporated in the PP were Irganox 1010 (I-1010), butylated hydrotoluene (BHT), octahydrophenanthrene (OP), and propylfluoranthene (Antirad)[1]. Their concentration in the matrix were 0.5 and 1*wt*%, and the film thickness were about 0.6-0.8 mm. The films were cut into dumb-bell shape specimens, put in the glass tube having breakable seal, evacuated, filled with 300 torr pure O_2, and sealed off. Samples, which were irradiated under vacuum, were sealed off without filling of O_2.

Irradiation. Gamma rays irradiation with ^{60}Co source was carried out at room temperature. The irradiation on liquid was carried out with a dose rate of 7kGy/h, and rotated during

irradiation. PP films were irradiated with 0.7kGy/h, and those irradiated under vacuum with a dose rate of 10kGy/h. The total absorbed dose was measured by alanine dosimeter[3].

***Analysis*. Gas products.** The pressure of the evolved gas was measured and analyzed by gas chromatography (GC). The schematic diagram and details of the analysis were described elsewhere[4]. Analysis was carried out isothermal at 50° C, and the carrier gas was He (30ml/min). The detectors were TCD (Thermal Conductometry Detectors).

Mechanical properties. Tensile strength, modulus, and elongation at break of PP samples were measured at room temperature by an INSTRON 4301. The cross head speed was 200 mm/min. The values were determined as an average of four measurements.

Liquid products. (a). **Total acid content.** The carboxylic acids present in the irradiated sample was determined by titration. A mixture of 0.50±0.02g of sample and 5.0ml of alcoholic (IPA) 0.1N KOH was diluted to 50 ml by a toluene/water/isopropanol(IPA) (4/1/5) solution. The neutralization reaction was carried out at 65° ±1° C for 20 min to accelerate the neutralization reaction. The remained KOH was then back-titrated after cooling to room temperature with a standard alcoholic (IPA) 0.1N HCl. The end point of titration was potentiometrically determined by an automatic titrator. (b). **Total carbonyl content.** The total carbonyl content was spectrometrically determined. Condensation reaction with DNPH (2,4-dinitrophenylhydrazine) has been carried out, and the procedure was adopted from ref.5. For quantitative analysis, butanone-2 and α-tetralone were used as the standard compounds. (c). **Total hydroperoxides content.** The total hydroperoxide content was determined by iodometry[6]. The standard compound was H_2O_2.

RESULTS AND DISCUSSION.

I. EFFECT OF ADDITIVES ON THE VACUUM RADIOLYSIS OF POLYMER MATRIX AND ITS MODEL COMPOUND.

Under vacuum condition, H_2 formation in the radiolysis of polymer matrix and its model compound are similar. The $G(H_2)$ of PP (2.9) is almost the same as that of squalane ($C_{30}H_{62}$, 3.0), and both are lower than that of n-$C_{16}H_{34}$ (3.5). It is suggested that H_2 evolution depends on the chemical structure rather than the physical state. Linear polymers produce larger amount of H_2, but undergo less main chain scission than the branched ones. It might be due to the localization of energy at C-H bond which breaks it,but is delocalized at the C-C bonds along the main chain of linear alkane. The presence of tertiary carbons in branched alkanes weaken the main chain , and causes bond rupture which induces more chain scission.

The presence of additives reduces the H_2 evolution as well as main chain scission, and the latter one results in the retardation of the PP deterioration. Aromatics are more effective than hydroaromatics in the liquids, and the antirad is more effective than antioxidants in PP (Fig.1). Energy and charge transfer to the added molecules take place both in the liquid and solid phase, due to the difference in the ionization potential (IP) and excited state (S_1) level between the solvent (matrix) and the additives[2]. The protection efficiency depends on degree of aromaticity, or concentration of aromatic rings in the matrix.

II. RADIATION INDUCED OXIDATION OF POLYMER MATRIX AND ITS MODEL COMPOUND.

The reaction of molecular O_2 with the formed free radicals is determined by the physical state as well as the geometry of the substrate such as film thickness and O_2 pressure, since oxidation is a diffusion controlled reaction regardless of its initiation mode.

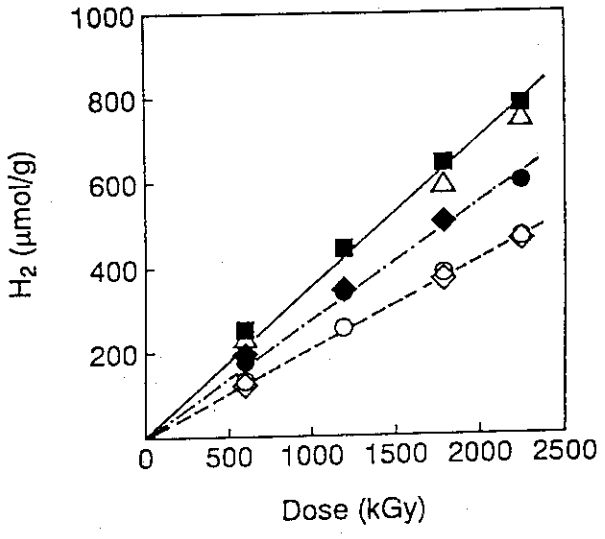


Fig.1a. Effect of additives on gas evolution of n-$C_{16}H_{34}$ (■) pure, and in the presence of(△) Decalin, (●) Tetralin, (○) Naphthalene, (◆) Octahydrophenanthrene, (◇) phenanthrene.

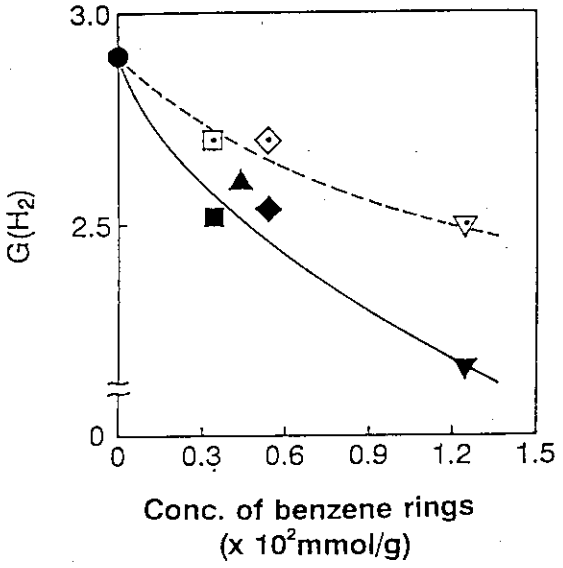


Fig.1b. Effect of additive concentration on $G(H_2)$ in the vacuum irradiation (□ BHT), (△ I-1010) (◇ OP), (▽ Antirad). (open:0.5wt%, solid:1wt%)

Table I. G-values of O_2 uptake and gas products of pure substrates

		Liquid		PP*	
		n-$C_{16}H_{34}$	$C_{30}H_{62}$	0.6mm	0.3mm
O_2 uptake		5.7	6.5	48.0	73.0
Products	CO	0.02	0.05	0.12	2.1
	CO_2	0.30	0.25	0.17	3.1
	H_2O	0.30	0.25	>0.20	>0.50
	H_2	3.0	2.6	2.9	2.9
	CH_4	0.02	0.07	0.14	0.24

*)initial O_2 pressure: 300 torr, G-values are calculated at 25kGy (0.7 kGy/h)

Table I shows that G-value of O_2 uptake in PP oxidation is very high (48-73) compared to that in liquid paraffins (ca. 6.0) despite of their same G-value of alkyl radical ($G(R\cdot) \approx 3.5$ at 77K). The value becomes larger when the film thickness is reduced (0.3mm, $G(-O_2) \approx 73.0$), which means that the oxygen diffusion into the film controls the over all oxidation. These data indicate that the oxidation step in PP is a long chain reaction, whereas in the liquid paraffins the chain is very short. Seguchi *et al.* assumed a "neighboring" oxidation in the solid phase to induce large O_2 uptake[7]. The evolved energy in the oxidation will induce free radical formation of the neighboring molecules and promotes the O_2 uptake. The existence of trapped radicals in PP might induce post-irradiation oxidation due to its migration to the crystalline surface with time. Since there are no trapped radicals in the liquid phase, no post-irradiation effect is observed.

Molecular H_2 is a radiolysis product in both substrates. The $G(H_2)$ of n=$C_{16}H_{34}$ and $C_{30}H_{62}$ are lower than those under vacuum (3.5 and 3.0,respectively). On the other hand, $G(H_2)$ in irradiated PP is not affected by oxygen (Table II). Then, O_2 is an energy and

electron scavenger in the liquid phase.

Table II. G-values of H_2 evolution

	Vacuum (10 kGy/h)	in 300 torr O_2 (1.0 kGy/h)	
film thickness (mm)	0.6	0.6	0.3
Pure PP	2.9	2.9	2.9
PP + BHT (1*wt*%)	2.6	2.9	3.3
PP + I-1010 (1*wt*%)	2.6	2.9	2.9
PP + OHP (1*wt*%)	2.6	2.9	2.9
PP + Antirad (1*wt*%)	2.2	2.4	2.8

Only less than 10% of the consumed O_2 are involved in the gas products as CO, CO_2, and H_2O. Condensed products analysis of oxidized PP has been carried out by Lacoste *et al.*[8] The oxidation products are converted into their derivates by gaseous reactions before the infrared (IR) analysis. The main product is reported to be *tert.*-PP hydroperoxide, because this compound is stable enough at room temperature. The carbonyl compounds detected at 1710 cm^{-1} are mainly ketones. On the other hand, liquid product analysis of the paraffins shows that hydroperoxides and ketones are minor, but more than 90% of the consumed O_2 are converted into carboxylic acids (G(acids)= 5.0).

Since the detected products in the liquid phase and PP are quantitatively and qualitatively different, it is suggested that the reactions in the oxidation step in both substrates are different. This difference is due to the physical state of the substrates (solid & liquid). The deterioration of the irradiated PP is enhanced by chain scission during oxidation.

III. PROTECTION IN THE RADIATION INDUCED OXIDATION.

Since H_2 evolution is assumed to be parallel with the alkyl radical formation, the presence of additive also reduces the alkyl radical formation. Table III shows the G-values of H_2, O_2 uptake and oxidation products of n-$C_{16}H_{34}$ systems. The reduction of H_2 evolution, acid formation and O_2 uptake are almost proportional, except for hydroaromatic compounds. The order of gas and acid reduction are similar to the order of gas reduction under vacuum. The reduction of H_2 evolution indicates the occurrence of energy and charge transfer. Hydroaromatics suppress the oxidation of paraffins, but they themselves are oxidized, therefore the O_2 uptake becomes larger. The hydroaromatic donates its allylic hydrogen, and the allylic radical itself is scavenged by O_2 molecules. This hydrogen donating effect agrees with that reported on inhibition of radiation degradation of polyolefins by Kubo and Otsuhata[9].

Unlike the reduction of O_2 uptake in the liquid, the reduction in PP is less dependent on the degree of aromaticity of the additive (Fig.2). Antioxidant (BHT) is more effective than Antirad and OP. The protection effectiveness is determined by the compatibility of the additive with the substrate. Although the additives reduce the O_2 uptake, they loss their protection effect at higher doses because they might be consumed by irradiation. The reduction of O_2 uptake is not proportional to that of H_2. Table II shows that H_2 evolution becomes larger in the presence of additives and if the oxidation condition becomes severe. It means that the additives evolve H_2 during their transformation under oxidation condition. Moreover, the reduction of O_2 uptake is more obvious in PP than in the liquid phase despite the less effective H_2 reduction. The effect of BHT is more obvious in PP than in the liquid phase. All the differences observed may be caused by the difference in the reactions of the

oxidation step. The peroxyl radicals are very mobil in the liquid phase, but not in the semi-crystalline polymers. Therefore, those in the semi crystalline ones are easier to be scavenged.

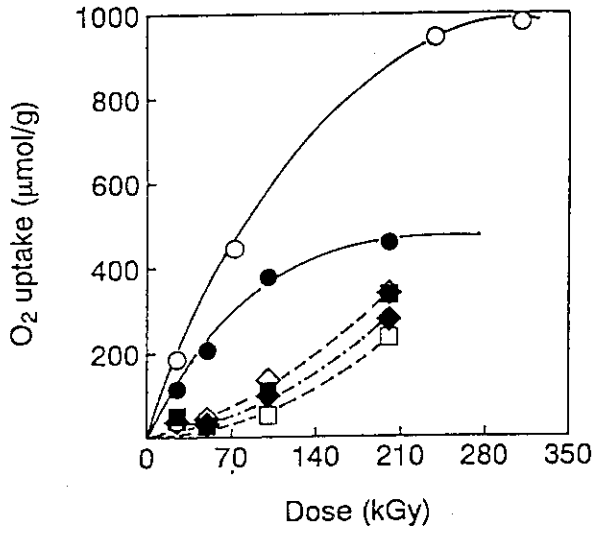


Fig.2. Effect of additives on the O_2 uptake (1kGy/h, 300 Torr O_2, 0.6mm films) Pure PP(●), PP in the presence of 1w% (□BHT) (■I-1010) (◇OP) (◆Antirad) (○0.3mm pure PP)

Table III. G-values of O_2 uptake and products of irradiated n-$C_{16}H_{34}$ in the presence and absence of additives.

	G(H_2)	G(-O_2)	G(CO)	G(CO_2)	G(H_2O)	G(carbonyl)	G(acids)
Pure $C_{16}H_{34}$ (C)	3.0	5.7	0.02	0.30	0.30	-	5.0
C + N (200mM)	2.2	3.8	0.02	0.20	0.20	-	3.0
C + P (200mM)	2.2	3.8	0.02	0.20	0.20	-	3.1
C + T (200mM)	2.4	6.2	0.02	0.20	0.25	6.5	3.7
C + OP (200mM)	2.4	7.4	0.03	0.20	0.25	5.1	4.3
C + BHT (108mM)	2.3	4.4	0.07	0.10	0.25	-	4.0

Sample vol./tube: 5.0ml/100ml, 600 torr O_2, 600 kGy (6-7 kGy/h)

CONCLUSION.

O_2 uptake in radiation induced oxidation of liquid paraffins are lower than that in the PP matrix, and the main oxidation products are carboxylic acids. The presence of additives reduces molecular degradation of both PP and its model compound, but the reduction efficiency depends on the physical state of the matrix.

REFERENCES.

1. Soebianto *et al.*(1994), submitted to *Polym. Deg. Stab.*
2. Soebianto *et al.*(1993), *Polym. Deg. Stab.***42**,29 and references therein.
3. Kojima T., and Tanaka R. (1989), *Appl. Radiat. Isot.***40**,851.
4. Hegazy *et al.*(1981), *J.Appl.Polym Sci.***26**,1361.
5. Jordan D.E., and Veatch F.C.(1964), *Anal.Chem.***36**,120.
6. Davis A.G.(1961), *Organic Peroxides,* Butterworths, London.
7. Seguchi *et al.*(1989), *Proceeding of International Symposium of Radiation Degradation of Polymeric Materials,* Takasaki.
8. Lacoste *et al.*(1993), *J.Polym.Sci.Polym.Chem.Ed.***31**,713.
9. Kubo J., and Otsuhata K., *Rad. Phys. Chem.39*,261.

4. Polymers (1)

4.1 *Relationship between Energy Profile and Chemical Structural Change in Polymers Irradiated by Ion-beam

Yoshimasa HAMA, Kenichi HAMANAKA, Hideya MATSUMOTO,
Hisaaki KUDOH*, Tsuneo SASUGA* and Tadao SEGUCHI*
Advanced Research Center for Science and Engineering, Waseda University,
3-4-1 Okubo, Shinjuku, Tokyo 169, JAPAN.
* Japan Atomic Energy Research Institute, Takasaki Radiation Chemistry Research Establishment, 1233 Watanuki, Takasaki 370-12, JAPAN.

ABSTRACT

The relationship between the energy profile and the chemical structural change in the effects of the ion-beam irradiation on some slabbed polyethylenes is investigated by using micro-FT-IR. Predominant species induced by ion-beam irradiation are trans-vinylene unsaturation, carbonyl and hydroxy groups. The origin of the carbonyl group is suggested to be the allyl radical which is stable in vacuum at room temperature. The depth profile of the species induced is like the Bragg curve, though the peak of IR absorption due to chemical species is not close perfectly to the Bragg peak. This suggests that the relation between the chemical reaction and energy transfer is very complex on ion-beam irradiation.

KEYWORDS: ion-beam irradiation effects, polyethylene, LET effect, micro-FT-IR.

INTRODUCTION

Ion-beam has larger stopping power compared with γ-ray or electron beam. Different irradiation effects from that by low stopping power beams has been expected. The energy deposition profile of the ion beam in a material should be represented by the Bragg curve along the track. If the ion beam deposites all energy in the material, the energy deposition profile of the ion beam comes to be different along the track. Therefore, if the stopping power effect (LET effect) is remarkable for polymers, the different chemical structural change along the track should be expected. This would be important for the degradation of polymers by ion-beam irradiation.

This work is concerning the depth profile of the change of the chemical structure induced in the slab of low density polyethylene (LDPE) and high density polyethylene (HDPE) by heavy ion-beam irradiation. Moreover, the relationship between the profile of chemical structural change and the energy profile of ion beam is discussed.

EXPERIMENTAL.

In this work, low density polyethylene (LDPE) and high density polyethylene (HDPE), which were formed in a slab of 2mm thick, were used.

H^+, He^{2+} and Ar^{8+} were irradiated in vacuum with AVF cyclotron in JAERI Takasaki

(TIARA). The absorbed dose at the surface was estimated by beam current.

The sample irradiated was sliced along the cross-section right-angled to the slab surface to get a thin film of about 100 μm for measurement.

The infrared spectrum data from the region of 10μm x 10μm of the thin film were accumulated stepwisely along the depth direction by using micro-FT-IR spectrometer (JEOL JIR micro-6000).

Results and discussion.

a. Species induced by ion-irradiation.

The predominant species induced by each ion-irradiation were trans-vinylene unsaturation (ca. 964cm^{-1}), carbonyl group (1712cm^{-1}) and hydroxy group (3400cm^{-1}) for all samples, though there were slight difference in the yield between LDPE and HDPE. In LDPE, the trans–vinylene unsaturation was produced more remarkably than the carbonyl group. But in HDPE, carbonyl group was produced remarkably. Assuming the precursor of the carbonyl group formation would be allyl radical produced by irradiation, the present result is reasonable. Because the allyl radicals produced in HDPE should be more stable in vacuum than those in LDPE, as reported in many works. The allyl radicals convert to any compounds with a carbonyl group by the reaction of the allyl radicals with oxygen molecules diffusing into the PE.

b. Depth profile of the species.

The depth profile of FT-IR absorption of the trans–vinylene unsaturation in LDPE irradiated by 20 MeV He^{2+} is shown in Fig.1. This profile is found to be similar to the Bragg curve. On H^+ and Ar^{8+} irradiations, a similar depth profiles also were obtained. On 175 MeV Ar^{8+} irradiation, however, the absorption peak appeared very close to the surface, because of the short range of the heavy ion with rather low energy.

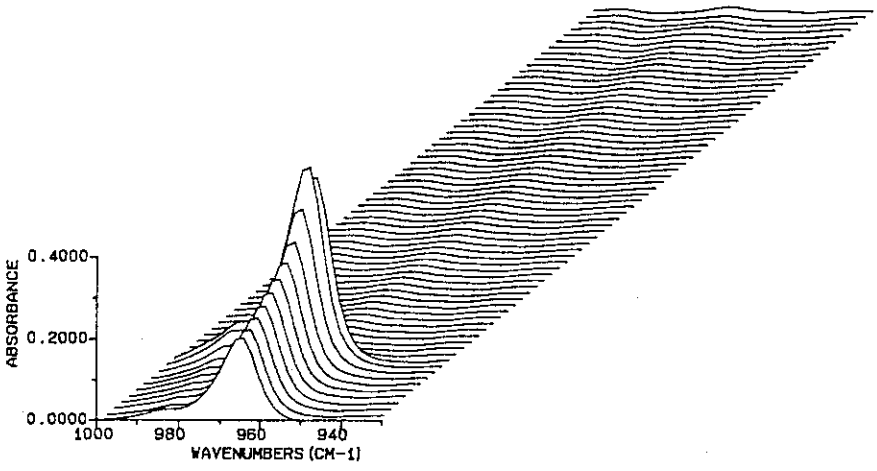


Fig.1. Depth profile of the IR absorption due to the trans–vinylene unsaturation induced in LDPE irradiated to a dose of 0.5 MGy by 20 MeV He^+.

Fig.2 shows the depth profiles of the trans–vinylene and carbonyl group absorptions on 10 MeV and 20 MeV H^+ irradiation, together with the profile of the stopping power calculated by Bethe formula. It can be found that the profile of the absorption shows good correspondence with one of the stopping power. On 20 MeV H^+ irradiation, however, the peaks appear slightly shorter depth than the peak of the stopping power calculated. This comes from the fact that in this observation two slabs of the sample were used, because of long range coming from the higher energy of H^+ ion.

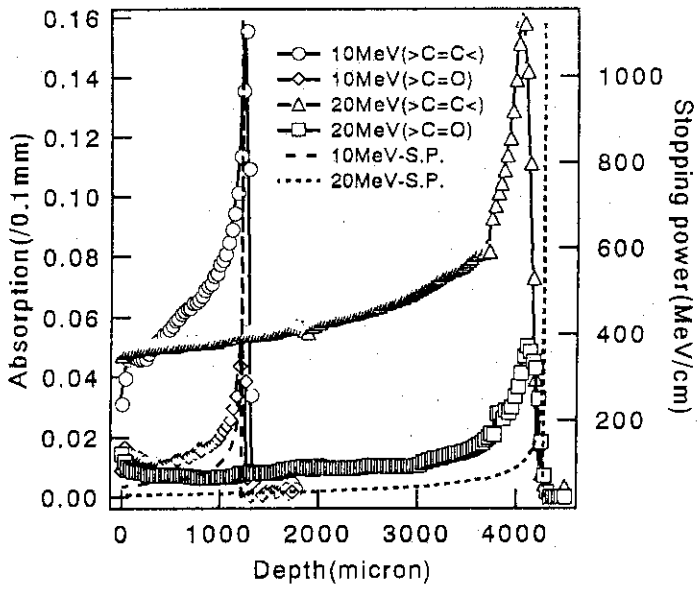


Fig.2. Depth profile of trans–vinylene and carbonyl group absorptions for LDPE irradiated by 10 MeV or 20 MeV H^+, together with stopping power calculated by Bethe formula.

c. Effect of fluence on the yield of the species.

Fig.3 shows the effect of fluence on the yield of the trans–vinylene for LDPE irradiated by 10 MeV H^+. The yield is evaluated by G value for the trans–vinylene calculated by the stopping power. It can be found that the yield decreases with fluence. Similar results were obtained in all other cases. Assuming that the tracks of all ions do not superpose each other and that the yield of the trans–vinylene is constant in each track, the yield should be proportional to the fluence. Therefore, the fact obtained in this work suggests that the track superposes each other and the yield in the overlapping region may be less than that in the lone track, since the yield of the trans–vinylene depends on the number of methylene group in the ion track.

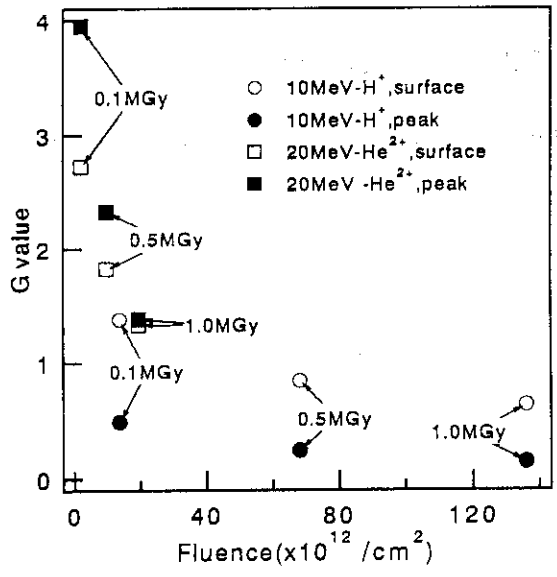


Fig 3. The relationship between G value for trans–vinylene and fluence for LDPE irradiated by H^+ or He^{2+}. Term of surface or peak in figure means the G value calculated by the stopping power at the surface or the peak of the absorption.

d. The relationship between energy transfer and depth profile of induced species.

As found in Fig.2, the relationship in the depth profile between the stopping power and the IR absorption due to species seems to be in good coincidence. In fact, the G value for the induced species, which was calculated by stopping power and the yield of the species, is almost constant along depth near to the peak of the absorption. On the other hand, the relationship between them around the absorption peak was found to be very complicated. According to detailed calculation by using Bethe formula and TRIM code which is in consideration of the charge balance, it is found that the profile around the peak is greatly dependent of the charge of the ion. In low charged ion, the peak of the IR absorption appears at shorter depth than each peak of the stopping power calculated by both codes and the absorption has rather long tail. In high charged ion (heavier ion), both peaks come to be near each other for TRIM code calculation, though in calculation by Bethe formula there is no coincidence in both peaks. In this case, however, the absorption also shows long tail beyond the peak. This suggests that more detailed calculation for the energy profile is required.

CONCLUSION

The depth profile of the chemical structural change for PE irradiated by heavy ion was observed clearly by micro–FT–IR. The yields of the trans- vinylene unsaturation and allyl radical were found to be more than those in γ–irradiation. The relationship in the depth profile between the chemical change and the energy profile calculated by Bethe formula and TRIM code suggests that the detailed mechanism should be considered in the calculation of the energy profile for lower energy heavy ions.

ACKNOWLEDGEMENT

This study was supported partly by Waseda University Grant for Special Research Projects.

4.2 WAXD and SAXS Study on Gamma-radiation Damage to Polyamide-1010 Crystal Structure

Lihua Zhang, Hongfang Zhang and Donglin Chen

Changchun Institute of Applied Chemistry, Chinese Academy of Sciences, Changchun, 130022. P. R. China

Abstract: In the present work we attempt to settle the controversy on the district wherein the radiation induced reaction preferentially occurs through examining the structural changes of the irradiated polyamide-1010 specimens on both the crystallographic and the supermolecular level by using WAXD and SAXS techniques. Experimental results indicated that the chain crosslinking and scission of the irradiated specimens occur mainly in the amorphous region and on the crystal surface (or interphase), and extend into the inner portion of the crystal with increasing radiation dose.

INTRODUCTION

A wide interest in the radiation effect on the semicrystalline polymer has been raised for many years. However, from the theoretical point of view, there remains a controversy on the district wherein the radiation induced reaction preferentially occurs and the mechanism wherewith the radiation damage i.e., the skin or core damage to polymer crystal takes place (Keller, 1982; Luo, 1985; Zhang, 1990). After we have reported the works on the aggregated structure dependence of chemical reaction in irradiated polyamide-1010 (PA-1010), which is a typical semicrystalline gamma-radiation crosslinkable polymer, and the decay of the trapped radicals in irradiated PA-1010 during post irradiation heat treatment etc. (Zhang, 1990; Zhou,1993), in this paper we attempt to settle the controversy through examining the structural changes of the irradiated PA-1010 specimens on both the crystallographic and the supermolecular level by using wide angle X-ray diffraction (WAXD) and small angle X-ray scattering (SAXS) techniques.

EXPERIMENTAL

PA-1010, a commercial product, was supplied by Jilin Union Chemical Works. Its glass transition temperature T_g is ca. 50 °C and melting temperature T_m within the temperature range of 205-210 °C (Zhang, 1991; Feng, 1989). The dried granules of PA-1010 were moulded at ca. 220 °C into sheets of 0.5 mm in thickness. Nearly 100 % amorphous specimens could be obtained by quenching in ice water. Specimens with various crystallinities were prepared through annealing amorphous specimens at temperatures between T_g and T_m for different times.

Specimens were subjected to gamma-irradiation with different dosage in vacuo at room temperature. The dose rate was 10 kG_y/h. Wide angle X-ray diffraction (WAXD) scans of the specimens were taken on a D/MAX-IIB diffractometer. Small angle X-ray diffraction (SAXS) of the specimens was examined on a Philips Pw-1700 diffractometer.

RESULTS AND DISCUSSION

1. Crystal structure of PA-1010 Recently we have studied the crystal structure of PA-1010 and found that it belongs to the triclinic system as shown in Fig.1. (Mo, 1993) From the model of structural arrangement of molecular chains in PA-1010 crystal, it is seen that the plane ac contains hydrogen bonds and is indexed as 010 plane, while bc or 100 plane is the surface absent from hydrogen bonding.

The WAXD intensity curves for PA-1010 specimens with various crystallinities are displayed in Fig.2. The diffraction peak intensities I_{hkl} and the ratios between I_{010} and I_{100} are varied with crystallinity W_c calculated by Ruland method (Ruland, 1961). The microcrystal sizes, L_{hkl} in different directions were calculated in accordance with Scherrer equation (Scherrer, 1969). The effect of annealing temperature on W_c, L_{100} L_{010} is summarized in Table 1, while the relationship between W_c and microcrystal sizes L_{hkl} in different directions is shown in Fig.3(a).

Table 1. Effect of annealing temperature on L_{100}, L_{010} and W_c.

Anneal. temp.(°C)	25	60	70	130	165	180	190
L_{100}, nm	0	8.3	9.2	10.2	12.4	10.8	14.3
L_{010}, nm	0	0	3.2	3.1	5.0	5.6	7.3
W_c, %	0	3.0	22.3	26.0	42.0	45.3	53.4

The results shown in Fig.2 and 3(a) indicate that both the intensity of diffraction peak I_{hkl}, and microcrystal sizes, L_{hkl} increase with W_c, and the L_{100}/L_{010} ratios of the specimens are greater than 2. Evidently, this is possibly due to the effect of hydrogen bonding, which stimulates a regular arrangement of molecular chains in the direction normal to 100 plane and parallel to 010 plane. Besides, the appearance of L_{100} precedes that of L_{010} in the early stage of crystal formation. From Fig.3(a) it is obvious that both L_{100} and L_{010} are directly proportional to W_c. The lowering of annealing temperature would result in lower W_c, smaller microcrystal size, and more imperfect crystal.

Recent theoretical considerations have led to the conclusion that for semicrystalline polymers, an interphase exists between the amorphous and crystalline phase (Flory, 1984). Among others, SAXS is a valuable technique to exhibit the existence of the interface. Fig.4 is a plot of the intensity of SAXS against scattering angle for PA-1010, from which the thickness of the interface d_{tr}, the crystalline lamella thickness $\bar{d}$ and long period L could be evaluated on the basis of one-dimensional electron density correlation function. Fig.3(b) shows the dependence of the above parameters on the crystallinity of PA-1010. From the figure it is noted that $\bar{d}$ and L increases with the increase of W_c, while d_{tr} remains nearly constant.

2. Variation of crystal structure of irradiated PA-1010

a. WAXD of irradiated PA-1010 specimens. Fig.5 shows the results evaluated from WAXD of irradiated specimens Pa-a (original crystallinity W_c° = 40.5%) and Pa-b (W_c° = 22.5%), it is found that for PA-a specimens irradiated with different amounts of radiation dose D, both the crystallinity W_c and microcrystal sizes L_{hkl} increase slightly in the beginning of irradiation when radiation dose is smaller than 1 MG_y. The result is thought to be a consequence of the local crystallization of radiation induced broken tie

molecules (Bhateja, 1990) under the action of hydrogen bonding and the local heating produced by collision of radiation particles within the structure (sherrer, 1967). With further increase in D from 1 to 5 MG_γ, L_{100} and L_{010} remain nearly unchanged irrespective of a little lowering of W_c. However, the crystallinity of the specimens is still somewhat higher than that of the original one. When D is greater than 5 MG_γ, the microcrystal sizes start to depress with radiation dose. Moreover, L_{100} decreases more drastically than L_{010} does. Thereafter, the crystallinity W_c continues to decrease with further increase in dose until it vanishes. The fact implies that only if with a dose above 5 MG_γ, a net deterioration of the crystalline region could be taken place.

Besides, the same result is also displayed in the Charlesby-Pinner's plot (Charlesby, 1950) of $(S + S^{1/2})$ against D, where a linear relationship appears when D is less than 5 MG_γ (see Fig.6). It is well recognized that Charlesby -Pinner's equation was derived upon the presumption that the chemical events take place randomly. Apparently, this prerequisite can only be fulfilled in the noncrystalline region. In addition, we have also found that the crosslinking yield G(X) is directly proportional to $(1 - W_c^\circ)$ of the specimen (Zhang, 1990). For comparison, the crystallinities of the irradiated specimens are also plotted as a function of 1/D in this figure. Evidently, the resulting curve is essentially flat before 5 MG_γ is reached.

In comparison with specimen PA-a, the onset of crystallinity lowering for the less crystallized specimen PA-b manifests itself rather earlier with a dose of ca. 2 MG_γ only (Fig.5(a)). Furthermore, the rate of variation of W_c and L_{100} with radiation dose for PA-b is much greater than that for PA-a. When D is greater than 0.5 MG_γ, the decrease in L_{100} for PA-b is more obvious than in L_{010}, which scarcely varies even when the dose is raised to 5 MG_γ. All the facts indicate that the crystal damage is related to the plane containing hydrogen bonds. Since a specimen with lower initial crystallinity possesses larger specific crystal surface or more interphase per unit volume of the crystal, the easiness of this specimen to be damaged gives evidence that the crystal surface is the start point of crystal damage.

b. SAXS of irradiated PA-1010 specimens. Fig.7 shows the variation of structural parameters obtained by SAXS with radiation dose for irradiated PA-a specimens. From the figure, it is known that the value L is independent of radiation dose and the $\bar{d}$ exhibits a tendency much the same as W_c as in the case of WAXD, only if with a dose above 5 MG_γ, the value $\bar{d}$ starts to decrease with dose. The variation of the interface thickness d_{tr} is quite unique, it decreases continuously from the very beginning of irradiation even though the magnitude of depression is rather small. The SAXS results support further the above viewpoint that in low dose range radiation reaction occurs solely in noncrystalline and interfacial regions and the crystal damage starts from the surface of the crystal.

In fact, other experimental techniques such as dielectric and ESR spectrum also gave results in favour of the above point of view (Zhang, 1990; Zhou, 1993; Zhang,1994).

To sum up, all the findings of the present work are in conformity with Keller's supposition (Keller, 1975; 1982) proposed in early days that gamma-radiation damage to crystal of semicrystalline polymer spreads from

the crystal fold surface inwards. So we can conclude that the skin damage is more possible, i.e. radiation reactions occur solely in the noncrystalline and interfacial regions in low dose range, only after being subjected to high radiation dose the crystal would be damaged from the outer to the inner portion and eventually completely amorphotized.

REFERENCES

Bhateja, S. K., Yarbrough, S. M. and Andrews, E. H., J. Macromol. Sci., -Phy., B29(1) (1990) 1.

Boyer, R. F., J. Polym. Sci., Symposium No. 50 (1975) 189.

Charlesby, A. and Pinner, S, H., Proc. R. Soc., A249 (1950) 367.

Feng, J., Zhang, L. and Chen, D., Chin. J. Polym. Sci., 7(1), 54(1989); Radia. Phys. Chem., 38(1) (1991) 105.

Flory, P. J., Yoon, D. Y., and Dill, K. A., Macromolecules, 17(1984), 862.

Jenkin, H., and Keller, A., Macromolecules, 14(1975), 1683.

Keller, A., "Developments in crystalline Polymers-1", Ed. Basset, D. C., Appl. Sci. Pub., London, 1982.

Luo, Y., Wang, G., Lu, Y., and Jiang, B., Radia. Phys. Chem., 25 (1985) 359.

Mo, Z., Meng, Q.,Feng, J., Zhang, H. and Chen, D., Polym. Int. 32, (1993) 53.

Petal, G. N. and Keller, J. Polym. Sci., Phys. Ed., 13 (1975) 305.

Ruland, W., Acta Cryst., 14 (1961) 1180.

Scherrer equation, cited from Alexander, L. E., "X-Ray Diffraction Methods in Polymer Science", Wiley-Interscience, New York, 1969, p.335;

Sherrer, A. E. and Kline, D. E., J. Appl. Polym. Sci., 11 (1967) 341.

Zhang, L. and Chen, D. et.al., Radiat. Phys. Chem., 36(6) (1990) 743.

Zhang, L. et. al., Preprints of the 9th Summer Symposium on Chemistry, (Changchun), A-5, 1990.

Zhang, L. and Chen, D. et. al., Ann. Report of Polym. Phys. Lab., Academia Sinica, p.35, 1990; chin. J. Appl. Chem., 7(2) (1990) 20-24.

Zhang, L, Li, S. Qi, Y. and Chen, D. Science in China, Ser. A, 33(9) (1991) 1115.

Zhang, L., Liu, Y. and Chen, D., Chn. J. Instr. Anal., 13(4) (1994) 28.

Zhou, M., Zhang, L., Liu, Y and Chen, D., Abstracts of the 5th China-Japan Bilateral Symposium on Radiation Chemistry (Beijing), p.69, 1991; Chin J. Polym. Sci., 11(1) (1993) 46-53.

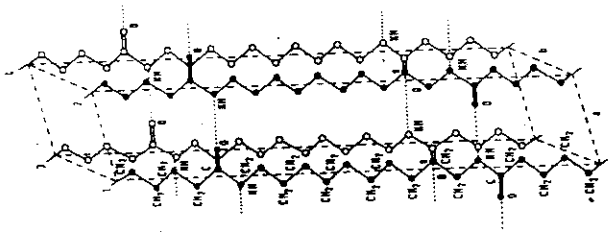


Fig. 1. Structural model showing the arrangement of molecular chains in PA-1010 triclinic crystal.

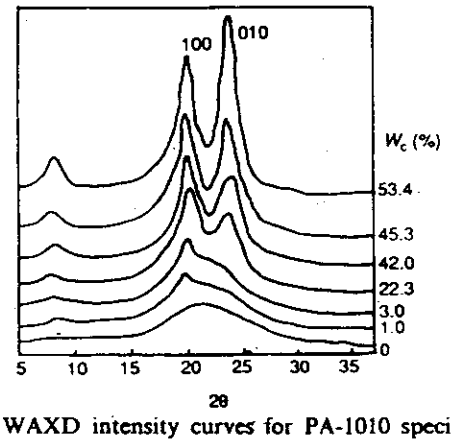


Fig. 2. WAXD intensity curves for PA-1010 specimens with various crystallinities.

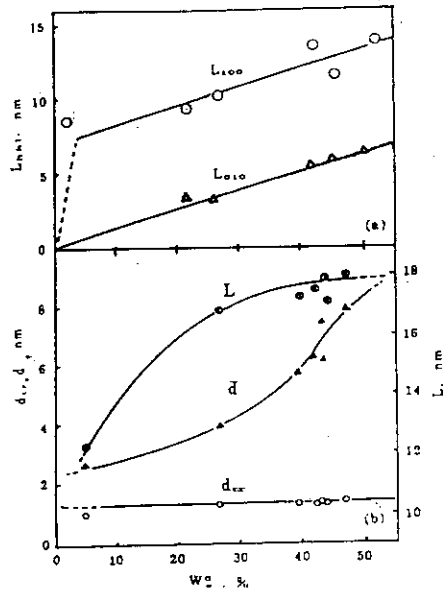


Fig.3 (a) Relationship between L_{100}, L_{010} and W_c^0 of PA1010
(b) Relationship between L, d, d_{cr} and W_c^0 of PA1010

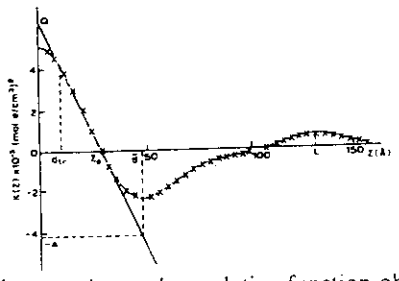


Fig. 4. Experimental correlation function obtained for Nylon-1010.

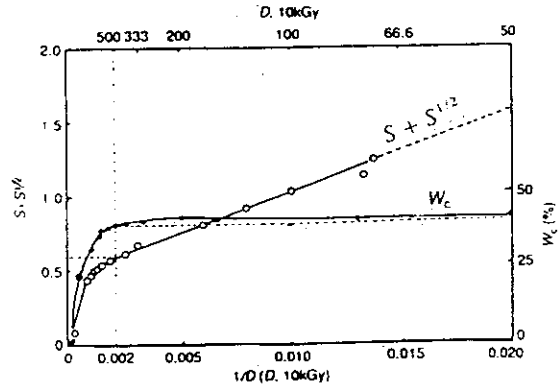


Fig. 6. (a) Plot based on Charlesby–Pinner's equation [$(S + S^{1/2})$ versus $1/D$] and (b) the corresponding variation of W_c with the reciprocal D for specimen PA-a. The fine broken horizontal line denotes the crystallinity before irradiation (W_c = 40·5%).

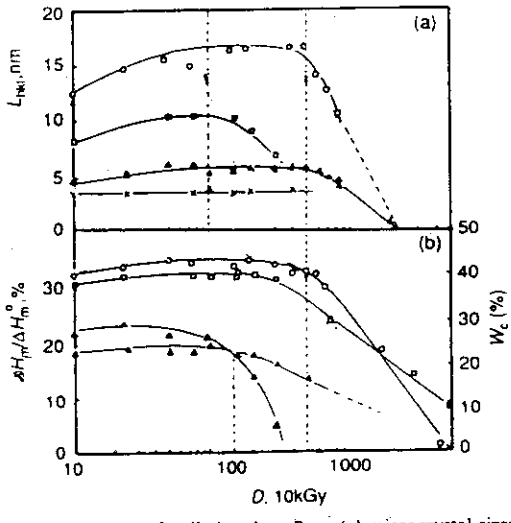


Fig. 5. Influence of radiation dose D on (a) microcrystal sizes L_{100} and L_{010} and (b) W_c and ΔH_m of specimens PA-a and PA-b. (a) PA-a: original W_c = 40·5%: (○) L_{100}, (△) L_{010}, PA-b: original W_c = 22·5%: (□) L_{100}, (×), L_{010}, (b) W_c(%): (○) PA-a; (△) PA-b. $\Delta H_m/\Delta H_m^0$(%): (□) PA-a; (▲) PA-b.

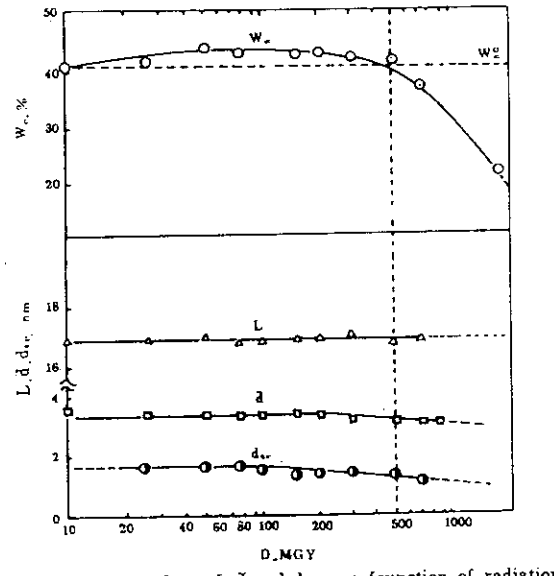


Fig.7 Variations of w_c, L, d and d_{cr} as a founction of radiation dose for PA-a

4.3 Radiation Damage of Polymers Studied by Positron Annihilation (Positron and Gamma-ray Irradiation Effects)

T. SUZUKI, Y. OKI, M. NUMAJIRI, T. MIURA, K. KONDO, and Y. ITO*

Radiation Safety Control Center, National Laboratory for
High Energy Physics, Tsukuba,305,Japan
* Research Center for Nuclear Science and Technology,
The University of Tokyo, Tokai-mura, Ibaraki 319-11,Japan

Abstract: Positron irradiation effects on polypropylene (PP) have been studied using positron sources (^{22}Na) during positron annihilation (PA) experiments. The irradiation effect was measured by the intensity (I_3) of the long-lived component of positronium (Ps). At a low temperature of around 100K, I_3 for unirradiated PP samples increased due to a termination of the thermal motion of the -CH_3 groups. However, the increase in I_3 for γ-ray irradiated samples was reduced in inverse proportion to the amount of irradiation. Although no increase in I_3 was observed for 1 MGy-irradiated PP with γ-rays, an increase was observed again after a 48 h irradiation by positrons emitted from ^{22}Na. This may be due to a reconstructing of the polymer chains.

INTRODUCTION

Positron annihilation (PA) in polymers has been extensively studied during the last decade, and the positron annihilation lifetime (PAL) technique has been recognize as being a useful method to study the characteristics of polymers. However, positrons emitted from ^{22}Na have sufficient energy to induce radiation damage in polymers, and the positron probe can thus affect the object to be investigated. It has been pointed out that the positron irradiation effect is quite significant in polyethylenes (PEs) and polypropylenes (PPs) (Walender and Maurer, 1992; Suzuki et al.,1994a) during PAL experiments. These polymers are considered to be easily affected by radiation, compared with such aromatic compounds as epoxy resins and polyimides. Radiation damage of these polymers induced by γ-rays has been studied by PAL (Suzuki et al.,1994b, Wang et al., 1988, Hsu and Hadley, 1971). Considering the radiation effect of positrons on the polymer samples, these results must be carefully analyzed.

It has been reported that at low temperature I_3 increased along with decreasing temperature, and that β-relaxation at 246 K and γ-relaxation at 200 K were observed (Suzuki et al., 1994c; Zhang and Ito, 1991; Reiter and Kindle, 1990). The former relaxation was associated with micro-Brownian motion and the latter with crankshaft-type motion of the methyl groups. After cooling the samples from room temperature to 100 K, the increase in I_3 took a few days to reach the maximum, at which point the polymer structures were considered to obtain the thermal equilibrium (Reiter and kindle, 1990). The time required to reach equilibrium is considered to be equivalent to the relaxation time of the polymer structures at low temperature.

In this study, the radiation effects on PPs due to both positrons and γ-rays were investigated by the PAL method. Hence, positrons are playing a role as probes to study

nano-meter polymer structures and, at the same time, serve as radiation to induce radiation damage. The temperature dependence of the radiation effect due to γ-rays is described. Although an increase in I_3 at low temperature became negligible in highly irradiated samples by γ-rays, it was again observed by reconstructing the broken polymer structures. Thus the effect of γ-rays is compared with the effect of positron irradiation.

EXPERIMENTAL

The PA experiments were conducted using a conventional fast-fast coincidence system having a time resolution of 270 ps full width at half maximum (FWHM). The details have been presented elsewhere (Suzuki et al., 1994a).

PP slabs (2mm thick) were cut into pieces to an area of 10×20 mm^2. Two kinds of isotactic PPs, of which crystallinities were determined by X-ray measurements as 55% (PPN: polypropylene normal) and 65% (PPHC: polypropylene with high crystallinity), were used. Positron sources were prepared by depositing ca. 1 MBq (30 μCi) of aqueous ^{22}NaCl on a 7 μm thick Kapton foil having a 10×10 mm^2 area. After drying, the foil was covered with the same size of foil; the edge was then glued with epoxy resins.

In order to measure the irradiation effect of positrons emitted from ^{22}Na by PA, it is important to start data-taking as soon as the positron source is placed between two samples. Hence, in these experiments the data collection was started within a minute after setting the sources. Every PA spectrum was automatically saved every hour. Thus, PA spectra were taken for about 70 h, resulting in 2 million events being collected in each spectrum. The PAL spectra were analyzed using POSITRONFIT EXTENDED (KirKegaard and Eldrup, 1974).

In order to study the effect of γ-ray irradiation, the samples were sealed in glass tubes under a vacuum and irradiated at room temperature at the ^{60}Co γ-ray irradiation facility, Japan Atomic Energy Research Institute. The same care as mentioned above was taken while conducting the PA experiments for the γ-ray irradiated samples.

RESULTS and DISCUSSION

Positron irradiation effect at room temperature

It has been shown that I_3 in PP decreased with two components: the decrease of the fast component was 4% within 10 h in a vacuum and 5% in air (Suzuki et al., 1994a); the decrease in the slow component was 1% in both air and a vacuum. Comparing the G values of cross-linkings (G(X)=0.18) with that of scissions (G(S)=0.27) (Quirk and Alsamarraie, 1989), it is expected that there are more scissions than cross-linkings in the radiation damage of PP. Due to a reduction in the Ps formation by -CH3 groups, we have temporarily ascribed the two decay components in PP as follows: the fast decay component is subject to the formation of new -CH_3 groups due to scissions and the slow decay component to form free radicals (suzuki et al., 1994a). The difference between air and vacuo irradiation may be due to radiation-induced oxidation, which forms carbonyl groups in polymers (suzuki et al., 1994c).

Positron irradiation effect at low temperature

Figure 1 shows I_3 for 6 different temperatures: for 100 K, the sample temperature was restored to 300 K after 93 h; for other low-temperature cases, it was after 48 h. These facts indicate the following: (1) the lower was the samples cooled, the greater did I_3 increase; (2) as soon as the temperature was restored to 300 K, I_3 reached the same value as that of samples irradiated at 300 K; (3) above 195 K, I_3 decreased first, and then in a few hours it started to increase. The increase at low temperature can be explained by a freezing of the thermal motions of the $-CH_3$ groups and other short branches (Zhang and Ito, 1991).

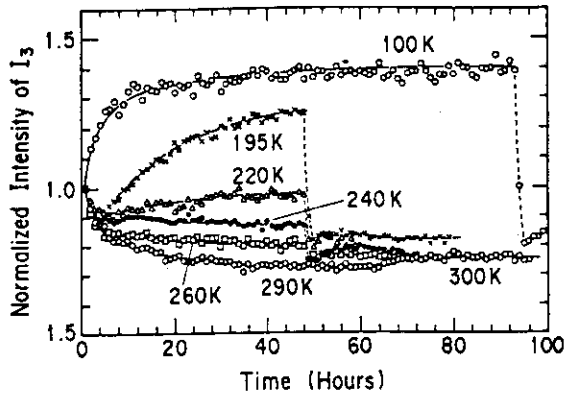


Figure 1, Normalized intensity of I_3 vs time for polypropylene. Data after 2 h are normalized to the first one-hour data. Samples were kept for 48 h for 195K～260K and 93h for 100K.

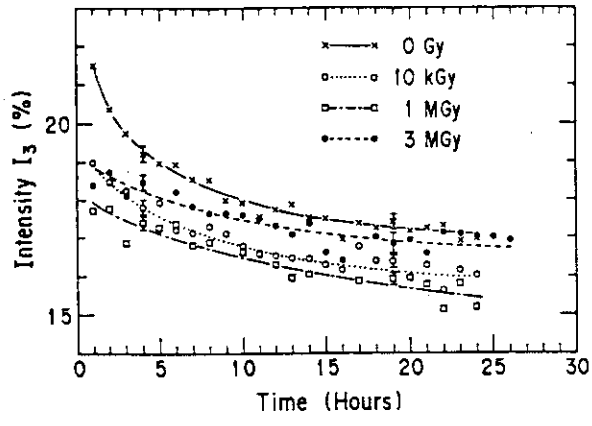


Figure 2, I_3 vs time for polypropylene irradiated by ^{60}Co γ-rays. Data were taken at room temperature.

γ-ray irradiation effect on I_3

PAL measurements of PP samples irradiated by γ-rays of ^{60}Co were conducted in a vacuum at room temperature for 24 h (Fig. 2). As described above, for the unirradiated samples, I_3 decreased by ca. 4% in 10 h. For 1 MGy irradiation with γ-rays, I_3 at 1 h was 3.7% smaller than I_3 of unirradiated samples; the decrease in I_3 within 10 h was only 1.5%. The time variation of I_3 of these irradiated samples was measured at 100K for 24 h (Fig. 3). Although a sharp increase was observed for the unirradiated samples, the increase became smaller in the irradiated samples with a larger dose; it was almost negligible for 1 MGy-irradiated samples. Since the increase has been explained by the termination of rotating thermal motions of the $-CH_3$ groups, the negligible observed increase may suggest the loss of thermal motion due to scissions of polymer structures. A rotating motion of short branches is possible in rigid polymer structures.

Positron irradiation effect on γ-ray irradiated samples

As discussed above, positron irradiation can induce radiation effects on I_3 for PP samples; at room temperature it decreased with the irradiation time. Figure 4 shows both positron and γ-ray irradiation effects in the following three temperature

regions: (1) 0～24 h, 100K; (2) 25～48 h, 300K; (3) 49～100 h, 100K. Although I_3 for the unirradiated sample increased sharply in the first region, I_3 for the 1 MGy irradiated sample with γ-rays showed a negligible increase, and was almost constant for 24 h. In the second region, I_3 became smaller than that in the first region and the value at 25 h was almost the same as that obtained after 25 h of positron irradiation at room temperature (Fig. 2).

These results indicate that the radiation effect on I_3 remained at 100 K and, as soon as the sample was heated up to room temperature, the effects appeared as the step decrease in I_3. In the third region, a gradual increase was observed. This increase could be fitted by the equation 1-exp(t/T), where t is the positron

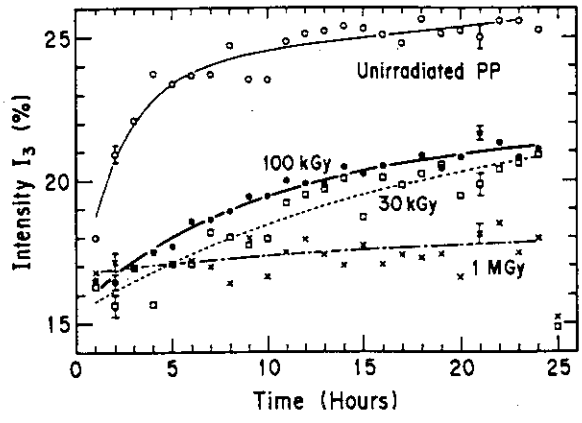


Figure 3, Radiation effect on the increase in I_3 at 100K.

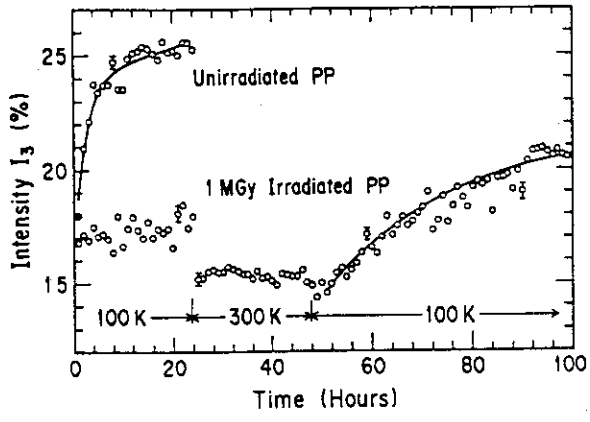


Figure 4, Positron irradiation effect on polypropylene irradiated by ^{60}Co γ-rays. The increase in I_3 for the unirradiated samples is shown to be compared with that for the irradiated one.

irradiation time in h and T a constant, which may be equivalent to the relaxation time related to the thermal motions of the $-CH_3$ groups. For the unirradiated case, two Ts, T1= 3 h and T2= 20 h, were obtained. On the other hand, for the irradiated case, only one T2 = 28 h was obtained. If there are a sufficient number of events to fit the PAL spectra with four components, two long-lived components can be found in the case of PP; one is contributed from Ps in the crystalline region, and the other in the amorphous region. From a previous study by Reiter and Kindle in 1990, T2 was considered to be equivalent to the relaxation time for the amorphous region. Hence

the T2 shown above for the third region may indicate that the amorphous region appeared again after 48 h of positron irradiation. This may be possible to induce cross-linkings so as to reconstruct broken polymer structures caused by radiation-induced scissions.

CONCLUSIONS

Positron irradiation effects on γ-ray irradiated PP have been studied with positron sources for positron annihilation experiments. The radiation effect at low temperature remained while irradiating the samples by positrons. As soon as a sample was heated from 100K to room temperature, I_3 decreased from 25% to 15% for unirradiated

samples, and from 17.5% to 16% for the 1 MGy irradiated samples with γ-rays.

The increase in I_3 was larger in samples cooled at a lower temperature, but increased as soon as the samples were cooled at 100K. The increase was fitted with two components of the relaxation time; the longer time was considered to be related to the amorphous region. Although the increase for the 1 MGy irradiated samples with γ-rays was not observed during the first stage of cooling at 100K, it increased during the second stage of cooling after heating the samples to room temperature. From the relaxation time, the amorphous region was considered to be reconstructed, suggesting that positrons induced cross-linkings of broken polymer structures caused by radiation-induced scissions.

Acknowledgments: For ^{60}Co γ-ray irradiation, the Inter-University Laboratory for the Common Use of JAERI facilities is acknowledged. This work was supported in part by a Grant-in-Aid of the Japanese Ministry of Education, Culture and Science.

REFERENCES

Hsu F.H. and Hadley J.H.(1971), Positron annihilation in irradiated teflon. Phys.Lett. 34A,317

KirKegaard P. and Eldrup M.(1974), POSITRONFIT EXTENDED: a new version of a program for analyzing positron lifetime spectra. Computer Physics Communication 7,pp.401-409

Quirk R.P. and Alsamarraie M.A.A. (1989), Physical constants of polypropylene and polyethylenes. Polymer Handbook edited by Brandrup J. and Immergut E.H., John Wiley & Sons, New York

Reiter G. and Kindl P.(1990), Positron lifetime investigations on linear polyethylene compared to branched polyethylene. Phys.Stat.Sol.(a)118,pp.161-168

Suzuki T.,Oki Y.,Numajiri M.,Miura T.,Kondo K., and Ito Y.(1994), Positron irradiation effects on polypropylene and polyethylene studied by positron annihilation, to be published in Radiat. Phys. Chem., KEK Preprint 94-3

Suzuki T.,Oki Y.,Numajiri M.,Miura T.,Kondo K., and Ito Y.(1994), Structure dependence of gamma-ray irradiation effects on polyethylenes studied by positron annihilation, to be published in Radiat. Phys. Chem.

Suzuki T.,Oki Y.,Numajiri M.,Miura T.,Kondo K.,Shiomi Y., and Ito Y.(1994), Effects of aging and oxidation on positronium formation in polyethylenes. Radiat. Phys. Chem. vol.43,pp.557-562

Wang G.H., Teng M.K., Shen D.X., Yi C.Y., Zhou Y.Y., Lu Y.Y., Wang H.W., Zhu Y.Z., and Dou L.(1988), Positron annihilation lifetimes and Doppler broadening studies of electron irradiated polypropylene Phys.Stat.Sol.(a) bf 106,K1

Walender M. and F.H.J. Maurer (1992), Decrease in o-Ps formation in polymers during positron lifetime measurements. Mat.Sci.Forum 105-110,pp.1811-1814

Zhang Z. and Ito Y.(1991), Micro-structures of gamma-ray irradiated polyethylenes studied by positron annihilation. Radiat.Phys.Chem. 38,pp.221-225

4.4 *The Radiation Chemistry of Poly(Arylene Ether Phosphine Oxide)s

D.J.T. Hill, J.L. Hopewell, J.H. O'Donnell and P.J. Pomery
Polymer Materials and Radiation Group, The University of Queensland, Brisbane, Australia 4072.

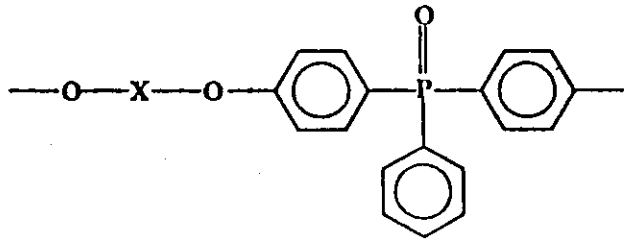
Abstract: Electron spin resonance spectroscopy has been used to study the radicals which are formed on the gamma radiolysis of selected poly(arylene ether phosphene oxide)s which have been irradiated either at 77 or 303 K. At 77 K both neutral and anionic radicals are formed, but the anionic radicals are unstable above 200 K. Two types of neutral radicals were observed. They were the phenyl and phenoxyl radicals formed by homolytic scission of the backbone ether bonds. ^{31}P NMR spectroscopy showed that no new structures involving phosphorus were formed, but there was an indication that crosslinking may take place at aromatic rings adjacent to phosphorus atoms. Solution viscosity measurements indicated that the polymers undergo nett chain scission on irradiation, but the nett scission yield is very small.

INTRODUCTION

In general, highly aromatic polymers with phenyl groups in the backbone chain have been demonstrated to exhibit good thermal properties and to have a high resistance to degradation by gamma radiation. This is believed to be due to their propensity to degrade the absorbed energy to heat with out the cleavage of bonds and to their ability to scavenge hydrogen atoms to form the less reactive cyclohexadienyl radicals. The radiation resistance of these polymers has resulted in their use in the structural components of space vehicles and as insulators in nuclear reactor applications.

The poly(arylene ether phosphine oxide)s, or PEPOs as they are commonly called, along with other aromatic polymers containing the phosphine oxide moiety, have two other desirable properties. First, the presence of the phosphorus imparts to the polymers an inherent flame retardancy. Second, under an oxygen atom flux the surface phosphorus is converted to phosphate, which renders the polymer surface resistant to further oxygen atom attack. These two properties are particularly useful for space applications in low earth orbits.

In this paper we report a study of the high energy radiation sensitivity of three PEPO polymers, using ESR spectroscopy to study the radical formation, ^{31}P NMR to probe cleavage of phosphorus carbon bonds, and solution viscosity to investigate the molecular weight changes. The generalized structure of the three PEPO polymers is given below. As well as the phosphine oxide groups, the polymers contain either hydroquinone, HQ, bisphenol-A, bis-A, or biphenol, BP, repeat units in the chains, which are indicated by the X in the generalized structure. The radiation chemistry of the poly(arylene ether sulfone), PSO, analogues of the three polymers has been reported previously (Hill, 1992).



EXPERIMENTAL

The PEPO polymers were synthesized in the laboratory of Professor J.E. McGrath at Virginia Polytechnic and State University. They possess glass transition temperatures in the range 200 to 250 °C, and they are thermally stable to approximately 500 °C. The M_n of the polymers was in the range 20–25 kg mol^{-1} prior to irradiation.

Samples of the powdered polymers were irradiated under vacuum in pyrex ampoules or quartz ESR tubes using an AECL Gammacell facility. The ESR spectra were obtained on a Bruker X–band spectrometer, and the radical concentrations were determined by comparison with a Varian pitch reference standard. The NMR spectra were obtained in $CDCl_3$ solvent on a Bruker AC200F FT–NMR spectrometer, and the molecular weight changes were monitored by measuring the limiting viscosity numbers of the polymers in dichloromethane at 298 K.

RESULTS AND DISCUSSION

The 77 K ESR spectra, obtained after irradiation of the PEPO polymers at 77 K, are characterized by broad featureless singlets centered at approximately g = 2.004. The spectrum for bis–A PEPO is shown in Figure 1 as an example. The observed spectra are similar to those reported previously for the polysulfone (Lewis, 1989), polyketone (Heiland, 1994a) and polycarbonate (Hama, 1970) analogues of the polymers, and show no evidence for the presence of any phosphorus centred radicals. The spectra have been analysed in terms of the formation of both anion radicals and neutral phenyl and phenoxyl radicals, the latter radicals being formed as a result of backbone scission.

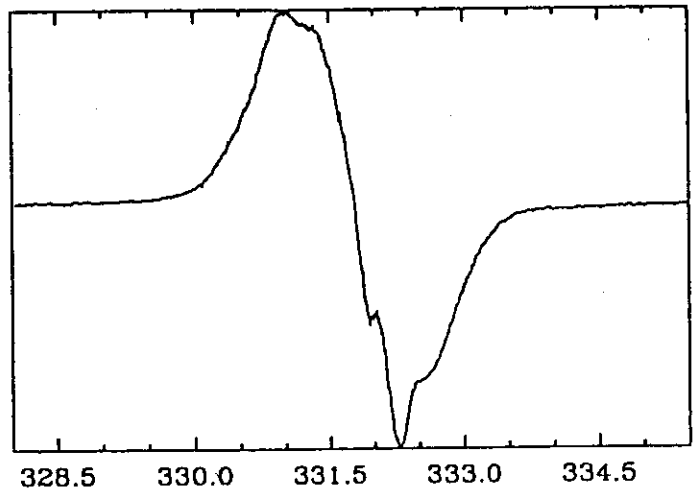


Figure 1: Radical spectrum of bis–A PEPO obtained at 77 K.

Photobleaching studies carried out at 77 K confirmed the presence of two anion radicals following radiolysis at this temperature. It is postulated that these two anions are located on the oxygen atoms of the phosphine oxide or on the aromatic rings of the main chain or the side chains. The anion radicals were shown to constitute approximately sixty percent of the total radical yield at this temperature.

The radical yield versus dose curves were determined at 77 K for low doses, and are shown in Figure 2. Dose saturation effects are clearly present, even at low doses. The dose curves are very similar for the three polymers, and the low dose G–values for radical

7MGy, indicating that while chain crosslinking takes place, the chain scission reaction dominates over crosslinking. This observation was confirmed by solution viscosity measurements. The limiting viscosity numbers for the polymers in dichloromethane were shown to decrease slowly with dose, as demonstrated in Figure 3 for HQ-PEPO. These observations indicate that the polymers are resistant to radiation damage but that the molecular weights of the polymers decrease slowly with increasing dose, indicating that G(S) is only slightly greater than 4G(X).

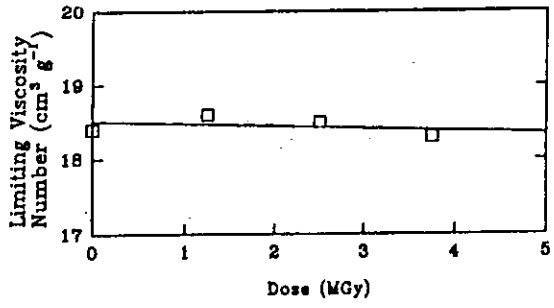


Figure 3: Limiting viscosity number versus dose plots for HQ-PEPO in dichloromethane.

It is of interest to compare the radical yields for the PEPO polymers with those for other polymers which contain the same comonomer back-bone groups. This has been done in Figure 4 for a range of polymers containing the bis-A and HQ comonomer groups. The figure shows that the radiation chemical yields for the PEPO polymers are very similar to those of their polysulfone analogues, but they are less resistant to radical formation than the polyketones and the polyimides, and they are significantly more resistant than Kevlar or bis-A polycarbonate, for which G-radical has been reported to be 1.8 at 77 K (Hama, 1970)

The relative sensitivity of the polymers shown in Figure 4 can be compared with the relative sensitivities as assessed by volatile gas formation, or on the basis of the changes in their tensile properties. Recently Hegazy et al. (Hegazy, 1992) reported that on the basis of the G-values for total gas formation on gamma radiolysis, the polymers could be ranked in terms of resistance to damage in the order Kapton > PEEK > bis-A PSO > bis-A polyester. In an earlier study of the tensile properties of many of the same polymers, Sasuga et al. (Sasuga, 1985) concluded that for e-beam irradiation the order of radiation resistance was PEEK> KAPTON > Ultem > bis-A PSO > PPO, based on a 50% decrease in tensile strength.

There is a great deal of correspondence between the order of radiation resistance as assessed by radical yield, gas formation and tensile property changes, except that on the basis of the radical yields the relationship is reversed for Kapton and PEEK compared to that found for the gas yields. The reason for this reversal in the order is not clear. However, the dose range used for the assement based on radical formation is of the order of 10 kGy, while the dose required for measurement of the gas yields or the tensile property changes is much higher, being of the order of 10 MGy. Thus for the latter measurements the doses are one thousand times higher than for the radical measurements, and the damage to the polymer would be correspondingly much greater.

formation for the polymers was determined from the plot to be 0.58 . This value is very similar to the values obtained for the polysulfones at low dose, which are HQ PSO 0.56, bis-A PSO 0.57 and BP PSO 0.51 (Heiland, 1994b).

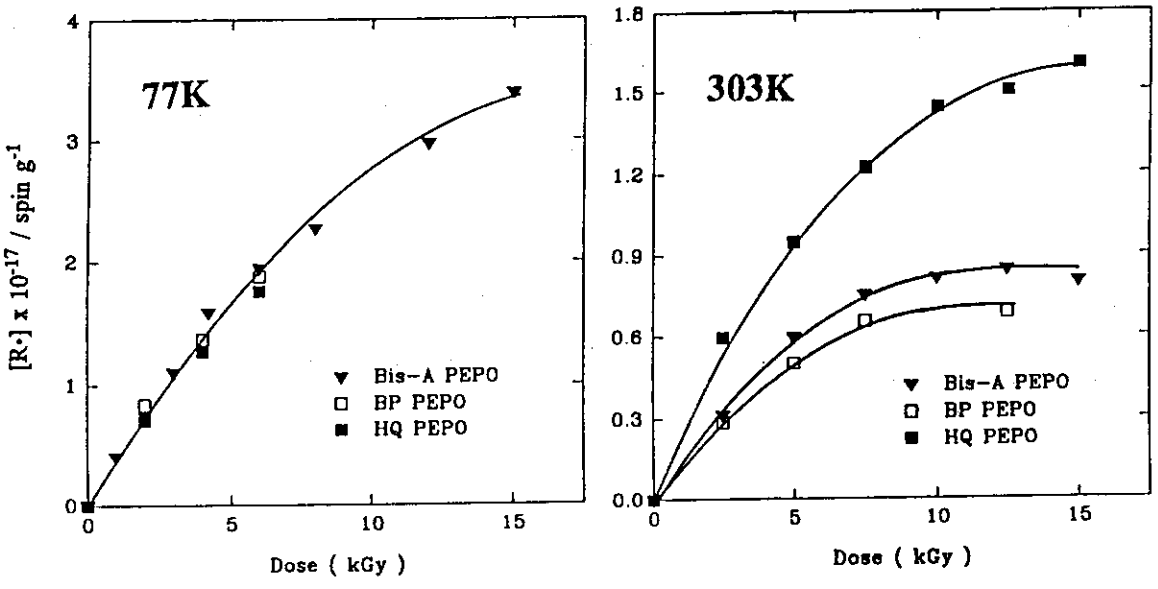


Figure 2: Radical yield plots for irradiation of the PEPO polymers at 77 and 303 K.

Thermal annealing of the samples after irradiation at 77 K demonstrated that radicals are lost over two thermal ranges. Over the temperature range 77 to 200 K the anionic species are lost, and above room temperature the phenyl and phenoxyl radicals both begin to decay concurrently.

Radiolysis at room temperature (303 K) produced radical spectra identical to those observed by warming to this temperature. The radical yield plots are shown in Figure 2. At 303 K the radical yields for HQ PEPO are much greater than those for bis-A PEPO and BP PEPO, which are of similar magnitude. Dose saturation effects were also evident at this temperature. The low dose radical yields were calculated from the plots in Figure 2 to be 0.35 for HQ PEPO, 0.22 for bis-A PEPO and 0.19 for BP PEPO. The somewhat higher G-value for HQ PEPO could reflect the higher ether oxygen content of this polymer as compared to the other two.

The ^{31}P NMR spectra of samples of the PEPO polymers which had been irradiated to 6.9 MGy at room temperature have been investigated, and were found to show no new phosphorus resonances. The only major phosphorus resonance observed in the samples was that due to the triphenyl phosphine unit at 29.1 ppm, indicating that the phosphorus-phenylene bonds are not broken during radiolysis. However, the spectra did show evidence of significant broadening of this phosphorus peak in the irradiated polymers, particularly towards lower field, which would be consistent with some deshielding of phosphorus atoms. The broadening could also be indicative of a lowering of the mobility of the groups adjacent to phosphorus. Both of these effects would be consistent with chain crosslinking at the phenyl rings attached to the phosphorus atoms in the chain.

The irradiated PEPO polymers remained soluble in dichloromethane to doses greater than

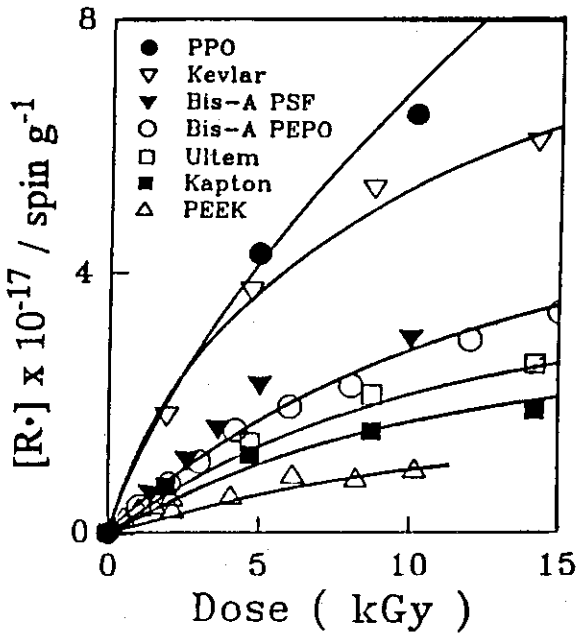


Figure 4: Comparison of the radiation chemical yields for related polymers at 77 K.

CONCLUSIONS

The radical yields on gamma radiolysis of HQ PEPO, bis-A PEPO and BP PEPO have been measured at 77 and 303 K. At 77 K both anions and neutral radicals are formed, but at room temperature only neutral radicals are observed. Two anion radicals were observed, one associated with the phosphine oxide units and one with the aromatic units. The neutral radicals were the mainly phenyl and phenoxyl radicals formed by cleavage of phenyl-oxygen bonds. At 77 K the yield of radicals was similar for all three polymers, but at 303 K the yield of radicals from HQ PEPO was higher than that for the other two polymers. The radiation sensitivity of the PEPO polymers was found to be similar to that of their PSO analogues.

REFERENCES

Hama Y. and Shinohara K. (1970) *J. Polym. Sci. A-1*, **8**, 651.
Hegazy E.A., Sasuga T., Nishii M., and Seguchi T. (1992) *Polymer*, **33**, 2897.
Heiland K., Hill D.J.T., O'Donnell, J.H. and Pomery P. (1994a) *Polym. Adv. Technol.*, **5**, 116.
Heiland K., Hill D.J.T., Hopewell, J.L., Lewis D.A., O'Donnell J.H., Pomery P.J. and Whittaker A.K. (1994b) *ACS Symposium Series*, American Chemical Society, Washington, D.C., In Press.
Hill D.J.T., Lewis D.A., O'Donnell J.H., Pomery P.J., Hedrick J.L. and McGrath J.E (1992) *Polym. International*, **28**, 233.
Lewis D.A. (1989) PhD Thesis, The University of Queensland.
Sasuga T., Hayakawa N., Yoshida K. and Hagiwara M. (1985) *Polymer*, **26**, 1039.

4.5 Mechanism of Radiation-induced Degradation of Poly(Methyl Methacrylate)

Tsuneki Ichikawa, Ken-ichi Oyama and Hiroshi Yoshida
Graduate School of Engineering, Hokkaido University
Sapporo, 060 Japan

Abstract- ESR and gel permeation chromatographic measurements of poly(methyl methacrylate) γ-irradiated between 77 K and 300 K have been carried out to elucidate the mechanism of radiation-induced degradation of the polymer. It is revealed that the scission of the main chain is not taken place immediately after the absorption of radiation energy but is induced by the intramolecular radical conversion of the side-chain $-COO\dot{C}H_2$ radical to the tertiary $-CH_2-\dot{C}(CH_3)-$ radical followed by the main-chain β-scission of the latter radical. The degradation is not taken place below 190 K, because the side-chain radical starts to convert only above 190 K. The residual monomer in the polymer reacts with the side-chain radical below 190 K to generate the stable propagating-type radical, so that the degradation is suppressed even after warming the polymer to the ambient temperature.

INTRODUCTION

Effect of ionizing radiation on polymers is generally divided into main-chain scission (degradation) and crosslinking. Although both processes are taken place in parallel in many polymers, if the scission predominates the crosslinking, they are termed degrading polymers. Degrading polymers such as poly(methyl methacrylate), PMMA, are possible to be used as high-resolution positive-type resist materials in X-ray and electron beam lithography.

The molecular structures of degrading-type polymers with alkane main chains are generally expressed as $[-CH_2-CRR'-]_n$, where one of alkyl groups, R or R', is possible to be replaced by a hydrogen atom. The function of the alkyl group is considered to introduce strain into the main chain. It has been believed that the strain prevents the recombination of primary alkyl radicals generated by direct rupture of a main chain, or accelerates conversion of primary polymer radicals into scission-type radicals accompanying the β-scission of the main chain.

The degradation efficiency of degrading-type polymers has been known to depend strongly on the irradiation temperature. For example, Wall and Brown (1957) fond about three-hold increase of degradation efficiency of PMMA by increasing the irradiation temperature from 77 K to 300 K. Although it is generally explained that the increase of the temperature causes the increase of chain mobility, which in turn causes the decrease of the recombination probability of radical pairs generated by homolytic chain cleavage, the detailed mechanism of degradation and the temperature effect is not known.

The present paper summarizes our recent studies on radiation-induced degradation of PMMA (Ichikawa and Yoshida, 1990, 1991, 1994, Tanaka et al.,

1990). We will prove that the decrease of the G value of main-chain scission at low irradiation temperature is not due to the change of the chain mobility but the addition of residual MMA monomer below 200 K to the primary-generated side-chain $-OCH_2$ radical which otherwise causes the scission of the main chain above 200 K by intramolecular radical conversion to the main-chain $-C(CH_3)-$ radical followed by conversion to the scission-type $C(CH_3)(COOCH_3)-$ radical by main-chain β-scission .

EXPERIMENTAL

Four types of PMMA samples were prepared from commercial PMMA with the average molecular weight of $\bar{M}_n$=15000: PMMA as received (crude PMMA), PMMA purified by repeated precipitation from tetrahydrofuran solution into methanol and vacuum-dried (purified PMMA), purified PMMA but was allowed to stand for 2 months before irradiation (aged PMMA), purified PMMA but was exposed to the vapor of methyl methacrylate monomer for 1 hr (monomer-doped PMMA). Deaerated PMMA sealed in a quartz tube was irradiated with ^{60}Co γ-rays with the dose rate of 20 kGy/hr. The irradiation temperature was controlled by immersing the sample in the slurry of organic solvents. The irradiated samples were then stored in liquid nitrogen.

The molecular weight was measured at room temperature by gel permeation chromatography using calibration with polystyrene standard and appropriate corrections. The ESR spectra of the samples γ-irradiated to a dose of 10 kGy were measured on a Varian E9 X-band spectrometer. The modulation width and the incident microwave power was carefully chosen to minimize the spectral distortion.

RESULTS and DISCUSSION

GPC analysis. The Dose-$\bar{M}_n$ curves of γ-irradiated PMMA followed a well-known equation of $1/\bar{M}_n(D)=1/\bar{M}_n(0)+G_s D/9.65$[2] The G values of the scission, $G(s)$, at 300 K irradiation temperature were the same for all the samples and was about 1.5. However, as

Table 1. Effect of pretreatment on the G value of the scission by 77K-irradiation

PMMA sample	G(s)
Crude, as received	0.30
Purified	1.50
Purified but aged	0.26
Purified but MMA-doped	0

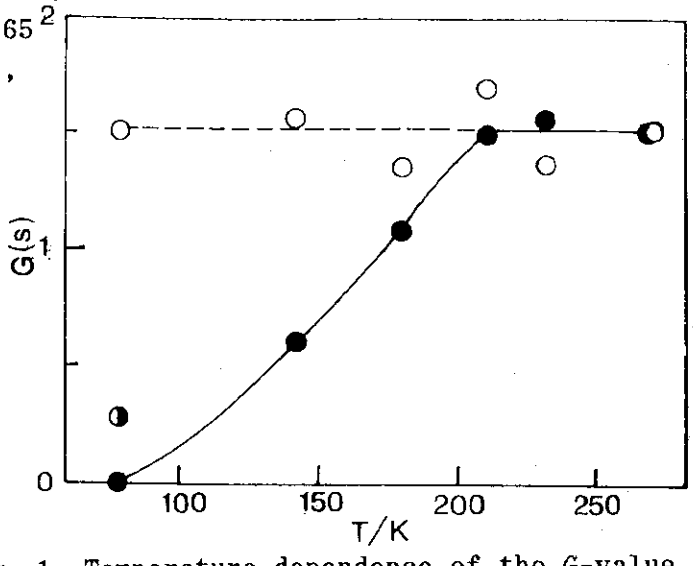


Fig. 1. Temperature dependence of the G-value of the scission for (○) purified, (○) crude and (●) MMA-doped PMMA.

summarized on Table 1. the G values at low temperature strongly depend on the samples. The main-chain scission was completely suppressed by the addition of MMA monomer. This indicates that MMA monomer, no matter whether it is remained in the crude PMMA, generated by unzipping during the storage period, or artificially added, acts as a scission prohibitor at low temperature. As shown in Figure 1. the function as scission prohibitor was completely lost above 200 K.

ESR analysis. Figure 2 shows the change of the ESR spectra during warming of the purified PMMA γ-irradiated at 77 K. As indicated in the Figure, γ-irradiation of the purified PMMA at 77 K causes the formation of three major radical species which are the side-chain $-\dot{C}(O^-)OCH_3$ radical anion with broad singlet ESR line, the side-chain $-COO\dot{C}H_2$ radical with triplet lines, and the main-chain $-\dot{C}H-$ radical with doublet lines. A small amount of formyl radical (doublet ESR) and methyl radical (triplet ESR) are also formed, but they do not play any role in the main-chain scission. These radicals are thermally stable at least up to 170 K, so that the ESR spectrum below 170 K consist of the overlapping spectra of these radicals. The side-chain radical anion starts to convert to the scission-type $-CH_2-\dot{C}(CH_3)COOCH_3$ radical (5+4 lines) by the detachment of the side chain followed by β-scission of the main chain, as,

$$-COO\dot{C}H_2 \longrightarrow -CH_2-\dot{C}(CH_3)(COOCH_3)-CH_2- + CO,\ CH_2O$$

$$-CH_2-\dot{C}(CH_3)(COOCH_3)-CH_2- \longrightarrow -CH_2-C(CH_3)(COOCH_3)=CH_2 + \cdot C(CH_3)(COOCH_3)-CH_2-$$

Only the scission-type radical and the main-chain radical are therefore observed at 270 K.

Figure 3 shows the ESR spectra for the crude PMMA γ-irradiated at several temperatures. The ESR spectra for the monomer-doped PMMA and the aged PMMA are essentially the same as those for the crude PMMA. The ESR spectrum markedly changes between 163 K and 192 K. The spectra were measured at 77 K because of preventing the gradual change of the ESR spectra due to reaction between impurity molecules and radical species during the ESR measurements. The major radical observed above 192 K seems the scission-type radical. The ESR spectrum of the scission-type radical is much sharper than that for the purified PMMA, which indicates that at least a part of the radical is generated by the addition of the monomer to another radical, as,

$$CH_2=C(CH_3)(COOCH_3) + \cdot R \longrightarrow R-CH_2-\dot{C}(CH_3)(COOCH_3)\ .$$

Although the generated radical is not the scission-type but a propagating-type, the molecular structure and the ESR spectrum of the propagating-type radical are the same as those of the scission-type radical. The main-chain radical converts to the propagating-type radical by increasing the temperature to 273 K.

The major spectral component for the crude PMMA irradiated below 163 K is

a sharp triplet which can be assigned to the allyl-type radical anion of the monomer molecule generated by electron capture, as

$$H_2C=C(CH_3)(COOCH_3) + e^- \longrightarrow H_2C-C(CH_3)-C(O^-)OCH_3 \ .$$

Exposure of the samples to visible light at 77 K eliminates the allyl-type radical anion. The ESR spectra of the photo-illuminated sample are much more complex than those for the purified PMMA. They show more than seven ESR lines. The radical species remaining after the illumination are probably the side-chain radical, the main-chain radical, the scission-type radical generated by reaction (2) during γ-irradiation, and the monomer radical (septet ESR spectrum) generated by the addition of a hydrogen atom to the monomer. Warming of the 77K and 163 K irradiated samples to 273 K gives the same ESR spectrum as that of the 273 K irradiated sample, which indicates that the scission-type or the propagating-type radical is the most stable radical in monomer-contaminated PMMA.

The experimental results mentioned so far undoubtedly indicate that the monomer molecules in PMMA act as an inhibitor of the radiation-induced main-chain scission at low temperature. Scission of the main chain necessitates the presence of the side-chain radical and survival of the radical up to 180 K. The side-chain radical may be generated by direct action of ionizing radiations:

$$-COOCH_3 + \gamma \longrightarrow -COO\dot{C}H_2 + H \ , \qquad (1)$$

by proton transfer of the side-chain radical cation:

$$-COOCH_3 + \gamma \longrightarrow -COOCH_3^{\cdot +} + e^- ,$$
$$-COOCH_3^{\cdot +} \longrightarrow -COO\dot{C}H_2 + H^+ \ , \qquad (2)$$

which can be suppressed by charge transfer to MMA, as

$$-COOCH_3^{\cdot +} + CH_2=C(CH_3)(COOCH_3) \longrightarrow -COOCH_3 + CH_2=C(CH_3)(COOCH_3)^{\cdot +} \qquad (2')$$

or by hydrogen abstraction:

$$-COOCH_3 + H \longrightarrow -COO\dot{C}H_2 + H_2 \ . \qquad (3)$$

which can be suppressed by hydrogen-atom addition to MMA. as

$$CH_2=C(CH_3)(COOCH_3) + H \longrightarrow \cdot C(CH_3)_2(COOCH_3). \qquad (3')$$

Since the activation energies for reactions (2') and (3') are lower than those for reactions (2) and (3), respectively, suppression of side-chain radical formation is favorable at lower temperature.

The side-chain radical converts to the scission-type radical during warming the sample to room temperature, as,

$$-COO\dot{C}H_2 \longrightarrow -CH_2-\dot{C}(CH_3)(COOCH_3)-CH_2- + CO, CH_2O \ ,$$
$$-CH_2-\dot{C}(CH_3)(COOCH_3)-CH_2- \longrightarrow -CH_2-C(CH_3)(COOCH_3)=CH_2$$
$$+ \cdot C(CH_3)(COOCH_3)-CH_2- \ . \qquad (4)$$

which competes with reaction:

$$-COO\dot{C}H_2 + CH_2=C(CH_3)(COOCH_3) \longrightarrow -COOCH_2-CH_2-\dot{C}(CH_3)(COOCH_3), \quad (4')$$

Reaction (4') is approximately the reverse reaction of (4) and is exothermic by approximately 13 kcal/mol (heat of polymerization). Reaction (4') is therefore preferable at lower and higher temperature. In any reaction mechanisms, the monomer molecules act as an efficient degradation inhibitor at lower temperature.

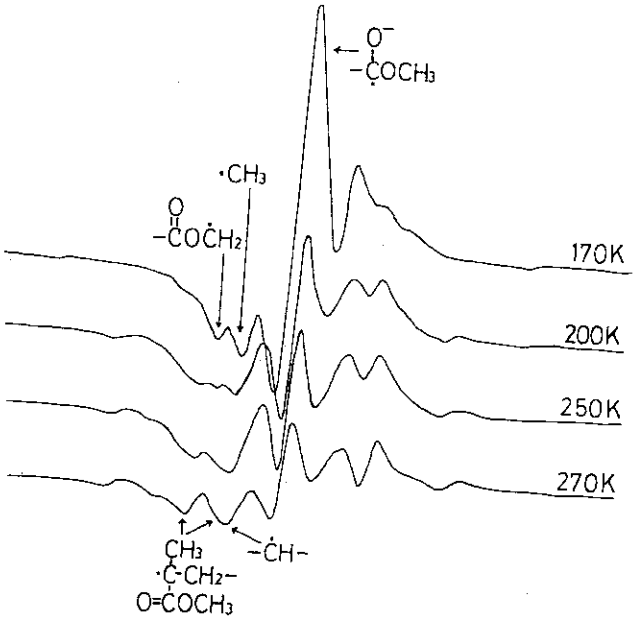


Fig. 2. Change of the ESR spectrum of Purified PMMA γ-irradiated at 77 K during warming the sample to room temperature.

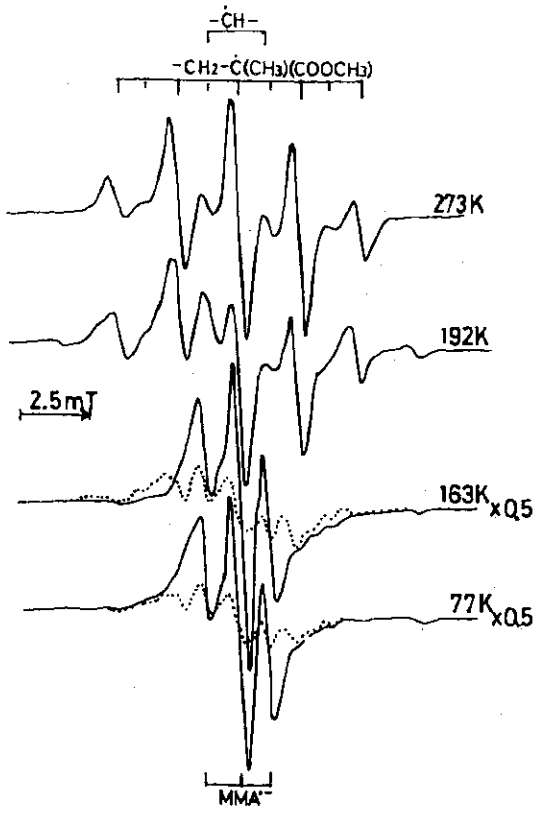


Fig. 3. Effect of irradiation temperature on the ESR spectrum for crude PMMA. Dotted line shows the spectra after photoillumination.

REFERENCES

Ichikawa T. and Yoshida H. (1990) J. Polym Sci. A, 28, 1185.
Ichikawa T. and Yoshida H. (1991) Radiat. Phys. Chem. 37, 367.
Ichikawa T., Oyama K., Kondoh T. and Yoshida H. (1994) J. Polym. Sci. A, 32, 2487.
Tanaka M. Yoshida H. and Ichikawa T. (1990) Polym. J. 22, 835.
Wall and Brown (1957) J. Phys. Chem. 61, 129.

4.6 Radiation Stability of Pyridine Resin for Reprocessing

M.Nogami, Y.Fujii and T.Sugo*

Research Laboratory for Nuclear Reactors, Tokyo Institute of Technology,
O-okayama, Meguro-ku, Tokyo 152, Japan
*Takasaki Radiation Chemistry Research Establishment,
Japan Atomic Energy Research Institute,
Watanuki-machi, Takasaki-shi, Gunma 370-12, Japan

Abstract The resistance against radiation of the tertiary pyridine resin synthesized for reprocessing was evaluated. As a result, after the irradiation of 10 MGy, less than 10 % of the exchange groups were deteriorated in HCl solutions regardless of their concentrations. But 30~40 % were deteriorated in HNO_3. Thus it has been revealed that this pyridine resin has remarkable resistance against radiation particularly in HCl. And it has been revealed as well, that the deterioration of pyridine type resins results from the scission of the principal chains.

INTRODUCTION

About 50 years ago, when the separation of the spent fuel was studied for the first time, the ion exchange method was considered as an alternative to the solvent extraction. But then, the organic ion exchange resins were too weak in radiation conditions to be applied to the radioactive elements.

Recently, however, the properties of organic ion exchange resins have been greatly improved. Then in order to investigate the applicability of the ion exchange resins to reprocessing, the authors of the present study paid attention to the pyridine type anion exchange resin. It is expected that this type of resin has strong resistance against radiation[1,2]. Though HNO_3 is better as the extractant in the present reprocessing, in the present work, our attention is placed on HCl solutions. Because anion exchange resins have better ion selectivities in HCl than in HNO_3.

Thus we have conducted the irradiation test and quantitatively evaluated the resistance against radiation in HCl on this resin we have synthesized. To make comparison, the same test and evaluation was done in HNO_3 which is used as the extractant in the present reprocessing. Moreover we intended to make the mechanism of deterioration clear, too.

EXPERIMENTAL

The samples used in the test were the tertiary pyridine resin which is macroporous, 20 % crosslinked and has the uniform diameter of 60 μm because it is imbedded into the porous silica beads. This silica was used to suppress the swelling or shrinking of. The method of synthesis is recently reported[3].

In the test, the samples were encapsulated in 15cm^3 of test tubes which were dry or containing the solution of H_2O or 0.1, 3, 6 M HCl or HNO_3. Under aeration they were irradiated up to 1, 3, 10 MGy by ^{60}Co γ ray. The durability was evaluated by calculating the deterioration rate of exchange groups which is derived from the exchange capacity measured before and after irradiation, defined as,

$$100\{(EC)_b - (EC)_a\}/(EC)_b \quad (\%)$$

where $(EC)_b$ and $(EC)_a$ are the exchange capacities before and after irradiation, respectively.

To make comparison, other three types of resins were also irradiated at the same conditions. They are tertiary pyridine type (macroporous, without silica), quaternary ammonium type (macroporous) and the same type (gel).

RESULTS AND DISCUSSION

The original color of the two pyridine resins was almost white. After irradiation, the resin with silica turned high green in HCl and high brown in HNO_3. On the other hand, the resin without silica turned orange and the degree was much higher in HNO_3 than in HCl. The reason, why the change in the color of the resin with silica was very much different from that without silica, seems to be due to MoO_3 which silica beads contain.

The pyridine resin with silica was deteriorated in proportion to the irradiation dose. After the irradiation of 10 MGy, only less than 10 % of the exchange groups were deteriorated in 3M HCl solution, but about 30 % in 3M HNO_3 (Fig.1). The deterioration rates were found to be independent of their acid concentrations. This pyridine resin has shown to be remarkable resistance against radiation particularly in HCl. Almost the same results were obtained on the pyridine resin without silica. This indicates that this silica has little influence on irradiation though there is a lot of difference on the change of the color of the resins.

In the case of conventional quaternary ammonium type resins, about 70 % of exchange groups were deteriorated in HCl and about 50 % in HNO_3 regardless of their acid concentrations. The deterioration rates of gel type in dry form and in 3M acids were shown in Fig.2.

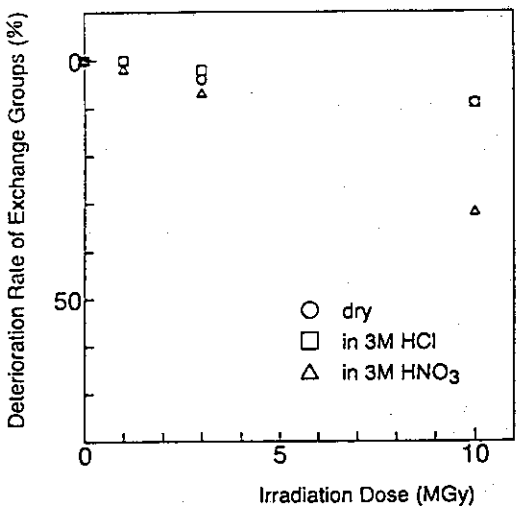


Fig.1 Deterioration of Tertiary Pyridine Resin (With Silica) by Irradiation of γ Ray

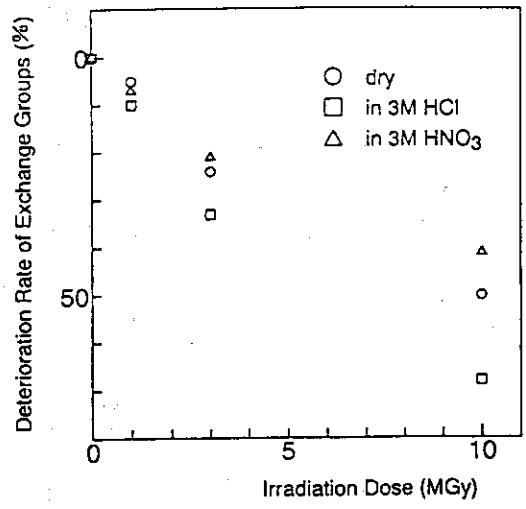


Fig.2 Deterioration of Quaternary Ammonium Resin (Gel) by Irradiation of γ Ray

The deterioration of the quaternary ammonium type resin was studied before, and it is mainly due to the scission of the C-N bond connecting $N(CH_3)_3$ groups with benzyl radicals which leads to the elimination of the exchange groups[4]. It has been revealed that this type of resin is more stable in HNO_3 than in HCl because HNO_3 scavenges hydrated electrons which cause the scission[5]. Our results agree with that.

In contrast, the pyridine resin was more stable in HCl in our test. To make the mechanism of the deterioration of this resin clear, the IR spectra were studied on the resin samples after irradiation of 10 MGy. As a result, the adsorption band around 1700 cm^{-1} which seems to come from carbonyl groups or carboxylic acids was observed particularly on the sample in HNO_3, where the deterioration was larger. In addition, in order to investigate more detail, the solutions in the sample tubes after irradiation of 10 MGy were subjected to the analyses of GC / MS. It was found by mass spectrometry that the detected species in the solutions was not pyridine but nicotinic acid (C_6H_4NCOOH).

From the experimentally observed facts, the mechanism of the deterioration would be suggested as follows. There are the two possible ways; the radiation of lower dose causes the scission of C-H bonds of the principal chains, and that of higher dose causes the scission of C-C bonds. In the former case, by addition of oxygen, carboxylic acids which work as cation exchange sites are formed. But we haven't confirmed yet. They make little indifference on the anion exchange in acid solutions. In the latter case, the addition of oxygen as well forms carboxylic acids and carbonyl groups. And by more breakage of the principal chains, the fragments of lower molecular weights such as nicotinic acid are dissolved to the acid solution. The more deterioration in HNO_3 would be due to the fact that HNO_3 is the stronger oxidant than HCl.

CONCLUSION

As mentioned above, it has been revealed that the tertiary pyridine resin we have synthesized has remarkable resistance against radiation particularly in HCl solutions. Thus it would be adaptable to reprocessing in HCl system. But there would be little advantage in HNO_3. The deterioration of this resin seems to result from the scission of the principal chains. If the resin, whose principal chains have a conjugation system is, developed, it would be more resistant against radiation.

REFERENCES

1. E. D. Kiseleva, V. M. Khasanova and K. V. Chmutov (1971) The Radiation Stability of AVKh-8P and AVI-8P Quinoline and Isoquinoline Anion-exchange Resins. *Russ. J. Phys. Chem.* **45-5,** 667

2. V. M. Khasanova, E. D. Kiseleva and K. V. Chmutov (1977) The Radiation Stability of the VP-1AP Anion-exchange Resin. *Russ. J. Phys. Chem.* **51-3,** 329

3. M. Nogami and Y. Fujii (1994) Synthesis of Ion Exchange Resin for Treatment of Radioactive Wastes and Ion Selectivity Test. *Abs. Int. Conf. Reactive Polymers, Xian,* 146

4. A. Kabi and P. G. Gray (1968) Gamma Radiolysis of Aqueous Solutions of Aryl Alkyl Amines. *Radiat. Res.* **34,** 680

5. A. R. Kazanjian and D. R. Horrell (1975) Radiation Effects on Ion-Exchange Resins-II. Gamma Irradiation of Dowex 1. *U. S. AEC, Rocky Flats Division, Golden, Colorado,* RFP-2354

4.7 Inhibition of Radiation-oxidation by Pure Hydrocarbon Type Radical Scavengers

Junichi Kubo*
Central Technical Research
Laboratory, Nippon Oil Company
Chidori-cho 8,Naka-ku,Yokohama,231 Japan
Kazushige Otsuhata
Raytech Corporation
Soshu Bldg 402,4-40-13 Takadanobaba
Shinjuku-ku,Tokyo,169 Japan

Abstract

Hydrogen-donating hydrocarbons derived from petroleum(HHAP) whose high radical scavenging ability was already confirmed in various tests were applied as inhibitors against radiation-oxidation of polyolefins and a petroleum products (base stock for lubricants), and the effects were compared with the conventional hindered phenolic antioxidantds. HHAP exhibited evident inhibiting effects and superior durability in these hydrocarbon products. These effects can be attributed to the high radical scavenging ability and the pure hydro-carbon constituent of HHAP without functional groups containing heteroatoms. These effects were also applied to crosslinking of polypropylene.

Introduction

Pure hydrocarbons without functional groups containing heteroatoms have seldom been used as radical scavengers except in such examples as coal liquefaction and heavy oil upgrading[1,2] in which hydrogen-donating hydroaromatics are used as hydrogen-donor solvents in reductive atmosphere.

Hydroaromatics, represented by tetralin, have been regarded as being easily oxidized, and they have not been applied as antioxidants to date. However, it was found that hydroaromatics exhibit the radical scavenging effects even in the presence of oxygen although closely related with the oxygen partial pressure at the reaction sites.[3,4] It was also found that the hydrogen-donating hydrocarbons(HHAPs) which have high radical scavenging abilities can be produced from petroleum, and the high radical scavenging abilities of HHAPs were confirmed in the reactions with DPPH(2,2-diphenyl-1-picrylhydrazyl) and in the practical tests for the inhibition of thermal and oxidative degradation of petroleum products[3], rubbers[5], plastics[6], and thermoplastic elastomers.[7]

The radiation degradation in hydrocarbon products such as petroleum products and plastics are considered to be radiation-induced oxidation.[8] Then, based on the facts mentioned above, a hydrogen-donating hydrocarbons derived from petroleum(HHAP) was applied as a inhibitor for radiation degradation.

The experimental results conducted with a petroleum product and polyolefins are reported in this paper compared with the conventional antioxidants. The outline of the test results for crosslinking of polypropylene are also reported.

Experimental

Application to Polyolefins

The additive effects of HHAP on high density polyethylene(PE, density:0.963, produced by Nippon Petrochemical Co.) and isotactic polypropylene(PP, density: 0.90-0.91, produced by Nippon Petrochemical Co.) were examined. HHAP, whose properties are shown in Table 1, was produced by the hydrogenation of a highly

aromatic heavy oil obtained from a heavy fraction of petroleum. It contains many components(more than 300 detected by gas chromatography), and it is difficult and meaningless to clarify the chemical structures of the individual components. Most of the components are inferred to have partly hydrogenated products of condenced aromatic rings, and it is oderless, yellowish brown in color, solid/liquid state at room temperature, boiling points above 350°C with average molecular weight of 398.

The added amount of HHAP was 0.3 wt% and 1.0 wt% to the base plastics. A conventional hindered phenolic antioxidant was also tested for the comparison. The test specimens were prepared sequentially by mixing, kneading and pressing. The dumbell specimens pressed out from the sheets were irradiated by an electron beam(EB) at 0.67kGy/s (2400kGy/h) in air at room temperature up to 0–500 kGy for PE and 0–100kGy for PP.

After irradiation, elongation at the break was measured at room tenperature by the extension tester (Model CS–183TE made by CSI).

For the post–oxidation, elongation at the break and the yield strength were measured for the specimens preserved for six months in air at room temperature after the irradiation of 50, 100, 150, 200 kGy for PE and 30, 50, 80 kGy for PP.

Table 1. Properties of heavy hydroaromatics from petroleum (HHAP)

Density (15°C, g cm^{-3})	1.028
Viscosity (100°C, m^2 s^{-1})	2.536×10^{-5} (25.36cst)
Carbon residue (wt%)	1.15
Pour point (°C)	27.5
Flash point (°C)	234
Elemental analysis (wt%)	
	C 89.7
	H 10.1
	S 0.08
	N —
H/C (atomic ratio)	1.35
Average molecular weight	398
Refractive index	1.5978
Distillation (°C)	
IBP/5%	348/374
10/30	385/420
50/70	447/478
90/EP	525/584
Composition (wt%)	
Saturates/aromatics	21.3/78.7
^{1}H-NMR of aromatics	
Hα/H	0.16
Hα/H	0.30
Hβ/H	0.37
Hγ/H	0.17
Fa (fraction of aromatic carbons)	0.38

Application to Oil Product

The additive effects of HHAP on a base stock (SAE–10), whose properties are shown in Table 2, were investigated. Samples (25g) were placed in glass bottles(inner volume:30ml), and irradiated by γ–ray in air at room temperature without mixing. The samples after the irradiation were analyzed by an acid balue analyzer(defined as JIS K2501; KOH(g) was used to neutralize the total acidic compounds in the samples(g), IR(JASCO FT/TR–7000, 0.1 mm fixed cell), and a gas chromatography (SHIMADZU GC–9A,column:methylsilicone 0.25mm×25m, carrier gas:He). The irradiation rate was 10kGy/h from Co–60.

A conventional hindered phenolic antioxidant (DBPC) was also tested for the comparison. The DBPC(di–t–butyl–p–cresol, produced by TOKYO KASEI KOGYO Co.) was more than 99% in purity, and it was used as received.

Table 2 **Properties of Base Stock (SAE-10)**

specific gravity	15/4 °C	0.8536
viscosity, cSt	at 40 °C	23.01
	at 100 °C	4.545
viscosity index		111
color	ASTM	L0.5
pour point, °C		–10
smoke point, °C		–8
aniline point, °C		107
refractive index	n_d^{20}	1.4691
nitrogen, wppm		3
sulfur, wppm		4
analyses by column chromatography, wt %		
saturates		95.1
aromatics		4.8
resins		0.1

Results and Discussion

The elongations at the breaks immediately after EB irradiation are shown in Fig.1 for PE and Fig.2 for PP. The effects of HHAP on PE are obvious in the addition of 1.0 wt%, but not so obvious with 0.3 wt% HHAP or 0.1 wt% of the conventional antioxidant.

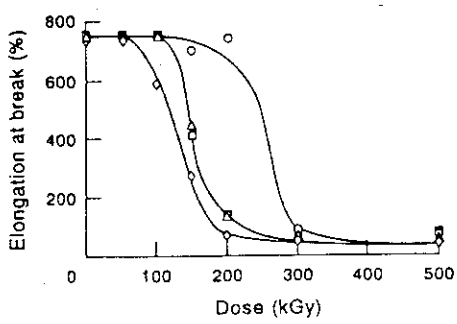


Fig. 1. Changes of elongation at the break by electron beam irradiation in air for polyethylene containing additives. ◇, Blank (no additive); □, commercial antioxidant (0.1 wt%); △, addition of HHAP (0.3 wt%); ○, addition of HHAP (1.0 wt%).

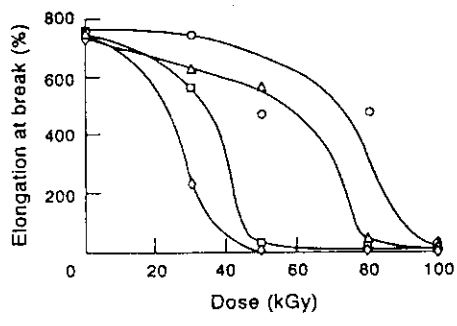


Fig. 2. Changes of elongation at the break by electron beam irradiation in air for polypropylene containing additives. Symbols are the same as in Fig. 1.

Elongation was maintained almost unchanged until 200 kGy for PE with 1.0 wt% HHAP. The effects of HHAP are more distinct in the case of PP(Fig.2); 0.3 wt% HHAP gives distinct effects, and elongation did not change up to 30 kGy with 1.0wt% HHAP.

The changes in the mechanical properties of these polyolefins by aging(post-oxidation) were investigated, and the results with PP are described in this paper as they are more distinct and meaningful. The changes in elongation by aging for PP are elucidated in Fig.3.

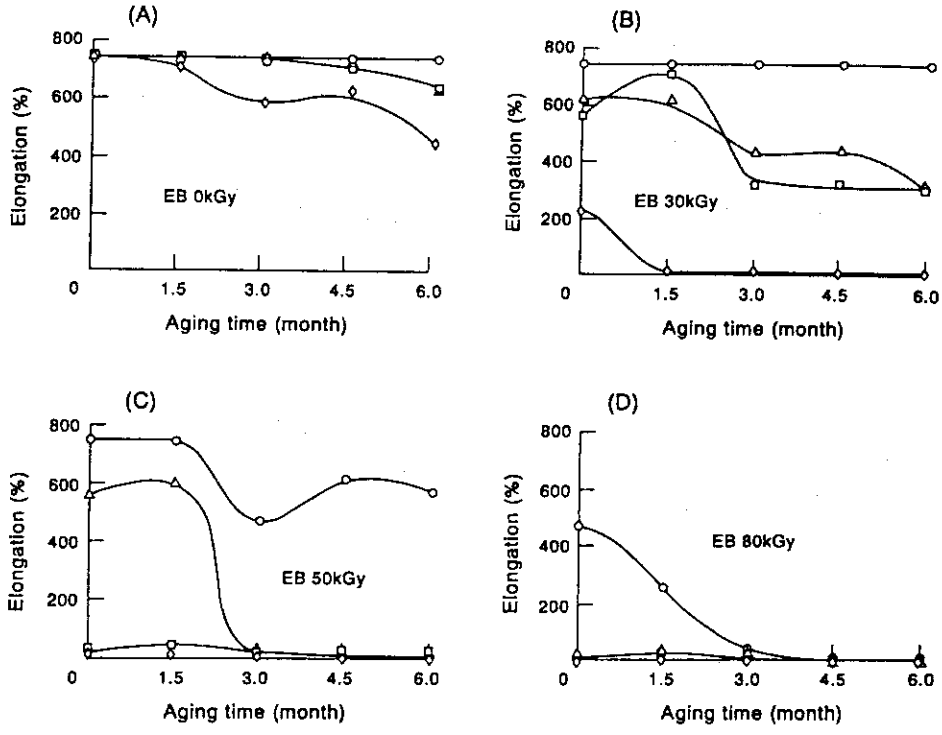


Fig.3 . Changes of elongation at the break by aging for polypropylene after electron beam irradiation in air. Symbols are the same as in Fig. 1.

An obvious decline in elongation can be observed by aging even for the sample without irradiation(A in Fig.3). At 30 kGy, the obvious differences can be observed among the cases, and the elongation was maintained unchanged by the addition of 1.0 wt% HHAP. At 50 kGy(C), a decline of elongation was seen for the sample added 1.0 wt% HHAP, however, as high as 80% of elongation was preserved for 6 months.

The results from the tests with a base stock are described, next. The changes of acid values by dose are illustrated in Fig.4. The additive effects of both DBPC and HHAP are obvious, and the effect of HHAP is higher than that of DBPC. The addition of HHAP(0.5 wt%) and DBPC(0.5 wt%) together exhibited an intermediate effect between those. The changes in carbonyl absorbances(1710 cm^{-1} by IR) with dose are shown in Figs.5 and 6. In the case of the addition of HHAP, the increase in carbonyl absorbance were clearly inhibited by HHAP until 2500 kGy, and the effects depended on the amounts of HHAP added(Fig.6). In the case of the addition of DBPC, on the other hand, the carbonyl absorbances were suppressed up to 1000 kGy; however, they were intensely increased at 2500 kGy, exceeding over the blank data(without addition). This can be considered that the increases of the carbonyl absorbances are due to quinones and other carbonyl compounds formed from the added DBPC[7]. This is supported by

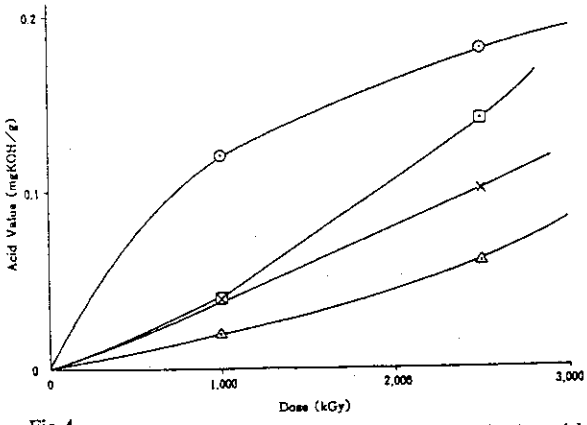


Fig.4 . Increases of acid values of mineral oil by irradiation with γ-rays in air at room temperature (irradiation rate 10 kGy/h from Co-60): ⊙, blank (without addition); ⊡, addition of DBPC (1.0 wt %); ▲, addition of HHAP (1.0 wt %); ×, addition of DBPC (0.5 wt %) and HHAP (0.5 wt %).

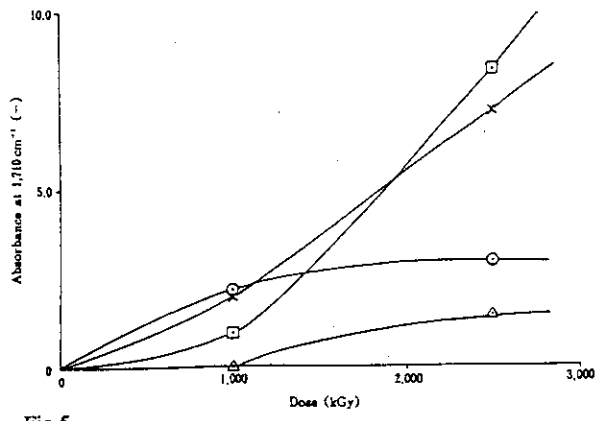


Fig.5 . Increases of carbonyl absorbance (1710^{-1} cm by IR) of mineral oil by irradiation with γ-rays in air at room temperature (irradiation rate 10 kGy/h from Co-60, cell thickness 0.1 mm): symbols are identical to those in Figure 4.

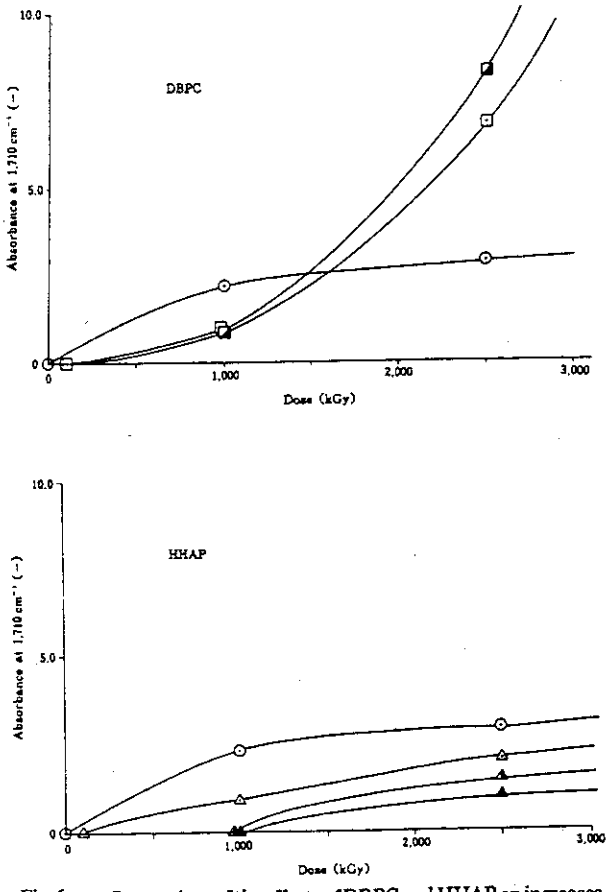


Fig.6 . Comparison of the effects of DBPC and HHAP on increases of carbonyl absorbance (1710^{-1} cm by IR) of mineral oil by irradiation with γ-rays in air at room temperature (irradiation rate 10 kGy/h from Co-60, cell thickness 0.1 mm): ⊙, blank (without addition); ⊡, addition of DBPC (0.3 wt %); ⧈, addition of DBPC (1.0 wt %); ▲, addition of HHAP (0.3 wt %); ▲, addition of HHAP (1.0 wt %); ▲, addition of HHAP (3.0 wt %).

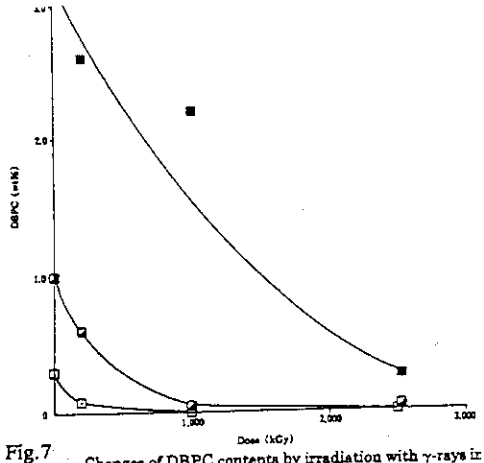


Fig.7 Changes of DBPC contents by irradiation with γ-rays in air at room temperature (irradiation rate 10 kGy/h from Co-60): ⊡, addition of DBPC (0.3 wt %); ⧈, addition of DBPC (1.0 wt %); ■, addition of DBPC (3.0 wt %).

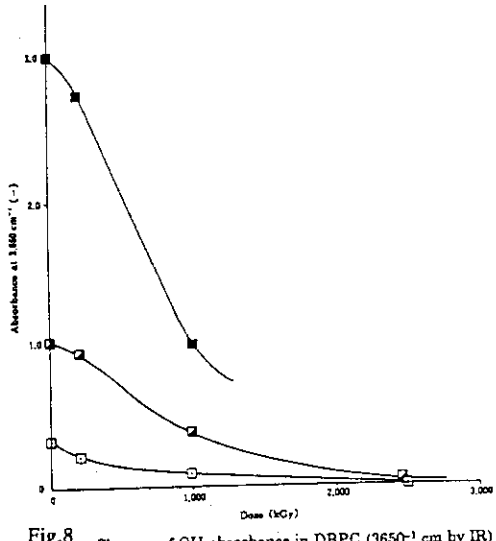


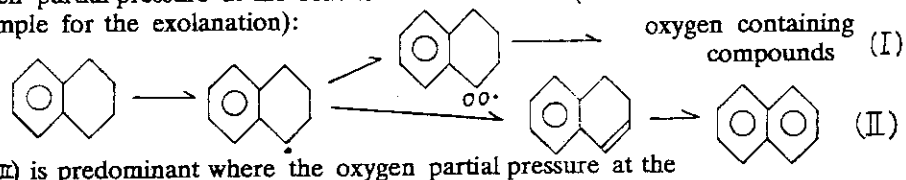
Fig.8 Changes of OH absorbance in DBPC (3650^{-1} cm by IR) by irradiation with γ-rays in air at room temperature (irradiation rate 10 kGy/h from Co-60, cell thickness 0.1 mm): symbols are identical to those in Figure 4.

the data of the addition of HHAP and DBPC together.

Next, the changes in DBPC contents (by gas chromatography) by dose are illustrated in Fig.7. The added DBPC(0.3, 1.0, 3.0 wt%) were certainly detected at dose 0, and the DBPC contents were abruptly decreased by the dose. The hydroxyl groups contained in DBPC(detected at 3650 cm^{-1} by IR) were also examined, and the results are shown in Fig.8. It can be understood that the hydroxyl groups were decreased by dose, in accordance with the DBPC contents. Information on the structural changes in HHAP could not be obtained because it has many components, but it can be inferred from Fig.5 that such structural changes as with DBPC did not occur in HHAP.

Radiation degradation of hydrocarbons can be considered to be radiation-induced oxidation[8], that is, radicals formed by irradiation are oxidized by oxygen in air. As already reported[4], the radical scavenging effects of hydro-aromatics were confirmed by the reactions with DPPH even in the presence of oxygen, and HHAPs have much higher radical scavenging ability than tetralin and octahydrophenanthrenes as follows[10]; tetralin: 1.11×10^{-3} min^{-1}, OHP: 5.60×10^{-3} min^{-1}, HHAP: 78.5×10^{-3} min^{-1}(reaction rate constants at 50 °C in air assuming 1st order). These effects have also been demonstrated as evident inhibiting effects against termal and oxidative degradation of petroleum products, rubbers, plastics, and thermoplastic elastomers. The additive effects of HHAP to the polyolefins and the base stock are attributable to the high radical scavenging ability of HHAP.

Hydroaromatics represented by tetralin have been regarded as being easily oxidized[11,12], and they have not been used as inhibitors in the presence of oxygen. However, it can be considered that the reaction pathways of hydroaromayics are changed by oxygen partial pressure at the reaction sites as follows(tetralin is taken as the example for the exolanation):



That is, route(II) is predominant where the oxygen partial pressure at the reaction site is relatively low, and when it comes to zero, the reactions approach to coal liquefaction. HHAP exhibited prominent effects in the tests described here, as well as the other performances already reported[3-8]. These effects are considered to be based on the reactions in route(II) as the oxygen partial pressures at the reaction sites are relatively low in these cases.

One more important fact shown from these results is the advantage of pure hydrocarbon constituent of HHAP. As elucidated in Figs.4 and 5, acid values and carbonyl absorbances are increased by dose in the cases of the addition of DBPC extending over the blank data. The structural changes can be deduced to be occurred in DBPC as the irradiation doses were accumulated. Judged from the papers already reported[8], the main oxidation products from DBPC are quinones; and the inhibiting effects on the formation of carboxylic acids are observed to decline as elucidated in Fig.4. This interpretation are supported by the changes in DBPC contents(Fig.7) and the hydroxyl groups in DBPC(Fig.8).

On the other hand, acid values and carbonyl absorbances were suppressed until 2500 kGy in the cases of HHAP. In addition, the suppressing effect is proportional to the amount of HHAP added(Fig.6). This can be understood because HHAP does not have functional groups containing heteroatoms which is liable to be attacked by oxygen. That is, it can be concluded that hindered phenols are prone to be structurally changed into quinones because of their OH groups; however, pure hydrocarbon type HHAP is more resistant to irradiation.

As already reported[6], the hindered phenolic antioxidant(Irganox 1010) exhibited very high inhibiting effects on the oxidative degradation of the same PP by the addition of 0.1 wt% as illustrated in Fig.9. However, as judged from Figs.1 and 3, the additive effects of 0.1 wt% of this conventional additive is not so eminent as HHAP on both the degradation during irradiation and post-irradiation. This can be deduced that the structural changes described above,

are related. That is, OH groups in DBPC were attacked and the phenols were changed to carbonyl compounds, and the inhibiting effects were declined. This deduction seems to be less exact because the testing conditions were not same in many respects; however, the facts reported by other researchers[13] seem to support this deduction. It was already pointed out that hindered phenolic anti-oxidants, including Irganox 1010, were destroyed at lower doses in PP, and that the extent of the destruction depended on the nature of the antioxidants and the polymers.

The eminent radical scavenging ability and durability of HHAP were applied to crosslinking of PP. PP was obviously crosslinked at lower doses by the addition of HHAP together with A-TMPT(trimethylpropane-tri- acryrate). In these cases, HHAP functions to suppress scissions caused by the irradiation, and consequently, high gelation and distinct changes in properties were apparent (especially in MFR and HDT).

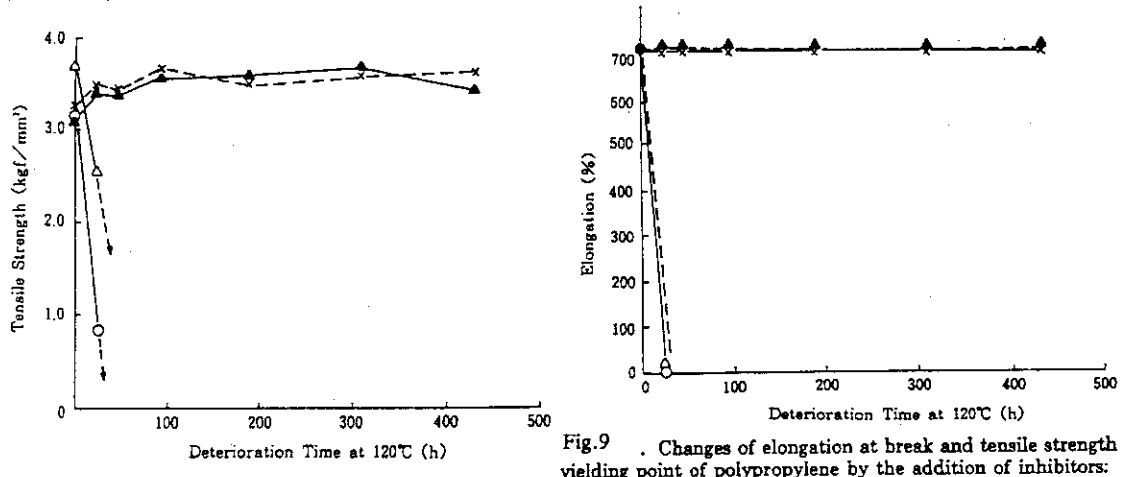


Fig.9 . Changes of elongation at break and tensile strength at yielding point of polypropylene by the addition of inhibitors: ○, blank (without addition); △, addition of HHAP (0.1 wt %); ▲, addition of HHAP (0.5 wt %); ×, addition of Irganox 1010 (0.1 wt %).

Conclusions

The additive effects of a pure hydrocarbon type radical scavenger derived from petroleum(HHAP) against radiation-oxidation of polyolefins and a petroleum product(base stock) were investigated, and the following results were obtained:

(1)The additive effects of HHAP to PE and PP were evident including post-irradiation oxidation; however, the ones of a hindered phenolic antioxidant were not so evident in the comparison with the effects against oxidation of the same PP.

(2)The additive effects of HHAP were maintained until high doses(2500 kGy); however, the effects of a hindered phenolic antioxidant was declined by the increase of dose in the tests for the base stock.

(3)The structural changes in the phenolic antioxidants by the attack of the hydoxyl groups were observed.

(4)The prominent inhibiting effects and the durability of HHAP seems to be attributable to its pure hydrocarbon constituent without functional groups containing heteroatoms.

References

1. Carlson,C.S.,Langer,A.W.,Stewart,J.,Hill,R.M., Ind.Eng.Chem.,50,1067(1958).
2. Fisher,I.P.,Southrada,F.,Wood,H.J., Prepr.Div.Petrol.Chem.,ACS Mtg.,27,838 (1982).
3. Kubo,J., Fuel Process.Technol.,27,263(1991).
4. Kubo,L., Ind.Eng.Chem.Res.,31,2587(1992).
5. Kubo,J., J.Appl.Polym.Sci.,47,925(1993).
6. Kubo,J., J.Appl.Polym.Sci.,45,51(1992).
7. Kubo,J.,Onzuka,H.,Akiba,M., Polym.Degr.Stab.,45,27(1994).
8. Clough,R.L.,Gillen,K.T., J.Polym.Sci.,19,2041(1981).
9. Cook,C.D., J.Org.Chem.,18,261(1953).
10. Kubo,J.,Miyagawa,R.,Takahashi,S., Energy Fuels,8,804(1994).
11. Larsen,R.G.,Thorpe,R.E.,Armfield,F.A., Ind.Eng.Chem.,34,183(1942).
12. Robertson,A.,Waters,W.A., J.Chem.Soc.,1574(1948).
13. Chuk Mak,Li,S.,Patel,A.,Farber,J., Rubber World,189,20(1983).

4.8 Degradation of Elastomers by Heat and/or Radiation

M. Ito

Japan Atomic Energy Research Institute, Nuclear Education Center
2-28-49, Honkomagome, Bunkyou-ku Tokyo, 113, JAPAN

Abstract This article studied some problems on the degradation of elastomers by heat and /or radiation. The changes in ultimate elongation, and the increase in C=O concentration show the existence of synergistic relationship between heat and radiation as the rate constant of chemical stress relaxation shows. The temperature dependence of radiation induced degradation of fluorine containing elastomers was found to be small. The florin containing elastomer have less radiation resistant properties than appropriately compounded EPDM.

INTRODUCTION

The electric cable and components in container vassal of nuclear power plant are exposed by radiation and heat simultaneously during normal service condition and a simulated loss of coolant accident. Elastomers are used as the materials for the electric cables and the components because of it's elastic and flexible properties. Therefor, it is important to study the temperature dependence of radiation induced degradation of elastomers. The synergistic relationship between heat and radiation is the functional problem to be also clarified. It is practically useful to investigate whether heat resistant elastomer have radiation resist prooperties. The article studied some problems on the degradation of elastomers by heat and/or radiation mentioned above.

EXPERIMENTAL

The fluorine containing elastomers used were AFLAS type(Asahi glass Co. Ltd.) and VITON type (Du pont). AFLAS type is copolymer of tetrafluoroethylene with propylene, and VITON type is copolymer of hexafluoropropylene with vinilyden fluoride. Each of the copolymers contains small amount of termonomer. Table 1 shows compounding receipts of those samples. The receipt of ethylene-propylene diene elastomer(EPDM) was shown elsewhere (Ito M.,1993). The sicknesses of the samples were about 0.5mm. The irradiation was performed by Co-60 ray at the constant temperature in air oven. The mechanical properties were measured by the tensile test at room temperature. The distance of jowl was 500mm, and the extension rate was 50mm/min. The volume resistivity was measured with applying electricity of 500V.

Table 1 compounding receipts of fluorine containing elastomers.

AFLAS Type		VITON Type	
Ingrediant	Parts	Ingrediant	Parts
AFLAS 150 (Asahi glass)	100	VITON B (Du pont)	100
1,3-Bis(ter-butyl peroxy		Lead monooxide	15
isopropyl)benzene	1.0	DAIAK No.3(Du pont)	3.0
Triallyl isocyanurate	5.0	Activated calcium carbonate	30
Sodume stearate	1.5		
Mistron vapor talc	30		

RESULT AND DISCUSSION

Synergistic relationship between heat and radiation on the degradation of elastomers.

Fig.1 shows increase in concentration of C=O of ethylene-propylene copolymer pure valcanizate by heat and/or radiation. If there is the simple additivity on the increase in C=O concentration by heat and radiation, the simultaneous additions of each of the deteriorate conditions gives the data on dotted line. The simultaneous addition results higher C=O concentration than the value expected from the basis of simple additivity. Therefore the result shows the existence of a synergism between heat and radiation. Clough and Gillen (1981), and Ito (1981) concluded that there is a synergistic relationship between heat and radiation on the degradation of polymers. The former measured the decrease in ultimate elongation by heat and/or radiation but they did not define the rate of decrease in ultimate elongation. On the other hand, the latter measured the rate of chemical stress relaxation. The method proposed " coefficient of synergism" to express the magnitude of synergism.

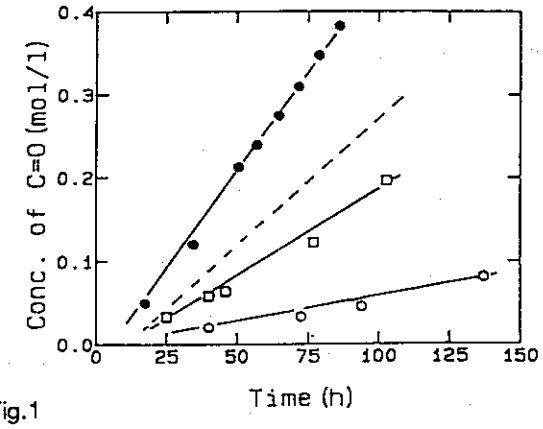


Fig.1

Increase in concentration of C=O of EP07P by heat and/or irradiation.

○ 70°C heat alone
□ 3kGy/h at room temperature
● 3kGy/h at 70°C
The extraporated line - - - - - - - - - -

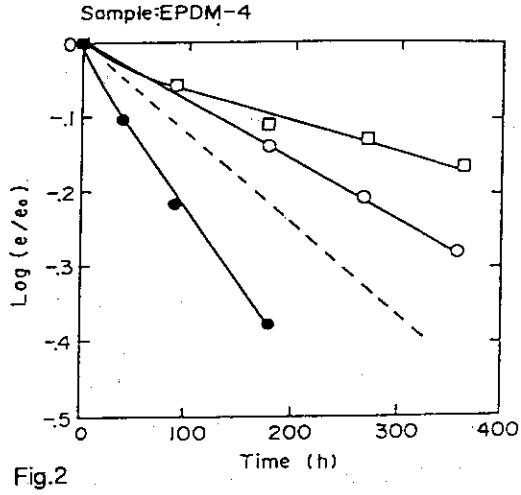


Fig.2

Synergism of Heat and Radiation on Elongation Changes.

□ Heat (140°C)
○ Radiation (0.5 Mrad/h at 70°C)
● Heat and Radiation (0.5 Mrad/h at 140°C)

Recently I found out that the rate constant of decrease in ultimate elongation can define for certain elastomers. As an example, decrease in ultimate elongation of EPDM-4 by heat and/or radiation is shown in Fig.2. The rate constant of decrease in ultimate elongation K defined by equation 1.

$$\mathrm{Log}\ (e/e_0) = -Kt \qquad (1)$$

where e is elongation at time t and e_0 is the initial elongation. A synergistic relationship exist on the decreasee in ultimate elongation. The slope for the simulatanious addition of heat and radiation is higher than that expected from the basis of simple additivity. The results suggests that the measurement of C=O concentration and elongation at break for the certain elastomers can give the degree of synergism.

Radiation induced degradation of fluorine containing elastomers at various temperatures.

Fig.3 and 4 show the relationship between the weight of the samples and dose. The weight decreases with increasing dose and temperature. The scission reaction by irradiation produced low molecular products. The diffusion of those volatile products from samples to air results in the weight loss at higher temperatures. The temperature dependence of the rate of weight loss was found to be discrete. The results show that the rate of scission reaction does not affect the weight loss directly, but the diffusion of low molecular weight products from the sample to air controls the rate of the weight loss. Fig.5 and 6 show the changes of volume resistivity by irradiation. At higher temperatures, irradiation does not affect the resistivity. This is due to the vaporization of polar molecules that decrease the value of resistivity from the samples at higher temperatures. The 25% modulus of two elastomers increases with increasing dose as shown in Fig.7 and. VITON type doses not show the temperature dependence. AFLAS types have temperature dependence, but not remarkable one. The decrease in ultimate elongation by irradiation at various temperatures was also studied. Fig.9 shows the dose when elongation at break decreases to 50% and when elongation decreases the half of initial values. The result shows that AFLAS type has better radiation resistant properties than VITON type.

Comparison of radiation resistant property with another elastomers.

Fig 10 shows the decreases in ultimate elongation of various elastomers by irradiation. EPDM-3 and acrylic elastomer(AC-1) have better radiation resistant properties on the view point of elongation retained. Thus, appropriately compounded EPDM and acrylic rubber were found to have excellent radiation resistant properties compared with fluorine containing heat resistant elastomers.

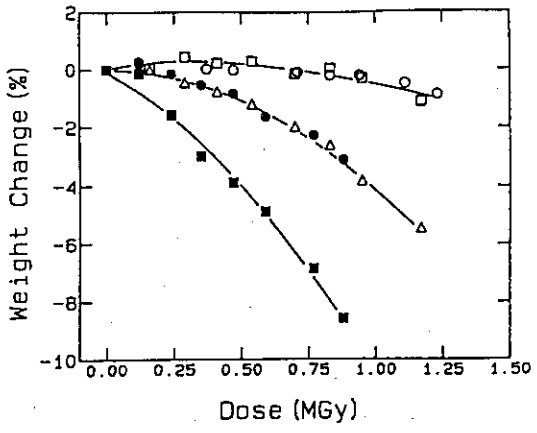


Fig.3 Weight chenge of AFLAS type elastomer by irradiation.

○ 90°C □ 120°C △150°C
●175°C ■ 200°C

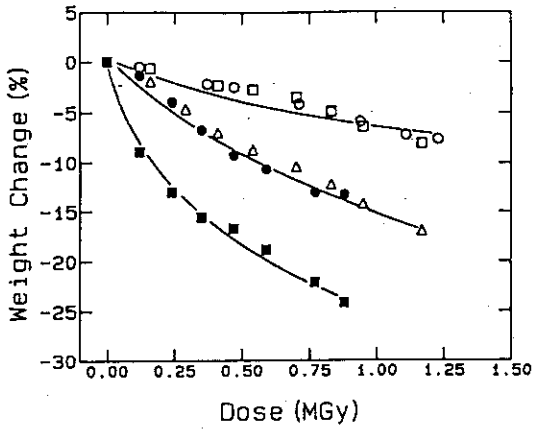


Fig.4 Weight change of VITON type elastomer by irradiation.

○ 90°C □ 120°C △150°C
●175°C ■ 200°C

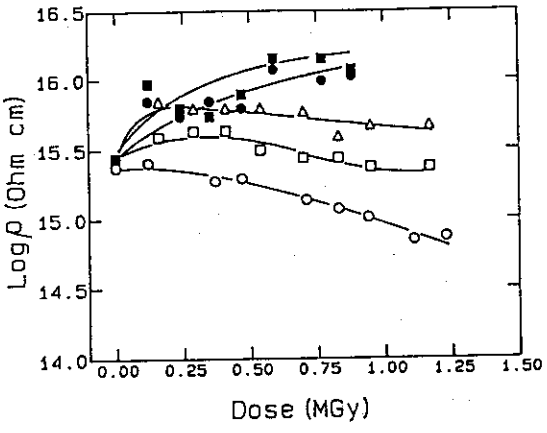


Fig.5 Changes of volume resistivity of AFLAS type elastomer by irradiation.

○ 90°C □ 120°C △150°C
●175°C ■ 200°C

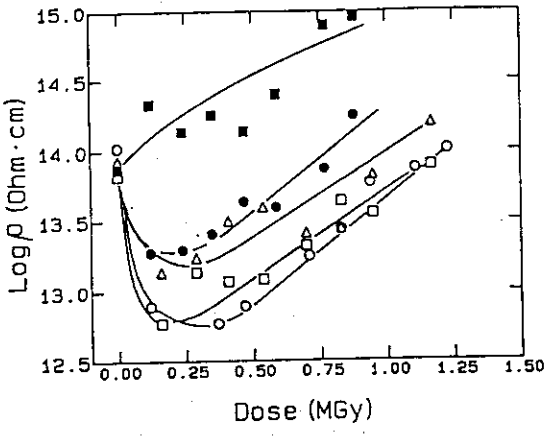


Fig.6 Changes of volume resistivity of VITON type elastomer by irradiation.

○ 90°C □ 120°C △150°C
●175°C ■ 200°C

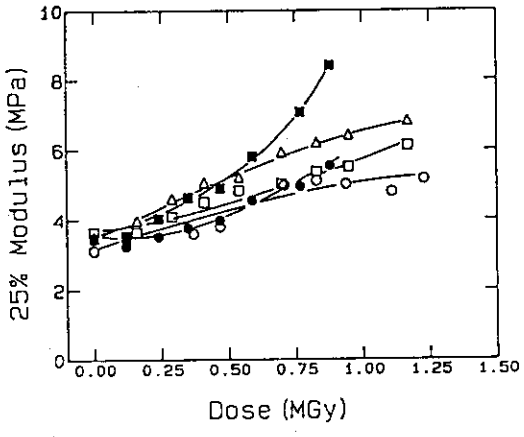


Fig.7 Changes of 25% modulus of AFLAS type elastomer by irrasiation.

○ 90°C □ 120°C △150°C
●175°C ■ 200°C

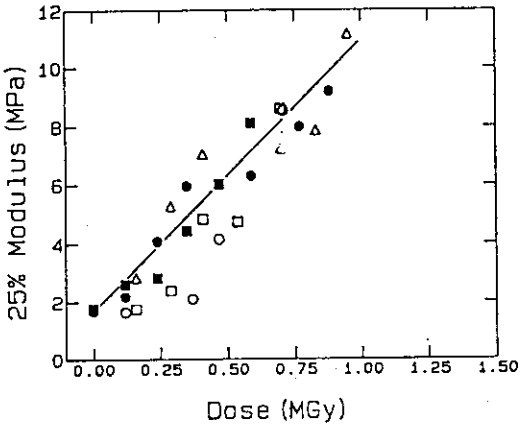


Fig.8 Changes of 25% modulus of VITON type elastomer by irradiation.

○ 90°C □ 120°C △150°C
●175°C ■ 200°C

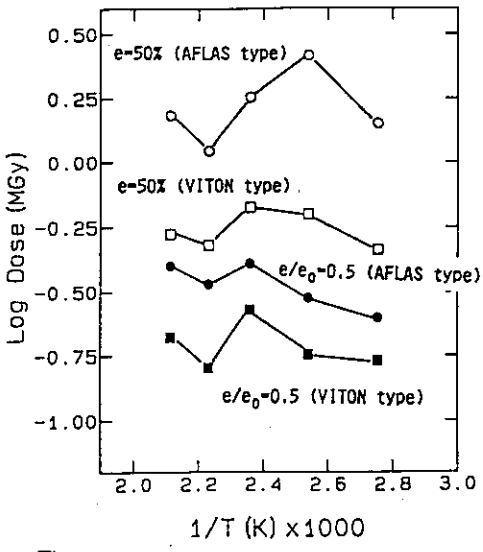


Fig.9 Relationship between critical dose and reciprocal of temperature.

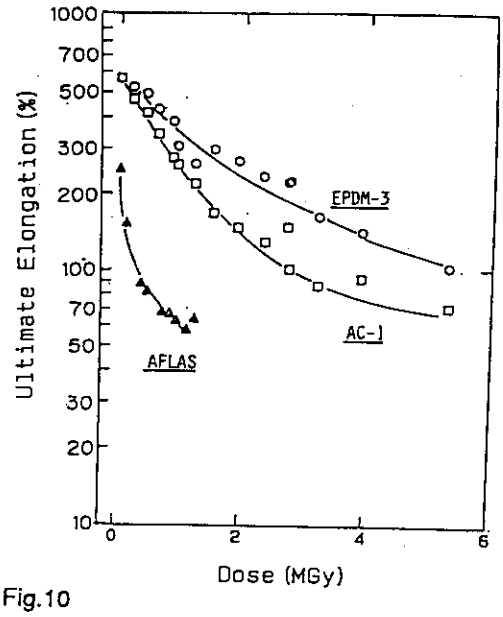


Fig.10 Decrease in ultimate elongation of various elastomers by irradiation. (3 kGy/h at 70°C)

REFERENCES

Clouh R.L. and Gillen K.T.(1981) Radiation-thermal degradation of PE and PVC mechanism of synergistic and dose rate effect. Radiat. Phys. Chem. 81 661-669

Ito M Chemorheology of rubber under heat and radiation. Radiat. Phys. Chem. 81 653-660

Ito M, Kusama, Y. ,Yagi,T. ,Okada S., and Yosida K.(1993) The methododology study of time accelerated irradiation of elastomer. Materials Life 5 18-24

4.9 Aging Effect on Radiation-induced Degradation of Polypropylene

M.Imai, M.Sekiguchi and M.Tabei

Tokyo Metropolitan Isotope Research Center
Fukazawa 2-11-1, Setagaya-ku, Tokyo 158, Japan

Y.Yamada, H.Shimizu

Saitama Institute of Technology
Fusaiji 1690, Okabe-cho, Osato-gun, Saitama 369-02, Japan

Abstruct PP sheets and films were irradiated with γ-ray and with high energy electron beam. The mechanical degradation, decay of peroxy radical and the variation of molecular weight with storage time were measured. The variation of molecular weight corresponded to mechanical degradation. The molecular weight of sheet sample at which elongation falls to zero was much higher than that of film sample. The relation between mechanical degradation and sample thickness was discussed.

INTRODUCTION

Polypropylene (PP) is extensively used in disposable medical equipment, but is severely degraded by the sterilization dose (normally 25 kGy). Degradation occurs not only during irradiation but also during the subsequent storage of irradiated articles. The post-irradiation degradation depends on the shape of polypropylene, a kind of additive, irradiation condition and radiation source.

Dunn T. S. (1979) reported that the variation of radical concentration corresponded to mechanical degradation after irradiation of PP. In the previous paper, it has reported that the mechanical degradation of PP film during storage after irradiation corresponds to the increase of carbonyl group (M.Imai et al. 1989). Tabei M. (1984) reported that PP surgical suture irradiated with γ-ray degraded during and after irradiation more than that irradiated with electron beam. Yoshii F. (1986) measured the depth of oxidation layer of irradiated PP sheets and reported that the oxidation occurs near the surface area. Babic D. (1983) reported that molecular weight of irradiated PP decreased with dose and storage time but he did not measure the mechanical degradation.

To elucidate the mechanism of degradation of polypropylene after irradiation, the investigation about the relations among mechanical degradation, peroxy radical decay and variation of molecular weight performed using PP sheet and film.

EXPERIMENTAL

PP pellets with and without additives (PPa),(PP0) , oriented PP film (OPP) and casted one (CPP) were used. CPP included 0.3 % ethylene component. PPa include 0.05 w% of Irgafos 168, 0.05 w% of Sumilizer GA-80, 0.20 w% of DMTP, 0.20 w% of calcium stearate and 0.1 w% of Chimassorb 944 LD (HALS). Both OPP and CPP included only 0.1 % butyl hydroxy toluene (BHT) and had a thickness of 25 μm. These materials were supplied from TOKUYMA Corporation. The pellets are moulded to the sheet by mixing extruder (CSI-Max Extruder Model CS-194). Then the sheets were pressed to even thickness of 0.5 mm at 180 °C. The sheets were immediately cooled in ice water. The crystallinities of PP0, PPa, OPP and CPP were 56, 56, 61 and 28 respectively.

These four samples were irradiated in air with ^{60}Co γ-ray with a dose rate of 10.7 kGy/h to a dose of 25 kGy and were also irradiated in air with high energy electron beam (HEEB) with accelerating voltage of 5 MV and beam current of 10 mA to a dose of 25 kGy. The samples for ESR measurement were stored at -78 °C till the first measuring time. OPP and CPP were also irradiated with low energy electron beam (LEEB) with acceralation voltage of 200 kV and beam current of 5.0 mA to a dose of 25 kGy. After irradiations, samples were stored at 25 °C in air in a dark box.

The samples were cut out to Dumb bell shaped pieces with the size of 40 cm (elongation direction) and 5 mm (width). Tensile strength and elongation of the cut samples were measured 1 day after irradiation, and 1 week, 1, 3 and 6 months after irradiation by using Shimadzu Autograph AG-100 with elongation speed of 100 mm/min.

The variation of radical concentration was also measured by electron spin resonance (ESR) spectrometer (JEOL RE-2X was used). As relative radical concentration, the peak height of the spectrum of peroxy radical to that of Mn^{2+} was used.

The molecular weight and molecular weight distribution were measured by Gel Permeation Chromatography (Waters 150C was used) at 135 °C. The flow rate of solvent ODCB was 1.0 ml/min and the amount of injected sample was 400 μml. As the standard polymer, 6 narrow standard polystyrenes were used.

RESULTS

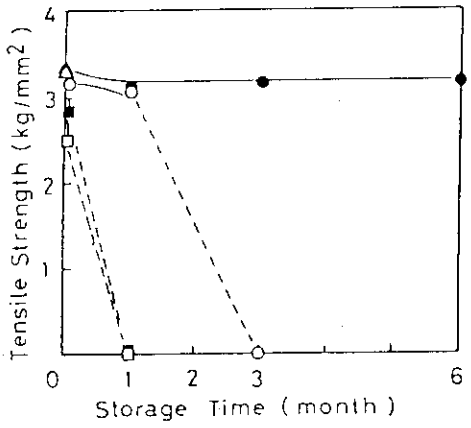


Fig. 1. Variation of tensile strength of PP0 and PPa with storage time:(○)PP0 with HEEB;(●)PPa with HEEB; (□)PP0 with γ-ray;(■)PPa with γ-ray;(△)PP0 unirradiated; (▲)PPa unirradiated

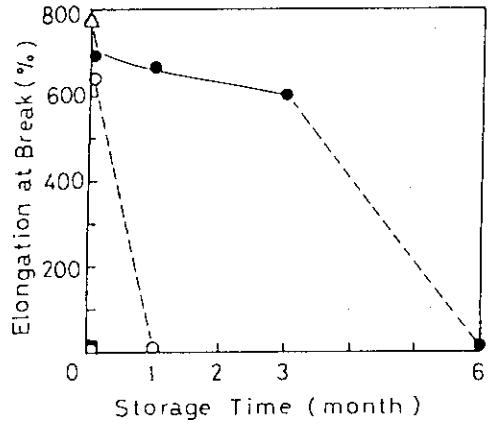


Fig. 2. Variation of elongation at break of PP0 and PPa with storage time:Symbols as Fig.1

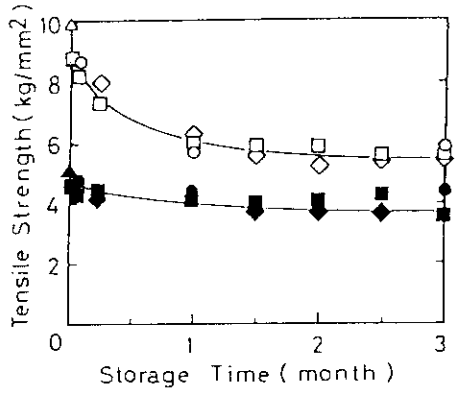


Fig. 3. Variation of tensile strength of OPP and CPP with storage time:(○)OPP with HEEB; (●)CPP with HEEB;(□)OPP with γ-ray;(■)CPP with γ-ray ;(◇)OPP with LEEB;(◆)CPP with LEEB; (△)OPP unirradiated;(▲)CPP unirradiated

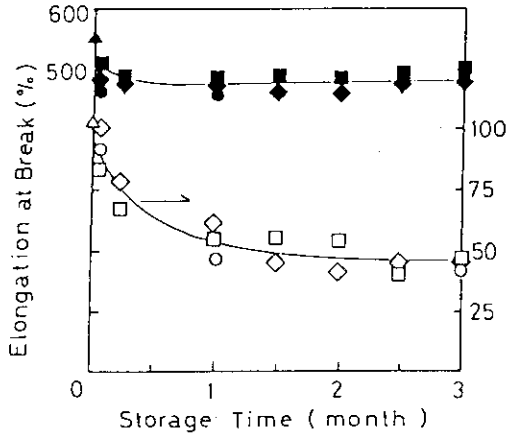


Fig. 4. Variation of elongation at break of OPP and CPP with storage time: Symbols as Fig.3.

Figures 1 and 2 show the variations of tensile strength and elongation at break of irradiated PP0 and PPa with storage time. Figures 3 and 4 show the variation of tensile strength and elongation at break of OPP and CPP with storage time. The tensile strength and elongation of PP0 decrease with storage time more rapidly than those of PPa. The tensile strength and elongation of PP0 and PPa irradiated with γ-ray decrease more severely than those with HEEB. The tensile strength and elongation of OPP decrease with storage time more rapidly than those of CPP. There are no remarkable difference among γ-ray, HEEB and LEEB in the case of OPP and CPP. The tensile strength and elongation of sheet samples decrease more than those of film samples remarkably.

Figure 5 shows the ESR spectrum of γ-irradiated OPP. The spectra of other samples were almost the same. Figure 5 indicates that 1 h after irradiation, there remain alkyl type radical or some other radical, but about 1 week after irradiation, only peroxy radical remains and it decays with storage time.

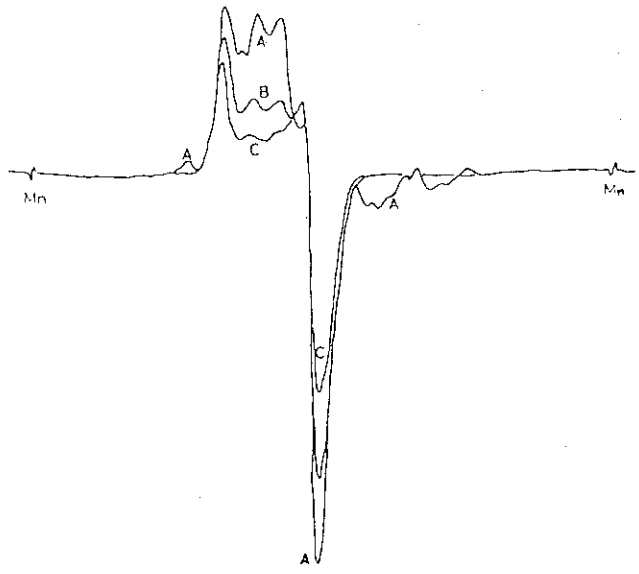


Fig. 5. ESR spectra of γ-irradiated OPP:(A)1 h after irradiation;(B) 1 day after irradiation;(C) 1 week after irradiation;(C) 4 months after irradiation;(Mn) signal of Mn^{2+}

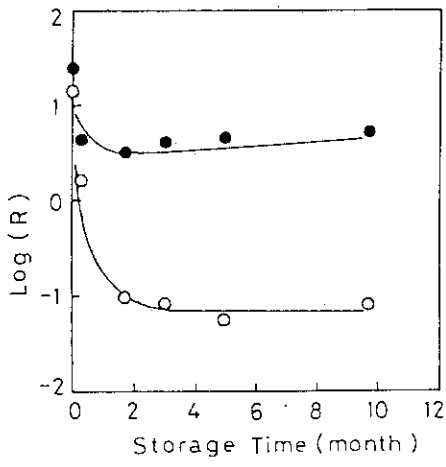


Fig. 6. Variation of relative radical concentration in PP0 and PPa irradiated with HEEB with storage time:(○)PP0;(●)PPa

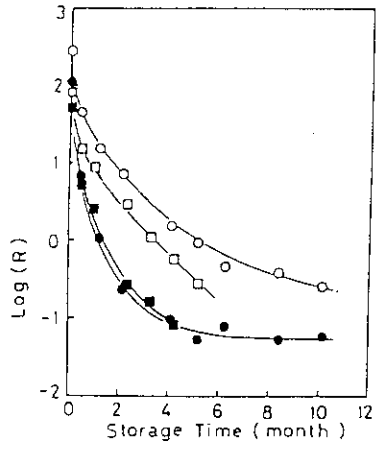


Fig. 7. Variation of relative radical concentration in OPP and CPP with storage time:(○)OPP with HEEB; (●)CPP with HEEB;(□)OPP with γ-ray;(■)CPP with γ-ray

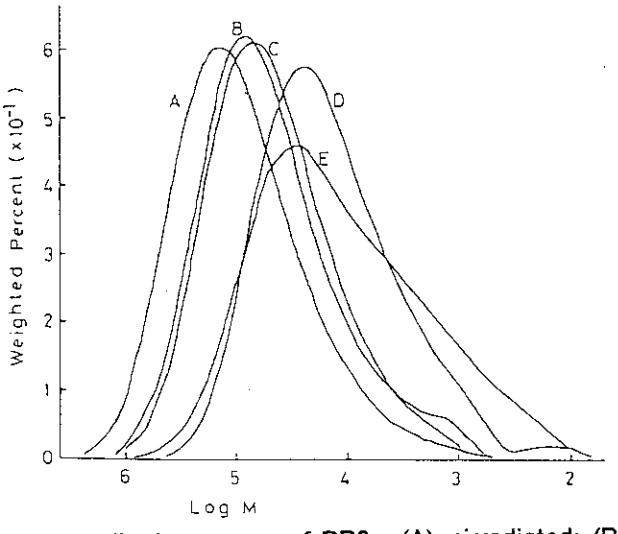


Fig. 8. Molecular weight distribution curves of PP0 : (A)unirradiated; (B)1 day; (C)1 month; (D)3 months; (E)6 months

Figures 6 and 7 show the variations of the relative radical concentration in PP sheet and in PP film with storage time. The radical decays more rapidly in PP0 than in PPa and more in CPP than in OPP. Figure 8 show the variations of the molecular weight distributions with storage time of the sample of PP0 irradiated with HEEB as the representation of 4 samples.

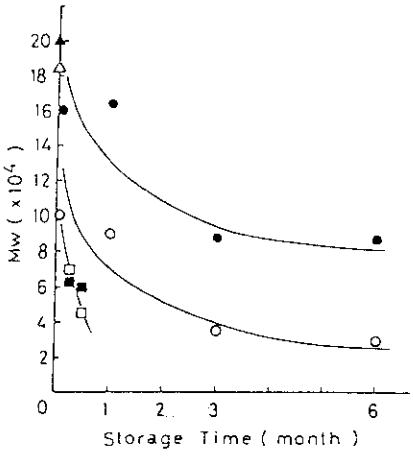


Fig. 9. Variation of weight averaged molecular weight (Mw) of PP0 and PPa with storage time : (○)PP0 irradiated with HEEB; (●)PPa with HEEB; (□)PP0 with γ-ray; (■)PPa with γ-ray

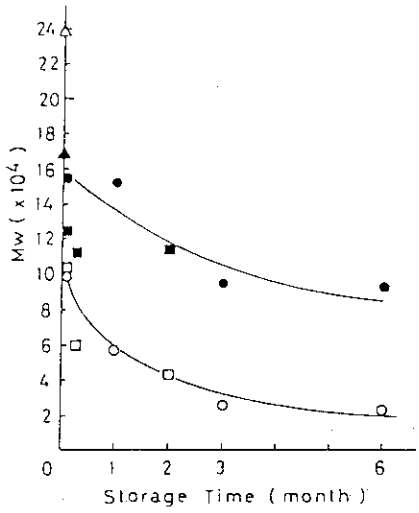


Fig.10. Variation of weight averaged molecular weight (Mw) of OPP and CPP with storage time : (○)OPP irradiated with HEEB; (●)CPP with HEEB; (□)OPP with γ-ray; (■)CPP with γ-ray

Figures 9 and 10 show the variations of the weight averaged molecular weights (Mw) with storage time of the samples of sheets and films respectively including the data irradiated with γ-ray.

The molecular weight of each sample decreases with storage time and the decreasing patterns correspond to mechanical degradation as shown in Figures 1 through 4.

DISCUSSION

The oxidation reaction during and after irradiation are summarized by some workers (Kagiya T. et al., 1985, Becker R. F. et al. 1988 and Falicki S. et al., 1994) as shown in the following equations.

$$RH \rightsquigarrow R\cdot + H\cdot \quad (1)$$

$$H\cdot + RH \rightarrow R\cdot + H_2 \quad (2)$$

$$R\cdot + O_2 \rightarrow ROO\cdot \quad (3)$$

$$ROO\cdot + RH \rightarrow ROOH + R\cdot \quad (4)$$

$$2ROO\cdot \rightarrow ROOR + O_2 \text{ or others} \quad (5)$$

$$ROOH \rightarrow R_1CHO + R_2\cdot + \cdot OH \quad (6)$$

$$ROOH \rightarrow R_1(C{=}O)R_2 + \cdot OH + \cdot H \quad (7)$$

In these equations, RH means PP.

In PP0, peroxy radical decays very rapidly, but in PPa, the radical remains at higher concentration for a long time as shown in Figure 6. This phenomena in PPa is thought to be due to one of the additives. One of the stabilizers in PPa is thought to react with peroxy radical of PP chain and change to another type of peroxy radical which cannot react with PP chain but can be observed by ESR. By this reason, PPa is excluded in the discussions below.

The radical decays more rapidly in CPP than in OPP as shown in Figure 7. The difference is thought to be due to the difference of the crystallinity shown in the Table. In the amorphous region, polymer chains are thought to be able to move rapidly and radicals on the chains can meet frequently and be terminated by recombination reaction as shown in the equation (5). Therefore, the radical decays more rapidly in CPP (low crystallinity) than in OPP (high crystallinity). It is also conceivable that the difference is due to the difference of crystal size or crystal structure. But, there are no data about the crystal size or the crystal structure of the samples to be argued. The radical decays more rapidly in PP0 than in PP films (OPP and CPP) as shown in Figures 6 and 7. But it is difficult to discuss the difference because not only method of moulding but also the thickness of the sample is different.

In the above equations, the value of the concentration of peroxy radical means the ability to induce degradation reaction at measured time in the sample by producing ROOH as expressed by equation (4) and induce chain scission as expressed by equation (6). The fact that the peroxy radical in OPP remains at

higher concentration than in CPP as shown in Figure 7, corresponds to the fact that the decreses of tensile strength and elongation of OPP is more rapid than those of CPP as shown in Figures 3 and 4. The patterns of radical decay in OPP and CPP also correspond to the decreasing patterns of weight averaged molecular weights as shown in Figure 10. The difference between OPP and CPP may be explained by the difference of morphology (Nishimoto et al., 1991),but there are no data about the morphology of these samples. In PP0, the concentration of peroxy radical becomes lower and leveled off at 2 months after irradiation as shown in Figure 6, the decrease of molecular weight of PP0 continues at that time as shown in Figures 8 and 9. This indicates that even small amount of peroxy radical is effective for chain scission or that the reactions expressed by equations (6) and (7) are remarkably slow.

The decreasing patterns of weight averaged molecular weights as shown in Figures 9 and 10 correspond to mechanical degradations shown in Figures 1 through 4. But the value of Mw at which the elongation falls to almost zero of the sheet samples is higher (about 90,000) than that (less than 30,000) of film samples. These differences between PP sheet and PP film are thought to depend on the difference of the thickness. In the films with a thickness of 25 μm, oxygen molecules can be supplied sufficiently to the inner part of the film even in the case of HEEB irradiation with high dose rate and there are no severe differences in oxidation degradation between surface area and inner part. Therefore, there is no strain in the film samples. On the other hand, in the sheet samples with a thickness of 500 μm, most of the oxygen molecules entered into the sample are consumed in the region near the surface and cannot enter into the inner part of the sheet and make oxidation layer even after irradiation as reported by Yoshii (1985). The oxidation layer is thought to make strain in the sheet, by which the sheet becomes easily breakable when tensile test is performed. As the result, the mechanical degradation of sheet samples are remarkably severe as shown in Figures 1 and 2. When irradiated with γ-ray, the dose rate is low and irradiation time is long, then oxygen molecule is supplied more sufficiently during irradiation time than in the case of irradiated with HEEB. Then the oxidation layer grow up more in the case of γ-ray than HEEB. Therefore, Tensile strength and elongation of the sheet samples decrease more rapidly than those of film samples and decrease more rapidly when irradiated with γ-ray than with HEEB as shown in Figures 1 and 2.

CONCLUSIONS

1. The mechanical degradations of sheet samples were more remarkable than those of film samples.
2. Radical decays in film samples corresponded to mechanical degradations and the decreases of molecular weight.
3. The variation of molecular weight corresponds to the mechanical degradation in all samples.
4. The value of the weight averaged molecular weight (Mw) at which elongation falls to zero was higher in the case of sheet samples than film samples.
5. The mechanical degradation depends not only on the decrease of molecular weight but severely on the sample thickness.

REFERENCES

Babic D., Safranj A., Markovic V. (1983) Radiation Degradation of Polypropylene-Molecular Weight and Melt Viscosity Change, Isotopenpraxis, 19, S. 228

Becker R. F., Carlsson D. J., Cooke J. M. and Chmela S. (1988) Stabilization of Polypropylene to γ-Initiated Oxidation, Polym. Degrad. Stab., 22, 313

Dunn T. S., Epperson B. J., Sugg H. W., Stannet V. T. and Williams J. L. (1979) Radical Structure and its Role in the Oxidative Degradation of γ-Irradiated Polypropylene Radiat. Phys. Chem. 14, 625

Falicki S., Gosciniak D. J., Cooke J. M., Cooney J. D., Carlsson D. J. (1994) Polypropylene Stabilization : During γ-Irradiation and During post-g Storage, Polym. Degrad. Stab., 43 117

Imai M., Lu G.,Ametani K. and Tutiya M.(1989),γ-Irradiation of Polypropylene in Vacuum and in Air, J. Polym. Sci. A: Polym. Chem., 27, 1763

Kagiya T., Nishimoto S., Watanabe Y. and Kato M. (1985), Importance of the Amrphous Fraction of Polypropylene in the Resistance to Radiation-Induced Oxidative Degradation, Polym. Degrad. Stab., 12, 261

Nishimoto S.,Kitamura K., Watanabe Y., Kagiya T. (1991), The Correlation between the Morphology and Radiation Resistance of Polypropylene Solid Materials, Radiat. Phys. Chem., 37, 71

Tabei M.,Sekiguchi M.,Minegishi A.,Sato K.,Katsumura Y. and Tabata Y (1984) Electron-Beam Sterilization of Surgical Suture J. Antibact. Antifung. Agents, 12, 611

Yoshii F., Sasaki T., Makuuchi K. and Tamura N.(1986), Durability of Radiation-Sterilized Polymers III. Oxidation Layer Determined by Chemiluminescence, J. Appl. Polym. Sci., 31, 1343

4.10 Effect of Isotacticity on Radiation Stability of Polypropylene

Qiao Jinliang and Zhang Fengru
(Beijing Research Institute of Chemical Industry, Beijing 100013, China)
Wei Genshuan, Zhang Juhong and Wu Jilan
(Department of Technical Physics, Beijing University, Beijing 100871, China)

Abstract: The relationship between radiation stability and isotacticity of polypropylene(PP), such as isotactic pentad ratio, was studied in this paper. It was found that the higher the isotacticity, the better the radiation stability. Compared with normal PP powder which has normal isotacticity, the special PP powder with higher isotacticity, such as, isotactic pentad ratio > 98%, can keep the Melting Index change less than normal PP after UV-light-oxygen aging or γ-irradiation in air. Furthermore, the special PP powder with higher isotacticity has lower intention of crosslinking or branching after 1KGy γ-irradiation in vacuum and has lower intention of degradation after 5KGy γ-irradiation in vacuum. The special PP powder with higher isotacticity also has lower content of carbonyl after 25 KGy γ-irradiation in air. These demonstrated that the special PP with higher isotacticity made from "special catalyst" is more suitable as the material for radiation sterilization than normal PP, because there are less "week points" in PP with higher isotacticity than that in PP with lower isotacticity. The random copolymer with 2.7% ethylene units made from the "special catalyst" mentioned above is even more stable in irradiation sterilization than homopolypropylene with higher isotacticity; therefore, it is reasonable that a random copolypropylene with about 4%wt ethylene made from the "special catalyst" should be the much more suitable PP material than normal PP for irradiation sterilization.

Introduction: Radiation sterilization of medical supplies made of polypropylene(PP) has been carried out widespreadly. Compared with ethylene oxide-sterilization method, radiation sterilization is a very safe method, but people still want better products, such as, the medical supplies made of PP with less additives. For this purpose, the PP resin(without additives) which has better radiation stability has to be used; therefore, it is important to know what kind of PP has better radiation stability.

The effect of PP microstructure on its radiation stability has been studied widely<1-9>. For example, it was said that the copolypropylene with 6% ethylene units has better radiation stability<8><9>, the PP with lower crystallinity<5><8> or with larger spherulite size<9> has better radiation stability, adding nucleate agent can make PP's radiation stability become worse. Besides, the effect of quenching<8>, molecular weight<7> ect. on radiation stability of PP has also been studied However, the study of effect of isotacticity of PP, such as, isotactic pentad ratio, relative length of helix structure, ect., on radiation stability has not been found up to now; therefore, this paper will discuss the effect of isotactic pentad ratio of PP on its radiation stability.

Experiment: 1. Material: HPP-1 is a homopolypropylene with higher isotacticity and MI=1.0 g/10min.; HPP-2 is also a homopolypropylene with general isotacticity and MI=2.0 g/10min.; HPP-3 is also a homopolypropylene with lower isotacticity and MI=2.0 g/10min.; And RPP is a random copolypropylene with about 2.7% ethylene units made from N-catalyst from which HPP-1 was made.

2. Experiment: The samples were irradiated with ^{60}Co γ-ray in air or in vacuum; Melting Index(MI) was measured at 230°C and antioxidant with ethanol was added into PP powder before measurement. The measurement was carried out after the sample was completely dried; The content of

carbonyl and relative length of helix structure were measured by FT-IR; The isotactic pentad ratio was measured by 100 MHz ^{13}C-NMR at 135°C; Rheograph was obtained by Rheometer at 230°C.

Result and Discussion: 1. Expression of isotacticity of PP: Isotacticity of PP is usually expressed by Isotactic Index which is measured by extraction with boiling n-heptane and this method is not precise enough; therefore, the isotacticity of PP will be expressed by isotactic pentad ratio and relative length of helix structure(10 or more isotactic units' relative contents) in this paper. Table 1 shows the isotacticity result of different commercial PP powder made from different commercial catalysts. In Table 1, HPP-1 with higher isotacticity was made by using N-catalyst and HPP-2 with general isotacticity was made by using GF-2A catalyst. It is obvious that isotacticity of HPP-1 made from N-catalyst is higher than that of HPP-2 made from general high efficiency catalyst.

Table 1. Isotacticity of Different PP

	HPP-1	HPP-2
Isotactic Pentad Ratio %	> 98	95.2
Relative Length of Helix	95.7	92.3

2. Effect of isotacticity on ultraviolet ray stability of PP powder: HPP-1, HPP-2 and HPP-3 powder with different isotaticity were irradiated by outdoor sunlight and MI of these PP was measured every other day. It is found that PP with different isotacticity has different ultraviolet ray stability (See Fig.1).

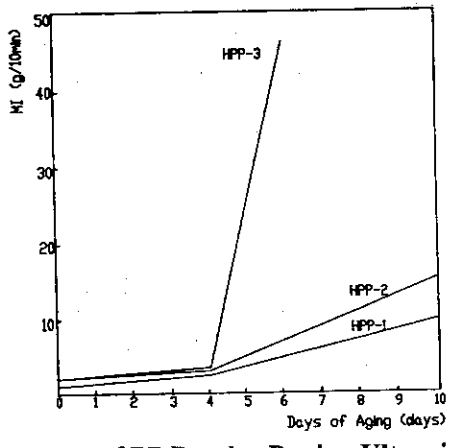


Figure1. MI Change of PP Powder During Ultraviolet Ray Ageing

It can be seen from Fig.1 that all 3 PP powders did not degrade obviously in 4 days' ageing; therefore, these 4 days could be called induction time of ultraviolet ray ageing. After 4 day-ageing, the speed of degradation is increased obviously and the speed of 3 different PP powders is much different: the slope(tgθ) of HPP-1 with higher isotacticity is only 1.2, and the slopes of HPP-2 and HPP-3 are 2.0 and 21.3 respectively; therefore, it is obvious that PP with higher isotacticity has better UV-stability.

3. Effect of isotacticity on γ-radiation stability of PP powder: PP powders were irradiated by γ-ray in air and in vacuum. The result is shown in Table 2. Normally the higher the crystallinity of PP is, the worse its radiation stability is. The abnormal phenomenon occurs here: the crystallinity of HPP-1 powder is 60.2%, and that of HPP-2 powder is only 54.3%, however the radiation stability of HPP-1 is better than that of HPP-2. This phenomenon suggests that isotacticity plays a very important role in radiation stability of PP and the higher the isotacticity of PP, the better the radiation stability of PP.

Table 2. Relationship Between Isotacticity and γ-radiation Stability ($\dot{D}$=1.0 Gy · s^{-1})

MI g/10min.	Before Irradiation	1KGy in Air	1KGy in Vacuum	5KGy in Vacuum
HPP-1	1.0	6.5	0.9	3.2
HPP-2	2.0	13	1.4	4.4

The result of radiation in vacuum is little bit different from that in air. Although PP belongs to crosslinking type polymer[8], it is easy to degrade during and after irradiation. It is largely dependent on the radiation condition of PP whether crosslink or degradation occurs predominantly. From the data in Table 2, it could be found that crosslinking or branching is predominant as the absorbed dose is less than 1KGy in vacuum, while the degradation becomes important as the absorbed dose increases. Rheology measurement conforms that PP powder has indeed been crosslinked or branched after 1 KGy irradiation in vacuum and the crosslinking or branching is more obvious in HPP-2 which has general isotacticity, than that in HPP-1 which has higher isotacticity (see Fig.2). For linear polymer molecule,

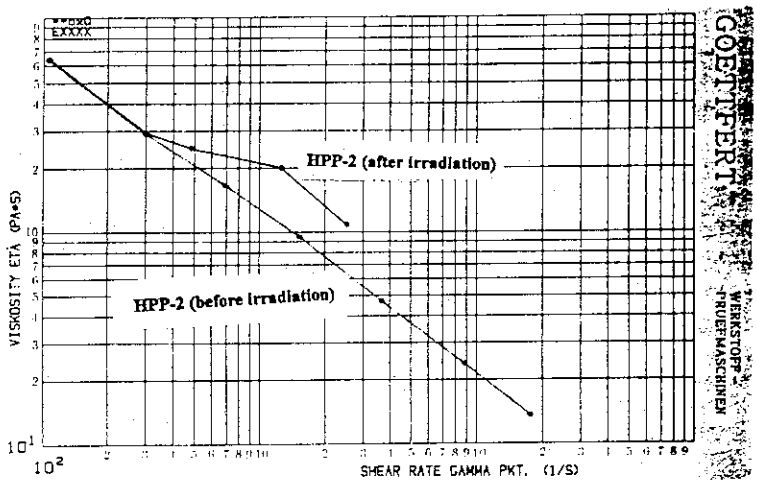


Figure 2. Rheograph of HPP-2 before and after irradiation at 230°C (D=1.0KGy, $\dot{D}$=1Gy · s^{-1}, in vacuum)

such as, polypropylene, its molecule can be oriented gradually when shear rate of rheometer is increased; therefore, the apparent viscosity of linear polymer can be found to decrease gradually. For the polymer with crosslinking or branching structure, the molecule is difficult to be oriented when shear rate of rheometer is increased; therefore, its apparent viscosity can be found to decrease less than that of linear polymer. Accordingly, Figure 2 indicates that HPP-2 has indeed been crosslinked or branched after 1 KGy irradiation in vacuum. Compared with HPP-2, only a little crosslinking or branching occurs in HPP-1 after 1 KGy irradiation in vacuum(see Fig.3). Apparent viscosity of it appears little increased

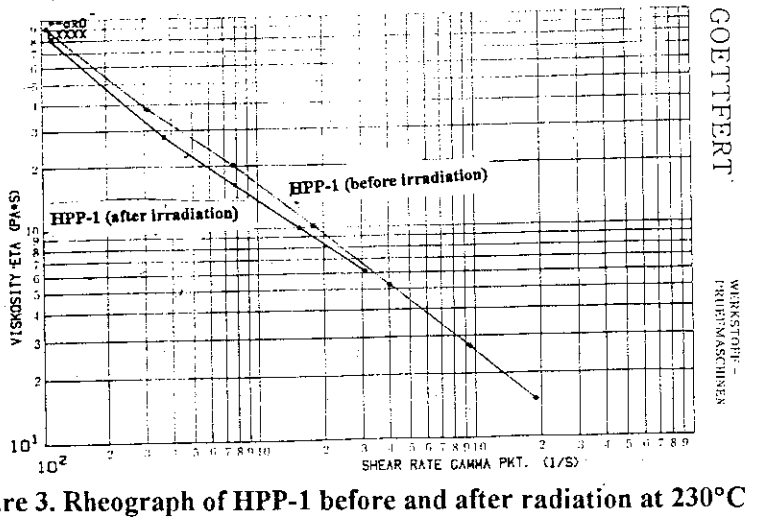


Figure 3. Rheograph of HPP-1 before and after radiation at 230°C (D=1.0 KGy, $\dot{D}$=1Gys^{-1}, in vacuum)

only when the shear rate of rheometer is very high. According to above information, it is not difficult to find that radiation stability of HPP-1 with higher isotacticity is better than that of HPP-2 with general isotacticity. For instance, molecular weight of HPP-1 is reduced less than that of HPP-2 after 1 KGy irradiation in air; Crosslinking or branching of HPP-1 is less than that of HPP-2 after 1 KGy irradiation in vacuum, and the degradation of HPP-1 is also less than that of HPP-2 after 5 KGy irradiation in vacuum.

4. Effect of isotacticity on the content of carbonyl of PP after irradiation: HPP-1 and HPP-2 with same kinds of additives were extruded at same condition, and then were compressed into film samples under same condition. These samples were measured by FT-IR immediately after 25 KGy irradiation in air The relative content of carbonyl S was obtained

$$S = \frac{\text{Peak area of } 1700\ cm^{-1}}{\text{Peak area of } 1460\ cm^{-1}}$$

S was measured every month and the results are shown in Table 3 and Fig..4. The result further confirms that the PP with higher isotacticity made from N-catalyst has better radiation stability than the PP with general isotacticity.

Table 3 Effect of Isotacticity on Content of Carbonyl of PP after 25 KGy Irradiation

S	Immediately	1 Month	2 Month	3 Month	4 Month
HPP-1	0.082	0.088	0.109	0.113	0.135
HPP-2	0.067	0.101	0.133	0.135	0.147

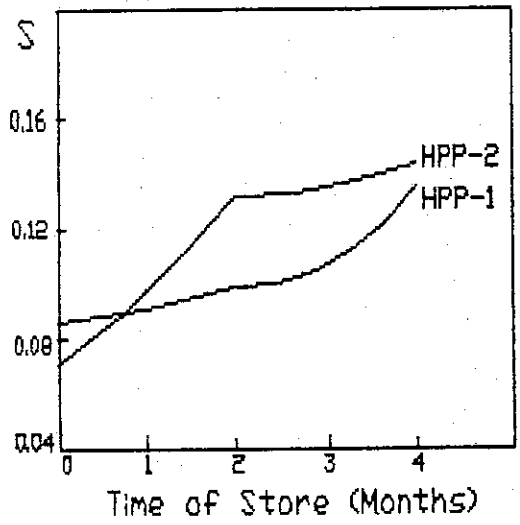


Figure 4. Effect of isotacticity on content of carbonyl after 25 KGy irradiation

5. Mechanical properties of PP with higher isotacticity after irradiation: In order to compare with commercial product Himont PD 626 which is a random copolypropylene and a special type for radiation sterilization, a special homopolypropylene was made from N-catalyst which has higher isotacticity (Isotactic pentad ratio is over 98%) and similar MI to that of PD 626. A certain type of additives were added to this homopolymer and test pieces were made by injection moulding. The measurement result is shown in Table 4. It can be seen that retaining rate of mechanical properties of the special

Table 4. Comparison of Mechanical properties between special homopolypropylene and commercial PP for irradiation sterilization

	PD 626, MI=12.7			Homopolypropylene, MI=13.2		
25KGy irradiatio	before	after 5 days	after 3 months	before	after 5 days	after 3 months
Flexural Modules10^3 MPa	1.1	1.1	1.2	1.6	1.7	1.8
Flexural Strength MPa	28.6	29.3	30.6	42.8	43.6	45.7
Izod Impact Notched, J/M	31.7	29.8	24.5	26.2	25.5	19.2
Tension Strength MPa	30.7	30.0	30.2	38.0	39.1	38.6

homopolypropylene listed in Table 4 are similar to that of PD 626, such as, the retaining rate of impact strength with notch which is considered to have closest relationship with practical use (see Table 5).

Table 5. Retaining rate of impact strength with notch after irradiation

	PD 626	Homopolymer
5 days after irradiation	94%	97%
3 months after irradiation	77%	73%

Why does the PP with higher isotacticity have so excellent radiation stability? It is proposed by the authors that there are less weak points(stress concerning points) in the PP molecule with higher isotacticity than that in normal PP molecule with general isotacticity and amount of weak points is the key factor which can make PP stable or not(see Fig. 5). It can be seen from Fig.5 that there are more weak points in the PP with general isotacticity because there are more trans-form units in this kind of PP.

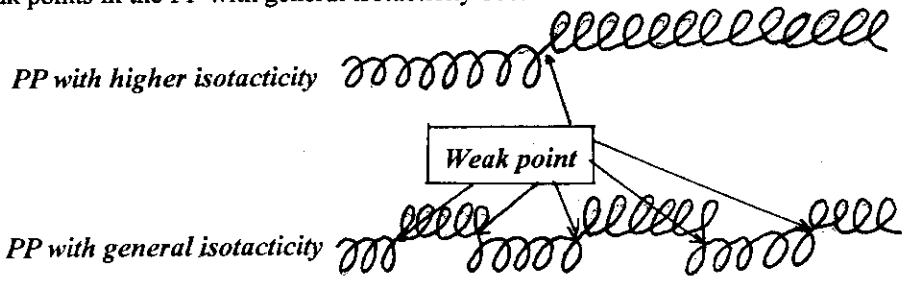


Figure 5. Sketch of PP molecular helix with different isotacticity

The weak points are easy to be broken when PP molecule is exposed to γ-ray; therefore, chemical reaction, such as, crosslinking or degradation, is easy to occur in the PP with general isotacticity when this kind of PP is irradiated. On the other hand, the PP with higher isotacticity is different from general PP. It has better radiation stability since there are less weak points in its molecule.

6. The radiation stability of random copolypropylene made from N-catalyst: It is known that the retaining rate of elongation of homopolypropylene is not as high as that of copolypropylene; therefore, a polypropylene with 2.7% ethylene units(RPP) made from N-catalyst was used. Although there is only 2.7% ethylene units in RPP, its radiation stability becomes much better than that of HPP-1 (see Table 6). The retaining rate of elongation of RPP is much higher than that of HPP-1. The result after

Table 6. Radiation stability of homo-PP and Co-PP

MI g/10min.	before irradiation	1 KGy in air	1 KGy in vacuum	5 KGy in vacuum
HPP-1	1.0	6.5	0.9	3.2
RPP	1.2	2.5	1.4	1.8

25KGy irradiation is shown in Table 7. It is proved that the random copolypropylene made from N-catalyst has good radiation stability. The reasons are that (1) the crystallinity of RPP is only 44.2%, much lower than that of HPP-1(60.2%); (2) there are less weak points in crystalline area because the N-catalyst was used. It can be expected that a random copolypropylene with excellent radiation stability can be obtained if the copolypropylene contains about 6% ethylene units as suggested by references <8> and <9>.

Table 7. Retaining rate of elongation of HPP-1 and RPP

elongation %	before irradiation	after irradiation	retaining rate
HPP-1	587	298	51%
RPP	554	480	87%

Conclusion: 1. The PP with higher isotacticity made from N-catalyst has better radiation stability than the PP with general isotacticity. The homopolypropylene with higher isotacticity has already had higher retaining rate of mechanical properties after γ-ray irradiation.

2.. The radiation stability of the PP with higher isotacticity can be improved if a certain amount of ethylene units is randomly copolymerized into its molecule.

Reference: 1. S.E. Chappell, J.A. Sauer and A.E. Woodward J. Polym. Sci. Part A 1, 2805 (1963)
2. T.S. Punn, B.J. Epperson, H.W. Sagg, V.T. Stannett and J.L. Williams Radiat. Phys. Chem. 14 625(1974)
3. Y.Hori, Y. Makino and H. Kashinabara Polymer 25, 1436(1984)
4. F. Yoshii, T. Sasaki, K. Makuuchi and N. Tamara J. Appl. Polym. Sci. 30, 3339(1985)
5. F. Yoshii, K. Makuuchi and I. Ishigaki J. Appl. Polym. Sci. 32, 5669(1986)
6. F. Yoshii, K. Makuuchi and I. Ishigaki Die Angewandte Makromolekulare Chemie 143, 25(1986)
7. F. Yoshii, K. Makuuchi and I. Ishigaki Polym. Commun. 29, 146(1988)
8. I. Ishigaki and F. Yoshii Radiat. Phys. Chem. 39(6), 527(1992)
9. Z.A. Kadir, F. Yoshii, K. Makuuchi and I. Ishigaki Radiat. Phys. Chem. 39(6), 535(1992)

4.11 Structural Changes in the Crystal-amorphous Interface of Isotactic Polypropylene Film Induced by Annealing and γ-irradiation

Sei-ichi Nishimoto,* Hideo Seike,* Malinee Chaisupakitsin,*
Fumio Yoshii,** and Keizo Makuuchi**

*Division of Energy and Hydrocarbon Chemistry, Graduate School of Engineering, Kyoto University, Sakyo-ku, Kyoto 606-01, Japan. **Japan Atomic Energy Institute, Takasaki Radiation Chemistry Research Establishment, Takasaki 370-12, Japan

Abstract Annealing and radiation effects on the microstructures of isotactic polypropylenes, homopolymer and ethylene (<2.3 wt%) incorporated random copolymers, in the solid state were studied to get mechanistic insight into the modification and degradation of mechanical properties. The growth of helical conformation of isotactic chains in the crystal-amorphous interface was induced to greater extent by γ-irradiation, while the transition from smectic to monoclinic modifications in the crystal phase occurred simultaneously by annealing. The yield stress of the polypropylene films increased with the increased content of helical conformation as the result of annealing and/or γ-irradiation.

INTRODUCTION

Isotactic polypropylene is a typical stereoregular polyolefin and shows polymorphism due to crystallization into a variety of modifications of different orders (Natta, 1960). A family of homo- and co-polymers of propylene in the solid state undergoes oxidation to produce several oxygen-containing products in the amorphous phase upon irradiation in air. Tie chains have been believed to be a critical target for oxidative degradation of polypropylene and other polymeric materials. It is likely that the oxidative tie-chain scission may stimulate structural changes in the crystal phase and the crystal-amorphous interfacial domain. Such microscopic structural changes give rise to either improvement or degradation of various macroscopic physical properties to considerable extent. Recently, we have demonstrated that the stability of polypropylene materials toward radiation damage shows a significant relationship with the primary morphology (Nishimoto *et al.*, 1991, 1992a).

In the present study, an annealing treatment of isotactic polypropylene (homopolymer and random copolymers with up to 2.3 wt% ethylene content) films has been performed to modify their primary morphologies that were obtained by conventional polymer processing. The main objective of this study is to get insight into (1) the correlation of radiation sensitivity of

polypropylene solid with varying secondary morphologies produced by the annealing treatment, and (2) the characteristics of radiation- and annealing-induced structural changes.

EXPERIMENTAL

The sample films (0.2 mm in thickness) were separately wrapped up with aluminum foils and then were annealed at several fixed temperatures (<150°C) in an air oven for various periods until reaching the respective maximum amount of a monoclinic crystalline modification. The annealed films were γ-irradiated in air over the dose range up to 15 Mrad at a dose rate of 0.1 Mrad/h, using a 60Co γ-ray source. The FT-i.r. spectrometry, the X-ray diffraction (XRD) analysis, and the differential scanning calorimetry (DSC) were carried out as reported previously (Nishimoto *et al.*, 1992b).

RESULT AND DISCUSSION

Negligible amount of thermal oxidation occurred during annealing of sample films in the temperature range of 50 to 150°C for up to 8 h. The melting temperature (T_m) of homopolymer films (165.4-165.7°C) without and with an additive (1.0-3.0wt% monoalkyldiphenyl ether) was invariant upon annealing, while that of copolymer films without and with an antioxidant (0.1wt% bis(2,2,6,6-tetramethyl-4-piperidinyl)sebacate) increased at annealing temperatures above 130°C.

I.r. absorption characteristic of helical conformation and isotactic regularity of a polypropylene chain appear at 998 and 973 cm^{-1}, respectively (Koening, 1980). The ratio of absorbances at both bands (A_{998}/A_{973}), which may be a spectroscopic measure of the amount of helical conformations forming in the sample films, increased with a rise in annealing temperature, while there was no change at room temperature. In the case of homopolymer films, apparent activation energy of the helical growth showed a big change at annealing temperature of near 80°C, becoming larger in the range of above 80°C compared with lower annealing temperatures. Such a pronounced secondary phase transition could not be observed for the copolymer films. Both additives showed negligible influence on the thermal growth of helical conformations. It is likely that isotactic polypropylene chains located at crystal-amorphous interfacial region can form the secondary helical conformations as a result of stimulated thermal motion of polypropylene segments by the annealing. In this association, the length of cooperatively mobile segments would increase with annealing temperature rise, so that the helical growth becoms easier to produce lamellar crystals with greater thickness.

Following the method of Zannetti *et al.* (1969) that was proposed for the characterization of the annealing effect, the reciprocal of the half-height broadening of the X-ray diffraction peak

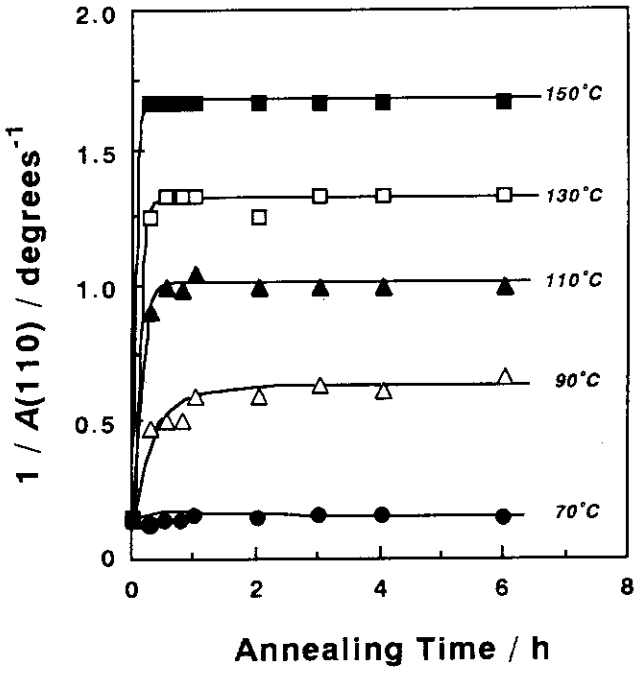


Figure 1 Time course of the transition to a monoclinic crystalline modification, measured by an XRD measurement, upon annealing at various temperatures.

at 2θ of about 15° ($1/A(110)$) was used to evaluate the relative degree of crystalline structural order: this peak is assigned to refraction from the monoclinic (110) plane. Thus, $1/A(110)$ value of homopolymer films increased rapidly to attain the maximum value characteristic of a given annealing temperature in the range of 70 to 150°C, while it was almost invariant upon annealing at below 70°C (Fig. 1). The apparent heat of fusion (ΔH_f), which is a measure of crystallinity, of homopolymer and 0.5 wt% ethylene incorporated copolymer films once decreased in the range of 70-90°C, then increasing progressively with increasing temperature (Fig. 2). These observations suggest that there is a first-order phase transition to cause disordering in the polypropylene solid, which can promote the crystal transition into the most stable structure of monoclinic modification. In the case of 2.3 wt% ethylene incorporated copolymer films, the ΔH_f value was invariant when annealed at below 80°C and increased monotonously with the increased annealing temperature in the range of >80°C (Fig. 2).

The homo- and co-polymer films underwent oxidation to produce hydroperoxide and carbonyl groups upon γ-irradiation in air. The rate of oxidation was smaller for the sample film annealed at higher temperature, probably due to decreased amount of amorphous and crystal-amorphous interfacial regions. Furthermore, the T_m depression was observed simultaneously with the oxidation, indicating the occurrence of main-chain scission (the entropy of fusion (ΔS_f) would increase) in both the crystal and amorphous phases. In accord with the behavior of

oxidation rate, the extent of T_m depression was smaller for the films annealed at higher temperature. It is also observed that both additives can inhibit the radiation-induced oxidation and the T_m depression.

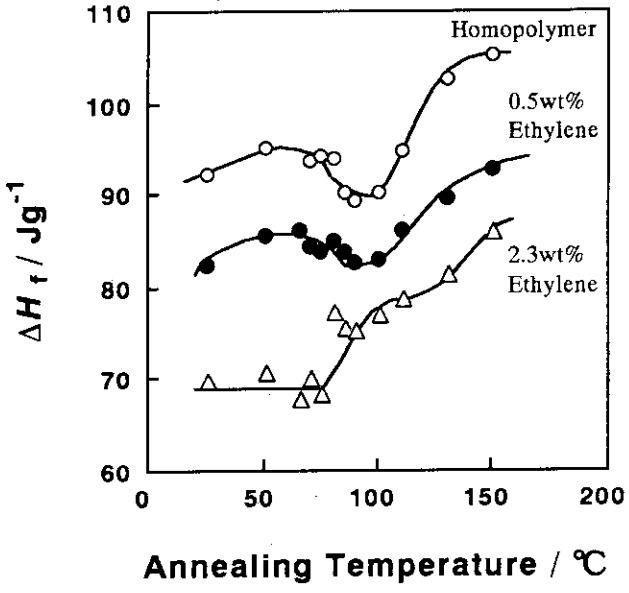


Figure 2 Variation in heat of fusion (ΔH_f), as measured by a DSC analysis, with increasing annealing temperature.

In contrast to the annealing effect, the transition to monoclinic crystalline modification was negligible when the films were irradiated up to 15 Mrad at room temperature in air. On the other hand, the secondary helical conformation growth, as measured by the A_{998}/A_{973} value, was readily induced upon γ-irradiation. The extent of the radiation-induced helical growth became smaller as the annealing temperature was raised. The superposition of the helical conformation growths due to annealing and γ-irradiation led to monotonous increase of the A_{998}/A_{973} value with increase in the reduced dose: the annealing effect was reduced to the dose of irradiation at room temperature by superposition of the maximum A_{998}/A_{973} value attained at a given annealing temperature on the dose response curve of unannealed films (Fig. 3). The antioxidant additives were also effective to inhibit the secondary helical conformation growth. It is therefore most likely that the interlamellar tie chains and the crystal-amorphous interfacial loop chains undergo radiation-oxidative scission to form the secondary helical conformation even at room temperature.

The yield stress of various sample films after annealing and/or γ-irradiation increased as the corresponding A_{998}/A_{973} value became greater. This result suggests that the increased thickness of lamellar crystals due to the secondary growth of helical conformations would result in high yield stress in the tensile test of the sample films.

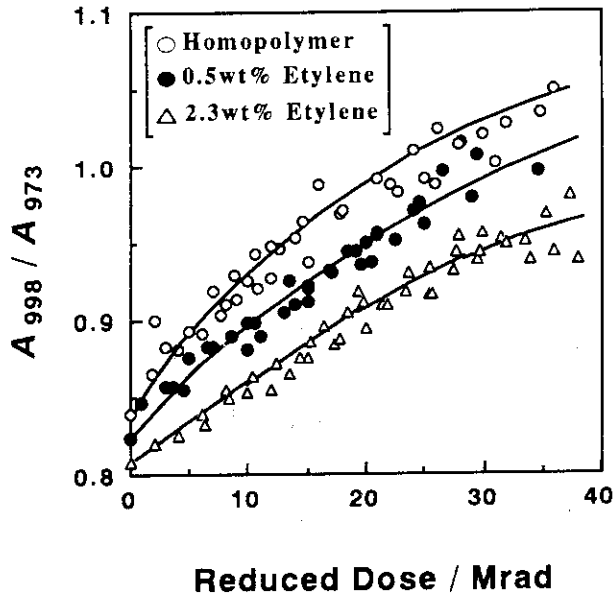


Figure 3 Superposed master curves for the secondary helical conformation growth, as measured by A_{998}/A_{973} value, upon annealing and γ-irradiation.

CONCLUSIONS

The secondary growth of helical conformations of isotactic polypropylene chains in the crystal-amorphous interface was induced not only by annealing but also by γ-irradiation, while the transition from smectic to monoclinic modifications in the crystal phase occurred to significant extent only by the former treatment. The amount of helical conformation was correlated to the yield stress of the polypropylene films.

REFERENCES

Koening, J. L. In *Chemical Microstructure of Polymer Chains*; Wiley: New York, 1980.

Natta, G. *Makromol. Chem.*, **1960**, *35*, 93.

Nishimoto, S.; Kitamura, K.; Watanabe, Y.; Kagiya, T. *Radiat. Phys. Chem.* **1991**,*37*, 71.

Nishimoto, S. ; Kagiya, T. In *Handbook of Polymer Degradation*; Hamid, S. H.;

Amin, M. B.; Maadhah, A. G. Eds.; Marcel Dekker: New York, 1992a; Chapter 1.

Nishimoto, S.; Chaisupakitsin, M.; Inui, T. *Radiat. Phys. Chem.* **1992b**, *39*, 413.

Zannetti, R.; Celotti, C.; Fichera, A.; Francesconi, R. *Makromol. Chem.* **1969**, *128*, 137.

4.12 The Effect of Monomer Molecular Weight on Grafting Reaction

Wu Minghong, Ding Zhongli, Ma Zueteh

Shanghai Applied Radiation Institute,
Shanghai University of Science and Technology,
Shanghai 201800, P.R. China

Abstract

In this paper, some condensed ethylene glycol acrylate monomers with different molecular weight being grafted to the PE film by means of pre-irradiation is reported. The effect of molecular weight of monomer on grafting reaction and the hydrophilicity of grafting sample have been discussed. The experimental results show: molar degrees of grafting decreased non-linearly with the increasement of molecular weight of monomer, the grafting reaction of polymer is greater effected by the swelling degree of PE film, the greater the swelling degree of grafting material, the higher the grating degree grafting is, the initial rate of grafting reaction decreased with the increasement of molecular weight of monomer.

Keywards:
pre-irradiation, grafting polymerization, biomedical material

Introduction

Currently many researchers have performed investigations on improving the biocompatibility of biomedical material. Improving the surface hydrophilicity of this kind of material is considered as one of the effective methods. Many reports about grafting hydrophilic monomer (for example methyl acrylic-β-hydroxyl ethylester, N-vinylpyrrolidone, acrylamide) are being published continuously,but in most of these grafting experiments,low molecular weight chemical as monomer was used[1-3], one disadvantage of such system is difficult to control the grafting chain structure. To make the grafting chains more regular and controlabe, it is a good way to graft polymers instead of low molecular weight monomer[4,5]. So it is most important to study the effect of molecular weight on grafting, so far, all about these havn't been reported. In our experiments we adopted the method of pre-irradiation to graft condensed ethylene glycol acrylate on PE film, and studied the effect of molecular weight on grafting reaction.

Experimental

Low density PE film ($50\times30\times0.08mm^3$, PE 579-50, Shanghai Plastic Film Factory) was used as substrate which was irradiated by EB at a dose rate of 667 Gy/s, dose of 50KGy in ambient condition. The grafting reaction was carried out in a test tube which contained monomer, condensed ethylene glycol acrylate (synthesized by our laboratory), cyclohexane-n-propynal mixture as grafting medium and the pre-irradiated PE film. The grafting reaction was achieved by storing the test tube at 90℃ for desired time under N_2 protection. The degrees of grafting and ratio of water absorption were defined as:

$$G = \frac{W_d - W_o}{W_o} \times 100$$

$$H = \frac{W_w - W_d}{W_o} \times 100$$

Where: G —— degree of grafting

H —— ratio of water absorption

W_d — net weight of grafted film

W_o -- net weight of ungrated film

W_w — weight of grafted film and its absorbing water

Results and Discussion

1.| The process of grafting reaction

Fig.1 is the kinetic curve of grafting reaction in 90℃, monomer concentration is 20% and the solvent proportion of cyclohexane/n-propynal is 2/1. Fig.1 indicates that the degree of grafting was proportional to reaction time in the initial stage, the reaction rate is constant. The reaction rate is controlled by monomer diffusion in grafting reaction, in the case of the lower change ratio of monomer, the monomer concentration is nearly constant,so the diffusion rate and the reaction rate are constant. The reaction rate reduces with the reaction going on, and finally it tends to zero. Because the active centers which come from pre-irradiation are gradually consumed till they are exhausted. The degrees of grafting tend to saturate.

The relationship between the initial reaction rate of grafting and molecular weight of monomer is shown in Fig.2 (Fig.2 and following figures are the same reaction condition as Fig.1). It is clear from Fig.2 that the initial rate of grafting linear decreased with the increasement of molecular weight of monomer. Under the same reaction condition, the diffusion rate becomes less as the

molecular weight of monomer is increasing, therefore the rate of grafting reaction controlled by monomer diffusion drops down.

2. The saturate degree of grafting and molecular weight of monomer

Fig.1 shows that the degrees of grafting are not increase in pace with the reaction time after it get to the maximum we call this maximum degree of grafting as saturate degree of grafting. Fig.3 is the relationship between the saturate degrees of grafting and molecular weight of monomer. The saturate degrees of grafting linear reduce with the growing of molecular weight of monomer. If divide degree of grafting by monomer molecular weight, we obtain:

$$G_m = \frac{G}{M} = \frac{W_d - W_o}{M \cdot W_o} = \frac{W_d - W_o}{M} \cdot \frac{1}{W_o}$$

where: M is molecular weight of monomer, $W_d - W_o$ can be considered as the weight of material which have been grafted on PE sample, so $(W_d - W_o)/M$ is the mole number of monomer forming grafting sample. We call G_m the molar grafting degrees which means the mole number of grafting monomer of the unit weight sample. Fig.4 shows the ralationship between the saturable molar grafting degree and the molecular weight of monomer. It's different from Fig.3 that the influence of molecular weight on the saturate molar grafting degrees is greater in the case of lower monomer molecular weight, but with the monomer molecular weight increasing, the influence on the saturate molar grafting degrees becomes smaller.

3. Solvation

In grafting reaction system, solvent influences greatly the grafting reaction, it is connected with grafting-depth, grafting reaction rate and grafting degree. We use the mixture of cyclohexane/n-propynal as solvent. Fig.5 shows how the change of solvent influences the grafting degree, each grafting degree of the three systems reduces with

the rising of the proportion of n-propynol. In addition, the change of grafting degrees tend to relax after one turn point of solvent proportion. The turn point goes in the direction of increasing of n -propynal constituent. n-propynal isn't good solvent of PE, but cyclohexane is. Therefore the reducing of n-propynal constituent leads the swell ability of PE to enhance and the monomer molecular to diffuse, so the degree of grafting rises. The higher the molecular weight of monomer, the more diffcult the diffusion is,so high molecular monomer is more sensitive to the swell ability and the turn point come to earlier (in the direction of increasing of the cyclohexane constituent)

4. Hydrophilicity of the sample

Ratio of water absorption can be considered as one of the expressions of hydrophilicity. The hydrophilicity of material becomes better as the ratio of water-absorption is increasing. Fig.6 shows the relationship between the ratio of water absorption and the grafting degree of sample.The ratio of water absorption is almost in proportion to the grafting degree. Each slope (k) of the line in Fig.6 is:

$$K = \frac{H}{G} = \frac{W_w - W_d}{W_d - W_b}$$

where K is the weight of water absorption of the unit weight, it's to be said absorption ratio. Fig.6 shows with the increasement of the molecular weight of grafting monomer, the absorption ability decrease because of the increasement of grafting monomer condensed ethylene glycol acrylate and the decreasement of proportion of the -OH whose hydrophilicity is the best.

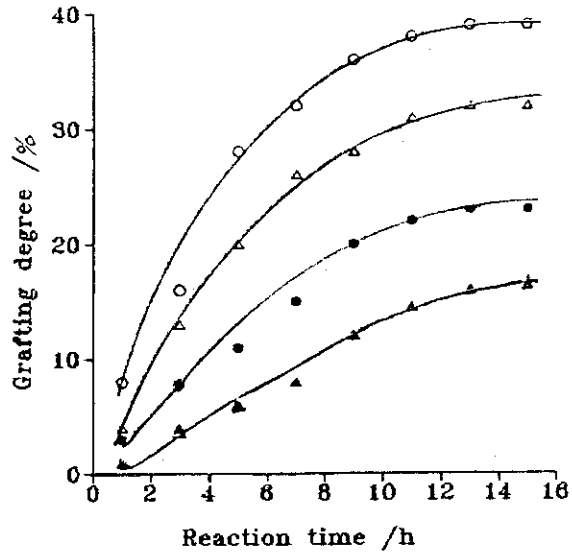


Fig.1 The kinetics curves of grafting reaction

- ○ acrylic acid
- △ ethylene glycol acrylate
- ● condensation diethylene glycol acrylate
- ▲ condensation triethylene glycol acrylate

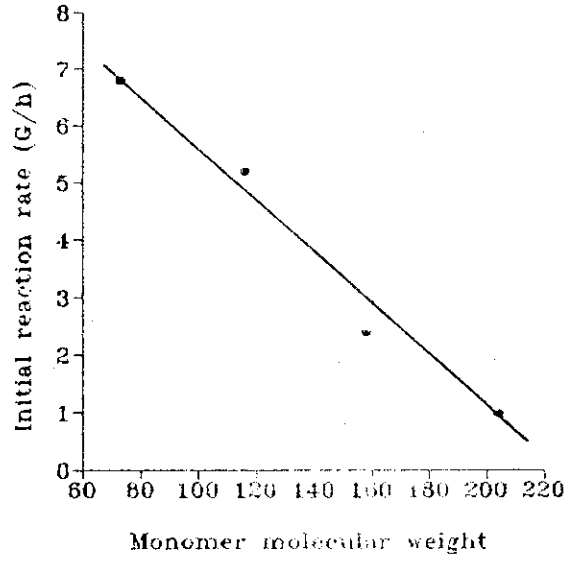


Fig.2 The relationship between molecular weight of momer and initial reaction rate

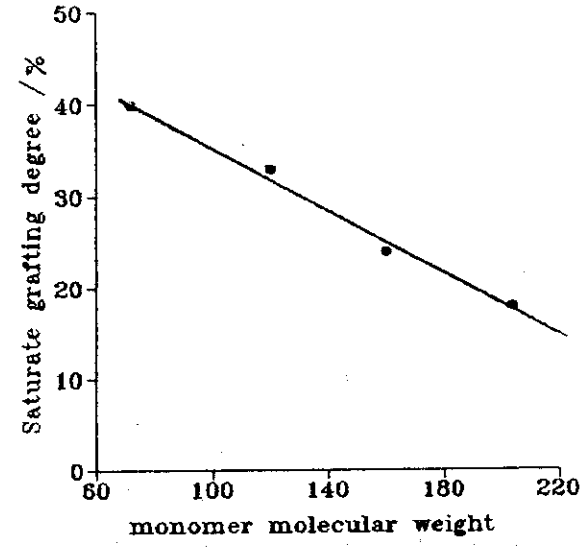


Fig.3 The influence of molecular weight of monomer on saturate degree of grafting

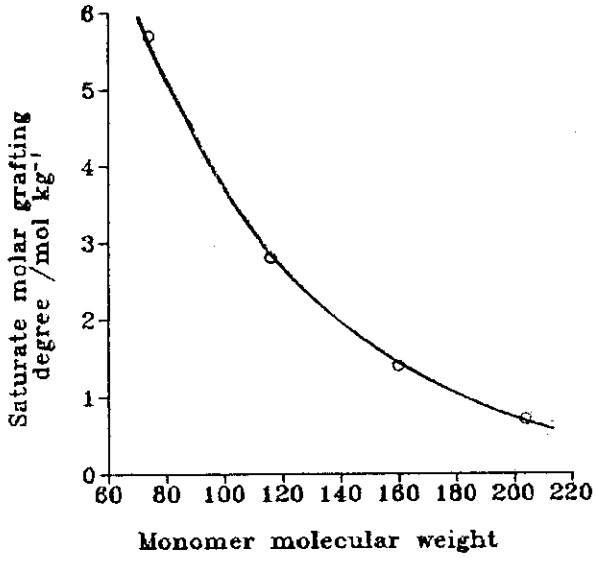


Fig.4 The influence of monomer molecular weight on the saturate molar grafting degree

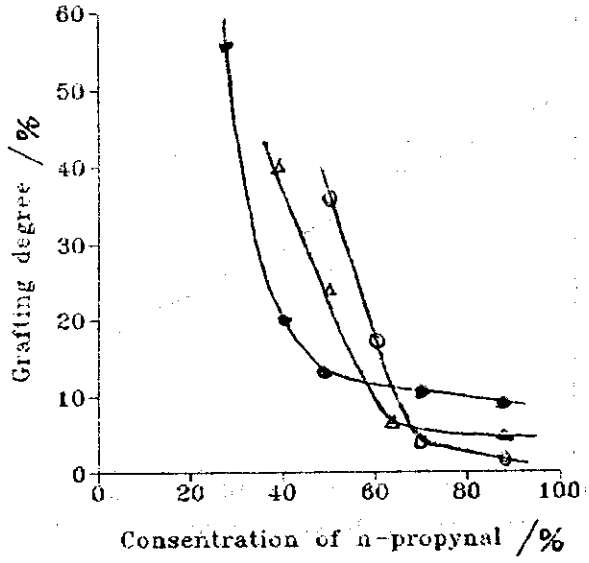


Fig.5 The influence of solvent on grafting degree

● -- acrylic acid,
△ -- ethylene glycol acrylate,
○ -- condensation diethylene acrylate.

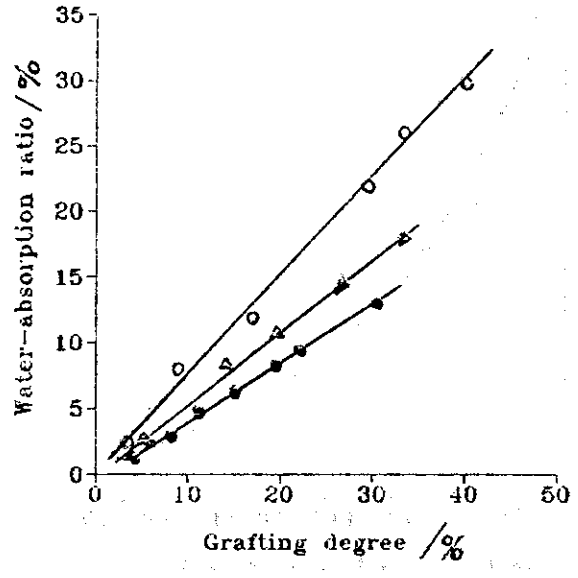


Fig.6 The relationship between the ratio of water absorption and grafting degree

○ -- acrylic acid,
△ -- ethylene glycol acrylate,
○ -- condensation diethylene glycol acrylate.

References

1 B.D.Ratner, A.S.Hoffman, J. Appl. Polym. Sci. 1974, 18, 3183.
2 V.T.Stannett, Radiat. Phys. Chem. 1990, 35(1-3), 82.
3 Chye H.Arg, John L.Granett, et al, Radit. Phys. Chem. 1985, 22(3-5), 831.
4 Sun Y.H, W.R.Gombotz, A.S.Hoffman, J. Bioactive and Biocompat Pols. 1986, 1, 316-334.
5 Sun Y.H, A.S.Hoffman, ACS Polymer Prepr. 1987, 28(1), 292-294.

5. Gas and Liquid Phase (2)

5.1 *Radiation and Photochemistry of Fullerenes

Jai P. Mittal
Chemistry Group
Bhabha Atomic Research Centre
Trombay, Bombay 400 085

Since the discovery of carbon clusters in laser ablated graphite vapours, fullerenes C_{60} and C_{70} have provided an unending source of excitement for experimental and theoretical scientists alike . Their brilliant colours in solutions and three dimensional aromaticity has fascinated photochemists. Our group has recently characterised singlet and triplet states of fullerenes using singlet-singlet ($S_1 \rightarrow S_n$) absorption spectra were studied in picosecond time domain and rates of intersystem crossing were established. Triplet states were produced directly by photoexcitation in laser flash photolysis experiments and by energy transfer in pulse radiolysis . Triplet-triplet ($T_1 \rightarrow T_n$) absorption spectra were characterised and rate constants for various triplet decay channels were measured.

The transient optical absorption spectra obtained on electron pulse radiolysis of de-aerated solutions of C_{60} and C_{70} in benzene have been assigned to the triplet states with $G(^TC_{60})$ = 0.52 and $G(^TC_{70})$ = 0.48. Low G ($-C_{60}$) and G($-C_{70}$) in the steady-state-γ radiolysis in benzene and hexane suggest their stabillity towards γ-radiation.

Pulse radiolytical studies on the water soluble γ-cyclodextrin C_{60} complex with primary radiolytic species such as OH, H and e_{aq}^- have also been carried out in aqueous solution. Rate constants for the formation of the transient species are determided by following the build up kinetics of the adduct transient species at the respective absorption maxima and the bleaching of the ground state C_{60} at 330 nm. Studies regarding the reaction of e_{aq}^- with γ-CD/C_{60} indicates the formation of γ-CD complexed C_{60}^- as confirmed by monitoring its characteristic aborption spectrum.

Other members of the Group include Dr. A.V. Sapre, Dr. T. Mukherjee, Dr. Hari Mohan, Dr. Indira Priyadarsini, Dr. D.K. Palit, Mr. H.N. Ghosh, Dr. H. Pal and D.K. Maity

5.2 The Research of Some Transient Species of Fullerenes with Pulse Radiolysis and Laser Photolysis

Si-de Yao, Zhi-rui lian, Wen-feng Wang, Jia-shan Zhang
and Nian-yun Lin

Laboratory of Radiation Chemistry, Academia Sinica, Shanghai Institute of Nuclear Research, P.O.Box 800-204, Shanghai 201800, CHINA

Abstract

The radical cation of C_{60} is generated either via hole transfer from radical cation of CCl_4 to C_{60} or via electron transfer from the triplet C_{60} to CCl_4. The radical adduct of $^{\cdot}CCl_3$ to C_{60} and C_{70} was also produced via two different mechanisms, namely the radical addition reaction and the reaction between triplet C_{60} and CCl_4 respectively. The pulse radiolysis and laser flash photolysis of C_{60} in other chlorinated methane solvents, $CHCl_3$ and CH_2Cl_2 presented the similar results.

1. Introduction

The discovery of facile laboratory synthesis and characterization [1-2] of C_{60} have triggered an intensive interest in exploring its basic properties. The excited state[3], cation radical [4-7], and anion radicals[8-11] of C_{60} have been studied. The electron transfer processes involved C_{60} both in the ground and excited states[7,12-23] have also been reported. In our previous work [24], we have reported the generation of radical cation of C_{60} ($C_{60}^{+\cdot}$) via an electron transfer reaction from the triplet excited state of C_{60} ($^3C_{60}^*$) to CCl_4 or CCl_3CF_3 for the first time and observed a transient absorption peak of $C_{60}^{\cdot +}$ at 650nm. In the past two years, the studies on the chemical reactivity of C_{60} have been becoming more and more intensive [25-27]. However the mechanism of the reactions involving C_{60} has just begun to be explored [28-34] and most of research works were carried out in non halogenated hydrocarbon solvents. Recently radiation induced addition of trichloromethyl radical ($^{\cdot}CCl_3$) or trichloromethylperoxyl radical ($CCl_3OO^{\cdot}$) to C_{60} were reported

[32]. In this paper,the absorption spectra of radiation and laser induced transient species of fullerens have been studied synergistically and found that the characteristic absorption peak of C_{60}^{+} at 650nm was different from that of radical adduct of $^{\cdot}CCl_3$ to C_{60} ($[C_{60}CCl_3]^{\cdot}$) at 430nm unambiguously. And a hole transfer mechanism to produce C_{60}^{+} with pulse radiolysis has also been suggested. In addition two different mechanisms of addition of $^{\cdot}CCl_3$ to fullerenes have been proposed.

2. Experimental

C_{60} was prepared and characterized according to a method similar to that discovered by Krätschmer et al. [1,2] as described previously [24]. C_{70} was purchased from Texas Fullerenes Corporation of USA,CCl_4,$CHCl_3$,CH_2Cl_2,C_6H_6(AR) were all commercially available and distilled before use.

The pulse radiolysis experiment was carried out using a 10 Mev linear accelerator which delivered an electron pulse with a duration of 8ns. The used maximum dose of a single pulse is 15 Gy determined by thiocyanate dosimetry and corrected for the electron density of the organic solvents employed (i.e., CCl_4, $CHCl_3$, CH_2Cl_2). The details of the equipment were described elsewhere [24].

The laser flash photolysis experiment was carried out using a home-built KrF excimer laser which provided a 248 nm pulse with a duration of 15ns. The maximum energy is about 50mJ per pulse.Detailed technical description of this facility have been given elsewhere[35,36].

3. Results and discussion

3.1. Pulse radiolysis of C_{60} in CCl_4

Carbon tetrachloride has been commonly used as an efficient solvent to oxidize the organic solutes [37-40] due to its high ionization potential (11.47ev) [41].It is generally accepted that the primary cations and radical species are $CCl_4^{\cdot+}$, $^{\cdot}CCl_3$, and the others are $CCl_3^{\cdot+}$, Cl^{-}, $:CCl_2$ and Cl etc. as summaried in reaction 1:

$$CCl_4 - \rightarrow CCl_4^{\cdot+},\ ^{\cdot}CCl_3,\ CCl_3^{\cdot+},\ Cl^{-},\ :CCl_2,\ Cl \qquad (1)$$

These radical species can react with solutes only if the concentration of dissolved substrate is high enough to compete with the natural decay of these species [32]. By monitoring at different time regions, one can selectively studied the reaction of $CCl_4^{\cdot +}$, or $^{\cdot}CCl_3$ with solute molecules. Neta et al have studied the one-electron oxidation of phenol and etc by pulse radiolysis of CCl_4 solutions and determined the G values of solute cations [37]. Dimitrijivic has recently studied the addition reaction of $^{\cdot}CCl_3$ or $CCl_3OO^{\cdot}$ with C_{60} in the time region of longer than 400μs using the pulse radiolysis techniques[32]. However he has not observed the absorption peak of $C_{60}^{\cdot +}$ on the time region of about several ten microseconds. Washio et al. has studied the pulse radiolysis of some aromatic molecules (denoted as M)in CCl_4 solution [42] and found that different transient species of cation ($M^{\cdot +}$), dimmer cation radical ($M_2^{\cdot +}$) or CT complex with Cl atom ($M^{\delta +}Cl^{\delta -}$),were produced somewhat relating to the ionization potential (IP) of solutes (reaction 2-4).

$$CCl_4^{\cdot +} + M \longrightarrow M^{\cdot +} + CCl_4 \qquad (2)$$

$$M^{\cdot +} + M \longrightarrow M_2^{\cdot +} \qquad (3)$$

$$M^{\cdot +} + Cl^- \longrightarrow M^{\delta +}Cl^{\delta -} \qquad (4)$$

C_{60} usually behaves as an aromatic and its IP (7.6ev [44]) is similar to that of pyrene (7.5ev [45])although it has not hydrogen atom [43]. Therefore, it can be expected that radiolysis of C_{60} in CCl_4 solution should also produce radical cation. Fig.1 shows the transient absorption spectrum recorded at 1 and 40μs after the pulse radiolysis of C_{60} in CCl_4. The characteristic spectra of $^3C_{60}^*$ did not exist as in the case of pulse radiolysis of C_{60} in benzene solution [3,18,24,46-49]. However an obvious absorption peak appeared at 650nm instead, which was in good accord with that of $C_{60}^{\cdot +}$ either predicated by CNDO/S calculation [4] or assigned from our previous pulse radiolysis of C_{60} in benzene containing CCl_4 or CCl_3CF_3 as electrophilic agents[24]. So the transient absorption peak at 650nm in this case should also be assigned to $C_{60}^{\cdot +}$. However, It is generated via a hole-transfer mechanism (reaction 5).

$C_{60} + CCl_4^{\cdot+} \longrightarrow C_{60}^{\cdot+} + CCl_4$ (5)

Ordinaryly $CCl_3^{\cdot+}$ derived from dissociation of $CCl_4^{\cdot+}$ should give less contribution to the production of $C_{60}^{\cdot+}$ because the ionization potential of $^{\cdot}CCl_3$ (8.78 eV) [44] is near to that of C_{60} (7.8 eV).

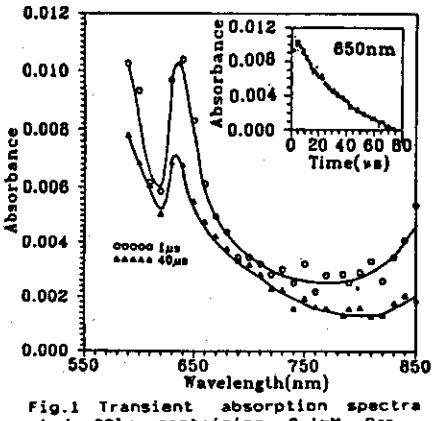


Fig.1 Transient absorption spectra of deaerated CCl_4 containing 0.1mM C_{60} at different times following the electron pulse. (●)1μs; (▲)40μs. Insert shows the absorption-time profile at 650nm.

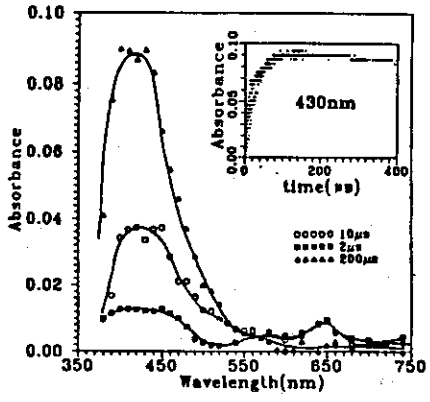


Fig.2 Transient absorption spectra of deaerated CCl_4 containing 0.1mM C_{60} at different times following the electron pulse. (■)2μs; (●)10μs; (▲)200μs. Insert shows the absorption-time profile at 430nm.

The absorption-time profile of the absorption peak at 650nm is shown in the insert of fig.1. Under the concentration of C_{60} (0.1mM) and dose (about 15Gy) employed,the rising time of $C_{60}^{\cdot+}$ is within 1μs, and its life time is around 40μs. From the rising trace at 650nm the generation rate constant of $C_{60}^{\cdot+}$ following reaction (5) is estimated to be about $3.5\times10^{10}mol^{-1}dm^3s^{-1}$. One may argue that this peak around 650nm may stem from the dimmer cation radical $(C_{60})_2^{+}$ or CT complex of C_{60} with Cl as in the case of aromatic molecules described above [42]. However, by carefully examining the experimental conditions and data obtained, this possibility can be excluded based on the following points. (1) The rising time of this transient species is about 1μs which is much longer than that of CT complex (about several ten ns)[42]. (2) Its life time is about 40μs which is much longer than that of CT complex(usually shorter than 1μs)[42].(3) Under the conditions employed in our experiment, the concentration of C_{60} (0.1mM) is much lower than that used in the study of radiolysis of aromatic molecules (i.e. several ten mM), so there is no sufficient amount of C_{60} to react with $C_{60}^{\cdot+}$ for production of $(C_{60})_2^{+}$ via reaction (3). (4) As shown in our previous work of pulse radiolysis of C_{60} in benzene with 3.5mM CCl_4 additive [24] which should produce much

lower concentration of Cl^- than that from pulse radiolysis of C_{60} in neat CCl_4 in this experiment, so in that case the concentration of Cl^- is too low to produce $C_{60}^{\delta+}Cl^{\delta-}$ via reaction 4, but the peak at 650nm still exists. This fact indicates that the peak at 650nm should not be assigned to $C_{60}^{\delta+}Cl^{\delta-}$.

In a longer time region of about several hundred μs after pulse radiolysis a broad absorption peak around 430nm was observed (Fig.2), which has a much longer growth time of around 100μs and a very long life time (>1000μs) as shown in the insert of Fig.2. The characteristic absorption maximum and its life time is in good accord with that from radical adduct of $^{\cdot}CCl_3$ to C_{60} ($[C_{60}CCl_3]^{\cdot}$) generated via the radical addition mechanism (reaction 6) as proposed by Dimitrijivic [32].

$$^{\cdot}CCl_3 + C_{60} \longrightarrow [C_{60}CCl_3]^{\cdot} \qquad (6)$$

The pulse radiolysis of C_{60} in other chlorinated methane solvents (i.e. $CHCl_3$ and CH_2Cl_2) also show similar absorption band around 400-500nm which are also similar to that observed and assigned to $[C_{60}CHCl_2]^{\cdot}$ and $[C_{60}CH_2Cl]^{\cdot}$ respectively by Dimitrijivic [32].

3.2. Laser flash photolysis of C_{60} in CCl_4

Fig.5 shows the transient absorption spectra recorded after the 248nm laser flash photolysis of 0.1mM C_{60} in CCl_4 solution. At 1μs after the laser pulse, the spectra presented was in good accord with the authentic spectra of $^3C_{60}^*$ [3,18,24,46-49].The $^3C_{60}^*$ was produced by direct excitation of C_{60} and the following intersystem crossing process (reaction 7).

$$C_{60} \xrightarrow{h\upsilon(248nm)} {}^1C_{60}^* \xrightarrow{isc} {}^3C_{60}^* \qquad (7)$$

Such a strong absorption spectra of $^3C_{60}^*$ has never been reported before.In a longer time region, with the decay of $^3C_{60}^*$ at 745nm, a new absorption peak around 650nm appeared which is very similar to the absorption peak of $C_{60}^{\cdot+}$ discussed above.Trace 6a and 6b in Fig 6 show the change of absorbance at 740nm, A_t^{740}, and the change of absorbance at 650nm, $A_t^{650}$with time respectively.Trace 6c is

corresponding to the absorbance contribution of $C_{60}^{\cdot+}$ at 650nm obtained by subtraction method [35],Where factor p is the ratio of the absorbance of $^3C_{60}^*$ alone at 650nm and 740nm,which was determined from the standard absorption of $^3C_{60}^*$ [3,18,24,46-49].From trace 6c it is found that the growth of the absorption of $C_{60}^{\cdot+}$ is also synchronous with the decay of $^3C_{60}^*$ at 740nm. Therefore, the generation of $C_{60}^{\cdot+}$ here can be considered via electron transfer (ET) with exciplex mechanism as proposed in our previous paper on the pulse radiolysis of C_{60} in benzene containing CCl_4 or CCl_3CF_3 [24] (reaction 8).

$$^3C_{60}^* + CCl_4 \underset{}{\overset{K_q}{\rightleftharpoons}} [C_{60}\cdots CCl_4]^* \rightleftharpoons [C_{60}^{\delta+}\cdots CCl_4^{\delta-}] \quad (8)$$

$$\downarrow$$

$$C_{60}^{\cdot+} + CCl_4^{\cdot-}$$

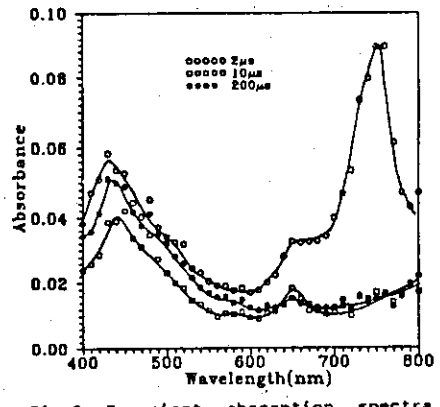


Fig.5 Transient absorption spectra of deaerated CCl_4 containing 0.1mM C_{60} at different times following the laser pulse. (●)2μs; (□)10μs; (▲)200μs.

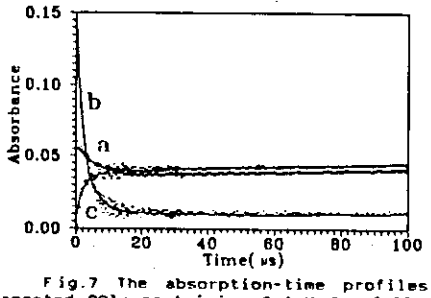


Fig.7 The absorption-time profiles of deaerated CCl_4 containing 0.1mM C_{60} following the laser pulse. Traces (a) and (b) were obtained at 650 and 740nm respectivnly. Trace (c) corresponding to the absorbance of C_{60} radical cation at 650nm was obtained from traces (a) and (b) by the subtraction method (see ref.[35]).

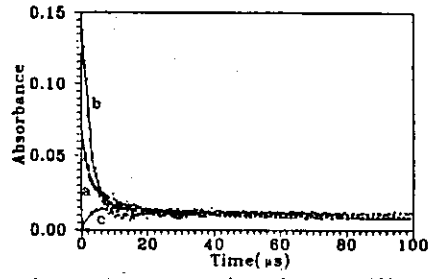


Fig.6 The absorption-time profiles of deaerated CCl_4 containig 0.1mM C_{60} following the laser pulse.Trace (a) and (b) were obtained at 650 and 740nm respectively.Trace (c) corresponding to the absorbance of C_{60} radical cation at 650nm was obtained from trace (a) and (b) by substraction method.

Since the one-electron reduction potential of CCl_4 is not available, the change of free energy (ΔG^0) of reaction (8) can not be estimated by the Rehm-Weller equation [50].

Also as shown in Fig.5, at 200μs after the laser pulse a new absorption band around 430nm clearly presented. Its absorption maxima and shape is very similar to the absorption band of $[C_{60}CCl_3]^{\cdot}$ from pulse radiolysis of C_{60} in CCl_4 as confirmed in part 3.1. So this absorption band should also be assigned to $[C_{60}CCl_3]^{\cdot}$.Trace of 7a and 7b show the change of absorbance at 740nm, A_t^{740}, and the one at 450nm, A_t^{450} respectively. Trace of 7c is corresponding to the absorbance contribution of $[C_{60}CCl_3]^{\cdot}$at 450nm obtained by subtracting method[35],Where factor p is the ratio of the absorbance of $^3C_{60}^*$ alone at 450nm and 740nm[3,18,24,46-49] and is determined to be 0.33.From trace of 7c it seems that the decay of $^3C_{60}^*$ is synchronous with the growth of $[C_{60}CCl_3]^{\cdot}$and the growth time of $[C_{60}CCl_3]^{\cdot}$ is about 10μs, which is much shorter than that of $[C_{60}CCl_3]^{\cdot}$ arising from the pulse radiolysis of same solution discussed above (reaction 6). The observed growth rate constant K_{obs} is estimated to be $6.4\times10^5 s^{-1}$, which is also much larger than that in the radical addition mechanism (reaction 6), i.e. $8.0\times10^4 s^{-1}$. Moreover, by carefully comparing Fig.2 and Fig.5, It is found that the ratio of absorption maximum at 450nm to that at 650nm, A_{450}/A_{650} of Fig.2 (i.e.10/1) is different from that of Fig.5 (i.e.3/1). So, it should be concluded that the mechanism of generation of $[C_{60}CCl_3]^{\cdot}$ from laser flash photolysis is different from the radical addition mechanism (reaction 6) in the case of pulse radiolysis. Fig.8 shows the transient absorption spectra at 200μs from the laser flash photolysis of C_{60} in CCl_4 solution saturated by O_2. It shows that the presence of dissolved O_2 greatly decreased the yield of $[C_{60}CCl_3]^{\cdot}$. This indicated that $^3C_{60}^*$ must be a precursor of the generation of $[C_{60}CCl_3]^{\cdot}$ in the photolysis of C_{60} in CCl_4 solution. Based on all the points above, we proposed the following mechanism as a novel path for the generation of $[C_{60}CCl_3]^{\cdot}$ in the laser flash photolysis of C_{60} in CCl_4 (reaction 9).

$$^3C_{60}^* + CCl_4 \underset{}{\overset{k_q}{\rightleftharpoons}} \underbrace{[C_{60}\cdots CCl_4]^*}_{\text{exciplex}} \longrightarrow [C_{60}CCl_3]^{\cdot} + Cl \qquad (9)$$

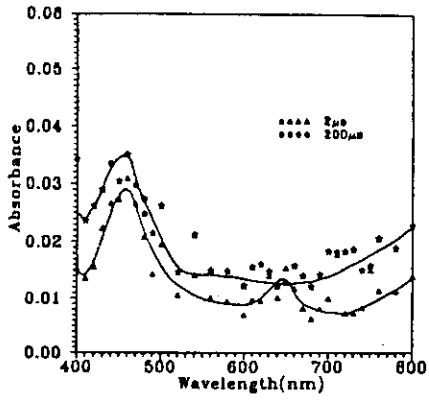


Fig.8 The absorption-time profiles of deaerated CCl_4 containing 0.1mM C_{60} following the laser pulse. Traces (a) and (b) were obtained at 450 and 740nm respectively. Trace (c) corresponding to the absorbance of radical adduct of $^{\cdot}CCl_3$ to C_{60} ($[C_{60}CCl_3]^{\cdot}$) at 450nm was obtained from traces (a) and (b) by the subtraction method (see ref.[35]).

The reaction (8) and (9) are competing reactions via an exciplex between C_{60} and CCl_4. It has been well recognized that electron transfer reaction via exciplex is a key process in many photo-induced reactions such as generation of cation, photocyclodation etc. [51] and hydrogen transfer reactions [52]. However, transfer of such a large group as $^{\cdot}CCl_3$ has never been reported. The detail of this mechanism needs to be further explored.

Based on the above mechanism and the reported absorption coefficients of $^3C_{60}^*$ and $[C_{60}CCl_3]^{\cdot}$, the conversion yield of $[C_{60}CCl_3]^{\cdot}$ from $^3C_{60}^*$, denoted as ϕ can be deduced from the following equation.

$$\frac{\phi\, A^{740}(\,^3C_{60}^*)|_{t=0}}{\varepsilon^{740}(^3C_{60}^*)} = \frac{A^{450}([C_{60}CCl_3]^{\cdot})|_{t=0}}{\varepsilon^{450}([C_{60}CCl_3]^{\cdot})} \qquad (10)$$

Dimitrijivic [32] has given the $G\varepsilon^{450}$ value of $[C_{60}CCl_3]^{\cdot}$ from pulse radiolysis of C_{60} in CCl_4 as 200000, but did not give the corresponding G value. In order to obtain the $\varepsilon^{450}([C_{60}CCl_3]^{\cdot})$, we should estimate the G value of $[C_{60}CCl_3]^{\cdot}$ from pulse radiolysis of C_{60} in CCl_4 here. Since the G value of $^{\cdot}CCl_3$ from the pulse radiolysis of CCl_4 was 3.5 [37], so the the G value of $[C_{60}CCl_3]^{\cdot}$ from pulse radiolysis of C_{60} in CCl_4 should be lower than 3.5. Therefore the $\varepsilon^{450}([C_{60}CCl_3]^{\cdot})$ was then deduced from the $G\varepsilon^{450}$

value to be $\geq 5714 M^{-1}cm^{-1}$. The $\varepsilon^{740}(^3C_{60}^*)$ is taken as 16000 $M^{-1}cm^{-1}$[18]. The $A^{740}(^3C_{60}^*)|_{t=0}$ and $A^{450}([C_{60}CCl_3]^\cdot)|_{t=0}$ was obtained by extrapolating Fig.7b and 7c to t=0 as,

$$A^{740}(^3C_{60}^*)|_{t=0} = 0.2$$

$$A^{450}([C_{60}CCl_3]^\cdot)|_{t=0} = 0.05$$

Therefore, the conversion yield ϕ was deduced from equation (10) to be ≤ 0.7.

Since the $^\cdot CCl_3$ can be produced from laser flash photolysis of CCl_4 [39], so another possible mechanism is the direct addition of $^\cdot CCl_3$ to $^3C_{60}^*$ (reaction 11),but it is less possible than the mechanism(9) and should be excluded.

As shown in Fig 3,almost the same spectrum like the one of triplet of C_{70}(Fig 4) has been observed in laser photolysis of CCl_4 solution containing 0.05mM C_{70},but growing process and the lif time of the species is much different from tha of triplet of C_{70}.according to above results of C_{60},It may be proposed that the species is C_{70}-CCl_4 adduct radical with the generating mechanism as:

$$CCl_3 + C_{70} \text{---} C_{70}\text{-}CCl_3 \qquad (11)$$

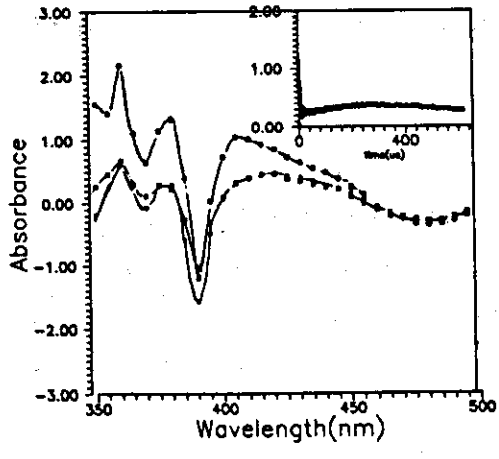


Fig.3 Transient absorption spectrr of deaerated CCl_4 containing 0.05mM C_{70} at different times following the laser photolysis (□)0.5μS;(■)100μS;(*)500μS
insert shows the absorption-time profile at 405nm

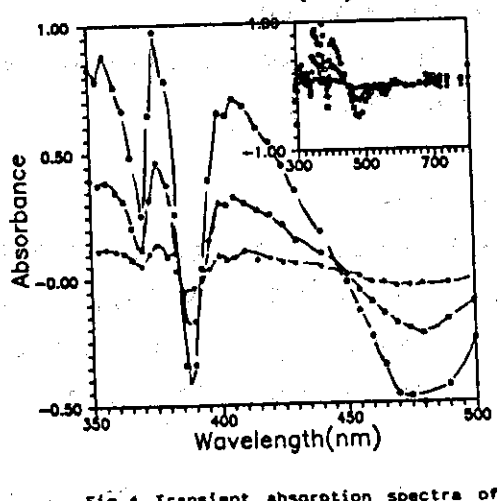


Fig.4 Transient absorption spectra of deaerated C_6H_{12} containig 0.05mM C_{70} at different times following the laser photolysis (□)0.5μS;(■)2μS;(*)5μS
insert shows all spectra of triplet of C_{70}.

When $CHCl_3$ and CH_2Cl_2 were employed instead of CCl_4, the similar transient absorption spectra of cation and adduct radical were obtained.The bimolecular quenching rate constants of $^3C_{60}^*$ was determined to be 6.4×10^9, 4.8×10^9 and $2.8\times10^9 mol^{-1}dm^3s^{-1}$ for

CCl_4, $CHCl_3$ and CH_2Cl_2 respectively, which are in accord with their electron affinities (EA) value as gathered in Tabel 1.

Table 1. Quenching rate constant of $^3C_{60}^*$ by CCl_4 (k_q), $CHCl_3$ and CH_2Cl_2 and their electron affinities (EA).

	CCl_4	$CHCl_3$	CH_2Cl_2
k_q ($mol^{-1}dm^3s^{-1}$)	6.4×10^9	4.8×10^9	2.8×10^9
EA(ev)[53]	2.12	1.76	1.36

4. Conclusion.

$C_{60}^{\cdot+}$ was generated via hole-transfer and electron-transfer via exciplex mechanism arising from pulse radiolysis and laser photolysis respectively. The radical adduct of $^{\cdot}CCl_3$ to fullerenes was also produced via two different mechanisms including radical addition mechanism and a novel mechanism via exciplex between C_{60} and CCl_4 respectively. In the later mechanism, the yield of $[C_{60}CCl_3]^{\cdot}$ from $^3C_{60}^*$ was estimated to be ≤ 0.7. The pulse radiolysis and laser flash photolysis of C_{60} in other chlorinated methane solvents, $CHCl_3$ and CH_2Cl_2, presented similar results.

5. Acknowledgement

This study was supported by National Nature Science Foundation of China (NNSFC).

References

[1]H.M.Kroto,A.M.Allaf,and S.P.Balm,Chem.Rev.91(1991)1213.

[2]R.F.Curl,and R.E.Smalley,Scientific American, 265(1992)32.

[3]R.V.Benson, T.Hill, C.Lambert, E.J.Land, S.Leach, T.G.Truscott,Chem.Phys.Letters, 201(1993)326 and references therein.

[4]T.Kato, T.Kodam, T.Shida, T.Nakagawa, Y.Matsui, S.Suzuki, H.Shiromaru,K.Yamauchi,Y.Achiba,Chem.Phys.Lett.180(1991)446.

[5]T.Kato, T.Kodama, T.Shida, Chem.Phys.Letters 205(1993)405.

[6]Z.Gasyna,L.Andrews and P.N.Schatz,J.Phys.Chem.96(1992)1525.

[7]S.Noell,J.W.Arbogast and C.S.Foote, J.Phys.Chem.96(1992)4170.

[8]T.Kato, T.Kodama, T.Shida, Chem.Phys.Letters 205(1993)405.

[9]L.Biezok, H.Linschitz, Chem.Phys.Letters 195(1992)339.
[10]N.D.Dimitrijivic, P.V.Kamat, J.Phys.Chem.97(1993)7623.
[11]M.V.Mirkin,Luis O.S.Bulhoes,A.J.Bard,
J.Am.Chem.Soc.115(1993)201 and references theirin.
[12]R.J.Sension, A.Z.Szarka, G.R.Smith, R.M.Hochstrasser,
Chem.Phys.Letters, 185(1991)179.
[13]J.W.Arbogast,C.S.Foote and M.J.Kao,J.Am.Chem.Soc.114(1992)227
[14]Y.Wang,J.Phys.Chem.,96(1992)704.
[15]A.Samanta, P.V.Kamat, Chem.Phys.Letters, 199(1992)635.
[16]M.Gevaert, P.V.Kamat, J.Phys.Chem.,96(1992)9883.
[17]M.Gevaert, P.V.Kamat, J.Chem.Soc.Commun., (1992)1470.
[18]L.Biczok, H.Linschitz, R.I.Walter, Chem.Phys.Letters,
195(1992)339.
[19]D.Dubois,K.M.Kadish,S.Flanagan,R.E.Haufler,L.P.F.Chibante,
L.J.Wilson, J.Am.Chem.Soc.113(1991)4364.
[20]D.Dubois, K.M.Kadish,, S.Flanagan, L.J.Wilson, J.Am.Chem.Soc.
113(1991)7773.
[21]P.M.Allemmand,A.Koch,F.Wudl,Y.Rubin,F.Diederich,M.M.Alvaez,
S.J.Anz,R.L.Whetten,J.Am.Chem.Soc.113(1991)1050.
[22]N.S.Saciciftci, L.Swilowitz, A.J.Heeger, F.Wudl, Science,
258(1992)1474.
[23]P.V.Kamat,J.Am.Chem.Soc.113(1991)9705.
[24]H.Q.Hou,L.Chang,Z.X.Liu,D.M.Mao,Q.Z.Qin, Z.R.Lian,
S.D.Yao,W.F.Wang, J.S.Zhang, N.Y.Lin, Chem.Phys.Letters,
203(1993)555.
[25]H.A.Schwarz, Chem.Int.Ed.Engl.31(1992)293.
[26]F.Wudl, Acc.Chem.Rec.25(1992)157.
[27]F.Wudl, A.Hirsch, K.C.Khemani, T.Suzuki, P.M.Allemand, A.Koch,
H.Echert, G.Srdanov, H.M.Webb, A.C.S.Symp.Ser.481(1992)161.
[28]P.J.Krusic,E.Wasserman,B.A.Parkinson,B.Malone,Jr.E.R.Holler,
J.Am.Chem.Soc.113(1991)6274.
[29]P.J.Krusic,E.Wasserman,P.N.Keizer,R.J.Monton,K.F.Preston,
Science 254(1991)1183.
[30]R.J.Morton, K.R.Preston, P.J.Krusic, S.A.Hill, E.Wasserman,
J.Am.Chem.Soc.14(1992)5454.
[31]R.J.Morton, K.R.Preston, P.J.Krusic, S.A.Hill, E.Wasserman,
J.Phys.Chem.96(1992)3576.
[32]N.M.Dimitrijivic, Chem.Phys.Letters 194(1992)457.

[33]N.M.Dimitrijivic,P.V.Kamat,R.W.Fessenden,
J.Phys.Chem.97(1993)615.
[34]D.M.Guldi,H.Hungerbuehler,E.Janta,K.D.Asmus,
J.Chem.Soc.Commun.1(1993)84.
[35]L.Jian,W.F.Wang,Z.D.Zheng,S.D.Yao,J.S.Zhang,N.Y.Lin, Research on Chemical Intermediates,15(1991)293.
[36]Z.H.Zuo,S.D.Yao,L.Jian,W.F.Wang,J.S.Zhang,N.Y.Lin,
J.Photochem.Photobiol.B:Biol.,15(1992)215.
[37]J.Grodkowski,P.Neta, J.Phys.Chem.88(1984)1205.
[38]R.E.Bühler, Radiat.Phys.Chem. 21(1983)139.
[39]M.Wahio, S.Tagawa, Y.Tabata, Radiat.Phys.Chem.21(1983)239.
[40]O.Brede,J.Bös,W.helmstreit,R.Mehnert,
Radiat.Phys.Chem.19(1982)1.
[41]D.R.Lide(ed.), " CRC Handbook of Physics and Chemistry "(72th edietion), CRC Press (1991). p.10-216.
[42]M.Wahio,S.Tagawa,K.Furuya,N.Hayashi,Y.Tabata,
Radiat.Phys.Chem.34(1989)533.
[43]D.L.Lichtenberger,K.W.Nebesney,C.D.Ray,D.R.Huffman and
L.D.Lamb,Chem.Phys.Lett.176(1991)203.
[44]V.A.Vedeneyev, L.V.Gurvitch, V.N.Kondratyev, V.A.Medvedev, Ye.L.Frankevich, "Bond Energies, Ionization Potentials and Electron Affinites".St.Martin's Press: New york,1966.
[45]P.J.Fagan,J.C.Calabiese,B.Malone,Science 252(1991)1160.
[46]N.D.Dimitrijivic, J.Phys.Chem.96(1992)4811.
[47]Y.Kajii,T.Nakagawa,S.Suzuki,Y.Achiba,K.Obi and K.Sbibuya,
Chem.Phys.Lett.181(1991)100.
[48]R.J.Sension,C.M.Phillips,A.Z.Szarka,W.J.Romanow,A.R.Mcghie,
J.P.McCauley,A.B.Smith,R.M.Hochstrasser,
J.Phys.Chem.95(1991)6075.
[49]J.W.Arbogast and C.S.Foote,J.Am.Chem.Soc.113(1991)8886.
[50]D.Rehm, A.Weller, Ber.Bunsenges.Phys.Chem.73(1969)834.
[51]F.Müller, J.Mattay, Chem.Rev.93(1993)99.
[52]For example, H.Gruen,H.N.Schott,G.W.Byers,H.G.Giles,
J.A.Kampmeier, Tetrahedron.Letters 37(1972)3925.
[53]A.F.Gaines, J.Kay, F.M.Page, Trans.Faraday Soc.62(1966)874.

5.3 Radiolytic Reduction Reaction of Colloidal Silver Bromide Solution

Yasuhisa Oya, Takehiro Zushi*, Kunihiko Hasegawa* and Tatsuo Matsuura**

Research Laboratory for Nuclear Reactors, Tokyo Institute of Technology, Tokyo 152, Japan

* Radiochemistry Research Laboratory, Shizuoka University, Shizuoka 422, Japan

** Institute for Atomic Energy, Rikkyo University, Yokosuka 240-01, Japan

Abstract The reduction reaction of colloidal silver bromide $(AgBr_3)^{2-}$ in nitrous oxide gas saturated solution of some alcohols: methanol, ethanol, 2-propanol and 2-methyl-2-propanol by γ-irradiation was studied spectrophotometically in order to elucidate the mechanism of the formation of colloidal silver bromide $(AgBr_3)^{3-}$ at ambient temperature . The amount of colloidal silver bromide formed increases in the order: i-PrOH, EtOH, MeOH. In t-BuOH, colloidal silver bromide did not form. The relative reactivities of alcohols for colloidal silver bromide was also studied kinetically.

INTRODUCTION

The reduction reaction of colloidal silver bromide $(AgBr_3)^{2-}$ in aqueous solution by γ-ray irradiation has been known to form colloidal silver. However, the mechanism of the formation of colloidal silver bromide $(AgBr_3)^{3-}$ adding alcohols in N_2O saturated solution has not been revealed.

In present paper, the reduction of colloidal silver bromide by γ-irradiation saturated solution in the presence of alcohols, viz., methanol, ethanol, 2-propanol, 2-methyl-2-propanol was studied. The mechanism of reduction of colloidal silver bromide was also studied.

EXPERIMENTAL

All reagents were obtained from Wako Pure Chemical Industries Ltd. methanol, ethanol, 2-propanol, 2-methyl-2-propanol were purified by distillation. Other reagents were used without further purification. Water from a Milli RO60 Millipore filtering system was used throughtout the study. Colloidal silver bromide suspensions were prepared by adding 2×10^{-2}M $AgNO_3$ and adding very slight excess of 2×10^{-2}M ion concentration of KBr solution in 0.05% gelatine solution and then stirring the solution to prepare a homogeneous collidal solution. The colloidal silver bromide solution was produced to a negative charge colloid in the solution. N_2O gas passed through the solution for 10 min to study the reaction between OH radical and colloidal silver bromide. Hydroxy radical, OH, and hydrated electrons, e_{aq}^- are formed by the radiolysis of water. In N_2O saturated solution hydrated electrons are converted to OH radical:

$$e_{aq}^- + H_2O + N_2O \rightarrow N_2 + OH^- + OH. \qquad (1)$$

To prevent the effect of UV radiations the solution was quickly wrapped in black paper and then irradiated at the room temperature. The amount of colloidal silver obtained by the irradiation was determined spectrophotometically at the maximum wave length of 405~410 nm, ε = 11500 mol $dm^{-3}cm^{-1}$ and that of 410~420 nm, ε = 13500 $mol^{-3}cm^{-1}$(Johnson, *et al.*,1970). ^{60}Co γ -ray source, 1.35kCi, was used for the irradiation. Dose rate measured with Fricke dosimeter (G=15.5) was 1.3×10^{17}~3.0×10^{17}eV · g^{-1} h^{-1}.

RESULTS AND DISCUSSION

The wave lengths of maximal absorption of colloidal silver bromide $(AgBr_3)^{3-}$ in 0.1M MeOH was 409 nm at the absorbed dose 1.8×10^{18}eV · s^{-1}. The absorption maximum is shifted to long wave lengths upon increasing the dose. The range of maximum absorption was 409~420 nm. The dose rate for colloidal bromide solution was studied. The amounts of $G(Ag^\circ)$ was found to increase with the dose rate and colloidal silver bromide formed at a given dose in the order: i-PrOH, EtOH and MeOH (Johnson, 1978). The stability of colloidal silver bromide produced by γ -ray irradiation was studied for about 200 hrs. It was found that colloidal silver bromide reduced by irradiation diminished with pseudo first order reaction. After finishing for irradiation, the colloid is stable within about 1 h. For one example, in

case of silver bromide solution to add $1.0\times10^{-3}\sim1.0\times10^{-1}$M MeOH, the relation between Ag° (=$(AgBr_3)^{3-}$) produced and the absorbed dose is shown in Fig.1. As can be seen from figure, for MeOH, the amount of Ag° produced is increase with the concentration of alcohol. The initial $G(Ag^{\circ})$ was obtained from the slope of curve in the figure.

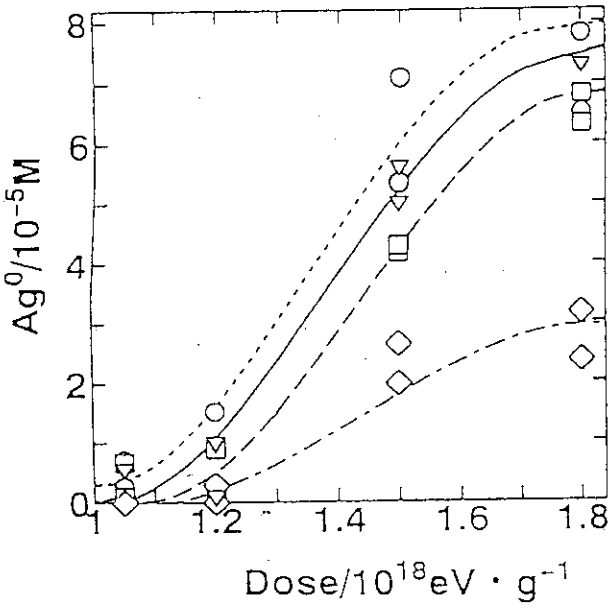


Fig.1 Radiolytic reduction reaction of colloidal silver bromide with methanol; Concentration of MeOH, ○:1.0×10^{-1}M, □:1.0×10^{-2}M, ▽:5.0×10^{-2}M, ◇:1.0×10^{-3}M

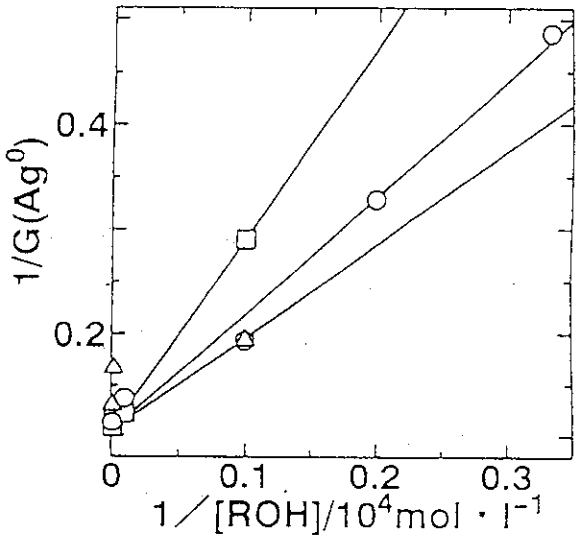


Fig.2 $1/G(Ag^{\circ})$ vs. 1/ [ROH] ; □: MeOH, ○: EtOH, △: i-PrOH.

As described above, when excess Br^- ion was added to the solution, the colloidal silver bromide forms $(AgBr_3)^{2-}$ as a chemical form. First of all, this colloid solution was irradiated by γ-ray irradiation:

$$(AgBr_3)^{2-} \rightarrow [(AgBr_3)^{2-}]^{*}. \qquad (2)$$

OH radical(1) produced reacts alcohol to form radical:

$$RCH_2OH + OH \rightarrow RCHOH + H_2O. \qquad (3)$$

The produced radical(3) reacts with $[AgBr_3)^{2-}]^{*}$ to form $(AgBr_3)^{3-}$, rate constant k_1 is reaction (4):

$$[(AgBr_3)^{2-}]^{*} + RCHOH \xrightarrow{k_1} (AgBr_3)^{2-}\cdots RCHO + H^{+}. \quad (4)$$

On the other hand, the excited colloidal silver bromide make up to the stable colloid, rate constant k_2 is reaction (5):

$$[(AgBr_3)^{2-}]^{*} \xrightarrow{k_2} (AgBr_3)^{2-}, \quad (5)$$

where the radiation yield(G) of colloidal silver denotes $G(AgBr_3)^{2-} = G(Ag^{\circ})$, the intensity of γ-ray is I and the reaction efficiency a , $G(Ag^{\circ})$ can be discribed as follows:

$$G(Ag^{\circ})\, I = k_1 [(AgBr_3)^{2-}]^{*} [RCHOH] . \quad (6)$$

When the rates of production equals to the rate of disapperence in excited colloidal silver bromide, the following equation (7) can be written by the use of stationary state method:

$$G(Ag^{\circ}) = \frac{ak_1 [RCHOH]}{k_1 [RCHOH] + k_2} . \quad (7)$$

In order to find a relation $G(Ag^{\circ})$ and the rate constants, k_1 and k_2, eq.(7) is rearranged as:

$$\frac{1}{G(Ag^{\circ})} = \frac{1}{a} + \frac{k_2}{ak_1 [RCHOH]} . \quad (8)$$

Therefore, if a plot of $1/G(Ag^{\circ})$ against the concentration of alcohol gives a straight line, a and relative rate constant of k_1 and k_2 can be determined from the intercept and slope respectively. This relations is shown in Fig.2.

$$CH_3OH + OH \xrightarrow{k_m} CH_2OH + H_2O, \quad (9)$$

$$CH_3CH_2OH + OH \xrightarrow{k_e} CH_3CHOH + H_2O, \quad (10)$$

$$(CH_3)_2CHOH + OH \xrightarrow{k_p} (CH_3)_2COH + H_2O. \qquad (11)$$

The rate constants of the reaction between OH radical and MeOH, EtOH and i-PrOH, respectively, are the following 0.5, 1.0 and 1.5 $\times$ 10^9 M^{-1} s^{-1} (Anbar *et al.*, 1967). Thus, the following relation roughly can be expressed:

$$\frac{1}{3}k_p = \frac{1}{2}k_e = k_m = k_R' \qquad (12)$$

Considering OH radical reacts with radical produced from alcohol, we can derive from (7) equation:

$$\frac{1}{G(Ag^\circ)} = \frac{1}{a} + \frac{k_2}{ak_1k_R\,[RCH_2OH]\;[OH]}. \qquad (13)$$

For one example of EtOH and MeOH, we can obtain the following relation:

$$\frac{ak_1(EtOH)k_e\,[OH]}{ak_1(MeOH)k_m\,[OH]} = \frac{1.84\times10^{-4}}{1.12\times10^{-4}}. \qquad (14)$$

The relative rate constant of MeOH, EtOH and i-PrOH are found to be 1 : 2 : 3 for OH radical and 1 : 3.3 : 6.2 for the reduction by the radicals produced from alcohols by γ -ray irradiation. It became evident that colloidal silver bromide solution can be reduced to faciliate by EtOH and i-PrOH radicals more than MeOH radical. This result show that the relation of the reduction ability is established in the both aqueous solution and colloidal solution.

REFERENCES

Anbar M. and Neta P. (1967) *Intl. J. Appl. Radiation & Isotope* 18, 493.

Johnson F.J.,Mehrotra K.N. and Huh.Y.(1970) *Radiation Res.* **44**, 323.

Johnson F.J. (1978) *Radiation Res.* 75, 286.

5.4 Simulation of Radiation-induced Ozone Decomposition in Water in the Presence of Organic Compounds

H. Arai, H. Namba, T. Miyata, M. Arai, A. Sakumoto, and H. Sunaga

Takasaki Radiation Chemistry Research Establishment,
Japan Atomic Energy Research Institute
1233 Watanuki-machi, Takasaki-shi, Gunma-ken 370-12 Japan

Abstract Ozone decomposition in water by electron beam irradiation in the presence of acetic acid and *t*-butanol was studied by the direct measurement of ozone concentration using a spectroscopy equipped with optical fiber light guides and the computer simulation based on 80 reactions. The calculated data were in fair agreement with the observed data for acetic acid aq. solution. For *t*-butanol high concentration aq. solution, the calculated data became closer to the observed data when the decomposition of peroxide were assumed to occur to produce HO_2 or O_2^-. At low concentration of the organic solutes, the presence of HCO_3^- or CO_3^{2-} disturbs the ozone decomposition substantially. The concentrations of active species such as OH radicals during the irradiation were also estimated from the simulation.

INTRODUCTION

Some organic compounds in water are easily decomposed by gamma-ray irradiation combined with ozone (Sakumoto and Miyata, 1984). Some times, G values of decomposition of organic compounds exceed 10 – 30, suggesting that chain reactions take place in this system. Based on the ozone decomposition mechanism in water proposed by Staehelin and Hoigné (Staehelin and Hoigné, 1985), the chain reactions were thought to be due to regeneration of OH radical through the decomposition of HO_3 radical formed by the reaction of O_3 with O_2^- which is produced from the decomposition of peroxide of the organic compounds (Arai et al., 1986). In this report, we studied the ozone decomposition by electron beam irradiation in water in the presence of acetic acid and *t*-butanol from the direct measurement of ozone concentration and the computer simulation based on the above mechanism.

REACTION MODEL AND SIMULATION

Staehelin and Hoigné (1985) proposed the reaction model for the decomposition of ozone in water in the absence and in the presence of organic solutes (SBH model). We modified this model by adding the decomposition of water by electron beam irradiation as follows.

Initiation Step. Water molecule is decomposed by electron beam irradiation to produce OH radical, hydrated electron, hydrogen atom etc. At the same time, ozone is decomposed by the reaction with OH^- to produce perhydroxyl radical (HO_2) or superoxide ion (O_2^-).

Propagation step. OH radical is also produced by the next sequence of reactions. That is, HO_2 or O_2^- is converted to O_3^- by the reaction with ozone. The O_3^- reacts with H^+ to form HO_3 which decomposes to OH radical. OH radical is consumed by the reaction with ozone or organic compounds (RH) in the solution. In the former case, HO_2 or O_2^- is produced via the formation of HO_4. In the latter case, organic peroxide (ROO) is formed by the addition of oxygen to R radical. For some organic compounds, ROO decompose to produce O_2^- or HO_2. Then, HO_2 or O_2^- is used to reproduce OH radical via reaction with ozone.

Termination step. The above sequence of reactions is terminated by recombining of the radicals to produce stable products.

80 reactions and 22 molecular species including HO_2, HO_3, HO_4, O_3^-, O_2^-, H, e_{aq}^-, H_2O_2, CO_3^{2-} and HCO_3^- were considered in the simulation with a semi-implicit Runge-Kutta method (Watanabe et al., 1989) using a FACOM M-780/20 computer. Some of the main reactions in each step were summarized in Table 1. Reactions (13) and (21) were reported to take place for *t*-butanol aqueous solution (von Piechowski et al., 1992). The initial pH of the sample solution was assumed to be 7 in the simulation.

Table 1 Rate constants for several important reactions

Elementary reaction	Rate constant	Reference
Initiation		
1) $H_2O \sim\!\!\!\!\rightarrow OH$	G = 2.8	1
2) $H_2O \sim\!\!\!\!\rightarrow e_{aq}^-$	G = 2.7	1
3) $O_3 + OH^- \rightarrow O_2^- + HO_2$	70 $M^{-1}s^{-1}$	3
4) $HO_2 \rightleftharpoons H^+ + O_2^-$	pKa = 4.8	2
.....		
Propagation		
5) $O_3 + O_2^- \rightarrow O_3^- + O_2$	1.6 x 10^9 $M^{-1}s^{-1}$	4
6) $O_3^- + H^+ \rightarrow HO_3$	5 x 10^{10} $M^{-1}s^{-1}$	4
7) $HO_3 \rightarrow OH + O_2$	1.1 x 10^5 s^{-1}	5
8) $OH + O_3 \rightarrow HO_4$	3 x 10^9 $M^{-1}s^{-1}$	4
9) $HO_4 \rightarrow O_2 + HO_2$	2.8 x 10^4 s^{-1}	6
.....		
10) $OH + RH \rightarrow H_2O + R$	a	
11) $R + O_2 \rightarrow RO_2$	1.4 x 10^9 $M^{-1}s^{-1}$	7
12) $RO_2 \rightarrow R + O_2^-$	a	
13) $RO_2 + RO_2 \rightarrow 2HO_2$ + products	9 x 10^6 $M^{-1}s^{-1}$	7
Termination		
14) $HO_4 + HO_2 \rightarrow O_3 + O_2 + H_2O$	1 x 10^{10} $M^{-1}s^{-1}$	4
15) $OH + OH \rightarrow H_2O_2$	5 x 10^9 $M^{-1}s^{-1}$	6
16) $HO_2 + HO_2 \rightarrow H_2O_2 + O_2$	2.5 x 10^6 $M^{-1}s^{-1}$	2
17) $O_2^- + O_2^- \rightarrow H_2O_2 + O_2$	5 x 10^7 $M^{-1}s^{-1}$	2
18) $HO_3 + OH \rightarrow H_2O_2 + O_2$	5 x 10^9 $M^{-1}s^{-1}$	6
19) $HO_3 + HO_3 \rightarrow H_2O_2 + 2O_2$	5 x 10^9 $M^{-1}s^{-1}$	6
20) $HO_3 + HO_4 \rightarrow H_2O_2 + O_3 + O_2$	5 x 10^9 $M^{-1}s^{-1}$	6
21) $RO_2 + RO_2 \rightarrow$ products	1.7 x 10^8 $M^{-1}s^{-1}$	7
.....		

a: depending on compounds.

[1] O'Donnel H. and Sangster D.F. (1970) *Principles of Radiation Chemistry*, Edward Arnold Ltd., London. [2] Spinks J.W.T. and Woods R.J. (1976) *An Introduction to Radiation Chemistry*, 2nd ed., p. 292, John Wiley & Sons, New York. [3] Staehelin J. and Hoigné J. (1982) *Environ. Sci. Technol.*, **16**, 676. [4] Staehelin J. and Hoigné J. (1985) ibid., **19**, 1206. [5] Bühler R.E., Staehelin J. and Hoigné J. (1984) *J. Phys. Chem.*, **88**, 2560. [6] Bühler R.E., Staehelin J. and Hoigné J. (1984) ibid., **88**, 5999. [7] von Piechowski M., Thelon M., Hoigné J. and Bühler R.E. (1992) *Ber. Bunsenges. Phys. Chem.*, **96**, 1448.

EXPERIMENTAL

Acetic acid or *t*-butanol aqueous solutions were saturated with ozone by introducing ozone-containing oxygen gas from an ozone generator. The ozone-saturated solutions were placed in a quartz cell (inner dimension: 38 mm x 12.5 mm). The cell was covered with a thin polymer film and immediately irradiated with 3 MeV electron spot beams (diameter ca. 50 mm). The depth of water

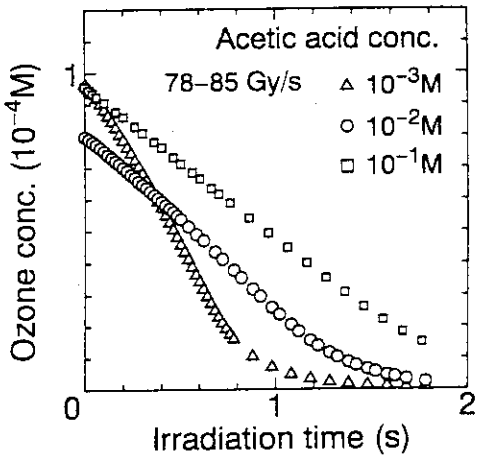


Fig. 1. The changes of ozone concentration in acetic acid aqueous solutions by electron beam irradiation.

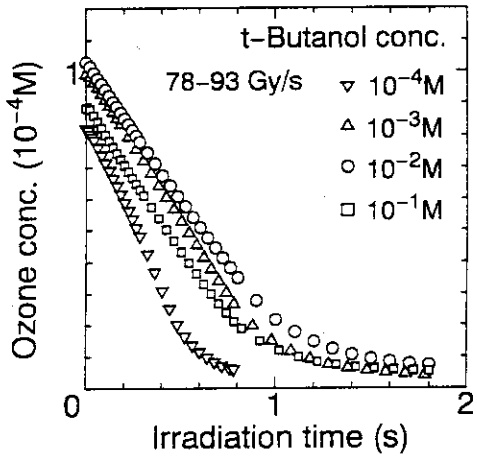


Fig. 2. The changes of ozone concentration in *t*–butanol aqueous solutions by electron beam irradiation.

layer was 12 mm. The ozone concentration in the solution under the irradiation was monitored by measuring the optical density at 260 nm with a spectrometer manufactured by Otsuka Electronics Co. Ltd. in which the light was guided with optical fibers from the cell. The optical densities were converted to the ozone concentration using the molar extinction coefficient of 2900 cm^{-1} (Hoigné and Bader, 1976). The dose was determined with a Fricke dosimeter. The dose rate was 71 – 690 Gy/s.

RESULTS AND DISCUSSION

Ozone decomposition data

Figs. 1 and 2 show the change of the ozone concentration, which was measured directly, by electron beam irradiation for acetic acid and *t*–butanol aqueous solutions, respectively. In the both solutions, the ozone concentration decreased almost linearly at the beginning of the irradiation except for in low concentration. In the low concentration solutions, the ozone concentration decreased more rapidly than linearly.

Simulation for acetic acid aq. solution

The value of 7.5 x 10^7 $M^{-1}s^{-1}$ (Spinks and Woods, 1976) was used as the rate constant for reaction (10) for this system, and the reactions (11) and (21) were assumed to take place similarly as in *t*–butanol system (von Piechowski et al., 1992). Reaction (13) was assumed not to occur.

In Fig. 3, the ozone concentrations calculated by the above reaction scheme are shown with dotted lines for 10^{-2} M aq. solution at the dose rate of 85 Gy/s together with the observed data. The calculated data are in fair agreement with the observed data. Similar agreement was also obtained at the dose rate of 270 and 690 Gy/s for the same concentration. For the concentration of

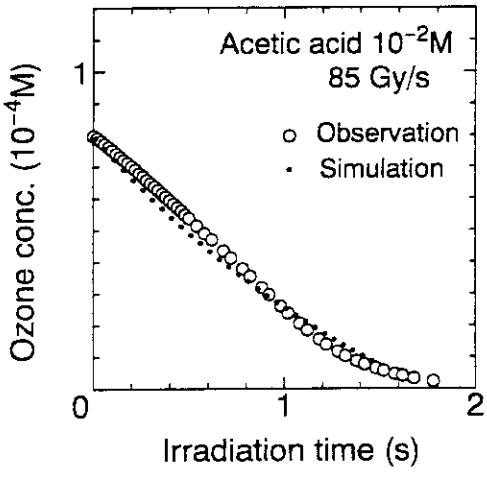


Fig. 3. Comparison of the calculated ozone concentration with the observed data for 10^{-2} M acetic acid aqueous solution irradiated by electron beams.

10^{-1} M, the calculated data were somewhat larger than the observed data. On the contrary, when the acetic acid concentration is as low as 10^{-3} M, the calculated data (the curve of Sim.1) are much smaller than the observed data as shown in Fig. 4. In order to know the reason for this large discrepancy, the presence of HCO_3^- and CO_3^{2-} in the solution were considered in the simulation. The curves of Sim.2, 3 and 4 are the calculated data when the scavenging reactions toward OH radical by these ions were considered and correspond to the HCO_3^- concentration of 10^{-3} M and 10^{-2} M and the CO_3^{2-} concentration of 10^{-3}M, respectively. The HCO_3^- and CO_3^{2-} ions were revealed to change the ozone decomposition substantially.

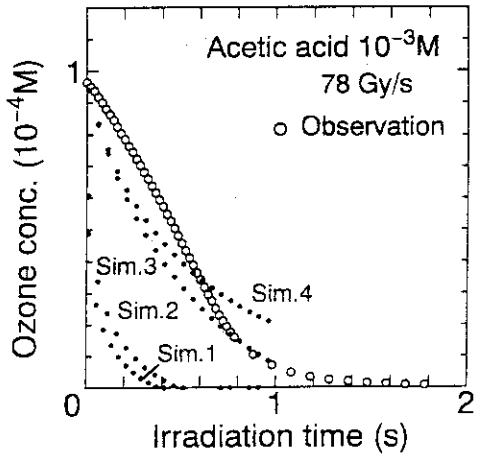


Fig. 4. Comparison of the calculated ozone concentration with the observed data for 10^{-3} M acetic acid aqueous solution irradiated by electron beams.

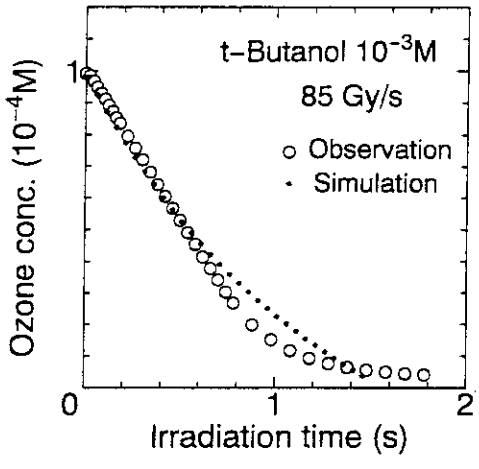


Fig. 5. Comparison of the calculated ozone concentration with the observed data for 10^{-3} M *t*-butanol aqueous solution irradiated by electron beams.

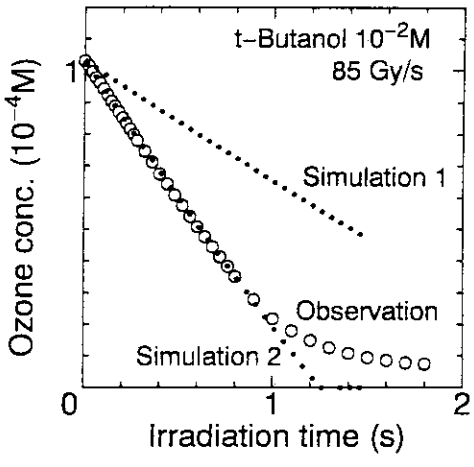


Fig. 6. Comparison of the calculated ozone concentration with the observed data for 10^{-2} M *t*-butanol aqueous solution irradiated by electron beams.

Simulation for t-butanol aq. solution

For this system, a fair agreement was obtained between the calculated data and the observed data for 10^{-3} M concentration at the dose rate of 85 Gy/s as shown in Fig. 5. However, when the *t*-butanol concentration is as high as 10^{-2} and 10^{-1} M, the calculated data are fairly larger than the observed data (the curve of Sim.1) as shown in Fig. 6. In the above reaction model, only the decomposition of peroxide due to reaction (13) was assumed, but some organic peroxides decompose to HO_2 or O_2^- (Ilan et al., 1976). If the next reaction is assumed to occur, the calculated data are in fair agreement with the observed data as shown by the curve of Sim.2 in Fig.6.

$$ROO \rightarrow R' + HO_2 \text{ or } O_2^-, \qquad k = 65\ s^{-1}$$

On the contrary, when the *t*-butanol concentration is 10^{-4} M, the calculated data were also much smaller than the observed data just as for acetic acid system. In this case, if HCO_3^- and CO_3^{2-} were considered, the calculated data became closer to the observed data.

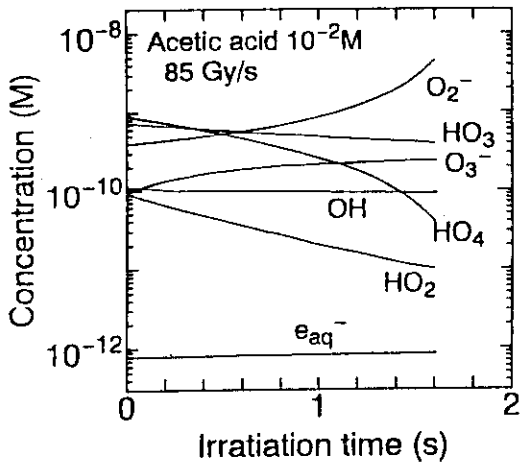


Fig. 7. The calculated concentrations of active species during the electron beam irradiation for 10^{-2} M acetic acid aqueous solution.

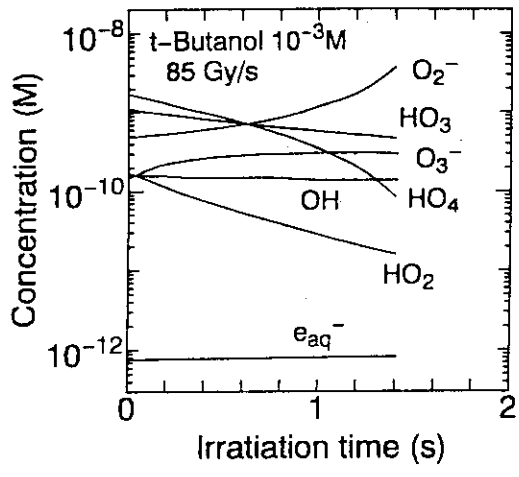


Fig.8. The calculated concentrations of active species during the electron beam for 10^{-3} M *t*–butanol aqueous solution.

Calculated concentrations of active species

The concentrations on the relevant molecular species during the irradiation were also estimated from the simulation. In Figs. 7 and 8, the data for OH, e_{aq}^-, HO_2, HO_3, HO_4, O_2^- and O_3^- are shown for acetic acid and *t*–butanol systems under the same conditions as Figs. 3 and 5, respectively. According to the calculation, the concentrations of OH, e_{aq}^- and O_3^- attain steady state concentrations immediately after starting of the irradiation. The O_2^- concentration increases gradually with irradiation time, but the HO_2 concentration decreases steadily.

CONCLUSION

From this study, it was confirmed that the modified SBH model explain well the ozone decomposition in water in the presence of acetic acid by electron beam irradiation. In the low acetic acid concentration, the presence of HCO_3^- and CO_3^{2-} disturbs the ozone decomposition substantially. For *t*–butanol high concentration aqueous solution, the calculated data became closer to the observed data when the decomposition of peroxide was assumed to occur to produce HO_2 or O_2^-. The concentrations of active species such as OH radicals during the irradiation were also estimated from the simulation.

REFERENCES

Arai H., Arai M. and Sakumoto A. (1986) *Water Res.*, **20**, 885.
Hoigné J. and Bader, H. (1976) *Water Res.*, **10**, 377.
Ilan Y., Rabani J. and Henglein A. (1976) *J. Phys. Chem.*, **80**, 1558.
Sakumoto A. and Miyata T. (1984) *Radiat. Phys. Chem.*, **24**, 99.
Staehelin J. and Hoigné J. (1985) *Environ. Sci. Technol.*, **19**, 1206.
Watanabe T. et al. (1989) *Softwares for Numerical Simulation by Fortran77*, pp.182–189, Maruzen, Tokyo (in Japanese).

5.5 The Model of Initial Intratrack Chemical Processes of Water Radiolysis

M. Domae[1], Y. Katsumura[1], K. Ishigure[1] and V. M. Byakov[2]

[1] Department of Quantum Engineering and Systems Science, Faculty of Engineering, University of Tokyo, 7-3-1 Hongo, Bunkyo-ku, Tokyo 113, Japan

[2] Institute for Theoretical and Experimental Physics, B. Tcheremushkinskaya, 91, Moscow, 117259, Russia

Abstract A new spur model of water radiolysis is proposed by extending the spur diffusion model to sub-picosecond time region. In this model, H_2 formation is attributed to the result of reaction of quasi-free electron with H_2O^+, from positronium formation data. This model explains the experimental decrease in $G^0(e_{aq}^-)$ and $G(H_2)$ in the presence of NO_3^- by taking into account the reaction of quasi-free electron with NO_3^-. The calculated results of radiolysis of nitrate solutions are compared with experimental results.

INTRODUCTION

At present spur diffusion model (Schwarz, 1969; Kuppermann, 1967) is known as a powerful tool to explain the experimental results of radiolysis of aqueous solutions: especially dependence of yields of each species on solute concentration and LET. However, this model hardly explains the following facts: (i) decrease in initial yield of hydrated electron in the presence of special solutes (Wolff et al., 1970; Jonah et al., 1977), (ii) significant decrease in $G(H_2)$ in the presence of some kinds of solutes such as NO_3^-, CrO_4^{2-} (Peled et al. 1970). Thus, more general spur model is necessary. Additional knowledge on hydration time of electron and life of hole (H_2O^+) observed by laser photolysis is available (Gauduel et al. 1991; Long et al. 1990). Therefore, it seems possible to modify the conventional spur diffusion model. In this study, a new spur model of radiolysis of aqueous solution is proposed by extending the conventional spur diffusion model to sub-picosecond time region.

after the incidence of radiation. Hole (H_2O^+) recombines with e^- or reacts with water molecule. Excited water molecule (H_2O^*) formed by recombination of H_2O^+ with e^- decomposes into H + OH, H_2 + 2OH or H_2O. The coefficients of decomposition channels are selected by fitting (see below). Most of e^- which escape recombination will be hydrated. In the presence of solute, it is possible that e^- and/or H_2O^+ react with the solute. The former is the cause of decrease in $G(H_2)$ in the presence of solute.

The value of 3.3×10^{12} s^{-1} is used as k_{hyd}, which seems the mean value of hydration time of electron evaluated by laser photolysis. It is also reported that the life of H_2O^+ is less than 100 fs (Long et al. 1990); k_{imr} is more than 1.8×10^{11} M^{-1} s^{-1}. This lower limit is used as k_{imr}. Some researchers think that diffusion is not necessary for the reaction of H_2O^+; H_2O^+ reacts with adjacent molecule. It is an approximation to introduce second order rate constant for ion-molecule and recombination reaction in this model. Other parameters $r^0(H_2O^+)$, $r^0(e^-)$, $D(H_2O^+)$, $D(e^-)$, and k_{eh} are determined by fitting (see below).

The sub-picosecond simulation begins with the initial condition at 1×10^{-15} s, and is terminated at 5×10^{-12} s, when initial species H_2O^+ and e^- are almost annihilated. The initial conditions are following: (i) $G(H_2O^+) = G(e^-)$, (ii) the distribution of H_2O^+ and e^-(Gaussian is assumed), (iii) radii of H_2O^+ and e^-. After the sub-picosecond simulation, calculated results are substituted for the initial condition of the conventional spur diffusion model. Finally, we obtain the primary yield (at 1×10^{-6} s) of each species.

RESULTS and DISCUSSION

First the combination of diffusion coefficients ($D(H_2O^+)$ and $D(e^-)$) and initial radii ($r^0(H_2O^+)$ and $r^0(e^-)$) was selected so that the distribution of H_2O^+ and e^- at 1×10^{-12} s(or 5×10^{-12} s) without reactions almost coincides with that of OH and e_{aq}^- used in the conventional spur diffusion model, respectively. The reason for this procedure is following. Hydrated electron and most of OH are formed from e^- and H_2O^+, respectively. Hydrated electron and OH formed hardly move in sub-picosecond time region due to their small diffusion coefficients. Thus, the distribution of e^- and H_2O^+ at 1×10^{-12} s without reactions nearly indicates that of

MODEL

There are clear correlations between decrease in positronium formation yield I_3, primary yield of hydrogen molecule and initial yield of hydrated electron, in the presence of solutes (Byakov et al. 1986). The results of picosecond pulse radiolysis of aqueous solutions strongly suggest the reaction of solute with the precursor of hydrated electron, e^-, which we call quasi-free electron. We do not classify the electrons by their energy for simplification. It is known that e^- is one of positronium precursors. Therefore, it is considered that positronium, hydrogen molecule and hydrated electron have common precursor, e^-. However, it is assumed that some parts of hydrogen molecule are formed in the time region of 10^{-12}-10^{-6} s through the following spur reactions,

$$e_{aq}^- + e_{aq}^- \rightarrow H_2 + 2OH^- \quad (1)$$

$$e_{aq}^- + H \rightarrow H_2 + OH^- \quad (2)$$

$$H + H \rightarrow H_2 \quad (3)$$

since the conventional spur diffusion model is available for many systems, especially in the case of low solute concentration. The new spur model shown in Fig. 1 is considered. Ionization of water molecule occurs within 1×10^{-15} s

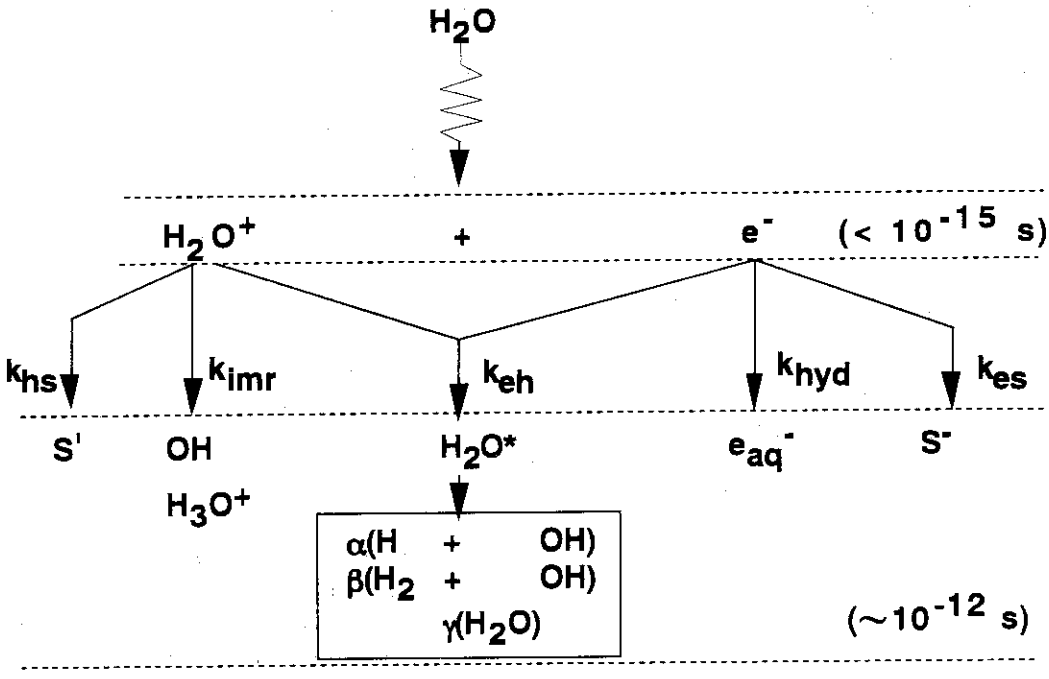


Fig. 1 The scheme in sub-picosecond time region in radiolysis of water.

e_{aq}^- and OH, respectively. The value of k_{eh} is determined so that $G(H_2O^*) = 1.2$ at 5×10^{-12} s is induced. Furthermore, the coefficients α, β and γ are determined so that $G(H_2) = 0.11$ and $G(OH) = 5.7$. This value corresponds to the initial yield of H_2 in the conventional spur diffusion model. The validity of these parameters are tested by calculating primary yield of each species in pure water (Fig. 2). Calculated primary yields are in good agreement with experimental results. Parameters employed in this calculation are listed in Table 1. Then, we calculate decrease in $G(e_{aq}^-)$ at 30 ps in the presence of NO_3^- with the same parameters, in order to

Table 1 Parameters used in the calculation

Energy to produce a spur	62.5 eV	
G value	$G(H_2O^+) = G(e^-) = 6.3$	
Diffusion coefficient	$D(H_2O^+) = 1.0\times10^{-3}$ cm^{2}s^{-1}	$D(e^-) = 1.0\times10^{-1}$ cm^{2}s^{-1}
Initial radius	$r^0(H_2O^+) = 0.75$ nm	$r^0(e^-) = 0.75$ nm
Rate constant	$k_{eh} = 2.4\times10^{13}$ M^{-1}s^{-1}	$k_{imr} = 1.8\times10^{11}$ M^{-1}s^{-1}
	$k_{hyd} = 3.3\times10^{12}$ s^{-1}	$k_{es} = 1.0\times10^{13}$ M^{-1}s^{-1}

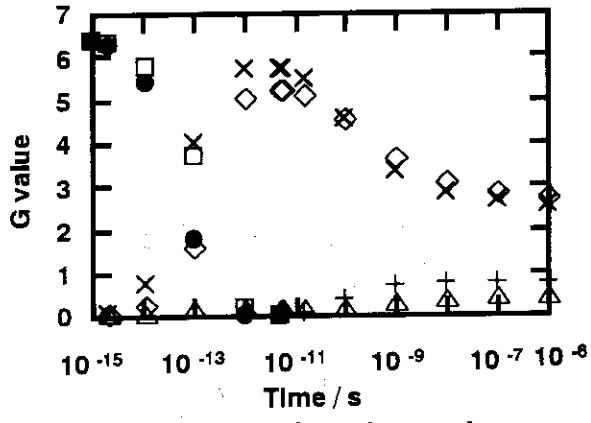


Fig. 2 G value of each species as a function of time:
(□) e^-, (●) H_2O^+, (◇) e_{aq}^-, (×) OH, (+) H_2O_2, (△) H_2.

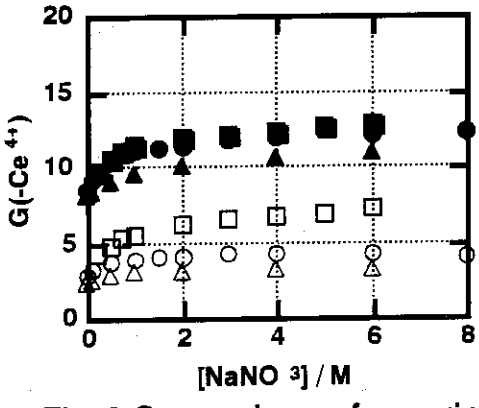


Fig. 3 Comparison of experimental and calculated G(-Ce4+) depending on [NaNO3]:
(open) in the absence of Tl^+,
(closed) in the presence of Tl^+,
(square) experimental,
(circle) calculated by new model,
(triangle) calculated by conventional model.

determine the rate constant of reaction of NO_3^- with e^- (Table 1). With this rate

constant decrease in primary yield of hydrogen molecule in the presence of NO_3^- are calculated; results agree rather well with experimental data.

Finally, we calculated G(-Ce^{4+}) in nitric acid and sodium nitrate solutions containing 0.4 M sulfuric acid using parameters determined by above procedure. The redox reactions of Ce^{3+} and Ce^{4+} with decomposition products of water are well known, and reactions of these ions with nitrogen compounds are described elsewhere (Nagaishi et al. 1994). Results calculated by the new and conventional model in sodium nitrate system containing 0.4 M sulfuric acid are shown in Fig. 3 with the experimental data. In Fig. 3, each calculated point contains the contribution of direct effect of radiation on solute (Jiang et al. 1994). The conventional model cannot explain the drastic increase in G(-Ce^{4+}) in low concentration of NO_3^-. By contrast, the new model reproduces the increase in G(-Ce^{4+}). Thus, this increase in G(-Ce^{4+}) is considered due to reaction of e^- with NO_3^-. However, the experimental values are still larger than calculated ones, probably because the actual initial G value of water decomposition is larger than 6.3 as pointed out by Nagaishi et al. (Nagaishi et al. 1994).

REFERENCES

Byakov V. M. and Grafutin V. I. (1986) *Radiat. Phys. Chem.* **28**, 1.

Gauduel Y., Pommeret S., Migus A. and Antonetti A. (1991) *J. Phys. Chem.* **95**, 533.

Jiang P. Y., Nagaishi R., Yotsuyanagi T., Katsumura Y. and Ishigure K. (1994) *J. Chem. Soc. Faraday Trans.* **90**, 93.

Jonah C. D., Miller J. R. and Matheson M. S. (1977) *J. Phys. Chem.* **81**, 1618.

Kuppermann A., In *Radiat. Res., Proc. 3rd Int. Congr.* June-July 1966(Edited by Silini G.), pp. 212-234. North Holland, Amsterdam, 1967.

Long F. H., Lu H. and Eisenthal K. B. (1990) *Phys. Rev. Lett.* **64**, 1469.

Nagaishi R., Jiang P. Y., Katsumura Y., Ishigure K. (1994) *J. Chem. Soc. Faraday Trans.* **90**, 591.

Peled E. and Czapski G (1970) *J. Phys. Chem.* **74**, 2903.

Schwarz H. A. (1969) *J. Phys. Chem.* **73**, 1928.

Wolff R. K., Bronskill M. J. and Hunt J. W. (1970) *J. Chem. Phys.* **53**, 4211.

5.6 Radiolysis of Concentrated Nitric Acid Solutions

R. Nagaishi, P.Y. Jiang, Y.Katsumura, M.Domae and K.Ishigure

Department of Quantum Engineering and Systems Science,
Faculty of Engineering, The University of Tokyo
Hongo 7-3-1, Bunkyo-ku, Tokyo 113, Japan

Abstract A study on electron pulse- and ^{60}Co γ-radiolysis of concentrated nitric acid and nitrate solutions has been carried out to elucidate the radiation induced reactions taking place in the solutions. Dissociation into NO_2 and $O(^3P)$ was proposed as a direct action of the radiation on nitrate and gave the G-values were dependent on the chemical forms of nitrate: $g_{S2}(-NO_3^-)=1.6$ and $g_{S2}(-HNO_3)=2.2$ (molecules/100eV). Based on the experimental yields of HNO_2 and reduced Ce^{IV}, the primary yields of radiolysis products of water, g_W, were evaluated to clarify the effects of nitrate on spur reactions of water in various nitrate solutions.

INTRODUCTION

While the understanding of the radiolysis of diluted aqueous solutions was well established, that of concentrated solutions is far from complete. Because the solute as well as water can absorb the energy of radiation in the solutions and intermediates are directly formed from the solute (direct action), which react with the radiolysis products of water(indirect action) leading the reaction scheme in the solutions to be complicated. We have been studying the radiolysis of concentrated acid solutions to understand and predict the radiation induced reactions taking place in the solutions.

In the present experiment, the radiolysis of concentrated nitric acid and nitrate solutions has been studied and reported[1-3], which is practically related to the radiation effects in the nuclear spent fuel reprocessing. NO_3 radical was observed using the pulse radiolysis method with electron pulses and yields of HNO_2 formed and Ce^{IV} reduced in γ-radiolysis were obtained. On the basis of the experimental results, the radiolytic processes of nitrate were proposed together with the yields and the radiation induced reactions were discussed quantitatively.

EXPERIMENTAL

Electron pulses of 100 ns and 28 MeV from a linear accelerator at Nuclear Engineering Research Laboratory and γ-ray from 3kCi ^{60}Co at Rearch Center for Nuclear Science and Technology, University of Tokyo, were used.

Details of the pulse radiolysis system have been described elsewhere.[1] The absorbance of NO_3 radical was followed at 640 nm, where the spectrum of NO_3 have a peak($\varepsilon=1300\pm100$ $M^{-1}cm^{-1}$). For the dosimetry, a 10 mM KSCN aqueous solution saturated with N_2O was used with G=6.1 (molecules/100eV) and $\varepsilon(472nm)=7580$ $M^{-1}cm^{-1}$ for the radical anion $(SCN)_2^-$.

Ar-purged nitric acid solutions were irradiated by γ-ray with the dose rate of 1.4 $Gy\cdot s^{-1}$ to determine the yields of HNO_2 formed as the final product, and aerated nitrate solutions containing Ce^{IV} ion irradiated with 0.02-0.14 $Gy\cdot s^{-1}$ to determine yields of reduced Ce^{IV}. HNO_2 was determined using Shinn's method with some modification with the

ε(543nm)=53400 $M^{-1}cm^{-1}$ as estimated in this study.[2] The absorption coefficients of Ce^{IV} in various nitrate solutions were also estimated.[3] For the dosimetry, the Fricke dosimeter was used with G=15.5 and ε(304nm)=2164 $M^{-1}cm^{-1}$ for Fe^{3+}.

All experiments were carried out at room temperature(around 20 °C) unless otherwise stated. The energy deposition was assumed to be proportional to the electron density of the solutions and was corrected accordingly.

RESULTS AND DISCUSSION

Expression of observed G-value

When a species P is formed in the radiolysis of concentrated nitrate solutions, the yield of P, G(P), can be expressed as a function of electron fraction of nitrate(f_S) as a solute :

$$G(P) = g_W \cdot f_W + g_S \cdot f_S \qquad ; f_W + f_S = 1 \quad . \qquad (I)$$

, where g_W and g_S are the yields of radiolysis products originated from nitrate(ion form NO_3^- and acid form HNO_3) and water, respectively, which form P after escaping from spurs. f_S is given by $f_S=[SN_S/M_S]/[SN_S/M_S+ (1-S)N_W/M_W]$, where S is the wt.% of nitrate, N_S(=32) and N_W(=10) are the molecular numbers of nitrate and water, and M_S and M_W the molecular weights of nitrate and water, respectively. The energy of radiation was assumed to be absorbed not by only valence electrons but by all valence and inner-sphere electrons.

Radiolytic processes of nitrate

NO_3 radical has been observed as an intermediates from nitrate, which has characteristic peaks at 600, 640, and 675 nm in its spectrum.[1] It was found in the pulse-radiolysis experiments that NO_3 was formed through a dissociation of nitrate(fast process)(1) and the reaction of undissociated HNO_3 with OH radical(slow process)(2) :

$$NO_3^- \rightsquigarrow NO_3 + e_{aq}^- \qquad (1)$$

$$OH + HNO_3 \rightarrow H_2O + NO_3 \qquad ; k = 1.4 \times 10^8\ M^{-1}s^{-1} \quad . \qquad (2)$$

Fig.1 shows the experimental yields of NO_3, $G(NO_3)$, against f_S. The fast process was independent of chemical forms of nitrate and gave a relation of $g_{S1}(NO_3)=g_{S1}(e_{aq}^-)=g_{S1}(-NO_3^-)=g_{S1}(-HNO_3)=4.8$ (molecules/100eV).

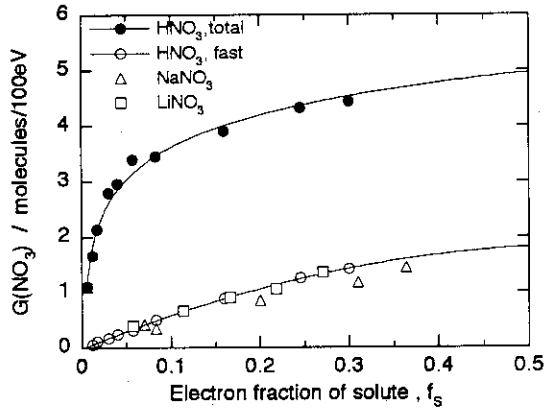


Figure 1 Dependence of $G(NO_3)$ on nitric Acid and nitrate concentrations.

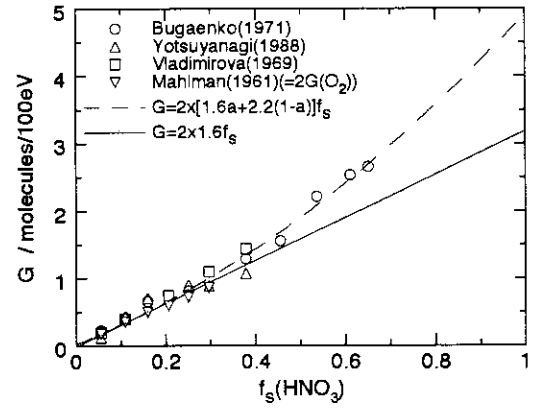


Figure 2 G-values of HNO_2 and O_2 in nitric acd solutions.
a : dissociation degree of nitric acid

HNO_2 and O_2 are formed as final products in γ-radiolysis of concentrated nitrate solutions. The experimental yields of HNO_2 and O_2 have been reported by us and the other groups as shown in Fig.2.[2] There are not any contributions of water radiolysis and the fast process of NO_3 (1), [2] suggesting the existence of other radiolysis process(es) leading to the formation of HNO_2 and O_2. Since at $f_S<0.4$ in Fig.2, the ratio of $G(HNO_2)/G(O_2)$ was 2 as reported by Mahlman[5], the following dissociation and reaction were proposed :

$$NO_3^- \rightsquigarrow NO_2^- + O\ (^3P) \qquad (3)$$

$$O(^3P) + NO_3^- \rightarrow O_2 + NO_2^- \qquad (4)$$

The formed $O(^3P)$ can react with NO_3^- but not with water. The dissociation of nitrate into NO_2 and $O^-(OH)$ as the other radiolysis process was not taken into account in the present work because of no formation of HNO_2 and O_2. Also Fig.2 shows that the experimental $G(HNO_2)(=2f_S \cdot g_{S2}(NO_2^-))$ did not increase linearly with f_S at $f_S>0.4$, suggesting that the dissociation was dependent on the forms of nitrate. g_{S2} could be expressed by the dissociation degree of nitric acid, α.

$$g_{S2}(NO_2^-) = g_{S2}(O) = \alpha \cdot g_{S2}(-NO_3^-) + (1-\alpha) \cdot g_{S2}(-HNO_3) \qquad (II)$$

$g_{S2}(-NO_3^-)=1.6$ (molecules/100eV) was evaluated from $G(HNO_2)$ at $f_S<0.4$ and $g_{S2}(-HNO_3)=2.2$ at $f_S> 0.4$.

Radiolytic reduction of Ce^{IV}

Since NO_3^- is well known to be a strong scavenger of pre-hydrated(e_p^-) and hydrated (e_{aq}^-) electrons, the primary yields of water radiolysis may change with nitrate concentration.

$$e_p^- / e_{aq}^- + NO_3^- + H_2O \rightarrow NO_2 + 2OH^- \rightarrow 1/2\ HNO_2 \qquad (5)$$

In order to understand the effects of nitrate on the primary yields of the radiolysis products of water, aerated 0.4 M sulfuric acid with nitric acid or sodium nitrate solutions containing cerium ion were irradiated and analysed for the yield of Ce^{IV}. Fig.3(a) shows the yields of reduced Ce^{IV}, $G(-Ce^{IV})$, in the absence(G_1) and presence(G_2) of Tl^+. [3]

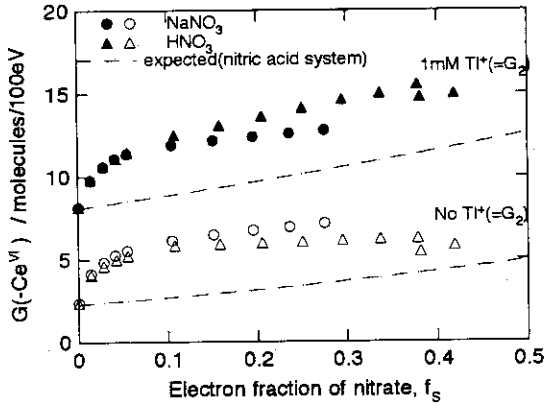


Figure 3(a) The yield of Ce^{IV} reduced in 0.4M H_2SO_4

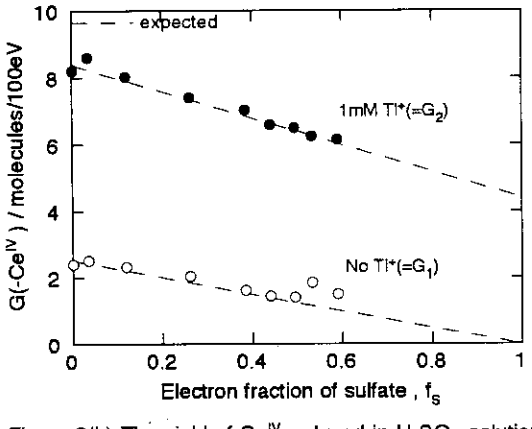


Figure 3(b) The yield of Ce^{IV} reduced in H_2SO_4 solutions

In the radiolysis, the redox of cerium ions with the radiolysis products of water and nitrate could occur as follows :

$$Ce^{IV} \underset{OH,\ NO_3(\text{with}(\rightarrow)\ \text{and without}(\leftarrow)\ Tl^+)}{\overset{e_{aq}^-,\ H,\ H_2O_2/2,\ HNO_2/2}{\rightleftharpoons}} Ce^{III} \qquad (6)$$

Consequently, the $G(-Ce^{IV})$, could be expressed using the yields of the radiolysis products :

$$G_1(-Ce^{IV}) = f_W\cdot[g_W(e_{aq}^-+H) - g_W(OH) + 2g_W(H_2O_2)] + f_S\cdot[g_{S1}(e_{aq}^-) - g_{S1}(NO_3)] + 4f_S\cdot[\alpha\cdot g_{S2}(-NO_3^-) + (1-\alpha)\cdot g_{S2}(-HNO_3)] \qquad (III)$$

$$G_2(-Ce^{IV}) = f_W\cdot[g_W(e_{aq}^-+H) + g_W(OH) + 2g_W(H_2O_2)] + f_S\cdot[g_{S1}(e_{aq}^-) + g_{S1}(NO_3)] + 4f_S\cdot[\alpha\cdot g_{S2}(-NO_3^-) + (1-\alpha)\cdot g_{S2}(-HNO_3)] \qquad (IV)$$

When the primary yields of radiolysis products of water in 0.4M sulfuric acid were used as g_W in eqn.(III) and (IV), G_1 and G_2 could be expected, plots of which are shown as dotted lines(nitric acid) in Fig.3(a). However, the lines did not agree with the experimental $G(-Ce^{IV})$.

On the other hand, $G(-Ce^{IV})$ in sulfuric acid solutios agreed well with the expected lines as shown in Fig.3(b), where the dissociation into SO_4^- and e_{aq}^- only takes place as the radiolysis of sulfate.[4] These results suggests that NO_3^- and HNO_3 have influences on the spur reactions of water and that the respective g_W vary with the concentration of nitrate.

The primary yields of radiolysis products of water

The respective g_W of $-H_2O$, e_{aq}^-+H, OH, and H_2O_2 can be evaluated from the material balance(V) and the experimental yields of g_{S1}, g_{S2}, G_1 and G_2 in the following equations : [3]

$$g_W(-H_2O) = g_W(e_{aq}^-+H) + 2g_W(H_2) = g_W(OH) + 2g_W(H_2O_2) \qquad (V)$$

$$g_W(OH) = \{[G_2(-Ce^{IV}) - G_1(-Ce^{IV})]/2 - f_S\cdot g_{S1}(NO_3)\}/f_W \qquad (VI)$$

$$g_W(-H_2O) = \{G_2(-Ce^{IV}) + 2G(H_2) - 2f_S\cdot g_{S1}(NO_3) - 4f_S\cdot[\alpha\cdot g_{S2}(-NO_3^-) + (1-\alpha)\cdot g_{S2}(-HNO_3)]\}/(2f_W) \qquad (VII)$$

$$g_W(e_{aq}^-+H) = g_W(-H_2O) - 2g_W(H_2) \qquad (VIII)$$

$$g_W(H_2O_2) = [g_W(-H_2O) - g_W(OH)]/2 \qquad (IX)$$

, where $g_W(H_2)$ is obtained from $G(H_2)$ $(=g_W(H_2)\cdot f_S)$ reported by Mahlman.[5] Fig.4 shows the g_W in 0.4M sulfuric acid with nitric acid(a) and sodium nitrate(b).

In both the nitric acid and sodium nitrate systems, the $g_W(-H_2O)$ and $g_W(e_{aq}^-+H)$ concurrently increase with the concentration of nitrate, while the $g_W(H_2)$ decreases. It indicates clearly that the electron scavenging of NO_3^- in spurs suppresses recombinations between e_{aq}^- and OH into water and H_2 formation from the reaction of a pair of e_{aq}^-. Furthermore, the $g_W(-H_2O)$ at higher f_S is larger than the recommended initial yield of water decomposition(=5.7), suggesting the yield larger than 5.7 in concentrated nitrate solutions just after water

decomposition by radiation.

Consequently, the yields of OH escaping from spurs and H_2O_2 formed from a pair of OH would be expected to increase. However, the tendency of the $g_W(OH)$ and $g_W(H_2O_2)$ in the nitric acid system are different from those in the sodium nitrate system. Because not only NO_3^- but also HNO_3 exsists in the nitric acid system, the OH scavenging of HNO_3 suppresses the H_2O_2 formation. Therefore, the $g_W(OH)$ increases and the $g_W(H_2O_2)$ does not vary in the nitric acid system, while the $g_W(OH)$ decreases and the $g_W(H_2O_2)$ increases in the sodium nitrate system.

Also the yield of O_2, $G(O_2)$, in nitrate solutions in the absence(X) and the presence(XI) of Ce^{IV} can be evaluated:

$$G(O_2) = f_S \cdot g_{S2}(O) \qquad (X)$$

$$G(O_2) = f_W \cdot g_W(H_2O_2) + f_S \cdot g_{S2}(O) = [G_1(-Ce^{IV}) + 2f_W \cdot g_W(H_2)]/4 \qquad (XI)$$

$G(O_2)$ evaluated in 0.4M sulfuric acid with Ce^{IV}-sodium nitrate is found to increase with f_S and agree well with that reported by Mahlman.[5]

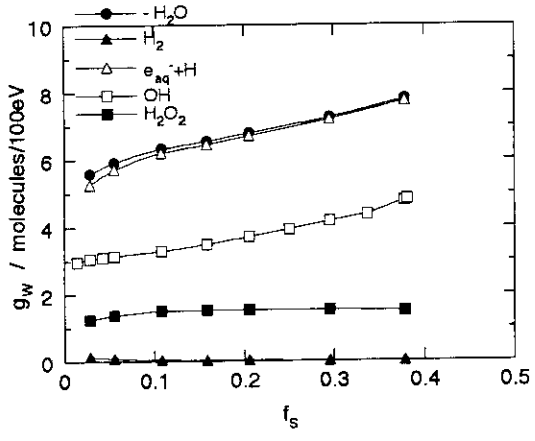


Figure 4(a) The primary yields of water radiolysis in 0.4M sulfuric acid solution with nitric acid

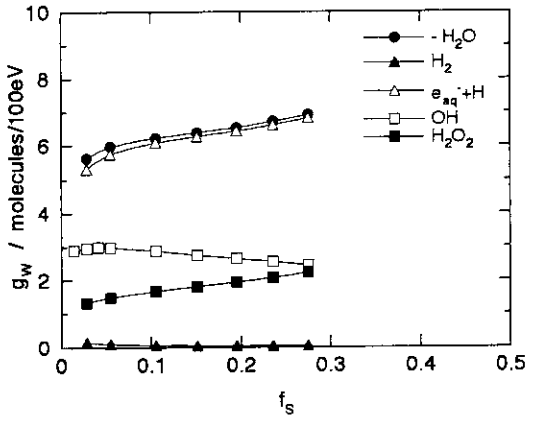


Figure 4(b) The primary yields of water radiolysis in 0.4M sulfuric acid solution with sodium nitrate

REFERENCES

1 Y.Katsumura, P.Y.Jiang, R.Nagaishi, T.Oishi, K.Ishigure and Y.Yoshida, *J.Phys.Chem.*,1991,**95**,4435-4439.

2 P.Y.Jiang, R.Nagaishi, T.Yotsuyanagi, Y.Katsumura and K.Ishigure, *J.Chem.Soc. Faraday Trans.*,1994, **90**(1),93-95.

3 R.Nagaishi, P.Y.Jiang, Y.Katsumura and K.Ishigure, *J.Chem.Soc. Faraday Trans.*, 1994, **90**(4),591-595.

4 P.Y.Jiang, Y.Katsumura, R.Nagaishi, M.Domae,K.Ishikawa, K.Ishigure and Y.Yoshida, *J.Chem.Soc. Faraday Trans.*,1992,**88**,1653-1658.

5 H.A.Mahlman, *J.Chem.Phys.*,1961,**35**,936.

5.7 Radiolysis of Water at Elevated Temperatures with γ-rays and Fast Neutrons

Y. Katsumura, G. R. Sunaryo, D. Hiroishi and K. Ishigure

Department of Quantum Engineering and Systems Science,
Faculty of Engineering, The University of Tokyo
Hongo 7-3-1, Bunkyo-ku, Tokyo 113 Japan

Determination of G-values of water decomposition products in neutral water produced by irradiation with gamma-rays and fast neutrons at elevated temperatures up to 250°C was carried out by a combination of $NaNO_2$, acetone + methanol, and $HClO_4$ + methanol solutions. In the gamma-radiolysis, the G-values obtained in the present experiment are in good agreement with recently reported ones except G_{OH} and G_{H2O2}. In the fast neutron radiolysis, although a similar change of the G-values with temperature was observed, the higher molecular yields of G_{H2} and G_{H2O2} and lower radical ones of G_H and, especially, $G_{e\text{-}aq}$ were determined. It was made clear that the LET effect still remains even at elevated temperatures. It suggests that the spur size would expand at higher temperatures and the fraction of the intraspur reactions decreases. Furthermore, in order to clarify the characteristics of the determined G-values, computer simulations under the simplified conditions in nuclear reactors have been carried out. The G-values for fast neutron radiolysis give a significant influence to the result. It was pointed out by the simulations that reverse reactions for $H_2 + OH \rightarrow H + H_2O$ and $e^-_{aq} + H^+ \rightarrow H$, which can be neglected at room temperature, become important at higher temperatures.

Introduction

The radiolysis of water at elevated temperature is practically important from the view point of the quality control of the coolant in the nuclear power reactors, where the chemical condition of the coolant is predominantly controlled by the radiolysis of water not only with γ rays but also with fast neutrons up to 300°C. Quality control of the coolant is highly required in order to avoid radiation accumulation of the primary circuits and to keep integrity of the reactor operation. The temperature dependence of the G-values of water decomposition and the change of spur structure at elevated temperatures are also interesting from the point of radiation chemistry. Over these ten years much work has been made and several sets of G-values for water decomposition at high temperatures have been determined and reported in γ radiolysis of acid and neutral aqueous solutions (Burns, 1981a, b; Elliot *et al.*, 1993; Kabakchi and Lebedeva, 1989; Katsumura *et al.*, 1989, 1992; Kent and Sims, 1992a,b).

In the present experiment, a combination of three kinds of aqueous solutions have been employed to determine the G-value for the decomposition products of neutral water up to 250°C in both γ and fast neutron radiolysis. It was found that there remained a big LET effect of the water decomposition in fast neutron radiolysis not only at room temperature but also at high temperature. The temperature dependencies of water decomposition products indicate that spur size would be expanded with increasing temperature, which was confirmed by an additional experiment. By using the values determined in the present experiment, several computer simulations were made to characterize the values and compared with reported G-values. It was noticed that the dose evaluation in the reactor is inevitably important. It has been revealed that the simulation of the radiation induced reaction at elevated temperature needs much more reliable rate constants for the reactions of $H_2 + OH \rightarrow H + H_2O$ and $e^-_{aq} + H^+ \rightarrow H$, which can be neglected at room temperature.

Experimental

In the present experiment, G-values are expressed in the unit of molecules formed or destroyed per 100 eV energy absorbed. The primary yield of water decomposition is expressed by G with a subscript, such as G_H and $G_{e\text{-}aq}$ and, on the contrary, the yields experimentally determined are expressed by the G-values with brackets, such as $G(H_2)$ and

$G(H_2O_2)$.

Samples:

Three kinds of aqueous solutions were taken: (a) 2mM $NaNO_2$, (b) 1mM acetone + 10mM methanol, and (c) 1mM $HClO_4$ + 10mM methanol solutions. After irradiation, H_2 evolution for all solutions, the formation of H_2O_2 in (a) and the formations of H_2O_2, ethyleneglycol and formaldehyde in (c) were measured. The yields of H_2 evolution is proportional to G_{H2}, $G_{H2} + G_H$ and $G_{H2} + G_H + G_{e\text{-}aq}$ in (a), (b) and (c) solutions, respectively. From the H_2 evolution, the G_{H2}, G_H and $G_{e\text{-}aq}$ are derived and the total water decomposition is also calculated based on the material balance relation. For the separation of G_{OH} and G_{H2O2}, calculations were fitted to the experimental results of the yields for H_2O_2 (a) and H_2O_2, ethyleneglycol and formaldehyde obtained in solutions of (c), respectively. Thermal stability of the solutes and products were checked by an independent experiment. All the solutes except proton are stable up to 250°C and the proton concentration is decreasing at elevated temperatures probably due to the exchange reaction of the proton with ampoule surface. The ethyleneglycol is slowly decomposed into formaldehyde by first order at 250°C. It is known that H_2O_2 is decomposed into $H_2O + O_2/2$ at elevated temperatures and, in fact, the H_2O_2 was not detected at elevated temperatures. These were taken into consideration for the simulation.

Irradiations:

Sample solutions were prepared using the ultra pure water provided through a Millipore equipment and sealed into glass ampoules with a breakable seal under Ar atmosphere. The samples were irradiated with γ ray source under the dose rate of 0.5 - 0.25 kGy/hr, which were calibrated by a Fricke dosimeter. Irradiation at elevated temperatures were done with oil bath and in a specially designed pressure vessel. In fast neutron radiolysis, a fast neutron source reactor named "YAYOI" was taken and dose rate was set as 1.9 kGy/hr. More than 95% of the total dose comes from fast neutrons. Concerning the recoil protons, the average LET in the reactor for water was calculated as 6 eV/Å. The dosimetry for the fast neutron radiolysis was reported elsewhere (Katsumura *et al.*, 1989).

Simulations:

Simulations of chemical reactions induced by irradiation were made by using FACSIMILE calculation code developed at Harwell. The reactions and their rate constants at room temperature and elevated temperatures were taken from the references (Buxton *et al.* 1988; Buxton and Elliot, 1989). The rate constants unknown at elevated temperatures were estimated by using the activation energy of 12.6 kJ/mole.

Details of the procedures are reported elsewhere.

Results and Discussion

Room temperature radiolysis:

As a first step, room temperature radiolysis was done. In Fig.1, H_2 evolution as a function of irradiation dose at room temperature is shown. As expected, the yield increases linearly with dose and from the slopes, the values of G_{H2}, G_H and $G_{e\text{-}aq}$ were derived. For the separation of G_{OH} and G_{H2O2}, the calculations were fitted to the experimental results of the yield of H_2O_2 in the $NaNO_2$ solution and H_2O_2, ethyleneglycol and formaldehyde in the $HClO_4$ + methanol solution. Final evaluation of the G-values are summarized in Table together with the established reported values. It is clear that the values of G_{H2}, G_H and $G_{e\text{-}aq}$ evaluated in the present experiment are in excellent agreement with established values. But the values for OH are slightly higher than the expected due to the higher concentration of the OH scavengers, methanol and $NaNO_2$, than recommended (Draganic and Draganic, 1973). The experimental limitations forced us to take higher concentration of methanol and $NaNO_2$, and this affects the spur reactions partially. During the evaluation, the rate constants for the reactions of (1): $2(\bullet CH_2OH) \rightarrow (CH_2OH)_2$, (2): $2(\bullet CH_2OH) \rightarrow CH_2O + CH_3OH$ and (3): $\bullet CH_2OH + H_2O_2 \rightarrow CH_2O + H_2O + \bullet OH$ were determined as 2.25×10^9, 1.5×10^8 and 5×10^4 $M^{-1}s^{-1}$, respectively.

The method was directly applied to the fast neutron radiolysis and the data is also

involved in the Table. Unfortunately, there exists no experimental evaluation of the fast neutron radiolysis and the data was compared with those obtained by ion beam radiolysis. It is surprising that there are a few reports on the radiolysis of neutral water with ion beam in spite of much accumulated data for 0.4M H_2SO_4 solutions (Allen, 1961; LeVerne and Schuler, 1994). The data evaluated in the present study is parallel to the ion beam radiolysis data reported by Appleby and Schwarz (1969). The larger yield of molecular products and smaller yield of radical products, especially for hydrated electron, characterize the fast neutron radiolysis. This is the first experimental evaluation of the fast neutron radiolysis of water.

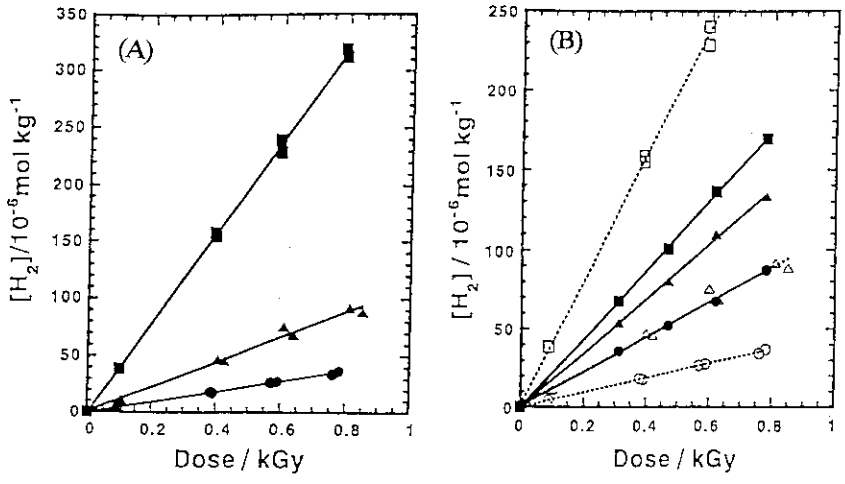


Fig. 1
The H_2 yields produced by irradiation with γ -rays (A) and fast neutrons (B) at 25°C in ● (a) ; ▲ (b) ; and ■ (c) ; solutions (see text).

TABLE: G-values of water decomposition by irradiation with γ -rays, fast neutrons and ion beams at room temperature.

sources		G_{H2}	G_H	$G_{e\text{-}aq}$	G_{OH}	G_{H2O2}	G_{-H2O}
γ rays	present	0.45	0.63	2.75	(3.12)[a,b]	(0.58)[a,b]	4.28
0.023 eV/Å	Elliot *et al.* (1990)	0.45	0.60	2.7	-	-	4.20
	Spinks &Woods (1976)	0.43	0.61	2.7	2.86	0.61	4.14
fast neutrons	present *6eV/Å*	1.07	0.58	0.43	(0.86)[a] (0.70)[b]	(1.14)[a] (1.22)[b]	3.15
	Burns & Moore (1976) [c]	0.88	0.50	0.93	1.09	0.99	3.15
	Gordon *et al.* (1983) [c]	0.85	0.41	0.15	0.37	0.95	2.27
ion beams	Appleby & Schwarz (1969)						
	18MeV D^+ *0.50 eV/Å*	0.68	0.64	1.48	1.66	0.91	3.48
	32MeV He^{2+} *2.3 eV/Å*	0.96	0.42	0.72	1.00	1.00	3.06
	12MeV He^{2+} *4.8 eV/Å*	1.11	0.27	0.42	0.75	1.08	2.91
	Elliot (1992)						
	23MeV D^+ *0.42 eV/Å*	0.57	0.51	1.55	-	0.75	3.2

a: the values derived from $NaNO_2$ solutions
b: the values derived from $HClO_4$ + methanol solutions
c: theoretical estimation d: average LET e: initial LET

High temperature radiolysis:

The method confirmed its validity at room temperature was extended to higher temperature radiolysis. Although the slopes obtained at higher temperatures are different from the data at room temperature, linear increases of the evolution with dose were again observed. On the other hand, the H_2O_2 yields were much smaller at elevated temperatures due to the thermal degradation. The change of the yield of formaldehyde and ethyleneglycol in $HClO_4$ + methanol solution with dose were used as the reference for the simulation. The sum of the rate constants for the reaction of (1) + (2) were assumed to increase with the activation energy of 12.6 kJ/mol and ratio of these rates were varied. The rates of thermal degradation of the H_2O_2 were taken as 9.3×10^{-3} and 0.05 s^{-1} at 200 and 250°C, respectively (Hiroishi and Ishigure, 1989). Among the sets of the rate constants, a certain set which could reproduce

both γ and fast neutron radiolysis data was selected. Finally, The primary yields of G_{H2}, G_H, $G_{e\text{-}aq}$, G_{OH} and G_{H2O2} for γ and fast neutron radiolysis were shown in Figs. 2. All the G-values tend to increase with temperature except OH and H_2O_2. Up to now, there are a few reports on the G-values of water decomposition products at elevated temperatures in neutral pH. The $G_{e\text{-}aq}$ value with temperature was evaluated and reported up to the highest temperature of 300°C. They all increase linearly with temperature and our evaluation gives almost the same trend. However, at higher than 200°C, the increase saturates and it seems that the water decomposition does not increase anymore. The increasing yield of H radical with temperature is not significant, which is in agreement with recent Elliot's evaluation (1993).The H_2 increases slightly, again, similar to the recent reports by Elliot, and Kent and Sims (1992a, b). The pair of OH and H_2O_2 appears to be different from the reported and simulated ones. The present G_{OH} increase only slightly with temperature, which is contradict to the big increase reported by Elliot, and Kent and Sims.

In fast neutron radiolysis, the tendency of the change is similar to that observed in γ radiolysis in spite of the values are much smaller. It is surprising that, even at 250°C, there exists a significant LET effect remained; $G_{e\text{-}aq}$ is much less than unity. This is confirmed by the recent evaluation using four different ion beams at elevated temperatures and extrapolation of the LET values to the fast neutron radiolysis (Elliot, 1994). However, again our temperature dependence of OH is much smaller, as compared with Elliot's. This may be caused by the derivation method; simulation in the present and direct measurement for Elliot. Temperature dependence of other products are similar. Anyway, this measurement is the first experimental evaluation for the fast neutron radiolysis.

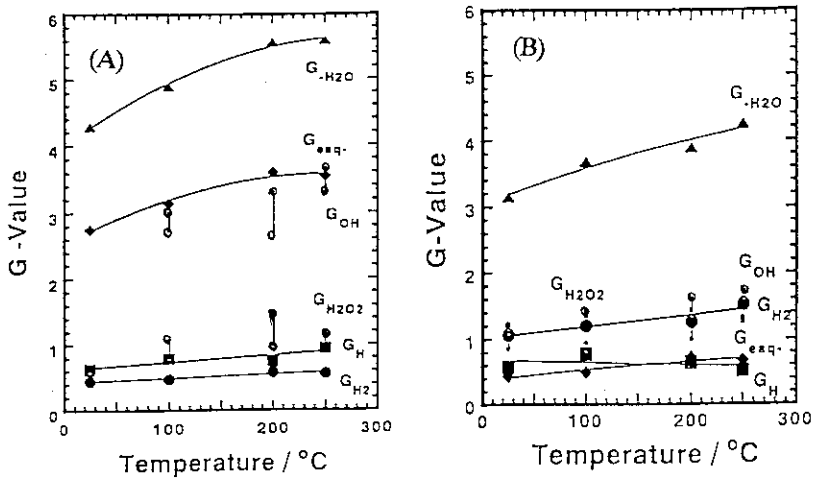


Fig. 2
The temperature dependence of the G_{-H2O}; ▲, G_{H2}; ●, G_H; ■ Geaq-; ◆, G_{OH}; ⟟ and G_{H2O2}; ⟟ in γ-radiolysis (A) and fast neutron radiolysis (B).

Spur and Track structure at elevated temperatures:

From the increase of water decomposition with temperature in both γ and fast neutron radiolysis, it is strongly suggesting that the spur might expand at elevated temperature. In order to check this hypothesis, an additional experiment was made. We took the solution containing 1mM $HClO_4$ + methanol solution and H_2 evolution was measured by changing the concentration of methanol. As expected, concentration effect of methanol on the hydrogen evolution at 250°C is much smaller than at room temperature (Fig. 3). Recent spur diffusion kinetic study also supports this picture (LeVerne and Pimblott, 1993). However, in fast neutron radiolysis, it was found that observed H_2 yields are much lower than in γ radiolysis because fast neutrons, namely recoil protons have high LET. Since the distance between the spurs formed in fast neutron radiolysis are significantly shorter, an experimental finding indicates that the effect of intra spur reactions still much larger than in γ radiolysis, even the spur expands at high temperatures.

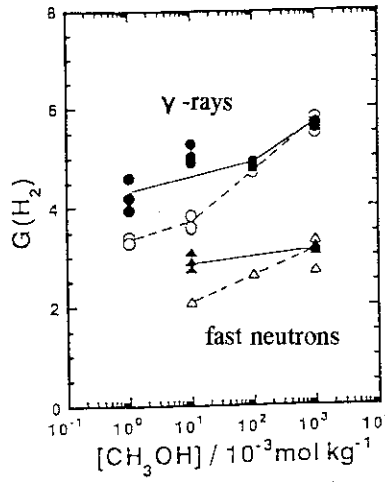


Fig. 3 Tha yields of G_{H2} in 10^{-3} mol • kg^{-1} $HClO_4$ at various concentration of CH_3OH irradiated at 25°C (open) and 250°C (closed) with γ-rays (○, ●) and fast neutrons (△, ▲).

Characteristics of the G values of water decomposition at elevated temperatures:

In order to clarify the characteristics of the G values of water decomposition at elevated temperatures, simulations of the chemical reactions induced by irradiation under various conditions imitated the nuclear reactors at 250°C were carried out. Dose rates, fraction of fast neutron dose to total absorbed one, concentrations of oxygen remained and hydrogen injected *etc.* were changed. For comparison, G-values reported by Elliot for γ (1993) and Burns for fast neutron radiolysis (1981a, b) were also taken for calculation. It was found that both sets of G-values evaluated by Elliot and in the present experiment for γ radiolysis is almost equivalent from the view point of simulation. But, for fast neutron radiolysis, calculations with the set reported by Burns give significant different results from that with G-values determined in the present experiment. In addition, much higher steady state concentrations of the decomposition products are obtained in fast neutron radiolysis than in γ radiolysis under the same dose rate due to the smaller yield of radical products and larger yield of molecular products. These concentrations are easily reduced by the contamination of γ ray to fast neutron dose. It indicates not only the importance of the experimentally determined G-values for fast neutron radiolysis but also the necessity of the precise evaluation of the neutron dose at the reactor core.

Through the simulations, it was found that some reactions normally negligibly small at room temperature become important at higher temperatures and the results are strongly effected by the values of their rate constants. The first reaction is a reverse reaction of $H_2 + OH \rightarrow H + H_2O$ and its rate constant was estimated before by Hartig and Getoff (1982). From the thermodynamical consideration, the rate would be 20 s^{-1} at 250°C and this affects strongly the steady state concentrations, especially in the presence of hydrogen: under hydrogen injection. Another one is a reverse reaction of $e^-_{aq} + H^+ \rightarrow H$, the equilibrium of which is shifted to H at room temperature, but the value of 1×10^5 s^{-1} for $H \rightarrow e^-_{aq} + H^+$ at 250°C was determined recently by Shiraishi *et al.* (1994). Both are key reactions for the hydrogen injection condition, further study would be expected.

This paper is a summary of the series of the papers (Sunaryo *et al.*, 1994, 1995a, b) accepted in *Radiat. Phys. Chem.* We wish to thank the staff of the reactor "YAYOI", Nuclear Engineering Research Laboratory, The Uinversity of Tokyo, who operated the reactor.

References

Allen, A. O. (1961) *The Radiation Chemistry of Water and Aqueous Solutions* Van Nostrand, Princeton
Appleby, A. and Scwarz, H. A. (1969) *J. Phys. Chem.* **73**, 1937
Burns, W. G. (1981a) *Water Chemistry of Nuclear Reactor Systems* **2**, 373, BNES, London
Burns, W. G. (1981b) *J. Chem. Soc. Fararay Trans.1* **77**, 197
Buxton, G. V., Greenstock, C. L., Helman, W. P. and Ross A. B. (1988) *J. Phys. Chem. Ref. Data* **17**, 513
Buxton, G. V. and Elliot, A. J. (1991) *Proc. JAIF Int. Conf. Wat. Chem. Nucl. Pow. Plants* 283, JAIF, Fukui
Draganic, Z. D. and Draganic, I. G. (1973) *J. Phys. Chem.* **77**, 765
Elliot, A. J. Chenier, M. P. and Quellette, D. C., (1993) *J. Chem. Soc. Faraday Trans.* **89**, 1193
Elliot, A. J., (1994) Private communication
Hartig, K. J. and Getoff, N. (1982) *J. Photochem.* **18**, 29
Hiroishi, D. and Ishigure, K. (1989) *Water Chemistry for Nuclear Reactor Systems* **5**, vol.1, 333, BNES, London
Kabakchi, S. A. and Lebedeva, I. E., (1989) *High Energy Chem.* **21**, 261
Katsumura, Y., Yamamoto, S., Hiroishi, D. and Ishigure, K. (1992) *Radiat. Pys. Chem.* **39**, 383
Katsumura, Y., Takeuchi, Y., Hiroishi, D. and Ishigure, K. (1989) *Radiat. Phys. Chem..* **33**, 299
Kent, M. C. and Sims, H. E. (1992a) *Water Chemistry of Nuclear Reactor Systems* **6**, 153, BNES, London
Kent, M. C. and Sims, H. E. (1992b) *AERE-RS-2302, PWR/CTG/P(92)084*, AEA Technolgy, Harwell
LeVerne, J. A. and Pimblott, S. M. (1993) *J. Phys. Chem.* **97**, 3291
LaVerne, J. A. and Schuler, R. H. (1994) *J. Phys. Chem.* **98**, 4043, references cited herein
Shiraishi, H., Sunaryo, G. R., and Ishigure, K. (1994) *J. Phys. Chem.* **98**, 5164
Sunaryo, G. R., Katsumura, Y., Shirai, I., Hiroishi, D. and Ishigure, K. (1994) *Radiat. Phys. Chem.*, **44**, 273
Sunaryo, G. R., Katsumura, Y., Hiroishi, D. and Ishigure, K. (1995a) *Radiat. Phys. Chem.*, **45**, 131
Sunaryo, G. R., Katsumura, Y. and Ishigure, K. (1995b) *Radiat. Phys. Chem.*, in press

6. Biological System (1)

6.1 *Excitation Transfer, Charge Transfer and Hydrogen Abstraction Reaction, Kinetics Studies of Modification of DNA Components

N.Y.Lin

Laboratory of Radiation Chemistry, Academia Sinica,
Institute of Nuclear Research, P.O.Box 800-204 Shanghai, China

Abstract Laser induced acetone-sensitized excitation of DNA components offered, for the first time, T-T absorption spectra and direct triplet states kinetics of cytosine, cytidine, and dCMP, adenine, adenosine and dAMP and guanosine . Mechansims and kinetics of electron transfer reactions between triplet acetone and purine bases and triplet thymine and electroaffinic modifiers have been elucidated. Rapid electron transfer from hydroxycinnamic acid derivatives to oxidizing OH adducts of pyrimidines have been performed. Fast reduction and repair of oxidizing damage of pyrimidines have been achieved accordingly.

INTRODUCTION

Extensive studies on the triplet states of pyrimidines and their nucleosides and nucleotides were performed.[1] However cytosine and purine base and their nucleosides, nucleotides have not yet observed.[1] Very recently a breakthrough for detection of absorption spectra and direct triplet state kinetics of cytosine and its two derivatives, adenine and its two derivatives and guanosine have been achieved at our laboratory.OH adduct of pyrimidines are the major cause of oxidizing damage of DNA.The oxidizing OH adduct can be reduced via electron transfer reaction by N.N.N',N' tetramethyl-p-phenyldiamine(TMPD) or ascorbate. Recently the oxidizing OH adducts of thymine, cytosine and polycytidylic acid (polyC) have been reduced and repaired via electron transfer from hydroxycinnamic acid derivatives to the adducts.

EXPERIMENTAL

DNA components including cytosine cytidine and dCMP,

guanosine and adenine adenosine and dAMP were obtained commercially and used without further purification.[2][3][4] Purity of acetone(Ac) and $Mncl_2$ were given elsewhere.[2]

RESULTS AND DISCUSSION

1.Novel triplet states of DNA components.

A new breakthrough of direct detection of triplet states of DNA components has been achieved under acetone-sensitization in aqueous solution. Since energy level of triplet acetone is higher than that of DNA bases, nucleoside and nucleotides. And due to very short life time of acetone,the composite spectra of triplet base and dehydrogenated radicals were observed several micosecond after laser pulse. The neat decay trace and T-T absorption spectra were obtained, for the first time, according to subtraction method suggested by us.[3] These species decay following pseudo-first order kinetics with the apparent decay rate constant (K_{obs}) as below:

$$K_{obs}=K_o+K_s[B]+K_q[Q]$$

The reaction mechanisms can be summarized as follows:

$$Ac \xrightarrow{248nm} {}^3Ac^*$$

$${}^3Ac^* + B \xrightarrow{K_{TT}} Ac + {}^3B^*$$

$${}^3B^* \xrightarrow{K_o} B$$

$${}^3B^* \xrightarrow{K_q} B + Q \qquad Q:Mn^{2+}$$

Several sets of direct kinetic parameters of triplet decay (K_o. K_s. K_q and K_{obs}) were obtained upon detailed kinetic analysis. The life times were derived accordingly.

1.1 Triplet state of guanosine [3]

The absorption spectra after laser photolysis of guanosine aqueous solution containing acetone as photosensitizer show that besides triplet acetone a new transient species appeared. Based on the subtraction method the neat transient absorption spectrum was obtained. Its decay follow first order kinetics with $K_{obs}=9.4\times10^4 s^{-1}$; $\tau_{1/2}=7.4\ \mu s$ at 1×10^{-4}M guanosine in the absence of triplet quencher. In addition, the species can be quenched by Mn^{2+} with rate constant $Kq=1.9\times10^{10} M^{-1}S^{-1}$.

1.2 Triplet states of cytosine.cytidine and dCMP[2]

The transient absorption spectra from laser flash photolysis of aqueous solution containing cytosine and acetone show that besides triplet acetone a new transient species appeared. Based on the subtraction method for the resolution of composite spectra the neat characteristic absorption was also recorded. Its decay follow the first order kinetics and can be quenched by Mn^{2+} . Similar transient absorptions have been recorded from laser photolysis of cytidine and dCMP in the presence of acetone. These novel species should be assigned to triplet cytosine cytidine and dCMP after quenching by Mn^{2+}. Their kinetics parameters of triplet decay were given in table 1.

Table 1
Kinetic parameters of triplet states of cytosine, cytidine, and dCMP

	k_o (s^{-1})	k_s ($dm^3mol^{-1}s^{-1}$)	k_q ($dm^3mol^{-1}s^{-1}$)	k_T ($dm^{-3}mol^{-1}s^{-1}$)
$^3Cyt^*$	$5.5x10^4$	$4.2x10^8$	$8.0x10^7$	$3.8x10^9$
$^3Cyd^*$	$7.6x10^4$	$2.4x10^8$	$2.5x10^8$	$4.5x10^9$
$^3dCMP^*$	$9.4x10^4$	$1.8x10^8$	$1.7x10^8$	$5.1x10^9$

The half life time ($\tau_{1/2}$) of triplet cytosine,cytidine and dCMP are 5.0,5.6, and 5.3ms respectively at the concentration of $2x10^{-4}M$ in the absence of triplet quencher. Utilizing energy transfer method and taking the molar absorption coefficient of $^3Ac^*$ as 600 $M^{-1}cm^{-1}$ at 300 nm as well as the kinetic parameters given in table 1, the molar absorption coefficient of triplet cytosine,cytidine and dCMP have been estimated to be 200 $M^{-1}cm^{-1}$(340nm),200$M^{-1}cm^{-1}$(350nm) and 400$M^{-1}cm^{-1}$ (450nm) respectively.

1.3 Triplet states of adenine, adenosine and dAMP

The transient absorption spectra from laser flash photolysis of aqueous solution containing adenine and acetone show that besides triplet acetone, a new transient species appeared. According to our subtraction method the neat transient absorption

spectrum was recorded. Its decay follow the first order kinetics and can be quenched by Mn^{2+}. Similar transient absorptions have been observed following the laser photolysis of aqueous solution of adenosine and dCMP respectively in the presence of acetone. After quenching by Mn^{2+}, these novel species should be assigned to triplet adenine, adenosine and dAMP with half life times of 2.7,2.8and 5.8 μs respectively in the absence of triplet quencher. Their kinetic parameters of triplet decay were deduced as shown in table 2.

Table 2.

Kinetic parameters of triplet states of adenine, adenosine and dAMP

	k_{obs} (s^{-1})	k_o (s^{-1})	k_{sq} ($dm^3mol^{-1}s^{-1}$)	k_q ($dm^{-3}mol^{-1}s^{-1}$)
$^3Adenine^*$	$2.6x10^5$	$1.1x10^5$	$6.9x10^8$	$4.2x10^8$
$^3Adeonsine^*$	$2.5x10^5$	$7.9x10^4$	$8.3x10^8$	$3.5x10^8$
$^3dAMP^*$	$1.2x10^5$	$3.7x10^4$	$3.6x10^8$	$6.0x10^8$

2.Electron transfer reactions between DNA components and modifiers

2.1 Reactions of triplet acetone with DNA components

Following the laser photolysis of guanosine aqueous solution containing acetone besides the triplet guanosine a long-lived absorption, quite similar to the transient absorption from reaction of dG with SO_4^- radical, had been assigned to G(-H) radical.[5] It was suggested that electron transfer from guanosine to triplet acetone occurred . Subsequent hydrogen abstraction occurred via following reaction:[3]

$$^3Ac^* + dG \longrightarrow Ac^- + dG^+ \longrightarrow \dot{A}c(+H) + \dot{d}G(-H)$$

After laser photolysis of adenine in the presence of acetone besides the absorption band from triplet adenine a long-lived absorption which decay following second order kinetics and was assumed to be a dehydrogenated adenine radical arising from electron transfer reaction between adenine and triplet acetone:

$$^3Ac^* + A \longrightarrow Ac^- + A^+ \longrightarrow \dot{A}c(+H) + \dot{A}(-H)$$

Similar transient absorption spectra have been obtained from

laser photolysis of adenosine and dAMP aqueous solution in the presence of acetone. Based on kinetic analysis the long-lived absorption should be assigned to the dehydrogenated radical of adenosine and dAMP respectively.[4]

On another hand the free energy change (ΔG) of these supposed electron transfer reactions were calculated according to Rehm-Weller equation.Calculated ΔG values indicated that electron transfer from purine bases or its nuclesides and nucleotides to triplet acetone should proceed spontaneously.[3][4]

2.2 Electron transfer reaction between triplet pyrimidines and electroaffinic modifiers

Laser induced electron transfer from triplet thymine or thymidine to a cyclic disulfide compound,lipoic acid,was studied. Laser induced transient absorption spectra of CH_3CN solution of thymine or thymidine and lipoic acid indicated that long-lived transient absorption is very similar to the anion radical of lipoic acid ($RSSR^{\cdot -}$). Based on the quenching of triplet thymine or thymidine by lipoic acid the electron transfer reaction rate constant was deduced to be $1.3\times10^{10}M^{-1}S^{-1}$ and $6.9\times10^{-9}M^{-1}S^{-1}$ for thymine and thymidine respectively.[6]

On the other hand laser induced electron transfer reaction between thymine or uracil and tetracyanoethylene(TCNE) was also studied. laser flash photolysis of CH3CN solution of TCNE and pyrimidines led to the formation of a species characterized with an absorption band very similar to anion radical of TCNE. The electron transfer reaction rate constant are $7.6\times10^{9}M^{-1}S^{-1}$ for thymine and $1.7\times10^{10}M^{-1}S^{-1}$ for uracil.[7]

3.Pulse radiolysis studies of the interaction of hydroxycinnamic acid derivatives with oxidizing OH adduct of pyrimidines[8]

The hydroxyl radical either generated by radiation decomposition of water in biological system or via redox cycling chemicals can cause DNA damage. There are two ways to inhibit the lesion of cell, either via scavenging OH radical or fast repair of the OH adducts. The reaction of OH radical with pyrimidines take place predominantly at C5-C6 double bond. The radical formed by addition of OH to C5 is reductive, while to C6 is oxidative. The reduction of oxidizing OH adduct of pyrimindes were performed by strong reductant TMPD.[8] The fast reduction and repair of

OH adducts of pyrimidines by hydroxycinnamic acid derivatives via electron transfer reaction have been performed at our laboratory.[9]

The transient absorption spectrum at 1μs after pulse radiolysis of 2 mM cytosine and 0.1mM sinapic acid aqueous solution saturated with N2O is stemming from OH adduct of cytosine predominately. At 10 μs after electron pulse accompanying the decay of the characteristic absorption band of OH adduct of cytosine a novel band appeared which was assigned to the phenoxyl radical of sinapic acid arising from electron transfer reaction between OH adduct of cytosine and sinapic acid. After capture of an electron the oxidizing OH adduct should be repaired by dehydroxylation or reduced to stable OH adduct .Similar transient absorption spectrum after pulse radiolysis of solution containing cytosine and caffeic acid or ferulic acid has been recorded. The characteristic absorption peak assigned to phenoxyl radical of caffeic acid or ferulic provided evidences of electron transfer from caffeic acid or ferulic acid to OH adduct of cytosine. The electron transfer reaction of hydoxycinnamic acid derivatives with oxidizing OH adduct of thymine have also been studied in the same way. After pulse radiolysis of 2mM thymine and 0.1mM sinapic acid or caffeic acid or ferulic acid in aqueous solution saturated with N2O the transient absorptions revealed similar absorption peaks assigned to the phenoxyl radicals of sinapic acid, cafferic acid and ferulic acid respectively. The electron transfer rate constants for reduction of oxidizing OH adduct of thymine by hydroxycinnamic acid derivatives have also been determined (see table.3)

Table 3.
The rate constants of electron transfer from hydroxycinnamic acid derivatives to oxidizing OH adducts of pyrimidinine

Substrate	$k[CytOH]_{ox}$	$k[ThyOH]_{ox}$
Sinapic acid	$1.1x10^9$	$1.3x10^9$
Caffeic acid	$1.2x10^9$	$1.3x10^9$
Ferulic acid	$1.0x10^9$	$1.1x10^9$

ACKNOWLEDGEMENT

This project was supported by the National Natural Science Foundation of China.

REFERENCES

[1]Cadet J. and Vigny P.(1990) in Morrison H.(ed), Bioorganic Photochemstry ,Vol 1 .Wiley,New York P 35.
Bensasson.R.V., Land.E.J., and Truscott.T.G., Flash photolysis and pulse radiolysis, pergamon, oxford, 1983.P 121 .

[2]Zuo.Z.H.,Yao.S.D.,Luo.J.,Wang.W.F,Zhang.J.S and N.Y.Lin,(1992) J.phtotchem.photobiol .B:Biol.15.215.

[3]Jian.L.,Wang.W.F., Zheng.Z.D., Yao.S.D., Zhang.J.S., and Lin.N.Y. (1991) Res.Chem.Intermed.15,293.

[4]Li.H.C.,Yao.S.D.,Zuo.Z.H.,Zhang.J.S., and Lin.N.Y.,J.Photochem Photobiol. B:Biol.to be published.

[5]Steenken.S.,(1989) Chem.Rev. 89,503.

[6]Lian.Z.R.,Yao.S.D.,Wang.W.F.,Zhang.J.S., and Lin.N.Y.,(1993) J.Photochem.Photobiol.B.Biol.20,113.

[7]Zhang.X.Y., Jin.S., Ming.Y.F., Fan.M.G., Lian.Z.R., Yao.S.D., and Lin.N.Y., J.Photochem.Photobiol. A:Chem. to be published.

[8]von Sonntag.C.,(1987),Radiat.Phys.Chem.30.313.

[9]Wang.W.F., Luo.J., Yao.S.D., Zhang.J.S., and Lin.N.Y., Radiat.Phys.Chem., to be published.

6.2 Kinetic Observation of Rapid Electron Transfer between Thymine and Thymidine Anion Radicals and Caffeic Acid: A Pulse Radiolysis Study

Z.H.Zuo, S.D.Yao, H.C.Lee, W.Z.Lin, J.S.Zhang and N.Y.Lin
Laboratory of Radiation Chemistry, Academia Sinica, Shanghai 201800, P.R.China

Abstract Rapid electron transfer from thymine or thymidine anion radicals to caffeic acid with rate constant of 1×10^{9} $M^{-1}s^{-1}$ was observed by pulse radiolysis, leading to the formation of anion radicals of caffeic acid which is characterized with absorption maximum at 360nm. Caffeic acid has a higher one-electron reduction potential than the target molecule (thymine or thymidine) and acts as a electrophilic protector which prevent the target anion radical from its irreversible protonation at C6 leading to its 5-yl radical via fast electron transfer. The kinetic demonstrations have provided dynamic evidence of charge transfer protection mechanism.

INTRODUCTION

Elucidation of mechanism of radioprotection and radiosensitization is an important subject in the field of radiation physics and chemistry of DNA. The "three transfer" mechanisms generalized by Lin in 1980s are the comprehensive principle of radioprotection and radiosensitization and quite useful to explain the protection and sensitization effects on DNA.[1] And the charge transfer protection mechanism, the major contribution to the foregoing mechanism, proposed that the charge transfer protector is a sort of modifier with higher electron affinities (EA) but lower ionization potentials (IP) than that of target molecule, thus the target molecule can be repaired from its anion and cation radicals via charge transfer.

Caffeic acid (3,4-dihydroxycinnamic acid) belongs to electrophilic phenylsubstituted unsaturated carboxylic acid. Pulse radiolysis, ESR and chemiluminescence studies have reported its antioxidant activity to scavenge superoxide anion radical and hydroxy radical.[2,3] In addition ESR detection and CNDO/2 calculation have explored its radioprotection effect to repair the target from its anion radicals via the charge transfer mechanism.[1]

In this paper efforts were made to observe the rapid electron transfer between thymine and thymidine anion radical and caffeic acid by pulse radiolysis and kinetic spectrophotometric monitoring techniques, in order to get direct evidence of the charge transfer protection mechanism.

EXPERIMENTAL

Caffeic acid (3,4-dihydroxycinnamic acid) and thymine and thymidine were recrystallized three times from triply distilled water. Tert-butanol were distilled and purified before used. All solutions were prepared with three distilled water and buffered with phosphate and saturated with high purity nitrogen gas by bubbling for 20 minutes.

Pulse radiolysis experiments were conducted by using a linear accelerator providing electron pulse with a duration of 8 nanosecond. The dosimetery of the pulse was determined by thiocyanate dosimeter containing 1×10^{-2} M KSCN solution saturated with air by taking ε and G value of $(SCN)_2^-$, 7600 M^{-1} cm^{-1} at 480nm and 2.9 respectively. The detailed technical descriptions of set-up were given elsewhere.[3]

RESULTS AND DISCUSSION

1. Observation of electron transfer

Figure 1(A) showed the transient absorption spectra arising from pulse radiolysis of the deaerated solution of 1×10^{-3}M thymine and 6×10^{-5}M caffeic acid, 0.2M tert-butyl alcohol and 2×10^{-3}M phosphate buffered at pH7. The weak spectrum recorded at 1μs with a maximum absorbance at 340nm, was similar to that of thymine anion radicals ($T^{-\cdot}$) observed from radiolysis of thymine solution alone. $T^{-\cdot}$ was measured to have a molar extinction coefficient of 1.8×10^{3} $M^{-1}cm^{-1}$ at 340nm, similar to that reported by Hayon.[4]

However the spectrum detected at 40μs has a maximum absorbance at 360nm, which is different from that of $T^{-\cdot}$, but similar to that of anion radicals of caffeic acid ($DHC^{-\cdot}$) arising from radiolysis of caffeic acid solution alone. The molar extinction coefficient of $DHC^{-\cdot}$ at 360nm (1.1×10^{4} $M^{-1}cm^{-1}$) is much larger than that of $T^{-\cdot}$ at 340nm.

The insert trace in Figure 1(A) showed the increase absorbance at 360nm which reaches the maximum value at 40μs, indicating the formation of $DHC^{-\cdot}$ via electron transfer between $T^{-\cdot}$ and DHC.

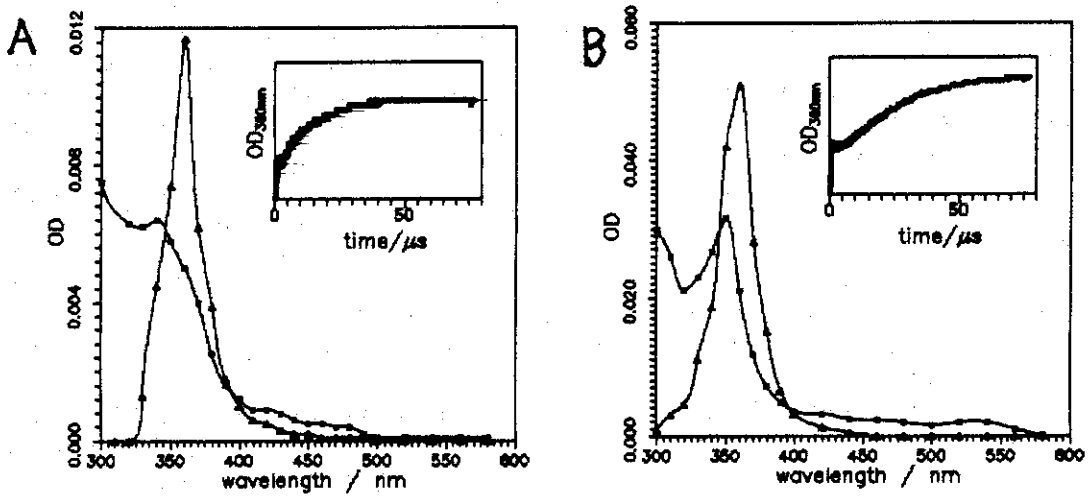


Figure 1. Transient absorption spectra observed upon irradiation of the solution containing 1mM thymine (A) or thymidine (B) with 0.06mM caffeic acid, 0.2M tert-butanol, 2mM phosphate buffer at pH7 and saturated with Nitrogen, at 1μs (solid square), 40μs (A) or 70μs (B) (solid triangle). Insert: trace of caffeic acid anion radicals at 360nm. The average dose absorbed was 3.5Gy determined by thiocyanate dosimetery.

Similar spectra were obtained from radiolysis of solution containing thymidine and caffeic acid, as shown in Figure 2(B) and also showed the formation of $DHC^{-\cdot}$ via electron transfer.

2. Thermodynamics analysis

(1) reaction of thymine with e^-_{aq}

The hydrated electron reacts with thymine with diffusion-controlled rates for production of $T^{-\cdot}$(reaction 1), which is subsequently protonated rapidly at O(4) (reaction 2) and slowly at C(6) (reaction 3).[5,6] Protonation at O(4) is reversible on the pulse-radiolysis time scale and the pK_a value of O(4)-protonated electron adducts of thymine or thymidine is 7.2 or 6.9 respectively.[4]

1 $T + e^-_{aq} \longrightarrow T^{-\cdot}$ $k_1=1.7\times10^{10}M^{-1}s^{-1}$ [7,8]

$E^1_{8.6}$= -1100mV/NHE, at pH8.6 [9]

2 $T^{-\cdot} \underset{OH^-}{\overset{H^+}{\rightleftharpoons}} TH^{\cdot}$ $k_2(H^+)=2.6\times10^{10}M^{-1}s^{-1}$[6]

$k_{-2}(OH^-)=10^{10}M^{-1}s^{-1}$ [10]

3 $T^{-\cdot} \xrightarrow{H^+} T'H^{\cdot}$ $k_3= 5\times10^3s^{-1}$ [6]

whereas in reaction 1 $E^1_{8.6}$ means the one-electron reduction potential of thymine at pH8.6 determined by Steenken et al.[9] The nucleosides and nucleotides of pyrimidine bases were reported to have the very similar reduction potential. In order to describe the pH-dependence of reduction potential, reactions 1 and 2 should be considered, and the value at pH7 for the system $E^1_7(T,H^+/TH^{\cdot})$ was calculated to be -1077mV from:[11]

$$E^1_7(T,H^+/TH^{\cdot})=E^1_{8.6}(T,H^+/TH^{\cdot}) + \frac{RT}{F}\ln\left(\frac{K_a + 10^{-7}}{K_a + 10^{-8.6}}\right) \qquad (1)$$

(2) reaction of caffeic acid with e^-_{aq}

Since caffeic acid has an electrophilic phenylsubstituted unsaturated carboxylic acid, hydrated electron could attack its carbonyl oxygen, leading to the formation of anion radicals of carboxylic acid:

4 $DHC + e^-_{aq} \longrightarrow DHC^{-\cdot}$ $k_4 = 1.4\times10^{10}\ M^{-1}s^{-1}$

E^1_7= -343mV at pH7 [12]

whereas the one-electron reduction potential of caffeic acid at pH7 was measured using duroquinone as the reference.[12]

$DHC^{-\cdot}$ decays by a first-order kinetics with the rate of $7\times10^3\ s^{-1}$, probably through its protonation process (reaction 5), followed by a

supposed bimolecular decay of the protonated forms (reaction 6) to a more stable products:

5 $DHC^{-\cdot} \xrightarrow{H^+} DHC(+H)^{\cdot}$ $\quad k_5 = 7.4\times10^3\ s^{-1}$

6 $DHC(+H)^{\cdot} + DHC(+H)^{\cdot} \longrightarrow P_2$

(3)electron transfer reaction

On account of rate constants of reaction 1 and 4, and the concentration of thymine and caffeic acid in the mixed solution, almost all of the initial hydrated electron were captured by thymine immediately after the electron pulse. However caffeic has an a higher one-electron reduction potential than thymine, consequently $DHC^{-\cdot}$ was formed via electron transfer from thymine anion radical to caffeic acid, as shown by reaction 8 :

8 $T^{-\cdot} + DHC \longrightarrow T + DHC^{-\cdot}$ $\quad k_8=1\times10^9 M^{-1}s^{-1}$

ΔE_0=734mV, ΔG_0=-70.8KJ/mol

whereas k_8 was measured from kinetic analysis of the decay process of $T^{-\cdot}$ at 300nm, and ΔE_0 and ΔG_0 is the difference in reduction potential and free energy at pH7 respectively.

The kinetic process of $DHC^{-\cdot}$at 360nm includes reaction 8 and 5, thus:

$$[DHC^{-\cdot}]_t = \frac{k_8[DHC]}{k_5 - k_8[DHC]}\,[X_0] \times (e^{-k_8[DHC]t} - e^{-k_5 t}) \qquad (2)$$

where as $[X_0]$ is the initial yield of $T^{-\cdot}$ which decays following electron transfer reaction. From the experimental data of the maximum value of $[DHC^{-\cdot}]_{tmax}$ at tmax , the value of $k_8[DHC]$ and k_5, $[X_0]$ was measured to be about 8×10^{-7} M, since the initial concentration of hydrated electron was 1×10^{-6}M, about 80% of hydrated electron were captured eventually by caffeic acid and $G(DHC^{-\cdot})$ was about 2.2.

CONCLUSIONS

Rapid electron transfer from thymine or thymidine anion radical to caffeic acid has been detected by kinetic spectrophotometric techniques with the rate constant of around $10^9\ M^{-1}s^{-1}$. The electron transfer reaction prevents C(6) protonation of thymine or thymidine anion radicals and eventually inhibites their damage by caffeic acid. The kinetic demonstrations have provided dynamic evidence of the charge transfer protection mechanism proposed based on our previous ESR and molecular orbital studies.

ACKNOWLEDGEMENT

This project was supported by the National Natural Science Foundation of China.

REFERENCES

1. Lin N.Y.,(1986) *Radiat.Phys.Chem.*,28(2),211 and reference there in.
2. Hu T.X., Chen J.W., Huang Z.D., Sheng M.L., (1990) *Symposium of radiation research and processing*, edt. Lin N.Y., Shanghai Medical University Press, Shanghai, China, 52.
3. Wang W.F., Luo J., Yao S.D., el al, (1993) *Radiat.Phys.Chem.*, 42,985.
4. Hayon E., (1969) *J.Chem.Phys.*, 51,4881.
5. Das S., Deeble D.J., Schuchmann M.N.and Sonntag C.V., (1979) *Int.J. Radiat. Biol.*, 35,449.
6. Deeble D.J, Das S. and Sonntag C.V., (1985) *J.Phys.Chem.*, 89, 5784.
7. Hart E.J., Gordon S. and Thomas J.K., (1964) *J.Phys.Chem.*, 68,1271.
8. Moorthy P.N., Hayon E., (1974) *J.Phys.Chem.*,78, 2615.
9. Deeble D.J. and Sonntag C.V., (1987) *Int.J.Radiat.Biol.*, 51, 791.
10. Steenken S., Telo J.P., Novais H.M. and Candeias L.P., (1992) *J.Am.Chem. Soc.*, 114,4701.
11. Wardman P., (1989) J.Phys.Chem.Ref.Data, 18(4), 1637.
12. Lee H.C., (1993) Determination of one-electron reduction potentials of hydroxycinnamic acid derivatives, M.A. thesis of Shanghai Institute of Nuclear Research.

6.3 Cellular Non-protein Thiol Depletion and Radiosensitization of Hypoxic Cells by Nitroazole Derivatives Possessing and NPSH-reactive Side Chain

Ling Zhou and Sei-ichi Nishimoto

Division of Energy and Hydrocarbon Chemistry, Graduate School of Engineering, Kyoto University, Sakyo-ku, Kyoto 606-01, Japan

Abstract A new class of dual-function hypoxic-cell radiosensitizers that are composed of electron-affinic nitroazole rings and thiol-reactive α,β-unsaturated carbonyl side chains were synthesized. Typically, methyl 4-(2'-nitroimidazolyl)crotonate (**1**) reacted with glutathione (GSH) in phosphate buffer solution to form the corresponding 1,4-addition products which have been isolated and fully characterized by spectroscopy. The same reaction took place within EMT6/KU cells with intracellular GSH to give the drug-GSH conjugates. The enhanced radiosensitizing activity of **1** on hypoxic EMT6/KU cells by alteration in both D_0 and n parameters of dose-survival curve was suggested as the result of the intracellular NPSH-depletion by the common α,β-unsaturated carbonyl side chain.

INTRODUCTION

Endogenous non-protein thiols (NPSH), mainly glutathione (GSH, γ-*L*-glutamyl-*L*-cysteinylglycine), play an important role in determining the response of cells to ionizing radiation, especially under hypoxic conditions (Britten *et al.*, 1992, Jordan *et al.*, 1987). The degree of ionizing radiation damage to cells is governed by the competitive processes between the actions of damage repair by thiols and the damage fixation by oxygen or oxygen-mimic chemical modifiers (Alper *et al.*, 1956, Howard-Flander, 1960). The enhancing effect on radiosensitivity of hypoxic cells under reduced thiol level has been observed when thiol-depleting agents are used alone (Biaglow *et al.*, 1983), or in combination with electron-affinic radiosensitizers such as misonidazole (**2**) (Bump *et al.*, 1982a, 1982b). A number of strategies have been sought to achieve NPSH depletion, including oxidation of GSH to GSSG (Harris *et al.*, 1973), formation of GSH conjugate through covalent bond (Han *et al.*, 1976), and inhibition of intracellular GSH synthesis (Biaglow *et al.*, 1983). However, little direct evidence has been hitherto obtained for the intracellular GSH reaction. In connection with our interests in developing electron-affinic compounds with thiol-depleting action for radiosensitization of hypoxic cells, we have synthesized a series of nitroazole derivatives bearing α,β-unsaturated carbonyl groups in the side chains. Among them, methyl 4-(2'-

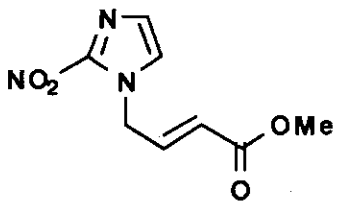
nitroimidazolyl)crotonate (**1**) demonstrated extraordinarily high enhancement ratio *in vitro*, compared with the corresponding saturated analogue. This paper reports on the reaction of **1** with GSH both in phosphate buffer solution and in biological cells, and the effect of intracellular NPSH depletion by **1** on radiosensitization of hypoxic EMT6/KU cells.

EXPERIMENTAL

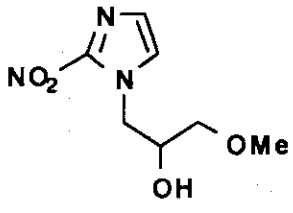
α,β-Unsaturated carbonyl compounds were synthesized by conventional methods. Typically, the compound **1** was derived from reaction of 2-nitroimidazole with methyl γ-bromocrotonate in absolute ethanol under basic conditions. The experimental details of the radiation survival studies on hypoxic EMT6/KU cells can be found in the previous paper (Shibamoto *et al.*, 1989).

RESULTS AND DISCUSSION

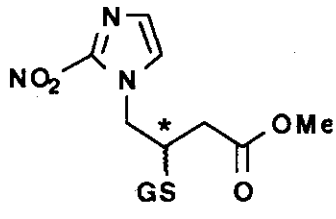
Reaction of **1** with GSH in phosphate buffer solution (pH 7.2, 37°C) followed a second-order kinetics with the rate constants (k_2) of 0.21 M^{-1} s^{-1}. The reaction mixture obtained from the solution of **1** and GSH was separated by HPLC (conditions: column, M&S pack C_{18}, F 4.6 x 150 mm; solvent, 15% MeOH in phosphate buffer solution (pH 4.5); delivery rate, 6.0 mL/min; detection, 320 nm; retention times for **(1-GSH)a,b** are 16.7' and 17.5', respectively) and the structures of the two products were determined by ^{13}C NMR and MS spectra to be the diastereomers of the conjugate addition products **(1-GSH)a,b** in ca. 1:1 ratio (**(1-GSH)a**: $[a]^{20}_D$ -20.11° (c = 0.22, H_2O); ^{13}C NMR (25 MHz, DMSO-d_6) d 176.2, 175.0, 174.4, 173.0, 172.5, 141.0, 127.8, 122.0, 54.6, 54.0, 53.9, 53.1, 42.5, 41.4, 37.3, 33.3, 31.8, 25.2; MS *m/z* 519 (M^++H). **(1-GSH)b**: $[a]^{20}_D$ +0.34° (c = 0.15, H_2O); ^{13}C NMR (25 MHz, DMSO-d_6) d 176.0, 175.0, 174.2, 173.0, 172.5, 141.0, 128.0, 122.0, 58.0, 54.5, 53.8, 53.0, 42.3, 41.4, 36.9, 33.4, 31.9, 25.2; MS *m/z* 519 (M^++H).). The absolute



1



2: misonidazole



(1-GSH)a,b

stereochemistry at the β-carbon of **(1-GSH)a,b** has not been established. Since equal amounts of diastereomers were formed, the chiral centers in GSH have no inductive effect on the newly

forming chiral center at the β-carbon atom of **(1-GSH)a,b**. This Michael addition reaction of intracellular GSH to **1** was also examined using EMT6/KU tumor cells. Figure 1 shows the dependence of total intracellular NPSH level in EMT6/KU cells on the concentration of compound **1** and **2**, when drug exposure was performed for 1 h at 37 °C in air. Thus, treatment of **1** resulted in gradual decrease of the intracellular NPSH level. Compound **1** at 1.0 mM depleted NPSH by more than 80% (from 68.8 nmol/10^7 cells to 12.3 nmol/10^7 cells, see also Fig. 1). Similar depletion of the total NPSH in cellular system was also obtained with **1** under hypoxic conditions (data not shown). On the other hand, treatment with **2** for 1 h at concentrations up to 5.0 mM did not change the intracellular NPSH level (Fig. 1). The remarkable effect of **1** on the reduction of intracellular NPSH level, in contrast to **2**, is attributable to a thiol-reactive function of the α,β-unsaturated carbonyl side chain of **1**. The ability of compound **1** to act as a substrate for glutathion-*S*-transferase was negligibly small, probably because of high electron affinity. In a separate experiment, formation of the conjugates **(1-GSH)a,b** between **1** and intracellular GSH within EMT6/KU cells was confirmed by HPLC, by reference to the authentic samples prepared from the reaction in phosphate buffer solution as above.

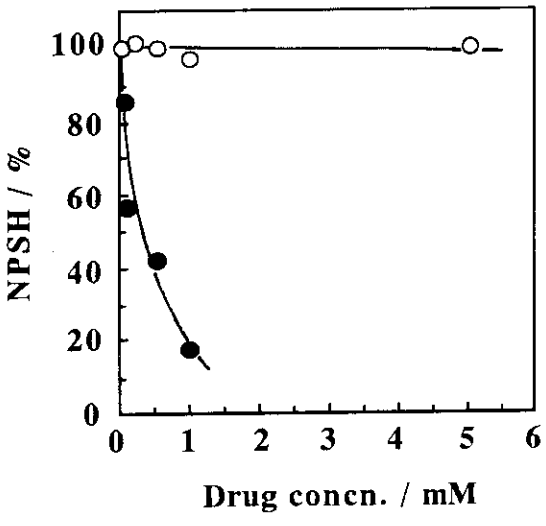


Figure 1. Changes in total intracellular NPSH level of EMT6/KU cells upon exposure to several concentrations of (●) **1** and (○) **2** for 1 h at 37 °C in air. Total amount of NPSH in EMT6/KU cells without drug exposure was 68.6 nmol / 10^7 cells.

The radiosensitizing effect of **1** possessing the NPSH-reactive side chain on the hypoxic EMT6/KU tumor cells was then investigated (Shibamoto *et al.*, 1989), comparing to **2** as a well-documented radiosensitizer. The profiles of dose-survival curves of EMT6/KU cells observed upon X-irradiation with compounds **1** and **2** are shown in Fig. 2. Treatment of hypoxic EMT6/KU cells with 1.0 mM of **1** for 1 h followed by X-irradiation resulted in cell sensitization with 50% decrease of the mean lethal dose (D_0: reciprocal of the slope of linear portion in the dose-survival curve) from 3.2 Gy of control to 1.6 Gy, and reduction of the extrapolation number (n) from 9.0 to 1.5 as well (Fig. 2(a)). Disappearance of the shoulder

(non-linear portion at lower doses) of survival curve indicates that compound **1** is capable of sensitizing hypoxic cells efficiently even in the lower radiation dose region. While treatment of 1.0 mM of **2** decreased the D_0 from 3.2 Gy to 2.0 Gy, little alteration of n value (n = 8.0) was achieved in the dose-survival curve, as shown in Fig. 2(b). The sensitizer enhancement ratio (SER: see the legend in Fig. 2) at 1.0 mM were 2.80±0.20 for **1**, which were comparable to the oxygen enhancement ratio (OER = 2.90±0.10), while the SER for **2** was 1.5. Obviously, the high sensitizing activity of the α,β-unsaturated carbonyl compounds originate from the combined effect on the shoulder and the slope of the dose-survival curve.

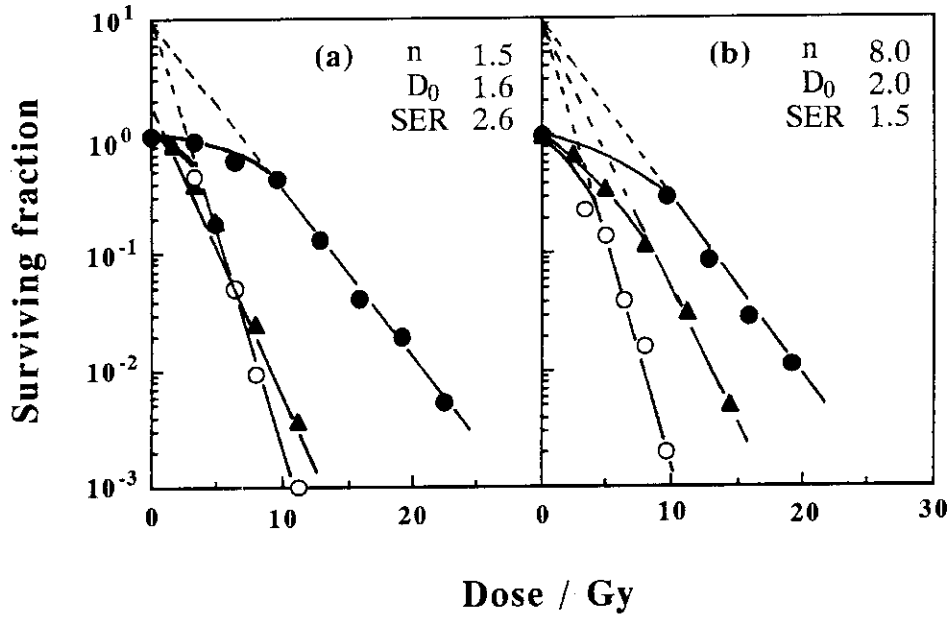


Figure 2. Survival of hypoxic EMT6/KU cells upon X-irradiation after 1h incubation with (▲) 1.0 mM of (a) **1** and (b) **2** under hypoxic conditions (95% N_2+5% CO_2): (●) hypoxic and (○) aerobic (95% air+5% CO_2) controls. The SER was calculated from the ratio of the doses reducing the survival to 1.0 % without and with drug. Oxygen enhancement ratio (OER) was 2.90±0.10. The n values for both hypoxic and aerobic controls were 9.0. The D_0 values were 3.2 Gy for hypoxic control and 1.4 Gy for aerobic control, respectively.

The finding of the distinct effects between compounds **1** and **2** on the profiles of dose-survival curves suggests the importance of NPSH depletion in the radiosensitization of hypoxic cells, particularly in lower radiation dose region. It is reasonable to predict that compound **1** sensitizes hypoxic cells by at least two mechanisms. The effect on the slope is apparently related to the electron affinity of the compound originating from the 2-nitroimidazole ring structure. Since **1** possesses the similar electron affinity with **2** (one-electron reduction potentials measured in DMF are -1.01 V and -1.04 V vs. Ag/Ag^+ for **1** and **2**, respectively), it is likely that compound **1** is able to exhibit oxygen-mimic activity in the process of radiation-

induced damage of DNA, thereby promoting the radiation inactivation of hypoxic cells (Adams, 1992). The effect of **1** on the reduction of shoulder in the dose-survival curve might be related to the depletion of cellular NPSH compounds to inhibit their radical scavenging or hydrogen donating action as the protectors (Held, 1988). In view of the clinical importance of dose fractionation regimens in the radiotherapy for tumor control, it is necessary to find less toxic sensitizers which can sensitize hypoxic cells in low radiation dose region. The high SER value of the novel compound **1** possessing a thiol-reactive side chain in both low and high radiation dose regions would provide potential application in the fractionation radiotherapy. Further studies in this direction are in progress (as the part 2 of this series: Zhou *et al.*, *in press*).

CONCLUSIONS

The higher radiosensitizing effects of the "dual-function" nitroazole radiosensitizers **1** than the ordinary electron-affinic nitroazoles such as misonidasole **2** are attributed to the NPSH reactivity of the α,β-unsaturated carbonyl side chain. The reaction of **1** with intracellular GSH was identified to form the corresponding 1,4-addition products.

REFERENCES

Adams, G. E. *Radiat. Res.* **1992**, *132*, 129.

Alper, T.; Howard-Flander, P. *Nature* **1956**, *178*, 978.

Biaglow, J. E.; Varnes, M. E.; Clark, E. P.; Epp, E. R. *Radiat. Res.* **1983**, *95*, 473.

Britten, R. A.; John, A. G; Warenius, H. M. *Int. J. Radiat. Oncol. Biol. Phys.* **1992**, *24*, 527.

Bump, E. A.; Yu, N. Y.; Brown, J. M. *Science* **1982a**, *217*, 544.

Bump, E. A.; Yu, N. Y.; Brown, J. M. *Int. J. Radiat. Oncol. Biol. Phys.* **1982b**, *84*, 39.

Han, A.; Sinclair, W. K.; Kimler, B. F. *Radiat. Res.* **1976**, *65*, 337.

Harris, J. W.; Power, J. A. *Radiat. Res.* **1973**, *56*, 97.

Held, K. D. *Pharmaco. Ther.* **1988**, *39*, 123.

Howard-Flander, P. *Nature* (London) **1960**, *186*, 485.

Jordan, J.; d'Arcy Doherty, M.; Cohen, G. M. *Br. J. Cancer* **1987**, *55*, 627.

Shibamoto, Y.; Nishimoto, S.; Shimokawa, K.; Hisanaga, Y.; Zhou, L.; Wang, J.; Sasai, K.; Takahashi, M.; Abe, M.; Kagiya, T. *Int. J. Radiat. Oncol. Biol. Phys.* **1989**, *16*, 1045.

Zhou, L.; Nishimoto, S. *Int. J. Radiat. Biol.*, *in press*.

6.4 A Study on Radiosensity of Listeria Monocytogenes in the Food

Hu Jinhui Wang Zhixin Du Qiang Yan Di

Beijing Radiation Application Research Center ,Yang Fang, An Ding Men Wai, Beijing, China.100012

ABSTRACT The research in the radiosensitivity of Listeriamonocytogenes in three kinds of food and one liquid medium has been made. The three kinds of food are milk,cooked beef and sweetened riceflour , the liquid medium is nutritional broth. Exponential regression analysis has proved that the four surviving curves of Listeria monocytogenes in four media accord with formulae:

$N/N_0=0.48e^{-3.280}$ $N/N_0=0.54e^{-2.480}$

$N/N_0=0.57e^{-2.340}$ $N/N_0=0.82e^{-4.230}$

Their correlation coefficients are respectively -0.9787,-0.9310,-0.8914 and -0.9928 with n: 9,9,9,15,their D_{10} have been given .

PREFACE

In recent years , there are more and more food poisonings caused by Listeria monocytogenes, which do much harm to mankind. So people pay more and more attention to it . The food poisonings caused by Listeria monocytogenes have led to a higher death rate. Listeria monocytogenes have been examined from dairy products and meat products. Listeria monocytogenes is still alive and breeding in refrigerator because it is addicted to cold so the ordinary store method can't restrain it.

EXPERIMENT

㈠ materials

1. Listeria monocytogenes: provided by Beijing Commodity Inspection Institute.
2. milk: milk powder " Read Star " 1 gram to 10 millilitre water.
3. cooked beef: provided by Da Hong Men meat process factory

㈡ methods

1.The examination method of Listeria monocytogenes provided by Beijing Commodity Inspection Institute.

2. The Contamination test: steriled sample was inoculated with Listeria monocytogenes 10^6 cfu/g(ml)

㈢ results

Liquid medium, milk , sweetened riceflour, cooked beef were irradiated with different dose and then examined the surviving colony. After that,make exponential regression equation with the logarithm of surviving ratio against irradiation dose and give correlation coefficients. see Table

Table I. Correlation coefficient and exponential regression equation of Listeria monocytogenes in four kinds of media.

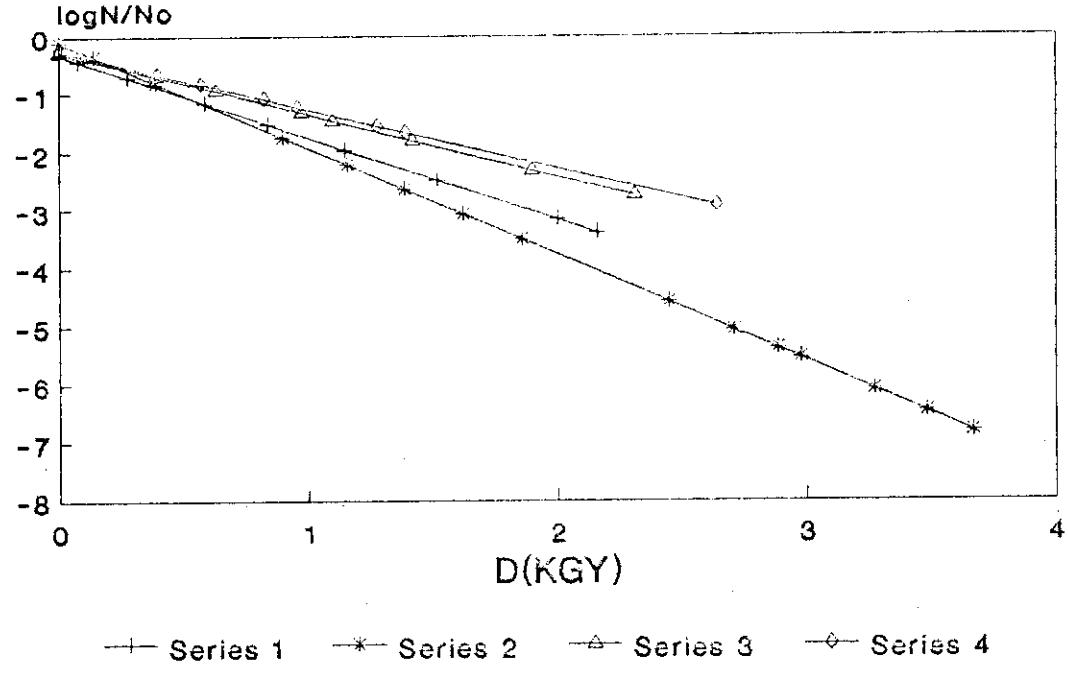
Medium	Exponential regression equation	Correlation coefficient
liquid medium	$N/No=0.82e^{-4.280}$	-0.9928
milk	$N/No=0.48e^{-3.280}$	-0.9784
cooked beef	$N/No=0.54e^{-2.480}$	-0.9310
sweetened riceflour	$N/No=0.57e^{-2.340}$	-0.8914

Make F examination to examine correlation coefficients, see Table II .

table II . F examination of correlation coefficients

Media	F examination	Judgement
liquid medium	F=1030.44>F0.01(1,16) =8.5	minus corredative
milk	F=127.36>F0.01(1,9)=10.6	minus corredative
beef filling	F=51.22>F0.01(1,9)=10.6	minus corredative
sweetened riceflour	F=51.68>F0.01(1,9)=10.6	minus corredative

This examination proved that all these equations can be founded. Plot a diagram , see Fig - I.



Note:liquid medium:-*- series 1
milk: -+- series 2
cooked beef: -△ - series 3
sweetened riceflour-◇- series 4

Plot the curves for four equations.
The curves of this series are all straightlines. Calculating D_{10} values respectively. See Table III

Table III . D10 value of four curves

Medium	D10 value (kGy)
liquid medium	0.54
milk	0.70
cooked beef	0.93
sweetened riceflour	0.98

DISCUSSION

Listing D10 Values of some microbe species in Table IV

Table IV. D_{10} values of some microbe species

Microbe	D_{10} (kGy)	Irradiation medium
Bacillus pumilus	1.72	physiological saline
Escherichia coli	0.29	physiological saline
Candida albicans	1.10	physiological saline
Staphlococcus aureus	0.93	physiological saline
Salmonella enteritidis	0.26	physiological saline
Bacillus cereus	1.79	meat

Listeria monocytogenes can't be alive in physiological saline and phosphoric acid buffer, the D_{10} value in liquid medium is regarded as the standard D_{10} value. Comparing Table III with Table IV, the D10 value of Listeria monocytogenes is lower than B. pumilus ,but is rather high in pathogenic bacteria's.

2. The water contents of four kinds of media are listed in Table V .

Table V. The water content of four kinds of media

Medium	Water content(%)
liquid medium	98.5
milk	91.0
cooked beef	72.9
sweetened riceflour	20.0

Comparaing the water content with D_{10} value and regression equation, we can see that the water content is in inverse proportion to D_{10} value and in direct proportion to absolute value of exponential. this means: water can enhance the sensetivity of Listeria monocytogenes to the γ -ray.

6.5 *The Effects of γ-irradiation on the Garlic Oil Contents in Garlic Bulbs and the Radiolysis of Allyl Trisulfide

WEI GENSHUAN, WANG GUANGHUI, YANG RUIPU AND WU JILAN
Dept. of Technical Physics, Peking University,
Beijing 100871, P.R.China

Abstract: The study of the effects of γ-irradiation on the garlic oil contents in the garlic bulbs and the radiolysis of allyl trisulfide and disulfide were carried out. The content of garlic oil in fresh garlic bulbs treated by gamma ray keeps nearly constant as stored for 10 months long. The main components of the garlic oil are allyl trisulfide (about 60%) and allyl disulfide (about 30%). The G values of radiolysis products of allyl disulfide and trisulfide in ethanol system were determined. The results show that allyl trisulfide is a very effective solvated electron scavenger and can oxidize $CH_3\dot{C}HOH$ radical into acetaldehyde, which causes that the formation of 2,3-butanediol is extensively inhibited.

Keywords: Garlic, Radiolysis, Allyl Trisulfide, Allyl Disulfide

INTRODUCTION

It is well known that garlic (Allium Sativum) has been used not only for a kind of flavour food but also for wide medical purposes[1,2]. Certain extracts from garlic are of antibacterial and antifungal effects, while other extracts are of antithrombatic, which can inhibit the aggregation of blood platelets. Therefore, a number of researchers have long been attracted by the magic functions of garlic and its products.

Garlic oil is one of the garlic relating active compositions and is composed of garlic decomposing products formed as the garlic was broken into pieces, which can be collected and purified by water steam distillation. Garlic oil is water insoluble, light yellow liquid and mainly composes of allyl disulfide and allyl trisulfide and exhibits a very strong antigerm property. γ-Irradiation can inhibit the sprouting of garlic bulbs in dormancy stage, which is generally used for commercial and marketable purpose. The effects of γ-irradiation on the garlic oil contents in garlic bulbs and the radiolysis of allyl disulfide and trisulfide are rarely reported. In the present work, the reactivities of allyl trisulfide and disulfide with the active species generated by γ irradiation in the ethanol system , such as H, e^-_{solv} and radicals, have been also studied as garlic oil is water insoluble and the radiolysis mechanism of ethanol is almost clear[3,4].

EXPERIMENTS

(1)The contents of garlic oil in bulbs were measured with: (a) steam distillation and extraction methods and (b) $Hg(NO_3)_2$ precipitation method. (2) Allyl disulfide and trisulfide were prepared by Brain Milliger method[5]. The identification and determination of the radiolysis products of disulfide and trisulfide in ethanol system were carried out by GC-MS with different capillary column and detectors for different products. (3) Irradiation samples of disulfide and trisulfide in ethanol were nitrogen saturated and oxygen free.

RESULTS AND DISCUSSION

(1)The effects of γ-irradiation on the contents of garlic oil in bulbs shown in Fig.1, the contents of garlic oil in irradiated bulbs with 50Gy in dormancy stage keep nearly constant during a storage period over 10 months; but in the untreated bulbs the contents fall down when the storage time is over 5 months, meanwhile the bulbs begin to sprout. γ-Irradiation treatment on the sprouted bulbs even with 100Gy is not helpful to prevent the loss of garlic oil. There are about two thirds allyl trisulfide(RSSSR) and one third disulfide(RSSR) of the original quantity in the garlic oil which was obtained with the methods mentioned above.

(2)G values of ethanol radiolysis products in containing RSSR and RSSSR system: the dependence of G values of H_2, CH_3CHO and 2,3-butanediol on the concentrations RSSR and RSSSR are shown in Fig.2 and Fig.3.

As the results shown above, some conclusions could be drawn:

A. G(diol): Both of RSSSR and RSSR can entirely inhibit the formation of 2,3-butanediol even at very low concentrations(about 5×10^{-5} mol dm^{-3}). This indicates that: (a) the precursor of 2,3-butanediol, hydroxyethyl radical was scavenged directly by RSSR and RSSSR or (b) H atom and e-solv was scavenged, which prevented the formation of hydroxyethyl radical.

$$RSSSR + CH_3\dot{C}HOH \longrightarrow RSSH(RSH) + RS\cdot(RSS\cdot) + CH_3CHO \quad (1)$$

$$RSSSR + H\cdot \longrightarrow RSS\cdot(RS\cdot) + RSH(RSSH) \quad (2)$$

$$RSSR + H\cdot \longrightarrow RS\cdot + RSH \quad (3)$$

B. G(CH_3CHO): The G values of CH_3CHO increase very quickly with the concentrations of RSSR and RSSSR and approach their maxima 3.9 and 5.7 respectively. According to the radiolysis mechanism of ethanol, the reason causing the increasing of G(CH_3CHO) is due to the competition of scavenging e^-_{solv} between RSSR/RSSSR and CH_3CHO. The reactions of RSSSR and RSSR with e^-_{solv} are much more fast, which caused the increasing of G value of CH_3CHO.

$$RSSR(RSSSR) + e^-_{solv} \longrightarrow RSSR^-(RSSSR^-) \quad (4)$$

$$CH_3CHO + e^-_{solv} \longrightarrow CH_3CHO^- \quad (5)$$

However, this may be only explainable for the reactivity of RSSR. In the case of RSSSR, there should be another way to form CH_3CHO, because the maximum increase of G(CH_3CHO) caused by the processes mentioned above is only 1.7. So the redox reaction(1) maybe exists and is important to the formation of CH_3CHO in the RSSSR-ethanol system.

C. G(H_2): The values of G(H_2) decrease slowly with the increasing of concentration of RSSSR and RSSR, can not approach 2[3], even [RSSR] and [RSSSR] as high as 10^{-2} mol dm^{-3}. This is reasonable because in the following reaction

$$CH_3\dot{C}H_2OH + H\cdot \xrightarrow{k_6} CH_3\dot{C}HOH + H_2 \quad (6)$$

k_6 is about 2×10^7 mol^{-1} dm^3 s^{-1}, the ratios of [RSSR] and [RSSSR] to [CH_3CH_2OH] are about

5×10^{-4} , thus reactions (2) and (3) are not comparable to reaction(6) under this condition. In another words, reaction(6) is still predominant over reaction (2) and (3).

(3) The radiolysis products of RSSR and RSSSR in ethanol system.

Irradiated samples were at first separated on GC, three different columns were used, 50m OV-1 capillary column, 25m SE-54 capillary column and 25m PEG-20M capillary column. By comparing the peak retention time with standard compounds on the three columns respectively, and by using FPD detector to check the compounds containing sulfur, and finally GC-MS were used for analysis the structure. The number of sulfur atoms in the molecule can be calculated by using the sulfur M+2 isotope peak intensity. The typical GC and GC-MS spectra are shown in Fig.3-5.

It can be expected that the radiolysis of RSSR and RSSSR should be rather complicated. The G values of main radiolysis products are listed in Tab.1

Tab. 1 The G values of sulfur containing radiolysis products of RSSR and RSSSR in ethanol. Absorbed dose: 4,300 Gy: Dose rate: 1.2 Gy s^{-1}; [RSSR] and [RSSSR] are about 1.0×10^{-3}mol dm^{-3}

Products	-Ge(1)	RSR(F)	RSSR(8)	RSSSR(9)	RSSSSR(K)	RSH(I)
RSSR	1.86	1.02	/	/?	0.10	0.4
RSSSR	2.86	0.2	1.48	/	1.18	1.20

RS_3H(J)	RS_4H(G)	RS_5H(P)	H_2S(L)	$RSOC_2H_5$(H)	ΔR(%)(2)	ΔS(%)(3)
0.2	/	/	1.0	0.40	85.0	90.1
0.15	0.28	0.11	0.90	0.18	88.0	103.0

(1) The total G values of RSSR or RSSSR radiolysis .
(2) The ratio of R (CH_2=CH-CH_2-) in radiolysis products to total R in decomposed RSSR or RSSSR.
(3) The ratio of S in radiolysis products to total S in decomposed RSSR or RSSSR.

The results shown in Tab.1 reveal that the main radiolysis products of RSSR and RSSSR result from attacking S-S bond by reactive species which are induced in the radiolysis of ethanol, such as e^-_{solv}, H· and $CH_3\dot{C}HOH$, though there are some differences in the G values of the products, and less products from attacking S-C and C=C bonds. This is the reason why the radiolysis product spectrum of trisulfide is more complicated than that of disulfide. From the values of the ΔR and ΔS, it can be seen that there are good material balances of allyl group(R) and sulfur atoms in the radiolysis products. So the radiolysis products of RSSR and RSSSR may be formed through reactions(1)-(4) and following reactions:

$$RSSSR^- + CH_3CH_2OH_2^+ \longrightarrow RSS\cdot(RS\cdot) + RSH(RSSH) + CH_3CH_2OH \quad (7)$$

$$RSSR^- + CH_3CH_2OH_2^+ \longrightarrow RS\cdot(R\cdot) + RSH(RSSH) \quad (8)$$

$$2RSS\cdot \longrightarrow RSSSSR \quad (9)$$

$$2RS\cdot \longrightarrow RSSR \quad (10)$$

$$RS\cdot + C_2H_5O \longrightarrow RSOC_2H_5 \quad (11)$$

$$RSH(RSSH) + H\cdot \longrightarrow (RS\cdot) + R\cdot + H_2S \quad (12)$$

CONCLUSION

(1)γ-Irradiation can inhibit the sprouting of garlic bulbs and does not cause the loss of garlic oil yield and the change of the composition of garlic oil in bulbs which have been irradiated during a long period of storage.

(2)Allyl trisulfide and disulfide exhibit strong reactivities to scavenge e^-_{solv}, H and hydroxyethyl radicals introduced by γ-irradiation in the ethanol system, trisulfide can oxidize $CH_3\dot{C}HOH$ radical into acetaldehyde.

(3)The main radiolysis products of RSSSSR(in both cases of trisulfide and disulfide) and RSSR(in trisulfide) can be expected to react with radicals subsequently. Therefore, the garlic oil exhibits remarkable reactivity with radicals.

(4)All of the main radiolysis products are related to the S-S bond breakup, which means that -S-S- is more sensitive to γ-radiation than S-C, C=C and C-H bonds.

References:

1. E.Block. J.A.C.S. Vol. 106, 8295-8296(1984)
2. E.Block. Scientific American Vol.252, 94-99(1985)
3. Wu Jilan et al. Acta Physico-Chemica Sinica Vol.7, NO.1(1991)
4. G.R.Freeman. NATO Adv. Study Lnst. Series C Vol.86, 399-416(1981)
5. B.Milligan. J.Chem.Soc. 4850-4853(1961).

Fig. 1 The Varies of Garlic Oil Contents with Storage Periods

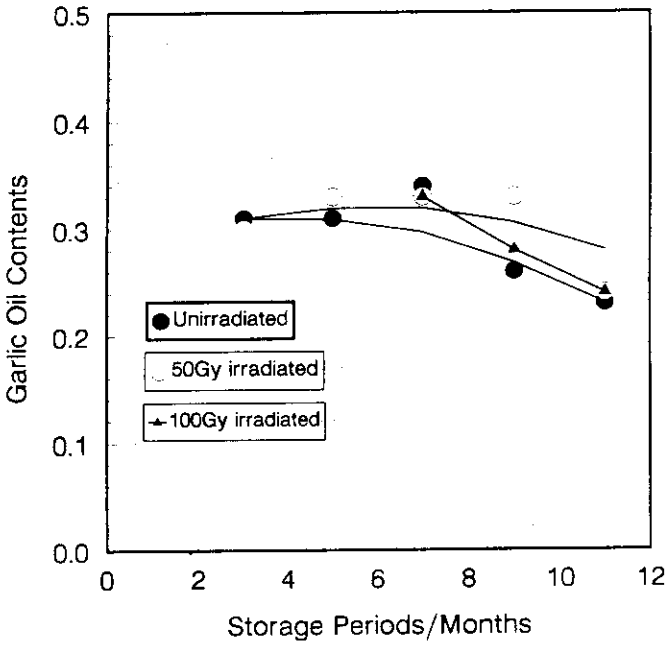


Fig. 2 The dependence of G values of Hydrogen, Acetaldehyde and 2,3-butanediol on [RSSR]; Dose rate = 1.2 Gy/s; Absorbed dose = 4,300 Gy

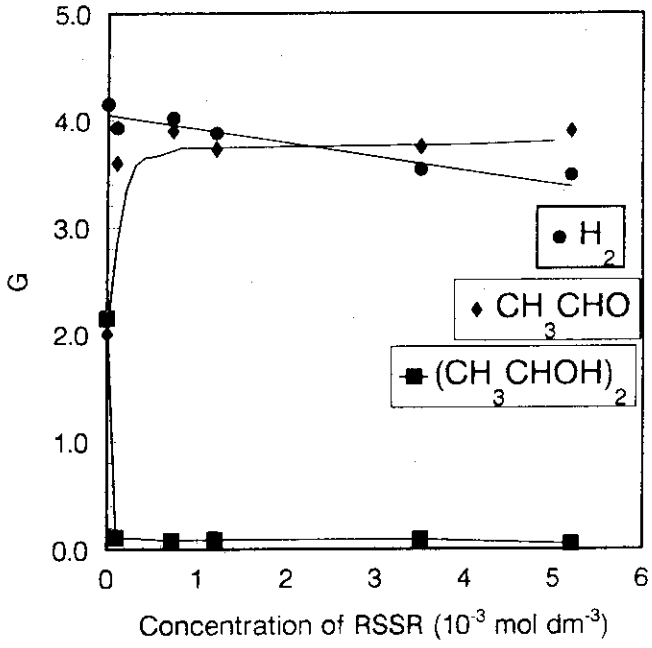
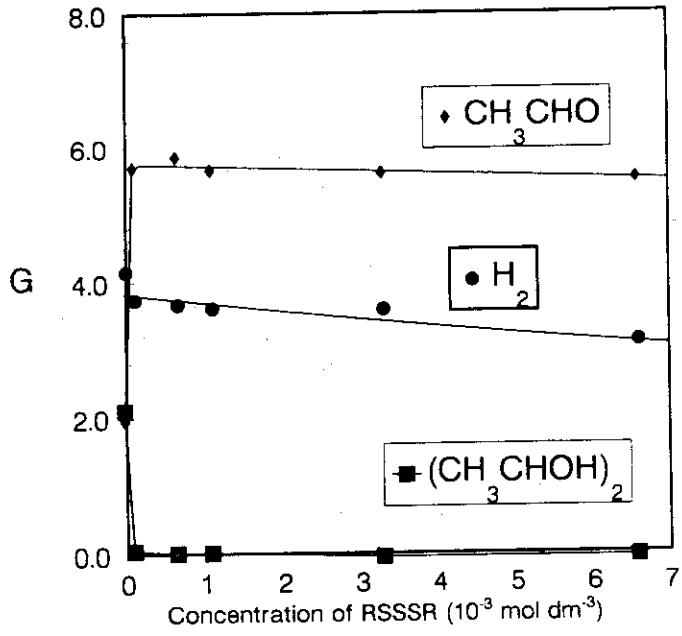


Fig. 3 The dependence of G values of Hydrogen, Acetaldehyde and 2,3-Butanediol on [RSSSR]; Dose rate = 1.2 Gy/s; Absorbed dose = 4,300Gy



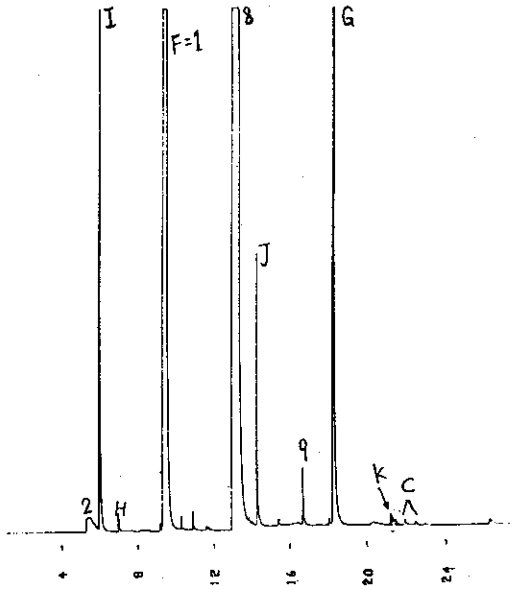


Fig. 4 The GC-spectra of radiolysis products of RSSR in ethanol (FPD). [RSSR] = $1x10^{-2}$ mol dm^{-3}, Dose rate = 1.2 Gy s^{-1} Absorbed dose = 16.000 Gy

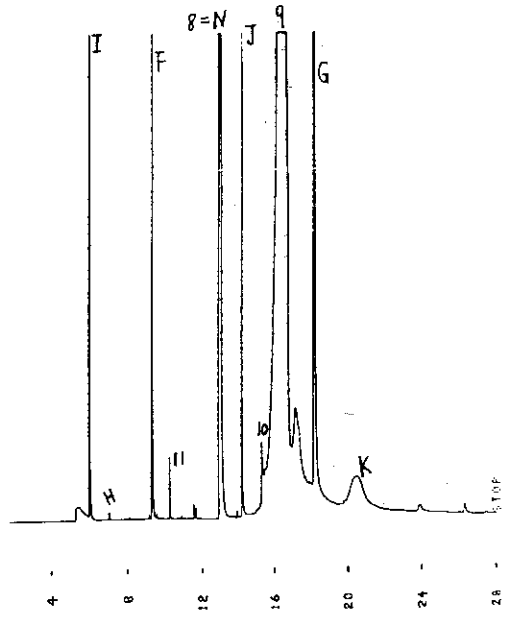


Fig. 5 The GC-spectra of radiolysis products of RSSSR in ethanol (FPD). [RSSSR] = $1x10^{-2}$ mol dm^{-3}. Dose rate = 1.2 Gy s^{-1} Absorbed dose = 16.000 Gy

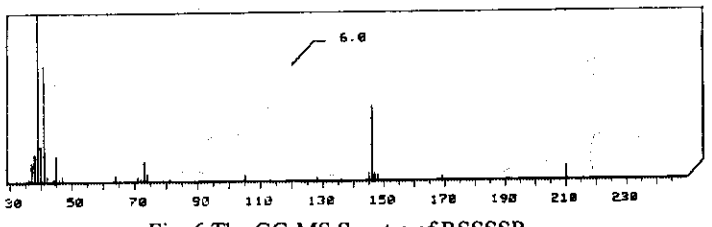


Fig. 6 The GC-MS Spectra of RSSSSR

m/e	210	169	146	136	105	73	43
Fragments	M^+	(M^+-R)	$(M-2S)^+$	$(RSSS^+-1)$	RSS^+	RS^+	R^+

6.6 Radiation Crosslinking for Signal Responsive Chemical Delivery Systems

ISAO KAETSU, KUMAO UCHIDA, SHINJI UETA,
KOICHI SUTANI AND GLYN O. PHILLIPS+

Faculty of Sciemce and Technology,
Kinki University, Kowakae 3-4-1, Higashi-osaka, Osaka, 577 Japan
+ NEWTECH Innovation centre, Croesnewydd Hall,
Wrexham Technology Park,Wrexham,Clwyd, U.K.

ABSTRACT

The authors proposed a signal responsive chemical delivery system(Kartsu, 1994). This system consists of biocoating, biosensor, actuator and substance reservoir. The crosslinked polymers are used for those parts and the radiation crosslinking has an important role for the purpose. The aqueous solution of vinyl monomer, crosslinker and polysaccharide was irradiated. Polysaccharide was entraped in a crosslinked vinyl polymer gel. The electro-responsive transformation and relaxation(volume shrinkage and expansion) of the gel was investigated. It was found that the crosslinking affected remarkedly on the electro-responsiveness as an actuator.

INTRODUCTION

The author's group has studied and developed an implantable drug delivery systems by radiation polymerization ,crosslinking and sterilization(Kaetsu,1988, 1992, 1993). However, the request for a signal responsive drug delivery,which means a timing controlled drug delivery by a signal from an environment, is increasing in recent years. From this point of view, the author proposed a novel chemical delivery system consisting of a biosensor and a drug delivery system (Kaetsu, 1991, 1994).

The concept of this system is shown in Fig.1 schematically.

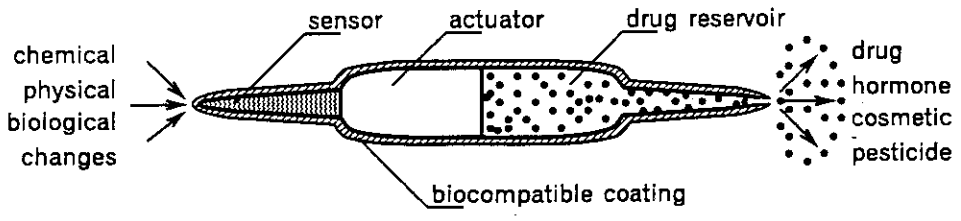


Fig.1 Model scheme of signal responsive chemical delivery system.

As shown in Fig.1, the signal responsive chemical delivery system consists of biocoating to give a biocompatibility to the device, biosensor to catch a signal from the used environment, actuator to transduce an electrical signal from the sensor into a mechanical energy to initiate a substance release from a reservoir and bioreactor to produce and provide a substance to the reservoir.Radiation immobilization techniques (Kaetsu, 1992, 1993) can be used for the biosensor to immobilize enzyme, antibody and receptor, for the bioreactor to immobilize a biocatalyst and also for the reservoir to immobilize a drug and other chemical substances to be released.

It is important that various kinds of polymeric gels are used as the basic materials for biocoating, biosensor, actuator and reservoir and most of those gels should be crosslinked for the uses. The reason would be described in the following sections. Therefore, the advantage of radiation to cause the crosslinking easily and efficiently can be noticed for the present purpose to construct the signal responsive chemical delivery system.

EXPERIMENTAL

UV light from 400W MercuryArc Lamp or gamma-ray from 5000 Ci Cobalt-60 source was irradiated on a mixture of monomer, polyfunctional monomer and polysaccharide aqueous solution to polymerize and crosslink the system. The formed gel was cut into 1.0 cm^3 cubic form and sandwitched between

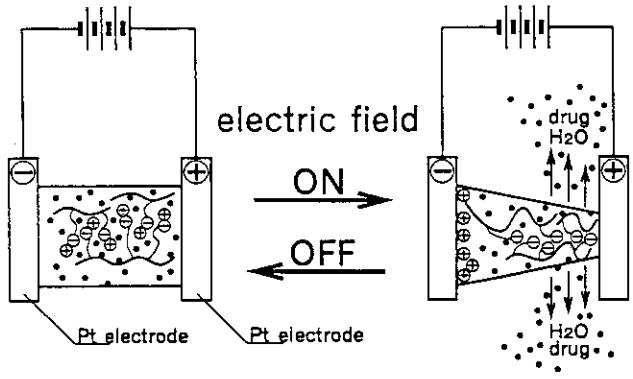


Fig.2 Model scheme of electro-responsive release in polyelectrolyte gel.

two platin electrodes . The changes in weight of the gel were measured with the on -off switching of electric field between the electrodes at a certain interval. The gel fraction and the swelling ratio of gel were measured by common method of weighing. The gel shrunk under electric field owing to an electrophoresis phenomenon and expanded again with off-electric field by a relaxation. The electroresponsiveness of the gel was evaluated by clearness and keenness of those changes due to electrophoretic transformation and the relaxation. Model scheme for electroresponsiveness test is shown in Fig.2.

RESULTS AND DISCUSSION

Entraping crosslinking of polysaccharide in polymethacrylate and polyacrylate gels

The mixture of monomers and polysaccharide aqueous solution was irradiated. The product was a homogeneous gel. The mechanism of gelation has not been clarified. But it was reduced that the polysaccharide molecule was entraped inside the crosslinked network of polymethacrylate or polyacrylate gel. A co-crosslinking between polysaccharide and other polymer, and a grafting of other polymer onto polysaccharide might be partly possible. However, a similar homogeneous gel formed also by a catalytic reaction of same system. The main principle of gelation might be the entraping of polysaccharide in the polymethacrylate or polyacrylate networked matrix. Fig.3 and Fig.4 show the results of gelation by the entraping crosslinking of hyaluronic acid sodium salt-methacrylates

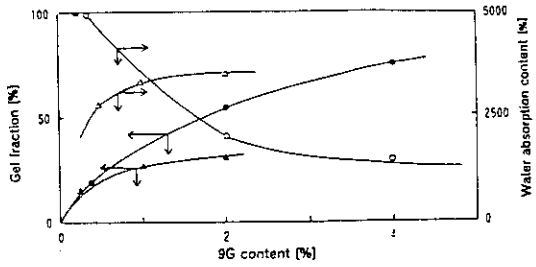


Fig.3 Relation between 9G content and gelation in entraping crosslinking of poly saccharide monomer system.
Composition, Hyaluronic acid sodium salt(HA)−N,N'−methylene−bis acrylamide(BIS)−polyethylenglycol #400 dimethacrylate(9G);
(△ , ▲):100−2−X;(○ , ●):100−4−X.

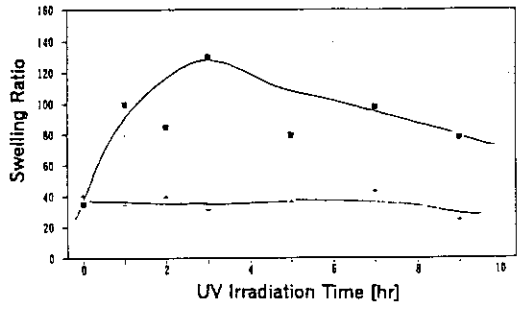


Fig.4 Effect of irradiation time on swelling ratio of entraping hydrogel
Composition, Hyaluronic acid sodium salt(HA)−N,N'−methylene−bis acrylamide(BIS)−polyethylenglycol #400 dimethacrylate(9G);(■):100−2−2;
HA−Polyethylenglycol dimethacrylate(2G)−2−hydroxyethyl methacrylate;
(+):100−0.04−4.

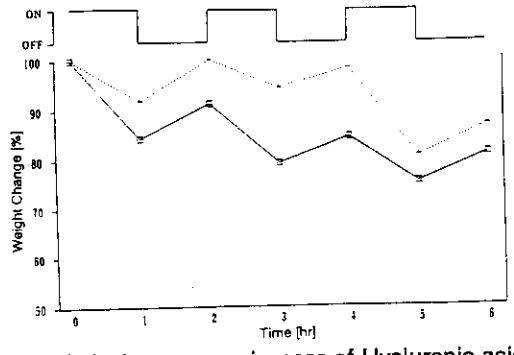


Fig.5 Change of electro−responsiveness of Hyaluronic acid sodium salt with changes of voltage.
Composition,HA−HEMA−9G;1−0.04−0.04. Voltage;(□):10V;(+):5V.

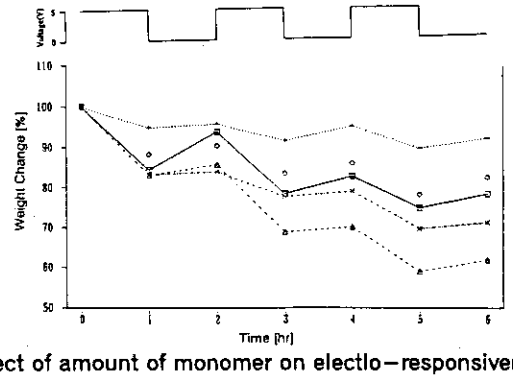


Fig.6 Effect of amount of monomer on electlo−responsiveness of carboxyl methyl cellulose sodium salt(CMC) under on−off switching of electric field.
Composition,CMC−HEMA−9G;(□):1−0−0.05;(+):1−0.05−0.05;
(◇):1−0.10−0.05;(△):1−0.15−0.05;(×):1−0.20−0.05.

system and alginate sodium salt-methacrylates system.

Electro-responsiveness of polysaccharide-polymethacrylate entraping gels

The electroresponsiveness of formed gels was measured and evaluated. The results were shown in Figs.5 and 6. As observed in those figures, a considerable electro-responsiveness was proved in the polysaccharide entraping gels. But it was not so keen as compared to the responsiveness in synthetic polyelectrolyte such as polyacrylic acid sodium salt(Kaetsu, 1992). The results also showed that the crosslinking affects importantly on the electro-responsiveness. For examples, the responsiveness of hyaluronic acid sodium salt and alginate sodium salt systems showed the optimum responsiveness at a certain amount of crosslinker composition. Fundamentally the crosslinked structure is necessary to keep polysaccharide molecule insoluble and unleakable from the matrix. Furthermore, the crosslinked structure is also reologically important to realize and control the electro-responsive reversible volume changes. Because, the responsiveness is the repetition of transforming and relaxing and the visco-elastic property of gel is related essentially to the transformation and relaxation behavior. The optimum viscoelastic property can be attained by an optimum crosslinked structure. The study to clarify the relation between the optimum responsiveness,viscoelasticity and crosslinking would be continued and reported in the near future.

REFERENCES

Kaetsu I., (1994) Radiat. Phys. Chem., in press
Kaetsu I. et all , (1988) Drug Develop. Industr. Pharmac., 14, 2519
Kaetsu I.,(1992) Radiation Processing of Polymers(Ed. by A. Singh and J. Silverman) Chapter 8,p149
Kaetsu I.,(1993) Advances in Polymer Science (Ed.by S. Okamura) vol.5, p81
Kaetsu I. et all (1991) Proc. 18th Intern. Symp. Controlled Release of Bioact. Mater., p449
Kaetsu I. et all (1994) Proc. 21st Intern. Symp. Controlled Release of Bioact. Mater., p.589
Kaetsu I., Uchida K., Morita Y., Okubo M., (1992) Radiat. Phys. Chem., 40, 157

7. Poster Presentation (1)

7.1 Variation in Yield Ratios of Fragment Ions and of Ion-pairs from CF_2Cl_2 Following Monochromatic Soft X-ray Absorption

I. H. Suzuki, N. Saito, and J. D. Bozek

Electrotechnical Laboratory, Umezono, Tsukuba-shi, Ibaraki 305, Japan

Abstract Fragment ions produced from CF_2Cl_2 have been measured from 44 to 1200eV using a time-of-flight mass spectrometer and monochromatized synchrotron radiation. Positively charged ion pairs from this molecule were observed in the inner-shell excitation regions using a Selected photoion-photoion coincidence technique. Obtained yield ratios of fragment ions indicate that the atomic chlorine ion, Cl^+, has the greatest intensity at all photon energies above 60eV and exhibits a steep increase at the Cl $L_{2,3}$-edges. Some fragment ions, in particular CF_2^+, have a clear intensity increase at the transitions of inner-shell electrons to unoccupied molecular orbitals. The ion pair F^+ - Cl^+ exhibits the highest yield at most photon energies, and some of the branching ratios for ion-pair production changed significantly near the Cl $L_{2,3}$-edges.

INTRODUCTION

When a molecule is irradiated with a soft X-ray, an inner-shell electron in the molecule is excited to unoccupied molecular orbitals, Rydberg orbitals or ionized continuum. Produced inner-shell holes are usually filled through the Auger transition, and the molecule turns into a highly excited molecular ion. Then the molecular ion decomposes to ionic fragments. Since the core hole is strongly localized around the particular atom, core-electron excitation in the molecule is expected to result in selective bond breaking. Several studies were carried out for understanding this site-selective reaction in molecules excited in core-hole states (Nagaoka et al., 1993). Since the molecule CF_2Cl_2 has three inner-shells in the soft X-ray region, it is very interesting to examine the fragmentation pattern of this molecule photoexcited using monochromatic soft X-rays. On the other hand, ionic fragmentation was studied in the vacuum ultraviolet radiation region, indicating that CF_2Cl^+ has the highest yield (Zhang et al., 1991). Inner-shell excitation spectra were also reported to show some pre-edge structures and ionization continuum transition (Chen and Sette, 1990 and Zhang et al., 1992). In the present study, ionic products from CF_2Cl_2 following selective inner-shell excitation have been measured using a time-of-flight (TOF) mass spectrometer and monochromatized synchrotron radiation.

EXPERIMENTAL

Synchrotron radiation from the electron storage ring at the Electrotechnical Laboratory was dispersed using a Grasshopper monochromator in the soft X-ray region (Saito et al., 1994, Suzuki et al., 1994a and Suzuki et al., 1994b). In order to reduce the stray light and higher-order contributions, the energy for the electron beam in the storage ring was appropriately selected and thin films of Be, Al, In and mylar were inserted into the soft X-ray beam. The monochromatic soft X-ray beam crossed an

effusive beam of the sample gas at right angles in the center of the TOF spectrometer. The electrons and ions produced were extracted in opposite directions and detected with micro-channel plates. The electric field applied at this center was set to be 80 V/mm in order to collect ions of all kinetic energies.

The spectrometer was operated in two measurement modes ; TOF mass spectrum mode and Selected photoion-photoion coincidence (PIPICO) spectrum mode. In the TOF mode, two time-to-amplitude converters (TAC's) were used for minimizing detection loss of heavier fragment ions because two ionic products are usually formed in the present photon energies and because the conventional technique usually detects only lighter fragment ions. In the Selected PIPICO mode, the conventional PIPICO technique was modified for obtaining a well separated PIPICO peak for each ion-pair. A gating signal was supplied to the TAC for selecting a particular fragment ion as the lighter partner of ion pairs.

RESULTS AND DISCUSSION

1) Time-of-flight spectra

Figure 1 shows TOF spectra of CF_2Cl_2 measured at photon energies of 50, 220, 320 and 800eV. These photon energies correspond to those being capable to induce ionizations of only valence electron, Cl 2p electron, C 1s electron and F 1s electron, respectively. The parent molecular ion $CF_2Cl_2^+$ was not observed here, which agrees with the result by Zhang et al. (1991). Since natural chlorine atom consists of two main stable isotopes, the peaks for the ions including one or two atoms are split into two or three components. The relative intensities of the peaks change dramatically with photon energy over this energy range. The widths of the peaks increase at higher photon energies, and this increase results from a greater release of kinetic energy in the ionic fragmentation of CF_2Cl_2 at the higher photon energies. Yield ratios for the production of fragment ions were determined from the areas of the peaks in the TOF mass spectra measured over the energy range 44-1200eV (Suzuki et al., 1994a).

2) Selected photoion-photoion coincidence spectra

For ion-pair production from CF_2Cl_2, the Selected PIPICO technique was used. Typical examples of ion-ion coincidence spectra are shown in Fig. 2 for a photon energy of 214eV. The conventional PIPICO spectrum is shown at the top panel of Fig. 2, where a number of structures are found in the difference spectrum of flight times. When we focused on the fragment ion C^+ as a lighter ion (faster ion), the spectrum measured with the Selected PIPICO is shown in Fig. 2 (b). The spectrum indicates the presence of $C^+ - F^+$ and of $C^+ - Cl^+$ clearly. Since the photon energy is above the Cl $L_{2,3}$-edges, it is natural that the intensity of $C^+ - Cl^+$ is considerably higher than that

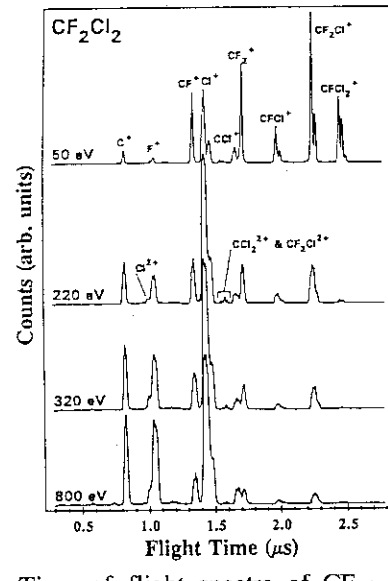


Fig. 1 Time-of-flight spectra of CF_2Cl_2 measured with some photon energies.

of $C^+ - F^+$. The central panel of the figure, Fig. 2 (c), depicts the Selected PIPICO spectrum when F^+ was selected, where the ion-pair of $F^+ - Cl^+$ has the highest intensity. The Selected PIPICO spectra for the selection of CF^+ and Cl^+ are given in Fig. 2 (d) and (e), respectively. As described here, the Selected PIPICO technique provides a clear spectrum in which we can easily assign each peak to the corresponding ion pair (Suzuki et al., 1994b).

3) Yield ratios of fragment ions

Yield ratios of fragment ion production are shown as a function of photon energy in Fig. 3 (a) and (b) (Suzuki et al., 1994a). Molecular ions composed of 3 and 4 atoms have high yield ratios below 100eV but show a steeply decreasing trend with increasing photon energy below the Cl $L_{2,3}$-edges. The atomic ions have the yield ratios exhibiting a significantly increasing curve below these edges. The ratio of Cl^+ suddenly increases at these edges, but that of F^+ shows a drop at these edges and a considerable increase at the F K-edge.

It is interesting to note that the yield ratios of molecular ions decrease below the Cl $L_{2,3}$-edges and that those of atomic ions increase. This phenomenon probably originates from fragmentation pathways which become open at or above excitation energies of 50eV. These pathways are presumably connected to excited states involving two valence electrons. A molecular ion with two holes in the valence shell has a greater probability of yielding a higher degree of fragmentation than the one with only a single valence hole.

Sharp changes in the yield ratios of the fragment ions across the inner-shell ionization edges may result from the different relative probabilities of two valence hole states being populated by double valence

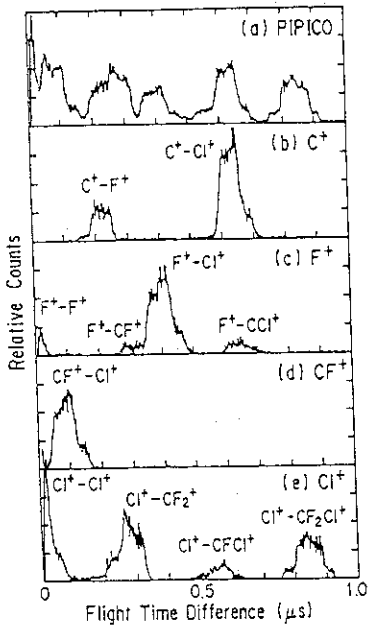


Fig. 2 Spectra of difference of flight times between fragment ions produced from CF_2Cl_2 using the Selected PIPICO techinique.

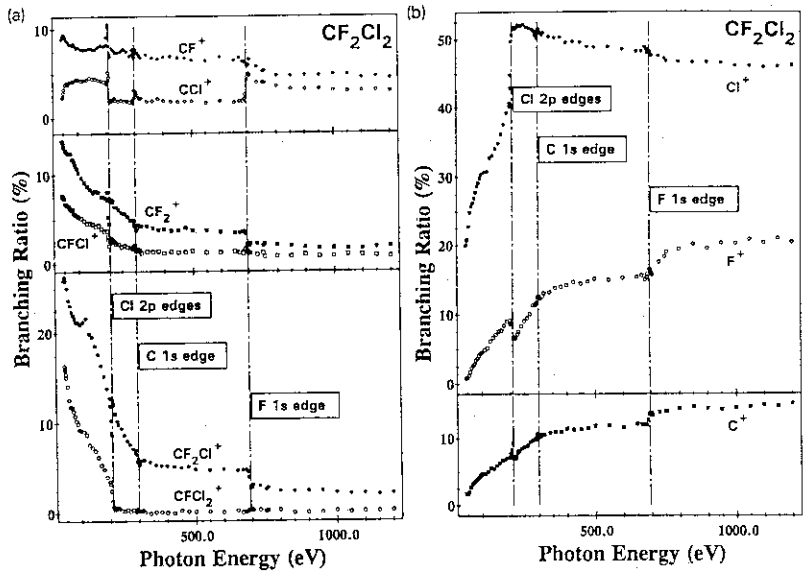


Fig. 3 Yield ratios of the fragment ions of CF_2Cl_2 over the photon energy range of 44 to 1200eV. (a) Molecular ions. (b) Atomic ions.

excitation or by the Auger decay of a core hole. The valence orbitals holding the spatial overlap with the core-hole have a greater pobability of being involved in the Auger transition. Then the excitation of Cl 2p electron tends to bring about the bond breaking near the Cl atom, i. e. the Cl^+ has a higher probability to be produced. A similar effect is found through the increase in the yield ratio of F^+ around the F K-edge, as shown in Fig. 3.

Measured partial yield spectra for fragment ions around inner-shell ionization edges show that atomic ions have a spectrum close to the total ion curve, which approximates the photoabsorption spectrum (Chen and Sette, 1990 and Zhang et al., 1992). The fragment ions CF_2^+ and CF^+ show a large peak at the excitation of Cl 2p electron into the unoccupied molecular orbital, $13a_1$. The $CFCl_2^+$ has a constantly decreasing curve across the Cl $L_{2,3}$-edges, indicating no production of this ion through the Cl 2p electron transition. The feature in the partial yield curves around the C K-edge is that the $CFCl_2^+$ exhibits a broad peak at the excitation into the molecular orbitals of $7b_1 + 14a_1$. The ions CF_2Cl^+ and CF_2^+ have partial yield spectra of constantly decreasing intensity around the F K-edge.

4) Yield ratios of ion-pairs

Yield ratios obtained at several photon energies are listed in Table 1 (Suzuki et al., 1994b). The ion pair $F^+ - Cl^+$ has the highest yield ratios at all the photon energies except 216eV, slightly above the Cl $L_{2,3}$-edges, and $C^+ - Cl^+$ shows the second highest. The most interesting finding is that the ratio of $Cl^+ - CF_2Cl^+$ exhibits a sharp increase at 216eV. This phenomenon is presumed to come from the following. The Auger transition following the Cl 2p electron ionization yields a number of low excited states of doubly charged molecular ions. These ions decompose to fragment ion pairs with a single bond breaking. If the molecular ion is produced in a highly excited state, the decomposition should take place more completely ; Lower yield of the $Cl^+ - CF_2Cl^+$ and higher yield of the ion-pairs composed of only atomic ions are expected than the measured results. This presumption is supported by the increase in the yield ratio of $Cl^+ - CF_2^+$ at 216eV. It is desireable that the Auger electron spectra are precisely measured from the inner-shell hole states of interest in the near future. The ion-pairs including F^+ show an increase in the yield ratio near the F 1s electron excitation. This finding is interpreted as a site specific effect ; The chemical bond around the fluorine atom is loosened to break and the atomic fluorine ion is yielded largely.

Partial yield spectra of individual ion pairs have been measured around the Cl $L_{2,3}$-edges, the C K-edge and the F K-edge. The spectra for many ion pairs show a similar curve to the photoabsorption spectra (Chen and Sette, 1990 and Zhang et al., 1992). Some spectra, however, exhibit a feature different from the photoabsorption ; Relative intensity of excitation into unoccupied molucular orbitals, compared to that of ionization, is very low for $Cl^+ - CF_2Cl^+$ near the Cl $L_{2,3}$-edges, for $Cl^+ - CF_2^+$ near the F K-edge. The yield of $Cl^+ - CF_2Cl^-$ shows a constantly decreasing trend near the F K-edge, indicating no production of this ion pair through the F 1s electron transition.

Table 1. Yield ratios (%) of ion-pair production from CF_2Cl_2 photoexcited around the inner-shell ionization thresholds. U denotes unoccupied molecular orbitals.

Energy	C-F	C-Cl	F-Cl	CF-Cl	Cl-Cl	Cl-CF_2	Cl-CF_2Cl
198	7.8	17.9	22.2	13.9	10.5	12.2	3.6
201(Cl_{2p}^{-1}U)	6.8	18.6	20.3	17.2	11.4	11.7	4.1
216	4.9	16.2	14.0	16.8	11.2	14.9	13.7
290	8.4	18.9	22.4	15.6	12.8	8.9	6.1
295(C_{1s}^{-1}U)	8.7	19.5	22.8	14.7	11.9	9.7	5.2
308	8.9	19.5	23.1	15.1	12.5	8.6	5.2
680	11.6	19.7	25.6	12.8	11.1	7.4	4.2
692(F_{1s}^{-1}U)	12.1	21.0	25.5	11.7	10.7	7.7	3.0
720	11.7	21.4	25.9	11.3	10.9	7.6	2.9

CONCLUSIONS

Variation in yield ratios of fragment ions and ion-pairs from CF_2Cl_2 have been found around the Cl $L_{2,3}$-edges, the C K-edge and the F K-edge. The yield ratio of Cl^+ increases steeply at the C $L_{2,3}$-edge, and F^+ exhibits an increase above the F K-edge. The yield ratio of $Cl^+ - CF_2Cl^+$ shows a significant change near the Cl $L_{2,3}$ - edges.

REFERENCES

Chen C. T. and Sette F. (1990) High resolution soft X-ray sepctroscopies with the Dragon beam line. Physica Scripta T31 119.

Nagaoka S., Oshita J., Ishikawa M., Masuoka T. and Koyano I. (1993) Ionic fragmentation processes following Si : 2p core level photoexcitation and photoionization of 1, 1, 1-trimethyltrichlorodisilane. J. Phys. Chem. 97 1488.

Saito N., Bozek J. D. and Suzuki I. H. (1994) Ionic fragmentation of CF_4 in the vacuum ultraviolet through the soft X-ray region. Chem. Phys. (in press).

Suzuki I. H., Bozek J. D. and Saito N. (1994) Ionic dissociation of CF_2Cl_2 photoexcited using monochromatic soft X-rays. Chem. Phys. 182 81.

Suzuki I. H., Saito N. and Bozek J. D. (1994) Variation in ion-pair yields from CF_2Cl_2 photoexcited in the inner-shell excitation regions. Int. J. Mass Spectrom. Ion Processes (in press).

Zhang W., Cooper G., Ibuki T. and Brion C. E. (1991) Excitation and ionization of freon molecules. Ⅲ. Absolute oscillator strengths for the photoabsorption (8.5-200eV) and the ionic photofragmentation (11.5-70eV) of CF_2Cl_2. Chem. Phys. 151 357.

Zhang W., Ibuki T. and Brion C. E. (1992) Absolute dipole differential oscillator strengths for inner shell spectra from high resolution electron energy loss studies of the freon molecules CF_4, CF_3Cl, CF_2Cl_2, $CFCl_3$ and CCl_4. Chem. Phys. 160 435.

7.2 The Specialty Committee of Radiation Processing of CIRA

Hou Fuzhen

The Speciality Committee of Radiation Processing
P.O.Box 45 No.30, Baishiqiao Road, Beijing 100081 P.R.C.

The Speciality Committee of Radiation Processing, of China Isotope and Radiation Association, is a socioeconomic organization which is organized on a voluntry basis, from industry sectors, institutions, scientific centers/labs, and academic universities in domestic radiation techniques and industry. The Committee which was established in Feburary 1992, has about 100 memeber units. Its works are directed by the China Isotope and Radiation Association (CIRA). Mr. Pan-Xiumiao is the director and Mr. Zhao-Wenyan is the permanent councilor of the Committee. The council consists of 30 memeber units, with a specialists' group of 13 experts, professors or research people, who could provide consulting services. A marketing network center of domestic radiation-treating processing was set up in 1993.

Radiation-treating processing industry is a new technology-based industry which uses high energy particles from a variety of nuclear radiation and accelerators for irradiating materials and products, including radiation-chemicals, radiation materials, sterilization of medical instrument, preservation of food, disposal of environment wastes, radiation control, and construction of radiation-treating equipment and their application technology.

Chief works done by the Committee:

It collects, counts, and sorts out the basic data or materials of radiation industry; investigates and analyses the developing tendency; proposes the plan, tech-economic policy and industry protection policy for the government; announces and conveys home and abroad tech-economic information and marketing information with the references of corresponding activities.

It organizes key research work, engineering projects and technical proof for the commission of responsible department.

It provides products appraisal and quality evaluation for the commission of some related departments.

It promotes cross-corporation between inner parts of the industry and between radiation industry and other industry; launches activities for exchanging techniques and management; provides consulting services for enterprises in producing and marketing; accelerates the technology process in radiation industry and improves the management.

It conducts various forms of activities in spreading the techniques, high-quality, management, teaching and evaluation; organizes personnel training courses and enhances professional quality in radiation-treating processing industry.

It contacts with other countries to enlarge co-orporation and exchanges on economic and technology and to meet the need of export and import within the radiation indutry.

Presently, the committee's memeber units have more than 40 Co-source irradiation equipments with 100k curie, spreading over 30 big cities. Now, China has more than 30 industrial accelerators with KW in 20 cities.

China has done a lot of research work on radiation-chemistry, chemicals, disinfection of medical instruments, preservation of food, radiation dosage and on the design and manufacture of radiation eqipment. There has been granted with hygenic standard of 18 kinds of irradiation-treating food by the State. Developed radiation -chemicals consist of about 20 items and irradition medical materials of over 20 items. Now, China has established State-standards for radiation dosage and has the ability to design or manufacture Co-Source equipment and large power irradiation accelerators independently. China has several times organized international academic symposium and training classes on radiation technology and has taken part in a lot of work in international services.

Among the 100 memeber units, have specialized chemical factories or corporation; have irradiation-treating workshops or assembly shops; have irradiation centers for manufacture and maintenance; the other are research institutions or colleges and universities, which aim at basic studies and applied usage of radiation processing, that can be carried out in some of their own corporations or factories.

Up to now, mone than 20 enterprises have eqiped with large power irradiation -treating accelerators for their irradiation of interconnect wires and cables.

Radiation chemical products includes heat-shrinkble materials, wires and cables, polyacrylamides, low-temperture bonders for textile printing and dyeing, lenses, functional films, medical silica rubber tubes, biological dressing, photographic emulsion supplemental agents, superfine powder of polyvinyl tetrafluoide, renew rubber, crystal/gem colouring. Polyvinyl actate has already been put into production; while foamed plastics, coat solidifying, rubber sulphrating, etc, are on their mid-term trial.

Radiation-treating disinfection of bacterium deals mainly with used-once only medical products, fur products, irradiating food includes 18 hygenic standard granted kinds, such as cereal crops, potatoes, etc.

"RedTech Asia '95 " — An international conference is going to be held by the Speciality Committee of Radiation Processing of CIRA in November 1995.

7.3 Photoionization Potentials of Fullerenes (C_{60}-C_{84}) in Non-polar Liquid

Iwao SHIMOYAMA, Kazumichi NAKAGAWA, [1]Chiemi FUJIKAWA,
[1]Katsuyuki MORII, [1]Tadaoki MITANI, [2]Ryuuzi KATO

Faculty of Human Development, Kobe University, Tsurukabuto, Nada-ku, Kobe 657, Japan
[1]Japan Advanced Institute of Science and Technology, Hokuriku, Tatsuguchi, Noumi-gun, Ishikawa 923-12, Japan
[2]Faculty of Science, Gakushuuin University, Mejiro, Tokyo 171, Japan

Abstract We measured ionization potential of fullerenes(C_{60}, C_{70}, C_{76}, C_{78A}, C_{78B}, C_{82}, C_{84}) in 2,2,4-trimethylpentane, and determined values of gas-phase ionization potential I_g of these fullerenes on the basis of electronic properties of nonpolar liquid. We found that with the increase of carbon number N, I_g values decreased at first and turned into increase at N>78. This result shows similar tendency to theoretical I_g data calculated by J.Cioslowski et. al.

INTRODUCTION

Since the discovery of C_{60}, fullerens were investigated so hardly in many fields. However, many basic physical and chemical properties of fullerenes are not revealed yet. One of those is the gas-phase ionization potential I_g, which is essentially important physical quantity. Although gas-phase UPS data are reported for C_{60} and C_{70}, such data for higher fullerenes are no tavailable because evaporation temperature of higher fullerenes is so high that experiment is very difficult. Therefore, instead of gas-phase UPS measurement, we tried to estimate I_g values of higher fullerenes from the result of measurements of photocurrent threshold energy I_P of fullerenes(C_{60}, C_{70}, C_{76}, C_{78A}, C_{78B}, C_{82},C_{84}) doped in 2,2,4-trimethylpentane(TMP). It is established tha tionization potential I_P of aromatic molecules doped in nonpolar liquid is wel ldescribed by an equation (Horlyd et al.,1983)

$$I_P = I_g + P + V_0 \qquad (1)$$

where V_0 is conduction band energy of liquid TMP, P is polalization energy of fullerenes in TMP. From Eq. (1), since V_0 of TMP is reported to be -0.24eV (Horloyd et al.,1983) I_g should be estimated when we measure I_P and estimate P value. Then we started experiment to measure I_P values.

EXPERIMENT

Fullerenes were prepared and purified in Japan Advanced Institute of Science and Technology, Hokuriku. Highly purified TMP were offered by Dr. Kengo Itoh at the University of Tokyo.

Experiments were performed at the BL-1B beamline of the UVSOR in the Institute for Molecular Science, Okazaki, Japan. The experimental arrangement is shown in the Figure 1. Monochromatized synchrotron radiation (SR) in the energy region of $2.4<h\nu<12.4$eV was introduced between two parallel-plate electrodes in the cell through the MgF_2 front window. After filling cell with TMP doped with fullerene, we measured photocurrent $i(h\nu)$ between the electrodes, and transmitted light intensity $T(h\nu)$ through the MgF_2 rear window of the cell.

Examples of absorption and photocurrent spectra of C_{78} are shown in the Figures 2 and 3. Because of strong absorption of the TMP above 6.7eV, we analyzed $i(h\nu)$ and $T(h\nu)$ in the region of $h\nu<6.7$eV.

RESULTS AND DISCUSSION

We determined I_P values using semi-empirical power law

$$Y(h\nu)=C(h\nu-I_P)^{5/2} \qquad (2)$$

where C is a constant, $h\nu$ is incident light energy, and $Y(h\nu)$ is photoionization quantum yield (Yakovlev and Lukin, 1985). $Y(h\nu)$ is defined as number of released electrons from the fullerenes divided by number of photons absorbed by the fullerenes. The former were calculated from $i(h\nu)$ and the latter were estimated from $T(h\nu)$. From the Eq.(2), a plot of $Y(h\nu)^{2/5}$ vs. $h\nu$ should have a linear portion. So, we determined I_P from the intersection of the linear line with the baseline. In Table 1 we show these values of I_P. Figure 4 shows obtained values of I_P vs. numbers N of carbon atoms of fullerenes.

We estimated experimental I_g values via eq.(1). V_0 value of TMP was reported to be -0.24eV[1]. P values of fullerenes were estimated via Born formula (Born, 1920)

$$P=-\frac{e^2}{2R}\left(1-\frac{1}{\varepsilon}\right) \qquad (3)$$

where e is the elementary charge, R the ion radius, and ε the dielectric constant of TMP, which is reported to be 1.936 at room temperature. Values of R were calculated by a simple relation

$$R = 0.355\sqrt{N/60} \qquad (4)$$

reported (Y.Saito et al., 1993), where N is the carbon number. Values of Ig estimated via Eq. (1), (3) and (4) are shown in the Figure 4 by a symbol ○. It is clear that with the increase of carbon number N, I_g values decrease at first and turns into increase at N>78. This result shows similar tendency to the theoretical I_g values calculated (J.Cioslowski et.al., 1992) , which are shown in the figure by a symbol △.

References 1)Holroyd R.A. et. al. (1983) J.Chem.Phys.79,1.
2)Yakovlev B.S. and Lukin L.V. (1985) Advances in Chem.Phys.60,99.
3)Born M. (1920) Z.Physik.1,45
4)Saito Y. et. al. (1993) Phys.Rev.B 48,12.
5)Cioslowski J. et. al. (1992) J.Chem.Phys.98,11.

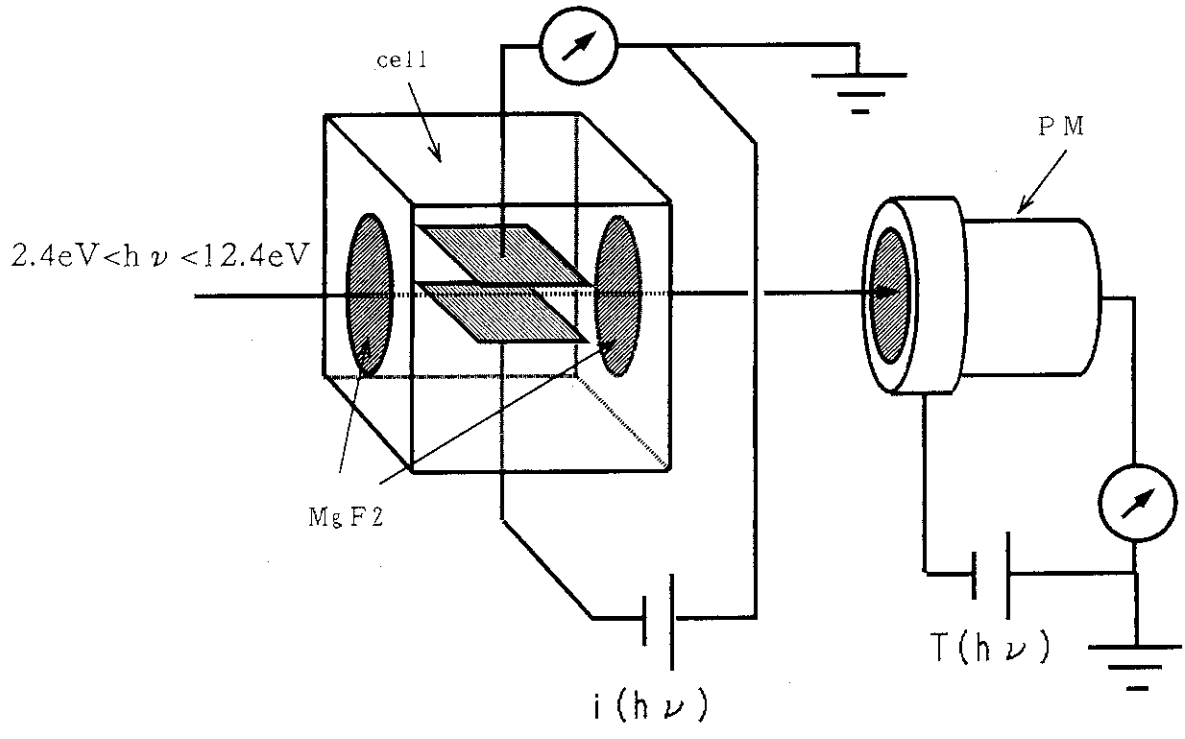


Fig.1. Experimental arrangement

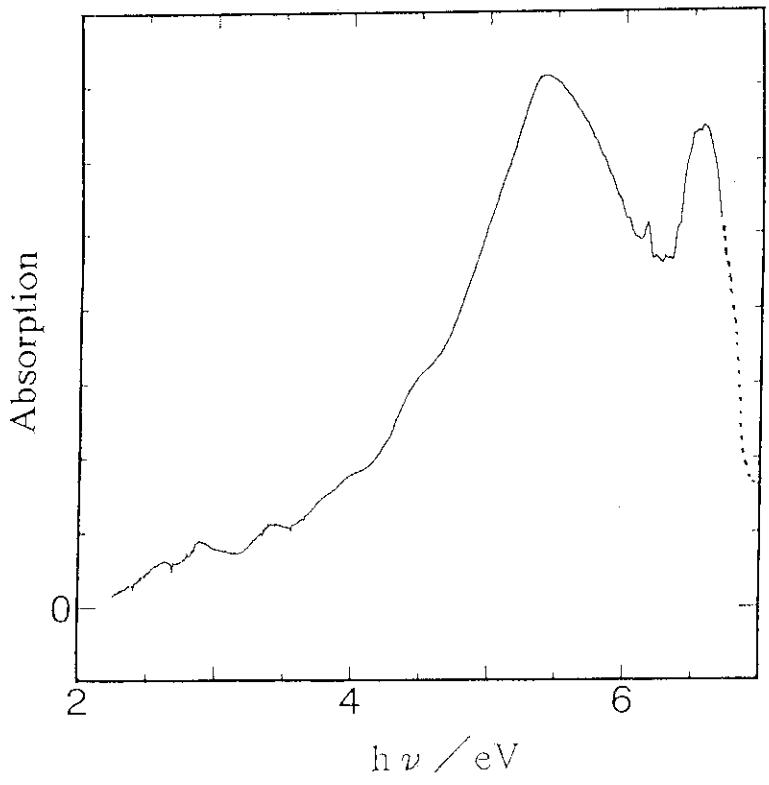


Fig.2. C_{78}/TMP absorption spectra

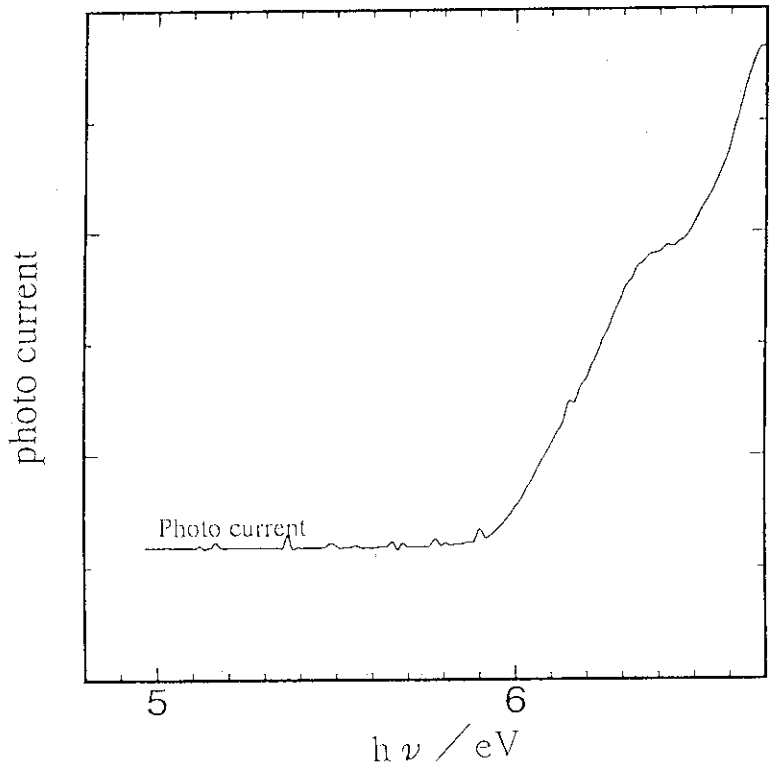


Fig.3. C_{78}/TMP photocurrent spectra

Table 1. Ionization potential of fullerene

	I_P(exp)	I_g(exp)	I_g(calc)
C_{60}	6.59	7.49	7.54
C_{70}	6.40	7.26	6.96
C_{76}	6.21	7.06	6.59
C_{78A}	6.11	6.96	6.91
C_{78B}	6.00	6.85	6.58
C_{82}	6.07	6.90	6.49
C_{84}	6.22	7.05	6.92 (D_2) 6.95 (D_{2d})

I_P(exp);our experimental data in TMP. I_g(exp);I_g data estimated from our I_P.
I_g(calc);theoretical I_g data by J.Cioslowski.

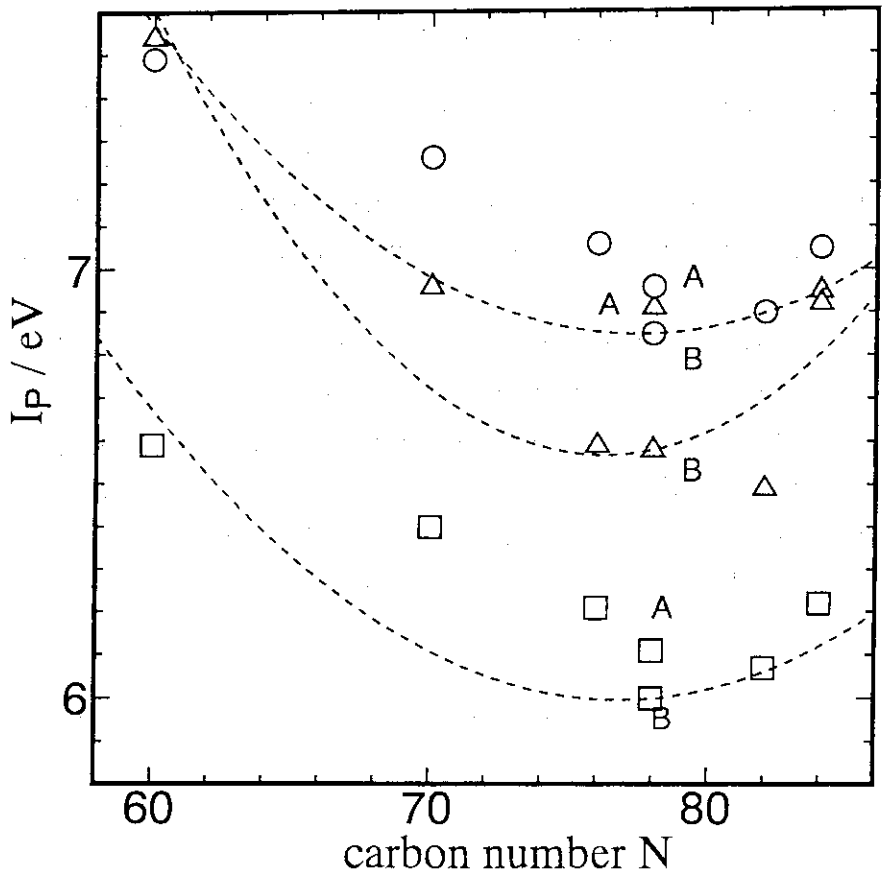


Fig.4. Ionization potential of fullerenes. □ ;our I_P data in TMP.
○; I_g data estimated from our I_P. △; theoretical Ig data by J. Cioslowski.

7.4 Radiation Damages on Superionic Conductors

T. Awano, M. Ikezawa* and T. Matsuyama**
Department of Applied Physics, Tohoku Gakuin University, Tagajo 985, Japan
*Research Institute for Scientific Measurements, Tohoku University, Sendai 980-77, Japan
**Research Reactor Institute, Kyoto University, Kumatori 590-04, Osaka, Japan

Abstract Irradiation coloration on superionic conductors of MA_4X_5 (M=K, Rb, NH_4; A=Ag, Cu; X=Cl, I) was observed. Five absorption bands were observed at 1.4, 1.8, 2.1, 2.3 and 2.9 eV in $RbAg_4I_5$. In these crystals, stable coloration was observed at lower temperature than in alkali halides. The absorption bands due to electronic centers and hole one were classified from the results of optical breaching and electron or hole doping. Growth rate and induced spectra by irradiation changed drastically at the temperatures just above the superionic phase transition. The growth rate increased drastically also at 40 K. ESR signal of γ-irradiated $RbCu_4Cl_3I_2$ showed that one of the induced defects is a hole trapped by a monovalent copper ion (Cu^{2+}).

INTRODUCTION

Superionic conductors contain a lot of ion vacancies. If the vacancies trap electrons or holes, color centers may be created as in alkali halides and coloration may occur easily. The induced defects may show characters which reflect the high ionic mobility. There have been, however, few studies on the radiation damages on superionic conductors.

MA_4X_5 (M=K, Rb, NH_4; A=Ag, Cu; X=Cl, I) have the highest ionic conductivity at room temperature and hold it even at the low temperature region, for example, above 122 K in $RbAg_4I_5$ (Owens and Argue, 1967). It has been reported that coloration occurs on $RbAg_4I_5$ in iodine vapor at room temperature (Andreev et al., 1984). This means that the critical temperature of additive coloration is very low comparing with that in alkali halides. We have investigated irradiation coloration at low temperature.

EXPERIMENTAL

Single crystals of MAg_4I_5 were grown from the hydroiodic acid solution saturated with the stoichiometric compounds. Crystals of $RbCu_4Cl_3I_2$ were grown from melt of stoichiometric compound. The crystals were composed of several small domain of single crystals. γ-Ray irradiation and ESR measurement were done at ^{60}Co facility of Research Reactor Institute, Kyoto University. X-ray irradiation was done under the condition of W-target, 40 kV and 20 mA.

RESULTS AND DISCUSSION

Irradiation induced absorption bands were at 1.35, 1.80, 2.05, 2.32 and 2.85 eV in $RbAg_4I_5$ and 1.71, 2.00, 2.35 and 2.95 eV in KAg_4I_5 and 1.75, 2.05 and 2.98 eV in $NH_4Ag_4I_5$ (Awano et al., 1990, 1992). Only the band around 2.9 eV appears by additive coloration by iodine vapor. This means that the 2.9 eV band is due to trapped holes and others are due to trapped electrons. This is supported by the results of coloration on electron or hole doped crystal. Electron doping enhanced the bands except the 2.9 eV band and hole doping enhanced the 2.9 eV band. The results of optical bleaching also support that. The intensities of all bands except the 2.9 eV band were decreased by illumination of the light of corresponding photon energies of each band.

A drastic increase of the coloration rate at temperatures just above the superionic phase transition was observed on MAg_4I_5. This seems to be due to the competition of the increase of the number of the vacancy of the conduction ion and the increase of the mobility of it.

Coloration rate by x-ray irradiation on $RbAg_4I_5$ increased drastically also at 45 K. Fig. 1 shows the growth rate of induced absorption bands by x-ray irradiation. No

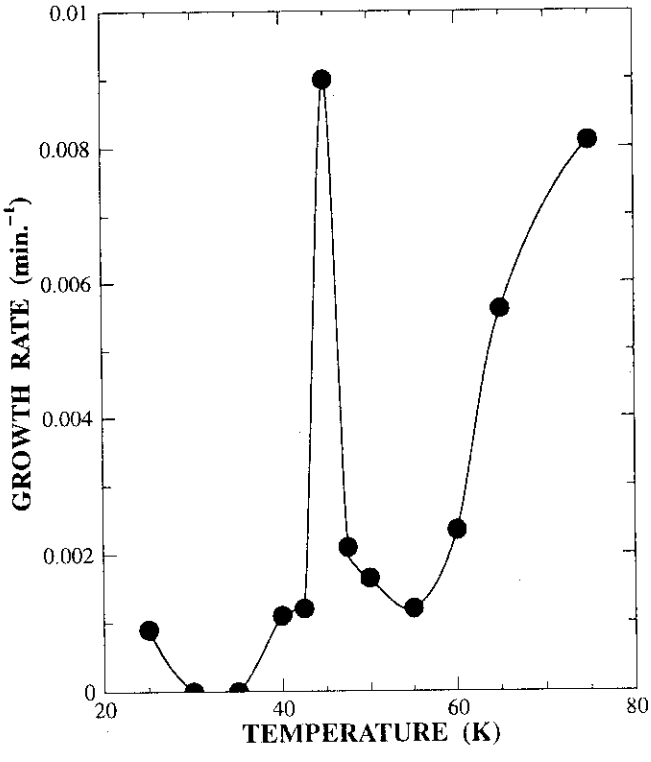


Fig. 1. Irradiation temperature dependence of the growth rate of each absorption bands induced by x-ray irradiation. No coloration was induced by irradiation at the temperature between 30 and 37 K. Below 30 K, the induced absorption bands were very broad as shown in fig. 2.

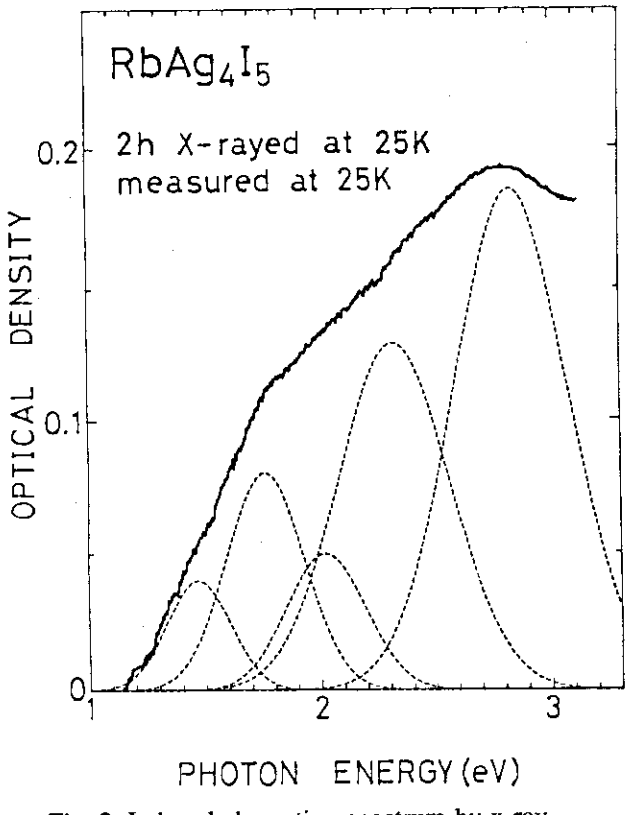


Fig. 2. Induced absorption spectrum by x-ray irradiation on $RbAg_4I_5$ at 25 K. The dashed lines show Gaussian components assuming the same peak energies as those above 45 K.

absorption bands were induced by irradiation at around 35 K. The induced absorption spectra by irradiation below 30 K were different from those above 40K. An example of the induced absorption spectra is shown in fig. 2. The dashed lines show Gaussian components assumed to have the same peak energies as those by higher temperature irradiation. The absorption bands by irradiation at temperature lower than 30K were very broad. This temperature is around the phase transitions in non-superionic phase at 44K and 30K, which were recently reported by Volkov et al. from the measurement of submillimeter transmission (Volkov et al., 1986).

In the case of $RbCu_4Cl_3I_2$, irradiation induced absorption spectrum were different from those of MAg_4I_5. Fig. 3 shows the induced net absorption spectrum of $RbCu_4Cl_3I_2$ x-ray irradiated at 77 K. Absorption bands were induced at 1.9, 2.4 and 2.8 eV. These bands were disappeared at 110 K in annealing process. Examples of ESR spectra from an irradiated crystal are shown in fig. 4. Angular dependence on the direction of external magnetic field was observed as shown by curve a and b. Curve b in fig. 4 has peaks at g = 2.43, 2.34, 2.26, 2.18 and 2.11. These g-values indicate that the defect is a hole. The spectrum b in the fig. 4 is similar to that of the hyperfine structure of Cu^{2+}, for example in AgCl crystal, which has four lines of the hyperfine structure by the nuclear spin of 3/2 (Fukui et al., 1973). Therefore, observed ESR spectra are able to be interpleted as that of a hole trapped by a Cu^{+} ion. The large width of lines seems to be due to the polycrystalline sample. This signal vanished at 160 K in annealing process and

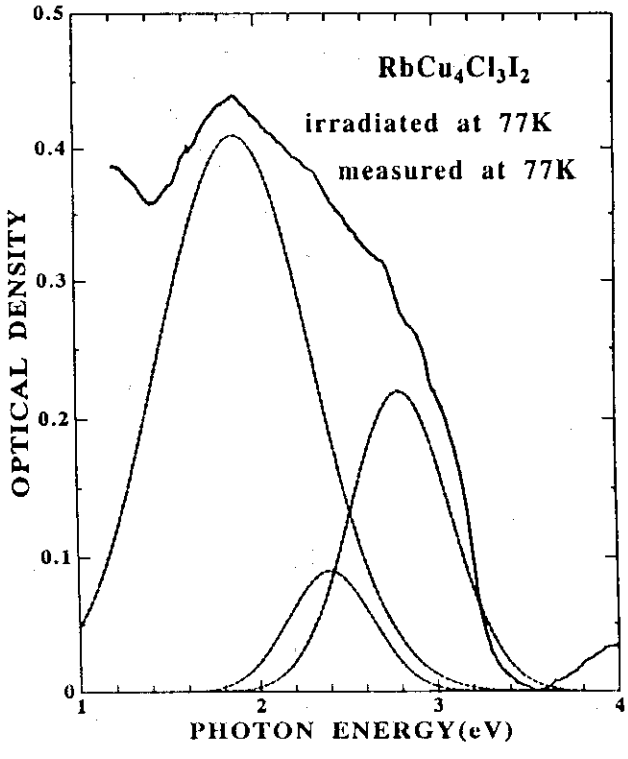


Fig. 3 Induced absorption spectrum by x-ray irradiation on $RbCu_4Cl_3I_2$ at 77 K. The dashed lines show Gaussian components.

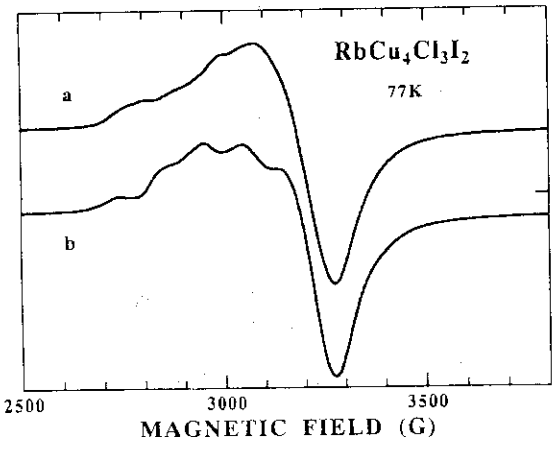


Fig. 4. ESR spectra of γ-irradiated $RbCu_4Cl_3I_2$ at 77 K. The direction of the magnetic field is 90 degrees apart from each other for lines a and b. The microwave frequency is 9.288 GHz.

another weak signal grew at g = 2.13. This new signal disappeared at 210K.

CONCLUSIONS

Irradiation induced signals of ESR and optical absorption were different between silver ion conductors and the copper ion conductor. This suggests that different electronic structure cause different radiation damages even in the crystals with the same crystal structure.

Acknowledgements-Authors thank to Dr. N. Lichkova of Institute of Solid State Physics, Russian Academy of Sciences for the sample preparation with the $RbCu_4Cl_3I_2$. A part of this work was executed under the visiting researcher program of Research Reactor Institute, Kyoto University.

REFERENCES

Andreev V. N. and Goffman V. G. (1984) Sov. Phys. Solid State **25**, 2004.

Awano T., Ikezawa M., Matsuyama T. and Yamaoka H. (1990) Solid State Ionics **40/41**, 324.

Awano T., Nanba T. and Ikezawa M. (1992) Solid State Ionics **53-56**, 1269.

Owens B. B. and Argue G. R. (1967) Science, **157**, 308.

Volkov A. A., Goncharov Y. G., Goffman V. G., Kozlov G. V., Mirzoyanz G. I. and Torgashev V. I.(1986) Zh. eksper. teor. Fiz. Pisma **43**, 280.

Fukui M., Hayashi Y. and Yoshioka H. (1973) J. Phys. Soc. Jpn., **34**, 1226.

7.5 Electron Transfer and Recombination Reactions of Polymer Anions Produced by Ionizing Radiation

M. Ogasawara

Hokkaido University of Education
Hachiman-cho 1-2, Hakodate 040, Japan

Abstract Reactions of radical anions of poly(4-vinylbiphenyl)(PVB), poly(methyl methacrylate) (PMMA), and aromatic substituted polyacetylenes produced by ionizing radiation have been studied in solution and matrix. Excess electron was localized on the side groups of PVB and PMMA, and its migration from one side group to another was observed in the solution of PVB. In aromatic substituted polyacetylenes, on the other hand, excess electron was delocalized over the main chain and the side group, although the delocalization was confined to only one or two monomer units because of twisted structure of the polymers.

INTRODUCTION

Excess electrons produced by ionizing radiation in solution and matrix attach to solute polymers, in appropriate conditions, to form polymer anions. We studied the reactivity and structure of the polymer anions of poly(4-vinylbiphenyl)(PVB), poly(methyl methacrylate)(PMMA), and aromatic substituted polyacetylenes, poly(1-phenyl-1-propyn)(PPPr) and polyphenylacetylene(PPA), by means of steady state and time-dependent optical and ESR spectroscopies. Unique intramolecular electron transfer reaction from one side group to another in PVB and delocalization of electron on a few monomer units in aromatic substituted polyacetylenes were observed. Part of the results has been published elsewhere (Ogasawara, 1992; Tanaka, 1992)

EXPERIMENTAL

Pulse radiolysis-optical absorption measurements were made with a 45 MeV linear accelerator at Hokkaido University. The pulse duration was usually 50 ns(ca. 200 Gy/pulse). Steady state optical absorption measurements were made by Shimazu MPS-5000 spectrophotometer quipped with a cryostat.

RESULTS AND DISCUSSION

(1)Electron Trapping by the Polymers

In 2-methyltetrahydrofuran(MTHF) containing PVB the polymer forms micro-domains as reported by Kato et al(Kato, 1988). In our pulse radiolysis measurement, very fast, but obviously disturbed geminate recombination in the polymer domains was observed.

In frozen MTHF matrices at liquid nitrogen temperature (LNT), excess electrons were mostly trapped by solvent molecules at first and then migrate to the solute polymer by tunneling

mechanism to form radical anion. The total yield of the polymer anion and the surviving trapped electron was found to decrease considerably with increasing polymer concentration. The lower yield was ascribed to lower trapped electron yield in the polymer domains.

In the same matrix containing PMMA at LNT, the logarithmic plot of the survival probability of the trapped electron vs. polymer concentration showed an S-shape curve with the critical concentration at ca. 0.1 base-unit mmol dm^{-3}. The result suggests a phase change of solution with increasing polymer concentration. Presumably, the polymer domains coagulated each other at higher concentration to form a network structure which occupied the whole system homogeneously.

(2)Intramolecular Electron Transfer in PVB

PVB anion produced by electron pulses in MTHF disappears by the neutralization reaction with solvent cation. To confirm whether the excess electrons trapped in PVB transfers to neighboring side groups of the polymers before disappearance, we synthesized poly(4-vinybiphenyl-co-1-vinylpyrene) in which a small number of biphenyl side groups were substituted by pyrenyl groups. Transient absorption spectra observed on pulse radiolysis of MTHF containing the copolymers indicated a growth of Py^- band and a concomitant decrease of the Bp^- band with the half-life of 0.2 μs after the pulse. The time-dependent spectra were analyzed on assuming one-dimensional well type potential for the copolymer at the sites where pyrene groups exist. The upper limit of one-dimensional diffusion coefficient of the electron was estimated as $4x10^{-10}m^2s^{-1}$. This value is 1-2 order smaller than that of the transfer coefficient of singlet energy migration in polystyrene and poly(2-vinylnaphthalene) via the Forster mechanism. From this value the average traveling distance of the electron for 1 μs is roughly estimated as 300 A.

(3) Electron Localization and Transfer in PPPr and PPA

Absorption spectrum observed from gamma-irradiated MTHF containing PPPr at LNT showed three bands peaking at 390, 560, and 1200 nm. The 1200 nm band is due to the electron trapped in the matrix. On warming the photobleached sample, the spectrum changed to another one peaking at 450 nm and 700 nm. ESR spectrum observed at 77 K from gamma-irradiated MTHF containing PPPr showed a sharp singlet with a linewidth of 4.0 gauss and an underlying septet. The singlet with the g-value of 2.002 is mostly due to the trapped electron in MTHF. Photo-

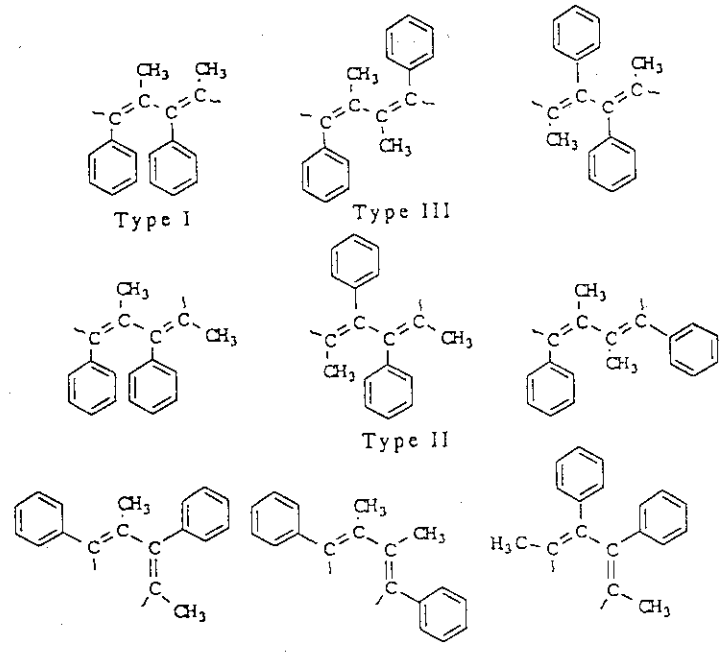


Fig.1 Possible chemical structures of electron trapping site in PPPr

bleaching with the light longer than 1000 nm reduced the intensity of the singlet to one third and increased the linewidth to 5.5 gauss. The singlet with a wider linewidth was assigned to $PPPr^-$ and correlated to the optical absorption spectrum with the maxima at 390 nm and 560 nm. By comparing these results with those obtained with model compounds, it was concluded that the excess electron in $PPPr^-$ was confined to only one monomer unit in the polymer. This limited delocalization of the electron is due to twisted main chain structure of PPPr arising from the repulsive interactions between bulky phenyl groups and methyl groups of the polymer.

The electrons produced by ionizing radiation are initially trapped by the type I sites(see Fig. 1) to form the radical anion which has absorption bands peaking at 390 nm and 560 nm. The polymer is abundant in this class of trapping site because of the smaller steric hindrance. The spectral change observed on warming the sample corresponds to the transfer of the excess electron from the type I site to the type II site. Trap-to-trap hopping of the electron must be assisted by the thermal motion of the polymers, because it occurs only in warmed matrices.

Absorption spectrum of the anion radical of PPA^- observed at 77 K showed a strong band at 1000 nm without overlapping electron band. The radical anion of styrene, a model compound of PPA, gives a different spectrum: it has a strong band at 400 nm and a weak one at 600 nm. The strong IR band in the PPA^- spectrum is ascribed to electronic transition between charge-resonance states of two monomer units. Thus the excess electron is delocalized at least two monomer units in this polymer. The difference is interpreted in terms of a relatively planar structure of PPA in comparison with that of PPPr.

REFERENCES

Ogasawara M., Suganuma T., Junke N., and Yoshida H. (1992) Radiat. Phys. Chem. 40, 111.
Tanaka M., Yoshida H., and Ogasawara M. (1992) Radiat. Phys. Chem. 39, 35.
Kato N., Miyazaki T., Fueki K., and Saito A. (1988) Int. J. Chem. Kinetics 20, 877.

7.6 Intramolecular Electron Transfer in Nitrite Reductase Studied by Pulse Radiolysis

K. Kobayashi[1], S. Tagawa[1], T. Kouzuma[2], Deligeer[2], K. Yamaguchi[2], N. Nakamura[2], S. Suzuki[2], and S. Shidara[3]

[1]The Institute of Scientific and Industrial Research, Osaka University, 8-1 Mihogaoka, Ibaraki, Osaka 567, Japan; [2]Department of Chemistry, Faculty of Science, Osaka University, 1-16 Machikaneyama, Osaka 560, Japan; [3]Department of Environmental Sciences, Faculty of Integrated Arts and Sciences, Hiroshima University, Naka-ku, Hiroshima 730, Japan

ABSTRACT We report the evidence for the electron-transfer reaction between two copper sites in nitrite reductase from *Achromobacter cycloclastes* IAM 1013 by pulse radiolysis. Type 1 Cu sites in native (type 1 Cu : type 2 Cu = 1 : 0.5) and type 2 Cu-depleted (T2D) nitrite reductase are reduced with N-methylnicotinamide radical generated by the hydrated electron. The reductions of the coppers in the both enzymes give second-order rate constants of (3.4 - 3.5) x 10^8 $M^{-1}s^{-1}$. In the case of the native enzyme, moreover, the recovery of the absorbance of reduced type 1 Cu is observed (about 35 %). This finding suggests the intramolecular electron transfer from type 1 Cu to type 2 Cu, because T2D nitrite reductase does not show the recovery of the absorption band at all. The electron-transfer occurs with an observed first order rate constant of 1400 s^{-1}. The incomplete electron transfer from type 1 Cu to type 2 Cu are due to the difference between the redox potential of two Cu sites.

INTRODUCTION

Nitrite reductase catalyzes the reduction of nitrite ion to nitric oxide as part of a denitrification pathway in which nitrate is sequentially reduced to nitrite, nitric oxide, and dinitrogen. Denitrification has become increasingly important in eutrophic ecosystem.

$$NO_3^- \longrightarrow NO_2^- \longrightarrow NO \longrightarrow N_2O \longrightarrow N_2$$

Copper-containing nitrite reductase isolated from *Achromobacter cycloclastes* IAM 1013 contains two electron-accepting sites per molecule of the protein, two different types of copper. Two copper atoms are distinguishable on EPR signal and the unique absorption spectrum having the intense bands near 460 and 600 nm, as belonging to type 1 (blue) and type 2 (nonblue) coppers (Iwasaki and Matsubara, 1972; Lin, *et al.* 1986). One of the interesting questions to be answered is how electrons are transferred within the enzyme during the catalytic cycle. Recently the crystal structure of the enzyme has been determined to 2.3 Å resolution by isomorphous replacement (Godden *et al.* 1991). The enzyme is a trimer, where the monomer (Mr = 36,000) contains two kinds of Cu. The type 1 Cu site having four ligands (2His, Cys, and Met) lies about 4 Å from the Connolly surface of the protein and its geometry is described as a flattened tetrahedron. The two Cu sites (T1Cu and T2Cu) are about 12.5 Å apart and are bound by adjacent residues in the sequence (T2Cu-His(135)-Cys(136)-T1Cu).

In this work, in order to elucidate the roles of two types of Cu of nitrite reductase, pulse radiolysis studies on *Achromobacter* nitrite reductase has been performed; the results are compared with type 2 Cu-depleted nitrite reductase (T2D). Pulse radiolysis is useful for investigations of electron transfers in proteins having multiple electron-accepting sites such as cytochrome oxidase (Kobayashi *et al.* 1989), xanthine oxidase (Kobayashi, *et al.* 1993), and ascorbate oxidase (Kyritsis *et al.* 1993). In these enzymes, it can be anticipated that the hydrated electron or organic radicals such as CO_2^- reduce the primary redox site and subsequently an electron flows to the other electron accepting site by intramolecular migration until equilibrium is reached. Here we succeeded in observation of intramolecular electron transfer from type 1 Cu to type 2 Cu in *Achromobacter* nitrite reductase (Suzuki et al.)

EXPERIMENTAL

Native nitrite reductase containing two kinds of Cu (type 1 Cu: type 2 Cu = 1 : 0.5) was isolated from *Achromobacter cycloclastes* IAM 1013 by the method of Iwasaki (1972). T2D nitrite reductase was prepared by the selective removal of type 2 Cu from the native enzyme (Avigliano, *et al.* 1979; Kohzuma *et al.* 1994). The EPR signal of T2D enzyme reveals that there is no residual type 2 Cu.

Pulse radiolysis experiments were performed with an electron linear accelerator at the Institute of Scientific and Industrial Research, Osaka University. The pulse width and energy were 8 ns and 27 MeV, respectively.

Pulse radiolysis was carried out in 10 mM phosphate buffer (pH 7.0) containing native or T2D nitrite reductase in the presence of 0.1 M *tert*-butyl alcohol for scavenging OH radical. The samples were deaerated by repeated evacuation and Ar gas flushing. The spectral data after the first or the second pulse were collected, since many pulses inflict damage on the protein.

RESULT and DISCUSSION

In the presence of 1 mM N-methylnicotinamide (NMA), a transient spectrum with an absorption maximum at 420 nm was observed at 100 ns after pulse radiolysis. Under the condition, the hydrated electron (e_{aq}^-) reacts with NMA to yield the NMA radical nearly quantitatively, since the concentration of NMA (1 mM) is much higher than that of nitrite reductase (70-200 μM). With the decay of NMA radical, the absorption in the blue bands of the enzyme was found to decrease. This suggests that NMA radical transfers an electron to type 1 Cu of the enzyme. The reaction obeys pseudo-first order kinetics when 8.6 μM NMA radical is generated in a solution containing 216 μM of the enzyme. The second-order rate constant of the reduction of type 1 Cu with NMA radical is estimated to be 3.4×10^8 $M^{-1}s^{-1}$ in the native enzyme. In contrast, e_{aq}^- hardly reduced the Cu chromophore in the enzyme. The difference cannot be explained by the redox potential of the radical. Rather charge type of the reductant may play an important role in the kinetics of reduction and in determining the site of interaction with the enzyme.

After the initial phase of the reduction, the recovery of the absorbance was observed with a half life of 580 μs, but it did not return to the initial level. Contribution to the recovery of absorption is 35 % of the total absorption change for the initial reduction. Moreover, the difference spectra (400-800 nm) obtained at 100 μs and 2 ms after the pulse are identical to the visible absorption spectrum of the enzyme. From these findings, it can be confirmed that type 1 Cu is initially reduced by NMA radical and subsequently reoxidized. On the other hand, no reoxidation process in T2D was observed, though the reduction process of type 1 Cu was not affected. In addition, a linear relationship between the amount of type 2 Cu and the percentage of the reoxidation of type 1 Cu was obtained. Therefore, it is supported that the slower process in the native enzyme is due to the intramolecular electron transfer from type 1 Cu to type 2 Cu. The first-order rate constant of the electron transfer is calculated to be 1.4×10^3 s^{-1} at pH 7.0. This value is independent of the enzyme concentration.

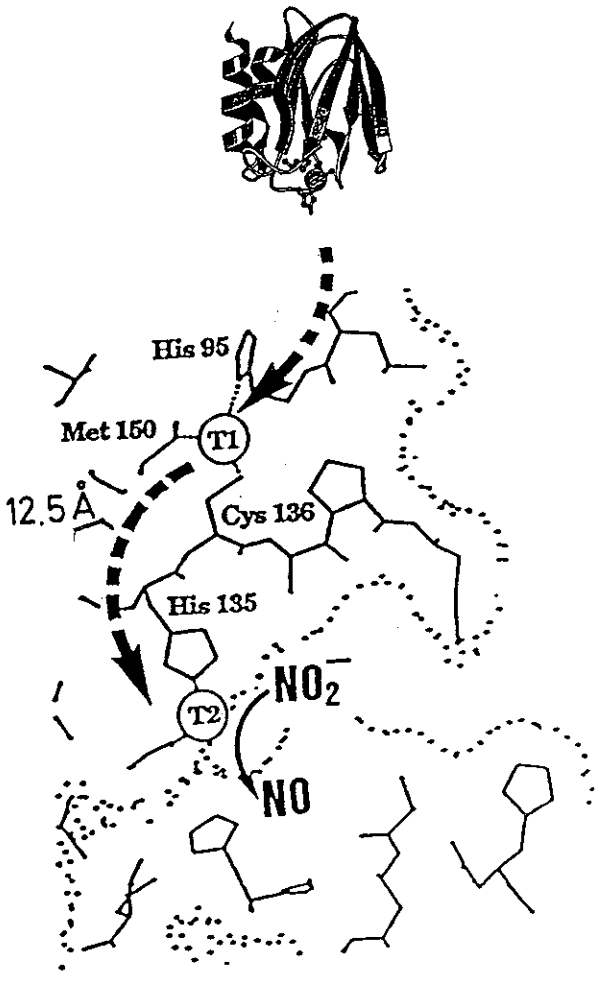
The recent pulse radiolysis study on the oxidized form of ascorbate oxidase from zucchini squash disclosed that there are two intramolecular electron transfer steps (fast process, 166 s^{-1} and slow second stage, 2.8 s^{-1}) between type 1 Cu site and trinuclear site composed of types 2 and 3 Cu (Kyritsis, *et al.* 1993); two sites are about 12 Å apart and are bound by adjacent residue in the sequence like nitrite reductase (Messerschmidt, *et al.* 1992). The observed rate constant of nitrite reductase is larger than that of the fast electron-transfer process in ascorbate oxidase by a factor of about 10.

The incomplete reoxidation of type 1 Cu can be explained by a rapid equilibrium for the electron transfer between two types of Cu. It is noted that the reoxidation of type I Cu was incomplete. This fact can be explained by a rapid equilibrium for the electron-transfer between two types of Cu. In the case of the intact form which contains type 1 Cu : type 2 Cu = 1 : 1, the reoxidation of reduced type 1 Cu is estimated by extrapolation to be 70 %. This might reflect the difference between the redox potentials of two Cu sites. The midpont potential (E1/2) of type 1 Cu in *Achromobacter* nitrite reductase was obtained to be + 240 mV (vs. NHE) by cyclic voltammetry (Kohzuma *et al.* 1994). Consequently, the $E_{1/2}$ value of type 2 is estimated to be ca. + 260 mV (vs. NHE). The electron transfer reaction is interpreted in terms of a rapid equiribrium.

$$\text{T1Cu (I) T2Cu (II)} \underset{k_{-1}}{\overset{k_1}{\rightleftharpoons}} \text{T1Cu (II) T2Cu (I)}$$

Therefore, the observed first order rate constant consists of the sum of k_1 (forward) and k_{-1} (backforward). The k_1 and k_{-1} are estimated to be 980 and 420 s-1, respectively, on the basis of 70 % reoxidation of the reduced type 1 Cu in the enzyme containing type 1 Cu: type 2 Cu = 1 : 1.

The results presented here provide important insight into the mechanism of nitrite reductase. The enzyme reaction can be schematized as follows. Type 1 Cu in native *Achromobacter* nitrite reductase mediates an electron from a blue copper protein, pseduazurin (a natural electron-donor) to type 2 Cu. Nitrite ion binds and is oxidized at type 2 copper site. The pulse radiolysis experiments of nitrite reductase from other denitrifying bacteria are currently in progress.



REFERENCES

Iwasaki, H., Mastubara, T. (1972) J. Biochem. (Tokyo) 71, 645-652

Kobayashi, K., Une, H., and Hayashi, K. (1989) J. Biol. Chem. 264, 7976-7980

Kobayashi, K., Miki, K., Okamoto, K., Nishino, T. (1993) J. Biol. Chem. 268, 24642-24646

Kohzuma, T., Shidara, S., and Suzuki, S. (!994) Bull. Chem. Soc. Jpn. 67, 138-143

Kyritsis, P., Messerschmidt, A., Huber, R., Salmon, A., and Sykes, A. G. (1993) J. Chem. Soc. Dalton Trans. 731-735

Lin, M. Y., Lin, M. C., Payne, W. J., and LeGall, J. J. (1986) J. Bacteriol. 166, 604-608

Messerschmidt, A., Ladenstein, R., Huber, R., Bolognesi, M., Avigliano, L., Petruzzelli, R., Rossi, A., and Finazzi-Agro, A.. (1992) J. Mol. Biol. 224, 179-205

Suzuki, S., Kohzuma, T., Deligeer, Yamaguchi, K., Nakamura, N., Shidara, S. Kobayashi, K., and Tagawa, S. J. Am. Chem. Soc. in press

7.7 Ion Beam Irradiation Effects on Aromatic Polymers

Satoshi Shukushima and Keiji Ueno

Sumitomo Electric Industries Osaka Research Laboratories Kanto Branch
3-3, Satsuki-cho, Kanuma, Tochigi, 322 Japan

Abstract We studied the optical and thermal properties of aromatic polymer films which had been irradiated with 1 MeV H^+, H_2^+ and He^+ ions. The examined aromatic polymers were polyetherether ketone(PEEK), polyetherimide (PEI), polyether sulfon(PES), polysulfon(PSF), and polyphenylene sulfide(PPS). The optical densities at 300nm of PES and PSF greatly increased after the irradiation. The optical densities at 400nm of all the examined polymer lineally increased with the irradiation dose. The PEEK film which had been irradiated with 1 MeV H^+ was not deformed above melting point. This demonstrates that cross-linking occurs in PEEK films by ion beam irradiation. As for the effects, depending on the mass of the irradiated ions, it was found that the ions with a high mass induced larger effects on the aromatic polymers for the same absorption energy.

1. Introduction

Ion beam applications for organic materials have not been put to practical use. One of the reasons is that the organic materials are less resistant than inorganic materials when irradiated with the ion beams. To reduce the damage caused by ion beams, we selected heat-resistant organic materials.

Aromatic Polymers, for example PEEK, PEI and PES are good heat-resistant materials. Therefore, we selected the aromatic polymers as the organic material to improve the performance using the ion beam irradiation.

2. Experimental

The aromatic polymer films were irradiated with 1MeV H^+, H_2^+ and He^+ ions. The examined aromatic polymers were PEEK, PEI, PES, PSF, and PPS. We studied the optical and thermal properties of the irradiated polymer films.

3. Results and discussion

3.1 Conversion of numbers of irradiated ions into absorption dose

In order to study the effect of ion beam species and ion beam energy, it is more convenient to express the quantity of implanted ions as the absorption energy rather than the number of ions. The number of irradiating ions could be converted into the absorption dose by calculating the stopping power for the implanted ions. The stopping powers for 1 MeV H^+, H_2^+, He^+ ions in the aromatic polymers were calculated from the stopping powers corresponding to

C, H, N, O and S [1] based on the additivity rule. The stopping power for 1 MeV H_2^+ is considered to be twice as high as that for 0.5MeV H^+, as the molecular ion of 1 MeV H_2^+ is broken into two atomic ions of 0.5MeV H^+ at the surface of a polymer film.

Using the stopping power, the absorption dose is calculated using the following equation [2]:

$$D=1.6\times10^{-13}\times S\times N \quad (1)$$

where D is the absorption dose in MGy, S the stopping power in MeV·cm^2 /mg and N the number of irradiated ions in ions/cm^2 .

As the stopping power is a function of the implantation depth, the average stopping power, Sav, is used to calculate the absorption dose in this experiment.

When the ion beam range is longer than the film thickness, Sav is calculated using the following equation:

$$Sav=\frac{\int_0^T S(l)dl}{T} \quad (2)$$

where T is the thickness of the polymer film and l the ion implantation depth.

When the range is shorter than the film thickness, Sav is calculated using the following equation:

$$Sav=\frac{\int_0^R S(l)dl}{R} \quad (2)'$$

where R is the range of the ion beam.

The average stopping powers for the ions in the examined aromatic polymer films are listed in Table 1.

Table 1 The average stopping powers for 1MeV ions in the examined aromatic polymer films

Polymer	Thickness [μm]	Range of 1MeV ions [μm]			Average stopping power [MeV cm^2 /mg]		
		H^+	H_2^+	He^+	H^+	H_2^+	He^+
PEEK	16	18.2	7.3	5.2	0.42	1.06	1.47
PEI	10	18.7	7.5	5.4	0.34	1.05	1.45
PES	8	18.6	7.5	5.4	0.30	0.98	1.36
PSF	9	19.2	7.7	5.5	0.33	1.05	1.46
PPS	8	18.0	7.3	5.3	0.32	1.03	1.41

3.2. UV and visible spectra

The aromatic polymer films that had been irradiated by the ion beams were all a brown color. The UV and visible spectra were measured. To examine the change in UV and visible spectra induced by the ion beam irradiation, a non-

irradiated film was used as reference. Therefore the obtained spectra are normalized with respect to the non-irradiated film. In this experiment, the optical density is obtained using the following equation:

$$OD=\log(In/Ii) \quad (3)$$

where OD is the optical density, In the intensity of the transmitted ray through the non-irradiated film and Ii the intensity of the transmitted ray through the irradiated film.

Fig. 1(a) shows the absorption spectra of the aromatic polymer films which had been irradiated with 1 MeV 1×10^{15} H^+/cm^2(about 50MGy). The spectra of only PES and PSF have large absorption peaks near 300nm. These absorption peaks are possibly related to the $-SO_2-$ group, because only PES and PSF contain the $-SO_2-$ group. The peaks near 300nm seemed to appear because of the decomposition of the $-SO_2-$ group.

The optical density of the irradiated films linearly increase with the numbers of implanted ions. The optical density at 400nm of the films was plotted as a function of absorption dose calculated by equation (1) in Fig.1(b). This figure shows that 1 MeV He^+ colored the films more efficiently than 1 MeV H^+.

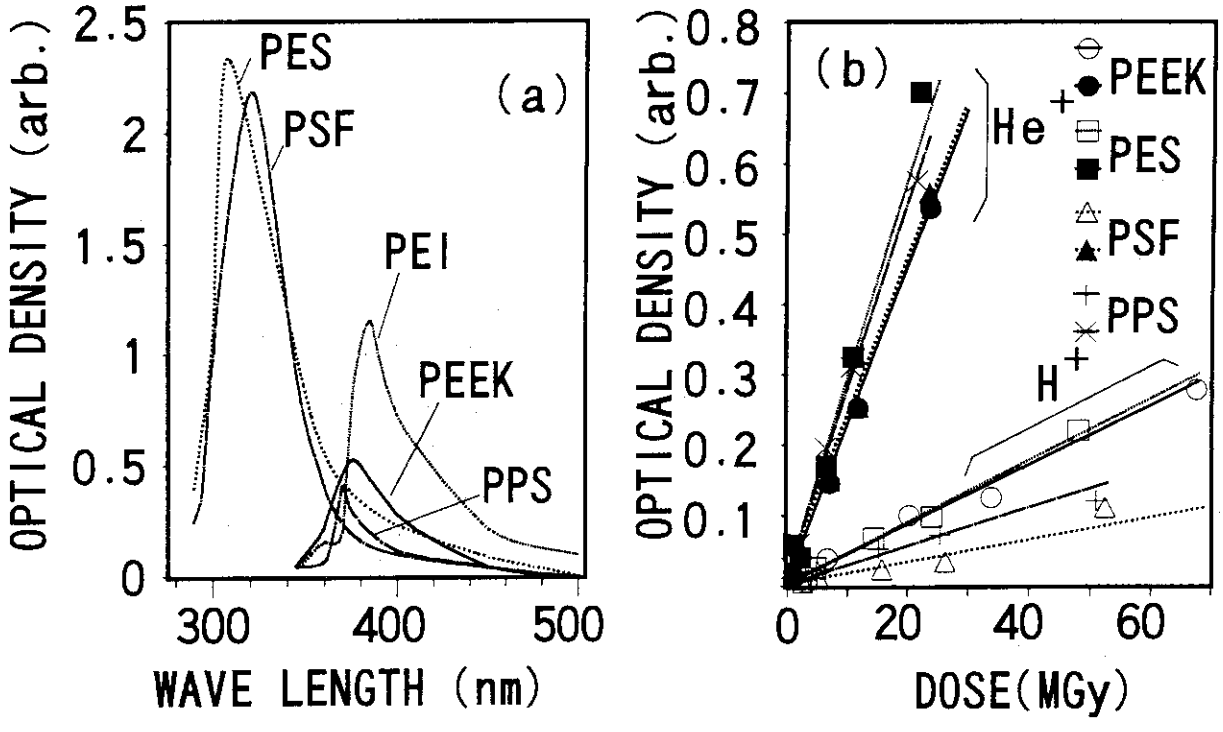


Fig. 1 (a)UV and visible absorption spectra of the aromatic polymer films which had been irradiated with 1 MeV $1\times10^{15}H^+ ions/cm^2$. (b)Optical Density at 400nm of the colored aromatic polymer films irradiated with a 1 MeV ion beam.

3.3. Gel fraction

The gel fraction, the insoluble part of the polymer, of the irradiated PEI film was measured. The films were immersed for 24 hours in Dimethyformamide at 120℃. Afterwards they were dried for 24 hours at 80℃.

Fig. 2 shows the gel fraction of the PEI as a function of absorption dose. As for the gel fraction, 1 MeV He^+ most efficiently formed the gel, in a similar way to UV and visible spectra. In other words, 1 MeV He^+ most efficiently crosslinked the PEI.

As listed in Table 1, the stopping power for 1 MeV He^+ is about four times higher than for 1 MeV H^+. As for the effects, depending on the stopping power, it was found that the ion whose stopping power is high efficiently crosslinks the polymer in same absorption dose. This effect is called the LET (Linear Energy Transfer) effect in radiation chemistry. A similar effect has been found in Polystyrene [2],[3] and some aromatic polymers [4],[5].

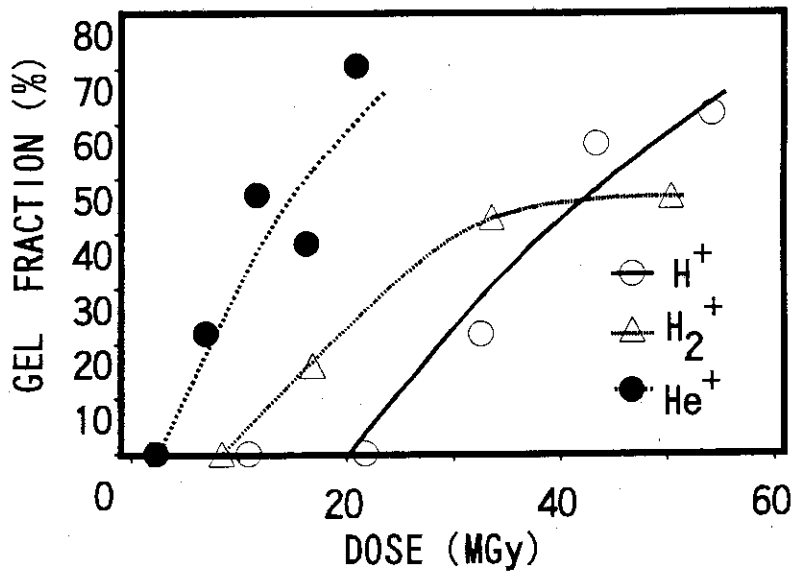


Fig. 2 Gel fraction of the PEI films irradiated with 1 MeV H^+, H_2^+ and He^+.

3.4 Deformation

Deformation of the irradiated PEEK film up to 500℃ under a load of 4.6kg/cm^2 was measured by Thermo Mechanical Analysis(TMA). The film was irradiated with 1 MeV H^+. The original thickness of the film was 25μm. The sample film was placed under a crystal rod with a flat face of 1mm in diameter. The temperature of the sample was raised up to 500℃ at 20℃ per minute. The deformation was obtained by measuring the film thickness during the test. The test results are shown in Fig.3.

PEEK is a crystalline polymer and its melting point is 334℃. The crystal melts and the polymer flows above the melting point. Therefore the non-

irradiated PEEK film has deformed rapidly above the melting point. However, the irradiated film did not deform as much as the non−irradiated one above the melting point. This suggests that crosslinking occurred in the PEEK by ion beam irradiation.

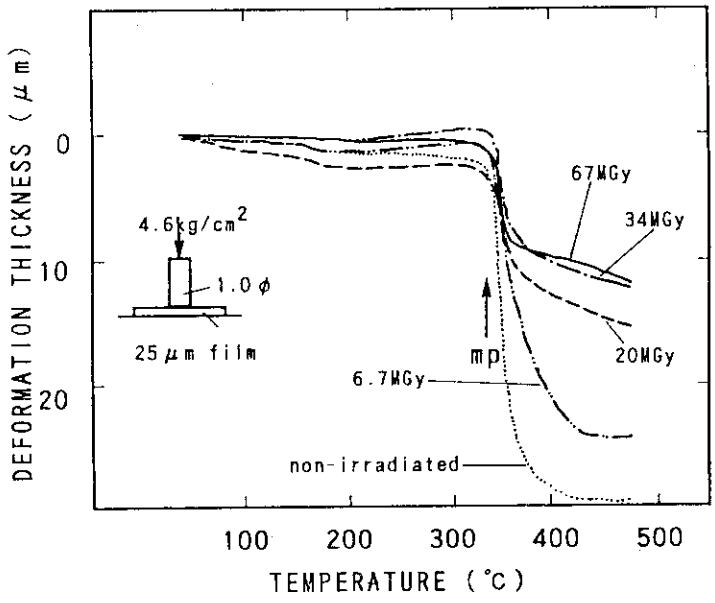


Fig. 3 Deformation of the 25 μm PEEK films irradiated with 1 MeV H^+, measured by TMA.

4. Conclusion

Various aromatic polymer films were irradiated with 1 MeV H^+,H_2^+, He^+ ions. It was found that the ion whose stopping power is high significantly changes the property of the aromatic polymers by the LET effect, this is also the case for coloration and gel formation. The absorbance at 300nm of both PES and PSF were greatly increased after irradiation.

The PEEK film which had been irradiated with 1 MeV H^+ was hardly deformed above the melting point. This demonstrates that crosslinking occurred in the PEEK film by ion beam irradiation.

References

[1] L.C.Northcliffe and R.F.Schilling, Nucl. Data Tables A7(1970)233
[2] Y.Aoki, N.Kouchi, H.Shibata, S.Tagawa, Y.Tabata and S.Imamura, Nucl. Instr. and Meth. B 33(1988)799
[3] L.Calcagno, G.Foti, A.Licciardello and O.Puglisi, Appl. Phys. Lett. 53(1988) 1495
[4] T.Sasuga, S.kawanishi, T.Seguchi and I.Kohno, Polymer 30(1989)2055
[5] S.Shukushima, S.Nishikawa, Y.Matsumoto and Y.Hibino, Nucl. Instr. and Meth. B 80/81(1993)1119

7.8 Ion-irradiated Polymer Studied by a Slow Positron Beam

Yoshinori Kobayashi, Isao Kojima

National Institute of Materials and Chemical Research, Tsukuba, Ibaraki 305, JAPAN

Shunichi Hishita

National Institute for Research in Inorganic Materials, Tsukuba, Ibaraki 305, JAPAN

Takenori Suzuki

National Laboratory for High Energy Physics (KEK), Tsukuba, Ibaraki 305, JAPAN

Abstract Poly(aryl-ether-ether ketone) (PEEK) films were irradiated with 1MeV and 2MeV O^+ ions and the positron annihilation Doppler broadening was measured as a function of the positron energy. The annihilation lines recorded at relatively low positron energies were found to become broader with increasing the irradiation dose, suggesting that positronium (Ps) formation may be inhibited in the damaged regions. A correlation was observed between the Doppler broadening and spin densities determined by electron spin resonance (ESR).

INTRODUCTION

Ion implantation is a useful technique to modify polarity, electron conductivity and other surface properties of organic polymers. Irradiation of the implanted ions, however, sometimes causes significant radiation damage, resulting in the final sample structure and composition much different from those of the original material (Itoh and Tanimura, 1994).

Variable energy positron beams, in combination with the Doppler broadening technique, have been successfully applied to damage and defect depth profiling of metals and semiconductors (Schultz and Lynn, 1988, Vehanen, 1989). The positrons injected into these materials strongly interact with the defects, resulting in the reduced Doppler broadening of the annihilation γ-rays with an energy of 0.511MeV. The usefulness of the technique, however, for the study of organic polymers has not been explored. Positron annihilation in polymers is known to be

more complex than the case of metals and semiconductors, because some of the positrons may bind an electron to form a hydrogen-like bound state, positronium (Ps) (Nakanishi, Jean, Smith and Sandreczki, 1989). In this paper, we report our attempt of using the positron beam technique to perform damage depth profiling of an ion-irradiated polymer.

The sample chosen for the present work was poly(aryl-ether-ether ketone) (PEEK), a radiation resistant polymer with a high glass transition temperature of about 420K. Semicrystalline PEEK films were irradiated by 1MeV and 2MeV oxygen ions (O^+) up to a dose of $6x10^{13}$ ions/cm^2. The Doppler broadening of the annihilation γ-rays was measured with a positron beam system as a function of the positron energy. The positron data were compared with free radical concentrations determined by electron spin resonance (ESR).

EXPERIMENTAL

Our slow positron beam system is shown in Fig. 1. Energetic positrons emitted from a 1.11GBq sealed ^{22}Na source (from Amersham) are moderated by a polycrystalline tungsten moderator with a thickness of 6μm. Slow positrons coming from the other surface of the moderator, because of the negative positron work function of tungsten (Schultz and Lynn, 1988), are separated from high energy positrons by a curved ExB filter (Hutchins, Coleman, Stone and West, 1986) and guided to the sample by a uniform longitudinal magnetic field of about 0.01T. The sample chamber and the beam line are electrically separated, so that the beam energy can be varied by simply floating the beam line to a desired electrostatic potential.

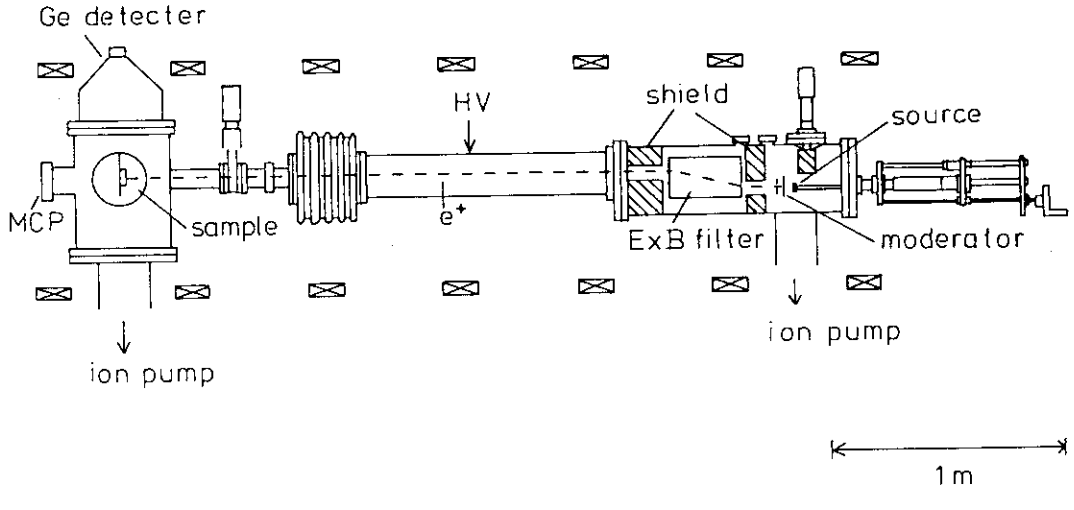


Fig.1 Variable energy positron beam system.

Semicrystalline PEEK films with a thickness of 25μm, which were kindly supplied by Sumitomo Chemical Co. Ltd., were irradiated with 1MeV and 2MeV O^+ ions up to a dose of $6x10^{13}$ions/cm^2. The ion current densities were 3-8nA/cm^2. The implantation depths of the oxygen ions with 1MeV and 2MeV energies were calculated by the TRIM code and found to be 1.7 and 2.6μm, respectively. The positron annihilation Doppler broadening was measured as a function of the positron energy (E) up to 35keV. The data were analyzed in terms of the S parameter, which is the relative fraction of counts in the central part of the 0.511MeV annihilation peak to the total counts contained in the whole peak.

RESULTS AND DISCUSSION

S-E curves for the ion-irradiated PEEK samples are shown in Fig. 2. The upper horizontal axis indicates the average positron implantation depth obtained by the formula

$$z=(0.04/\rho)E^{1.6},$$

where z is the depth in μm, E is the positron energy in keV and ρ is the material density in cm^3/g (Vehanen, 1989). The S parameters obtained at relatively low positron energies become lower with increasing the irradiation dose. The region, where the reduced S parameters are observed, extends to a deeper depth for the samples irradiated with 2MeV ions than those irradiated with 1MeV ions. This is consistent with the implantation depths calculated by the TRIM code, 1.7μm and 2.6μm for the 1MeV and 2MeV ions, respectively.

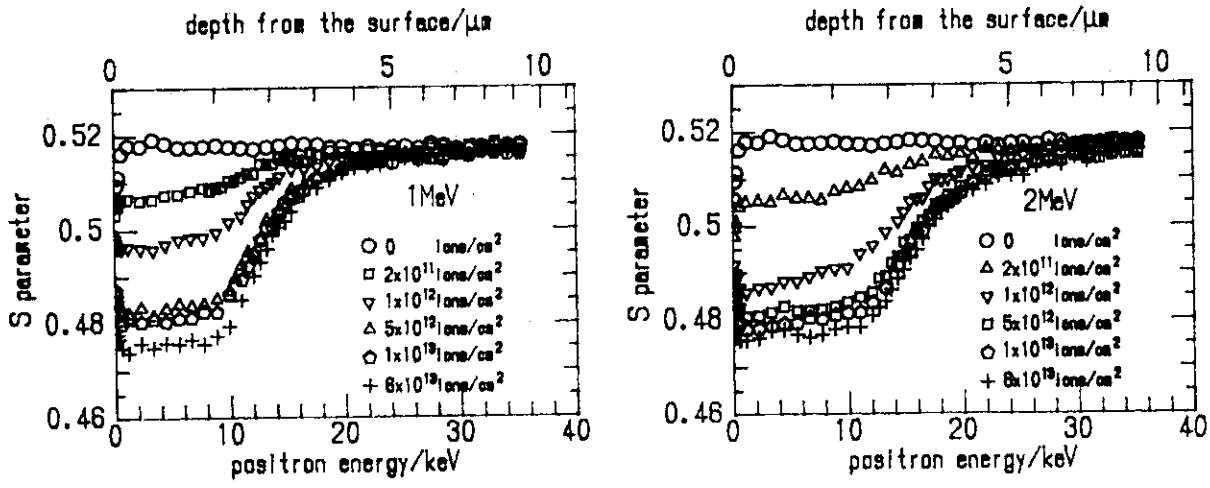


Fig. 2 S-E curves for PEEK, irradiated with oxygen ions.

In Fig. 3 are shown the variations of the *S* parameters at the positron energy of 2.2keV, corresponding to an average depth of 0.1μm from the surface, versus the ion dose. The *S* parameters for both sets of the samples, irradiated with the 1MeV and 2MeV ions, exhibit sharp decreases until the dose reaches $1x10^{13}$ions/cm^2. At higher doses, the *S* values are nearly constant around 0.48, which is close to the value for Kapton with no Ps formation. The *S* parameter is a good measure of the number of Ps atoms formed, because the self-annihilation of spin antiparallel *para*-positronium (*p*-Ps) atoms accompanies a very low momentum, giving a sharp annihilation peak with a large *S* value. It has been confirmed that some positrons do form Ps in PEEK (Nakanishi, Jean, Smith, Sandreczki, 1989); the fraction of spin-parallel *ortho*-positronium (*o*-Ps) atoms in our sample was about 18% (Kobayashi, Haraya, Hattori and Sasuga, 1994). Thus our results in Fig. 3 suggest that with increase in the irradiation fluence the Ps fraction decreases and at the dose of $1x10^{13}$ions/cm^2 it becomes zero. Some electron accepting species formed by the irradiation may scavenge Ps precursors such as electrons and/or hot Ps atoms in the terminal positron spur, leading to the chemical inhibition of Ps formation. The species responsible for the Ps inhibition should be rather stable because annealing of an irradiated sample at a nominal temperature of 490K for 10 hours did not change the *S*-*E* curve significantly.

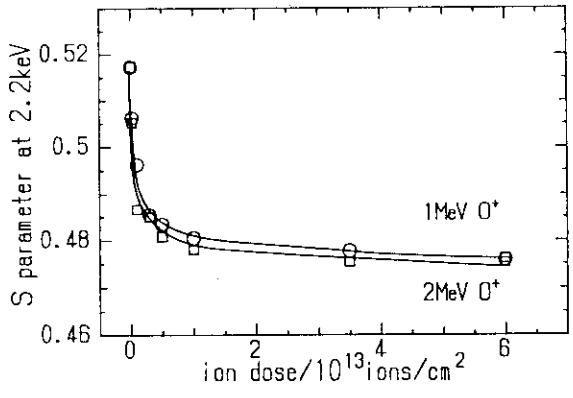


Fig.3 Plots of *S* parameters at the positron energy of 2.2keV versus irradiation dose.

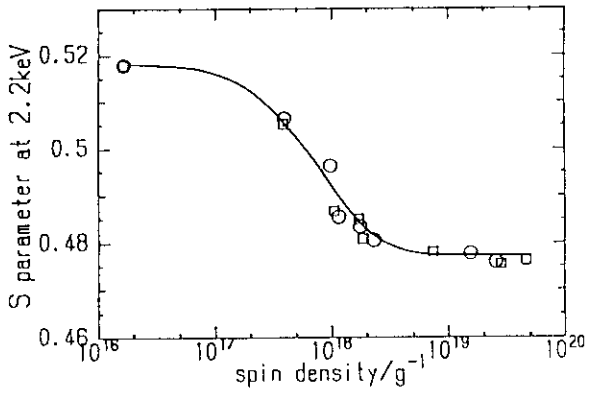


Fig. 4 Plot of *S* parameters at 2.2keV versus spin densities in the damaged regions. Symbols as in Fig. 3.

As polymer irradiation is known to produce free radicals, we determined radical concentrations in the damaged regions of the

ion-irradiated PEEK samples by ESR. It was assumed that free radicals were uniformly distributed from the surface down to the penetration depths of the irradiated ions and no radicals were produced beyond them. Fig. 4 shows the comparison between the *S* parameters at the positron energy of 2.2keV and the average spin densities determined under the assumption described above. Obviously, there is a correlation between the two quantities; data points for both 1MeV and 2MeV irradiation are fairly well reproduced by a single line. This result may indicate that both free radicals and active species responsible for the Ps inhibition are formed as the result of chain scission and their concentrations are somewhat correlated to each other.

CONCLUSION

Positron annihilation Doppler broadening was measured for O^+-irradiated PEEK as a function of the positron energy. The observed decrease of the *S* parameters at relatively low positron energies was attributed to the inhibition of Ps formation due to active species formed by irradiation. It may be concluded that the slow positron Doppler broadening technique is a useful non-destructive means for damage depth-profiling of Ps-forming polymers.

REFERENCES

Ito, N. and Tanimura, K. (1994) Radiation Effects in Insulators (REI-7), Proceedings of the Seventh International Conference on Radiation Effects in Insulators, North-Holland.

Hutchins, S. M., Coleman, P. G., Stone, R. J. and West, R. N. (1986) A Low-distortion Slow Positron Filter, *J. Phys.* E19, 282.

Kobayashi, Y., Haraya, K., Hattori, S. and Sasuga, T. (1994) Evaluation of Polymer Free Volume by Positron Annihilation and Gas Diffusivity Measurements, *Polymer* 35, 925.

Nakanishi, H, Jean, Y. C., Smith, E. G. and Sandreczki, T. C. (1989) Positronium Formation at Free Volume Sites in the Amorphous Regions of Semicrystalline PEEK, *J. Polym. Sci.* B27, 1419.

Schultz, P. J. and Lynn, K. G. (1988) Interaction of Positron Beams with Surfaces, Thin Films, and Interfaces, *Rev. Mod. Phys.* 60, 701.

Vehanen, A. (1989) Defect Profiling with Slow Positrons, Positron Annihilation, Edited by L. Dorikens-Vanpraet, M. Dorikens and D. Segers, World Scientific, Singapore, New Jersey, Hong Kong, p. 39.

7.9 One-touch Alanine Dosimetry System for Radiation Processing

S. KASHIWAZAKI[*1)], S. MATSUYAMA[*2)], H. YAGYUU[*1)], H. HARA[*3)], and T. KOJIMA[*4)]

*1)Power System Laboratory, The 2nd Department, Hitachi Cable, Co., Ltd.
5-1-1 Hitaka-machi, Hitachi-shi, Ibaraki-ken, Japan
*2)Hitaka Works, Insulated Wire and Cable Design Department, Hitachi Cable, Co., Ltd.
5-1-1 Hitaka-machi, Hitachi-shi, Ibaraki-ken, Japan
*3)Micro Device, Co., Ltd.
1-4-1 Komagome, Toshima-ku, Tokyo, Japan
*4)Advanced Radiation Technology Center, Japan Atomic Energy Research Institute,
1233 Watanuki-machi, Takasaki-shi, Gunma-ken, Japan

Abstract One-touch alanine/ESR dosimetry system which consists of mass-produced dosimeters, "AMINOGRAY™", and a new reader was designed, developed, and characterized for expansion of application of alanine dosimeter widely in radiation processing.

INTRODUCTION

Alanine/ESR(Electron Spin Resonance) dosimetry is based on ESR analysis of microcrystalline α-alanine which is de-aminated to the free radical by irradiation. The free radicals associated with unpaired electrons are stable at room temperature during and after irradiation, and its concentration proportional to the absorbed dose can be measured in terms of the main peak-to-peak amplitude of the first derivative of the ESR spectrum.

On the basis of the early works by Bradshaw *et al.* in 1962, and Bermann *et al.* in 1971, many studies on alanine dosimeter by several researchers has resulted in a well-known precise high-dose dosimetry method(Regulla and Deffner 1982). The advantages of this method include broad dose range(1Gy~100kGy), long-term stability, linear response, non-destructive analysis, tissue-equivalent properties and so on. However, difficulty of mass-production of uniform-sized dosimeter, and complicated and expensive reading system has hindered wide application of this method in radiation processing so far.

We has developed mass-productive uniform-sized and homogeneous alanine dosimeters with the shapes of rod(Kojima *et al.* 1989) and thin films(Kojima *et al.* 1993a). Rod-shaped dosimeters are now commercially available as "AMINOGRAY™"(Hitachi Cable, Co., Ltd.). Parallel to these developments, compact dose reading systems based on permanent magnet spectrometers were developed by reducing number of analytical parameters to the minimum(Kojima and Tanaka 1989: Kojima *et al.* 1993b, 1993c).

This paper briefly describes design, development and properties of the alanine/ESR dosimetry system which consists of mass-produced dosimeters, "AMINOGRAY™", and the latest developed an one-touch reader.

EXPERIMENTAL

(1)ALANINE DOSIMETERS

Alanine, a kind of amino acid, is provided as crystalline powder with grain size of about a few hundreds μm in diameter by pharmaceutical manufacturer. Uniform-sized and homogeneous dosimeters can be prepared with binders. We proposed to use polymers as binders(Kojima *et al.*, 1986), and molded admixture of alanine and polymer binders into dosimeters in various shapes: rod, sheet, film, chip and cord(Kojima *et al.* 1993d).

Among these dosimeters, rod-shaped dosimeter(DL-α-alanine 70 wt%, polystyrene 30wt%, 2.988±0.02 mm in diameter, 30 mm in length) have useful properties especially for high-dose region, and now play a important roll in IAEA international dose assurance service(IDAS). Detailed preparation procedure and main properties are described in the previous paper(Kojima and Tanaka 1989). Alanine dosimeter samples were irradiated by ^{60}Co-gamma rays under electron equilibrium at JAERI, to absorbed doses of 0.1, 1.0, 10 and 100 kGy at a dose rate of 1.0 or 10 kGy/h at 25°C, which are estimated by a parallel-plate ionization chamber calibrated at Electrotechnical Laboratory, the primary standard laboratory in Japan.

(2)DEVELOPMENT OF AN ONE-TOUCH READER FOR "AMINOGRAY™"

An one-touch reader dedicated to "AMINOGRAY™" was developed mainly on the basis of the development experiences of a prototype ESR reader(Kojima *et al.* 1993b, 1993c) with a permanent magnet by simplification of functions such as microwave frequency, magnetic field sweep range, microwave power, and magnetic field modulation amplitude.

The reader consists of two unit boxes, (a)sweep control/amplifier/power supply unit and (b)magnet/resonator/microwave unit, as shown in Fig.1. The main ESR parameters optimized aiming to measure only "AMINOGRAY™" are magnetic field:375±10 mT, microwave power:5 mW(10.5 GHz), magnetic field modulation amplitude:0.4 mT (100 kHz). As one of the special feature of the reader, it has a sub-cavity beside a main cavity so as to minimize change in Q-value with and without dosimeter sample in

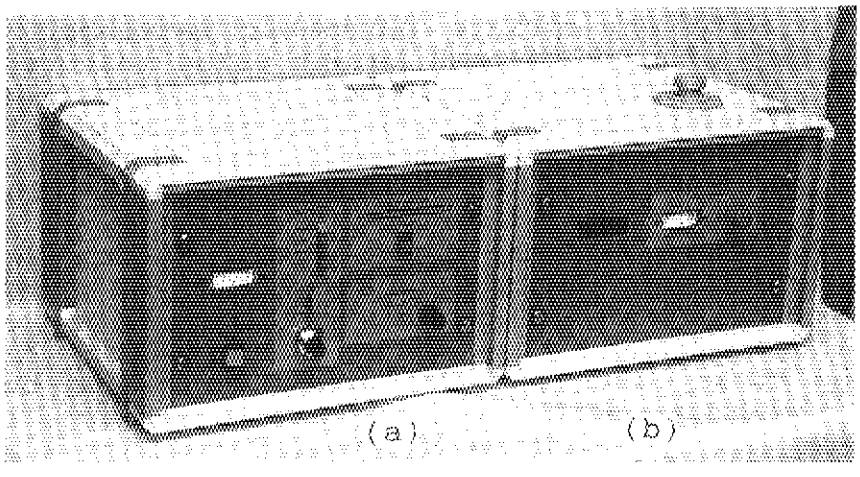


Fig.1 View of the one-touch reader dedicated to "AMINOGRAY™".
(a)sweep control/amplifier/power supply unit
(b)magnet/resonator/ microwave unit

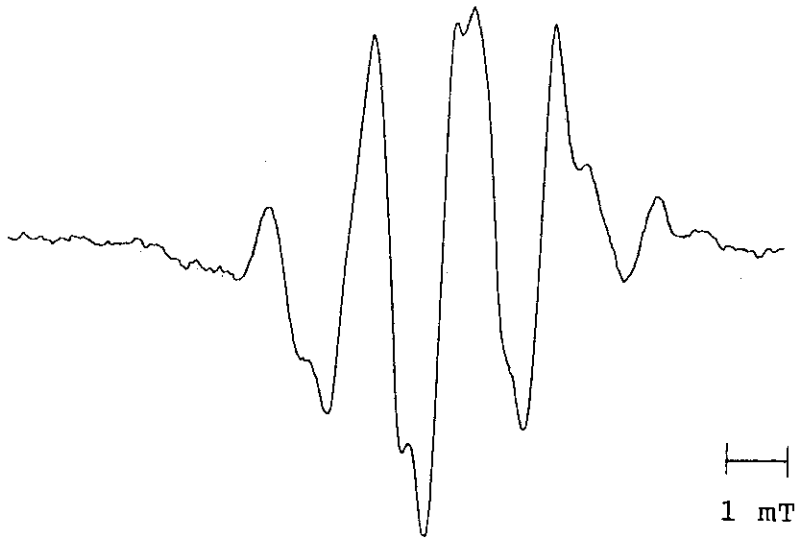


Fig.2 A typical first-derivative ESR spectrum of the "AMINOGRAY" irradiated to 5 kGy, which is measured by the one-touch reader.
magnetic field sweep:375±10 mT,
microwave power:5 mW(10.5 GHz),
magnetic field modulation amplitude:0.4 mT(100 kHz)

the main cavity. The improvement resulted into reduce the switching procedure of auto frequency control(AFC) function, although the procedure is necessary for conventional ESR spectrometers when samples are changed. The reader provides only ESR responses now, however it can be extended its function easily with an control electronic circuit board of data analysis.

RESULTS AND DISCUSSION

A typical first-derivative ESR spectrum of the irradiated dosimeter(5 kGy) measured above the dosimetry system is shown in Fig.2. The spectral shape, especially central two peaks is somewhat different from original one measured by a conventional spectrometer with appropriate parameter settings. However, reproducibility of peak-to-peak height value measured 20 times by repeating take-out/re-insertion of the same dosimeter sample is within ±1%(1σ) in terms of variation coefficients.

The dose response curve measured by the system is shown in Fig.3 with precision values in parentheses obtained by 20 measurements of the same dosimeter. The curve shape is similar to the typical dose response curve of alanine dosimeter(Kojima and Tanaka 1989), which has slight saturation tendency in higher dose region than about 10 kGy due to competitive reaction of generation and decomposition of free radicals by irradiation (Snipes and Horan, 1967). The precision values obtained at radiation processing dose level are within ±1%(1σ), except for the value at 1 kGy which is attributed to less signal/noise ratio. The precision at 1 kGy can be easily improved to meet requirements in process control dosimetry, within ±1%, by smoothing of a spectrum by using simple statistical data treatment(Kojima and Tanaka 1989).

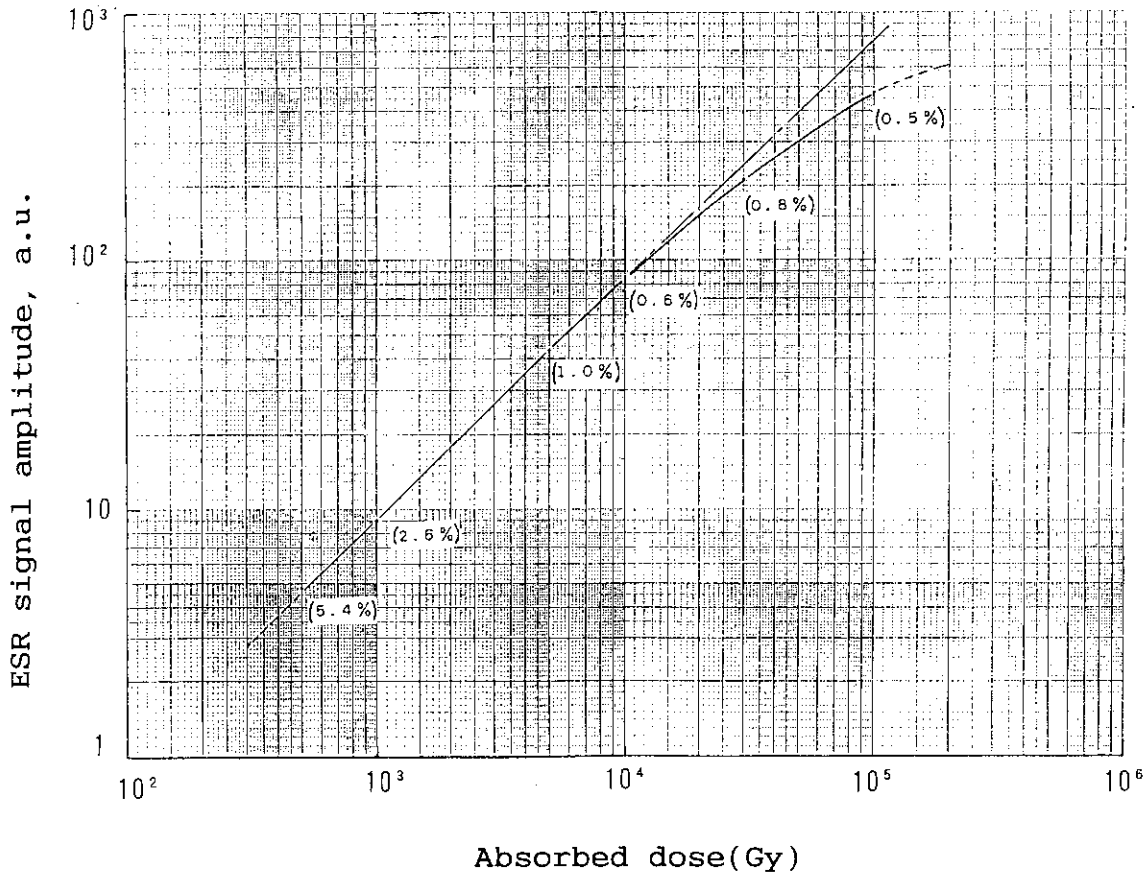


Fig.3 The dose response curve with precision values in parentheses which are estimated by 20 measurements of the same dosimeter.

CONCLUSION

The developed dosimetry system allows us to measure doses from 1 to 100 kGy with the precision of <±1%(1σ) in ~10 s by only one touch of the starting button. The reader which is commercially available as "AMINOGRAY™ dose reader", has additional advantages of small size(about 30-cm cube), low weight(14 kg) and reasonable cost(nearly equal to that of a standard UV spectrophotometer).

It is expected to be a trigger to expand application of alanine/ESR dosimetry in radiation processing.

REFERENCES

Bradshaw W.W., Cadena D.C., Crawford E.W. and Spetzeler H.A.W. (1962) *Radiat.Res.* 17, 11-21

Bermann F., De Choudens H. and Descours S.(1971) STI/PUB/269 (Vienna, IAEA), 311-325

Kojima T. and Tanaka R.(1989) *Appl.Radiat.Isot.* 40, 851-857

Kojima T., Ranjith H.L.A., Haruyama H., Kashiwazaki S. and Tanaka R.(1993a) *Appl.Radiat.Isot.* 44, 41-45

Kojima T., Haruyama Y., Tachibana H., Tanaka R., Okamoto J., Hara H. and Yamamoto Y.(1993b) *Appl.Radiat.Isot.*, 44, 361-365

Kojima T., Haruyama Y., Tachibana H., Tanaka R., Okamoto J., Yagi K., Tamura N., Hara H. and Kashiwazaki S.(1993c) *Radiat.Phys. Chem.*, 42, 757-760
Kojima T., Tachibana H., Haruyama Y., Tanaka R., and Okamoto J. (1993d) *Radiat.Phys.Chem.*, 42, 813-816(1993)
Regulla D.F. and Deffner U.(1982) *Int.J.Appl.Radiat.Isot.* 33, 1101-1114
Snipes W. and Horan P.K.(1967) *Radiat.Res.*, 30, 307-315

7.10 Radiation Induced Solid-state Polymerization of Long-chain Acrylates Containing Fluorocarbon Chain

Y. SHIBASAKI and ZHI-QIN ZHU

Department of Chemistry, Faculty of Science, Saitama University
Shimo-okubo 255, Urawa-shi, Saitama 338, Japan

ABSTRUCT

γ-Ray irradiation post-polymerizations of long-chain acrylates containing fluorocarbon chain, $H(CF_2)_{10}CH_2OCOCH=CH_2$ and $H(CF_2)_8CH_2OCOCH=CH_2$, were investigated and also the structures and thermal properties of comb-like polymers obtained were studied. It was found that these monomers exhibited very high polymerizability at wide temperature ranges around the melting points. Because the fluorocarbon chains are less flexible and thicker than the hydrocarbon chains, it can be expected that the aggregation force among the monomer molecules is strong and the conformational freedom of functional group for polymerization is large. According to the DSC and the X-ray diffraction measurements of the comb-like polymers obtained, the fluorocarbon chains are aggregated in a mode of hexagonal packing in the lamellar crystals. This situation can be considered as an optimum condition for the γ-ray irradiation post-polymerization.

KEYWORDS

γ-Ray-irradiation post-polymerization; solid-state polymerization; long-chain acrylate monomer; comb-like polymer; two-dimensional polymerization; lamellar crystal; polymorphism.

INTRODUCTION

In solid-state, the polymerization reaction of long-chain vinyl compounds will be influenced remarkably by the arrangement and packing mode of monomer molecules, because polymerization proceeds two-dimensionally in lamellar crystals and the polymerizability is controlled by the distance among the functional groups for polymerization and their local motion (Shibasaki et al.,1979; Shibasaki,1980; Shiozawa et al., 1992). Fluorocarbon chain is thicker than that of hydrocarbon chain and less flexible, since the van der Waals radius of fluorine atom is too big to make a trans zig-zag conformation of $-(CF_2-CF_2)_n-$ chain. Some monomer molecules containing long-fluorocarbon chains have a tendency to make a layered structure and the functional groups should be arranged in an effectively condensed state having a conformational freedom. Therefore, a monomer molecule, in which functional group is linked with a fluorocarbon chain by a CH_2 chain, may have good polymerizability in the solid-state. On the other hand, comb-like polymers containing fluorocarbon chain in the long-side chains have been interested from the viewpoint of new functional polymers with special electrical and chemical properties. In this work, γ-ray irradiation post-polymerizations of long-chain acrylates containing fluorocarbon chain were investigated and also the structures and thermal properties of

comb-like polymers obtained were studied.

EXPERIMENTALS

1H,1H,11H-icosafluoroundecyl acrylate ($H(CF_2)_{10}CH_2OCOCH=CH_2$, Abbr.:$F_{10}A$, mp 44.0-45.4 ℃) and 1H,1H,9H-hexadecafluorononyl acrylate ($H(CF_2)_8CH_2OCOCH=CH_2$, Abbr.:F_8A, mp -19 ℃) were bought from Daikin Chemical Co. $F_{10}A$ was purified by recrystallization from the ethanol solution, but F_8A was used as received. The samples of $F_{10}A$ and F_8A (1-2 g) were sealed in Pyrex tubes (i.d. 10 mm) under the nitrogen atmosphere or in vacuum and then crystallized by rapid cooling of the melt in liguid nitrogen. After γ-ray-irradiation of 2.58×10^2 -7.74×10^2 C kg^{-1} (1-3 Mrad, total dose) at -196 ℃, post-polymerizations at various temperatures were allowed to proceed for 24 h. The reaction mixtures of $F_{10}A$ were crushed and suspended in CCl_4 for 24 h, and further they were treated under the ultrasonic vibration for 4 h at room temperature to remove completely the unreacted monomer molecules from the polymer of $F_{10}A$ (Abbr.: $PF_{10}A$). In the case of F_8A, the polymerized samples were dissolved in acetone of 1-2 ml and poured into CCl_4 of 60-80 ml at room temperature (below ca. 20 ℃) to obtain the polymer of F_8A (Abbr.: PF_8A) as precipitation. Percent conversions were determined from the weights of polymers obtained. Thermal properties of monomers and polymers were measured using a Seiko Instruments Model DSC20 differential scanning calorimeter. IR spectra for monomers and polymers were measured using a JEOL Fourier transfer IR spectrophotometer (JIR 100). X-ray diffraction patterns were measured with a Rigaku diffractometer (RAD-B, Cu Kα radiation: 0.15405 nm).

RESULTS AND DISCUSSION

As shown in Fig.1, $F_{10}A$ exhibited a simple phase transition behavior in the DSC measurement. DSC curves for $PF_{10}A$ are also shown in Fig.1 for comparison with those of $F_{10}A$. Melting of $PF_{10}A$ occurred at a relatively wide temperature range. The melting temperature of $PF_{10}A$ estimated from the peak top of DSC curve was 118 ℃, which was higher than that of $F_{10}A$ about 73 ℃. Although, molar heat of fusion for constitutional unit of $PF_{10}A$ (Δ_fH=73.22 kJ mol^{-1}) was almost same with that of $F_{10}A$ (Δ_fH=75.31 kJ mol^{-1}), the entropy change for $PF_{10}A$ (Δ_fS=187 J K^{-1} mol^{-1}) was smaller than that for $F_{10}A$ (Δ_fS= 236 J K^{-1} mol^{-1}). These results indicate that arrangement of fluorocarbon

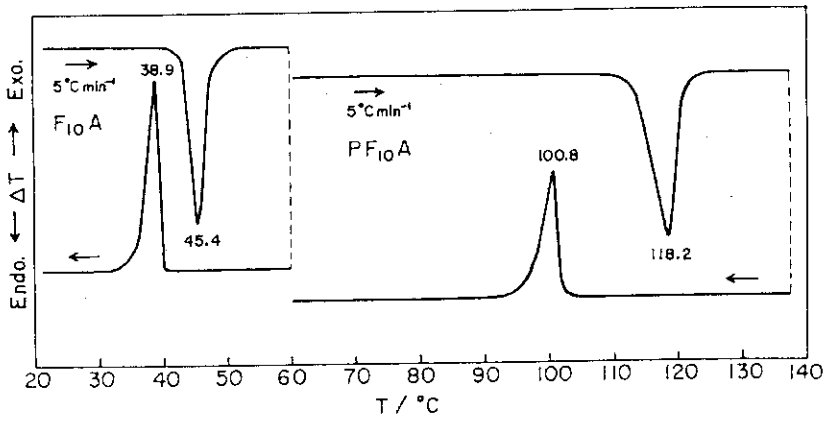


Fig.1 DSC curves for $F_{10}A$ and $PF_{10}A$.

chains in the comb-like polymer of $PF_{10}A$ may be somewhat disturbed by the conformation of the main chain. In addition, the value of entropy change for fusion $\Delta_f S$ of $F_{10}A$ is smaller than a critical value ranging from 270 to 310 J K^{-1} mol^{-1}, below which solid state polymerization may be allowed, reflecting the conformational freedom of the functional groups (Shibasaki et.al.,1988). In IR spectra of $F_{10}A$, with the progress of post-polymerization, the band at 1747 cm^{-1} for ester group $\nu_{C=O}$ shifted to 1759 cm^{-1} and intensities of $\nu_{C=C}$ band at 1637 cm^{-1}, δ_{CH}(in plane) bands at 1414 and 1300 cm^{-1}, and δ_{CH}(out-of-plane) bands at 983 and 806 cm^{-1} decreased remarkably.

In the X-ray diffraction pattern of $PF_{10}A$ obtained by powder method, two diffraction peaks appeared at $2\theta = 4.96°$ (vs) and $10.0°$ (w) indicating a layered structure of 1.78 nm distance and a very strong peak appeared at $2\theta = 17.96°$, which corresponds to a hexagonal packing of fluorocarbon chains (d=0.49 nm) and is larger than the dimension of hexagonal packing of hydrocarbon chains (d=0.42 nm). In addition, the $-CH=CH_2$ groups are arranged regularly in layered crystal of $F_{10}A$ and they have fairly large freedom for local motion. This situation can be considered as an optimum condition for the solid-state polymerization.

Results of post-polymerization of $F_{10}A$ at 0, 20, 40 and 60 ℃ are shown in Fig.2. At temperatures (40-60℃) around the melting point (45.5 ℃) the polymeization of $F_{10}A$ proceeded rapidly and reached to very high conversion. The polymerizability of $F_{10}A$ was rather high even at 0 ℃. From these results, it can be considered that conformational freedom of acrylic acid resides,i.e., local motions of functional groups for polymerization are relatively high, because diameter of the CF_2 sequence is relatively large comparing with those of CH_2 and $OCOCH=CH_2$ groups in the $F_{10}A$ molecule as shown schematically in Fig.3. Furthermore, at a temperature fairly above the melting point, the layered structure has been maintained owing to the strong aggregation force between fluorocarbon chains. Therefore, the polymerization of $F_{10}A$ proceeded two-dimensionally in a single layere and achieved very high conversions.

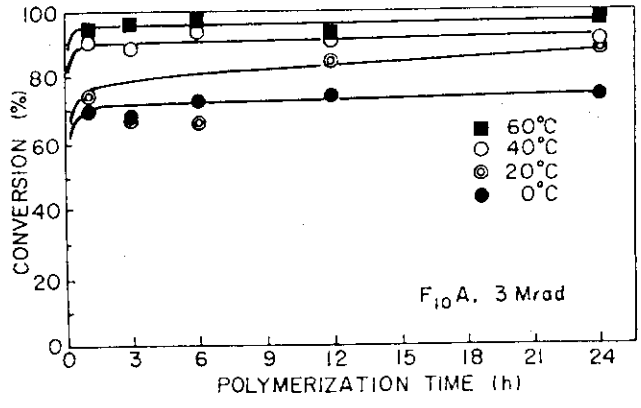


Fig.2 Polymerization curves for $F_{10}A$.

As shown in Fig.4, F_8A exhibited double peaks for fusion at -20.5 and -18.0 ℃ and crystallization at -20.9 and -24 ℃ in DSC curves, indicating an enantiotropic phase transition, such as crystal⇄mesophase⇄isotropic liquid. This feature differs from the phase transion behavior of $F_{10}A$. Packing mode of F_8A in the crystal may be similar to that of $F_{10}A$, although crystal structure of F_8A is not yet clarified by the X-ray diffraction measurement. It seems that

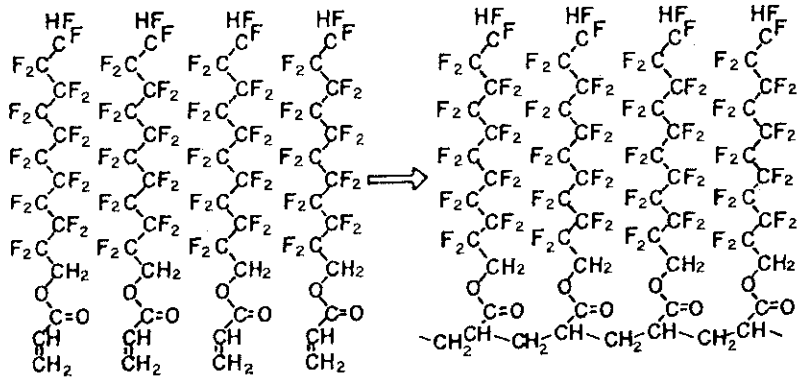


Fig.3 Schematic illustration for arrangements of $F_{10}A$ and $PF_{10}A$ in the lamellar structure.

the mesophase of F_8A observed is a kind of smectic liquid crystal. DSC curves of PF_8A are also shown in Fig.4. PF_8A melts at 65.5 ℃, which is higher than that of F_8A about 85 ℃, and crystallizes at 22.5 ℃. This wide difference in temperature between the melting and the crystallizing is an unexpected character of PF_8A. This phenomenon may be related to the very high polymerizability of F_8A in a wide temperature range around the melting point. The double peaks in the cooling curve seem to reflect the difference in microtacticity of the comb-like polymer obtained.

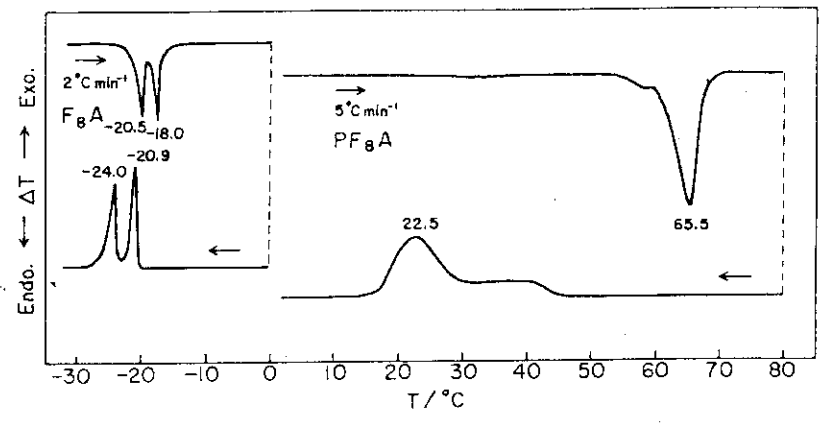


Fig.4 DSC curves for F_8A and PF_8A.

Results of post-polymerization of F_8A at -20 and 0 ℃ are shown in Fig.5. At temperatures just below (-20 ℃) and above (0 ℃) the melting point (-19 ℃) post-polymerization of F_8A proceeded rapidly and resulted in a comb-like polymer with very high conversions. In the case of post-polymerization of F_8A after γ-ray-irradiation of 2.58×10^2 C kg^{-1}, we can distinguish a difference in polymerizability of F_8A at 0 ℃ and -20 ℃. However, after a larg radiation dose of 7.74×10^2 C kg^{-1} any difference in polymerizability due to the polymerization temperature could not be observed, since the polymerizability of F_8A in the organized systems, such as lamellar crystal and mesophase, was too high. It can be considered that a part of F_8A molecules was frozen in the mesophase and polymerized rapidly.

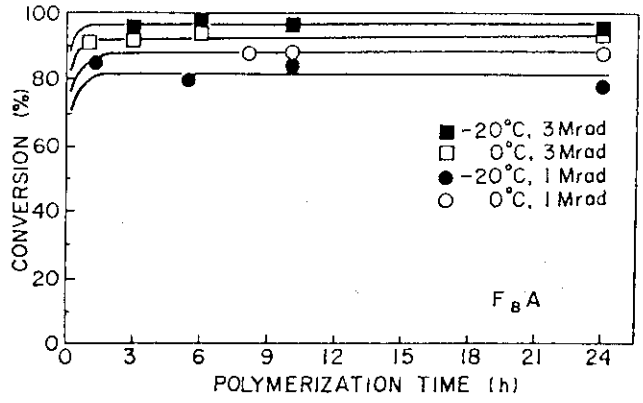


Fig.5 Polymerization curves for F_8A.

CONCLUSION

Radiation induced post-polymerization of long-chain acrylates containing fluorocarbon chain proceeds very fastly, because in the crystal with hexagonal packing of fluorocarbon chains the acrylic acid residue ($-COCH=CH_2$) are arranged regularly in layered structure and have fairly large freedom for local motion. The optimum condition for solid-state polymerization can be maintained up to temperatures fairly above the melting points of monomers, owing to the strong self-organizing property of comb-like polymers of F_8A and $F_{10}A$.

REFERENCES

Shibasaki Y. and Fukuda K. (1979). Solid-state polymerization of long-chain vinyl compounds. I. Effect of molecular arrangement on polymerizability of octadecyl methacrylate. J. Polym. Sci., Polym. Chem. Ed., 17, 2387-2400; II. Effect of molecular arrangement on polymerizability of octadecyl acrylate. J. Polym. Sci., Polym. Chem. Ed., 17, 2947-2959.

Shibasaki Y. (1980). Solid-state polymerization of long-chain vinyl compounds. III. Mechanism of γ-ray-initiated postpolymerization in layered structures of octadecyl methacrylate and acrylate. J. Polym. Sci., Polym. Chem. Ed., 18, 1693-1709.

Shiozawa T., Shibasaki Y. and Fukuda K. (1992). Molecular arrangement and polymerizability of n-alkyl acrylates in Langmuir-Blodgett films. Polym. Internat., 29, 9-16.

Shibasaki Y. (1988). Thermoanalytical study on the polymorphic behaviour of long-chain vinyl compounds. Thermochim. Acta, 123, 191-199.

7.11 Decolorization and Degradation of Melanoidins in Wastewater by Ionizing Radiation

M. SEKIGUCHI, T. TANABE and T. SAWAI

Tokyo Metropolitan Isotope Research Center,
2-11-1 fukazawa, setagaya-ku, Tokyo 158, Japan

ABSTRACT

Decolorization and degradation of molasses pigments (melanoidins) in wastewater from yeast factories by ionizing radiation were investigated. In the case of samples with the same value of chromaticity (4000), the reduction degree of chromaticity of dialyzed sample reached 27.5% and 75 % at a dose of 4.5 kGy and 14 kGy, respectively, and was greater than that of non-dialyzed sample. Organic acids such as oxalic acid, formic acid and glycolic acid were formed with increasing dose, and the biodegradability (BOD/COD) of wastewater was increased with decrease in pH. The relationships between the value of chromaticity/TOC and molecular weight of molasses pigments, were obtained from subsequent experiments using dialyzed and non-dialyzed samples with the same value of TOC.

KEYWORDS

radiation treatment, wastewater, recycled water, decolorization, degradation, COD, TOC, molasses pigment, melanoidin, organic acid, molecular weight distribution,

INTRODUCTION

In spite of lack of new sources, the large city such as Tokyo has consumed an increasing water. Therefore, recycling of municipal effluent has become increasingly important to support various usages as follows: washing, gardening, watering, agriculture and industry. However, the colored wastewater resistant to biological treatment, such as activated sludge treatment, is also known to discourage recycling water because the water is of low quality. Recently, the Ministry of Construction drafted a water quality standard for recycling water to improve the urban waterside environments, which presented the target value on choromaticity. From the view point of recycling, the developments and improvements of treatment process of colored wastewater is one of the most important and difficult problems. Effluent discharged from distillery and yeast factories to the public sewage system, contains molasses pigments (a kind of melanoidin), and which are hardly treated by conventional methods. As to decolorization of dark brown color of molasses pigments, numerous attempts, using hydrogen peroxide (Hayase F. *et al.*, 1984), ozone (Kim S. B. *et al.*, 1985), microorganisms (Ohmomo S. *et al.*, 1985) and others (Ichikawa M., 1991), have been carried out.

We have studied wastewater treatments with ionizing radiation and also reported on degradation of molasses pigment in effluent from a yeast factory (Sawai T. *et al*, 1993, Sawai T. *et al*, 1993).

In this paper, we investigated the decolorization and degradation of molasses pigments by ionizing radiation using wastewater without activated sludge treatment from a yeast factory.

MATERIALS AND METHODS

Sample
Colored wastewater without activated sludge treatment was obtained from a yeast factory, then part of the wastewater was dialyzed with permeable membrane. In our experiments, wastewater with the same value in chromaticity (4000) or TOC (about 300 mg/l) was prepared as a sample.

Dialysis and fractionation by permeable membrane
Seamless Cellulose Tubing (flat width: 25 mm, Union Carbide Corporation) and Spectra/Por membrane (No.1, 4 and 6, flat width: 25-45 mm, Spectrum Medical Industries INC.) were used as permeable membrane, and colored wastewater was dialyzed against distilled water at 4°C for more than 7 days.
The molasses pigments in wastewater were fractionated into 4 fractions with Spectra/Por membranes (FR1: above MW 1000, FR2: above MW 6000-8000, FR3: above MW 25000, FR4: above MW 50000).

Measurement of color
Decolorization was evaluated by chromaticity (1 unit is defined as the color of solution contained 1 mg of platinum and 0.5 mg of cobalt /1l water), color difference (ΔE^*: CIE $L^*a^*b^*$) and UV absorption at a wave length of 260 nm, and then UV-VIS spectrum was also measured. Color difference and UV-VIS spectrum were measured with Automatic Color Analyzer Model TC-1800 II (Tokyo Denshoku Co., LTD) and UV-VIS Spectrophotometer UV 3100S (Shimadzu CO., LTD), respectively.

Measurement of water quality (Japan Sewage Work Association, 1984)
Water quality was determined by COD (Chemical Oxygen Demand), BOD (Biochemical Oxygen Demand), TOC (Total Organic Carbon, TOC Analyser TC-500, Shimadzu CO., LTD.) and pH. Molecular weight distribution were obtained from gel-permeation chromatography (column: Sephadex G-25 fine, Liquid Chromatograph LC-10AD, Shimadzu CO., LTD). Organic acid analysis was performed with a Carboxylic Acid Analyzer Model S-300 (Tokyo Rikakikai CO., LTD), which used a ion exchange chromatography applied by a post-column derivative method.

Irradiation
Gamma ray radiation: Samples were irradiated under aerobic (aerated with air pumps) and anaerobic condition (saturated with nitrogen gas) by gamma rays (Co-60 source, capacity: 185 TBq, dose rates: about 3 kGy/hr). Electron beam radiation: Samples were agitated in order to saturate with air prior to irradiation, then irradiated by electron beams (5 MV Dynamitron accelerator, beam currents: 1.0-2.0 mA).

RESULTS AND DISCUSSION

Effect of radiation sources
The color difference and pH of non-dialyzed wastewater (NDW), irradiated under aerobic condition by gamma ray, were decreased with increasing dose (Fig.1). In other cases, any remarked change was not observed in pH. The color difference of wastewater , irradiated under anaerobic condition by gamma ray, was rapidly decreased to 4 kGy and slightly increased above the dose . However, that of wastewater irradiated by EB gradually decreased to 14 kGy and was almost constant above the dose.

Experiment on samples with the same value of choromaticity (4000)

Change of color
In the experiment using dialyzed (DW) and non-dialyzed wastewater (NDW) with a chromaticity of 4000, the reduction degree of chromaticity of DW reached 27.5% and 75 % at 4.5 kGy and 14 kGy, respectively, and which was greater than that of NDW (Fig.2). Furthermore, the change of color difference was similar to those of chromaticity and UV absorption at a wave length of 260 nm.
UV spectrum of both sample showed the shoulder at a wave length of about 260 nm and this shoulder disappeared with increasing dose.

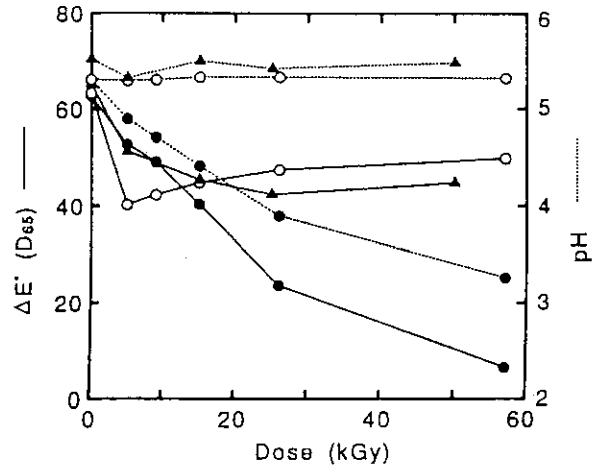


Fig. 1 Changes of color difference and pH in non-dialyzed wastewater irradiated by gamma rays and EB.
● : gamma ray (aerobic) ○ : gamma ray (unaerobic) ▲ : electron beam

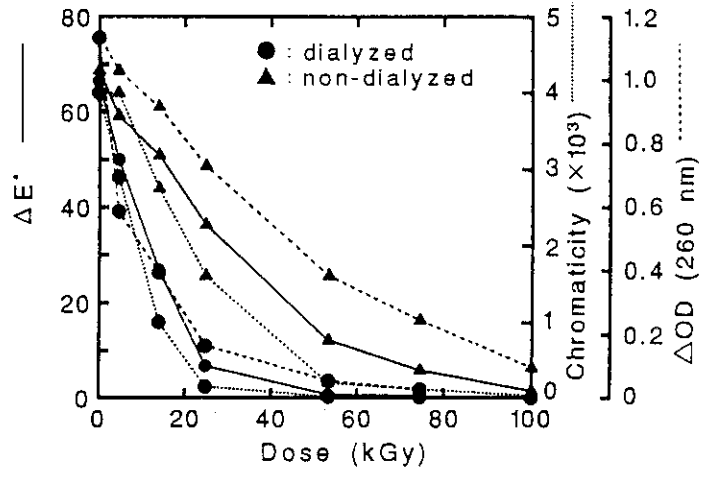


Fig. 2 Changes of chromaticity, color difference and optical density (260 nm) of wastewater irradiated by gamma rays

Change of water quality

The pH of DW decreased from the initial pH 5.3 to about 3 at 4 kGy and had a tendency to increase above about 80 kGy. On the other hand, the pH of NDW continued to decrease to 100 kGy and NDW reached pH 3 at this dose. Both COD and BOD values were also decreased with increasing dose, and the value of BOD/COD ,used as an indicator of biodegradability, showed the maximum at 75 kGy (Fig. 3).

The high molecular weight components of molasses pigment were degraded to lower molecular weight substances by ionizing radiation (Fig.4) and typical organic acids as an intermediate in degradation process were observed. The DW formed oxalic acid and glycolic acid at 5 kGy and the formation of those acid rose to the peak at 25 kGy (Fig. 5). The change of acid formation was closely related to that of pH.(Fig. 3)

Experiment on samples with the same value of TOC (about 300 mg/l)

Change of color

Samples with the same value of TOC had very different values of chromaticity as shown in Table 1. NDW showed the lowest value of chromaticity/TOC ,and FR1 and FR2 had higher values of chromaticity in comparison with those of FR3 and FR4. The former seems to be caused by a lot of low molecular weight and colorless substances. On the other hand, the latter may be closely relate to number of chromophores in melanoidin molecule. However, every sample showed similar result about the reduction rate of color by ionizing radiation.

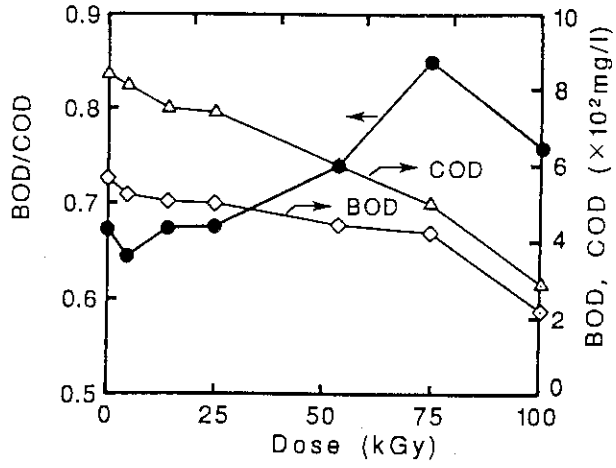


Fig. 3 Changes of BOD, COD and BOD/COD in non-dialyzed wastewater by gamma ray radiation.

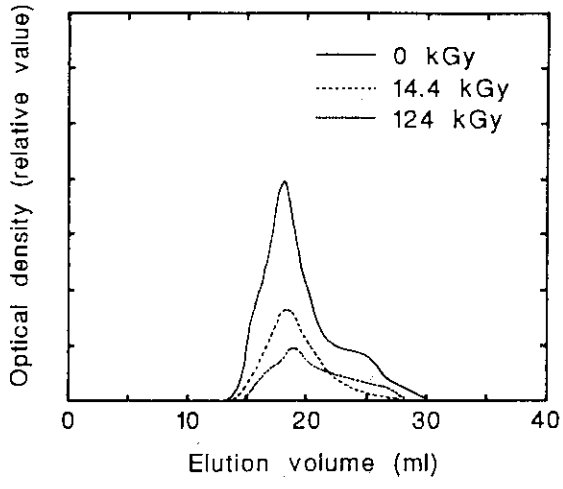


Fig. 4 Change of molecular weight distribution of molasses pigments by gamma ray radiation.

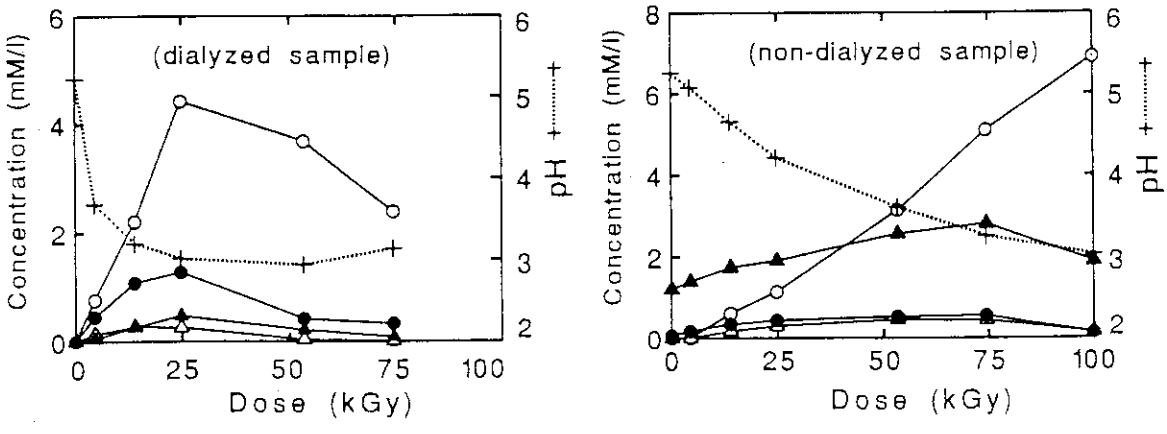


Fig. 5 Changes of organic acid formation and pH in dialyzed wastewater by gamma ray radiation.
● : formic acid ○: oxalic acid ▲: acetic acid △: glycolic acid

Table 1. The values of chromaticity, TOC and chormaticity/TOC in dialyzed fractions (FR1-4)

Sample	NDW	FR1	FR2	FR3	FR4
Chromaticity	1800	4500	4750	3750	3500
TOC (mg/l)	297	285	260	262	310
Chromaticity/TOC	6.06	15.79	18.27	14.31	11.29

Change of water quality

The change in pH of every sample was similar: the pH of NDW and five fractions (FR1-FR4) were decreased rapidly to 24 kGy, and showed the minimum (about pH 3) at 49 kGy. Organic acid formation also rose up the peak at 49 kGy. Furthermore, every sample irradiated by gamma rays was different in reduction rate of TOC (Table 2). The value of choromaticity/TOC was decreased rapidly with increasing dose because chromaticity was decreased more rapidly than TOC: for example, the values in Table 1 changed to 0.52 for NDW, 2.04 for FR1, 1.94 for FR2, 1.18 for FR3, and 1.28 for FR4 at 24 kGy, respectively.

Table 2. The change of TOC (mg/l) in dialyzed fractions irradiated by gamma ray

Dose (kGy)	NDW	FR1	FR2	FR3	FR4
0	297 (100)	285 (100)	260 (100)	262 (100)	310 (100)
9	295 (99.3)	275 (96.5)	262 (101)	260 (99.2)	285 (91.9)
24	279 (93.9)	245 (86.0)	258 (99.2)	211 (80.5)	235 (75.8)
49	237 (79.8)	200 (70.2)	209 (80.4)	154 (58.8)	163 (52.6)
75	221 (74.4)	114 (40.0)	143 (55.0)	69 (26.3)	75 (24.2)

note: the figures in parentheses represent percentage of residual TOC value.

CONCLUSION

Gamma ray radiation under aerobic condition was effective in decolorizing and degradating the molasses pigments in colored wastewater. However, it seems to be necessary to improve the irradiation condition for EB radiation. The decolorization efficiencies of DW by ionizing radiation were markedly increased in comparison with those of NDW. Change of pH is closely related to that of organic acid formation or biodegradability. Every wastewater with the same value of TOC showed the minimum in pH and maximum of organic acid formation at the same dose. The values of chromaticity/TOC of FR1 and FR2 were greater than those of other fractions and NDW.

REFERENCE

Hayase F., Kim S. B. and Kato H. (1984), Decolorization and Degradation Products of the Melanoidins by Hydrogen Peroxide., *Agric. Biol. Chem.*, 48, 11, 2711-2717.

Ichikawa M. (1991), Present and future technology for reduction of color materials of waste water from baker's yeast plant, *J. Environ. Pollution Control*, 27(8), 751-754.

Japan Sewage Work Association (1984), Gesui Shiken Houhou.

Ohmomo S., Itoh N., Watanabe Y., Kaneko Y., Tozawa Y. and Ueda K. (1984), Continuous Decolorization of Molasses Waste Water with Mycelia of *Coriolus versicolor* Ps4a., *Agric. Biol. Chem.*, 49, 9, 2551-2555.

Sawai T., Sekiguchi M., Shimokawa T. and Sawai T. (1993), Radiation treatment of municipal effluent, *Radiat. Phys. Chem.*, 42(4-6), 723-726.

Sawai T., Sekiguchi M., Tanabe H. and Sawai T. (1993), Radiation degradation of molasses pigment, Tokyo Metropolitan Research Center Annual Report, 1-9.

7.12 Discrimination of Damages Depending on the Types of Lactic Dehydrogenase Isozymes in Electron Beam Irradiation

Akishige Ohta[1], Takashi Matsubayashi[1], Liu Xiao-Lan[2], Haruki Takizawa[3]

1)Department of Radiology, Kitasato University School of Medicine, Sagamihara, Kanagawa, 228 Japan,
2)Department of Radiation Therapy, Third Hospital, Norman Bethune University of Medical Science, Chungchun, P.R.China,
3)Japan Atomic Energy Research Institute, Takasaki, Gunma, 370-12 Japan

ABSTRACT:

Lactate dehydrogenase(EC 1.1.1.27,LDH) was a tetrameric molecule. The five different combinations of two different polypeptide chains can be readily identified by electrophoresis and ion-exchange chromatography.

Injury patterns of LDH activity following electron-beam irradiation was investigated by assaying activities of three isozymes(pig heart LDH;M_4, rabbit muscle LDH;H_4, chicken heart LDH;M_3H_1). Following results were obtained in the electron beam irradiation to three kinds of LDH isozymes: 1) Each isozyme has respective different reactivities to the electron beam irradiation. 2) Among the isozymes, M_4 enzyme was increased its enzymatic activity by the irradiations of low-level doses. 3) For the H_4 enzymes, an increasing phenomenon of -SH group was found in the low-level doses of electron beam irradiation.

INTRODUCTION:

Lactic dehydrogenase (E.C. 1.1.1.27,LDH) catalyzes the following reaction:

$$\begin{array}{l} CH_3 \\ HCOH \\ COOH \end{array} + NAD^+ \rightleftarrows \begin{array}{l} CH_3 \\ C{=}O \\ COOH \end{array} + NADH + H^+$$

LDH is four-monomer-combined tetrameric macromolecule and its molecular weight is 140,000. Two different types of polypeptide chains, called H-type and M-type respectively, are present in the monomers. Five isozymes, M_4, M_3H_1, M_2H_2, M_1H_3 and H_4, are present in LDHs depending on the combination of M-type and H-type monomeric structures. These isozymes can be individually separated with ease

by means of electrophoresis or chromatography.[1,2] Following the principle of functional size analysis by radiation inactivation method[3], it is estimated that degrees of the loss of enzymatic activity by radiation exposure are also similar because the functional sizes of the five LDH enzymes are all in the same size. However, in the study to be reported here in which the sensitivity was compared among the isozymes by using LDH-M_4, LDH-H_4 and LDH-M_3H_1 enzyme preparations of LDH isozymes when the aqueous solutions of these preparations were irradiated by electron beam, it was indicated that there was an obvious discrimination among the enzymes for the loss of enzymatic activity by radiation exposure. Thus the experimental results are described in the following section.

MATERIALS AND METHODS:

Preparation of Enzyme Solution:

The enzyme preparations, LDH-H_4, LDH-M_4 and LDH-M_3H_1, are pure ones purified from of rabbit muscle, pig heart and chicken heart respectively; they were all purchased from Sigma Chemicals Co. Ltd. These enzyme preparations were dissolved in 0.05M phosphate buffer(pH 7.2) to prepare $1x10^{-8}$M, $5x10^{-8}$M and $1x10^{-7}$M solutions.

Electron Beam Irradiation:

3 MeV electron beam was used for irradiation, which was generated from the Cockcroft-Walton-type linear accelerator(0.01mA, 3 MeV) installed in Japan Atomic Energy Research Institute(Takasaki).

Measurement of Enzyme Activity:

LDH activities were measured by recording the decreasing rates of the optical density at 340nm for NADH that is consumed in associated with the reaction in which pyruvic acid is reduced to lactic acid.

Measurement of SH Group:

SH group contents in LDH molecules were photometrically estimated using 5,5'-dithiobis(2-nitrobenzoic acid)-reaction according to Ellman method.

Electrophoresis of LDH:

In order to detect the activity of enzyme proteins, 10 μl aliquots of the enzyme solutions irradiated by electron beam were applied polyacrylamide gels, then submitted to electrophoresis for one hour and

finally color visualizations were made by nitrotetrazolium-formazan staining method.

RESULTS AND DISCUSSION:

Fig.1A, B, C and D show the electrpphoregrams of LDHs, i.e. LDH-H_4, LDH-M_4 and LDH-M_3H_1, irradiated by 20, 30, 40, 50, 60, 80, 120 and 200 Gy doses of electron beam and non-irradiated LDH which were all concurrently electrophreted for each LDH in the same runs. From these Figures, it was found that the enzymes irradiated by electron beam were all decrease the coloring in proportionto the doses they reseived.

Fig. 2A, B and C represent dose-eefect relations obatined in the electron beam irradiation of the solutions of LDH-H_4, LDH-M_4 and LDH-M_3H_1. Each of these enzyme preparations was dissolved in phosphate buffer solution to make three different concentrations ($1x10^{-8}$M, $5x10^{-8}$M and $1x10^{-7}$M), then they were taken into polyethylene tubes of 1 cm diameter (wall thickness 1mm) and submitted to irradiation. The following four points become evident from these figures. 1) The solutions of higher enzyme concentration are less sensitive to the radiations compared to the solutionsof lower concentrations. 2) M_4 enzyme is more tolerable to the radiation damage than H_4 enzyme. 3) M_4 and H_4 enzymes are more tolerable to the radiation damage than M_3H_1 enzyme. 4) In M_4 enzyme, an activating phenomenon of enzymatic function that is called "low-dose effect" is caused in a range of low-level doses.

Fig. 3A, B and C represent dose-effect curves in the estimation of reactive -SH group contents in the electron beam irradiated enzyme molecules. In the estimating experiment of enzyme activities, it was observed that the -SH group content in the M_4 enzyme which showed a higher stability to the electron beam irradiation was less varied, while to the contrary, the -SH group content in the M_3H_1 enzyme molecule, having lost the activity easily electron beam irradiation, increased in proportion to the doses given to it. Meanwhile, the -SH group content in the H_4 enzyme molecule was increased by the irradiation in a low-level dose range, whereas the -SH group content decreased in proportion to the doses at the levels of above 80 Gy.

Since its birth on the earth, the living organism has had its species-specific evolution during such a long time until today in all aspects, for example, such as biological structure, function and external morphorogy, and thus various biological species we can see

nowdays have been formed. Through the long histry of biological evolution, biological molecules have also achieved so far their individual-specific evolutions. Consequently, the function of reactivity of biomolecules differs little by little among each other depending on their origins or histories of the substances even for biopolymer having the same functions. The specific signals of living organisms with their reactiveties or functions are stored in the primary structure of biopolymer as molecular signals.

In another previous paper, we have reported the results of studies ondamaging mechanisms of irradiations by X-rays, proton beams and ultraviolet rays by using two kinds of isozymes, i.e. yeast orogin alcohol dehydrogenase and lover origin alcohol dehydrogenase.[4,5] In the experiment, following three points were elucidated : 1) The liver origin enzyme is more tolerant to irradiation damages by X-ray, proton beams and ultraviolet rays compared with the enzymes originated from yeast. 2) In the liver origin enzyme, the enzyme activity rises by low-dose irradiations of X-rays and proton beams, while such a phenomenon is unable to be found in the yeast origin enzyme. 3) In the case of ultraviolet rays, the low-dose irradiation effects being caused by X-ray or proton beam irradiation are not observed.

CONCLUSIONS:

In the present experiment, the effect of electron beam irradiation to three kinds of LDH isozymes was examined, and thus demonstrated that the damaging mechanism of the LDH caused by the radiation is discriminated each other among the isozymes. As the LDH is a "-SH enzyme" in which the -SH groups of amino acid residues are involved in its active centers of reactions, the -S-S-bonds involved in the built-up of tetrameric structure of the M_3H_1 enzyme are weaker compared to those of the M_4 and H_4 enzymes, and thus it is inffered that the M_3H_1 enzyme holda its higher order structure though unstable chemical bonds.

Acknowledgement:

This work was supported in part by a research grant from the Reseach Center for Nuclear Science and Technology, University of Tokyo. Financial assistance from the Japan Atomic Energy Research institute is aknowledged with thanks.

References:

1)Schmidt,F.N. and Brush, H.A.:An efficient method for isolation of lactate dehydrogenase isozymes. Anal. Biochem. 38,158-163, 1970

2)Saito, M.:Subunit cooperativity in the action of lactate dehydrogenase. Biochim. et Biophy. Acta, 238,17-26, 1972

3)Kume, T.:Functional size analysis of bioactive materials by radiation inactivation(in japanease). Rad. Chem. 57,3-12,1994

4)Ohta, A. and Matsubayashi, T.:Effect of ultraviolet on alcohol dehydrogenase(in japanease). Annual report of radiation oncologist of jap. radiol. soc. 2,69-73,1989

5)Ohta, A. and Matsubayashi, T.:Recovery of activity in irradiated liver alcohol dehydrogenase, (Abstract, in japanease). Acta Radiol. Jap. 52(7),1053,1992

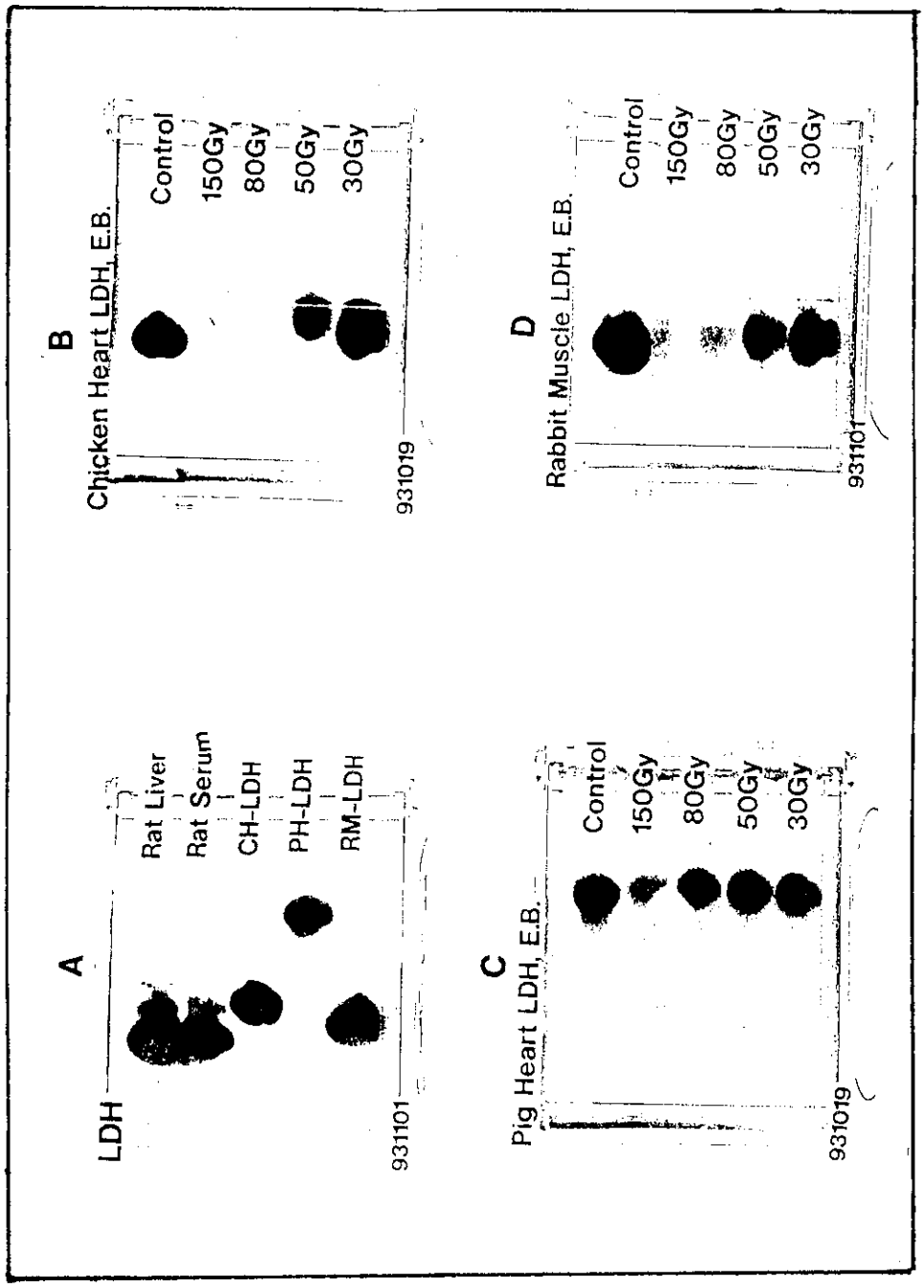


Fig. 1. Radiation inactivation disc gel electrophoretic piofiles of (B)chicken heart lactate dehydrogenase, (C) pig heart lactate dehydrogenase, (D) rabbit muscle lactate dehydrogenase. Irradiation was performed before electrophoresis of isozymes by electron beam. (A): The control electrophoregrams are the unirradiated rat liver cytosol LDH, rat serum LDH, chicken heart LDH, pig heart LDH and rabbit muscle LDH.

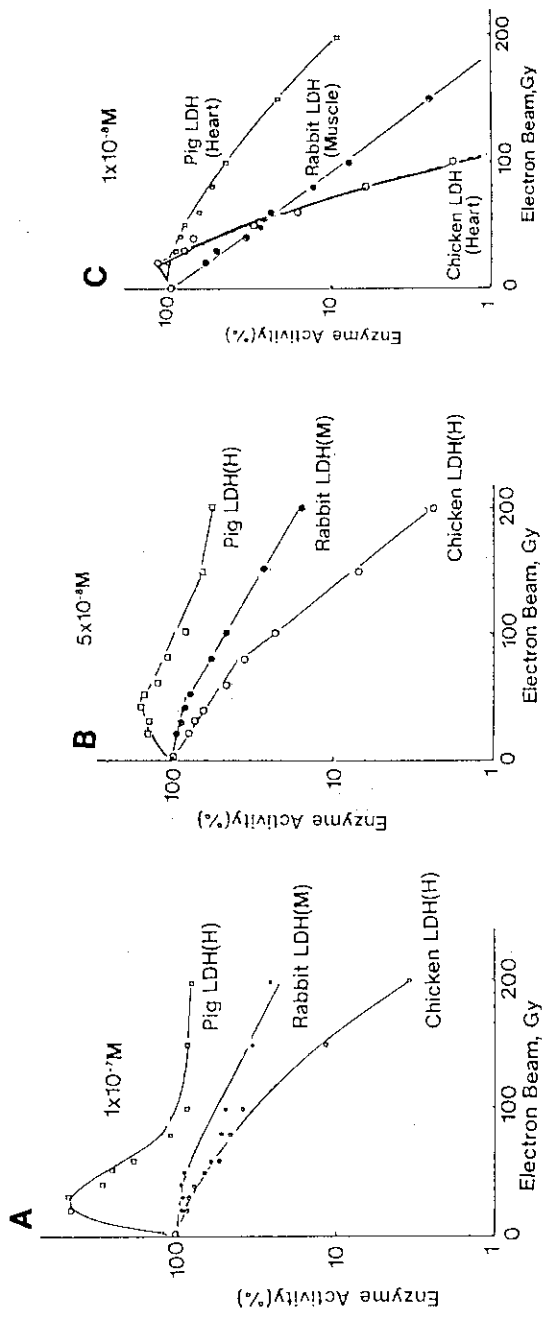


Fig. 2. Effect of electron irradiation on the rate of pyrvate reduction by chicken heart lactate dehydrogenase(○ — ○), pig heart lactate dehydrogenase(□ — □) and rabbit muscle lactate dehydrogenase(● — ●). The value of the enzyme activity is a mean value from three separate measurements. Enzyme concentration:$1x10^{-5}$M(A), $5x10^{-6}$M(B) and $1x10^{-5}$M(C).

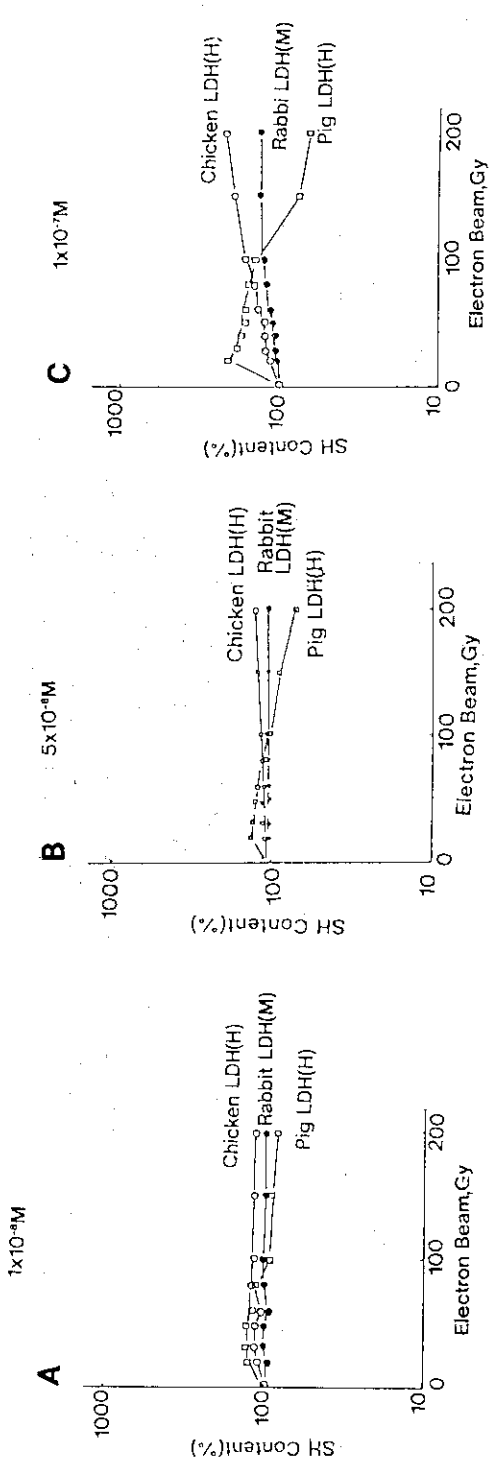


Fig. 3. Effect of electron irradiation on the content of SH group of chicken heart lactate dehydrogenase(○ — ○), pig heart lactate dehydrogenase(□ — □) and rabbit muscle lactate dehydrogenase(● — ●). Enzyme concentration: $1x10^{-8}$M(A), $5x10^{-6}$M(B) and $1x10^{-4}$M(C).

7.13 EPR Study of N^+-ion-induced Free Radical Formation in Antibiotic-producers

XIE LIQING, ZHANG YINFEN and CHEN RUYI
Radiation Beams & Material Engineering Laboratory
Institute of Low Energy Nuclear Physics
(Beijing Radiation Center)
Beijing Normal University
Beijing 100875, P. R. China

GAO JUNCHENG
Division of Ionizing Radiation, National Institute of Metrology
Beijing 100013, P. R. China

ZHANG PEILING and YING HENGFENG
Beijing Second Pharmaceutical Factory
Beijing 100022, P. R. China

ABSTRACT

Under the room temperature , electron paramagnetic resonance (EPR) spectrometer was used to study free radical formation in antibiotic-producers in order to investigate antibiotic-producer mutagenic breeding, which were induced by N^+ ion implanting into antibiotic-producers (e.g., Streptomyces ribosidificus, Streptomyces kanamyceticus and the phage-resistant culture of Streptomyces kanamyceticus). The results show that a lot of free radicals can be induced by N^+ ion implanting into antibiotic-producers, and the yields of the free radicals increase with implanting dose. The death rate of antibiotic-producers rises due to the increase of N^+-ion-induced free radical yields.

KEYWORDS

Ion beam; antibiotic-producer; EPR; strain ; free radical.

INTRODUCTION

Research works on "Potential use of heavy-ion radiation in crop improvement"

* Financial supported by NSFB, China.

showed that high LET heavy particle radiation can be highly mutagenic and can induce some regulatory mutation effectively (Yang and Tobias, 1979). Mutagenic breeding by heavy-ion radiation has been in progress in China (Wu, et al., 1989). The mutagenic breading of antibiotic-producers by means of ion implantation in pharmacy was developed in Beijing Radiation Center (BRC).

Free radicals as accessible and sensitive monitors of primary radiation damage in orange systems have played an indispensable role in the elucidation of damage mechanisms in cells at a molecular level. Quite extensive studies of free radical formation and reactions have been performed in the past under conditions of sparsely ionizing irradiation using the critical cell target DNA and its constituents as the specimen of investigation (Hüttermann and Schaefer, 1989). In order to investigate mutagenic mechanisms in antibiotic-producers, Electron paramagnetic resonance (EPR) spectroscopy as the method of means was used to study free radical formation in antibiotic-producer, which induced by heavy ion implantation. Dose-yield curves were obtained at room temperature. Therefore, the relation among implanting dose and free radical yield as well as death rate of produces was elucidated.

MATERIALS AND METHODS

Sample preparation

The materials studied were three kinds of antibiotic-producers, i.e., Streptomyces ribosidificus, Streptomyces kanamyceticus and the phage-resistant culture of Streptomyces kanamyceticus (Beijing Second Pharmaceutical Factory). Suspended spore solution of three produce strains was dropped on a filter paper, then dried in vacuum and put on an aluminum plate of < 50 mm diameter to be implanted. The size of the dry samples for EPR measurements was a tip of the filter paper with spores of 15mm long and 4mm wide.

Ion implantation

A 400keV ion implantor has been in operation at BRC since 1970. The samples of antibiotic-producer were implanted by N^+ ion beam with the energy of 100keV in the beam vacuum at room temperature, which has passed through a mass analyzer. The implanting dose range was of 1×10^{12}–1×10^{14} N^+/cm^2. The implanting doses were monitored using a beam current integrator with precision of ±1%.

EPR measurements

After one day of N^+ ion implantation, N^+—ion—induced free radicals were measured in dry samples of antibiotic producers at the room temperature using an electron paramagnetic resonance spectrometer (Model JES—FE—1XG, National Institute of Metrology) described elsewhere (Xie et al., 1993).

RESULTS AND DISCUSSION

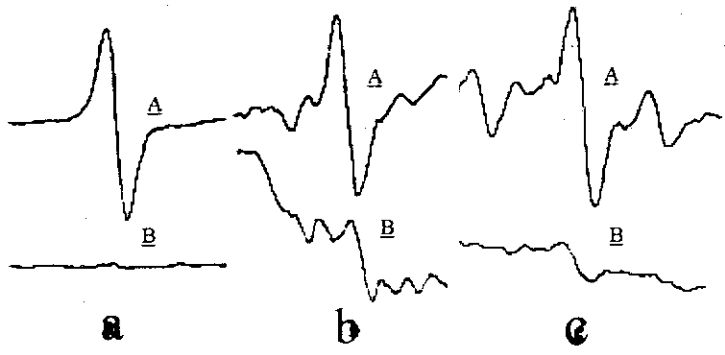


Fig. 1 ESR—spectra A Implanted, B No implanted
a : Streptomyces ribosidificus
b : Streptomyces kanamyceticus
c : the phage resistant culture of Streptomyces kanamyceticus

The corresponding EPR-spectra given in Figure 1 A showed that N^+ ion implantation induced a higher concentration of free radicals and destroyed some features in the produce strains. Figure 1B showed that a few of free radicals in these strains without N^+ ion implantation were much smaller than at N^+ ion implantation. The different EPR spectra of the different strains were observed. The EPR spectrum of ion implanted Streptomyces ribosidificus was characterized by a singlet-like pattern. The EPR spectra of ion implanted Streptomyces kanamyceticus and the phage-resistant culture of Streptomyces kanamyceticus were compound spectra with.

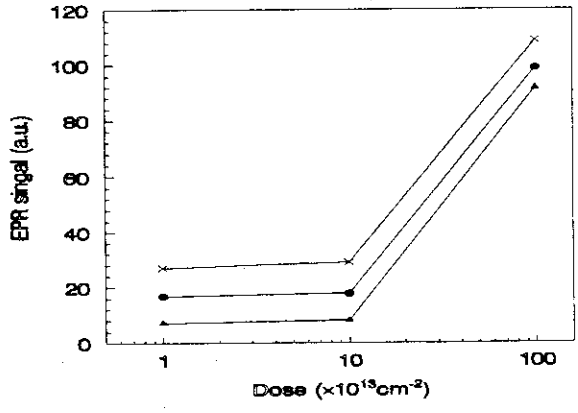


Fig. 2. Dose—free radical yield curve
▲: Streptomyces ribosidificus
•: Streptomyces kanamyceticus
×: the phage—resistant culture of Streptomyces kanamyceticus

central pattern and other outer lines. Results showed that the amount of free radicals induced was directly related to the ion implanting dose. Figure 2. showed the dose-yield curves obtained for there produce strains. The free radical yield increased with the increasing of implanting dose absorbed by these samples.

The death rates of these produce strains with different doses of N^+ ion implanting given in Figure 3. showed that the death rate of strain rose with increasing of implanting dose. Comparing Figure 2. and Figure 3, the death rate of antibiotic-producer strains rose mainly due to the increase of N^+-ion-induced free radical yield.

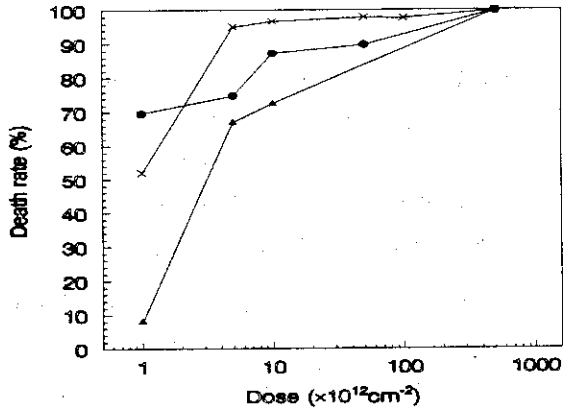


Fig. 3. Dose—death rate curve
▲: Streptomyces ribosidificus
●: Streptomyces kanamyceticus
×: the phage—resistant culture of Streptomyces kanamyceticus

The radiation susceptibility of three antibiotic-producers was different. The radiation resistance of Streptomyces ribosidificus was more than that of two others. Therefore, its death rate also was lower in the case of a similar dose.

CONCLUSIONS

Free radicals can be induced by N^+ ion implanting in antibiotic-produces. At room temperature, EPR spectra measured of implanted produces are complex, e.g., a singlet-like pattern or a composite pattern, mainly because of the different chemical structure of these produces. In fact, most of N^+-ion-induce free radicals were not long lived. Free radicals measured by EPR spectroscopy were long lived. Free radicals produced radiation damage in producers to result in mutation at a specific gene. Therefore, N^+ ion implantation can play a significant role of mutagenesis.

REFERENCE

Hüttermann, J. and A. Schaefer(1989). Heavy-ion-induced free radical formation in Solid DNA-constituents: quantitative and structural aspects Appl. Radiat. Isot. 40, 915-921

Wu , Y., Z. Yu and J. Deng (1989). Chinese J. Agricultural Science of Anhui , 2 , 10

Xie, L., Y. Zhang, J. Dai, T. Lu, R. Chen, H. Yang and J. Gao. (1993) Uses of polymer-alanine film / ESR dosimeters in dosimetry of ionizing radiation. Radiat. Phys. Chem., 42, 837-840

Yang, T. C. and C. A. Tobias (1979). Potential use of heavy-ion radiation in crop improvement. GAMMA-FIELD SYMPOSIA No. 18 'Crop Improvement by Induced Mutation'.

7.14 Adhesion of Yeast Cells on Surface of Polymers Produced by Radiation Polymerization

Zhaoxin Lu, Masaaki Takehisa
(Radia Industry Co. Ltd., Ooyagi 168, Takasaki, Japan 370)
Zongchuan Xie
(Institute of Atomic Energy, Jiangsu Academy of Agiricultural Sciences, Nanjing 210014, China)

ABSTRACT

The adhesion of yeast (Sacharomyces formesences) cells on plymers was studied thermodynamically. The polymers were laminally prepared by means of radiation polymerization.

By measuring contact angles, we calculated dispersion component and polar component of surface free energy of the polymers and the cells, and interfacial free energy between the polymer and the cells. Then interfacial free energy change of the cell adhesion to surface of the polymer was evaluated.

The adhesion behavior of yeast cells on the polymers was observed by optical microscope.

From above results, we conclude that the initial adhesion of the cells is related to the surface free energy of the polymer, but the irreversible adhesion may be close to the polar component in surface free energy. The high polar component is favourable the irreversible adhesion of yeast cells.

KEYWORDS: Adhesion; Yeast cell; Radiation Polymerization; Surface free energy.

INTRODUCTION

A microbial suspension may be interpreted as a living colloidal system and the microorganism adhesion to a carrier is often regared as solid-solid interaction. The physical chemistry of interfaces provides two theoretical frames for describing adhesion of a partical to a surface. The initial step of adhesion can in first approxiation be described by colloid chemical theories such as the DLVO theory, accounting for long-range interactions, point out the importance of electronstatic forces (Rutter and Vincent, 1980; Tadros 1980). The thermodynamic decripation of adhesion process emphasized the role of surface energy and hydrophobicity and accounts thus for short-range force (Busscher et al 1980; Absolom et al 1983).

In our previous work, the filamentous fungi, Trichoderma reesei were immobilized by adhesion onto ionic polymer carrier prepared by radiation polymerization. It was found that the ionic properties of polymer affected markedly adhesion of filamentous cells and the activity of adhered cells, and that the cationic property of polymer promoted the adhesion of the cells, indicated the importance of electrostatic interactions (Lu et al 1994). In present work, we prepared a series of acrylic and methacrylic esters using radiation polymerization technique in order to investigate on adhesion behavior of yeast cells

on the polymer surface and to discuss adhesion of the cells, thermodynamicly.

Materials and Methods

Microorganism and culture Saccharomyces formesensis was used in this work. The yeast cells were precultured under aerobic condition for 48 h at 28℃ in a medium consisting of 1% glucose, 0.1% molasses, 0.5% pepton, 0.3% yeast extract and 0.3% malt extract (pH 4.8). And Yeast cells after 48h of culture were gathered, washed by distilled water and centrifuged three times with 4000 rpm.

Carrier preparation Hydroxyethyl acrylate(HEA), hydroxypropyl methacrylate (HPMA), hydroxyethyl methacrylate(HEMA), and diethyleneglycol dimethacrylate (2G), tetraethyleneglycol dimethacrylate(4G), and nonaethyleneglycol dimethacrylate(9G) were obtained from Shin Nakamura chemicals Co. Ltd. Acrylamide (AM) was puchared from Beijing Dongfeng chemical plant, respectively.

The preparation of polymer piece was performed as following precedure: the monomer adding 10%(v/v) of methanol was poured between the two slide glasses, it was bound, then it was irradiated with 20kGy by γ-rays from Co-60 source at room temperature.

Contact angle measurement The contact angle measurement was carried out using sessile drop technique at 25℃ with bidistilled water and CH_2I_2 (DIM) as wetting agent. The contact angle was read in 3 sec. and measured three times. A series of contact angle (mean value) data on a given surface yields the solid surface energy by a least squre fitting procedure (Busscher et al 1983).

The centrifuged cells were coated on the slide glass as homogenuous and smooth as possible, dried in the room temperature and used for the measurement of contact angle of the cells. The measurement of the contact angel of the cells and the calculation of suface free energy of yeast cells were carried out by the same method as has been described above.

Adhesion test The polymer piece (1×1 cm) was placed horizontally into a flask (100ml), in which a cell- water suspension was poured and settle during 8, 24h. The carrier was then rinsed and lightly washed in the distilled water three times. Immediately, the adhesion state was examined by optical microscope (Olympus, Japan). The adhesion was characterized by a rough quatitative evalution of cell adhesion on the carrier. Four grades was used as grade 0, no adhesion; grade 1, low adhesion; grade 2, medium adhesion; grade 3, good adhesion.

Results and Discussion

Table 1 presented the surface free energy of polymers, dispersion compotnent, polar component, interfacial free energy of the cell adhesion and the test result of the adhesion of yeast cells on surface of the polymers produced by radiation polymerization and photographs show the adhesion behavior of cells on the surface of polymers. The surface free energy of cells was 42.63 erg/cm^2. The surface free energy of the polymers were in 40-60 erg/cm^2, in which the

dispersive component is about 40 erg/cm^2. The result is accordance with Van Pelt's result that γ^d is about 40 erg/cm^2 (an exception being polytetrafluoroethylene) for most materials (Van Pelt et al 1984).

The surface free energy of polymers is following order of decrease: HEA> HEMA> AM> 9G> 4G> 2G> HPMA. The degree of the cells adhered was in the order of HEMA= 9G> AM= HEA= HPMA> 4G> 2G (Table and Figure 1). The result indicates that yeast cells easily adhere on the polymer having high surface free energy. However, according to the thermodynamic approach, the adhesion process is considered as creating a new interface, cell-solid(cs), by disrupture of two preexisting interfaces, cell-liquid(cl) and solid-liquid(sl). This involves thus a molecular contact between the two adhering surface. The tendency of the surfaces to associate is expressed by the free energy change of the process. Adhesion may be expected by

$$\triangle G_{adh} = \gamma_{cs} - \gamma_{cl} - \gamma_{sl}$$

there, γ_{cs}, γ_{cl} and γ_{sl} are the interfacial free energy between cell and polymer, cell and liquid, polymer and liquid, respectively. If$\triangle G_{adh}<0$, the cell adhesion is favorable energetically.

From table 1, it can be seen that all $\triangle G_{adh}$(interfacial free energy change of adhesion) is less than zero, indicating the cell adhesion on these polymers is energetically favorable. But the degree of cell adhesion was not expressed the tendency that the smaller the cell adhesion, the lower ΔG_{adh}. For example, $\triangle G_{adh}$ of poly(2G) was lowest, but adhesion of the cells on this surface was hardly observed over 48h. On surfaces of the polymer having higher ΔG_{adh}, such as poly(HEMA), poly(AM), more cells adhered.

Table 1:interface free energy and the adhesion of yeast cells

polymer	γ	γ^d	γ^p	γ^p/γ^d	Δ_{adh}	grade
HEA	66.52	41.46	25.06	0.60	-16.72	2
AM	58.29	35.35	22.94	0.65	-17.53	2
HEMA	51.54	32.58	18.96	0.58	-20.17	3
9G	57.21	38.58	18.63	0.48	-21.10	3
4G	55.37	39.28	16.09	0.41	-23.25	1
2G	46.46	35.35	11.11	0.31	-27.42	1$^-$
HPMA	40.27	29.79	10.48	0.35	-27.42	2
YEAST	42.63	28.69	13.94	0.49		

γ : surface free energy (erg/cm^2), γ^d: dispersion component , γ^p: polar component, $\triangle_{adh}$: interface free energy of adhesion.

From above result, it was found that the thermodynamic approach may predict the initial adhesion of the cells, energetically, but it may be difficult to predict irreversible adhesion of the cells.

By further analysis, it was discovered that the larger γ^p/γ^d of polymer surface, the more the cells adhered on this surface, suggesting that the polar component in surface free energy of the polymer play an immpotant role in the irreversable adhesion of the cells on the surface. γ^p is related to polar group in molecule, which yield the dipole-dipole interaction and dipole-induced dipole interaction, so that strengthen the initial adhesion of the cells owing to the electrostatic interaction between the cells and the polymer. Another reason is assumed that the polymer having polar groups NH, OH, COOH may be recognized by the cells, whom surface has same polar groups, then induce the secretion of biopolymer to strengthen the initial adhesion and to promote subsequent multiplication. Suzuki has reported that the ion implanted polystyrene (PS) and segmented polyurethane(SPU) lead a dramatic increase in the extent of cell adhesion and spreading of endothelial cells comparing with unimplanted PS and SPU because the ion implantation broke the original chemical bond to form new radicals such as OH, >C=O, SiH and condensed rings (Y. Suzuki 1992).

References

Absolom D. R., Lamberti F. V., Policova Z., Zingg W., Van Oss C. J., and Neumann A. W., (1983) Surface thermodynamics of Bacterial Adhesion, Appl. Environ. Microbial 46:90-97

Busscher H. J., Weekamp A. H., Van Der Mei H. C., Vav Pelt A. W. J., De Jong H. P., and Arends J. (1980) Measurement of the Surfaces Free Energy of Bacterial Cell Surface And Its Relevance for Adhesion, Appl. Envoron. Microbiol., 48:980-983

Busscher H. J., Van Pelt A. W. J., De Jong H. P., and Arends J. (1983) Effect of Spreading Pressure on Surface Free Energy Determinations by Means of Contact Angle Measurement. J. Colloid Interface Science, 95(1):23-27

Lu Z-X and Minoru Kumakura (1994) Characteristics of Filamentous Cells Immobilized with Ionic-Hydrophobic Polymers Prepared by a Radiation Polymerization Method, Process Biochemistry, 29:191-196 (in print)

Rutter, P. R. and Vincent, B. (1980) The adhesion of microorganisms to surface: physico-chemical aspects. In Microbial adhesion to surfaces. Edi. by R. C. W. Berkeley, J. M. Lynck, J. Melling, P. R. Rutter, and B. Vincent. Ellis Horwood, London. pp. 79-91.

Tadros, Th. F. (1980) Particle-surface adhesion. In Microbial adhesion to surfaces. Edi. by R. C. W. Berkeley, J. M. Lynck, J. Melling, P. R. Rutter, and B. Vincent. Ellis Horwood, London. pp. 93-113

van Pelt, A. W. J., H. J. Busscher, M. H. W. J. C. Uyen, A. H. Weerkamp, H.P. de Jong, and J. Arends (1984) Adhesion of S. sanguis to polymers over a broad rang of surface free energy p167-177. In J. M. ten Cate, S. A. Leach, and J. Arends (ed.), Bacterial adhesion and preventive dentistry. IRL Press Ltd., London.

Y. Suzuki et al (1992) Endothelial Cell adhesion to ion implanted polymers Nuclear Instruments and Methods in Physics Reseach B65:142-147

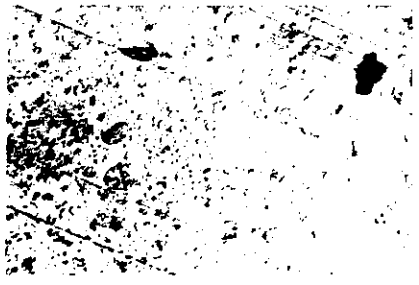
Figure 1: The adhesion of Yeast Cells on Surface of Polymers



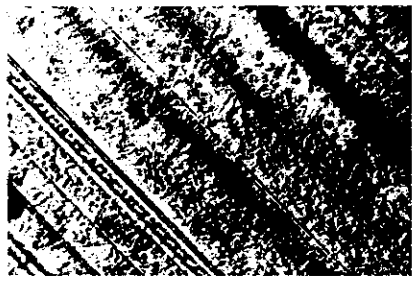
HEA polymer



AM polymer



HEMA polymer



9G polymer



4G polymer



2G polymer



HPMA polymer

8. Polymers (2)

8.1 Enhanced Interfacial Radiation-induced Reaction for Improving the Interfacial Adhesion of Incompatible Polymer Blend PP/BR

Liu Changhai Yang Huili Xu Jun
Changchun Institute of Applied Chemistry, Academic Science
Changchun 130022, People's Republic of China

Abstract γ-radiation induced interfacial changes of incompatible polymer isotactic polypropylene(PP) and cis1,4-polybutadiene(BR) blends containing polyfunctional monomer (PFM) triallyl isocyanurate(TAIC) were investigated. The results of the study are as following: PP is incompatible with BR; TAIC is hardly dissolved in both PP and BR; when blended with PP/BR, the concentration of TAIC in the interfacial region is higher than that in dispersion phase of BR or matrix of PP. The crosslinking and/or grafting of which TAIC occured under radiation in the interfacial region anchored the dispersed BR phase to PP matrix. The interaction between adjacent phases is changed from sole van der Waals force to co-action of both chemical bond and molecular forces. Crosslinking between adjacent phases links the dispersed phase with PP matrix, and grafting in the boundary regions increases the thickness of interface. These result in a good interfacial adhesion between dispersed phase and matrix.

INTRODUCTION

The interfacial condition and adhesion between different polymer phases obviously dominate the properties of polymer blend at some extent. The key of successfully preparing polymer blend is controlling the morphology and phase structure, solving the question of interfacial tension and adhesion between two adjacent phases.

In regard to incompatible polymer blends, the interaction is weak and the stability of phase structure is poor, and the interfacial adhesion is poor too. There is a tendency of phase separation from matrix. The stress cannot be well distributed and transferred between phases. Therefore improving the interfacial adhesion become one of the most important factors for preparing excellent polymer blend. It have been reported that the morphology of polymer blend can be affected by high energy radiation. Besides that each internal phase is influenced, the interfaces of blend are also influenced. Crosslinking and grafting will occur between different polymer blend components in the interfacial region. The former improves the force of adhesion of dispersed phase and matrix, the later increases the thickness of interface. However, for an immiscible or incompatible blend system, the crosslinking and grafting reaction between different components only occur in the interfacial region. Radiation initiate interfacial reaction simultaneously, it also act on each internal phase to initiate various radiation reaction, such as crosslinking, grafting and degradation; and only achieving some certain dose, it produce significant effect on the interface, whereas it may have produced serious effect on the dispersed phase and matrix at the same time

(S.Thomas, et al, 1987), which is unexpected sometimes. It is well known that the behavior of polymer showing at radiation field can be changed by addition of polyfunctional monomer (PFM), to change radiation reaction mechanism and assure crosslinking or grafting reaction being predominate (G. Odian, et al, 1964). At present there is no report on studying enhancement crosslinking and grafting reaction in the interfacial region of incompatible polymer blend to improve interfacial adhesion, and this work is very important for stabilizing morphology of blend, preparing excellent polymer alloy by high energy radiation. Therefore we selected blend of polypropylene(PP) and cis1,4-polybutadiene(BR) as our studying system. Transmission electron microscopy (TEM), scanning electron microscopy (SEM), differential scanning calorimeter (DSC), dynamic viscoelasticity techniques and gel measurement were used to study enhancement radiation induced interfacial reaction in this paper.

EXPERIMENTAL SECTION

The polymers used in this work are PP1330 (Mn 16888, Mw 306639) and BR9000 (cis1,4-polybutadiene, Ni as catalyst). Triallyl isocyanurate (TAIC) is used as PFM. PP, BR and TAIC were mixed at two roll mixer and kneaded at 180 ℃. The milled samples were then press-molded 1mm thickness sheet. The Samples packed with PE film subsequent were subjected to γ radiation at room temperature. Dose rate was 10KGy/hr. The gel fraction was determined by solvent extraction, using xylene as solvent at boiling temperature for 48hrs. The morphology studies involved scanning electron microscopy of fracture surface produced at liquid nitrogen temperature. These surfaces were evaporated onto thin layer of gold. In addition, polymer blends were examined by transmission electron microscopy, the ultrathin sections were stained with O_sO_4. The thermal properties were carried out in DSC-7, with raising temperature rate 10 ℃/min. The properties of dynamic viscoelasticity of blends were measured on DDV-Ⅱ-EA instrument, with raising temperature rate 3℃/min, temperature range -120℃ 200℃, frequency 3.5Hz.

RESULTS AND DISCUSSION

PP is a crystalline polymer, BR is a non-crystalline amorphous polymer. In the blend system consisted with them, PP crystalline phase is incompatible with BR non-crystalline phase and their aggregated state is very different. There is no strong interaction between them, the compatibility of blend system may be predicted bad. Fig.1 is TEM microphotograph of PP/BR blend. Here the black parts are BR particles, the white parts are PP continuous phase. It shows that PP and BR cannot form uniform phase. Fig.2 is SEM microphotograph of PP/BR blend. On the fracture surface the morphology and phase structure are clearly visible. The cavities and holes shown in microphotograph are rubber droplets which have been drawn out. The cavities and holes are more and well distributed, their edge are smooth, no inter-drawing has been

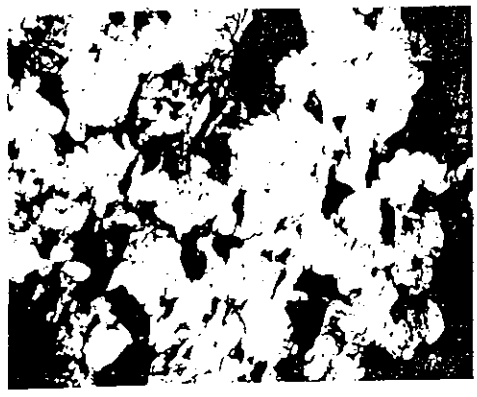


Fig.1 TEM microphotograph of PP/BR blend



Fig.2 Morphology of PP/BR/TAIC (80/20/2)

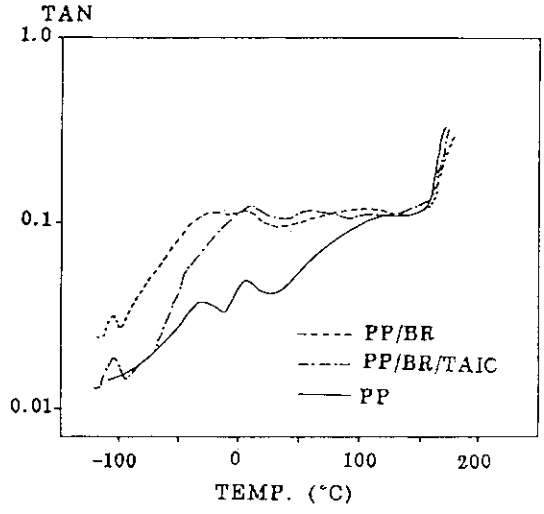


Fig.3 tg δ -T curves of PP/BR blend

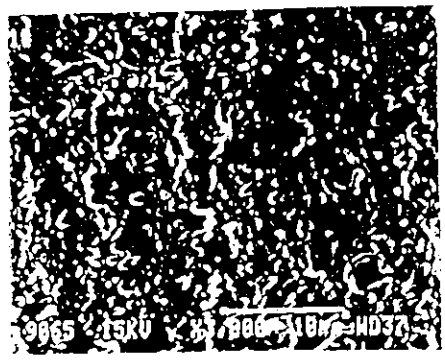


Fig.4 Morphology of PP/BR/TAIC (80/20/2): at 90KGy

found. It indicates that the rubber particles which adhered loosely to PP matrix are easily drawn out of PP matrix when stress fracture happened. We further investigate the compatibility of PP/BR blend by using dynamic viscoelasticity data, as showing in Fig.3. The tgδ-T curves of blend have three separate peaks, each of them is in correspondence to the tgδ peaks of PP and BR respectively. The Tg of PP in blend is basically in agreement with that in pure PP. These also illustrates the compatibility of PP/BR being bad.

We also study the compatibility of PFM TAIC blending with PP/BR system. We have found that TAIC would migrate, blooming (or"sweating") from the blends when blended with PP or BR. This demonstrates that the compatibility of TAIC with polymer PP or BR is poor. In addition, according to the solubility parameters, the compatibility of TAIC with polymer can be estimated. The δ of PP, BR and TAIC are 16.6, 17.8 and 22.0 respectively. There are larger differences between TAIC and PP or BR. TAIC has poor compatibility with them. According to Helfand and Tagami (1972), there is a lower density in incompatible blend interfacial region. So TAIC would migrate from dispersed phases and

matrix to the interface and surface when TAIC was blended with PP/BR, which induced higher concentration of TAIC in the interfacial region. So the crosslinking and grafting reaction would be enhanced in the incompatible interfacial regions when irradiated.

Fig.4 is SEM microphotograph of PP/BR/TAIC blend irradiated at 90KGy. The cavities and holes are dramatically less than that in Fig.2. The sum of BR particles being drawn out decrease, interface between BR phase and PP matrix is ambiguous (or"obscure"), BR phase and PP matrix are difficult to be distinguished. The case of one phase affected another can be seen in the fracture surface.

The changes of melting temperature of PP/BR/TAIC blend system irradiated at various dose are investigated, as showing in Fig.5. The main melting peak and sub-melting peak decrease 4.4K and 5.7K respectively when irradiated at 50KGy dose. At common case the damage of crystal by radiation is low at 50KGy dose. It shows that the PP crystalline phase is linked with amorphous BR phase by radiation induced interface reaction, which increases the interfacial adhesion and the interfacial thickness. Non-crystalline segments act on crystalline segments induced Tm decreasing.

Fig.6 is tgδ curves of PP/BR/TAIC blend irradiated at various dose. The peak of tgδ of BR move toward high temperature range with 40KGy dose irradiated, the original peaks of tgδ of PP move toward low temperature range, the gel of blend at this time is low, approximately 3 percent, the crosslinking degree is very limited, the adhesion between two phases is improved. At 90KGy dose, a new tgδ peak appear, the original peaks of tgδ of PP and BR disappear, the gel content of blend at this time is about 18 percent. PP and BR partly form crosslinking network. BR particles are anchored to PP matrix; the

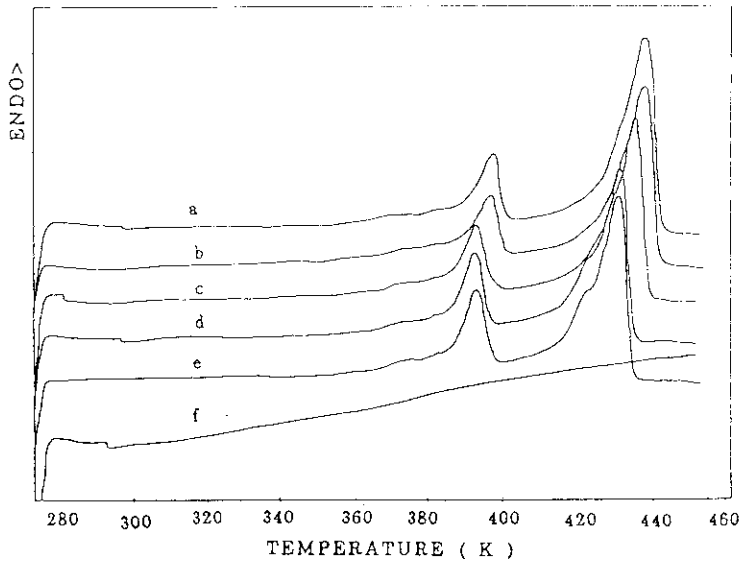


Fig.5 DSC curves of PP/BR blends a: PP b: PP/BR/TAIC, 0KGy
c: PP/BR/TAIC, 50KGy d: PP/BR/TAIC, 100KGy
e: PP/BR/TAIC, 150KGy f: BR

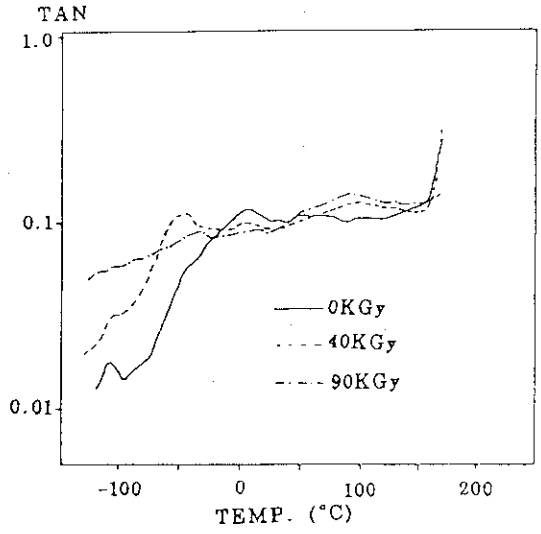


Fig.6 tg δ -T curves of PP/BR/TAIC blend: effect of radiation

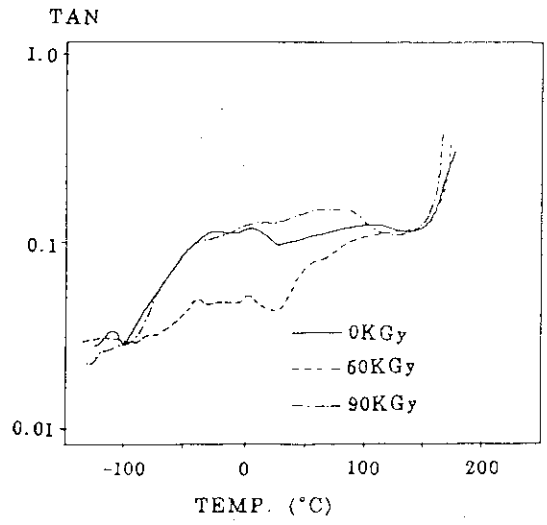


Fig.7 tg δ -T curves of PP/BR blend: effect of radiation

adjacent phases are linked by chemical bond and thick interface; the interfacial adhesion of blend is greatly improved. Nevertheless for PP/BR blend without TAIC, irradiation produce more effect on peak of tg δ of BR and less on PP tg δ peaks, as showing in Fig.7. It demonstrates that the radiation induced BR phase crosslinking but hardly affected on PP matrix, the degree of interface reaction is weakness.

CONCLUSIONS

PP/BR is incompatible blend system. TAIC is also incompatible with PP and BR. The distributing concentration of TAIC in blend is higher in interfacial region than that in BR phase and PP matrix. Crosslinking and grafting which is produced by TAIC when irradiated link the adjacent phases and increase the thickness of interface in the interfacial regions. Enhancement radiation-induced interfacial reaction is available to improve the interfacial adhesion of incompatible polymer blend.

REFERENCES

Helfand,E. and Tagami,Y. J. Chem. Phys. 1972, 56,3592
Odian,G. and Bernstein,B.R. J. Polym. Sci. part A, 1964, 2, 2835
Thomas,S., Gupta,B.R. et al, Polym. Degrad. Stab. 1987, 18, 189

8.2 *Morphology and Properties of Polyurethane/poly(ST) or Poly(MMA) Interpenetrating Polymer Networks by Co60 γ-ray

ZHI-PING ZHANG , GENG-CHAO WANG , SHENG-KANG YING

Institute of Material Science and Engineering,East China University of Science and technology,shanghai 200237,P.R.China

Introduction

Interpenetrating polymer networks,IPN's,ideally are a mixture of two or more cross-linked polymers which are dispersed or mixed in the segmental level. In general,due to the low entropy of mixing segmentally dispersed networks is difficult.

We were able to increase further the degree of interpenetration in the incompatible polyurethane-poly(methylmethacrylate) IPN's by applying Co^{60}-r radiation polymerization. No articles have been published concerning the synthesized PU/PMMA IPN's by Co^{60}-r radiation. By use of the simultaneous polymerization process under radiation a transparent, nearly segmentally dispersed mixture of the IPN could by obtained.

Herein a study of IPN's prepared under radiation by small-angle X-ray scattering,SAXS,and transmission electron microsocopy TEM micrographs showed that radiation initiated Polymerization was an effective way to obtain PU/PMMA IPN with high extent of interpenetration. The IPN's with two continuous phase structure were obtained. The observation of a SAXS maximum clearly demonstrates that phase separation is occurring via a spinodal mechanism.The ability of interpenetration increased with increasing the content of the crosslinking agents.The glass transition temperature at high temperature range shifted inwardly due to interpenetration. While the enhanced radiation dose reduce the spatial extent of phase separation, increasing the crosslink density of the component further reduces the size scale of the phase separation and the fracture stress increased. Furthermore,the ultimate elongation of the IPN's containing more than 50% PU(by wt) would be greater than that of the pure PU.

@ This work was supported by the national natural science foundation of China.

Experimental

Materials

Hydroxyl-Terminated polybutadiene(HTPB)
Mn=3067 OH No:=38.1 Fn=2.48
Diisocynamate Toluene(TDI) Stannous Octoate(OcSn)
Divinyl benzene(DVB) Azobisisobutyrontrile(AIBN)
Poly(propylene oxide), endcapped with ethylene Oxide(PPo-Eo)
Mn=3100, Fn=3.05
Trimehtylel propane (TMP) Methyl mthacrylate(MMA)
Trimethlyol-1 1,1- propane trimethacrylate(TMPTMA)

Synthnesis:

Precisely weighted amount of various reagents were mixed thoroughly by ultrasonic wave. The mixtrue was cast into a mold made by two glassplates, sealed with rubber, and polymerized by Co^{60}-r radiation at appropriate radiation dose and dose rate,and then putin a oven at 100℃ for 4 h.

Results and Discussion

1. The Morphology of IPN's

The transmission electron micrographs of PU(HTPB)/P(st) and PU(HTPB)/PMMA-IPN. are shown in Fig.1. The PU phase is stained by Osnnium tetroxide and appears black. The unstained Ps, PMMA,phase appears white in the Micrographs.

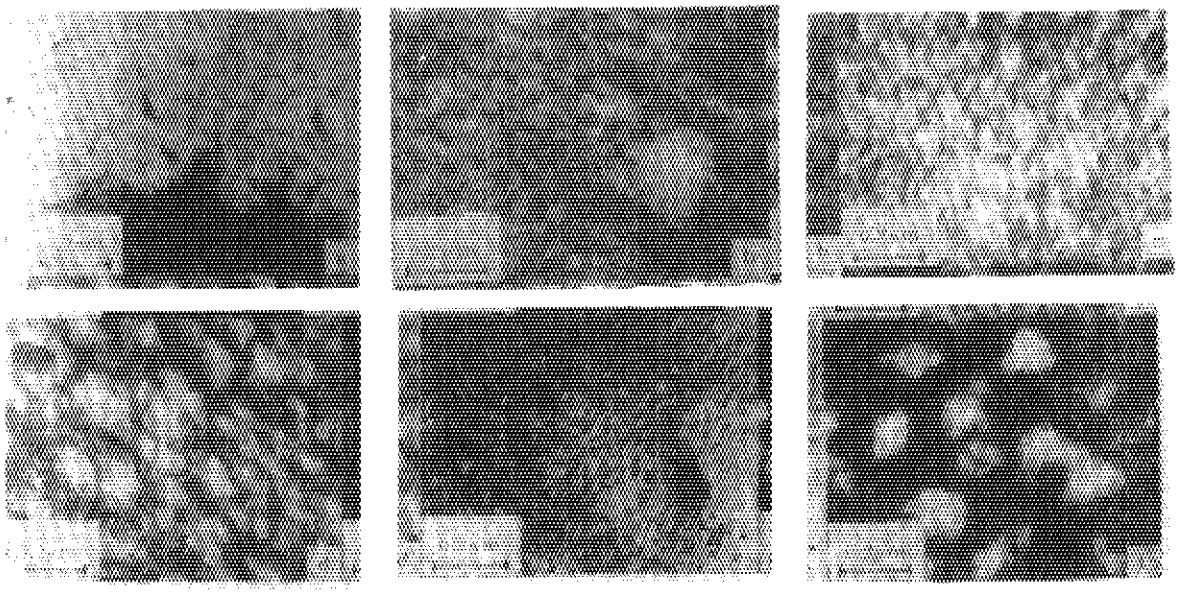


Figure 1 Morpology of PU(HTPB)/PSt IPNs

(a) PU(HTPB)/PSt=10/90, NCO/OH=1.5, DVB/St=2/100; (b) PU(HTPB)/PSt=25/75, NCO/OH=1.5, DVB/St=2/100; (c) PU(HTPB)/PSt=50/50, NCO/OH=1.5, DVB/St=2/100; (d) PU(HTPB)/PSt=50/50, NCO/OH=1.5, DVB/St=0/100; (e) PU(HTPB)/PSt=50/50, NCO/OH=1.8, DVB/St=2/100; (f) PU(HTPB)/PSt=50/50, NCO/OH=1.5, TRIM/MMA=2/100.

The morphology of PU(HTPB)/P(st)-IPN at 10/90 composition ratio. P(st) is the continuous phase. The distribution of domain ofwide ranges from 40 to 600 nm. the phase inversion ofthe system appears about the concentration of 25% PU(HTPB).The compatibility between two polymers is enhanced at 50/50,its sizes of domain is smaller(about 40nm).

The domain sizes of P(st) gradually decrease with increasing DVB content.It showes that increasing crosslinking degree of P(st) phase could enhance interpenetration of two phases and compatibility between two polymers. Increasing NCO/OH ratio could depress.The dispersed phase domain size of PU(HTPB)/P(st)-IPN.The domain size is about 10nm-20nm.It has more compatible structure, and depends on the reaction kinetics of each component.

Fig.2. showed the electron micrographs for IPN's with the different PU/PMMA rations. For IPN with the PU/PMMA ratio less than 40/60, the PMMA phase is continuous , while the PU phase is dispersed (see Fig. 2a)and the domain size is about 30nm. when the PU/PMMA ratio range is between 40/60 and 70/30.The IPN sample showed two continuous phase structure(see Fig.2b,2c,2d).The fact of the indistinguishable interface reflected that the extent of interpenetrationis maximum at the PU/PMMA ratio 50/50.

The extent of interpenetration increase with increasing the TMPTMA and TMP content (Fig.3).

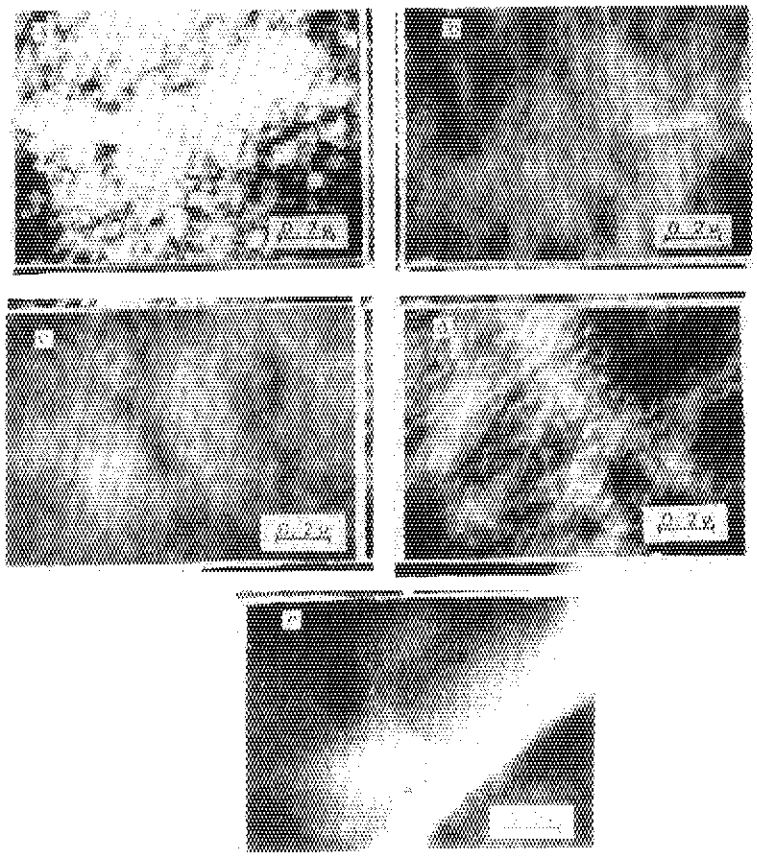


Figure 2 TEM micrographs for IPNs with the PU/PMMA ratio (by wt) of: (a) 25/75; (b) 40/60; (c) 50/50; (d) 70/30; (e) 75/25.

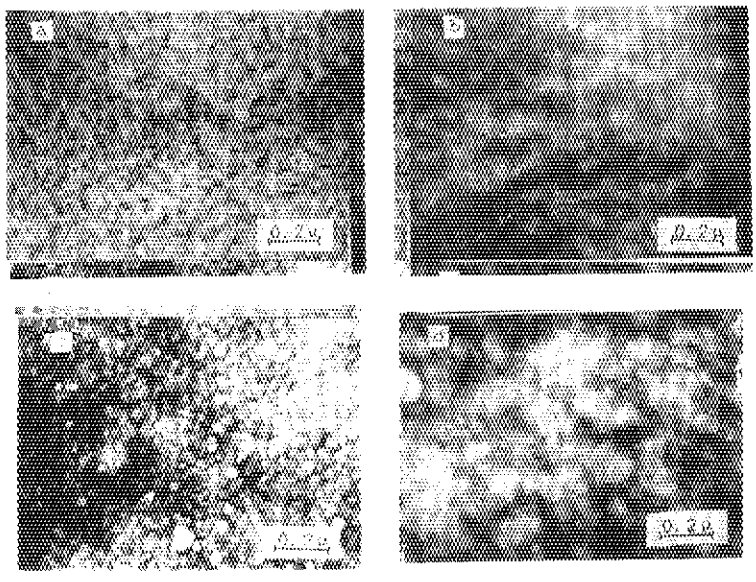


Figure 3 TEM micrographs for IPNs with different contents of TMPTMAor TMP:
(a)TMP/(Polyether +TDI) = 5/100, TMPTMA/MMA = 3/100; (b) TMP/(Polyether + TDI) = 1/100, TMPTMA/MAA = 3/100; (c) TMP/(Polyether + TDI) = 3/100, TMPTMA/ MMA = 5/100; (d) TMP/(Polyether + TDI) = 3/100, TMPTMA/MMA = 1/100.

The two continuous phase structure of IPNs, prepared by two incompatible polymers, is difficult to attain. By the control of Radiation dose, dose rate and reaction temperature during the radiation process, the formation rates of PU and PMMA could be kept almost the same, and the two networks could be formed simultaneously. Thus, in proper composition range, the IPN with two continuous phase structure could be prepared.

Small-angle X-Ray scattering SAXS results for IPN's investigated is this study are shown in table(1-3).

Table I Fraction of Hydrogen Bond, Thickness of the Transition Layer Range & Mechanical Properties for IPN [PU/P (St-An) = 40/30 — 30] in Different Synthesized Method

Synthesized ,method	$(X_b)_{c=0}$	σ/Å	τ/MPa	ε/%
Radiation	0.259	37.4	21.4	83.4
Initiator	0.276	29.2	18.6	78.5

σ: Thickness of the Transition layer range; τ: Fracture Stress; ε: Ultimate Elongation.

Table II Fraction of Hydrogen Bond, Thickness of the Transition Layer Range & Mechanical Properties for IPNs with Different PU/P (St-An) Ratio (by W.)

PU/ P(St-An)	$(X_b)_{c=0}$	σ/Å	τ/MPa	ε/%
20/40-40	0.289	28.3	27.4	21.2
40/30-30	0.259	37.4	21.4	83.4
60/20-20	0.300	25.2	18.3	248.2
100/0-0	0.455		8.5	201.5

σ: Thickness of the Transition layer range; τ: Fracture Stress; ε: Ultimate Elongation

Table III Fraction of Hydrogen Bond, Thickness of the Transition Layer Range & Mechanical Properties for IPNs with Different content of Acrylonitrile

PU/ P(St-An)	$(X_b)_{c=0}$	σ/Å	τ/MPa	ε/%
40/60-0	0.365	16.2	19.2	108.5
40/45-15	0.301	27.3	20.3	94.2
40/30-30	0.259	37.4	21.4	83.4
40/15-45	0.234	41.6	23.6	75.1

σ: Thickness of the Transition layer range; τ: Fracture Stress; ε: Ultimate Elongation

It was expected that the transition zone width would be much large since any factors that would compatibilte components would also produce an increase in the interfacial widths. This was found the transition layer Range for IPN in radiation polymerization larger than initialor.It is important to note that the size scale of the phase seperation isquite small, the PU phase domain size decreases as the intermixing increase. Infact the fraction of banded hydron bond is large, thickness of the transition layer range small, coarsening of the phase must have occurred so as to reduce the width of interface, the data suggest that radiation polymerization tends to promote compatibility. Conseguently,a coarsing of the domains has not occured and the phase separation has been arrested. The abservation of a scattering maximum clearly demontstrates that phase separation is occurring via a spinodal mechanism.

2. Glass Trasition of IPNS

The glass transition temperatures (Tgs) of PU/PMMA IPNs are listed in Table 4. The Tgs in low temperature range (Tg1), relating to the soft segment of PU network, are almost the same.This is because interpenetraion of PU and PMMA, which is actually the interpenetration of PMMA and the hard segment of PU as PU network was produced from the crosslinking of the hard segment,have little influence on the soft segment of PU. Only one glass transition in the high temperature range (Tg2) appeared; it was located between the Tg ofpure PMMA (401 K) and the Tg of hard segment in pure (378 K). In other words, the Tg2 shifted inwardly. This suggested that he high extent of interpenetraion could be obtained by means of radiation.

3. Mechanical Properties of IPNs

The stress-strain curves of different components of PU/PMMA IPNs are shown in Figure 4 .The fracture stress and ultimate elongation of PU/PMMA IPNs are listed in Table 4 .From Table 4 it can be seen that with increasing PU content in the system the ultimate elongation increased while the fracture stress decreased; the fracture stress,however was still higher than of pure PU . Furthermore, the ultimate elongation of the IPNs with appropriate composition could be higher than that of pure PU. This was due to the synergistic behavior of interpenetrating networks. The function of PMMA in the IPNs was the reinforcement on PU elastomers.

Table Ⅳ The Glass Transition Temperatures and Mechanical Properties for IPNs of Different PU/PMMA Ratio (by Wt)

PU/PMMA	T_g1 (K)	T_g2 (K)	Fracture Stress (MPa)	Ultimate Elongation (%)
0/100	—	401	58.2	3.0
25/75	226	395	28.7	33.5
40/60	227	389	24.1	94.5
50/50	228	386	22.8	213.4
75/25	228	392	15.4	308.4
100/0	227	378*	8.5	201.5

* The T_g of hard segment of pure PU is 378K.

Table Ⅴ Effect of TMPTMA and TMP Content on Mechanical Properties of IPNs with PU/PMMA = 50/50

Contents of Crosslinker		Fracture Stress (MPa)	Ultimate Elongation (%)
TMP/(Polyether + TDI)	TMPTMA/MMA		
3/100	1/100	21.4	221.6
3/100	3/100	22.8	213.4
3/100	5/100	24.1	199.1
1/100	3/100	18.7	294.2
5/100	3/100	24.5	191.3

The reinforcement through interpenetration is generally better than filler reinforcement.Filler reinforcement effect was produced by physical crosslinking among polymer chains, which resulted from surface absorption of filler particles on polymer chains. The filler reinforcement could disperse stress originally concentratedon one macromolecular chain to other chains. The reinforcement of IPNs was produced by the interlocking of dual crosslinking networks in IPNs system. The combining force of interlocking is much greater than the surface absorption force.The concentrated stress can be converged to macromolecular chains homogenously through interlocking networks.Even if there are cracks somewhere, IPNs can limit the enlargement of cracks through interlocking networks. This induces the fracture strss of PU/PMMA IPNs higher than that of pure PU and the ultimate elongation ofIPNs at proper composition greater than that of pure PU.

The data of mechanical properties for IPNs with different content of TMPTMA and TMP is listed in Table(4-5). The fracture stress for IPNs increased , but the ultimate elongation decreased with increasing the content of the crosslinking agents (TMPTMA and TMP). With increasing the content of the crosslinging agents,the crosslinking extent increased and the entanglement of the networks also increased.so the slipping among macromolecular chains can be prevented. Thus the rigidity and fracture stress of INPs were enhanced while ultimate elongation decreased.

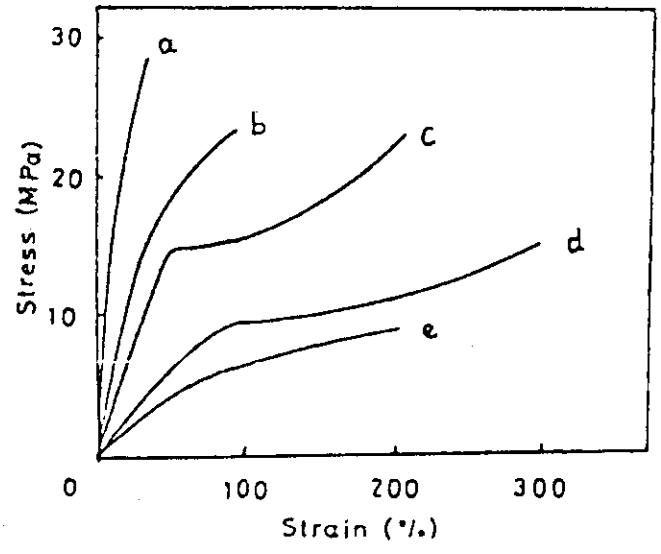


Figure 4 Stress vs. strain for IPNs with the PU/PMMA ratio (by wt) of : (a) 25/75; (b) 40/60; (c) 50/50 ; (d) 75/25; (e) 100/0.

CONCLUSION

The morphology, glass transition behavior, and mechanical properties of PU/PMMA IPNs synthesized by radiation, have been studied.TEM micrographs showed that radiation initiated polymerization was a effective way to obtain PU/PMMA IPN with high extent of interpeneration. The IPNs with two continuous phase structure were obtained in the PU/PMMA ratio range of 40/60 to 70/30 . The ability of interpenetration increased with increasing the content of the croslinking agents. The glass transition tempeature at high temperature range shifted inwardly due to interpenetration. With increasing PU content in the system, the fracture stress decreased andthe ultimate elongation increased.Furthermore, the ultimate elongation of the IPNs containing more than50% PU (by wt) would be greater than that of the pure PU. With increasing the content of the crosslinking agents (TMPTMA and TMP), the fracture stress increased while the ultimate elongation decreased.

It has been shown by a combination of FTIR and small-angle x-ray scattering that the synthesis of IPNS under Radiation can yield relatively homogeneous dispersions of two incompatible polymers.The extent of mixing of the components can be enhanced and the size scale of heterogeneities in the system can be reduced by the application of radiation during the systhesis.

REFERENCES

1. E.F.Cassidy, H.X.Xiao, K.C.Frisch, and H.L.Frisch, Polym.Chem.Ed., 22, 1839(1984).
2. K.C.Frisch, D.Klempner, and T.Antczak, J.Appl.Polym.Sci., 18,683 (1974).
3. G.M.Jordhamo,J.A.Manson, and l.H.Sperling, Polym. Eng.Sci., 26,517 (1986).
4. T.J,Hsu and T.Lee, Polym. Composition, 25, 951 (1990).
5. T.Pascal, R.Mercier, and b.Sillion, Polymer, 31 ,78, (1990).
6. D.S.Lee and S.C.Kim, Macromolecules, 18, 2173 (1985).
7. B.S.Kim, D.S.Lee, and S.C.Kim, Macromolecules, 19, 2589 (1986).
8. T.P.Russell and D.S.Lee, Macromolecules, 26, 1929 (1993).

8.3 Radiation Crosslinking Film

WU XIAN RADIATION PRODUCTS FACTORY. SUZHOU. CHINA

After irradiation by electron beam the linear molecular chain becomes network polymer so that the thermal mechanical properties are improved. Mechanism, chemical and physical changes of crosslinking and the factors which have an effect to crosslinking are reported (1,2). Four kinds of crosslinking polyethylene film which possess better thermo-contractibility, thermal resistance and insulating property and are proper to be used in cable work, production of cables, transformers and adhesive tapes have been developed by technique of irradiation with industral accelerator in our factory. Irradiation performed in the air at room temprature has the advantage of high effeciency and quick process. For continuous irradiation processing there is no necessity to stop operation for change roles of film so that it has the advantage of time saving, decreasing material which does not accept enough irradiation dose and preventing unfavorable effect on the accelerator caused by stopping operation. The technique charateristics of the crosslinking polyethylene film and the procedure undertaken in production also have been reported in this paper.

I. Procedure of manufacture

The technique procedure is a contribution of plastic processing and irradiation technology. The procedure is as follows:

material selecting-casting-irradiation-thermal pulling-cutting-test-packaging

Selection of material: when material is selected the properties of the products e.g. intensity degree of branching and feasibility have been considered.

Casting:Blowing, flowing and rolling technique has been applied in the casting of plastic according to requirement. In casting proper thickness should be considered for the film becomes thin during the process of stretching.

Stretching: Stretching can be achieved by heating with oil or far infra radiation. The ratio of stretching can be adjusted.

Cutting: The film can be cut by cutter according to the special specification.

II. Electron beam irradiation

1. Advantage

Electron beam irradiation builds on the principle of turning electric energy into electron beam with high energy and carrying irradiation in the air that has advantage of carrying out irradiation with high speed and efficiency, controlling the crosslink degree with dose and monitoring the crosslinking process with instruments.

2. Determination of electron beam parameters

In order to carry out irradiation in a proper way determination of beam

current, energy, scan distribution and penitration depth must be performed. The results of determination for our accelerator are as follows:
length of scan: 100cm, deviation of distribution 12%, the penitration depth at the 0.5 MeV accelerator valtage after operation: 0.176g/cm^2. This indicates that energy to the film is 0.4 MeV after electron passes titanium window and air layer. Calculation from these data shows that the best thickness for single face irradiation is 1.24mm(o.114g/cm^2) and double face irradiation is 2.92mm(0.268g/cm^2)

3. Product handling systems:

Because there are a lot of faults for interrupted irradiation a double face successive irradiation is applied. When the workshop was designed an access window has been laid out to allow the film to be rolled and unrolled on the same handling equipment. The whole system is consisted of stainless steel irradiation roller, guide roller and rolled and unrolled equipment (fig. 1). After several times of refraction the radiation coming out of the window becomes very weak so that people with simple radiation protection lay-out can work at the equipment.

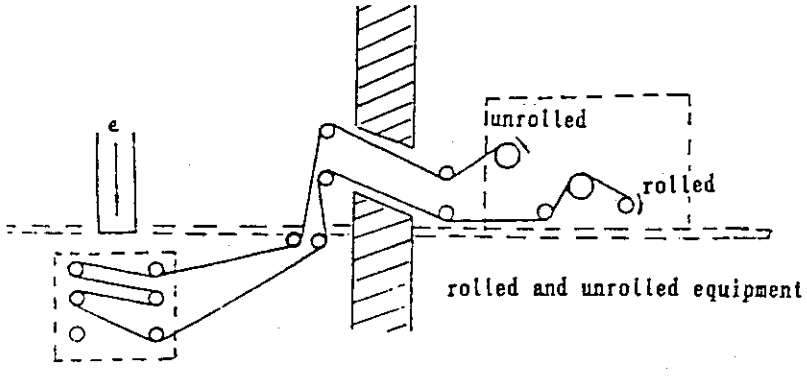


fig.1 successive irradiation system

4. Dose

When the best irradiation thickness is applied the average absorbed dose is given by:

$$D = \frac{1.3\ I\ E\ n\ 10^6}{bVR}$$

D is absorbed dose

I is irradiation beam current, mA

E is energy of incident electrons, MeV

N are layers of film

b is scan length, cm

R is distance of electron emission, g/cm^2

V is rolling speed cm/s

In general speaking the most of them are constant for operation. Only parameter which need to be controlled to change dose is V.

5. Technique specifications for process of crosslinking

The Specification of handling system consisted of electron accelerator and successive irradiation equipment are shown in the table 1.

Table 1. radiation crosslinking line specification

radiotion to film	Technical charateristics energy 0.4 Mev beam current 11mA		
Penitration depth	R=0.176g/cm^2	R_e=0.604x10^{23}e/cm^2	Rh=1.91mm
The best irradiation depth for single face irradiation	d=0.114g/cm^2	d_e0.392x10^{23}e/cm^2	d_h=1.24mm
The best depth for double face irradiation	d=0.268g/cm^2	d_e=0.92x10^{23}e/cm^2	d_h=2.92mm
Scan	The largest length of scan is 100cm unstability 12%		
Irradiation device	The largest length of successive irradiation is 100cm. Speed can be adjusted		

The thickness of irradiation film mm	0.1x2	0.2x2	0.4	0.6	0.8
width 100cm , weight kg/m^2	0.184	0.368	0.368	0.552	0.736
Linear valocity M/min	4	4	4	24	2.4
Dose 10^5GY	1.95	1.95	1.95	1.63	1.63
Percentage of gel formation %	65	65	65	60	60
Weight of irradiated material/hr Kg	44	88	88	79.5	106
Weight of irradiated material/15hr Kg	660	1320	1320	1190	1590

III. Charcteristics of irradiated pothylene film

Presented in table 2 the properties of crosslinked polyethylene produced in our factory. These products meet various requirements and will be developed to be serious products. In order to give the assurance to the quality of the product measure for quality control must be taken.

Table 2. Characteristics of crosslinked polyethylene

	RCF-1	RCF-2	RCF-3	RCF-4
application	cable work	cable production	transformer insulation	adhesive tape
thickness mm	0.08-0.2	0.05-0.20	0.10-0.12	0.25-1.00
length mm	25,50,80 250,300	5,8,10,15 20,25,960	10,20,104 180,230	460,960
diameter of the role mm	60,80,100 150	the largest role	the largest role	the largest role
gel fraction %	50-70	50-70	55-70	55-70
longitutional contraction rate %	20-40	20-40	20-40	20-60
tensile strangth longitutional transverse Mpa	18	20	20	18
vertical tensile strength longitutional/transverse N/cm	400	400	400	400
elongation at break %	300	300	300	300
volume resistivity Ω-cm	$1x10^{14}$	$1x10^{14}$	$1x10^{14}$	$1x10^{14}$
dielectric strangth KV/mm	100	100	100	30
dielectric loss angular tengent mHZ	$1x10^{-3}$	$1x10^{-3}$	$1x10^{-3}$	$5x10^{-3}$
rate of water absorption %	0.1	0.1	0.1	0.1

After maintenance and replacement of filament of electron gun energy and scan distribution must be measured. The standards of products and the strictly controled process of production and tests have been worked out. Gel fraction, thermal contraction rate and technique specifications of products must be determined before shipping. Transverse and longitutional distribution of gel fraction are often determined.

References:

1. Sun Jia Zhen, Radiation Chemistry of Crosslinking, Editted by Changchun Institute of Application Chemistry, Chinese Academy of Science
2. Ma Rui De, Radiation Processing Technique
3. Cheek, C. H, Linnenbam, V. J, Calculation of Absorbed Dose, NRL Rent. 5448 (1960)

8.4 Low Temperature Gamma-ray Irradiation Effects on Polymer Materials

H.Kudoh, N.Kasai, T.Sasuga and T.Seguchi

Takasaki Radiation Chemistry Research Establishment,
Japan Atomic Energy Research Institute
Takasaki, Gunma, 370-12, Japan

Abstract The gamma radiation induced degradation of glass fiber reinforced plastic (GFRP) and polymethylmetacrylate (PMMA) at 77K was examined by flexural test and gas analysis after irradiation and compared by the irradiation at room temperature. The decrease in flexural strength at break was much less at 77K than at RT. The evolution of CH_4, CO and CO_2 was also depressed at 77K. The temperature dependence of the degradation closely relates to the local molecular motion of matrix resin during irradiation. Polytetrafluoroethylene (PTFE) was also studied by irradiation at RT, 77K and 4K in terms of tensile elongation and molecular weight. The degradation was much less at 77K and 4K than at RT, and the same between 77K and 4K.

INTRODUCTION

Polymer and organic composite materials are planned to be used as the insulators for super conducting magnet in a fusion reactor. The radiation resistance of the materials must be evaluated at cryogenic environment. On this view point, low temperature gamma rays irradiation effects on glass fiber reinforced plastic(GFRP), polymethylmetacrylate(PMMA) and polytetrafluoroethylene(PTFE) were studied on mechanical properties, molecular weight and gas evolution, and compared with those by irradiation at room temperature(RT).

EXPERIMENTAL

Materials used in this work are bis-phenol A type epoxy resin GFRP of 2mm thick specimen (6mm width, 70mm length), PMMA of 3mm thick and PTFE of 0.1mm thick. They were irradiated by Co-60 gamma rays at 77K in liquid nitrogen and RT in nitrogen gas atmosphere at a dose rate of 30kGy/h at 77K and 10kGy/h at RT. PTFE was irradiated also at 4K. The irradiation at 77K and 4K was carried out using a low temperature irradiation equipment installed at JAERI Takasaki (Kasai et al., 1990, Kudoh et al., 1994). The mechanical properties were tested by three point flexural strength measurement at 77K for GFRP and PMMA with span length 50mm and crosshead speed 2mm/min and by tensile tests for PTFE at RT with a dumbell shaped specimens and crosshead speed 200mm/min.

Samples of GFRP and PMMA for gas analysis was irradiated in an evacuated glass ampule. Decomposed gas accumulated in the tube was analyzed by gas chromatography (GC) at RT.

RESULTS and DISCUSSION

1. Mechanical properties

Figure 1 shows the change in flexural strength of GFRP measured at 77K as a function of dose. Flexural strength at break of GFRP decreased with dose and reached the half of the original strength at 25MGy for 77K irradiation and 1MGy for RT (Kudoh et al., 1994). For specimens irradiated and measured at 77K, the strength scarcely changed by the annealing at room te,mperature after irradiation. These facts indicate that the radiation induced reactions is extremely depressed at 77K and almost completes during irradiation.

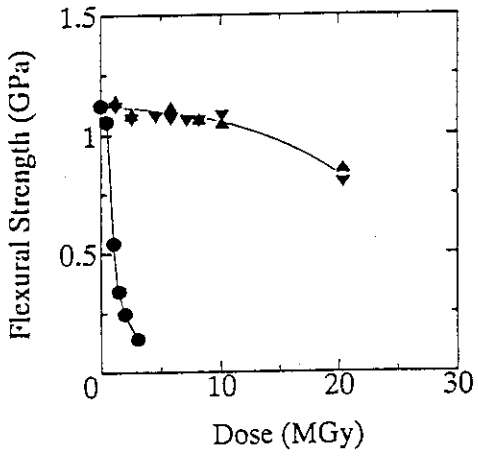


Fig.1 Flexural strength of GFRP at 77K irrad. at RT(●),irrad. at 77K and measured at 77K without warming(▲),irrad. at 77K and measured at 77K after annealing(▼)

Figures 2 and 3 show the change in flexural strength of PMMA measured at 77K and elongation at break of PTFE measured at RT as a function of dose, respectively (Kudoh et al., 1994). In both cases large difference by irradiation temperature is observed; the degradation by 77K irradiation is much less than that by RT irradiation. Moreover, the degradation by 4K irradiation is the same with that by 77K irrdiation for PTFE.

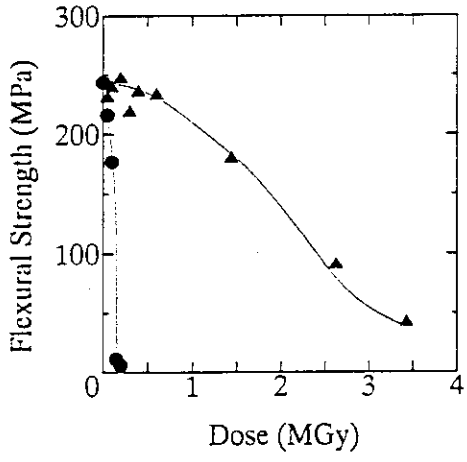


Fig.2 Flexural strength of PMMA measured at 77K irrad. at RT(●),77K(▲)

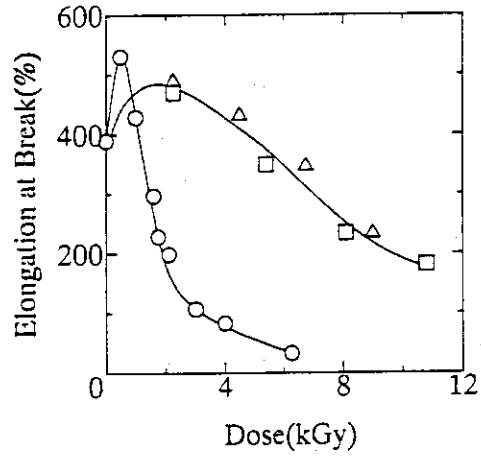


Fig.3 Elongation at break of PTFE measured at RT irrad. at RT(○),77K(△),4K(□)

The degradation of GFRP is mainly attributed to destruction of matrix resin. Figure 4 shows the change in glass transition temperature (Tg) of GFRP determind by DSC. Tg of GFRP corresponds to that of epoxy resin and decreases with dose indicating the destruction of network structure of epoxy resin with chain scission. The bahavior of Tg to the dose is the same with flexural strength; the degradation by 77K irradiation is much less than that by RT irradiation, which means the less probability of the chain scission at 77K.

Figures 5 and 6 shows the number average molecular weight of PMMA measured by gel peemeation chromatograophy (GPC), and that of PTFE determined by the heat of recrystallization measured by DSC (Suwa et al., 1973), respectively. Molecular weight decreased with dose indicating that the chain scission occured. The scission probability is less at 77K than at RT for both of PMMA and PTFE. Especially for PTFE, the probability is the same between 77K and 4K.

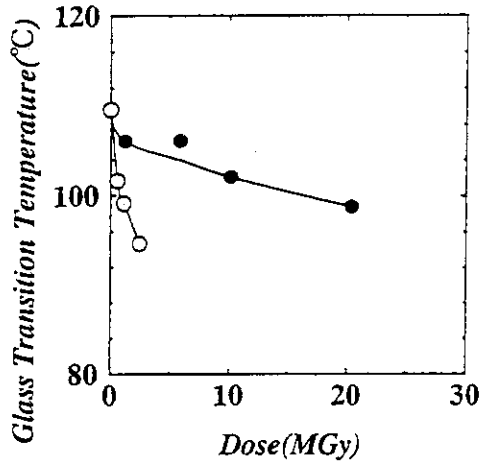


Fig.4 Glass transition temperature of GFRP irrad. at RT(○),77K(●)

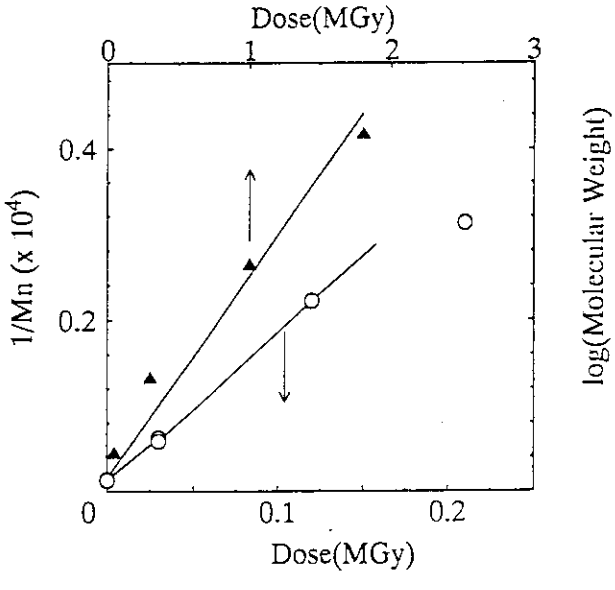


Fig.5 Molecular weight of PMMA irrad. at RT(○),77K(▲)

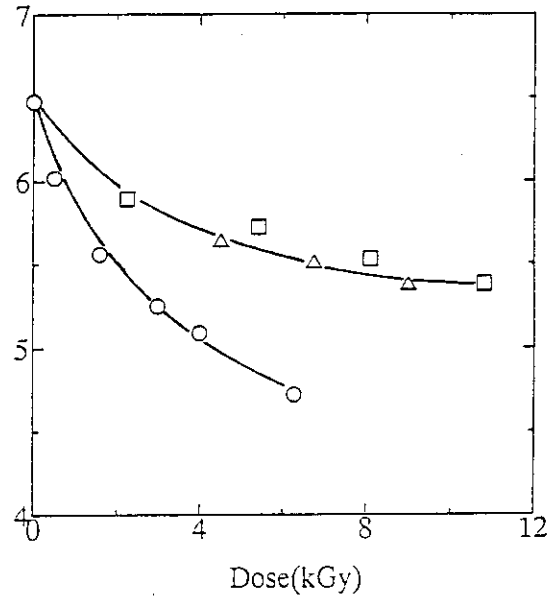


Fig.6 Molecular weight of PTFE irrad. at RT(○),77K(△),4K(□)

2. Gas evolution (Kudoh et al., 1993)

Figure 7 shows gas evolution from GFRP, total gas and component gases of H_2, CO and CO_2. H_2 evolution is almost the same between 77K and RT irradiation. However, CH_4, CO and CO_2 evolutions at 77K are much less than those at RT. It means that H_2 evolution from the cleavage of C–H bond is less dependent on irradiation temperature because the molecular motion of C–H bond is allowed even at 77K. The formation of CH_4, CO and CO_2 from the clevages of $-CH_3$, >C=O and –CO– bonds depend on the mobility of those bonds in bis-phenol A epoxy resin which are closely related to main chain scission. The transition temeperature in local molecular motion is around 170K (Sasuga et al., 1991) although glass transition of epoxy resin is around 370K. The local molecular motion is restricted at 77K and allowed at RT which reflects to the scission of those chemical bonds. The probability of radiation induced degradation of GFRP depends on the molecular motion of epoxy resin during irradiation. The transition in molecular motion at 170K would be related to the large difference in flexural strength change and gas evolution between 77K and RT irradiations.

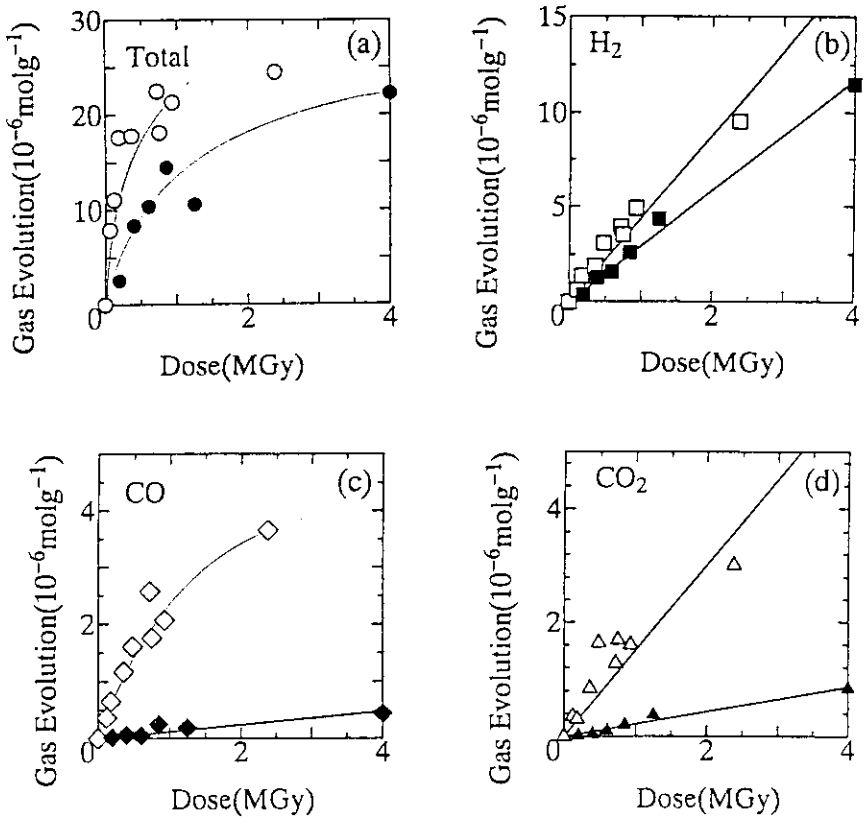


Fig.7 Gas evolution from GFRP
(a)Total,(b)H_2,(c)CO,(d)CO_2
open symbols denote RT irradiation and
solid symbols denote 77K irradiation, respectively.

Table 1 shows G values of gas evolution from PMMA. H_2 evolution is almost the same at 77K and RT. CO and CO_2 evolutions are much less at 77K than at RT. The same tendency with the case of GFRP is observed. Since the transition temperature of ester side group of PMMA is around 270K (Wundlich, 1989), the molecular motion of ester branch is restricted at 77K and allowed at RT. This transition would relate to the large difference in flexural strength and gas evolution between 77K and RT irradiations.

The irradiation temperature dependence would be related to molecular motion as decscribed above. The difference between 77K and 4K irradiation is not observed for PTFE. Considering that there is no transition in the molecular motion related to chain scission between 4K and 77K, the degradation at 4K would be the same with that at 77K for other polymers.

Table 1 G values of evolved gas from irradiated PMMA

Temperature	Total	H_2	CH_4	CO	CO_2
RT	1.3	0.27	0.038	0.33	0.047
77K	0.60	0.25	0.003	0.023	0.011

CONCLUSION

The irradiation temperature dependence on the degradation of GFRP, PMMA and PTFE was studied by irradiation at RT, 77K and 4K in terms of the change in mechanical properies, molecular weight and gas evolution. The degradation of mechanical properties at 77K was much less than at RT. Annealing effect up to room teperature after 77K irradiation is scarce for GFRP. The degradation at 4K is the same with that at 77K for PTFE. The gas evolution of CO and CO_2 well reflected the irradiation temperature dependence of flexural strength for GFRP and PMMA. The less degradation at low temperature is attributed to less probability of chain scission and relates to the local molecular motion. The probability of scission decreases with decreasing molecular motion at lower temperature, but it becomes constant below 77K where local molecular motion is restricted.

REFERENCES

Kasai N. and Seguchi T.(1990) JAERI-M, 90-155
Kudoh H., Kasai N., Sasuga T. and Seguchi T. (1993) The proceedings of 36th Symposium on Radiation Chemistry, Japan, Tokyo, Hachioji, p53
Kudoh H., Kasai N., Sasuga T. and Seguchi T. (1994) Radiat. Phys. Chem. vol.43, 329
Sasuga T. and Udagawa A.(1991) Polymer, vol.32, 402
Suwa T., Takehisa M. and Machi S.(1973) J. of Apply. Polym. Sci., vol.17, 3253
Wundlich K.(1989) The proceedings of international symposium of Radiation Degradation of Polymers and The Radiation Resistant Materials, Japan, Gunma, Takasaki, p159

8.5 Radiation Effects on Epoxy Composites at Cryogenic Temperatures

H. Yamaoka[1], K. Miyata[2], S. Nishijima[3] and T. Okada[3]

[1]Department of Polymer Chemistry, Kyoto University, Kyoto 606-1, Japan, [2]Research Reactor Institute, Kyoto University, Kumatori, Osaka 590-04, Japan and [3]Institute of Scientific and Industrial Research, Osaka University, Osaka 567, Japan

Abstract Radiation effects on glass-fiber reinforced epoxy composites at cryogenic temperatures has been studied by measuring the changes in interlaminar shear strength of the specimens. The scanning electron microscope observation has also been performed on fracture surface of the specimens. At 8.5 MGy of absorbed dose, only 10 % decrease of the strength was observed in the case of gamma irradiation, whereas over 80 % decrease of the strength was found on the reactor irradiated specimen. The difference of degradation behavior between gamma and reactor irradiations is attributed to the additional absorbed dose in the latter from the nuclear reaction due to boron-10 contained in the glass fibers by capture of thermal neutrons.

INTRODUCTION

Design studies for several fusion reactors and devices have become more detailed in recent years. One of the important aims of design engineering is to select suitable materials which perform reliably under the most severe conditions. Among several conceptual designs of fusion reactors, the machines based on magnetic confinement are planning to utilize a variety of superconducting magnets which are operated at cryogenic temperatures. The components of superconducting magnets are exposed to intense radiation of fast neutron and secondary γ-rays. Because of the brittleness and the difficulty of fabrication techniques in inorganic materials, the application of various organic materials has been considered for electrical insulators, thermal insulators and a part of structural supports in the magnets (Clinard and Hurley, 1981; Coltman, 1982; Hurley and Coltman, 1984).

Most of organic materials in fusion reactors must be designed to employ organic-matrix composites as it appears doubtful that conventional polymers can withstand the severe radiation environment for a long operation time. In the present paper, radiation effects on glass-fiber reinforced epoxy composites at cryogenic temperatures have been studied with mechanical measurements and scanning electron microscope observations.

EXPERIMENTAL

Materials

The specimens used in this work were basically glass-cloth-reinforced epoxy laminates. Both Lamiverre-A^R (Sample A) and Hoxan^R (Sample B) were commercially available diglycidyl ether of bisphenol A liquid-type epoxy resin laminates, and contained 60 to 62 % of E-glass woven fabrics by weight. Sample C and Sample D were specially prepared epichlorohydrin-bisphenol A solid-type epoxy resin laminates reinforced with E-glass cloth and T-glass (boron-free) cloth, respectively. E-glass contains the element of boron as a form of B_2O_3. Glass cloth content of both specimens were 50 % by weight.

Irradiation

γ-Irradiation of the specimens was done at room temperature and 77 K at a dose rate of 2 x 10^4 Gy/h with a ^{60}Co source of Osaka University. Reactor irradiation of the specimens was performed at a low-temperature irradiation facility of Kyoto University Reactor, the average temperature of which was about 20 K under reactor operation at 5 MW. The highest fast (E > 0.1 MeV) and thermal neutron fluences of the facility were 2.5 x 10^{15} n/m^2/s and 2.3 x 10^{16} n/m^2/s, respectively. The γ-ray dose rate at the same position was 1.2 x 10^5 Gy/h. After irradiation, the specimens were stored in liquid nitrogen (77 K) without warming up to room temperature and subjected to mechanical tests.

Measurements

Measurements of interlaminar shear strength (ILSS) of composites were performed with the use of specially prepared specimen shown in Fig. 1. The mean value of ILSS was obtained by compressing the specimen, although there are many problems of cryogenic ILSS testing arrangements (Becker, 1990). The displacement speed of Shimadzu Autograph Testing Machine, Model AG-500, was set at 1 mm/min. The fracture surface of specimens was observed with a JXA-50A scanning electron microscope (Japan Electron Optics Lab.) operated at 50 KeV.

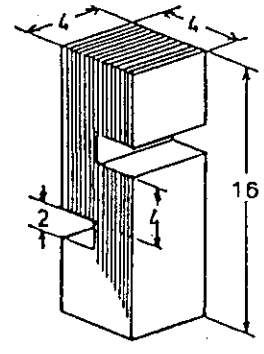


Fig. 1. Shape and size of specimens (in mm).

RESULTS AND DISCUSSION

The study on the mechanism of radiation-induced deterioration in organic composites has elucidated that the essential property which contributes the deterioration is the change in ILSS of composites (Okada *et al.*, 1986). An example of radiation effect on the mechanical properties of epoxy composites at room temperature is shown in Fig. 2. After γ-irradia-

tion of Sample A to 20 MGy, the ILSS of the specimen was reduced to approximately 75 % of the initial value, although the tensile strength of the same specimen kept constant (Nishijima *et al.*, 1988). This means that the tests on ILSS are more sensitive as a measure of radiation-induced deterioration of composites than those on tensile strength.

The changes in ILSS of Sample B at different irradiation conditions are represented in Fig. 3, where the absorbed doses due to fast neutrons were estimated under the conversion factor of 1 Gy = 10^{15} n/m^2 (E > 0.1 MeV). When this conversion factor was used, the absorbed dose due to neutrons was given to be one order of magnitude smaller than the absorbed dose of -radiation from the reactor, indicating that the absorbed dose due to fast neutron irradiation can be neglected. Nevertheless, the remarkable difference between - and reactor irradiations was observed. After cryogenic irradiation up to 8.5 MGy, over 80 % decrease of strength was found on the reactor irradiated specimen, although only 10 % decrease of the strength was observed in the case of -irradiation.

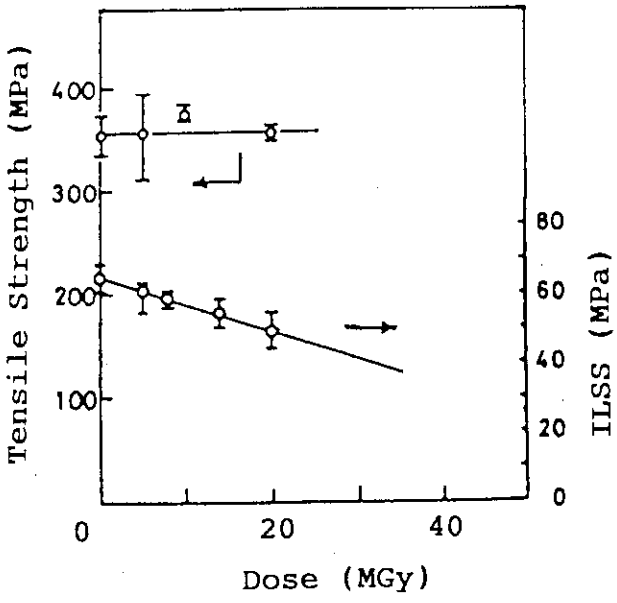


Fig. 2. Effect of γ-irradiation on tensile strength and ILSS of Sample A.

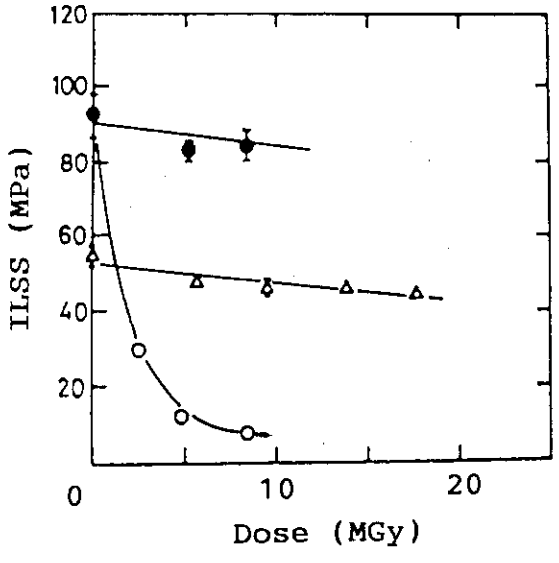


Fig. 3. Changes in ILSS of Sample B at different irradiation conditions. (o : Reactor irradiation at 20 K, tested at 77 K; ● : γ-irradiation at 77 K, tested at 77 K; Δ : γ-irradiation at room temperature, tested at room temperature.)

In order to clarify this different effect, the reactor irradiations of Sample C and Sample D were carried out at 20 K. The results obtained are shown in Fig. 4. The ILSS of Sample C reinforced with E-glass cloth markedly decreased with an increase of dosage, whereas that of Sample D reinforced with T-glass showed rather small effect on irradiation. The difference of radiation damage between two samples seems

to be attributed to the additional absorbed dose in Sample C from the fission of boron-10 in E-glass through a nuclear reaction of $^{10}B(n,\alpha)^{7}Li$ by capture of thermal neutrons (Okada *et al.*, 1992). Similar effects were also observed in the flexural tests of epoxy composites (Coltman and Klabunde, 1983) and the fatigue tests of various composites (Schmunk *et al.*, 1984).

The results of scanning electron microscope (SEM) observation on the fracture surface of irradiated specimens of Sample D revealed that the good adhesive nature with the matrix resin and the T-glass cloth were still maintained even after cryogenic reactor irradiation of 7.4 MGy. On the contrary, the SEM photograph of the specimens of Sample C showed that the surface of E-glass cloth at the same irradiation conditions was very smooth, indicating the debonding with the matrix resin. These fact are consistent with the results obtained in ILSS tests.

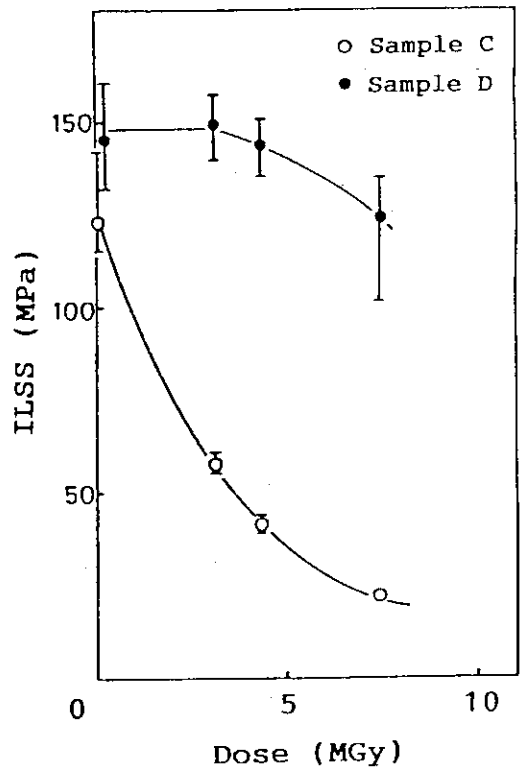


Fig. 4. Reactor irradiation of Sample C and Sample D at 20 K. (Tested at 77 K.)

CONCLUSION

In the epoxy composites reinforced with E-glass cloth, the remarkable difference in deterioration behavior was observed between gamma and reactor irradiations at cryogenic temperatures.

The drastic reduction in the ILSS of S-glass reinforced epoxy composites arose from a marked debonding in the matrix-glass cloth interface due to the additional absorbed dose resulted in the thermal neutron fission of boron-10 atoms. The SEM observation of fracture surfaces of irradiated specimens gave another evidence for the difference in radiation damage between E-glass and T-glass reinforcements.

The results obtained in this work suggest that the boron-free glass as reinforced fibers should be applied for polymer composites used in intense neutron fields.

REFERENCES

Becker H. (1990) Adv. *Cryog. Eng. (Mater.)* **36**, 827

Clinard F. W. and Hurley G. F. (1981) *J. Nucl. Mater.* **103/104**, 705

Coltman, Jr. R. R. (1982) *J. Nucl. Mater.* **108/109**, 559

Coltman, Jr. R. R. and Klabunde C. E. (1983) *J. Nucl. Mater.* **113**, 268

Hurley G. F. and Coltman, Jr. R. R. (1984) *J. Nucl. Mater.* **122/123**, 1327

Nishijima S., Okada T., Miyata K. and Yamaoka H. (1988) *Adv. Cryog. Eng. (Mater.)* **34**, 35

Okada T., Nishijima S. and Yamaoka H. (1986) *Adv. Cryog. Eng. (Mater.)* **32**, 145

Okada T., Nishijima S., Nishiura T., Miyata K and Yamaoka H (1992) *Adv. Cryog. Eng. (Mater.)* **38**, 241

Schmunk R. E., Miller L. G. and Becker H. (1984) *J. Nucl. Mater.* **122/123**, 1381

9. Dosimetry

9.1 *Dosimetry Systems for Radiation Processing in Japan

N. Tamura

Takasaki Establishment, Radiation Application Developmemt Association
1233 Watanuki-machi, Takasaki, Gunma-ken, 370-12 Japan

Abstract The present situation of dosimetry systems for radiation processing industry in Japan is reviewed. For gamma-rays irradiation the parallel-plate ionization chamber in TRCRE, JAERI has been placed as a reference standard dosimeter for processing-level dose. Various solid and liquid chemical dosimeters are used as routine dosimeters for gamma processing industries. Alanine dosimeters is used for the irradiation purpose which needs precise dosimetry. For electron-beam irradiation the electron current density meter and the total absorption calorimeter of TRCRE are used for the calibration of routine dosimeters. Plastic film dosimeters, such as cellulose triacetate and radiochromic dye are used as routine dosimeters for electron processing industries. When the official traceability systems for processing-level dosimetry now under investigation is completed, the ionization chamber of TRCRE is expected to have a role of the primary standard dosimeter and the specified alanine dosimeter will be nominated for the secondary or reference standard dosimeter.

INTRODUCTION

Reliabale methods of evaluating the radiation dose are required in the radiation processing industries. Various dosimeters have been developed so far in Takasaki Radiation Chemistry Research Establishment (TRCRE), JAERI and other research institutions for the validation of gamma-rays and electron-beam irradiations mainly in the industries of product sterilization, food irradiation, and polymer processing and the radiation resistance tests of materials used in nuclear facilities and space environments.
Through the experiences and investigations on the use of dosimeters at many irradiation facilities in Japan, the characteristics and role of each dosimeter have been clarified. The local intercomparisons of dose measurement between TRCRE and other research institutions or industries in Japan, and also the international or bilateral intercomparisons carried out by IAEA and TRCRE have contributed greatly to the reliability of dose measurement at the industrial irradiation facilities in Japan.
This paper will show the present situation of dosimetry systems for radiation processing industry in Japan. The official traceability system for processing-level dosimetry now under investigation will be also presented.

STANDARD DOSIMETERS AND CALIBRATION LABORATORY FOR RADIATION PROCESSING

Radiation dosimeters can be classified according to their characteristics and position in the dose traceability system: primary standard dosimeter, reference standard dosimeter, routine dosimeter and transfer dosimeter. The transfer dosimeter is selected usually from reference standard dosimeters which are

intended for transport between different locations used as an intermediary to compare absorbed dose measurements.

Primary Standard Dosimeter

In Japan the Electro Technical Laboratory (ETL) responsible for the standard on radiation dosimetry has the primary standard on exposure with ionization chambers (National standard instrument). In the processing-level dosimetry the parallel-plate ionization chamber in TRCRE was developed in cooperation with ETL (Tanaka et al. 1985). This ionizaton chamber is used virtually as a standard dosimeter instead of the ETL's ionization chamber, although it is classified still as a reference dosimeter at present. Concerning the electron-beam dosimetry the ETL dose not provide a standard dosimetry system. Under such circumstances the electron current density meter (Tanaka et al. 1980) and the total absorption calorimeter (Tanaka and Sunaga, 1985) in TRCRE are often used for the calibration of dosimeters.

Reference Standard Dosimeter

Although the position and the role of reference standard dosimeter have not been strictly defined so far in Japan, the chemical dosimetry systems whose response to radiation and other environmental factors is reproducible and elucidated will occupy such position. Table 1 shows the reference dosimeters which have been used so far in Japan.

The Fricke dosimeter has been used as both reference and also routine dosimeters at gamma irradiation facilities for sprout inhibition of potatoes in Shihoro, Hokkaido, since the dosage necessary for the sprout inhibition is rather low, less than 150Gy, and in this dose range the Fricke dosimeter is the most reliable and well characterized. The inspection using Fricke dosimeter is carried out by the local public health center under the direction of Ministry of Health and Welfare (MHW).

For the sterilization of medical appliances both physical and chemical dosimeters are used in industrial gamma irradiation facilities as a reference dosimeter. In some irradiation facilities the physical dosimeters such as ionization chambers and N/P type silicon solar cells (Tanaka et al. 1976) have been used. The ceric/cerous dosimeters have been partly used in Nordion-type commercial irradiation facilities. The reliability of the dosimetry in the irradiation facilities as well as the result of routine dose measurement is inspected by MHW through a documentary examination.

Electron-beam irradiation has been applied mainly for the processing of polymeric materials so far and is now expanding to the sterilization of medical supplies. In this application field the electron current density meter and the total absorption calorimeter in TRCRE are used as a reference dosimeter as already mentioned.

The alanine/ESR dosimetry system has been recognized as the precision-grade dosimeter in Japan, which is measurable in a wide dose range from 1 to 10^5Gy (Kojima et al. 1986; Kojima and Tanaka, 1989). The alanine dosimeter is made by molding with polystyrene (PS) binders. Now this PS-alanine/ESR dosimeter system is under discussion as a role of the reference dosimeter and will be nominated as a new reference standard dosimeter. Internationally it has been already recognized as reference standard dosimeter (ASTM, 1994).

A High-Dose Radiation Dosimetry Calibration Laboratory

Although the ETL provides a ^{60}Co gamma dosimetry calibration laboratory, a

radiation field with a dose-rate appropriate to radiation processing is not available. Recently a high-dose gamma radiation calilbration laboratory has been installed at the Irradiation Room No. 5 in TRCRE, which is calibrated by the pararell-plate ionization chamber. Figure 1 shows the plan view of the Irradiation Room No. 5, where a plaque source consisting of ^{60}Co pencils is lifted up to the irradiation position in the room from the source storage pool. The parallel-plate cavity ionization chamber previously described is installed on an automatic positioning stand within an accuracy of $\pm$0.2 mm and covers a wide dose-rate range from 0.1 to 10kGy/h. The dosimeters to be calibrated are irradiated in a movable sample chamber where the temperature and relative humidity are controlled (Tachibana et al. 1989).
The electron accelerators for the dosimetry calibration is not provided in the ETL. At present the calibration of routine dosimeters for electron beam is carried out by use of the electron current density meter and the total absorption calorimeter of TRCRE.

ROUTINE DOSIMETRY FOR INDUSTRIAL IRRADIATION FACILITIES

Many different routine dosimeters have been developed and tested so far at national and public research institutions for processing-level dosimetry. Table 2 shows the routine dosimeters, including the imported dosimeters, widely used at the industrial irradiation facilities in Japan.

Routine Dosimeters for Gamma Irradiation

In the gamma irradiation facilities for the sterilization of medical supplies dyed and undyed polymethylmethacrylate (PMMA) are mostly used, since these dosimeters were developed specially for the routine use in sterilization dosimetry. At present Red Perspex 4034, a dyed PMMA dosimeter, and Radix RN15, an undyed PMMA dosimeter, are mainly used in the sterilization industries.
For the radiation resistance test which needs more precise dose estimation the PS-alanine dosimeter known as Aminogray is frequently used for gamma irradition. The alanine dosimeter is applicable to the higer dose range than PMMA dosimeter.

Routine Dosimeters for Electron Beam Irradiation

For EB irradiation plastic film dosimeters are used as a routine dosimeter, since thin films are suitable for the measurement of depth profiles in the irradiated materials. Cellulose triacetate (CTA FTR-125) is the most widely used in EB processing industries in Japan and radiochromic dye dosimeter (FWT-60) is used mainly for low energy EB processing.
The CTA dosimeter has been developed in JAERI in collaboration with CEA, France and manufactured by Fuji Photofilm Co. (Tamura et al. 1981, Tanaka et al. 1984). The CTA film for dosimeter contains 15% triphenyl phosphate with no other additives. The absorbed dose is determined from the optical density change at 280nm before and after irradiation. The mechanism of the radiation-induced coloration of the CTA dosimeter was clarified (Matsuda and Nagai, 1991). A compact and precise readout system for CTA using the manganese hollow-cathode lamp as a monochromatic light source was developed and manufactured.

HIGH-DOSE INTERCOMPARISON BETWEEN THE IRRADIATION FACILITIES

The first high-dose intercomparison between the irradiation facilities in Japan was carried out in 1975 sponsored by the Radiation Application Development Association (RADA) after three industrial irradiation facilities had started; two are for sterilization of medical appliances and one is Shihoro potato irradiation facilities, where the irradiation process is assured by dosimetry. The aim of intercomparison was to improve the reliability of the irradiation process in industries and at the same time to harmonize the dosimetric measurement systems mutually between the irradiation facilities in the research institutions in Japan. Thirteen irradiation facilities, seven from national or public research institutes, two from universities and four from industries, participated in the intecomparison test. The Fricke dosimeter was used as a transfer dosimeter. Assuming the ETL value is a standard, the deviations from the ETL value were compared. The results show that the values of ten out of thirteen facilities agree with the standard value within ±5 % (Kawashima et al. 1978).

The second high-dose intercomparison was carried out by RADA in 1985 to harmonize and standardize the methods of dosimetry specially for low-enegy electron irradiations (Tanaka et al. 1989). The CTA (FTR-125) and radiochromic dye (FWT-60) dosimeters were used as transfer dosimeters. Ten irradiation facilities from research institutes, accelerator makers, and irradiation plants participated in this intercomparison. It was found that the transfer dosimetry by use of the thin film dosimeters, CTA and radiochromic dye, was useful and reliable for low energy electron-beam when care is taken for the environment such as humidity of the dosimeter films.

The dose intercomparison by using the PS-alanine/ESR dosimeter system was carried out with ten gamma irradiation facilities including the commercial plants. The main aim is to testify that the newly developed alanine dosimeter is appropriate for a reliable transfer dosimeter. The result of the intercomparison shows that the nominal doses agree with the estimated ones within ±5 % for most facilities and the variation coefficients for the dose response of five samples were within about ±1 % at all facilities (Kojima and Tanaka, 1989). This result demosnstrated that the PS-alanine/ESR dosimeter system has excellent characteristics for transfer dosimetry.

SCHEME OF THE NEW TRACEABILITY SYSTEM OF DOSIMETRY IN JAPAN

Now the official traceability systems for processing-level dosimetry are under investigation in Japan according to the New Measurement Law enforced in November 1993. In case this traceability system is completed , the parallel-plate cavity ionization chamber of TRCRE is expected to play a role of the primary standard dosimeter (National subsiduary standard instrument) in Japan. The specified alanine dosimeter is expected to be nominated for the reference standard dosimeter (Secondary standard instrument), which will have a role for the calibration of routine dosimeters used in gamma-rays and electron-beam irradiation industries. These dosimeter systems would provide the traceability from industry to national standards as shown in Fig. 4. It is important that they must be compatible with the dosimetry system of other countries through the international intercomparisons.

Table 1 Reference dosimeters used in Japan

Dosimeter	Readout System	Useful Absorbed Dose	Remarks
Gamma-rays			
Ionization chamber	Ammeter	10 to 3 $\times 10^4$ Gy/h	Parallel plate or cylindrical
Solar cell	Ammeter	10 to 10^5 Gy/h	Radiation resistant cell
Ceric-cerous sulphate solution	UV spectrophotometer or electrochemical potentiometer	10^3 to 10^5 Gy	
Ferous-sulphate solution (Fricke)	UV spectrophotometer	10 to 4 $\times 10^2$ Gy	
Alanine	ESR spectrometer	1 to 10^5	Polystyrene-molded
Electron beam			
Calorimeter	Thermometer	10^3 to 10^5 Gy	
Electron current-densitometry	Ammeter	0.01 to 10 μA/cm^2	

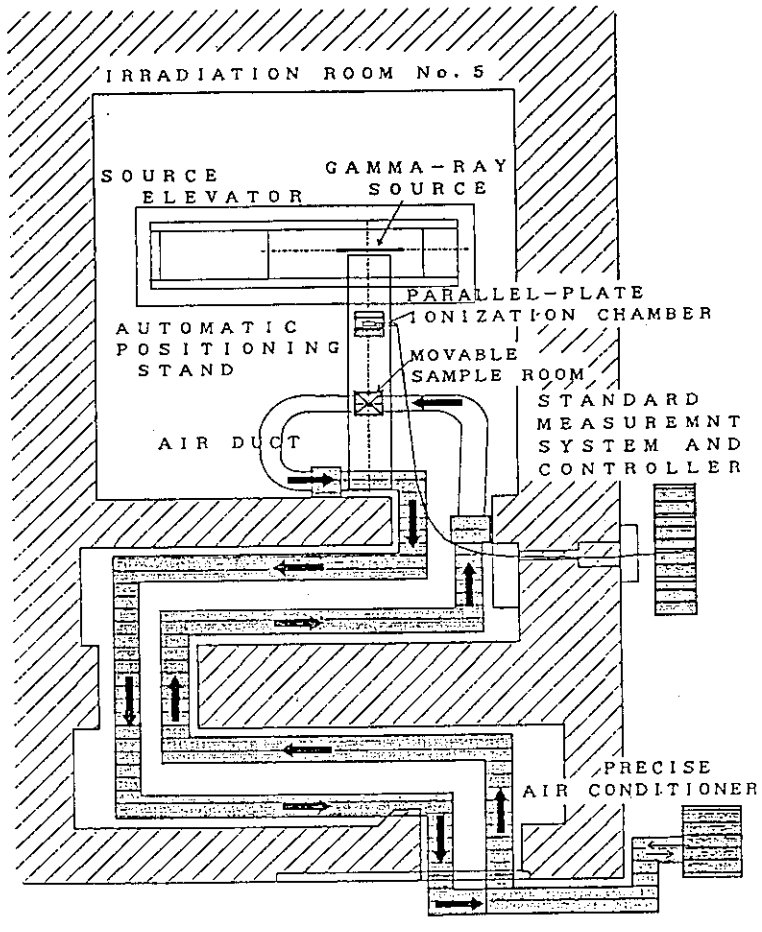


Fig. 1 Plan view of the high-dose gamma radiation calibration laboratory in TRCRE, JAERI (Tachibana et al. 1989)

Table 2 Routine dosimeters used in irradiation industries in Japan

Dosimeter	Readout System	Useful Absorbed Dose(Gy)	Remarks
Dyed polymethyl-methacrylate	Visible spectrophotometer	10^3 to 5×10^4	"Red Perspex4034" for γ-rays
Undyed (clear) polymethylmethacrylate	UV spectrophotometer	10^3 to 10^5	"Radix RN15" for γ-rays
Ceric-cerous sulphate solution	Potentiometer	10^3 to 10^5	for γ-rays
Ferous-sulphate solution (Fricke)	UV spectrophotometer	10 to 4×10^2	Potato irradiation for γ-rays
Alanine	ESR spectrometer	1 to 10^5	Polystyrene-molded
Cellulose triacetate	UV spectrophotometer Special reader	10^4 to 3×10^5	"FTR-125" for EB
Radiochromic dye films	Visible spectrophotometer Special reader	10^3 to 10^5	"FWT-60" for EB

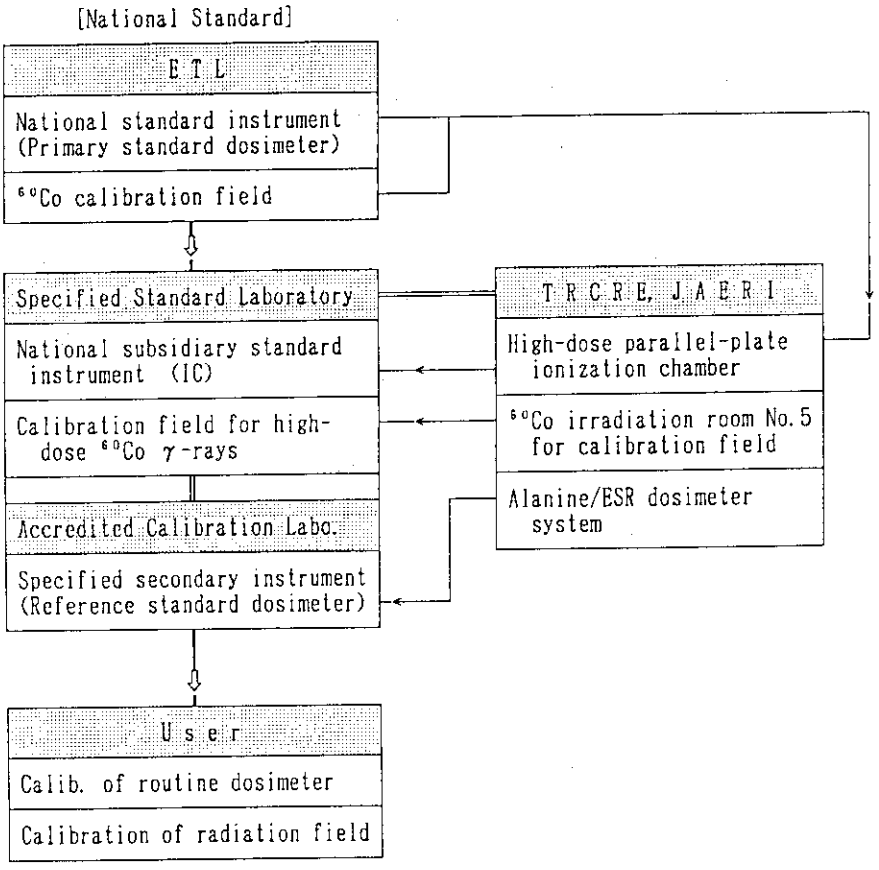


Fig. 2 Traceability system of high-dose dosimetry in Japan under consideration

REFERENCES

ASTM E 1607-94 (1994). Standard practice for use of the alanine-EPR dosimetry. Annual Book of ASTM Standards, Vol 12.02, p.855

Kawashima, K, K.Hoshino and M.Matsui (1978). Fricke dosimeters. "Practical Methods for processing-level radiation dosimetry" edited by Y.Moriuchi (RADA) p.27 (in Japanese)

Kojima, T., R.Tanaka, Y.Morita, and T.Seguchi (1986). Alanine dosimeters using polymers as binders. Appl. Radiat. Isot. **37**, 517

Kojima, T and R.Tanaka (1989). Polymer-alanine dosimeter and compact reader. Appl. Radiat. Isot. **40**, 851

Kojima, T., N.Haneda, S.Mitomo, H.Tachibana and R.Tanaka (1992). The gamma-ray response of clear polymethylmethacrylate dosimeter Radix RN15®. Appl. Radiat. Isot. **43**, 1197

Matsuda, K. and S.Nagai (1991). Studies on the radiation-induced coloration mechanism of the cellulose triacetate film dosimeter. Appl. Radiat. Isot., **42**, 1215

Tachibana, H., T.Kojima, R.Tanaka and K.Yoshida (1989). Standard dosimetry and irradiation system for high-dose rates gamma-rays. Proc. of the 26th Annual Meeting on Radioisotopes in the Physical Sciences and Industries, p.82 (in Japanese)

Tamura, N., R.Tanaka, S.Mitomo, S.Matsuda, and S.Nagai (1981). Properties of cellulose triacetate dose meter. Radiat. Phys. Chem., **18**, 947

Tanaka, R., S.Tajima, and A.Usami (1976). A simplified instrument for solid-state high-gamma dosimetry. Appl. Radiat. Isot., **27**, 73

Tanaka, R., S.Mitomo, and N.Tamura (1984). Effects of temperature, relative humidity, and dose rate on the sensitivity of cellulose triacetate dosimeters for electrons and γ-rays. Appl. Radiat. Isot., **35**, 875

Tanaka, R., H.Kaneko, N.Tamura, A.Katoh, and Y.Moriuchi (1985). Standard measurement of processing level gamma ray dose rates with a parallel-plate ionization Chamber. High-Dose Dosimetry (Proc. Symp. Vienna, 1984), IAEA, Vienna, p.203

Tanaka, R., H.Sunaga, I.Kuriyama and Y.Moriuchi (1989). Intercomparison study on low energy electron beam dosimetry. Radiat. Phys. Chem., **33**, 407

Tanaka, R., H.Sunaga, T.Kojima (1991). Simultaneous electron energy and dosimeter calibration method for an electron beam irradiator. High Dose Dosimetry for Radiation Processing (Proc. Symp. Vienna, 1990), IAEA, Vienna, p.189

9.2 Dosimetry of A 3-5 MeV Linear Electron Accelerator for Radiation Processing

XIE LIQING, SONG HONGBIN, WANG PENGCHENG, ZHANG YENFEN, GU HONGCHUN and LIU XIAOGUANG

Radiation Beam & Material Engineering Laboratory
Institute of Low Energy Nuclear Physics
(Beijing Radiation Center)
Beijing Normal University
Beijing 100875, P.R. China

ABSTRACT

With the multiple uses of a 3—5 MeV linear electron accelerator of the Institute of Low Energy Nuclear Physics (Beijing Radiation Center) at Beijing Normal University, the dosimetry of the linac for radiation processing has been studied. The graphite and water calorimeters have been used for routine dosimeter calibrations and reference measurements of absorbed dose for 4 MeV electron beam. Under the same irradiation condition, the polymer—alanine/ESR film and RCD dosimeters were calibrated in order to be used for routine process control. The polymer—alanine/ESR film dosimeter was also used as a transfer dosimeter for both ^{60}Co gamma rays and 4 MeV electron beam because of its good dosimetric properties.

KEYWORDS

Dosimetry; calorimeter; alanine dosimeter; radio chromic dye film dosimeter; absorbed dose.

INTRODUCTION

Electron beams (EB), generated by a 3—5MeV linear electron accelerator (Type BF—5) at Institute of Low Energy Nuclear Physics (Beijing Radiation Center) of Beijing Normal University (BNU), are widely used in polymer processing, in EB irradiation power devices, in sterilization of medical products, in food irradiation, in EB radiation mutagenic breeding and so on. Dosimetry is very important both for characterization the linac and for routine processing control. Calorimeter in water and graphite absorbers has been used for reference measurements of absorbed dose with 3—5 MeV electrons. The water calorimeters and graphite calorimeters were also used for calibrations of some dosimeters, e.g., polymer—alanine/ESR film (Xie et al., 1993) and radio chromic dye film (RCD), FWT—60—00 (from Far West Technology, Inc.,

Goleta, USA) under conditions that are similar to those of the intended use. Measurements with alanine and RCD film dosimeters for industrial 10 MeV electron reference dosimetry was reported (Miller et al., 1989). The polymer—alanine/ESR film dosimeters and RCD films, FWT—60—00, were calibrated by irradiation with ^{60}Co gamma rays and 3—5MeV EB to used for reference measurement and routine radiation process control. The purpose of these measurements was mainly to study the relation between the film dosimeter and calorimeter dose readings.

DOSIMETERS AND METHODS

The dosimeters were irradiated at the 3—5 MeV linear electron accelerator at BNU. The main accelerator parameters are shown in Table 1.

Table 1. Main characteristics of the 3—5 MeV linear electron accelerator.

Electron energy (MeV)	3—5
Average electron current (μA)	200
Maximum pulse electron current (mA)	200
Pulse repetition frequency (Hz)	100—500
Scanner frequency (Hz)	50
Maximum scan width (cm)	66
Power (kW)	0.78

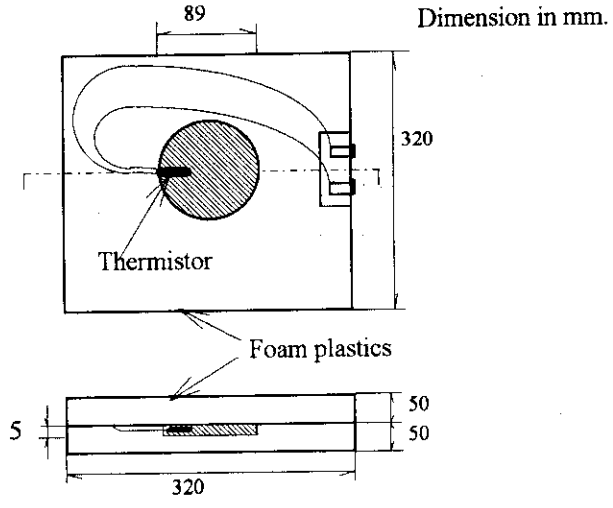


Fig. 1. The construction of a graphite calorimeter

The construction of a water calorimeter is simple (Yang and Xie, 1987), and the construction of a graphite calorimeter (Fig. 1.) was like the water calorimeter . A disc (89 mm diameter and 5 mm thickness) of the graphite calorimeter was also placed in foam plastics (polystyrene), and the temperature of the disc is monitored by a calibrated thermistor that was embedded in the middle of the graphite disc. The foam plastics maintain the temperature of the absorber so that change in temperature is very slow. For irradiation at BNU the readout can be made on—line to determine the temperature rise (Fig. 2.).

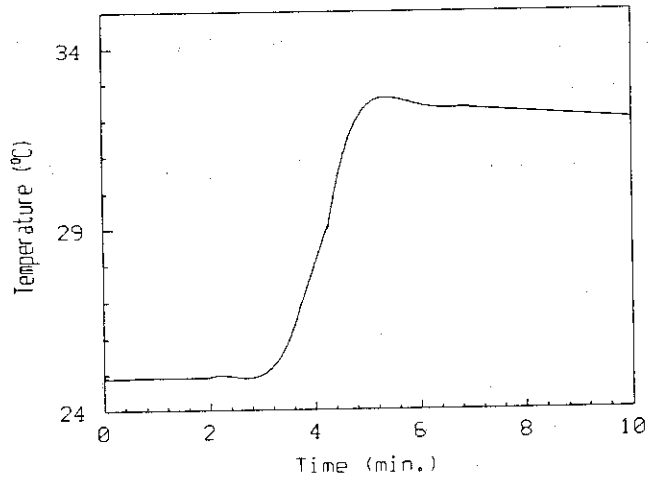
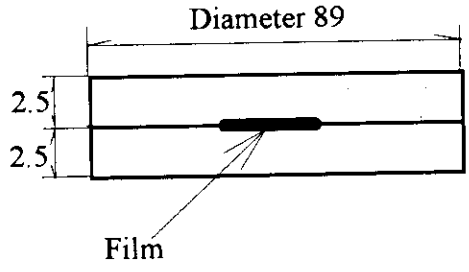


Fig. 2. The temperature rise curve of graphite .

Measurements of the depth—dose distribution (Xie et al., 1993) showed that the local dose in the half—depth of graphite disc is practically same as the average dose within the disc, so that the film dosimeter can be calibrated between two layers of the same graphite as



Dimension in mm .

Fig. 3. The situation of film in graphite .

that of the calorimeter disc but having half (2.5 mm) the thickness (Fig. 3.), which were placed in same foam plastics, namely because the measurements of the depth dose in the graphic disc showed that the dose increases almost linearly with depth.

The response of the FWT—60—00 film dosimeters and polymer-alanine film dosimeters was calibrated by irradiation at room temperature at BNU ^{60}Co γ—rays source. The dose rate in water of the gamma source was calibrated using Fricke dosimeters both from BNU and National Institute of Metrology (NIM). The total uncertainty of nominal doses at BNU ^{60}Co γ—source was estimated to ±2%(2σ). The ^{60}Co gamma ray irradiation was performed in terms of dose to water. The dose to the dosimeters in 5 mm graphite phantoms irradiated with 3—5 MeV electrons must be considered to do the stopping ratio correction at 3—5 MeV, respectively.
The polymer—alanine film dosimeters were read at NIM.

RESULTS AND DISCUSSION

The dose response variation of 4 water calorimeters for 4 MeV electrons is shown in Table 2.

Table 2. Dose response of 4 water calorimeters

Calorimeter No.	Dose kGy	Average dose kGy	Variation
1	21.54		-1.6
2	22.31	21.89	1.9
3	21.70		-0.9
4	22.01		0.5
1	15.81		2.0
2	15.25	15.50	-1.6
3	15.36		-0.9
4	15.57		0.4
1	7.99		1.8
2	7.89	7.85	0.5
3	7.73		-1.5
4	7.80		-0.6

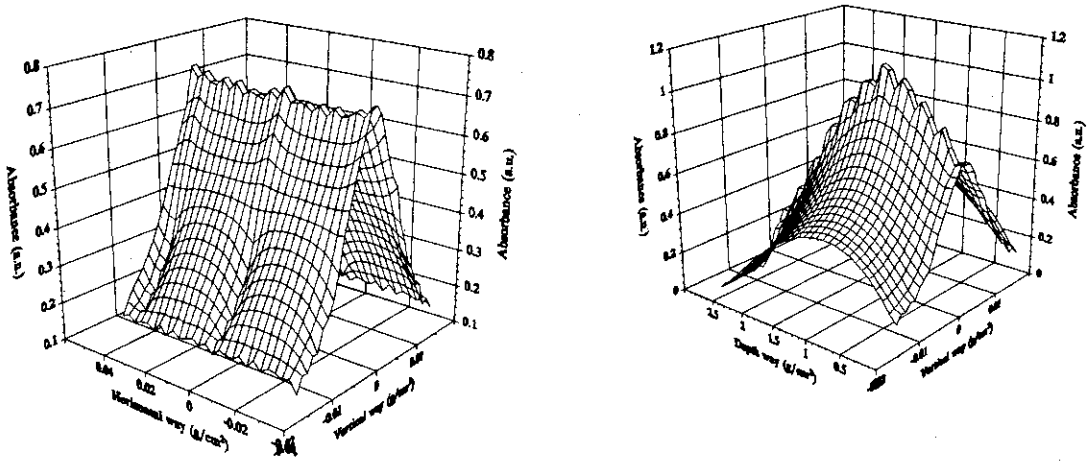
Table 2. showed that deviation of dose response among calorimeters is within ±2%. The water calorimeter can be used for reference measurements of absorbed dose for 4 MeV electrons processing. The polymer—alanine/ESR film dosimeter was also used as transfer dosimeter for both ^{60}Co gamma— rays and 4 MeV electron beam because of its good dosimetric properties. (Xie et al., 1993).

The ratios between the calorimeter and the film dosimeter readings are shown in Table 3. The results showed that for the two layer phantoms, the ratios between nominal dose as measured by calorimeter and the FWT—60—00 film and alanine film dosimeter readings are within ±2% of each other to be well within the experimental error.

Table 3. The ratios between the film and calorimeter readings

Approx. dose (kGy)	Phantom thickness (cm)	Ratios of measured dose	
		Calorimeter / FWT—60—00	Calorimeter / alanine
21	5	1.02	0.98
10	5	1.01	0.99

Fig. 4. showed a three dimensional plot of dose distribution on an aluminum plane



(a) (b)

Fig. 4. 3-D plot of dose distribution
(a) Horizontal and vertical (b) Depth and vertical

perpendicular to the electron beam obtained from irradiated FWT—60—00 film with electrons on the plane and in an aluminum phantom on the plane. It is proved that FWT—60—00 film is a convenient and valid dosimeter for measurements of dose

distribution. Fig. 4. (a) showed the horizontal and vertical dose distribution. Fig. 4. (b) showed the depth and vertical dose distribution.

CONCLUSION

These results indicate that the water and graphite calorimeters are suitable for reference measurements at the 3—5 MeV electron accelerator. Both alanine and RCD film dosimeters can be also used for reference measurements at the linac.

REFERENCE

Miller, A., A. KOVACS, A. WIESER and D. F. REGULLA (1989). Measurements with alanine and film dosimeters for industrial 10 MeV electron reference dosimetry. Appl. Radiat . Isot., 40, 967—969.

Xie, L., Y. Zhang, J. Dai, T. Lu, R. Chen, H. Yang and J. Gao (1993). Use of polymer alanine film/ESR dosimeters in dosimetry of ionizing radiation. Radiat . Phys . Chem., 42, 837—840.

Yang, G. and L. Xie (1987). Absorbed dose measurement with a water calorimeter for electron beam. In: Proc. of the 3rd China—Japan bilateral symposium on radiat. chem. Changchun, China, 495—497.

9.3 Dosimetry Study for Electron Beam Irradiation in Radiation Processing

H.SUNAGA, Y.HARUYAMA, H.TAKIZAWA, T.KOJIMA
and K.YOTSUMOTO

Takasaki Radiation Chemistry Research Establishment,
Japan Atomic Energy Research Institute
1233 Watanuki, Takasaki, Gunma, 370-12 Japan

Abstract For certain critical applications such as medical device sterilization and food irradiation, accurate calibration of electron energy and absorbed dose is required to assure the quality of irradiated products. To meet this requirement, TRCRE, JAERI has carried out research and development on high dose radiation dosimetry for electron beams in the energy range used in radiation processing (0.15 - 3.0 MeV). JAERI has developed a simultaneous electron beam energy and dosimeter calibration system that consist of a total absorption calorimater, an electron current density meter, and a stacked thin-film dosimeter set.

For low energy electrons, where it is important to measure the depth-dose profile in materials with high depth resolution, we studied the feasibility of a method using Gafchromic film dosimeters. This film, which has an 8-μm thick sensitive layer, is combined with a stepped array of absorber films of the same thickness to produce a high-resolution depth-dose profile on the Gafchromic film. The depth-dose profile obtained in this manner has about five times greater resolution than conventional radiochromic film dosimetry.

INTRODUCTION

Studies of radiation processing using electron beams have been carried out widely at Takasaki Radiation Chemistry Research Establishment (TRCRE), JAERI using three accelerators that cover the energy range from 0.15 to 3.0 MeV. For R & D studies of radiation processing, it is very important to establish reliable dosimetry methods because absorbed dose measurements are necessary to compare radiation effects quantitatively. Also, in industrial applications, accurate dose evaluation is necessary to ensure the quality of the process.

Dosimetry studies in radiation processing, including dose distribution measurements using film dosimeters and a calibration system for secondary routine dosimeters, have been reported in a previous publication (Tanaka et al., 1985). This study reports on a new method to simultaneously measure electron energy and calibrate the response of routine

dosimeters. We also describe a method for obtaining high-resolution measurement of the depth-dose distribution of low-energy electrons.

SIMULTANEOUS CALIBRATION SYSTEM FOR ELECTRON ENERGY AND ROUTINE DOSIMETERS

Electron beam radiation processing requires reliable measurement of absorbed dose in order to satisfy regulatory and quality control requirments. This demands periodic calibration of the response of dosimeters and the measurement of electron energy.

We have developed a simple system for simultaneous measurement of electron energy and calibration of routine dosimeters for medium energy (1 – 5 MeV) electron beam irradiation (Tanaka et al., 1991). The system consist of a total absorption calorimeter, an electron current density (ECD) meter (Tanaka et al.,1980) and a stack of un-calibrated film dosimeters with sufficient thickness to cover the electron range of interest. The same electron fluence is given to each by moving the three detectors across the irradiation zone

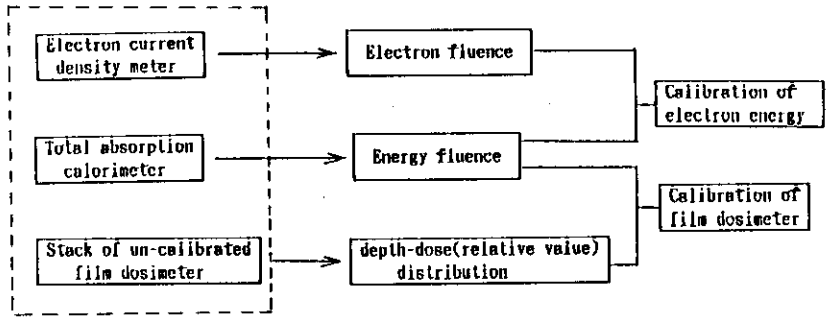


Fig.1 Schematic diagram of the simultaneous calibration system.

of the electron beam simultaneously or successively. Each detector experiences the exact same energy fluence, electron fluence and depth-dose (in relative value) profile, respectively. Figure 1 shows a schematic diagram of the system. For calibration of electron energy, the energy fluence (J/cm^2) and electron fluence (cm^{-2}) are combined,

$$E = 10^6 \cdot \frac{\phi_0}{\phi_0} \cdot \frac{1}{e} \qquad (1)$$

where E is the mean energy of the electrons in MeV, e = 1.602 x 10^{-19} is the charge of per electron, ϕ_0 (J/cm^2) is the measured electron energy fluence corrected for energy backscattering and radiation loss, and ϕ_0(cm^{-2}) is the electron fluence corrected for number of electrons backscattered.

The electron energy obtained in this manner is the mean energy of the electrons that enter the detectors. Therefore, this method is particularly well adopted to the measurement of the electron energy of dc accelerators in which the energy spread is low.

In addition to the energy measurement, routine film dosimeters are simultaneously calibrated by combination of energy fluence and depth-dose (in relative value) distribution

data. Especially, for the dosimeters which have linear relation between the absorbed dose and change in optical density, such as CTA film dosimeter, the calibration can be carried out using the following relation simply.

$$K = \frac{t \cdot \Sigma(\Delta OD_i)}{\phi_0} \qquad (2)$$

where

K : response of the film dosimeter, K–value, change in optical density per unit dose $(kGy)^{-1}$

t : thickness of a film dosimeter (g/cm^2),

ΔOD_i : change in optical density for each film,

Performance of the total absorption calorimeter has been tested to determine effects of different materials and chamber size (Sunaga et al., 1995). Figure 2 shows the

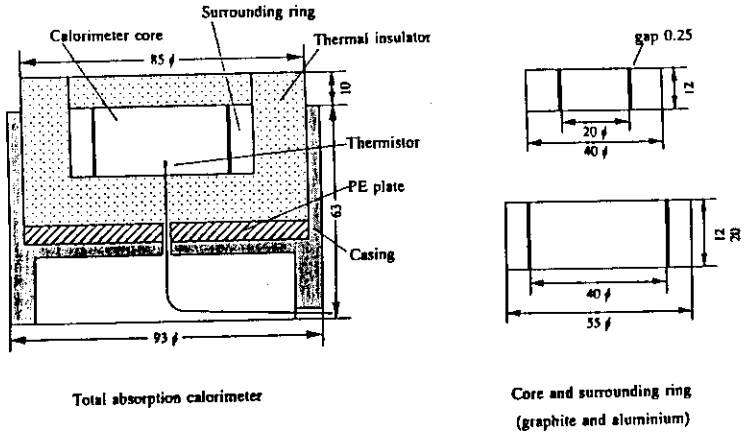


Fig.2 The cross–sectional view of the total absorption calorimeter.

cross–sectional view of the total absorption calorimeter. If the method is reliable, calorimeters made in various sizes and with different materials should provide the same energy fluence for measurements made in the same radiation field. Graphite and aluminium calorimeters were prepared. Drawing of the calorimeters are shown in Fig.2. The gap between the side wall of the absorber and the inner wall of the surrounding ring was set to 0.25 mm for all cases.

The calorimeters were irradiated together with the ECD meter, and electron energy per electron, i.e., the mean energy of the electrons, was compared. Table 1 shows the results of the measurement for accelerator voltage setting of 2.0 and 2.8 MV. The results in both materials and both sizes of the absorbers agreed.

We conclude that the absorber which consist of graphite with a 40 mm diameter opening and 12 mm thickness is optimum for 1 – 3 MeV scanning electron beams from the view point of correction of backscattering, radiation yield and resolution of measuring position.

Table 2 shows the result of calibration of CTA film dosimeter as an example of routine dosimeter calibration. The calibration yields the value, K = 0.0063 (kGy^{-1}) as the

K-value for CTA FTR-125 dosimeter. The ECD meter can be used as a monitor of the energy fluence when the electron energy is well known.

Table 1 Measured electron energy for 2.0 and 2.8 MV set in acceleration voltage.

calorimeter core		Evaluated electron energy	
material	size	accel. volt. set 2.0 (MV)	2.8 (MV)
Graphite	20 mmφ - 12 mmt	1.96 MeV	2.79 MeV
	40 mmφ - 12 mmt	1.85	2.70
	40 mmφ - 20 mmt	1.93	2.82
Aluminium	20 mmφ - 12 mmt	1.93	2.83
	40 mmφ - 12 mmt	1.85	2.71
	40 mmφ - 20 mmt	1.91	2.82

Table 2 Calibration of CTA dosimeter as an example.

E_e = 2.0 MeV, I = 3 mA, v = 4 m/min x 5 passes

$$K = \frac{t \cdot \Sigma(\Delta OD_i)}{\phi}$$

ϕ (Joule/cm^2)	$\Sigma(\Delta OD_i)$	t (g/cm^2)	K (kGy)$^{-1}$
32.86	12.62	0.0164	0.0063

HIGH-RESOLUTION DEPTH-DOSE DISTRIBUTION MEASUREMENT FOR LOW-ENERGY ELECTRON BEAM IRRADIATION

High accuracy depth-dose distribution measurements of low energy (150 - 300 keV) electros are technically difficult. Traditionally, these measurements are not very important because low energy electrons are only used for surface treatment. However, it is possible that the development of a measuring method with high resolution will lead to new applications of low-energy electron beams.

Gafchromic^R dosimeters consist of a very thin, 8 μm, radiation sensitive layer on a 100 μm thick PET film. Gafchromic film has high radiation sensitivity even though the thickness of the sensitive layer is very small. The film has been shown to have excellent characteristics as a routine dosimeter. High resolution depth-dose profiles of low-energy electrons were obtained by a method that makes use of the thin radiation sensitive layer of the Gafchromic film.

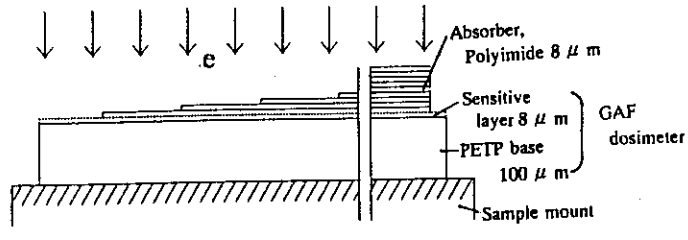


Fig.3 Experimental arrangement to measure the depth-dose distribution.

To measure the depth-dose distribution of low-energy electrons, a stepped array of absorbing material was assembled and placed upon a single layer of Gafchromic film. The step size of absorber is chosen comparable to the thickness of the sensitive layer of the dosimeter. In our experiment, we chose 8 μm Polyimide film because it has high registance to radiation exposure and it can be used repeatedly for several experiments. Figure 3 shows a drawing of the assembly and how it is oriented during exposure to the electron beam.

The assembly was irradiated by moving it through the radiation field. Figure 4 shows the results of measurements for irradiation of 200 kV and 250 kV in acceleration voltage. In the same figure, the depth-dose distributions measured using stacks of radiochromic dosimeter (FWT-60-00) are shown for comparison. It can be seen that the Gafchromic dosimeter method results in a 500 % improvement of depth resolution when compared to the conventional method.

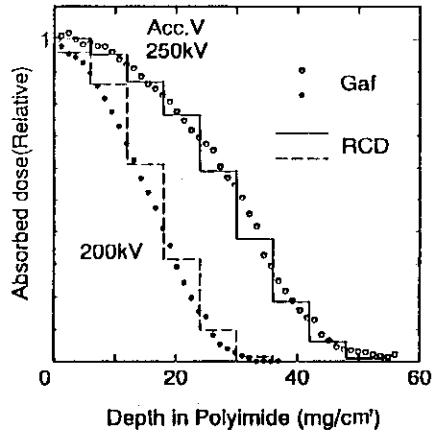


Fig.4 Depth-dose distribution in electron beam irradiation for 200 and 250 kV in acceleration voltage measured by new method.

SUMMARY

This paper reports on recent dosimeter studies at TRCRE, JAERI. It describes new methods for 1) simultaneous measurement of electron energy and calibration of routine dosimeters and 2) measurement of depth-dose distribution on low-energy electron beam irradiation with high-resolution. The energy measurement and dosimeter calibration is a simple, reliable and useful tool for standardization of irradiation parameters. The new method for generating high resolution depth-dose distribution profiles yields results that are about five times better than conventional methods. These R&D studies will cotribute to progress of radiation processing.

ACKNOWLEDGEMENT

The authers are grateful to Dr. Ryuichi Tanaka of TRCRE,JAERI and Dr.J. Paul Farrell of BROOKEHEVEN TECHNOLOGY GROUP, INC. for useful discussion in this work.

REFERENCESES

Sunaga H., R.Tanaka, N.M.Ali, and K.Yotsumoto (1995). Proceedings of 9th IMRP, to be published in *Radiat.Phys.Chem.*

Tanaka R., K.Mizuhashi, H.Sunaga and N.Tamura (1980). *Nucl.Instr.Meth.*,174,201-208.

Tanaka R., H.Sunaga and T.Agematsu (1985). *STI/PUB/671,(IAEA,Vienna),* 317-331.

Tanaka R., H.Sunaga and T.Kojima (1991). *STI/PUB/846(IAEA,Vienna),* 189-201.

9.4 The Status of Radiation Processing Dosimetry in China

Chen Wenxiu
Department of Chemistry, Beijing Normal University
Beijing 100875, China

Li Chenghua, Pang Ruicao and Zhang Yanli
Ioniz. Radiat. Div.,National Institute of Metrology
Beijing 100013, China

INTRODUCTION

Radiation processing is a rapidly expanding technology in China since 1970s. About 50 facilities of Co-60 source with the designed capacity more than 3.7PBq have been set up in Beijing, Shanghai, and 36 cities. The total charged activity of sources is more than 862PBq some facilities are shown in Table 1. More than 26 electron beam (EB) irradiation facilities have been established as listed in Table 2. The total power of electron beams had reached about 926 kW. The effectiveness of the process depends on the proper application of dose and its measurement. The importance of dosimetry events on the processing control of irradiation technology and the quality assurance of irradiated products has been acknowledged in China, which was introduced in this paper.

STANDARDIZATION AND REGULATORY CONTROL

The Provisional Regulation of Metrological Supervision and Management for Radiation Processing have been joinly issued by State Bureau of Technical Supervision (SBTS) and the State Commission of Science and Technology (SCST) on April 18, 1990 for implementing of the Law on Metrology of the People's Republic of China. This regulation stipulate to practise measurement licence for radiation processing units. Meanwhile a series of national standards,verification regulations, verification scheme and metrology technical norm have been enacted, these documents are listed as follows:

(1) Verification scheme of ^{60}Co γ-rays water absorbed dose mersuring instrument for radiation processing level;

(2) Verfication regulation of γ-rays radiation source;(for radiation processing)

(3) Verfication regulation of electron beams radiation source; (for radiation processing)

(4) Verfication regulation of the standard dosimeter of water absorbed dose for γ-rays;(radiation processing level)

(5) Verfication regulation of working dosimeter for γ-rays radiation processing;

(6) Standard method for using the Fricke dosimetry to measure absorbed dose in water;(Standard)

(7) Standard method for using the Ceric-Cerous Sulfate dosimeter to measur γ-rays absorbed dose in water;(Technical norm)

(8) Standard method for using the Potassium (Silver) dichromate dosimeter to measure γ-rays absorbed dose in water;(Technical norm)

(9) Monitoring method of dose assurance for radiation processing with gamma rays; (Technical norm)

(10) Standard method for using the Silver dichromate dosimeter to measure r- rays absorbed dose in water;(Technical norm)

(11) Verfication regulation of working dosimeter for electron beams radiation processing;

(12) Standard method for use of the radiochromic film and the polymethylmethacrylate dosimetry systems;(Standard)

(13) Pratical guide of dosimetry in a gamma irradition facility for food processing;(National standard, to be valid)

(14) Conversion method of absorbed doses in different materials irradiated by x. γ -rays and electron beams;(Standard)

(15) Terminology relating to radiation processing dosimetry; (Standard, to be valid)

(16) Guide for the selection and calibration of dosimetry systems for radiation processing; (Standard, in drafting)

(17) Standard pratice for dosimetry in an electron beam facility for radiation processing at energies 100-300keV and >300keV;(Standard, in drafting)

(18) Guide for estimating uncertainties in dosimetry for radiation processing; (Standard, in drafting)

(19) Standard practice for characterization and performance of a high dose gamma radiation dosimetry calibration laboratory;(Standard, in drafting)

(20) Method for use of the Alanine/EPR dosimetry system.(Standard, in drafting)

Those will play significant role in the dose measurement standardlization and the regularity control.

TRACEABILITY

The start points -National standards for EB measurement are established and maintained by the Primary Standard Laboratory, National Institute of Metrology(N.I.M), such as supply of the standard calorimeters from graphite and/or water. The graphite calorimeter for calibrating thin-film also supplied by the Secondary Standard Laboratory, Shanghai Insititute of Metrological Technology. A high-dose dissemination system have been trially performed as follows:

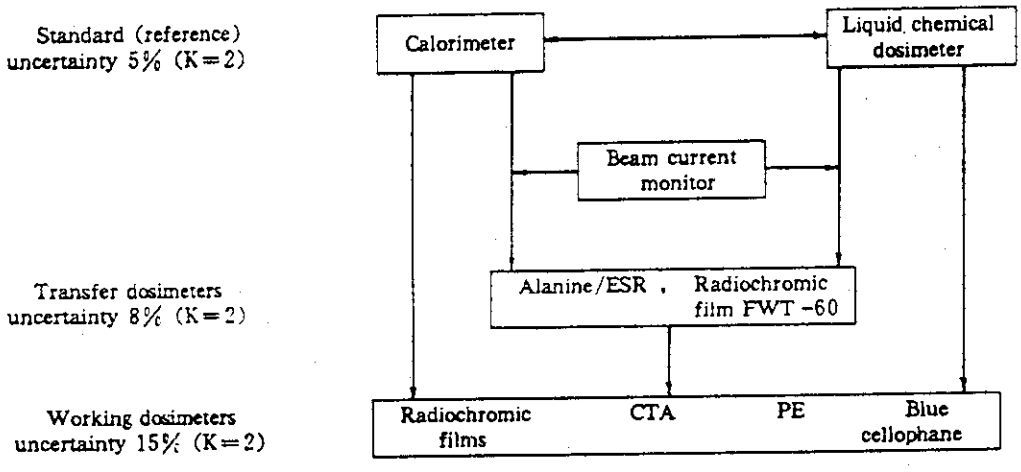


Fig. 1. The high-dose dissemination system of electron beams

The high dose measuerment system for gamma rays, including primary standards, transfer stndards and working dosimeters, has been established. The schema of dosimetry tracebility to primary standards for gamma rays is illustrated in Fig.2.

Primary standard uncertainty 2% (K=2)	Graphite calorimeter (1-20)Gy	Graphite Cavity ionization Chamber (1-20)Gy	Water calorimeter (2-50)Gy	Fricke dosimeter (40-200)Gy
	Substitution method			
Transfer standard uncertainty 4% (K=2)	Alanine/ESR dosimeter (0.05-40)Gy	LAgdc dosimeter (0.4-5)kGy	HK(Ag)Dc dosimeter (4-40)kGy	Ceric-cerous dosimeter (4-25)kGy
	Substitution method			
Working standard uncertainty 10%(K=2)	Solid working dosimeter (0.05-100)kGy		Liquid working dosimeter (0.04-50)kGy	

Fig.2. The schema of dosimetry tracebility to national primary standards for gamma rays.

Several solid dosimeters have been selected as transfer and working dosimeters in above system.

ROUTINE AND TRANSFER DOSIMETER

In 1985-1987 a series of program for routine and transfer dosimeter and relative products have been organized by the State Bureau of Metrology (SBM is a previous agent of SBTS) and completed by several institutions listed as table 3.

The radiochromic multipurpose reader(RCR-86, by BSRDW), film reader in 510, 600 and 650nm (FB-1. μ c-FB, by SIMT) and radiochromic dye (PR-CN.HPR-CN, by RICD) were also completed at the same time.

PLASTICS FLIM DOSIMETER ON DOSE MEASUREMENT

Plastics dosifilm was started in 1970s,it was suitably used on radiation processing as a routine dosimeter with reasonable cost for the convenience of dose mapping and for the possibility of file keeping, its density closed to water and tissue.

A series of dosifilm(PE. PE-MG. PE-CV. PE-MB. PVA-MG. PVA-MB. PVT and PVG) have been investigated or manufactured in Radiation Chemistry Group, BNU for dose measurement.

Dosifilm is particularly suit to EB dose measurement due to EB in less penetrability. The Alanine/ESR dosefilm started in 1980s, it also must be made as a dosifilm for EB dose measurement by blended with a matrix material plastics,the brief request of EB measurement was light stability, measurement of high-dose with high dose-rate and calibrated possibility.

The improvement and development of various plastics film were laid a strong emphasis upon EB dose measurement as its traceability were mentioned.

SUMMARY

The radiation processing business including radiation sterilization, food irradiation and polymer modification are very active in China. The national standards of dosimetry for quality assurance were documented and drafted, in reference with the standards of ASTM and in compliance with the demands of ISO standards. The radiation measurement can be made traceable to national standards, its precision and accuracy are satisfactory. There is a continue effort to improve the dosimetry. Recently the plastic dosifilm were emphasized using for EB dose measurement also were made understanding of the impact of various influence parameters on the performance of the routine dosimetry.

REFERENCE

1. C.Li, Y.Zhang, R.Pang, Z.Liu, X.Xia and J.Wu, *Radiat.Phys.Chem.* Vol.42, No.4-6,pp.823-826, 1993.
2. R.Pang, Y.Zhang, C.Li and J.Gao, *ibid* pp.857-858(1993).
3. W.Chen, G.Lu, H.Jia, H.Bao, *IAEA-SM-314/4*, Vienna, Nov, 1990.
4. H.Jia, A.Liu, Y.tian, W.Chen, Z.Meng, *Journal of Beijing Normal Univ.* (Natural) 30(2), p.237-240 (1994).
5. W.Chen, A. Liu, Two papers to be presented in *the 6th Japan-China Bilateral Symposium of Radiation Chemistry*, Tokyo, Nov. 6-11(1994)
6.The ducuments of national standarelizations and regulations.
7.Private communications between C.Li and W.Chen.

Table.1. The facilities of Co-60 (Activity charge at present more than 3.7PBq) with numerous applications

Location	Charged Activity(PBq)	Application
Henan (Zhengzhou)	3.7	(1).(3)
Jiangsu(Nanjing)	7.4	(1).(3)
Shanghai	6.55	(1).(3)
Shandong(Qingdao)	11.8	(1).(2).(4)
Guangdong(Shenzhen)	45	(1)
Ganshu(Lanzhou)	3.7	(1).(4)
Tianjin	3.7	(1).(2).(4)
Heilongjiang(Daqing)	3.7	(1).(2).(4)
Beijing	18.5	(1).(2).(4)
Beijing(A.E.I)	6.0	(2).(4)
Heilongjiang(Harbin)	3.7	(1).(2).(4)
Sichuan(Chengdu)	4.07	(3).(4)
Shanxi(Xi'an)	3.7	(4)
Sichuan(Dianjiang)	3.2	(3)
Beijing(M.M.I)	3.44	(3).(4)
Shanghai(S.N.I)	4.44	(4)
Jilin(Changchun)	6.22	(2).(4)
Anhui(Hefei)	1.74	(4)
Guangdong(Guangzhou)	5.11	(1).(3).(4)
Xinjiang(Wulumuqi)	4.07	(3).(4)
Henan(Zhongmou)	3.7	(2).(4)
Yunnan(Kunming)	4.1	(1).(2).(4)

(1):Medical products strilization;
(2):Polymer modification;
(3):Food processing;
(4):Multipurpose (including research work).

A.E.I: Atomic Energy Institute.
M.M.I: Military Medical Institute
S.N.I: Shanghai Nuclear Institute

Table 2. The facility of electron beam(power>1kW)

Facility(Location)	Energy (MeV)	Beam current (mA)	Application
China Institute of Atomic Energy(Beijing)	0.5	6	Wire, Film
Beijing Electron Radiation UnionCorp(Beijing)	2	10	Wire, Cable
Research Inst. of Automation for Machine Building Industry(Beijing)	0.2	15	Coating curing Film processing
Tianjin Cable Plant (Tianjin)	1.5	10	Wire, Cable
Inst. for Radiat.Protection, China(Shanxi, Taiyuan)	2.5	30	Heat-shrinkable material
Shenyang Special Cable Plant (Shenyang)	2	10	Special cable
Liaoyuan Cable Plant (Jilin)	2.5	20	Powercable
Changchun Inst. of Appl. Chem. (Jilin, Changchun)	1	20	Heat-shrinkable material
Jilin City Radiat. Chem. Res. Inst. (Jilin)	1.5	10	Heat-shrinkable material
Jilin City Radiat. Chem. Res. Inst. (Jilin)	3	40	Heat-shrinkable material
Shanghai Irrad. Tech. Devel. Centre(Shanghai)	1	20	Heat-shrinkable material
Shanghai Univ. of Sci. and Tech. (Shanghai)	0.3	30	Multiservices
Fengqiao Radiat. Product Plant(Suzhou)	0.3	30	Wire, Film
Changshu Cable Plant (Jiangsu)	2.5	30	Cable, Heat-shrinkable material
Yantai Cable Plant (Shandong)	2.5	30	Wire, Cable
Shanghai Cable Works (Shanghai)	2.5	30	Wire, Cable
Shanghai Cable Works (Shanghai)	2	10	Wire, Cable
Jiangxi Cable Plant (Jiangxi)	2	10	Wire, Cable
Shenzhen Changyuan Appl. Chem Co., Ltd. (Guangdong)		20	Heat-shrinkable material
Sichuan Univ. (Sichuan, Chengdu)	0.4	5	Multiservices
Chengdu Cable Plant, Shuang liu subplant(Sichuan)	2	10	Heat-shrinkable material
Sichuan Cable Plant (Chengdu)	2	10	Heat-shrinkable material
Kunming Cable Plant (Yunnan)	2.5	30	Heat-shrinkable material, Cable
Xian Electric Wire Central Plant(Shanxi)	2	30	Wire, Cable
Tianshui Cable Plant (Ganshu)	2.2	25	Wire, Cable
Southwest Inst. of Nucl. Phys. and Chem. (Sichuan)	3	10	Heat-shrinkable material
Total Power		926kW	

Table 3 The completed dosimeters organized by SBM in1985-1987

Dosimeter or product	Type	Dose range (kGy)	Institution*
Dyed PE dosifilm	PE-Mg	0.3-80	BNU
Radiochromic film	PVT	0.2-50	BNU
Radiochromic film	BC	0.8-100	IC&IAE
Radiochromic film	PC-85	1-50	BIRM&NIM
Radiochromic film	NF-86	1-100	BSRDW
Radiochromic OWG dosimeter	OWG-86	0.01-20	RICD
Lyoluminescence dosimetry system	JR-101	0.01-10	IB&BIM
Radiation indication labels	SN1-4	0.1-100	SINR

*: BNU: Beijing Normal University
IC: Institute of Chemistry
IAE: Institute of Atomic Energy on Agriculture
BIRM & NIM: Beijing Inst. Radiat. Med. and Natl. Inst. Metrol.
BSRDW: Beijing Shiying Radiation Detector Works
RICD: Research Institute of Chemical Defence
SIMT: Shanghai Institute of Metrology Technology
IB & BIM: Institute of Biophysics and Beijing Institute of Metrology
SINR: Shanghai Inst. Nucl. Res.

9.5 *Effects of Additives on PVG Dosifilm

CHEN Wenxiu LIU Aiguo
Department of Chemistry
Beijing Normal University
Beijing 100875 CHINA

ABSTRACT

Dosifilm PVG is a new radiochromic film dosimeter composed of matrix material polyvinyl butyral(PVB), leuco malachite green (LMG) and additive halogenated organic compound (RX), etc. The control of the dose range on PVG dosifilm was examined. The addition of halogenated compounds played an important role in the radiation reaction of LMG beyond the concentration of LMG. Bromide is more effective than chloride in this system, the oxidative species are $X\cdot$ and $X_2\cdot^-$. PVB with N-bromosuccinimide (NBS) can induce the oxidation of LMG before irradiation. The reaction mechanism of PVG was discussed.

Different linear ranges of radiation response on PVG dosifilm could be controlled by alternating the relative concentrations of halogenated compounds and LMG.

KEYWORDS

polyvinyl butyral; leuco malachite green; halogenated compounds; radiation oxidation; dosimeter.

INTRODUCTION

Leuco malachite green (LMG) in various systems has been utilized for radiation processing dosimetry purpose (Liu Aiguo et al.,1994;Wang Yanqiao et al., 1985; Stoltz et al., 1965). The discolor mechanism of LMG in polystyrene (PS) was also studied (Stoltz et al., 1965). The radiation chemistry in LMG organic solution has been reported (Vereshchinskiis et al., 1957; Bakh et al., 1960; Dejehet et al., 1972,1973; Grodkowski et al., 1990). Other leuco triarylmethane compounds have been studied, too (Armstrong et al., 1958; Bobrowski et al., 1985).

Polyvinyl butyral (PVB) film containing LMG and halogenated organic compounds as a dosimeter PVG has been developed and characterized (Liu Aiguo et al., 1994). Oxidation of LMG into its cation malachite green MG^+ with green color can be induced by gamma ray; its accumulation was proportional to the radiation dose.

Detailed study of LMG-PVB system in the presence of different halogenated organic compounds (RX) was carried out in this paper. By alternating the matrix and the concentration of LMG or RX, the linear relations of $\Delta A/L$ [i.e, $(A-A_0)/L$, mm^{-1} , see EXPERIMENTALS] vs dose (kGy) were obtained. The optimum composition and control of PVG dosifilm was deduced. The mechanism of radiation discoloration in the systems was discussed.

EXPERIMENTALS

Leuco malachite green (LMG, SIGMA, USA), polyvinyl butyral (PVB, Tianjing Organic Chemistry Industrial Experimental Factory, CHINA). $CCl_3CHO\cdot H_2O$ (A.R), C_2Cl_6 (A.R), CBr_4 (C. P), N-bromosuccinimide (NBS, A.R), PVC powder (Industrial Grade) and tetrahydrofuran (THF, A.R) were all manufactured in the Beijing Chemical Factory. The manufacture procedure of PVG dosifilm has been reported (Liu Aiguo et al., 1994). Irradiations were carried out using a 5.55×10^{14} Bq ^{60}Co-γ irradiation facility at Beijing Normal University with a dose rate of 16.2kGy/h. All the samples were kept in eletronic equilibrium during irradiation. Dose was calibrated by Fricke dosimeter. The dose values are expressed in terms of dose in water.

After irradiation the films were stored in a brown desiccator at room temperature(i.e, in air about 25-30℃). Absorbance of the films before (A_0) and after (A) irradiation was read out at a given wavelength using a HITACHI 200-20 double-beam UV spectrophotometer. The absorbance of each film was measured immediately after irradiation. The thicknesses (L) of the film pieces were measured using an Elecont micrometer made by Mitutoyo (JAPAN) with a reproducibility of $\pm0.2\,\mu m$.

RESULTS AND DISCUSSIONS

1. Formation of MG^+ in Irradiated PVB-LMG Film Containing Additive Halogenated Compounds (RX)

Exposed to ^{60}Co-γ, the PVB-LMG film with RX turned green owing to the formation of MG^+ (shows two absorption bands in the visible range with maximum absorption at 425 and 627nm). The PVB-LMG film without RX didn't change color after irradiation. Plots of ΔA/L vs dose were shown in Fig. 1 and Fig.2.

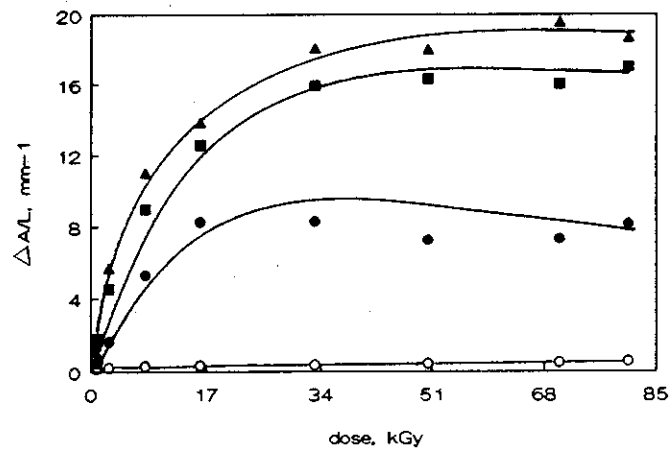


Fig.1 Response functions (ΔA/L,mm-1 vs dose, kGy) for PVB-LMG film with LMG concentration as 2×10^{-5} mole per gram PVB and varied halogenated compound (RX), in which RX:LMG > 50:1 (mole:mole), as CBr_4 (▲), C_2Cl_6 (■), $CCl_3CHO \cdot H_2O$ (●) and no additive (○).

As illustrated by Fig. 1, even the absorbed dose was up to 80 kGy, the ΔA/L in irradiated PVB-LMG system without RX increased far less than others. ΔA/L increased obviously with the increasing of dose in PVB-LMG systems with additives CBr_4, C_2Cl_6 or $CCl_3CHO \cdot H_2O$. The effect of these additives were in the order as bromide > chloride and C_2Cl_6 > $CCl_3CHO \cdot H_2O$ in the case of RX : LMG > 50:1 (mole : mole). The maximum doses related with ΔA/L in linearity in the three systems were no more than 20 kGy.

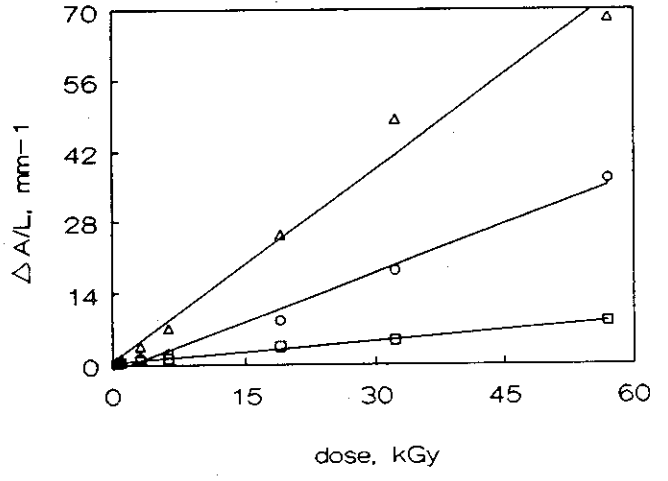
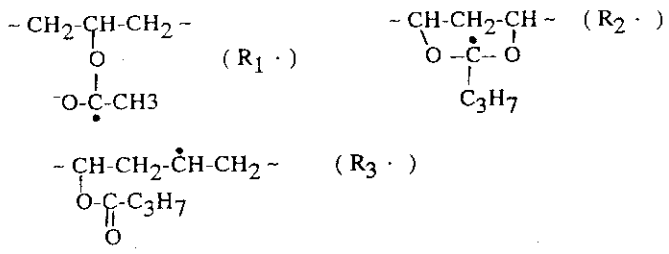


Fig.2 Response functions for PVB-LMG film with additives (RX:LMG=2:1, mole:mole) CBr_4 (△), C_2Cl_6 (□) and $CCl_3CHO \cdot H_2O$ (○) dye concentrations 1×10^{-4} mole LMG per gram PVB.

As shown in Fig.2, the maximum doses in the linear ranges expanded to about 60 kGy in the systems with higher concentration of LMG and lower concentration of RX (i.e, RX:LMG=2:1, mole : mole).

Irradiation of PVB without any additives radicals $R_1 \cdot$, $R_2 \cdot$ and $R_3 \cdot$ were as follows (Mikhallik et al., 1981):



$R_1 \cdot$, $R_2 \cdot$ and $R_3 \cdot$ were reductive intermediate species, LMG can not be oxidized by them. So that MG^+ can not be produced in the film without RX, as shown in Fig. 1. Addition of CBr_4, C_2Cl_6 or $CCl_3CHO \cdot H_2O$ to PVB-LMG system induced the radiation oxidation of LMG to MG^+ by the reactions:

$$RX + e^- \rightarrow R \cdot + X^-$$
$$\rightarrow R \cdot + X \cdot + e^-$$
$$X^- + P^+ \rightarrow X \cdot + P \cdot$$
$$X \cdot + X^- \rightarrow X_2 \cdot^-$$
$$X_2 \cdot^- + LMG \rightarrow MG^+ + 2\,X^-$$

Here, RX represented one of the halogenated compounds, $X \cdot$ and $X_2 \cdot^-$ were the oxidizing species.

Because the bond energy of C-Br is lower than that of C-Cl, so that the oxidative effect was in the order as $CBr_4 > C_2Cl_6$ and $CCl_3CHO \cdot H_2O$. In $CCl_3CHO \cdot H_2O$, atom Cl located on the α-carbon of ` =C=O ', the C-Cl bond was weakened so that the yield of MG^+ was higher in the composition with $CCl_3CHO \cdot H_2O$. The RX was much excessive in the system with RX : LMG > 50 : 1 (mole : mole), the reductive group -CHO in $CCl_3CHO \cdot H_2O$ may diminish the oxidation of LMG. Thus the linearity relation of radiation response (seen in Fig. 2) were limited at dose about 25kGy. If the system contained RX : LMG = 2:1 (mole : mole), the maximum dose of linearity went up to 60 kGy due to less amount of reductive group -CHO.

2. Formation of MG^+ in Irradiated Polyvinyl Chloride (PVC) - LMG Film

In view of what mentioned above, the $X \cdot$ and $X_2 \cdot^-$ derived from additive RX played an important role in the discoloration of irradiated PVB-LMG system. If PVC was used as the matrix, whether the chlorine induced by irradiation from PVC-LMG system will also play a similar role as above?

The PVC-LMG system was composed of as follows:

2.5 g PVC
0.0826 g LMG (1×10^{-4}mol LMG / g PVC)
35 ml THF

After irradiation, the colorless film turned green with the similar spectrum as in PVB-LMG system. The relation of Δ A/L vs dose can be seen in Fig. 3.

The linearity was good up to about 60 kGy. This meant that MG^+ was formed by reaction of LMG with chlorine from irradiated PVC.

$$PVC \rightarrow [P^+, e^-]$$
$$\rightarrow P^*$$
$$P^* \rightarrow P \cdot + Cl \cdot$$
$$P + e^- \rightarrow P \cdot + Cl^-$$
$$Cl \cdot + e^- \rightarrow Cl^-$$
$$Cl^- + P^+ \rightarrow Cl \cdot + P$$
$$Cl \cdot + Cl^- \rightarrow Cl_2 \cdot^-$$

i.e, PVC provided oxidative species Cl · and $Cl_2 \cdot^-$ during irradiation, and then LMG was oxidized:

$$Cl \cdot + LMG \rightarrow MG^+ + Cl^-$$
$$Cl_2 \cdot^- + LMG \rightarrow 2Cl^- + MG^+$$

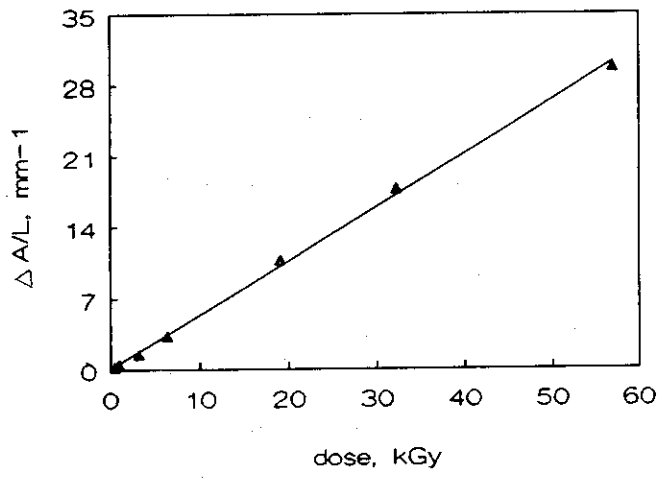


Fig.3 Response function for PVC-LMG film with LMG concentration as 1×10^{-4} mole per gram PVC. Its absorbance was measured at 627 nm.

3. Formation of MG^+ in PVB-LMG with Additive N -bromosuccinimide (NBS)

To confirm the oxidization mechanism furthermore, NBS was used as an oxidative species source. PVB-LMG film with NBS was composed as follow:

1×10^{-4} mol LMG per g PVB
LMG : NBS = 1 : 2 (mole : mole)

The PVB-LMG-NBS film turned green immediately without irradiation and and showed two absorbed bands (λ_{max}=629 nm and 427 nm, respectively) similar to that in section. 1 irradiated systems. It meant that LMG can be oxidized by NBS directly, because NBS was a Br · donor initiated by light or heat.

4. Effect of LMG Concentration in PVB-LMG Film with RX

Dye LMG concentrations were adopted as 8×10^{-5}, 4×10^{-5} and 2×10^{-5} mol per g PVB with RX : LMG > 50:1 (mole : mole). As shown in Fig. 4, the maximum doses in the linear relations of △A/L vs dose in three systems were about 20 kGy due to excessive concentration of RX which limited oxidation of LMG. The slopes of the linear part of the response functions 1.63, 1.10 and 0.51 corresponded to the LMG concentrations of 8×10^{-5}, 4×10^{-5} and 2×10^{-5} mole per g PVB, i.e, the higher the concentration of LMG was, the higher sensitivity of response was.

5. Effect of RX Concentration in PVB-LMG Film with RX

As derscribed above, the concentration of RX also affected the dose range of linear relation in PVB-LMG film.If the dye LMG concentration was kept as 1×10^{-4} mol per gram PVB in three systems, the RX concentrations varied as RX : LMG=10:1, 5:1 and 2:1 (mole : mole). After irradiation, the results were illustrated by Fig. 5 and table. 1. The sensitivity of reponse functions (i.e, `b' values in Table. 1) increased with the increasing of RX concentrations (RX:LMG) and the maximum dose of linear relation (second column in Table. 1) decreased from 70 to 40 kGy though the concentrations of LMG were same.

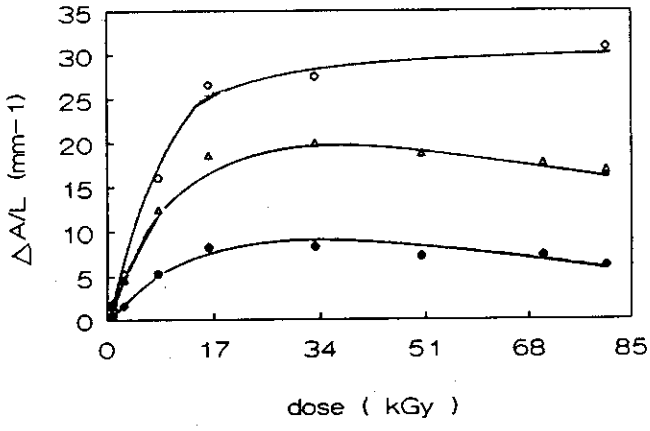


Fig.4 Response functions for PVB-LMG film with LMG concentrations $.8 \times 10^{5}$ (○), 4×10^{-5} (△) and 2×10^{-5} (●) mol per gram PVB with additive RX : LMG > 50:1 (mole : mole).

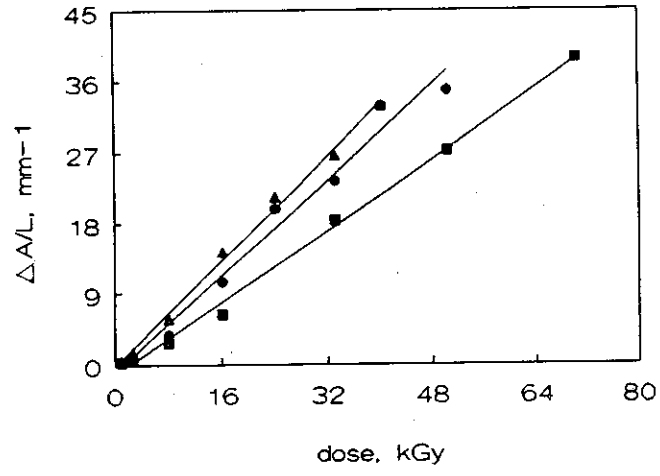


Fig.5 Response functions for PVB-LMG film containing LMG 1×10^{-4} mole per gram PVB with RX concentrations as RX:LMG=10:1 (▲), 5:1 (●) and 2:1 (■).

Table.1 Effect of RX concentration on the dose range of linear relation in PVB-LMG system (△A/L=a+bD, a and b were constant)

RX : LMG (mole:mole)	Dose range (kGy) in linear relation	Linear correlation coefficient	a (Intcp)	b (Slope)
10:1	1 ~ 40	0.9987	-0.3751	0.8238
5:1	2.5 ~ 50	0.9966	-1.0757	0.7063
2:1	5 ~ 70	0.9991	-1.8250	0.5803

CONCLUSION

Addition of halogenated organic compounds was extremely necessary for the radiation oxidation of LMG to MG^{+} in PVB-LMG system. By alternating the halogenated compounds RX, the relative concentrations of RX and LMG in PVB-LMG system, different sensitivities and dose ranges of linear relation of △A/L vs dose were obtained. These were important factors to select the optimum composition of PVG dosifilm. Oxidation of LMG occured in PVB-LMG-NBS system without irradiation was an evident to illustrate that MG^{+} generated from reactions of LMG with oxidizing species in irradiated PVG dosifilm or PVC film.

REFERENCE

Armstrong, W. A. and G. A. Grant. (1958). Radiation Chemistry of Solutions. 1. Use of Leuco Triarylmethane Compounds for Chemical Dosimetry. *Radiat. Res.*, 8, 375-387.

Bakh, N. A., G. G. Babicheva and V. A. Larin. (1960). Radiation Oxidation of Leuco Bases in Ketones in the Absence of Oxygen. *Doklady Akad. Nank S.S.S.R.* 134,1079-82.

Bobrowski, K., G. Dzierzakowska, J. Grodkowski, Z. Stuglik, Z. P. Zagorski and W. L. McLaughling. (1985). A Pulse Radiolysis Study of the Leucocyanide of Malachite Green Dye in Organic Solvents.*J. Phys. Chem.*, 89, 4358-66.

Dejehet, F. G., F. G. Coget, D. J. Apers and P. C. Carpron. (1972). Radiolytic Oxidation of MG Leuco Base in Acetone solution. *Radiochem. Radioanal. Lett.*, 9(2), 93-103.

Dejehet, F. G., A. G. De Kimpe and D. J. Apers. (1973). Radiation-induced Oxidation of the Malachite Green Leucobase in Acetone Solution in the Presence of Calcium Chloride.*Radiochem. Radioanal. Lett.*, 15(3), 177-86.

Grodkowski, J., Z. Stuglik and W. Czajkowski. (1990). Oxidizing Properties of CCl_3O_2 · Radicals Studied by Pulse Radiolysis. *Radiat. Phys. Chem.*, 36(2), 177-9.

Liu Aiguo, Chen Wenxiu and Jia Haishun. (1994). A New Leuco Dye Dosifilm PVG (in press).

Mikhailik, O. M., Ye. N. Seropegina, M. Ya. Melnikov and N. V. Fock. (1981). The Kinetics amd Mechanism of Photoageing of Polyvinylbutyral. *Eur. Polym. J.*, 17, 1011-9.

Stolz, W. and K. Prokert. (1965). Chemishe Dosimetrie Ionisieren der Strahlungen mit den Leukoverbindungen eniger Triphenylmethanfarbstoffe in Polystyrol. *Kernenergie*, 8(7), 425.

Vereshchinskii, I. V., L. T. Karpushkin and V. N. Shcheglov. (1959). Synthesis and Reaction of Leuco compounds of Dye under the Effect of Co-60 gamma Irradiation. *Proc. All-Union Conf. Radiat. Chem.*, 1st, Moscow, Pt. 5, 237-41 (English translation).

Wang Yanqiao, Zhou Xiaomin, Tang Zhangxiong and Zhang Gongming. (1986). CN 85,104,437

9.6 Recent Progress in Application of JAERI Alanine/ESR Dosimetry System

T. KOJIMA

Advanced Radiation Technology Center, JAERI
1233 Watanuki-machi, Takasaki-shi, Gunma-ken, Japan

Abstract Feasibility studies of application of JAERI alanine/ESR dosimetry system were performed on radiotherapy level dosimetry, low dose-rate dosimetry for residual life estimation of cable insulators used in nuclear power facilities, and dose monitoring for electron processing.

INTRODUCTION

Alanine/ESR(Electron Spin Resonance) dosimetry systems, which consist of rod or film alanine dosimeters molded with polymer as binders and compact precise ESR reading systems, has developed at JAERI mainly for reference and transfer dosimetry method (Kojima *et al.* 1989, 1993a). Alanine/ESR dosimetry has basically useful properties such as wide measurable dose range(1 Gy~100 kGy), relatively high precision, long-term stability after irradiation, tissue-equivalent composition, and incremental dose measurement based on non-destructive read-out(Regulla and Deffner 1981). Application field of JAERI system has been focussed on use for reference class high-dose(rate) dosimetry so far, although the system has above other useful properties.

On the basis of experiences of its application to high-dose dosimetry, feasibility studies to expand application of the JAERI alanine/ESR dosimetry system were performed on the dosimetry fields in radiotherapy(1~100 Gy)(Kojima and Tsuda, 1995), dosimetry at low dose rates of 50~200 Gy/h for residual life estimation of cable insulators(Haruyama *et al.*, 1995), and dose monitoring for MeV level electrons by using rod-shaped dosimeters (DL-α-alanine: 70wt%, Polystyrene: 30wt%, 3 mm in diameter)(Hou and Kojima, 1995).

In this paper, these recent studies are briefly described.

EXPERIMENTAL, RESULTS AND DISCUSSION

(1)Application to radiotherapy dose level(1~100 Gy)

Our developed alanine/ESR system is not designed to measure in the dose range of 1~100 Gy. However, it could be possible to measure these dose range by determination of individual zero-dose value and its subtraction from net dose response.

Rod alanine dosimeters(10 mm in length) were irradiated in water phantom at room temperature by a linear accelerator(Clinac 2100C, Varian, electrons:6~20 MV, X-rays:18 MV) at the Tokai university Hospital up to doses in the range from 5 to 40 Gy(in water) which are measured by a thimble-type ionization chamber calibrated at the Electrotechnical Laboratory(ETL), the national standard laboratory in Japan. Dose responses, in terms of main peak-to-peak height, were measured by using a conventional ESR

spectrometer(FE-3X, JEOL) at room temperature with appropriate tuning of measuring parameters. Dose values were estimated referring to dose response at 1 kGy, which is estimated by a JAERI parallel-plate ionization chamber calibrated at the ETL.

Fig.1 shows the typical first derivative ESR spectra of alanine dosimeters un-irradiated and those irradiated up to 5 or 40 Gy. The spectra of lower dose region associate with noise which is equivalent to about 0.3 Gy. The zero-dose responses are estimated within 3.5±1 Gy and subtracted from net dose responses after irradiation individually. Variation coefficients of five irradiated dosimeter responses in this dose range were about 2 to 4%(1σ) as shown in Table 1, although our estimated doses were about 3% lower than nominal doses of the hospital. Similar results is obtained for electrons with different energies(6, 9, 12, 16, and 20 MV) at about 40 Gy without energy dependence. These results shows that our developed alanine dosimeters can be used dose estimation down to 10 Gy. Further efforts on reduction of zero-dose response, improvement of the sensitivity of the ESR spectrometer, and statistical data treatment to smooth spectra with noise are necessary for expansion to doses below 5 Gy.

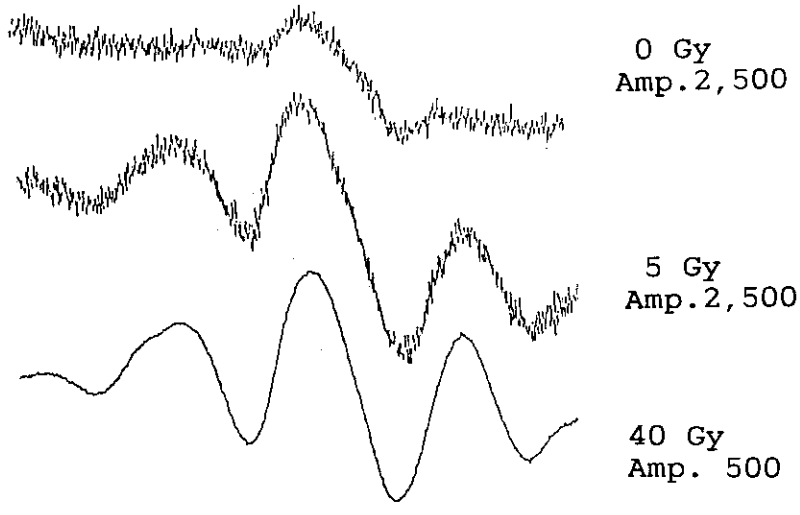


Fig.1 The typical first derivative ESR spectra of alanine dosimeters unirradiated and irradiated up to 5 and 40 Gy.
mignetic field sweep:334±5 mT)
microwave power:4 mW(9.4 GHz)
modulation amplitude:1 mT(100 kHz)

Table 1 Dose comparison for 18 MV X-rays

Nominal dose	Estimated dose	V.C.*	ratio
5 Gy	4.6 Gy	4.1 %	0.91
10	9.8	3.1	0.98
15	14.3	2.2	0.95
40	38.1	1.6	0.97

* V.C.:Variation coefficients(1σ) of dose responses are obtained by five dosimeters irradiated to the same absorbed dose.

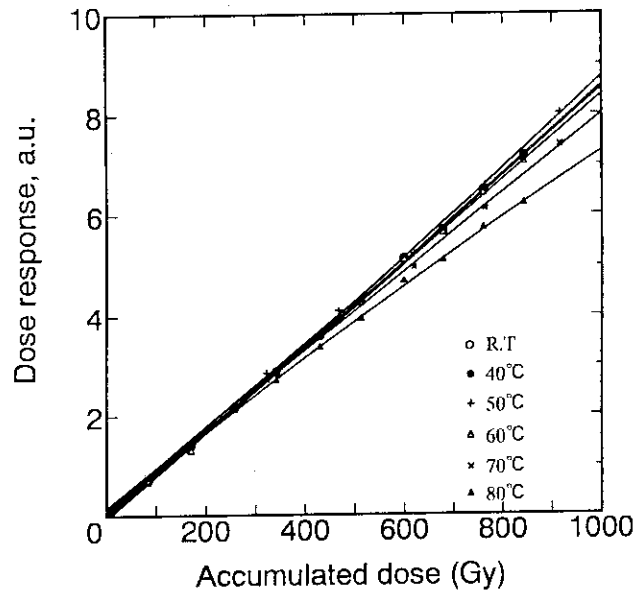


Fig.2 One example of incremental dose response curve for about 2,000 h under irradiation at the dose rate of 0.5 Gy/h and elevated temperatures.

(2)Incremental dose measurement at low dose-rates

For the residual life estimation of cable insulators used in nuclear power facilities, measurement of accumulated dose incrementally is required to evaluate residual life reffering to the relationships between mechanical or electric resistance properties and absorbed dose obtained by testing under simulated environment. Advantage to use alanine dosimeter in this field is ability of dose readings between annual-checks of the facilities for one year span, which are only chances to step into the facility.

Alanine dosimeters(30 mm in length) were irradiated by ^{60}Co γ rays cylindrical source(0.4 TBq) at JAERI under simulated condition to environment of cable insulators in a nuclear power facilities: dose, dose rate, and ambient temperature are roughly <1 kGy, 0.5-200 Gy/h, and room temperature to 80°C, respectively.

Figure 2 shows one example to measure incremental dose under above condition at 0.5 Gy/h for about 2,000 h. Dose response increases linearly up to 1 kGy at temperatures below 60°C.

Alanine dosimeters has irradiation temperature dependence of +0.24%/°C, and relatively fast fading at more than 40°C(Kojima *et al.* 1992). The dose responses shown in the figure may include these effects. However, from practical point of view, alanine dosimeter can be useful for dosimetry in such a low dose-rate field.

(3)Routine dose monitoring for MeV level electrons

As reference class dosimetry for electrons with energies below 4 MeV, we have developed thin alanine film dosimeter of 230 ±15 μm in thickness(Kojima *et al.* 1993b). However, rod-shaped dosimeters have advantages of easy-handling and suitable physical properties such as ruggedness.

In one-sided irradiation processing for electron beams, dose monitoring at specific position of products could be performed by rod-shaped alanine dosimeter after determination of coefficient based on relation between surface dose and measured dose which may work to correct contribution of depth-dose distribution in dosimeter itself. Dosimeters were inserted in polyethylene(PE) block with cylindrical holes so as to be positioned horizontally against vertical incident electron beams. Irradiation was performed by using an electron accelerator (Dynamitron, RDI, 1~3 MeV, 25 mA) at JAERI.

Figure 3 shows ratios of surface dose estimated by cellulose-triacetate(CTA) dosimeters(Tanaka *et al.* 1984) stack and averaged dose in terms of dose measured by rod-shaped alanine dosimeters, as a function of electron energies. The relation obtained for alanine dosimeters irradiated without surrounding materials is also shown in Fig.3. Coefficients of dosimeter responses in PE block and without surrounding materials are 0.83±4% and 0.87±3% for above 1.2 MeV, respectively. The latter value may include contribution of scattered electrons and of electrons come from oblique directions. However, once coefficients are given under specific condition similer to acutual irradiation processing, rod-shaped dosimeter can be practically used as a dose monitor for the processing using electrons with energies above 1.2 MeV.

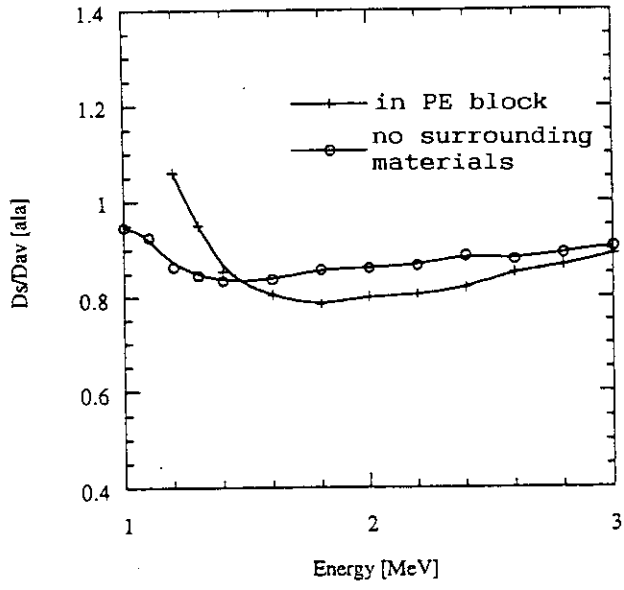


Fig.3 The relation of ratios of surface dose estimated by using cellulose-triacetate(CTA) dosimeters stack and averaged dose in terms of dose measured by rod-shaped alanine dosimeters in the PE phantom, as a function of electron energies.The relation obtained for alanine dosimeters irradiated without surrounding materials is also shown in the figure.

CONCLUSION

As preliminary results, the followings were obtained:

1)Low doses from 5 to 40 Gy can be estimated with the precision of about ±3%(1σ) by subtracting of the background signal(~3.5 Gy) and by dose estimation method on the basis of the dose response at 1 kGy.

2)Incremental dose measurement for residual life estimation of materials used in a nuclear power facilities, in which the low dose rate is 0.5 Gy/h and total dose is up to 1 kGy, can be performed by alanine dosimeter under ambient temperatures lower than 60°C without any correction.
3)Rod-shaped dosimeter can be also used as a dose monitor for one-sided electron processing with energies above 1.2 MeV, by determination of the coefficient attributed to contribution of dosimeter shape and geometry of irradiation field.

Alanine/ESR dosimetry has potential to expand its application more widely to various dosimetry fields also by development of new ESR techniques such as ESR imaging and pulse ESR spectrometry(Ikeya 1993).

ACKNOWLEDGEMENT

The author wish to thank Tsuda M. of the Tokai University Hospital, Hou H. of Shanghai Irradiation Center, Haruyama Y. and Tachibana H. of JAERI, Okamoto J. of Radiation Application Development Association, Kashiwazaki S., Matsuyama S. and Yagyuu H. of Hitachi Cable, Co., Ltd. for their collaborative works.

REFERENCES

Chu S., Weiser A., Feist H. and Regulla, D.F.(1989) *Appl.Radiat. Isot.* 40, 993-996
Haruyama Y., Tachibana H., Kojima T., Okamoto J., Kashiwazaki S., Matsuyama S. and Yagyuu H.(1995)to be published in *RADIOISOTOPES*
Hou H. and Kojima T. (1995) to be published in *Appl.Radiat.Isot.*
Ikeya M.(1993) "New application of electron spin resonance, --dating, dosimetry and microscopy--", World Scientific, Singapore
Kojima T. and Tanaka R.(1989) *Appl.Radiat.Isot.* 40, 851-857
Kojima T., Chen L., Haruyama, Y., Tachibana, H. and Tanaka R. (1992) *Appl.Radiat.Isot.* 43, 863-867
Kojima T., Tachibana H., Haruyama Y., Tanaka R. and Okamoto J. (1993a) *Radiat.Phys.Chem.*, 42, 813-816(1993)
Kojima T., Ranjith H.L.A., Haruyama H., Kashiwazaki, S. and Tanaka R.(1993b) *Appl.Radiat.Isot.* 44, 41-45
Kojima T. and Tsuda M.(1995) to be published in *RADIOISOTOPES*
Regulla D.F. and Deffner U.(1982) *Int.J.Appl.Radiat.Isot.* 33, 1101-1114
Tanaka R., Mitomo S. and Tamura N.(1984) *Int.J.Appl.Radiat.Isot.* 35, 875-881

9.7 Dosimetry Study on A p-n Junction Semiconductor Detector

Zheng Zheng Zhao Yongfu Dai Honggui Xie Zongchuan

Institute of Atomic Energy, Jiangsu Academy of Agricultural Sciences, Nanjing, Jiangsu 210014 PRC

ABSTRACT

A p—n junction semiconductor may be used as a radiation detector. Such a study is reported here. Its dosimetry specifities, include dose, dose rate, precision, stability, depth dose distribution and directional response, were studied in a ^{60}Co field, It is shown that the detector performs well. It exhibited a precision of ±0.05% (std dev.) and a stability of ±0.16% (std dev.), respectively.

KEYWORDS

p—n juncion; detector; ^{60}Co irradiator; radiotherapy.

INTRUDUCTION

Many researchers have reported their studies on various p—n juncion semiconductor detectors (3,6,7). Dixon & Ekstrand (1) reported their work of using a silicon diode to develop a small battery—operated dosimeter with a memory. Their opinion is that it may be used as on alternative to mailed TLD. Grusell & Rikner (2) showed why detectors based on n—type silicon, when radiation damaged, develop a sensitivity drop and a dose—rate non—linearity in pulsed radiation fields. With p—type detectors, the dose—rate non—linearity was eliminated and the radiation damage offect was limited to a moderate loss of sensitivity (4). They also reported how to select shieldings of a p—Si detector for quality independence (5). This kind of work was also done in our institute. With a p—silicon semiconductor, a radiation detector has been developed. It can be used for the dosimetry of photons of moderate dose—rate (the upper limit is about 70Gy/min) in agricultural ^{60}Co irradiators. In China most ^{60}Co irradiators belong in such kinds. It is impossible for them to by "expensive" Farmer lonization chambers, but there is a great need for such dosimeters. When they plan to do some works on radiation chemistry, food irradiation and sterilization of medical products, they can use the p—n junction semiconductor dosimeters to choose proper positions before irradiating samples or products.

DESCRIPTION OF THE DOSIMETRY SYSTEM

Structure of the p—n Junction Semiconductor Dosimeter

A p—type silicon detector with a sensitive volume less than 0.3mm^3 were encapsulated in epoxy resin of density 1.2g/cm^3. A 0.6mm thick copper cylinder is put around the detector as a cap. Outside is another cap which is made of 4mm thick perspex. Outside diameter of the dotector is 15.14mm, just same to 0.6cc Farmer—2571 micro ionization chamber.

Circuit Description

Designing the circuit, two stages integral micro current amplifiers were adopted, for the current is very weak. Integral voltage is monitored by a comparator. When the voltage reaches a set value, a pulse is generated. This pulse ofter shaped is delivered to the counter for counting. In the meantime the pulse is used to trigger a analog switch which discharges the capacitor, thereby starting the next integration period. The meter is controlled by a microcontroller which is a popular one in China. Its block diagram of the hardware system is shown in fig. 1.

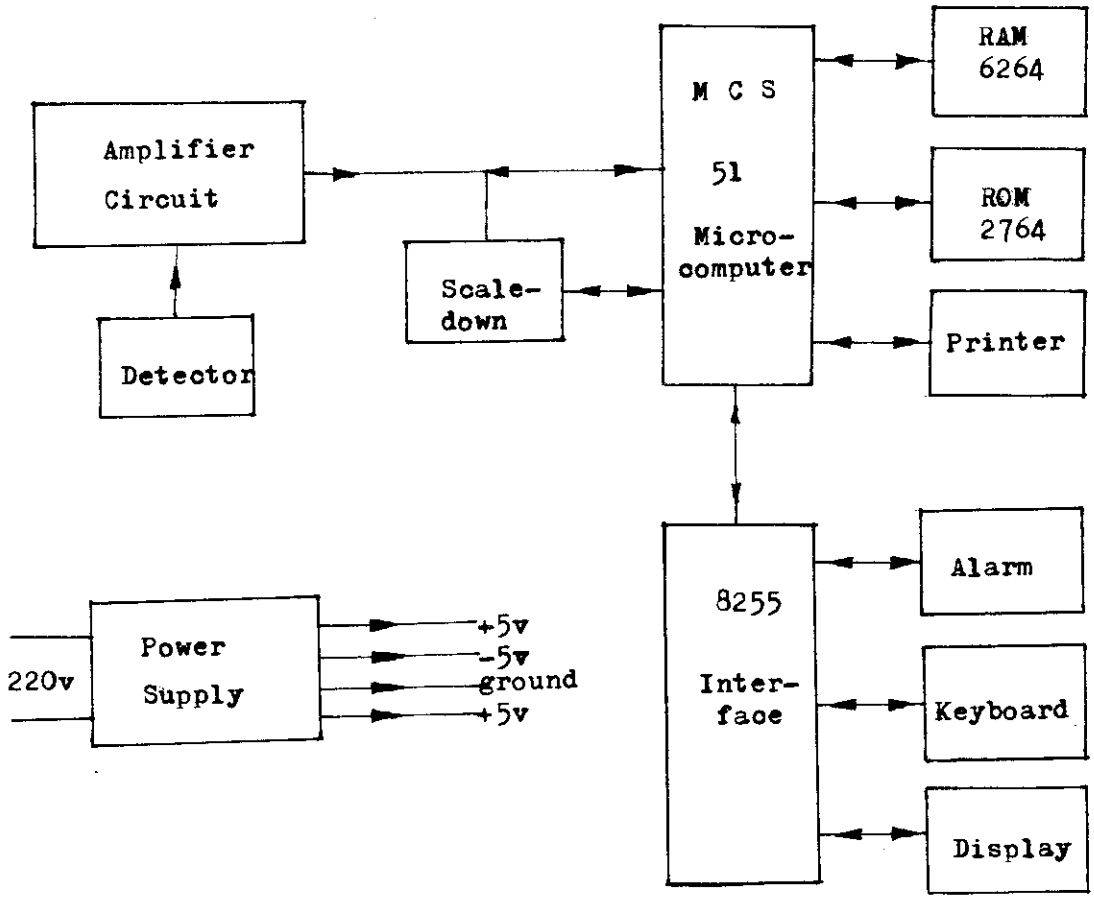


Fig. 1. Block diagram of the hardware system

The hardware system consists of a film keyboard, a microprinter, 7 segment LED displays, a 8031 chip, a 82C55 I/O chip, a ROM 27C64 and a RAM 6264 et al. This dosimeter is named as SDI—100 Radiation Dosimeter.

RESULTS AND DISCUSSIONS

Radiation Field and Comparison Dosimeter

Most dosimetry experiments were made in these two radiation fields. One is a single plate ^{60}Co source, its activity is 9.2×10^{15} Bq (250k Ci), ranked third in China. Another is a 2.96×10^{14}Bq (8k Ci) single stick ^{60}Co source. The dosimeters we used for comparison are Farmer 2560, Farmer 2570 and Fricke Dosimeters. They were calibrated by The UK National Physical Laboratory and The Chinese Academy of Metrology.

Relation Between Irradiation Time and Dose

The detector was fixed at a position which is 100cm from the source to measure cumulate doses. Results is shown in table 1.

TABLE 1 Irradiation Time and Dose

Time (S)	10	20	30	40	60	80	100
Dose (Gy)	0.2159	0.4312	0.6476	0.8633	1.292	1.729	2.162

Linear correlation coefficient is 0.999997.

Dose Rate

In the range 15—30cm from source 6 positions were chosen. At each position SDI—100 detector was fixed there to measure a dose rate, then instead of it Farmer 2571 Ionization Chamber was used to measure a dose rate. Table 2 shows the uniformity between these two meters. The main reason for the variance is probably the position can not be repeated well when detectors were exchanged. The source position when it was raised again also cause a variance.

TABLE 2 Comparison Between Two Groups of Dose Rates (Gy/min)

No	1	2	3	4	5	6
SDI—100	31.67	9.733	4.360	1.292	0.336	0.169
Farmer—2571	31.66	9.664	4.402	1.298	0.338	0.167

Precision

Put the detector at a position and read dose repeatly for many times. The positions of detector and source all were not changed. Result shows a precision of $\pm0.05\%$ (std dev.).

TABLE 3 Presision of the p—n Junction Detector

Dose (Gy)					Precision (std dev.)
0.7882	0.7882	0.7885	0.7882	0.7875	±0.05%
0.7888	0.7882	0.7888	0.7882		

Stability

Put the detector at a chosen position and fixed the ^{60}Co source. From a.m. 9 : 00 to p.m. 4 : 00 the dosimeter continued worked for 7 hours and every 35 minutes a datum was read. The variation observed over the period was ±0.16% (std dev.) for ^{60}Co irradiation.

TABLE 4 Stability of the p—n Junction Detector

Dose (Gy)					Stability (std dev.)
0.7881	0.7882	0.7898	0.7908	0.7910	±0.16%
0.7879	0.7883	0.7886	0.7910	0.7903	
0.7906	0.7892	0.7881			

All the 4 tables above are obtained based on the experiments made by Professor Gao Juncheng of Chinese Academy of Metrology, Senior Engineer Han Youdao of Jiangsu Provincial Standards Bureau and Dr. Yang Guangze, director of Lianyungang City Radiohygiene and Radiation Protection.

Depth Dose Distribution

Measurements of depth dose distributions were alternatively performed with the semiconductor detector and the 0.6cc micro chamber Farmer 2571 in a 30×30×30cm phantom in a wide open one single stick ^{60}Co source radiation field. Distance of source to phantom is 95cm. Detectors and source were at a same height (45cm). At each position two data were read by semiconductor detector and Farmer 2571, respectively. Then put a detector backward along the central axis and read data again. This experiment shows that these two groups of data coincide with each other well. Only a slight variation were observed and part of it is probably caused by the uncertainty of detectors displacement and raising source.

TABLE 5 Depth Dose Distribution

d(cm)	2	5	9	13	17	21	26
S/F	1.000	0.999	1.003	1.004	1.011	1.011	1.017

S/F means the ratio in depth doses between semiconductor detector and Farmer 2571 0.6cc micro detector.

Directional Response

The directional response of the semiconductor detector was measured in a single stick ^{60}Co source radiation field. Fig. 2 shows a slight directional dependence of the detector, but this will not cause any practical problems because the detector is always perpendicular to the line between the detector and the source.

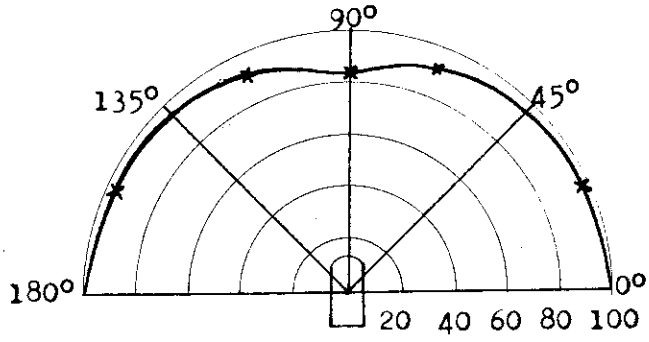


Fig. 2. Directional response of the detector

CONCLUSIONS

A p—n junction can be used as a semiconductor detector to develop a dosimeter. This detector performs as good as a Farmer 2571 micro ionization chamber in some ways, but not all ways. It will be useful in some moderate and small size ^{60}Co irradiators in China, for it has many advantages, such as high sensitivity, ruggedness, not so expensive and et al. Researehers who study on radiation chemistry, radiation processing and food irradiation may measure dose rate with it to choose the proper positions before irradiating samples and products.

REFERENCES

1. Dixon R. L. and K. E. Ekstrand (1980). A silicon diode dosimeter with a memory—on alternative to mailed TLD. Nucl. Instr. Meth. 175, 112—114.
2. Grusell E. and G. Rikner (1984). Radiation damage induced dose rate non—linearity in an n—type silicon detector. Acta Radiol. Oncology 23, 465.
3. Guldbrandsen T. and C. B. Madsen (1961). Radiation disimetry by means of semiconductors. Acta Radiol. 58, 226.
4. Rikner G. and E. Grusell (1983). Radiation damage effects on p—type silicon detectors. Phys. Med. Biol. 28, 1261.
5. Rikner G. and E. Grusell (1985). Selective shielding of a p—Si detector for quality independence. Acta Radiol. Oncology 24, 65—69.
6. Sharf M. A. (1967). Exposure rate measurements of x—and γ—rays with silicon radiation detectors Hlth . Phys. 13, 575.
7. Trump M. A. and A. P. Pinkerton (1967). Application of p—n junction diodes to the measurement of dose distribution of high energy radiation. Phys. Med. Biol. 4, 573.

10. Biological System (2)

10.1 Capturing of *Staphylococcus aureus* onto an Interface Containing Graft Chains

William Lee,[a] Kyoichi Saito,[b] Shintaro Furusaki,[a] Takanobu Sugo,[c] and Keizo Makuuchi[c]

[a]Department of Chemistry and Biotechnology, Faculty of Engineering, University of Tokyo, 7-3-1 Hongo, Bunkyo-ku, Tokyo 113, [b]Department of Specialty Materials, Faculty of Engineering, Chiba University, 1-33 Yayoicho, Inage-ku, Chiba 263, [c]Japan Atomic Energy Research Institute, Takasaki Radiation Chemistry Research Establishment, Takasaki, Gunma 370-12, Japan

Abstract—A microbial-cell-capturing material was prepared by radiation-induced grafting of glycidyl methacrylate onto a polyethylene-based fiber before the introduction of diethylamine. The prepared fiber was tested against a *Staphylococcus aureus* and *Escherichia coli* solution. The results showed that the grafted-type fiber had a capturing rate constant 1000-fold higher than the commercial crosslinked-type bead for *S. aureus* and that an activation energy of 39 kJ/mol was obtained for the microbial-cell-capturing action.

INTRODUCTION

For water purification, although chlorine has been widely introduced after the discovery of its antibacterial activity, hazardous levels of trihalomethane analogues and carcinogens are produced in chlorinated water containing organic materials. As a result, some researchers have been searching for an alternative water disinfectant such as an insoluble polymeric substance with antimicrobial activity in order to avoid the problem of residual toxicity of soluble chlorine (Kawabata, 1983; Tashiro, 1991).

Usually, most of the insoluble antimicrobial materials prepared were derived from the copolymer beads crosslinked with divinylbenzene, where the functional groups were immobilized directly onto the polymeric support. However, a study on the interaction of microbial cells with a graft-chain-containing polymer has not yet been reported. The functional groups of this polymer are not immobilized directly onto the polymeric support but the grafted polymer branches. These graft chains provide the microbial cell a flexible network for interaction. Tsuneda et al. (1994) reported that the sulfonic-acid(SO_3H)-group-containing polymer chains grafted on a polyethylene-based membrane provided a three-dimensional adsorption site for lysozyme. Mizota et al. (1994) reported that a 10-fold higher catalytic activity of the SO_3H-group anchored to the flexible grafted polymer chains can be obtained for the hydrolysis of sucrose as compared to a commercial SO_3H-type crosslinked resin. These kinds of functional materials can be easily prepared by radiation-induced graft polymerization.

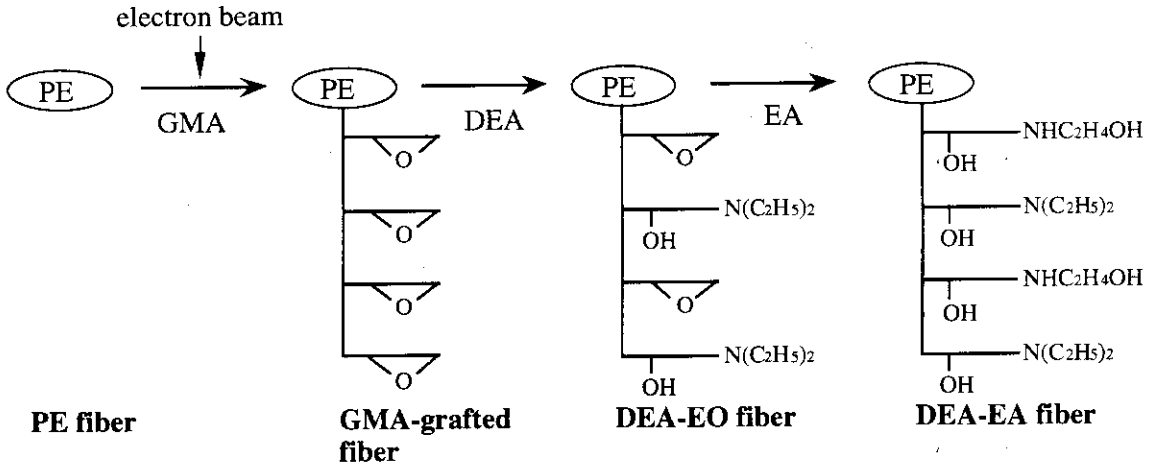
The radiation-induced graft polymerization (RIGP) has enabled the preparation of a novel polymeric material containing functional moieties on the branches grafted onto a variety of trunk polymers such as films, fibers, nonwoven cloth and hollow fibers (Sugo, 1989; Sugiyama, 1993). To date, we have developed various functional materials by applying RIGP, for instance, a chelating porous hollow-fiber membrane for the removal of metals from ultrapure water (Konishi, 1992), a urea-permeable anion-exchange membrane for the regeneration of dialysate in the peritoneal dialysis system (Lee, 1993), and a cation-exchange membrane for the separation of protein from biological fluids (Tsuneda, 1994).

Our previous paper (Lee, 1994) described that a grafted-type diethylamino-group-containing fiber had an adsorption rate constant of *Staphylococcus aureus* 1000-fold higher than the commercial crosslinked beads. Hence, the objectives of this study were threefold: (1) to propose a method for preparing an insoluble microbial-cell-capturing material which has a three-dimensional footing site by RIGP, (2) to study the influence of two coexisting functional groups, i.e., an epoxy group and an ethanolamino group, on the capturing of microbial cells, and (3) to measure the activation energy of the microbial cell-graft chain interactions in order to obtain some information on the mode of the microbial-cell-capturing action.

EXPERIMENTAL

Preparation of tertiary-amino-group-containing material

A commercial available polyethylene (PE) membrane of a hollow-fiber form (Asahi Chemical Industry Co., Ltd., Japan) was used as the trunk polymer for grafting. The inner and outer diameters of the hollow fiber are 1.9 mm and 3.2 mm, respectively, with a porosity of 70%. Figure 1 shows the chemical structure of the microbial-cell-capturing material prepared. A vinyl monomer, glycidyl methacrylate (GMA, CH_2=$CCH_3COOCH_2CHOCH_2$), was grafted onto the PE fiber by applying the RIGP method. The



PE: polyethylene GMA: glycidyl methacrylate DEA: diethylamine
EO: epoxide group EA: 2-aminoethanol

Fig 1. Chemical structure of the microbial-cell-capturing material prepared.

degree of GMA grafting was set to about 110%. The GMA-containing fiber was reacted with diethylamine (DEA, $HN(C_2H_5)_2$) for the introduction of cationic graft chains. The resulting fiber will be referred to as a DEA-EO fiber. The reaction conditions for radiation-induced grafting of GMA and subsequent introduction of tertiary amino groups (DEA) are described elsewhere (Lee, 1993). On the other hand, the residual epoxy group of DEA-EO fiber was hydrophilized by ethanol amine (EA, $H_2NCH_2CH_2OH$) and the resulting fiber will be referred to as a DEA-EA fiber.

For comparison, commercial GMA beads (FP-4000; Organo Co., Japan) crosslinked with ethylene glycol dimethacrylate were obtained and the same tertiary amino groups, DEA groups, were also introduced according to the same reaction conditions. The resulting beads will be referred to as DEA beads.

Bacterium culture and growth conditions

Escherichia coli IFO 3301 and *Staphylococcus aureus* IFO 12732 obtained commercially from the Institute for Fermentation, Osaka, were used as model microorganisms for the microbial-cell-capturing studies. One loopful of the bacteria was inoculated into a 10 mL of rehydration fluid (polypeptone 1.0%, yeast extract 0.2%, $MgSO_4 \cdot 7H_2O$ 0.1%, pH 7.0) and cultured at 32 °C for 18-24 h in a test-tube shaker at 100 strokes/min. After the cells in the cultured cell suspension were collected by centrifugation at 5600 × g for 15 min in a centrifuge refrigerated below 4 °C, and washed twice with 10 mL of distilled, deinoized, and sterilized water, they were again suspended in 10 mL of fresh sterilized water. The cells in the stationary state were serially diluted in sterilized water to the desired cell concentration (about 10^{5-6} cells/mL) before contact with the prepared fibers.

Batch experiment for capturing of microbial cell by DEA-EO and DEA-EA fibers, DEA beads

Forty milliliter of the cell suspension prepared were added into a 100 mL flask. The DEA beads, DEA-EO and DEA-EA fibers were brought into contact with the cells by shaking at 130 rpm at 25 °C.

One-tenth milliliter of the contact suspension was pipetted out from the flask at specific time intervals, inoculated into a 9.9 mL of sterilized water, and serially diluted with sterilized water. One-tenth milliliter of the diluted suspension was spread on an agar plate made of growth media. The plate was incubated at 37 °C for 18-20 h, and the number of viable cells in the contact suspension was calculated from that of the colony-forming units per milliliter (CFU/mL) on the plate.

Activation energy of microbial-cell-capturing action

The microbial-cell-capturing action of the DEA-EO (89% of DEA conversion) fiber was tested in the same batch mode at a temperature ranging from 15 to 37 °C. The values of the microbial-cell-capturing rate constant were determined from the slopes of the logarithm of viable cells vs contact time plots, and then the activation energy of the action was obtainable from the Arrhenius plot.

RESULTS AND DISCUSSION

Conversion of tertiary amino group (DEA) for the

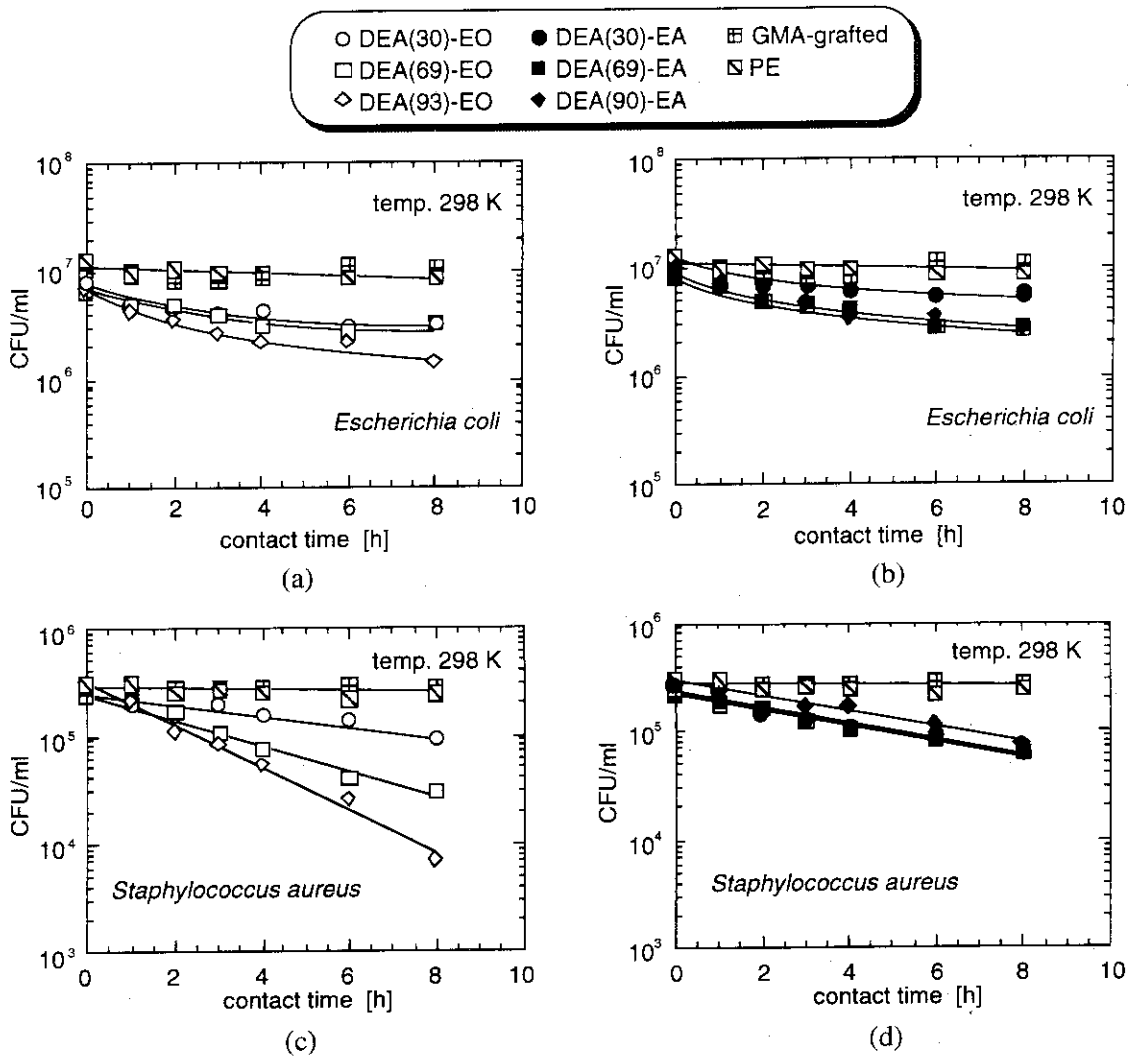


Fig 2. Effect of DEA-EO and DEA-EA fibers on the capturing of *Escherichia coli* and *Staphylococcus aureus.*

materials prepared

For the introduction of the tertiary amino group onto the fiber, the conversion of DEA increased with the reaction time. The fibers with the DEA conversion from 24% to 93%, i.e., the density of the DEA group from 0.8 mmol/g-product to 2.7 mmol/g-product, were obtained. The final DEA group density for the beads was 2.5 mmol/g-product.

Comparison of the capturing rate of microbial cells among the DEA-EO and DEA-EA fibers, and DEA beads

Both the DEA-EO and DEA-EA fibers with DEA conversion of 30, 69 and 93% were brought into contact with *E.coli* in batch mode, and the results showed that though both fibers captured *E.coli*, density of the DEA group and the coexisting of EA group had no significant influence on the capturing of *E.coli* (Fig. 2a and 2b). Whereas, for the DEA-EO and DEA-EA fibers (DEA conversion: 30, 69 and 93%) tested against *S.aureus* in the same batch mode, the DEA-EO fiber with a higher conversion of DEA captured the Gram-positive bacteria faster (Fig. 2c). However, when the DEA-EO fiber was hydrophilized with EA (DEA-EA fiber), the mode for capturing of microbial cell was retarded (Fig. 2d).

It is usually recognized that microbial cells have predominantly negative charges, and proposed that microbial cells can be adsorbed on solid surfaces by electrostatic interaction. And, the Gram-positive microbial cells (*S.aureus*, 2.56×10^{-16} g·eq/cell) have a higher surface charge density than the Gram-negative microbial cells (*E.coli*, 0.24×10^{-16} g·eq/cell) (Kawabata, 1992). The graft

Table 1. Comparison of capturing rate constant between crosslinked-type and grafted-type materials for the capturing of *S. aureus* in batch mode.

		This study	
	Tashiro	DEA beads	**DEA(93)-EO fibers**
type of material	chloromethylated, divinylbenzene crosslinked polystyrene bead	ethylene glycol dimethacrylate crosslinked GMA bead	**fiber containing graft chain**
functional group	polyethyleneimine	diethylamine	**diethylamine**
polymer structure	crosslinked	crosslinked	**grafted**
surface area (m^2)	1.08	0.10	**5.54×10^{-3}**
functional group density (mmol/g-product)	1.00	2.89	**2.69**
bacteria solution condition	in sterilized physiological saline	in sterilized water	**in sterilized water**
temperature (°C)	37	37	**37**
capturing rate constant, k*[1] (m/s)	1.18×10^{-9}	3.83×10^{-9}	**1.16×10^{-6}**

*[1] $k=-(V/A)(1/t)\ln(C/C_0)$ where V, A, t, C and C_0 are the volume of viable cell suspension (m^3), the contact surface area (m^2), the contact time (s), the viable cell number (CFU/mL) at contact time t and the initial viable cell number (CFU/mL), respectively.

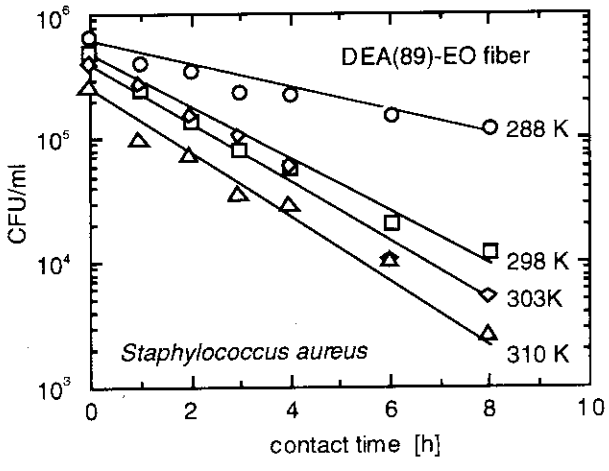


Fig 3. Temperature effect of DEA(89)-EO fiber on the capturing of *Staphylococcus aureus*.

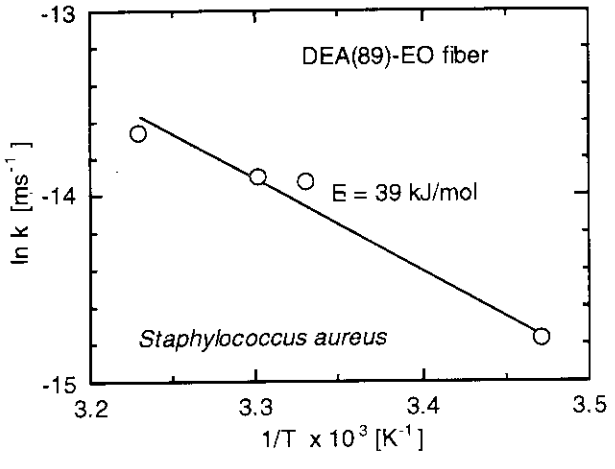


Fig 4. Arrhenius plot: microbial-cell-capturing rate constant of DEA(89)-EO fiber (ln k) *vs* 1/T.

chains of the DEA-EO fiber are partially protonated in water at pH 7 to yield cationic nitrogen atoms. Therefore, it may conclude that the microbial cells can be captured by the DEA-EO fiber mainly due to electrostatic interaction during the contact with the *S.aureus* cell suspension. As a result, the DEA-EO fiber prepared by RIGP exhibited good microbial cell capturing activity.

Similar experiment was also performed for the DEA beads. A slow capturing rate was observed for the DEA beads as compared to the DEA(93)-EO fiber. Comparison of capturing rate

constant among the polyethyleneimine beads of Tashiro (1991), the DEA beads and the DEA(93)-EO fibers is shown in Table 1. The DEA group densities for the DEA beads and DEA-EO fiber (2.6 and 2.7 mmol/g-product, respectively) used in the experiment were almost the same. Also, it was found that the DEA(93)-EO fiber has a capturing rate constant 1000-fold higher than the DEA beads (Table 1).

Temperature effect for capturing of S. aureus by DEA-EO fiber

Figure 3 shows that the microbial-cell-capturing rate of DEA(89)-EO fiber increased as the temperature is raised from 15 to 37 °C. The activation energy of the microbial-cell-capturing action for the DEA(89)-EO fiber was 39 kJ/mol (Fig. 4). This level of activation energy indicated that the interfacial interaction between *S. aureus* and the DEA(89)-EO fiber involved not only a physical process but a chemical reaction process as well. Kourai et al. (1985, 1986) reported that the activation energies of bactericidal action against *E. coli* for 12-alkylpyridinium iodides and 12,12'-dialkyl-γ,γ'-dipyridinium diiodides were 115 and 127 kJ/mol, respectively.

CONCLUSION

The coexisting of the epoxy group is an important factor for the capturing of *S. aureus* onto the interface containing cationic graft chains. The grafted-type DEA-EO fiber captures the cells 1000-fold faster than the crosslinked-type DEA beads. And, from the activation energy obtained, this study shows that the interaction between the DEA-EO fiber and *S. aureus* involved both the physical process and chemical reaction process.

Acknowledgments—We thank Makoto Chiwa of Organo Co., Japan, for providing the commercial GMA beads and Dr. Tamikazu Kume of Japan Atomic Energy Research Institute for his advice on the antimicrobial experiment. Lee W. is a research fellow of the Japan Society for the Promotion of Science (JSPS).

REFERENCES

Kawabata N., Hayashi T. and Matsumoto T. (1983) Removal of bacteria from water by adhesion to cross-linked poly(vinylpyridinium halide). *Appl. Environ. Microbiol.* **46,** 203.

Kawabata N. (1992) Capture of micro-organisms and viruses by pyridinium-type polymers and application to biotechnology and water purification. *Prog. Polym. Sci.* **17,** 1.

Konishi S., Saito K., Furusaki S. and Sugo T. (1992) Sorption kinetics of cobalt in chelating porous membrane. *Ind. Eng. Chem. Res.* **30,** 2722.

Kourai H., Takechi H., Horie T., Uchiwa N., Takeichi K. and Shibasaki I. (1985) The antimicrobial characteristics of quaternary ammonium salts. Parts. X. Antimicrobial characteristics and a mode of action of n-alkylpyridinium iodides against *Escherichia coli* K12. *J. Antibact. Antifung. Agents.* **13,** 3.

Kourai H., Takechi H., Horie T., Kume M., Takeichi K. and Shibasaki I. (1986) The antimicrobial characteristics of quaternary ammonium salts. Parts. XII. Antimicrobial characteristics of n,n'-dialkyl-γ,γ'-dipyridinium diiodides. *J. Antibact. Antifung. Agents.* **14,** 55.

Lee W., Saito K., Furusaki S., Sugo T. and Makuuchi K. (1993) Design of urea-pemeable anion-exchange membrane by radiation-induced graft polymerization. *J. Membrane Sci.* **81,** 295.

Lee W., Saito K., Furusaki S., Sugo T. and Makuuchi K. (1994) Adsorption of *Staphylococcus aureus* onto an interface containing functional graft chains. submitted to *Appl. Environ. Microbiol.*

Mizota T., Tsuneda S., Saito K. and Sugo T. (1994) Hydrolysis of methyl acetate and sucrose in SO_3H-group-containing grafted polymer chains prepared by radiation-induced graft polymerization. *Ind. Eng. Chem. Res.* **33,** 2215.

Sugiyama S., Tsuneda S., Saito K., Furusaki S., Sugo T. and Makuuchi K. (1993) Attachment of sulfonic acid group to various shapes of polyethylene, polypropylene and polytetrafluoroethylene by radiation-induced graft polymerization. *React. Polym.* **21,** 187.

Sugo T. and Saito K. (1989) Functionalization of filtration membrane by radiation-induced graft polymerization. *Bull. Seawater Sci. Jpn.* **43,** 3.

Tashiro T. (1991) Removal of *Escherichia coli* from water by systems based on insoluble polystyrene-poly(ethylene glycol)s, -polyethyleneimines, and -polyethylenepolyamines quaternized. *J. Appl. Polym. Sci.* **43,** 1369.

Tsuneda S., Shinano H., Saito K., Furusaki S., Sugo T. and Makuuchi K. (1994) Binding of lysozyme onto a cation-exchange microporous membrane containing tentacle-type grafted polymer branches. *Biotechnol. Bioeng.* **10,** 76.

10.2 An Intelligent Biopolymer Gel with Pendant L-proline Methyl Ester

Masaru Yoshida[a], Agneza Safranj[a], Hideki Omichi[a], and Ryoichi Katakai[b]

[a]Department of Material Development, Takasaki Radiation Chemistry Research Establishment, Japan Atomic Energy Research Institute, Watanuki-Machi 1233, Takasaki, Gunma 370-12, Japan
[b]Department of Chemistry, Faculty of Engineering, Gunma University, Kiryu, Gunma 376, Japan

Abstract: Linear poly(acryloyl-L-proline methyl ester, A-ProOMe), obtained by radiation-induced polymerization of its monomer in ethanol, exhibits a lower critical solution temperature (LCST) at 14°C. A-ProOMe was copolymerized with a minor amount of 2-hydroxypropyl methacrylate (HPMA) or 2-hydroxyethyl methacrytlate (HEMA), to obtain intelligent biopolymer gels for application in drug delivery systems. The poly(A-ProOMe/HPMA) gel was characterized by an initial rapid shrinkage at the surface in the swollen state, as resulting in formation of a rigid membrane barrier devoid of micropores. This gel is called a surface regulated matrix. In the case of poly(A-ProOMe/HEMA), no such a barrier formed, instead, the whole matrix shrunk without the disappearance of micropores. This gel is called a matrix pumping gel. Testosterone (T) was incorporated into the poly(A-ProOMe/HPMA) gel, and it was found that the daily dose of T released *in vivo* from this formulation remained constant at approximately 30 μg/day throughout an experimental period of 54 weeks. On the other hand, 9-β-D-arabinofuranosyladenine (Ara-A) was incorporated into the poly(A-ProOMe/HEMA) gel to evaluate the pulsatile drug release when cycled at 10 and 37°C. The *in vitro* release rate of Ara-A was found to be 11 ng/h at 10°C and 33 ng/h at 37°C.

INTRODUCTION

As an investigastion direction for the development of functional polymers, many researchers have actively prepared polymer gels which are responsive to external stimuli such as temperature, pH, electric field, and chemicals (Alhaique *et al.*, 1981, Bae *et al.*, 1989, Ito *et al.*, 1989,Tanaka *et al.*, 1982, Winnik *et al.*, 1990). It is well-known that living organisms contain various sensory systems with response function for external stimuli, and that α-amino acids, nucleic acids, and lipids play essential roles in the manifestation of responsive functions to physiological metabolism. Accordingly, as the first step, we decided to synthesize N-acryloyl and methacryloyl derivatives with pendant α-amino acids, and to investigate their polymerization and intelligent function. We found that the resulting polymer gel based on L-alanine showed reversible swelling-deswelling behavior when cycled in solution between different temperatures (Ding *et al.*, 1994, Safranj *et al.*, 1993). We now describe the synthesis and properties of poly(A-ProOMe). For this L-proline based polymer, there was a drastic volume collapse when the temperature was changed. We describe the reversible shrinkage and swelling kinetics of the gels containing A-ProOMe and also report the *in vivo* release of T from the poly(A-ProOMe/HPMA) gel and *in vitro* release of Ara-A from the poly(A-ProOMe/

HEMA) gel responsive to change in temperature.

EPERIMENTAL

A-ProOMe of R_f = 0.54 (ethyl acetate, Merck kieselgel 60F254) and $[\alpha]_D$ = 133.7° (c = 1, methanol) was synthesized by a coupling reaction of HCl•H-ProOMe and acryloylchloride (Yoshida *et al.*, 1993). HEMA and HPMA was purchased from Shin-Nakamura Chemical Co.

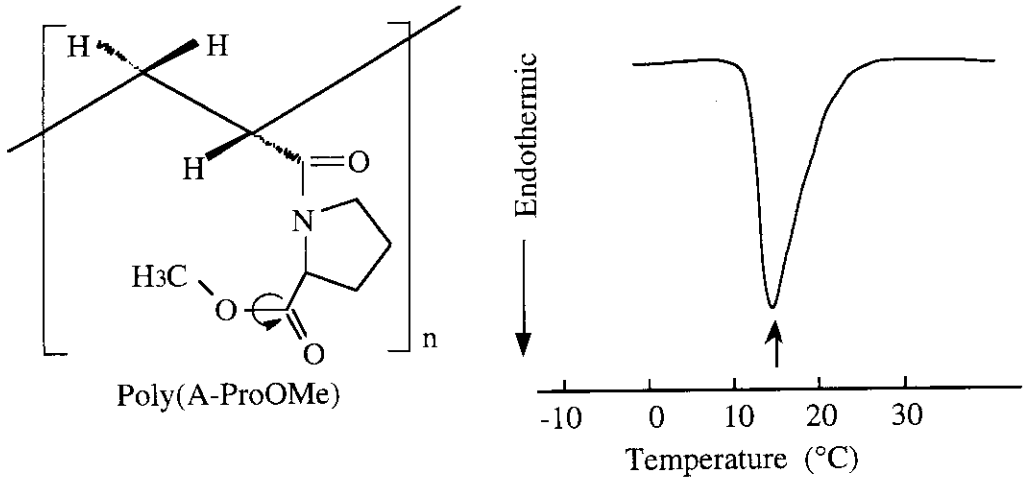


Fig. 1 DSC curve of poly(A-ProOMe) in 10 % (V/w) aqueous solution.

T (17β-hydroxy-4-androsten-3-one) was obtained from Sigma Chemical Company.

In the case of the preparation of thermo-responsive gel with T, A-ProOMe/HPMA monomer (80/20 vol. %, 0.25 ml) was mixed with T (30 mg) to give the homogeneous solution, and the solution was charged into an 8 mm internal diameter glass ampoule with a flat bottom. The ampoule was sealed under nitrogen and then irradiated for 3 hours at a dose rate of 10 kGy/h at 25°C using γ-rays from a ^{60}Co source. After the irradiation, a solid and transparent copolymer matrix with drug was obtained in tablet form by separating the product from the mold. It was washed with excess ethanol at 10°C to remove unreacted monomer. The polymer gel was allowed to swell in distilled-deionized water at 10°C just before use. The content of T in the swollen gel immediately before its implantation was found to be 27.85 ± 0.01 mg (n = 50). Drug concentration was assayed at 238 nm using a Hitachi U-3210 spectrophotometer. The poly(A-ProOMe/HPMA) gel with T was implanted under the back skins of male Wistar strain rats weighing 300 ~ 350 g at 3rd week from castration (one tablet/rat, five rats/group).

On the other hand, Ara-A was loaded into a lyophilized polymer gel consisting of A-ProOMe, HEMA, and a minor amount of crosslinker nonamethylene glycol dimethacrylate (Miyajima *et al.*, 1993). The weight of drug loaded in the gel was estimated from the weights of gels before and after loading. The *in vitro* release of Ara-A from thermo-responsive gels was determined in water by repeating measurements between 10 and 37°C at 60-minute intervals. The amount of drug released was assayed spectrophotometrically at 259 nm.

RESULTS AND DISCUSSION

The linear poly(A-ProOMe) with a chemical structure as shown in Fig. 1 was obtained by radiation-induced polymerization in the presence of ethanol at a dose rate of 10 kGy/h (a total

dose of 30 kGy) at 25°C, under nitrogen atmosphere. The LCST temperature of linear polymer was determined by DSC measurements, from the maximum of the endotherm, which gave us 14°C as a result (Fig. 1). Below the LCST, poly(A-ProOMe) exhibits the extended coil structure with strong interaction between the ProOMe group and water, in which the radius of

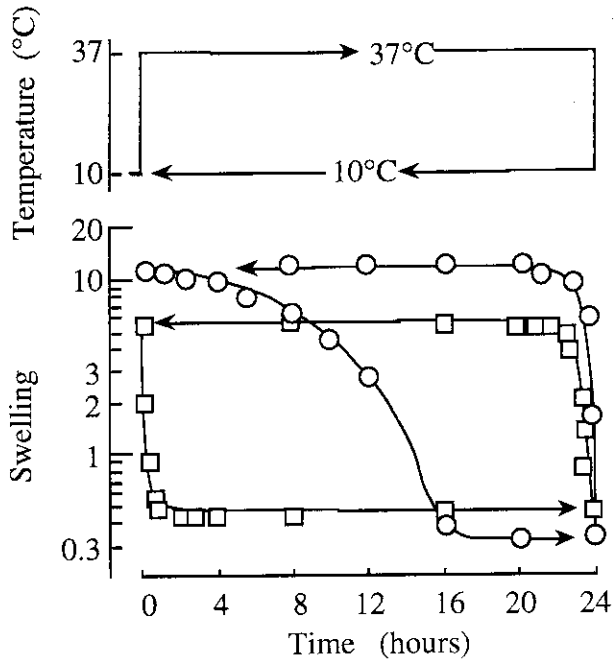


Fig. 2 Swelling-deswelling profiles of (O) poly(A-ProOMe/HPMA) gel and (□) poly(A-ProOMe/HEMA) gel between 10 and 37°C in water.

gyration $\langle S \rangle^{1/2}$ and apparent volume were found to be 40 nm and 270,000 nm^3 at 10°C, respectively. With increasing temperature, the hydrophobic interactions between proline groups become dominant and, at temperatures above the LCST, lead to inter- and intramolecular interactions forming compact clusters with a radius of gyration $\langle S \rangle^{1/2}$ = 8 nm and apparent volume of 2,100 nm^3 at 50°C.

Having established that the A-ProOMe gel is characterized by a thermo-responsive function, the swelling-deswelling kinetics of the gel between two fixed temperatures with the passage of time was next studied using two types of gels such as A-ProOMe/HPMA and A-ProOMe/HEMA. The swelling-deswelling profile between 10°C and 37°C at 24-hour intervals is shown in Fig. 2. The water temperature was first kept at 10°C to swell the gel, adjusted to 37°C for a period of 24 hours, and then re-adjusted to 10°C for 24 hours. The shrinkage of poly(A-ProOMe/HPMA) gel occured gradually throughout the experimental period of 24 hours, in contrast to a rapid shrinkage in the first 2 hours for the poly(A-ProOMe/HEMA) gel. On the other hand, reswelling equilibrium was reached within 2 hours in both cases. The results following repeat of the swelling-deswelling procedure at this temperature cycle show that the thermo-response of this gel is reversible. In order to clarify the difference in the swelling-deswelling kinetics, the appearance and cross sectional structure of this gel were investigated microscopically. Both gels were translucent in the swollen state at 10°C, but in the deswollen state their appearances differed markedly. The deswollen poly(A-ProOMe/HPMA) consisted of two layers, a transparent layer at the surface and opaque layer inside the matrix. In contrast, no such phase separation was seen in the case of deswollen poly(A-ProOMe/HEMA). The

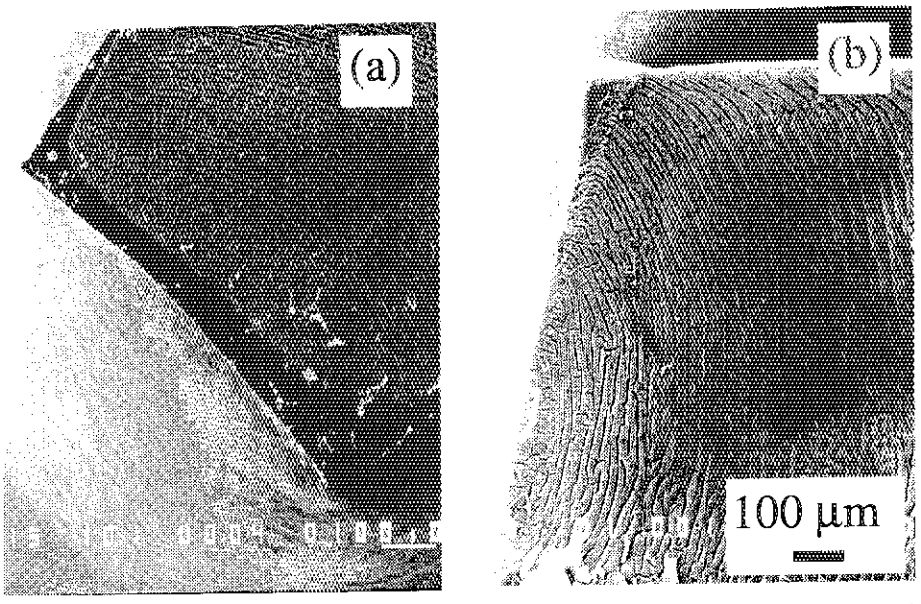


Fig. 3 SEM photographs of cross-sectional structures of poly(A-ProOMe/HPMA) gel (a) and poly(A-ProOMe/HEMA) gel (b) after deswelling for 8 hours at 37°C (both saturated previously with water at 10°C).

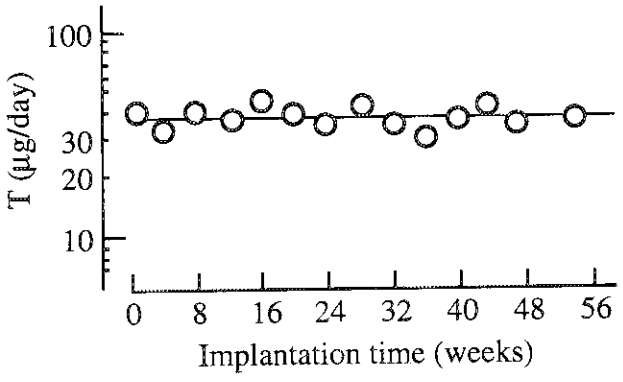


Fig. 4 Daily dose of T released *in vivo* from poly(A-ProOMe/HPMA) gel with a surface regulated function.

SEM photographs of cross sectional structures of the gels in the deswollen state are in Fig. 3. Deswelling of the poly(A-ProOMe/HPMA) gel leads to the formation of a rigid membrane barrier at the surface which lacks pores, and a number of pores in the interior of the matrix. The thickness of the barrier formed during the deswelling increased with time, and a small mass devoid of micropores was the eventual result. These finding imply that the dehydration of poly(A-ProOMe/HPMA) gel occurs from the surface of the matrix accompanying an initial rapid shrinkage, suggesting that the existence of a rigid barrier at the surface markedly retards the rate of passage of water from the interior of the gel. For reswelling , no such a barrier exists because of the regeneration of porous gel, suggesting that the microporous structure of the gel which can be freely changed in water by temperature cycle memorizes the event as a matrix, namely, a surface regulated matrix. In the case of poly(A-ProOMe/HEMA), no barrier

blocking the passage of water from the interior of the gel is present in the deswollen state; the micropores survive throughout the experimental period of 24 hours, despite a remarkable change in the shape of the gel and a marked decrease in the size of the micropore. In the

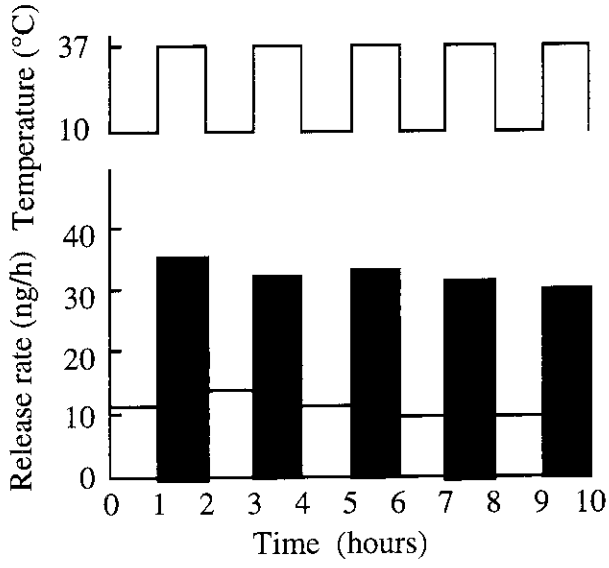


Fig. 5 *In vitro* release behavior of Ara-A from poly(A-ProOMe/HEMA) gel with a matrix pumping function

reswelling of this gel, both the pore size and the shape were restored to their initial states. We conclude from these results that deswelling of poly(A-ProOMe/HEMA) gel is accelerated by the passage of water from the inside matrix via pumping through the porous structure, namely a pumping matrix.

Testosterone (T) was incorporated into the gel by means of radiation-induced polymerization, to provide a T-loaded poly(A-ProOMe/HPMA) gel with 'surface regulating' function. In order to examine the thermo-response as a means for controlled drug release, tablet forms of the copolymer-drug gels were implanted subcutaneously into the backs of castrated rats. As can be seen clearly in Fig. 4, the *in vivo* daily dose of drug released from the gel was constant at approximately 39 μg/day throughout 54 weeks. Controlled drug release over a long period arises, we believe, because the gel blocks the initial rapid release of the drug owing to the formation of a rigid barrier at the surface of the matrix.

Ara-A was incorporated into a poly(A-ProOMe/HEMA/9G, 9/1/0.02 mmol) gel with a matrix pumping function to evaluate the *in vitro* release behavior. The gel employed, which has a size of 8 mm in diameter and 5 mm length, involves approximately 4.5 mg of Ara-A. The *in vitro* dose of Ara-A released from the gel was found to occur in the form of unstable release accompanying an initial burst during the first 24 hours period, followed by a constant release of approximately 11 ng/h at 10°C for 9 days from day 1 to 10. On the basis of this result, we decided to pretreat the drug-loaded gel in water at 10°C during the first 24 hours period in order to avoid the unstable period of release. Using this pretreated gel, the *in vitro* release behavior of Ara-A from the gel when cycled between 10 and 37°C at 60-minute intervals was examined and is depicted in Fig. 5. The *in vitro* release rate of Ara-A from the gel treated for 60 minutes at 10°C was approximately 11 ng/h, in contrast to approximately 33 ng/h at 37°C, suggesting that the release behavior of drug when cycled at different temperatures is reversible. The cause

of the high release rate of Ara-A at 37°C could readily be explained on the basis of the "matrix pumping" mechanism of the shrinking of the gel.

REFERENCES

Alhaique, F., Narchetti, M., Piccieri, F.M. and Santucci, F. (1981). A polymeric film responding in diffusion properties to environmental pH stimuli: a model for a self-regulating drug delivery system. ***J. Pharmacol.***, 33, 413-418.

Bae, Y.H., Okano, T. and Kim, S.W. (1989). Insulin permeation through thermo-sensitive hydrogels. ***J. Controlled Release***, 9, 271-279.

Ito, Y., Casolaro, M., Kono, K. and Imanishi Y. (1989). An insulin-releasing system that is responsive to glucose. ***J. Controlled Release***, 10, 195-203.

Miyajima, M., Yoshida, M., Sato, H., Omichi, H., Katakai, R. and Higuchi, W.I. (1993). Controlled release of 9-β-D-arabinofuranosyladenine from thermo-responsive devices based on acryloyl-L-proline methyl ester. ***Intern. J. Pharm.***, 95, 153-160.

Safranj, A., Yoshida, M., Omichi, H. and Katakai, R. (1993). Surfactant effect on the inverse volume phase transition of a polymer with amino acid side chains. ***Langmuir***, 9, 3338-3340.

Tanaka, T., Nishio,I., Sun, S.T. and Umeno-Nishio, S. (1982). Collapse of gels in an electric field. ***Science***, 218, 467-468.

Yoshida, M., Omichi, H., Kubota, H. and Katakai, R. (1993). Studies of coil-globule transition and cross-linking of poly(acryloyl-L-proline methyl ester) prepared by radiation-induced polymerization. ***J. Intel. Mater. Sys. Struc.***, 4, 223-228.

Winnik, F.M., Ringsdorf, H. and Venzmer, J. (1990). Methanol-water as a co-nonsolvent system for poly(N-isopropylacrylamide). ***Macromolecules***, 23, 2415-2416.

10.3 *IAEA Education and Training Programs in Radiation Technology

Ma Zue Teh

Shanghai Applied Radiation Institute
Shanghai University, Jiading Campus
Shanghai 201800, P.R. China

In order to assist with promoting industrial application of Isotopes and Radiation in Southeast Asia and Pacific Region, A Regional IAEA/UNDP/RCA project was formed since 1982. 1982-1986 was the phase I, 1987-1991 was phase II, now entered the phase III from 1993-1997.

15 countries joined the project, they are: Australia, Bangladesh, China, India, Indonesia, Japan, Rep. of Korea, Malaysia, Mongolia, Thailand, Vietnam. In these countries, Japan and Australia was the donor countries, now expand to five or more donor countries including China, Korea and India.

Radiation technology is one of the subproject of the Regional project, for aiming to transfer this technology from developed countries to developing countries and promote this technology to industrialization. Technical personel and skills are essential for the successful transfer of technology and implementation of industrial project. Technical knowledge plays a significant role in all the phase of project. IAEA support and supplement educational and training program in developing countries by providing specialized training education in subjects related to different aspects of radiation technology such as radiation Sterilization of medical supplies, radiation crosslinking wire and cable, radiation curing, radiation vulcanization of natural rubber latex, radiation engineering, recently emphasized the radiation pollution treatment (flue gas, sludge and waste water)

EMS (Executive Management Seminar), NW (National Workshop) and RTC & NTC (Regional Training Course and National Training Courses) are the main component of this education program.

Executive management seminars and national workshop

Generally organized at the national level, IAEA assist in the preparation of the program and supports the participation of key guest lecturers with significant scientific and industrial experience, the local counterpart (project national coordinator) is responsible for its organization announcement within the country, selection of participants and any local costs involved.

The seminars & workshop are meant to promote radiation technology and to initiate industrial projects and technology transfer, participants come from medium and high level management, representing industry, users, research organization, academic and national atomic energy authorities. The program consists typically of several lectures and with sufficient time left to discussions and a half day allotted to round table discussions on topics such as the feasibility of industrial radiation projects. A number of these seminars & workshop have been organized and planed in different countries on various subjects.

Between 20-80 participants have attended each seminar or workshop. Participant agreed in general that the seminars contribute significantly to the awareness of benefits and problems associated with the transfer and application of radiation technology even in countries where transfer had already taken place to certain extent, feedback was positive and provided valual input for further programming of agency training activities.

Training courses

There are directed toward technical personel involved in the identification and implementation of radiation technology projects. The training course is partly promotional and partly oriented towards technology transfer. However within the time limits of a typical training course the knowledge may not be sufficient for in-depth understanding of all aspects of the technology (Individual fellowships and expert missions provide the dimension of training).

Training courses are usually programmed for 2-4 week period or a total 80-160 hrs of intensive training, approximately equivalent to an average full semester academic course. Consists a series of lectures, experiments, demonstration and exercise. Typically 15-20 participant attend from local country.

Regional training

For the regional project was initiated by member state from Asia and Pacific with the support from IAEA, UNDP, Australia and Japan. The focus of activities has been on well-established industrial applications (Sterilization, Crosslinking, Curing) and on one of the developing areas of special interest to the region RVNRL.

Training centers on different technology have been established throughout the region, through IAEA, UNDP and participating government support.

* Industrial Radiation Sterilization
  (India, Rep. of Korea, Thailand)

* Radiation Curing (Indonesia)
* Radiation Crosslinking (China)
* RVNRL (Indonesia, Japan)
* Radiation Engineering (India, Japan)

Training activities organized within the region were based to the extend possible on actual interest and needs. During the first phase of the project, general introduction training courses were held.

China as a number country of the there region project, since 1985, more than hundreds Chinese young technician and engineer have benefited from these educational activities for their attendance on different aspects of radiation technology activities. Since 1984, SARI was nominated as one of the training demonstration facilities and counterpart institution for Radiation Crosslinking Wire & Table Industry, under the direction and support of IAEA and CAEA. We have hosted 6 times RTC and 4 times NTC. More than 400 participants including 100 foreign participants.

Through this training activities, great enhanced the linage between the regional and bilateral cooperation relationship. Indonesia has purchased a EB machine from China Shanghai Xian-Feng Electron Motor Factory. Through IAEA education and training, we got some laboratory equipment from IAEA, improved the experimental condition in our institute and research capability of younger scientist put forward our scientific research.

IAEA education and training provided a unique opportunity and powerful mechanism for supporting and supplementing standard academic curricula in developing countries by providing specialized training in subject related to different aspect of radiation technology and which normally are not available in standard University curricula in developing countries.

It was agreed that the IAEA educational program going well the actual needs and interest to participating countries, and should be continuous in future. It have become an important link on the effective transfer of Radiation Technology. It was apparent from results of evaluation more training at the basic level is needed throughout the region, and it was realized that the status of development in region require a more in-depth and more specialized type of training, education and training on radiation application in environmental protection and treatment should pay more attention.

A REGIONAL UNDP PROJECT
FOR
THE ASIA AND PACIFIC
ON
INDUSTRIAL APPLICATION OF ISOTOPES AND RADIATION

PHASE I —— 1982 - 1986

PHASE II —— 1987 - 1991

PHASE III—— 1993 - 1997

14 countries join this project:

AUSTRALIA, BANGLADESH, CHINA, INDIA, INDONESIA
KOREA,REP.OF, MALAYSIA, MONGOLIA, PAKISTAN
PHILIPPINS, SINGAPORE, SRILANKA, THAILAND
VIETNAM, **JAPAN**

Activities:

Training Course — **Workshop**

Expert Mission — **Seminar (Symposium)**

Fellowship

Scientific Visit

IAEA/UNDP/RCA

Industral Application of Isotopes and Radiation.

Radiation Processing

— Radiation Vulcanization of Natural Rubber Latex

— Radiation Curing of Wood Surface Coating

— Radiation Cross-linking of Insulating Materials for Wire and Cable

— Radiation Sterilization of Disposable Medical Products

— Rad. ENGINEERING

Technology transfer in industrial radiation processing in Southeast Asia and the Pacific

- ***Radiation sterilization of medical products***

Commercial facilities are in operation in India, Republic of Korea, Malaysia, Singapore, Thailand, Pakistan, People's Republic of China.

They are in the planning or construction stage in Bangladesh, People's Republic of China, Malaysia, Indonesia, India (2).

- ***Radiation crosslinking in the wire and cable industry***

Commercial facilities are in operation in the Republic of Korea (3) and People's Republic of China (3).

They are in the planning or construction stage in India (2) and Pakistan (1).

- ***Radiation curing***

A demonstration facility is operating in Indonesia.

- ***Radiation vulcanization of rubber latex***

A demonstration facility is operating in Indonesia.

Training demonstration facilities and counterpart institutions for the various sub-projects as follows

Radiation Processing

* Rubber — Center for the Application of Isotopes and Radiation, Jakarta Indonesia

* Wood — Centre for the Application of Isotopes and Radiation, Jakarta Indonesia

* Wire and Cables — Shanghai University of Science and Technology, China

* Medical Products — Bhabha Atomic Research Centre, India
— Korea Advanced Energy Research Institute, Korea

EDUCATIONAL AND TRAINING ACTIVVITIES IN SARI SINCE 1985

RTC - Regional training course; NTC - National training course; NS - National seminar

DATE	NAME	SUBJECT	PARTICIPANT NUMBER
1985. 10.	RTC	Radiation crosslinking in wire and cable	16
1986 . 9. 8 - 26	RTC	Radiation crosslinking in wire and cable	15
1987. 6	NS	Radiation curing	40
1988	RTC	Radiation crosslinking in wire and cable	15
1989. 9. 18 - 29	RTC	Formula technology for radiation crosslinking in wire and cable	13
1990. 10. 8 - 11	NS	Radiation crosslinking for industrial application	68
1990.10. 11- 18	NTC	Radiation crosslinking for industrial application	67
1991. 8. 26 - 9. 6	RTC	EB radiation processing technology	15

EDUCATION ACTIVITIES ON RADIATION TECHNOLOGY IN 1993 - 1994

Date		Item		Participants	Experts
93.10.1 1-15	RW	Radiation processing economic benefits	BNEI Beijing	14 foreigners and 50 local	G. R. Malkoshi (Canada) Peter Neijisen (Netherland) Niklaus Studer (Switzerland) George C. West (Australia) Wang Bin Lin and Qi Cheng Yun
93. 12. 7 - 9	NEMS	On radiation treatment of Flue gas	SNRI Shanghai	30 local	O. Tokunage (Takasaki, Japan) Chemilewski (poland)
94. 4. 25 - 29	NW	On radiation crosslinking wire and cable	SARI Shanghai	40 local	Bernie Kestler (RDI, USA) Jim Hackett (RDI, USA) Richard Hosier ((Huber & Suhner, Australia) Yang Qi Ru and Yan Yong Chang
94. 5. 9 - 12	NS	On radiation curing	BNU & RCS Beijing	42 local	Istvan Czalik (Hungry) D. J. French (USA) Wang Liang Zhi , Jing Yang Quan
94.12 12 - 16	RS	On radiation technology in biomedical application	SARI Shanghai	11 foreigners 10 local	V. Markovic (IAEA) A. Hoffman (USA), L. C. Dong I. Kaetsu (Japan), M. Yoshida (Japan) Rosiak (Poland) Ha Hong Fei and Cao Jin

10.4 Feasibility Study on Utilization of Vitrified Radioactive Waste as Radiation Sources

K. Makuuchi, F. Yoshii and K. Hyakutake

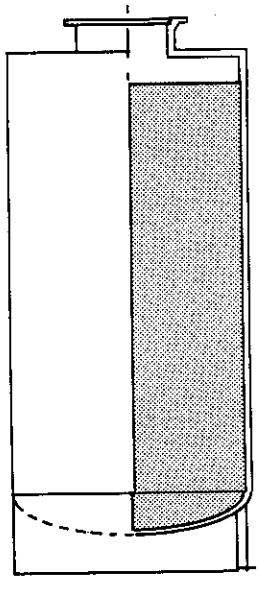
Takasaki Radiation Chemistry Research Establishment, JAERI
1233 Watanuki, Takasaki, Gunma, 370-12 Japan

A feasibility study on utilization of vitrified high level radioactive waste (VW) as radiation source has been carried out. Natural rubber latex was radiation vulcanized with VW to demonstrate the feasibility. The dose rate was 0.1 kGy/hr. As a sensitizer, n-butyl acrylate was added. Negligible small activation of natural rubber (NR) latex by neutron from the VW was observed. The residual sensitizer in the irradiated latex and physical properties of film molded from the irradiated latex were the same level with the conventional radiation vulcanization of NR latex with γ-rays from Co-60. Surgical gloves and protective rubber gloves for radioactive contamination were produced from 20 litters of NR latex vulcanized with 2 VWs. The physical properties of both gloves were acceptable. These results suggested that vitrified high level waste can be used as an industrial radiation source.

KEYWORDS
Vitrified high level waste, radiation source, RVNRL

1. VITRIFIED HIGH LEVEL WASTE

Vitrified high level radioactive waste (VW) is solidified liquid high level radioactive waste arisen from reprocessing of spent fuel to immobilize the radionuclides. The VW will be stored for 30 to 50 years to let radioactivity decay. Then the VWs are disposed of deep underground to isolate the waste from the biosphere. Figure 1 shows an example of the canister that will be produced by the Tokai Vitrification Facility (TVF) of the Power Reactor & Nuclear Fuel Development Corporation (PNC) (IAEA, 1992). About 30 VWs are produced as a result of 1GW of nuclear power generation for one year. It is expected that more than 40,000 VWs will be stored in Japan in A. D. 2030 - 2040. The outline of interim storage facility is illustrated in Fig. 2.



Content : Borosilicate glass
Weight : 380 kg incl. Canister weight
Volume : 110 liter

Canister : Vertical cylinder type
Material : Stainless steel

Outer diameter : 430 mm
Height : 1040 mm

Radioactivity : 1.5 X 10^7 GBq
Heat generation : 1.4 kW

Fig. 1 Vitrified high level radioactive waste canister of Tokai Vitrification Facility

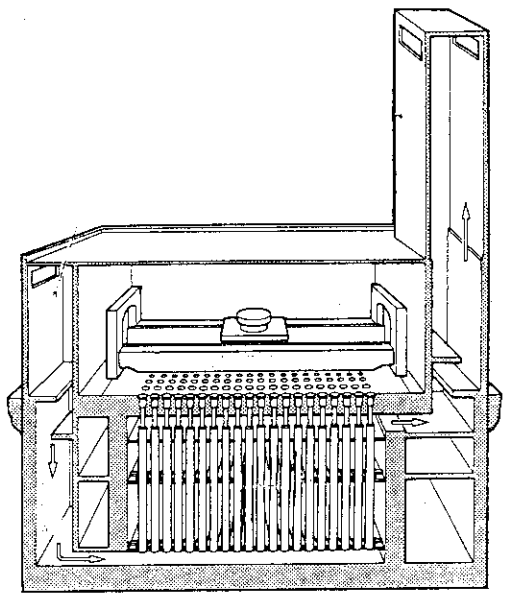


Fig. 2 Interim storage facility

One canister holds more than 10^6 GBq of Cs-137. Utilization of VW as radiation source is an interesting subject for those people who are working in radiation processing. Characteristics of VW as a radiation source are 1) large volume, 2) lower energy and dose rate compared with Co-60, and 3) activation of irradiated materials due to release of neutrons. Therefore there is limitation for utilization of VW as an industrial radiation source. The radiation process that meets the following conditions can utilize VW.

1) low dose rate irradiation
2) irradiation for raw materials (not consumer products)

So far there is no industrial process that meets the above conditions. The radiation vulcanization of NR latex seems to meet the above conditions among the radiation processes under developing.

2. RVNRL

The RVNRL means crosslinking of natural rubbers (cis-1,4- polyisoprene) dispersed in the form of microscopic particles in an aqueous medium. The RVNRL procedure consists of two steps (Makuuchi and Tsushima, 1985): mixing NR latex with sensitizer and irradiating. The resulting radiation vulcanized (RV) NR latex can be used for the manufacture of latex products by the conventional coagulant dipping process. Usually n-butyl acrylate (n-BA) is used as a sensitizer. The irradiation dose for vulcanization can be reduced to 15 kGy from 250 kGy by addition of 5 phr of n-BA. The radiation vulcanized NR latex and products from it have the following advantages over convention sulfur vulcanization (Makuuchi and Markovic, 1991);

1) Absence of N-nitrosamines
2) Very low cytotoxicity
3) Low emission of SO_2 and less formation of ashes
4) Transparency and softness
5) Degradable under the environment

3. RVNRL FACILITY WITH VW

A facility for RVNRL with VW was designed based on the concept of the utilization of interim storage of canisters as an irradiation facility to avoid the construction of irradiation facility for the reduction of vulcanization cost. Irradiation vessel having the same size with the VW canister put into the vertical pit of the storage. The vessel is placed alternately with VW so that one irradiation vessel is surrounded by 6 VWs as shown in Fig. 3. The moving of the canister can be operated automatically. The specifications of the facility are shown in Table 1.

Table 1 Specification of RVNRL facility with VW

Processing rate	1,000 tons/year
Materials of irradiation vessel	Stainless steel
Number of irradiation vessel	36 (112 kg latex/vessel)
Number of VWs	104
Operation days	250 days/year
Operation hours	17 hours/day

The flow sheet of the facility is shown in Fig. 3. The facility will be attached to the interim storage facility of VWs. The NR latex to be irradiated and irradiated NR latex will be

transported by tank truck. The capacities of storage tanks of NR latex and irradiated NR latex are $30m^3$.

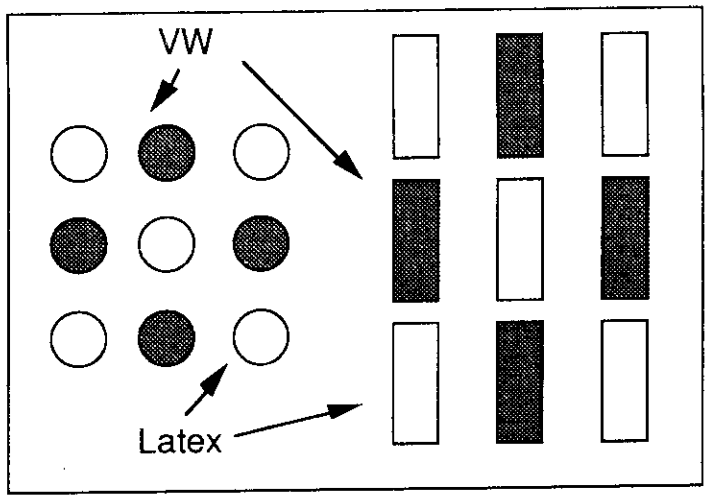


Fig. 3 Configuration of VW canister and irradiation vessel

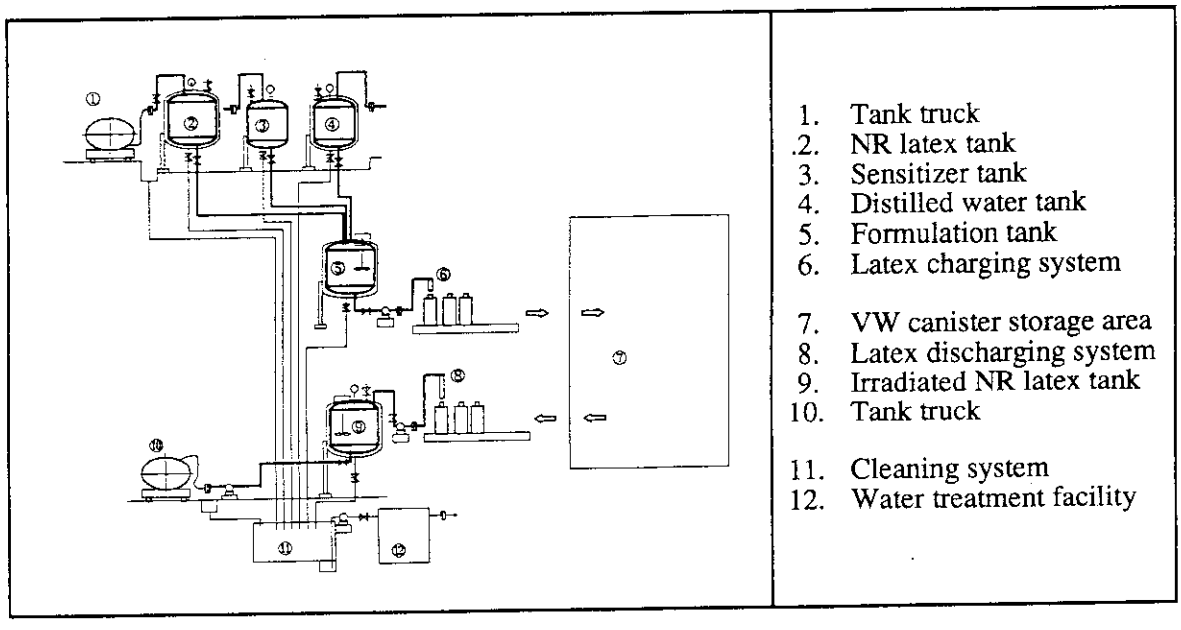


Fig. 4 Flowsheet of RVNRL with Vitrified High Level Waste

The construction cost and the operation cost of the facility were calculated in view of the respective element by adopting average investment method. The unit processing cost was estimated to be ¥31/kg. It was expected that this value will be acceptable for the latex industry.

4. RVNRL WITH VW

To verify the feasibility of utilization of VW as irradiation source RVNRL was carried out with small VW produced by the Chemical Processing Facility (CPF), PNC. The dimensions of the VW were 76 mm (outer diameter) and 500 mm (height). This VW contains 3.1 kg of glass and 5.9×10^4 Bq of γ-emitters. The dose rate measured with a alanine dosimetry was 0.1 kGy/hr. NR latex was irradiated in a polyethylene bottle having a capacity of 100 ml. The bottle was wrapped with polyvinylchloride. As a sensitizer 5 phr of n-BA was used. Dose was 5-30kGy. Activation of NR latex and bottle were negligible. The residual sensitizer in the irradiated latex was the same level with the conventional RVNRL with γ-rays from Co-60. Figure 5 shows typical example of the relationship between dose and tensile strength (Tb) of

Malaysian NR latex (IOTEX HA). Results obtained with Co-60 irradiation with the same dose is also shown in this figure for comparison. In the case of Co-60 irradiation the maximum Tb was achieved at 15 kGy. While it needed about 25 kGy in the case of VW irradiation in this NR latex. Hence, RVNRL needs more dose than Co-60 does. Probably this is due to lower energy of γ-rays from VW (0.66 MeV from Cs-137). Though VW is slightly inferior to Co-60 in terms of vulcanization dose, physical properties of the obtained rubber meet Japanese Industrial Standard. For example the maximum Tb and elongation at break were 31.5 MPa and 970 %, respectively. Comparison of RVNRL with Co-60 and VW is shown in Table 2. It can be said that VW can be used as an irradiation source for RVNRL.

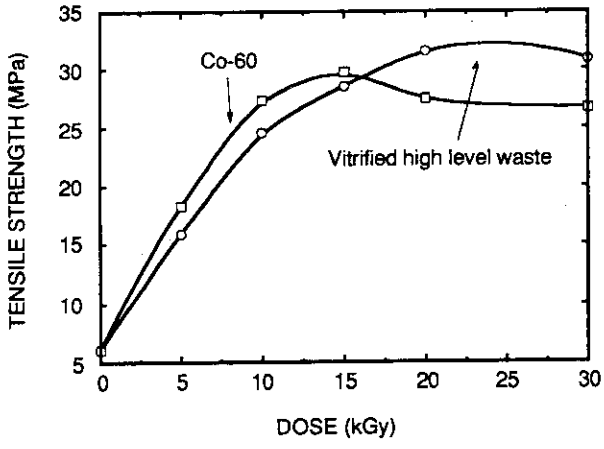


Fig. 5 RVNRL with VW and Co-60

Table 2 Comparison of RVNRL with VW and Co-60

	Irradiation source	
	Vitrified high level waste	Co-60
Vulcanization dose (kGy)	25	15
Tensile strength (MPa)	32	30
Elongation at break (%)	970	930

Test production of surgical gloves and protective rubber gloves for radioactive contamination were carried out successfully. For this purpose 20 liters of NR latex were vulcanized with 2 small VWs. Bottles made of polyethylene terephthalate were used as irradiation vessels. Physical properties such as Tb and elongation at break meet the Japanese Industrial Standards.

5. CONCLUSION

Vitrified high level waste is slightly inferior to Co-60 as radiation source from the point of view of vulcanization dose. However NR latex vulcanized with VW possessed practical physical properties. Vitrified high level waste can be used as a radiation source for RVNRL.

ACKNOWLEDGMENT

The authors thank the Science and Technology Agency (STA) for financial supportt and Mr. Yamada of PNC for the irradiation with VW.

REFERENCES

IAEA (1992). *Design and Operation of High Level Waste Vitrification and Storage Facilities.* IAEA Technical Report Series No. 339, pp. 75-78.

Makuuchi, K., and Tsushima, K. (1988). Radiation Vulcanization of Natural Rubber Latex with Acrylic Monomers. *International Rubber Conference 1985, Kuala Lumpur.* Proceedings, 2, 502-509.

Makuuchi, K. and Markovic, V. (1991). Radiation Processing of Natural Rubber Latex. *IAEA Bulletin*, 33, No. 1, pp. 25-28.

10.5 Production of an Intense Slow Positron Beam using a Compact Cyclotron

Masakazu Washio, Masafumi Hirose and Kazuyoshi Takahashi

Research and Development Center, Sumitomo Heavy Industries, Ltd.
63-30 Yuuhigaoka, Hiratsuka, Kanagawa 254, Japan
Tel: +81-463-21-8486 Fax: +81-463-21-8990

ABSTRACT Recently, we have developed a new method to produce an intense slow positron beam using a compact cyclotron. An intense positron source has been produced by making use of the $^{27}Al(p,n)^{27}Si$ reaction on a so-called on-line mode. A transmission type target system has been developed in order to avoid decreases in the slow positron beam intensity due to the damage induced in the moderator by proton irradiation. The number of the slow positron beam obtained by this method has been up to around 10^6/s in the preliminary experiment. According to the theoretical estimation, around 10^7/s can be expected. This method can give higher intensity of a slow positron beam than the RI method. And this method can provide the more inexpensive and smaller system than the LINAC method.

INTRODUCTION

In recent years, slow positron beams have been developed in many laboratories in order to apply them to the research of material surfaces using methods such as positron diffraction, positron microscopy, positron annihilation induced Auger electron spectroscopy, and so on. In those cases, two methods have been applied for the production of a slow positron beam. One is using radioisotopes (RI)(Aruga et al.,1992; Brandes et al.,1988; Frieze et al.,1985; Liszkay et al.,1992; Lahtinen et al., 1986) such as ^{22}Na and the other is an electron linear accelerator (LINAC)(Ito et al., 1991; Akahane et al.,1990; Hulett et al.,1989; Ley et al. 1985; Paridaens et al. 1992). Generally the former is compact and inexpensive, but the intensity of the slow positron beam is not so high (10^4-10^6 slow e^+/sec). On the contrary, the latter method can give an intense slow positron beam (10^7 - 10^9 slow e^+/sec), but its cost is to be very high and the system is normally very large.

Under these conditions, we have succeeded in developing a compact and inexpensive intense slow positron beam production system using a compact cyclotron by producing and using activity-saturated radioisotopes.

A comparison of primary sources for the production of a slow positron beam is given in table 1.

METHOD

The fundamental aim of this study is to produce β^+ decay radioisotopes from a nuclear reaction caused by ion beam irradiation of a target material and to utilize the radioisotopes to produce a slow positron beam.

There are two methods with which to use a slow positron beam created by the compact cyclotron produced ion beam irradiation of a target material. One is off-line mode (i.e. using the slow positron beam after the completion of the irradiation) and the other is on-line mode (i.e. using the slow

positron beam during the irradiation). The off-line mode has the merit of avoiding damage induced in the moderator by the ion irradiation, but the intensity of the slow positron beam decreases according to the half-life of the radioisotopes. Therefore, radioisotopes with a short half-life, and which in general have a high radioactivity, cannot be used in this mode. On the contrary, the on-line mode has the merit that radioisotopes with a short half-life can be used. However there had been a problem of a decrease in the slow positron beam intensity due to damage induced in the moderator by the irradiation. In order to avoid this problem, we have invented a "transmission type target system" instead of a "reflection type target system"(Stein et al.,1974). This system eliminates damage induced in the moderator by the ion irradiation and makes it possible to produce an intense slow positron beam continuously by the on-line use of the compact cyclotron.

The requirements for the target materials in which a nuclear reaction occurs are as follows: (1) High yield of the β^+ decay radioisotopes. (2) High branching ratio for the β^+ decay of the radioisotopes. (3) High maximum energy of the β^+ rays emitted from the radioisotopes. (4) A short half-life. (5) High thermal conductivity.

We have chosen aluminum as the target material which best meets the above mentioned requirements for a proton beam. The reaction $^{27}Al(p,n)^{27}Si$ has a threshold energy of 5.8 MeV. The branching ratio for the β^+ decay of the ^{27}Si is unity. The ^{27}Si has a half-life of 4.1 seconds. The maximum energy of the β^+ rays emitted from the ^{27}Si is 3.85MeV. Fig. 1 shows the range of 18MeV protons in the aluminum target. From the figure, it is clear that the thickness of aluminum target should be 1.8mm or more for the transmission type target system. Under the condition, direct damage of the moderator by proton irradiation can be avoided.

RESULTS

1) Calculated Radioactivity

The saturated radioactivity of the ^{27}Si is shown in fig. 2, and the slow positron beam intensity calculated from the values given in fig. 2 is shown in fig. 3 for the transmission type target. The saturated radioactivity for a proton current of 1 μA is evaluated at 8.5 GBq, and as shown in fig. 2 the radioactivity is distributed widely from the proton injected surface to a depth of about 1.5 mm.

Fig. 3 shows the calculated intensity of the slow positron beam which is generated by the β^+ rays emitted from the opposite surface to the proton injected surface (Transmission Type). The slow positron beam intensity is calculated as 4.3×10^5 slow e^+/sec for a proton current of 1 μA. The overall conversion efficiency from β^+ rays to slow positrons was tentatively fixed at 10^{-4} in the above calculations.

2) Experimental Setup

2)-1. Target System

The characteristics of the target system are as follows. (1) The

transmission type target system has been invented in order to avoid the damage induced in the moderator by the proton irradiation and produce an intense slow positron beam continuously by on-line use of the compact cyclotron. (2) Aluminum has been selected as the target material because the maximum energy of the β^+ rays emitted from the ^{27}Si is high. It is thus possible to make use of the saturated radioactivity efficiently. (3) Separate vacuum chambers for the compact cyclotron and the slow positron beam line have been provided. With this arrangement, the aluminum target can be cooled directly and efficiently with low temperature helium gas so that intense proton beam irradiation of the aluminum target is made possible. As a result, the intensity of the slow positron beam comes high. In addition, the safety of the system comprising the separate chambers is assured.

2)-2. Compact Cyclotron

This study has been performed by using the compact cyclotron (CYPRIS MODEL-370 manufactured by Sumitomo Heavy Industries, Ltd.) of SHI Examination & Inspection, Ltd. The cyclotron can accelerate protons and deuterons up to 18 MeV and 10 MeV, respectively and it can also accelerate He ions. The maximum beam current is 70 μA. The approximate size of the compact cyclotron is only 5 m long, 4 m wide and 3 m high. In the present study, protons with an energy of 18 MeV and an aluminum target with a thickness of 2.0 mm have been applied in the transmission type target system.

2)-3. Beam Line

The slow positron beam is generated from the 25 μm thick tungsten moderator set behind the aluminum target and is transported to the detector using a magnetic field produced by solenoid coils. The detector is composed of a microchannel plate (MCP) and a phosphorescent plate. At present, the intensity of the slow positron beam is determined by stopping all the beam and measuring the annihilation gamma-rays with an ionization chamber. A Ge semiconductor detector is also introduced in order to measure the intensity of the slow positron beam accurately.

3) Slow Positron Beam

The slow positron beam profile obtained by using the compact cyclotron is shown in fig. 4. It has been confirmed that the observed beam is a slow positron beam by controlling both the magnetic field of the steering coils and the electric potential of the tungsten moderator.

A slow positron beam intensity of about 3×10^6 slow e^+/sec has been achieved using a proton current of 30 μA. This value should be compared to the theoretical maximum intensity of 1.1×10^7 slow e^+/sec. The intensity is expected to be improved in the future by refinement of various adjustments.

Using the slow positron beam from the compact cyclotron, variable-energy positron lifetime measurement system is under construction. The

pulsing system is being tested at the moment.

CONCLUSION

An intense slow positron beam has been produced for the first time by applying a compact cyclotron. The output slow positron beam intensity is 3 x 10^6/sec at the present under the condition of proton current with 30 μA. This DC beam has been transported more than 10 m (from the target to experimental port) successfully using the solenoid coil under the vacuum at 10^{-7} torr.

TABLE 1
A comparison of primary sources for the production of a slow positron beam

Primary sources	Production processes	Slow e^+ beam intensity	Features
long half-life RI	β^+ decay	10^{4-6} slow e^+/sec	•compact •inexpensive •DC beam •low intensity
electron LINAC	pair production	10^{7-8} slow e^+/sec	•large •expensive •pulsed beam •high intensity
compact cyclotron	β^+ decay	10^{7-9} slow e^+/sec	•compact •inexpensive •DC beam •high intensity

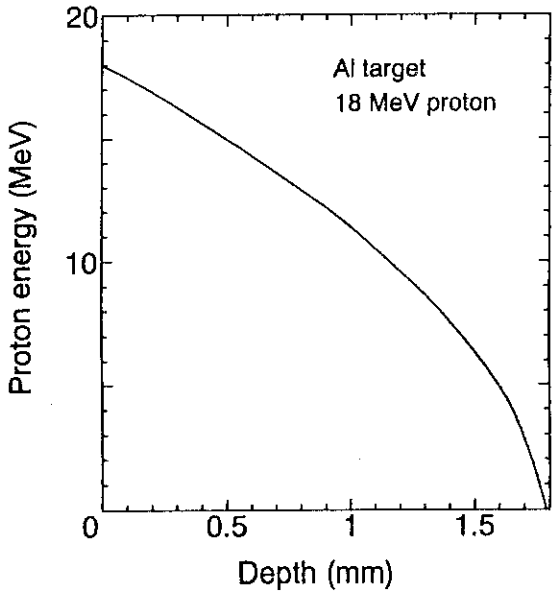


Fig. 1 Range of 18 MeV protons in aluminum target

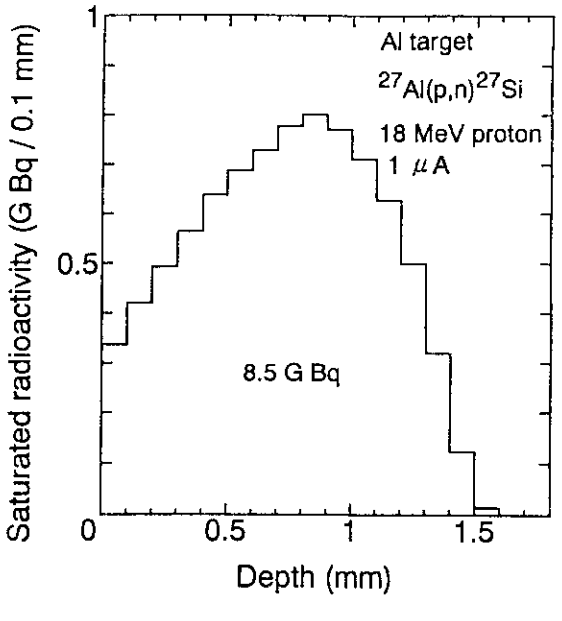


Fig. 2 Saturated radioactivity of the ^{27}Si formed by the ^{27}Al(p,n)^{27}Si reaction for a proton current of 1 μA

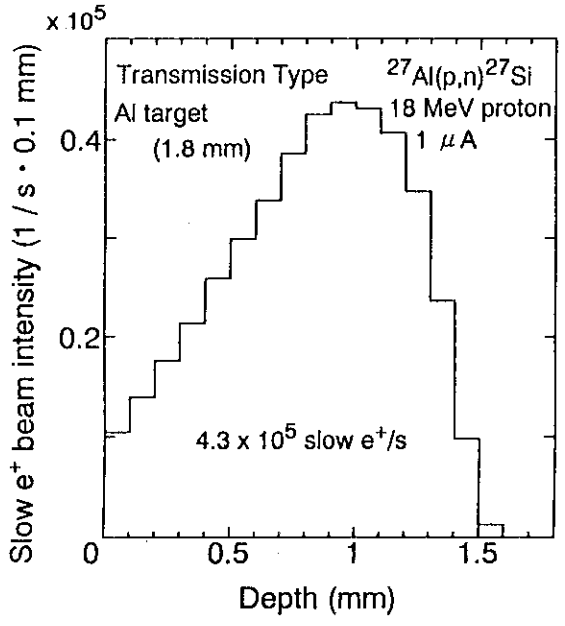


Fig. 3 Calculated intensity of the slow positron beam formed by the $^{27}Al(p,n)^{27}Si$ reaction for a proton current of 1 μA

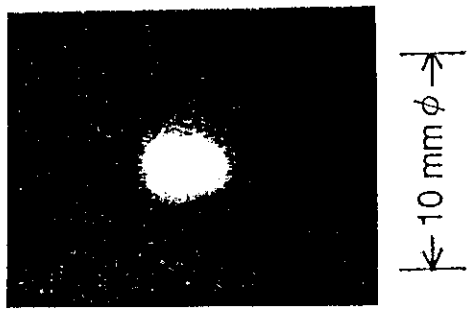


Fig. 4 The slow positron beam profile observed at the center of the MCP by using the compact cyclotron

REFERENCES

Aruga T., Takamura S.,Hirose M. and Itoh Y., (1992) Phys. Rev., **B 46**, 14411

Brandes G. R., Canter K. F. and Mills Jr. A. P., (1988) Phys. Rev. Lett. **61** 492

Frieze W. E., Gidley D. W. and Lynn K. G., (1985) Phys. Rev. **B 31** 5628

Liszkay L., Huomo H., Ronka K., Rytsola K. and Hautojarvi P., (1992) Positron Annihilation, Eds. Kajcsos Zs. and Szeles Cs. (Trans Tech Publications, Switzerland), 1931

Lahtinen J., Vehanen A., Huomo H., Makinen J., Huttunen P., Rytsola K., Bentzon M. and Hautojarvi P., (1986) Nucl. Instr. Meth. **B 17**, 73

Ito Y., Hirose M., Takamura S., Sueoka O., Kanazawa I., Mashiko K., Ichimiya A., Murata Y., Okada S., Hasegawa M. and Hyodo T., (1991) Nucl. Instr. Meth. **A 305**, 269

Akahane T., Chiba T., Shiotani N., Tanigawa S., Mikado T., Suzuki R., Chiwaki M., Yamazaki T. and Tomimasu T., (1990) Appl. Phys. **A 51**, 146

Hulett Jr. L. D., Lewis T. A., Donohue D. L. and Pendyala S., (1989) Positron Annihilation, Eds. Dorikens-Vanpraet L., Dorikens M. and Seger D., (World Scientific Publishing, Singapore), 586

Ley R., Niebling K. D., Osippowicz A., Picard A. and Werth G., (1985) Positron Annihilation, Eds. Jain P. C., Singru R. M. and Gopinathan K. P., (1985) (World Scientific Publishing, Shingapore), 996

Paridaens J., Segers D., Dorikens M. and Dorikens-Vanpraet L., (1992) Positorn Annihilation, Eds. Kajcsos Zs. and Szeles Cs. (Trans Tech Pbulications, Switzerland), 1951

Stein T. S., Kauppila W. E. and Roellig L. O., (1974) Rev. Sci. Instr.**45**, 951

10.6 The Recent Industrial EB Applications in Japan

KOJI NAKAI, MASAYUKI KASHIWAGI AND KENICHI MIZUSAWA

Nissin-High Voltage Co., Ltd.
Kyoto, Japan

ABSTRACT

The conventional applications of electron beam processing such as, crosslinking of electric wire and cable insulations, polyethylene foam, and of rubber tire components have been the main part of the EB business for many years. New applications are continuing to appear, however, the growth of the new applications has been relatively slow. Nissin High-Voltage, as one of the worlds leading manufacturers of electron beam equipments, continues to develop and improve EB equipment to meet the requirements of these new applications. In this paper recent EB applications and its improvements are described.

KEYWORDS

Electron Beam, Electron Processing, X-ray, EB curing, self-shielded, flue gas treatment

1. INTRODUCTION

Electron Beam Processing Systems have been in use in a variety of applications, such as: improving heat resistivity of electrical wire insulations, improving green strength of rubber tire materials, crosslinking of PE sheet for foam products, sterilizing of medical devices, curing of paints and printing inks. These technologies have also been a basic ones for modification of industrial materials. Most of these applications had their beginnings two or more decades ago. During those years, user requirements have continued to push EB manufacturers into providing equipment that will meet very specialized demands; systems have become more dedicated to these specific processes.

This paper will introduce the recent industrial EB applications and developments of electron beam processing systems at Nissin High Voltage, and will describe these developments as they relate to low-energy systems, medium-energy systems, and high-energy systems, respectively.

2. INDUSTRIAL EB APPLICATION IN JAPAN

2-1. Crosslinking

This technology is to modify polymer properties by rendering heat resistivity etc. and has been applied for long time in the production of heat resistant wire insulation, heat resistant sheet and film, heat shrinkable tube and film, foamed plastics and automobile tires as well known.
The features of this technology are:
1) Reduce chance of containing foreign materials in the product since catalyst is not required in general, although crosslinking aid material is added in some case.
2) Crosslinking density can be adjusted easily as the reaction is controlled by dose and dose rate.
However, to improve crosslinking efficiency, suitable crosslinking agent should be studied for the polymer material.

Recently, attention is paid to modified PP. which makes radical reaction. One example is the co-polymer with vinyl-silane compounds, the other is the co-polymer with non-conjugated compounds.

2-2. Grafting

There are two methods for graft polymerization. pre-irradiation in which monomers are grafted after developing radicals in base polymer by irradiation and simultaneous irradiation in which mixture of base polymer and monomer is irradiated at the same time to have grafting reaction.
Buttery separators and Ion exchanging membrane are made by pre-irradiation and non-cellular type flame retardant PE foam is made by simultaneous irradiation.
Recently, co-graft polymerization which is a kind of graft polymerization, is being studied. This technology is to have graft polymerization putting 2 kinds of monomers at the same time into base polymer. The feature of this to furnish 2 functions at once to the base polymer is assumed to be a useful technology to produce new functional materials comparing to conventional single monomer graft polymerization. The examples of functional materials development using co-grafting are shown in Table-1. The table shows reactions with various base polymers that means radiation grafting can be applied to any base polymers.

Table-1 RECENT STUDIES ON RADIATION CO-GRAFTING

base material	irradiation method	monomer	purpose
poly-tetra-fluoroethylene	simultaneous	MAA/AN	improving electric conductance
poly-propylene	pre-irradiation	VP/AN	improving heat resistance
silicone rubber	simultaneous	NIPAAm/AAm	developing organic adaptability
poly-urethane	simultaneous	HEMA/BA	developing organic adaptability
poly ethylene	simultaneous	VCA/VIMA	developing organic adaptability

NIPPAm:N-isopropyl acrylamide MAA:methacrylic acid BA:butyl acrylate
AAm: VP:4-vinyl pyridine VCC:vinylene carbonate AN:acrylonitrile
HEMA:2-hydroxy ethyl metacrylate VIMA:N-vinyl-N-methylacetamide

2-3. Curing

In Japan, R&D of paint curing by EB started in late 1960s. Next active period was 1980s when surface coating of roof tiles by Nakazato Sangyo stimulated the application field and number of industrialization followed being supported by the development of hi-qualified paint together with the development of compact electron processing equipments. Table 2 shows the brief history. EBC painted steel palate, anti-foggy film and transfer film followed and became practical application after Table 2.
The main stream of EB curing resin is radical polymerizing using acrylate resin. The disadvantage of the resin is PII and strong smell. Recent studies have improved PII below 1 by applying alkylene-oxide or lactones to alcohol. And, from the point of the preservation of natural environment development of aqua-resin is also active, that is the origin of no pollutant system without using VOCs.

EB curing is generally done in inert gas, mostly nitrogen, atmosphere because of the dominant radical polymerization. In order to reduce nitrogen gas consumption recycling system is utilized. On the other hand, cationic polymerization which cures in the air has not been used much because of less curability but vinyl-ether resins are being developed actively.

Table-2 SHORT HISTORY OF EB CURING

late 1960s ~early 1970s	: Start of studies (first active stage)
1973	: Curing of motor-cycle parts coating(SUZUKI)
late 1970s ~early 1980s	: Stagnation period
1979	: Curing of roof tile coating(NAKAZATO)
1982	: Curing of pre-coat metal(NIPPON STEEL)
middle 1980s	: Second active stage(linear cathode test machine)
1984	: Curing of gypsum tile coating(ACHILLES)
1985	: Curing of plastic film printing(MITSUMURA)
1986	: Curing of floppy disk coating(TDK)
1987	: Curing of metal coating(NIPPON STEEL)
1988	: Curing of metal coating(NISSIN STEEL)
1989	: Development of transfer film(DNP)
1990	: Development of anti-foggy film(DNP)

2-4.Sterilization

In Japan, most of radiation sterilization facilities for medical supplies use Co-60. But a few facilities use 10 MeV linac or 5 MeV electrostatic EB equipment with X-ray converter. EB equipment is assumed as safer radiation source but has smaller penetration than Co-60. Both Co-60 and EB sterilization will co-exist featuring each advantages. Other than sterilization of medical supplies, feed for experimental animals and dry flowers are disinfected by EB or Co-60.

2-5.Preservation of natural environment

Irradiation has been applied to wast water, sewage and its composting. A few test and pilot plant were built but none of them were brought to commercial scale except one facility Munich which use Co-60.

De-NOx, De-SOx of flue gas by EB irradiation have been paid attention and number of pilot plants were built and torn down. There are several competing technologies however it is expected that at least a few commercial sized plant will be build for electric power plant or incinerator of urban waste.

3. FUTURE OF EB APPLICATION TECHNOLOGY

The future of EB application technology in general is,

1) Crosslinking : is matured technology, but has continuing important role toward future.

2) Curing : has possibility to flourish greatly. there are 2 expected fields for curing technology.One is to apply to the field where conventional heat curing is difficult to be applied, that is, the field of hi-functioning. Another is innovation of heat curing that EB curing system enables the least VOCs, energy and space saving applying the feature of EB advantages.

3) Grafting : There seems to be no limits to furnish new functions to popular materials. Development of new functional materials will grow in the future.

4) Sterilization/ Disinfection : Higher energy, 5-10 MeV or X-ray conversion may co-exist with Co-60 and other technologies such as H_2O_2 plasma.

5) Conservation of environment : To remove SOx, NOx from flue gas, which is the cause of acid rain, EB may have some share in the competition with other technologies. The application in the water treatment field has variations. Some of the variations may have chance to be realized.

6) Others : There are number of applications studied other than the above.

Among them, improvement of thyristor switching is promising but the size of EB market for the application is rather small. As the future technology, super diffusion is one of the expected technology being studied which may become semiconductor manufacturing technology of the next generation.

4. RECENT DEVELOPMENT OF EB EQUIPMENTS

4-1 Lower Voltage Operation (100kV- 140 kV)

In low-energy EB curing applications, the thickness of the coating layer on the substrate is usually 100 micro-meter or less. The required acceleration energy level to cure these coatings is generally below 150 kV. At 150 kV much of the electron energy gets delivered into the substrate rather than the coating, this is especially true when thinner coatings are employed. In many cases electron energy deposition in the substrate has to be minimized because of potential damage to the substrate materials. To meet this demand, NHV developed a system which has an available operating range between 100 kV to 140 kV. In addition to reducing the substrate damage, these lower energy systems provide the user with advantages in smaller size and lower cost. Figure 1 shows the penetration curves of electrons accelerated from 100 kV to 150 kV. These measurements were made at NHV using thin film dosimetry. These curves may be used as a reference to obtain the most suitable energy available when substrates sensitive to EB are an issue. Lower energy technology allows the user more flexibility in the selection of substrate materials.

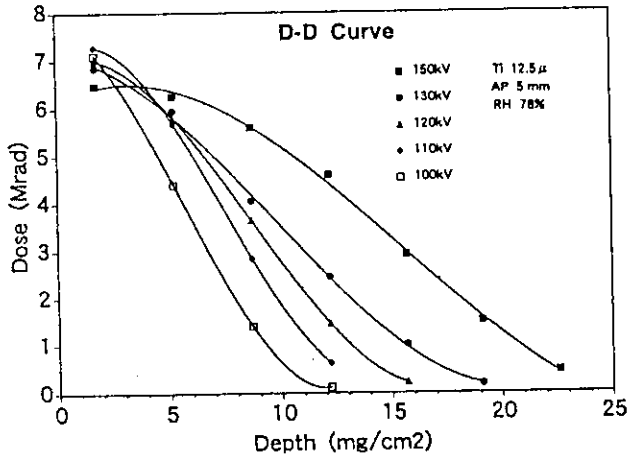


Figure 1

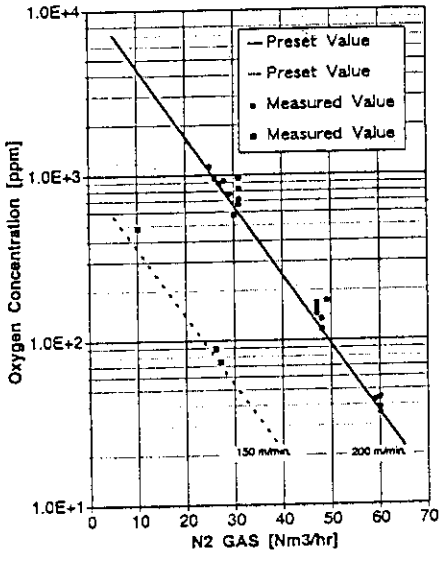


Figure 2

4-2 Nitrogen Control

Generally, EB curing applications require inert gas be used in the process chamber. The main reason to use an inert gas, mostly nitrogen, is to remove oxygen from the beam processing area, and oxygen is likely to prohibit radical polymerization. Inert gas consumption is regarded as one of the major factors in the operating cost of EB system. Therefore, it is a very important consideration for production line operation. To reduce nitrogen gas consumption, NHV introduced a nitrogen circulating system in 1986. Since then, further work has been done to minimize nitrogen consumption. Recent work was done on a test facility running at a web-speed of 200m/min, nitrogen consumption of 0.008 - 0.013m^3/min./m^2 was achieved. A new automatic gas flow control system proved effective in maintaining the oxygen concentration at a preset values, even when the operating conditions change, such as: a speed, a dose, or temperature.
Figure 2 shows how the oxygen concentration in the process chamber follows a preset value.

4-3 Rapid Beam Ramp-Time

Providing a uniform dose on a product that is running under the beam is very important. Controlling the beam current in proportion to the running speed provides the user with a constant dose system. In some cases line speed will change quickly, requiring the beam to ramp-up and/or down very fast. To meet this demand, a bias voltage system is applied to the cathode grid, this at the same time is used to control the beam current. The grid control system allows the rapid beam ramp-up or down.

4-4 Self-Shielded Unit

The first self-shielded electron beam system, in a production application, was installed in Japan in 1968 by the Nissin Electric Co., Ltd.. We are not sure but, we think, this might be the first self-shielded unit in the world installed. Since then, NHV has produced many types of self-shielded systems, these machines are now available for a wide range of voltage from 100 kV to 1000 kV. The advantage of the self-shielded design is its very suitability for in-line operations, where the EB system is installed with other production equipment, such as extruders, calendars, or others. The most unique feature of self-shielded systems is its compactness. The small size allows the equipment to fit into an existing production line, generally this is not possible with a concrete vault facility. Figure 3 shows a new 500 kV system NHV developed recently. The system occupies a space of: 3.4mH x 2.4 mW x 2. 6 mL.

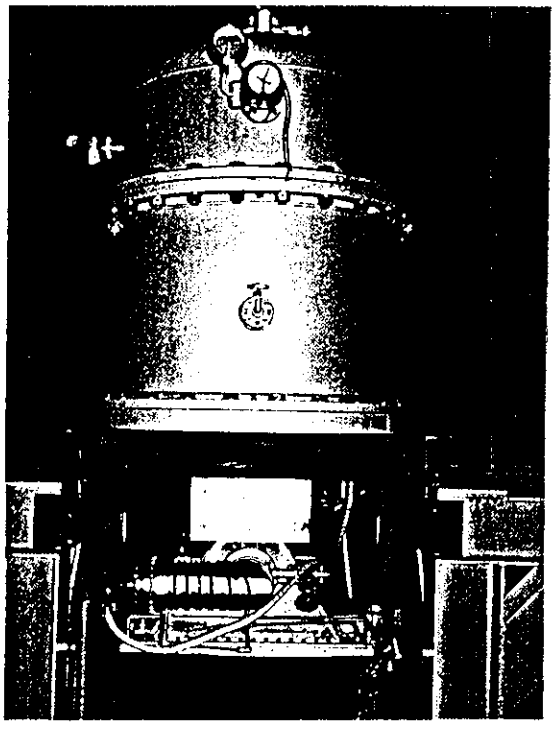


Figure 3

4-5 High Power Conversion Efficiency/High Power Output

Power conversion efficiency is an important factor when high speed and high electron beam currents are required. The use of EB technology in these applications is feasible, provided the economics work. A prime example is flue or stack gas treatment. In this application, the users are usually Electric Power Generation Stations, and in most cases, they are concerned with how much energy is consumed by the EB System. In this application most of the energy required must be used to generate and accelerate the electron beam, therefore, power conversion efficiency is

very important. To process large volumes of material, a higher power output is necessary while reduction in the cost per kW is essential. In addition, there are key technologies to achieve high powered electron beams. The factors that must be considered are: the DC Power Supply Design, the Filament, and the Window design. Today we have the designs and technology to build a system with a 400 - 500 kW output, the DC Power Supply would have a capability of 750 kW to 1000 kW. The Filament and Window technology is available for a 500 mA system using a scan beam and an air-cooled window. We have also developed several types of DC Power Supplies for these EB applications. The two most common types of DC power supplies used are:

1) Transformer Type
2) Cockcroft - Walton Type

Both provide very good power conversion efficiency from commercial line power. Recently, we achieved 92% efficiency, as reported by a customer using an NHV system in a flue gas treatment application. This may be the best fit system for flue gas applications.

4-6 X-ray Irradiation Target

The new NHV 5 MeV system provides an extremely high throughput capability in a sterilization application, but are limited to relatively thin materials, because of the electrons low penetrating power. To process thicker products, it is desirable to convert the energetic electrons into X-rays. To accomplish this, NHV started a joint study in 1983 with Japan Atomic Energy Research Institute to develop an effective X-ray conversion system. Figure 4 shows the X-ray conversion system installed at Radia Industries company that provides Irradiation Services in Japan. Figure 5 shows the dose rate distribution of X-rays under the target, the measured data is in good agreement with the computer simulation. Figure 6 shows a depth dose curve in a material with a bulk-density of 0.23g/cm^3. The data indicates the system is capable of processing 40 cm thick material with 0.23 g/cm^3.

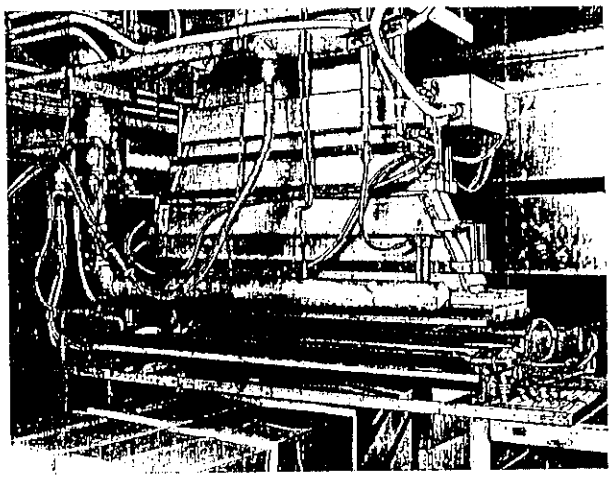


Figure 4

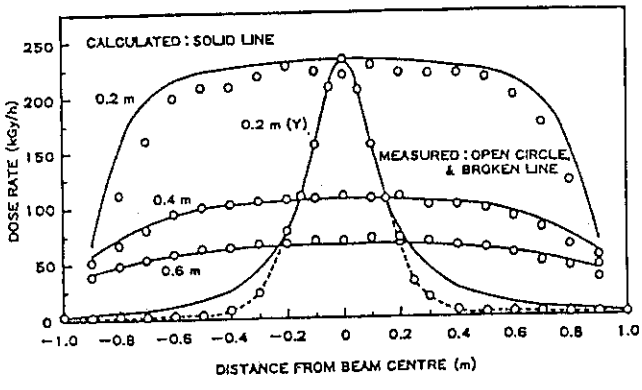


Figure 5

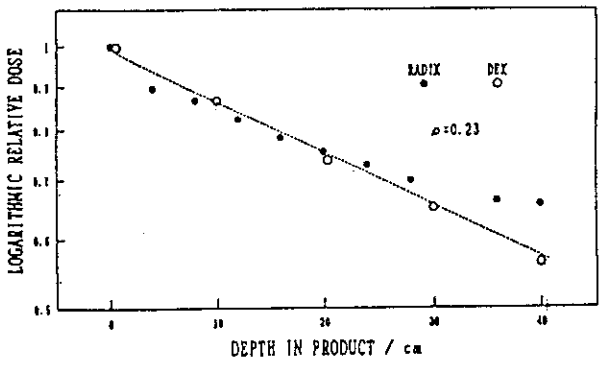


Figure 6

5. CONCLUSION

NHV continues to develop a variety of electron beam processing systems to meet future demands. Today, more than 200 systems have been installed in industrial applications by us. We accomplished this with the cooperation of our customers, and will continue these efforts for the future development of EB technologies.

11. Radiation Processing (1)

11.1 *Effect of Irradiation on PTC Performances of Carbon Black Filled Polymer Composites

Chen Xinfang, Jia Wentao, Tang Hao and Yang Huali
Institute of Materials Science, Jilin University, Changchun, 130023, China

Li Shuhua
Changchun Institute of Applied Chemistry, Changchun, 130022, China

Abstract *The influences of irradiation on Positive Temperature Coefficient (PTC) functions of polymer- carbon black composites are studied systematically, using HDPE, LDPE, PE/EPDM, PE/EEA as polymer matrixes and carbon black as conductive fillers. The results show that under a certain radiation dose, a remarkable improvment of the PTC intensity and the reproducibility of PTC curves of most polymer blends can be achieved,and Negative Temperature Coefficient (NTC) effects are decreased or eliminated. The mechanism of crosslinking structure on improving and stabilizing the PTC functions of polymer blends is also discussed through modern structural analysis methods. In this paper, an interesting and significant phenomenon is discovered. The PTC curve of PE/EPDM/CB composite presents an obvious NTC phenomenon as the dose exceeding 2 MGy.*

INTRODUCTION

Polymer composite PTC materials doped with conductive carbon blacks can be used as self- regulating heaters, current limiters and overcurrent protectors, etc.
One fact of great importance in applications of composite PTC materials is their stability under operating conditions. In our earlier work (Yang Huali et al., 1993), the influences of radiation crosslinking on the PTC effects of PE/CB blends have been studied. In this article, the problems on the stability of PTC characteristics of PE/CB, PE/EPDM/CB, PE/EEA/CB blends after radiation crosslinking and the stability mechanism of crosslinking structure on PTC effects are discussed in more detail. We also study the temperature dependence of resistivity of the PTC materials under much higher dose. As the dose exceeds 2MGy, the

NTC effects of PE/EPDM/CB composites have been found after the melting point. This new result is explained reasonably by the mechanism of radiation degradation.

EXPERIMENTS

The structure parameters of polymer matrixes and the specification of carbon black are shown in Tables 1 and 2, respectively. Polymer and carbon black were mixed in a Brabender for 5-6 min., roll- milled for 5-6 min., and compression-molded to about a 1-mm-thick sheet. The mixing and molding temperatures are shown in Table 1.
The samples were irradiated in ^{60}Co- γ -ray at room temperature with a certain dose rate in air. The gel fraction was determined by the method of solvent extraction. The ESR spectra of the irradiated samples were obtained from a Bruker ER 200D EPR.
A digital multimeter was used to measure lower electrical resistivity. When it exceeded $10^8\,\Omega$, an insulating resistance tester with a programmed temperature controller was used.

Table 1 The Parameters of Polymer Matrixes and Processing Temperature

Polymer	Melting Index (g/10min.)	Density (g/cm^3)	Melting Point (℃)	Processing Temperature	
				Mixing	Molding
HDPE1	1.2	0.954	130.8	150	150
HDPE2	0.2	0.950		150	150
HDPE3	2.0			150	150
LDPE	2.0	0.925	107.1	140	140
EEA	6.0	0.930	89.8	140	140
EPDM	EPT-4050				

Table 2 Physical and Chemical Properties of Carbon Blacks

	Average Size (nm)	Surface Area (m^2/g)	DBP Value (ml/100g)	pH Value
CSF-III	70	230	280	7.0-9.0

RESULTES AND DISCUSSION

The influences of radiation crosslinking on stability of PTC functions

It is clear from Fig.1 and Fig.2 that the stabilities of PTC fuctions of HDPE/CSF and LDPE/EPDM/CSF blends are improved significantly after a certain radiation dose. This can be reflected from two aspects. First, the high reproducibility of polymer blends is obtained undergoing many heating/cooling cycles. Second, the NTC effect is eliminated and the PTC intensity increases.

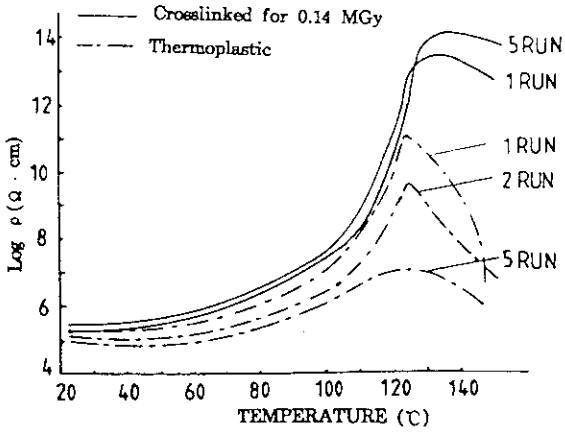


Figure 1 The effect of radiation crosslinking on the PTC intensity and reproducibility of HDPE/CB composite

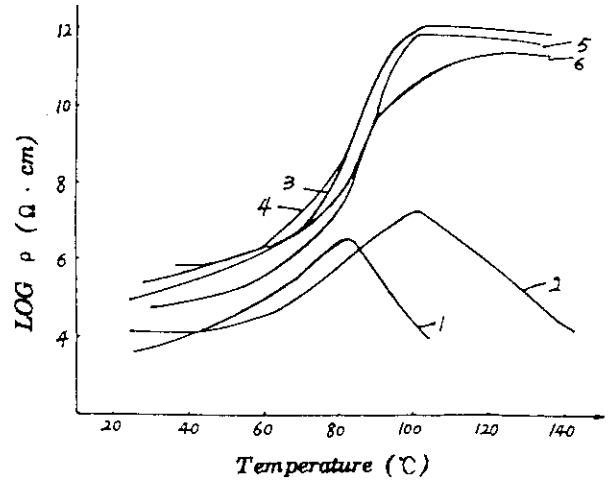


Figure 2 The PTC effect of LDPE/EPDM/CB composite crosslinked for (MGy):(1) 0; (2) 0.01; (3) 0.05 (4) 0.15; (5) 0.5; (6) 0.8

The mechanism of the stability of PTC functions

Though researchers have known earlier that the PTC stability of polymer-CB composite can be improved by radiation croslinking, it has not systematic studies up to date about the micromechanism of how crosslinking structure can affect PTC effects. The authors suggest the crosslinking structure can stabilize the PTC effect of polymer-CB composite from three aspects.

(1) During the croslinking process of linear polymer matrix, CB particles or aggregates participate partly in the crosslinking reactions, thus obviously increase the chemical bindings or physical adsorptions of CB particles on polymer matrix, that is, some CB particles participate directly in the reactions of intermolecular crosslinks, the others agglomerate at the surroundings of these reacted ones, therefore making CB fillers more stable in the polymer networks, and preventing them from reagglomerate at higher temperatures, thus eliminating NTC effects and improving the reversibility of PTC curve.

The experimental results listed below give strong support to this argument.

Table 3 The Effect of Carbon Black on the Gel Content of Polymers

Polymer Matrix (0.14MGy)	*HDPE*			*LDPE*			*EEA*		
CB content (w/w%)	*5*	*10*	*20*	*5*	*10*	*20*	*5*	*10*	*20*
Gel content (%)	*58*	*60*	*70*	*30*	*34*	*42*	*33*	*40*	*67*

Table 3 shows that under the same radiation dose, the gel fractions of three kinds of polymer composites increase with the increase of CB content. It demonstrates that some CB particles participate directly in the intermolecular crosslinking of polymer. This can also be proved by ESR spectra shown in Fig.3. The free radical concentration of HDPE/CSF compound shows considerable decrease compared with that of pure HDPE.



Figure 3 ESR spectra of the samples for crosslinked 0.2 MGy. The weights of the matrixes for all samples were equal. The spectra were obtained 30 min. after irradiation. (a) HDPE; (b) HDPE/CSF-III.

(2) Much more intensive interactions between CB particles and polar polymer segments can be produced due to the hydroxylic, carbonyl or carboxyl groups which may exist at the surfaces of CB particles. So the PTC functions of composite prepared from polar polymer and carbon black are relatively stable. Fig.4 shows the PTC curve of LDPE/EEA/CB composite. All the samples have not NTC effects at temperatures

exceeding melting point. This is due to the intensiveinteractions between the polar groups of CB particles and the ethoxycarbonyl groups of EEA segments. Part CB particles play a role of physical crosslinking bridge through such fairly intensive interactions.

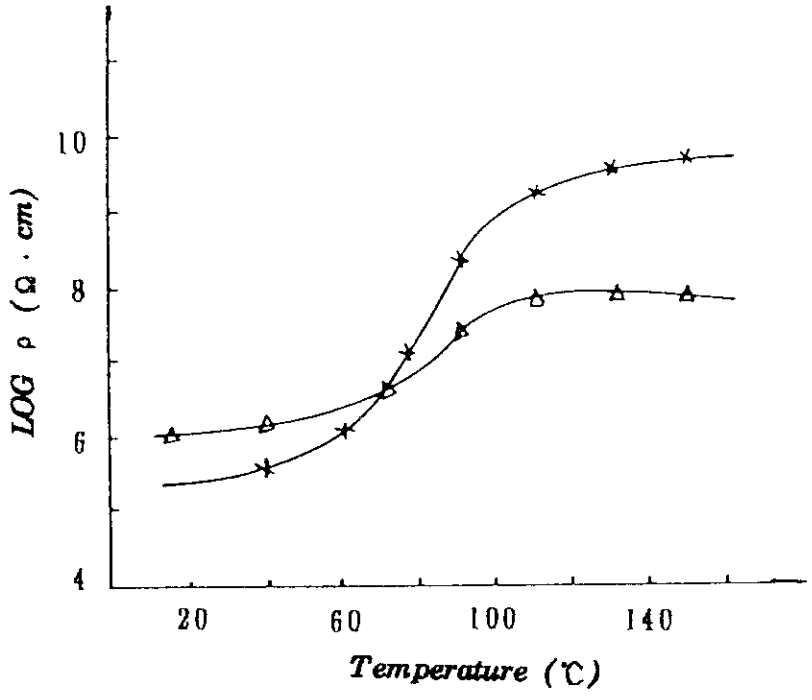


Figure 4 The PTC effect of LDPE/EEA/CSF composite (△) thermoplastic; (×) crosslinked for 0.1 MGy

(3) For radiation doses above the critical value for incipient gel formation, the polymeric system breaks into two phases of sol and gel, and the gel fraction increases with the dose. The gel is composed of crosslinked polymers having an infinite tri- dimentional network structure, which no longer melts above the melting temperature of initial linear polymer. Therefore, for the polymer- CB composite subjected to a certain radiation dose, the whole intermolecular movement at high temperatures disappears when the gel fraction exceeds a definite value. For this network system, at the melting temperature region of its initial linear polymers, the relatively stable distribution of CB particles in polymer matrixes remains, and the redistribution or reagglomerate of CB particles can be much weakened or eliminated, resulting in the disappearance of NTC phenomenon and the enhancement of reproducibility. The opinion mentioned above is proved satisfactorily by the experimental results shown in Fig.2.

Effect of Radiation Degradation

It has been observed in Figure 5 that the NTC effects are particularly pronounced in LDPE/EPDM/CB composites irradiated at much larger doses. In the opinion of the authors the reappearance of NTC phenomenon results from oxidative degradation of the main chains of polymer matrixes. Chapiro (Chapiro, 1962) had indicated that when irradiation is carried out in air, some of the polymeric radicals, which would otherwise lead to crosslinking, react with oxygen to form peroxidic structures which eventually decompose and cause oxidative degradation of the main chains.

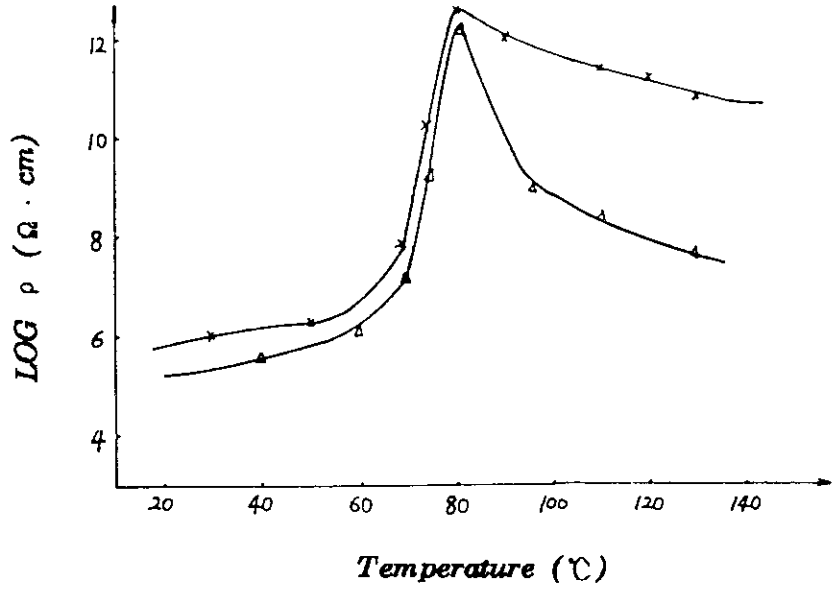


Figure 5 The PTC effect of LDPE/EPDM/CB composite after radiation crosslinking. Crosslinked for:
(×) 2 MGy; (△) 4 MGy.

Because the molecular chains of polymer matrix used contain some structure of polypropylene which can be easily oxidized, the fact that the main chains degradation of LDPE/EPDM polymer matrix occurs under irradiation of the doses higher than 2 MGy is believable. Therefore, the above interpretation on the reproduction of NTC effects of composites under highly radiation dose is reasonable.

REFERENCES

Yang Huali, Tang Hao and Chen Xinfang (1993), Radiat. Phys. Chem., 42 (1-3), 135

Chapiro. A (1962), Radiation Chemistry of Polymeric Systems, P360, John Wiley & Sons, New York, London.

* *The work was supported by National Natural Science Foundation of China*

11.2 An Investigation on Radiation Crosslinked Foam of LDPE/EVA Blends

SIQIN DALAI, CHEN WENXIU

Department of Chemistry, Beijing Normal University, Beijing 100875, China

ABSTRACT

LDPE/EVA blend, irradiated by γ— ray then expansed by heat as a foam material, the EVA content in LDPE/EVA blend was benefited to form gelation. The gel fraction on irradiated LDPE/EVA blend increased with the increasing of its EVA content in a given dose. The gel fraction values of LDPE/EVA blend with 30% EVA content were higher than those of other blends in a same given dose, its gel fraction value was 1.7 times as those values of LDPE without EVA. The gel fractions on LDPE/EVA blend were increased with dose in oxygen, in air and in nitrogen, the formation of gel was limited by oxygen. The oxidation products on foam of LDPE/EVA blend were observed in nitrogen, in air and in oxygen by FTIR spectra. The LDPE/EVA blend system has no protection effect from oxidation comparison with the LDPE system without EVA which has less oxidation product than those without EVA in a same given gel fraction. The gel fraction on foam of LDPE/EVA blend around 25—35%, dose 25±5kGy, irradiated by γ— ray in air or in nitrogen, with higher expansion ratio(19), smaller cell diameter (0.175mm), lower apparent density (0.042g/cm^3), higher tensile strength (0.40MPa) and longer elongation at break (290～360%) on foam of LDPE/EVA blend were selected. It was opitimun condition for application in this systems. The relations among gel fraction on LDPE/EVA blend, expansion ratio, apparent density, average cell diameter and mechanical properties of foamed sheet were discussed.

KEYWORD: Radiation crosslinking, foam, low density polyethylene, ethylene — vinyl acetate copolymer, blend.

INTRODUCTION

The application of crosslinked polyethylene (PE) foamed sheet has expanded, due to its insulation of heat and resistance to shock. The traditional manufacture of polyethylene containing foaming agent and peroxide crosslinking agent was foamed by heating[1]. If polyethylene containing foaming agent and crosslinking by irradiation without crosslinking agent, and then foamed by heating[3], compare with the traditional, which had smooth surface due to the uniform of crosslinking[2]. Radiation crosslinked PE foam also induced by electron beam (EB)[4][5]. High energy was requested, owing to the limitation of penetrating of EB for the thickness of sheet[2]. High expansion ratio PE foam, crosslinked by irradiation, was in the range 25— 35% of gel fraction. This paper examined emphasis to irradiated dose, mechanical properties, the benefit of EVA content on LDPE/EVA blend. The influence of atmospheres and the effect of dose rate have been studied. The Fourier transform infrared (FTIR) spectra of foamed sheets revealed the oxidation level. The relations among gel fraction of LDPE/EVA blend, expansion ratio, apparent density, average cell diameter, and tensile properties of foamed sheet were discussed.

EXPERIMENTAL

It was omited by limited space.

RESULTS AND DISCUSSION

1. The gel fraction of foam.

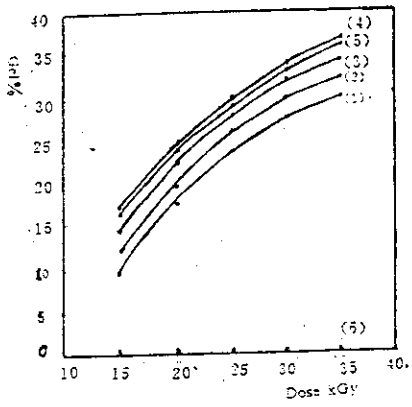


Fig. 1

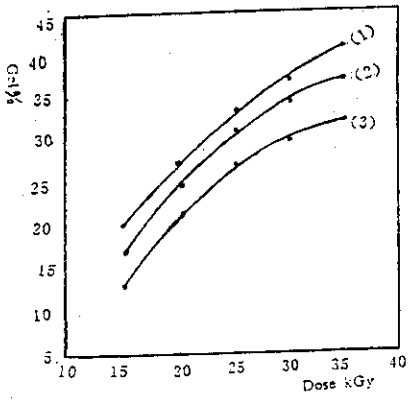


Fig. 2

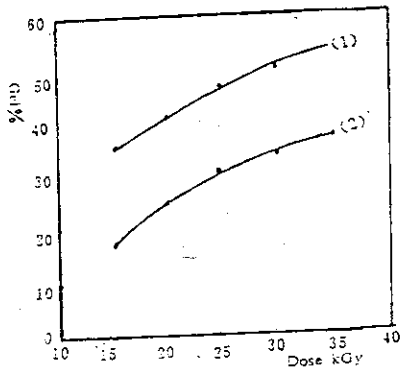


Fig. 3

Fig. 1 Gel% in LDPE/EVA blend with different EVA content versus dose, irradiated by γ— ray in air, dose rate 16.2 kGy/h. With EVA content 0(curve 1), 20%(curve 2), 25%(curve 3), 30%(curve 4), 50%(curve 5) and 100%(curve 6) respectively.

Fig. 2 Gel% in LDPE/EVA(70/30) blend versus dose in nitrogen (curve 1), in air (curve 2), and in oxygen (curve 3), irradiated by γ— ray, dose rate 16.2 KGy/h.

Fig. 3 Gel% in LDPE/EVA blend (70/30) versus dose, irradiated by EB (curve 1) and γ— ray (curve 2) in air, dose rate 360 kGy/h and 16.2 kGy/h respectively.

The benefit of EVA content.

Fig. 1 shown the relation of Gel% versus dose that the gel fraction on irradiated LDPE/EVA blend increased with the increasing of its EVA content in given dose. The gel fraction values of LDPE/EVA blend with 30% EVA content were higher than those of other blends in a same given dose, its gel fraction values were 1.7 times as those values of LDPE without EVA. If the EVA content in blend was increased up to 50%, the gel fractions of LDPE/EVA blend haven't increased further, there was a maximum value of gel fraction in the LDPE/EVA blend with 30% EVA content in each given dose, i.e. the gel fraction value of blend was not composed by each component of blend additionally. Curve 6 shows that no gel was formed in EVA without LDPE in given dose. That means the EVA content in irradiated LDPE/EVA blend system possessed sensitive effect to gel fraction, this effect was favourable to drop the request dose for gelation.

The influence of the atmospheres.

Fig. 2 shown that gel fractions of irradiated LDPE/EVA blend versus dose in oxygen, in air and in nitrogen, the gel fractions irradiated in oxygen were less than those of in air and in nitrogen, due to oxygen as a scavenger of radicals inhibiting the crosslinking of blend by diffusion. So, the effect of radiation atmospheres must be considered in LDPE/EVA blend system.

The effect of dose rate.

Fig. 3 shown that the Gel% versus dose in various dose rate. In higher dose rate, irradiated by EB, the gel fraction of LDPE/EVA blend was higher than those in lower dose rate, irradiated by γ— ray, because the reaction rate of radicals was accelerated in higher dose rate compare with the diffusion controlled of oxygen. Suitable dose rate was favourable to irradiated foamed sheet of LDPE/EVA blend.

2. The oxidation product in irradiated sheet of LDPE/EVA blend.

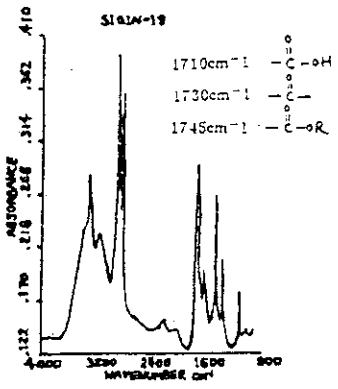


Fig. 4

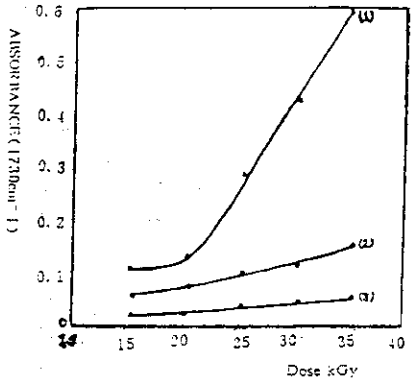


Fig. 5

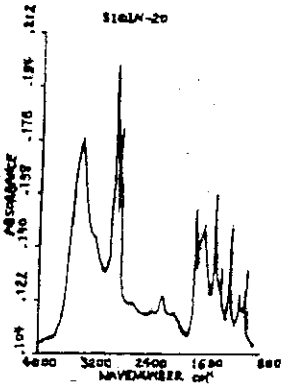


Fig. 6

Fig. 4 FTIR spectra on LDPE without EVA, irradiated by γ— ray in air.

Fig. 5 Absorbance in the 1730cm⁻1 on LDPE Without EVA versus dose in oxygen (curve 1), in air (curve 2) and in nitrogen (curve 3), irradiated by γ— ray.

Fig. 6 FTIR spectra on LDPE/EVA blend, irradiated by γ— ray in air.

For comparison, the FTIR spectra of irradiated LDPE samples without EVA in air was shown in Fig. 4. The spectra in the 1700cm⁻1 region with three bands were observed, i. e. 1710cm⁻1, 1730cm⁻1 and 1745cm⁻1, indicated various ketonic groups were formed by oxidation during irradiation[6]. The absorbance of the >c=o band at 1730cm⁻1 in different atmospheres versus irradiated dose was shown in Fig. 5. The absorbance in the 1730 cm⁻1 increased with the increasing of dose in oxygen, in air and also in nitrogen. The absorbance of ketonic groups in oxygen was stronger than those in air and in nitrogen, especially a sharp slope was observed above 20 kGy in oxygen. The reaction machanism has explained by Torikai[7].

The oxidation product of LDPE/EVA blend (70/30) was also examined by high resolution FTIR spectrometer, as shown in Fig. 6. The absorbance in the 1730cm⁻1 in different atmospheres, dose 25 kGy, was listed in table 1.

Table 1. Absorbance in the 1730cm⁻1 on LDPE/EVA blend (70/30), irradiated by γ— ray in different atmospheres, dose 25 kGy.

atmospheres	oxygen	air	nitrogen
absorbance	0.3012	0.1042	0.0467

The absorbance of LDPE/EVA blend (70/30) (Table 1) compared with of LDPE without EVA (Fig. 5) was similar in a given dose. The absorbance on LDPE/EVA blend in different atmospheres was slightly higher than that of LDPE without EVA, it means there was no protection from oxidation in the blend system with EVA. In accordance with Fig. 1, the request dose for gelation of LDPE/EVA blend (curve 4), was lower than those of LDPE without EVA (curve 1) in a given gel fraction, indicated blend system has less oxidation in comparison with the LDPE system without EVA in a same gel fraction.

3. The physical and mechanical properties on foam of LDPE/EVA blend

Apparent density and expansion ratio

Fig. 7 shown that the apparent density on foam of LDPE/EVA blend increased with the increasing of gel fraction in LDPE/EVA blend. The apparent density on foam of LDPE/EVA blend irradiated in oxygen was smaller than those in air and

in nitrogen.

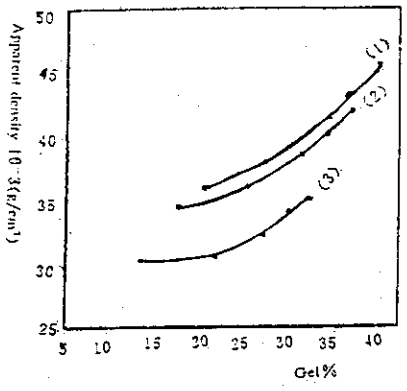


Fig. 7

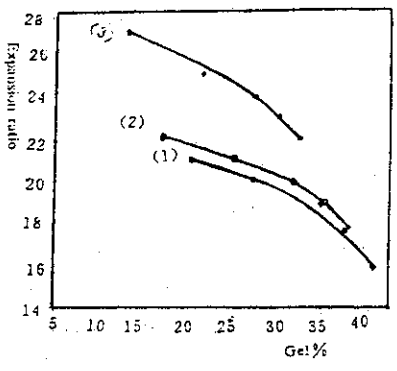


Fig. 8

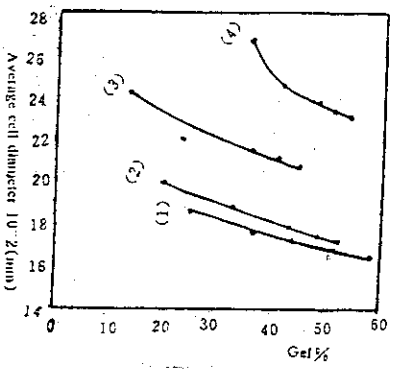


Fig. 9

Fig. 7 Apparent density on foam of LDPE/EVA blend versus gel fraction irradiated by γ — ray in nitrogen (curve 1), in air (curve 2) and in oxygen (curve 3)

Fig. 8 Expansion ratio on foam of LDPE/EVA versus gel fraetion irradiated by γ— ray in nitrogen (curve 1), in air (curve 2) and in oxygen (curve 3).

Fig. 9 Average cell diameter on foam of LDPE/EVA blend versus gel fraction irradiated by γ- ray in nitrogen (curve 1), in air (curve 2) and in oxygen (curve 3), and irradiated by EB in air (curve 4).

Fig. 8 shown that the expansion ratio on foam of LDPE/EVA blend, decreased with the increasing of gel fraction in LDPE/EVA blend. The expansion ratio on foam of LDPE/EVA blend irradiated in oxygen was the highest among them, the expansion ratio on foam of LDPE/EVA blend in air was close on in nitrogen with a higher expansion ratio value of 19, when gel fraction in LDPE/EVA blend was around 25—35%. The apparent density of foamed sheet was 0. 042g/cm3 in the same gel fraction as shown in Fig. 7.

Average cell diameter on foam.

Fig. 9 shown that the average cell diameter on foam of LDPE/EVA blend versus gel fraction which decreased with the increasing of Gel% on LDPE/EVA blend. The average cell diameter on foam of LDPE/EVA blend irradiated in air was close on the value in nitrogen. The smaller average cell diameter on foam was, the higher tensile strength (Fig. 10), longer elongation at break (Fig. 11), and the more smooth surface were.

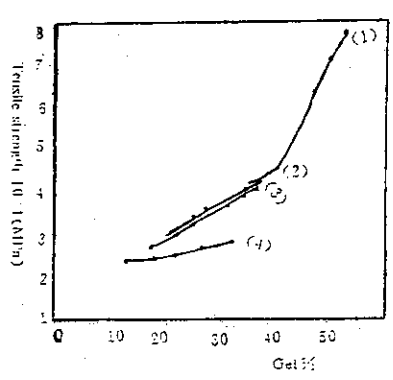


Fig. 10

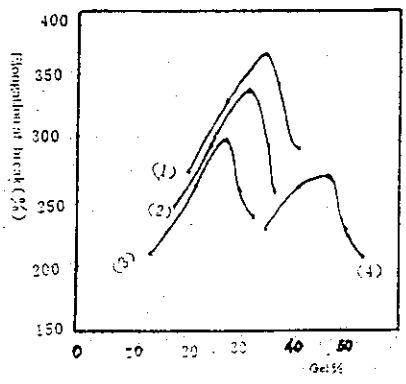


Fig. 11

Fig. 10 Tensile strength on foam of LDPE/EVA blend versus gel fraction irradiated by γ — ray in nitrogen (curve 2), in air (curve 3) and in oxygen (curve 4), and irradiated by EB in air (curve 1).

Fig. 11 Elongation at break on foam of LDPE/EVA blend versus gel fraction irradiated by γ— ray in nitrogen (curve 1), in air (curve 2) and in oxygen (curve 3), and irradiated by EB in air (curve 4).

Tensile strength and elongation at break

Fig. 10 shown that the tensile strength on foam of LDPE/EVA blend inereased with the increasing of gel fraction on LDPE/EVA blend. Tensile strength on foamed sheet irradiated in nitrogen was extremely close on the tensile strength in air. Tensile strength in oxygen was the lowest among them, because the peroxide (—0—0—) chain was easily formed during irradiation in oxygen, so that the tensile strength was decreased by above weak peroxide chain, which coincided with the results of FTIR spectra as shown Fig. 5. In comparison with Fig. 10, if the gel fraction around 25—35%, besides the higher expansion ratio(19), smaller cell diameter (0.175mm), lower apparent density (0.042g/cm3), the tensile strength value of foam was 0.40 MPa during irradiation in nitrogen or in air. So, the physical properties on foam in above conditions irradiated in air were similar as in nitrogen.

Fig. 11 shown the elongation at break on foam of LDPE/EVA blend versus gel fraction. There was maximum value of elongation at break on curves 1、2、3 and 4, whether irradiated in various atmospheres or in different radiation. If the dose was fixed around 25±5kGy, the values of elongation at break were 200～300% with reproducibility, but it will be less reproducibility beyond above dose range. The tensile strength on foam in 25 kGy was similar as the result of EB, so the crosslinking of LDPE/EVA blend can be irradiated by γ—ray or EB.

CONCLUSION

The gel fraction on irradiated LDPE/EVA blend increased with the increasing of its EVA content in given dose. The gel fraction values of LDPE/EVA blend with 30%EVA content were higher than those of other blend in a same given dose. The content of EVA in blend was benefited to gelation.

The gel fractions on LDPE/EVA blend irradiated in oxygen were less than those in air and in nitrogen.

In higher dose rate irradiated by EB, the gel fractions on LDPE/EVA blend were higher than those in lower dose rate irradiated by γ— ray, due to the acceleration of radicals reaction compared with the diffusion controlled of oxygen.

The oxidation products on foam of LDPE/EVA blend were observed by FTIR spectra in nitrogen, in air and in oxygen. The LDPE/EVA blend system hasno protection from oxidation but comparison with the LDPE system without EVA which has less oxidation products in a same given gel fraction, due to which benefited to gelation.

The gel fraction on foam of LDPE/EVA blend was around 25 to 35%, dose 25±5kGy, irradiated by γ— ray in air or in nitrogen, the higher expansion ratio (19), smaller cell diameter (0.175mm), lower apparent density (0.042g/cm3), higher tensile strength (0.40 MPa), and longer elongation at break (290%～360%) on foam of LDPE/EVA blend were obtained. It was optimum condition for application in this system.

REFERENCE

[1] Jia, Guo Xing; Plastics (China), 22(1), 45—48 (1993).

[2] T. Kemmotsu et al; Radiat. Phys. Chem, 42(1—3), 97—100(1993)

[3] Demoutev, A.G et al; Plast. Massy, (7), 34—5 (1991)

[4] Chen, Wenxiu et al; J. Radiat. Research and Processing (China), 2(1), 17—21 (1984)

[5] N. Sagane et al; Radiat. Phys. Chem, 18(1—2), 99—108 (1981)

[6] Geuskens, G and kabamba, S; Polym. Degrad. Stab., 4, 1277(1982).

[7] A. Torikai et al; Polym. photochem. 7, 199～211(1986).

11.3 Radiation Modification of LDPE Sheets and its Application

Li Chaoshun Zang Zhihui Rao Zhigong
Zeng Xinmiao Xu Ziyian Wang Binglin

Beijing Radiation Application Research Center
Beijing 100012, China

ABSTRACT

Blend Radiation Graft (BRG), Mutual Radiation Graft (MRG) and Chemical Oxidization (CO) methods were used to modify the surface of Low Density Polyethylene (LDPE) sheets in order to enhance their shear-bond strength in tension load τ (MPa). The results of different methods and their application are compared and analyzed in this paper.

KEYWORDS

Blend radiation graft; Mutual radiation graft; Chemical oxidization; LDPE surface modification; Shear-bond strength

INTRODUCTION

It's very difficult for thermoplastics to be adhered to, such as LDPE, because of their unpolar surface and lower surface tension. There is a broad applying prospects for the composites of LDPE with metal and unmetal materials, so it's important for us to enhance the surface bond strength of LDPE sheets. Many methods, such as chemical modification[1,2,3,4,5], blending modification[6], plasma modification[7,8], light grafting[9] and radiation grafting[10,11,12] etc, had been used by the researchers in the world to enhance the surface affinity of LDPE sheets. Much work of them focused on modification of LDPE particle marterial and membranes. Little had been done in LDPE sheets and its application to industry is also limitted. Here we want to find a suitable way to enhance the surface adhensivity of LDPE sheets through comparing BRG, MRG and CO methods.

EXPERIMENTS

BRG: The polar organic compounds, SMA, EVA and IA were chosen to be blended with LDPE particles respectively by a plasticator at LDPE melting temperature for ten minutes, then the blended samples of sizes 100mm×25mm×1.2mm with frosted surface were separately dipped in water(H), irradiated with ^{60}Co γ-ray(R), dipped in water after irradiated(RH), dipped in 2%NaOH liquid after irradiated(RS) and dipped in methanol liquid with 2%NaOH after irradiated(RA), then were dried for later use. Table 1 shows the components of each blended sample.

Table 1. Components of each blended sample (w/w)

Line	LDPE	SMA	IA	EVA
0	100	0	0	0
1	100	0.46	0.91	0
2	100	0.46	0	0.91
3	100	0	0	2.50

MRG[14]: LDPE samples of sizes 100mm×25mm×1.2mm were put into the grafting bottles with acrylate acid (AAC), methanol, Mohr's salt and water as grafting monomer, chain adjusting agent, inhibitor and solvent respectively. After bubbled N_2 gas for 20 minutes, the bottles were sealed, then irradiated with

^{60}Co γ-ray. The rates of grafting and swelling of some grafted samples were measured, the other samples were washed by water and dried for later use.

$$\text{Graft\%} = \frac{\text{sample weight after grafted - sample weight before grafted}}{\text{sample weight before grafted}} \times 100\%$$

$$\text{swell\%} = \frac{\text{swelled sample weight - unswelled sample weight}}{\text{unswelled sample weight}} \times 100\%$$

CO: LDPE samples of sizes 100mm×25mm×1.2mm were dipped in oxidizing liquid, which is composed of 5 weight fraction $K_2Mn_2O_7$, 8 weight fraction water and 100 weight fraction 98% sulfuric acid, at different temperatures for some minutes, then washed the oxidized samples to PH=6 and dried them for shear-bond strength test.

Shear-Bond Strength Test: Ten samples (as one group) treated by the same methods were separately adhered to the steel sheets of sizes 100mm×25mm×1mm by epoxy resin adhesive agent . The τ values were measured according to ISO-4587-79 method. The average τ value of each group is given in this paper.

RESULTS AND DISCUSSION

BRG: The polar organic compounds transfered to the surface of blended sheets to enhance the surface affinity, and the polar environment could accelorate the polar organic compounds transferation. Comparing τ_{H0} with τ_{H1-3} in Table 2, We find easily that the blended polar organic compounds can enhance the adhensivity of LDPE sheets. However, there is a thin interface at the surface of sheets made by the transfered moleculars which would be peeled out with the fixed adhensives in tension load, which will decrease the modification effects. In order to eliminate the thin interface, the blended sheets were irradiated with ^{60}Co γ-ray, and the transfered polar organic compounds were grafted to the surface of LDPE sheets. The τ values of irradiated blended sheets are higher than that of unirradiated LDPE sheets (comparing the τ_{R1-3} with τ_{H1-3} in Table 2). Oxide is very important to the LDPE sheets modification during irradiation. Unsaturated chemical bonds and/or peroxides as surface active spots are produced when the LDPE sheets are irradiated, thus the active spots can enhance the surface affinity and the shear-bond strength of the LDPE sheets(comparing τ_{1H} with τ_{1RA}); On the other hand, the polar molecules, such as water, sodium hydroxide, methanol and expoxy resin, can react with the LDPE matrix at the active spots. The τvalues of the irradiated sheets after treated by water, sodium hydroxide and methanol are higher than that of unirradiated sheets as well(see Table 2.).

Table 2. τ (MPa) of LDPE sheets in BRG

Line	H	R	RH	RS	RA
0	0.77	1.57	1.24	1.97	2.76
1	0.90	1.64	1.59	2.20	3.65
2	1.21	1.59	1.47	2.14	3.18
3	1.27	1.62	1.51	1.77	3.39

MRG: The rate of grafting is affected by monomer concentration, radiation dose, dose rate and chain adjusting agent concentration in the grafting system. The reaction results are shown from Fig.1 to Fig.4. The grafting reaction is controlled by the difussion of monomers and radicals, so the lower dose rate and long time is necessary for grafting (see Fig.4). Methanol is very important to inhibit the homopolymerization of monomers and to decrease the viscosity of the reaction system, so the monomers are easy to diffuse to the surface and inner of the LDPE sheets, and the grafting reaction is also from the surface to the inner of the LDPE sheets at the same time[13]. From the plots of the rate of swelling against the rate of grafting (see Fig.5), we get the same result as indicated above. The grafting system with methanol can be used again(see Table 3),but more methanol moleculors will inhibit the grafting reaction. From Fig. 3, we find that the best concentration of methanol as chain adjusting agent is about 15%(m/m).

Table 3. Graft% of the grafting system used once and once again

Sample No.	dose rate (Gy/h)	dose (Gy)	AC%	methanol%	Mohr's salt%	Graft%
1	4.8×10^3	2.0×10^4	40	15	0.5	6.05
2	1.0×10^4	2.0×10^4	40	15	0.5	4.65
1[a]	4.8×10^3	2.0×10^4				5.58
2[a]	1.0×10^4	2.0×10^4				3.87

a: grafting system used once again.

Although methanol is great advantageous to grafting and can increase the rate of grafting, it is not advantageous to enhance the shear-bond strength. The shear-bond strength associates with not only the rate of grafting but also the number of the grafted function groups on the surface of LDPE sheets. From Table 4 and Table 5, we find that the τ value of the LDPE sheet at lower rate of grafting (1.22%) without methanol in the grafting system is higher than that of higher rate of grafting (6.25%) with methanol, because the grafting reaction without methanol is focused on the surface of LDPE sheets. Certainly, the shear-bond strength of the modificated LDPE sheets which is higher than the tension strength of LDPE matrix itself has no practical use for adhension.

Table 4. τ values of grafed samples[a]

Graft%	1.22	21.35
τ (MPa)	>7.23[b]	>7.25[b]

a: grafting system without methanol.

b: LDPE matrix was torn.

Table 5. τ values of grafted samples[a]

Graft%	0	2.78	6.25	12.81	16.51	23.64
τ (MPa)	0.84	6.23	6.67	>7.26[b]	>7.10[b]	>7.15[b]

a: grafting system with methanol.
b: LDPE matrix was torn.

CO: The surface adhensivity as well as the surface affinity increased with the surface oxidization, but the mechanical properties and surface adhensivity decreased with undue oxidization. From Table 6 and Table 7, we find that the appropriate oxidizing conditions for the modification of LDPE sheets are 5 minutes at 65℃ or 10 minutes at 55℃.

Table 6. Change of τ value with temperature in CO
(the oxidization time is 5 minutes)

Temp. (℃)	55	60	65	70	75
τ (MPa)	5.78	6.21	6.26	6.11	6.95

Table 7. Change of τ value with time in CO
(the oxidization temperature is at 55℃)

Time (min)	5	10	15	20	25
τ (MPa)	6.71	7.38[b]	7.10	7.48[b]	7.00

b: LDPE matrix was torn.

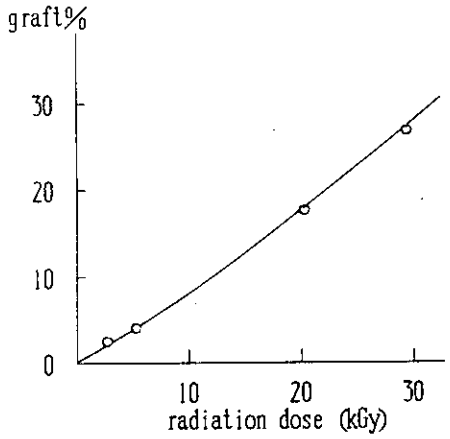


Fig.1 Effect of radiation dose on graft
Dose rate: 1×10³Gy/h; Methanol: 15%(m/m)
AAC: 40%(m/m); Mohr's salt: 0.5%(m/m)

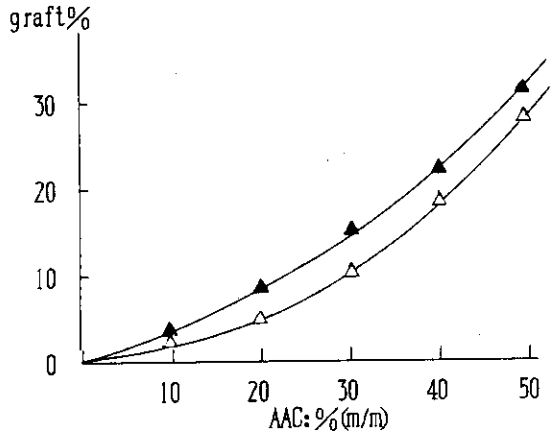


Fig.2 Effect of AAC on graft
Dose rate: 1×10³Gy/h; Totaldose: 2×10⁴Gy
▲: with 15%(m/m)methanol; △: without methanol
Mohr's salt: 0.5%(m/m)

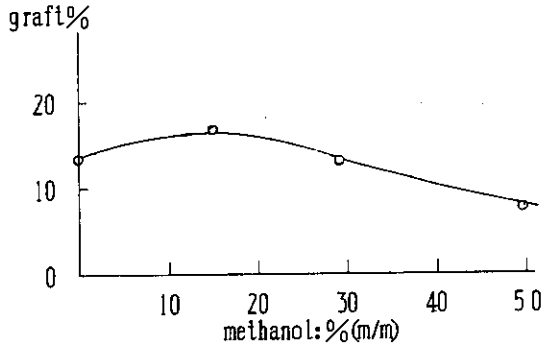


Fig.3 Effect of methanol on graft
Dose rate: 1×10³Gy/h; Total dose: 2×10⁴Gy
AAC: 40%(m/m); Mohr's salt: 0.5%(m/m)

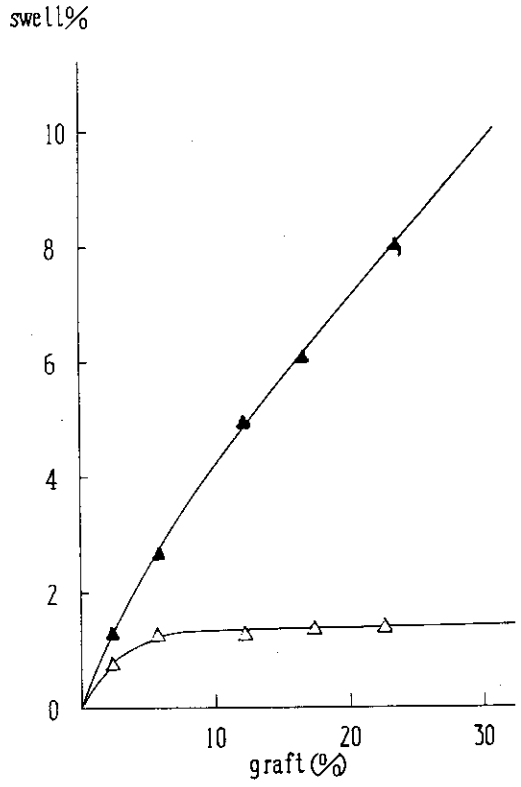


Fig.5 Plot of graft against swell
Methanol: 15%(m/m); AAC: 40%(m/m)
Dose rate: 1×10³Gy/h; Mohr's salt: 0.5%(m/m)
△: Swelling for 10min.; ▲: Swelling for 24h.

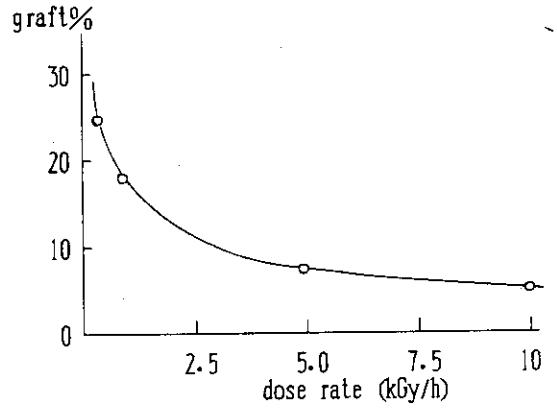


Fig.4 Effect of dose rate on graft
Total dose: 2×10⁴Gy; Methanol: 15%(m/m)
AAC: 40%(m/m); Mohr's salt: 0.5%(m/m)

CONCLUSION

The τ values of the samples modified by BRG are 3-5 times as much as that of unireated LDPE sheets, and BRG method is easy to apply to industrial processing. MRG method is better for the modification of LDPE sheets and the τ values changed with the rate of grafting, it is very suitable to modify some smaller samples because of the limit of their complex grafting technique and conditions. In CO method, the oxidizing agent, if penetrates the inner of LDPE sheets, will decrease the life-span and mechanical properties of LDPE sheets, and it also pollute the environment when the oxidizing liquid is heated. So the oxidizing agent adhering to the surface of LDPE sheets must be washed off completely. But the method is only suitable to processing a small amount of LDPE sheets.

REFERENCES

1 Blais P, Colloid J. Interface Sci, 1974,47:636.
2 Briggs D. J Modern Sci, 1976, 11:1927.
3 Ludwig P. J Modern Plastics, 1983, 1:78.
4 Liu Yuming. J Chem, 1990, 5:50.
5 Wang Mengzhong, et al. ADHENSIVES APPLICATION HANDBOOK, 1987, 436-440.
6 Qian Fengzhen. Plastics Sci and Techn, 1990, 5:50-54.
7 Hau JR. J polym Sci, 1972, 16:1465.
8 Hansen RH. J POlym Sci, 1966,4:203.
9 Fu Qiang, et al. Micromolecular Material Sci and Eng, 1989, 2:69-73.
10 Yamakawa S, Yamamoto T, J Appl Polym Sci, 1980,25:25.
11 Pekala W, et al. Radiat Phys Chem, 1986, 28(2):173-176.
12 Sidorova LP, et al. Radiat Phys Chem, 1986, 28(4):407-413.
13 Soebianto YS, et al. Angew Makromol Chem, 1987, 152:149-158.
14 Rao Zhigong, et al. J Isotopes,1994, 1:5-9.

11.4 Electron Beam Curing of Dimer Acid-based Urethane Acrylates for Pressure Sensitive Adhesives

Takashi Sasaki*1, Satoe Takeda*2 and Katsutoshi Shiraishi *2

*1Takasaki Radiation Chemistry Research Establishment,
Japan Atomic Energy Research Institute,
1233 Watanuki-machi, Takasaki, Gunma, 370-12 Japan
*2Research Laboratries, Sanwa Chemical Industries Co., Ltd.,
15 Suzukawa, Isehara, Kanagawa, 259-11 Japan

ABSTRACT

Polyester urethane diacrylate prepolymers prepared from dimer acids (DUA) were cured with low energy electron beams to investigate adhesive properties of cured films.Among various type monomers added, monofunctional methacrylates such as isobornyl methacrylate (IBX-MA) were effective for higher peel strength cured films although the dose-to-cure for the mixtures increased to 100 kGy or more.The increase in the molecular weight of prepolymers resulted in lower curing rates but higher peel strength. Aging tests up to 80 °C for four weeks proved good stability in peel strength of the stored products.

KEYWORDS

Electron beam; curing; urethane acrylate; dimer acids, pressure sensive adhesives

INTRODUCTION

Dimer acids, derived from unsaturated higher fatty acids, have been well known as raw materials for polyamide resins which have such industrial uses as hardners for epoxy resins and binders for gravure-inks. Due to their chemical structures, hexagonal alicyclic ring with long hydrocarbon chains, the polymers from the dimer acids have lower glass trasition temperatures (Tg) and flexibility. In the scope of widely utilizing the dimer acids which are available from natural-based and renewable resources, i.e. vegetable oils, research and development work on converting them into radiation-curable prepolymers have been carried out. The preceeding papers from our research group demonstrated the unique properties of cured oligomers based on dimer acids. Such properties are of essencial for pressure sensitive adhesives (PSA) which have a wide range of uses. Thus, in order to develope a non-solvent manufacturing system for PSA products, polyester urethane diacrylate prepolymers prepared from dimer acids (DUA) were cured with low energy electron beams to investigate adhesive properties of cured films.

EXPERIMENTAL

Materials

DUA prepolymers used in the present work were prepared as follows. Initially, polyester was prepared by the reaction of dimer acids with a diol. The polyester was then reacted with isophorone diisocyanate (IPDI), and finally the resulting urethane was allowed to react with 2-hydroxyethyl acrylate (HEA) to give an urethane diacrylate .

Irradiation

A sample solution (DUA or DUA/monomer mixture) was coated on PET film with a baker type applicator at about 25 μm thickness. The coated films were irradiated to be cured using a 60 cm wide Curetron (NHV) at an acceleration voltage of 250kV and a beam current of 30 mA in nitrogen atmosphere.

Mesurements and Testing

Adhesive properties evaluated were 180° peel strength, ball tack and holding power. The 180° peel strength was evaluated on strips of 25 mm width pasted onto a stainless steel panel (SUS 304) at a crosshead speed of 300 mm/min by using a Strograph-W2 (Toyo Seiki Co., Ltd.). The ball tack was measured by the J. Dow method at 30° slope. Holding power was evaluated for a sample adhered onto a SUS 304 panel with an area of 25 mm x 25 mm at 40 °C under a load of 1kg. Gel fraction was measured by Soxhlet's extraction with boiling acetone. Molecular weight was determined by using a Shodex DS-4 (Showa Denko Co., Ltd.). The Tg was measured by using a DSC/5200 (Seiko Instruments Inc.).

RESULTS AND DISCUSSION

Monomer Selection

The adhesive properties of DUA mixed with various monomers are shown in Table 1. The DUA oligomer used here was prepared from dimer acid, 1,6-hexanediol, IPDI, and HEA It can be seen that DUA without monomer can be cured at comparatively low dose and that the

Table 1 Adhesive properties of the oligomer mixed with monomers

Monomer*1	Dose (kGy)	Peel strength*2 (g/25mm)	Ball tack (No.)	Holding power*3 (hr)	% Gel (%)
None	30	7	5	> 24	90
	50	6	5	> 24	92
THF-A	50	25	4	> 24	91
IBX-A	50	540	2	> 24	83
L-A	50	7	5	> 24	79
ID-A	50	5	5	> 24	80
EDCP-A	50	40	6	> 24	79
DCP-DA	20	3	<2	> 24	88
NP-DA	20	4	<2	> 24	89
THF-MA	100	350	10	> 24	75
IBX-MA	100	420	7	> 24	80
L-MA	100	295	16	> 24	78
ID-MA	100	400	13	> 24	74
EDCP-MA	100	100	7	> 24	86

*1 DUA/A = 70/30 DUA/DA = 80/20 DUA/MA = 80/20
A:monoacrylate DA:diacrylate MA:monomethacrylate
THF:tetrahydrofurfuryl IBX:isobornyl L:lauryl ID:isodecyl
EDCP:ethylene oxide modified dicyclopentenyl DCP:dicyclopentenyl
NP:neopentyl-glycol
*2 on stainless steel(SUS 304)
*3 at 40℃, 1kg load

cured film has low peel strength. As for DUA /monomer mixed systems, it seems that the structure of monomer influences the adhesive properties and the curing speed. DUA with mono-acrylate is more reactive than DUA with mono-methacrylate, while the result is reverse as for the peel atrength. DUA with di-acrylate is much more reactive than those with others, but the cured film has low peel strength and tack. As for the structure of mono-acrylate,monomers having cyclic structure (IBXA, THFA and IDA) showed higher peel strength than monomers with linear structure (LA and IDA). Among these monomers IBXA gave the highest peel strength. However, IBXA is unfavorable for practical use because of the strong smell and toxicity. Therefore, isobornyl methacrylate (IBXMA), having moderate smell and toxicity, was selected for diluent of DUA in the following investigations.

Effect of Molecular Weight of DUA

The relationship between moleclar weigth of DUA and the adhesive properties of the cured oligomers are shown in Table 2. These oligomers have the same components (dimer acid, 1,6-hexanediol, IPDI, and HEA) and are mixed with 20% of IBXMA. Table 2 clearly shows the tendency that the oligomer with lower molecular weight is more reactive and the cured film has lower peel strength than the oligomer with higher morecular weight. Therefore, in the design of the adhesive, the oligomer with moderate molecular weight should be chosen in cosideration of the use.

Table 2 Relationship between molecular weight and adhesive properties

Molecular weight of DUA	6,100	17,500	21,200	28,600
Dose (kGy)	10	50	100	150
Peel strength (g/25mm)*1	3	70	600	990
Ball tack (No.)	< 2	< 2	3	11
Holding power (hr)*2	>24	>24	>24	>24
Gel fraction (%)	73	88	89	87

*1 stainless steel(SUS 304)

*2 at 40 ℃, 1kg load

Propeties of DUA Based on Various Diols

Table 3 shows the adhesive properties of cured DUA prepolymers prepared from dimer acids and various diols. These oligomers except the one based on PPG are mixed with 20% of IBXMA. The oligomer based on PPG mixed with 20% of IBXMA was not curable even at the dose of 200 kGy. From Table 3, it is found that oligomer based on various diols showed moderate peel strength and adequate holding power. The oligomer based on PPG seems to be suitable for removable type adhesives.

Table 3 Properties of DUA based on various diols

Diol	Molecular Weight (Mw)	Dose (kGy)	Peel strength*1 (g/25mm)	Ball tack (No.)	Holding power*2 (hr)	% Gel (%)
diethylene glycol	16,300	100	480	10	>24	65
1,5-pentanediol	20,700	100	550	13	>24	78
1,6-hexanediol	21,200	100	600	3	>24	89
polypropylene glycol	26,500	20	135	8	>24	85

*1 stainless steel(SUS 304)

*2 at 40 ℃, 1kg load

Tg of the Cured DUA

Fig. 1 shows the DSC thermograms of cured DUA and DUA/IBXMA mixture. The Tg values determined from the thermograms are below -50 °C. It is rather surprizing that the latter has such a low Tg in spite of high Tg(180 °C) of poly-IBXMA. The high peel strength of the cured DUA/IBXMA mixture is probably due to its low Tg value.

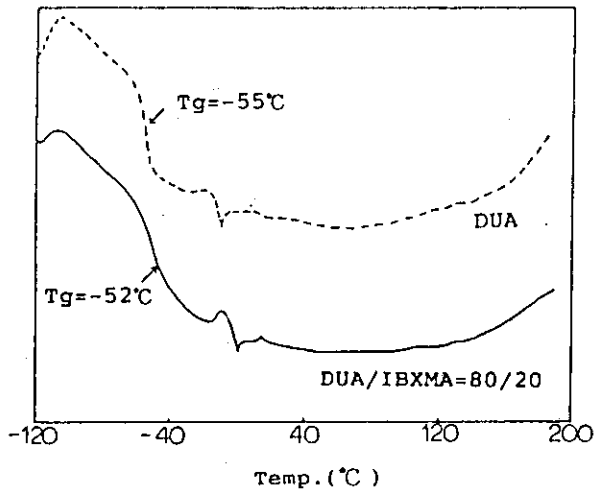


Fig.1 Tg of the cured DUA

CONCLUSION

The present work demonstrated that the EB cured DUA formulations showed high cohesion strength (holding power) and a wide range of peel strength depending upon the chemical structure and molecular weight of the DUA and diluent momers used. It should also be noted that the products had excellent thermal stablity. Thus it can be concluded that EB curing of DUA is one of most potential candidates for non-solvent processing of PSA products.

REFERENCES

1) A.Shakri and T. Sasaki, Proceedings of CRCA '88, pp.202-206
2) K Zaman and T.Sasaki, Proceeding of Radtech Asia '91, pp.359-364

11.5 *The Application of FT-IR Spectrum Method in Photocuring Process for Polyester Acrylate

Cao Jin Lu Xianliang Zhang Zhenli
East China University of Scince and technology
Shanghai 200237 China

Abstract This paper describles that the UV curing process of polyester acrylate can be monitored by measuring the degree of bouble bonds conversion with FT-IR spectroscopy. The various factors effect the UV curing rate. The relation between the curing rate and the concentration of photoinitiator , crosslinking agent , UV light intensity was discussed.

INTRODUCTION

Recently the UV curing technology was widely used in paint、coating 、printed board、ink、opticalfiber、adhesion agent and tooth material etc. field. C. Decker reported that Laser-induced polymerization of mono and multiacrylate monomer has been studied by using infrared spectroscopy. and degree of double bonds conversion was deterimened with the absorbance at 810 cm on IR specturm. This paper describles that the UV curing rate can be expressed by measuring the degree of bouble bonds conversion with FT-IR spectroscopy for polyester acrylate system. It was discussed that curing rate was related mutually to concentration of photoinitiators and crosslinking agent 、UV light intensity.

EXPERIMENT

Material:

The polyester acrylate has been prepared by the easterification with glycol and hexandioic acid. The photoinitiator, Irgacure 651(2, 2 - dimethoxy- 2- phenylacetophenone) and Irgacure 184 (hydroxycyclohexylphenyl acetone) is obatined from Ciba Geigy Co. Ltd. The active diluent, TMPT(trimethylolpropane triacrylate)、EDGA(ethyl diethylene glycol acrylate)、HDDA(hexanediol acrylate), can be get from the market.

Equipment:

The irradiation was carried out with UV radiator which consist of high pressure mercury (power 500W, 1000W, Model GG2) and Al reflect plate and ventilating device for aim at cooling.

Sample preparation and analysis method

According to various molar ratios for polyester, active diluent and initiator were mixed to form photocuring paint. It is plated on KBr disk then UV curing and deterimining degree of double bonds with FT- IR spectroscopy. It exhibited absorption at 810 cm^{-1}(-CH= CH- twisting) under UV irradiation. The decreasing of peak at 810 cm^{-1} will refect the extent of the photocuring processes since the $(A810)_o - (A810)_t$ is directly proportional to the number of acrylate functions. Thus, can be accounted degree of conversion for unsturated double bonds.

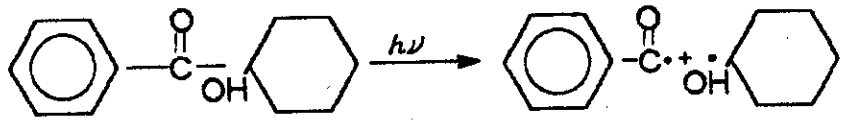
$$C\% = \frac{(A810)_o - (A810)_t}{(A810)_o} \times 100\%$$

RESULTS AND DISCUSSION

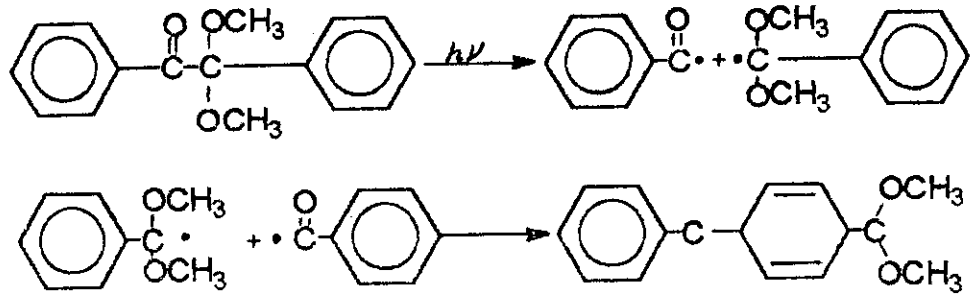
1. Influence of the kinds and concentration of photoinitiators on photocuring rate

The curing rate closely related to the kinds and concentration of initiators in system of paint upon UV irradiation. The initiators absorbed the incident light which lead to production of active radical as a consequence of the reaction of polymerization and crosslinking. The results showed that initiaton rate is in order of Irgacure 184 > Irgacure 651 > Benzophenone(BP). Since Irgacure 184 can straight cleaves to generate two free radical which induce the polymerization reaction. But Irgacure 651 cleaves to generate two free radical which the radical easily recompose to form yellow quinoid compound, decreasing the induce-polymerization rate.

Irgacure 184



Irgacure 651



The influence of the concentration of photoinitiator was illustrated by Fig. 2. The photocuring rate increased with increasing the concentration of initiator. The relation of curing rate and concentration ofinitiator can be represented of $R \propto [S]^{\frac{1}{2}}$

2. Influence of the construction of active diluent curing rate

Three kinds of active diluent were compared with each other. The initiation rate was illustrated as Fig. 3. The double bonds number for trifunctional monomer is more than difunctional monomer or monofunctional monomer. Because trifunctional- have more viscosity than difunctional- or monofunctional- so that the air diffuse difficulty in the system of paint, inhibiting effect of O on radical polymerization at induced step. After the induced reaction, the curing rate decreased with advanceing of initiated reaction for system of coatining trifunctional monomer. It is explained that amount of gel enhanced introduing curing rate droping. In the practical operation, monofunctional-、 difunctional- and trifunctional- were mixed, applied on the coating system.

3. Influence of ratio of oligomer(polyester acrylate) with active dulent on curing rate

It is important that the ratio of oligomer as main component with active diluent applied to photocuring system of paint. The experiment showed that when the molar ratio of oligomer to diluent is 1:1, the curing surface apparent the smooth and bright. The relation of curing rate and concentration of oligomer expresses $R \propto [M]$. Fig. 4.

4. The curing rate relation with UV light intensity

The samples were exposed under high mercury lamp, study the influence of UV intensity which was adjusted by distance of sample from UV lamp on curing rate. The results lead to increase the curing rate in proportion to light intensity. The Fig. 5. recored the relation of curing rate and light intensity $Rp \propto I^{\frac{1}{2}}$

5. For the system of radical polymerization, the presence of O_2 inhibits reaction progress as can be interpreted at Fig. 6. The double bond conversion % when the sample exposed to 5 sec in N_2 can be evaluated to reach near upon 100 %.

6. The post-polymerization was observed when the sample exposed to 5 sec in presence of O_2 then put it in dark at room temperature after one hour, The degree of double bond conversion reached 89. 5%, two hour 90.0%, twenty two hour 92. 0%.

CONCLUSIONS

1. It is found that initiated efficiency for photoinitiator in the system of polyester acrylate arranges Irgacure 184〉 Irgacure 651〉 BP.

2. The relational formula for curing rate and concentration of initiator or concentration of oligomer or light intensity were: $Rp \propto [S]^{1/4}$ $Rp \propto [M]$, $Rp \propto [I]^{1/2}$.

3. The sequence of avtive diluent which advance initiated rate was TMPTMA>TEGDA>HDDA.

REFERENCE

[1] C. Decker and Moussa, Real-Time Kinitic Study of Laser- Induced polymerization Macromolecules. Vol. 22. 4455(1989)

[2] I. K. Shahidi and J. A. Vona, Mod. Paint. Coating. Vol. 21(1975)

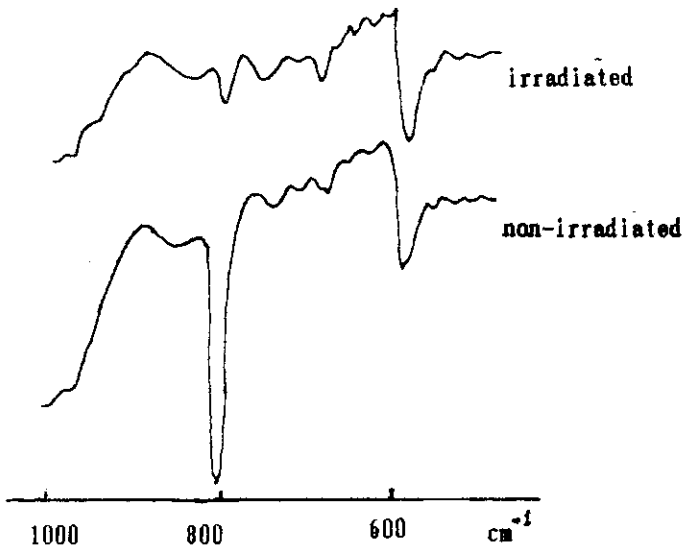


Fig.1. FT-IR spectrum of the sample for irradiated and non-irradiated

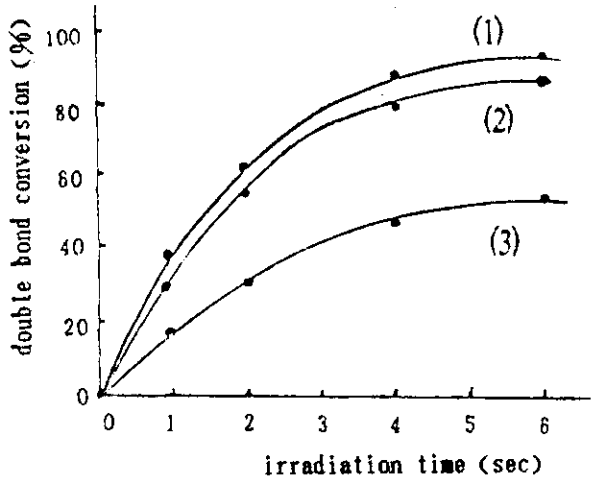


Fig.2. The effect of concentration of photoinitiator on curing rate
Irgacure 184 (1) 5% (2) 3% (3) 1%
oligomer/diluent=1:1

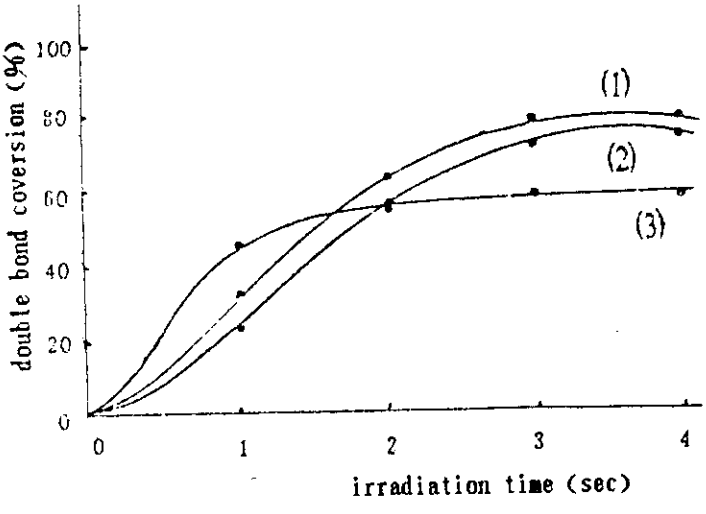


Fig.3. The effect of various diluent on curing rate
(1) HDDA (2) TEGDA (3) TMPTMA
Irgacure 184 3%

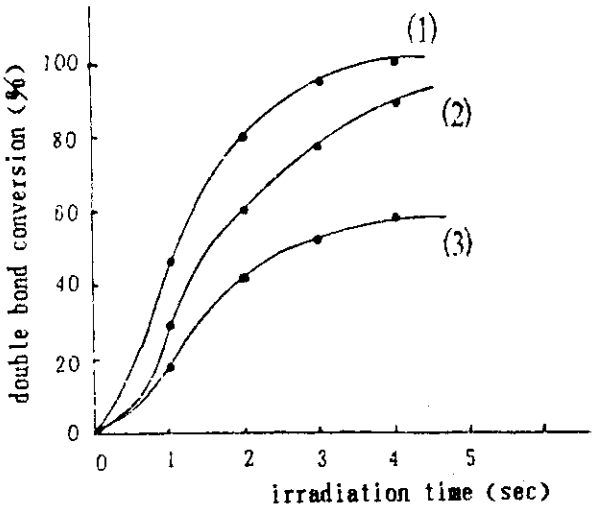


Fig.4. The effect of ratio of oligomer/diluent on curing rate
(1) 2:1 (2) 1:1 (3) 1:2 diluent HDDA

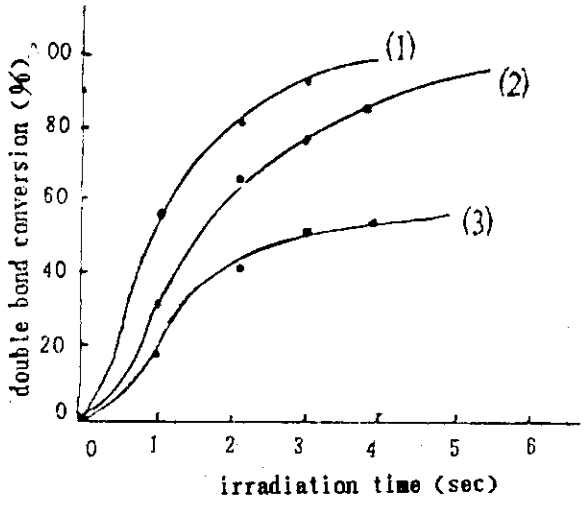


Fig.5. The curing rate relation with light intensity
(1) 93.7(mj.cm) (2) 50.4(mj.cm) (3) 26.7(mj.cm)
oligomer/diluent=1:1

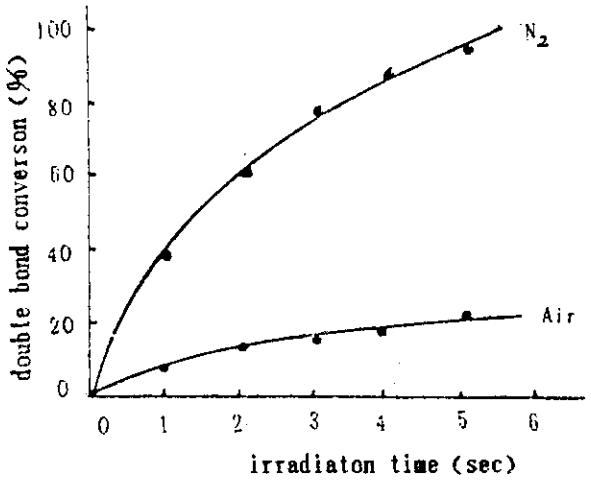


Fig.6. The effect of atomosphere on curing rate
oligomer/diluent=1:1

11.6 Radiation Polymerization and Crosslinking of *N*-isopropylacrylamide in Aqueous Solution and in Solid State

Agneza Safranj[1], Noriyasu Nagaoka[2], Masaru Yoshida[1], Hitoshi Kubota[2], Hideki Omichi[1] and Ryoichi Katakai[2]

[1] Department of Material Development, Takasaki Radiation Chemistry Research Establishment, Japan Atomic Energy Research Institute, 1233 Watanuki, Takasaki, Gunma 370-12, Japan
[2] Department of Chemistry, Faculty of Engineering Gunma University, Kiryu, Gunma 376, Japan

Abstract: Poly(N-isopropylacrylamide) hydrogels were synthesized by radiation induced simultaneous polymerization and crosslinking. Aqueous monomer solutions and pure monomer, without crosslinker, were irradiated in nitrogen atmosphere at a ^{60}Co gamma source. The conversion from monomer to polymer and crosslinked gel was investigated as a function of temperature and monomer concentration. The swelling behavior of the gels showed clear dependence on the synthesis conditions.

INTRODUCTION

Poly(N-isopropylacrylamide) (PNIPAAm) shows a typical thermal reversibility of phase transition in aqueous solutions. That is, it precipitates from solution above a critical temperature called the lower critical solution temperature (LCST) and dissolves below this temperature. When it is crosslinked, the obtained hydrogel collapses above LCST, while it swells and expands below LCST (Hirokawa and Tanaka, 1984). The poly(NIPAAm) hydrogel was used as a model system for thermally induced volume phase transition of gels (Otake *et al.*, 1989) and was proposed for various biomedical applications (Hoffman, 1987).

Crosslinking of linear polymers or polymerization and crosslinking of monomers either by chemical means or gamma radiation has been used to produce these gels. Gehrke (1993) reviewed the study of the variables which can influence the properties of the chemically crosslinked poly(NIPAAm) gels. Monomer purity, reaction temperature, initiator type and concentration and total reaction time all had significant effects on the swelling properties of the gels.

We are interested in the synthesis of PNIPAAm hydrogels by radiation polymerization and crosslinking (Nagaoka *et al.*, 1993). Here we describe the synthesis of this hydrogel by radiation polymerization and crosslinking in aqueous monomer solution and in pure monomer. Since there is no crosslinker in these systems, we refer to such gels as "self-bridged" gels. The mechanism of the gel formation is different in the aqueous solution from the crosslinking in the pure monomer. In the case of the aqueous solution, the monomer radicals are mainly formed by the indirect effect of radiation based on the reaction of the products of water radiolysis with the monomer. When bulk monomer is irradiated, the radicals are formed by the direct radiation effect. The difference in the radical formation and the mechanism of polymerization and crosslinking in these different systems, depending also on irradiation temperature and dose, are responsible for the different microstructures of the gels that results in different swelling behavior.

The results described here are part of a systematic study of the mechanism of crosslinking and swelling behavior of self-bridged poly(NIPAAm) gels, that started recently in our laboratory.

EXPERIMENTAL

In the work reported here, the synthesis was done by irradiating a 10 % w/w aqueous solution of NIPAAm (Eastman Kodak), in a glass tube with 3 mm inner diameter. All irradiations were carried out under nitrogen atmosphere at 25 °C with a ^{60}Co gamma source with doses up to 1000 kGy at dose rate of 10 kGy/h. The pure monomer was also irradiated under the above mentioned conditions, at several different temperatures in the range from 0 to 80 °C (The melting point of N-isopropylacrylamide is 65 °C).

After the polymerization the gels were removed from the tubes and washed in distilled-deionized water for three weeks. The gel fraction was measured after Soxhlet-type extraction in ethanol for 24 h and drying the extracted gel in vacuum to constant weight. The swelling is determined gravimetrically after 24 h equilibration of gels in water at fixed temperature, then calculated as a weight ratio of the swollen sample to the dry one.

RESULTS AND DISCUSSION

When the monomer is irradiated in aqueous solution, monomer radicals are mostly generated by the indirect effect based on the reactions of the products of water radiolysis with the monomer [Chapiro, 1962]. Some of these intermediates will form monomer radicals, while others undergo recombination or other reactions. Radicals are also generated by the direct radiation effect, but to a much lesser extent. After these initial processes, monomer radicals combine and propagate to form a linear or slightly branched, but soluble polymer (sol fraction) until the dose reaches the gel point. Once the polymer is formed, it is itself radiolyzed, since the primary $H^{\cdot}$ and $OH^{\cdot}$ radicals are very efficient for abstracting hydrogen from the polymer molecule. These polymer free radicals also contribute to chain initiation and cross-link formation. Once the gel point is reached, the amount of the gel grows rapidly (Fig. 1).

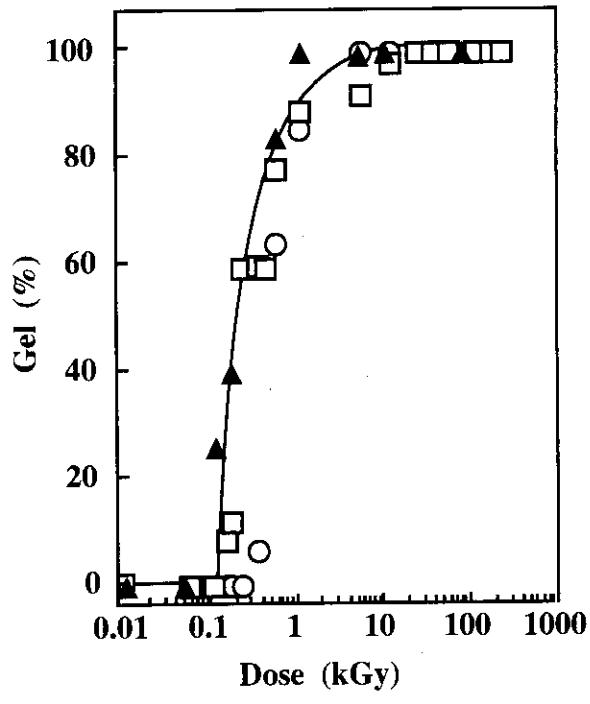


Fig. 1. Gel formation during irradiation of: (○) 5 w/w %; (□) 10 w/w %; and (▲) 20 w/w % aqueous solutions of NIPAAm.

PNIPAAm gels can also be obtained by radiation polymerization and cross-linking of the pure monomer. In this case, the radicals are formed only by the direct radiation effect, and they mobility is low, thus the gel doses are much higher than in the case of polymerization in aqueous solutions (Fig. 2). For example, the gel dose for pure monomer is about 13 kGy at 25 ° C, as compared to 71 Gy in 10 w/w% aqueous solution, at the same temperature. The radiolysis of the polymer also occurs, and these polymer radicals will to some extent contribute to the further polymerization and crosslinking. With the increase in temperature the mobility of the molecules increase and the gel dose becomes as low as 1.5 kGy near the melting temperature at 60 °C, and only about 8 Gy when the monomer is irradiated in the molten state at 70 °C.

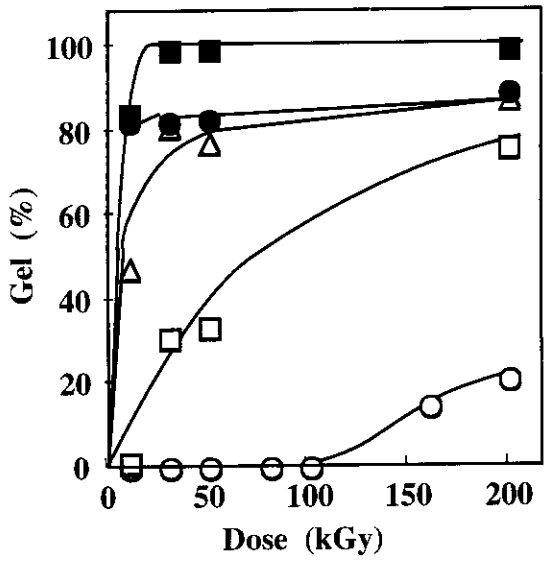


Fig. 2. Gel formation in the irradiated pure monomer at the following temperatures: (○) 0; (□) 25; (△) 60; (●) 70, and (■) 80 °C.

The most important property of PNIPAAm hydrogels is their temperature -induced inverse volume phase transition in aqueous solutions. The volume phase transition of the gels is similar to the coil-globule transition of the polymer chains [Dusek and Patterson, 1968], and the thermoshrinking behavior is caused by a critical balance of hydrophobic and hydrophilic groups at the polymer chain [Taylor and Cerankowski, 1975; Otake *et al*, 1984]. At low temperatures a strong hydrogen bonding between these hydrophilic groups and the surrounding water will cause the formation of a highly organized water layer around the polymer chains [Shild and Tirrell, 1990]. This enables the good solubility of the polymer chains, as well as the swelling of the gels. With increasing temperature the hydrogen bonding weakens, leading to a reduction in the structuring of water around the hydrophobic groups. As this structured water is released, the interactions between hydrophobic side groups of the polymer increase. Above the LCST, which is around 32 °C for PNIPAAm, these hydrophobic interactions become dominant, and the refolding of the polymer chains will cause the shrinking of the gel.

The swelling behavior of the self-bridged PNIPAAm gels is illustrated on Figs 3 and 4. Figure 3 shows the swelling of the gels synthesized from aqueous solutions, while on Fig. 4, the swelling of gels obtained by irradiation of the pure monomer, can be seen. All gels show high swelling at temperatures below 32 °C, and shrinking above this temperature. Besides this expected temperature dependent swelling of PNIPAAm gels, Fig. 3 shows an interesting effect of absorbed dose on the swelling of the gels that shows a difference between PNIPAAm gels synthesized by chemical crosslinking method and by radiation of a pure monomeric system. When gels are crosslinked chemically, usually the lower the crosslinking percentage, the higher the swelling ability of the gels. Above the critical temperature, however, all gels shrink to a similar volume, independently from the crosslinking percentage. In our case, when aqueous solutions of the

monomer are irradiated, the gels synthesized at high doses (high crosslinking percentage), collapse to a much smaller volume than the gels synthesized at low doses. Besides, the change in the swelling with the increase in temperature becomes continuous. This effect reflects the microscopical structure of the gel network, that changes with dose [Nagaoka *et al*, 1993].

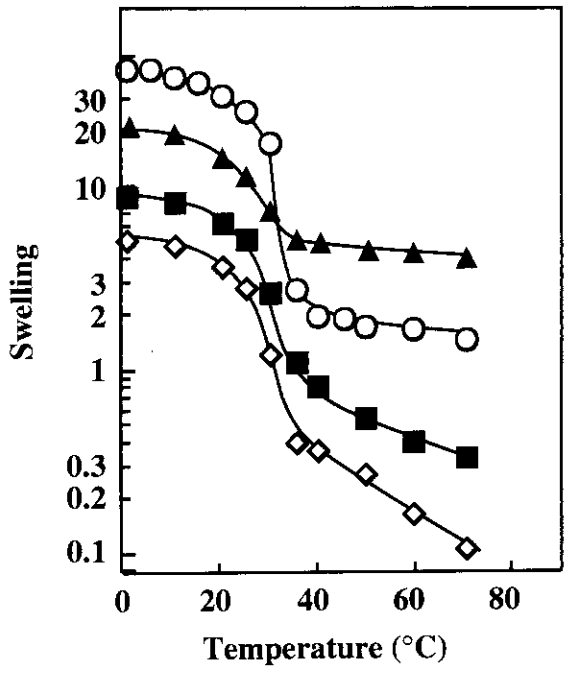


Fig. 3. Swelling characteristics of PNIPAAm gels crosslinked during the radiation induced polymerization of a 10 w/w % aqueous solution of NIPAAm. The solutions were irradiated at the following doses: (O) 20; (▲) 50; (■) 160; and (◇) 320 kGy.

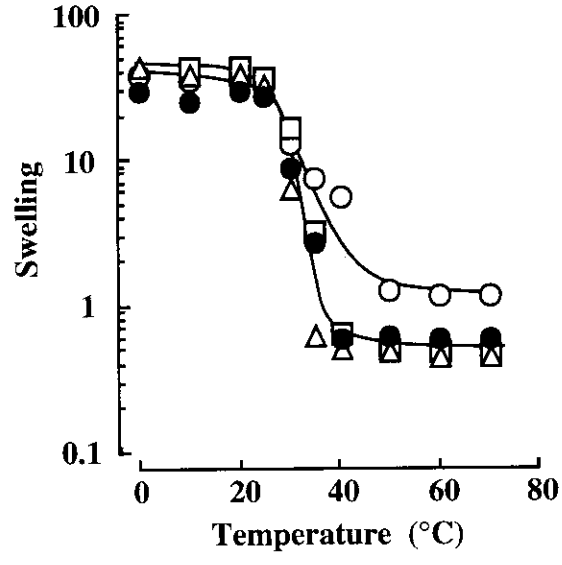


Fig. 4. Swelling characteristics of PNIPAAm gels synthesized by radiation polymerization and crosslinking of a pure monomer at 80 °C and at the following doses: (O) 10; (□) 30; (△) 50, and (●) 200 kGy.

At the start of the polymerization, the network consists only of polymer chains forming giant molecules with branches and entanglements and with very few real crosslink. We call this structure "tree" structure. When the gel swells below LCST, the polymer chains tend to distance from each other. The swollen coils will exclude one another from the volume defined by their radius of gyration. With increasing dose, the fraction of real network ("ladder" structure) would increase. The chains are then forced together by their crosslink points and will overlap somewhat. The higher the fraction of the ladder over the tree structure, the lower the flexibility of the chains, and the gel swells less. At still higher doses, a radiation-induced degradation of the previously formed ladder structure will take place. This degradation will lead to a network structure which we call "broken ladder". This change affects only the shrinking of the gel, because this increased flexibility of chains near the braking point would facilitate the hydrophobic interactions between the polymer chains above the volume phase transition temperature. Besides, in the broken ladder, the pores of the gel became bigger. As a result, more water could be expelled from the network, and the gel collapses to a smaller volume.

On the other hand, when the gels are obtained by irradiating a pure monomeric system above the melting temperature, all gels synthesized with doses between 30 and 200 kGy, have similar swelling behavior (Fig. 4). This fact indicates, that no major changes in the microstructure of these gels occurs under these irradiation conditions. The changes in the crystallinity and the microstructure of these gels is presently under investigation.

REFERENCES

Chapiro, A. (1962). Radiation chemistry of polymeric systems. Interscience, New York.

Dusek, K. and Patterson, D. (1968). Transition in swollen polymer networks induced by intramolecular condensation. *J. Polym. Sci. Part A-2,* 6, 1209-1216

Gehrke, S.H. (1993) Synthesis, equilibrium swelling, kinetics, permeability and applications of environmentally responsive gels. *Adv. Polym. Sci.,* 110, 81-144

Hirokawa, Y. and Tanaka, T. (1984). Volume phase transition in nonionic gel. *J. Chem. Phys.,* 81, 6379-6380

Hoffman, A.S. (1987). Applications of thermally reversible polymers and hydrogels in therapeutics and diagnostics. *J. Controlled Release,* 6, 297-305

Nagaoka, N., Safranj, A., Yoshida, M., Omichi, H., Kubota, H. and Katakai, R. (1993). Synthesis of poly(N-isopropylacrylamide) hydrogels by radiation polymerization and crosslinking. *Macromolecules,* 26, 7386-7388

Otake, K., Inomata, H., Konno, M. and Saito, S. (1989). A new model for thermally induced volume phase transition of gels. *J. Chem. Phys.,* 91, 1345-1350

Schild, G. H. and Tirrell, D. A. (1990). Microcalorimetric detection of lower critical solution temperature in aqueous polymer solutions. *J. Phys. Chem.,* 94, 4352-4356

Taylor, L. D., and Cerankowski, L. D. (1975) Preparation of films exhibiting a balanced temperature dependence to permeation by aqueous solutions - a study of lower consolute behavior. *J. Polym. Sci., Polym. Chem. Ed.,* 13, 2551-2570

12. Poster Presentation (2)

12.1 Collisional Deexcitation Processes of Ne($^3P_2$) by Rare Gas Atoms

Deba Bahadur Khadka, Yuji Fukuchi, Masashi Kitajima, Masatoshi Ukai, Noriyuki Kouchi and Yoshihiko Hatano.

Department of Chemistry, Tokyo Institute of Technology, Meguro-ku, Tokyo 152, Japan.

ABSTRACT

The temperature dependence of the rate constants for the deexcitation of Ne($^3P_2$) by Ar and Kr has been measured in the temperature range from 143 to 296K using a pulse radiolysis method and thus the collisional energy dependence of the deexcitation cross sections is obtained. The collisional energy dependence obtained in this experiment is much different from that obtained by crossed beam experiments. The magnitude of the cross section values are discussed in terms of an electron-exchange mechanism.

INTRODUCTION

Collisional deexcitation processes of excited rare gas atoms by atoms and molecules are one of the fundamental chemical reactions in the gas phase, which provide information to understand the fundamental processes in the interaction of ionizing radiation with matter and the phenomena in ionized gases such as reactive plasmas and upper atmosphere. Excited neon atoms have a large amount of internal energies enough to ionize heavier rare gas atoms, M, (see Fig. 1.) even in thermal energy collisions. The following collisional ionization as divided into Penning ionization (1) and associative ionization (2):

$$Ne(^3P_2) + M \rightarrow Ne + M^+ + e^- \quad (1)$$
$$\rightarrow NeM^+ + e^-. \quad (2)$$

are exclusively dominant in the deexcitation of Ne($^3P_2$).

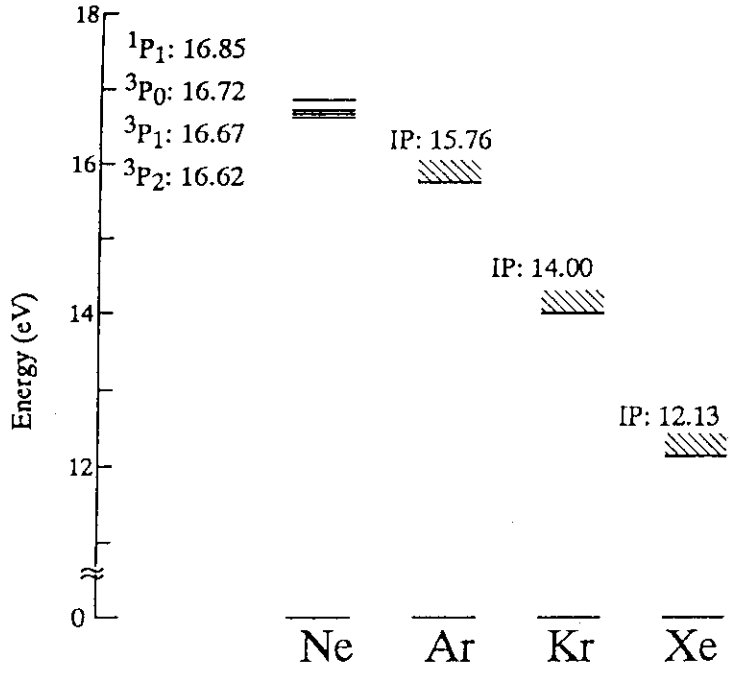


Fig. 1 Energy level diagram of Ne, Ar, Kr, and Xe; excitation energies of Ne*($^1P_1$,$^3P_0$,$^3P_1$ and $^3P_2$) as compared with the first ionization potentials of Ar, Kr, and Xe.

RESULTS AND DISCUSSION

In the deexcitation of $Ne(^3P_2)$ in a Ne–SF_6–M system, the following reactions are exclusively dominant in the present experimental condition (Yokoyama and Hatano, 1981; Yoshida et al., 1993; Hatano, 1983, 1991; Ukai and Hatano, 1991),

$$Ne(^3P_2) \xrightarrow{\tau_0^{-1}} Ne(\text{in pure Ne}), \quad (5)$$

$$Ne(^3P_2) + SF_6 \xrightarrow{k_{SF6}} \text{Products}, \quad (6)$$

$$Ne(^3P_2) + M \xrightarrow{k_M} \text{Products}, \quad (7)$$

where τ_0 is the effective lifetime of $Ne(^3P_2)$ in pure Ne, and k_{SF6} and k_M are the deexcitation rate constants of $Ne(^3P_2)$ by SF_6 and M, respectively. Since the total deexcitation rate of $Ne(^3P_2)$, τ^{-1}, is written as

$$\tau^{-1} = \tau_0^{-1} + k_{SF6}[SF_6] + k_M[M], \quad (8)$$

where $[SF_6]$ and [M] are the densities of SF_6 and M in a Ne–SF_6–M system, respectively. Each slope of τ^{-1} vs. [M] plots in Fig. 2 gives the deexcitation rate constant, k_M, under a constant $[SF_6]$. The velocity averaged (or thermally averaged) cross section is given as

$$\sigma_M = k_M / (8k_BT / \pi\mu)^{1/2} \quad (9)$$

at a mean collisional energy, $E = (3/2)k_BT$, where k_B is the Boltzmann constant, T is the absolute temperature, and μ is the reduced mass of Ne–M, respectively.

The obtained collisional energy dependence of the deexcitation cross section of $Ne(^3P_2)$ by Ar is shown in Fig. 3 together with those obtained by crossed beam experiments (Baudon et al., 1991; Verheijen and Beijerinck, 1986). The present cross section is in good agreement within the experimental errors with those obtained by Yokoyama and Hatano (1981) and West et

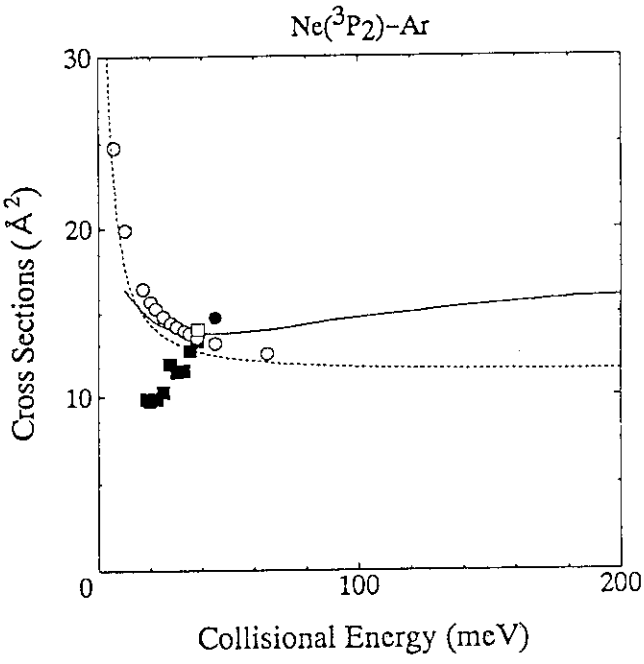


Fig. 3. A comparison of the cross sections for $Ne(^3P_2)$–Ar with those in beam experiments.
■ : represents the present results; ····· (Baudon et al.,1991) and ○ velocity averaged (Baudon et al., 1991); □ (Yokoyama and Hatano, 1981); ● (West et al., 1975); —— (Verheijen and Beijerinck, 1986).

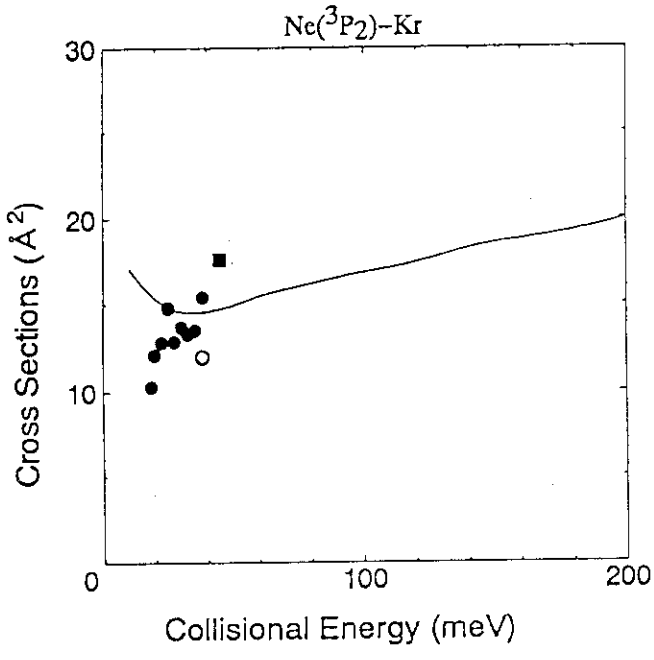


Fig. 4. A comparison of the cross sections for $Ne(^3P_2)$–Kr with those in beam experiment. ● : represents the present results;—— (Verheijen and Beijerinck, 1986); ○ (Yokoyama and Hatano, 1981);■ (West et al., 1975).

The mechanism of Penning ionization can be understood by an electron-exchange interaction between $Ne(^3P_2)$ and M. The mechanism is expressed as (Yokoyama and Hatano, 1981; Aguilar et al., 1990; Van den Berg et al., 1987; Hotop et al., 1981).

$$Ne(^3P_2)[1] + M[2] \rightarrow Ne[2] + M^+ + e^-[1], \qquad (3)$$

where [1] and [2] denote the excited 3s electron in $Ne(^3P_2)$ and an orbital electron of M, respectively. The transition probability of electron-exchange interaction, $W_{ex}(R)$, is given by

$$W_{ex}(R) = \Gamma_{ex}(R) / \hbar = C \exp(-d.R) \qquad (4)$$

where R is the intermolecular distance between $Ne(^3P_2)$ and M, and C and d are constants. The transition probability $W_{ex}(R)$ related to the overlap of target orbitals and the 2p vacant orbital of $Ne(^3P_2)$ increases exponentially with the decrease in R. It has been shown that the spatial electron distribution of M is one of the important factors in the determination of absolute values of the deexcitation cross sections for Ne^*-M (Yoshida et al., 1993).

Experiments of Ne^*-M have been relatively very few as compared with those of He^*-M and Ar^*-M (Yencha, 1984). Measurements of the collisional energy dependence of cross sections have been further limited. There have been reported recently the collisional energy dependence of cross sections for metastable neon atoms by crossed beam experiments. Since, however, pulse radiolysis methods are clearly advantageous to obtain the absolute values of the rate constants or cross sections for the collisional deexcitation of excited rare gas atoms (Hatano,1983; 1991), the temperature dependence of the rate constants for the deexcitation of $Ne(^3P_2)$ by Ar and Kr is measured in this experiment in the temperature range from 143 to 296K, and thus the collisional energy dependence of the cross sections is obtained.

EXPERIMENT

The apparatus and procedure in the present pulse radiolysis experiment have been described in detail previously (Hatano, 1991; Ukai and Hatano, 1991). Briefly, after irradiation by an intense nano-second electron beam pulse onto a mixture of Ne with a trace amount of SF_6 and M in a gas cell, the time-resolved optical absorption of $Ne(^3P_2 \rightarrow 2p_8)$ at 633.44 nm was measured, thereby, the time dependent variation of the density of $Ne(^3P_2)$ was obtained.The trace amount of SF_6 was added to remove thermal electrons produced in irradiated sample gases. The temperature of a sample gas, which corresponds to a mean collisional energy, was controlled by introducing cold N_2 vapor onto the gas cell. The temperature was varied from the room temperature (296K) down to 143K. Sample gases used were commercially available Ne(99.9%), Ar(99.999%), Kr(99.95%), and mixtures (SF_6 / Ne = 0.000731).

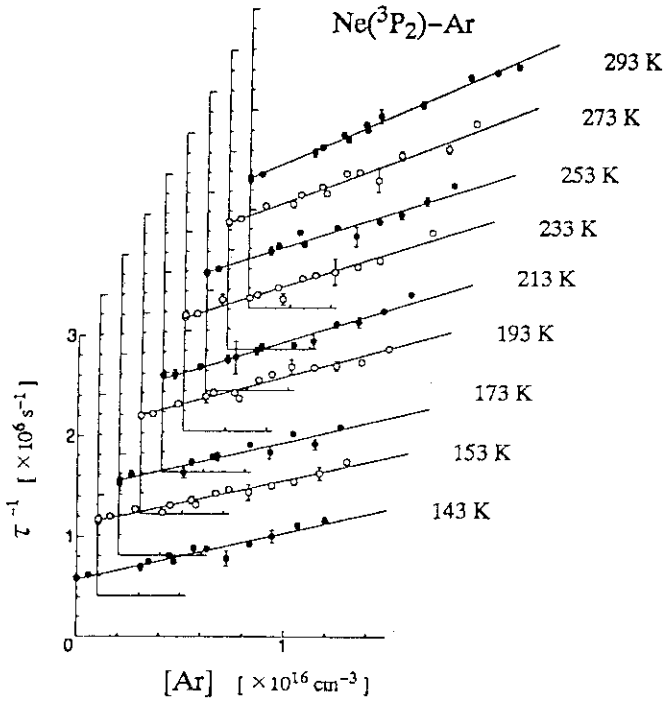


Fig. 2. Kinetic plots for deexcitation rates vs. number densities of Ar.

al. (1975) at room temperature. The present cross sections increase with increasing the collisional energy, whereas the crossed beam result shows a different collisional energy dependence, i.e., the cross sections decrease with increasing the collisional energy. A significant discrepancy exists also in the crossed beam results between the result obtained by Baudon et al. (1991) and that obtained by Verheijen and Beijerinck (1986). The deexcitation cross sections of $Ne(^3P_2)$ by Kr shown in Fig. 4 are again in good agreement with those by Yokoyama and Hatano (1981) and West et al. (1975) at room temperature. The difference in the collisional energy dependence with a beam experiment (Verheijen and Beijerinck, 1986) is also shown. The reason for these discrepancies is not clear at present. Further studies are greatly needed of experiments by means of both pulse radiolysis methods and crossed beam methods as well as of theories concerning the collisional deexcitation of $Ne(^3P_2)$ by M.

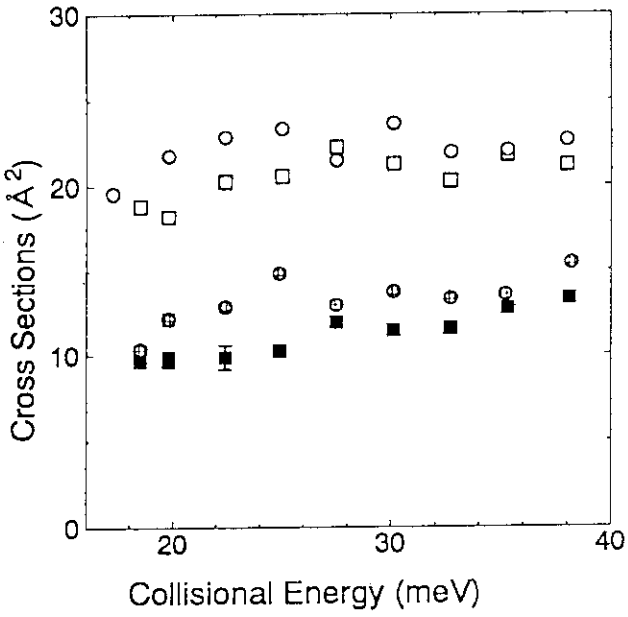


Fig. 5. Collisional energy dependence of the cross sections for the deexcitation of $Ne(^3P_1)$: □ Ar, ○ Kr and $Ne(^3P_2)$: ■ Ar, ● Kr.

The cross section values for $Ne(^3P_2)$ by Ar are slightly smaller than Kr, which is ascribed to the difference in the ionization potential between Ar and Kr. The decrease of the ionization potential of M (see Fig. 1) should increase the electron density outside of the rigid surface of M, i.e.,. the more electron density is possible for Kr than Ar which overlap with the 2p vacant orbital of $Ne(^3P_2)$, leading to the greater probability of Penning ionization due to the electron-exchange mechanism. This interpretation is in good agreement with the autoionization rate for Ne^*-M obtained by a scattering experiment by Gregor and Siska (1981); the value for Kr is greater than that for Ar at the repulsive wall of the interaction potential between Ne^* and M at a given collisional energy. The collisional energy dependence of the cross sections for $Ne(^3P_2)$ by Ar and Kr shown in Fig. 5 together with that for $Ne(^3P_1)$ by Ar and Kr. For both $Ne(^3P_2)$ and $Ne(^3P_1)$, the cross section values slightly increase with increasing the collisional energy. The cross section values for $Ne(^3P_2)$ by Ar and Kr are slightly smaller than those for $Ne(^3P_1)$ by Ar and Kr (Hidaka,1994). This indicates that although the cross sections for $Ne(^3P_1)$ are enhanced by a weakly allowed dipole-dipole interaction, the deexcitation of $Ne(^3P_1)$ by M is dominated also by the collisional ionization due to an electron-exchange interaction.

REFERENCES

Aguilar A., Brunetti B., Gonzalez M. and Vecchiocattivi F. (1990) Chem. Phys. 145 , 211.
Baudon J., Feron P., Miniatura C., Perales F., Reinhardt J., Robert J., Haberland H., Brunetti B. and Vecchiocattivi F. (1991) J. Chem. Phys. 95 , 1801.
Gregor R. W. and Siska P. E. (1981) J. Chem. Phys. 74 , 1078.
Hatano Y. (1983) in The Third International Symposium of the Dynamics of Molecular Collisions, Kaiserslautern.
Hatano Y. (1991) Pulse Radiolysis, chap. 9 (edited by Tabata Y.), p.199. CRC, Boca Raton, FL.
Hidaka K. (1994) Master Thesis, Tokyo Institute of Technology.

Hotop H., Lorenzen J. and Zastrow A. (1981) J. Electron Spectrosc. 23 , 347.
Ukai M. and Hatano Y. (1991) Gaseous Electronics and Its Applications, (edited by Crompton R. W., Hayashi M., Boyd D. E. and Makabe T.), p.51. KTK Scientific, Tokyo.
Van den Berg F. T. M., Schonenberg J. H. M. and Beijerinck H. C. W. (1987) Chem. Phys. 115 , 359.
Verheijen M. J. and Beijerinck H. C. W. (1986) Chem. Phys., 102 , 255.
West W. P., Cook T. B., Dunning F. B., Rundel R. D. and Stebbings R. F.(1975) J. Chem. Phys. 63, 1237.
Yencha A. J. (1984) Electron Spectroscopy–Theory, Techniques and Applications, Vol. 5 (edited by Brundle C. R. and Baker A. D.), p.197. Academic Press, New York.
Yokoyama A. and Hatano Y. (1981) Chem. Phys. 63 , 59.
Yoshida H., Kitajima M., Kawamura H., Hidaka K., Ukai M., Kouchi N. and Hatano Y. (1993) J. Chem. Phys. 98 , 6190.

12.2 Studies of Some Elementary Processes Involving Electrons in the Gas Phase by Pulse-radiolysis Microwave-cavity Technique

Takeyoshi Sunagawa, Takeshi Makita, Hirofumi Musasa, Yoshitsugu Tatsumi, and Hiroshi Shimamori

Fukui Institute of Technology, 3-6-1 Gakuen, Fukui 910, Japan

Abstract The pulse radiolysis-microwave cavity technique has been employed for detection of free electrons in the gas phase. Presented are results of the observation of electron disappearance by attachment to molecules,the electron thermalization (energy loss) processes in the presence of an electron-attaching compound, and the formation of electrons by Penning ionization.

INTRODUCTION

Radiation effects on gaseous media involve a number of elementary reactions associated with reactive intermediates such as electrons, positive ions, free radicals, and atoms or molecules in electronically excited states. It is important to investigate these elementary reactions in order to clarify their specific roles in the chemical consequences of the radiation effects. The pulse radiolysis method has long been used for such purpose. Most intermediates can be detected by measurements of optical absorption or emission, but electrons are hard to be monitored by ordinary means. In order to observe the time variation of the electron density the microwave conductivity method has been combined with the pulse radiolysis and have been successfully applied to studies of electron attachment reactions, electron thermalization, and the Penning ionization process in the gas phase (Shimamori, 1991). The present work presents some new results on these elementary processes, which are brought through further improvement of the experimental and analytical procedures associated with the microwave cavity method.

EXPERIMENTAL

The details of the method and the apparatus were described elsewhere (Shimamori, Tatsumi, Ogawa, and Sunagawa, 1992 a, b). The gas sample in a microwave cavity was irradiated by 3 ns X-ray pulse from Febetron 706, and the change in the microwave conductivity was detected. The output signal from detectors in circuit, which is proportional to the shift of the resonant frequency of the cavity was amplified and fed to a digital oscilloscope. In the electron attachment measurement, the heating mi-

crowaves were additionally applied to the cavity in order to vary the mean electron energy.

RESULTS AND DISCUSSION

(i) Electron attachment

A trace amount of sample compound is added to 70 Torr of Xe, and the lifetime is measured for the first-order decay of electrons due to an attachment reaction. The two-body attachment rate constant is determined from the lifetime so obtained. Varying the heating power we can determine the rate constant as a function of the mean electron energy. The results are shown in Fig.1 for CCl_4, $CFCl_3$, and $CHCl_3$. It has been established that the data of rate constants as a function of the mean electron energy can be converted to the cross sections as a function of the electron energy by "unfolding" the rate constants. The details of the unfolding procedure was described elsewhere (Shimamori, Sunagawa, Ogawa, and Tatsumi, 1994).

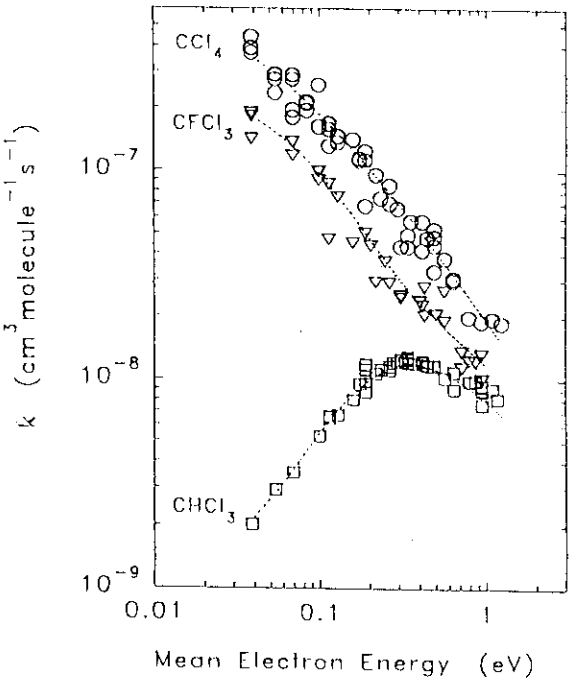


FIG.1 Rate constants for electron attachment to CCl_4, $CFCl_3$, and $CHCl_3$ as a function of the mean electron energy.

Shown in Fig.2 are the cross sections for CCl_4, $CFCl_3$, and $CHCl_3$. Both CCl_4 and $CFCl_3$ show a peak at 0 eV, and the latter has another peak at 0.8eV. $CHCl_3$ exhibits a peak at 0.3eV. These compounds are known to undergo dissociative electron attachment, and the peaks at 0 eV correspond to the formation of Cl^- ion and that at 0.8eV in $CFCl_3$ to the production of Cl_2^-, which is in accord with the result of the electron-impact study (Illenberger, 1982). The peak at 0.3eV in $CHCl_3$ also corresponds to the Cl^- production. The cross sections

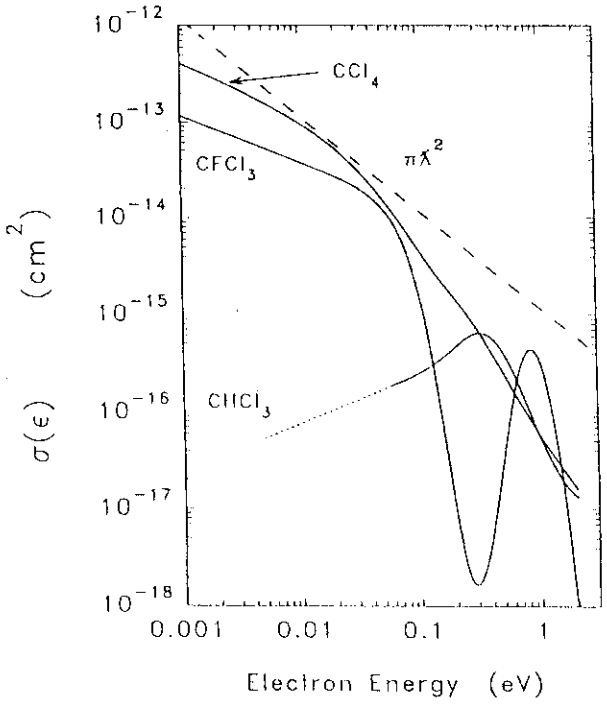


FIG.2 Cross sections for electron attachment to CCl_4, $CFCl_3$, and $CHCl_3$ (solid lines) and the s-wave maximum cross section (dashed line).

for CCl_4 are in good agreement with most previous data.

(ii) Electron thermalization in the presence of electron-attaching gas

Following pulsed X-ray irradiation of Ar atoms, high-energy electrons produced by ionization lose their energies by collisions with Ar atoms and are eventually thermalized. The electron thermalization during electron attachment to C_6F_6 in Ar buffer gas has been observed. Time profiles of the conductivity signals observed for pure Ar (70 Torr) and Ar (70 torr) containing C_6F_6 are shown in Fig.3(A). For pure Ar the signal increases slowly. This is ascribed to the presence of the Ramsauer minimum in the electron energy dependence of the momentum transfer cross section for Ar. When electrons are thermalized the signal becomes flat. The signals for mixtures with C_6F_6, on the other hand, show decreases by the electron attachment reaction. This reaction may be influenced by the electron thermalization process. The signals can be converted to the electron densities dependence on time, as shown in Fig.3(B). Generally the rate of disappearance of electron by attachment to a molecule is given by Eq.(1).

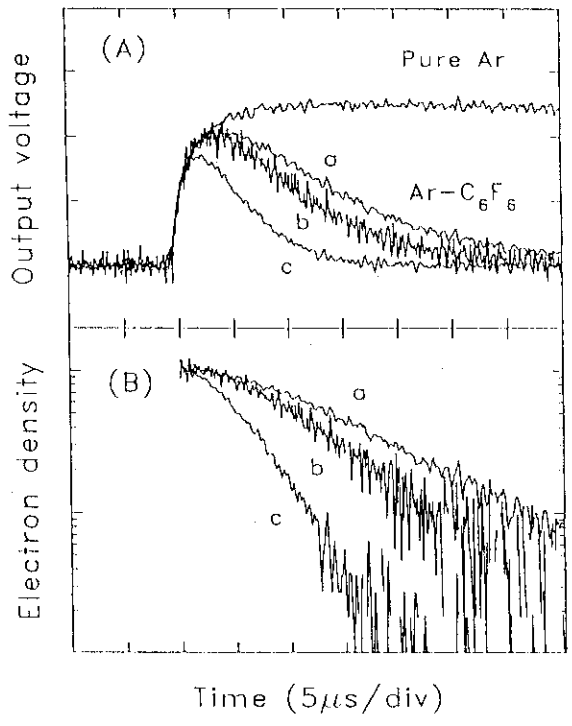


FIG.3 (A) Microwave conductivity signals for pure Ar (70 Torr) and those for mixtures containing C_6F_6 at different pressures; (a) 1.29 x 10^{-5} Torr, (b) 3.71 x 10^{-5} Torr, and (c) 9.08 x 10^{-5} Torr. (B) The electron density as a function of time.

$$\frac{d \ln[e^-]}{dt} = -k(\langle\varepsilon\rangle)[C_6F_6] \quad (1)$$

where $[C_6F_6]$ is the concentration of C_6F_6, $k(<\varepsilon>)$ is rate constant as a function of mean electron energy, $<\varepsilon>$. If the results of electron densities dependence on time

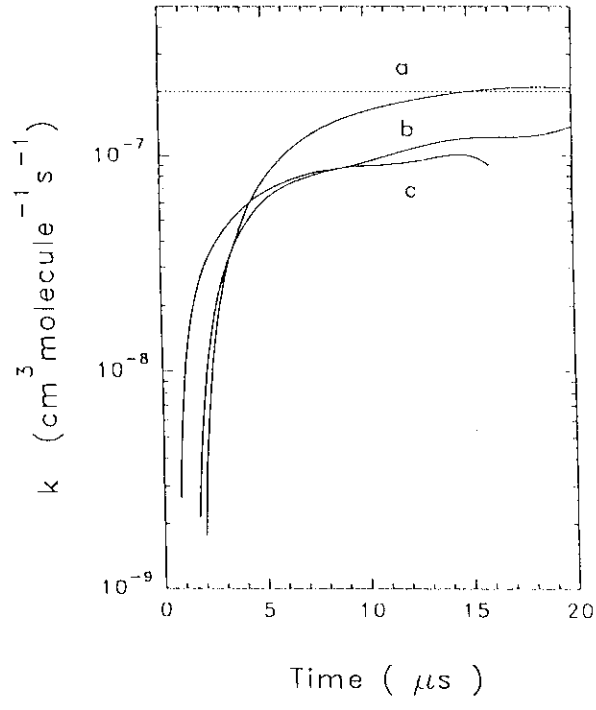


FIG.4 Rate constants for electron attachment to C_6F_6 as a function of time. The dotted line represents the value for thermal electrons.

are the first-order decay, differential equation (1) can be solved to obtain the rate constants. Since, however, the decays are not of the first-order, the attachment rates must be dependent on time. Thus, we have differentiated the $\ln[e^-]$ vs t curve directly to obtain the derivative $-k(<\varepsilon>)[C_6F_6^-]$ at respective time. The rate constants as a function of time so obtained are shown in Fig.4. Since the rate constants of electron attachment to C_6F_6 as a function of mean electron energy is known (Shimamori, Sunagawa, Ogawa, and Tatsumi, 1994), the time-variation the rate constants can be converted to that of the mean electron energy, as shown in Fig.5. This shows that at a high concentration of C_6F_6 the electrons are captured before they are thermalized.

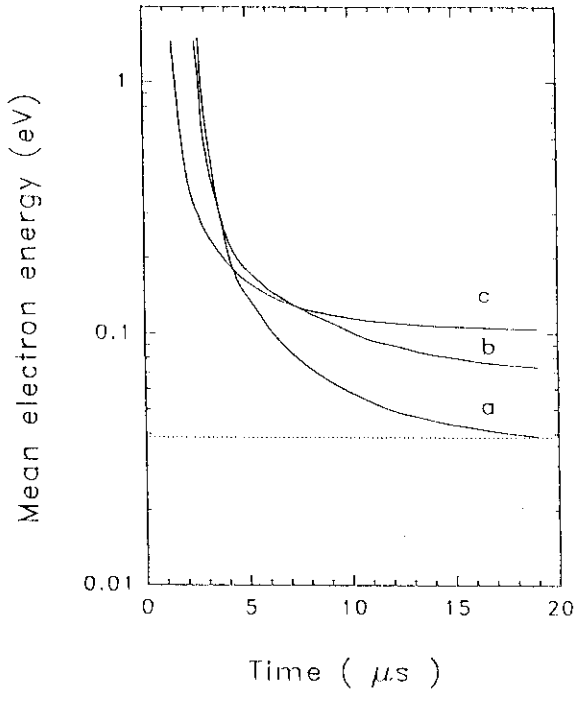


FIG.5 Mean electron energies vs time. The dotted line corresponds to the thermal energy.

Such behavior may be true of electron degradation process in the presence of other electron-attaching compounds.

(iii) Penning ionization

Penning ionization of neo-C_5H_{12} by metastable neon atom Ne^* has been investigated. The rate constant for this process has been obtained from an analysis of observed microwave conductivity signals representing the variation of electron density.

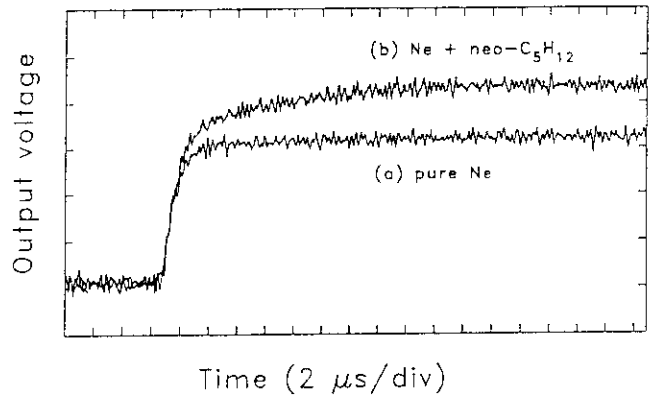


FIG.6 Microwave conductivity signals observed for (a) pure Ne 400 Torr and (b) 4.85×10^{-3} Torr neo-C_5H_{12} in 400 Torr Ne.

The decay of Ne^* through de-excitation processes are as follows:

$$Ne^* + AB \rightarrow Ne + (AB)^+ + e^- \quad (2)$$

$$\rightarrow (Ne\ AB)^+ + e^- \quad (3)$$

$$\rightarrow Ne + A^+ + B + e^- \quad (4)$$

$\rightarrow$ Ne + A + B (5)

where Ne^* is a metastable neon atom, AB is neo-C_5H_{12}. The solution of differential equation representing the time-variation of electron density is.

$$[e^-] = [Ne^*]_0 \left(\frac{k}{k+k_5}\right)\{1-e^{-(k+k_5)[AB]t}\} \quad (6)$$

where the brackets [ ] stand for the concentration, subscript 0 means the initial concentration immediately after pulse irradiation, and $k(=k_2+k_3+k_4)$ and k_5 are the rate constant for the ionization processes and the dissociation process, respectively. The microwave conductivity signals, which are proportional to electron density, as a function time is shown in Fig.6(a) for pure Ne (400 torr) and (b) for Ne (400 torr) containing neo-C_5H_{12}. The first-order growth rate is determined by analysis of the electron production process, which is obtained by subtracting the microwave conductivity signal (a) from that of (b). The slope of the plot of the growth rates against [neo-C_5H_{12}] gives $k+k_5=3.0 \times 10^{-10}$ cm^3 $molecule^{-1}$ s^{-1}. This value is rather lower than the known value (8.4×10^{-10}) for the Penning ionization of He metastable atoms by neopentane (Ueno, Yokoyama, Takao and Hatano, 1980). .

REFERENCES

Illenberger E. (1982) Energetics of negative ion formation in dissociative electron attachment to CCl_4, $CFCl_3$, CF_2Cl_2, and CF_3Cl. *Ber. Bunsenges. Phys. Chem.* **86**, 252.

Shimamori H. (1991) Microwave Conductivity Technique. In *CRC Handbook of Radiation Chemistry,* p.131, CRC Press, Boca Raton.

Shimamori H., Tatsumi Y., Ogawa Y. and Sunagawa T. (1992 a) Electron-energy dependence of electron attachment to c-C_7F_{14}, CH_3I and CH_2Br_2 studied by the pulse-radiolysis microwave-cavity technique combined with microwave heating. *Chem. Phys. Lett.* **194**, 223.

Shimamori H., Tatsumi Y., Ogawa Y. and Sunagawa T. (1992 b) Low-energy electron attachment to molecules studied by pulse-radiolysis microwave-cavity technique combined with microwave heating. *J. Chem. Phys.* **97**, 6335.

Shimamori H., Sunagawa T., Ogawa Y. and Tatsumi Y. (1994) Low-energy electron attachment to C_6F_5X (X=F, Cl, Br and I). *Chem. Phys. Lett.* **227**, 609.

Ueno T., Yokoyama A., Takao S. and Hatano Y. (1980) De-excitation rate constants of $He(2^3S)$ by atoms and molecules as studied by the pulse radiolysis method. *Chem. Phys.* **45**, 261.

12.3 Photoredox Chemistry of Chloro Complexes of Main Group Metals

N. Shinohara and M. Ohshima

Department of Chemistry, Yokohama City University,
Seto 22-2, Kanazawa-ku, Yokohama 236, Japan

Abstract The photoredox reactions of chloro complexes of the main group metals with electron configurations s^2 (e.g. Tl(I), Sn(II), Pb(II), Sb(III)) and s^0 (e.g. Tl(III), Sn(IV), Sb(V)) were studied. The transient species of electron configurations s^1 (e.g. Tl(II), Sn(III), Pb(III), Sb(IV)) are formed by the flash photolysis of aqueous hydrochloric acid solutions containing the corresponding s^2 or s^0 metal complexes. The optical characteristics of these transient complexes were determined. UV-light irradiation of s^2 chloro complexes of antimony, bismuth, and lead in the presence of a large amount of 2-propanol led to the formation of corresponding metal colloid.

INTRODUCTION

Generally, the main group metals exist in stable states in which the ground state electron configuration is either s^2 or s^0. The absorption spectra of the complexes of s^2 and s^0 metals are characterized by metal to ligand charge transfer (MLCT) and ligand to metal charge transfer (LMCT) bands, respectively (Jørgensen, 1964; Jørgensen, 1969). The complexes of the main group metals with s^0 and s^2 electron configurations undergo photoredox reactions upon UV-light irradiation, which involve successive one-equivalent step, and frequently, the s^2 and s^0 complexes are interconverted (Vogler et al., 1986a; Paukner et al., 1987). Very little is known about the photochemistry of complexes of the main group metals. The present paper reports the data on the formation of s^1 chloro complexes from photolysis of aqueous solutions of s^0 or s^2 metal ions of thallium, tin, antimony, lead etc.

EXPERIMENTAL

All chemicals used were of chemically pure grade. Sn(IV) solutions were obtained by the oxidation of Sn(II) with oxygen. The deaerations of the solutions used for photolysis were carried out by bubbling with pure nitrogen. Absorption spectra were recorded on a Shimazu UV-2100 spectrophotometer. Transient absorption spectra of unstable species were measured using a flash photolysis apparatus as described previously (Shinohara et al., 1986b). The steady irradiation was carried out by using a ultrahigh-pressure mercury lamp. Hydrogen was determined gaschromatographically.

RESULTS AND DISCUSSION

s^2 complexes: Photoredox reactions of chloro complexes of Sb(III) and Sb(V) in CH_3Cl have been studied (Vogler et al., 1989) and it has been reported that Sb(III) and Sb(V) complexes are interconverted by the following reactions.

$$[Sb(Cl)_6]^{3-} + O_2 \xrightarrow{h\nu} [Sb(Cl)_6]^{-} + O_2^{2-} \qquad (1)$$

$$[Sb(Cl)_6]^{-} \xrightarrow{h\nu} [Sb(Cl)_4]^{-} + Cl_2 \qquad (2)$$

However, no study on transient species generated in the photolysis of Sb(III) and Sb(V) has been carried out. Flash photolysis studies of Sb-(III) and Sb(V) have been carried out in 1 to 5 M hydrochloric acid solutions. It seems that under these conditions several different chloro complexes of Sb(III) are present. However, the same type of absorption spectra were obtained at[HCl]>2 M as shown in Fig 1. The transient species produced after a flash has absorption maxima at 322 and 380 nm. The shape and the ratio of the optical densities at 322 and 380 nm are the same during disappearance of the absorption as shown in Fig. 2.

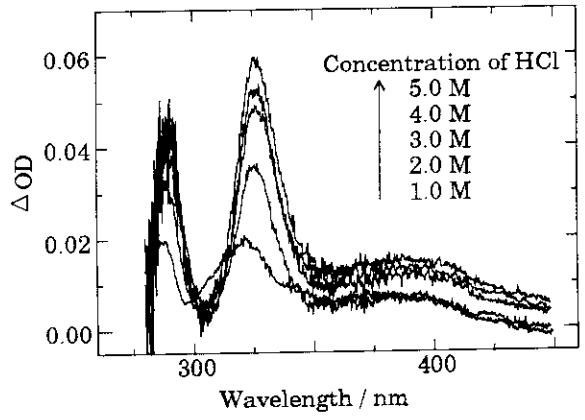


Fig. 1. Transient absorption spectra obtained in the flash photolysis of Sb(III) in deaerated solutions of various hydrochloric acid concentration. [Sb(III)]=5.0 x 10^{-5} M, Recorded 50 μs after the flash.

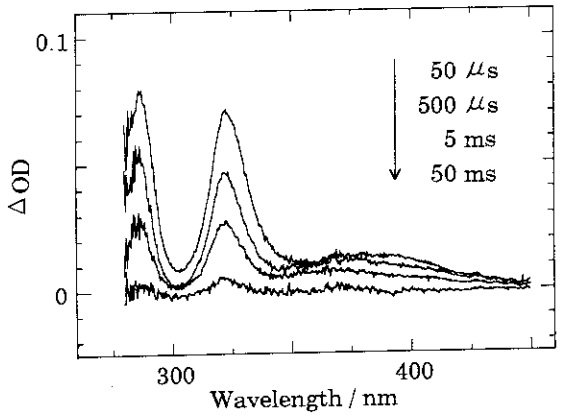


Fig. 2. Transient absorption spectra produced from the flash photolysis of 1.0 x 10^{-4} M Sb(III) in deaerated hydrochloric acid solutions.

Hence, this spectrum is caused by one species which can be assigned as a Sb(IV) complex. The formation of Sb(IV) could be attributed to the following reaction.

$$Sb(III) \xrightarrow[H^+]{h\nu} Sb(IV) + H \qquad (3)$$

It has been reported that an unstable Sn(III) was similarly produced by UV-irradiation of Sn(II) in deaerated aqueous hydrochloric acid solutions (Shinohara et al.,1986b; Shinohara et al., 1989). The absorption spectrum of Sn(III) complex has an absorption maximum at 280 nm in a hydrochloric acid solution (Fig. 3).

Henglein et al. have studied the Pb(III) formation in the radiolysis of Pb(II) and Pb(IV) (Henglein et al., 1990). They have reported that Pb^{2+} ions in acidic solution do not produce Pb(III) since Pb^{2+} does not react with OH radicals. However, in neutral and more alkaline solutions where hydroxlated Pb(II) species are present, the OH radicals rapidly react with them to yield Pb(III) species, $Pb(OH)_2^+$ or $Pb(OH)_4^-$, of which transient absorption spectra were measured. We have found that a transient species attributable to a chloro complex of Pb(III) is formed in a deaerated hydrochloric acid solution in the flash photolysis of Pb(II). The transient spectra of the chloro complex has an absorption maximum at 320 nm.

The absorption spectra of Tl^{2+} (Cercek et al., 1966) and $[Tl(OH)]^-$

(O'Neill et al., 1975) in aqueous solution have been measured using the pulse radiolysis technique. It was reported that the absorption spectrum of the transient Tl^{2+} has absorption maxima near 260 nm and 400nm(sh). In the present study, absorption spectrum of a chloro complex of Tl(II) has been measured in the aqueous hydrochloric acid solutions containing Tl(I) using a flash photolysis technique, and it has been found that the spectrum has absorption bands at 290 and 360 nm (Fig. 4). This spectrum is attributed to the Tl(II) produced by the reaction (4).

$$Tl(I) \xrightarrow[H^+]{h\nu} Tl(II) + H \qquad (4)$$

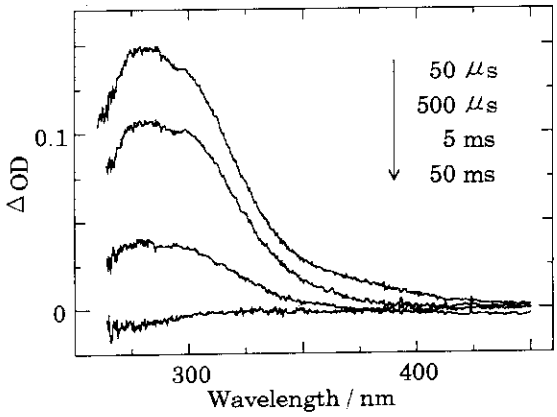


Fig. 3. Transient absorption spectra produced from the flash photolysis of 1.0×10^{-4} M Sn(II) in deaerated hydrochloric acid solutions.

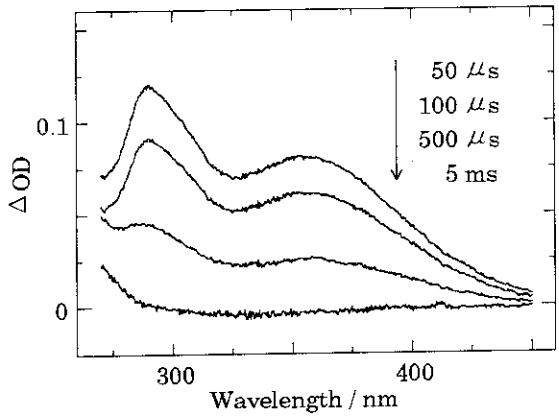


Fig. 4. Transient absorption spectra produced from the flash photolysis of 1.0×10^{-4} M Tl(I) in deaerated hydrochloric acid solutions.

s^0 complex: Upon irrradiation of chloro complexes of s^0 main group metals such as Tl(III), Sn(IV) and Sb(V), s^1 complexes are also produced together with Cl_2^-. Transient spectra obtained in the photolysis of Sb(V) are given in Fig. 5. A shoulder was observed near 340 nm which is attributed to Cl_2^-. The shoulder decayed more rapidly than other absorption bands, and the spectra obtained after the decay is similar to the transient spectrum obtained in the flash photolysis of Sb(III) (Fig. 1). This fact supports that the shoulder near 340 nm is due to the Cl_2^-. These results are consistent with the following reactions.

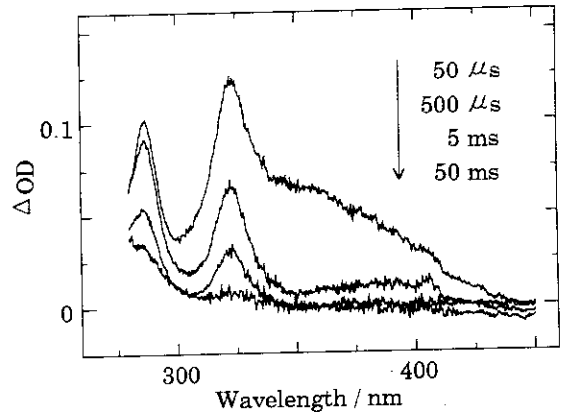


Fig. 5. Absorption spectra of transient species in the flash photolysis of 1.0×10^{-3} M Sb(V) in deaerated hydrochloric acid solutions.

$$Sb(V)\text{-}Cl \xrightarrow[Cl^-]{h\nu} Sb(IV) + Cl_2^- \qquad (5)$$

A similar absorption band which is attributable to Cl_2^- was observed in the photolysis of other s^0 complexes such as Tl(III) or Sn(IV).

The effect of additive: It has been found that UV-light irradiation of Sb(III), Bi(III) or Pb((II) solution containing a large amount of 2-propanol led to the formation of metal colloid together with hydrogen and acetone. The colloids are relatively stable in the absence of oxygen even in 5 M hydrochloric acid solution, and act as a catalyst for the formation of hydrogen from radicals.

CONCLUSIONS

Chloro complexes of main group metals with s^1 electron configuration can be produced easily upon UV-irradiation of the corresponding s^0 and s^2 chloro complexes. The absorption spectra of the transient s^1 chloro complexes were measured using a flash photolysis technique. Further, it was found that UV-light irradiation of Sb(III), Pb(II), or Bi(III) led the formation of colloidal metal which acts as a catalyst for the formation of hydrogen by reducing radicals.

REFERENCES

Bonifacic M. and Asmus K.-D. (1976) On the equilibrium between thallium-(II) hydroxide and hydroxothallium(II) ion: A Pulse-radiolysis study. *J. Chem. Soc., Dalton*, 2074.

Buxton G. V., Rhodes T. and Sellers R. M. (1982) Radiation chemistry of dilute aqueous solutions of thallous ion. *J. Chem. Soc., Faraday Trans.* I, 78, 3341.

Cercek B. Ebert M. and Swallow A. J. (1966) Novel valence states of thallium as studied by pulse radiolysis. *J. Chem. Soc.* (A), 612.

Ershov B. G., Akinshin M. A., Gordeev A. V. and Sukhov N. L. (1986) A pulse radiolysis study of the chloride complexes of Bi(II) and Bi(IV). *Radiat. Phys. Chem.*, 27, 91.

Jørgensen, C. K. (1964) Absorption spectra and chemical bonding in complexes. Pergamon Press, Oxford.

Jørgensen, C. K. (1969) Oxidation number and oxidation states. Springer, Berlin.

Mosseri S., Henglein A. and Eberhard J. (1990) Trivalent lead as an intermediate in the oxidation of Pb^{II} and the reduction of Pb^{IV} species. *J. Phys. Chem.*, 94, 2722.

Paukner A., Kunkely H. and Vogler A. in Yersen H. and Vogler A. (eds.) (1987) Photochemistry and photophysics of coordination compounds. Springer, Berlin.

Shinohara N., Mori K. and Inoue M. (1986) Aqueous chemistry of tin(III). A flash photolysis study. *Chem. Lett.*, 661.

Shinohara N. and Inoue M. (1989) Photochemical generation of Sn(III) in hydrochloric acid solutions. *Bull. Chem. Soc. Jpn.*, 62, 730.

Vogler A., Quitt C., Paukner A. and Kunkely H. (1986) Photochemical reductive elimination of hexaazido complexes of tin(IV) and lead(IV). *J. Am. Chem. Soc.*, 108, 8263;

Vogler A. and Paukner A. (1989) Photoredox chemistry of chloro complexes of antimony(III) and (V). *Inorg. Chim. Acta*, 163, 207.

12.4 Photoionization of C_{60} and C_{70} in Alkane Liquids

Ryuzi Katoh *, Klaus Lacmann and Werner F. Schmidt

Hahn-Meitner-Institut Berlin, Abteilung Strahlenchemie,

D 14109 Berlin - Wannsee, Germany

Published in Z. Naturforsch, **49a**, 793-796 (1994).

* on leave from Faculty of Science, Gakushuin University, Mejiro, Tokyo 171, Japan.

Abstract Single photon ionization of C_{60} in 2,2-dimethylpropane (neopentane, NP), 2,2,4,4-tetramethylpentane (TMP), 2,2-dimethylbutane (neohexane, DMB) and 2,2,4-trimethylpentane (isooctane, iso-OCT) and of C_{70} in TMP have been studied by photoconductivity measurement. Threshold energies of the photoconductivity were determined. From these results the polarization energies of the cations are discussed with respect to Born's formula. Absorption spectrum of C_{60} and C_{70} in VUV range are also reported.

INTRODUCTION

Photoconductivity measurements on solutions of aromatic solutes in liquid alkanes have been performed by several authors in order to study the influence of an inert dielectric medium on the process of photoionization (Bottcher and Schmidt, 1984, Holroyd et al., 1984, Tweeten and Lipsky, 1989). It was found that the photoconductivity threshold, I(liq), was reduced on account of the electron affinity of the liquid alkane, V_0, and of the polarization energy of the cation, P_+,

$$I(liq) = I(gas) + V_0 + P_+ \qquad (1)$$

where I(gas) denotes the ionization potential of the solute molecule in the gas phase. P_+ is always negative while V_0 can be positive or negative depending on the type of alkane (Allen, 1976). Born expressed the polarization energy of a ion by the dielectric constant of the solvent, ε_r, and by the apparent radius of the ion, R_+ (Born, 1920),

$$P_+ = -\frac{e^2}{8\pi\varepsilon_0 R_+}\left[1-\frac{1}{\varepsilon_r}\right] \qquad (2)$$

e denotes the electronic charge, ε_0 is the permittivity of the vacuum. From the value of P_+ obtained from photoconductivity measurements, R_+ was extracted and compared to the van der Waals radius, R_{vdW}, of the solute molecule. In the case of small aromatic molecules in alkane solvents,

$$R_+ \approx R_{vdW} \qquad (3)$$

was found to be valid (Holroyd et al., 1983 and Katoh et al., 1994). It seemed to be interesting to study the photoconductivity of solutions of molecules with well known ionization potentials and

van der Waals radii. The fullerenes C_{60} and C_{70} are well characterized and, here, we wish to report photoconductivity threshold energies obtained for fullerene solutions of several alkanes.

EXPERIMENTAL

A deuterium discharge lamp with MgF_2 window (Hamamatsu, L1835) followed by a vacuum ultraviolet monochromator (Acton, VM502) was used as a light source. The wavelength resolution of the system was 1nm. The relative intensity distribution of the light source was determined by using sodium salicylate, the fluorescence of which was detected with a photomultiplier (Hamamatsu, R928). The photoconductivity cell was the same as in a previous study (Bottcher and Schmidt, 1984). Exciting light entered the cell through the front electrode, which consisted of a gold thin film (thickness: 7 nm) deposited on a MgF_2 plate. The back electrode was separated by a teflon spacer (thickness: 4 to 5 mm) from the front electrode. Bias voltages between + 500 and +1000 V were applied to the front electrode. The photocurrent was measured with a pico-ammeter (Keithley, Model 617). Wavelength change and photocurrent readings were controlled and recorded by a Macintosh™ computer, model IIsi.

The hydrocarbon solvents were 2,2-dimethylpropane (neopentane, NP) and 2,2-dimethylbutane (neohexane, DMB) from Phillips Petroleum Co., 2,2,4,4-tetramethylpentane (TMP) from Wiley Organics , and 2,2,4-trimethylpentane (isooctane, iso-OCT) from Merck. They were purified by percolation through activated silica gel and molecular sieves (pore size, 0.4 nm). C_{60} (Fluka) and C_{70} (Fluka) were used as obtained. The concentrations of the solutions are listed in Table 1.

Table 1: Concentrations of Fullerenes employed in the present work

	Concentration (mol / l)
C_{60} / NP	1×10^{-5}
C_{60} / TMP	9×10^{-5}
C_{60} / DMB	5×10^{-5}
C_{60} / iso-OCT	5×10^{-5}
C_{70} / TMP	5×10^{-5}

RESULTS AND DISCUSSION

The figures 1 and 2 show action spectra of the photoconductivity of C_{60} in various solvents and of C_{70} in TMP, respectively. The photocurrent increases gradually above the threshold (arrows in the Figs.1 and 2) with photon energy. At higher photon energies the photocurrent decreases steeply due to absorption by the solvent itself. The photoconductivity spectrum reflects the relative ionization efficiency as a function of photon energy when the

exciting light is absorbed completely between electrodes. In the case of NP, the shape of the spectrum is affected by absorption coefficient since the concentration of the saturated solution is not sufficient (Fig. 3 (a)).

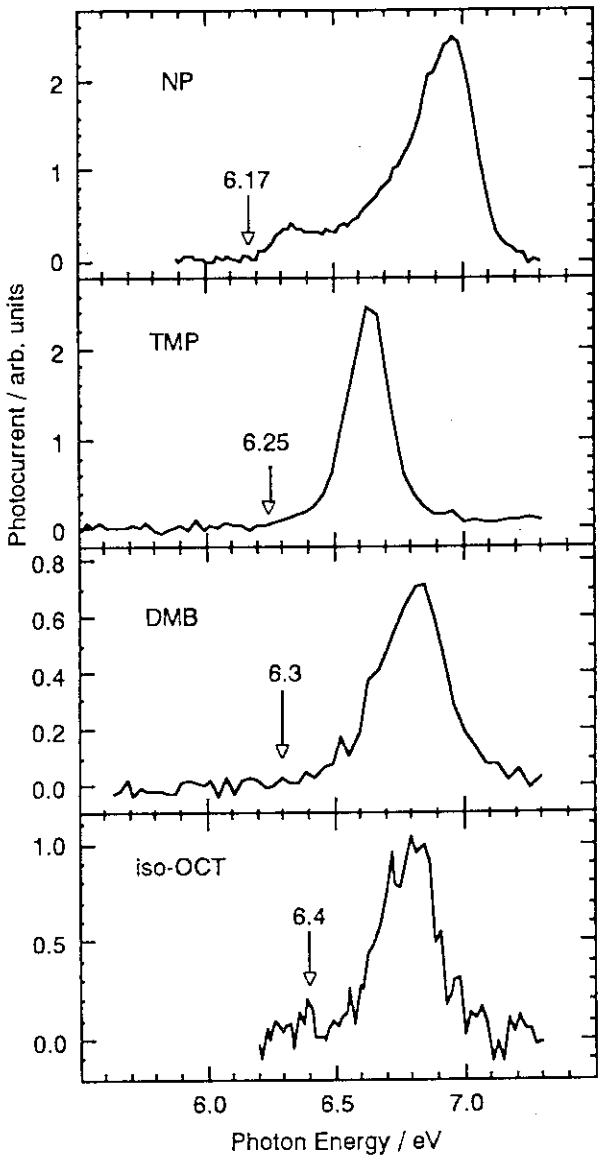


Figure 1: Action spectra of photoconductivity of C_{60} in various solvents at room temperature; threshold energies in eV are indicated by arrows; NP: C_{60}- Neopentane; TMP: C_{60}- 2,2,4,4 Tetramethypentane; DMB: C_{60} - Neohexane; iso-OCT: C_{60}- iso-Octane.

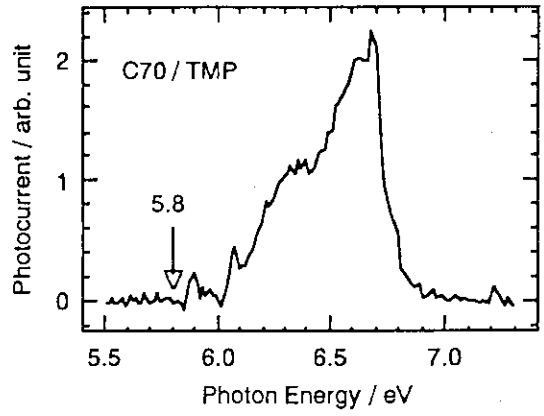


Figure 2: Action spectrum of photoconductivity of C_{70} in 2,2,4,4 Tetramethylpentane; the threshold energy in eV is indicated by an arrow

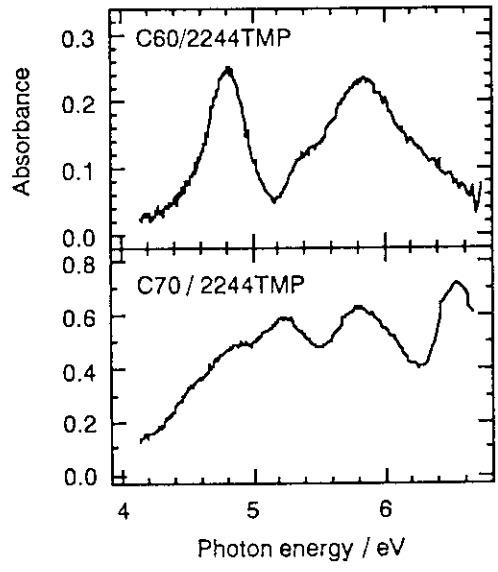


Figure 3: Absorption spectra of C_{60} and C_{70} in 2,2,4,4 tetramethylpentane.

In the case of C_{70} (Fig. 2) the exciting light is absorbed completely. The photoconductivity spectrum exhibits a shoulder at 6.3 eV. A possibility may be the auto-ionization of a highly excited state. It is interesting to note that the peak in the action spectrum does not correspond with absorption peak (Fig. 3 (b)). Therefore, the auto-ionizing state is not highly neutral excited state but may be semi-ionized state, such as Rydberg state.

For the estimation of the threshold energy of photoionization from the photoconductivity action spectrum a power function is used (Holroyd et al., 1983),

$$Y = A\,[h\nu - I(liq)]^n \qquad (4)$$

Y is the apparent efficiency of photoionization, A is a constant and hν is the photon energy of the exciting light. In the case of alkane solutions, an exponent of n = 2.5 yields good agreement of the data with eq. 4. The values of I(liq) reported in Table 2 and indicated by the arrows in Figs.1 and 2 were determined in this way.

Since the V_0 -values of the solvents used in this work and the photoionization energies, I(gas), of C_{60} and C_{70} are known, values of P_+ and R_+ can be obtained. They are included in Table 2. On the other hand, the van der Waals radii of the fullerenes are available from the literature (Dravid et al., 1992, T.Kato et al., 1003). Comparison of R_+ and R_{vdW} (see Table 2) shows that the ionic radii obtained here are much smaller than the van der Waals radii. A priori, we would have expected that the positive charge would be distributed evenly over the whole molecule and that the apparent radius of the charge would be identical to the van der Waals radius.

Table 2:

Ionization potential of fullerene in the gas phase I(gas), conduction band energy of solvent, V_0, threshold energy of photoconduction of fullerene solution, I(liq), n refractive index, polarization energy , P_{+exp} and ionic radius R_{exp} determined experimentally and polarization energy, P_{+vdW} estimated from the van der Waals radius R_{vdW}

Solute	Solvent	I(gas) (eV)	V_0 (eV)	I(liq) (eV)	$\varepsilon_r=n^2$	P_{+exp} (eV)	R_{exp} (nm)	P_{+vdW} (eV)	R_{vdW} (nm)
C_{60}	NP	7.54[a]	-0.43[b]	6.17	1.816	-0.94	0.34	-0.63	0.51
C_{60}	TMP	7.54[a]	-0.33[b]	6.25	1.979	-0.96	0.37	-0.70	0.51
C_{60}	DMB	7.54[a]	-0.20[b]	6.3	1.874	-1.0	0.35	-0.66	0.51
C_{60}	iso-OCT	7.54[a]	-0.24[c]	6.4	1.936	-0.9	0.4	-0.68	0.51
C_{70}	TMP	7.3[a]	-0.33[b]	5.8	1.979	-1.2	0.30	-0.67	0.53

a) Hertel et al., 1992 b) Allen, 1976 c) Holroyd et al., 1975

In the case of solution of aromatic compounds in non-polar liquids, the ionic radius (from Born's equation) and the van der Waals radius were found to agree in magnitude (Holroyd et al., 1983). For the fullerene molecules, however, this relation is not valid. It is possible that the photoionization occurs in two steps. First an electron-hole pair is produced on a fullerene molecule by optical transition, and second, thermal dissociation of this complex takes place. Fullerenes are large molecules and have large polarizabilities (Maltsev et al., 1993), therefore, the ion-pair is easily dissociated by thermal energy. Recently, Schlag and Levine proposed such a model for the photoionization of large molecules and clusters Schlag and Levine, 1992).

REFERENCES

Allen A.O. (1976) Drift Mobility and Conduction Band Energies of Excess Electrons in Dielectric Liquids, NSRDS-NBS-58, US Natl. Bur. Stand.

Born M, (1920) Volumen und Hydratationswarme der Ionen.Z. Physik **1**, 45.

Böttcher E.H. and Schmidt W.F. (1984) Photoconductivity of nonpolar liquids induced by vacuum-ultraviolet light. J. Chem. Phys. **80**,1353.

Dravid V.P., Lin X., Zhang H., Liu S. and Kappes M.M. (1992) Transmission electron microscopy of C70 single crystal at room temperature. J. Mater. Res. **7**, 2440.

Hertel I.V., Steger H., Vries J. de, Weisser B., Menzel C., Kamke B. and Kamke W. (1992) Giant plasmon excitation in free C60 and C70 molecules studied by photoionization. Phys. Rev. Lett. **68**, 784.

Holroyd R.A., Tames S. and Kennedy A. (1975) Effect of temperature on conduction band energies of electrons in nonpolar liquids. J. Phys. Chem. **79**, 2857.

Holroyd R.A., Preses J.M. and Zevos N (1983) Single-photon induced conductivity of solutes in nonpolar solvents. J. Chem. Phys. **79**, 483.

Holroyd R.A., Preses J.M., Böttcher E.H. and Schmidt W.F. (1984) Photoconductivity induced by single-photon excitation of aromatic molecules in liquid hydrocarbons. J. Phys. Chem. **88**, 744.

Kato T., Kikuchi K. and Achiba Y. (1993) Measurement of the self-diffusion coefficient of C60 in benzene-d6 using pulsed-gradient spin echo. J. Phys. Chem. **97**, 10251.

Katoh R., Lacmann K. and Schmidt W.F., Polarization energies of molecular cations in alkane solutions. Z. Phys. Chem. submitted.

Maltsev V.A., Nerushev O.A., Novopashin S.A. and Selivanov B.A. (1993) Anomalous polarizability of fullerene. Chem. Phys. Lett. **212**, 480.

Schlag E.W. and Levine R.D. (1992) Ionization, charge separation, charge recombination, and electron transfer in large systems. J. Phys. Chem. **96**, 10608.

Tweeten D.W. and Lipsky S (1989) Photoconductivity of anthracene in liquid hydrocarbons. J. Phys. Chem. **93**, 2683.

12.5 Magnetic Field Effects in the Ion-pair Recombination Process

Kunihiro Kokubu, Hiroshi Hasegawa and Yoshimasa Hama

Advanced Research Center for Science and Engineering,
Waseda University
3-4-1 Okubo, Shinjuku, Tokyo 169, Japan

Abstract The present paper is concerned with the evolution of the singlet character of correlated ion pairs. Quantum beats induced by the difference in *g*-factors between a pair of *p*-terphenyl anion and diphenylsulfide cation have been detected in recombination fluorescence kinetics. Cyclohexane and *trans*-decalin are found to be suitable solvents to detect clear beats. The kinetics behavior of geminate recombination of solute ions in producing excited states to throw light on the role of hole transportation are discussed.

INTRODUCTION

The concept of singlet-triplet transitions in radical-pair recombination plays an important role in our understanding of the influence of magnetic fields on the rate of radical reactions[1]. The transitions occur periodically with frequencies determined both by hyperfine interaction between the unpaired electrons of a radical-pair and magnetic nuclei (the so-called hfi mechanism) and by differences in the Zeeman frequencies between the radicals of a pair (the so-called Δg mechanism). Accordingly, the probability of forming the pair of recombination products with a certain multiplicity changes with time. This phenomenon was given the name "Quantum beats" in radical recombination[2].

The simultaneous formation of an ensemble of such pairs in a certain spin state is a necessary condition for experimental observation of quantum beats[2]. This condition can be realized in practice if geminate radical pairs are generated by pulse ionizing radiation in non-polar solutions containing electron and hole acceptors. When such pairs recombine, the excited molecules appear in singlet or triplet state. Since only excited singlet molecules makes fluorescence in a liquid, the intensity of the fluorescence will oscillate at a frequency determined by hfi and Δg mechanisms.

In the case of the Δg mechanism, the luminescence intensity will oscillate at a frequency (ω_{ST_0}) equal to the difference between the Larmor-precession frequencies of both radicals[1]:

$$\omega_{ST_0} = \omega_1 - \omega_2 = (g_1 - g_2)\beta_e \hbar^{-1} H_0 \equiv \Delta g\, \beta_e \hbar^{-1} H_0 \quad (1)$$

where ω_1, ω_2 and g_1, g_2 are the Larmor frequencies and *g*-factors, respectively, of each radical in a pair and H_0 is the external magnetic field. It can be seen from Eq.(1) that the oscillation frequency increases with increasing the strength of the external magnetic field.

The radical-pair (diphenylsulfide)$^+$/(*p*-terphenyl)$^-$ formed from diphenylsulfide and *p*-terphenyl solution in a non-polar solvent by radiolysis, capturing a free electron and a hole in the track of an ionizing particle, fulfills these conditions[4]. The singlet-pair formed by recombination product a excited singlet *p*-terphenyl to scintillate the fluorescence.

EXPERIMENTAL

The time-resolved recombination fluorescence were measured by using a single-photon counting technique taken by Klein *et al* [5]. The block-diagram of the set-up is shown in Fig.1.

In the present work, the sample is excited by β particle from a 10 μCi source of ^{90}Sr-^{90}Y plunged into the solutions contained in cylindrical cells. Sample was degassed by the freeze-pump-thaw technique. All measurements were made at room temperature.

RESULTS AND DISCUSSION

Fig.2 shows the time dependence of the fluorescence intensity $I(t)$ observed for a *trans*-decaline solution involving 60mM diphenylsulfide and 1mM *p*-terphenyl,

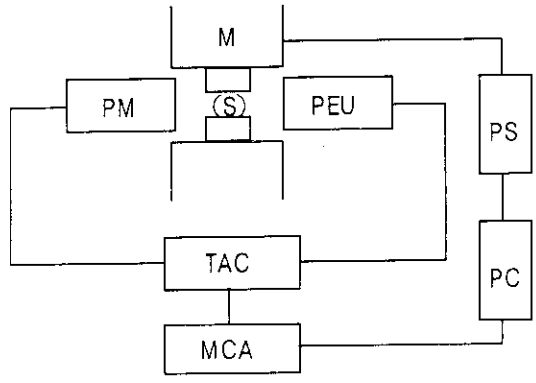


Fig.1 : Block-diagram of magnetically modulated single photon counting method.

irradiated by fast electrons in 500, 300mT and zero magnetic fields. Even if these decay curves have rather low value of signal-to-noise, an obvious difference can be found among the curves for zero-field and high field. In high fields, there are small rises of fluorescence intensity in the decay curves. That is obviously the effect of magnetic field, because there are no rises in zero field. Fig.2 (d) also shows $I(t)$ observed in cyclohexane solution, involving the same solutes as mentioned above, at high magnetic field (500mT). Similar oscillations are also observed here. However, the beat amplitude is smaller than that of *trans*-decalin solution. Following the technique described before[4], we consider the ratio of oscillations ($\Delta I(t)=[I(t)-F(t)]/F(t)$). This ratio of *trans*-decalin solution is shown in fig.3(a) and (b) for two different external magnetic field (500 & 300mT). To calculate this ratio, the smooth curve $F(t)$ was simulated[3] as

$$F(t)=A+B\exp(-t/t_1)+C/(1+t/t_2)^{\alpha} \quad (2)$$

where t_1, t_2 and α are the parameters. The numerical parameters of the functions are chosen by a computer. The signal-to-noise ratio is increased by smoothing the original curve. The time dependence of the oscillation ratio have a "dip" at initial time stage. With increasing magnetic field, the amplitude of the "dip" increases and the position of the maxima shifts to the short region of time. This behavior may be explained by assuming the existence of the Δg-oscillations in the pair

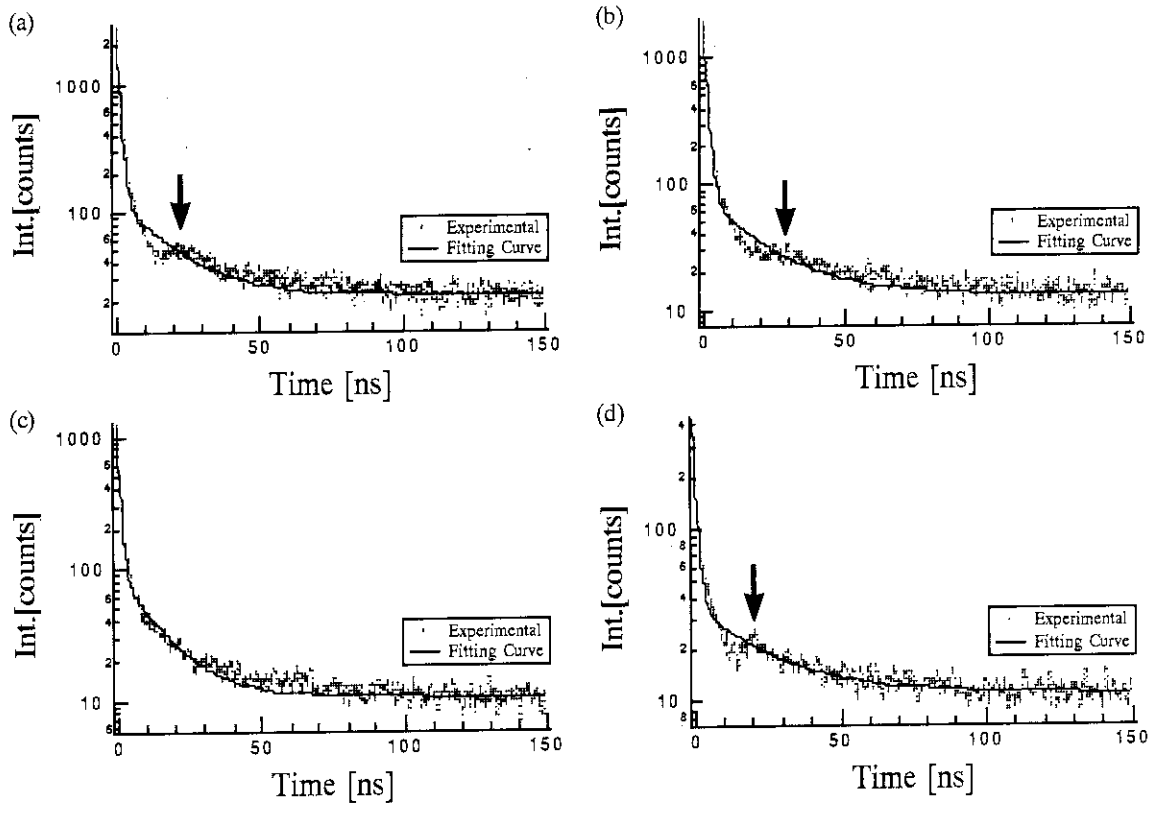


Fig.2 : Time dependence of the recombination fluorescence intensity in *trans*-decalin[(a)~(c)] and cyclohexane[(d)] solution in the external magnetic field of 500mT[(a),(d)], 300mT[(b)] and 0mT[(c)].

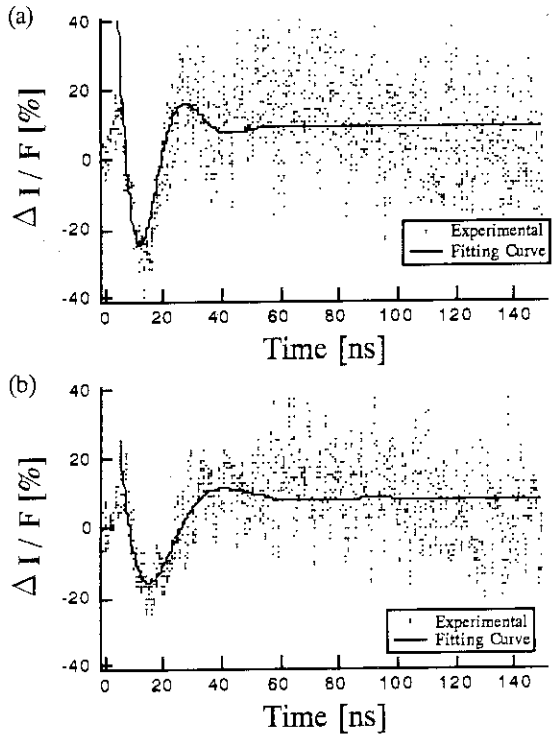


Fig.3 : The oscillation shapes in *trans*-decalin solution in the external magnetic field of (a)500mT and (b)300mT.

(diphenylsulfide)$^{+}$/(*p*-terphenyl)$^{-}$. Too short lifetime of the beats in present observation is possibly caused by the effect of hfi due to hydrogen atoms of the solutes. Most experiments to detect quantum beats have been done for deuterated solutes. However, it can be seen from Fig.3 that the period T of observed oscillation depends on the external magnetic field. The oscillation period was obtained from the observed curves by computation. The formula used is of the next form[5],

$$F(t)=A+B\cos(\omega t+C)\exp(-t/t_1) \quad (3)$$

where t_1 is the decay time of the oscillation. The oscillation periods obtained are shown in

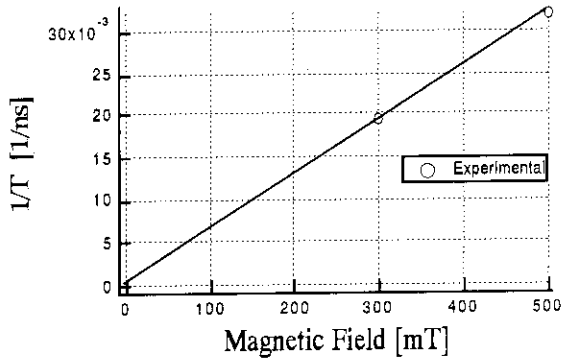


Fig.4 : The dependence of 1/T on $H0$

Table 1. Fig.4 shows the H_0 dependence of $1/T$. The experimental points lie on a straight line passing through the origin. This is a conclusive evidence that the beats in the recombination luminescence are induced by the Δg mechanism. Taking Eq.(1) and the relation $\omega_{ST_0}=2\pi/T$, the difference in g factors between radicals of the pair can be calculated from the slope in Fig.4. The value obtained is Δg=0.0046, which agrees within experimental error with the Δg value estimated from the OD ESR signal of the same pair by Veselov *et al*[1].

As mentioned above, the simultaneous formation of an ensemble of solute ion-pairs in a certain spin state is the necessary condition for experimental observation of quantum beats. In other words, when quantum beats could be observed, electrons and holes induced by radiation should diffuse immediately to be captured by solute molecules. Electron mobility may be almost the same for most solvents. So the migration to be process of the primary hole captured by diphenylsulfide, must play the principal role. It is well known that fast hole transport does take place in cyclohexane[6]. Furthermore, it is reported that cyclohexane and *trans*-decalin radical cations are the shortest lived in most liquid alkanes[7]. This fact agrees with and supports our conclusion that the positive

Table1:Experimental and theoretical oscillation periods

	t-decalin 500mT	t-decalin 300mT	c-hexane 500mT
Oscillation Period [ns] (Experimental)	31.178	51.000	25.945
Oscillation Period [ns] (Theoretical)	29.7	49.6	29.7

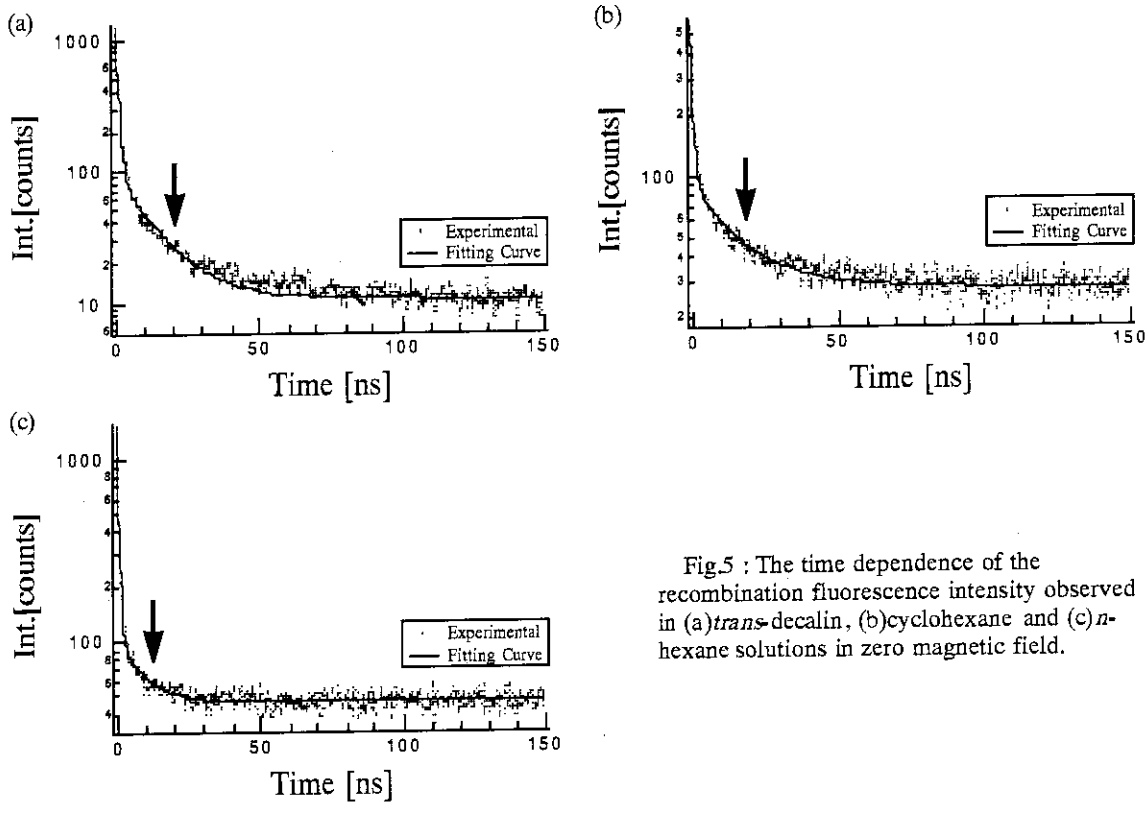


Fig.5 : The time dependence of the recombination fluorescence intensity observed in (a)*trans*-decalin, (b)cyclohexane and (c)*n*-hexane solutions in zero magnetic field.

charges generated in these solvents transfer quickly and stabilize by forming the solute cations. In our experiment, the beat amplitude in *trans*-decalin solution exceeds the one in cyclohexane. This suggests that the hole mobility in *trans*-decalin may be faster than that in cyclohexane.

Fig.5(a), (b) and (c) represents that the third component of the fluorescence decay (see equation (2)) in *n*-hexane is much smaller than one in the other solvents. The second component of the equation(2) may corresponds to the fluorescence from (solvent cation)/(solute anion) pair, and the third component probably refers to the solute anion and cation pair. So the slow decay of fluorescence in cyclohexane and *trans*-decalin must be due to rich existence of solute ions. This also supports our conclusion.

CONCLUSION

We observed quantum beats originated from Δg-mechanism in cyclohexane or *trans*-decalin solution of *p*-terphenyl and diphenylsulfide. From our experimental results, cyclohexane and *trans*-decalin, especially *trans*-decalin, are characterized by anomalously large hole mobility.

The observation of quantum oscillations of high intensity allows the method of quantum beats to be used for detailed investigations of positive charge transfer mechanisms. By increasing the S/N ratio, we will progress this studies.

REFERENCE

1.A.V.Veselov, V.I.Melekhov, O.A.Anisimov and Yu.N.Molin, Chem. Phys. Lett. 136 (1987) 263.
2.O.A.Anisimov, V.L.Bizyaev, N.N.Lukzen, V.M.Grigoryants and Yu.N.Molin, Chem. Phys. Lett. 101 (1983) 131.
3.J.Klein and R.Voltz,Can.J.Chem.55(1977)2102.
4.A.V.Veselov, V.L.Bizyaev, V.I.Melekhov, O.A.Anisimov and Yu.N.Molin, Radiat. Phys. Chem. 34 (1989) 567.
5.K.M.Salikhov, Yu.N.Molin, Spin Polarization and Magnetic Effects in Radical Reactions., Elsevier, Amsterdam., (1984)
6.W.R.Simon Appleton and B.Brocklehurst, Radiat. Phys. Chem., 32 (1988) 245.
7.M.C.Sauer Jr., D.W.Werst, C.D.Jonar and A.D.Trifunac, Radiat. Phys. Chem., 37 (1991) 461.
8.Veselov,A.V.; Anisimov,O.A.; Molin,Yu.N., Pulse Radiolysis, Y.Tabata(ed.), CRC Press, Boca Raton, FL, 1991, P27-51

12.6 Pulse Radiolysis of Cyclodextrin Inclusion Complexes

Y. Yamamoto, Y. Naka,* Y. Yoshida and S. Tagawa

The Institute of Scientific and Industrial Research, Osaka University,
8-1 Mihogaoka, Ibaraki, Osaka 567, Japan
*Faculty of Biology Oriented Science and Technology, Kinki University,
Nishimitani 930, Uchidachyo, Nagagun, Wakayama 649-64, Japan

Abstract Pulse Radiolysis of argon-saturated aqueous solutions of biphenyl-4-sulfonate, biphenyl-4-carboxylate, biphenyl-4-acetate, pyrene-1-sulfonate, pyrene-1-carboxylate, 4-pyren-1-ylbutyrate results in the one-electron reduction of the biphenylyl and pyrenyl moieties of the solutes by the hydrated electron. Effects of the cyclodextrin (CD) inclusion complexation of the hydrophobic aromatic groups of the sulfonates and carboxylates have been investigated by using α-, β- and γ-CDs.

INTRODUCTION

Cyclodextrins (CDs) possess hydrophobic cavities and form inclusion complexes with organic molecules in aqueous solution.[1,2] The most common of them are α-, β- and γ-CDs consisting of six, seven and eight glucose units, respectively. The host/guest stoichiometry depends on sizes of CD cavities and of guest molecules.

Pulse radiolysis is expected to provide significant information regarding the effects of CD complexation on reactions of guest molecules. This study is concerned with the one-electron reduction of aromatic sulfonates and carboxylates by the hydrated electron, e_{aq}^-, in the presence of CDs. The guest electrolytes are biphenyl-4-sulfonate (BPS^-), biphenyl-4-acetate (BPA^-), biphenyl-4-carboxylate (BPC^-), pyrene-1-sulfonate (PyS^-), 4-pyren-1-ylbutylate (PyB^-) and pyrene-1-carboxylate (PyC^-). The transient absorption spectra of the one-electron reduction products are similar to those of the radical anions of the corresponding aromatic hydrocarbons, indicating that the radical anion sites are located on the aromatic moieties of the electrolytes. The rate constants for the one-electron reduction of the biphenyl and pyrene derivatives are effectively reduced by the CD complexation with β- and γ-CDs, respectively, whose cavities best fit to the respective aromatic groups.[3,4]

EXPERIMENTAL

BPS^-Na^+ was prepared by adding sodium methoxide to a methanol solution of BPS^-H^+, which was synthesized according to a published procedure, and was recrystallized from water. BPA^-H^+ (Tokyo Kasei) was recrystallized from methanol. BPC^-H^+ (Wako Chemicals) and biphenyl-2-carboxylic acid (Tokyo Kasei) were recrystallized from benzene-methanol mixtures. PyS^-Na^+, PyB^-H^+ and PyC^-H^+ (all Molecular Probes) were used without further purification. α- and β-CDs (both Wako Chemicals) were recrystallized from a water-methanol mixture and from water,

respectively. γ-CD (Wako Chemicals) was used without further purification. Water was deionized and then distilled or was purified by using a Millipore Milli-Q system. Solutions were saturated with argon or nitrous oxide. The pH was adjusted with NaOH at around pH 6 - 7, otherwise noted.

An L-band linear accelerator operating at 28 MeV was used for the pulse radiolysis. The pulse width was 8 ns (the beam diameter, ca. 1 cm). The pulse radiolysis was carried out at room temperature kept at *ca.* 22 °C. Dosimetry was performed with an aerated aqueous solution of 1 x 10^{-5} mol dm^{-3} KSCN taking the $G\varepsilon$ value of $(SCN)_2^-$ to be 2.23 x 10^{-4} m^2 J^{-1}. The dose per pulse was ca. 43 - 100 Gy (1 Gy = 1 J kg^{-1}) producing e_{aq}^- concentrations *ca.* (1.2 - 2.8) x 10^{-5} mol dm^{-3}.

RESULTS AND DISCUSSION

Pulse radiolysis of argon-saturated aqueous solutions of the aromatic sulfonates and carboxylates results in the one-electron reduction of the solute by e_{aq}^-. The reactive species primarily formed by electron-beam irradiation of aqueous solutions are

$$H_2O \text{ -}\!\!\wwvy\!\!\rightarrow H,\ OH,\ e_{aq}^-,\ H_3O^+ \qquad (1)$$

The yields of the above species are: G(H) = 0.6, G(OH) = 2.7, $G(e_{aq}^-)$ = 2.7 and $G(H_3O^+)$ = 2.7. The radical anions and neutral radicals are produced by the reactions of the primarily generated e_{aq}^-, OH and H with the solutes. The transient absorption spectra of the reduced aromatic sulfonates and carboxylates are analogous to those of the radical anions of the corresponding aromatic hydrocarbons, suggesting that the radical anion site is located on the aromatic moieties.

$$e_{aq}^- + ArX^- \longrightarrow (Ar)^-X^- \qquad (2)$$

$$OH\ (\text{or } H) + ArX^- \longrightarrow {}^-Ar(OH \text{ or } H)X^- \qquad (3)$$

where Ar denotes biphenylyl or pyrenyl and X^- denotes SO_3^-, CH_2COO^-, COO^-, or $(CH_2)_3COO^-$. Fig. 1 shows the transient absorption spectra of the argon-saturated aqueous solutions of BPS^-. Fig 2 shows the effects of *t*-butyl alcohol and N_2O, used as radical and electron scavengers, respectively, on the transient absorption spectra. The sharp peak at 405 nm and the broad band at 620 nm disappear when the solution is saturated with N_2O and are assigned to the one-electron reduction product, the radical anion. The spectral shape is similar to that of the biphenyl radical anion, indicating that the radical anion site is located on the biphenylyl group. Similarly, the one-electron reduction was proved for the solutions of the other sulfonates and carboxylates.

The one-electron reduction of the biphenyl and pyrene derivatives are effectively reduced by β- and γ-CDs, respectively, whose cavities best fit to the respective aromatic groups. Figs. 3 and 4 show the effects of α-, β- and γ-CDs on the rise of the absorption of the radical anions of BPS^- and PyS^-, respectively, at the peak positions. Remarkable effects are observed for the BPS^-/β-CD and PyS^-/γ-CD solutions. Similar results were obtained for the carboxylates.

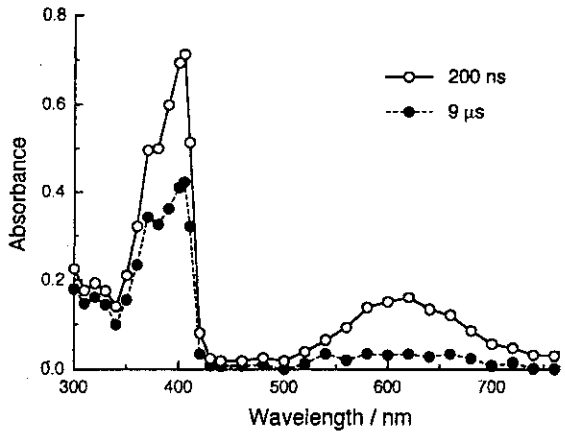


Fig. 1. Transient absorption spectra for the argon-saturated aqueous solution of 5 x 10^{-3} mol dm^{-3} BPS^-.

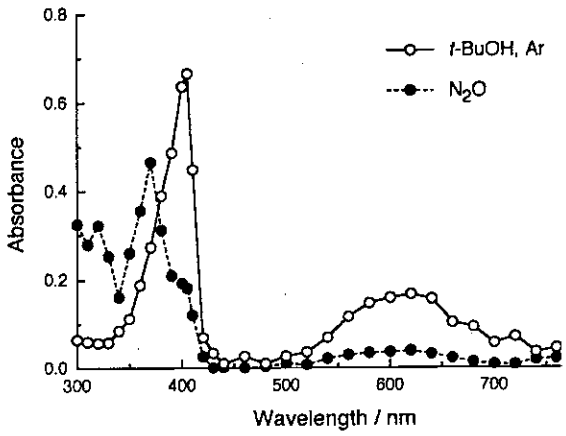


Fig. 2. Transient absorption spectra at 200 ns for the BPS^- solutions saturated with argon and containing 1.0 mol dm^{-3} *t*-BuOH and saturated with N_2O.

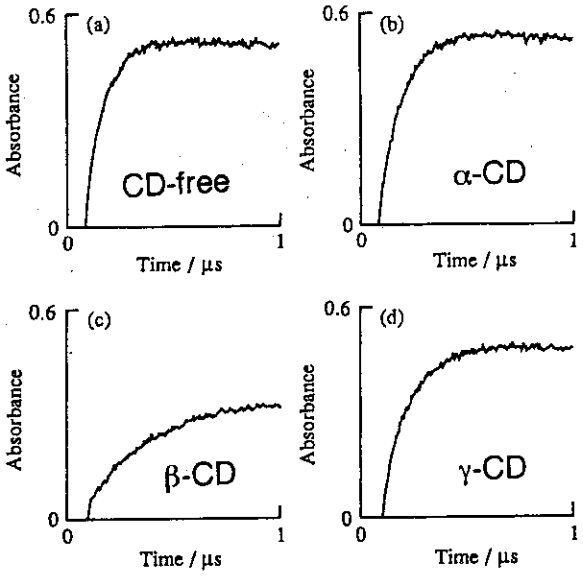


Fig. 3. Rises in the absorption of the radical anion at 405 nm for the 1 x 10^{-3} mol dm^{-3} BPS^- in the absence and presence of 1 x 10^{-2} mol dm^{-3} CDs.

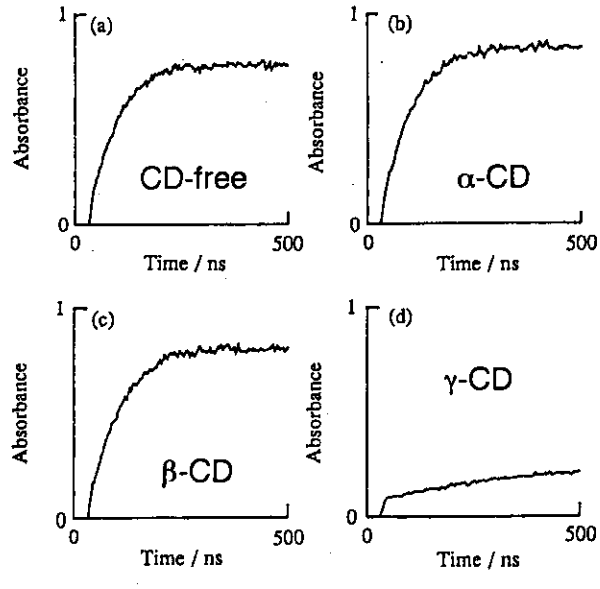


Fig. 4. Rises in the absorption of the radical anion at 490 nm for the 1 x 10^{-3} mol dm^{-3} PyS^- in the absence and presence of 1 x 10^{-2} mol dm^{-3} CDs.

The rises of the absorption of the radical anions were consistent with the decay of e_{aq}^-. Their formation and decay behaviour obeyed first-order kinetics. The bimolecular rate constants for the one-electron reduction of the aromatic sulfonates and carboxylates were determined from the slopes of the linear plots of the pseudo-first-order rate constants against substrate concentration. The pseudo-first-order rate constants were obtained by the kinetic analysis of the decay of e_{aq}^-. Similarly, the bimolecular rate

constants for the one-electron reduction of their inclusion complexes with β- or γ-CD were determined in the presence of an excess of the CDs. The rate constants of the one-electron reduction of the aromatic electrolytes ($k_{CD\text{-}free}$) and those of their inclusion complexes (k_{CD}) are listed in Table 1 together with their ratios ($k_{CD\text{-}free}/k_{CD}$), which are taken as a measure of the effect of the CD complexation on the one-electron reduction.

The $k_{CD\text{-}free}/k_{CD}$ ratios for BPA⁻ and BPC⁻ are 7.3 and 3.6, respectively, indicating that the effect of the CD complexation is smaller for BPC⁻ than for BPA⁻. This can be interpreted in terms of the occurrence of the one-electron reduction of BPC⁻ through the attachment of e_{aq}^- to the carboxyl group being placed outside the CD cavity. On the other hand, in the case of BPA⁻, the attachment of e_{aq}^- is limited to the biphenylyl group by the presence of the methylene spacer between the biphenylyl and carboxyl groups. The attachment of e_{aq}^- to the carboxyl group of BPA⁻ may be as slow as that to the acetate ion with the rate constant of 4.3×10^4 dm^3 mol^{-1} s^{-1} reported in the literature. The contribution of the carboxyl group to the one-electron reduction of BPC⁻ is also demonstrated by the $k_{CD\text{-}free}$ value of BPC⁻ larger than that of BPA⁻.

It is known that 2:2 complexes are formed between the pyrenyl groups and γ-CD at higher host and guest concentrations. The 2:2 complexes dissociate into the 1:1 complexes in strongly alkaline solution. This is due to ionic repulsion between the anionic forms of the secondary hydroxyl groups of the γ-CDs facing each other to form the 2:2 complexes. The rate constants for the one-electron reduction of the inclusion complexes of PyS⁻, PyB⁻ and PyC⁻ with γ-CD drastically increased at pH > 12.5. This can be attributed the dissociation of the 2:2 complexes into the 1:1 complexes, which are much less protected against the one-electron reduction than the 2:2 complexes.

Figs. 5 and 6 show the transient absorption spectra for the solutions of 5×10^{-3} mol dm^{-3} PyS⁻ and PyC⁻, respectively, in the presence of 5×10^{-2} mol dm^{-3} γ-CD. The absorption spectra are shifted to shorter wavelengths with time after the pulse. Such a spectral shift was not observed for PyB⁻. Neither was it observed at pH above 12.5 for PyS⁻ and PyC⁻. It is suggested that the 2:2 complexes of PyS⁻ and PyC⁻ with γ-CD undergo a structural change upon the one-electron reduction. The structural change is caused by the introduction of the negative charge to one of the guest molecules completely surrounded by the hydrophobic cavities. On the other hand, in the case of PyB⁻, the methylene chain between the pyrenyl and carboxyl groups may disturb the formation of the rigid 2:2 complex like those of PyS⁻ and PyC⁻.

Table 1. The Rate Constants for the One-electron Reduction of the Aromatic Electrolytes ($k_{CD\text{-}free}$) and their Inclusion Complexes (k_{CD}).

Aromatic electrolytes	$k_{CD\text{-}free}$/dm^3 mol^{-1} s^{-1}	k_{CD}/dm^3 mol^{-1} s^{-1}	$k_{CD\text{-}free}/k_{CD}$
BPS⁻	9.3×10^9	1.0×10^9	9.3
BPA⁻	3.3×10^9	4.5×10^8	7.3
BPC⁻	9.0×10^9	2.5×10^9	3.6
PyS⁻	1.7×10^{10}	1.3×10^9	13
PyB⁻	1.1×10^{10}	5.8×10^8	19
PyC⁻	1.5×10^{10}	1.5×10^9	10

Effect of β- anf γ-CDs on the electron transfer from the reduced BPS$^{\cdot}$ to PyS$^{\cdot}$ was also investigated with 1 x 10^{-2} mol dm^{-3} BPS$^{\cdot}$ solutions containing (2 - 10) x 10^{-4} mol dm^{-3} PyS$^{\cdot}$ in the absence and presence of 5 x 10^{-2} mol dm^{-3} γ-CD. The transient absorption spectra for these solutions in the early stage were similsar to those for the BPS$^{\cdot}$ solution not containing PyS$^{\cdot}$. The formation of the reduced PyS$^{\cdot}$ is due to exclusively electron transfer from the initially produced radical anion of BPS$^{\cdot}$ to PyS$^{\cdot}$. The bimolecular rate constants for the electron transfer were determined by kinetic analysis of the decay of the 405-nm absorption of the reduced BPS$^{\cdot}$ in the absence and presence of 5 x 10^{-2} mol dm^{-3} γ-CD. The rate constants for the electron transfer from BPS$^{\cdot}$ to PyS$^{\cdot}$ and to the inclusion complex of PyS$^{\cdot}$ with γ-CD were 1.2 x 10^{9} and 5 x 10^{7} dm^{3} mol^{-1} s^{-1}, respectively. The $k_{CD\text{-}free}/k_{CD}$ ratio for the electron transfer is *ca.* 24. It can be said that the 2:2 complex of PyS$^{\cdot}$ with γ-CD is more effectively protected against electron transfer than against the one-electron reduction, probably because of a difference in the reducing power between BPS$^{\cdot}$ and e_{aq}^{-}.

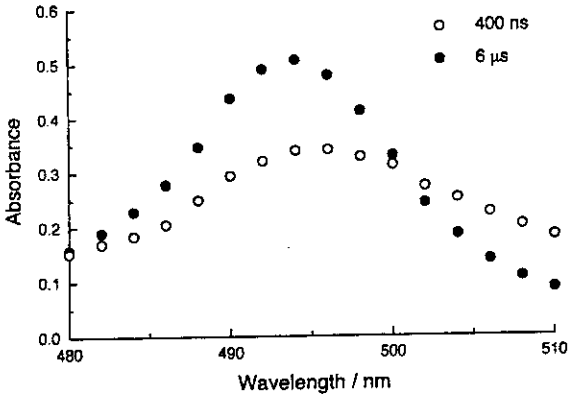


Fig. 5. Transient absorption spectra for the 5 x 10^{-3} mol dm^{-3} PyS$^{\cdot}$ solution containing 5 x 10^{-2} mol dm^{-3} γ-CD.

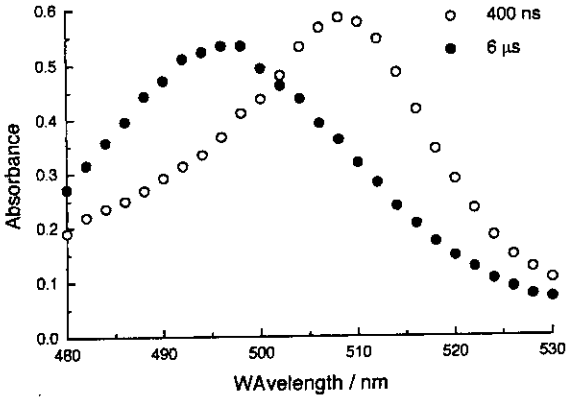


Fig. 6. Transient absorption spectra for the 5 x 10^{-3} mol dm^{-3} PyC$^{\cdot}$ solution containing 5 x 10^{-2} mol dm^{-3} γ-CD.

REFERENCES

(1) M. L. Bender and M. Komiyama, *Cyclodextrin Chemistry*, Springer-Verlag, Berlin, 1978.
(2) J. Szejtli, Cyclodextrins and Their Inclusion Complexes, Akademiai Kiado, Budapest, 1982.
(3) Y. Yamamoto, S. Shiraki and Y. Kawamura, *J. Chem. Soc., Perkin Trans. 2*, 1992, 2241-2245.
(4) Y. Yamamoto, *J. Chem. Soc., Perkin Trans. 2*, 1994, 1555-1559.

12.7 Uniform Irradiation of High-energy Intense Ion Beams to Large Area by Two-dimensional Beam Scanning

TAKASHI AGEMATSU, SUSUMU OKUMURA and KAZUO ARAKAWA

Takasaki Radiation Chemistry Research Establishment
Japan Atomic Energy Research Institute
Watanuki-cho, Takasaki-shi, Gunma 370-12, Japan

Abstract ---- JAERI AVF cyclotron is equipped with ion beam scanners for large area irradiation. The cyclotron beam is two-dimensionally scanned by using a pair of laminated electromagnets. Cellulose triacetate (CTA) film dosimeter has been successfully applied as an integral method to measurement of the two-dimensional relative fluence distributions of the scanned ion beams, proton, He, C, Ar and Kr. The measured result showed that the fluence was not uniform within the scanned area. We have developed a beam scanning simulator to evaluate fluence distribution by calculation, and the simulation result was compared with the measured distribution. The un-uniformity was found to result from the distortion of the current wave form of the scanner. On the basis of this result, the power supply of the scanner was improved. A good uniformity of fluence distribution was available within ±4%.

INTRODUCTION

Large AVF cyclotrons have been used so far mostly for fundamental nuclear physics and medical application to radiation therapy and radioisotope production. An AVF cyclotron dedicated to R&D in materials science, biotechnology and other irradiation purposes was constructed firstly in JAERI (Arakawa, *et al.*, 1992). In these applications, the uniform irradiation of high-energy, intense ion beams over a large area is required especially for evaluation of radiation resistance of materials and solar cells.

We have four methods for making uniform irradiation area by a pencil-like narrow beam; i.e., defocusing, scattering, beam scanning and mechanic scanning methods. The defocusing method is a simple, but it can not make a uniform irradiation on a large area and does not give a good reproducibility of distribution. A scattering method using double scattering foils and a occluding ring (Chu, *et al.*, 1985a) makes loss of particle energy and beam current at the scattering foils. Wobbler scanning method (Chu, *et al.*, 1985b) and raster scanning method can be easily extended to heavier ions as electromagnetic scanning method, because the ion beam does not suffer any scattering or energy loss. Spot scanning method (Kanai, *et al.*, 1980) has been developed for proton radiotherapy. The spot beam is digitally controlled by micro-computer and directed at any point by scanning magnets. It is difficult to realize large area irradiation of high-energy ion beams by electrostatic scanning method. Mechanic scanning method needs to drive the sample in a vacuum chamber. We adopted raster scanning method with electromagnets in view of the fact that a large area uniform irradiation can be realized easily without loss of particle energy and beam current. In this paper, the method of measuring fluence distribution, the method to make the distribution uniform and its improvement are reported.

SCANNING SYSTEM

The cyclotron beam is two-dimensionally scanned by using a pair of laminated electromagnets fed with excitation current alternating in triangular wave form as shown in Fig. 1. The horizontal scanning frequency is 50 Hz and the vertical one is 0.5, 1.0, 2.5 and 5.0 Hz. Beam scanners were installed on three beam courses (HY, LD, LX) as shown in Fig. 2. The maximum scanned area of 100 x 100 mm^2 is available at the beam course LD.

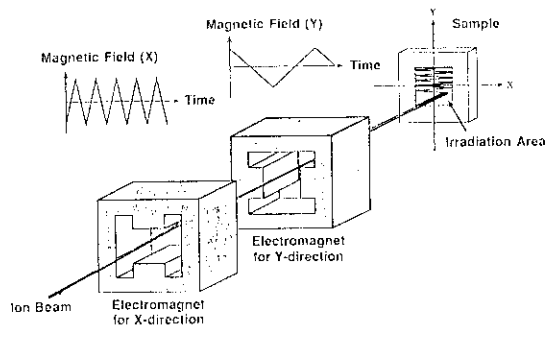


Fig. 1 Raster scanning method by electromagnets.

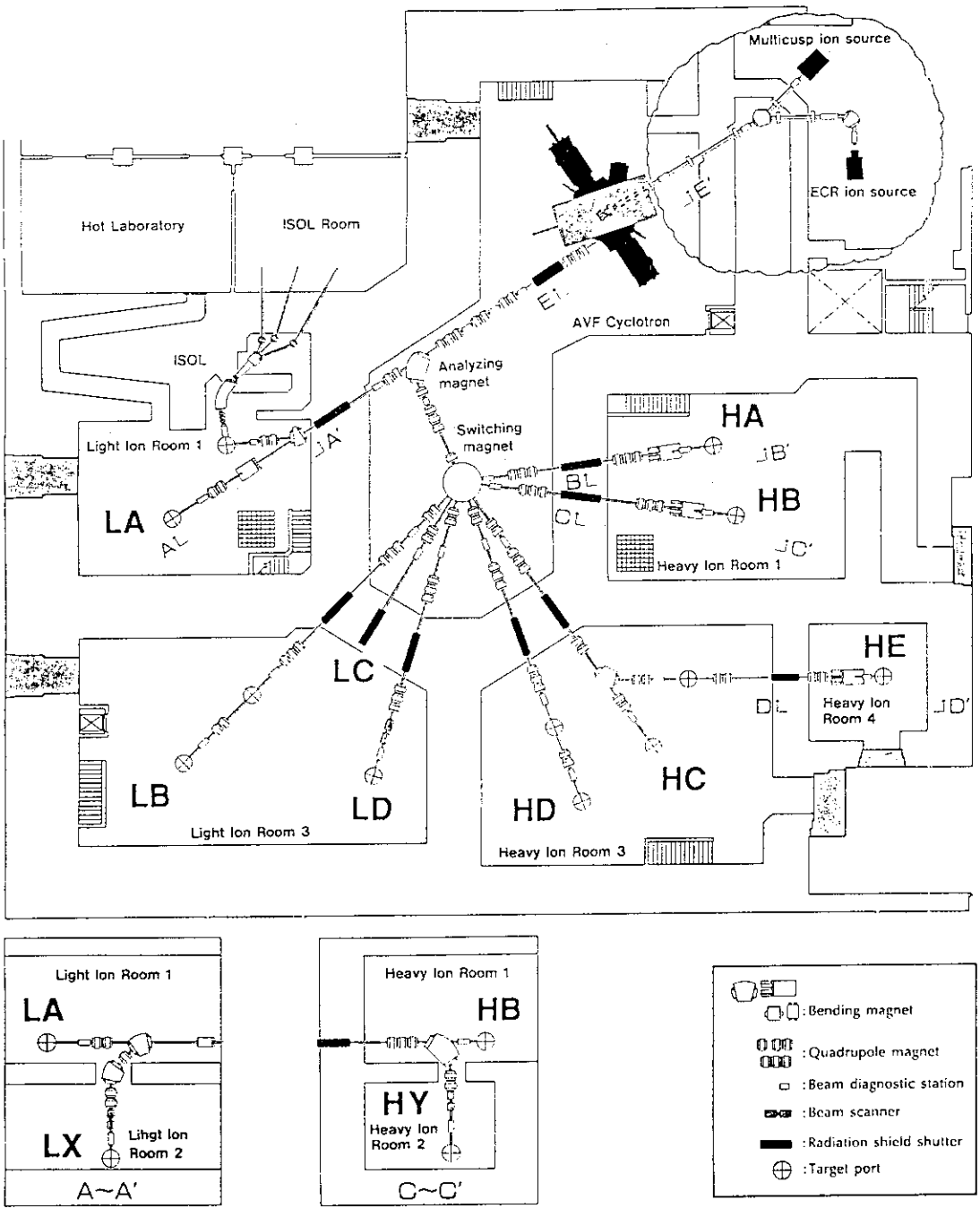
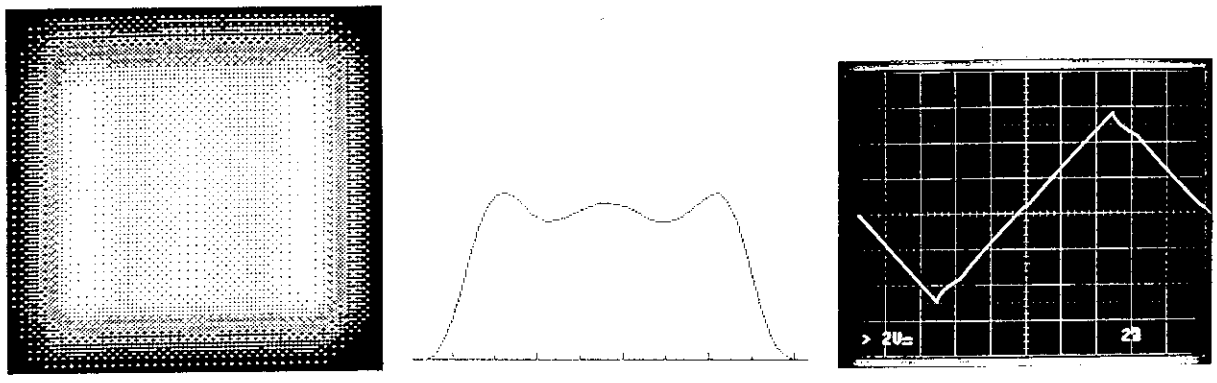


Fig. 2 Layout of JAERI AVF cyclotron beam courses.

MEASUREMENT OF FLUENCE DISTRIBUTION

Film dosimeters widely used for radiation processing with electron beams and γ-rays are suitable for measurement of dose distribution because of their high spatial resolution and simplicity in the measurement. Cellulose triacetate (CTA) film dosimeter (Tanaka, *et al.*, 1984) has been successfully applied to dose measurement of electron beams and γ-rays as an integration method. A commercial film dosimeter with 125 μm in thickness, FTR-125 of Fuji Photo Film Co., Ltd., was used for the experiment. The dosimetry is based on radiation-induced optical densities change at 280 nm in the linear dose response region. Measurement of optical density distribution was carried out with a double-scanning micro-spectrophotometer (Tanaka, *et al.*, 1985). The data collection and the analysis were performed by a personal computer.



(a) Two-dimensional fluence distribution.

(b) Fluence profile in horizontal direction.

(c) Current wave form of the scanning magnet in the horizontal direction.

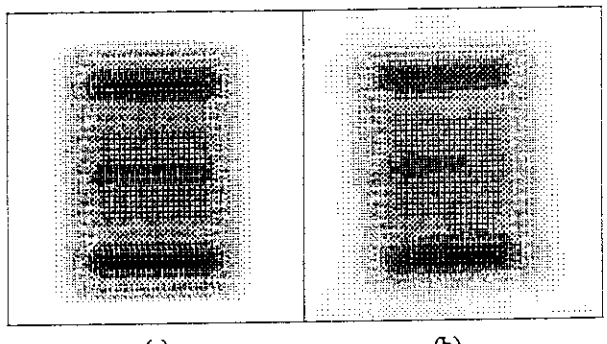
Fig. 3 An example of fluence distribution, before improvement of the scanner, measured by CTA film dosimeter. A 45 MeV proton beam was scanned in the area of 35 x 55 mm^2 with a beam condition of 1 μA for 200 sec. The scanning frequency was 50 Hz in the horizontal and 0.5 Hz in the vertical direction.

CTA film dosimeter have been applied to measure absorbed dose of proton beams (Sunaga, *et al.*, 1987), He, C and N ions (Sasuga, *et al.*, 1991). It was revealed in these experiments that this dosimeter does not provide absolute dose because of the lack of data of dose dependence on linear energy transfer (LET), but it is enough to measure a relative dose distribution. The dose distribution corresponds to relative fluence distribution, because the dose is approximately given by the product of the mass stopping power and the fluence.

Fluence distributions of the scanned beam were evaluated by CTA film dosimeter for the following beam conditions: 10 MeV proton, 45 MeV proton, 20 MeV $^4He^{2+}$, 50 MeV $^4He^{2+}$, 220 MeV $^{12}C^{5+}$, 175 MeV $^{40}Ar^{8+}$, 520 MeV $^{84}Kr^{20+}$. Figure 3(a) and (b) shows an example of relative fluence distributions measured for the scanned 45 MeV proton beam. It indicates that the fluence distribution is not enough uniform within the scanned area.

THE SIMULATOR OF BEAM SCANNING

The film dosimetry does not give fluence distribution in real time. For this reason, we have developed a simulation method to evaluate the fluence distribution from scanned beam dynamics on the basis of the wave form of the scanning coil current. The simulated distributions were compared with the measured ones. The both were in good agreement as shown in Fig. 4 and we can optimize the beam scanning condition for uniformity irradiation by using this simulation.



(a) (b)

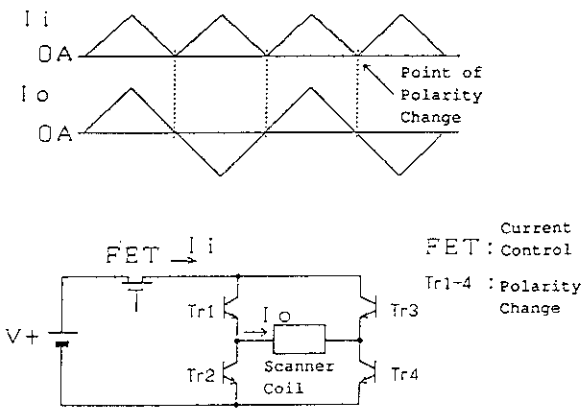
Fig. 4 Comparison of fluence distribution, (a): Simulation and (b): CTA film dosimetry. A 50 MeV $^4He^{2+}$ ion beam was scanned in the area of 56 x 34 mm^2. The scanning frequency was 0.5 Hz in the horizontal and 50 Hz in the vertical direction.

IMPROVEMENT OF THE SCANNER

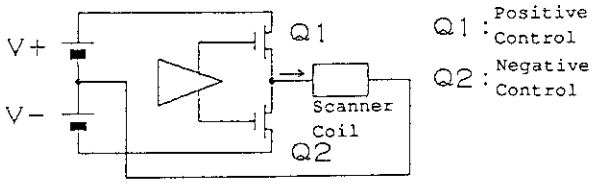
In Fig. 3(a) and (b), the fluence profile has three peaks at the both edges and the center along the horizontal direction. The similar profiles are

commonly observed in most irradiation results in the direction. The simulated distribution demonstrated that the distortion of the wave form of the scanning coil current, shown in Fig. 3(c), results in the three peaks in fluence distribution. The distortion at the maximum current results from the induced counter electromotive force and the one at the zero-cross point is caused by polarity change of the transistor.

For removing the distortions, we improved the power supply of the circuit system for the direction of 50 Hz scanning. The circuit system was replaced by a single end push pull (SEPP) circuit system without polarity change. Figure 5 shows the two circuit systems : (a) before and (b) after improvement. As shown in Fig. 6(a) and (b), the fluence distribution measured at the same irradiation condition as shown in Fig. 3(a) and (b) has no peak in the fluence profile. The wave form of the scanning coil current has no distortion as shown in Fig. 6(c). The improvement of the power supply resulted in a good uniformity of fluence distribution within ±4%. The fluence distributions for various ion beams indifferent scanning conditions have been measured by using CTA film dosimeter for 10 MeV proton, 20 MeV $^{4}He^{2+}$, 50 MeV $^{4}He^{2+}$, 220 MeV $^{12}C^{5+}$, 175 MeV $^{40}Ar^{8+}$ and 520 MeV $^{84}Kr^{20+}$.

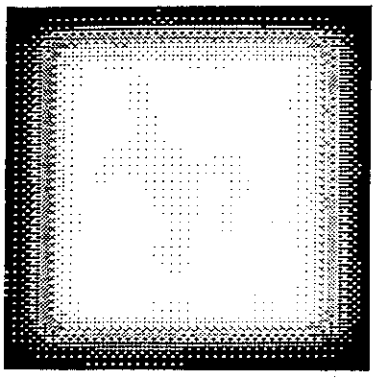


(a) Circuit system before improvement.

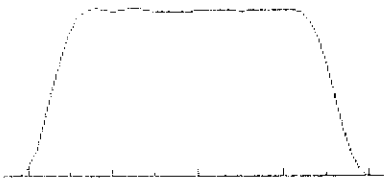


(b) Circuit system after improvement.

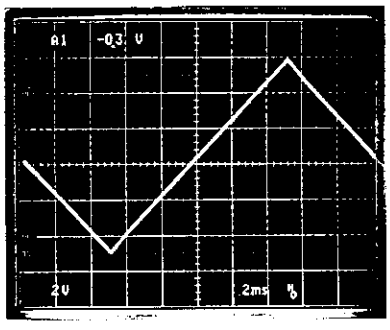
Fig. 5 Circuit system of scanner power supply, before and after improvement.



(a) Two-dimensional fluence distribution.



(b) Fluence profile in horizontal direction.



(c) Current wave form of the scanning magnet in the horizontal direction.

Fig. 6 An example of fluence distribution, after improvement of the scanner, measured by CTA film dosimeter. Uniformity is ±4% within the scanned area. A 45 MeV proton beam was scanned in the area of 35 x 55 mm^2 with a beam condition of 1 μA for 200 sec. The scanning frequency was 50 Hz in the horizontal and 0.5 Hz in the vertical direction.

SUMMARY

A good ion fluence uniformity within ±4% over the scanned area of 100 x 100 mm^2 was achieved. To analyze the uniformity, cellulose triacetate (CTA) film dosimeter has been successfully applied to measurement of the two-dimensional relative fluence distribution as an integration method for ion beams, proton, He, C, Ar and Kr. We have developed a beam scanning simulator to evaluate the fluence distribution. These scanning system and the measurement method are useful for R&D in materials science and other irradiation purposes.

The accuracy limit of uniformity analysis is about ±4% from the signal to noise ratio of the double-scanning micro-spectrophotometer which has been used for CTA dosimetry of the fluence distribution. We are planning to develop a new high-precision double-scanning micro-spectrophotometer. Since CTA film dosimeter can not be used for real time measurement, we are developing a parallel plate avalanche counter (PPAC) as a two-dimensional fluence distribution in real time.

REFERENCES

Arakawa K., Nakamura Y., Yokota W., Fukuda M., Nara T., Agematsu T., Okumura S., Ishibori I., Karasawa T. and Tanaka R. (1992) Construction and First Year's Operation of the JAERI AVF Cyclotron. *Proc. 13th Int. Conf. on Cyclotron and their Applications,* Vancouver, Canada, p.119.

Chu W. T., Curtis S. B., Llacer J., Renner T. R. and Sorensen R. W. (1985a) Wobbler Facility for Biomedical Experiments at the BEVALAC. *IEEE Trans. Nucl. Sci.* **NS-32**, 3321.

Chu W., McEvoy M., Nyman M., Renner T., Gonzales B., Singh R. P. and Stradner R. (1985b) Wobbler Dosimetry for the Biomedical Program at the LBL BEVALAC. *IEEE Trans. Nucl. Sci.* **NS-32**, 3324.

Kanai T., Kawachi K., Kumamoto H., Ogawa H., Yamada T. and Matsuzawa H. (1980) Spot Scanning System for Proton Radiotherapy. *Med. Phys.* **7**, 365.

Tanaka R., Mitomo S. and Tamura N. (1984) Effects of Temperature, Relative Humidity, and Dose Rate on the Sensitivity of Cellulose Triacetate Dosimeters to Electrons and γ-Rays. *Int. J. Appl. Radiat. Isot.* **35**, 875.

Tanaka R., Sunaga H. and Agematsu T. (1985) Methods for Measuring Dose and Beam Profiles of Processing Electron Accelerators. In *High-Dose Dosimetry, Proc. Symp.,* Vienna, 1984. p.317 IAEA-SM-272/18. IAEA, Vienna.

Sunaga H., Agematsu T., Tanaka R., Yoshida K. and Kohno I. (1988) Dosimetry by a Cellulose Triacetate Film Dosimeter in Proton-beam Irradiation. *Radioisotopes* **37**, 84.

Sasuga T., Kawanishi S., Nishii M., Seguchi T. and Kohno I. (1991) Effects of Ion Irradiation on the Mechanical Properties of Several Polymers. *Radiat. Phys. Chem.* **37**, 135.

12.8 High Energy Ion Irradiation Effects on Polymer Materials

H. Kudoh, T. Sasuga and T. Seguchi

Takasaki Radiation Chemistry Research Establishment,
Japan Atomic Energy Research Institute,
Takasaki, Gunma, 370-12, Japan

Abstract The changes in mechanical properties of several polymers induced by high energy protons(10, 30 and 45MeV) were studied and compared with those by 2MeV electrons and Co-60 gamma rays. The elongation at break in tensile test for polytetrafluoroethylene (PTFE) showed the same behavior with absorbed dose between proton and electron irradiations. The flexural strength at break of polymethylmetacrylate (PMMA) and glass fiber reinforced plastic (GFRP) also showed no difference between proton and Co-60 gamma rays irradiations.

INTRODUCTION

The evaluation of radiation resistance of polymer materials to ion irradiation is necessary to select and apply suitable materials for space and fusion reactor environment where materials are subjected to high energetic ions. The radiation resistance of polymer materials has been studied extensively with gamma rays or electron beam. The radiation effects has been assumed to be different between ion and gamma ray or electron beam due to the difference in linear energy transfer (LET). Radiation resistance of polymer materials is determined in terms of change in mechanical properties such as tensile elongation and flexural strength. For the evaluation by these test, the materials must be irradiated in the wide area with uniform dose. However, there are few facilities for it and lacks of data. On this view point, ion accelerators and ion irradiation chamber for uniform irradiation were prepared in JAERI Takasaki (Sasuga et al., 1993). In this work, the changes in mechanical properties induced by proton irradiation were studied for several polymers and compared with those by 2MeV electron or Co-60 gamma rays irradiations.

EXPERIMENTAL

Polymers used in this work is polytetrafluoroethylene (PTFE), polymethylmethacrylate (PMMA) and glass fiber reinforced plastic (GFRP; Glass/bisphenol A type epoxy resin). PTFE are 0.1mm thick for tensile test. PMMA is 3mm thick and GFRP is 2mm thick for flexural test. Proton spot beams of 10mm diameter from Cycrotoron was scanned uniformly in 100 x 100mm wide area. Thin films of PTFE were irradiated with 10MeV protons, and PMMA and GFRP were irra-

diated with 30MeV protons, respectively, in order that protons pass throughout specimens. The materials were placed on the water cooled holder and irradiated at room temperature under vacuum. LET of 10MeV protons is as large as 24 times than that of 2MeV electrons or gamm aary, and those of 30 and 45 MeV protons is 9 and 7 times larger, respectively. Absorbed dose by proton irradiation was evaluated as the product of fluence and Bethe's mass stopping power. For comparison with proton irradiation, 2MeV electron irradiation was carried out for PTFE under vacuum, and Co-60 irradiation for PMMA and GFRP in nitrogen gas atmosphere at room temperature. After irradiation, PTFE were examined by tensile test and PMMA and GFRP were by three points flexural tests at room temperature. Molecular weight of PMMA were measured by gel peameation chromatography (GPC). Glass transition temperature (Tg) of GFRP was measured by differential scanning calorimeter (DSC).

RESULTS and DISCUSSION

(1)PMMA (Kudoh et al., 1994)

Figure 1 shows the change in flexural strength of PMMA measured at RT as a function of absorbed dose. The flexural strength decreases with dose above 0.1MGy, and this behavior to dose is the same among gamma rays, 45MeV and 30MeV protons. Figure 2 shows the change in molecular weight(Mn) as a function of absorbed dose. Mn decreases in the same way among gamma rays, 45MeV and 30MeV protons. The ratio of weight average molecular weight to number average one, Mw/Mn was about 3 before irradiation and around 2 after small dose irradiation, which means that the molecular weight distribution is random. The G value of chain scission of PMMA calculated from Fig. 2 is 1.7 and agrees well with values in literatures (Yates et al., 1993). The experimental results of flexural strength, Mn and Mw/Mn indicate that the chain scsission takes place in the same way in number and spatial distribution among the irradiation of gamma rays and 45MeV and 30MeV protons, and that the decrease in

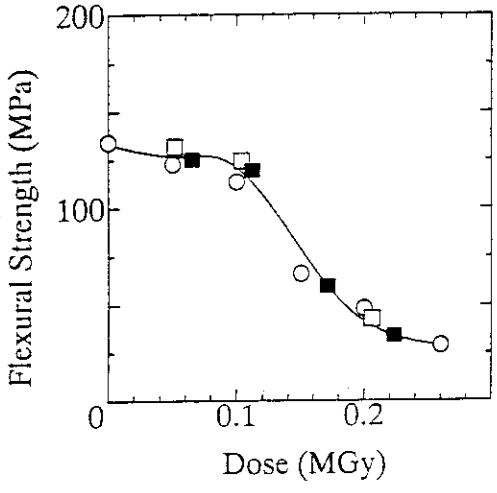


Fig.1 Flexural strength of PMMA measured at RT

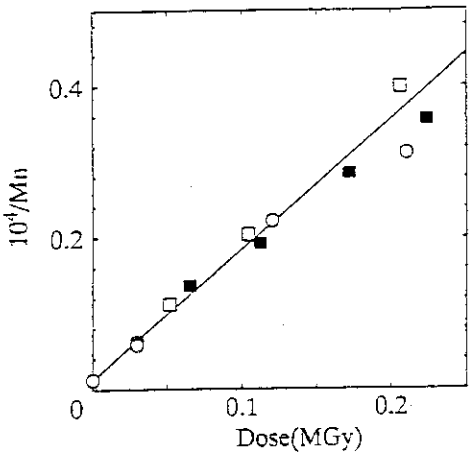


Fig.2 Number average Molecular weight irradiated by gamma ray(○), H^+45MeV(□),H^+30MeV(■)

mechanical properties depends only on dose. LET effect on PMMA degradation is not observed in the range of this work.

(2)GFRP (Kudoh et al., 1994)

Figure 3 shows the change in flexural strength of GFRP measured at RT as a function of absorbed dose. The strength increased about 20% at 0.5MGy to 0.6MPa from the initial strength of 0.5MPa and decreased with dose above 1MGy. The behavior to the dose is the same between 30MeV protons and gamma rays irradiations. The radiation degradation of GFRP is attributed to the degradation of matrix resin. Figure 4 shows the change in Tg of epoxy resin deterimind by DSC. The decrease of Tg means the destruction of network structure of epoxy resin. The scission probability is the same between gamma rays and 30MeV proton irradiations.

(3)PTFE

Figure 5 show the change in elongation at break and tensile strength of PTFE measured at RT. PTFE specimens are so thin that high LET ions can pass through them. The degradation is not sensitive to LET showing almost the same behavior to dose in spite of the large difference in LET. Since PTFE degrades undergoing the chain scission by radiation, the scission probability does not depend on LET so much.

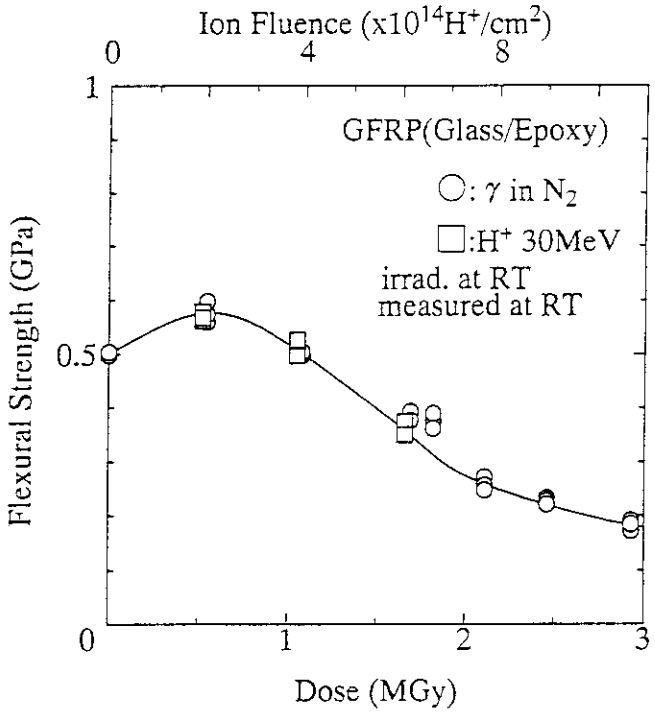


Fig.3 Flexural strength of GFRP measured at RT irrad. by gamma ray(○),H$^+$30MeV(□)

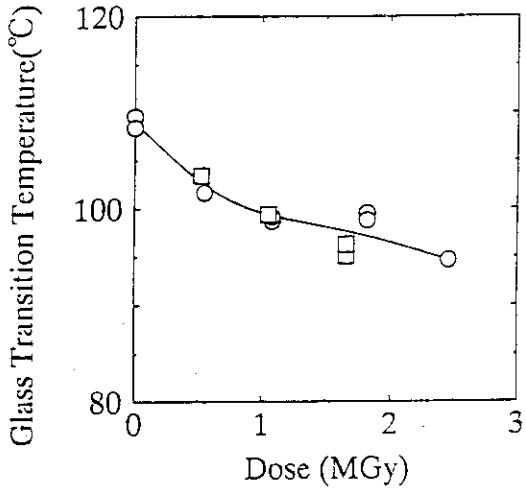


Fig.4 Glass transition temperature(Tg) irrad. by gamma ray(○),H$^+$30MeV(□)

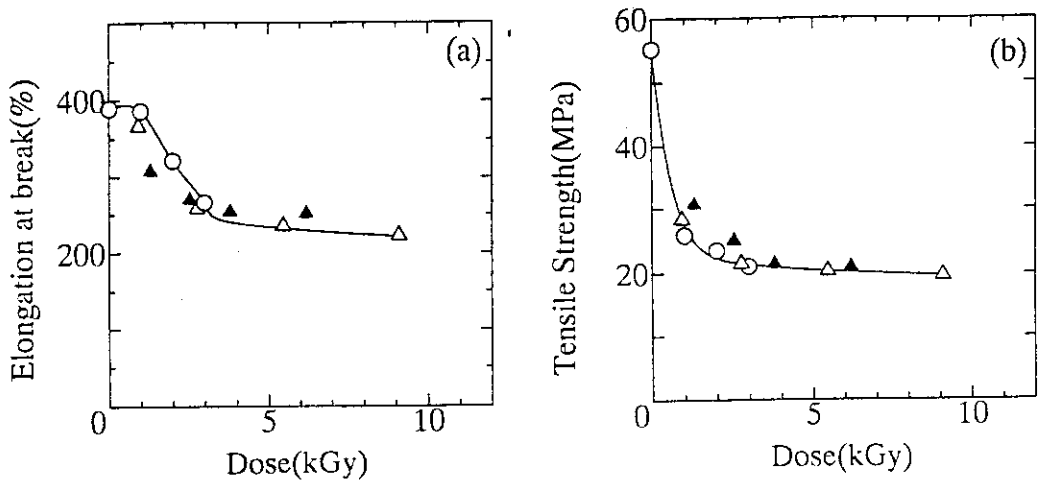


Fig. 5 (a)Elongation at break of PTFE
(b)Tensile strength at break of PTFE
irradiated by e^- 2MeV(○),
H^+ 10MeV(△), H^+ 45MeV(▲)

CONCLUSION

High energy ion irradiation effects on polymer materials such as PMMA, GFRP and PTFE were studied by mechanical properties molecular weight and glass transition temperature changes after irradiation by using Cyclotoron and ion irradiation chamber prepared in JAERI Takasaki. The changes in mechanical properties showed the same behavior to absorbed dose between protons and electron or gamma rays irradiations, which means that the LET effects on the degradation of these polymers are very small.

REFERENCES

Kudoh H., Sasuga T. and Seguchi T.(1994) The proceedings of 37th Symposium on Radiation Chemistry, Japan, Hokkaido, Sapporo, p73
Sasuga T., Kudoh H. and Seguchi T.(1993) JAERI-M 93-047, 117
Yates B.W. and Shinozaki D.M.(1993) J.Polym.Sci.B,vol.31, 179

12.9 Space Charge Distribution in Gamma-irradiated Low Density Polyethylene

M. Kojima, Y. Tanaka, T. Takada and Y. Ohki*

Musashi Institute of Technology
1-28-1 Tamazutsumi, Setagaya-ku, Tokyo 158, Japan
*Waseda University
3-4-1 Ohkubo, Shinjuku-ku, Tokyo 169, Japan

Abstract - The present paper discusses the residual space charge distribution in gamma-irradiated polyethylene formed with dc voltage, which was measured using the pulsed electroacoustic (PEA) method. The PEA method is one of advanced non-destructive techniques to measure the space charge distribution with a high sensitivity and reproducibility. From the experimental results, it became clear that a large amount of positive charges existing near the cathode in gamma-irradiated polyethylene enhance the electric field at the cathode interface. Under short circuit condition, the strength of this electric field by the space charge is sometimes more than two times of the applied field. On the other hand, almost no space charge was observed in the non-irradiated sample.

INTRODUCTION

The research on the effect of irradiation on the electrical properties in polymeric dielectric materials is important when these materials are used in space or a nuclear power plant. We have reported on the relationship between the amount of space charge formed in irradiated polymer dielectrics and its radiation resistance [1]. In this previous report, we suggested that the amount of charge remained in the irradiated polymers was obviously associated with the radiation resistance of the polymers. However the amount of charge was estimated from the results of dc conduction current, thermally stimulated current (TSC), residual voltage and thermal pulse current measurements. With these measurement methods, only the differences in the total amount of residual charges among the samples could be estimated. Therefore, to measure not only the total space charge but also its distribution accurately and precisely, similar measurements were carried out by the pulsed electroacoustic (PEA) method. The present paper discusses space charge formation characteristics in low density polyethylene0 irradiated by low-dose γ-rays.

SAMPLES AND EXPERIMENTAL PROCEDURES

Samples used in this experiment are commercially available low-density polyethylene (LDPE), supplied from Nippon Petrochemicals. All of the samples are hot-pressed sheets of about 600 μm thick, with two evaporated gold electrodes with a diameter of 20 mm. Gamma irradiation was carried out using a ^{60}Co source in air at room temperature, at a dose rate of 100 Gy/h to a total dose of 2.4 kGy, the dose which is large enough to excite carriers and low enough to avoid chemical change or structure damage during the irradiation [1]. All of the experiments were begun one hour after the γ irradiation.

To measure the space charge distribution, the PEA method was employed. In this method, a high voltage short-duration pulse (of about 13 ns) is applied to the sample, which generates an acoustic pressure wave from a charge layer. By detecting such a pressure wave with a piezoelectric transducer, we can obtain the space charge distribution formed in the sample. Details of the principle were described elsewhere [2].

At first, the following experimental procedure was used to study the dependence of space charge distribution on the application time of dc field. DC voltage of 15 kVdc was applied for certain durations from 1 to 240 minutes to the 2.4 kGy irradiated sample and the space charge profile was collected. During the measurement, immediately after the voltage was turned off, the space charge profile was recorded. Then, the original voltage was applied. By repeating above procedure, the time dependence of space charge distribution under short circuit condition was obtained.

RESULTS

Figure 1 shows the time dependence of space charge distribution in non-irradiated LDPE during the voltage application of dc 15 kV. Almost no space charge is observed in the bulk even at 240 min.

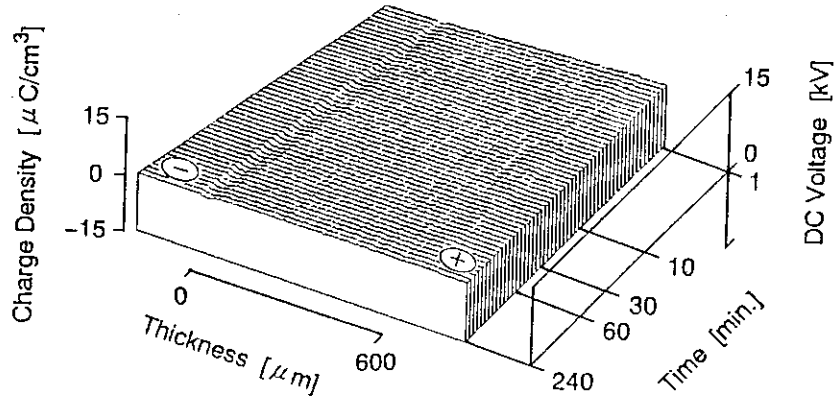


Fig.1. Time dependence of space charge distribution in non-irradiated LDPE.

Figure 2 shows the space charge distribution in γ-irradiated LDPE before dc voltage application. No space charge is observed. Similarly space charge was not observed in all the samples before application of dc voltage, irrespective of being γ-irradiated or not.

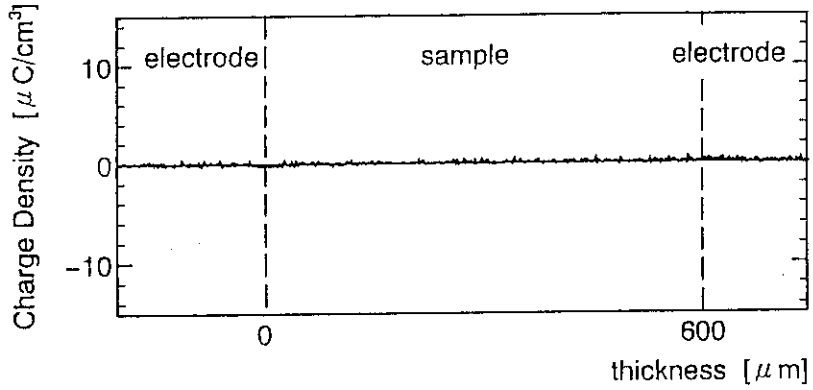


Fig.2. Space charge distribution in γ-irradiated LDPE before dc voltage application.

Figure 3 shows time dependence of space charge distribution in the 2.4 kGy irradiated LDPE with dc voltage of 15 kV (= 25 kV/mm). Immediately after dc voltage application to this sample, positive charge is observed near the cathode and become larger with increasing the voltage application time. On the other hand, a small amount of negative charge is observed near the anode around 10 minutes after voltage application, but its value is much smaller compared with the positive charge near the cathode. The change of the space charge distribution seems to be saturated around 60 minutes after voltage application.

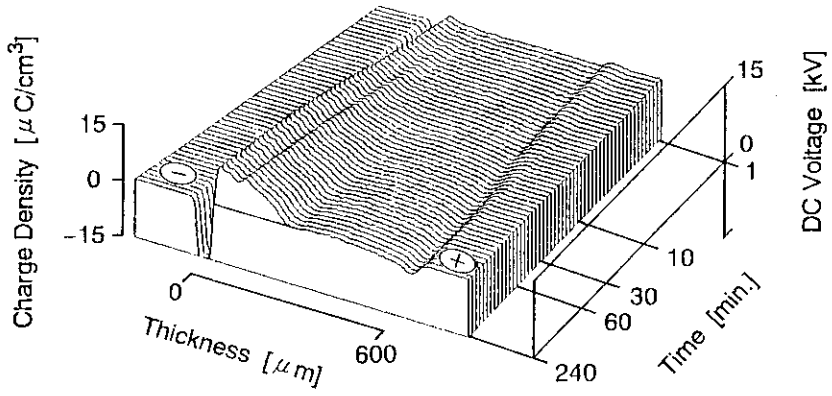


Fig.3. Time dependence of the space charge distribution in γ–irradiated LDPE with dc voltage applied.

Figure 4 shows time dependence of space charge distribution in the 2.4kGy irradiated LDPE under short circuit condition, which follow the above measurement shown in Fig.3. After short circuit, a part of the positive charge existed at a remote position from the cathode decreases with time, but the positive charge near the cathode still remained for 4 hours under short circuit condition. The negative charge near the anode immediately disappears after short circuiting, and a positive charge gradually appears.

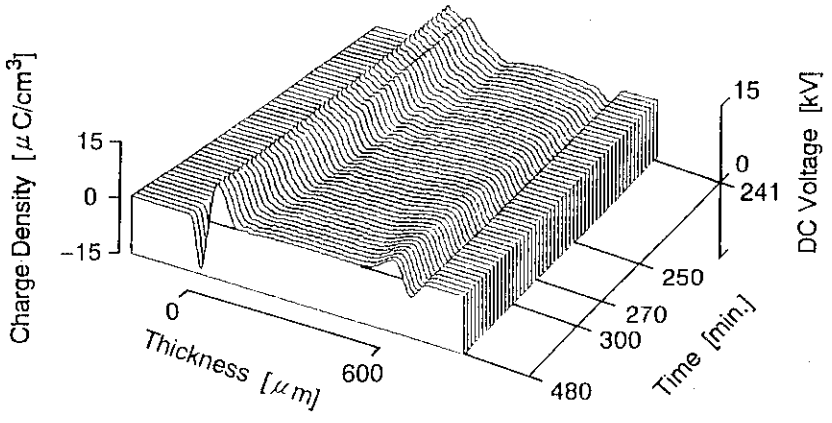


Fig.4. Time dependence of the space charge distribution in γ-irradiated LDPE under short circuit condition.

Figure 5 shows time dependence of electric field at the cathode interface for the 2.4 kGy irradiated LDPE with 15 kVdc applied and under short circuit condition, which were obtained by calculation from the results shown in Figs. 3 and 4 [3]. The electric field increases with increasing voltage application time up to around 60 minutes. Then the field becomes saturated at the value of about 60 kV/mm, although the applied field was about 25 kV/mm. Consider the value was obtained from the measurement done under short circuit condition, it means that the positive charge formed in this sample near the cathode enhances the electric field to more than three times of the applied field. After the sample was short circuited, the field decreases gradually. However, almost the same value as the applied field still remained for 4 hours.

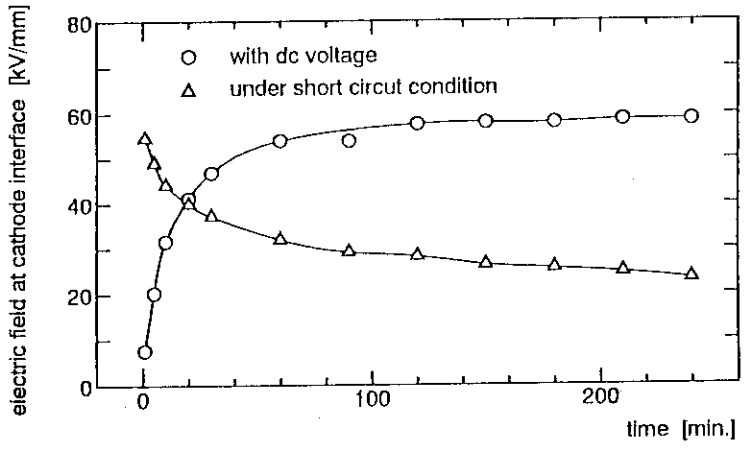


Fig.5. Time dependence of the electric field
at the cathode interface of the γ-irradiated LDPE.

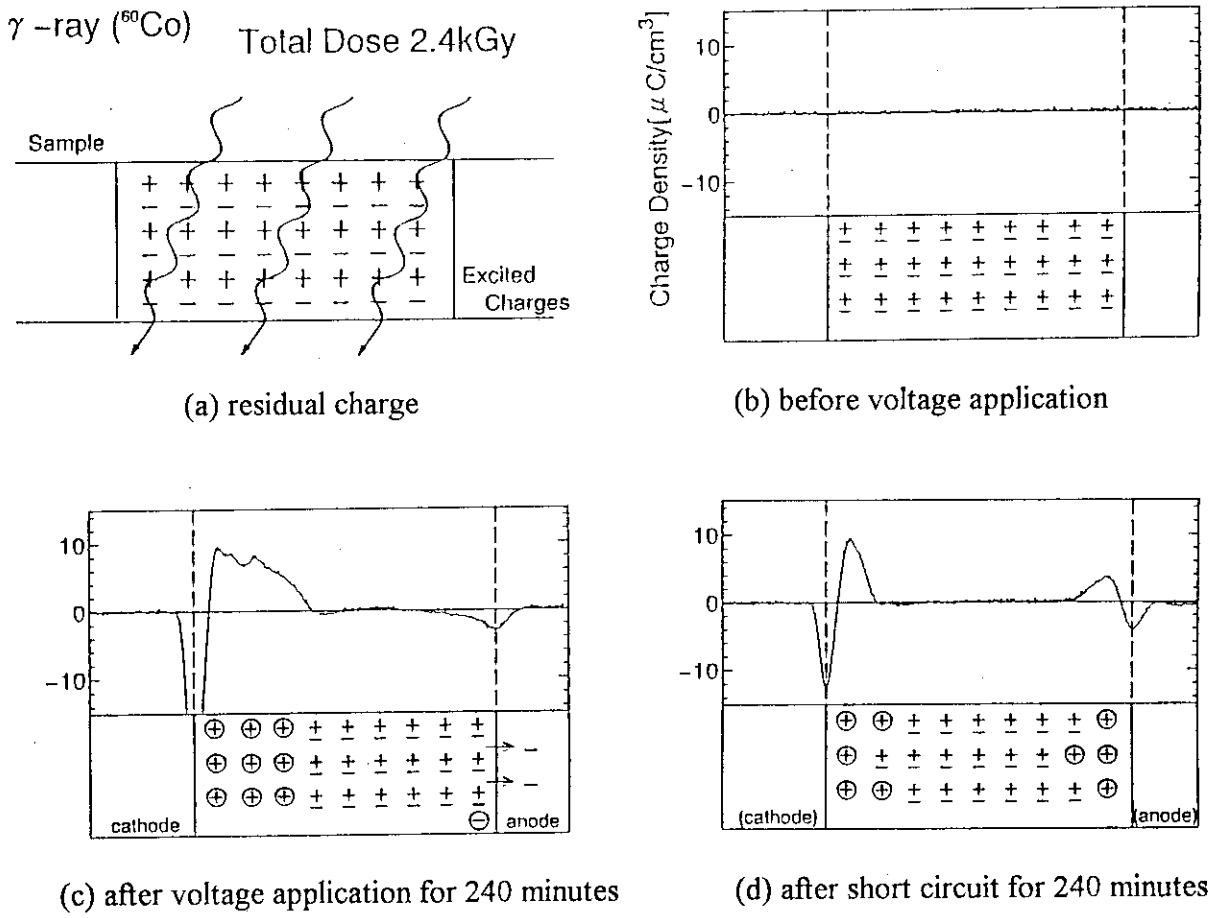
DISCUSSION

A large amount of positive charge is observed in the γ-irradiated LDPE, while space charge is scarcely observed in non-irradiated LDPE. From the results of our previous works, the density of space charges formed in polyethylene with dc voltage was usually less than 5 μ C/cm^3 even in the samples with additives and/or impurities [2-4]. In the γ-irradiated LDPE, more than 10 μ C/cm^3 of charge density was observed. As such a large amount of positive charge was not observed in the non-irradiated LDPE in Fig. 1, the appearance of these positive charges in the irradiated LDPE must be resulted from the effect of γ-irradiation. Assuming that the injection condition does not change by γ-irradiation, the positive charges must be generated from the bulk. Part of the charge pairs excited by γ-rays and escaped from recombination are considered to become observable.

Figure 6 shows the observed distribution (upper in Figs. 6(b)-(d)) and schematic models (lower in Figs. 6(b)-(d)) of space charge formation in the 2.4 kGy irradiated LDPE. From the result of Fig. 2, no space charge was observed before the application of dc voltage. Therefore, after γ-irradiation, the remained charge pairs may be distributed homogeneously (see Figs. 6(a) and (b)). By the applied dc voltage, electrons from these excited charge pairs were swept off from the bulk into the anode. Therefore, the remained positive charges near the cathode side are observed (see Fig. 6(c)). This formation model is almost the same as the one assumed in the previous report [1]. After the circuit was shorted, the electrons remained in the bulk move toward the former cathode, and as a result, positive charges become observable near the former anode (see Fig. 6(d)). The electric fields at the cathode interface in the γ-irradiated samples were remarkably high as shown in Fig. 5. The electric fields must affect high field phenomena such as electrical breakdown and surface discharge.

CONCLUSION

Space charge distributions formed in low density polyethylene (LDPE) irradiated by low dose γ-rays were observed using the pulsed electroacoustic method. In the γ-irradiated LDPE, large amounts of positive charges were observed near the cathode, whereas the same phenomenon was not observed in the non-irradiated LDPE. This is probably because there exist many survived γ-excited charges, which escaped from recombination, in the γ-irradiated LDPE. Therefore, it seems that the dc voltage applied to the sample swept off the negative charges from the bulk into the anode, leaving positive charges behind.



(a) residual charge

(b) before voltage application

(c) after voltage application for 240 minutes

(d) after short circuit for 240 minutes

Fig.6. Observed distribution of space charge and the estimated models of distribution of electrons and holes(or positive ions) in γ–irradiated LDPE.
After γ–irradiation (a), before dc voltage application (b), after dc voltage application for 240 min. (c), and under short circuit condition for 240 min.(d).

Besides of study about the above space charge formation mechanism, the electric field which was generated from the space charge formed near the cathode was calculated from the measurement results. In the non-irradiated LDPE, the electric field is only less than 5 % of the applied field. On the other hand, the electric field formed in the γ–irradiated LDPE is more than twice of the applied field. It decreases under short circuit condition, but still remain to be almost the same value as the applied field for several hours. Such remaining electric field seems to affect high field phenomena such as electrical breakdown and surface discharge.

ACKNOWLEDGMENT

This work was supported in part by a Grant-In-Aid for Scientific Research from the Ministry of Education, Science, and Culture, Japan (# 06750332).

REFERENCES

[1] Y. Tanaka, Y. Mita, Y. Ohki, H. Yoshioka, M. Ikeda and F. Yazaki, J. Phys. D: Appl. Phys.,23, 1491(1990).
[2] Y. Li and T. Takada, Proc. 6th DMMA, 104(1992).
[3] Y. Li and T. Takada, J. Phys. D:Appl.Phys., 25, 704(1992).
[4] Y. Li, T. Takada, H. Miyata and T. Niwa, J. Appl. Phys., 74, 2725(1993).

12.10 A New Leuco Dye Dosifilm PVG

LIU Aiguo, CHEN Wenxiu and JIA Haishun
Department of Chemistry
Beijing Normal University
Beijing, 100875 CHINA

ABSTRACT

A leuco dye film dosimeter for dose measurement on Co-60 gamma radiation processing was developed. The matrix material polyvinyl butyral (PVB) with leuco malachite green (LMG) and additive halogenated compounds (RX) were manufactured as the PVG dosifilm. Its response (Δ A/L vs dose) at 627nm showed a linearity (correlation coefficient r > 0.999) in the dose range from 0.5 to 80 kGy. The calibration coefficient of temperature during irradiation was + 0.053/ ℃. The response increased slightly with the increasing of relative humidities (0-96.4%); and the the calibration coefficient was +0.006/ Δ r.h(%). From 54.9% to 96.4% the deviation was less than 4%.

The PVG dosifilm was stable before and after irradiation when it was stored in the dark at a given relative humidity. The deviation of response on PVG dosifilm kept in a brown desiccator was less than 4% after 40 days. It was suitable to serve as a routine dosimeter.

KEYWORDS

Polyvinyl butyral; Leuco malachite green; Halogenated organic compounds; Radiochromic film dosimeter; Radiation processing.

INTRODUCTION

Polyvinyl butyl (PVB) has been used as the matrix of dyed plastic film dosimeters(McLaughling et al., 1977; Miller et al., 1981, 1988), which based on one of several dye precursors of similar chemical structure, i.e, three benzene rings and a cyanide group surround a central carbon atom, such as hexa(hydroxyethyl) pararosaniline cyanide (HPR-CN) and pararosaniline cyanide (PR-CN). But these radiochromic dosimeters are sensitive to UV light and must be protected from fluorescent lights and sunlight (McLaughling et al.,1988).

Leuco malachite green (LMG) has been used for dosimetry purpose (Stolz et al., 1965; Dejehet et al., 1972,1973; Wang Yanqiao et al.,1985). LMG is less light sensitive compared with HPR-CN or PR-CN. This paper describes the initial investigations of films composed of PVB, LMG and halogenated organic compounds (RX). The effects of some factors such as temperature and relative humidities (r.h) during irradiation or storage on PVG dosifilm were introduced.

EXPERIMENTALS

Different compositions of LMG, RX and polymer base material have been tested. For the development of commercial routine dosimeters, a PVB film with LMG and RX was chosen. The requests for above materials were the solvents with less toxicity on mankind, PVB with high transparent and flexibility and the good compatibility among them.

Two components of dosimeter for different dose ranges were studied:

Components A (A #):	Components B (B #):
--2.5g of PVB	--2.5g of PVB
--0.0827g of RX	--1.5g of RX
--0.0826g of LMG	--0.0165g of LMG
--mixed solvent	--mixed solvent

Films were cast by pouring the above solutions on glass surfaces and till dry. Then the films were stripped off from the plates and stored in the dark. Finally dry films with thickness 70-100 μ m were obtained, from which samples were cut into 1 × 1 cm^2 pieces and put in a brown glass desiccator. These pieces were named as PVG dosifilm.

Absorbance data were measured using HITACHI 200-20 UV spectrophotometer at given wavelengths.The dosifilm thickness was measured using an Elecont micrometer made by Mitutoyo, with a reproducibility of ± 0.2 μm. Irradiations were carried out using a 5.55×10^4 Bq ^{60}Co- γ irradiation facility at Beijing Normal University and the dosifilm was kept in electronic equilibrium during irradiation. Dose was measured by Fricke dosimeter. All the dose values are expressed in terms of dose in water.The absorbed dose rate was 16.2 kGy/h.

After irradiation all the samples were stored in a brown desiccator at room temperature.

RESULTS AND DISCUSSIONS

Absorption Spectrum and Dose Response

Upon irradiation the PVG dosifilm developed into green and showed two absorption maximum at 627 and 425 nm respectively. The absorbance change at 627 nm was more sensitive to dose than that at 425 nm(see Fig. 1). The dosifilm was irradiated within dose range from 0.25 to 90 kGy.

Three parallel samples of PVG dosifilm were irradiated at each given dose and the absorbance values were recorded 24hr after irradiation. The dose response plots were shown in Fig.2, 3.

The linearity of $\Delta A/L$ vs dose was in the range from 0.5 to 80 kGy with good reproducibility in same batches.

The dosifilm A # was used in the following tests. Its absorbance was measured at 627 nm. The stability of dosifilm PVG before and after irradiation during storage at various temperatures (T), relative humidities (r.h) and light conditions were listed. The response of dosifilm irradiated at various T and r.h was studied, too.

Stability After Irradiation

The radiation-induced color (absorbance at 627 nm) on dosifilm developed in the first 24 hours after irradiation, as shown in Fig. 4. The color development tendency depended on the total absorbed dose. The color faded slightly after 24 hours of storage. The radiation responses ($\Delta A/L$, mm^{-1}) 42 days after irradiation decreased about 4% compared with that of 1 day after irradiation.

Light Stability During Storage

Exposed to sunlight, the color of unirradiated PVG dosifilm changed into green (absorbance at 627 nm increased) immediately. If it was exposed to ambient light (i.e, in room) for 48 hours, there was no change in color. After 16 days of exposure, the absorbance of PVG dosifilm increased from about 0.1 to 0.2. However the absorbance of dosifilms kept constant during storage in the dark. (Fig. 5)

Temperatures Effect Before Irradiation

All samples were stored in the dark in this experiment. Fig. 6 showed the change of absorbance vs temperatures. The dosifilm showed no change for two months at storage temperatures lower than 35 ℃. There was no change in the dosifilm stored at 40℃ for 5 days. But when the temperature was as high as 60℃, the absorbance increased about 20% after 24 hours of storage.

Relative Humidity Effect Before Irradiation

PVG dosifilm was not sensitive to relative humidity (r.h) before irradiation except for high r.h (>96.4%). (Fig. 7)

The deviation of absorbance of unirradiated dosifilm is less than ±4% stored a month at r.h <75.7%. The absorbance of samples stored at r.h 96.4% increased with time at the first two weeks ($\Delta A \approx 0.1$).

Temperature Effect During Irradiation

Six sets of dosifilm samples were irradiated by Co-60 γ with dose 16.9 kGy at temperatures (T) of 0, 15, 25, 35, 45 and 50℃, respectively. The relation of $\Delta A/L$ vs T was shown in Fig. 8.

The response upon irradiation increased with the increase of irradiation temperature and the approximate calibration coefficient is +0.053/℃ at the temperature range of 0-50 ℃.

Relative Humidity(r.h) Effect During Irradiation

Fig. 9 showed the relation of Δ A/L vs r.h. The response Δ A/L increased slightly with the increase of r.h during irradiation, and an approximate coefficient of $+0.006/\Delta$ r.h(%) can be used. All of the samples were irradiated 8.84 kGy.

CONCLUSIONS

A new PVG dosifilm has been developed. Its irradiation response (Δ A/L vs dose) showed a good linearity (correlation coefficient $r > 0.999$) within dose range from 0.5 to 80 kGy. PVG dosifilm was low light sensitive and color stable before and after irradiation. The measured doses increased slightly with temperatures and relative humidities during irradiation, the calibration coefficients were introduced. It was suitable to serve as a routine dosifilm for radiation processing dosimetry purpose.

REFERENCES

Dejehet, F. G., F. G. Coget, D. J. Apers and P. C. Carpron. (1972). Radiolytic Oxidation of MG Leuco Base in Acetone solution. *Radiochem. Radioanal. Lett.*, 9(2), 93-103.

Dejehet, F. G., A. G. De Kimpe and D. J. Apers. (1973). Radiation-induced Oxidation of the Malachite Green Leucobase in Acetone Solution in the Presence of Calcium Chloride. *Radiochem. Radioanal. Lett.*, 15(3), 177-86.

McLaughlin, W. L., A. Miller, S. Fidan, K. Pejtersen and W. Batsberg Pedersen. (1977). Radiochromic Plastic Films for Accurate Measurement of Radiation Absorbed Doses and Dose Distributions. *Radiat. Phys. Chem.*, 10, 119-27.

McLaughlin, W. L., J. C. Humphreys, Dene Hocken and W. J. Chappas. (1988). Radiochromic Dosimetry for Validation and Commissioning of Industrial Radiation Processes. *Radiat. Phys. Chem.*, 31, 505-14.

Miller, A. and W. Batsberg Pedersen. (1981). Dose Distribution in Electron Irradiated Plastic Tubing. *Radiat. Phys. Chem.*, 18, 967.

Miller, A., W. Batsberg Pedersen and W. Karman. (1988). A New Radiochromic Thin-film Dosimeter System. *Radiat. Phys. Chem.*, 31(4-6), 491-6.

Stolz, W. and K. Prokert. (1965). Chemishe Dosimetrie Ionisieren der Strahlungen mit den Leukoverbindungen eniger Triphenylmethanfarbstoffe in Polystyrol. *Kernenergie*, 8(7), 425-9.

Wang Yanqiao, Zhou Xiaomin, Tang Zangxiong and Zhang Gongming. (1985). CN 85,104,437.

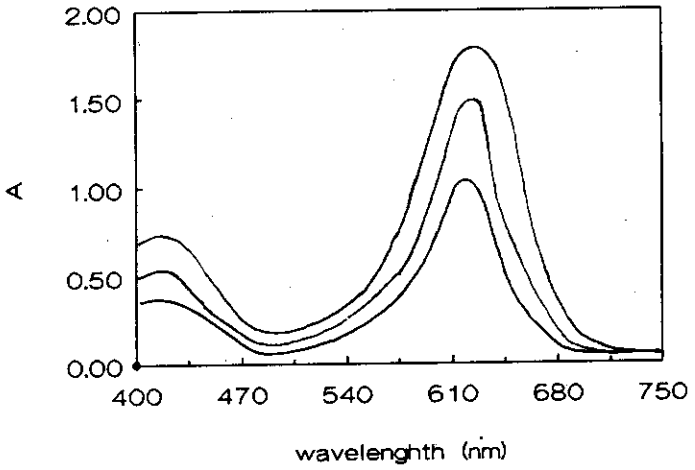


Fig.1 Absorption spectra of the PVG dosifilm, irradiated at a Co-60 source to absorbed doses as indicated.

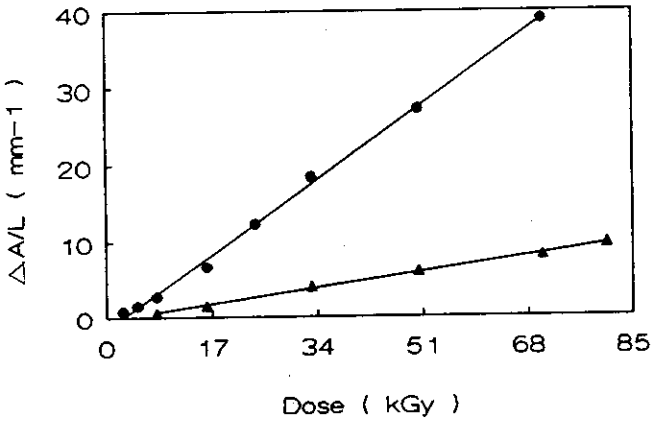


Fig.2 Response functions (Δ A/L, mm^{-1} vs dose, kGy) for A # PVG dosifilm at λ =627 nm (●) and 425 nm (▲).

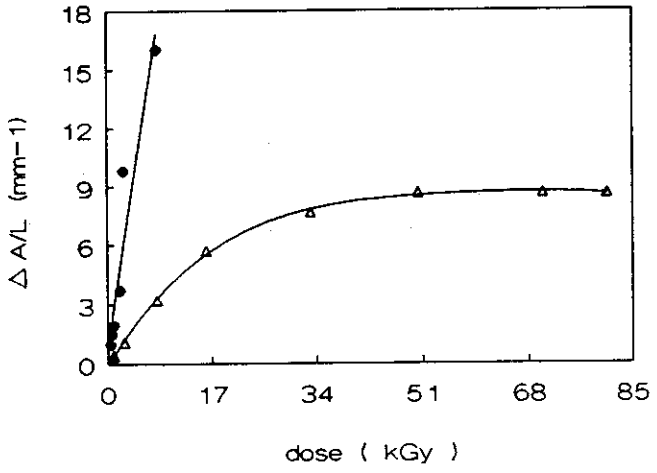


Fig.3 Response functions (Δ A/L, mm^{-1} vs dose, kGy) for B # PVG dosifilm at λ =627nm (●) and 425nm (Δ).

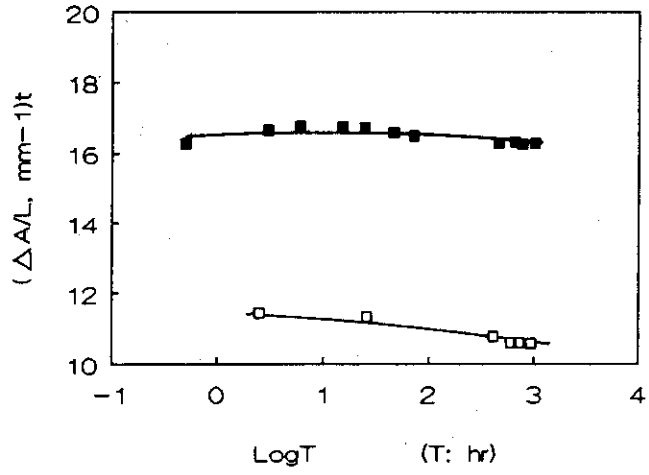


Fig.4 Stability of irradiated A # PVG dosifilm with absorbed dose 21.0 kGy (□) and 31.4 kGy (■).

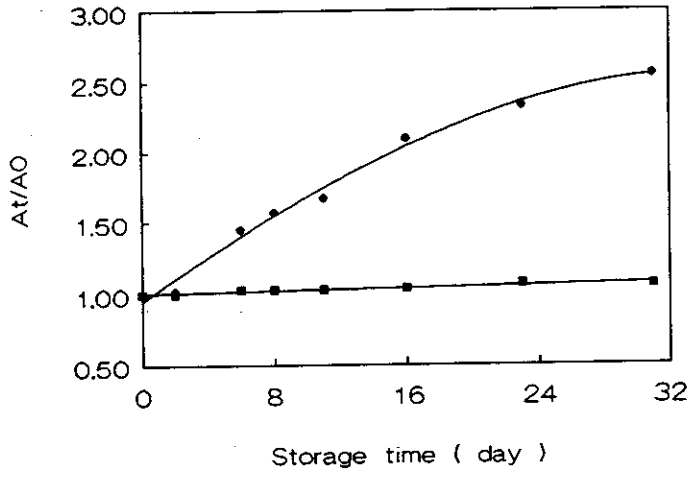


Fig.5 Changes in relative values of absorbance (A_t/A_0, A_t: exposure time t, A_0: exposure time 0) for A # PVG dosifilm exposed to ambient light (●) and stored in darkness (■).

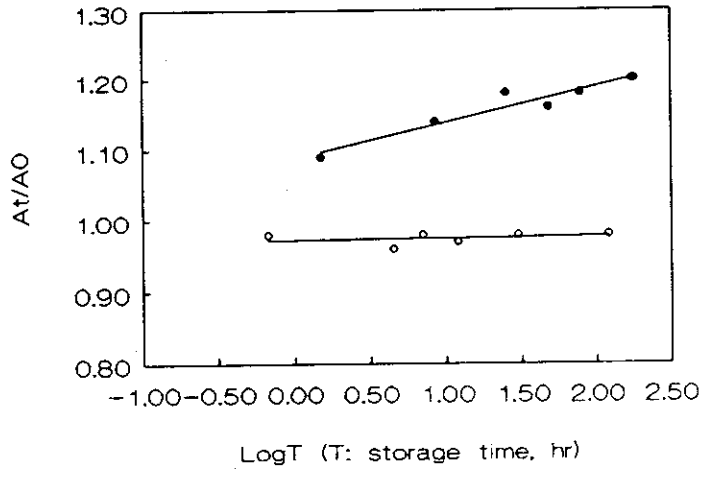


Fig.6 Changes in relative values of absorbance (A_t/A_0) for unirradiated A # PVG dosifilm stored in the dark at 40℃ (○) and 60 ℃ (●).

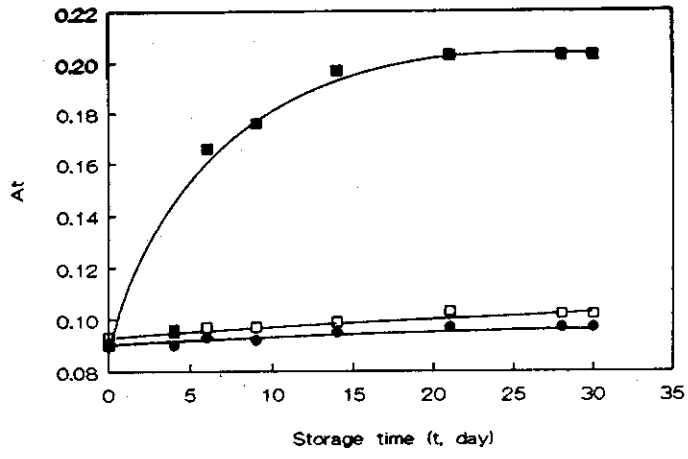


Fig.7 Changes in absorbance (A) for unirradiated A # PVG dosifilm stored in the dark at relative humidity (%) 54.9(●), 75.5 (□) and 96.4 (■).

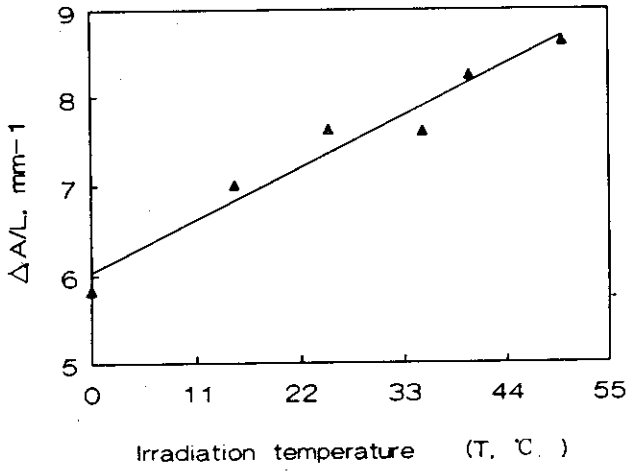


Fig.8 Changes in the response (Δ A/L, mm^{-1}) for A # PVG dosifilm irradiated at different temperatures (T, ℃). (absorbed dose were 16.9 kGy)

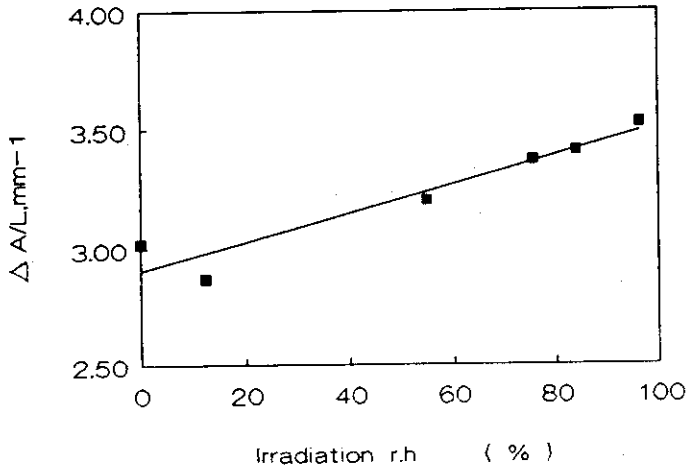


Fig.9 Changes in the response (Δ A/L, mm^{-1}) for A # PVG dosifilm irradiated with 8 .84 kGy at different relative humidites (r.h).

12.11 Radiation Induced Crosslinking of Polytetrafluoroethylene

Akihiro OSHIMA, Yoneho TABATA, Shigetoshi IKEDA*,
Kazushige OTSUHATA*, Hisaaki KUDOH**,
and Tadao SEGUCHI**

Faculty of Engineering, Tokai University, Hiratsuka Kanagawa 259-12 Japan
* RAYTECH CORPORATION, Shinjuku Tokyo 169 Japan
** Japan Atomic Energy Research Institute, Takasaki Radiation
Chemistry Research Establishment, Takasaki Gunma 370-12 Japan

Abstract — The Irradiation temperature effect on polytetrafluoroethylene (PTFE) from room temperature to 380°C was investigated by tensile test and thermal analysis. The behavior of tensile properties and changes of crystallinity on irradiation indicated the formation of a network structure in PTFE by radiation induced crosslinking in inert gas in the molten state just above the melting temperature of PTFE (327°C). The crosslinked PTFE showed a much improved radiation resistance in an atmospheric radiation field.

INTRODUCTION

PTFE has been well recognized as a typical polymer which undergoes chain scission by ionizing irradiation. The mechanical properties decay with a small dose either in air or even under vacuum irradiation(Dole,1973). Therefore, PTFE has limited use as a material in radiation fields such as in a nuclear facility or a space environment.

In recent studies, it was shown that the temperature of irradiation influenced the irradiation effect on polymers. For example, at very low temperature(e.g. 77K) for γ irradiation for PTFE, the probability of chain scission is reduced to 1/5 times, as compared with room temperature irradiation (Kudoh *et al.*,1994).

In the previous studies of irradiation effects on PTFE, some phenomena indicating the possibility of crosslinking were observed. Tutiya (1972) found that abnormal behavior occurred for irradiation around the melting temperature, but concluded it was due to changes in the morphology. Zhang(1988) proposed the possibility of crosslinking of PTFE, and recently the experimental details were disclosed (Sun *et al.*,1994). In Tabata's laboratory at Tokai University, experimental evidence for network formation by radiation crosslinking was observed (Tabata,1992).

In this work, electron beam(EB) irradiation effects on PTFE were investigated for a wide range of irradiation temperatures on the basis of experimental evidence obtained in our laboratory. This paper describes the technique of PTFE crosslinking by EB irradiation, and reports the mechanical and the thermal properties of the crosslinked polymer.

EXPERIMENTAL

Sample; PTFE sheets(Daikin Kogyo Co.Ltd.) with thickness of 0.5mm were used for the

experiments. The molecular weight was about 12 million, which was determined by the heat of crystallization using the differential scanning calorimeter (DSC) measurement technique developed by Suwa *et al.*(1973).

Irradiation; PTFE was set in a vessel with a heating device(Kanazawa *et al.*,1992), and irradiated up to 10kGy-5MGy with a dose rate of 0.5kGy/s using an EB accelerator of 2MeV at various temperatures ranging from room temperature(25°C; RT) to 380°C in an argon gas atmosphere. For assessment of the radiation resistance of the crosslinked PTFE, ^{60}Co-γ irradiation was carried out with a dose rate of 10kGy/h at RT in air.

Measurement; Tensile tests was carried out at RT, and the stress-strain(S-S) relations of the dumbbell (ASTM D-1822L) specimens were obtained with a cross head speed of 200mm/min. The yield strength, tensile strength, elongation at break, and modulus were determined from the S-S relations.

The melting and the crystallization temperatures, and heat of crystallization were measured by DSC under an atmosphere of nitrogen. Both heating and cooling rates in the DSC measurement were 20°C/min.

RESULTS and DISCUSSION

Figure 1 shows the elongation at break and tensile strength against dose for PTFE after EB irradiation to 100kGy at various temperatures in Ar. For the original PTFE, the elongation at break and tensile strength are 400% and 55MPa, respectively. Both elongation at break and tensile strength decreased to a large extent by irradiation at any temperature below the melting point. The both values decrease with increasing temperature until around 325°C, but they change drastically around the melting temperature of 327 °C. The maximum of each peak in Fig.1 was at about 340°C. The elongation at break is rather higher than that of unirradiated PTFE. At temperatures higher than 350°C, both elongation at break and tensile strength decrease sharply, and the mass loss was accelerated with dose, especially, at the surface of the sheets.

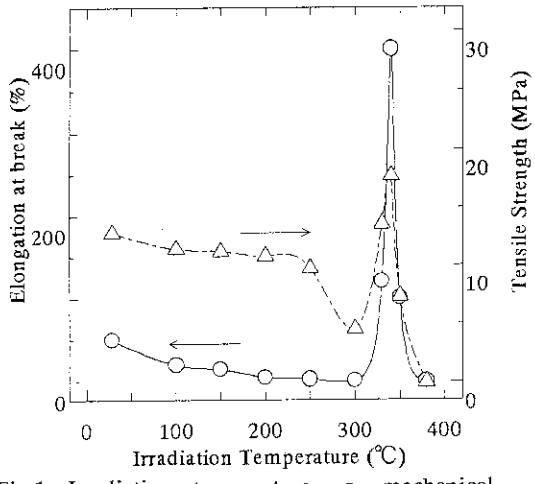


Fig.1 Irradiation temperature vs. mechanical properties for PTFE irradiated by electron beam to 100kGy in Ar gas

The degradation of PTFE is due to chain scission by irradiation, so the experimental results indicate that the probability of chain scission increases with irradiation temperature below the melting temperature. Above 350°C, the chain scission process may be accompanied by thermal depolymerization. At around 340°C, the radiation induced chemical reactions are changed very much, where the chain scission is much reduced or other reactions such as crosslinking may proceed with irradiation.

On the bases of the above experiments, the dose dependency at these temperatures was investigated. Elongation at break against dose is shown in Fig.2, for EB irradiated PTFE up to 5MGy in Ar at RT and 340°C. For the irradiation at RT, the elongation at break and tensile

strength decrease sharply with dose within 50kGy, as has been well known. However, for the irradiation at 340°C the elongation at break remains over 150% at 2MGy irradiation. The tensile strength decreases with dose at small dose up to 100kGy, then tends to increase with dose up to 5MGy.

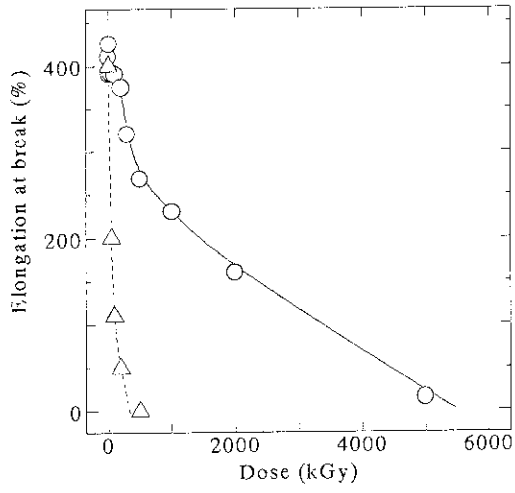


Fig.2 Elongation at break vs. dose for PTFE irradiated by electron beam in Ar gas at 340°C and at RT ; ○: irradiated at 340°C, △:irradiated at RT

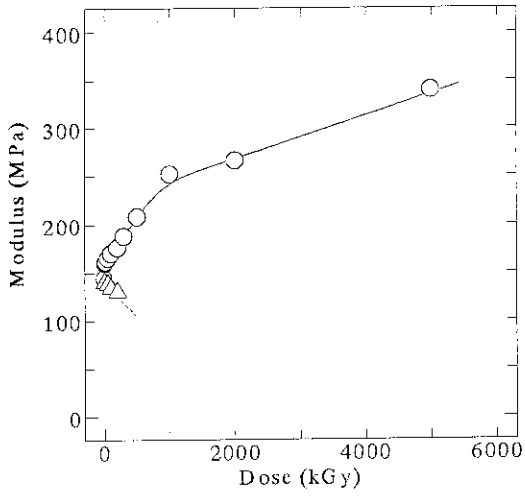


Fig.3 Modulus of PTFE irradiated by electron beam in Ar gas at 340°C and at RT ; ○: irradiated at 340°C, △:irradiated at RT

The yield strength, the stress at the knee point of S-S curve at the strain of about 10%, increases with dose. The modulus, which is determined from the slope of the initial line in the S-S curve increases with dose as shown in Fig.3. These results indicate that the crosslinking takes place preferentially in the molten state and a network structure is formed by the crosslinking.

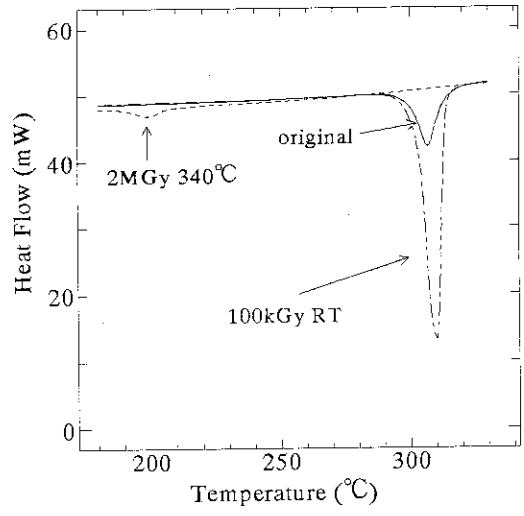


Fig.4 DSC thermograms of crystallization for PTFE irradiated in Ar gas at 340°C and at RT

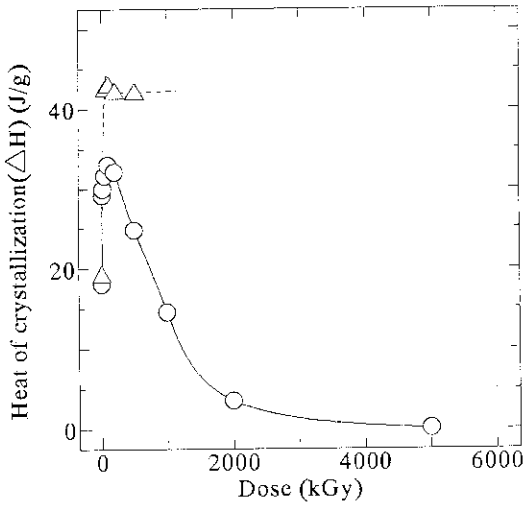


Fig.5 Heat of crystallization(ΔH) for PTFE irradiated in Ar gas at 340°C and at RT ;○: irradiated at 340°C, △:irradiated at RT

Figure 4 shows the DSC thermograms and the crystallization peaks for specimens irradiated

by EB in Ar at 340°C and at RT. The crystallization of unirradiated PTFE begins at 315°C. However, for the irradiation at RT, the temperature of the peak for crystallization is the same as the original sample but the peak intensity increases with dose. In the case of irradiation at 340°C, with increasing dose the crystallization temperature shifts to lower temperatures, and the peak intensity decreases.

The heat of crystallization(ΔH) determined from the peak area in the DSC thermograms is plotted in Fig.5. The ΔH reflects the amount of the crystalline component in PTFE, so the result indicates that the crystallization is much depressed with increase of dose in the molten state. Above 350°C, the crystallinity also decreased with dose. As the properties of the crystalline component decreased with the increase in the network density, the PTFE sheet became transparent and had a rubber like property.

Figure 6 shows the relative elongation against dose for various crosslinked PTFE samples after γ irradiation up to 600kGy in air at RT. The dose for half decay of ultimate elongation for crosslinked PTFE(500kGy) was about 300kGy, while the dose was only 3kGy for the original PTFE. The radiation resistance at RT increases with the crosslinking density. The crosslinked PTFE showed that the radiation resistance in an atmospheric radiation field was very much improved.

It was found that the changes in the tensile properties and the crystallization behavior of PTFE irradiated at around 340°C in the molten state were completely different from the solid state irradiation. The changes and the behavior in the molten state irradiation strongly suggest that the network is formed by radiation induced crosslinking in PTFE. Especially, the increase in the yield strength and in the modulus indicates an increase in the network density in PTFE. Generally, it is accepted that these values increase with increasing crosslinking density for linear polymers.

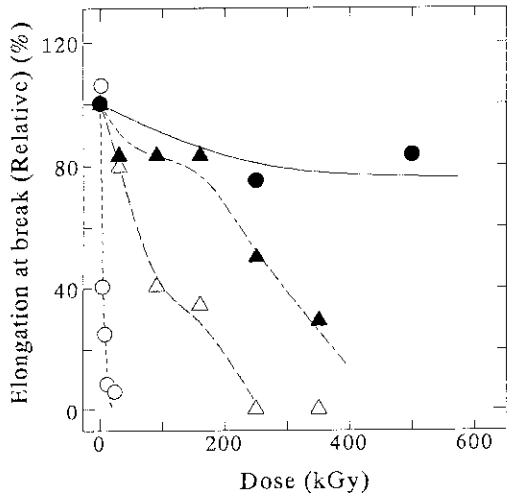


Fig.6 Elongation at break(relative) vs. dose γ-irradiation in air for PTFE crosslinked with various conditions ;○:0kGy at 340°C, △:300kGy at 340°C, ▲:500kGy at 340°C,●: 2MGy at 340°C

The crosslinking between PTFE polymer chains should prevent the crystallization of the chains from the molten state. When the crosslinking density is small, the chains with rather long segments between the crosslinking points may crystallize, but the crystal size becomes smaller with an increase in the crosslinking density. The shift of the crystallization temperature and the decrease in the crystallization enthalpy are well explained by the above model.

Since the PTFE molecule has a helical coil structure in the crystalline state below the melting temperature, the free radicals formed by radiation are restricted in their ability to react with the radicals formed on neighbor molecules by the steric hindrance of the molecular chain. Above the melting temperature molecular mobility would be much improved, and radical could combine more easily with other radicals to form crosslinks.

At temperatures higher than 350°C, the thermal depolymerization of PTFE is accelerated by irradiation, and it may exceed the crosslinking. Then, the mechanical properties decrease greatly

with irradiation dose.

As the radiation resistance of crosslinked PTFE is markedly improved, it is expect to find applications as a material for use in the radiation fields.

CONCLUSION

Main chain scission of PTFE is the predominant reaction on irradiation and tends to increase with irradiation temperature below the melting temperature. On the other hand, network formation proceeds on by irradiation in the molten state just above 340°C. At higher temperature than 350°C, the depolymerization proceeds because of the combined effects of thermal stress and radiation. By network formation through the crosslinking of PTFE, the crystallinity was decreased and the mechanical properties, such as yield strength and modulus, were improved. As the crystalline component decreases with crosslinking density, the crosslinked PTFE will become transparent. The radiation resistance of PTFE is improved significantly by the crosslinking.

REFERENCES

Dole M.(1973), Chap.9, pp.167-178 in "The radiation chemistry of Macromolecules vol. II " Edited by Dole M., Academic Press.

Kanazawa T., Haruyama Y. and Yotsumoto K.(1992) , Report of Japan Atomic Energy Research Institute, JAERI-M 92-062.

Kudoh H., Kasai N., Sasuga T. and Seguchi T., Radiat.Phys.Chem.,Vol.43 ,1994,pp.329-334,

Sun J., Zhang Y., Zhong X., Zhu X., Radiat.Phys.Chem.,Vol.44 ,1994,pp.655-659,

Suwa T., Takehisa M. and Machi S.(1973) J.Appl.Polym.Sci.,Vol17,3253.

Tabata Y.(1992) Proceedings of "Solid State Reactions in Radiation Chemistry" in The Taniguchi Conference, pp.118-120, June 22-26,1992, Sapporo, Japan.

Tutiya M. (1972) Japanese J.Appl.Phys., Vol.11, 1542.

Zhang Y. Private Communication, (1988) IAEA Workshop

12.12 Kinetic Behavior of Nitric Oxide in Biological System Studied by Pulse Radiolysis

M. Miki, K. Kobayashi, and S. Tagawa

The Institute of Scientific and Industrial Research, Osaka University, Mihogaoka 8-1, Ibaraki, Osaka 567, Japan

Abstract With pulse radiolysis technique, nitric oxide (NO) can be produced by the reaction of hydrated electron with NO_2^-. This is verified by the formation of the NO complex of ferrous myoglobin after pulse radiolysis of the ferric form in the presence of NO_2^- under deaerated condition. By the use of this technique, the reaction of superoxide anion (O_2^-) with NO was followed directly in oxygen saturated solution containing NO_2^-. It was found that O_2^- reacted with NO with a second-order rate constant of 3.8×10^9 M^{-1} s^{-1} at pH 7.5 to form peroxynitrite ($ONOO^-$) with an absorption maximum around 300 nm. Peroxynitrite thus formed decomposed with a first-order rate constant 0.8 s^{-1} at pH 7.5. The reactivity of peroxynitrite against various biological molecules was also studied. Peroxynitrite was found to react with NADH and GSH with second-order rate constants of 4×10^3 $M^{-1}s^{-1}$ and 6.5×10^2 $M^{-1}s^{-1}$ at pH 7.4, respectively, but did not react with either ascorbate or hydroquinone. These results suggest that peroxynitrite does not act a strong oxidant.

INTRODUCTION

Nitric oxide (NO) has been shown to be produced by many mammalian cell types and to be involved in a variety of important cellular process (Moncada, et al. 1991). The reaction between NO and superoxide anion (O_2^-) in Reaction 1 has received considerable attention, since activated macrophages and neurophils are capable of production and release of these two radical species simultaneously. It has been demonstrated that peroxynitrite ($ONOO^-$), which is formed by Reaction 1, has a potent oxidant in macrophage-induced cytotoxicity against bacteria (Ischiropoulos, et al. 1992).

$$NO + O_2^- \longrightarrow ONOO^- \qquad (1)$$

In other tissues, potentially toxic levels of peroxynitrite can be achieved, when NO and O_2^- productions are stimulated. However, there is no direct evidence of the occurrence of Reaction 1 in biological systems.

Many reports suggest that the product of Reaction 1, peroxynitrite ($ONOO^-$), or its proposed decomposition products are strongly oxidizing species. It is shown that peroxynitrite mediates oxidation of both sulfhydryls of nonprotein and protein (Radi, et al. 1991), and initiates lipid peroxidation (Hogg, et al. 1991), and DNA cleavage (King et al. 1992). In contrast to these studies, it has been proposed that NO can act as a free radical scavenger of O_2^- (Rubanyi, et al. 1991). Furthermore, Wink et al. (1993) reported that the cytotoxic effects in Chinese hamster cells resulting from O_2^- or H_2O_2 are protected by NO. To solve the controversy, it is necessary to investigate the reactivity of peroxynitrite toward various biological molecules in a simple system.

By pulse radiolysis technique of aqueous solution of NO_2^-, it is possible to produce NO to follow reactions of NO spectrophotometrically. The present paper describes the formation and decay process of peroxynitrite by the use of pulse radiolysis.

EXPERIMENTAL

Pulse radiolysis experiments were performed with an electron linear accelerator in the Institute of Scientific and Industrial Research Osaka University (Kobayashi, et al. 1991; Kobayashi, et al. 1989). The pulse width and energy were 8 ns and 27 MeV, respectively. The dose was in the range of 100-15 Gy.

A sample of ferric myoglobin (Mb) for pulse radiolysis was prepared as follows. A solution of 8 μM ferric Mb in 5 mM phophate buffer at pH 7.5, 1mM $NaNO_2$, and 0.1 M *tert*-butyl alcohol (scavenging OH radical) was deoxygenated by repeated evacuation and flushing with argon. To study the reaction of O_2^-, a sample of 1-5 mM $NaNO_2$ in 5 mM phosphate buffer (pH 5-8), or 10 mM borate buffer (pH 8-10), and 0.1 M sodium formate, or 0.1 M *tert*-butyl alcohol (scavenging OH radical) was saturated with oxygen by bubbling with oxygen gas.

RESULTS and DISCUSSION

We followed the time course of optical absorption changes after pulse radiolysis of ferric Mb in the presence of NO_2^- under the deaerated condition. A faster and a slower absorption changes, due to the reaction of hydrated electron (e_{aq}^-) with ferric Mb (Reaction 2) and the ligand binding process of NO to ferrous Mb, (Reaction 3) were observed after the pulse.

$$Fe^{3+} + e_{aq}^- \longrightarrow Fe^{2+} \quad (2)$$

$$Fe^{2+} + NO \longrightarrow Fe^{2+}\text{-}NO \quad (3)$$

It is, therefore, concluded that NO is formed in the reaction of e_{aq}^- with NO_2^-, as shown in Reaction 4.

$$NO_2^- + e_{aq}^- \longrightarrow NO_2^{2-} \xrightarrow[H^+]{} NO + OH^- \quad (4)$$

By the use of this technique, the reaction of O_2^- with NO was followed in oxygen saturated solution containing 5 mM NO_2^-. The absorption at 280 nm increased rapidly and then increased slowly, whereas only slow absorption change was observed at 320 nm. The difference spectrum between 400 ns and 50 μs has an absorption maximum at 300 nm is similar to that of peroxynitrite ($ONOO^-$) reported (Blough and Zafiriou, 1984). Therefore, it is concluded that the pulse radiolysis used here has permitted a direct demonstration of the reaction between O_2^- and NO in Reaction 1.

For determination of the rate constant in Reaction 1, the dependence of the apparent first order rate constant in the concentration of O_2^- was examined under the condition of $[O_2^-] >> [NO]$. The second-order rate constant in Reaction 1 is calculated to be 3.8×10^9 $M^{-1}s^{-1}$ at pH 7.5. The value is two-orders magnitude greater than that reported before (3.7×10^7 $M^{-1}s^{-1}$) (Saran et al. 1990), but simialr to that determined by flash photolysis (6.7 x 109 M-1s-1) (Huie and Padmaja, 1993). The discrepancy between our results and the study of Saran et al. (1990) is considered to arise from the experimental condition. They followed the time course of absorption changes of aerobic solution containing NO. Under their conditions, the formation of NO^- due to the reaction of e_{aq}^- with NO and the subsequent reactions occur to form various species such as $N_2O_2^-$, and therefore it is difficult to determine the rate constant of Reaction 1. In our experimental conditions, on the other hand, NO and O_2^- can be produced concomitantly after the pulse. In addition, we can avoid the reaction of NO and O_2^- prior to the pulse.

The formation of $ONOO^-$ was found to be inhibited upon the addition of superoxide dismutase (SOD). In the presence of 50 μM SOD, the absorption at 320 nm remained unchanged, whereas a rapid increase of the absorption at 300 nm was not affected. Half-maximal inhibition was observed was observed at 15 μM SOD, when the concentration of O_2^- and NO generated are approximately 50 μM and 10 μM, respectively. This suggests that a 5-10 μM level of SOD in tissue would not effectively prevent Reaction , if sufficient NO is released from cells.

The peroxynitrite thus formed was found to decay with a first-order rate constant of 0.8 s^{-1} at pH 7.5. The values increased with a decrease in the pH range from 8.5 to 5.5. Above pH 11, peroxynitrite was very stable and could be kept for 5 min without changes in the absorption spectrum.

The absorption changes at 320 nm after the pulse were noticeably decrease with a decrease in pH, though the rates of the formation of peroxynitrite were not affected by pH. This result cannot be explained in terms of pH-dependent formation of NO by the pulse, since a similar result was obtained by the stopped-flow method. The pK value of this transition is found to be approximately 6.8. The effect of pH can be explained by the fact that the spectrum of peroxynitrite acid (ONOOH) has a much lower extinction coefficient than that of peroxynitrite ($ONOO^-$) with a pK value of 6.8, as shown in Reaction 5.

$$ONOO^- + H^+ \rightleftharpoons ONOOH \qquad (5)$$

The pK value in the transition is in good agreement with that determined based on the rate of peroxynitrite decomposition (Koppenol, et al. 1992).

On pulse radiolysis of an O_2-saturated solution containing 5 mM $NaNO_2$, 100-400 μM NADH, and 0.1 M *tert*-butyl alcohol, at pH 7.4, resulting absorbance at 320 nm decreased after the decay of peroxynitrite. The result was tentatively ascribed to reaction as Reaction 6.

$$ONOO^- + NADH \xrightarrow[H^+]{} NO_2^- + NAD^+ + H_2O \qquad (6)$$

This reaction proceeds nearly quantitatively, suggesting that peroxynitrite acts as an effective two-electron oxidant in the reaction. The second-order rate constant for the reaction of peroxynitrite with NADH is calculated to be 4 x 10^3 M^{-1} s^{-1} at pH 7.4. The rate constant decreased with the increase of pH, giving a pK value of 6.8.

The reactions of sulfhydryl compounds such as cysteine and GSH with peroxynitrite were performed. The rate of decay of peroxynitrite followed at 300 nm increased with the increase of the concentrations of cysteine and GSH. The rate constants of the reaction of peroxynitrite with cysteine and GSH are 2.6 x 10^3 $M^{-1}s^{-1}$ and 6.5 x 10^2 $M^{-1}s^{-1}$ at pH 7.4, respectively. On the other hand, we could not detect the reactions of peroxynitrite with ascorbate, hydroquinone, trolax, tyosine, and ferric hemoproteins such as met Mb and horseradish peroxidase. The rate in the decay of peroxynitrite were not affected upon the addition of these compounds.

In the present experiments we have not obtained the data showing that peroxynitrite is a strongly oxidizing species. Even in the oxidation of NADH or sulfhydryl compounds, the rate constants are much smaller than those of other radicals such as thiyl radical (Forni & Wilson, 1986). These results suggest that peroxynitrite does not act as a strong oxidant, and are conflict those obtained by using peroxynitrite prepared in the quenched flow reactor (Beckmann, et al. 1991; Radi, et al. 1991). It may be simply due to technical problem relating to the purity of peroxynitrite. Rather, NO is converted into peroxynitrite unreactive to various components of cells by the reaction between NO and O_2^-. Therefore, present findings are in accordance with the proposal that NO can function as a chemical barrier to cytotoxic free radical.

REFERENCES

Beckman, J. S., Beckman, T. W., Chen, J., Masshall, P. A., and Freeman, B. A. (1990) Proc. Natl. Acad. Sci. U. S. A. 87, 1620-1624

Blough, N. V. and Zafiriou, O. C. (1984) Inorg. Chem. 24, 3504-3505

Forni, L. G. and Wilson,R. L. (1986) Biochem. J. 240, 897-903

Hogg, N., Darley-Usmar, U. M., Wilson, M. T., and Moncada, S. (1993) Biochem. Soc. Trans. 21, 358-362

Huie, R. E. and Padmaja, S. (1993) Free Radical Res. Commun 18, 195-199

Ischiropoulos, H., Zhu, L., and Beckman, L. S. (1992) Arch. Biochem. Biophys. 298, 446-451

King, P. A., Andeson, V. E., Edwards, J. O., Gustafso, G., Plumb, R. C., and Suggs, J. W. (1992) J. Am. Chem. Soc. 114, 5340-5342

Kobayashi, K., Harada, Y., and Hayashi, K. (1991) Biochemistry 30, 8310-8315

Kobayashi, K., Hayashi, K., and Sono, M. (1989) J. Biol. Chem. 264, 15280-15283

Koppenol, W. H. , Moreno, J. J., Pryor, W. A., Ischiropoulos, H., and Beckman, J. S. (1992) Chem. Res. Toxicol. 5, 834-842

Moncada, S., Palmer, R. M. J., and Higg, E. A. (1991) Pharmacol. Rev. 43, 109-142

Radi, R., Beckman, J. S., Bush, K. M., and Freeman, B. A. (1991) J. Biol. Chem. 266, 4224-4250

Rubanyi, G. M., Ho, E. H., Cantor, E. H., Lumma, W. C., and Botrlho, H. P. (1991) Biochem. Biophys. Res. Commun. 181, 1392-1397

Saran. M., Michel, C., and Bors, W. (1990) Free Radical Res. Commun. 10, 221-226

Wink, I. A., Hanbauer, I., Krishna, M. C., DeGraff, W., Gamson, J., and Mitchele, J. B. (1993) Proc. Natl. Acad. Sci. U. S. A. 90, 9813-9817

12.13 Radicals of Some Aminoacids and Their Derivatives at 77K Produced by Synchrotron Radiation in Vacuum Ultraviolet Range Ⅱ. N-acetyl-DL-alanine

Atsuko Minegishi, Junkichi Sohma, and Kiminori Ushida*

Research Institute for Integrated Sciences, Kanagawa University, 2946 Tsuchiya, Hiratsuka, Kanagawa 259-12 Japan, and * The Institute of Physical and Chemical Research, 2-1 Hirosawa, Wako, Saitama 351-01 Japan.

ABSTRACT

Two radicals were confirmed from the ESR spectra of N-Acetyl-DL-alanine ($CH_3CONHCHCH_3COOH$) irradiated at 77K with 155 and 160nm SR light (near the ionization threshold). One of them is identified as decarboxyl radical ($CH_3CONHCHCH_3$). The other is identical with the radical formed on SR-irradiation with 235nm light and at 77K which identified as ($CHCH_3COOH$). We discuss the role of superexcited states that are able to form these two radicals.

INTRODUCTION

N-acetylamino acid is one of the simplest molecules containing biologically important peptide linkages, -CO-NH- . The effects of ionizing radiation on these simple peptides have been examined with electron spin resonance(ESR) technique. In the case of of X- or γ -irradiated N-acetylglycine and N-acetylalanine, observed radicals were the stable radicals at room temperature and their ionic precursor radicals. [1-7]

Recently by HPLC, we have investigated the final products of N-acetylglycine and N-acetyl-D, L-alanine γ -irradiated at 77K and at room temperature, and found the two types of final products with different dependence on irradiation temperature. [8,9,10] The first type of products exhibits remarkable dependence on irradiation temperatures, and their yield were remarkably lower at 77K than at room temperature. This results should be based on the tunneling charge recombination of anion and cation radicals during irradiation for their lifetime should be quite long at low temperatures.

The yield of the second type of produts were independent on irradiation temperatures and they should be generated by the neutral fragmentation via super excited states formed in the sample during the ionizing irradiation as pointed out by Platzman. [11]

Hatano and his group have been researching intensively on superexcitation of simple polyatomic moecules. According to Hatano[12], with photo-energy near ionization threshold, the probability of the neutral fragmentation via superexcited states is higher than that for the ionization and becomes almost 100%.

Hatano's experimental results described above prompted us to carry out irradiation with synctrotron radiation(abbr. SR) in the vacuum ultraviolet region (115nm-160nm) near the ionization threshold on N-acetylglycine and N-acetyl-D, L-alanine. The same product of the second type was obtained for N-acetylglycine and for N-acetyl-D, L-alanine, respectively (Minegishi [9,10], and the product of N-acetyl-D, L-alanine showed maximum yield at 235nm[13].

Now, we have condensed our interest to find precurser radicals from neutral fragmentation via superexcited states, and planned to construct SR-ESR Dewar vessel for the irradiation 77K with SR-light near ionization threshold and measuring the ESR at 77K.

EXPERIMENTAL

1) SR-ESR Dewar

A Dewar vessel(named as SR-ESR Dewar) was designed for SR-irradiation with VUV light and sequencial off-line ESR measurement in X-band, avoiding unfavorable elevation of the temperature. Both SR-irradiation and ESR measurement were performed at 77K. Saturated aqueous solution of samples was spread on a plate of fused silica (0.5mm x 5mm x 30mm) and dried completely. The sample plate was attached to the sample holder at the bottom of the liquid nitrogen trap, kept in the vacuum (10^{-6} Torr) and cooled down to 77K by heat conduction.

The irradiation was performed at Beam Line 5 of SOR ring (0.4 GeV) at the Institute for Solid State Physics, the University of Tokyo. During SR-irradiation, SR-spot (5mm x 5mm) was moved to several positions on the sample plate by using an up-and-down adjusting mechanism of SR-ESR Dewar.

2) Materials and Condition of SR-irradiation

N-Acetyl-DL-alanine ($CH_3CONHCHCH_3COOH$) was SR-irradiated at 77K. SR-irradiation was performed at 155, 160 and 235nm and their total fluences were 10^{16}-10^{17} photon/(sample plate).

The SR-irradiated specimens were carried from the institute for Solid State Physics to Kanagawa University or the Institute of Physics and Chemical

Research by automobile and then, ESR measurement was performed. Therefore more than 4 hours passed during irradiation and transportation.

RESULTS and DISCUSSION

The ESR spectrum at 77K of N-acetyl-D, L-alanine, which irradiated with 160nm SR-light at 77K, was observed with magnetic field modulation width of 0.1mT and microwave power of 1mW. The spectrum is shown in Fig. 1 which is named as 160nm-ESR in this article. Total intensity of Fig. 1 decreased gradually and the shape was changed close to the six-line pattern, which is similar to that obtained at room temperature for N-acetyl-D, L-alanine after γ-irradiation at room temperature in vacuum, as shown in Fig. 2 (named as six-line ESR). Broadness and slight changing of 160nm-ESR suggest the excistence of superimposed signals due to some other radicals.

With 235nm-SR light, another pattern of ESR spectrum was obtained as shown in Fig. 3 (named as 235nm-ESR). As is shown in Fig, 4 we could satisfactorily reproduce the 160nm-ESR spectrum as a sum of a six-line ESR and 235nm-ESR. The six-line ESR, observed for N-acetyl-D, L-alanine γ-irradiated at room temperature was first studied by Katayama[1], who attributed it to the back-bone radical ($CH_3CONHCCH_3COOH$). Saxebøl[3] suggested the six-line ESR could be explained by the excistence of ether the decarboxyl radical ($CH_3CONHCHCH_3$) or the deamination radical ($CHCH_3COOH$). Authors[6], however, identified the six-line ESR to decarboxyl radical ($CH_3CONHCHCH_3$) by spin-trapping technique using t-nitrosobutane (tNB, 2-methyl-2-nitrosopropane), since obtained spin-adduct was CH_3-COND-$CHCH_3$-(NO-tBu). A simulation spectrum for (CH_3-CONH-$CHCH_3$) almost agreed with the six-line ESR, with an assumption of hfs(N)=1.0mT, hfs(H)=2.0mT, hfs(each H of $-CH_3$)=1.7mT, hfs(H of-N)=0.15mT, and unpaired electron localized on C, eventhough without anisotropies.

The 235nm-ESR is resemble to the five-line ESR spectrum of L- and DL-alanine powder γ-irradiated and measured at room temperature (Fig. 5, named as five-line ESR) which was previously identified as deaminated radical ($CHCH_3COOH$, or $CHCH_3COO^-$) by Miyagawa and Gordy[14]. However, there is still some ambiguity with this identification because of the broadness of signals. The radical in 235nm-ESR may be produced by the excitation of forbidden $n-\pi^*$ transition of -NH- or -CO- in a -CO-NH- bond, and be formed by neutral fragmentation via π^* state. The absorption spectrum of aqueous N-acetyl-D, L-alanine rises sharply from 245nm to the VUV region and the peak of this $n-\pi^*$ transition are not

distinguished due to overlapping with this high absorption. Since 235nm-ESR seems to be involved in 160nm-ESR spctrum, however, some radicals are formed via this π^* state generated from higher excited valence states.

The radical for six-line ESR which was found as the main radical in N-acetyl -D, L-(and L-) alanine by γ-irradiation at room temperature, seems to come from ion radicals which were found clearly at 77K. We could not find any signals from ion radicals in 160nm-ESR (77K) but could have seen them on γ-radiolysis at 77K.

Therefore we conclude that the radical for six-line ESR found on 160nm-SR irradiation should be from the neutral fragmentation via superexcited state, not through ionizing processes.

CONCLUSION

1) The radical formed after 235nm SR-irradiation at 77K is also found in the 160nm and 155nm SR-irradiated spectra at 77K. This radical seems to be formed from the $n-\pi^*$ transition at 235nm. The formation in the range near ionization threshold should be from neutral fragmentation via highly excited valence states related to the $n-\pi^*$ transition.

2) The main radical produced by 155 and 160nm SR irradiation at 77K coincides with the radical ($CH_3CONHCHCH_3$) formed by γ-irradiation at room temperatures. No ion-radicals were observed in 150nm, 160nm and 235nm ESR at 77K. From these results, it is concluded that the radical ($CH_3CONHCHCH_3$) is formed through superexcited state like as Rydberg states, and not through ionization process.

REFERENCES

1) Katayama, M. (1962) J. Molec. Spectroscopy 9, 429-435.
2) Saxebøl, G. (1973) Int. J. Radiat. Biol. 24, 475.
3) Saxebøl, G. (1975) Int. J. Radiat. Biol. 27, 293.
4) Saxebøl, G., Melo, T. B., and Henriksen, T. (1973)Radiat. Res. 55, 356.
5) Sinclair, J., and Codella, P. (1973)J. Chem. Phys. 59, 1569.
6) Minegishi, A., Bergene, R., and Riesz, P. (1980) Int. J. Radia. Biol. 38, 627.
7) Box, H. C., Budzinski, E. E., and Lilga, K. T. (1970)J. Chem. Phys. 57, 4295.
8) Minegishi, A., Minami, K., Matsuyama, H., Watanabe, M., and Kinjo, Y. (1990)Bull. Tokyo Metropolitan Isotope Research Center 7, 119.
9) Minegishi, A., Matsuyama, H., Saito, H., Azumi, A., and Hieda, K. (1990)Activity Report of Synchrotron Radiation Laboratory The University of Tokyo 1990. 47.
10) Minegishi, A., Minami, K., Matsuyama, H., Saito, H., Azumi, A., Hirono, T., Takakudra, K., and Hieda, K. (1990)Activity Report of Synchrotron Radiation Laboratory, The University of Tokyo, 1990, 50.
11) Platzman, R. L., (1962) Radiat. Res. 17, 419.
12) Hatano, Y. (1988)Radiochimica Acta 43, 119.
13) Minegishi, A. to be published.
14) Miyagawa, I. and Gordy, W. (1960)J. Chem. Phys. 32, 255.

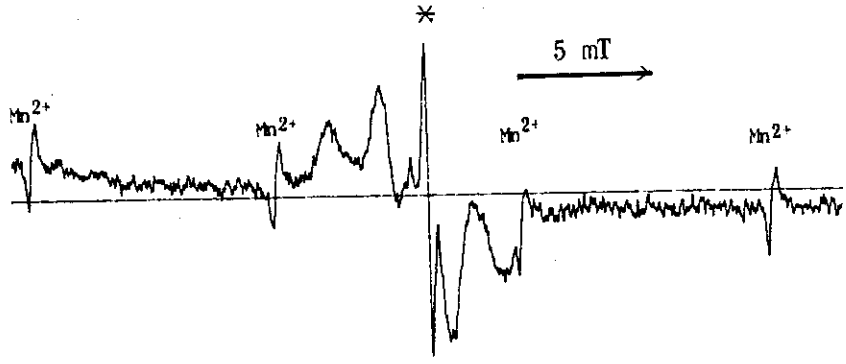


Fig. 1. ESR spectrum at 77K of N-acetyl-D, L-alanine irradiated with 160nm synchrotron radiation at 77K. (named as 160nm-ESR).
* signal of irradiated fused-silica plate

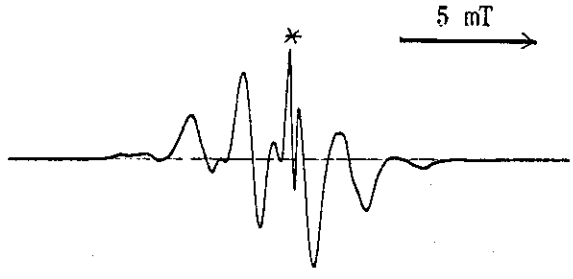


Fig. 2. ESR spectrum measured at room temperature of N-acetyl-D, L-alanine γ-irradiated in a vacuum at room temperature. (named as six-line ESR).
* signal of fused-silica plate.

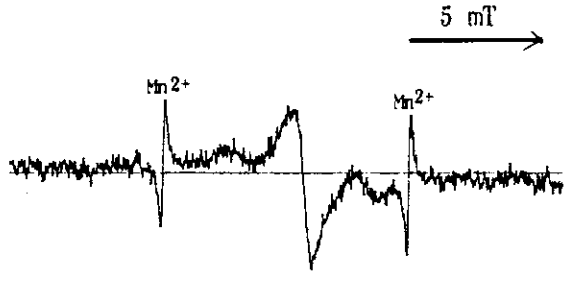


Fig. 3. ESR spectrum at 77K of N-acetyl-D, L-alanine irradiated with 235nm synchrotron radiation at 77K. (named as 235nm-ESR).

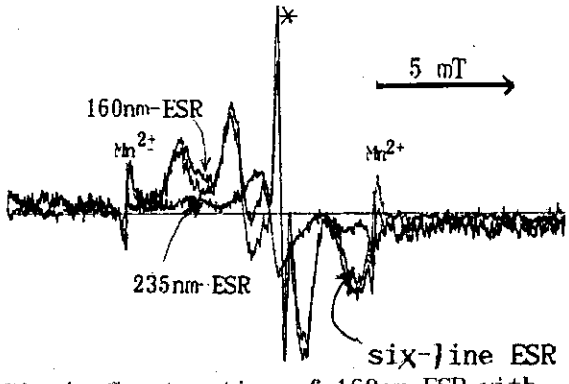


Fig. 4. Construction of 160nm-ESR with two components, six-line ESR(Fig. 2) and 235nm-ESR.
* signal of fused-silica plate.

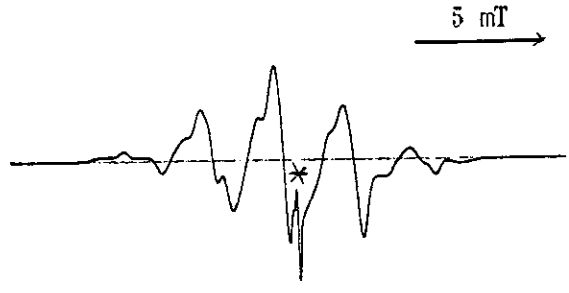


Fig. 5. ESR spectrum of L-alanine γ-irradiated and measured at room temperature. (named as five-line ESR)
* signal of fused-silica plate.

12.14 Protecting Effect on Gamma-ray Damage of DNA by Tea Catechin

H. Yoshioka, G. Akai, H.Yoshioka*, K. Yoshinaga**, K. Hasegawa

Radiochemistry, Research Lab., Faculty of the Science, Shizuoka University, Ooya 836,Shizuoka 422, Japan,
*Division of Environmental Health Science, University of Shizuoka, 395 Yada, Shizuoka 422, Japan,
**Department of Chemistry, Faculty of the Science, Shizuoka University, Ooya 836, Shizuoka 422, Japan

Abstract

The protecting effect of the tea catechin on the radiation induced scission of DNA *in vitro*. was examined. In addition, ESR spin-trapping method was used to make clear the mechanism of the protection.

INTRODUCTION

Recently, it has been shown *in vivo* and *in vitro* [1), 2)] that tea catechin suppress mutation and carcinogenesis. Main components of the catechin is (-)-epigallocatechin gallate(EGCg). The content of EGCg exceeds 50% of the total catechin and show in many cases the strongest activity of the suppression on the mutation and the carcinogenesis. However, the mechanism is not sufficiently clarified. It is well known that carcinogenesis, mutation and aging include the chemical process of DNA scission and the DNA scission is induced by radiation as well as chemical carcinogenesis. Therefore, we examined quantitatively the protecting effect of the tea percolate and EGCg on the radiation induced scission of DNA *in vitro*. In addition, we tried to make clear the mechanism of the protection using ESR spin-trapping method.

EXPERIMENTAL

Preparation of the Samples and the Reagent: Plasmid pUC18 DNA was prepared from *E.coli by a* conventional method. EGCg(WAKO, guaranteed reagent) was dissolved into SSC buffer solution(0.15M NaCl, 0.015M Na-citrate, pH7) to be $1x10^{-1}$ M just before the experiment, then diluted to the required concentration. Specially purified spin trapping agent, 5,5-dimethyl-1-pyrroline N-oxide (DMPO), was obtained from

LABOTEC Co. Ltd. All other reagents used are guaranteed reagents.

Apparatus: Gamma irradiation was carried out with ^{60}Co source at Shizuoka University. Radiation doses at various points from the source were measured by Fricke dosimeter. Mini-gel electrophoresis system (Mupid, ADVANE Co. Ltd.) and densitometer (Atto-DCD-16) were used. ESR spectra were measured by JEOL RE3X spectrometer (X-band) with 100 kHz field modulation.

Procedure: (1) 4 μl of SSC buffer solutions of DNA (0.019 μg/ μl) were placed in micro-tubes. (2) To them, 6 μl of tea percolate or SSC buffer solutions containing various amounts of EGCg were added. (3)Those samples were irradiated with ^{60}Co source for 2h. (4) After finishing irradiation, DNA was separated to each forms explained later by electrophoresis. (5)Each bands stained by etidium bromide were photographed. (6)Degree of the darkening of the bands on the film were measured by a densitometer and the integrated area were calculated with a computer. (7) Survival percentage of CCC form DNA used as a index of the protecting effect was calculated with the following equation.

$$\text{Survival } (\%) = \frac{1.42 \times [\text{CCC}]}{1.42 \times [\text{CCC}] + [\text{OC}] + [\text{L}]} \times 100$$

Here, L means linear form DNA formed by the double strand scission, but it was not detected in this experiment. The values in the brackets mean the degree of darkening and the factor, 1.42, is a correction coefficient for CCC form.

Spin trapping experiments were carried out as follows. (1)75 μl of aqueous $FeCl_2$ solutions were placed in a number of micro-tubes, then 15 μl of DMPO were added. (2)Next, 35 μl of water or SSC buffer or 35 μl of the solutions containing the protecting agents were added and vortexed for mixing. (3)75 μl of H_2O_2 solutions(1×10^{-3} M) were added and mixed quickly. Time was measured from the mixing. (4)The mixtures were sucked into capillary glass tubes (Drummond 75 μl micropipette, 0.8 mm i.d.) and the one end of the tubes was sealed with teflon tubes and ERS spectra were measured.

RESULTS AND DISCUSION

Protection by Tea Percolate Fig. 1 shows the protecting effect of green tea percolate. The photograph is the electrophoresis pattern showing native covalently closed circular (CCC) and open circular (OC) form DNA. Sample 5 is the control, which was non-irradiated, not containing tea percolate, contains only CCC form. As shown in the sample 4, CCC form DNA was decomposed perfectly into OC form under this irradiation condition. However, CCC form still remains in the samples 1 ~ 3 and the survival ratios depend on the quantities of the tea percolate. In the samples containing the same amounts of tea percolate as samples 1 ~ 4 and having been stood for 2 h without irradiation, DNA scission was not observed, showing that tea percolate really protected irradiation-induced scission. The survival (%) were tabulated in Table 1.

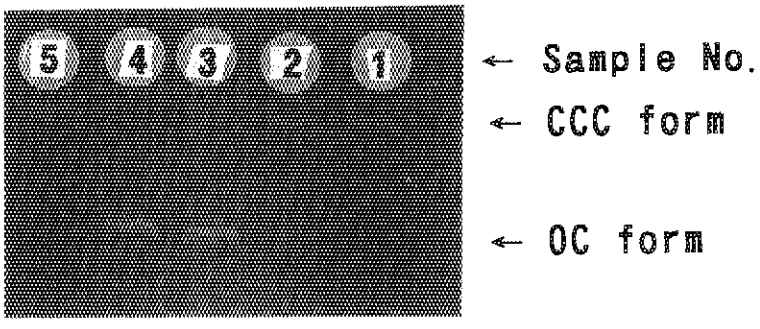


Fig. 1 Electrophoresis pattern of γ -ray irradiated DNA.

Table 1 Protecting effect of green tea percolate on DNA scission by γ ray

Sample No	Relative cocentration of tea percolate *	CCC DNA survival (%)
1	1.00	95.3 (irrad.)
2	0.1	77.0 (irrad.)
3	0.01	45.2 (irrad.)
4	0	0 .0 (irrad.)
5 (control)	0	100 .0 (not irrad.)

Green tea (4g) was percolated with hot water (75 °C, 50 ml, 3 min). Sample 1 is the original percolated solution, and 2 and 3 are diluted 10 and 100 times of the original.

Protection by EGCg. Fig. 2 shows the protecting effect of EGCg and the dependency on the EGCg concentration and the radiation dose. The protecting effect increased with

increase in the EGCg concentration. But, DNA scission increased with increase in the radiation dose in all the samples containing different amounts of EGCg.

Duration of the Protecting Effect of EGCg. EGCg is susceptible to the autoxidation even at the room temperature and browning is observed while it is stood as aqueous solutions for a few days. Therefore, it is a problem whether the protecting effect is kept while standing. To ascertain it, we compared the protecting effect of a freshly prepared EGCg solution and the solution stood for a day at room temperature. Difference was not observed between them, showing that the effect was kept at least for a day.

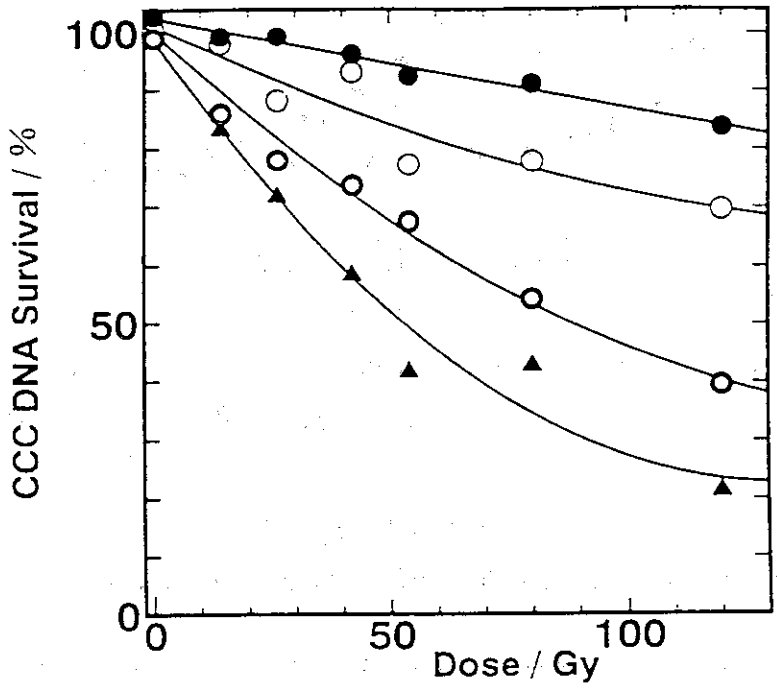


Fig. 2 Dependence of CCC Survival on the radiation dose under various concentrations of EGCg. (DNA) : 0.019 μg／μl, Irradiation time : 2h
▲ 0 M, ◎ 3×10^{-4} M, ○ 1×10^{-3} M, ● 3×10^{-3} M

Spin Trapping Experiment. It is generally accepted that the radiation-induced scission of DNA is caused mainly by OH radical formed from water molecule. For example, t-butanol known as a scavenger of OH radical suppressed DNA scission. Therefore, it is reasonable to consider that the protecting effect of EGCg is attributed to the scavenging effect of OH radical. We examined the OH radical scavenging activity of EGCg. Here, OH radical was generated by Fenton reaction and was trapped with

DMPO. Fig. 3 shows the results, where the intensity of the spin adduct, DMPO-OH, was decreased when EGCg was coexistent, suggesting that EGCg acts as the scavenger.

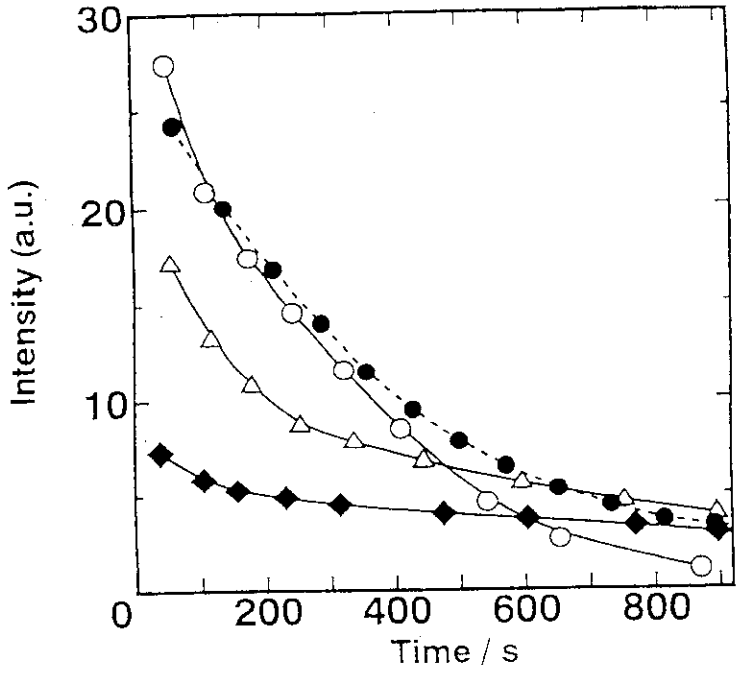


Fig. 3 ESR intensity of DMPO-OH under various EGCg concentrations
○ 1×10^{-4} M, △ 1×10^{-3} M, ◆ 1×10^{-2} M, ● 0 M

CONCLUSIONS

1) Tea percolate and the main ingredient EGCg suppress the radiation-induced scission of DNA.
2) Spin-trapping method showed that EGCg acted possibly as a OH radical scavenger.
3) Protecting effect of EGCg on the radiation-induced scission of DNA is attributable to the OH radical scavenging activity.

REFERENCES

1) S. Taniguchi, H. Fujiki, H. Kobayashi, H. Go, K. Miyado, H. Sadano, et al.,(1992). Cancer Letters, 65, 51-54, Effec of (-)-epigallocatechin gallate, the main constituent of green tea, on lung metastasis with mouse B16 melanoma cell lines.
2) Zhi Yuan Wang, Jun-Yan Hong, Mou-Tuan Huang, Kenneth R.Reuhl,Allan H.Conney, and Chung S.Yang (1992) CANCER RESEARCH 52, Inhibition of N-Nitrosodiethylamine-and 4-(Methylnitrosoamino)-1-(3-pyridyl)-1-butanone -induced Tumorigenesis in A/J Mice by Green Tea and BlackTea.

12.15 γ-radiation Induced Polymerization of Unsaturated Liposomes Containing Unsaturated Lipid, Cholesterol, and Saturated Aliphatic Acid

F.Hosoi[1], H.Omichi[1], K.Akama[2], S.Tokuyama[2], and Y. Nakano[2]

[1]Takasaki Radiation Chemistry Research Establishment,JAERI
1233 Watanuki-machi, Takasaki, Gunma 370-12, Japan
[2]Tsukuba Research Laboratory, NOF Corporation
5-10 Tokodai, Tsukuba, Ibaragi 300-26, Japan

Abstract γ-Radiation induced polymerization of mixed-lipid liposomes consist of 1,2-bis[(2E, 4E)-2,4-octadecadienoyl]-*sn* - glycero-3-phosphocholine(DODPC), diparmitoyl phosphatidyl choline(DPPC), cholesterol(CHol), and stearic acid(SA) was studied from the point of view the kinetics and mean molecular area on the water surface. All the polymerization was carried out at temperature of 4°C. The polymer yield and molecular weight of soluble polymer increased when compared with those of poly-DODPC liposomes. The overall rate of polymerization increased linearly with decreasing the molar fraction of DODPC in the membrane. The mean molecular area on the water surface of mixtures DODPC with DPPC, CHol, and SA gave the ideal line indicating immiscibility.

INTRODUCTION

Biological membranes consist of phospholipids, proteins, cholesterol, and other compounds. When phospholipid contact with water, its assembly makes spherical particles consist of bimolecular membrane containing aqueous cores called liposomes[1]. The liposomes have a same characteristic as that of natural biocell membranes. One of the disadvantage of liposomes is their short life time and low stability for the physical stimuli such as out side pressure. It is necessary to improve these properties for utilize the liposomes as a functional material.

The stable liposomes that are more suited as cell membrane can be prepared by introducing polymerizable groups such as diene or diacetylene in a acyl chain of phospholipid[2]. The polymerization of liposomes can be initiated by various means such as organic initiators[3], UV[4], and γ-irradiation[5]. In particular, γ-irradiation method is much suitable for this purpose because the polymerization can be initiated without any initiator. However, there are few reports that have discussed on the reaction mechanism from the standpoint of the correlation for the polymer yield and the molecular weight to obtain useful information concerning the property of final products. In previous report, we studied the polymerization of 1,2-bis[(2E,4E)-2,4-octadeca-dienoyl]-sn-glycero-3-phosphocholine (DODPC) as liposomes using γ-ray and found that respective acyl chains polymerize selectively at a hydrophilic or hydrophobic region in bilayer[6].

The present investigation was under taken to determine the mixing effect of saturated phospholipid, cholesterol, and saturated aliphatic acid onto the polymerization of DODPC liposomes in connection with a kinetic treatment and the occupied area of mixed-lipid on the water surface.

EXPERIMENTAL

Mixed-lipids were prepared by mixing 1,2-bis[(2E,4E)-2,4-octadecadienoyl]-sn-glycero -3-

phosphocholine(DODPC) with L-α-dipalmitoyl phosphatidyl choline(DPPC), cholesterol(CHol), and stearic acid(SA) in benzene solution. A freeze-dried powder of mixed lipid was suspended in distilled water. The suspension was extruded through the filters to adjust the vesicle size to ca. 200nm. The average diameters of the liposomes were 200±10nm.

The mixed-lipid suspension sealed in a glass tube after bubbling with Ar gas through the solution. The polymerization of liposomes by γ-radiation was carried out using ^{60}Co at dose rate 1.65 - 10kGy/h at a temperature of 4°C. The polymerization yield was estimated from measuring the decrease in UV absorption intensity at 255nm due to the diene chromophores. The degree of polymerization was determined by the molecular weight of poly-2,4-octadecadienoic acid that derived from the hydrolysis of irradiated liposomes using gel permeation chromatography (GPC).

RESULTS AND DISCUSSION

Polymerization There was no marked difference in vesicle size distribution in liposomes before and after irradiation. The phosphatidyl choline group that linked to glycerol by ester-bonding act as surface active agent in the water. This fact shows that the ionic end of phospholipid is stable for γ-irradiation. The polymer yield versus time curves for various compositions of the liposomes is shown in Fig.1 and 2. The polymer yield increased with increasing the irradiation time and once gets saturated at near 50%, and then increased gradually following further irradiation. This fact shows that the reactivity of two unsaturated acyl groups is different from each other and the polymerization of unsaturated groups of 1 or 2 acyl chains is carried out selectivity in a different area (step[1] or [2]) due to two acyl chains of phospholipid are located with different distance from the water-fatty acid interface as described in previous paper. Furthermore, the polymer yield for mixed-lipid liposomes at a certain time increased significantly when compared with that of DODPC liposomes though the DODPC concentration in the bimolecular membrane decreased with mixing DPPC and others to DODPC. These phenomena could be observed clearly at DPPC/DODPC ratio over 3/7 as shown in Fig.2.

Fig.3 shows that the number average molecular weight ($\overline{Mn}$) of soluble polymer obtained by hydrolysis of irradiated mixed- lipid

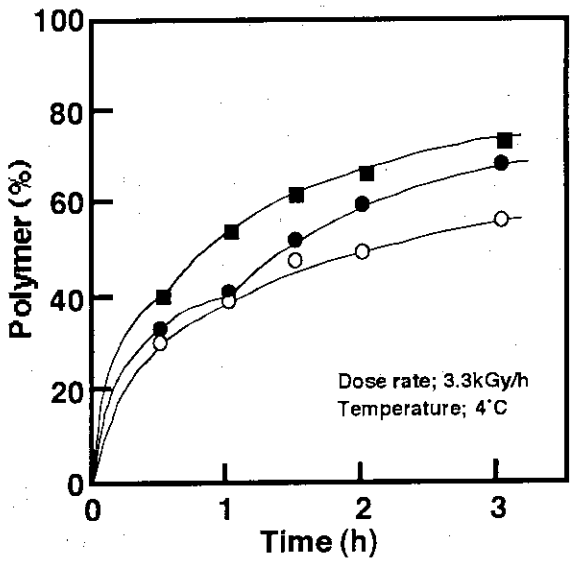


Fig.1 γ-Ray induced polymerization of unsaturated liposomes consisit of various compositions: ■ (DODPC/DPPC)/ CHol/SA=(3.5/3.5)7/2; ● DODPC/DPPC = 5:5 ; and ○ DODPC.

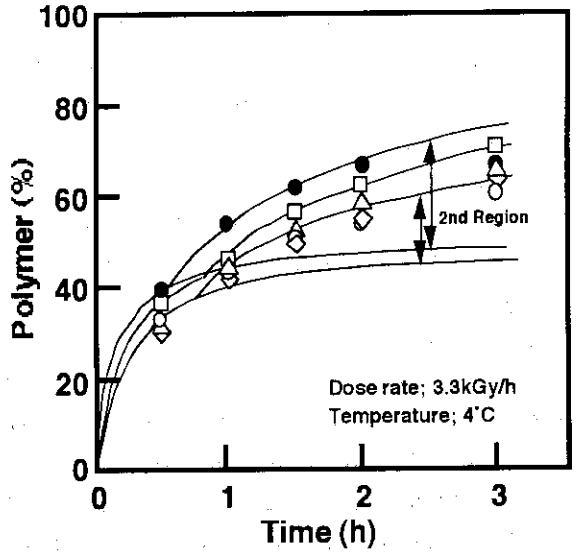


Fig.2 γ-Ray Induced polymerization of unsaturated liposomes consist of mixed-lipid liposomes: mixing ratio of (DODPC/DPPC)/ CHol/SA=7/7/2: mixing ratio of DODPC/DPPC, ○ 10/0; ◇ 9/1 △ 8/2; □ 7/3; ● 5/5.

liposomes consists of DPPC/DODPC ratio 0/10 or 5/5 decreases with increasing the irradiation time and is ranging in about 14500 to 6130. Where the molecular weight of 2,4-octadecadienoic acid converted to that of poly-styrene is 557. This result indicates that the polymerization degree of DODPC is the range of about 26 to 11. These values may be rather low when compared those with that of polymers obtained by polymerization of general monomers. $\overline{Mn}$ decreased with increasing the irradiation time and $\overline{Mn}$ for DPPC/DODPC ratio 5/5 obtained at a certain time is increased significantly when compared with that of soluble polymer obtained for DPPC/DODPC ratio 0/10.

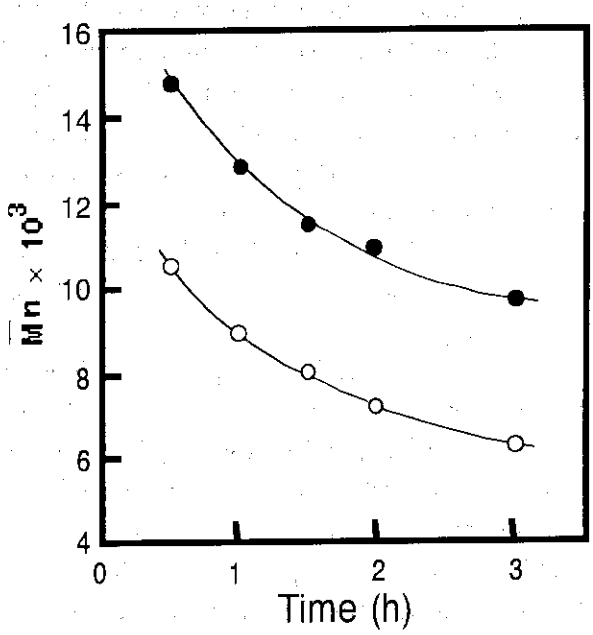


Fig.3 Number average molecular weight of soluble polymer obtained for mixing ratio (DODPC/DPPC)/CHol/SA= 7/7/2; mixing ratio of DODPC with DPPC,○ 10/0 ; ○ 5/5.

Kinetic treatment In previous report, we described the polymerization of DODPC liposomes was classified as stationary state polymerization with slow initiation from the facts that the rate of polymerization was proportional linearly to the dose rate and the degree of polymerization decreased with increasing the irradiation time though the initiation reaction took place continuously in the course of polymerization. Since the similar kinetic features to the polymerization of DODPC liposomes were observed in the polymerization of mixed-lipid liposomes consist of DODPC, DPPC, CHol, and SA, the reaction mechanism in eqs.(1)-(6) is also assumed for this polymerization.

Initiation

$$H_2O \xrightarrow{Irrad} H\bullet + \bullet OH \qquad Rd=k_{di}\cdot\rho H_2O\cdot I \qquad (1)$$

$$H\bullet + \bullet OH \xrightarrow{kdi} H_2O \qquad Rdt=kdt[H\cdot][\cdot OH] \qquad (2)$$

$$\bullet OH + M \xrightarrow{ki} R1\bullet + H_2O \qquad Ri=k_i[\bullet OH][M] \qquad (3)$$

Propagation

$$R1\bullet + M \xrightarrow{kp} R2\bullet$$

$$Rn\bullet + M \xrightarrow{kp} Rn+1\bullet \qquad Rp=k_p[Rn\bullet][M] \qquad (4)$$

Termination

$$Rn\bullet + Z \xrightarrow{kt} Pn \qquad Rt=k_t[Rn\bullet][Z] \qquad (5)$$

Transfer

$$Rn\bullet + M \xrightarrow{ktr} Pn + R\bullet \qquad Rtr=k_{tr}[Rn\bullet][M] \qquad (6)$$

Where M, $R1\cdot$, $Rn\cdot$,and Z are monomer, monomeric radical, growing radical, and the substance by

which R_n is deactivated, respectively: R_d, R_{dt}, R_i, R_p, R_t, and R_{tr} denote the rate of radical formation from the water, its back reaction, initiation of polymerization, propagation, termination, and chain transfer with rate constant k_{di}, k_{dt}, k_i, k_p, k_t and k_{tr} respectively. because the amount of hydroxyl radical is much larger than that of monomeric liposomes. It is not so difficult to assume that the concentration of hydroxyl radical is as equilibrium between the two reactions (1) and (2). Then the concentration of hydroxyl radical is expressed as follows;

$$[\bullet OH] = k_{di}\cdot\rho H_2O\cdot I/k_{dt}[H\bullet] = KI \quad \text{where, } K=k_{di}\cdot\rho H_2O/k_{dt} \qquad (7)$$

Since the rate of polymerization is proportional linearly to the dose rate, the overall rate of polymerization **R** is expressed as follows;

$$R = -d[M]/dt = k_p\cdot k_i\cdot KI[M]^2/k_t[Z] \qquad (8)$$

The integration of equation(8) from time 0 to t is given by following equation;

$$1/[M]_t = (k_p\cdot k_i\cdot KI/k_t[Z])\cdot t + 1/[M]_0 \qquad (9)$$

If it is possible to treat [Z]=constant, the plot of $1/[M]_t$ against the irradiation time gives a straight line with an intercept on the y ordinate 1. According to the result of polymerization shown in Fig.2, the equation (9) was applied to region I and II separately as the same as polymerization of liposomes consist of DODPC. Fig.4 shows that the plot of $1/[M]_t$ against the time for region I gives straight lines with an intercept on the y ordinate 1 under all compositions. A similar result obtained for region II though the straight line did not start from t=0. It corresponds to the time that start the polymerization in region II. These results indicate that equation(9) is reasonable and the polymerization of mixed-lipid liposomes is carried out with the same mechanism as DODPC liposomes.

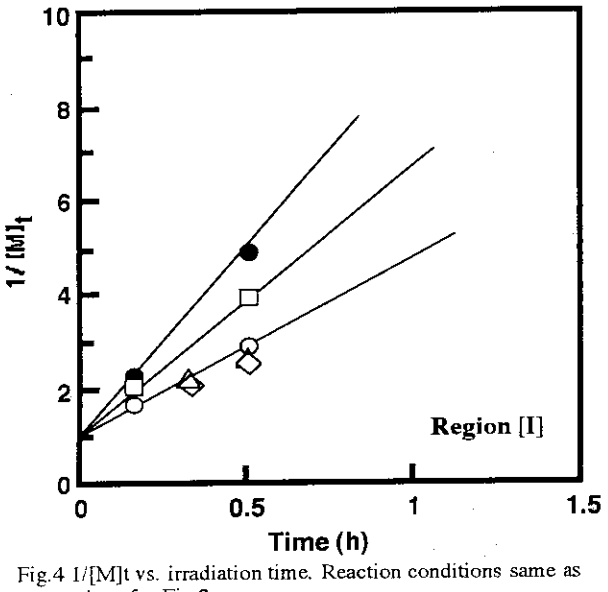


Fig.4 1/[M]t vs. irradiation time. Reaction conditions same as given for Fig.2.

Fig.5 is the plot of the slope obtained Fig.4 against the molar fraction of DODPC in the mixed-lipid membrane. The overall rate constant presented by $k_p\cdot k_i\cdot KI/k_t[Z]$ increases linearly with decreasing the molar fraction of DODPC. A similar result was obtained for region II. Since the concentration of hydroxyl radical which contribute to the initiation of polymerization can be treated as a constant regardless of liposomes composition because the amount of water is excessive when compared with that of monomers and the polymerization of DODPC is classified as a steady state polymerization, the value of $k_i\cdot k_p\cdot KI/$

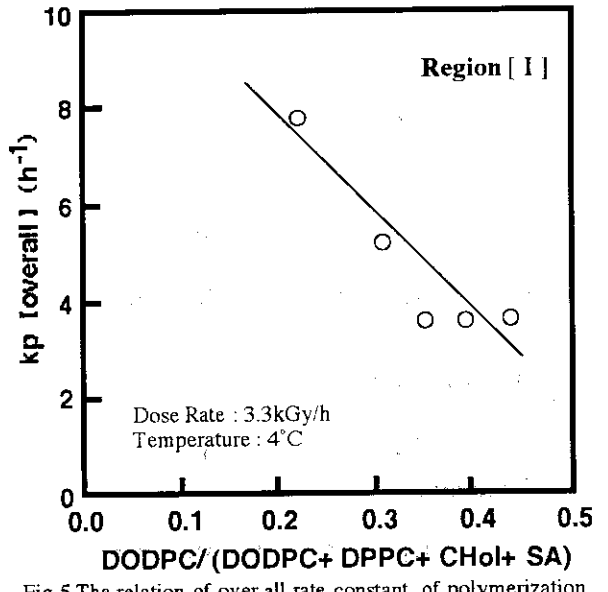


Fig.5 The relation of over all rate constant of polymerization to the molar fraction of DODPC in the mixed-lipid membrane.

$k_t[Z]$ is expected as a constant for the all of mixed-lipid composition, if DODPC is miscible with DPPC, CHol, and SA completely. From these results, it is concluded that DODPC is immiscible with DPPC, CHol, and SA, and each component forms its own domain. These results could be derived easily from the p-A plot on the water surface, considering the two dimensional phase rules of Defay-Crisp. In Fig.6 the mean molecular area is plotted against the monolayer composition of DODPC and CHol, which demonstrates that the measured data fit with the ideal line indicating immiscibility. The same results obtained for mixtures DODPC with DPPC, and SA. Ringsdorf et al. reported that no polymer formed when the miscible unpolymerizable component exceeds 75% in the mixed-membrane, since the all of polymerizable lipid are only surrounded by unpolymerizable molecule. On the basis of these results, it can be concluded that each component forms its own domain.

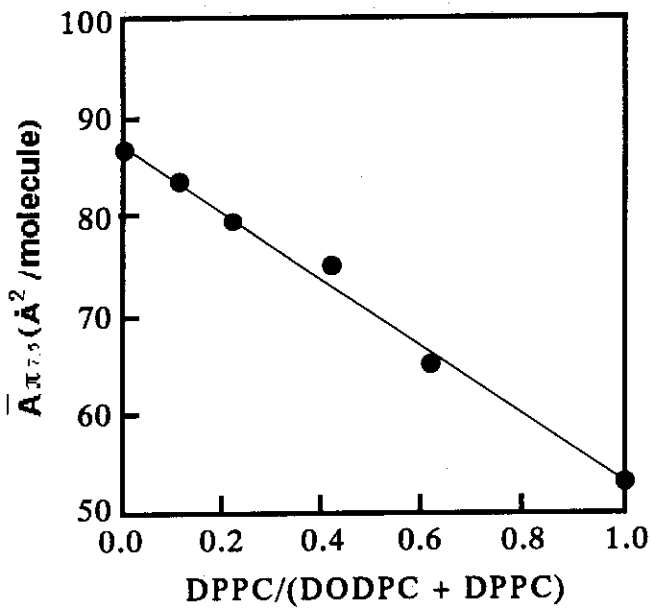


Fig.6 Mean molecular area as a function of the composition DODPC with DPPC at a surface pressure of mN/m.

CONCLUSION

Two acyl chains of DODPC in the mixed-lipid liposomes polymerized independently from each other as the same as DODPC liposomes due to two acyl chains located in different distance from the water-lipid interface. The both of polymer yield and molecular weight of polymer at a certain time increased significantly when compared with those of DODPC. From the results of kinetic treatment and mean molecular area of mixtures, it can be concluded that DODPC immiscible with DPPC, CHol, and SA, and the polymerization of DODPC in the mixed membrane is enhanced by the interaction between the hydrophobic chains of DODPC and that of the components, in which the ordering of unsaturated acyl chains of DODPC is promoted to form the polymer easily.

REFERECES

[1] A.D.Bangham, M.M.Standish, and J.C.Watkins, J. Mol. Biol., 13(1965)238.
[2] A.Akimoto, K.Dorn, L.Gros, H.Ringsdorf, and H.Schupp, Angew. Chem.,93(1981)108.
[3] P.Tundo, D.Kippenberger, and J.H.Fendler, J. Am. Chem. Soc., 104(1982)456.
[4] H.Ohno, Y.Ogata, and E.Tsuchida, Macromolecules, 20(1987)929.
[5] E.Tsuchida, E.Hasegawa, N.Kimura, M.Hatashita, and C.Makino, Macromolecules, 25 (1992)207.
[6] F.Hosoi, H.Omichi, K.Akama, and S.Tokuyama, 35th Symposium on Radiation Chemistry, (1993)189.
[7] T.Kagiya, M.Izu, S.Machi, and K.Fukui, Bull. Chem. Soc. Japan, 40(1967)1049.
[8] H.Ringsdorf, and H.Schupp, J. Am. Soc., Org. Coat. Plast. Chem., Pap.,42(1980)379.
[9] B.Huper, H.Ringsdorf, and H.Schupp, Macromol. Chem., 182(1981)247.

12.16 Microemulsion Polymerization of Butyl Acrylate Irradiated by γ-ray

Zhicheng ZHANG, Xiangling XU, Lei SHI and Manwei ZHANG

Department of Applied Chemistry, University of Science and Technology of China, Heifei 230026, China

ABSTRACT Radiation polymerization of butyl acrylate was carried out in microemulsion with high monomer and low emulsifier content. The rate of polymerization shows three intervals--the increasing period, the plateau period and the decreasing period for most cases. The length of nucleation period is independent of monomer content and temperature, and becomes longer with the increase of dose rate and the decrease of emulsifier content. The length of Rp plateau region increases with the increase of monomer and emulsifier content and with the decrease of dose rate. By studying the kinetics, the following formula were derived: $R_p \propto [M]^{0.93} D^{1.27} [E]^{-1.07}$; $M_n \propto [M]^{0.65} D^{0.28} [E]^{-1.66}$.

INTRODUCTION

Microemulsion polymerization has been investigated quite extensively since the first report in 1980 (Stoffer and Bone, 1980) . Many researchers got the spherical and monodisperse latex particles by the polymerization of styrene (St) and methyl methacrylate (MMA) in o/w microemulsion with sodium dodecyl sulfate (SDS) as the emulsifier and pentanol as the coemulsifier (Tang, et al, 1984; Holdsroft, et al, 1990; Johnson, et al, 1984). It was found that there are two intervals of polymerization , which related to particle nucleation and growth respectively. Recently, long alkyl chain cationic emulsifiers such as dodecyltrimethylammonium bromide (DTAB) and cetyltrimethylammonium chloride (CTAC) were used as emulsifier without coemulsifier in microemulsion polymerization of St (Antoniett, et al, 1991; Gan, et al, 1993; Puig, et al, 1993). It was found that a new period with constant polymerization rate appearred at a lower initiator concentration or a lower temperature.

In the microemulsion polymerization systems cited above, the ratio of monomer-to-emulsifier was less than 0.6 and the concentration of emulsifier usually larger than 10wt%. In this paper butyl acrylate (BA) was polymerized in a microemulsion when monomer-to-emulsifier ratio is about 2.5 and BA content about 30wt%, the kinetics and mechanism of BA microemulsion were aslo discussed.

EXPERIMENTAL

Materials

BA from Dongfang Chemical Factory was distilled at 10mmHg to remove inhibitor. 12-butinoyloxy-9-octadecenoic acid (BOA) was synthesized by direct esterfication of butanoic acid with 12-oxy-9-octadecenoic acid (OOA) with H_2SO_4 as catalyst.

Polymerization

Dilatometric method was used to study the kinetics of microemulsion

polymerization. The microemulsion was first degassed at about 10 mmHg for two times and then fed directly into the dilatometer specially made for radiation polymerization. The polymer conversion was calculated from the volume change of liquid in the capillary. The resulted microemulsion remains stable and reddish.

Molecular weight determination

The polymerized microemulsion latices were precipitated in a large quantity of methanol. The polymer was dissolved in acetone, and then precipitated with water to remove emulsifier completely. The molecular weight was measured with Ubbelode capillary viscometer: $[\eta]=6.85\times10^{-3}[Mn]^{0.75}$ (ml/g).

RESULT AND DISCUSSION

Effect of BA concentration

Microemulsion polymerization rates at different content of BA are depicted in Fig. 1. The overall polymerization rate (Rp) increases with the increase of monomer concentration. There are three intervals observed. In interval I, the rate increases with the increase of the number of

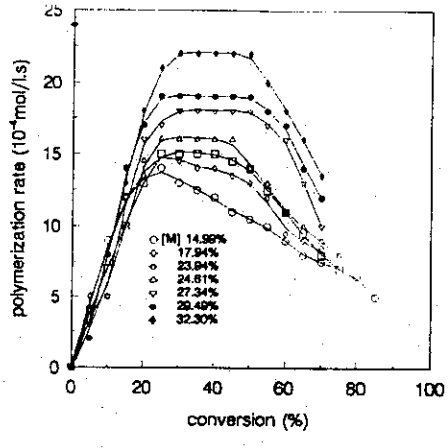


Fig.1 The rate of microemulsion polymerization vs conversion at different monomer content. [E], 10.1wt%; PH=7.5; Dose rate, 46.42Gy/min; T=311K

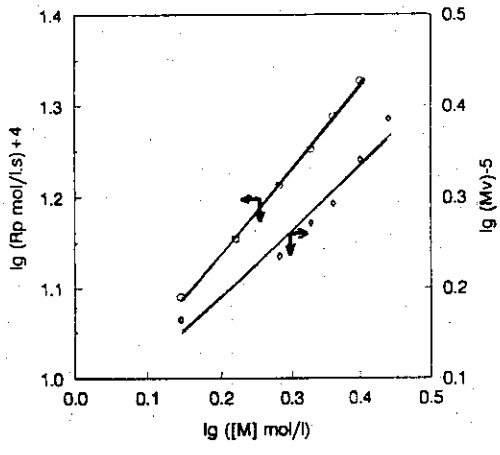


Fig.2 The effect of monomer concentration on Rp and Mn at the same condition listed in Fig.1

polymerization loci, which are continuously nucleated by the free radical (H, OH) flux generated by γ ray. The length of interval I seems to be independent of monomer concentration. In interval II, the Rp plateau region is due to a constant supply of monomer from the uninitiated microemulsion droplets to the initiated ones. In this circumstance, the uninitiated microemulsion droplets serve as monomer reservoirs, just like monomer droplets in emulsion polymerization. The length of plateau depends on the monomer concentration and increases with the increase of monomer concentration. When the BA concentration is lower than 20 wt%, the plateau disappeared completely. The decrease of Rp in interval III is caused by the diminishing of BA concentration in growing particles.

It is found that Rp is 0.93 order with respect to BA concentration and polymer molecular weight (Mn) is 0.65 order as shown in Fig. 2. It is conjectured that the increase of Rp and Mn is due to the high rate of monomer

diffusing into the polymerization loci at the higher monomer content.

Effect of emulsifier

Fig. 3 shows that with the increase of emulsifier concentration [E] from 10 to 15 wt%, the polymer conversion at which the polymerization rate plateau appears changes from 15% to 40% and the length of plateau is shortened. The dependence of Rp and Mn on emulsifier concentration are -1.07 and -1.66 power respectively (Fig. 4). It also do not conform to the Smith-Ewart theory which predicts 0.6 power for both Rp and Mn.

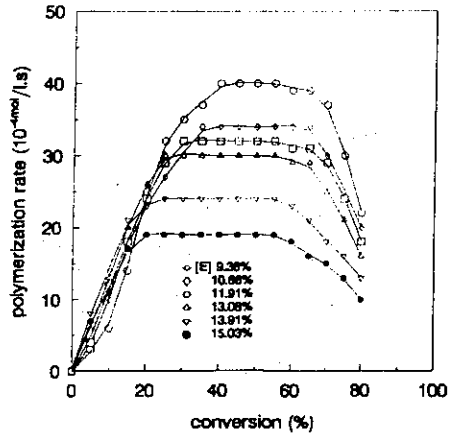


Fig.3 The rate of polymerization vs conversion at different emulsifier content. [M], 30wt%; PH, 7.5; Dose rate, 46.42Gy/min.; T, 311K

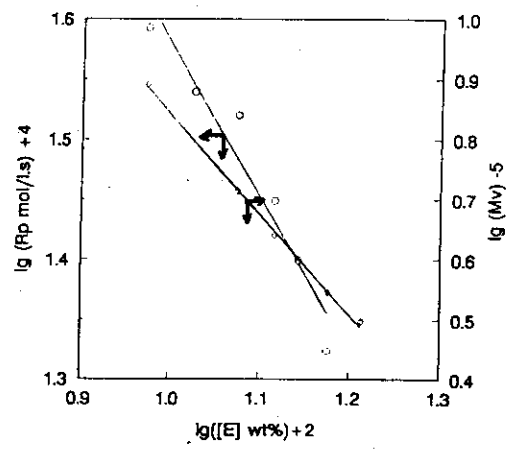


Fig.4 The effect of emulsifier content on Rp and Mn at the same condition listed in Fig.3

Because the emulsifier content in this system is high and surpasses the amount needed to form a mono-molecular-layer around the microemulsion droplets. Increasing of emulsifier concentration leads to form a thicker layer and retards the entry of radical generated in aqueous phase. As a result, the initiating rate is limited and Rp decreases. Meanwhile, the transferring of growing polymer chains to emulsifier may be important and it also contributes to the decrease of Rp and Mn.

Effect of dose rate

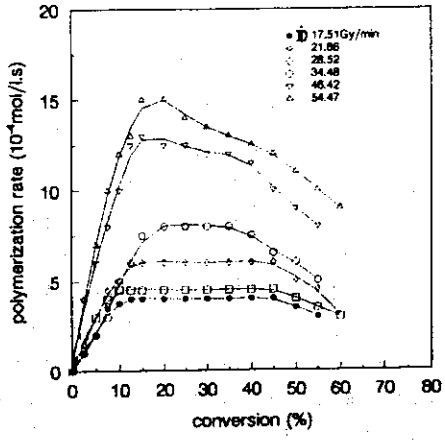


Fig.5 The rate of polymerization vs conversion at different dose rate. [E], 10.8wt%; [M], 26.0wt%; water, 63.2wt%; PH=7.5; T=308K

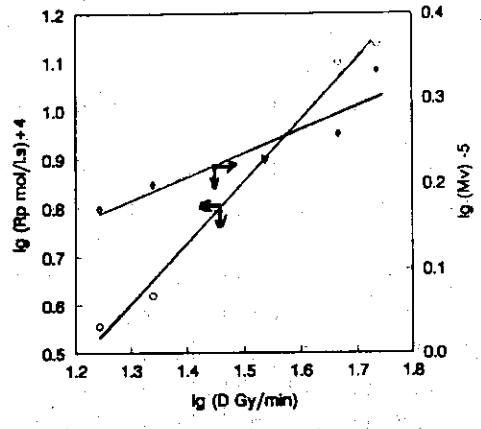


Fig.6 The effect of dose rate on Rp and Mn at the same condition as in Fig.5

The effect of dose rate on the polymerization is shown in Fig. 5. As expected, a much larger fraction of microemulsion droplets would be initiated with the the increase of dose rate due to a larger radical flux when the composition of microemulsion remained unchanged, so the length of interval I would become longer. Meanwhile, the increase of dose rate leaves a smaller fraction of uninitiated droplets for monomer recruiting and the length of interval II become shorter naturally. As shown in Fig. 5, the Rp plateau region almost disappeared with dose rate up to 50 Gy/min corresponding to the rate of radical generation 1.89×10^{14} /l. s.

The dependence of Rp and Mn on dose rate was found to be 1.27 and 0.28 power respectively, as shown in Fig. 6. It is quite out of expectation, that Mn increases with the increase of dose rate. It may be caused by two competitive factors with opposite effects. On one hand, Rp and Mn should conform to the Smith-Ewart theory for emulsion polymerization ($Rp \propto D^{0.4}$, $Mn \propto D^{-0.6}$); On the other hand, the emulsifier layer around the polymerization locus would become thinner for the number of loci increases with the increase of dose rate, and the thinner emulsifier should make Rp and Mn increase according to the effect of emulsifier discussed above. In fact, the powers for both Rp and Mn are about 0.9 higher than that expected from Smith-Ewart theory.

Effect of temperature

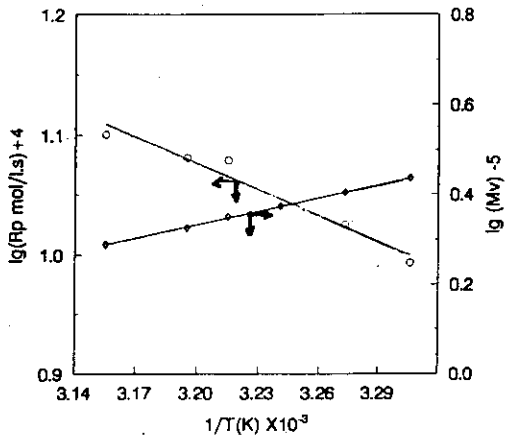


Fig.7 The Arrhenius plots of log Rp and log Mn vs 1/T. [E],10.8 wt%; [M],26.0wt%; Dose rate, 46.4Gy/min.; PH=7.5

As expected, the effect of temperature on radiation microemulsion polymerization is less obvious than on polymerization initiated by chemical initiators, since the activation energy of radical generation by radiation is zero. The nucleation period (until 20-25% conversion) is not affected by the change of temperature. The Arrhenius plots of log Rp and log Mn versus 1/T are shown in Fig. 7. The overall activation energy (Ea) of Rp and Mn are 14.0 and -7.8 kJ/mol respectively.

REFERENCES

Antoniett M., Bremser W., Muschenborn D., Rosenauer C., Schupp B. and Schmidt M. (1991) *Macromolecules*, 24, 6636

Gan L. M., Chew C. H., Lee K. C. and Ng S. C. (1993) *Polymer*, 34, 3064

Holdcroft S. and Guiliet E. L. (1990) *J. Polym. Sci. Polym. Chem. Ed.*, 18, 1823

Johnson P. L. and Gulari E. (1984) *J. Polym. Sci. Polym. Chem. Ed.*, 22, 3967

Puig J. E., Perez-luna V. H., Perez-Gonzalez M., Macias E. R., Rodriquez R. E. and Kaler E. W. (1993) *Colloid Polym. Sci.*, 271, 114

Stoffer J. O. and Bone T. (1980) *J. Polym. Sci. Polym. Chem. Ed.*, 18, 2641

Tang H., Johnson P. I. and Gulari E. (1984) *Polymer*, 25, 1357

12.17 The Measurement of Dose Distribution in the Product Boxes by Alanine/ESR Dosimeter

XIE LIQING, ZHANG YINFEN, LAN LIQIAO and ZHOU RUIYING

Radiation Beams & material Engineering Laboratory
Institute of Low Energy Nuclear Physics (Beijing radiation Center)
Beijing Normal University
Beijing 100875, P. R. China

MA SHIMING
Beijing Radiation Application Center, Beijing 100012, P.R. China

GAO JUNCHENG
National Institute of Metrology, Beijing 100013, P.R. China

ABSTRACT

The dose distribution in the irradiation product boxes is measured with the alanine/ESR dosimeter. The activity of ^{60}Co gamma radiation source is 11.4PBq, which used for radiation processing at Beijing Radiation Application Center. The size of the irradiation product box is 460mm×550mm×913mm. The dummy product is the newspaper and its bulk density is 200kg/m^3. We measured the dose distribution with both of the alanine/ESR dosimeters of Beijing Radiation Center (BRC) and Gesellschaft für Strahlen-und Umweltforchung(GSF) and the ratios of the maximum and minimum doses in the product boxes were 1.45(BRC) and 1.47 (GSF), respectively.

KEYWORDS

Alanine/ESR dosimeter; ESR spectrometer; ^{60}Co gamma radiation source; absorbed dose distribution; product box.

INTRODUCTION

An alanine/ESR dosimeter is solid free radical dosimeter. When organic solids are exposed to ionizing radiation, free radicals are induced and accumulated. By the electron spin resonance (ESR) technique the free radicals are detected qualitatively and quantitatively, thus providing a potential dosimetry. Because of its excellent radiation response characteristics, wide useful dose range, good linearity, Similarity to the tissue equivalency, non-destructive reading, long-term stability and so on, therefore, alanine dosimeters have been mainly applied to transfer dosimetry in the high gamma radiation

dose region and have been also applied for routine dosimetry in quality control of radiation processing.

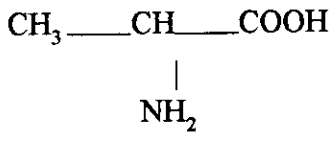
An alanine/ESR dosimetry method was used by Bradshaw et al., in measuring high dose (Bradshaw et al., 1962). The method has been improved and developed by Regulla and Deffner (Regulla and Deffner, 1980, 1981, 1982, 1985). IAEA decided , not long ago , that the alanine/ESR dosimeter of GSF was used as the International Dose Assurance Service of gamma radiation facilities in the high dose measuring for the member countries of IAEA.

In this work, the dose distribution in irradiation product boxes is measured by the alanine/ESR dosimeter which made in BRC. The basic property of alanine/ESR dosimeter has been studied (Zhang et al., 1990a).

EXPERIMENTAL PROCEDURES

Dosimeter Preparation

Alanine is an amino acid of formula:



Polycrystalline samples can be used for dosimetry measurements. For practical reasons, the pellets of the samples chosen are 3mm diameter and 7.0mm long (Zhang et al., 1990b), based on purified polycrystalline material mixed with paraffin, with an alanine content to 80% by weight. The average mass was 70.46±0.64mg (Zhang et al., 1990b). Paraffin was found to add negligible ESR signal after irradiation.

The Alanine Dosimeter Calibration

So far, the dosimetry method based on alanine/ESR analysis is a relative method, for calibration against a reference or standard dosimeter, e.g., standard Fricke dosimeter. The alanine that is exactly the same as that in the sample measured is used in a "reference sample". The calibration of dosimeter was performed in the irradiation field of the 0.38PBq ^{60}Co gamma radiation source at Beijing Normal University. It is calibrated by means of Fricke dosimeter in terms of absorbed dose in water. The absorbed dose rate was $0.36GyS^{-1}$. The relationship between ESR signal and absorbed dose was shown in Fig. 1 for ^{60}Co gamma radiation with a dose range for the alanine/ESR dosimeter from 0.1-10kGy. The ESR signal height was proportional to the absorbed dose up to 10 kGy.

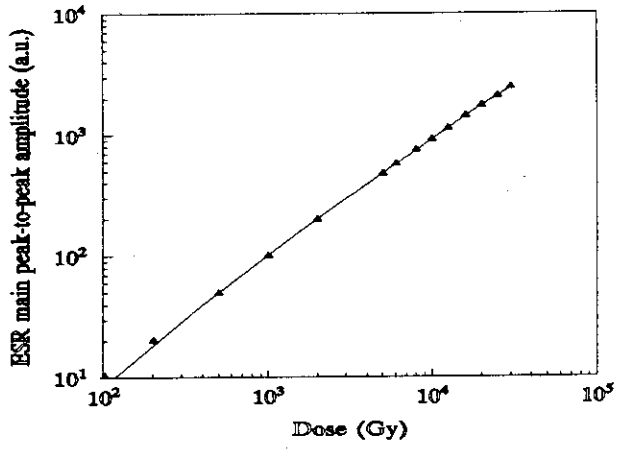


Fig. 1. Dose response curve of alanine/ESR dosimeter.

The Measurement of ESR signal

After being irradiation, the dosimeter was put into a tube, having a thin wall, made from quartz and inserted into a resonant cavity. The measurement is carried out by a JES-FE-1XG spectrometer at National Institute of Metrology. The microwave frequency is 9425MHz. The magnetic field setting is 334mT , and the field scan range is 25mT. The modulation amplitude is 0.36mT and the power of the microwave is 2mW. The ESR signal amplitude all need to be normalized for the sample mass and the gain of the ESR spectrometer , so as to eliminate the nonlinear effect between the mass dispersivity and the gain. The spectrometer sensitivity is checked before and after every series of measurements with irradiated reference samples that has been exposed at the reference position of known absorbed dose.

RESULTS AND DISCUSSION

The Intercomparison of the Alanine/ESR dosimeters

The ratios between alanine/ESR dosimeter of Beijing Radiation Center (BRC) and alanine/ESR dosimeter of IAEA and National Institute of Metrology (NTM) irradiated are obtained at ^{60}Co gamma radiation source of Beijing Normal University. The deviations of the ratios are -1.4% and +1.0%, respectively, for the alanine/ESR dosimeter of BRC and IAEA as well as BRC and NTM. These results were within their experimental error.

When the absorbed dose was measured by an alanine/ESR dosimeter, the uncertainty of dose-response data consists of random uncertainty (RU) of the ESR and weight measurements and a systematic error (SE) of dose calibration. At the measuring position of dose 1.1kGy the overall uncertainty is $\pm 4.5\%(2\sigma)$.

Dose distribution in product boxes is measured by alanine/ESR dosimeter.

The activity of ^{60}Co gamma radiation source is 11.4PBq to used for radiation

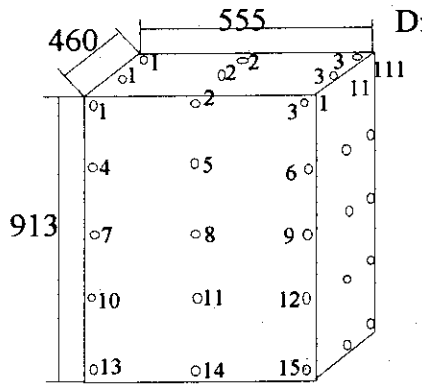


Fig. 2. Dose distribution in product boxes, measured by the alanine dosimeter.

processing at Beijing Radiation Application Center. The size of the irradiated cardboard box is 460mm×555mm×913mm. The dummy product is the newspaper and its bulk density is 200kg/m³. The two alanine dosimeters sealed in the perspex holder having a wall of 4mm thick. The alanine dosimeter of GSF provided by

Table 1. The measurement of dose distribution in the product boxes by alanine dosimeter

NO.	Dhi		Dhi		Dhi	
	BRC	GSF	BRC	GSF	BRC	GSF
1	1.35	1.38	1.12	1.13	1.45	1.47
2	1.31	1.31	1.08	1.13	1.37	1.37
3	1.33	1.35	1.11	1.14	1.43	1.46
4	1.16	1.21	1.10	1.10	1.21	1.27
5	1.17	1.21	1.09	1.11	1.19	1.26
6	1.22	1.22	1.07	1.10	1.26	1.26
7	1.13	1.14	1.07	1.04	1.14	1.19
8	1.09	1.12	1.09	1.06	1.12	1.16
9	1.16	1.13	1.07	1.05	1.30	1.19
10	1.22	1.22	1.06	1.05	1.20	1.31
11	1.22	1.23	1.06	1.05	1.22	1.27
12	1.22	1.24	1.06	1.07	1.24	1.28
13	1.19	1.25	1.03	1.01	1.24	1.28
14	1.27	1.28	1.04	1.01	1.28	1.31
15	1.24	1.23	1.00	1.00	1.25	1.28

Dhi: local overdose ratio (local dose / $dose_{min}$)

Dummy product density: 200kg/m³

Sulzer Company, Switzerland. One dosimeter put into the perspex holder. The results are showed in Fig.1 and Table 1.

The experiment results shows: The exact places of the minimum and maximum doses in the boxes are determined, which by BRC and GSF is in the same place. It explains that the property of the alanine dosimeter of BRC suited for the radiation processing. Due to its good reproducibility, long-term stability, high accuracy, the measure error is small. It is also as a reference dosimeter, or a transfer dosimeter.

Acknowledgments —The authors thanks Yan Aoshung, Gao Wei, Liu Huiping and Zeng Xinmiao,Beijing Radiation Application Center; Zhong Xinmin and Yuan Guodong, Lu Gongxu, Institute of Low Energy Nuclear Physics and Chemistry Department, Beijing Normal University; Li Chenghua and Zhang Yanli, National Institute of Metrology; Pan hongbin, Beijing Laboratory of Industrial Hygienc, Ministry of Public Health; and H.Herrnhut ,Sulzer Company, Switzerland; for supporting and assistance to this work.

REFERENCES

Bradshaw W.W., D.G. Cadena , G.W. Crawford and H.A.W. Spetzler (1962). The use of alanine as a solid dosimeter . Radiat. Res., 17, 11.

Regulla D.F and U. Deffner (1982). Dosimetry by ESR spectroscopy of alanine . Int . J. Appl. Radiat. Isot., 33, 1101-1114

Regulla D.F and U. Deffner (1985). Progress in alanine/ESR transfer dosimetry. In High-Dose Dosimetry, Proc. Symp., Vienna, 1984, P. 221, IAEA-SM-272/39. IAEA, Vienna.

Deffner U. and D.F. Regulla (1980). Influences of Physical parameters on High-Level Amino Acid Dosimetry. Nuclear Instruments and Method , 175 ,134.

Regulla D.F , U. Deffner and H. Tuschy (1981). A practical high-level dosimetry based on tissue-equivalent alanine . High-Dose Measurements in Industrial Radiation Processing , 139-151

Zhang Yingfen, Hongbin Pan, Liqing Xie and Ruiying Zhou (1990a). The DL-alanine/ESR dosimeter in the radiation processing. Radiat. Phys. Chem. Vol 35 , Nos 4-6,783-788.

Zhang Yinfen, Hongbin Pan, Liqing Xie and Ruiying Zhou (1990b). A Study of the basic dosimetric property of the alanine for ESR dosimeter. J. of Beijing Normal University (National Science) , 4 , 39-44.

13. Solid Phase

13.1 Quantum Mechanical Tunneling Reaction in Solid Hydrogen and Solid Alkane at Low Temperature, Tunneling of Hydrogen Atom and Hydrogen Molecule

Tetsuo Miyazaki

Department of Applied Chemistry,
School of Engineering, Nagoya University,
Furo-cho, Chikusa-ku, Nagoya 464-01, Japan

Abstract Tunneling reactions of hydrogen-atom-transfer and hydrogen-molecule-transfer were studied by use of γ-irradiation and ESR in solid hydrogen at 4 K and solid 2,3-dimethylbutane at 77 K, respectively.

INTRODUCTION

According to a classical theory of chemical reaction, a reaction takes place by passing over a potential energy barrier for the reaction and thus it cannot occur at very low temperature. A chemical reaction, however, does take place even at 4 K by a quantum-mechanical tunneling, in which the reaction occurs by passing through a potential barrier by a wave character of particles. Two kinds of tunneling reactions will be reported here; tunneling reaction involving hydrogen-atom-transfer (part 1) and tunneling reaction involving hydrogen-molecule-transfer (part 2).

EXPERIMENTAL

n-H_2(75% ortho-H_2; 25% para-H_2), HD(98 %), D_2(99.5 %), and p-H_2(>95% p-H_2) were solidified at 4 K. p-H_2 was synthesized by passing normal hydrogen gas through a column of molecular sieve at 14 K. 2,3-Dimethylbutane(h-DMB) was greater than 99 mol%. 2,3-Dimethylbutane-2,3-d_2(d-DMB) was synthesized by a reaction of tetramethylethylene(TME) and D_2 gas in the presence of activated alumina-5 wt% Pd catalyst at room temperature. The samples of hydrogen and DMB were irradiated with γ-rays at 4 K and 70 K, respectively. The reactive species, produced by the radiolysis, were measured with ESR.

RESULTS AND DISCUSSION

1. Transfer of Hydrogen Atom by Tunneling

The role of quantum mechanical tunneling in a hydrogen atom-hydrogen molecule reaction has been important in the theory of chemical kinetics. When solid hydrogen, such as HD, D_2-H_2 mixtures and H_2, is irradiated by γ-rays at 4 K, H and D atoms are produced. The amounts of H (D) atoms change upon storage of the irradiated samples at 4 K by tunneling reaction. The rate constants (k^{tunnel}_{exptl}) were obtained by the change of amounts of hydrogen atoms in the irradiated solid hydrogen (Miyazaki et al. 1992). In Table 1 the rate constants obtained experimentally are compared with theoretical rate constants (k^{tunnel}_{calc}) for tunneling reactions (Takayanagi and Sato 1990; Hancock et al. 1989) and those ($k^{classical}_{calc}$) estimated for classical reactions in which reactions take place by passing over the barriers. k^{tunnel}_{exptl} is approximately similar to k^{tunnel}_{calc}, but much larger than $k^{classical}_{calc}$.

There are two kinds of H_2, i.e., para-H_2 and ortho-H_2. Rotational quantum states (J) of p-H_2 and o-H_2 at 4 K are 0 and 1, respectively. Thus, the effect of rotational quantum states on tunneling reaction can be studied by use of p-H_2 and o-H_2. Table 2 shows the effect of rotational quantum states on rate constants for tunneling reactions (Miyazaki et al. 1991). The reaction H_2(J=0, 1) + T was studied by use of recoil T atoms in Xe-H_2-D_2 mixtures (Fujitani et al, 1993). H(T) atoms react faster with H_2(J=0) than H_2(J=1). The orientation of H_2 molecules at J=0 is isotropic, while H_2(J=1) molecules rotate at some orientation. H(T) atoms can react all of H_2(J=0) molecules, but they react only a part of H_2(J=1) molecules whose orientation is suitable for the tunneling reaction.

2. Transfer of Hydrogen Molecule by Tunneling

Most of tunneling reactions have been limited to an atom-transfer reaction. The tunneling reaction of H_2-molecule transfer has not been reported previously. The significant isotope effect on hydrogen-molecule elimination reaction from h-DMB^+ cations was observed by ESR at 77 K (Miyazaki et al. 1994). When a h-DMB-SF_6(0.6 mol%) mixture is γ-irradiated at 70 K, h-DMB^+ ions in addition to h-DMB radicals are produced. When the irradiated mixture is stored at 77 K for 10 min, TME^+ cations are produced by the following H_2-elimination reaction from h-DMB^+ ions.

$$(CH_3)_2CHCH(CH_3)_2^+ \rightarrow (CH_3)_2C=C(CH_3)_2^+ + H_2$$

The rate constant (k_{exptl}) for this reaction was measured as 1.1×10^{-3} s^{-1} at 77 K (cf. Table 3). When a d-DMB-SF_6(0.6 mol%) mixture is γ-irradiated at 70 K and then stored at 77 K, TME^+ ions are scarcely produced upon storage of the irradiated mixture at 77 K even for 5 days. The rate constant for the D_2-elimination reaction from d-DMB^+ ions was measured as 6.5×10^{-8} s^{-1}. Thus, the isotope effect on the reaction amounts to the extremely large value of $1.1\times10^{-3}/6.5\times10^{-8}=1.7\times10^4$.

The rate constant for the H_2-elimination reaction was calculated by two models. First, H_2-elimination takes place by passing over the barrier for the reaction. The rate constant ($k_{calc}^{classical}$) can be estimated by the following equation.

$$k_{calc}^{classical} = \int_{Eo}^{\infty} A\cdot(1-E_o/W)^{S-1}\cdot(1/RT)\cdot\exp(-W/RT)\,dW$$

where A and S are the frequency factor (10^{12} s^{-1}) and the number of vibration freedoms of the ions. Seconds, H_2-elimination takes place by tunneling of H_2 molecule. The rate constant (k_{calc}^{tunnel}) for the tunneling elimination can be obtained by the following equation.

$$k_{calc}^{tunnel} = \int_{0}^{\infty} A\cdot G(Q+W)\cdot(1/RT)\cdot\exp(-W/RT)\cdot dW$$

G(Q+W) is the tunneling permeability through the barrier, which is approximated by an unsymmetrical truncated parabolic curve. In Table 3 the experimental rate constant (k_{exptl}) for H_2-elimination is much larger than $k_{calc}^{classical}$, but is the same as k^{tunnel} for tunneling elimination. In Table 4 the extremely large isotope effect on the reaction was explained qualitatively by the model of tunneling elimination.

REFERENCES

Miyazaki T., Kitamura S., Morikita H. and Fueki K. J. Phys. Chem. (1992) 96, 10331.

Takayanagi T. and Sato S. J. Chem. Phys. (1990) 92, 2862.

Hancock G.C., Mead C.A., Truhlar D.G. and Varandas A.J.C. J. Chem. Phys. (1989) 91, 3492.

Miyazaki T., Hiraku T., Fueki K. and Tsuchihashi Y. J. Phys. Chem. (1991) 95, 26.

Fujitani Y., Miyazaki T., Masaki N.M., Aratono Y. and Tachikawa E. Chem. Phys. Lett. (1993) 214, 301.

Miyazaki T., Kitamura S., Kozono Y. and Matsunaga H. J. Phys. Chem. in press (1994).

Table 1. Comparison of experimental rate constants with theoretical ones for tunneling reactions at 4 K

reaction	rate constant, $cm^3\ mol^{-1}\ s^{-1}$			
	k^{tunnel}_{exptl} Miyazaki et al.	k^{tunnel}_{calc} Sato et al.	k^{tunnel}_{calc} Truhlar et al.	$k^{classical}_{calc}$
$n\text{-}H_2 + D \rightarrow H + HD$	0.27 - 0.49	1.2	18	6×10^{-426}
$n\text{-}H_2 + H \rightarrow H + H_2$	26 21	0.46	13	2×10^{-464}
$HD + D \rightarrow H + D_2$	0.0019 0.0023	0.0027	0.039	1×10^{-454}

Table 2. Effect of rotational quantum states on rate constant for tunneling reactions

	ratio	temperature
$k(H_2(J=0)+H)\ /\ k(H_2(J=1)+H)$	3.6	4.2 K
$k(H_2(J=0)+T)\ /\ k(H_2(J=1)+T)$	4 ± 2	77 K

Table 3. Rate constants for formation reaction of TME^+ ions in h-DMB at 77 K

	rate constant, s^{-1}
k_{exptl}	1.1×10^{-3}
k_{calc}^{tunnel}	1.1×10^{-3}
$k_{calc}^{classical}(S=33)$	9.4×10^{-59}
$k_{calc}^{classical}(S=1)$	8.8×10^{-23}

Table 4. Isotope effect on formation reaction of TME^+ ions in h-DMB and d-DMB at 77 K

	isotope effect
$(k_{h\text{-}DMB} / k_{d\text{-}DMB})_{exptl}$	1.7×10^{4}
$(k_{h\text{-}DMB}^{tunnel} / k_{d\text{-}DMB}^{tunnel})_{calc}$	1.4×10^{6}

13.2 Asymmetrical Distorted Structure, Dynamics, and Reactions of the Silacyclohexane and Related Radical Cations: ESR and *ab-initio* MO Study

Kenji Komaguchi, Masaru Shiotani, and Mitsuo Ishikawa
Faculty of Engineering, Hiroshima University
Higashi-Hiroshima 724, Japan

Introduction

The σ-type radical cations generated by one electron oxidation of the saturated hydrocarbon have been attracted much attention because of their fundamental importance as primary reactant species in radiation chemistry[1,2]. Our studies on σ-type radical cations were recently extended to the silacyclohexane (*c*SiC5), silacyclopentane (*c*SiC4), and silacyclobutane (*c*SiC3) radical cations. Their electronic structure, dynamics, and reactions were investigated by means of low temperature matrix isolation ESR technique combined with ionizing radiation (γ-rays from ^{60}Co) [3].

In the preceding paper, the 1-methylsilacyclohexane (1-Me-*c*SiC5) radical cation has been found to take an asymmetrically distorted C_1 structure with one of two Si-C bonds elongated in which the unpaired electron mainly resides (^{2}**A** in C_1) [3a]. This conclusion was based on the 4.2 K ESR spectra of radical cations of selectively deuteriated and/or methyl-substituted silacyclohexanes, *i.e.*, *c*SiC5-2,2,6,6-d_4^+, 1-Me-*c*SiC5$^+$, 1-Me-*c*SiC5-2,2-d_2^+, 1-Me-*c*SiC5-2,2,6,6-d_4^+, 1,1-Me$_2$-*c*SiC5$^+$, and 4,4-Me$_2$-*c*SiC5$^+$, in a frozen CF_3-*c*C_6F_{11} matrix. Here we report further experimental and theoretical results on 1-methylsilacyclohexane radical cation, especially on the *ab initio* MO results and matrix effects on the structural distortion, as well as thermal reactions of the radical cations. The results will make it clear that the distorted C_1 structure of the 1-Me-*c*SiC5$^+$ is the intrinsic nature at the ground electronic state.

Experimental

Solid solutions containing *ca.*0.1 mol % of the solute in halocarbon matrix molecules were prepared in Suprasil ESR sample tube on a vacuum line and then irradiated by γ-rays at 77 K. This method is well established to generate the solute radical cation [1-3]. The ESR spectra were recorded on a Bruker ESP300E spectrometer from 4 K to the temperature at which all solute radicals decayed. The *ab initio* MO calculations were carried out on a Convex C3240 computer at Information Processing Center, Hiroshima University.

Results and Discussion

We have proposed, for 1-Me-*c*SiC5$^+$, the asymmetrically distorted SOMO (singly occupied molecular orbital), ***a*** in C_1, with one of the Si-C bonds elongated based on the analysis of experimental 4.2 K ESR spectra observed in CF_3-*c*C_6F_{11} matrix (Fig.1 (a)) [3a]. In the low temperature halocarbone matrix isolation, however, matrix effects should be always took into account on the electronic ground state of the radical cation. In fact the electronic ground state of some alkane radical cations has been sometimes affected by matrix used. The theoretical approach to the static electronic structure is useful to clarify the matrix effect on the ground electronic state.

MO Calculation The geometrical structure of 1-Me-*c*SiC5$^+$ was optimized by the *ab initio*

MO method (Gaussian 90 / STO-3G basis set). The calculations resulted in the asymmetrically distorted C_1 structure. The results are summarized in Fig.1 (b). In the C_1 structure one of the Si-C bonds is 2.175 Å, which is elongated by 0.308 Å (16 %) longer, while the other Si-C bond is contracted by 0.005 Å (0.3 %) compared with the "normal Si-C bond length", 1.867 Å, of the neutral molecule. The other C-C bonds are unchanged.

Consistent with the experiments the electronic ground state of ^{2}**A** in C_1 was theoretically calculated: the ^{2}**A** state resulting in more stable by 0.33 eV in the total energy than the ^{2}**A"** state in a symmetrical C_s structure. Furthermore, our systematic theoretical calculations for a series of silacyclohexane radical cations lead to distorted C_1 structures in preference to symmetric C_s structures and this preference is not altered by introducing methyl groups to Si atom.

The ^{1}H hf splittings were evaluated by INDO-MO method for the optimized C_1 structure (in parentheses in Fig. 1 (b)). The calculated hf splittings for four equatorial hydrogens, H_{3e}, H_{5e}, H_{2e}, and H_{6e}, are compared with the experimental ones as follows: 7.40 mT (cal.) vs. 7.3 mT for H_{3e}, 0.36 mT (cal.) vs. 2.4 mT for H_{5e}, 2.59 mT (cal.) vs. 3.0 mT for H_{6e}, and 0.32 mT (cal.) vs. 2.0 mT for H_{2e}. The coincidence between the experimental and calculated values are not perfectly good. But, taking the approximations used in the calculation into consideration, one might say that the coincidence were rather good. Thus, an asymmetrically distorted C_1 structure of cSiC5$^+$ was concluded both experimentally and theoretically.

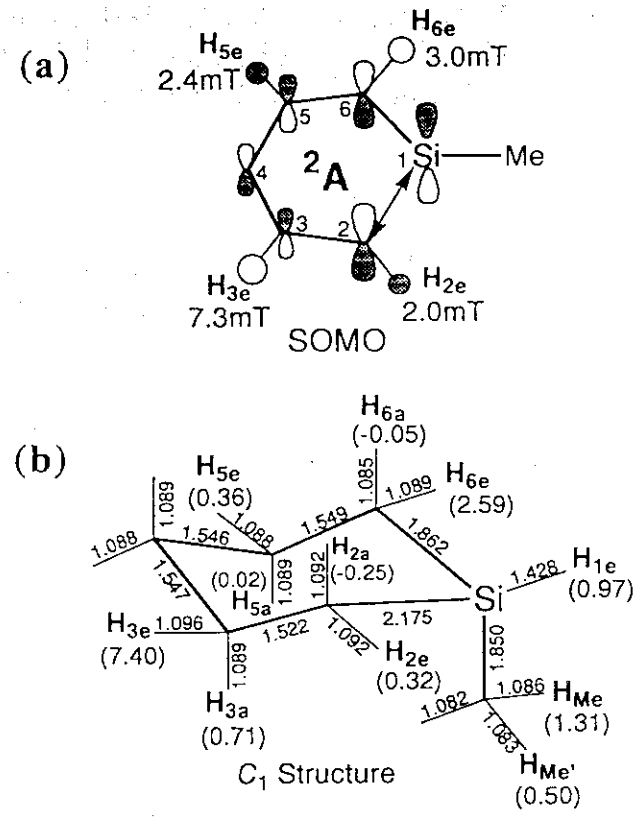
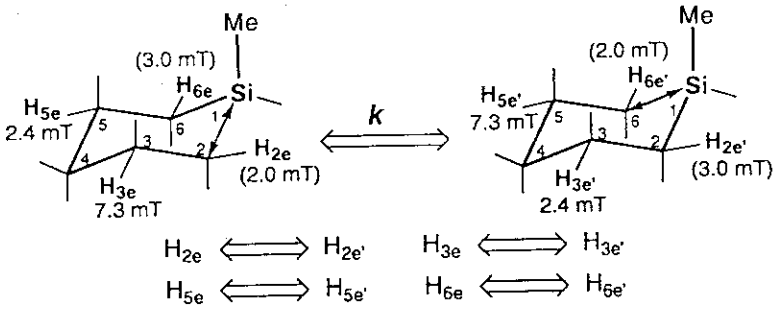


Fig. 1. (a) A proposed SOMO for the 1-Me-cSiC5$^+$ together with the isotropic ^{1}H hf splittings observed in CF_3-cC_6F_{11} matrix at 4.2 K. (b) C_1 geometrical structure optimized by ab initio MO method at UHF / STO-3G level of Gaussian 90. The values in parentheses are the isotropic ^{1}H hf splittings (in mT) calculated by the INDO MO method for the optimized geometry.



Scheme 1

Temperature dependent ESR Spectra: matrix effect The temperature dependent ESR spectra were observed for 1-Me-cSiC5$^+$ in CF_3-cC_6F_{11} matrix as shown in Fig.2 (a). They were reversibly changed in the temperature range 4 K - 140 K. The spectral line shapes were successfully analyzed in terms of Si-C bond length alternation between two mirror imaged distorted C_1 structures (Scheme 1) [3a]. The rate constants (***k***) for the dynamics were

evaluated by the spectral line shape simulations: for example, k = 1.2 x 10^7 s^{-1} at 4.2 K, k = 2.5 x 10^8 s^{-1} at 140 K. The rate constant at 4.2 K was found to become one third compared with that of cSiC5$^+$.

Fig. 2 (b) shows the temperature dependent ESR spectra observed for 1-Me-cSiC5$^+$ in CF_3CCl_3 matrix. In the temperature range of 4.2K to 140K, the spectral line shapes reversibly changed with the constant total hfs of 9.7 mT. The observed temperature dependency in CF_3CCl_3 is quite different from that in CF_3-cC_6F_{11}. That is, the doublet of 8.8 mT at 4.2K reversibly changed to the doublet of doublets with hf splittings of 7.0 mT and 2.7 mT at 140K. The 140 K spectral line shape is rather close to that in CF_3-cC_6F_{11} at 4.2 K although amplitude of the inner doublet is more intense. With increasing temperature from 4 K to 140 K the inner doublet shifts toward the center, but its signal intensity being kept almost constant. This process is reversible with temperature. The spectral line shape change can not be reproduced by a dynamic model of the Si-C bond length alternation. Instead, we propose a modified model to explain the spectral change: the structural distortion becomes larger with increasing temperature. This suggests that the interaction between matrix molecules and the radical cation become weaker with increasing temperature. The very similar temperature dependent spectral line shapes were also observed for cSiC5$^+$ in CF_2BrCF_2Br matrix. The line shapes can be successfully reproduced by the simulation method employing two parameters of the rate constant and a degree of structural distortion.

Thermal Reaction The irreversible ESR spectral change was observed, when the radical cation of 1,1-Me_2-cSiC5 warmed to 120 K in $CF_2ClCFCl_2$. The spectrum observed at 120 K is shown in Fig. 3 (b), and can be analyzed in terms of isotropic hf splittings of 4.64 mT (1 H), 2.08 mT (1 H) 1.59 mT (1 H). These ^{1}H hf splittings can be assigned to the neutral radical formed by the geo-selective deprotonation at the carbon next to the Si atom with two methyl groups. It have been reported for primary alkane radical cations that the hydrogen

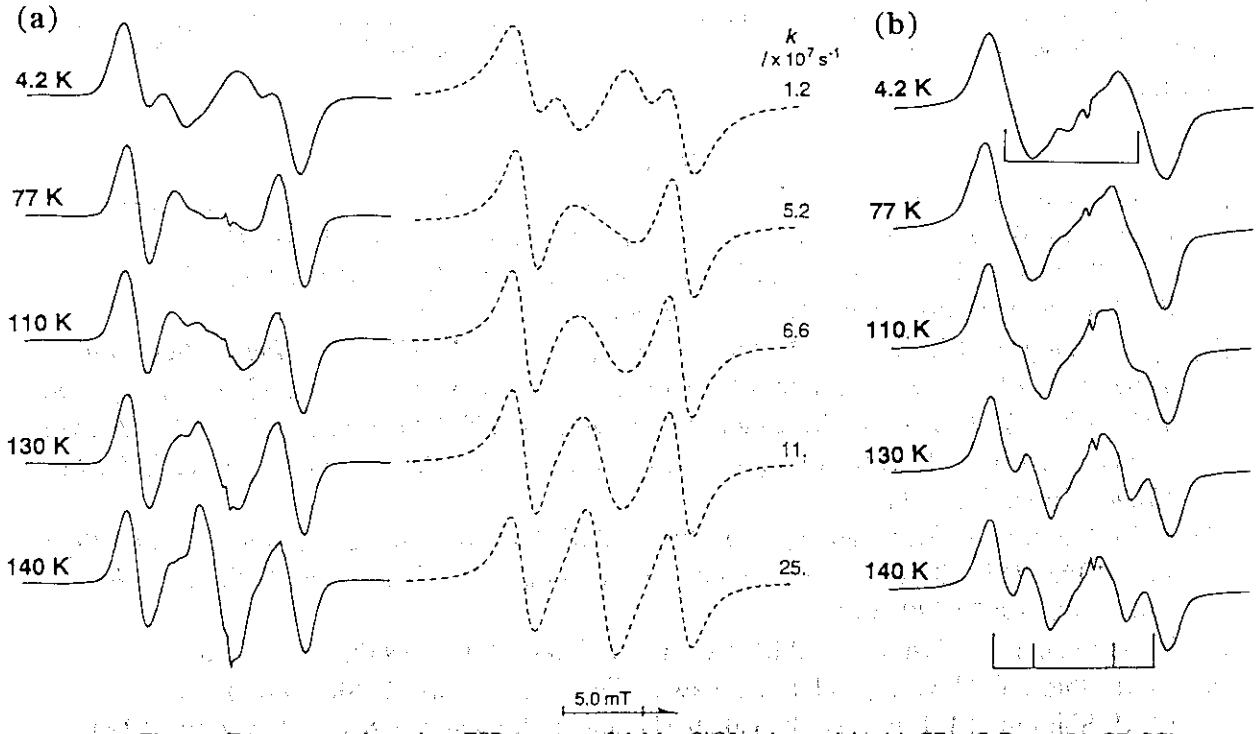


Fig. 2. Temperature dependent ESR spectra of 1-Me-cSiC5$^+$ observed in (a) CF_3-cC_6F_{11} (b) CF_3CCl_3 matrices. The broken lines are simulated spectral line shapes corresponding to (a) together with the rate constant k (in 10^7 s^{-1}) employed.

having the higher spin density are predominantly deprotonated in the thermal reaction [4]. In the present 1,1-Me_2-cSiC5$^+$ there is no correlation between deprotonation site and the spin density distribution [5].

Conclusions

The asymmetrically distorted C_1 structure with one of two Si-C bonds elongated was concluded to be an intrinsical nature for the 1-Me-cSiC5$^+$. Its electronic ground state was found independent of introducing methyl group to the Si atom. Effect due to the matrix used can be neglected, especially on the structural distortion. However, the effect is not strong enough to alter the electronic states of radical cation; it affects only the degree of the structural distortion. The radical cations of cSiC4 and cSiC3 are also found to have a distorted C_1 structure similar to that of 1-Me-cSiC5$^+$ in their electronic ground state. The further results will be published elsewhere.

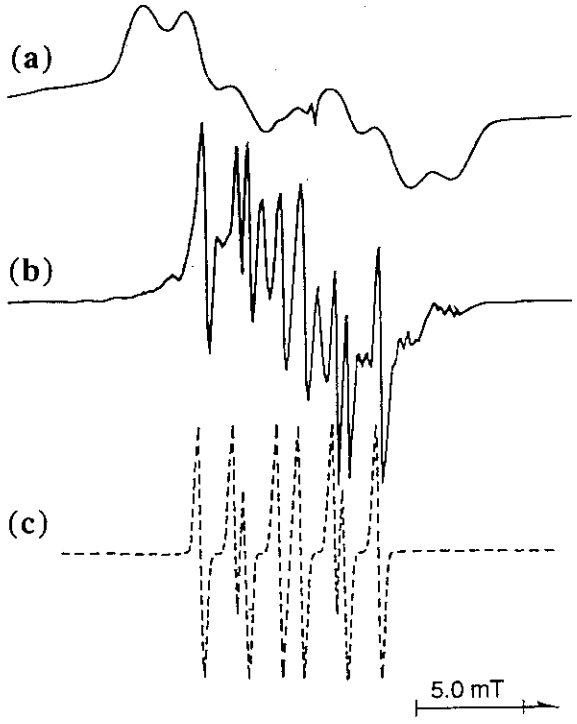
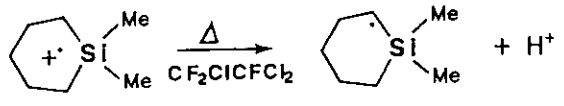


Fig. 3. The ESR spectrum of 1,1-Me2-cSiC5$^+$ observed at 77 K in $CF_2ClCFCl_2$ matrix. (b) ESR spectrum of a neutral radical formed by the deprotonation of 1,1-Me2-cSiC5$^+$ at 120 K. The broken lines show a simulated spectrum using the hf splittings of 4.64 mT (1 H), 2.08 mT (1 H), 1.59 mT (1 H).



Acknowledgment

One of the authors (K K) thanks the JSPS Fellowships for Japanese Junior Scientists.

References

[1] a) A. Lund and M. Shiotani, eds., *Radical Ionic Systems* (Kluwer, Dordrecht, **1991**).;
b) M. Iwasaki, K. Toriyama, and K. Nunome, *J. Am. Chem. Soc.*, **1981**, *103*, 3591.;
c) K. Toriyama, K. Nunome, and M. Iwasaki, *J. Chem. Phys.*, **1981**, *71*(12), 5891.;
d) M. C. R. Symons, *Chem. Soc. Rev.*, **1984**, 180.

[2] a) M. Lindgren, M. Shiotani, N. Ohta, T. Ichikawa, and L. Sjöqvist, *Chem. Phys. Lett.*, **1989**, *161*, 127.; b) M. Shiotani, M. Lindgren, and T. Ichikawa, *J. Am. Chem. Soc.*, **1990**, *112*, 967. ; c) M. Shiotani, M. Lindgren, N. Ohta, and T. Ichikawa, *J. Chem. Soc. Perkin Trans. 2*, **1991**, 711. d) M. Lindgren, K. Komaguchi, M. Shiotani, and K. Sasaki, *J. Phys. Chem.*, **1994**, *98*, 8331.

[3] a) M. Shiotani, K. Komaguchi, J. Ohshita and M. Ishikawa, and L. Sjöqvist, *Chem. Phys. Lett.* **1992**, *188*, 93.; b) K. Komaguchi, M. Shiotani, M. Ishikawa and K. Sasaki, *Chem. Phys. Lett.* **1992**, *200*, 580.

[4] K. Toriyama, K. Nunome, and M. Iwasaki, *J. Chem. Phys.*, **1982**, *77*(12), 5891.

[5] a) M. Shiotani, N. Ohta, and T. Ichikawa, *Chem. Phys. Lett.*, **1988**, *149*(2), 185. ;
b) M. Shiotani, M. Lindgren, F. Takahashi, and T. Ichikawa, *Chem. Phys. Lett.*, **1990**, *170*(2,3), 185.

13.3 *The Factor that Determines Photo-induced Crystalline-state Reaction

Y. Takenaka

Hokkaido University of Education, Hakodate
Hachiman 1–2, Hakodate, Hokkaido 040, Japan

Abstract The photo-induced crystalline-state reaction of cobaloxime complexes were investigated by X-ray diffraction method. The reactivity or the reaction rate is dependent only on the volume of the reaction cavity. The hydrogen bond formation of the reactive group and the difference of the base ligand have no effect.

INTRODUCTION

Solid-state reaction is very useful to obtain functional materials, for example asymmetric compounds or crystalline polymers, that cannot be obtained from solutions. Among the solid-state reactions, crystalline-state reaction of cobaloxime complexes are very outstanding because the reaction proceeds without degradation of the single crystal form.

It has been found that the chiral 1-cyanoethyl group bonded to the cobalt atom in the crystal of cobaloxime complex is racemized by exposure to visible light keeping the single crystal form (Ohashi and Sasada, 1977). Figure 1 shows a cobaloxime complex with (*S*)-1-phenylethylamine as axial ligand. The cobalt atom is surrounded by the dimethylglyoxime plane, a chiral cyanoethyl group, and the base ligand. If this crystal is irradiated by light, the chiral cyanoethyl group changes its configuration to the disordered racemate, that is (*R*)- and (*S*)-cyanoethyl groups are distributed randomly in the crystal, both of the cyanoethyl groups are superimposed in Fig. 1. For various base ligands, various reactions have been observed. These reactions are initiated by the Co–C bond cleavage (Ohashi, Yanagi, Kurihara, Sasada, and Ohgo, 1981). In this study the relationships between the reactivity or the reaction rate and the packing of the reactive group were investigated for some cobaloxime complexes with various amines or phosphines as axial base ligands by X-ray diffraction method, and was examined what is the responsible factor for the crystalline-state photo-reaction.

EXPERIMENTAL

The various cobaloxime crystals, pyrrolidine (pyrr), (*S*)-phenylethylamine (pea), and dimethylphenylphosphine (dmpp) as axial ligands with (*R*)-1-cyanoethyl group, and pea with (*S*)-1-cyanoethyl group (S-pea), were prepared. The integrated intensities of diffracted X-rays were measured using four-circle diffractometer. Based on the intensity data, the crystal structures were determined. The changes of cell dimensions with exposure time were also measured continuously using four-circle diffractometer.

RESULTS and DISCUSSION

The variation in cell dimensions for pyrr were shown in Fig. 2. It indicates that the variation follows first-order kinetics. The reaction rates were calculated by least-squares fitting procedure. The values are shown in Table 1.

It has been proposed that the packing around the cyanoethyl group plays an important role in crystalline-state reaction. The reaction cavity was defined in order to estimate the packing of the reactive group more precisely (Ohashi, *et al.*, 1981); the space limited by a concave surface of the surrounding atoms around the reactive group in the crystal, the radius of each sphere is taken to be 1.2 Å greater than the van der Waals radius of the corresponding atom (Fig. 3). The cavity of pyrr is shown in Fig. 4.

In order to investigate the relationship between the reactivity or the reaction rate and the packing of the reactive group, the nine cobaloxime complexes were compared; diethylphenylphosphine (depp; Tomotake, Uchida, Ohashi, Sasada, Ohgo, and Baba, 1984), diphenylethylphosphine (dpep; Tomotake, *et al.*, 1984), tributylphosphine (tbp; Kurihara, Uchida, Ohashi, Sasada, Ohgo, and Baba, 1983), triphenylphosphine (tpp; Kurihara, *et al.*, 1983), pyrr, S-pea, pea, and dmpp, of which S-pea has two polymorphs. Of these nine cobaloxime complexes, tpp, pyrr, and one of the S-pea crystals have hydrogen bonds between the N atom in the cyanoethyl groups and the solvent water molecules. The volume of the reaction cavity and the reaction rate are shown in Table 1.

Comparing the various cobaloxime complexes, it found that the reactivity and the reaction rate were dependent only on the volume of the reaction cavity, other factors, for example hydrogen bond formation between reactive group and the surrounding atom, could be neglected. There are no exceptions on this rule. Furthermore, the volume of the reaction cavity required to carry out the reaction can be determined to be 11.5 $Å^3$. This value, 11.5 $Å^3$, is appreciable to all of the crystalline-state reactions of cobaloxime complexes with cyanoethyl groups (Takenaka, Arisawa, and Ohashi, 1995).

This fact is contrast to the solid-state photo-isomerization of 2-cyanoethyl group in cobaloxime complex. If the cobaloxime complex with β-cyanoethyl group is irradiated by light in solid-state, isomerization of cyanoethyl group is observed (Fig. 5). In that case, if the cyanoethyl group has N–HO hydrogen bond with water molecule, the reaction is accelerated compared to the crystal without the hydrogen bond. This acceleration was attributed to the stabilization of the β-cyanoethyl radical to the α-radical by the hydrogen bond (Sekine and Ohashi, 1991). But in the case of racemization, the created α-cyanoethyl radical is already stable. The unpaired electron does not transfer to any other atom in radical. Furthermore, because the methyl group in cyanoethyl group moves most drastically in crystalline-state racemization, the hydrogen bond is not an obstacle of the inversion of the cyanoethyl group. So the hydrogen bond has no effect in racemization.

CONCLUSIONS

The crystal is constructed in the consequence of the equilibrium of many forces, for example electrostatic force, or van der Waals force, and so on. But in the case of crystalline-state racemization of cobaloxime complex with cyanoethyl group, the reaction proceeds dependent only on the packing of the reactive group. Although the number of cyanoethyl radical created by the cleavage of the Co–C bond may differ according to the base ligand or the hydrogen bond formation between the reactive group, these effects are found to be negligible. It can be concluded that the packing of the reactive group is responsible factor for photo-induced crystalline-state reaction.

The experiments were carried out in Tokyo Institute of Technology under the guidance of Prof. Y. Ohashi. The author also thanks to him and co-workers for their useful discussion.

REFERENCES

Kurihara T., Uchida A., Ohashi Y., Sasada Y., Ohgo Y., and Baba S. (1983) *Acta Cryst. B39*, 431–437.

Ohashi Y. and Sasada Y. (1977) *Nature 267*, 142–144.

Ohashi Y., Yanagi K., Kurihara T., Sasada Y., and Ohgo Y. (1981) *J. Am. Chem. Soc. 103*, 5805–5812.

Sekine A. and Ohashi Y. (1991) *Bull. Chem. Soc. Jpn. 64*, 2183–2187.

Takenaka Y., Arisawa M., and Ohashi Y. (1995) *Acta Cryst. B*, in preparation.

Tomotake Y., Uchida A., Ohashi Y., Sasada Y., Ohgo Y., and Baba S. (1984) *Acta Cryst. C40*, 1684–1687.

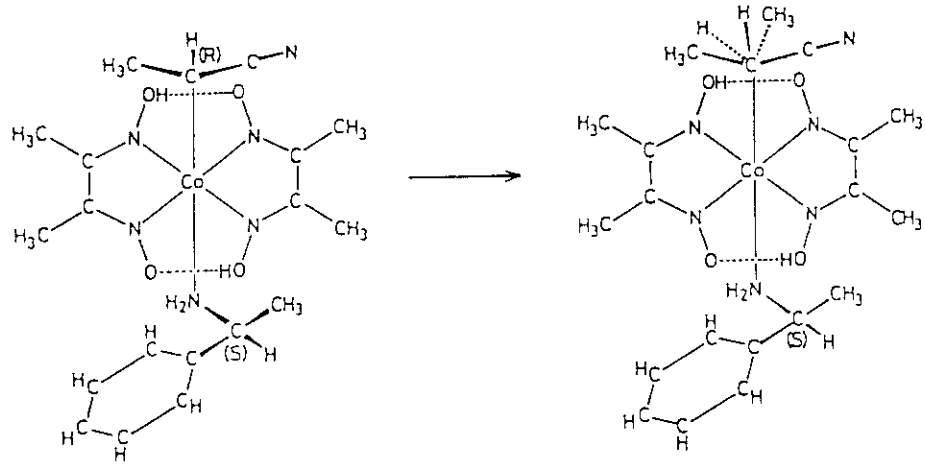


Figure 1 Crystalline-state racemization of cobaloxime complex, [(*R*)-1-cyanoethyl][(*S*)-phenylethylamine]cobaloxime (Ohashi and Sasada, 1977).

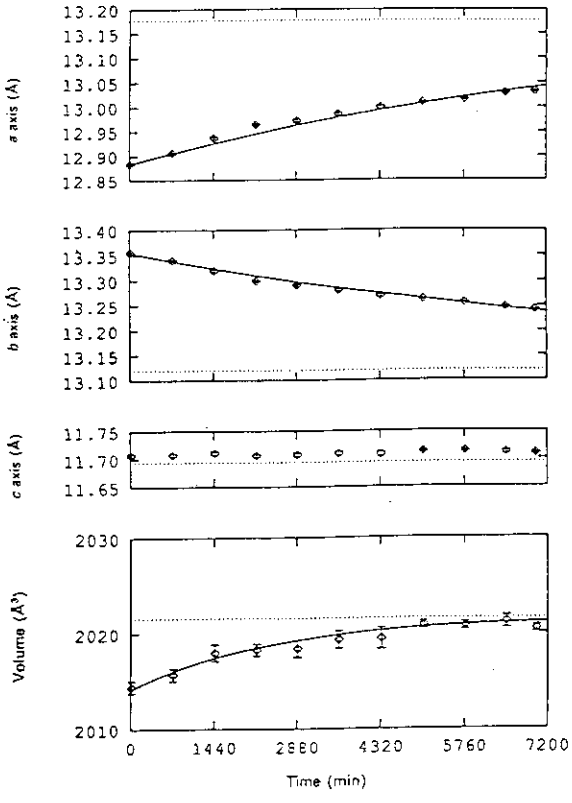


Figure 2 Change of the unit cell dimensions on exposure time. Solid curves represent the first-order kinetics and dotted lines indicate the final parameters.

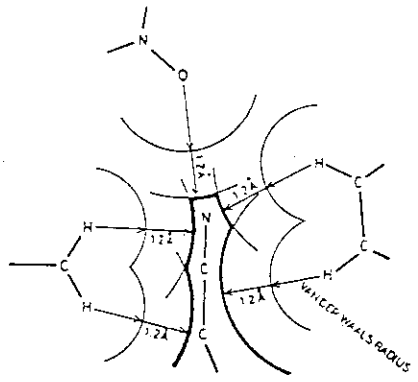


Figure 3 The definition of the reaction cavity (Ohashi, *et al*, 1981).

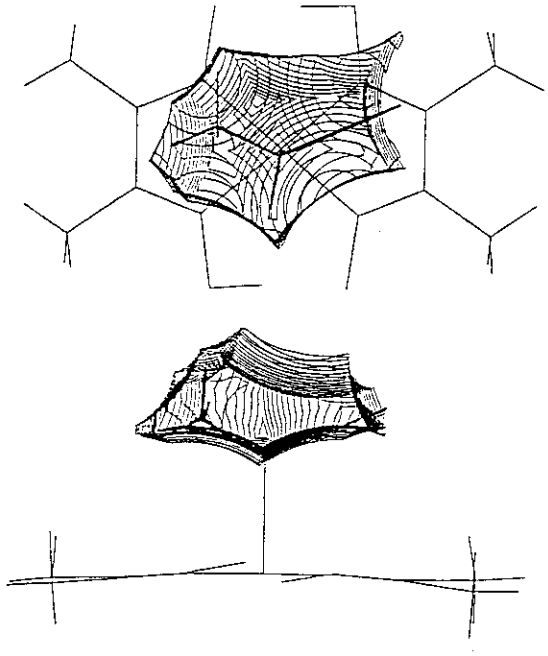


Figure 4 The reaction cavity of [(*R*)-1-cyanoethyl](pyrrolidine)cobaloxime projected onto the cobaloxime plane and the side view. Contours are drawn in sections separated by 0.1 Å.

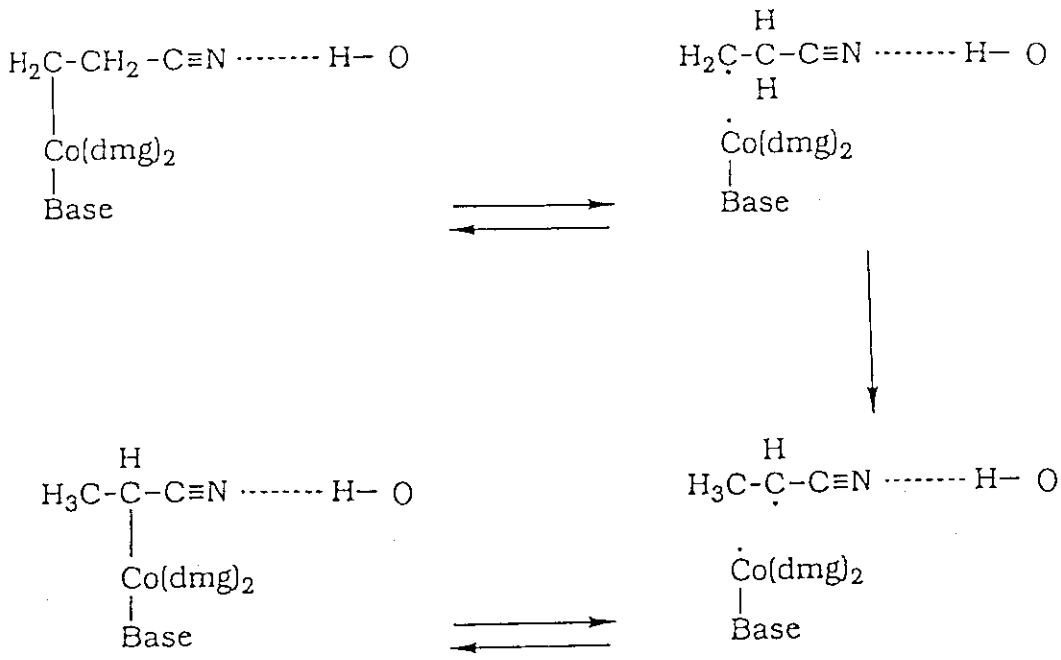


Figure 5 The β-α photo-isomerization of cobaloxime complex (Sekine and Ohashi, 1991).

Table 1 The size of the reaction cavity and the reaction rate.

	V_{cav} (Å^3)	reaction rate ($\times 10^{-6} s^{-1}$)
depp	8.4	–†
S-pea(II)	8.6	–
dpep	10.2	–
tbp	10.6	–
tpp	11.3	–
pyrr	11.6	1.69
S-pea(I)	12.8	2.38
pea	15.3	3.13
dmpp	18.0	4.80‡

†: Racemization was not observed at room temperature.

‡: The value determined from the site occupancy factor of the cyanoethyl group.

13.4 Optical Absorption Analysis on Diamond Crystals Modified by H_2^+ Implantation and Subsequent Annealing

Z. Q. Ma , H.Naramoto , Y. Aoki , S. Yamamoto , T. Takeshita and P. C. Goppelt -Langer

Establishment, JAERI, 1233 Watanuki, Takasaki Functional Materials Lab.2, Department of Materials Development, Takasaki Radiation Chemistry Research, Gunma 370-12 , Japan.

Abstract :The optical absorption analysis on synthetic diamond irradiated by molecular hydrogen ions (H_2^+) with 40 keV, 10^{15}-10^{17} H/cm^2, at 100 K, showed that the absorption coefficient (α) of modified layer in UV-VIS range was increased with the implanted dose and decreased with thermal annealing. While its relative optical band gap ($E_{r,opt}$) was decreased with ion fluence and proportional to the annealing temperature. The possible microstructure of atomic coordination for as-implanted and subsequent annealing samples was discussed tentatively. In addition the optical inhomogeneity of the type Ib diamond has been revealed by absorption topograph at λ=430 nm.

INTRODUCTION

The potential use of diamond in many areas is now well appreciated and is reflected by the growing interest in diamond by materials researchers. This has been the result of a long time study of diamond over the past few decades. As such, many properties of diamond are well established. However, there are also many questions which remain to be answered, both on the growth and on the characterization of diamond. A simple example is the understanding of the broad luminescence bands and absorption bands centered around infrared and UV-VIS regions in type-Ib diamond (Nazare and Neves 1987, Collios et al 1989). Besides this, the systematic studies of radiation damage in diamond and the extensive optical and paramagnetic resonance studies have produced a considerable amount of information on the radiation damage centers (Clark et al 1992).

In this paper, we are concerned primarily with the radiation effect by ion bombardment.. A type-Ib diamond has been irradiated with H_2^+ ions and examined by means of optical transmission spectrum in order to get comprehensive understanding of the damaging process of ion irradiated layer and the effect of implanted species, especially for dose dependent hydrogen.

EXPERIMENTAL DETAILS

The type-Ib diamond samples with volume of 3.5x3.5x0.5 mm^3 had a (100) surface. The transmission intensity imaging (topology) at 430 nm was used to survey the distribution of nitrogen concentration because the considerable variations of nitrogen impurity in the different growth sectors in submicrometer scale affected the corrected quotient value in very sensitive ultraviolet-visible region during optical transmission measurement. All of the diamonds were irradiated with 40 keV H_2^+ ions at 100 K except two of them at room temperature. Implanted doses ranged from $1x10^{15}$ to $1x10^{17}$ H/cm^2 and, each sample was covered one half area of surface along a diagonal line for the comparison between virgin and implanted areas.

The projected ranges and longitudinal straggling of the implanted H_2^+ and the other collision damage distribution were calculated with TRIM program with surface binding energy of 4.5 eV (Smith and Webb 1991). The maximum range of the possible damage caused by projectiles in diamond is approximate 140 nm, which means any change of atomic structure and electronic states distinguished from originals. The optical absorption measurements were performed at room temperature using a micro-spectrophotometer.

RESULTS AND DISCUSSION

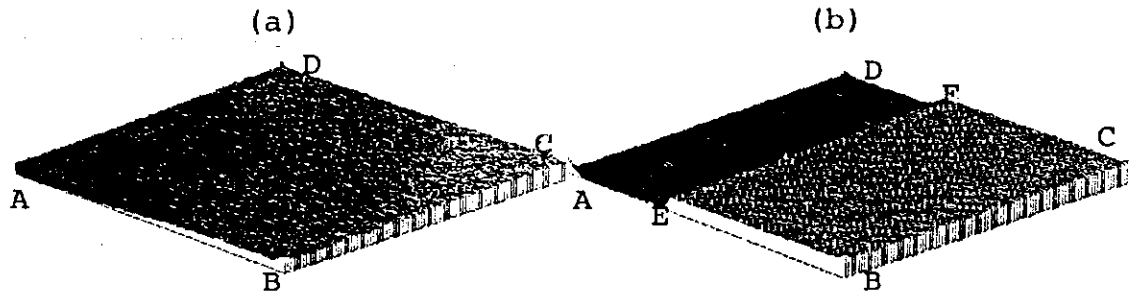


Fig.1 Near visible (λ=430 nm) absorption topograph of a synthetic diamond plate, (a) the un-implanted sample, (b) the sample as (a) but implanted with 40 keV H_2^+ and a dose of $1.3x10^{17}$ H/cm^2.

Diamond are notorious for their optical inhomogeneity, which is caused by a non-uniform distribution of point defects (van Enckevort and Visser 1990, Burns et al 1990) . To select a more transparent position for standard spectrum measurement, an optical absorption topography, which employs the enhanced near UV-VIS absorption by the single-substitutional nitrogen centers, is capable of imaging the distribution of this impurity in the diamond. Figure 1 (a and b) shows a typical micrograph of one of the synthetic diamond specimens, before and after implantation with H_2^+ ions, respectively. The each area measured by a directly incident focused light of which the diameter is about 20 μm during automatic surface scanning carefully chosen to be $1800x1800\ \mu m^2$.

The topographies were obtained by photographing the specimen plates via an optical transmission microscope fitted with a monochromatic VIS (λ=430 nm) light source. In Fig.1a, the optical absorption is gradually increased at different positions from A to C. So that the distribution of morphotropy of the nitrogen concentration in diamond crystal can be reflected in this 2-dimension diagram. The variation of absorption of diamond processed by ion implantation was showed in Fig.1b. The virgin and implanted areas were marked by AEFD and BCFE respectively. From the stiff change of absorption between implanted and un-implanted regions in this topography, it can be inferred that the optical absorption of ion-processed diamond is not only associated with the nitrogen impurity but also with the new defects induced by ions, and the latter might play an important role.

During ion implantation, especially at low temperature, many defects are produced by ion collision cascades with target atom and recoils. The radiation damage profile induced by energetic ion in solids (de Souza et al 1994 and Shwe et al 1993) and in diamond (Spits 1992) were determined by some techniques as well as predicting calculation with TRIM program. Presently, TRIM-91 with a surface binding energy of 4.5 eV, mass density of $3.52\ g/cm^3$ and atomic displacement energy of 45 eV was used to indicate the distribution of the vacancies, ion and final target atom recoil ranges. Because diamond possesses a very low diffusivity at normal conditions the extension of damage profile should be neglected during optical measurement. Thus an approximately 1400 Å damaged layer from the diamond surface to the end of the range was used in the following optical band gap calculations.

The spectra shown in Figure 2 were the ion fluence dependence of the absorption coefficient of the damaged layer mentioned-above in wavelength ranging 250 – 800 nm. The approximate absorption coefficient α was calculated from formula

$$\alpha = (1/t)\ \ln [\ I_s(\lambda)/I_i(\lambda)\ ] \qquad (1)$$

where the t was a effective thickness of that modified layer of diamond, and the transmission spectra $I_s(\lambda)$ and $I_i(\lambda)$ were always obtained at a positioned virgin point and another fixed point in implanted region, respectively. In Fig.2 we can see that the absorption coefficient increases with the dose implanted from 10^{15} to 10^{17} H/cm^2 in whole wavelength, except the difference between the doses of $5x10^{15}$ and $6.3x10^{16}/cm^2$ in ultraviolet region. The reason caused this difference is that the inhomogeneity of nitrogen concentration among the different diamond wafers, because the single-substitutional nitrogen donor defects demonstrated a strong absorption property in this region.

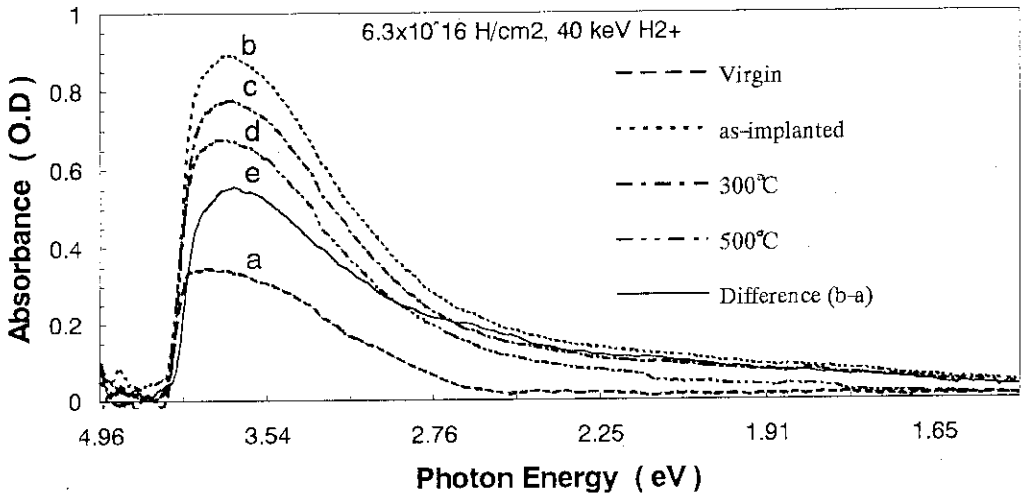


Fig.3 Absorbance (O.D) vs photon energy for type Ib diamond irradiated with $6.3x10^{16}$ H/cm^2 and following warm up to R.T, and anneals at 300 and 500°C.

In the same way, the optical densities in fig.3 were also converted into the estimation of the optical band gap as shown in fig.4b , and the approximate values of 1.88, 1.96 and 2.05 eV, corresponding to as-implanted, 300°C and 500°C, were obtained at room temperature, respectively. The plot, marked with virgin and represented a value of 2.4 eV, was a reference for comparison with those optical band gap values taken after implantation and following annealing. Hence its amount should be not identical for any two points on the same sample and/or for different samples, and its actual meaning is a reflection of the distribution of nitrogen concentration in type Ib diamond.

In fig.4b, we found an obvious annealing effect of $E_{r,opt}$ at relative low temperature. The relative optical band gap of the damaged layer increases with annealing temperature. Referring to the recently experimental results obtained by others (Kushita et al 1992 and Niwase 1994) with EELS and Raman spectra, the C-H bonds were formed during D and H_2^+ implantation at room temperature. Thus, if the hydrogen atom is still exist in diamond in subsequent annealing process, the bonding between carbon and implanted hydrogen should occur after thermal annealing, because the increase of optical band gap with temperature and very low diffusivity for impurity in diamond support this possibility. In addition the production of C-H bonds is helpful for getting more tetrahedral coordination structure (sp^3) network and decreasing the graphitic structure (sp^2) or the likely carbon chain (sp^1) of small clusters in this modified mixing layer, and the larger optical gap is associated with the high concentration of sp^3 state.

Figure 5 is a plot of the annealing temperature dependence of relative optical gap of the damaged layer. The fact that the relative optical gap increases with annealing temperature is just contrary to the result of annealing-experiment by (Smith 1984) using a-C:H film. This means the behavior of amorphous layer in diamond obtained here by implantation of H_2^+ is different from that of plasma depositioned a-C:H film. Probably, the modified diamond layer by H_2^+ ions at low temperature possesses both properties of i-C (ion-beam deposition carbon) and a-C:H if the hydrogen present, basing on the evolution of optical band gap.

Interestingly, we can get an derived correlation from the relative optical gap ($E_{r,opt}$) and annealing temperature (T_a) as follows

$$E_{r,opt} = \xi T_a + \zeta \qquad (3)$$

where the parameters ξ and ζ have been fitted to the value of $3.45x10^{-4}$ eV/°C and 1.87 eV, respectively. Replacing the $E_{r,opt}$ with referential value of 2.4 eV as relative optical gap measured before implantation in formula (3), a derived temperature of about 1550°C is obtained.

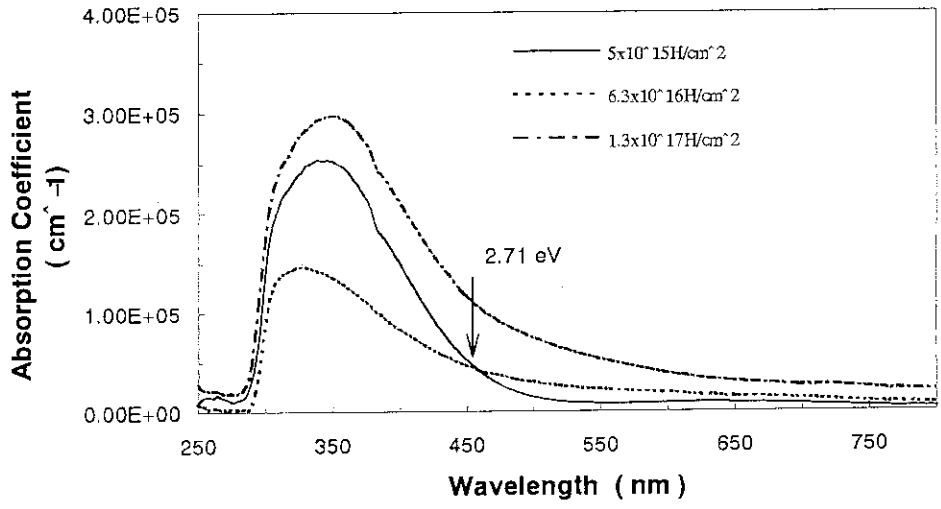


Fig.2 Absorption spectra recorded with the samples at room temperature for as-implanted diamond by H_2^+ (40 keV, $5x10^{15}$, $6.3x10^{16}$, and $1.3x10^{17}$ H/cm^2, respectively).

However, a regular change of absorption dependent on ion fluences in visible region was obtained in all of the experiments. A typical result for the optical density (O.D) , defined as $\log_{10}$(1/Transmittance), as a function of the photon energy from 1.55 to 4.96 eV , was shown in Figure 3 for the sample implanted with a dose of $6x10^{16}$/cm^2, and a subsequent thermal annealing process at 300°C and 500°C for two hours was performed. The curve (a) in this illustration, corresponding to the inhomogeneous distribution of the single-substitutional nitrogen impurity contained in the synthetic diamond crystals, was obtained before ion implantation. The curve (b) was a much more increase in the absorbance for the same sample and the exactly identical positions for $I_s(\lambda)$ and $I_t(\lambda)$ measurements as (a), but it was derived from the transmittance after implantation under 100K and naturally warm up to room temperature. The variation of absorbance after thermal annealing at 300°C and 500°C was shown as (c) and (d) respectively, and the (e) was a representation of the difference of (b) from (a). It is apparent that an enhancement of absorption in ion-irradiated layer has been produced in whole wavelength, and the absorbance was reduced by subsequently thermal annealing, even if the annealing temperature was not high enough. The results manifested that the electronic density of state as well as the atomic structure in diamond has been changed by ion irradiation because the optical density is sensitively associated with the variation. In order to elucidate the microscopic atomic structure characteristic of varying in absorption, a very useful parameter, optical band gap suitable to absorption edge, has been used for plotting $(\alpha E)^{1/2}$, in Fig.4a, as a function of photon energy (Savvides 1986)

$$(\alpha E)^{1/2} = G (E - E_{t,opt}) \qquad (2)$$

where E is the photon energy, G is a constant, and $E_{t,opt}$ is the optical band gap obtained by extrapolation of the linear part of the curves to α=0. Owing to the different background arise from the distribution of the nitrogen concentration in different diamond wafer a cross point at 455 nm (2.71 eV) in figs.2 and 4a was present between two samples for doses of $5x10^{15}$ and $6.3x10^{16}$H/cm^2, respectively. However, a regular decrease of optical band gap with increase of ion fluence was obtained in fig.4a using formula (2). But this result contradicted to the optical band gap measurement by (Robertson and O Reilly 1987 and Yoshikawa et al 1988) for the hydrogenated amorphous diamond like film (a-C:H), in which the decrease of the optical band gap was correlative to the decrease of hydrogen content in a-C:H film. The concentration of C-H bonding was considered as an advantage for forming the fourfold coordination (sp^3) state. Therefore, in the present the hydrogen -hybridized carbides in those damaged layers of diamond through molecular hydrogen ion implantation were actually different from a-C:H film in structure. The optical band gap of these layers was dominantly determined by some kinds of stable defects at room temperature induced by ionization, excitation and displacement of target atom during implantation. Furthermore, this means that there is no more bonding of carbon and hydrogen atom as well as chemical effect.

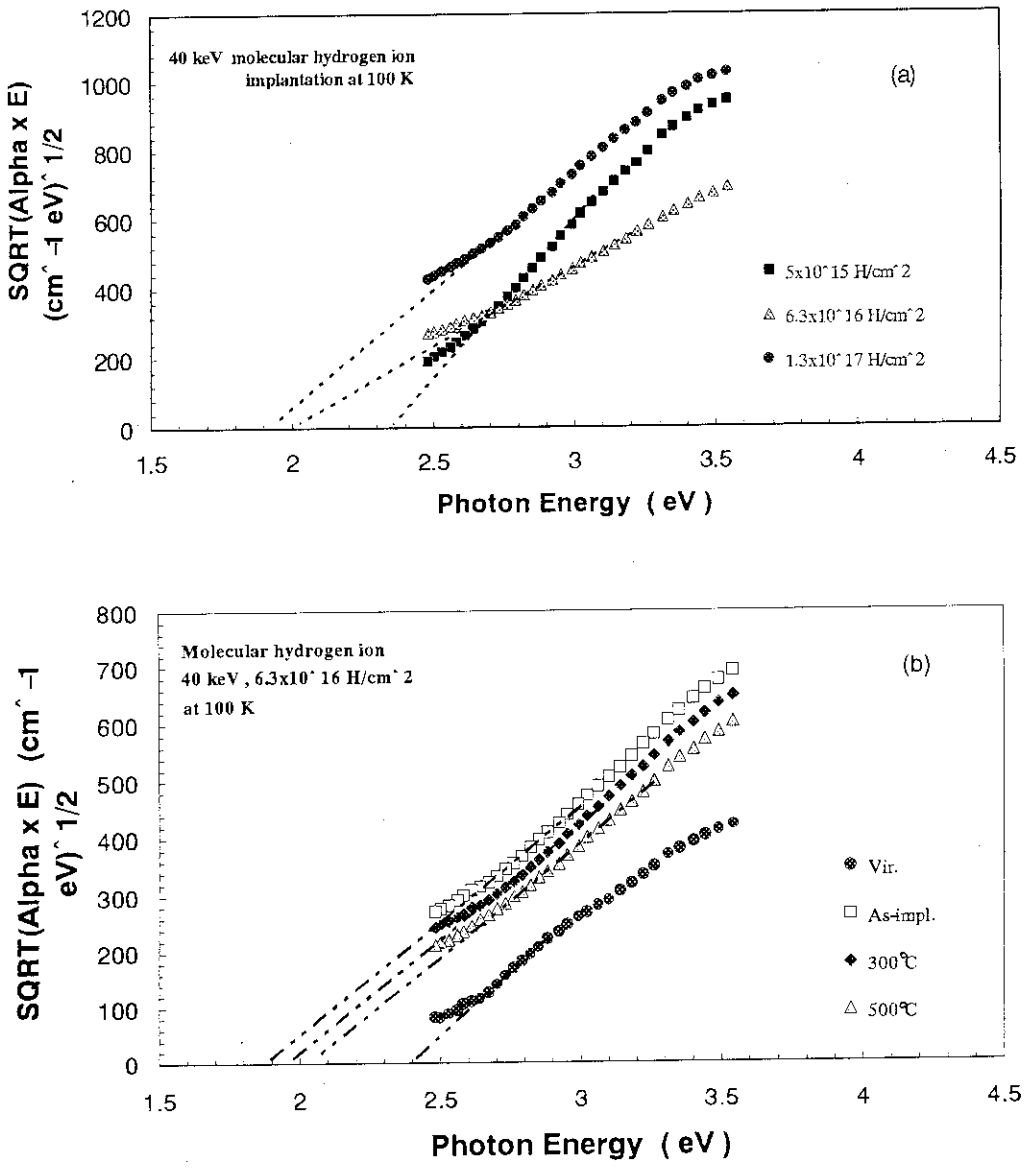


Fig.4 Tauc plots of the photon energy dependence of the optical absorption coefficient (α) for : (a) three different doses (H/cm^2) of 40 keV H_2^+, and the sample temperature during implantation was kept at about 100 K; (b) naturally warm up to room temperature and subsequent annealing at 300 and 500°C.

It is just the temperature at which the isolate-substitutional nitrogen atom starts moving in irradiated type Ib diamond (Collios 1980). Therefore, the temperature dependence of relative optical gap in Fig.5 shows a relationship of some optical absorption components and atomic structure development in subsequently thermal annealing. A possible explanation for this thermodynamical process in microscope is that the clustered size of sp^3 or sp^2 sites has been changed upon temperature driving, but the identification of different kind of the optical components contributing to the broaden absorption band is still remained for investigation.

.

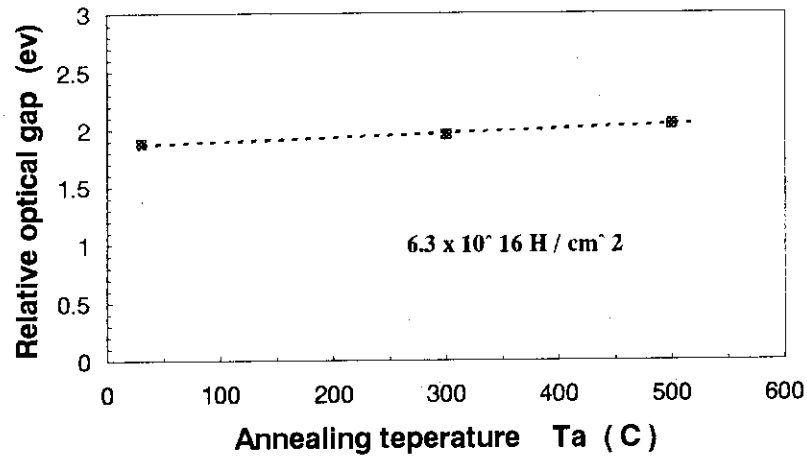


Fig.5 Relative optical band gap ($E_{T,opt}$) of modified layer in diamond by H_2^+ (40 keV, 6.3x10^{16} H/cm^2) vs annealing temperature T_a(°C).

CONCLUSIONS

The implantation of hydrogen in type-Ib diamond by H_2^+ ion at low temperature with several dose levels has been carried out and characterized through optical absorption spectra in UV-VIS wavelength range at room temperature. The enhancement of absorption density in whole wavelength indicated that the surface implanted layer was amorphized by displacement damage. The dose and temperature dependence of relative optical band gap $E_{T,opt}$ in absorption edge showed that the atomic structure in the amorphized layer was ascribed to the mixing site network of fourfold (sp^3) and threefold (sp^2) states, and the thermal evolution of $E_{T,opt}$ was much different from that of a-C:H (DLC) films made by plasma deposition. However, the presence of C-H bonds and chemical effect during subsequent thermal annealing might be possible resulting from the increase of $E_{T,opt}$ if the hydrogen composition was still remained in that buried layer till to 500°C or more. But the further confirmation of absorption components as well as defects associated with color center, combing with other approaches, is necessary in future.

Acknowledgments : We gratefully acknowledge the staffs of Takasaki-TIARA for their good corporation in ion implantation. This work was conducted under STA program.

REFERENCES

Burn R.C. et al., (1990) J. Cryst. Growth **104**, 257.
Clark C.D. Collios A.T. and Woods G.S. (1992) in The Properties of Natural and Synthetic Diamond, edited by Field J.E (Academic, London) p.30
Collios A.T. (1980) J. Phys. 13, 2641.
Collios A.T.Kamo M. and Sato Y. (1989) J. Phys.: Condens. Matter **1**, 4029.
De Sousa J.P. Bondinov H. and Fichtner P.F.P. (1994) Appl.Phys. Lett. **64**, 3596.
Kushita K.N.,Hojou K.,Furuno S. and Otsu H. (1992) J.Nucl.Mat. **191-194**, 346.
Niwase K., Kakimoto.,Tanaka I. and Tanabe T. (1994) Nucl.Instr.Meth. B**91**, 78.
Robertson J. and O Reilly E.P. (1987) Phys.Rev. B**35**, 2946.
Savvides N. (1986) J.Appl.Phys. **59**, 4133
Shwe C. et al., (1993) J.Appl.Phys. **74**, 6587.
Spits R.H., Derry T.E. and Prins J.F. (1992) Nucl. Instr. Meth. B**64**, 210.
Smith F.W. (1984) J.Appl.Phys. **55**, 764.
Smith R. and Webb R.P. (1991) Nucl Instr.Meth. B**59/60**, 1378.
van Enckevort W.J.P. and Visser E. (1990) Phil. Mag. **62**, 597.
Yoshikawa M. et al., (1988) J. Appl. Phys. **64**, 6464.

13.5 Generation and Bleaching of γ-ray-induced Loss of Er^{3+}-doped Silica-core Optical Fiber

Takeshi Koyama, Nobuyuki Dohguchi, Yoshimichi Ohki, Hiroyuki Nishikawa[1], Yasuo Kusama[2] and Tadao Seguchi[2]

Department of Electrical Engineering, Waseda University, 3-4-1 Ohkubo, Shinjuku-ku, Tokyo 169, Japan
[1] Department of Electrical Engineering, Tokyo Metropolitan University, 1-1 Minami-Ohsawa, Hachiohji-shi 192-03
[2] Takasaki Radiation Chemistry Research Establishment, Japan Atomic Energy Research Institute, 1233 Watanuki-cho, Takasaki 370-12

Abstract Erbium-doped silica optical fibers were irradiated by γ-rays, and their loss-increasing characteristics were analyzed. The loss is mainly induced by Er^{2+} created by the reduction of Er^{3+}. The loss increase is described by two saturating exponential terms and one linear term, which can be derived from the yield equation of E'γ centers and another species induced by hole trapping. It is considered that hole trapping supplies electrons to induce the reduction, and plays an important role in the loss increase.

INTRODUCTION

Recently, research has been actively carried out on doping photoactive rare-earth elements such as Er, Nd, Tm and Yb into optical fibers with a view to utilizing them as functional fibers such as fiber amplifiers[1,2] and fiber lasers.[3,4] In particular, Er^{3+}-doped fibers have brought about a breakthrough in optical communication since the amplification wavelength corresponds to the minimum loss wavelength, 1.55 μm, of silica-core optical fibers.

A thermoluminescence dosimeter is another application of rare-earth doped materials,[5,6] based on the principle that rare-earth ions trap electrons induced by irradiation and become metastable states with different valences, from which luminescence occurs upon being heated, with an intensity proportional to the total dose of radioactive rays. Such reduction by irradiation and oxidation by heating have been reported for many rare-earth ions doped into crystals.[7,8]

Imamura *et al.*[9] have reported a radiation sensing system, which utilizes the induced transmission loss of Nd^{3+}-doped silica fiber upon γ-ray irradiation. While the dose-rate dependence, or the effects of photobleaching and irradiation temperature were reported in their paper, no explanation was given on the mechanism of the loss increase induced by irradiation.

We report on the optical loss of an Er^{3+}-doped fiber induced by γ-ray irradiation and discuss the loss-increase mechanism.

EXPERIMENTAL

The sample fiber used in experiments is an Er^{3+}-doped pure-silica-core fiber with an F-doped silica cladding. The Er^{3+} concentration is 920 ppm, and the core and cladding diameters are 7.5 μm and 125 μm, respectively. As a bulk sample, the preform rod of this fiber, which is of a disk shape with a diameter of 15 mm and a thickness of 2.4 mm, is also used. The core diameter, in which Er^{3+} is doped, is 7 mm. Both sides of the disk are mirror-polished.

To measure optical loss, single-mode fibers with a Ge-doped silica core were connected at both ends of the sample fiber, and the transmitted light intensity was monitored continuously during irradiation of ^{60}Co γ-rays with dose rates between $0.5X10^5$ to $2.7X10^5$ R/h. The light source was a 0.85 μm LED with an input power of -40 dBm. For the measurement of absorption spectra of the bulk sample, a ^{60}Co source with a dose rate of $3.9X10^3$ R/h was used. The spectra were obtained with a Shimadzu UV-160 spectrometer after the sample had been irradiated for 200 h.

To investigate the recovery of light transmission by sample annealing, bulk samples which had been irradiated by γ-rays for 100 h were annealed at high temperatures, or by irradiation with an ArF excimer laser or an Ar ion laser.

RESULTS

The absorption spectra of the bulk sample before and after γ-irradiation of 780 kR are shown in Fig.1. Two sharp peaks are due to f-f transition of Er^{3+}. Upon irradiation, the optical loss is increased drastically at wavelengths shorter than 800 nm, showing a greater loss at a shorter wavelength. Curve (a) in Fig.2 is the spectrum of γ-ray-induced loss, obtained from Fig.1 by subtracting the spectrum before irradiation from that after irradiation. The absorption peak at 215 nm is due to the E'γ centers ($\equiv Si\cdot\ {}^{+}Si\equiv$) induced in the host material (SiO_2) by γ-irradiation.[10] Here, "≡" and "·" denote bonds with three separate oxygen atoms and an unpaired spin, respectively.

Figure 3 shows an example of loss increase during irradiation and the following recovery as a function of time observed for the fiber sample. The induced loss was measured for 600 min with a dose rate of $1X10^5$ R/h, while the recovery was measured for 300 min. The loss which increased rapidly upon the start of irradiation gradually slows down, and finally shows a slow and almost constant increase.

The results of annealing experiments are shown in Fig.4. The loss induced by γ-rays bleaches almost completely by the thermal annealing, but some of the loss remains after the photoannealing. The absorption at 215 nm due to E'γ centers decreases in accordance with the bleaching at other wavelengths, either by the thermal annealing and by the ArF excimer laser. However, in the case of Ar ion laser, the absorption at 215 nm scarcely disappears.

DISCUSSION

When a material with doped trivalent rare-earth ions is irradiated by γ-rays, the trivalent ions are known to be reduced to become divalent.[7,8] It is, in fact, reported that divalent rare-earth ions have very strong and broad absorption due to f-d transition from the near-infrared or visible to the ultraviolet regions.[11-13] The induced loss spectrum by γ-irradiation of 780 kR obtained for pure SiO_2, the host material of the sample, is shown by curve (b) in Fig.2. The γ-ray-induced loss of pure SiO_2 from 300 nm to 1000 nm is much smaller than that of Er^{3+}-doped SiO_2, except for the absorption near 215 nm due to the E'γ center. Therefore, it seems that Er^{2+} produced by γ-irradiation mainly causes the induced loss.

As shown in Fig.1, the intensities of the two sharp peaks due to f-f transition of Er^{3+} do not appreciably change after γ-irradiation. This indicates that the reduction rate from Er^{3+} to Er^{2+} is low. Since f-d transition is allowed, its oscillator strength is by far larger than that of the f-f forbidden transition. Therefore, it is reasonable that a small amount of Er^{2+} brings about significant induced loss. When Er^{3+} is reduced to Er^{2+}, it traps one electron. By γ-ray irradiation, many electron-hole pairs are created, but soon most of them are geminately recombined. To prevent recombination, respective trap centers for electrons and holes are necessary. This suggests that hole traps are responsible for the induced loss.

As mentioned above, the E'γ centers are induced. It is believed that the E'γ center is induced by the following reaction:

$$\equiv Si\text{-}Si\equiv + h^{+} \rightarrow \equiv Si\cdot \; {}^{+}Si\equiv . \qquad (1)$$

Namely, the E'γ center is created through trapping of a hole at an oxygen vacancy site (≡Si-Si≡).[10] If the oxygen vacancies trap holes induced by γ-rays, electrons will be left behind. Such electrons are considered to be trapped by Er^{3+}, thus creating Er^{2+}.

From the above-mentioned viewpoint that the induced loss is governed by hole trapping, the loss increase can be expressed as follows:[14]

$$\alpha(t)= \sum_{i=1}^{2} A_i[1-\exp(-\lambda_i t)]+\alpha_L t \qquad (2)$$

where $\alpha(t)$ is the loss magnitude as a function of time(t). One of the two saturation components and the linear component in eq.(2) are led from the generation of the E'γ centers and the other saturation component is led from the existence of a hole trap other than the oxygen vacancy. Therefore, it is considered that two kinds of hole traps, one being the oxygen vacancy, are involved in the loss generation.

As mentioned above, while the induced loss bleaches in accordance with the decrease in the E'γ centers in the cases of thermal annealing and photoannealing with the ArF excimer laser photons, it does not show such a clear dependence in the case of the Ar ion laser. This supports the assumption that

two kinds of hole traps, one being the precursor of the E'γ centers, are responsible for the loss induced by γ-rays.

CONCLUSIONS

Gamma-ray-induced loss of an Er^{3+}-doped silica-core optical fiber has been investigated. The induced loss is mainly caused by Er^{2+} which is created by the reduction of Er^{3+}. The loss increase can be expressed by

$$\alpha(t)= \sum_{i=1}^{2} A_i[1-\exp(-\lambda_i t)]+\alpha_L t,$$

which can be derived from the yield equation of the E'γ centers and another species induced by hole trapping. By the thermal and the photo-induced annealing experiments, the results which support this mechanism were obtained. It is considered that hole trapping is a source of electrons to reduce Er^{3+} to Er^{2+}, and thus plays an important role in the loss increase.

REFERENCES

1) R.J.Mears, L.Reekie, I.M.Jauncey and D.N.Payne: Electron. Lett. 23 (1987) 1026.
2) M.Nakazawa, Y.Kimura and K.Suzuki: Appl.Phys.Lett. 54 (1989) 295.
3) L.Reekie, R.J.Mears, S.B.Poole and D.N.Payne: J.Lightwave Technol. LT-4 (1986) 956.
4) M.Shimizu, H.Suda and M.Horiguchi: Electron.Lett. 23 (1987) 768.
5) R.Huzimura and K.Atarashi: Phys.Status Solidi a70 (1982) 649.
6) T.Yamashita, N.Nada, H.Onishi and S.Kitagawa: Health Phys. 21 (1971) 295.
7) D.S.McClure and Z.Kiss: J.Chem.Phys. 39 (1963) 3251.
8) W.Hayes: Crystals with the Fluoride Structure (Clarendon, 1974).
9) K.Imamura, T.Suzuki, T.Gozen, H.Tanaka and S.Okamoto: Proc. SPIE 787 (1987) 62.
10) D.L.Griscom: Phys.Rev. B22 (1980) 4192.
11) Z.J.Kiss and D.L.Staebler: Phys.Rev.Lett. 14 (1965) 691.
12) E.Loh: Phys.Rev. 175 (1968) 533.
13) D.L.Wood and W.Kaiser: Phys.Rev. 126 (1962) 2079.
14) T.Koyama, N.Dohguchi, Y.Ohki, H.Nishikawa, Y.Kusama and T.Seguchi: Jpn.J.Appl.Phys. 33 (1994) 3937.

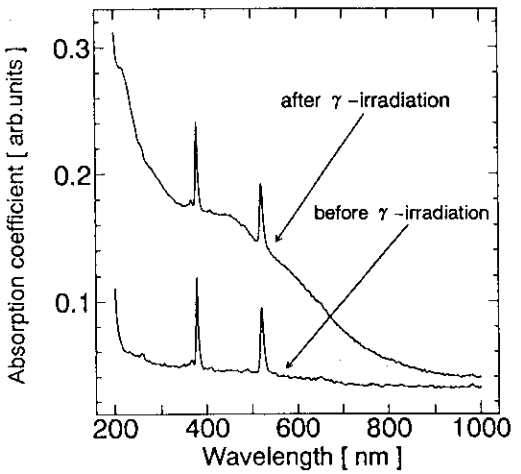


Fig.1. Absorption spectra before and after γ -ray irradiation.

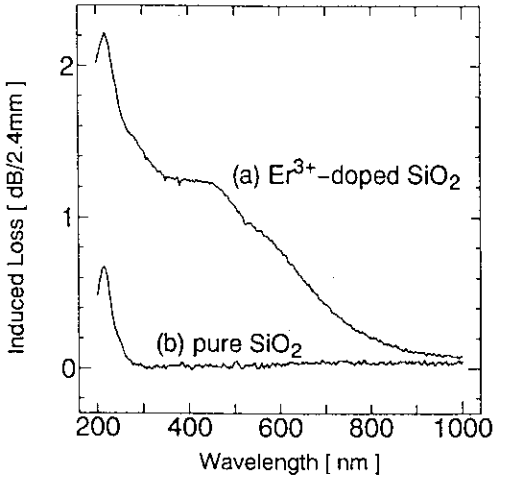


Fig.2. Spectra of γ -ray-induced loss for Er^{3+}-doped SiO_2 (a) and pure SiO_2 (b).

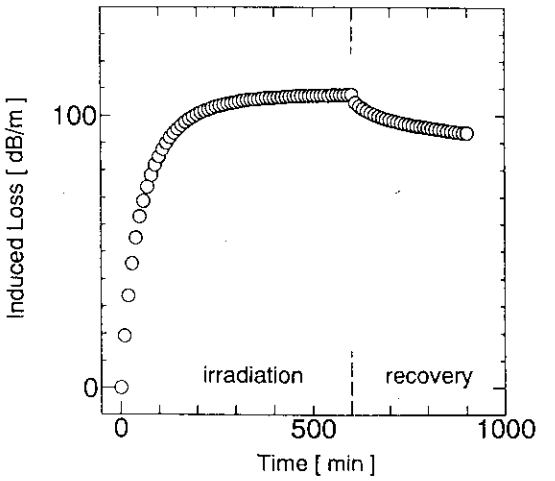
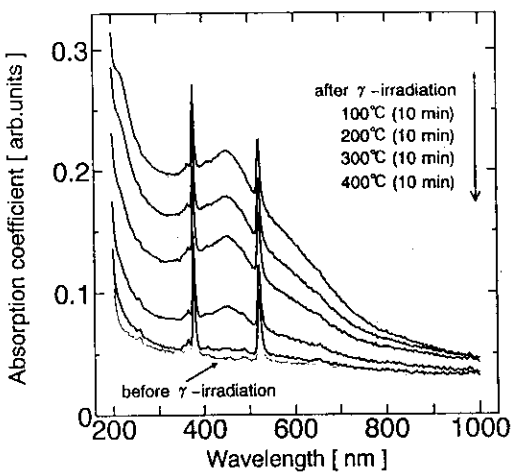
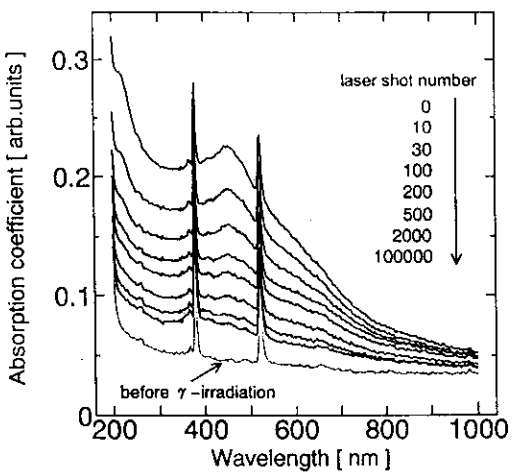


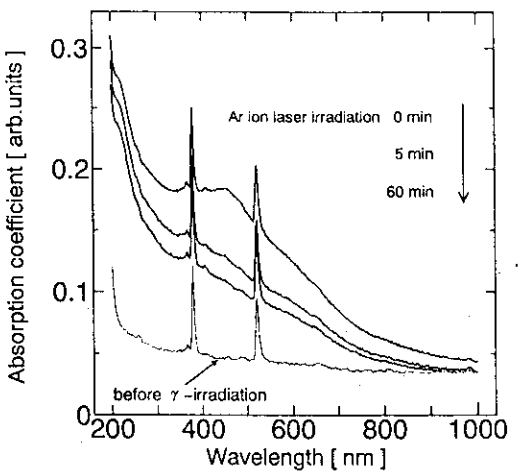
Fig.3. Loss increase and recovery of Er^{3+}-doped silica fiber by γ -irradiation with a dose rate of 1×10^5 R/h.



(a) high temperature annealing



(b) annealing by ArF excimer laser (193nm)



(c) annealing by Ar ion laser (488nm)

Fig.4. Effect of sample annealing on the recovery of transmission (*i.e.* decrease in loss) induced by γ -ray irradiation of 390 kR.

13.6 Self-trapped Holes in Alkali Silver Halide Crystals

T. Awano, M. Ikezawa *and T. Matsuyama**

Department of Applied Physics, Tohoku Gakuin University, Tagajo 985, Japan
*Research Institute for Scientific Measurements, Tohoku University, Sendai 980-77, Japan
**Research Reactor Institute, Kyoto University, Osaka 590-04, Japan

Abstract γ-Ray irradiation at 77 K induces defects in M_2AgX_3 (M=Rb, K and NH_4; X=Br and I) crystals. The irradiation induces self-trapped holes of the form of I^0 in the case of alkali silver iodides, and $(halogen)_2^-$ and $(halogen)^0$ in the case of ammonium silver halides. The $(halogen)^0$ is weakly coupled with the nearest alkali metal ion or ammonium ion. It is able to be denoted as RbI^+, KI^+, NH_4I^+or NH_4Br^+. The directions of hole distribution of $(halogen)_2^-$ and $(halogen)^0$ were different in each case of the alkali silver iodides, ammonium silver halides and mixed crystal of them. The $(halogen)^0$ decayed at 160 K in annealing process. The $(halogen)_2^-$ was converted into another form of $(halogen)_2^-$ at 250 K and this decayed at 310 K. A formation of metallic layers was observed on the crystal surface parallel with the *c*-plane of $(NH_4)_2AgI_3$ irradiated at room temperature.

INTRODUCTION

Alkali silver halide or ammonium silver halide crystals of the formula of M_2AgX_3 (M=Rb, K and NH_4; X=Br and I) are orthorhombic and belong to the space group of D_{2h}^{16} (Brinc and Kroase, 1954). A unit cell contains four molecules as shown in Fig. 1, which shows a projection of a unit cell along the *b*-axis of the crystal. A silver ion is surrounded by a tetrahedron formed by halogen ions. This tetrahedron is connected along the *b*-axis.

The top of the valence band is mainly composed of the *p*-orbital of the halogen ion and the lowest conduction band is *s*-orbital of the silver atom. The energy levels of Ag(4*d*) and X(*p*) are close and they are mixed to form the uppermost valence band (Edamatsu et al., 1989).

This crystal structure and energy band structure are different from those of alkali halides, in which defect formation process has been well investigated. We have investigated the structure of defects in M_2AgX_3 by ESR measurements to study the relation between the defect formation and the energy band structure.

In the case of alkali halides and ammonium halides, there is no difference in the structure of the self trapped holes (STHs). It was found by this study that different forms of STHs are stable in alkali silver halides and ammonium silver halides. It is interesting to investigate the reason why those STHs have different stable forms in alkali silver halides from

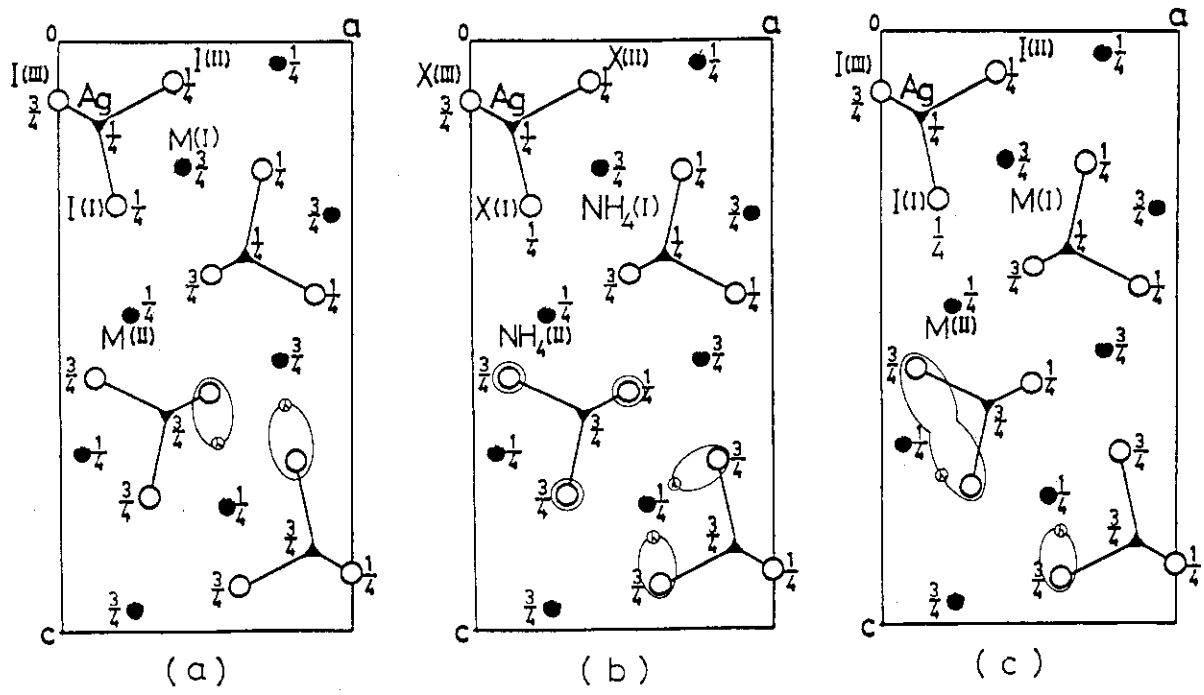


Fig. 1. Crystal structure of (a) alkali silver iodides, (b) ammonium silver halides and (c) alkali-ammonium silver halides. A unit cell is projected on *ac* plane. Figures show *b*-coordinates of each ion. "M" in (a) denotes alkali metal ion. "X" in (b) denotes halogen ion. "M" in (c) denotes rubidium or ammonium ion. Schematic distributions of self-trapped holes are shown in the figure. In (b), X_2^- is parallel to the normal of the *ac* plane of the crystal. It is shown as simple circle in the figure. (See text.)

those in ammonium silver halides. Thus, we also have investigated the structures of self-trapped holes in the mixed crystal of alkali silver halides and ammonium silver halides of the formula of $(M_x(NH_4)_{1-x})_2AgX_3$.

EXPERIMENTAL

Single crystals of M_2AgX_3 were prepared from saturated aquaous or hydrohalogenoid acid solution of stoichiometric compounds of MX and AgX. The dimension of obtained crystal was 7×15 ×30 mm^3 at maximum. γ-Ray irradiation was done by the ^{60}Co facility at the Research Reactor Institute of Kyoto University. The dose was about 50 Mrad in ammonium silver halides and 200 Mrad in alkali silver halides. Mixed crystals of alkali silver iodide and ammonium silver iodide were grown in saturated aqueous solution of a mixture of NH_4I, MI (M=K, Rb) and AgI. A part of alkali metal ions seems to be substituted by ammonium ions in the crystal considering from x-ray diffraction analysis. The concentration ratio of Rb and NH_4 was determined by neutron activation analysis.

RESULTS AND DISCUSSION

The characteristic feature of ESR spectra of M_2AgI_3 γ-irradiated at 77 K was as follows (Awano et al., 1989). Each of four sets of component has six hyperfine structures of

an equal intensity. Each set of hyperfine structure is due to a single iodine nucleus which has a nuclear spin of 5/2. The g tensor and the hyperfine tensor have the uniaxial symmetry whose axes are almost coincident with directions between I(I) and the nearest alkali metal ion M(II) or I(III) and M(I) in the fig. 1(a). Super-hyperfine structure is due to a nearest alkali metal nucleus. The main contribution is due to ^{39}K of which natural abundance is 93.2 % and nuclear spin is 3/2 in the case of K_2AgI_3. The above results show that the defect formed in both crystals is a pair of iodine ion and an alkali ion at the sites I and III but not in the site II. It can be denoted in a simple way as KI^+ and RbI^+ molecule. The mixing of Ag 4*d*-orbital with the I 5*p*-orbital may be larger at the site II and this may be the reason of the difficulty of the localization of a hole.

In the ESR spectra of $(NH_4)_2AgI_3$ γ-irradiated at 77 K, each of two sets of component has six hyperfine structures of an equal intensity (Awano et al., 1993). The super-hyperfine structure of the three lines of an equal intensity and splitting is due to a nitrogen nucleus. The hole is located at I(I) or (II) and slightly distributed to the nearest NH_4(I) as shown in fig. 1(b). Hyperfine parameters of I^0 are almost the same as those in alkali silver halides. Beside the hyperfine structure of I^0, hyperfine structure of I_2^- is observed. The I_2^- has its axis parallel with the *b*-axis of the crystal. Hyperfine parameters of I_2^- are almost the same as those in alkali iodides.

In the case of $(NH_4)_2AgBr_3$, each of two sets of several lines has four hyperfine structures with an equal splitting and an almost equal strength, beside the large structure centered at g=2 (Awano and Matsuyama, 1994). The former signal is due to Br^0 weakly coupled with a nitrogen nucleus and hydrogen nuclei. The uniaxial directions of Br^0s are coincide with the direction between each Br^- ion located on the sites I and II and the nearest NH_4(I) ion as in the case of $(NH_4)_2AgI_3$.

In the case of $(Rb_{0.9}(NH_4)_{0.1})_2AgI_3$, hyperfine parameters of I^0 and I_2^- are approximately the same as those in the alkali silver iodides and the ammonium silver iodide (Awano and Matsuyama, 1994). Uniaxial directions of I^0 and I_2^- are, however, different from those in the alkali silver iodides and the ammonium silver halides. In $(Rb_{0.9}(NH_4)_{0.1})_2AgI_3$, I^0 exists only in iodine ion (II) and slightly distributes the nearest NH_4^+ (I) as shown in the fig. 1(c). I_2^- is in two iodine ions on the horizontal edge of the iodide tetrahedron.

The $(halogen)^0$ decays at 150 K in the alkali silver iodides and the ammonium silver halides. The $(halogen)_2^-$ decays at 180 K in the ammonium silver halides. The structural conversion of the $(halogen)_2^-$ occurs in the ammonium silver halides. Fig. 2 shows an example of ESR spectra of $(NH_4)_2AgI_3$ γ-irradiated at 77K and annealed up to 190 K. Magnetic field was applied in directions in the *ac* plane of the crystal. Angles from the *a*-axis are shown in the fig. 2. This new $(halogen)_2^-$ was stable up to 250K and disappeared at 280 K. This has small hyperfine parameters and large line width comparing with $(halogen)_2^-$ in alkali halides. The same phenomena occurred in the case of $(NH_4)_2AgBr_3$. Fig. 3 shows an example of ESR spectra of $(NH_4)_2AgBr_3$ γ-irradiated at 77K and annealed up to 258 K.

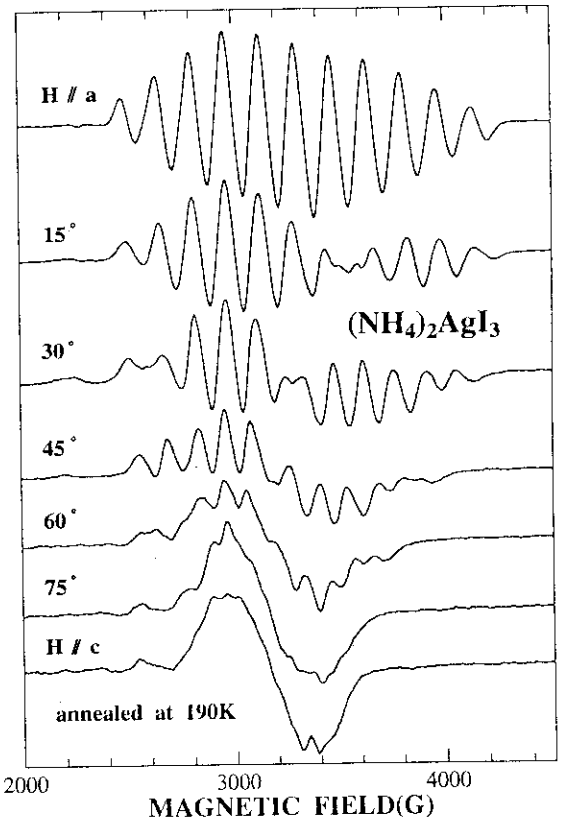


Fig. 2. ESR spectra of $(NH_4)_2AgI_3$ γ-irradiated at 77K and annealed up to 190 K. Magnetic field was applied in directions within *ac* plane of the crystal. Angles from the *a*-axis are shown in the figure. The temperature of measurement was 77 K. The microwave frequency was 9.290 GHz.

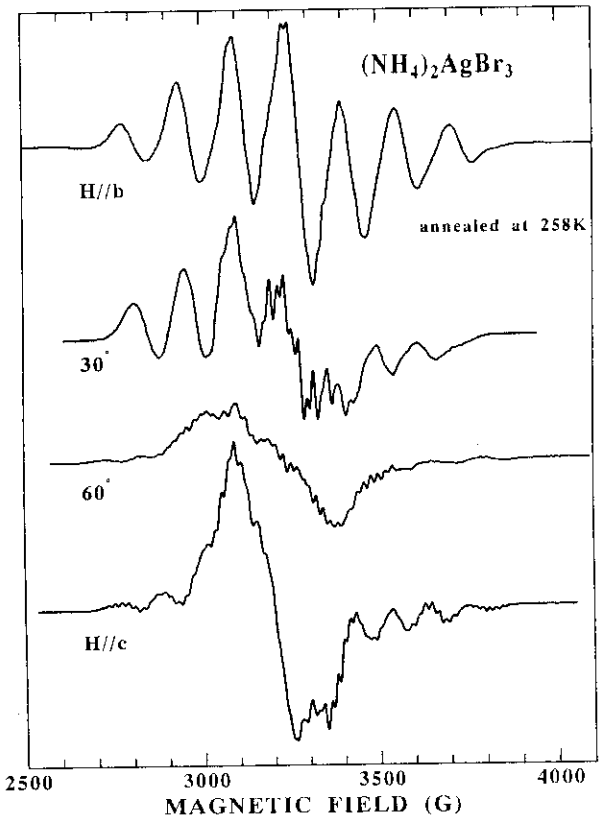


Fig. 3. ESR spectra of $(NH_4)_2AgBr_3$ γ-irradiated at 77K and annealed up to 258 K. Magnetic field was applied in directions within *bc* plane of the crystal. Angles from the *b*-axis are shown in the figure. The temperature of measurement was 77 K. The microwave frequency was 9.290 GHz.

Magnetic field was applied in directions in the *bc* plane of the crystal. Angles from the *b*-axis are shown in the fig. 3. This new V_K center disappeared at 310 K. This conversion did not occur in the $(Rb_{0.9}(NH_4)_{0.1})_2AgI_3$ crystal. Each of the I_2^- and I^0 in $(Rb_{0.9}(NH_4)_{0.1})_2AgI_3$ crystal decayed at 250 K and 240 K in an annealing process. Comparing with the alkali silver iodides and the ammonium silver iodide, I_2^- and I^0 were stable in the mixed crystal in the annealing process.

$(NH_4)_2AgI_3$ crystal turned in brown color by irradiation at room temperature. The *c* plane of this crystal showed silvery luster. The *a* plane also showed a little silvery luster. The *b* plane, however, showed no luster. Such a metallic coloration was reported on alkylammonium chlorides (Yoshinari et al., 1985). This phenomenon is probably due to the deposition of microcrystal layers.

CONCLUSION

A self-trapped hole of the form of I^0 was stable in Rb_2AgI_3 and K_2AgI_3 among alkali silver halides. The I^0 was weakly coupled with the nearest alkali ion and it is denoted by RbI^+ or KI^+. On the other hand, both of X_2^- and X^0 were stable in $(NH_4)_2AgX_3$. The structures of self-trapped holes induced in the mixed crystal of the alkali silver iodide and the ammonium silver iodide are almost the same as those in each component crystal. Their orientations are, however, different from those in each component crystal. They are thermally stable comparing with those in each component crystal. These facts indicate that small differences of site energies, which is due to the energy band structures, resulted in rather large differences of the stability of the STHs.

Acknowledgements-This work was executed under the visiting researcher program of the Research Reactor Institute of Kyoto University.

REFERENCES

Brinc C. and Kroase H. A. S. (1951) Acta Cryst. **5**, 433 .

Awano T. , Nanba T., Ikezawa M., Matsuyama T. and Yamaoka H. (1989) J. Phys. Soc. Jpn. **58**, 2570.

Awano T., Ikezawa M., Matsuyama T. and Yamaoka H. (1993) Defect in Insulating Materials, World Scientific, Singapore.

Awano T. and Matsuyama T. (1994) Nucl. Instrum. Methods **B91**, 227.

Awano T. and Matsuyama T. (1994) Proc. 7th europhysical conference on defects in insulating materials, Lyon (in press).

Edamatsu K., Nanba T. and Ikazawa M. (1989) J. Phys. Soc. Jpn. **58**, 314.

Yoshinari T., Matsuyama T., Yamaoka H. and Aoyagi K. (1985) Jpn. J. Appl. Phys. **24**, L720.

13.7 Ion Beam Induced Luminescene and Damage Study on Single-and Poly-crystalline Al_2O_3:Cr

N.T. My*, Y.Aoki, H. Takeshita, S. Yamamoto, P. Goppelt-Langer, and H. Naramoto

Dept. of Materials Development, JAERI-Takasaki, Watanuki, Takasaki, Gunma, Japan
*Vietnam National Atomic Energy Commision 59 Ly Thuong Kiet, Hanoi, Vietnam

Abstract Luminescence and Damage induced by Ar^+ and He^+ ion bombardment for a luminescent oxide of Al_2O_3:Cr has been studied. Both, single- and poly-crystalline Al_2O_3:Cr gave an intense luminescence at 695 nm due to Cr^{3+} excited states. But the light intensity decreased rapidly with dose. The rate of decrease depends on the sample and the incident ions. In addition, enhancement of the luminescence yield was observed. RBS-Channeling results show that the extent of disorder in the crystals increases in the dose range of 1×10^{15} to 1×10^{16} ions/cm^2. It is concluded that the luminescence efficiency is closely associated to damage produced in the crystals.

INTRODUCTION

When an energetic ion penetrates a solid, it will lose its kinetic energy by elastic collision with target atoms and by inelastic proscesses such as excitation and ionization of target atoms, until it comes to rest at some depth within the target. The inelastic processes are responsible for electronic processes, for example luminescence or charge transfers in materials, while the elastic collision causes production of defects such as vacancies, interstitials and these complex states. Earlier studies have shown that the structure and the concentration of these defects influence the luminescence yield (Klicks and Schulman, 1951; Dexter and Schulman, 1954) and ion beam induced luminescence can be used to monitor defects produced during ion implantation(Townsend,1987; Abu-Hassan and Townsend, 1988; Al Ghaamdi and Townsend,1990; Jacque and Townsend, 1990). Al_2O_3:Cr is one of luminescent materials which is often used for looking at the beam spot in accelerator facilities, because it gives intense red luminescence by irradiation of high energy electrons and ions. However, in the case of ion irradiation, the yield of luminescence decreases depending on the kind of incident ion and irradiation dose. The degradation of luminescence efficiency is not clear yet.

In this work, luminescence induced by Ar^+ and He^+ ion irradiation at room temperature was measured for single- and poly-crystalline Al_2O_3:Cr as fuctions of irradiation dose and ion energy. The aim of this study is to find out the relationship between the luminescence yield of the impurity and the damage roduced in the oxide during ion irradiation. Here, Ar^+ and He^+ ions were chosen as incident ions in order to elucidate the effects of the elastic and the inelastic collisions on excitation of the luminescent impurity.

EXPERIMENTAL

Poly-crystal (AF995R, Desmarquest) and single-crystal, grown by Verneuil method, of Al_2O_3:Cr samples were used in this study. The latter was cut and polished to mirror-like finish and then annealed in air at 1400°C for 12h. Ar^+ and He^+ irradiation was done by a 200 kV ion implanter (Danfysik) at room temperature in vacuum (ca. 2×10^{-6} Torr). The ion beam was swept over the sample surfaces horizontally and vertically to get uniform

irradiation. The incident angle was about 45° to the normal to the surface. The emitted light during irradiation was collected by a quartz lens and guided to monochrometer/spectrograph (HR250, Jovin-Yvon) through 1.5 m quartz fibers. Then the luminescence spectrum was detected by a 1024ch photodiode array detector with image intensifier (OMH-42, ATAGO BUSSAN). All spectra were corrected for the photo-sensitivities of the grating on HR250 and the photodiode array detector. Although there were no correction for the transmittant characteristics of the collecting lens and the optical fibers, the measured spectrum should not be distorted because their transmitting properties in the wavelength region measured here (630-830 nm) are rather constant(~100%). For escaping from charging effect during irradiation, sample surface was covered with Al-foil having a hole of 2mmϕ for irradiation. The fixed area of hole worked for comparison of luminescence yields from different types of irradiation using different types of sample and different ion energies. Rutherford backscattering analysis under channeling condition (RBS-C) was done for single crystal samples with 2 MeV $^4He^+$ beam from 3 MV single-ended accelerator in the TIARA facility (JAERI-Takasaki), in order to observe the damage produced in the crystals by ion irradiation.

RESULTS AND DISCUSSION

a. Dose dependence

Fig. 1 shows typical spectra of luminescence induced by 200 keV He^+ ion irradiation on poly-crystalline Al_2O_3:Cr at room temperature. The spectral position and the shape are the same as those obtained by photoexcitation. The main band centered at 695 nm can be ascribed to the R-line due to the electronic transition from ^2E states to $^4A_2$ states of Cr^{3+}, since its excitation spectrum corresponds to the electronic energy structure of Cr^{3+} in ruby (Nelson and Sturge, 1965). The luminescence yield changed with the irradiation dose, depending on the ion species, the enrgy and the type of the samples as shown in Fig. 2 and Fig. 3. In the case of Ar^+ irradiation, the luminescence yield decreases monotonously and rapidly with dose. The higher decreasing rate is obtained using lower ion energy. The rate of decrease is seen much higher for the single crystals than that for the poly-crystalline one. On the other hand, the intensity of the R-line induced by He^+ beam increases at the beginning of irradiation and then decreases with lower rate than that observed in Ar^+ irradiation. Similar results which show decreases of luminescence yield by ion irradiation are found in the previous works (Levy and Spie, 1985; Hollerman et al., 1992) for other crystals. The observed decrease of luminescence yield is considered to be related to radiation damege by ion irradiation, especially via elastic collisions. Most of kinetic energy is deposited to electronic system in He^+ irradiation while nuclear stoping power is relatively high in Ar^+ irradiation.

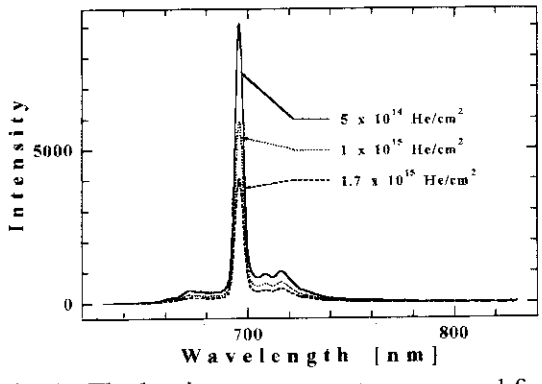


Fig. 1 The luminescence spectra measured for polycrystalline Al_2O_3:Cr during 200 keV He^+ irradiation at room temperature.

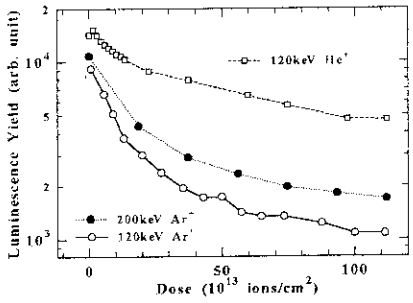


Fig. 2 The dose dependence of luminescence observed around 695 nm for Ar^+ and He^+ irradiated polycrystalline Al_2O_3:Cr.

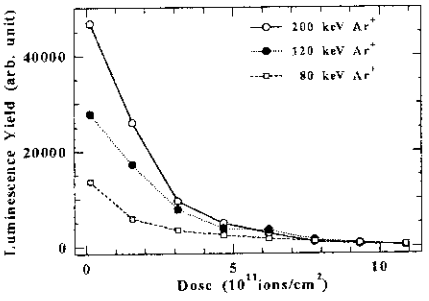


Fig. 3 The dose dependence of luminescence observed around 695 nm for Ar^+ irradiated single crystalline Al_2O_3:Cr.

b. Energy dependence

The energy depositing process by energetic ions is a function of the energy of ions as well as ion species. Then, the luminescence yield around 695 nm was measured for a short time repeatedly on the same sample with changing the incident energy, increasing and decreasing. For comparison, the same measurement was done for virgin samples.

Fig. 4, and 5 show the energy dependence of the yield of the ion beam inducesd luminescence of poly-crystalline sample for Ar^+ and He^+ irradiations, respectively. The irradiation time for each plot was 2.5 sec with ion current density of 25 and 64 nA/cm² for single crystals and polycrystals, respectively. In the case of Ar^+ irradiation, the curves of the yield for repeated irradiations are lower than that for the virgin sample at every ion energy. It shows that damage is accumulated in the samples by ion irradiation. Temperature effect is negligible here because of such short irradiation with relatively low energy and low current. On the other hand, the curve for decreasing energy of He^+ shows higher yields than those for virgin samples at the higher energy side. Together with the increase of the yield for He^+ irrdiation observed in Fig. 2, some enhancement mechanism seems to work via inelastic collisions in He^+ irradiation. Furthermore, the faster decrease of luminescence yield is seen in Fig. 3 for the single crystals than that for polycrystalline ones in Fig. 2. It can be also an evidence for the enhancement of luminescence yield occured by ion irradiation even for Ar^+

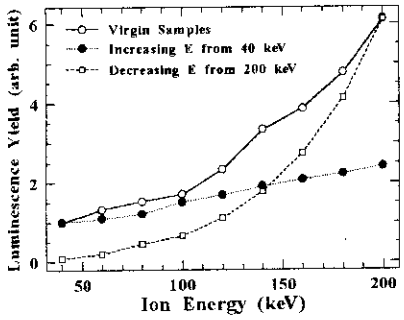


Fig. 4 The energy dependence of luminescence yield observed aroub 695 nm for Ar^+ irradiated Al_2O_3:Cr.

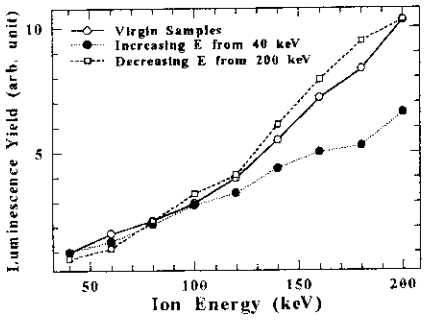


Fig. 5 The energy dependence of luminescence yield observed around 695 nm for He^+ irradiated Al_2O_3:Cr.

irradiation. As a mechanism for the enhancement, charge transfer can be consider to occur on Cr atom or the ion to produce Cr^{3+}. But there is no further experimental results which supports this possibility yet.

d. RBS-C analysis

Fig. 6 shows the random and the aligned RBS spectra of ruby single crystals irradiated at various doses with 200 keV Ar^+ ions. The aligned spectra show that the damage on the atomic structure by Ar^+ irradiation increases in the dose range of 10^{15} to 10^{16} ions/cm^2 and then the region extends to deeper region with the dose. The aligned spectrum of Al_2O_3:Cr with the lowest dose of 5 x 10^{14} ions/cm^2 shows very little damage in the surface layer. But the luminescence yield decreases by about two orders of magnitude at the dose of 10^{12} ions/cm^2. It may show that the luminescence process under ion irradiation is very sensitive to point defects in the single crystal.

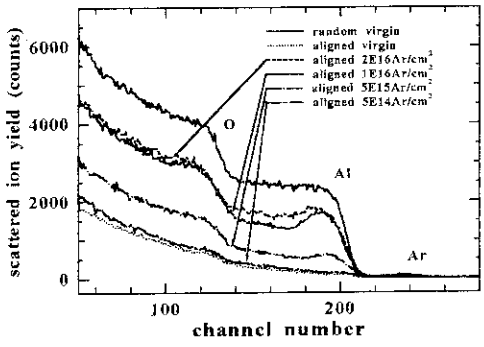


Fig. 6 The random and the aligned RBS spectra obtained with 2 MeV $^4He^+$ for single crystals of Al_2O_3:Cr irradiated with 200 keV Ar^+.

CONCLUSION

Luminescence spectrum during ion irradiation was measured for single- and poly-crystaline Al_2O_3:Cr as a function of irradiation dose at room temperature. Intense R-line luminescence of Cr^{3+} was observed at 695 nm in the spectrum and the yield was changed differently with irradiation dose, depending on the ion species, the energy and the type of sample. These results suggested that (1) damage induced by elastic and/or inelastic collision between incident ions and the crystals reduces the luminescence yield and (2) some electronic process induced by the inelastic collision, for example charge transfer process, forms Cr^{3+} to enhance the luminescence yield in the polycrystal of Al_2O_3:Cr. In addition, results of RBS-C analysis for Ar^+ irradiated single-crystalline Al_2O_3:Cr suggested that (3) the degradation of the luminescence process is much sensitive to damage produced by elastic collisions

References:

Abu-Hassan L.H., and Townsend P.D. (1988) Luminescence efficiency of silica during excitation. Nucl. Instr.and Meth. **B32**, 293.

Al Ghamdi A. and Townsend P.D. (1990) Ion beam excited luminescence of sapphire. Nucl. Instr. and Meth., **B46**, 133.

Dexter D.L. and Schulman J.H. (1954) Theory of concentration quenching in inorganic phosphors. J. Chem. Phys., **22**, 1063.

Hollerman W.A., Fisher J.H., Shelby G.A., Holland L.R. and Jenkins G.M. (1992) Spectroscopic analysis of proton-induced fluorescence from yttrium and gadolinium oxysulfide phosphors. IEEE Trans. Nucl. Sci., **39**, 2295.

Jaque F. and Townsend P.D. (1981) Luminescence during ion implantation of silica. Nucl. Instr. and Meth., **182/183**, 781.
Klick C.C. and Schulman J.H. (1951) Luminescence in solids. in "Solid state physics Vol.5" Eds. Seitz F. and urnbull D. Academic Press, N.Y., 119.
Levy P. and Spie P. (1985) Radiation Effects in Optical Materials., **541**, 22.
Nelson D.F. and Sturge M.D. (1965) Relation between absorption and emission in the region of the R lines of Ruby. Phys. Rev., **137**, A1117.
Townsend P.D. (1987) Optical effects of ion implantation. Rep. Prog. Phys., **50**, 501.

13.8 *Effect of Carbon K-shell Excitation on H^+ Desorption and Color Center Formation in Anthracene Crystal

Iwao SHIMOYAMA, Kazumichi NAKAGAWA, Aiko KIMURA, [1]Ryuzi KATO, [1]Masahiro KOTANI, [2]Tetsuji SEKITANI, [3]Jun'ya MARUYAMA and [2]Ken'ichiro TANAKA

Faculty of Human Development, Kobe University, Tsurukabuto,Nada-Ku,Kobe 657, Japan
[1]Faculty of Science, Gakushuin University, Mejiro, Toshima-Ku, Tokyo 171, Japan
[2]Photon Factory(KEK-PF), National Laboratory of High Energy Physics, Tsukuba 305, Japan
[3]Faculty of Engineering, Chiba University, Inage-Ku, Chiba 263, Japan

Abstract

we measured absolute values of quantum yield $\eta_c(h\nu)$ of color center formation and quantum yield $\eta_s(h\nu)$ of singlet excitons in anthracene single crystals as a function of soft X-ray photon energy $h\nu$. $\eta_c(h\nu)$ shows a resonance at the carbon K-shell energy, while $\eta_s h\nu)$ shows no resonance. A model to describe the energy dependence of $\eta_c(h\nu)$ and $\eta_s(h\nu)$ is suggested. Moreover, we report a result of our recent experiment on photo-stimulated desorption for condensed phase of benzene.

1. Introduction

Soft X-ray is a useful tool to study the effects of inner-core excitation on color center formation at the intermediate energy region between hard X-ray and ultraviolet light. At the energy region higher than K-shell energy, effects by secondary electrons are important and thus total amount of radiation effects are characterized by the magnitude of incident photon energy. For example, an effect produced by one photon with energy of 4 MeV is equal with that produced by a summation of one photon processes of two 2 MeV photons irradiated at different time. This is a key concept of the radiation chemistry. On the contrast, at the energy region at which the photochemistry is established, resonance is a key concept. For example, a 8 eV photon can ionize an anthracene molecule, but two 4 eV photons irradiated at different timing cannot.

The interesting subject at the soft X-ray energy region would be; which chemistry is important for inner-core excitation, i. e., radiation chemistry or photo-chemistry? In an attempt to study this subject, we measured absolute values of quantum yield $\eta_c(h\nu)$ of color center formation and quantum yield $\eta_s(h\nu)$ of singlet excitons in anthracene single crystals as a function of soft

X-ray photon energy $h\nu$. A model to describe the energy dependence of $\eta_c(h\nu)$ and $\eta_s(h\nu)$ is suggested. Moreover, we report aresult of our recent experiment on photo-stimulated desorption for condensed phase of benzene.

2. Experimental procedure and result

First, we describe for the experiments of measurements of absolute values of quantum yield $\eta_c(h\nu)$ of color center formation and quantum yield $\eta_s(h\nu)$ of singlet excitons[Kimura A. et. al. 1994].

Anthracene single crystals grown by the sublimation method were cooled to 200K in a cryostat.

Experiments were performed at the beamlines BL-11A and BL-12C of the Synchrotron radiation facility KEK-PF (Photon Factory of National Laboratory of High Energy Physics, Tsukuba, Japan). Monochromatized soft X-ray beams with $100 < h\nu < 600$ eV was irradi-ated to the sample and the florescence intensity $F_{sx}(h\nu)$ of S_1 exciton was measured by the photomultiplier with a V-Y45 glass filter and that intensity was compared with the fluorescence intensity Fs_{365} excited by the 365 nm light from a mercury lamp with a U-360 glass filter. Assuming the total number Ns_{365} of S_1 excitons produced by the 365 nm photons equal with the 365 nm photon number, we estimated the total number $N_{sx}(h\nu)$ of S_1 excitons produced by soft X-ray photons with energy $h\nu$ by $N_{sx}(h\nu)=Ns_{365}F_{sx}(h\nu)/Fs_{365}$. The quantum yield $\eta_s(h\nu)$ of singlet exciton formation was calculated by $\eta_s(h\nu)=N_{sx}(h\nu)/I_x(h\nu)$, where $I_x(h\nu)$ is the absolute intensity of the soft X-ray measured via photoelectron yield of a Au plate. The quantum yield $\eta_c(h\nu)$ of color center formation was calculated by $\eta_s(h\nu)=N_{cx}(h\nu)/I_x(h\nu)$, where $N_{cx}(h\nu)$ is the absolute values of total number of the color centers produced by the irradiation of soft X-rays with energy $h\nu$. Values of $N_{cx}(h\nu)$ were estimated via S_1 exciton fluorescence quenching technique [Kimura A. et. al. 1994]. Fig. 1 and 2 show absolute values of $\eta_s(h\nu)$ and $\eta_c(h\nu)$.

Desorption of H^+ and other ions from condensed benzene were measured at 77 K by a custom chamber designed by M. C. K. Tinone and K. Tanaka, which equipped with a powerful quadrapole mass spectrometer. Figures 3 and 4 show the mass spectra obtained with excitation energy of 380 eV and 600 eV. Quantum yield of H^+ ion desorption is shown in Fig. 5.

3. Discussion

3-1. Quantum yields of formation of color center and singlet excitons

We assumed that both singlet excitons and color centers are produced via both primary resonance effects and secondary effects due to secondary electrons.

The former includes conversion of an anthracene ion with a hole in the valence level due to resonance ionization of the valence electron to the color center and so on. We assumed proportional relation of the magnitude of the secondary effect to the electron energy, which was the key concept of the radiation chemistry. The final form of our model equations are;

$$\eta(h\nu)= \frac{\mu_v}{\mu}\{\eta_v+\eta_2\cdot(h\nu-E_v)\}+\frac{\mu_K}{\mu}\{\eta_{vv}+\eta_2\cdot(h\nu-E_K)+\eta_2\cdot(E_K-2E_v)\}$$

where μ_v and μ_K is absorption coefficient of valence and K-shell electrons, respectively. μ_v and μ_K are functions of $h\nu$. E_v and E_K is binding energy of valence and K-shell electron. η_v and η_{vv} is conversion yield of anthracene molecules with one and two holes at valence levels to color center. Solid lines in Fig. 1 and 2 show best fit curves of above equations to experimental values. The best fit values of parameters are $\eta_2=1.2\times10^{-4}$ (color centers/eV), $\eta_v=4.6\times10^{-2}$ (color centers/photon) and $\eta_{vv}=0$ (color centers/photon) for the case of $\eta_e(h\nu)$; $\eta_2=1.2\times10^{-4}$ (S_1 excitons/eV), $\eta_v=0$ (S_1 excitons/photon) and $\eta_{vv}=0$ (S_1 excitons/photon) for the case of $\eta_s(h\nu)$. As seen from the figures, experimental results were well produced by our models.

The next problem is why η_e decreases just above the carbon K-shell energy. Since the color center detected by our method is a hydrogen-added type radical [Chong and Itoh, 1976], we can make a postulate in which hydrogens can escape easily from anthracene surface and this easiness should be enhanced at energies near carbon K-shell energy because strong absorption at k-edge energy means the small penetration depth of soft X-ray photons of these energies. In an attempt to check this postulate, we made the experiment in which we measured the quantum yield of H^+ ion desorption as a function of excitation energy.

3-2. Desorption of H^+ and other ions from condensed benzene.

From figures 3, 4 and 5, it is clear that H^+ ion desorption is not dominant at the energies near the carbon K-shell energy. Fig.3 seems to imply that fragmentation reaction is dominant at this energy region. We are planning the next experiment to study what is happening by the irradiation of soft x-ray to these materials.

Reference

Chong T. and Itoh N., Phys. Status Solidi B74(1976)111.
Kimura A. et. al., Nucl. Instr. and Meth. B91(1994)67-70.

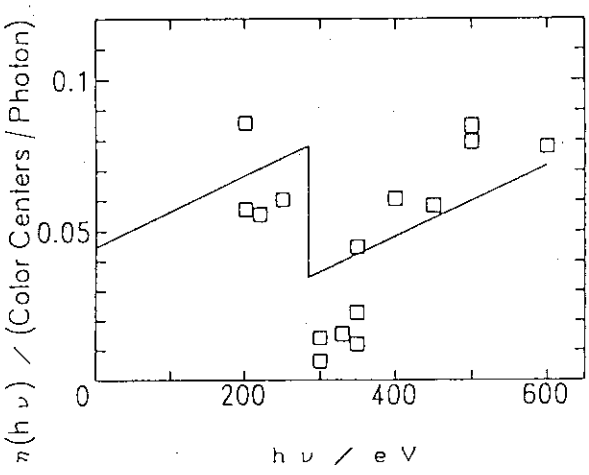


Fig. 1 Color center formation quantum yield η_c.

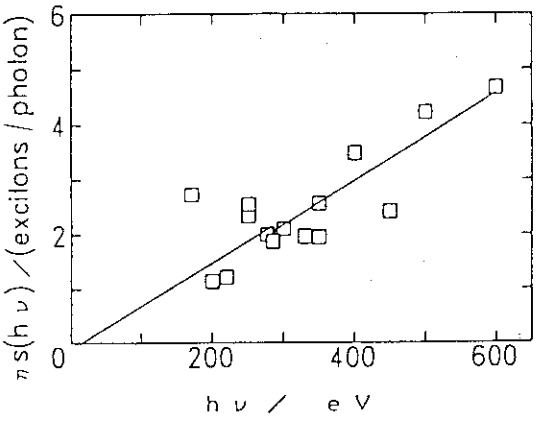


Fig. 2 S_1 Exciton formation quantum yield η_e.

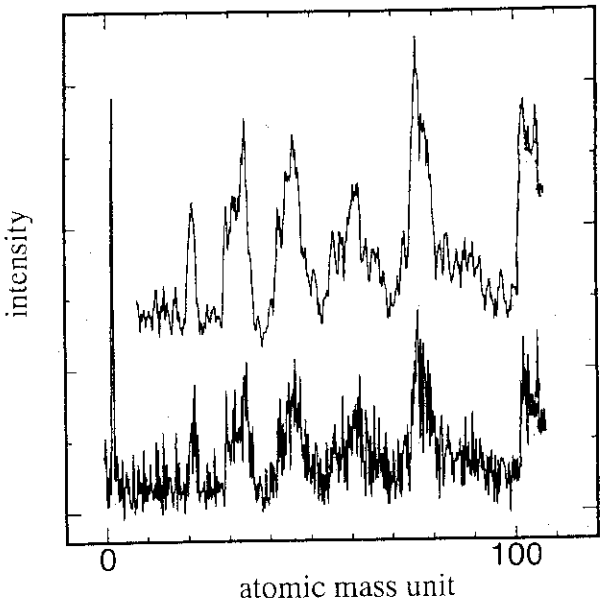


Fig. 3 Mass spectrum at $h\nu$ = 380 eV.

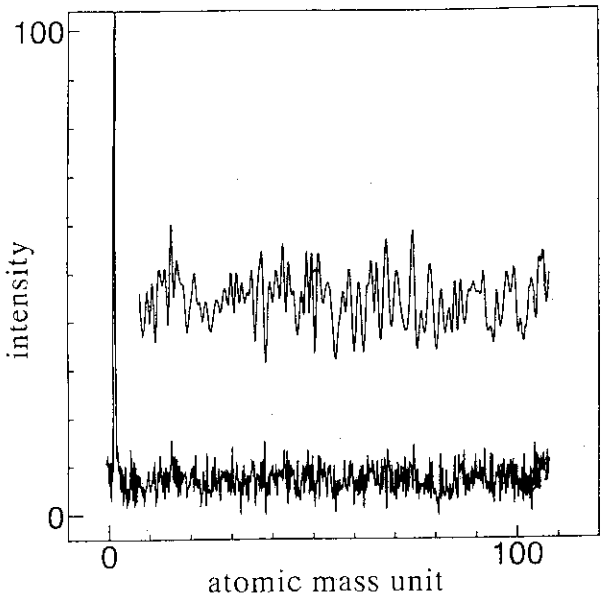


Fig. 4 Mass spectrum at $h\nu$ = 600 eV.

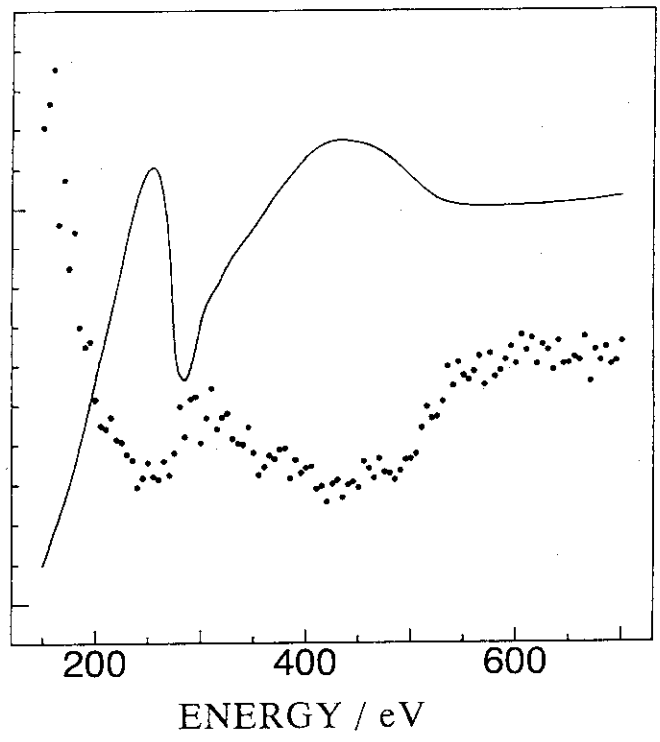


Fig. 5 Yield spectrum of H^+ ion(•).

14. Radiation Processing (2)

14.1 *A Research on Gas-phase Grafting of Acrylic Acid onto Polytetrafluoroethylene by Preirradiation

Hu Fumin, Fen wen

Chengdu Research Centre for Silicone, Ministry of Chemical Industry, Chengdu, 610041 P. R. China

Wang Yufang, Huang Guanglin

Sichuan University, Chengdu, 610064, P. R. China

Abstract The gas-phase grafting of acrylic acid by preirradiadition onto polytetrafluoroethylene was studied kinetically. The correlation between the degree of grafting and preirradiation conditions, grafting temperature, time and film thickness was analyzed. The effect of t apped radical formed upon preirradition on grafting was discussed.

INTRODUCTION

Gas-phase grafting techique by preirradiation is an effective approach for modification of polymer materials and preparation of functional polymer materials. Recently more attention has been paid to modification of fluoro-containing polymer because of its excellent chemical stability, high physical and thermo-mechanical properties. Grafting of acrylic acid (AA) onto these polymer materials may provide them with a series of special properties such as hydrophilic, ion-exchange property and increased adhesiveness. Many studies have been reported for preirradiation grafting onto fluoro-containng polymer in liquid phase(1. 2. 3.). However there are few papers dealing with grafting in gaseous phase(4).

In the present paper the gas-phase grafting of acrylic acid by preirradiation onto polytetrafluoethylene was studied kinetically. The relation between preirradiation conditions, grafting temperture, grafting time, film thickness and the degree of grafting was analyzed. The effect of trapped radical formed upon preirradiation grafting was discussed by ESR method.

EXPERIMENTAL

Materials

PTFE film (specific gravity 2. 2g/cm^3, Chenguan Plant of Chemical Industry) was washed with ethynol and dried at room temperature. Reagent-grade acrylic acid (Beijiang plant of chemical reagent) are added with appropriate quantity of hydroquinone as an inhibitor before use.

Preirradiation

A piece of accurately weighted PTEE film was charged into a special glass ampoule, evacuated for 4 hr under reduced pressure 1×10^{-3} mmHg, and then subjected to γ-ray irradiation from ^{60}Co at room temperature.

Post-graft polymerisation

The irradiated ampoule was once again jointed with vacuum system, to which the vessel containing AA was attached. When reduced pressure was reached to $1x10^{-3}$ mmHg, the monomer was frosen and refrosen by liquid nitrogen to remove air from the monomer. This procedure was repeated three times. Afterward, the monomer was transfered into the special ampoule under high vacuum by low temperature distillation. After the ampoule was sealed off from the vacuum system, it was put in water bath to start graft polymerisation under certain conditions. The grafted PTFE film thus obtained was removed and washed thoroughly with hot distilled water. The film was then dried in vacuum at 60℃ for 24hr and weighed. The degree of grafting was determined by its percentage increase in weight. The concentration of radicals was taken on a BRUKER ESR Spectrometer.

RESULTS AND DISCUSSION

Effect of Preirradiation Dose

Figure 1 shows the graft-time curves at various preirradidation dose. The degree of grafting at first increases rapidly with time and then comes a constant value gradually. We can see that the degree of grafting increases with increasing preirradiation dose when the dose is lower then 48kGy (Fig. 1a) and decreases with dose when higher than 48kGy (Fig. 1b). The dose exponents of the grafting rate was found to be approximately 0. 35 and -0. 17 order for lower and higher dose respectively (Fig. 2).

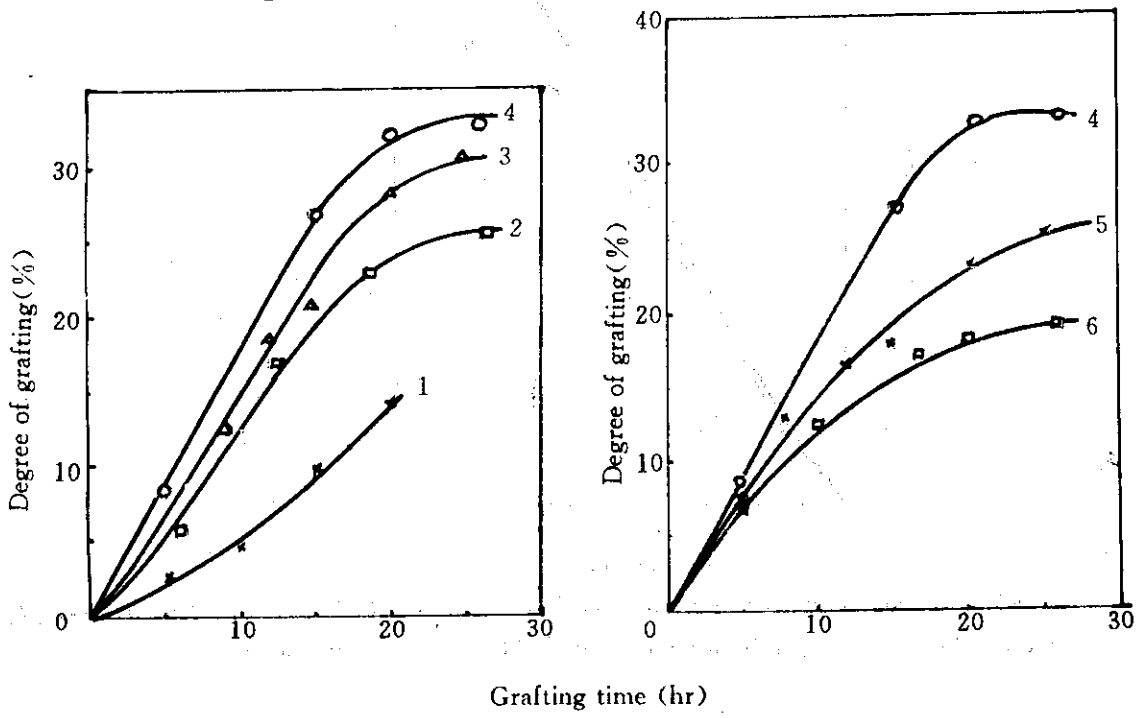


Fig. 1 Graft yield vs. time at various preirradiation doses. (1. 10kGy; 2. 12kGy; 3. 27kGy; 4. 48kGy; 5. 70kGy; 6. 96kGy); Grafting temp., 50℃; film thickness, 0. 10mm, dose rate, 1. 32kGg/sec.

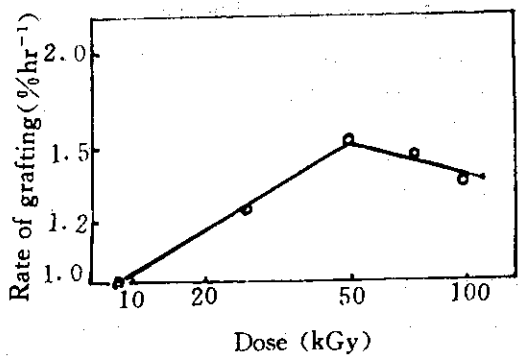


Fig. 2 Logarithmic plots of grafting rate vs. preirradiation dose. Grafting conditions same as in Fig. 1

Irradiation of initial fluoro-containing polymer under vacuum results in accumulation of radical. When dose reaches a certain does (50kGy) the accumulation of radical will be ended due to the recombination of themselves (4). Meanwhile the rate of radical accumulation slightly decreases with increasing preirradiation does rate (Tab. 1). This is due to increasing of the radical concentration at increased dose rate and easiness of recombination of themselves. The effect of does rate on the grafting of PTFE at the same dose is shown in Fig. 3.

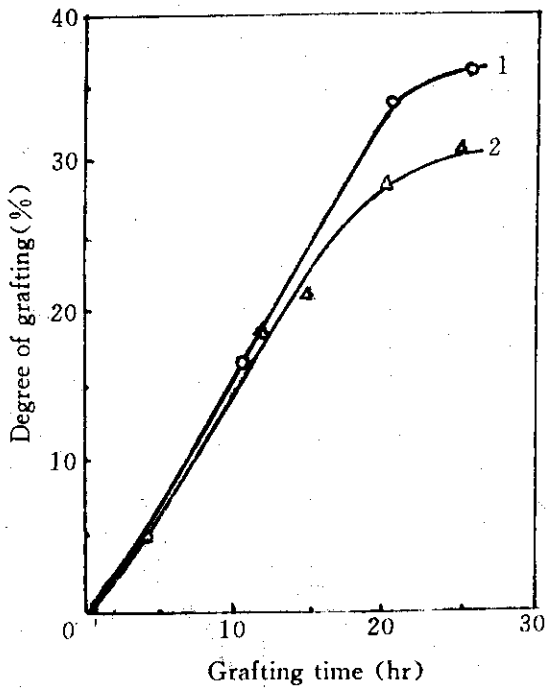


Fig. 3. Graft yield vs. time at various preirradiation dose rate (1. 0.51kGy/sec; 2. 1.32kGy/sec.); preirradiation dose, 25kGy; grafting temp., 50℃; film thickness, 0.10mm.

Table 1. ESR measurment of irradiated PTFE at different dose rate

irradiation does (kGy)	dose rate (Gy/sec)	Spin N×10^{17}/g
26	1.32	6.3
24	0.513	7.1

Effect of Grafting Temperature

Fig. 4 shows the graft yield-time curves obtained at different temperature. We can see that the rate of grafting increases with increasing temperature until 50℃ and then decreases with increasing temperature. It may be explained by the increasing of monomer vapour concentration, diffusibility into PTFE matrix and reactivity of trapped radicals. When the grafting temperature is higher than 50℃ the rate of grafting decreases with the increasing of temperature (Fig. 5). It is concerned not only with the temperature dependence of growth and destruction of kinetical chains, but also the increasing of initial radicals termination with the increasing of temperature and also the temperature dependence of monomer diffusion and sorbtion coefficient. These factors are competitable between themselves at various temperature.

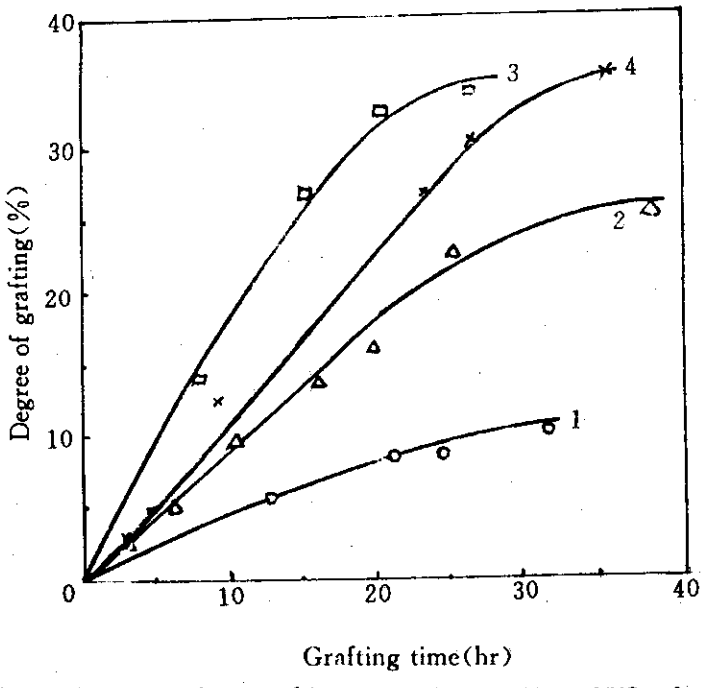


Fig. 4 Graft yield vs. time at various grafting temperatures (1. 25℃; 2. 40℃; 3. 50℃; 4. 60℃). Preirradiation dose, 48kGy; dose rate, 1.32Gy/sec; film thickness, 0.1mm.

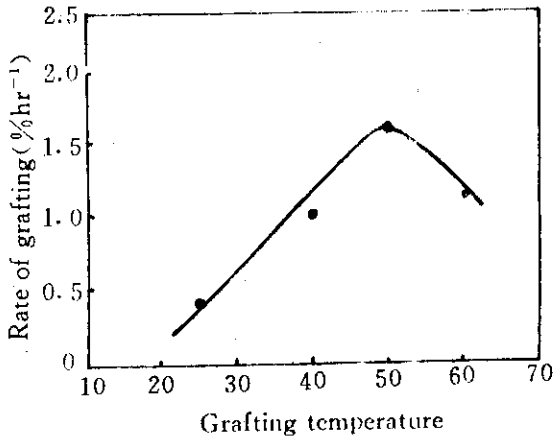


Fig. 5. Rate of grafting vs. grafting temperature
Grafting condiation same as in Fig. 4.

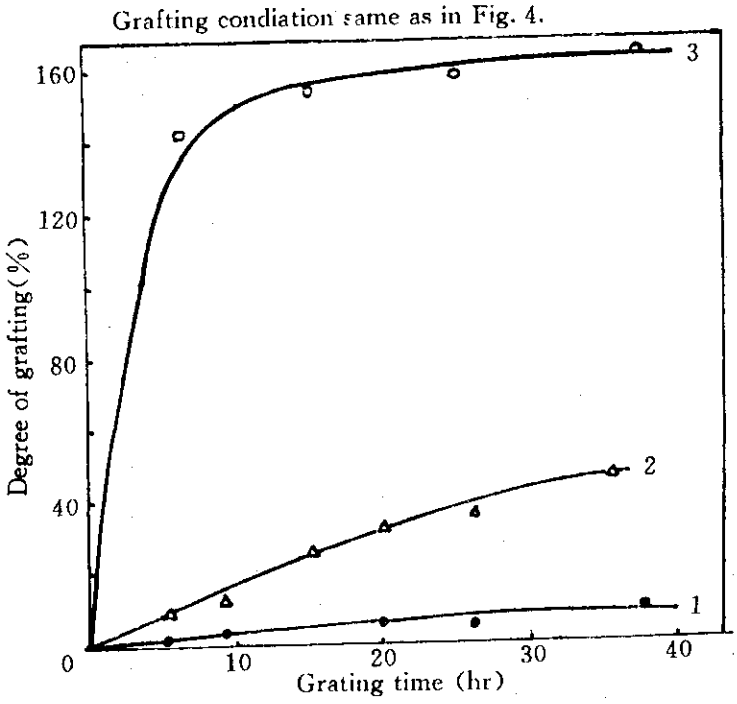


Fig. 6. Graft yield vs time at various film thickness (1. 0.5mm; 2. 0.1mm; 3. 0.015mm)
Preirradiation dose, 48kGy; dose rate, 1.32Gy/sec; grafting temperature, 50℃.

Effect of Film Thickness

Figure 6 shows the graft yield-time curves for the film with various thickness. We can see in Fig. the grafting rate and degree of limited grafting decrease with increasing film thickness. The results shown in Fig. 6 were analyzed by taking account of weight increase per unit surface area of the film as shown in Fig. 7. The initial rate of weight increase per unit surface area was found to be a slightly linear decrease with increasing film thickness. The final weight of grafted polyacrylic acid per unit surface area is linearly proportional to the thickness.

All these results mentioned above show that, in this gas-phase grafting system, the grafting begins at the region close to the surface and then proceeds gradually into the center of

the film. Just as in the liquid phase grafting, the gas-phase grafting system is mainly controlled by the monomer diffusion.

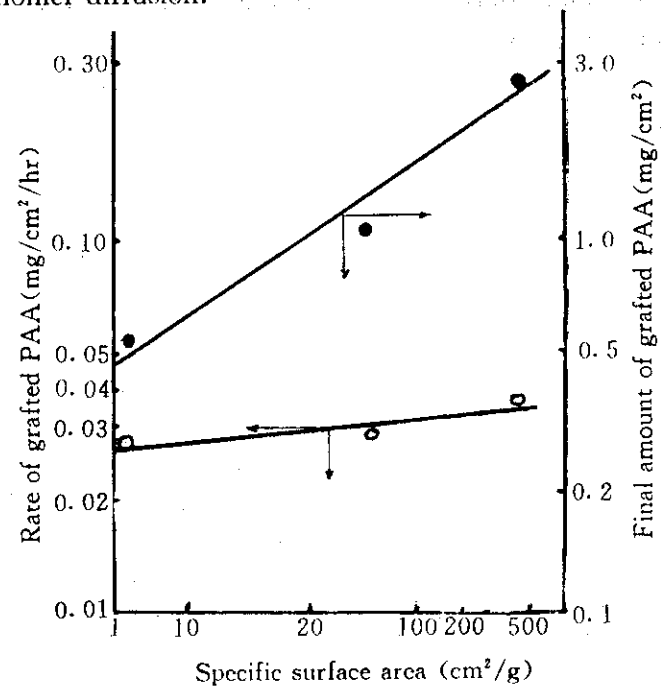


Fig. 7. Logarithmic plots of rate of grafted PAA and final weight increase per unit surface area vs. specific surface area of film. Grafting condition same asin Fig. 6.

CONCLUSIONS

The gas-phase grafting of acrylic acid onto polytetrafluoroethylene film has been studied by using a preirradiation technique. From the experimental results mentioned above we can make the following conclusions:

(1) The dependences of the gas-phase grafting rate on preirradiation dose were found to be 0.35 and ~0.17 order for lower and higher dose respectively.

(2) The dependences of the grafting rate showed that the lower the dose rate, the deeper the grafting proceeds.

(3) The grafting temperature affects both the reactivity of radical and the gaseous pressure of monomer.

(4) The relationship between the grafting and film thickness was found to give a certain linear dependence.

References

1. El-SAYED A. HEGAZY, ISAO ISHIGAKI, and JIRO OKAMOTO, J. Appl. Polym. Sci., 26, 3117-3124 (1981)
2. S. A. Pavlov, Ye. A. Ragol'skaya, A. A. Abyshew, E. N. Teleshov Vysokomol. soed., Ser A 32, 2438-2445 (1990)
3. Ye, A. Ragol'skaya, S. G. Prutchenko, S. A. Pavlov, E. N. Teleshov. Vysokomol.

Soed., Ser A. 32, 495-501 (1990)
4. S. A. Pavlor, Ye, A. Ragol'skaya, A. A. Alyshev, E. N. Teleshov. Vysokomol, Soed., Ser B 31, 864-867 (1989)

14.2 Radiation Induced Graft of Acrylonitrile on Silk Protein in $ZnCl_2$ Solution

Zhicheng Zhang and Jiegen Chu

Department of Applied Chemistry, University of Science and Technology of China, Hefei 230026, China

Abstract Camma-ray induced graft of acrylonitrile on silk protein in the solution of 60wt% $ZnCl_2$ was carried out. The effects of absorbed dose (D), dose rate (I), the concentrations of monomer, silk protein and certain metal ions (Cu^{++}or Fe^{3+}) were examined. It was found and discussed that the initial graft efficiency is mainly determined by [S]/([S]+[M]), where [S] and [M] are the concentrations of silk protein and monomer, respectively; furthermore, the graft efficiency increases with the increase of absorbed dose. It was noticed that the existence of Cu^{++} or Fe^{3+} has a strong inhibition effect on the molecular weight of grafted chain, and almost no effect on graft yield and efficiency. An attempt to spin the filament of the copolymer by solution spining method has been made.

INTRODUCTION

Grafting of vinyl monomer onto silk has been investigated by several groups (Nayak et al, 1978; Nayak et al, 1981; Pati et al, 1979; Tsukada, 1990; Tsukada, 1988; Arai, 1971). All of the graft copolymerization were carried out in heterogeneous systems composed of two phases: certain monomer solutions and silk fibers as the bases. In that case, both the ratio of surface area to mass of silk fiber and the diffusion rate of monomer into the fiber must be the importand factors which affect the graft reaction seriously and bring about a complicated mechanism. Moreover, from the point of view of waste silk reutilization, the heterogeneous graft method is unsuitable, because the resultant can not be used directly.

Very little attention has been paid for the grafting copolymerization in homogeneous system (Yamamoto et al, 1975). In fact, no reference about graft copolymerization of silk protein in homogeneous system has been found. In this paper we presental the results of studies of grafting acrylonitrile on silk protein in 60% $ZnCl_2$ solution, γ-ray radiation was used to induce the grafting copolymerization.

EXPERIMENTAL

Materials: Silk fibroin fibers were obtained by scouring raw silk in an aqueous solution containing 0.4% soap for 2hr and washing with 0.05% sodium carbonate solution followed by boiling water. Acrylonitrile (AN) was distilled under normal pressure before use, zinc chloride (A.R.), copper chloride (A.R.), ferric chloride (A.R.), N,N-dimethylformamide (DMF) (A.R.) and acetic acid (A.R.) were used directly. The purified silk fibers were dissolved in 60% zinc chloride solution at the temperature of 60~70℃. After the solution cooling down, the required amount of monomer, $CuCl_2$ or $FeCl_3$ were added in.

Irradiation: The solution as prepared above were irradiated by ^{60}Co-γ-ray at 25℃ and at certain dose rates for 10~70 minutes, and the graft copolymerization were carried out during the irradiation period. After irradiation the samples were kept in static state for 2hr.

Measurements: The resultants were poured on a plate glass and made into membranes, which were washed with water and then with 2% acetic acid. The washed membranes were dried and weighed (W_1), then extracted with DMF for 48 hr to remove the homopolymers, dried again and weighed (W_2).

$$\text{Grafting}(\%) = (W_2 - W_0)/W_0 \times 100\% = \Delta W/W_0 \times 100\% \quad (A)$$

where W_0 is the original weight of silk fibroin, ΔW for the inceease of weight. The conversion of AN was calculated as follows:

$$\text{Conversion}(\%) = [W_1 - W_0)/W_M] \quad (B)$$

where W_M is the weight of added monomer. The grafting efficiency was obtained from:

$$\text{Grafting efficiency}(\%) = (W_2 - W_0)/(W_1 - W_0) \quad (C)$$

The dried membrane of graft copolymer was immersed in 6N HCl solution at 95℃ for 2 hr to make the substrate polymer hydrolysis. The residua were washed, dried, weighed and ground to powder. Then the average molecular weight of PAN graft side chains was measured viscometrically by its DMF solution at 30℃ and calculated from:

$$[\eta] = 3.976 \times 10^{-4}[\overline{M_\eta}]^{3/4} \quad (D)$$

Moreover, some additional measurements, such as IR, TGA were also carried out. An attempt to spin the filament of the copolymer by solution spining method was made.

RESULTS AND DISCUSSION

The factors affecting γ-ray induced grafting copolymerization of AN onto silk protein were investigated. Variable studied included absorbed dose rate, monomer concentrations, silk protein concentration, Cu^{++} or Fe^{3+} concentrations. The solution of 60% $ZnCl_2$ were used as the solvent for all of the cases due to its capability of dissolving the silk protein and monomer as well as the resultant.

1. Theoretical preparation

A probable mechanism of radiation induced grafting copolymerization can be described as follows:

Initiation

$$H_2O \longrightarrow 2R^{\cdot}\ (\text{including } H^{\cdot},\ {}^{\cdot}OH, \cdots\cdots) \quad (1)$$

$$\sim SH + R^{\cdot} \longrightarrow \sim S^{\cdot} + HR \quad (2)$$

$$\sim S^{\cdot} + M \longrightarrow \sim SM^{\cdot} \quad (3)$$

$$R^{\cdot} + M \longrightarrow RM^{\cdot} \quad (4)$$

Propagation

$$\sim SM_n^{\cdot} + M \longrightarrow SM_{n+1}^{\cdot}\ (\text{grafting}) \quad (5)$$

$$RM_m^{\cdot} + M \longrightarrow RM_{m+1}^{\cdot}\quad (\text{homoplymerization}) \quad (6)$$

Termination

$$\sim SM_n^{\cdot} + R^{\cdot} \longrightarrow \text{grafted polymer} \quad (7)$$

$$RM_m^{\cdot} + R^{\cdot} \longrightarrow \text{homopolymer} \quad (8)$$

$$RM_m^{\cdot} + RM^{\cdot} \longrightarrow \text{homopolymer} \quad (9)$$

$$\sim SM_n^{\cdot} + \sim SM_{n'}^{\cdot} \longrightarrow \text{grafted polymer} \quad (10)$$

$$\sim SM_n^{\cdot} + RM_m^{\cdot} \longrightarrow \text{grafted polymer} \quad (11)$$

where ~SH=silk protein, M=monomer.

2. Effects of absorbed dose and dose rate.

From Fig. 1 it can be seen that the graft yields increase with the increase of irradiated time and then reach a plateau in the higher dose range. The higher dose rate is, the higher graft yield is for a certain irradiation time. It is

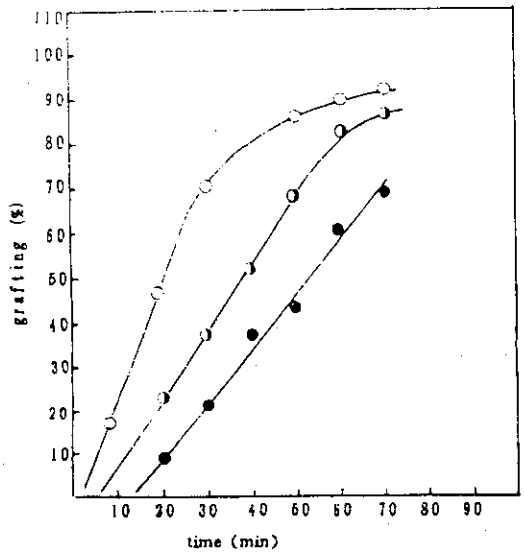


Fig. 1. Grafting yield vs irradiation time for several sose rate; a) 23.32Gy/min; b) 6.30Gy/min; c)3.16Gy/min; Silk protein; monomer; solvent = 4; 8.866; 100, T = 25℃

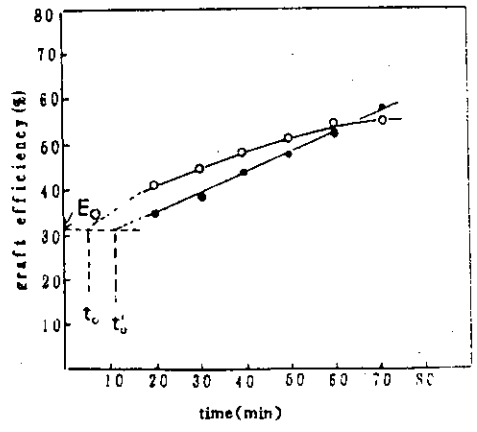


Fig. 2. Graft efficiency vs irradiation time for the dose rates; (○) 6.30Gy/min; (●) 3.16Gy/min, t_0 and t_0' show the induction periods for the corresponding dose rate, R_0 shows the initial graft efficency. Silk protein; monomer; solvent = 4; 8.866; 100, T = 25℃

easy to understand because that a higher dose rate means a higher radical concentration, so that a higher reaction rate. Several additional informations can be obtained from Fig. 2: (a)The grafting efficiency increases with the increase of

irradiated time (or absorbed dose), it can be considered as the result of reaction(11). The second possible reason for the increase of the grafting efficiency is the radiation induced closelinking between the copolymer and homopolymer. (b)The initial grafting efficiency (E_0) is about 31% which just equals $W_0/(W_0+W_M)=4/(4+8.866)$. It means both the initial reactions (2)and (4)are controled by the diffusion of $R^{\cdot}$, so that they have the same rate canstant. (c) A higher dose rate corresponds to a higher grafting efficiency for a certain irradiation time, it can be ascribed to the relatively higher conversion of monomer and so that to reaction (11).

From Fig. 3 and Fig. 4 it is seen that; a) the average molecular weight of the grafted chains decrease with the increase of the irradiation time (Fig. 3) and the conversion of AN(Fig. 4), b) a higher dose rate corresponds to a lower molecular weight. As we know from the theoretical preparation section, the molecular weight of grafted chain is mainly determined by both the propagation rate of reaction (5) and the termination rate of reaction (7), i. e. molecular weight$\sim k_5[M]/k_7[R^{\cdot}]$. A longer irradiation time corresponds to a higher conversion of monomer, as a result the laterly produced side chain has a smaller molecular weight than the formerly formed one, thus the average molecular weight decreased. A higher dose rate gives a higher $[R^{\cdot}]$, so that a smaller molecular weight.

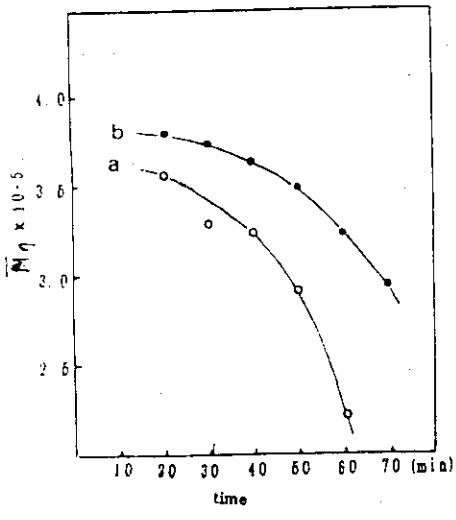


fig. 3. $\overline{M\eta}$ vs irradiation time for the dose rates (○) 6. 30Gymin; (●) 3. 16Gy/min. Reaction system is the same as that for Fig. 1

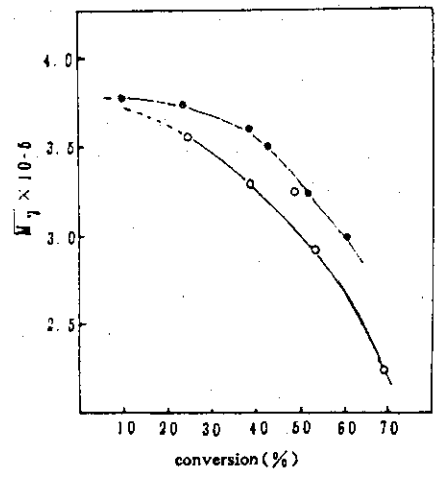


Fig. 4. $\overline{M\eta}$ vs the conversion of monomer at the same conditions as that for Fig. 3

3. Effects of the concentrations of monomer and silk protein

It has been noticed that the moment graft efficiency is mainly determined by the rates of reactions(2) and (4), i. e. $E_g=R_2/(R_2+R_4)$. For the diffusion controled mechanism, both reactions (2) and (4) have the same rate constants, then the above relationship can be rewrited as;

$$E_g=[S]/([M]+[S]) \qquad (D)$$

where [S] can be seen as a constant (i. e. $[S]\approx[S]_0$) for a certain system, while [M] decreases with the reactions carried out. From the above equation, it is easy to understand the fact shown in Fig. 5, i. e. the grafting efficiency decreases with the increase of AN concentration. As a qualitative evaluation, using the relationship (D) for a certain conversion we can obtain;

$$\text{graft yield}\sim[M]/([M]+[S]) \qquad (E)$$

From the above relationship, it is clear that the graft yield increases with the increase of monomer concentration as the fact shown in Fig. 5, and on the other hand it decreases with the increase of silk protein concentration as shown in Fig. 6. Another fact shown in Fig. 6 is the average molecular weight dcreases with the increase of [S]. A probable explanation for this is that the increase of silk protein concentration brings about the increase of total concentration of various radicals because the recombination of initial radical ($H^{\cdot}$ and $^{\cdot}OH$....)is inhibited to a lelatively larger extent by reaction (2). According to the relationship;

$$(X_n)_g\approx R_S/R_t=k_5[M]/k_7[R^{\cdot}] \qquad (F)$$

where $[R^{\cdot}]$ shows the total concentration of all radicals, the average molecular weight of side chain decreases with the increase of $[R^{\cdot}]$. By the above relationship, we also can explain the fact shown in Fig. 7. i. e. the average

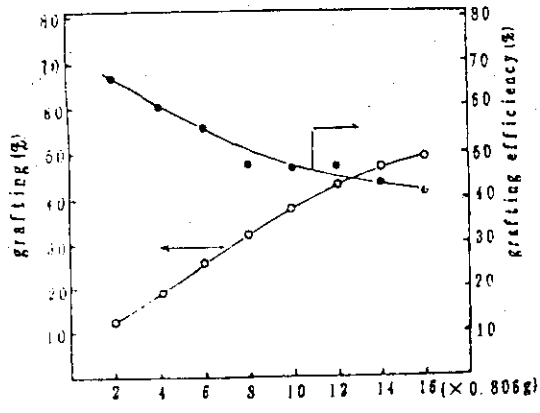


Fig. 5. Effects of monomer concentration on grafting yield (○) and grafting efficiency (●). Silk protein/Solvent = 4/100; I = 6. 30Gy/min, t = 30min; T = 25℃

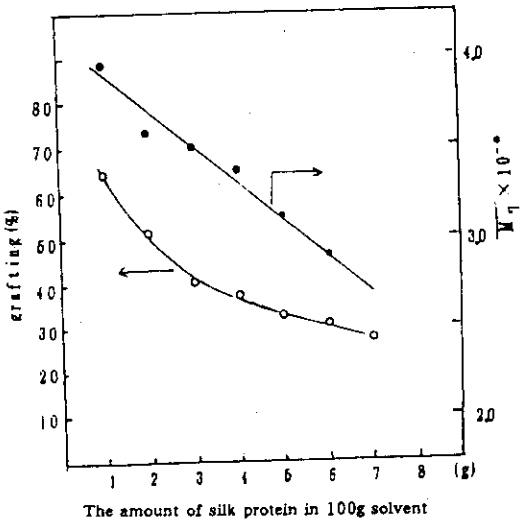


Fig. 6 Effects silk protein concentration on grafting yield (○) and $\overline{M\eta}$ (●). Monomer/Solvent = 8. 866/100; I = 6. 30Gy/min; t = 300min; T = 25℃

molecular weight increases with monomer concentration up to about 6% and than decreases with further increase of monomer concentration due to the increasing k_7 caused by the decrease of the system viscosity.

4. Effects of Cu^{++} and Fe^{3+}

From Fig. 8, it can be found that the existence of Cu^{++} or Fe^{3+} in solution can cause a large decrease of average molecular weight. A probable mechanism for this is described as follows:

$$\sim SM^{\cdot} + Cu^{++}\,(\text{or } Fe^{3+}) \longrightarrow \sim SM^{+} + Cu^{+}\,(\text{or } Fe^{++}) \quad (12)$$

$$\sim SM_n^{+} + Cl^{-} \longrightarrow \text{dead chain} \quad (13)$$

$$Cu^{+} + H^{+} + \sim SH \longrightarrow \sim S^{\cdot} + Cu^{++} + H_2 \quad (14)$$

According to the above scheme, the existence of Cu^{++} and Fe^{3+} can decrease the molecular weight by reaction (12) followed by reaction (13). The Cu^{+} produced in reaction (12) is oxidated to Cu^{++} again in reaction (14), at the same time a new active radical is produced. As a result, Cu^{++} shows a much larger efficiency to regulate the side chain molecular weight than Fe^{3+} at the lower concentration region. According to the above mechanism, it can be predicted that the effect of Cu^{++} on graft yield must be very small, it is testified by the data shown in table 1.

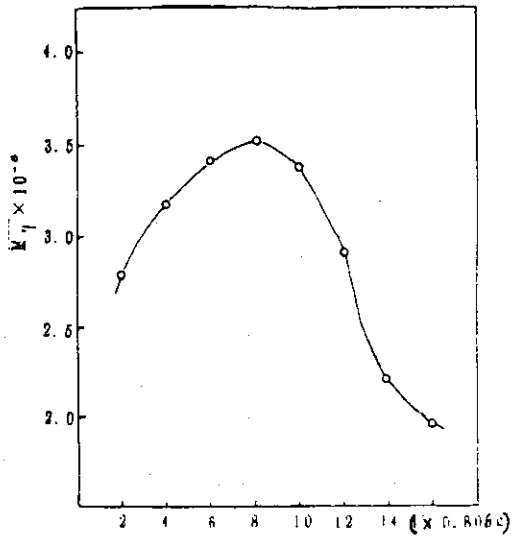


Fig. 7 $\overline{M\eta}$ vs monomer concentration at the same condition for Fig. 5

In fact, existence of Cu^{++} brings about an increase of the conversion, it can be ascribed to an increase of reaction rate due to the lower viscosity which is corresponding to the lower molecular weight of produced polymer and copolymer. The decrease of grafting efficiency can be ascribed to that reaction (11) is cut out due to the chain transfer action of Cu^{++}.

Table 1. Effects of Cu^{++} on graft reaction

$[Cu^{++}]$(ppm)	0	11. 62	23. 24	34. 88	46. 48	58. 1
graft yield (%)	37. 5	36. 8	37. 5	37	38	36. 4
conversion of AN (%)	38	45	46. 1	45. 8	46. 5	44. 6
grafting efficiency (%)	44. 5	36. 9	36. 7	36. 5	36. 9	36. 8

I = 6. 30Gy/min, t = 30min; T = 25℃; silk protein : monomer : Solvent = 4 : 8. 866 : 100

5. Properties of graft copolymer

The infrared spectra of grafted copolymer (a) and silk protein (b) are shown in Fig. 9. The strong absorption

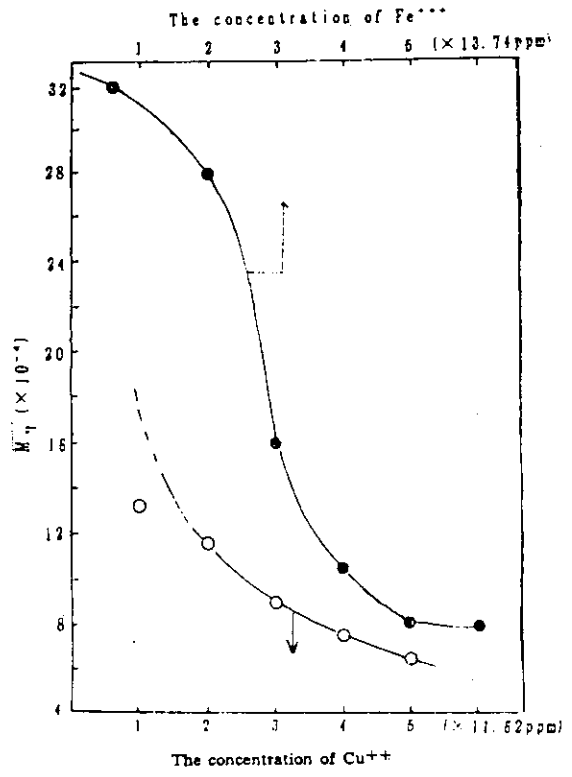


Fig. 8 Effect of [Cu++] (○) and [Fe3+] (●) on $\overline{M_\eta}$. silk/monomer/solvent = 4; 8.66; 100; I = 6.30Gy/min; t = 30min; T = 25℃

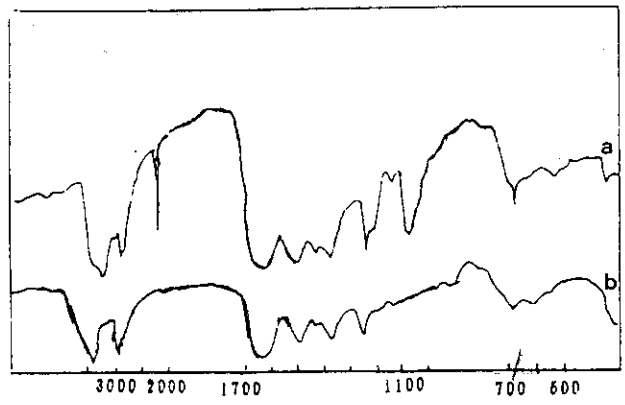


Fig. 9 Infrared spectra of copolymer (a) and silk protein (b)

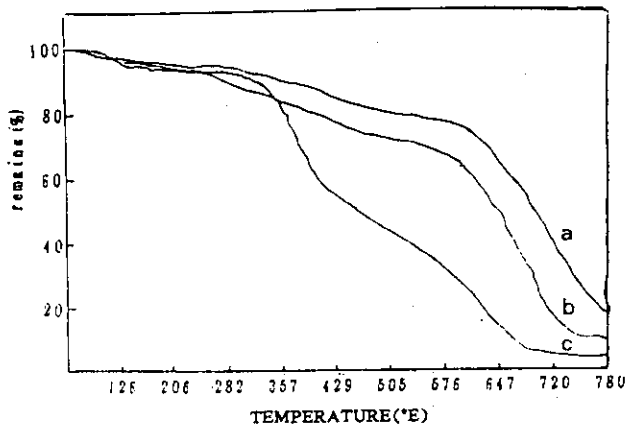


Fig. 10 TGA curves of grafted copolymer(a), PAN(b) and silk(c)

peak at 2200cm^{-1} of grafted copolymer is ascribed to -CN. Fig. 10 gives us the TGA curves of grafted copolymer (a), PAN (b) and silk (c), it is very interesting to note that the grafted copolymer shows the best thermostability among them.

An attempt to spin the filament of copolymer by solution spining method was made, the main parameters were shown in Table 2. The strength of obtained fiber was ~4g/den.

Table 2: Parameter of spining solution

$[polymer]_{total}$	grafted copolymer in polymers	graft yield	$\overline{M}_\eta$	aperture diameter	total draw ratio
6.8%	71.5%	37.2%	3.2×10^5	0.1mm	11.4

REFERENCES

Arai K., Negishi M., Komino S., and Tankada K. (1971) *Appl. Polym. Symp.*, **18**, 545.

Nayak P. L., Lenka S. and Pati N. C. (1981) *Angew. Makromol. Chem.*, **96**, 131.

Nayak P. L., Lenka S. and Pati N. C. (1979) *J. Appl. Polym. Sci.*, **23**, 1345.

Pati N. C., Lenka S. and Nayak P. L. (1979) *J. Macromol. Sci.-Chem.*, **A13**, 1157.

Tsukada M. (1988a) *J. Appl. Polym. Sci.*, **35**, 2133.

Tsukada M. (1988b) *J. Appl. Polym. Sci.*, **35**, 965.

Tsukada M. (1990) *J. Appl. Polym. Sci.*, **39**, 1289.

Yamamoto K. et al (1975) *Kobunshi Ronbunshu*, **32**, 295.

14.3 Effects of Preirradiation Graft Polymerization of Acrylic Acid onto Polyethylene Film

Feng Wen, Hu Fumin
Chengdu Research Center for Silicones, Ministry of Chemical Industry, Chengdu, 610041, China
Yuan Lihua, Zhu Po, Chen Zefang
Sichuan University, Chengdu, 610064, China

ABSTRACT

With the aid of preirradiation method of grafting onto low-density polyethylene film, a systematic investigation was made of grafting of aqueous acrylic acid under conditions such as monomer concentrations, irradiation dose, dose rate, reaction time, the effect of concentrations of Mohr's salt and sulphuric acid on the graft reaction.

KEYWARDS

Preirradiation Graft, Acrylic Acid, Polyethylene Film.

INTRODUCTION

The radiation grafting was developed in 1950's and has so far progressed in a large scale[1]. Its application in industry at prescent embodies modification of fibres, synthesis of biological macromolecules in medicine and selective osmosis membrane, and adhesion improvement for polymers. In 1980's, our institute commenced on the researches of graft polymerization of acrylic acid onto low-density polyethylene by the direct radiation grafting method and has found practial uses in the battery separators, cationic exchange membranes and superabsorbed materials in industry. However, because of the formation of large amounts of homoplymer on the film surface of LDPE, the post-handling was very tedious, the product quality was unstable and also it resulted in waste of raw materials. Therefore, we turn to employ the preirradiation method and examine the effects of various factors on the grafting process.

EXPERIMENTAL

Materials

A commercial low-density polyethylene film, 35μm thick, obtained from Lanzhou Chemical Industry Co. of China, was used for grafting. Acrylic acid (C. R) supplied by Shanghai Chemical Reagent Factory of China, was used without further purification. Sulphuric acid (C. R) Mohr's salt (A. R) and deionized water were used as received.

Irradiation

Weighed polyethylene films were exposed to cobalt-60 gamma rays at a dose rate of 0. 795 Gy/sec. All irradiations were carried out at room temperature in air.

Grafting Procedure

The weighed and preirradiated polyethylene film was first immersed in the aqueous monomer solution with known concentrations of acrylic acid, Mohr's salt and suphuric acid. The solution

was deaerated by bubbling nitrogen in a water bath at 70°c. After the desired period, the film was taken out, washed with water, and dried in vacuum to constant weight.

The degree of grafting was obtained through the weight increase of the film according to the following equation:

$$\% \text{ Grafting} = \frac{W_g - W_0}{W_0}$$

where, w_g and w_o are the weights of grafted and ungrafted film respectively.

Swelling Measurement

Swelling of the grafted films was determined gravimetrically after immersion in 0. 1N NaOH for 48h at room temperature. The films were then removed, pressed between sheets of blotting paper to remove the excess liquid on the surface and weighed. The percent swelling was calculated as follows:

$$\% \text{ Swelling} = \frac{W_s - W_g}{W_g}$$

where, w_s is the weight of swollen film.

Water Absorbency

The grafted films were first immersed in deionized water for 24h, and then taken out. Upon removal of the excess water on the surface, they were weighed. The percent absorbency of water was calculated as follows:

$$\% \text{ Absorbency} = \frac{W_h - W_g}{W_g}$$

where, w_h is the weight after absorbing the water on the film surface.

RESULTS AND DISCUSSION

Influence of monomer concentration

The curves representing the relationship of various concentrations of aqueous acrylic acid solution and percent grafting are shown in Fig. 1. From these curves, it is known that for each one there is an induction period for peroxide decomposition in different degrees at the initial stage of the grafting reaction, followed by rapid grafting with increasing time. After 40 min, these curves

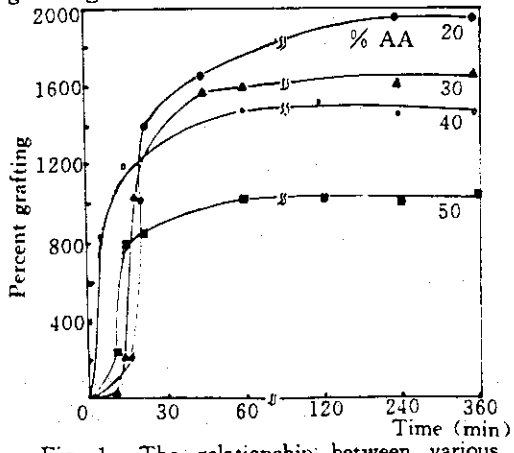


Fig. 1. The relationship between various monomer concentrations and percent grafting Radiat. dose: 100 kGy; Mohr's Salt: 0. 1wt%; sulphuric acid: 0. 2mol/L; grafting tempt. : 70°C

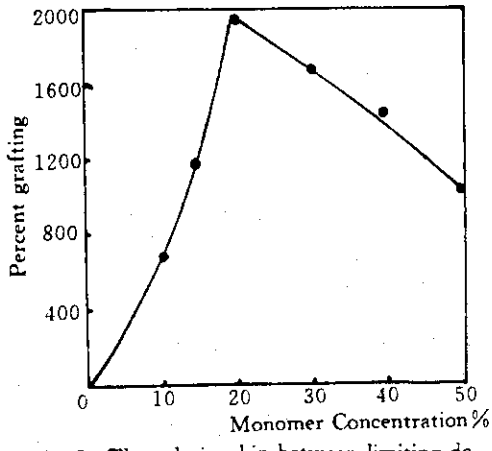


Fig. 2. The relationship between limiting degree of grafting and monomer concentration

begin to level off by degrees. The maximum grafting rate is found at 40% of monomer concentration, and the minimun at 20%. From the relationship between limiting degree of grafting and monomer concentration as shown in Fig. 2, it can be seen that the limiting degree of grafting increases significantly with the increase of monomer concentration within the concentration range of 0～20%, whereas it falls after 20%. Possibly this is due to the larger opportunity for homopolymerization with the increment of monomer concentration, leading to the increasing viscosity in the reaction system and unfavorable to the diffusion of monomer into the graft films. A. Chapiro and I. Ishigki obtained the similar results[2,3].

Influence of Mohr's salt

The addition of Mohr's salt in the reaction system not only can effectively prevent homopolymerization, but accellarate the decompositions of peroxides via a redox proeess aided by Fe^{2-} of Mohr's salt[2].

As shown in Fig. 3, the grafting system with 0.25% concentration of Mohr's salt provides the maximum initial grafting rate, and that with 0.1% the minimum but the limiting degree of grafting of the latter is higher(0.1%) than that of the former (Fig. 4).

Figure 4 shows the influence of ferrous sulphate on the limiting degree of grafting with increasing its concentration. The decrease in the degree result from both the exerted influence of Mohr's salt of various concentrations on the decomposition of peroxides on the film, and its inhibition to the grafted chain propagation[2].

$$R\text{-}CH_2\cdot + Fe^{2-} + H_2O \longrightarrow R\text{-}CH_3 + Fe^{3+} + OH^-$$

Mohr's salt functions in two opposite directions. They influence and regulat each other. With the higher concentration of Mohr's salt, the lower degree of grafting occurred due to the chain termination by Fe^{2-}.

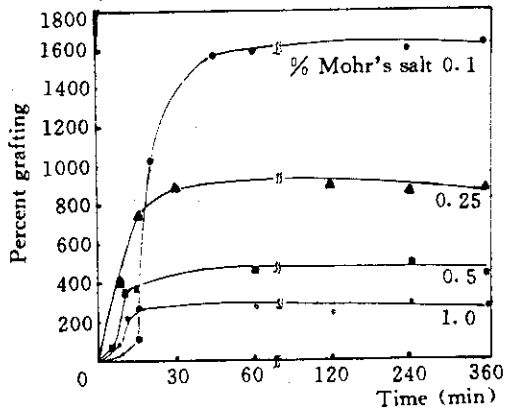


Fig. 3. The relationship between various concentration of Mohr's salt and percent grafting Monomer concentration: 30%; other condition as for Fig. 1.

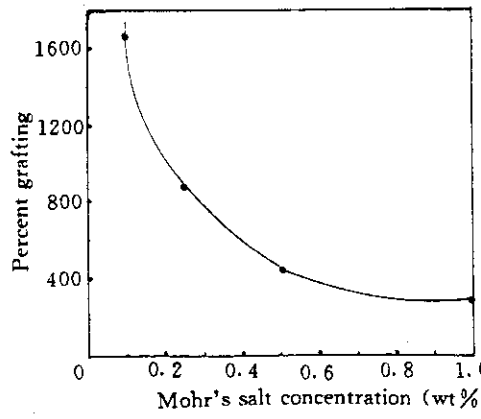


Fig. 4. The relationship between Mohr's salt concentration and limiting degree of grafting Monomer concentration: 30%; other conditions as for Fig. 1.

Influence of pre-irradiation dose

The relationship between dose and limiting degree of grafting is shown in Fig. 5. At lower dose, partial breakdown of molecules in non-crystalline domain of LDPE films happened, leading to fewer formation of peroxide and thus relatively lower limiting degree of grafting. With the increase of dose, the breakdown of molecules both in non-crystalline and crystalline occurred, and more peroxides were formed, resulting in a higher limiting degree of grafting.

Influence of dose rate

Shown in Fig. 6 are the two curves representing various dose rate for a given dose. It demonstrates that only a lower dose rate is obtained with a long period of radiation time at the same dose. Oxygen molecules has enough time to diffuse into the surface of the film to form peroxides. At the dose of 100 kGy, and the dose rate of 27. 8Gy/Sec with electron pre-irradiation, the grafting reaction proceeded 4h and the percent grafting only reached 3. 5%. This confirms the above conclusion.

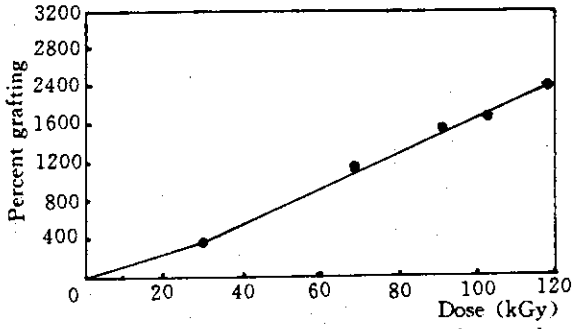


Fig. 5. The relationship between dose and limiting degree of grafting
Monomer concentration: 30%; other conditions as for Fig. 1.

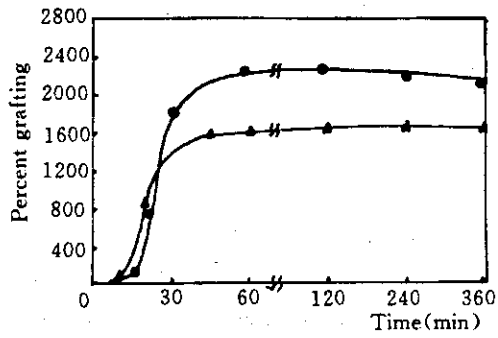


Fig. 6. The influence of dose rate on the degree of grafting
Dose rate (Gy/sec): (•) 0. 27; (▲) 0. 795
monomer concentration: 30%; other conditions as for Fig. 1.

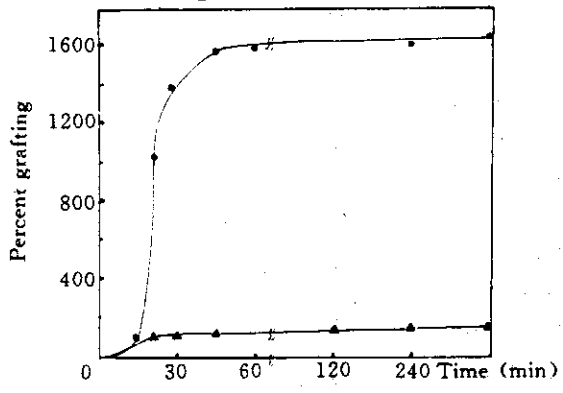


Fig. 7. The influence of sulphuric acid on the degree of grafting
(•) With added H_2SO_4: 0. 2mol/L; (▲) without H_2SO_4; monomer concentration: 30%; other conditions as for Fig. 1.

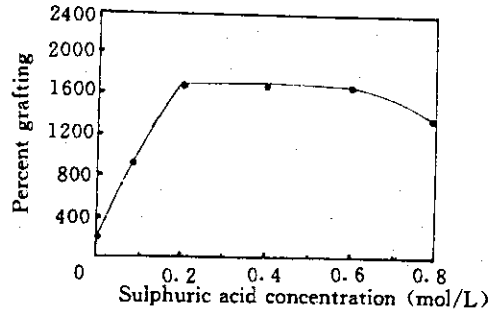


Fig. 8. The relationship between the concentration of sulphuric acid and limiting degree of grafting
Monomer concentration: 30%; other conditions as for Fig. 1.

Influence of sulphuric acid

It was documented that the addition of inorganic acides accelerates graft-copolymerization in many systems[4,5,6]. In our study as shown in Fig. 7, the limiting degree of grafting is only 164% without the presence of sulphuric acid, and the film thus obtained is not so smooth, whereas a yield of 1671% is arrived at with 0. 2mol/L of sulphuric acid, nearly ten times that of the former. Furthermore, an initial grafting rate rise to some extent was observed. But dose it mean that the more the added sulphuric acid, the better? Figure 8 shows that the limiting degree of grafting obviously increases with the increase of concentrations of sulphuric acid in the range of 0 ~ 0. 2 mol/L. The curve begins to level off beyond 0. 2mol/L. Further enhancement of concentrations of sulphuric acid (0. 6~0. 8mol/L) leads to a decline of the limiting degree of grafting. Therefore, we think that the proper amount of added sulphuric acid can give rise to the destruction of ordered arrangement of molecules in crystalline domain of LDPE films which accelerates the penetration of grafted monomer into crystalline region accordingly.

Water absorbency of the grafted films

The surface of LDPE films was known to be non-polarized and hydrophobic. After grafting acrylic acid onto the film, the water absorbency was greatly improved(Fig. 9). For grafted films with various percent grafting, the ability to absorb water per unit grafting yeild was not constant. As shown inFig. 10, the multiple of water absorbency of per unit grafting yield falls with the rise of percent grafting.

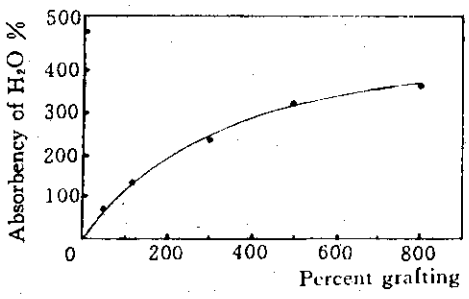


Fig. 9 The relationship between water absorbency and the degree of grafting

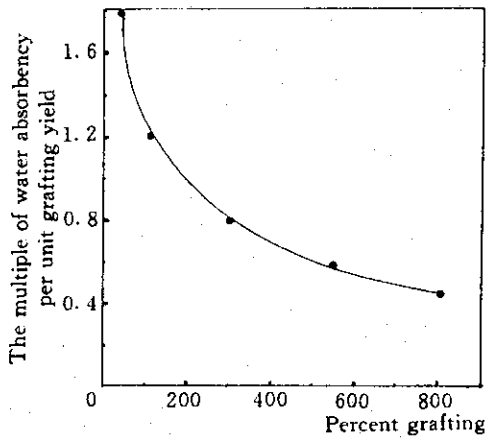


Fig. 10. The relationship between the multiple of water absorbency of per unit grafting yield and percent grafting

Swelling of the grafted films

Percent swelling is plotted as a function of percent grafting as shown in Fig. 11. It can be found that the membranes swelled to a very large extent when they was immersed in 0. 1N NaOH. For the grafted film with the degree of grafting at 894%, the percent swelling arrives at 2179%. In the meanwhile, the percent swelling increases significantly with percent grafting in the grafting range of 0～300%, whereas it tends to level off beyond 300%. But if the grafting goes to a very large extent, the film tends to break readily after 48h of swelling.

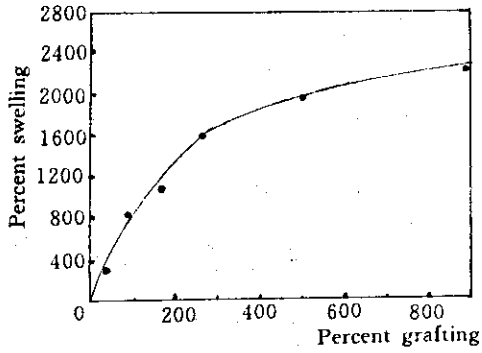


Fig. 11. The relationship between the percent swelling and the degree of grafting

REFERENCE

1. H. M. Chen(1982), Nuclear Technology 6. 1
2. B. D. Gupta, A. Chapiro(1989), J. Eur. Polym., 25, 1137
3. I. Ishigaki, T. Sugo, K. Senoo, T. Okada, J. Okamoto, S. Machi(1982), J. Appl. Polym. Sci., 27, 1033
4. J. L. Garnett, N. T. Yen(1974), J. Polym. Sci.: Polym. Lett., 12, 225
5. J. L. Garnett, S. V. Jankiewicz, M. A. Long(1985), J. Polym. Sci:Polym. Lett., 23, 563
6. W. J. Chappas, J. Silverman(1979), Radiat. Phys. Chem., 14, 847

14.4 Preparation of Carboxy-group-contained Polyvinyl Alcohol Amidoxime Chelate Fiber by Preirradiation Grafting and its Adsorbability for Au(Ⅲ) Ions

Lei Rao, Jun Xu, Wenbing Xie and Jinyu Yao
Changchun Institute of Applied Chemistry, Chinese Academy of Science,
Changchun 130022, P. R. China

ABSTRACT

Carboxy-group-contained polyvinyl alcohol amidoxime chelate fiber (PVAAO-AAc) was synthesised by preirradiation graft copolymerization and amidoximation. The radiation dose and ratio of monomers, acrylonitrile and acrylic acid, influence the value of grafting rate, amidoxime group component and adsorption capacity. The properties of adsorbing Au(Ⅲ) ions was systematic studyed in the paper.

Keywords: amidoxime, carboxy, radiation, gold, graft.

INTRODUCTION

Chelate fibers and resins are effective adsorbents which are used to enriching and separating some metal ions[1-5]. Amidoxime chelate fiber, amidoxime chelate group [-C=NOH(NH_2)] contained functional group can chelate some metal ions and create stable chelators, so that very pure metal ions are obtained by elution. Amidoxime chelate fiber is very useful in recoverying uranium from sea water[4-6] and enriching or separating noble ions.

The adsorption rate of amidoxime chelate fiber is influenced by fiber's hydrophilicity. Therefore, it is necessary to increase the hydrophilicity of the amidoxime chelate fiber. H. Omich et al[7,8] reported that adsorbents containing both amidoxime groups and carboxyl groups were synthesized by grafting acrylic acid in the first step and acrylonitrile in the second step. Carboxy-group-contined polyvinyl alcohol amidoxime chelate fiber was prepared in our laboratory. The mainchain, polyvinyl alcohol (PVA) fiber, is a hydrophilic one because of hydroxy groups in its chains. Carboxy induced by preirradiation grafting acrylic acid is the other hydrophilic factor. It is the reason that PVAAO-AAc fiber possessed so many properties as high hydrophilicity, fast adsorption rate and good selectivety for some metal ions. In addition, the damage of the fiber can be reduced since acrylonitrile (AN) and acrylic acid (AAc) were grafted in the same step. PVAAO-AAc chelate fiber and its preparation have not been seen in literatures.

The Au(Ⅲ) ions uptaked with this fiber was investigated in the paper. The fact is that the fiber adsorbs Au(Ⅲ) ions with high selectativity and fast adsorption rate.

EXPERIMENTAL

Synthesis: Polyvinyl alcohol fiber was irradiated with ^{60}Co-γ rays, which were produced by 100,000 curie ^{60}Co-γ source in air at room temperature. Then the fiber was immersed in AN and AAc mixture solution at 80℃ for 4 hours to copolymerize AN, followed by amidoximation of cyano groups of grafted chains by connecting the grafted fiber with a 3% hydroxylamine aqueous solution at 80℃ for 2 hours. PVA, a commercial products, was cut into 5mm long before experiment. Acrylonitrile (A.R.) has been distilled before use.

Copper adsorption capacity: PVAAO-AAc fiber adsorbed copper ions was obtained through that 0.25g PVAAO-AAc samples were equilibrated with excess copper ions solution at room temperature for 2.5 hours, then, filtered, rinsed and dryed.

The adsorption of gold and measurement: 0.20g PVAAO-AAc samples were immersed into de-ionized water for 24 hours, washed with alcohol in stirring, then with HNO_3 and at last with the amount of de-ionized warer. The fiber treated as above is loaded in chromatograph column for enriching Au(Ⅲ) ions. The volume of water phase is 25 ml and PH value is 2. Chromatograph column is 0.7 x 10 cm glassy column with 100-120 mesh sintered glass stand siveve plate in the end of it. The elution is finished by the mixture solution of 1% thioureu and 3M HCl. Quantitative analysis is followed to determine the amount of gold by P-4 403 type flame atomic adsorption spectrophotometer. The determination condition is that the electron current of KY-1 type Au hollow cathode light is 8 mA, wavelength is 242.8 nm, spectral bandwidth is 0.7 nm, air mass flow is 18 l/min, acetylene mass flow is 5 l/min and

10s integration is adopted.

Saturated adsorption capacity of Au(Ⅲ) ions: Every sample, 0.2g PVAAO-AAc dry fiber, was submerged into de-ionized water for 24 hours in the separation funnel. Excessive Au(Ⅲ) ions were put into it when volume of water phase was 25 ml and PH value was 2. Shaked then the sample were equilibrated with the Au(Ⅲ) ions solution at room temperature for 24 hours. The supernatant liquor was concentrated, determined and calculated the fibers adsorption capacity on Au(Ⅲ) ions with following function. W_{Au}: weight of all Au ions put into. W_{Au}': weight of Auions supernatant. W_{fiber}: weight of the PVAAO-AAc fiber.

$$\text{Adsorption Capacity of the fiber with Au (mg/g)} = \frac{W_{Au}-W_{Au}'}{W_{fiber}}$$

RESULTS AND DISCUSSION

1. Synthesis of PVAAO-AAc Fiber

Fig.1 shows the synthesis course of the fiber. It can be devided into three steps, preirradiated initiation, grafting copolymerization and amidoximation. The key step in the synthesis of PVAAO-AAc fiber is whether or not grafting copolymerization is successful. From the FT-IR results of the product of grafting copolymerization, we found that -CN and -COOH groups did be grafted because -C≡N and -C=O stretching vibration peaks at 2240 cm-1 and 1710cm-1 exist obveriously. We draw another conclutions from table 1 and table 2 that the irradiation dose and ratio of monomers (AN/AAc) influence the value of grafting rate, amidoxime group componen and adsorption capacity.

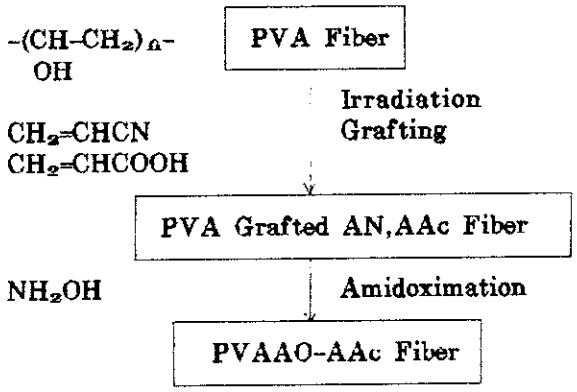


Fig.1 Synthesis Course of PVAAO-AAc Fiber

Table.1 Influence of Irradiation Dose

Irradiation Dose (Mrad)	25	20	16	10	5
Grafting Rate (%)	182.4	121.0	55.4	68.8	76.5
AN (%)	57.1	51.0	34.1	39.1	35.8
-C=NOH(NH_2) (%)	39.8	34.8	29.6	26.9	27.6
Adsorption Capacity ($mgCu^{2+}$/g fiber)	50.8	49.5	35.6	32.4	36.2

Table.2 Influence of the Ratio of AN/AAc

$M_{AN/AAc}$	1:4	1:2	1:1	2:1	4:1
-C=NOH(NH_2)	22.3	26.2	34.4	26.7	28.9
Adsorption Capacity ($mgCu^{2+}$/g fiber)	33.7	41.3	45.1	43.2	45.7

2. The Properties of PVAAO-AAc Fiber

(1) Adsorption Rate

The adsorption rate of PVAAO-AAc fiber adsorbed Au(Ⅲ) ions is shown as fig.2. It is found that the adsorption rate has reached more than 99% since the vibration time is 6 minunes. It indicats that the speed of PVAAO-AAc chelate fiber adsorbed Au(Ⅲ) ions is quite fast.

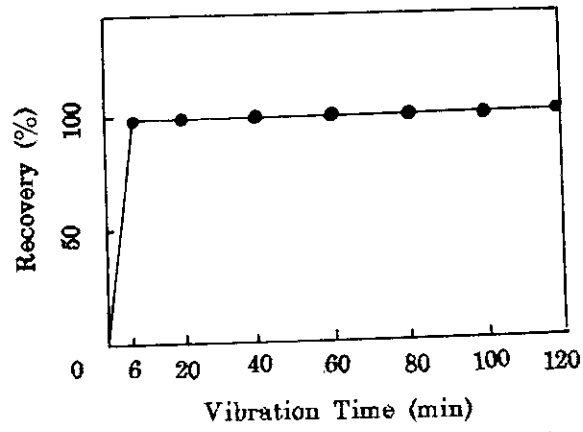


Fig.2 The Adsorption Rate of PVAAO-AAc Fiber with Au Ions

(2) The acidity of enriching and eluting

PH value is an important factor in adsorption reaction. the PH values of enrichment and elution were studied in this part. We took a serious of standard solution containing the same amount of Au(Ⅲ) ions, adjusted the range of PH value from 1-6 separatly. The adsorption was finished on chromatograph column. The elution was followed by mixture of 5 ml 1% thiouteu and 3M HCl. The results of analyses and calculation are listed in the table 3 and table 4. We can see that the influence of PH value on PVAAO-AAc fiber is very samll and in a wide range of PH value, PH=1-5, the fiber can be used in adsorbing Au(Ⅲ) ions. It illustrates that the enriching PH value of the fiber adsorbing Au(Ⅲ) ions is easy to chose.

Table 3 The Influence of Acidity on Enrichment

PH value	1	2	3	4	5	6
W_{Au} (add)			0.122			
W'_{Au} (eluent)	0.108	0.133	0.111	0.104	0.101	0.053
Recovery (%)	89	93	91	85	83	43

Table 4 The Influence of PH Value on Elution

PH value	1	2	3	4	5
W_{Au} (add)	0.192	0.193	0.148	0.148	0.148
W'_{Au} (eluent)	0.174	0.176	0.158	0.148	0.151
Recovery (%)	91	91	107	100	102

(3) Saturated Adsorption Capacity

The saturated adsorption capacity of PVAAO-AAc chelate fiber is 49.5mg Cu^{2+}/g dry fiber and 96.9 mg Au^{3+}/g dry fiber respectively.

(4) The Selectivety of the Fiber

Whether the fiber with single selective adsorbability is the key index for the properties of chelate fiber. Table 5 give the separate factors of Au(Ⅲ) ions with usual metal ions. Obviously, the separate factors of Au(Ⅲ) ions and many metal ions are big, but it is small between Au(Ⅲ) ions and Fe(Ⅲ) ions. There is a good way to solve the problem that the amount of Fe(Ⅲ) ions were put into the solution. The fact is that no effects on adsorption capacity of Au(Ⅲ) ions exist when the concentration of Fe(Ⅲ) ions is more than 10 mg/ml in the sample.

Table 5 The Separative factors of Au (Ⅲ) ions and usual metal ions

Element	Au	Mn	Pb	Cu	Zn	Fe	Cr	Ni	Ag
Capacity	9923	14.38	87.59	94.45	16.88	180.2	6.7	52.5	100
Separative factors		690	113	105	588	54.8	148	189	99

(5) The Adsorption from the Solution Containing Different Quantity of Au(Ⅲ) ions

Table 6 Enriching from Solution with Various Concentration

$W_{Au\ add}$ (ng)	5	10	20	50	100	200	300	1000
Recovery (%)	100	100	100	98	97	97	98	98

Table 6 is enriching experament results from different quantity Au(Ⅲ) solution. It shows that PVAAO-AAc fiber can adsorbed Au(Ⅲ) ions from solution containing various concentration of Au(Ⅲ) ions.

(6) The Elution of Au(Ⅲ) ions

Quantitive Au(Ⅲ) ions were adsorbed by PVAAO-AAc fiber and eluted by 2ml mixture solution of 1% thiouren and 3M HCl every time. The contant of Au in eluent was determined and elution curve was drawn.

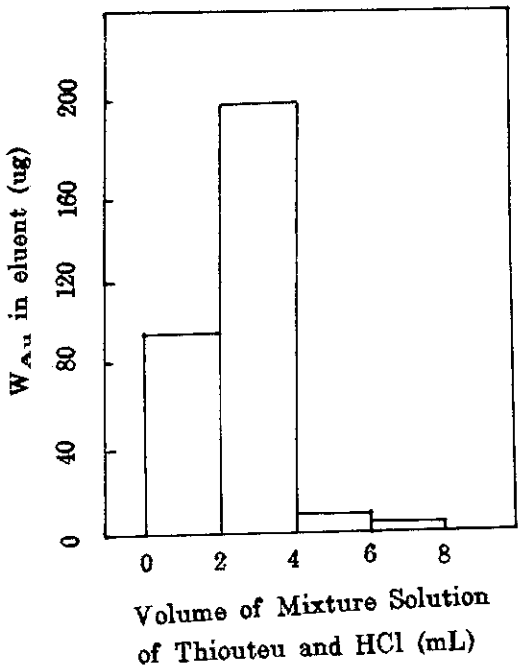


Fig.3 Elution Curve of Au (Ⅲ) Ions

3. Analyses of Ore Sample

(1) Standard Curve

Au(Ⅲ) ions standard solution was compound as 2. 4. 6. 8. 10 ug/ml respectively. It was determined by atomic adsorption spectrometry and a standard curve was drawn.

(2) Pretreatment of the Sample

We weighed Au ore sample 3.00g and put it into 50ml beaker. The sample have soluted

with aqua regia, filtered, concentrated liquor to 1ml, diluted with water, adjusted PH=2 and adsorbed by PVAAO-AAc fiber on the column.

(3) The results

The result is that rate of recovery on Au is between 86%-102%. This is evident in table 7. Therefore, PVAAO-AAc fiber is a good adsorbent for adsorbing Au(Ⅲ) ions.

Table 7 Results of Analysis of Ore Sample

W_{Au} in sample (ug/g)	W_{Au} in eluent (ug/g)	Recovery (%)	RSD (%)	X (ug/g)
4.3	4.4	102	79	4.2
	4.4	102		
	3.7	86		
	4.2	97		

CONCLUSION

PVAAO-AAc fiber have been prepared by preirradiation graft copolymerization and amidoximation.

PVAAO-AAc fiber is a good adsorbent for adsorbing Au(Ⅲ) ions. The adsorption rate is fast and the saturated adsorption capacity is satisfied. It is true that the fiber can adsorb Au(Ⅲ) ions with single selecitive property. In Addition, it can adsorbed Au(Ⅲ) ions from solution containing various concentration of Au(Ⅲ) ions, and it is easy to elution.

It is also obtained good results from the examination of Au ore sample.

REFERENCE

[1] J. Okamoto et al, J. Appl. Sci., 1985, 30:9673
[2] Shi Honggao and Rao Lei, Gongneng Gaofenzi Xuebao, 1992, 5(1):42
[3] M. B. Colella and S. Siggia, Anal. Chem., 1980, 52:967
[4] K. Sugasaka et al, Sep. Sci. Technol. 1984, 16(9):971
[5] Kyoichi Saito et al, J. Appl. Polym. Sci., 1990, 39:2153
[6] C. Bernido et al, Sep. Sci. Technol., 1988, 23(1-3):35
[7] H. Omichi et al, Sep. Sci. Technol., 1985, 20(2&3):163

14.5 Stability of Guest Molecules in Urea Canal Complexes by Canal Polymerization

Fumio YOSHII and Keizo MAKUUCHI
Takasaki Radiation Chemistry Research Establishment
Japan Atomic Energy Research Institute
1233 Watanuki-machi, Takasaki-shi, Gunma-ken, 370-12 Japan

Abstract It was found that various organic materials are attracted into urea canal by hexanediol diacrylate (HDDA) and long chain compounds. This means that materials which does not form complex by itself are induced in canal by HDDA and long chain compounds. To include with stability perfumes, insecticides, attractants and repellents in urea canal, leaf alcohol was used as a model compound for guest molecules in the canal. The leaf alcohol from the canal released gradually over many days and the release was inhibited for 15 days by long chain compounds and for 30 days by polymerized HDDA after irradiation. After releasing, the leaf alcohol in the canal remained 25 % stable for long chain compounds and 40 % for polymerized HDDA. The dose required for stabilization of leaf alcohol in the urea canal by canal polymerization of HDDA was 30 kGy.

INTRODUCTION

It is well known that a urea (host molecule) canal complex is formed with paraffin and fatty acid (guest molecules) . From x-ray analysis, the structure of this complex is hexagonal. When a urea canal complex is formed, urea undergoes crystal transition from original structure of tetragonal to hexagonal structure. The hexagonal structure of the canal complex decomposes at temperature before melting of the tetragonal urea (133°C). The polymerization (canal polymerization) of monomer in the urea canal complex gave a polymer with excellent steric regularity . For instance, canal polymerization produces isotactic polymer for acrylonitrile (Inoue Y. and Nishioka A., 1972 ; Matsuzaki K. et al., 1968; Minagawa M. et al., 1988; Yoshii F. et al., 1975), syndiotactic polymer for vinyl chloride (Yoshii F, Abe T. and Hayakawa N., 1975) and 1,4-trans polymer for butadiene (Chatani Y. and Kuwata S, 1975).

In the previous paper (Yoshii F. and Kaetsu I. 1978), it was found attracting effect that hexanediol diacrylate (HDDA) attracted various monomers into the canal and copolymerization occurred between HDDA and those attracted monomers by irradiation. It was expected that the urea canal complex is effective in the control of slow release of substances attracted from canal complexes, when perfumes, insecticides, attractants and repellents are included in the canal complex by the attracting effect. In this article, leaf alcohol was used as a model compound of guest molecules attracted in the canal and stabilized with long chain compound and polymerized HDDA in canal polymerization.

EXPERIMENTAL

Materials

Urea, leaf alcohol, lauryl alcohol, cetyl alcohol, stearyl alcohol, oleic acid and stearic acid utilized were special grade. HDDA was obtained from Nippon Kayaku Co. Ltd. (Japan). These materials were used without further purification.

Preparation of urea canal complex

Solid materials of long chain compounds such as lauryl alcohol, cetyl alcohol, stearic acid, oleic acid and paraffin (melting point, 52-54 °C) attracted leaf alcohol in to the canal by grinding in a mortar with urea and leaf alcohol. The molar ratio of urea, HDDA or long chain compounds and leaf alcohol is 15 : 1 : 1.

In the case of HDDA, a mixture of HDDA and leaf alcohol was added to solid urea, then stored at room temperature. Formation of the urea canal complex attracting could be determined from the fact that those mixtures changed to a fluffy powder state from a slurry state.

Canal polymerization and stability of leaf alcohol in the canal

The urea canal complex was irradiated to include strongly leaf alcohol in the canal by polymerization. Gamma irradiation from a Co-60 source was carried out with a dose rate of 10 kGy/hr.

The decomposition temperature of the urea canal complex including leaf alcohol was estimated using a DSC (Perkin-Elmer DSC 7). The release of leaf alcohol from the canal versus storage was determined by measuring weight reduction.

RESULTS AND DISCUSSION

Stability of leaf alcohol attracted in the canal by long chain compounds

DSC analysis is well used to elucidate formation of urea canal complexes. Figure 1 shows the change in DSC curves of urea canal complexes attracted leaf alcohol by oleic acid. Curve 1 is decomposition of single oleic acid urea canal complex. Melting of urea (peak temperature, 133 °C) appear after decomposition of canal complex. DSC curves of the canal complex including leaf alcohol are shown in curves 2 and 3. Decomposition of the canal complex shifts to higher temperatures than that of a single oleic acid canal complex. The melting point of urea after decomposition of the canal complex attracted leaf alcohol was similar to tetragonal urea, showing that the crystal lattice changes from hexagonal to tetragonal during the decomposition. From these findings, it is guessed that the peak of decomposition appears at slightly higher temperatures by the influence of leaf alcohol induced in the canal by grinding in the presence of long chain compounds.

To confirm the stability of leaf alcohol in the canal complex, weight reduction of canal complex versus storage time was estimated (Figure 2). The release of leaf alcohol from the canal continued up to 17 days and then was inhibited, while in the mixture of urea and leaf alcohol, almost all leaf alcohol (95 %) is released after the same period. In the case of oleic acid, the release of leaf alcohol from the canal is slower than that of the mixture of urea and leaf alcohol. After release, the leaf alcohol remains 20 % for stearyl alcohol and 25 % for oleic acid in the canal as shown in Figure 2. The leaf alcohol remains stable in the canal even after 45 days. The release rate for leaf alcohol attracted with cetyl alcohol and paraffin was examined. Release rate of leaf alcohol from these canal complexes was almost the same as that of the canal complex attracted with stearyl alcohol. Accordingly, it is concluded that approximately 20 - 25 % of the leaf alcohol attracted with long chain compounds in the canal remains after release.

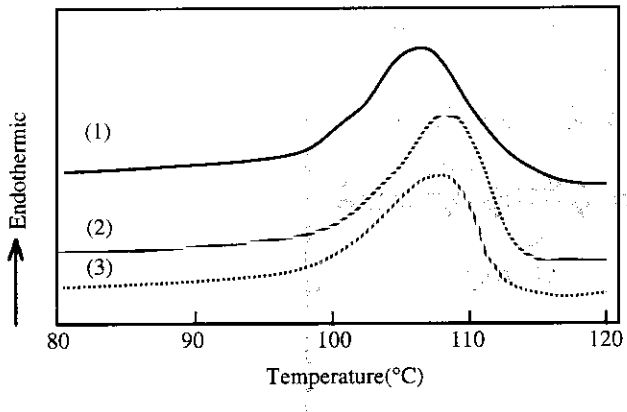


Fig.1 DSC curves of urea canal complex attracted leaf alchol by oleic acid.
Molar ratio of Urea/Oleic acid/Leaf alchol,
(1) Urea/Oleic acid=15/1
(2) Urea/Oleic acid/Leaf alchol=15/1/0.5,
(3) Urea/Oleic acid/Leaf alchol=15/1/1.

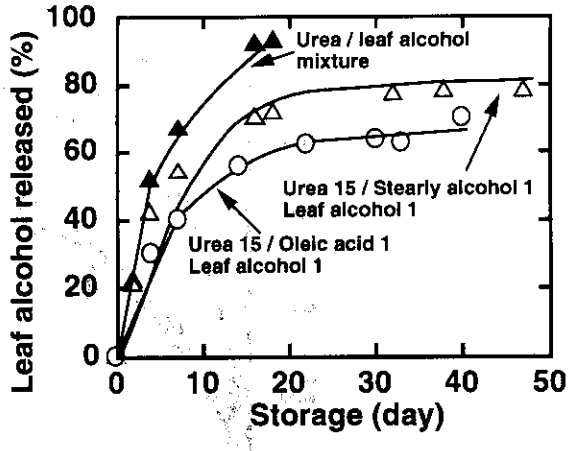


Fig.2 Release curves of leaf alcohol attracted in canal by long chain compounds

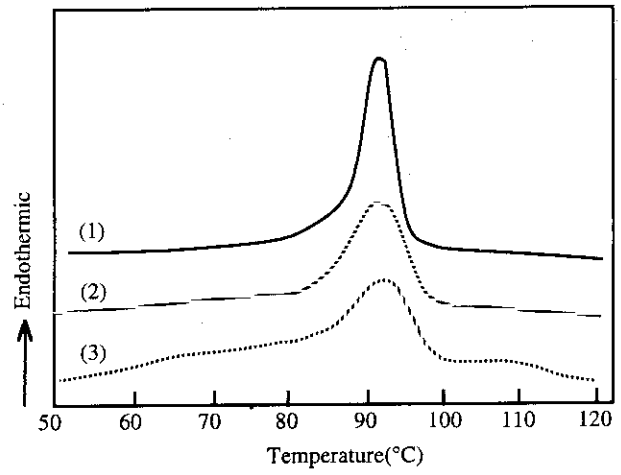


Fig.3 DSC curves of urea canal complex attracted leaf alcohol by HDDA.
Molar ratio of Urea/HDDA/Leaf alchol,
(1) Urea/HDDA=15/1
(2)Urea/HDDA/Leaf alchol=15/1/0.5,
(3)Urea/HDDA/Leaf alchol=15/1/1.

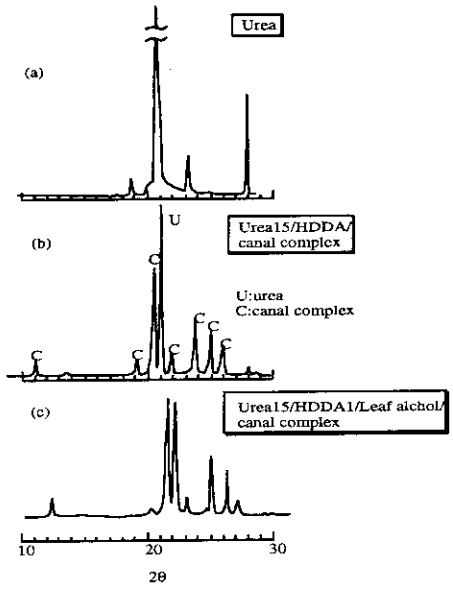


Fig.4 X-ray powder patterns of urea canal complex attracted leaf alchol by HDDA.

Stability of leaf alcohol by canal polymerization

Figure 3 shows DSC curves of the urea canal complex attracted leaf alcohol in the canal by HDDA. Decomposition of the canal complex is affected by attracted leaf alcohol. The endothermic curve of the decomposition become broader and shifts to slightly higher temperature than that of the single HDDA canal complex as well as attracting of long chain compounds. The reflections of 2q in X-ray powder patterns of canal complex attracted leaf alcohol by HDDA are shown in Figure 4. Profile (a) is reflection of tetragonal urea. The HDDA urea canal complexes showed new large reflection peak due to HDDA at 12.2°, 21.4°, 23°, 25°, 26° and 24.2°. The urea canal complex of single HDDA is hexagonal analogous to well-known n-paraffin-urea canal complexes. In canal complex attracted leaf alcohol by HDDA, reflection at 22.5° of urea decrease remarkably with respect to the single HDDA urea canal complex, suggesting that leaf

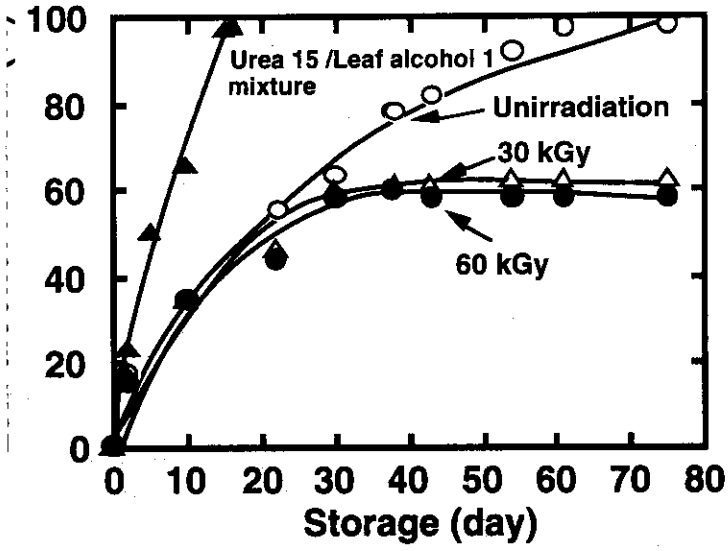


Fig. 5 Release curves of leaf alcohol in canal after canal polymerization of HDDA.
Urea 15 / HDDA 1 / Leaf aocohol 1

alcohol is attracted into canal.

In order to elucidate the stability of leaf alcohol in the urea canal complex, reduction of leaf alcohol released from the canal at 20°C was measured. Figure 5 shows stability of the leaf alcohol attracted in the canal. The leaf alcohol of nearly 100 % in the urea mixture is released for 17 days. The leaf alcohol in the unirradiated canal is released gradually over days and leaf alcohol of 95 % is released for 75 days. The release rate of leaf alcohol from the canal in the unirradiated sample is slower in HDDA canals than for long chain compounds canal complex. On the other hand, the leaf alcohol in the irradiated canal complex is gradually released over 35 days, then the release of leaf alcohol ceases. After 35 days, no leaf alcohol is released from the canal and 40 % leaf alcohol remained in the canal. In the previous paper (Yoshii F. and Kaetsu I., 1978), HDDA in the canal by irradiation began to polymerize at 80 kGy. As shown in Figure 5, the dose for stabilization of leaf alcohol in the canal is sufficient at 30 kGy. Thus, solid polymer of HDDA is not produced at this dose. However, after irradiation, when leaf alcohol urea canal complex with HDDA is added into methanol, the solution became turbid. From this finding, lower molecular weight polymer (oligomer) dissolved in methanol results from a lower dose of 30 kGy. Reduction of HDDA released from the canal versus storage and radiolysis of leaf alcohol during irradiation were not observed. Hence, it is assumed that 40 % leaf alcohol retains between HDDA oligomer in the canal after release. In Figure 2, approximately 20 % of the leaf alcohol included in the canal by stearyl alcohol remained stable in the canal after release. Accordingly, it is apparent that polymerized HDDA kept stable more leaf alcohol in the canal compared with that for long chain compounds.

CONCLUSION

It was found that HDDA or long chain compounds attract various organic compounds into urea canal . Stability of leaf alcohol attracted in urea canal complex by these materials were examined. After releasing in canal, leaf alcohol were stably trapped 25 % between long chain compounds and 40 % between polymerzed HDDA in canal.

REFERENCES

Chatani Y., and Kuwata S. (1975) Structual investigation of radiation- induced urea canal polymerization of 1,3-butadiene. Macromolecules **8**, 12

Inoue Y., and Nishioka A. (1972) Nuclear magnetic resonance spectroscopy of polyacrylonitrile. Polymer J. **3**, 149

Matsuzaki K., Uryu J., Okada M. and Shiroki H. (1968) The stereoregularity of polyacrylonitrile and its dependence on polymerization temperature. J. Polym. Sci. **6**, 1475

Minagawa M., Miyano K., Takahashi M. and Yoshii F. (1988) Infrared characteristic absorption bands of highly isotactic poly(acrylonitrile). Macromolecules **21**, 2387

Yoshii F., Abe T. and Yoda O. (1975) Radiation-induced post polymerization of acrylonitrile in urea canal complex. Kobunshi Ronbunshu **32**, 399

Yoshii F., Abe T. and Hayakawa N. (1975) Radiation-induced polymerization of vinyl chloride in urea canal complex as studied by broad line NMR. Kobunshi Ronbunshu **32**, 429

Yoshii F. and Kaetsu I. (1978) Trailing effect and copolymerization of long chain monomers and various monomers trailed in canal irradiated by gamma ray in urea canal complex. Angew. Makromol. Chem. **69**, 15

Yoshii F. and Kaetsu I. (1978) In-source and post-polymerization of long chain monomers gamma-irradiated in urea canal complexes. Angew. Makromol. Chem. **69**, 1

14.6 Preparation of Polymer Microspheres by Radiation-induced Polymerization

Y. Naka, *Y. Yamamoto, *Y.Yoshida, and *S. Tagawa

Faculty of Biology Oriented Science and Technology, Kinki University,
Uchitachyo, Nagagun, Wakayama, 649-64, Japan.
*The Institute of Scientific and Industrial Research, Osaka University,
Mihogaoka, Ibaraki city, Osaka, 567, Japan.

Abstract Cross-liking monomer, diethylene glycol dimethacrylate gives microspheres from organic solution by radiation-induced polymerization. /One of the remarkable result is that the number of the microspheres is not changing during the polymerization. Ethyl methacrylate, maleic anhydride, styrene and acrylamide are used as comonomers. These comonomers give the microspheres in the range of 0 to 0.4 as mol fractions.

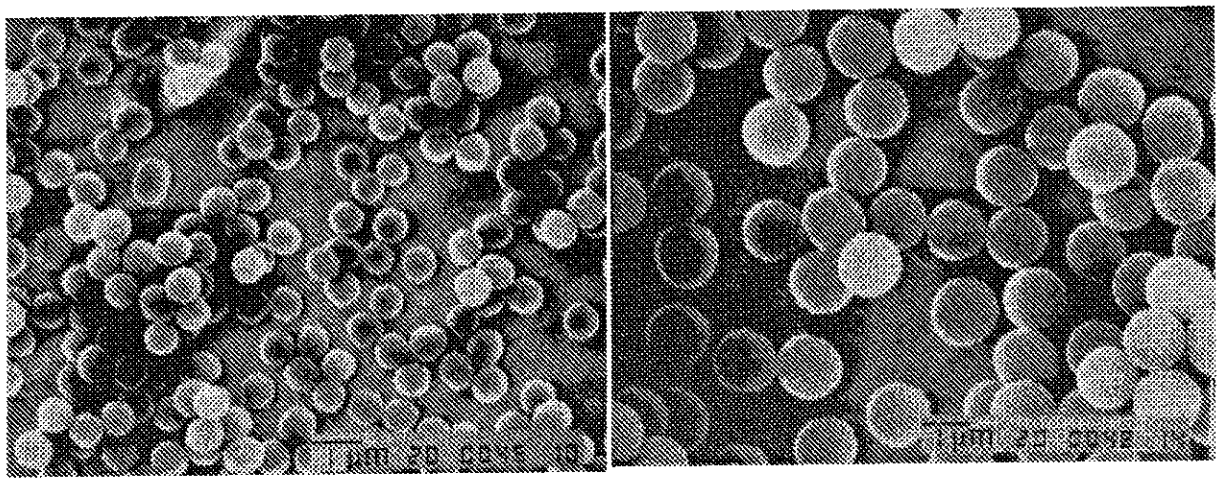
INTRODUCTION

Recently, microspheres (fine particles with spherical shape) are getting new interests as functional materials. Applications of the microspheres have been expanding in many fields. Remarkable applications of the microspheres are in the biological and medical fields as immuno-assays, cell labeling, and drug carriers. Emulsion- and dispersion-polymerizations are well-known as the methods for the preparation of polymer particles. A unique method has been reported which gives monodisperse microspheres by the radiation-induced polymerization.[1] It is characteristic that a mixture of a monomer and a solvent gives monodisperse microspheres in the absence of any kind of additives. The mechanism is considered to be different from those of the conventional methods, but the details of the formation mechanism have not yet been known. This report deals with the development of the monodisperse microspheres by the radiation-induced polymerization and the possiblity of thier applications. [2-5]

EXPERIMENTAL

Diethylene glycol dimethacrylate (2EGDM), supplied from Shin Nakamura Kagaku, was purified by passing through active alumina. Ethyl methacrylate (EMA), styrene, maleic anhydride, and acrylamide, were purchased from Wako Pure Chemical. Ethyl methacrylate and styrene were purified by distillation. Maleic anhydride and acrylamide were purified by recrystallization from benzene. Organic solvents, purchased from Wako Pure Chemical, were used without further purification otherwise noted.

In a typical experiment, solutions of 2EGDM (10 vol %) in organic solvents were degassed



(a) (b)

SEM photographs of poly-2EGDM microspheres. (a) 15 min, (b) 120 min. 4 kGy h^{-1}. 10 vol % of 2EGDM in ethyl acetate.

and sealed in 20 ml glass vessels. The degassing was carried out by five-times freeze-melt repeatings. The samples were irradiated with 60Co γ rays without stirring. The dose rate was 4 kGy h^{-1} and the irradiation time was 2 h otherwise noted.

Teflon filters of a 0.2 μm pore size (Advantest) were used for the separation of the microspheres from the irradiated solutions. The microspheres were washed with the solvents and dried under vacuum. The microspheres were photographed by using a scanning electron micrograph (SEM) (JELO, JST-300).

RESULTS AND DISCUSSION

Figures 1(a) and 1(b) show the SEM photographs of the microspheres prepared in ethyl acetate. The microspheres both obtained at 15 min as Fig. 1(a) and 2 h as Fig. 1(b) have a complete spherical shape. The diameter increases with irradiation time. The microspheres grow with narrow size distribution. This means that the microspheres grow independently during the polymerization.

Figure 2 shows the time-conversion curve for the microspheres. The monodisperse microspheres are obtained with the yields more than 80 % by 2h polymerization. The size of the microspheres can be controlled by irradiation time. The easiness of the termination of the polymerization must be one of the advantages of the radiation-induced polymerization.

The number of the microspheres was calculated by assuming that the specific gravity of the microspheres is the same as that of the polymer obtained by the radiation- induced bulk polymerization of 2EGDM. The specific gravity of the 2EGDM polymer block was determined to be 1.24. Figure 3 shows the number of the microspheres plotted against irradiation time. The number of the microspheres is constant through the irradiation period. This agrees with the expectation from the monodispersity of the microspheres. The number of the microspheres

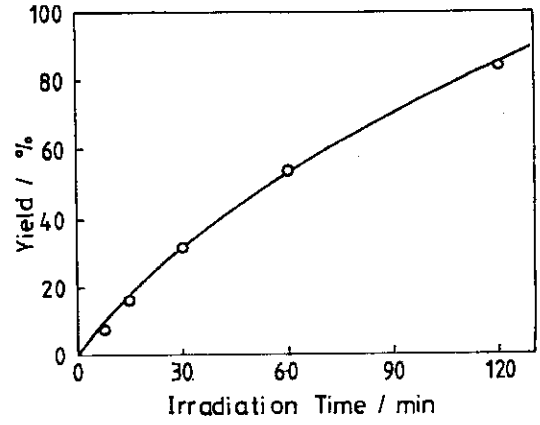


Figure 2. Time-conversion curve of the microsphere. Concentration of 2EGDM was 10 vol %, in ethyl acetate. Dose rate was 4 kGy h^{-1}.

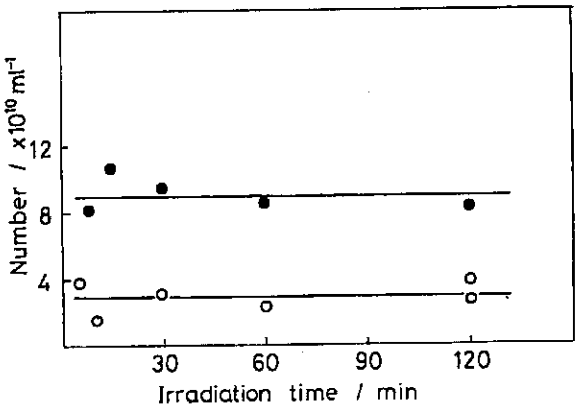


Figure 3. Relationship between irradiation time and number of microspheres. (●) 10 vol %, at room temperature, (○) 5 vol % at 40 °C, with ethyl acetate. 4 kGy h^{-1}.

becomes constant at the conversion below 10 % within the irradiation time of 5 min. The radicals produced after the irradiation time of 5 min do not contribute to the formation of the nuclei of the microspheres. That is to say, the formation of the nuclei is inhibited by the presence of the microspheres.

The results of the radiation-induced polymerization of 2EGDM monomer in various solvents are presented in Table 1 together with the viscosities and the solubility parameters of the solvents. The solubility of the monomer in the solvents increases with decreasing difference in their solubility parameters between 2EGDM and the solvents. The solubility parameter of the 2EGDM monomer was calculated to be 8.9. The solvent of which solubility parameter is close to 8.9 is considered to be a good solvent for 2EGDM monomer. Monodisperse microspheres and polymeric gel are produced depending on the solvents. It seems that the solubility parameters of the solvents giving separate microspheres are relatively close to that of 2EGDM. It is suggested that good solvents for the monomer are suitable for the formation of the microspheres. Thus, it is considered that the good solvent makes growing microspheres stable in the solution to avoid the aggregation of the microspheres.

Table 1. Solvent Effect on the Formation of Microspheres[a]

Solvents	Result	Yield %	Size μm	δ[b] %	Viscosity cp (25°C)
Methyl formate	Microspheres	50.4	4.80	10.2	0.33
2-Butanone	Microspheres	64.1	4.01	9.4	0.38
THF	Microspheres	72.6	2.81	9.9	0.46
Ethyl acetate	Microspheres	82.3	1.30	9.1	0.43
Ethyl caprylate	Microspheres	94.7	1.01	7.3	
Ethyl propionate	Microspheres	85.2	0.98	8.4	0.56[c]
Benzene	Gel			9.2	0.87
Ethanol	Gel			12.8	1.08
1,4-Dioxane	Gel			10.1	1.08[c]
Acetic anhydride[d]	Gel			10.3	0.78[c]

a Concentration of 2EGDM was 5 vol %. (4 kGy h^{-1} and 4 h)
b Solubility parameter ($cal^{-1/2} cm^{-3/2}$)
c 30 °C
d Irradiation time were 2h.

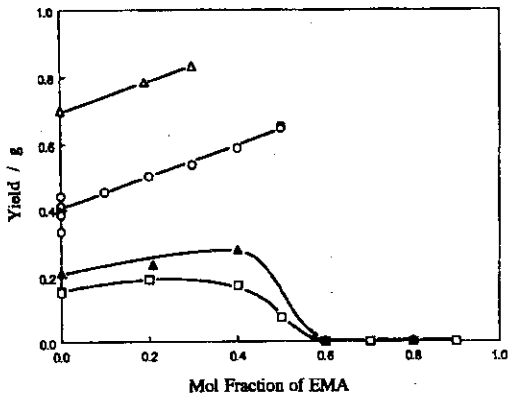


Figure 4 Effect of EMA on the yield of 2EGDM based copolymer microspheres. Each feed solution contains (□) 5 vol %, (▲) 7 vol %, (○) 10 vol %, and (△) 15 vol % 2EGDM.

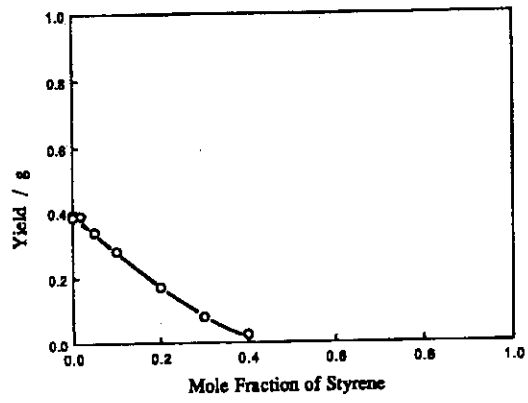


Figure 5 Effect of styrene on the weight yield of copolymer microspheres. Feed solution contains 10 vol % 2EGDM.

The formation of the microspheres is also affected by the viscosities of the solvents. The microspheres are obtained in the solvents with relatively low viscosities. This is probably due to the large mobility of the monomer and oligomer molecules and the propagating radicals in the solvents. The size of the microspheres varies with the solvents. It seems that the size increases with decreasing viscosity.

Figure 4 shows the copolymerization effect of EMA on the formation of 2EGDM based microspheres, i.e., the relationship between monomer composition in the feed solution and the weight yield of the microspheres. The mole fraction was changed under keeping the 2EGDM concentration constant. Thus each feed solution in a series of runs contains the same concentration of 2EGDM monomer. (This is because the decrease of 2EGDM concentration also causes the decrease of the microsphere yield)

The yield curves show two different manners due to the concentration of 2EGDM monomer. The weight yield of microspheres increases with increasing mole fraction of EMA in the feed solution until 0.4 for the solutions containing the low concentrations of 2EGDM (5 and 7 vol %). The weight yield decreases rapidly when the mole fraction of EMA exceeds 0.4 and then no microspheres are obtained when the mole fraction exceeds 0.6. The formation of copolymer microspheres is not favorable for the solution containing low 2EGDM (5 and 7 vol %). On the other hand, instead of the decrease of the weight yield, the gelation occurred at the high mole fractions of EMA in the feed solution containing high concentration of 2EGDM (10 and 15 vol %). The yield of the microspheres increased simply with increasing amount of EMA. But the gelation occurred when the mole fraction of EMA exceeded 0.6 for the 10% 2EGDM solution and 0.4 for the 15 vol % 2EGDM solution. The allowed region for the mole fraction of the solutions containing 10 vol % 2EGDM monomer is wider than the solutions containing 15 vol % 2EGDM. Therefore the suitable basic concentartion of 2EGDM for copolymerization is considered to be arround 10 vol %.

In the case of copolymerization effect for 2EGDM and maleic anhydride, yield of microspheres was not affected by the addition of maleic anhydride. The yield of microspheres is

not zero even the mole fraction of maleic anhydride exceeds 0.5 in the case of both the solutions containing 5 and 10 vol % 2EGDM monomer. No gelation was observed in the whole range of mole fraction of maleic anhydride. These results were different from those for the other comonomers.

In the case of copolymerization with acrylamide, yield increases slightly with increasing mole fraction of acrylamide. The decrease of yield was not observed, but gelation was observed when the mole fraction of acrylamide exceeded about 0.5. The size of the microspheres decreases with increasing amount of acrylamide. The addition of acrylamide causes the reduction in size.

Figure 5 shows the effect of copolymerization with styrene on the formation of the 2EGDM based microspheres. The weight yield of microspheres decreases rapidly with increasing mole fraction of styrene in the feed solution. This rapid change was not observed for the other comonomers mentioned in this paper. The effect of the addition of styrene is different from that of the copolymerization with EMA as the standard case and styrene seems to disturb the polymerization.

The copolymerization of 2EGDM and styrene seems to be a poor combination from the productive point of view. However, it can be a possible procedure for the preparation of large size microspheres, because there remains unreacted monomers in solutions under the 2 h irradiations. The low yield can be supplemented by enlonging the irradiation time. The size of copolymer microspheres, obtained from the feed solution of 10 vol % 2EGDM containing 0.2 mole fraction of styrene by 4 h irradiation, is 2.6 μm and the weight yield is 60 %.

Conclusion

The combination of closs-linking monomer such as 2EGDM, good solvent and radiation-induced polymerization is effective to obtain monodisperse microsphere. Copolymer microspheres of 2EGDM with EMA, acrylamide, maleic anhydride and styrene are obtained successively. Although the ratio of comonomer to 2EGDM is limited, the copolymerization make it possible not only to give functional group onto the microspheres, but also to controll the size of the microspheres.

(1) M.Yoshida, et.al.,*Radiat. Phys. Chem.*, **30**, 39 (1987)
(2) Y. Naka, et. al , *J. Polym. Sci., Part A, Polym. Chem.*, **29**, 1197-1202 (1991).
(3) Y. Naka and Y. Yamamoto, *J. Polym. Sci., Part A, Polym. Chem.*, **30**, 1287-98 (1992).
(4) Y. Naka and Y. Yamamoto, *J. Polym. Sci., Part A, Polym. Chem.*, **30**, 2149-58 (1992)
(5) Y. Naka, et.al., in preparation.

14.7 *Synthesis of Nanometer Metallic Powders or its Oxides by γ-ray Reduction of Salts Aqueous Solution

Zhang Manwei, Zhu Yingjie, Qian Yitai and Chen Zuyao
Department of Applied Chemistry USTC, Hefei, Anhui 230026, P. R. China

Abstract The nanocrystal powders of pure Ag, Cu, Ni, Pt, Au, Pd, Cd, Sn, Pb and Co were obtained by γ-radiation reduction of their salt aqueons solution. The average particle sizes of them are 5-45 nm respectively. the factors affecting the particle size and the formation and growth of the nanocrystal particles into single crystal are illustrated and discussed. the pure nanocrystal Cu_2O powders were also successfully prepared. The mechanism of its formation is discussed.

INTRODUCTION

Compared with the conventional materials the nanocrystal particles have certain special physical and chemical properties, such photosensitivity, magnetism, semiconductivity, superconductivity, catalysis ..... etc.. These outstanding properties of them have aroused greate interest for their applications in various fields. For example, in the electronics industry, ultrafine silver powder constitute the active parts of conductive inks, pastes and adhesives used in manufacture of various electronics parts[1], conductive silver pastes and inks form the basis for the thick-film technology for producing electronic components such as hybrid microcircuits[2], and the internal electrodes of multilayer ceramic capacitors[3]. Ultrafine powders of Pd and Ni are very high effective catalysts in petrochemical industry. Extremely fine particles of cuprous oxide can be used as catalysts, coatings, antifouling paints, semiconductor (to rectify alternating currents or use in some photoelectric cells), in the manufacture of coloring porcelain or paper, ... etc. Therefore, a great attention of the scientists has attracted to prepare, then to produce the nanocrystal powders.

Various non-radiation methods have been found for the preparation of superfine metal powders[4-5]. Conventionly, the methods of condensation with inert gases and the methods of pressurization in situ under vacuum are adopted to prepare the nanocrystal metal materials. However, the very expensive installations, the necessary of high vacuum and the low yields of metals restrict the applications of those methods to produce the nanocrystal powders. The metal cations can be reduced in radiolytic aqueous solution to form the nanocrystal particles[6-13] by e_{aq}^- or H. ; The reaction rate constants of them are in order of magnitude of 10^9-10^{10} [14-15]. The metal nanocrystal particles produced by radiolysis in solutions are present in colloidql state. Therefore further treatment for the formation of ultrafine powders is needed, although the nanocrystal aggregates can be obtained by one-step at room temperature and under ambient pressure. The pure nanocrystal powders of Ag[16], Cu[17], Pd, Ni, Pt, Au, Cd, Sn, Pb, Co and Cu_2O[18] were obtained in USTC Laboratory by combined method of γ-radiolysis with hydrothermal synthesis. It is sure that any metallic pure ultrafine powders can be obtained in principle by this method under suitable conditions.

EXPERIMENTS

The nitrate, sulfate or chloride or an other salt of Ag, Cu, Ni, Co, Cd, Sn, Pb, Au, Pt or Pd in analytic grade was dissolved in distilled water. A complexing agent (EDTA), a surfactant (sodium dodecyl sulfate SDS, PVA or sodium multiphosphate) and a OH radical scavenger (isopropanol IPol) were added into the salt solution. Then it was deaerated with N_2 and was irradiated by ^{60}Co γ-radiation. Finally the irradiated solution was put to hydrothermal synthesis. The ultrafine powders were washed with distilled water or (and) 25% ammonia aqueous solution, and dried.

The photoabsorption spectrum, the X-ray diffraction (XRD) patterns and the transmission electron microscope (TEM) microphotographs and electron diffraction patterns were used to study the radiolysis process of the solutions, the nanocrystal structures and the nanocrystal particle size and their shape, respectively. The XRD patterns Were taken from a Japan Rigaku Dmax γ_A X-ray diffractometer with high-intensity Cu Kα radiation ($\lambda = 1.54178$ Å) and a graphite monochrometer at a scanning rate of 0.05° s^{-1} in 2θ range from 20°—85°. The TEM microphotographs were recorded by a Hitachi model H-800 TEM with 200kv. The distribution of the nanocrystal particle size was determined by Perkin- Elmer microdensitometer and IBM PC-386 computer to analyse the microstructure densitometry of the TEM images.

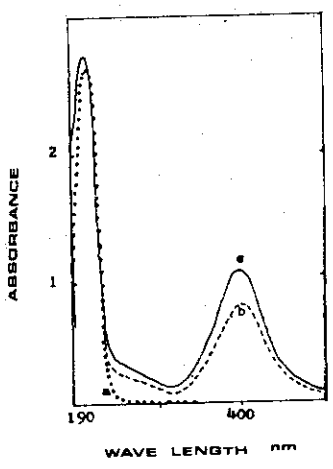


Fig. 1 Absorption spectrum of the 0. 01M $AgNO_3$ solution at different absorbed dose (dose rate 1. 0×10^2Gy/min): a. 0; b. 500Gy; c. 1000Gy.

RESULTS AND DISCUSSION

Creation, Formation and Growth of the Metal Aggregates

The metallic superfine particles can be created by the reduction transient species e_{aq}^- and H in radiolysis of aqueous solutions under γ-irradiation. The metallic atoms were produced one by one in earliest stage, which then were collected together each other by Van der Waals force to form the metallic cluster, finally, were assambled to grow up to be the metallic aggregates. The experimental data indicted that Ag colloidal aggregates were quickly formed in a few minutes after the starting of γ-irradiation, such as showned in Fig. 1. At the wave length 400 nm a new absorbance has appeared with absorbed dose 500 Gy, and the UV absorption intensity is increased with the increasing of the absorbed dose, i. e. the silver colloidal aggregates are increased with the increasing of the dose.

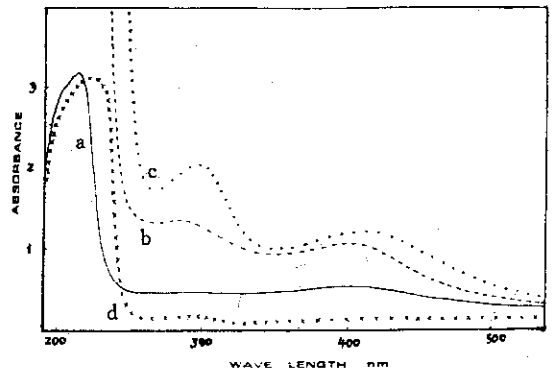


Fig. 2 UV absorption spectra of γ-irradiated $AgNO_3$ solution with different composition (dose 100 Gy, dose rate 20 Gy/min): a. 0. 001M $AgNO_3$+1. 2M IPol+0. 01M SDS; b. the same as (a) except $AgNO_3$ 0. 01M; c. the same as (a) except $AgNO_3$ 0. 1M; d. the same as (b) without SDS.

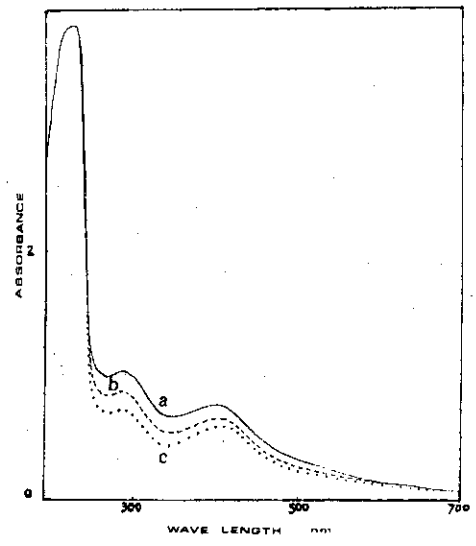


Fig. 3 The decay of the absorbances of Ag clusters and aggregates after their formation.
a/. 30 hrs after irradiation;
b/. 72 hrs after irradiation;
c/. 150 hrs after irradiation.

When dose rate was reduced to 20 Gy/min and the total dose 1×10^2Gy was absorbed, a new absoorption peak closing to 300nm appeared in colloidal $AgNO_3$ solution with 0. 01M SDS after irradiation immediately (see Fig. 2). From Fig. 2 it is clear that a new absorption peak at 289nm appears in solution (b), but it isn't observed in solutions (a) and (d). However, the peak strengthened and tended to shift to 300nm in solution (c). Perhaps it is the silver clusters with 4 atoms Ag_4^{2+} which should have observed at 275nm[12]. But it is probable that they are silver clusters with more atoms than 4. And it can predict that the absorption peak will shift to red with the increasing of the atoms in clusters, finally, till to 400nm which means the formation of the Ag aggregates with a few hundred to thousand silver atoms.

Fig. 3 shows that UV absorbances of the silver clusters and aggregates are step by step decayed with the time after their formation. It is certain that the absorbances at 289 nm and 400nm will be fully disappeared after a few weeks.

The metallic colloidal aggregates formed in irradiating aqueous solution will continueously grow

up to be a single crystal with the increasing of the radiation dose. The growth process of nanpcrystal Cu induced by electron irradiation into single crystal was observed by TEM, which is illustrated in Fig. 4. Fig. 4(a) and (b) are the original nanocrystal Cu particles with an average 16nm diameter. Fig. 4(c), (d), (e) and (f) show the Cu particles growed up progressively after electron irradiation of 3s, 6s, 9s and 12s, respectively. Finally, the Cu particles became a large spheroid single crystal about 1.5μm in diameter, i. e. the particles about 100 times growed up in diameter. It was fully proved by the electron diffraction that the spheroid is a single crystal of pure Cu (see Fig. 4 (h) and (g)). From these it may come to the conclusion that the radiation dose and dose rate strongly influence the nanocrystal metallic particle size, and therefore, it's properties.

Particle Size Distribution of Metallic Nanocrystal And Influence Factors On Them

Radiation—hydrothermal synthesis of the nanometallic powders and their oxide is an effective method. The ultrafine particles obtained in experiments are shown in Table 1.

Table 1. The conditions for preparing of nm powders

solution composition	PH	radiat. dose*, KGy	T, ℃	t, h	prod-t & av. size, nm
0.05M SN+0.1M SDS+6.0M IPol	5	24	105	1	Ag, 8
0.01M CS+0.1M SDS+3.0M IPol+0.01M EDTA	3.5	36	110	2	Cu, 16
0.01M PC+0.05M SDS+3,0M IPol	3	88	110	1	Pd, 10
0.001M H_2PtCl_6+0.01M SDS+2.0M IPol		1.8			Pt, 5
0.01M NS+0.01M SDS+2.0M IPol+0.1M AW	9.5	60			Ni, 9
0.01M $HAuCl_4$+0.01M SDS		0.75			Au, 10
0.01M CS+0.01M SDS+2.0M IPol+ 0.02M AcA+0.03M SAc	4.5	24			Cu_2O, 14
0.01M CdS+0.01M AS+1M AW+ 0.01M SDS+6.0M IPol	9—10	29			Cd, 20
0.01M TC+0.5M SH+2M IPol	12	25			Sn, 20
0.01M LA+0.05M SDS+2M IPol		12			Pb, 45
0.01M CC+0.5M AC+0.1M AW+2M IPol	~10	25.6			Co, 22

* Dose rate 92.5 Gy/min. SN—$AgNo_3$; CS—$CuSO_4$; PC—$PdCl_2$; NS—$NiSO_4$; AW—aqueous ammonia; AcA—CH_3COOH; SAc—CH_3COONa; EDTA—ethylenediamine tetraacetic acid; CdS—$CdSO_4$; AS—$(NH_4)_2SO_4$; TC—$SnCl_2$; SH—NaOH; LA—lead acetate; CC—$CoCl_2$; AC—NH_4Cl.

From Table 1 it may be affirmed that any metallic nanocrystals and their oxides can be prepared by radiation method if the reaction conditions are appropriate.

Firstly, the kind of salts seriously affects the reduction reaction, for instance, nitrates solutions are more difficult to produce the metallic particles than sulfates, because the reaction rate constants of nitrate with e_{aq}^- is about 10^4 times larger than sulfate. Therefore, selection of salt kind, is very important for reduction processes.

Secondly, a suitable surfactant is necessary to use to limit the aggregation of metallic particles. SDS is usually applicated in the experiments. When there was no SDS in solution, for example, the average particle size of Ag powders was 47nm, but it decreased to about 10nm if 0.1M SDS was added into the solution. Others can also be used sometimes as surfactant.

Thirdly, for some metals, such as copper, a complex agent is favorable for producing nano metallic powders. The average particle size is about 70nm from the solutions without EDTA. However, it is reduced to 16nm when EDTA was added. This phenomenon may be caused by relative lower reduction reaction rate of Cu^{++}—EDTA complexation ligands with e_{aq}^- than Cu^{++}.

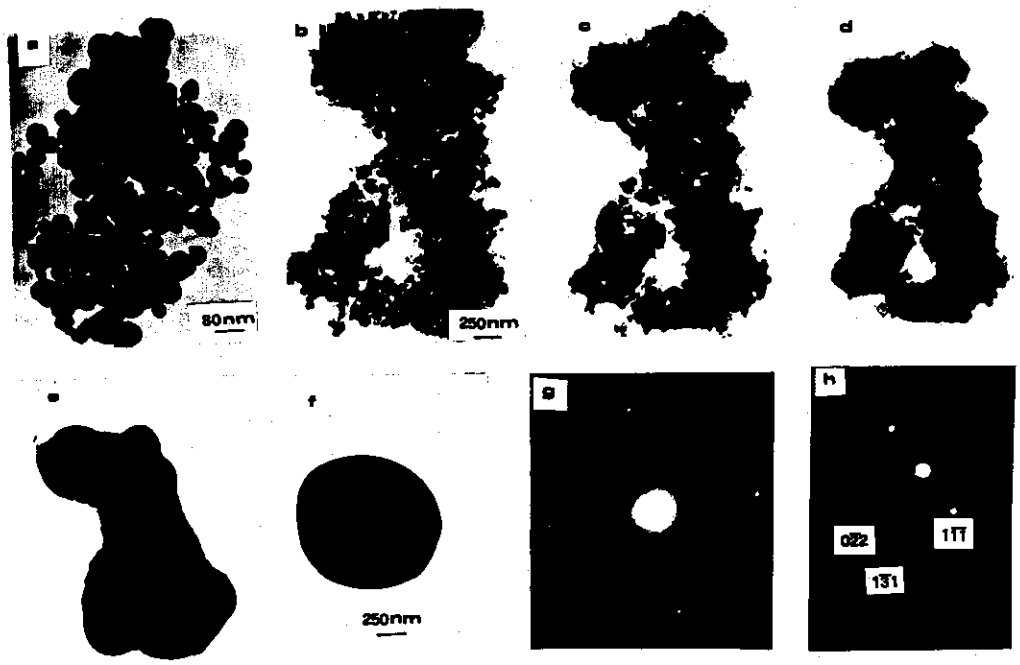


Fig. 4 TEM images of the samples prepared by γ-radiation- hydrothermal synthesis. a/ and b/ —— the same original sample with an average 16nm diameter; c/,d/,e/ and f/—— the same sample of b/ after 3s, 6s,9s and 12s of electron irradiation; g/ and h/——the electron diffraction images of the sample g/ in [001] direction and in [211] reciprocal lattice plane.

The experimenal data of temperature effect on the synthesis of Ag nanocrystal powders are shown in Table 2. 105℃ and 1h is the optimum conditions for collecting nanocrystal Ag powders. The Ag particle size increases from 9nm to 31nm to 43nm with the increasing of the temperature from 105℃ to 150℃ to 210℃. The absorbed dose in solution not markedly affects the Ag particle size in range 7.7——30 KGy.

Table 2. The influence of the temperature on Ag particle size

Solution	absorbed dose,kGy	hydrotherm. synthes.		particle size, nm
		temp,℃	time, h	
0.05M $AgNO_3$+6.0M IPol +0.1M SDS	30	105	1	15
	24	105	1	8
	11	105	1	9
	7.7	105	1	10
	11	room temp.	7 days	23
	11	150	1	31
	11	150	26	35
	11	210	1	43

The distribution of Ag particle sizes of the sample measured by TEM is showed in Fig. 5. The Ag particle sizes range from 6 to 40 nm, the largest percentage is about 35% in range 10 to 15nm. The average particle size is 16nm, which is in good agreement with that calculated from XRD patterns, 13nm.

Purity Identification of the Synthesized Materials

The XRD patterns of the products synthesized by γ-radiation—hydrothermal method are as the same as the XRD patterns of the standard pure Pd, Ag, Ni, Co, Cd, sn, Pb, Pt, Au, Cu and Cu_2O, respectively, i. e. they show that the products are single phase of Pd, Ag, Ni, Co, Cd, Sn, pb, pt, Au, Cu and Cu_2O, respectively. The formation of the pure metallic nanocrystal particles in solutions is not difficult to understand if the radiation reduction reaction was completd. However,

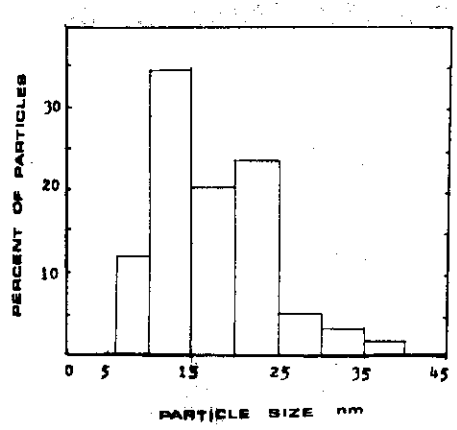


Fig. 5 nm Ag Particle size distribution

Cu^+ ions are very unstable in solution because they may further be reduced by e_{aq}^- to form Cu^0 or be dismutated each other to form Cu^0 and Cu^{++}. Then why can be obtained the pure Cu_2O in solution? The natural pH of the solution without buffer pair is 3.0—3.5, the product is the mixture of Cu^0 and Cu_2O because there are three competitive reactions: the reduction and dismutation of Cu^+ ions and the formation of CuOH in the solution. While pH value is over 4.0 to 4.5, the final product in solution is pure Cu_2O because the reduction and dismutation of Cu^+ are completely suppressed and CuOH decomposes immediately to Cu_2O after its formation. On the other hand, $Cu(OH)_2$ will form and precipitate at pH>5. So the pH value should be controlled in range 4.0——5.0 for preparation of Cu_2O. It is achieved by CH_3COOH/CH_3COONa buffer solution.

CONCLUSIONS

The nanocrystal powders of pure Ag, Pd, Ni, Co, Cd, Sn, Pb, Pt, Au, Cu metals were synthesized by γ-radiation.

The pure Cu_2O particles were obtained first of all by γ-radiation synthesis.

The creation, formation and growth processes from clusters to metallic aggregates and to single metal crystal are showed and discussed.

The metallic nanocrystal particle size distribution and the influence factors on them are illustrated and discussed.

All synthesized nanometer powders identified by XRD are absolute pure.

REFERENCES

(1). H. D. Glicksman, (1984)Metals Handbook, 9th Ed. V. 7, p. 147, American Society for metals, Metals Park, OH.
(2). Larry, J. R., Rosenberg, R. M. and Uhler, R. G., (1980) IEEE Trans. Compon. Hybrids Manuf. Technol. CHMT-3, 211.
(3). Fisher, G., (1983)Ceram. Ind. (chicago), 120, 80.
(4). Davis, S. and Klabunde, k. J., (1982) Chem Rev., 82, 153.
(5). Gleiter, h., (1989) Prog. Mater. Sci., 33, 223.
(6). Jujita, H., Izawa, w. and Yamazak, H., (1962)Nature, 196, 666.
(7). Belloni, J., Delcourt, M. O. and Leclere, C. M(1982) Nouv. J. Chim. (New J. Chem.), 6, 507; Delcourt, M. O., Keghouche, N. and Belloni, J., (1983) ibid, 7, 131; Delcourt, M. O., Amouyal, E. and Georgopoulos, M., (1986) ibid, 10, 607.
(8). Delcourt, M. O., Belloni, J., Marignier, J. C., Mory, C. and Collex, C., (1984) Radiat. Phys. Chem., 23, 485.
(9). J. L. Marignier, J. Belloni, M. O. Delcourt, and J. P. Chevalier, (1985)Nature, 317, 344.
(10). Bruneaux, J., Cachet, H., Froment, M., Amblard, J., Belloni, J., Mostafavi, M., (1987) Electrochimioa Acta, 32, 1533.
(11). Ershov, B. G., Janata, E., and Henglein, A., (1993) ibid, 97, 5457.
(12). T. Linnert, P. Mulvaney, A. Henglein, and H. Weller, (1990)J. Am. Chem. Soc., 112, 4657.
(13). Chen Zuyao, Chen Bo, Qian Yitai, Zhang Manwei, Yang Li and Fan Chenggao, (1992) Acta Metall. Sinica B, 5, 407.
(14). M. Anbar, M. Bambenek and A. B. Ross, (1973)NSRDS—NBS 43; A. B. Ross, (1975)ibid suppl.
(15). Anbar, M., Farhataziz and Ross, A. B., (1975) NSRDS—NBS 51.
(16). Zhu Y., Qian Y., Zhang M., Chen Z., Lu B. and Wang C., (1993) Mater. Lett., 17, 314.
(17). Zhu Yingjie, Qian Yitai, Zhang Manwei, Chen Zuyao, Lu Bin and Zhou Guien, (1994) Mater. Sci. Engn. B, 23, 116.
(18). Zhu Yingjie, Qian Yitai, Zhang Manwei, Chen Zuyao, Xu Dengfeng, Yang Li, Zhou Quien, (1994) Materials Res. Bulletin, 29, 377.

14.8 Preparation of a New Thermo-sensitive Material by Preirradiation Grafting

Minghong Wu, Zhongli Ding, Hongding Pu, Zue-teh Ma

Shanghai Applied Radiation Institute
Shanghai University of Science and Technology
Shanghai 201800, P.R.China

Abstract In this paper, a new thermo-sensitive material that NIPAAm was grafted onto EVA by preirradiation grafting was obtained, and the effects of reaction condition on grafting reaction were discussed. The experimental results showed that the swelling of the grafted EVA were reversible and the lower critical solution temperature (LCST) of the surface was 32°C, compared with the poly-NIPAAm gel, the grafted EVA with high mechanical strength behave the similar thermo-sensitivity and the more swift response to the change of temperature. When acrylic or acrylamide was added to NIPAAm, the LCST of the grafted surface shifts to higher with the increasement of the grafted component hydrophilicity.

INTRODUCTION

Thermo-sensitive hydrogel, one kind of external stimuli response hydrogel, collapse at elevating temperature through the LCST. The large change of volume happens within a quite narrow temperature range[1-5]. The gel swift absorb and release water in a way of switch on-off with the change of temperature. So this kind of material could be highly useful in many fields such as drug delivery[6-7], extraction[8], catalytic reaction rate control[9] and enzyme activity control[10].

The most important factors of thermo-sensitive hydrogel are phase transition temperature, phase transition rate and the mechanical strength, crosslinked poly-NIPAAm with a LCST about 32°C has attracted much attention for its representative thermo-sensitivity, but in swelling state, the mechanical strength is weak. To improve the mechanical strength, copolymerization and the interpenetrating polymer networks (IPN) have been tried [6,7,11]. The experimental showed the thermo-sensitivity is depended on the surface of hydrogel, the LCST may be kept at the same temperature as that of poly-NIPAAm, so we expect to get a new material with high mechanical strength and thermo-sensitive surface through the grafting of NIPAAm onto a trunk polymer. In experiments, we prepared the material that NIPAAm was grafted on EVA. The grafted EVA with high mechanical strength preformed the similar thermo-sensitive to the poly-NIPAAm gel. The effects on grafting and thermo-sensitive property were discussed.

EXPERIMENTAL

Trunk polymer, EVA slices in size of 8mm×20mm×1mm were carried out at a dose rate of 100 Gy/sec and a dose of 100kGy with EB of 0.9Mev energy from a Van de Graff accelerator at room temperature in the present of air. The irradiated slice and solution of NIPAAm with concentration of 20 Wt% in deionized water were added to test tube, then pump the atmosphere out of tube and added nitrogen to it. Then the test tube was placed in constant temperature water pool which has already reached the reaction temperature for desired hours, the grafting reaction was achieved.

The grafting yield and the swelling ratio were defined as:

$$G = (W_d - W_0)/W_0 \times 100\%$$

$$R = (W_i - W_d)/W_d \times 100\%$$

where W_0 -- the weight of the slice before grafting
W_d -- the weight of the slice after grafting
W_i -- the weight of the slice after equilibration in water
G -- the grafting yield
R -- the swelling ratio

RESULTS AND DISCUSSION

1 The influence of reaction condition on the grafting reaction

In grafting reaction, we discussed the influence of reaction temperature, reaction time, monomer concentration, preirradiation dose and dose rate on the grafting reaction. The results shown: common characteristic of preirradiation grafting reaction are reflected in NIPAAm-EVA system, for example, the grafting yield increases with the increasement of reaction temperature, reaction time and monomer concentration. When the reaction conditions were selected as: radiation dose rate is 280kGy/s, dose is 100kGy, monomer concentration is 20 Wt%, reaction temperature is 90 °C, after 5 hours grafting reaction, the grafting yield get 79%.

2 The select of trunk polymer

Fig.1 shows the swelling-deswelling curve of the surface of EVA and PE after grafted with NIPAAm. It is clear from Fig.1: with the increasing of temperature, the swelling ratio of the grafted EVA and PE happen abrupt change around 32 °C, it does not change with the different grafting trunk polymer. The swelling ratio of the grafted EVA is much higher than that of grafted PE. The volume of grafted EVA happens much larger

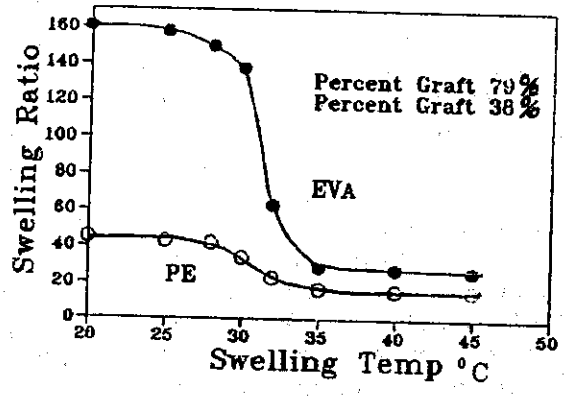


Fig.1 The influence of temperature on swelling ratio of EVA and PE sheet grafted by NIPAAm.

change within 2 ~ 3°C narrow temperature range through the LCST.

The difference of the swelling ratio between the grafted EVA and PE is connected with the grafting yield on the trunk polymer,the grafting yield is changed with the trunk: 1) The ventilatency of EVA is much better than that of PE. Oxygen diffuse easilier in preirradiation of the EVA slices, and it is favorable to the formation of peroxide. 2) In the other hand, the water pool temperature of grafting reaction is 90 °C, it is just nearby the softening temperature (Tm) of EVA and far from the Tm of PE. So it is convenient for the diffusion and absorption of the grafting monomer to EVA. Therefore, the grafting yield of NIPAAm on EVA is much higher than that on PE, the grafting yield of EVA can be get 79% while the grafting yield of PE is only 38%. So the grafted EVA with NIPAAm show the better thermo-sensitive.

3 Influence of grafting yield on thermo-sensitivity

The relationship between the swelling ratio and grafting yield is shown in Fig.2, it's clear from the change of swelling as a function of temperature that LCST of the surface grafted with NIPAAm does not change with the variation of grafting yield. The swelling ratio increase with increasing of grafting yield. As the grafting increase,the surface of trunk polymer become more and more hydrophilic below LCST, so the swelling ratio increase. As to above LCST, the shrinked grafting copolymer contains water, through much less than it does below LCST. The more graft, the more water is contained.

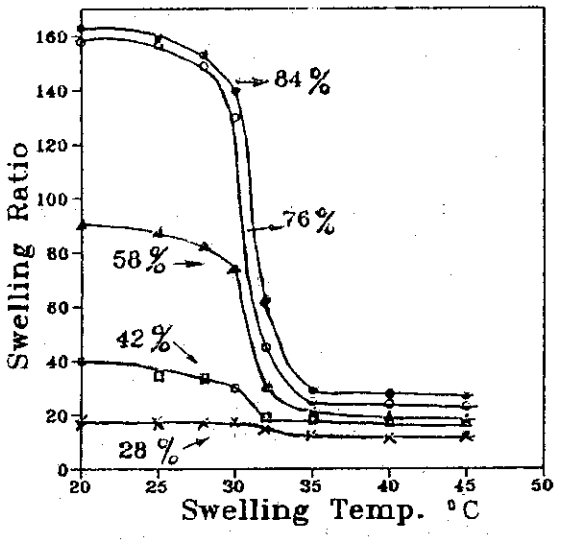


Fig.2 The swelling of EVA-g-NIPAAm changes as a function of NIPAAm grafting yield.

4 Influence of component of the grafting monomer on thermo-sensitivity

Fig.3 ~ Fig.5 are the DSC curves that the grafted surface happened phase separation around 30°C. They show the effect of hydrophilic monomer AAm on LCST and the swelling behavior of the surface co-grafted with NIPAAm-AAm. With the increasement of AAm component from 0%, 5% to 15%, correspondingly, the temperature of the phase change starting point

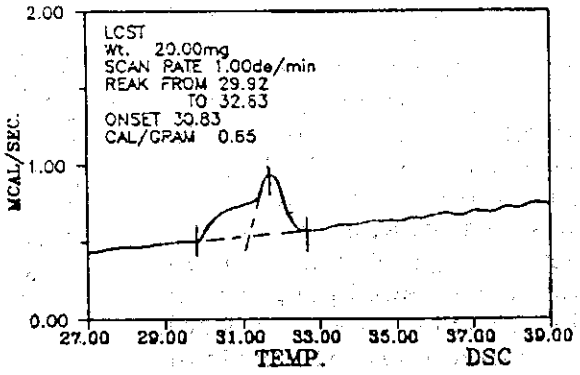


Fig.3 DSC thermogram for the surface layer EVA-g-(AAm-NIPAAm) equilibrated in deionized water at 15 C (100 NIPAAm).

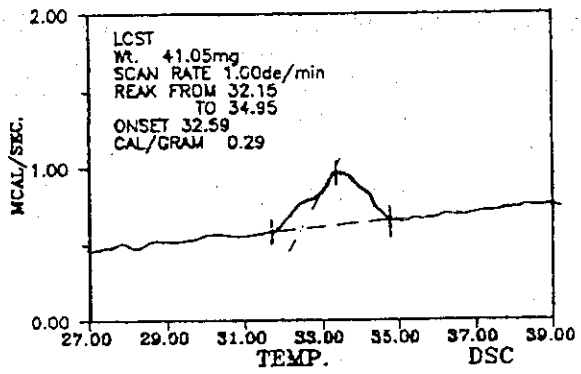


Fig.4 DSC thermogram for the surface layer EVA-g-(AAm-NIPAAm) equilibrated in deionized water at 15°C (95% NIPAAm, 5% AAm).

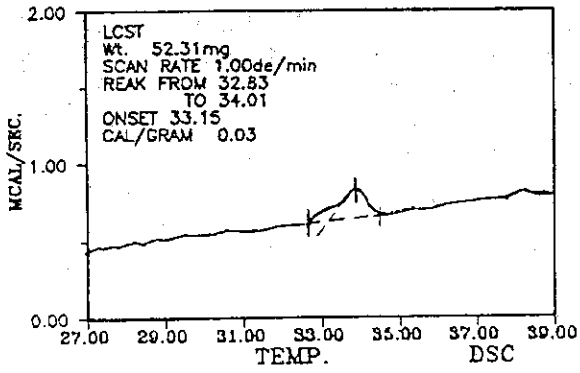


Fig.5 DSC thermogram for the surface layer EVA-g-(AAm-NIPAAm) equilibrated in deionized water at 15 C (85 NIPAAm, 15 AAm).

(ONSET) that stand for LCST enhance from 30.63 °C, 32.59 °C, 33.25 °C. In the meantime, the heat of phase separation that stand for the ratio of swelling decrease from 0.65, 0.29, 0.03 cal/g. So when hydrophilic monomer AAm was added to NIPAAm grafting solution, the LCST of grafted surface shift to higher temperature and the swelling ratio of grafted surface decrease with the increasement of AAm conponent.

5 Swelling and deswelling kinetics

The swelling-deswelling kinetics of EVA grafted with NIPAAm is shown in Fig.6. It indicate the swelling and deswelling of the grafted EVA were reversible. After several revesible swelling-deswelling change, both of the equilibration swelling ratio of swelling state and deswelling state basically keep constant. The response to temperature change is very quick. An abrupt decrease of swelling ratio is observed when the temperature is modulated from 20°C to 40°C, It takes only 15 minutes to squeeze out 80% of water. The reswelling is relatively slow and needed 25 minutes to reach 80% of full swell.Poly-NIPAAm gel took about one hour to extrude 70% water it contained in response to temperature from 25°C to 40°C. In reswelling, 2 hours are needed to absorb 80% of water. Compare with poly-NIPAAm, the EVA surface grafted with NIPAAm is more sensitive to temperature. Because when the temperature raising through the LCST, the out

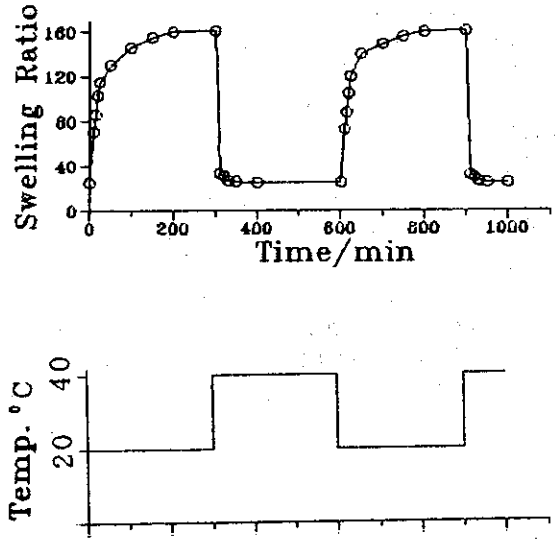


Fig.6 The swelling-deswelling kinetics of EVA surface grafted with NIPAAm.

layer of poly-NIPAAm is the first area to be affected, skin is formed, which retards the flux of water out. The decrease rate of swelling ratio is slow. In contrast, the NIPAAm grafted on the EVA surface is quite thin and loose, no skin is formed as the temperature increase pass LCST. The water in the grafting polymer is very easy to pass through when it shrinks. Therefore, EVA-g-NIPAAm would be useful for immobilization of enzymes to have their activities thermally controllable.

CONCLUSIONS

1 The grafting reaction on EVA with NIPAAm has common characteristics of preirradiation grafting reaction.
2 EVA surface grafted with NIPAAm present typical thermo-sensitivity similar to that of P-NIPAAm gel. The volume happen abrupt change within 2~3°C around its LCST of 32°C.
3 The grafting on EVA with NIPAAm-AAm mixture, the LCST of the grafted shifts to higher temperature, and the swelling ratio diminishes.
4 The response of EVA surface grafted NIPAAm to the change of temperature is more swift than that of poly-NIPAAm.

REFERENCES

1 Tanaka T, Phys.Rev.Lett., 1978, 40:820.
2 Hirotsu S, Hirokawa Y, Tanaka T, J.Chem.Phys., 1987,87:1392.
3 Matsuo E.S, Tanaka T, J.Chem.Phys., 1988, 89:1695.
4 Havasky M, Hrouz J, Havlicek.I, Polym., 1985, 26:26.
5 Ulbrick K, Kopeek I, J.Polym. Sci. Polym. Symp., 1979, 66:206.
6 Hoffman A.S, Affrassiabi A, Dong L.C., J.Controlled Release, 1986, 4:213.
7 Bae Y.H, Okano T, Kim S.W. Makromol, Chem., Rapid.Commun., 1987, 8:481.
8 Freitas R.F.S, Cussler E.L, Sep.Sci.Technol., 1987, 22:911.
9 Hoffman A.S, Affrassiabi A and Dong L.C, Paper Presented at American Chemical Society Meeting, New York,April,14-18(1986).
10 Dong L.C, Hoffman A.S, J.Controlled Release, 1986, 4:223.
11 Mukae K, Bae Y.H, Okano T, Kim S.W, Poly.J., 1990, 22:206.

14.9 International Standard of Radiation Sterilization Current Trend of Dose Setting and the Issues

Masaaki TAKEHISA

Radia Industry Co., Ltd.
168 Ooyagi, Takasaki, Gunma, 370 Japan

ABSTRACT

Current devices produced in a clean environment have low bioburden. However, a sensitivity of verification test of ISO method 1 declines at a low bioburden. Validation of the verification test in low bioburden region should be studied further. A dose setting using D_{10} of bioburden isolate should be reevaluated and be included in the ISO dose setting method.

KEYWORDS

bioburden, dose setting, D_{10} value, international standard, radiation sterilization, sterility test

INTRODUCTION

An international standard (ISO) of medical device sterilization "validation and routine control of radiation sterilization of health care products" is published shortly. The standard consists of a mandatory main body, requirement for validation and routine control, and informative annexes consisting of device and packaging material, sterilization dose setting, and dosimetry. ISO participating countries agreed the main body unanimously, and the standard will penetrate into the world shortly. However, the dose setting methods have problems because each country has their national methods according to the historical background.

Dose setting using bioburden and sublethal sterility test at SAL of 0.01 of natural contaminants was materialized as AAMI B1 dose setting (AAMI, 1984) using with a standard resistance distribution known as AAMI population C. The reference distribution of radiation resistance was obtained using isolates D_{10} of medical devices of cellulosic origin under conditions giving the highest values (Whitby, J., 1979), and should be represented that of natural bioburden with a margin of safety.

Many medical devices are now made of artificial materials, which are less contaminated than the natural products. An automated production line in a clean environment markedly reduces bioburden of medical devices less than 10. The method 1 was developed during late 1970's and bioburden of 1000 was used as a typical value. A verification condition of SAL=0.01 means that one of the 10^5 microbes survives in the bioburden of 1000, while one of the 100 microbes survives for bioburden of one. These will have quite different statistical significances. We have to seek about a modified verification test analysis for low bioburden devices.

PROBLEMS OF DOSE SETTING METHOD USING STERILITY TEST

Sensitivity of verification test for low bioburden devices

Figure 1 shows decrease in acceptance of verification test as a function of increasing radiation resistance of bioburden. The radiation resistant bioburden is calculated by assuming that D_{10} of each microbes in reference population C increases by factor of F (Takehisa M., 1994).

The results shown in Fig. 1 indicate that how the sensitivity of verification test at SAL=0.01 using 100 samples decreases with decreasing bioburden. Purpose of verification test is to confirm that the bioburden resistance is weaker than the reference population. Validation of the verification test has to show that the increased radiation resistance of bioburden results a failure of the verification test at more than 50% probability. If acceptance probability of verification decreases down to 50%, continuous success of audit is impossible. Figure 1 also suggests that the reference population must have safety margin corresponding to F at the rejection point of verification test.

Safety margin for reference population to bioburden resistance and validation of verification test

The 10 years experience of verification test acceptance in the US industry is reported that only 2.2% failed among 806 audits (Hansen J., 1993). A horizontal arrow in Fig. 1 suggests that the F of the real microbial resistance distribution is in the range of 0.93 to 0.80 for the bioburden range of 1000 to 0.1. This corresponds to margin of safety of the reference population of 1.08 to 1.25. The paper didn't refer the failure percentage of verification test as a function of bioburden, Anyhow, population C has 10 to 20% margin of safety for the bioburden resistance.

Under the 50% criterion of verification failure, F increases from 1.13 to 1.70 with decreasing bioburden from 1000 to 0.1 for the validation. In principle, the reference distribution should have the above margin of safety to real resistance distribution of bioburden microorganisms.

Figure 2 shows relation between bioburden in logarithmic scale and necessary factor of resistance (F) of reference population to bioburden at the 50% acceptance criterion. As seen in Fig. 1 success of verification test declines to 50% within the proper margin of safety of 1.1 - 1.2 (average value of 1.15 is shown in Fig. 2) in the F for high bioburden devices. The verification only declines, however, to 70 - 80% at low bioburden in this range of F values; where the test may be resulted in a false acceptance of verification. Such a false judgement in the boundary region is inevitable in a statistical method.

There are two ways to estimate the proper margin of safety of population C for criteria of validation from US experience (Hansen J. R., 1993). One is the overall value of 1.15 is applied for all bioburden, and the other is that the margin of safety is calculated for each bioburden values assuming an acceptance of verification was 97.8% for each bioburden. It can be said that the safety margin for validated verification is not assured at low bioburden in both cases.

The lack of the sensitivity of verification is obvious in low bioburden range lower than 1, where the difference exceeds beyond 20%. Use of present verification for bioburden less than two should be restrained until the efficacy of the safety margin becomes clear (AAMI, 1984, 1991). We have to develop a sophisticated logic for the validation.

A D_{10} DISTRIBUTION FOR LOW BIOBURDEN DEVICES

The above analysis conclude that sensitivity of verification test decreased for low bioburden products. On the other hand, verification test of low bioburden products tended to fail when exact (median) verification dose was delivered. Recent findings of bioburden and D_{10} distribution of hypodermic needles (Tabei *et al.*, 1994) shows that the D_{10} distribution has two peaks. The ratio of weak cells over strong one is smaller than the ratio of AAMI population C. A change in D_{10} distribution in a low bioburden range seems the cause of above discrepancy. Further study is necessary to clarify the assumption.

A practical solution, compatible to the ongoing standard is modifying the population C for low D_{10} microbes. If we unify D_{10} <1.0kGy and 1.0 - 1.5kGy microbes as <1.5kGy microbes with

frequency of 0.8798, which is the sum of frequencies of <1.0kGy and 1 - 1.5kGy microbes of AAMI population C (AAMI, 1992), the verification doses in low bioburden region increases. However, the sterilization doses at SAL of 10^{-6} are kept as they are, because the low D_{10} microbes already decayed in low dose region than 10^{-6} SAL dose as shown in Table 1 (Takehisa, M.,1994-2). This will add a margin of safety for reference distribution for dose level of verification test and increases sensitivity.

STERILIZATION DOSE SETTING USING ISOLATE RADIATION RESISTANCE (D_{10})

Dose setting with use of bioburden and isolate radiation resistance

The dose setting with use of device bioburden and radiation resistance (mostly D_{max}) of isolates is popularly used in many countries. Merits of the bioburden isolate method are needs of small sample sizes, direct reflection of radiation resistance of bioburden to sterilization dose, and sufficient margin of safety of sterilization dose by using D_{max}. Demerit of the method are man power oriented D_{10} measurements. Issues of this dose setting method are unknown relationship of radiation resistance of isolate to that of natural state, and existence of resistant microbe in small fraction that is scarcely found in the bioburden. An existence probability of the resistant microbes higher than 3.1kGy (1.3% of microbes are in this range in AAMI population C) is 12.7% or 1.3% of devices with bioburden of 10 or 1. It can be said that such resistant microbes contribute to high bioburden product but negligible for low bioburden product.

A joint research project between government and industrial sectors for D_{10} accumulation

A three years joint research project has started in 1994 in cooperation with National Institute of Hygienic Sciences, two public research institutes, and 10 device manufacturers. Aims of the research project is to accumulate D_{10} of contaminants from medical devices using the harmonized methodology. A radiation resistance measurement of bioburden isolate is carried out using harmonized method used for AAMI population C that represents radiation resistance of natural bioburden (Davis, K.W. *et al.*, 1981). This is also compatible to D_{10} measurement method in Manchester (Yan, A., *et al.*, 1994). In the present research project we clarify a resistance distribution for isolates from devices made of artificial materials, and water filled devices such as a wet type hemodialyzer. An initiation of similar research project is expected to clarify that the resistance distribution is homogeneous around the world or not. This will help the future harmonized dose setting method in the international trade. We expect the isolate method is to be included in the annex of ISO after new D_{10} distribution is clarified. This also contribute the refinement of verification test method of ISO method 1.

REFERENCES

AAMI, (1984). *Process control guideline for gamma radiation sterilization of medical devices* (AAMI RS), Arlington, VA., AAMI.
AAMI, (1992). *Guideline for gamma radiation sterilization* (ANSI/AAMI ST32-1991, 2nd. Ed.), Arlington, VA., AAMI.
Hansen, J.M. (1993). AAMI dose setting: Ten years experience. *Sterilization of medical products*, Vol. VI, (Morrissey R.F. , Ed.), Polyscience Publications Inc., Morin Heights, Canada, pp. 273 -281.
Tabei, M., Sekiguchi, M., (1994). Evaluation of sterilization dose for disposable hypodermic needles manufactured under ultra-clean condition, *Radiat. Phys. Chem.* (presented at IMRP9)
Takehisa, M., (1994). A versatile method of verification test for radiation sterilization, *Radiat. Phys. Chem.* (submitted)
Takehisa, M., (1994-2). International Standard (ISO) of Radiation Sterilization and Issues in the Sterilization dose Setting, *J. Radiation Phys. Chem.* (presented at IMRP9).
Whitby, J.L., (1979). Radiation resistance of microorganisms comprising the bioburden of operating room packs. *J. Radiat. Phys. Chem.* 14, 285 - 288
Yan, A., and Tallentire, A., (1994). Distribution of radiation resistance of microbiological contaminants of a cotton-based medical product, *Radiat. Phys. Chem.* (presented at IMRP9).

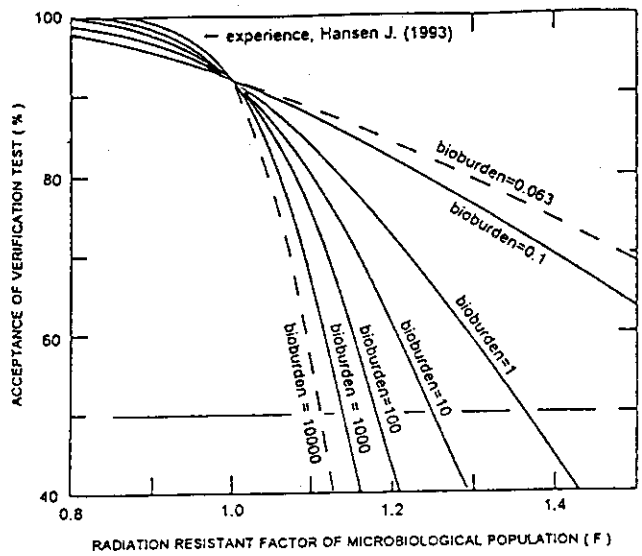


Fig. 1. Sensitivity of verification test at SAL of 0.01 using 100 samples

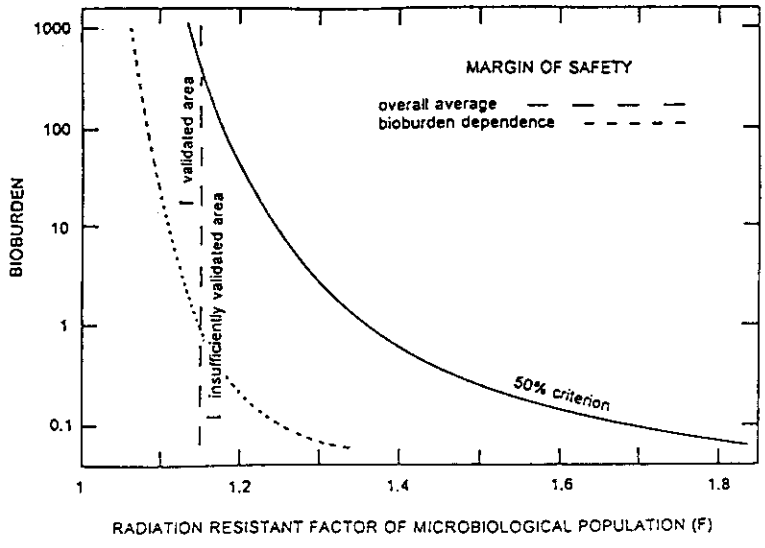


Fig. 2. Region of validated verification test as function of bioburden at SAL of 0.01 using 100 samples

Table 1. Change in verification dose by unifying D=1 and D=1.5kGy microbes as 1.5kGy microbes in AAMI population C (Frequency = 0.8798)

Bioburden	Verification dose (kGy)			10^{-3} SAL dose (kGy)			10^{-6} SAL dose (kGy)		
	ISO/AAMI		this work	ISO/AAMI		this work	ISO/AAMI		this work
0.1	1.3	<	1.6	3.0	<	3.4	11.0	=	11.0
1.05	3.0	<	3.4	5.4	<	5.5	14.3	=	14.3
10.69	5.3	<	5.5	8.1	=	8.1	17.8	=	17.8
104	8.0	=	8.0	11.0	=	11.0	21.3	=	21.3

presented at JCBSRC, Waseda Univ., Tokyo, on Nov. 10, 1994

14.10 Electron Beam Sterilization for Dishes

WANG DE-REN FANG MEI-ZHEN

WU XIAN RADIATION PRODUCTS FACTORY SUZHOU, CHINA.

Modern biological science often needs various fine strike devices which are often made from non-toxic transparent plastic. The application of high temperature steam to the sterilization as a tradi tional methods often causes deformation and colour change. When chemicals are applied to the sterilization residure of chemical grain often causes toxicity. Only application of radiation to the sterilization can overcome this faults and carry out with sterility assurance at room temperature. In this research 1.3 MeV electron beam coming from Model JJ-2 accelerator was applied for sterilization to 96-well tissue culture plates. After clean packaging the plates were irradiated with 31.7 KGy and operational voltage 1.3 MeV and 100 μA on the PY device. Repeated tests demonstrate that the products are sterile. The output is 2×10^5 pieces for each year.

1. Principle

Irradiation of electron beam with high energy can cause formation of free ions and radicals and various chemical and biochemical reactions the process of which are complex and are still not clear yet. The present theory of sterillization is achieved by destroy of life that is caused by DNA chain break and inhibition of protein synthesis. But application of irradiation to sterilization was discovered much earlier than this and it has been applied and developed on technology. Economic advantage has been obtained.

2. Technique process

Requirements for manufacture of device for tissue culture are very strict. There is strict specification for the volume of wells on the plates so that not visible deformation should exist. It must be transparent PS plastic. Scratches and colour change are not permitted. Besides it must be sterile and nontoxic without toxic residue on them. Numbers of organism surviving must meet the standards. Only the strict controled process can meet such a kind of requirement. The procedure undertaken in production is as follows:

Injection of plastic-cleaning-drying by heating-packaging and seaking-irradiation sterilization-tests.

Injection of plastic: Equipment and material used for injection of plastic should be clean and free of dust. After removing from cast the devices are put in plastic bags. The numbers of organism surving on it must meet the standards.

Cleaning: The devices are soaked in non-toxic detergent for some time then washed thoroughly with water.

Dry: Deformation should be prevented from over heat at high temperature. After drying the devices are packed in the purification hood with ultra-violet lamp and air purifying device. The bags containing the plates are sealed

immediately. All operation should be conducted by operators with sterile medical gloves.

3. Electron irradiation

Irradiation is the key link in the process.

(1) Determination of dose

A large amount of investigation has been carried out by medical scientists. Sterilizing dose has been known. In considering the margin of safety the 12 D_{10} value has been taken into account. This is the dose that will reduce given population by a factor of 10^{-12}. The lowest absorbed dose for routine radiation steripization permitted by authority in U.S.A. Japan and Europian counties is 25KGy. This regulation satisfys with the margin of safety. Tests with spore of Bacillus subtilis were carried out by Hung-Fu Shi et al. D_{10} and $12D_{10}$ were obtained: D_{10}=2.09KGy, $12D_{10}$=25KGy. This indicates that when dose reaches to 25KGy the population will be reduced by a factor 10^{-12} e.i., irradiated at this dose all organism excèpt spore of Bacillus Subtilis are killed. Of couse, if the dose is larger than this organism will be killed but it will cause energy waste, or deformation and damage of irradiated devices. So this is the margin of the lowest absorbed dose which is economise for irradiation.

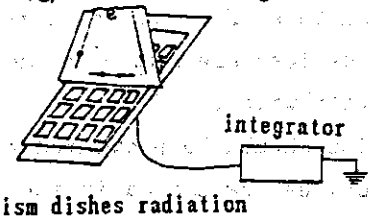
(2) Irradiation

Electron beam irradiation was conducted with the Model JT-2 accelerator under condition of accelerator valtage 1.3 MeV and length scan 10cm. In order to use electron beam fully a movable PY device was installed at the electron window. At the bottom of the device is a stainless steel tray on which 4 rows of plates, 8 for each row, e.i., 32 plates in total. Because the electron beam was not large enough irradiation must be carried out in a cumulative way by conducting interval and repeated irradiation. When irradiation finished for one batch a new batch was replaced during the time of operation intervals. Irradiation dose was monitored by integrator from which a sire leads to the tray. The process was monitored by ITV. The operator must concentrate on the operation.

(3) Dose control

In according to the smallest radiation sterilization absorbed dose 25KGy and electron beam 1.3MeV integral results can be worked out. The 96 well plate was made from PS plastic. Specific gravity of which is 1.04g/cm^3. Total thickness of cover and base is 3.5mm. The mass thickness is 0.364g/cm^2. The electron density of PS is Pe=3.24x10^{23}e/g. When E=1.3 MeV the range of electron ejection can be caculated as $R=\frac{1.5/E}{P_e}=0.606 g/cm^2 > 0.364 g/cm^2$. The integration can be expressed as

$$\phi=\frac{DbeR}{1.3E}$$



When $\emptyset$ is integral value expressed as μC, length of scan E is electron energy, D is the smallest radiation-sterilization absorbed dose, e is the range of electron penitrating in PY, R is ejection distance. In this case b=40cm, D=25KGy, e=110cm, R=0.606g/cm^2, caculation is carried out in according to the above given parameters. The result is $\emptyset$=39444 micro c. In considering the thickness of the thickest part of the plate we take the $\emptyset$ as 50,000 micro c D=31.7 KGy.

This dose does not cause deformation of PS. When irradiation reaches to the half dose we turn plates over and continued irradiation. When the reading get to 50,000 micro c irradiation is stopped. The process of irradiation ends.

If operation is carried out at 100 micro A irradiation time is 500 seconds. In considering time of stopping operation and replacement cycle of irradiation for 32 plates is 15 minutes. It means 128 plates can be irradiated per hr. and 2×10^5 plates per year.

4. Tests

After package of 72 well plates they were tested for radiation sterilization with brogh-agar plate culture method by medical school. All results were negative. The validation of radiation sterilization was also tested by H^3-TdR corperation method. RPMI 1640 medium and H^3-TdR were put in wells on the plate and incubated in the CO_2 incubator at 37°C for definte time. After incubation radioactivity of H^3-TdR in each well was determined by cintilation counter. Radioactivity in un-irradiated samples in plates were taken as control. Activity of samples in the irradiated plates was at background level. The counts of samples in the un-irradiated plates were 2 million cpm. The processed plates have been sent to the Chinese Cytology Institute, the Chinese Fundermental Medical Science Institute and hospitals to have tests. These tests indicate that the plates are sterile, non-toxic and proper for cell growing. Microbiological tests were conducted by the epidemic disease provention station too. The results are negative. In the tests 6 indicators of bacteria with 10^6 "4001" bacillus which were in different parts in the bag were applied. The test results are negative.

Conclution

By application of process for irradiated organism plates validation of sterilization can be achieved. It has the advantage of efficient, high speed and undeformation.

References:

1. Bin-Ling Wang: Radiation sterilization of medical supplies Reference material compiled by Society of Nuclear Scince and Radiation Applications.
2. Hung-Fu Shi et al: Technique of radiation sterilization of ready use medical supplies. Report of Chinese Nuclear Technology
3. Ross. E. W. Jr.: J. Food. Sci 1974,39,800

14.11 Evaluation of Sterilization Dose for Disposable Hypodermic Needles Manufactured under Ultra-clean Condition

Masae TABEI and Masayuki SEKIGUCHI

Tokyo Metropolitan Isotope Research Center, 2-11-1 Fukazawa, Setagaya-ku, Tokyo, Japan

ABSTRACT

Relationship between characteristics of bioburden and sterilization dose setting for disposable hypodermic needles, produced on same manufacturing lines, is presented in this study. The number of bioburden for 512 needles (18 lots) was changed from 0 to 6 and its distribution was extremely shifted to 0. Most of isolates (401 strains) were Gram positive cocci (60.3%) and spore forming bacteria (31.7 %). The distribution of gamma radiation resistances (D_{10}) showed two peaks at about 1.1 kGy and 0.4 kGy. The sterilization doses estimated by Japan log formula method on the basis of above data became higher than those by AAMI B2 (UDS) and B3 methods.

KEYWORDS

disposable hypodermic needle, radiation sterilization, sterilization dose, bioburden, radiation resistance

INTRODUCTION

Generally speaking, the lack of informations for bioburden brings about undesirable results in sterilization dose setting. Recently, following with GMP control, medical products with a very low bioburden have been mass-produced, but such products essentially have difficulties to obtain sufficient informations for bioburden. In AAMI methods (AAMI,1984; AAMI,1991), known as a flexible dose setting method, a low bioburden may influence the estimation of the extrapolation factor or the results of auditing experiments.
Therefore, to establish a resonable sterilization dose with a large safety margin for such products, the dose setting method should be carefully selected or developed. From above reasons, the investigation on characteristics of bioburden in such products have increasingly become important.
We have examined a relationship between characteristics of bioburden in a product manufactured by ultra-clean condition and differences of sterilization dose estimated with several dose setting methods.

MATERIALS AND METHODS

Needles
About 9500 samples (20 lots) of disposable hypodermic needles (18G×$1^1/_2$ - 27G ×23 mm, Misawa Medical Industry), produced on the same manufacturing lines for about 3 years , was used.

Measurements of Bioburden
One needle and 10 ml of washing solution (0.1% Tween 80 + 0.85% NaCl in distilled water) in a screw-cocked test

tube (30 ml) were agitated by a shaker for 5 min. (about 360 strokes / min). Moreover, efficient collecting microorganisms, 10 samples and 30 ml of washing solution in a Duran bottle (100 ml) were agitated by the same condition as above. After agitating, washing solution was filtrated with membrane filter (MF: Toyo Advantech, pore size: 0.45 μm). MF was incubated on a paper filter pad immersed with 2 ml of Trypticase Soy Broth (TSB, BBL) at 35 °C for 7 days, and these bioburden were calculated from viable counts of colony on MF. Sterility tests of pre-sterililized needles were carried out with TSB at 32°C for 14 days and the probability of positive culture was examined.

Simple classification of microorganisms

After Gram's and spore staining, microorganisms were classified with regard to morphology by microscopic observation.

Samples for irradiations

After simple classification of bioburden by microscopic observation, spore forming microorganisms were incubated on Trypticase Soy Agar medium (TSA, BBL) contained 10 ppm of Mn^{2+}, and non-spore forming microorganisms were incubated on TSA at 35 °C for 2-10 days. Fungi and yeasts were incubated on Potato Dextrose Agar medium (PDA: Difco) at 25 °C for 14 days. Microorganisms grown on the culture media were scratched with a glass spreader. Microorganisms were filtrated with glass wool, and then washed by centrifugation (6000 rpm, 20 min., 4 °C , 3 times) with 0.85 % saline water.

20 μl of harvested washed microorganism suspensions were dropped on a glass fiber paper (Toyo Advantech, GA-100, about 1×1 cm) or a piece of polypropylene (PP) cap of needle (about 1×1 cm) with a micropipette. After drying in a clean bench, these test pieces were enclosed in sterilized bags (Hogi Medical, HM-301) one by one.

Irradiation

Gamma ray was irradiated by Co-60 source (185 TBq). Dose range of 1-15 kGy and dose rates of 0.36-2.2 kGy/hr were used. Electron beam (EB) was irradiated by a 5 MV Dynamitron accelerator. Beam currents were 0.8-1.0 mA, cart speed under the beam were 9.5-17.5 m/min and dose range were 1-16 kGy. Dosimetry for gamma ray and EB radiation were done using Fricke dosimeter and radiochromic film dosimeter (FWT-60), respectively.

Radioresistance of microorganisms

Irradiated test pieces were agitated for 5 min. with 3 ml of washing solution and about 15 glass beads (Ø: 2-3 mm) in test tube by an automatic mixer. Homogenized suspensions of glass fiber paper and agitated suspensions of PP cap were adequately diluted with 0.85 % saline water. An adequate amount of diluted suspension was mixed in a petri dish with TSA at about 50 °C and shaked ,and then incubated at 35°C for over 40 hours. Fungi and yeasts were incubated at 25°C for 5 days after spreading on PDA.

Survival curves were made from viable colony counts on the agar culture, and were approximated to linear or quadratic expression with least squares method. D_{10} values were calculated from survival curves as the average values of 6D/6.

RESULTS AND DISCUSSION

Bioburden

On the bioburden experiments of 512 needles (18 lots) by MF method, the number of bioburden was from 0 to 6 and its distribution extremely shifted to 0 (total average bioburden: 0.123). Furthermore, the average probability of detecting microorganisms (8.0%) of all lots was larger than that of positive cultures in sterility tests (3.8%), and both were independently changed from lot to lot (Fig.1). Following AAMI B2 (UDS) method (AAMI, 1984), needles randomly sampled from 3 lots, which probability of positive sterility test in non-irradiated needle was 2 %, were separately irradiated in the incremental dose experiments by EB and gamma ray. All samples were negative except the sample irradiated at a dose of 1 kGy by EB (one positive). The results of sterility test experiments for non-irradiated 1800 needles (18 lots × 100 samples), which were carried out for the same lots as the bioburden experiments, and some of AAMI auditing experiments were shown in Table 1. The number of positive culture was changed from 0 to 11 of 100 samples. In AAMI auditing experiments, 5 of 17 auditing experiments showed more than 3 positive, that original sterilization dose was not accepted. Usually, we observed microscopically the existence of limited types of microorganisms. 401 contaminants isolated from MF and sterility test experiments were classified

into four groups with regard to morphology: Gram positive cocci (60.3 %), spore forming bacteria ,*Bacillus*, (31.7 %), yeasts and fungi (3.5 %) and unclassified microorganisms (4.5 %).

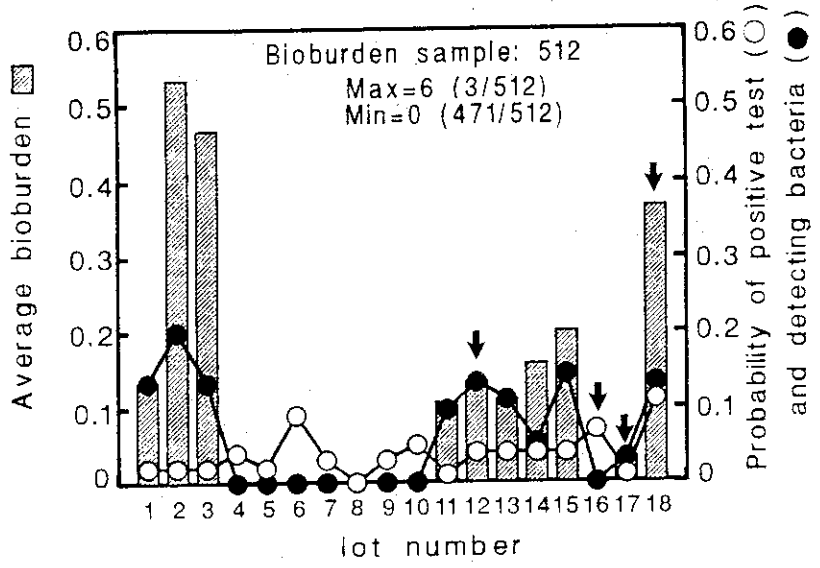


Fig. 1. Relationship between bioburden and sterility test
↓ : failed lot in AAMI audit experiments

Table 1. Results in AAMI audit experiments

	Positive number of 100 samples											
	0	1	2	3	4	5	6	7	8	9	10	11
Non-irradiated	1	2	4	1	5	1	0	1	0	1	0	1
Gamma ray (1 kGy)	4	2	1	1	2	0	0	0	0	0	0	0
Electron beam (1 kGy)	4	1	0	1	1	0	0	0	0	0	0	0

* The number in column show frequencies of audit experiments

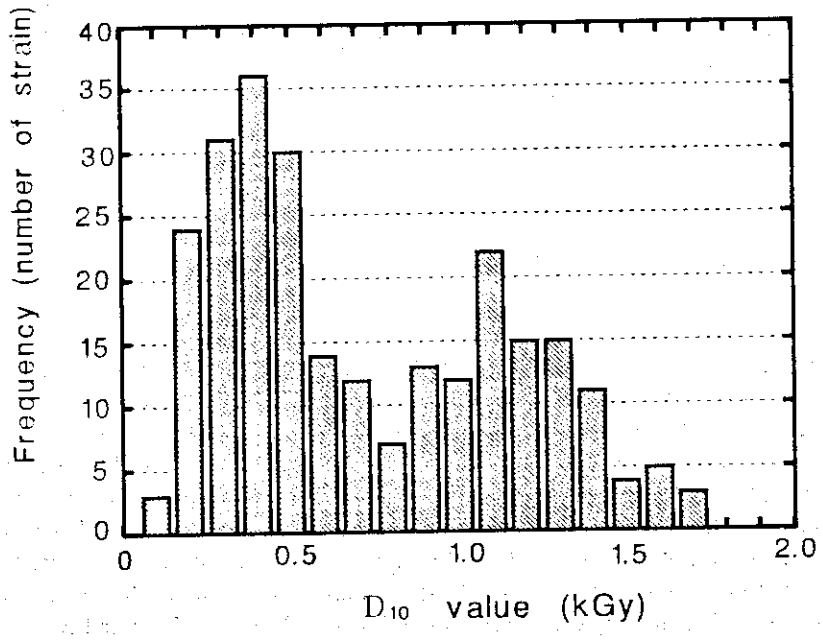


Fig. 2. D_{10} value distribution of natural bioburden (257 strains) on the hypodermic needles for gamma ray irradiation. (carrier material : glass fiber paper)

Table 2. Radioresistances of microorganisms isolated from hypodermic needles

	D_{10} value for electron beam (kGy)		D_{10} value for gamma ray (kGy)	
	glass fiber paper	PP test piece	glass fiber paper	PP test piece
Baccilus pumilus ATCC 27142	1.55	1.52	1.51	1.55
No.1 (*Bacillus*)	1.38	1.55	1.40	1.51
No.10 (Gram positive cocci)	1.67	1.97	1.61	1.93
No.21 (*Bacillus*)	1.78	1.88	1.68	1.68
No.24 (*Bacillus*)	1.50	1.73	1.59	1.98

Radioresistance of isolated microorganisms

Distribution of radioresistances (D_{10}: 6D/6, carrier: glass fiber paper) for isolated microorganisms showed two peaks at about 1.1 kGy and 0.4 kGy. The maximum and minimum D_{10} values were 1.76 kGy and 0.15 kGy, respectively (Fig.2). Spore forming bacteria and a part of Gram positive cocci were contained in the former peak, and fungi, yeasts, and the rest of Gram positive cocci were contained in the later peak.

And then four strains of high radioresistant bacteria that were selected from a series of experiments and reference bacteria (*Bacillus pumilus* ATCC 27142) were used to the estimation of radioresistances by EB and gamma ray irradiation: Three strains (No.10, 21 and 24) were isolated from bioburden experiments, and one strain (No.1) was isolated from the experiment followed AAMI-B3 method. Radioresistances of those bacteria were influenced by carrier material (Table 2). Radioresistance of bacteria inoculated on PP cap of needle were higher than that on glass fiber paper. The maximum D_{10} value was less than 2 kGy.

Estimations of sterilization doses

Sterilization doses of needles were estimated based on above data. When the sterilization dose was calculated by Japan log formula method (Ministry of Health and Welfare, Japan, 1993), 1.97 kGy (EB) and 1.98 kGy (gamma ray) as the maximum D_{10} values, and 10 organisms per needle as the safety estimation value instead of the maximum of bioburden (6 organisms per needle) were used. As the results, sterilization doses were 13.79 kGy (EB) and 13.86 kGy (gamma ray), respectively.

The maximum D_{10} values obtained by AAMI B3 method were 1.55 kGy (EB) and 1.51 kGy (gamma ray), respectively. The sterilization doses calculated from those data were 8.95 kGy (EB) and 9.00 kGy (gamma ray).

On AAMI B2 (UDS) method, D^{**} were 0.95 kGy (EB) and 1.00 kGy (gamma ray) , and UDS of both were 1.8 kGy. And then, sterilization doses were 8.15 kGy (EB) and 8.2 kGy (gamma ray). When AAMI method 1 (AAMI, 1991) was used to these samples, sterilization dose correspondent to the average bioburden (0.53) was 13.5 kGy, provided that the verification test was passed. The sterilization doses estimated by Japan log formula method were higher than those by AAMI B2 (UDS) and AAMI B3 method, and almost equal to those by AAMI method 1 by chance.

As shown in Fig.1 and Table 1, the auditing of sterilization dose in AAMI B2 and B3 method was sometimes failed by fluctuation of bioburden. If AAMI method 1 is applied to low bioburden products, the sterilization and auditing dose may be changed remarkably with fluctuation of bioburden. The increase of the difference between average and maximum bioburden may bring about the decrease of the efficacy of the auditing as shown in Table 1. The radioresistant distribution of AAMI population C was obtained with sub-lethal screening and expressed as populations with D_{10} values of more than 1 kGy (Whitby *et al.*, 1979). Therefore, if populations with D_{10} values of less than 1 kGy are omitted from the radioresistant distribution of the hyperdermic needle bioburden (Fig.2), the survival curve of the residual populations (average bioburden=1) is plotted as shown in Fig.3.

The survival curve for PP cap carrier (solid line) was estimated by multiplying radioresistances of the residual populations by 1.245, which value was the ratio of the D_{10} value of 1.98 kGy to that of 1.59 kGy for No.24 strain in Table 2 and also the muximum ratio of the D_{10} values for PP cap to those for glass fiber paper in Table 2. The auditing dose obtained from the survival curve for PP cap carrier was greater than that of AAMI population C.

If dried samples of bacteria suspended in TSB, as Whitby's experiments, have great radioresistances compared with those in distilled water, the auditing dose obtained by the survival curve for PP cap carrier may be further increased. Therefore, those methods are undesired to apply to medical products with a very low bioburden. On the other hand, Japan log formula method, using a maximum D_{10} and safety value instead of maximum bioburden, is thought to be relatively stable against fluctuation of bioburden and providing a reasonable sterilization dose with a satisfactory safety margin.

From above reasons, microbiological informations by routine control following with GMP, are very important to estimate a sterilization dose for ultra-clean medical products.

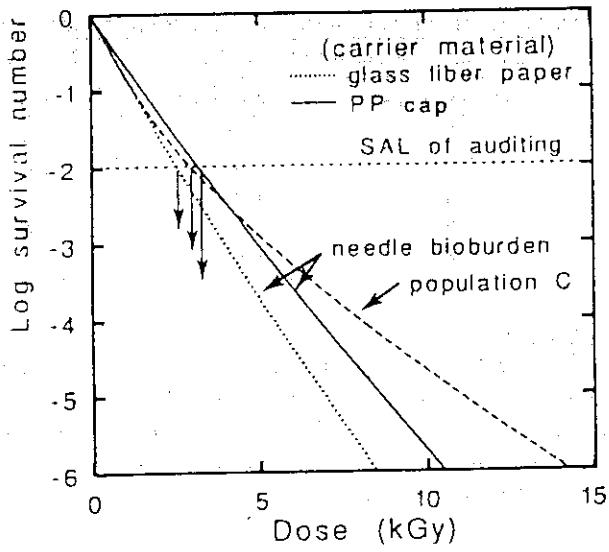


Fig. 3 Survival cureves for the hypdermic needle bioburden and AAMI population C, and auditing doses (average bioburden = 1)

REFERENCES

Association for the Advancement of Medical Instrumentation (1984), Process control guideline for gamma radiation sterilization of medical devices RS-3/84 .

Association for the Advancement of Medical Instrumentation (1991), Guideline for gamma radiation sterilization (ANSI/AAMI ST32-1991, 2nd edition).

Ministry of Health and Welfare, Japan (1993), Guide to Medical Registration in Japan, 7th edition.

Whitby J. L. and Gelda A. K. (1979), Use of Incremental doses of cobalt 60 radiation as a means to determine radiation sterilization dose, *J. Parent. Drug. Assoc.*, 33, 144-155.

14.12 Removal of Gaseous Xylene by Electron Beam Irradiation

Koichi HIROTA,[1] H. MÄTZING[2] and H. -R. PAUR[2]

[1]Japan Atomic Energy Research Institute, Takasaki Radiation Chemistry Research Establishment, 1233 Watanuki, Takasaki, Gunma 370-12, Japan and [2] Kernforschungszentrum Karlsruhe GmbH, Laboratorium für Isotopentechnik, Postfach 3640, D-76021 Karlsruhe 1, Germany

Abstract—Gaseous xylene was irradiated with electron beam in the dose range of 0-10 kGy at ambient temperature. The concentration of xylene was measured with a gas chromatograph for the evaluation of the irradiation effect on removal of xylene. Input concentration of 22.5 ppm xylene decreased to 3 ppm at the dose of 10 kGy. The irradiated xylene gave gaseous products and solid aerosols. The analyses of the gaseous products by ion chromatography revealed that formic, acetic, propionic, and butyric acids were formed by the xylene-irradiation. The concentration of the aerosols constituted approximately 50 % of the xylene removed. Mass balance for the xylene-irradiation was calculated on the basis of mgC/Nm^3 unit. More than 80 % of the recoveries were obtained in all experiments.

INTRODUCTION

Various kinds of treatment methods for pollutants have been applied to meet the regulations established by the Japanese Government for environment and our health. New technologies and/or the developed methods are required to meet more strict and new regulations which will be drawn up in the future. Electron beam irradiation has been proposed as the new technology for treating VOC (Volatile Organic Compounds) (Paur et al., 1991), where VOC was removed to form aerosols and gaseous products at ambient temperature. High performance for the VOC treatment was confirmed through their studies. Strict regulation and effective treatment method for VOC emission are not completely established in Japan yet. Hence, the electron beam treatment of VOC is expected to be a new technology which can be operated at ambient temperature leading to energy saving.

The treatment by electron beam irradiation is based on the reactions of VOC with radicals:

$$\text{VOC} + \text{OH} \longrightarrow \text{aerosols} + \text{gaseous products} \qquad (1)$$

Hydroxyl radicals yielded by the irradiation of humid off-gas react with VOC to give aerosols and gaseous products which may be removed readily. Therefore, the electron beam irradiation may treat various kinds of organic compounds together in one process. This is one of the merits for the method as well as the operation at ambient temperature. Since application of the method requires basic information of the reactions, typical aromatic hydrocarbon, xylene was selected for the irradiation experiments.

In the course of the present study, dose dependence of the xylene removal was studied with quantitative analyses of the aerosols and the gaseous products. Mass balance for the xylene-irradiation is calculated.

EXPERIMENTAL

The experiments on the xylene-irradiation were carried out at ambient temperature using the AGATE II plant of KfK in Germany. The schematic flow chart of the plant is shown in Fig. 1. Gaseous xylene was obtained by the feeding of 150 °C nitrogen into liquid xylene which contained the o- (17.33 %), m- (43.82 %) and p- (19.50 %) isomers and ethylbenzene (17.67 %). The set of the flow rate of the xylene-contained nitrogen gave a constant xylene concentration of about 100 mgC/Nm^3, i.e., 22.5 $\pm$ 0.5 ppm in the air stream of the AGATE II (1000 Nm^3/h). The irradiation of xylene was performed in the dose range of 0-10

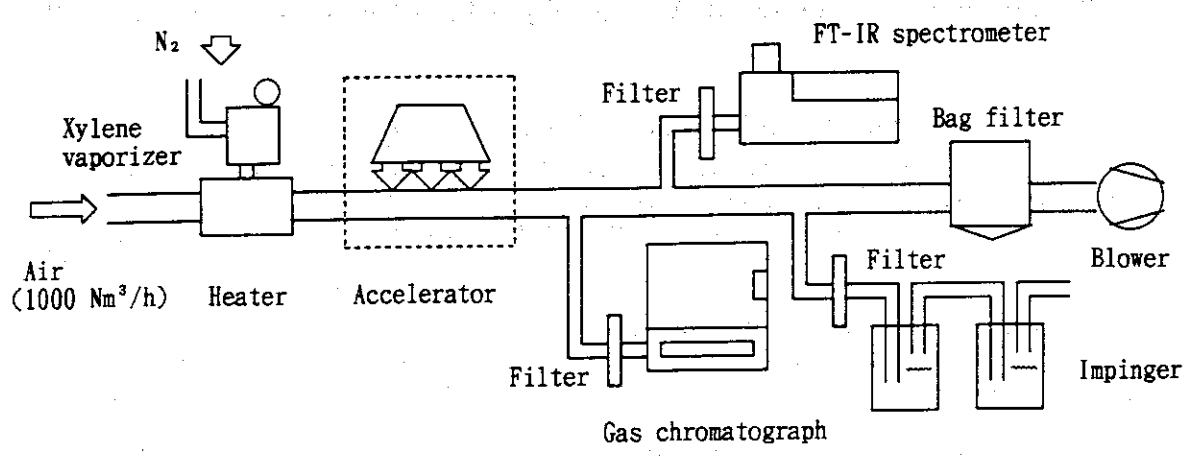


Fig. 1. Schematic flow chart of the AGATE II plant

kGy with an electron beam accelerator supplied 550 keV with current up to 30 mA. The removal of xylene was calculated from the concentration of xylene remaining quantified with a gas chromatograph (Carlo Erba Instruments GC 6000 Vega Series 2). The temperature of the column was increased from 45 to 110 °C at 3 °C intervals per minute for the detection of three isomeric xylenes and ethylbenzene separately. In addition to the GC measurements, a FT-IR spectrometer (Bruker ; ISF 48) was arranged to analyze the by-products such as CO and CO_2 for mass balance estimation of the irradiation experiments.

For the quantitative analyses of the reaction products from the xylene-irradiation, a sampling system was attached in the line of the AGATE II. The system consisted of a filter holder in which a piece of filter was put and two bottle of impingers filled with 40 ml 0.1 N sodium hydroxide. The sample gas was introduced into the alkaline solutions through the filter. The solid aerosols formed were collected on the filter, which is followed by elemental analysis. The alkaline solution was analyzed after the irradiation with a Dionex AI 400 chromatograph for the identification of the gaseous reaction products.

RESULTS AND DISCUSSION

Dose dependence of xylene removal

The results obtained with the GC showed that the electron beam irradiation led to the removal of xylene. The concentration change in gaseous xylene measured with the GC is shown in Fig. 2 as a function of dose. The concentration of xylene remaining decreased markedly in the dose of 0-5 kGy and gradually up to 10 kGy. Approximately 3 ppm of remaining xylene concentration, equal to 87 % of removal efficiency, was obtained at 10 kGy. The remaining xylene concentration approached the constant at higher dose. Since the removal of xylene occurs through the reactions with radicals described above, the staying of the xylene concentration indicates that OH radicals were consumed by the reactions with not only xylene itself but also other species

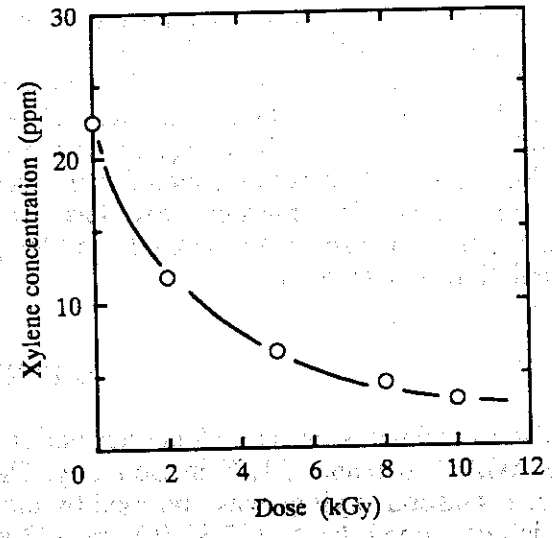


Fig. 2. Concentration of xylene remaining in the air of the AGATE II after electron beam irradiation as a function of dose.

such as reaction products formed much at higher dose.

Dose dependence of three isomeric xylenes

Although the temperature-programmed column of the GC was conducted, the separation of m- and p-xylenes was not obtained. Figure 3 shows concentration changes in three isomeric xylenes with electron beam as a function of dose. The initial concentrations of o-, m- and p-, and ethylbenzene were normalized to 22.5 ppm. The lowest remaining concentration of xylene was obtained from the m- and p-xylenes irradiation, and the highest from the ethylbenzene irradiation in the investigated dose range. Assuming that the initial reactions with OH radicals lead to their removals, this result indicates that m- and p- xylenes are favorable for the reactions with OH radicals. Actually, the OH rate constants of m- (24.5×10^{-12} cm^3 molecule^{-1} s^{-1}; 25 °C) and p- xylenes (15.2×10^{-12}) are higher than those of o-xylene (14.7×10^{-12}) and ethylbenzene (7.5×10^{-12}) (Finlayson-Pitts and Pitts, 1986).

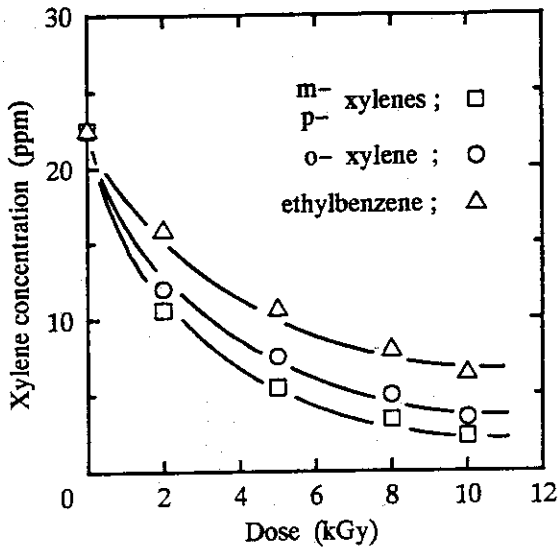


Fig. 3. Concentration change in three isomeric xylenes by electron beam irradiation as a function of dose.

Reaction mechanism

The xylene irradiation gave yellow colored particulates and gaseous products. Four carboxylic acids, i.e., formic, acetic, propionic and butyric acids, were identified as gaseous products with the IC chromatograph. The fact of the yielding of the four carboxylic acids from the xylene-irradiation suggests that the reactions of xylene with OH radicals may lead to the ring cleavage. The reactions of OH radicals with xylene occur via addition of OH radicals to the aromatic ring at temperatures below 320 K (Finlayson-Pitts and Pitts, 1986):

$$C_6H_4(CH_3)_2 + OH \longrightarrow OH\text{-}\cdot C_6H_4(CH_3)_2 \quad (2)$$

The OH-adduct of xylene is formed through initial attack of OH radical. The intermediate, then, has two ways to react with oxygen in air, that is, hydrogen abstraction and oxygen addition reactions (Darnall et al., 1979):

$$OH\text{-}\cdot C_6H_4(CH_3)_2 + O_2 \longrightarrow C_6H_3(CH_3)_2OH + HO_2 \quad (3)$$

$$OH\text{-}\cdot C_6H_4(CH_3)_2 + O_2 \longrightarrow \cdot OO\text{-}C_6H_4(CH_3)_2(OH) \quad (4)$$

$$\cdot OO\text{-}C_6H_4(CH_3)_2(OH) \xrightarrow[O2, NO]{\text{Ring cleavage}} \text{Carboxylic acids etc.} \quad (5)$$

Oxygen addition reaction of (4) may give the ring cleavage of aromatic, which leads to the yielding of various organic compounds through the reactions with NO and/or oxygen. The predominant primary products of the ring opening reactions are simple aldehydes under tropospheric reaction conditions (Shepson et al., 1984). In the present study, further oxida-

Table 1. Elemental analyses of aerosols formed by xylene irradiation

Dose (kGy)	C (%)	H (%)	O (%)	N (%)
5	51.14	6.14	38.80	1.73
10	48.42	5.75	40.70	2.24

Table 2. Carbon balance for xylene irradiation

Dose (kGy)	HCOOH (mgC/Nm³)	CH_3COOH (mgC/Nm³)	C_2H_5COOH (mgC/Nm³)	C_3H_7COOH (mgC/Nm³)	CO (mgC/Nm³)	CO_2 (mgC/Nm³)	Products on the filter (mgC/Nm³)	Unreacted xylene (mgC/Nm³)	Xylene input (mgC/Nm³)	Recovery (%)
10	2.48	6.26	2.58	1.76	5.25	6.31	40.56	13.98	97.02	81.6
8	2.59	5.79	6.05	1.58	6.43	2.37	38.69*)	18.86	95.65	86.1
5	3.41	6.80	26.59	—	4.27	2.70	34.48	29.20	98.27	109.9
2	1.51	3.12	19.21	—	2.52	0.11	22.20*)	49.01	93.75	104.2

tion of the aldehydes has obviously produced the carboxylic acids as secondary products.

The weight of the particulates collected on the filter increased with the dose. The elemental analyses of the particulates showed that they contained approximately 50 % C and 40 % O by weight, as shown in Table 1. Since xylene consists of only carbon and hydrogen, the fact of the existence of oxygen and nitrogen in the particulates suggests that addition reactions of oxygen and nitrogen oxide to the aromatic ring occur with help of electron beam irradiation. Figure 4 shows the concentration fraction of aerosols against xylene removed. Here, it was estimated that aerosols formed with the dose of 2 and 8 kGy contained 50 % C on the basis of the results shown in Table 1. The straight line indicates that 50 % of xylene removed forms aerosols, being independent of the investigated dose range. The fact is expected that VOC can be removed by the filtration of aerosols formed with electron beam at lower dose.

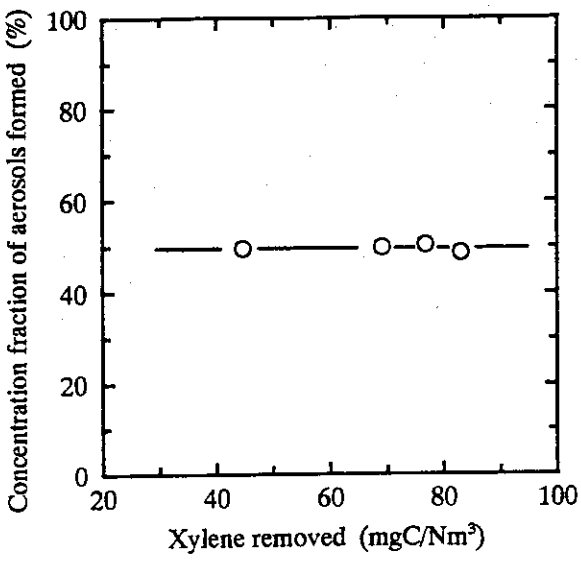


Fig. 4. Concentraiton fraction of aerosols formed by electron beam irradiation of air containing 22.5 ppm xylene against xylene removed.

Mass balance

Mass balance for the xylene-irradiation was calculated on the basis of mgC/Nm³ unit. The results are shown in Table 2. In addition to the gaseous products and the .rm 15.8cm aerosols, CO and CO_2 were formed as carbon-containing by-products. Recoveries of 95 ± 15 % were obtained in all experiments.

CONCLUSIONS

Gaseous xylene was irradiated with electron beam in the dose range of 0–10 kGy. Approximately 85 % of xylene was removed at a dose of 10 kGy. The ion chromatographic analyses identified formic, acetic, propionic and butyric acids as the gaseous products. The major products from the xylene-irradiation were aerosols which constituted 50 % of xylene removed on the basis of mgC/Nm³ unit. Mass balance for the xylene-irradiation showed 95 ± 15 % recoveries in all experiments.

REFERENCES

Darnall K. R., Atkinson R. and Pitts J. N. Jr. (1979) Observation of biacetyl from the reaction of OH radicals with o-xylene. Evidence for ring cleavage. *J. Phys. Chem.* **83**, 1943.

Finlayson-Pitts B. J. and Pitts J. N. Jr. (1986) *Atmospheric Chemistry*. Wiley, New York.

Paur H.-R., Mätzing H. and Woletz K. (1991) Removal of volatile organic compounds from industrial offgas by irradiation induced aerosol formation. *J. Aerosol. Sci.* **22**, S509.

Shepson P. B., Edney E.O. and Corse E. W. (1984) Ring fragmentation reactions on the photooxidations of toluene and o-xylene. *J. Phys. Chem.* **88**, 4122.

14.13 On the Mechanism for Chemical Reactions in the Electron Beam Irradiated Fuel Gas

Shin-ichi Ohno,[1] Hideki Namba,[2] and Okihiro Tokunaga[2]

[1]Inst. Res. Develop., Tokai University, 2-28 Tomigaya, Shibuya-ku, Tokyo 151 and [2]TRCRE, Japan Atomic Energy Research Institute, 1233 Watanuki-machi, Takasaki 370-12

Abstract--- To obtain information on removal efficiency for SO_2 and NO in the coal-fired flue gas by electron beam irradiation, we investigated theoretically a scheme of chemical reactions taking place during irradiation. The yields of primary radiolysis products from N_2 which is the main component (70-80%) of the flue gas were first calculated on the basis of the binary encounter model: $G(N_2^+)$= 2.3, $G(N^+)$=0.4, $G(e^-)$=2.7, $G(N;^4S)$=3.6, and $G(N;^2P$ or $^2D)$=1.4. Then, the fate of these species in the presence of a certain amount of various substances such as O_2, H_2O, CO_2, NH_3, SO_2 and NO was studied with the aid of the rate constants in the literature for ion-molecule reactions and also for N-atom reactions with these molecules. They eventually form aerosols and will be stabilized at the time of say 10^{-3}s after the energy deposition. The G-value for the total reactive species which we can utilize for our purpose is estimated to be 10~11.

INTRODUCTION

Radiation processing can be used for conservation of environment---one such example is electron beam cleaning of flue gases. Since most fossil fuels from which we get energy contain sulfur and nitrogen as impurities, emission of SO_2 and NO will be accompanied and may cause acid rain. Removal of SO_2 and NO from coal-fired flue gas with added ammonia(NH_3) is now regarded as promising among such electron beam processings and several pilot scale tests have been performed (DOE Contract, 1988; BMFT Contract, 1990; Chmielewski et al, 1993; Namba et al, 1993). However, theoretical work which would enable us to estimate maximum G-value for removing SO_2 and NO is still important for the evaluation of energy efficiency for this process.

In the present study, primary radiolysis yields from nitrogen were first calculated using the binary encounter model for collision between incident electron and target electrons, i.e. electrons in the nitrogen molecule combined with the continuous slowing-down approximation (Sato et al, 1974; Okazaki et al, 1975; Ohno et al, 1975). This approximation is known to give primary yields with the accuracy of 20% for the cases of simple molecules such as N_2. Based on these results, together with available rate constant data on relevant ion-molecule reactions and excited nitrogen atom reactions, we will present a figure in which various chemical species appear in the medium under irradiation as a function of time starting from the radiation energy deposit. With this figure we can deduce the maximum expected G-value for removing SO_2 and NO.

PRIMARY YIELD CALCULATION

Suppose an incident electron having the kinetic energy T collides with an electron in the molecule whose ionization energy is I_i and kinetic energy in the molecule K_i and transfers the energy of E. The cross-section for this is given as

$$\sigma_E(T)dE = \frac{\pi e^4}{T+I_i+K_i}\left(\frac{1}{E^2} + \frac{4K_i}{3E^3}\right) dE \qquad (1)$$

After the collision the kinetic energy of the incident electron becomes T-E, while the target electron, on receiving the energy E, is ejected from the molecule and can now move freely in the medium with the kinetic energy of $E-I_i$ and the molecule becomes ionized. In principle, we can treat this problem using quantum mechanics, but in this case we can only solve for the case of H_2 and He. For the cases of more complex molecules such as N_2, use of classical mechanics is very useful (Vriens, 1969).

The ionization energy I_i of the N_2 molecule may be known from the ESCA and PES data. If the energy received by an electron in the molecule is not sufficient enough to be ejected, the electron remains in the molecule but in a higher molecular orbital, thus giving an excited state. The ejected electron in turn enter into exciting and ionizing collisions if it has still sufficient energy. Calculation procedure is rather simple (Sato et al, 1974). Moreover, it should be mentioned that double collisions can be also included in the calculation. The double collision occurs when an incident electron succesively collides with two electrons in a molecule or else the ejected electron from the first collision collides with a second electron in the same molecule. The 6-valence electrons in N_2 are assumed to be situated uniformely on the surface of the sphere with a radius of 1Å. The 2nd ionization or excitation level is tentatively taken to be 2xI(1) or 2xE_i(1), respectively.

FATE OF PRIMARILY PRODUCED IONIC SPECIES AND EXCITED N-ATOMS

Radiolysis of N_2-molecules produces various ionic species and N-atoms as primary products. It would be convenient to know first the time after the primary energy deposition at which charge neutralization between positive and negative ionic species takes place. This time can be estimated by the equation:

$$t_{1/2} = 1/\, k_{rec}[n_i] \qquad (2)$$

where k_{rec} is rate constant for charge recombination reation and $[n_i]$ is the concentration of ionic species (positive or negative) during irradiation. At the steady-state irradiation with dose rate of D(kGy/s) and the density of the medium ρ,

$$dn_i/dt = G_{ion}\, D\, \rho - k_{rec}\, n_i^2 = 0 \qquad (3)$$

holds and $[n_i]$ can be estimated. Thus, charge neutralization time ($t_{1/2}$) may be determined as in Eq. 2. By this charge neutralization time, positive and

negative ions initially produced would have changed into different ions through seeral ion-molecule reactions. We can get information about what ion-molecule reaction is most dominant over others by comparing the reported rate constants (Ikezoe et al, 1989; Tabata et al, 1990) of all the existing impurities (Table 1). For example, N_2^+ ion would react with N_2 ($2\times10^{19}cm^{-3}$; 70%), H_2O ($2.7\times10^{18}cm^{-3}$; 10%) and CO_2 ($2.7\times10^{18}cm^{-3}$; 10%) with rate constant 1.6×10^{-9}, 1.6×10^{-9}, 2×10^{-9},and 8×10^{-10} mole$^{-1}cm^3s^{-1}$, respectively, the reaction time being respectively 3.5×10^{-11}, 1.3×10^{-10}, and 3×10^{-10}s. One may also deduce from these figures that the initially produced N_2^+ becomes to N_4^+(80%), H_2O^+(14%) and CO_2(5%) at the time of 3×10^{-11}~10^{-10}s. We can make similar estimation for N^+, N_4^+, H_2O^+ and other ions and other reactive species to know what species appear as time goes by.

Table 1. Concentration of gas components in the flue gas used in the present calculation. NH_3 is added to the system to form aerosols.

Component	N_2	O_2	H_2O	CO_2	NO	SO_2	NH_3
%	70	10	10	10	0.01	0.1	0.1

Table 2. Ionization yields from each M.O. of the N_2 molecule.

M.O.	No. of electron	G-value	Mode of decomposition
$3\sigma_g$	2	0.59	$N_2^+ + e$
$1\pi_u$	4	0.93	
$2\sigma_u$	2	0.47	
$2\sigma_g$	2	0.13	$N^+ + N + e$
KK	4	0.014	$N^+ + N^+ + 2e$

Table 3. Excitation yields from each M.O. of the N_2 molecule.

M.O.	No. of electron	G-value	Mode of decomposition
$3\sigma_g$	2	1.24	$N(^4S) + N(^4S)$
$1\pi_u$	4	1.12	$N(^4S) + N(^2P,^2D)$
$2\sigma_u$	2	0.26	$N_2^+ + e$
$2\sigma_g$	2	0.05	$N^+ + N(^2P,^2D) + e$
KK	4	0.0004	$N^+ + N^+ + 2e$

Table 4. Double excitation and/or ionization of valence M.O.(σ_g, π_u, σ_u) of the N_2 molecule

	G-value	Mode of decomposition
N_2^{++}(ioni.-ioni.)	0.025	$N^+ + N^+ + 2e$
N_2**(excit.-excit.)	0.039	$N_2^+ + e$
N_2^+*(ioni.-excit.)	0.11	$N^+ + N(^2P,^2D) + e$

RESULTS AND DISCUSSION

[Primary yields] Table 2-4 include the results of the present calculation of primary products in G-value, namely yields of ionization and excitations from each M.O. and double excitation and/or ionization of valence M.O. of the N_2 molecule. Probable decomposition mode of these electronically excited states are also indicated in the figures. According to the mode of decomposition, we can

deduce: $G(N_2^+) = 2.3$, $G(N^+) = 0.4$, G(e) 2.7, G(N: ^4S) = 3.6, and G(N: ^2P or ^2D) = 1.4. The primary radiolysis yields had been given by Willis and Boyd (Willis et al, 1976). They utilaized the reported W-values, that is to say the experimental total ionization yield, and also usd reported relative cross-sections of each excitations for a fixed electron energy(100 eV) instead of attempting an integration of a whole range from an incident electron, for example 800 keV, to zero energy. Nevertheless, their results: $G(N_2^+) = 2.27$, $G(N^+) = 0.69$, G(e) 2.96, and G(N: ^4S, ^2P, ^2D) = 5.41 are in good agreement with the present ones.

[Ion-molecule reaction] Electrons after thermalization will be captured by H_2O, O_2, and CO_2 to form negative ions. Positive (N_2^+ and N^+) and negative ions undergo ion-molecule reactions with existing molecules in the flue gas and eventually they will disappear through charge recombination. As the charge neutralization rate constant k_{rec} is known to be 10^{-6}~10^{-8} cm^3s^{-1} (Tabata, 1991) and, for the most typical cases, D is 10kGy/s with ρ = 1 kg/m^3 and G_{ion} = 2.7 as above, we get $[n_i] = \sim 10^{11}\,cm^{-3}$. Therefore, the charge neutralization, from Eq.2, should be expected to occur at 10^{-4}~10^{-5}s after the energy deposition. By this time the positive ions primarily produced, N_2^+ and N^+ with G-value of 2.7, will have reacted with N_2 and H_2O to form $H_3O^+(H_2O)_n$ and OH, and, furthermore, the $H_3O^+(H_2O)_n$ will change into $NH_4^+(H_2O)_n$ by reacting with ammonia.

$$N_2^+ + N_2 + N_2 \rightarrow N_4^+ + N_2,\ k = 8\times10^{-29}\,mole^{-2}cm^6s^{-1}$$
$$N_4^+ + nH_2O \rightarrow H_3O^+(H_2O)_n + OH + 2\,N_2$$
$$H_3O^+(H_2O)_n + NH_3 \rightarrow NH_4^+(H_2O)_n$$

The OH radical produced is known to react with NO and SO_2 at the time 2×10^{-5}s with G = 2.45; see Fig. 1. Negative charge changes through $H_2O^-(H_2O)_n$, $O_2^-(H_2O)_n$ and then further into SO_4^- with associated water molecules:

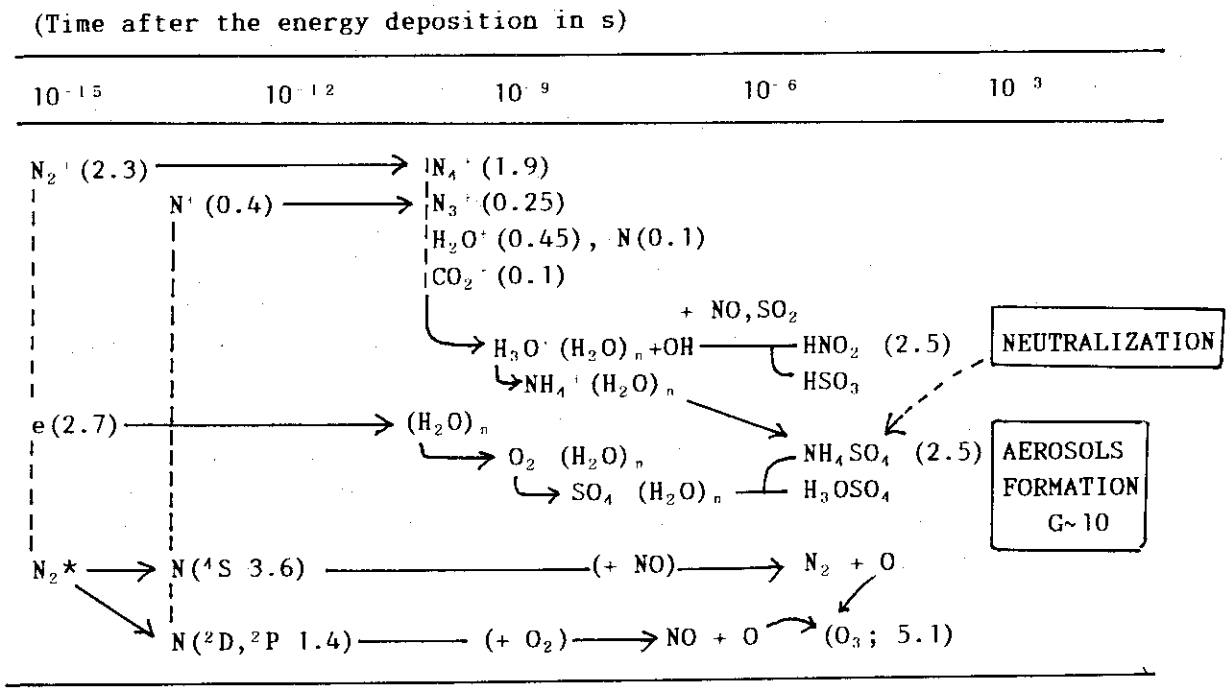
$$O_2^-(H_2O)_n + SO_2 \rightarrow SO_4^-(H_2O)_n \text{ with } k\sim2\times10^{-9}\ mole^{-1}cm^3s^{-1}.$$

Thus, the ion neutralization occurs most probably between $H_3O^+(H_2O)_n$ or $NH_4^+(H_2O)_n$ and $SO_4^-(H_2O)_n$ (with G~ 2.4) by the time after ~ 10^{-4}s. The resulting molecule H_3OSO_4 or NH_4SO_4 would further oxidize NO or SO_2 to become chemically stabilized.

[The fate of the N-atoms] The N-atom reacts somewhat differently depending on the electronic state of the N-atom. ^2P or ^2D state will react mainly with O_2 to produce NO and O (G~1.4). The N-atom in the ^4S ground state will react with NO at ~3×10^{-5}s to produce N_2 and O-atom (G~3.6). The O-atom in turn reacts with O_2 to produce O_3. The G-value of O_3-formation will amount to 5.1.

The products yields which can be used to oxidize SO_2 and NO will amount to about G = 10. However, if the reaction intermediates such as H_3OSO_4 or NH_4SO_4 regenerate reactive radicals which may oxidize NO or SO_2, higher G-values than 10 may be expected. They recombine with each other to be stabilized and to form possibly aerosols at the time after ~10^{-3}s. In conclusion, we should like

Fig 1. Ionic and radical species appearing as a function of time after the energy deposition in the flue gas; They finally form aerosols at ~10^{-3}s with maximum G-value(~10) of removing SO_2 and NO.



to stress the importance of basic research on the behavior of aerosols as well as its formation mechanism under irradiation for a better understanding of radiation chemistry of the flue gas.

REFERENCES

BMFT Contract(1990), 03E-6354-A.
Chmielevski A.G. et al(1993), Radiat. Phys. Chem., 42, 663.
DOE Contract(1988), AE22-830PC60259.
Ikezoe Y. et al(1987), "Gas Phase Ion-Molecule Reaction Constants Through 1986," Maruzen, Tokyo
Namba H. et al(1993), Radiat. Phys. Chem., 42, 669.
Ohno S. et al(1975), Bull. Chem. Soc. Jpn., 48, 2153.
Okazaki K. et al(1975), Bull. Chem. Soc. Jpn, 48, 1141.
Sato S. et al (1974), Bull. Chem. Soc. Jpn., 47, 2174.
Tabata Y. et al ed.(1991) "Handbook of Radiation Chemistry," CRC Press.
Vriens L. et al(1969), "Case Studies in Atomic Collision Physics," North Holland, Amsterdam, p. 335.
Willis C. and Boyd A.W.(1976), Radiat. Phys. Chem., 8, 71.

List of Participants

Agneza, S., サフランニ・アグネサ	JAERI Takasaki
Aoki, Y., 青木 康	JAERI Takasaki
Agematsu, K., 上松 敬	JAERI Takasaki
Arai, H., 新井 英彦	JAERI Takasaki
Arakawa, K., 荒川 和夫	JAERI Takasaki
Awano, T., 淡野 照義	Tohoku Gakuin University
Cai Zhongli, 蔡 中麗	Xiamen Torch High-Tech Indus.Devel.Corp.
Cao Jin, 曹 瑾	East China University of Science and Technology
Chen Wenxiu, 陳 文秀	Beijing Nomal University
Chen Xinfang, 陳 欣方	Institute of Material Science, Jilin University
Deba Bahadur Khadka, テバ・バハドゥル・カドカ	Tokyo Institute of Techno1ogy
Dohke, T., 道家 忠義	Waseda University
Domae, M., 堂前 雅史	The University of Tokyo
Fang Meizhen, 方 美珍	Suzhou Wu Xian Radiation Products Factory
Feng Wen, 馮 文	Chengdu Research Center of Silicones, Mini. of Chem. Indus.
Fukuchi, Y., 福地 雄士	Tokyo Institute of Technology
Fujita, K., 藤田 和利	Sumitomo Electric Industries, LTD.
Fu Zhonghua, 傅 中華	Southwest Institute of Nuclear Physics and Chemistry
Futami, T., 二見 達也	Sumitomo Metal Mining Co., LTD.
Goppelt-Langer, P., ピーター・ゴッペルトランガー	JAERI Takasaki
Hama, Y., 浜 義昌	Waseda University
Hara H., 原 秀元	Micro Device Co., LTD.
Hasegawa K., 長谷川 圀彦	Shizuoka University
Hatano, Y., 旗野 嘉彦	Tokyo Institute of Technology
Hill, D.J.T., ディビット・ジェイムス・ヒル	The University of Queensland
Hirade, T., 平出 哲也	JAERI Tokai
Hirota, K., 広田 耕一	JAERI Takasaki
Hou Fuzhen, 侯 福珍	The Specialty Committee of Radiation Processing
Hosoi, F., 細井 文雄	JAERI Takasaki
Hu Fumin, 胡 福敏	Chengdu Research Center of Silicones, Mini. of Chem. Indus.
Hu Jinhui, 胡 金慧	Beijing Radiation Application Research Center
Ichikawa, T., 市川 恒樹	Hokkaido University
Imai, M., 今井 正彦	Tokyo Metropolitan Isotope Research Center
Imamura, M., 今村 昌	Riken (The Institute of Physical and Chemical Research)
Inamura, T., 稲邑 豊昭	Sumitomo Heavy Industries, LTD.
Ishigure, K., 石榑 顕吉	The University of Tokyo
Ito, M., 伊藤 政幸	JAERI Takasaki
Ito, Y., 伊藤 泰男	The University of Tokyo
Jin Haofang, 金 浩芳	Peking University
Kaetsu, I., 嘉悦 勲	Kinki University
Kashiwazaki, S., 柏崎 茂	Hitachi Cable, LTD.
Kataoka, T., 片岡 忠孝	Eikosha, LTD.
Katoh, R., 加藤 隆二	Gakushuin University
Katsumura, Y., 勝村 庸介	The University of Tokyo

Kawakami, K., 川上 和市郎	JAERI Takasaki
Kimura, K., 木村 一宇	Riken (The Institute of Physical and Chemical Research)
Kobayashi, K., 小林 一雄	Osaka University
Kobayashi, Y., 小林 慶規	Nationa1 Institute of Materials and Chemica1Research
Kojima, M., 小嶋 雅之	Musashi Institute of Technology
Kojima, T., 小嶋 拓治	JAERI Takasaki
Kokubu, K., 国分 晋裕	Waseda University
Komaguchi, K., 駒口 健治	Hiroshima University
Kouchi, N., 河内 宣之	Tokyo Institute of Techno1ogy
Koyama, T., 小山 武志	Waseda University
Kubo, J., 久保 純一	Nippon Oil Company LTD.
Kudoh, H., 工藤 久明	JAERI Takasaki
Li Chaoshun, 李 朝順	Beijing Radiation App1ication Research Center
Li Li, 李 莉	The University of Tokyo
Lin Nianyun, 林 念芸	Inst. Nucl. Res. Shanghai
Lugão, A. B.; エイ・ビー・ルガオ	JAERI Takasaki (IPEN, Brazil)
Lu Zhaoxin, 陸 兆新	Radia Industry Co., LTD.
Machida, H., 町田 寛子	Niigata Kohnan High School
Majima, T., 真嶋 哲朗	Osaka University
Makuuchi, K., 幕内 恵三	JAERI Takasaki
Matsuum, T., 松浦 辰男	Rikkyo Universfty
Matsuyama, T., 松山 奉史	Kyoto University
Ma Zhongquan., 馬 忠権	JAERI Takasaki
Ma Zue-Teh., 馬 瑞徳	Shanghai University of Science and Technology
Miki, M., 三木 美弥子	Osaka University
Minegishi, A., 峯岸 安津子	Kanagawa University
Mittal, J. P.; ジェイ・ピー・ミッタル	Bhabha Atomic Research Centre
Miyazaki, T., 宮崎 哲郎	Nagoya University
Mizusawa, K., 水澤 健一	Nissin-High Voltage Co.,LTD.
Naka, Y., 仲 幸彦	Kinki University
Nakai, K., 中井 康二	Nissin-High Voltage Co., LTD.
Nagaishi, R., 永石 隆二	The University of Tokyo
Nagasawa, K., 長沢 可也	Shonan Institute of Tech.
Nakagawa, K., 中川 和道	Kobe University
Nishikawa, M., 西川 勝	Kanagawa Institute of Technology
Nishimoto, S., 西本 清一	Kyoto University
Nogami, M., 野上 雅伸	Tokyo Institute of Technology
Odaka, T., 小高 貴浩	Tokyo Institute of Technology
Ogasawara, M., 小笠原 正明	Hokkaido University of Education
Ohki, Y., 大木 由美	Tohtsu Co., LTD.
Ohki, Y., 大木 義路	Waseda University
Ohno, S., 大野 新一	Tokai University
Ohta, A., 太田 顕成	Kitasato University
Oshima, A., 大島 明博	Tokai University
Ota, S., 太田 晋一	Sumitomo Electric Industries, LTD.
Otsuhata, K., 乙幡 和重	Raytech, LTD.
Oya, K., 大矢 恭久	Tokyo Institute of Technology
Qiao Jinliang, 喬 金梁	Beijng Res. Inst. of Chem.Indus., Mini. of Chem. Indus.
Rao Lei, 饒 蕾	Changchun Institute of Applied Chemistry

Sasaki, T., 佐々木 隆	JAERI Takasaki
Sawai, T., 沢井 健	Tokyo Metropolitan Isotope Research Center
Sawai, T., 沢井 照子	Tokyo Metropolitan Isotope Research Center
Seguchi, T., 瀬口 忠男	JAERI Takasaki
Sekiguchi, M., 関口 正之	Tokyo Metropolitan Isotope Research Center
Shibasaki, Y., 柴崎 芳夫	Saitama University
Shigeta, M., 繁田 道男	Koga Isotope, LTD.
Shiotani, M., 塩谷 優	Hiroshima University
Shimamori, H., 嶋森 洋	Fukui Institute of Technology
Shimoyama, I., 下山 巌	Kobe University
Shinohara, N., 篠原 信好	Yokohama City University
Shinsaka, K., 新坂 恭士	Kanazawa Institute of Technology
Shukushima, S., 宿島 悟志	Sumitomo Electric Industries, LTD.
Silverman, J., ジョゼフ・シルバーマン	University of Maryland
Siqin Dalai, 斯欽 達来	Beijing Nomal University
Soebianto, Y.S., ソエビアント・ヤンテイ・サバリナ	The University of Tokyo
Song Xiu Feng	Shanghai Duo Yuan Engineering Materials Co., LTD.
Sugoh, T., 須郷 高信	JAERI Takasaki
Sunaga, H., 須永 博美	JAERI Takasaki
Sunagawa, T., 砂川 武義	Fukui Institute of Technology
Sun Jiazhen, 孫 家珍	Changchun Institute of Applied Chemistry
Suzuki, I., 鈴木 功	Electrotechnical Laboratory
Suzuki, T., 鈴木 健訓	KEK(National Laboratory for High Energy Physics)
Takamuku, S., 高椋 節夫	Osaka University
Tagawa, S., 田川 精一	Osaka University
Takenaka, Y., 竹中 康之	Hokkaido University of Education
Takehisa, M., 武久 正昭	Radia Industry Co., LTD.
Tanaka, Y., 田中 康寛	Musashi Institute of Technology
Tanabe, H., 田辺 寛子	Tokyo Metropolitan Isotope Research Center
Tabata, Y., 田畑 米穂	Atomic Energy Commission
Tabei, M., 田部井 雅枝	Tokyo Motropolitan Isotope Research Center
Tamura, N., 田村 直幸	Radiation Application Development Association
Tsuchimoto, H., 土本 浩子	Shizuoka University
Tomita, K., 富田 恵一郎	Radia Industry Co., LTD.
Ueno, K., 上野 桂二	Sumitomo Electric Industries, LTD.
Ukai, M., 鵜飼 正敏	Tokyo Institute of Technology
Ushida, K., 丑田 公規	Riken (The Institute of Physical and Chemical Research)
Wang Binglin, 王 炳林	Beijing Radiation Application Research Center
Wang Deren, 王 徳仁	Suzhou Wu Xian Radiation Products Factory
Washio, M., 鷲尾 方一	Sumitomo Heavy Industries, LTD.
William Lee, ウィリアム・リー	JAERI Takasaki
Wei Genshuan, 魏 根栓	Peking University
Wu Guozhong, 呉 国忠	The University of Tokyo
Wu Jilan, 呉 季蘭	Peking University
Wu Minghong, 呉 明紅	SARI/SUST
Xie Liqing, 謝 立青	Beijing Normal University
Xu Jun, 徐 俊	Changchun Institute of Applied Chemistry
Yamamoto, S., 山本 幸男	Osaka University

Yamaoka, H., 山岡 仁史	Kyoto University
Yamase, Y., 山瀬 豊	Sumitomo Heavy Industries, LTD.
Yao Side, 姚 思徳	Inst. Nucl. Res. Shanghai
Yokogawa, K., 横川 薫	Beam Operation Co., LTD.
Yoshida, H., 吉田 宏	Hokkaido University
Yoshida, M., 吉田 勝	JAERI Takasaki
Yoshida, Y., 吉田 陽一	Osaka University
Yoshii, F., 吉井 文男	JAERI Takasaki
Yoshioka, H., 吉岡 閤江	Shizuoka University
Zhang Lihua, 張 利華	Changchun Institute of Applied Chemistry
Zhang Manwei, 張 曼維	University of Science and Technology of China
Zhang Zhicheng, 張 志成	University of Science and Technology of China
Zhang Zhiping, 張 志平	East China University of Science and Technology
Zheng Zheng, 鄭 正	Institute of Atomic Energy, Jiangsu Acad. of Agri. Sci.
Zhou Ling, 周 玲	Kyoto University
Zhong Xiaoguang, 鐘 暁光	Changchun Institute of Applied Chemistry
Zushi, T., 圖師 丈裕	Shizuoka University

AUTHOR INDEX

Agematsu, T. 467
Aikawa, Y. 46
Akai, G. 502
Akama, K. 507
Aoki, Y. 536, 552
Arai, H. 184
Arai, M. 184
Arakawa, K. 467
Awano, T. 248, 547
Azami, K. 96
Bahadur, Khadka Deba 439
Bozek, J. D. 236
Byakov, V. M. 189
Cai, Zhongli 91
Cao, Jin 428
Chaisupakitsin, M. 152
Chen, D. 105
Chen, Ruyi 293
Chen, Wenxiu 349, 356, 414, 481
Chen, Xinfang 408
Chen, Zefang 574
Chen, Zuyao 593
Chu, Jiegen 569
Dai, Honggui 367
Deligeer, 255
Ding, Zhongli 157, 598
Dohguchi, N. 542
Domae, M. 189, 194
Du, Qiang 221
Fang, Xingwang 4, 81
Fang, Meizhen 317, 607
Feng, Wen 562, 574
Fujii, Y. 125
Fujikawa, C. 243
Fukuchi, Y. 439
Furusaki, S. 372
Gao, Juncheng 293
Gopinathan, C. 35
Goppelt-Langer, P. C. 536, 552
Gu, Hongchun 338
Hama, Y. 101, 458
Hamakawa, S. 96
Hamanaka, K. 101
Hara, H. 270
Haruyama, Y. 344
Hasegawa, K. 179, 502
Hasegawa, H. 458
Hatano, Y. 21, 69, 439
He, Yongke 91
Hill, D. J. T. 115
Hirade, T. 64
Hiroishi, D. 199
Hirose, M. 396
Hirota, K. 615
Hishita, S. 265
Hopewell, J. L. 115
Hosoi, F. 507
Hou, Fuzhen 241
Hu, Jinghui 221
Hu, Fumin 562, 574
Huang, Guanglin 562
Hyakutake, K. 392
Ichikawa, T. 120
Ikeda, S. 487
Ikezawa, M. 248, 547
Imai, M. 141
Inamura, T. 46
Ishida, A. 76
Ishigure, K. 96, 189, 194, 199
Ishikawa, M. 527
Isoda, K. 69
Ito, Y. 110
Ito, M. 136
Jia, Wentao 408
Jia, Haishun 481
Jiang, P. Y. 194
Jin, Haofang 81
Kaetsu, I. 231
Kasai, N. 321
Kashiwagi, M. 401
Kashiwazaki, S. 270
Katakai, R. 377, 434
Kato, R. 243, 453, 557
Katsumura, Y. 96, 189, 194, 199
Kawakami, W. 29
Kimura, A. 557
Kitajima, M. 439
Kobayashi, K. 255, 492
Kobayashi, Y. 265
Kojima, I. 265
Kojima, T. 270, 344, 362
Kojima, M. 476
Kokubu, K. 458
Komaguchi, K. 527
Kondo, K. 110
Kotani, M. 557
Kouchi, N. 69, 439
Kouzuma, T. 255
Koyama, T. 542
Kubo, J. 96, 129
Kubota, H. 434
Kudoh, H. 96, 101, 321, 472, 487
Kusama, Y. 542
Kusuhata, I. 96
Lacmann, K. 453
Lan, Liqiao 517
Lee, H. C. 211
Lee, William 372
Li, Chenghua 349
Li, Shuhua 408
Li, Chaoshun 419
Lian, Z. R. 167
Lin, Nianyun 167, 211, 204
Lin, W. Z 211
Liu, Xiaolan 285
Liu, Changhai 303
Liu, Xiaoguang 338
Liu, Aiguo 356, 481
Lu, Zhaoxin 298
Lu, Xianliang 428
Ma, Zueteh 157, 383, 598
Ma, Z. Q. 536
Majima, T. 76
Makita, T. 444
Makuuchi, K. 152, 372, 392, 584
Maruyama, J. 557
Matsubayashi, T. 285
Matsumoto, H. 101
Matsuura, T. 179
Matsuyama, T. 248, 547
Matsuyama, S. 270
Miki, M. 492
Minegishi, A. 497
Mitani, T. 243
Mittal, J. P. 35, 166
Miura, T. 110
Miyata, T. 184
Miyata, K. 326
Miyazaki, T. 522
Mizusawa, K. 401
Morii, K. 243
Musasa, H. 444
My, N. T. 552
Mätzing, H. 615
Nagaishi, R. 194
Nagaoka, N. 434
Naka, Y. 462, 588
Nakagawa, K. 243, 557
Nakai, K. 401
Nakamura, N. 255
Nakano, Y. 507
Namba, H. 184, 620

Naramoto, H. 536, 552
Nishijima, S. 326
Nishikawa, H. 542
Nishimoto, S. 152, 216
Nogami, M. 125
Numajiri, M. 110
O'Donnell, J. H. 115
Odaka, T. 69
Ogasawara, M. 36, 252
Ohki, Y. 476, 542
Ohno, S. 620
Ohta, A. 285
Okada, T. 326
Oki, Y. 110
Okumura, S. 467
Omichi, H. 377, 434, 507
Oshima, M. 449
Oshima, A. 487
Otsuhata, K. 129, 487
Oya, Y. 179
Oyama, K. 120
Pang, Ruicao 349
Paur, H.-R. 615
Phillips, G. O. 231
Pomery, P. J. 115
Pu, Hongding 598
Qian, Yitai 593
Qiao, Jinliang 146
Rao, Zhigong 419
Rao, Lei 579
Safranj, A. 377, 434
Saito, N. 236
Saito, K. 372
Sakumoto, A. 184
Sasaki, T. 424
Sasuga, T. 101, 321, 472
Sawai, T. 280
Schmidt, W. F. 453
Seguchi, T. 96, 101, 321, 472, 487, 542
Seike, H. 152
Sekiguchi, M. 141, 280, 610
Sekitani, T. 557
Shi, Lei 512
Shibasaki, Y. 275
Shidara, S. 255
Shimamori, H. 444
Shimizu, H. 141
Shimoyama, I. 243, 557
Shinohara, N. 449
Shinsaka, K. 69
Shiotani, M. 527
Shiraishi, K. 424
Shukushima, S. 260
Siqin, Dalai 414
Soebianto, Y. S. 96
Sohma, J. 497
Sudani, K. 231
Sugo, T. 125, 372
Sun, Jiazhen 11
Sunaga, H. 184, 344
Sunagawa, T. 444
Sunaryo, G. R. 199
Suzuki, T. 110, 265
Suzuki, H. 236
Suzuki, S. 255
Tabata, Y. 1, 487
Tabei, M. 141, 610
Tagawa, S. 59, 255, 462, 492, 588
Takada, T. 476
Takahashi, K. 396
Takamuku, S. 76
Takeda, S. 424
Takehisa, M. 298, 603
Takenaka, Y. 531
Takeshita, T. 536, 552
Takizawa, H. 285, 344
Tamura, N. 337
Tanabe, T. 280
Tanaka, Y. 476
Tanaka, K. 557
Tang, Hao 408
Tatsumi, Y. 444
Tokunaga, O. 620
Tokuyama, S. 507
Uchida, K. 231
Ueno, K. 260
Ueta, S. 231
Ukai, M. 54, 69, 439
Ushida, K. 497
Wang, Binling 51, 419
Wang, W. F. 167
Wang, Zhixing 221
Wang, Guanghui 225
Wang, Gengchao 308
Wang, Deren 317, 607
Wang, Pengcheng 338
Wang, Yufang 562
Washio, M. 396
Wei, Genshuan 146, 225
Wu, Jilan 4, 81, 91, 146, 225
Wu, Minghong 157, 598
Xie, Liqing 293, 338, 517
Xie, Zongchuan 298, 367
Xie, Wenbing 579
Xu, Jun 303, 579
Xu, Ziyan 419
Xu, Xiangling 512
Yaguu, H. 270
Yamada, H. 69
Yamada, Y. 141
Yamaguchi, K. 255
Yamamoto, Y. 462, 588
Yamamoto, S. 536, 552
Yamaoka, H. 326
Yamase, Y. 46
Yan, Di 221
Yang, Ruipu 225
Yang, Huili 303
Yang, Huali 408
Yao, S. D. 167, 211
Yao, Jinyu 579
Ying, Hengfeng 293
Ying, Shengkang 308
Yoshida, Y. 59, 462, 588
Yoshida, H. 120
Yoshida, M. 377, 434
Yoshii, F. 152, 392, 584
Yoshinaga, K. 502
Yoshioka, H. 502
Yoshioka, H. 502
Yotsumoto, K. 344
Yuan, Lihua 574
Zhang, Xujia 81
Zhang, H. 105
Zhang, L. 105
Zhang, Fengru 146
Zhang, Juhong 146
Zhang, J. S. 167, 211
Zhang, Peiling 293
Zhang, Yinfen 293, 338
Zhang, Zhiping 308
Zhang, Yanli 349
Zhang, Zihui 419
Zhang, Zhenli 428
Zhang, Zhicheng 512, 569
Zhang, Manwei 512, 593
Zhang, Yinden 517
Zhao, Yongfu 367
Zheng, Zheng 367
Zheng, Xinmiao 419
Zhou, Ling 216
Zhou, Ruiyng 517
Zhu, Zhiqin 275
Zhu, Po 574
Zhu, Yingjie 593
Zuo, Z. H. 211
Zushi, T. 179